Silicon Compounds in Low Oxidation States Supported by a Cyclic (Alkyl)(Amino)Carbene: Synthesis, Structure and Reactivity

---

Dissertation

Submitted in the fulfillment of the degree

doctor rerum naturalium

(Dr. rer. Nat.)

of

The Faculty of Mathematics and Natural Sciences

of

the University of Bonn

by

Fabian Gstrein, M. Sc.

born in Schlanders-Silandro, Italy

Bonn, 2022

Prepared with the consent of the Faculty of Mathematics and Natural Sciences of the University of Bonn.

Thesis committe members:

Prof. Dr. Alexander C. Filippou (1st Examiner)

Prof. Dr. Robert Glaum (2nd Examiner)

Prof. Dr. Dirk Menche (3rd Examiner)

Prof. Dr. Diana Imhof (4th Examiner)

Date of dissertation defense: 27th February 2023

Year of publication: 2023

Acknowledgements

I would like to express my gratitude to Prof. Dr. Alexander C. Filippou for his invaluable guidance and for the opportunity to work in his well-equipped laboratory on this highly challenging research topic. In this context, I would like to thank Dr. Ujjal Das, who not only layed the fundations for this work, but also encouraged the progress of my dissertation by many valuable suggestions and for proofreading the first draft of the thesis.
I would like to thank:

- Prof. Dr. Olav Schiemann and Hamed Alei for the EPR spectroscopic studies and for the valuable discussions, which provided a deeper understanding of the nature of the measured radicals.
- Prof. Dr. Sven Schneider and Dr. Daniel Delony, in the university of Göttingen, for the opportunity to perform isothermal titration experiments of my compounds.
- The NMR department, Dipl.-Ing. Karin Prochnicki, Hannelore Spitz, Ulrike Weynand and Dr. Senada Nozinovic for recording solution NMR spectra and for their guidance in the recording of countles variable temperature measurments.
- Kerstin Kühnel-Lysek, Hannelore Spitz, Anna Martens and Dr. Sabine Rings for the preparation and measurement of the elemental analysis samples.
- Charlotte Rödde and Dr. Gregor Schnakenburg for the X-ray crystallographic measurements and molecular structure solutions.
- Jens Rump, Leonard Maurer and Dr. Gregor Schnakenburg for the quantum chemical calculations, providing a deeper insight into the nature of the electronic structure of my compounds.
- Andreas Lülsdorf and Leonard Maurer for UV-Vis measurements.
- Max Bogner and Jens Rump for cyclic voltammetric measurements.
- Dr. Jürgen Tirrée for the competent technical support and for keeping the lab running.
- All research group members for the friendly atmosphere and productive scientific and non-scientific discussions.
- The University of Bonn for the financial support of this work.

Finally, I would like to thank my mom for constant emotional support and my dad for inspiring me to work harder for my goals.

"Quality is not an act, it is a habit."
– Aristotle

Table of Contents

1 Introduction

Silicon is the eighth most common element in the universe by mass, it is the most abundant heavier main group element in the solar system and it is widely distributed in cosmic dusts, planetoids and planets in various forms of silicon dioxide (SiO_2) or silicates. More than 90% of the Earth's crust is composed of silicate minerals, making silicon the second most abundant element in the Earth's crust (26.3% by mass), after oxygen.[1] Besides its close proximity in the periodic table to carbon it differs remarkably in terms of its physical and chemical properties, which can be attributed to the different electronegativities (C: 2.55, Si: 1.9)[1] and atomic radii (C: 1.90 Å, Si: 2.32 Å).[2] Also, on the molecular level their compounds differ drastically. For example, C–C bond is one of the most naturally abundant chemical bonds involving main group elements, whereas, compounds featuring Si–C bonds are very rare in nature presumably due to high oxophilicty of Silicon.

Elemental silicon is essential for the semiconductor and solar cell industry and occurs in our daily life in form of silicones. In most of its compounds, inter alia, silicones it features four substituents at the silicon centers. Contrary if it features less than four bonds then a low valent silicon compound would result. These mostly highly reactive compounds play an essential role in the industry: Two-coordinate dihalosilylenes (SiX_2), for example, are key intermediates in the Müller-Rochow process in the synthesis of alkyl(chloro)silanes.[5,6] Silicon radicals, such as the SiH_x ($x = 1 – 3$) and Si_2H_x ($x = 1 – 5$) molecules, are transient intermediates in the chemical vapor deposition (CVD) of silicon or silicon-containing thin films,[7] which play a crucial role in the synthesis of highly pure polysilicon, that is extensively used in the semiconductor industry. Therefore, besides the high academic interest, the research of such compounds is crucial for the investigation and optimization of large scale processes in the industry.

---

1 Electronegatvity scale according to Pauling, see reference [2].

2 atomic radii derived using relativistic all-electron density functional theory calculations, given in references [3,4]. The atomic radii correlate well with van der Waals radii derived from crystal structures.

1.1 Chemistry of low valent silicon

1.1.1 Multiple bonds to silicon

The major difference between carbon and its heavier homologues is its ability to from multiple bonds with itself (alkenes, alkynes, aromatic compounds, graphite, fullerene) or other elements (imines, nitriles, ketones) leading to a plethora of stable unsaturated carbon compounds. Multiple bonds to the heavier homologues of carbon (and to the elements beyond the second period in general), in contrast, were not known until synthetic strategies were developed to stabilize such labile species. These strategies involve the use of sterically high demanding substituents for the kinetic stabilization of otherwise highly reactive functionalities.

Prior to the development of such synthetic strategies, researches believed for a long time in the "Double bond rule",[8–10] which states that the heavier main group elements with a principal quantum number greater two (i. e. aluminum onwards) would not form multiple bonds with themselves or other elements. This roule was disproved by Lappert and co-workers in 1976 by the isolation and characterization of the distannene $Dsi_2Sn{=}SnDsi_2$ (Dsi = $CH(SiMe_3)_2$), which features the first example of a tin compound containing a multiple bond.[11] In this context, in 1981 West et al. and Brook et al. reported the first stable disilene (**I-1**)[12] and silene (**I-2**)[13], featuring a Si=Si and Si=C double bond, respectively, which layered the foundation of the silicon chemistry in low oxidation states. In the same year the first stable diphosphene (**I-3**)[14] and phosphaalkyne (**I-4**) [15], featuring a P=P and P≡C bond, was accessed by Yoshifuji and Becker. Since then the chemistry of low valent main group compounds, especially of silicon, rapidly evolved and was subjected to several review articles.[16–20] The major advantage of low valent main group elements is their transition metal-like behavior, which enables them to activate small molecules and thus enables them to be used as an alternative to transition metal catalysts in catalytic processes. However, thus far their use in catalysis is currently limited to very few examples.[20]

In contrast to carbon, which features usually planar or linear multiple bonded structures, the heavier multiple bonded tetrylenes feature *trans*-bent geometries, as it can be seen in the case of bent angles in disilene **I-1** (Θ = 12°, 14°).[21]

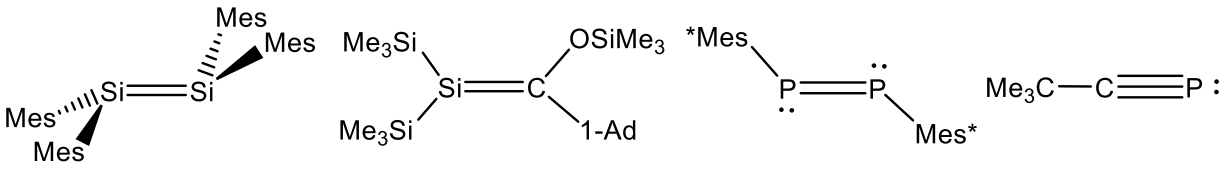

Figure 1.1. First examples of a disilene (**I-1**), silene (**I-2**), diphosphene (**I-3**) and phosphaalkyne (**I-4**).

Upon descending the tetrylenes in the periodic table, the non-bonded electron pair character of the elements increases and as such the degree of pyramidalization or bending at the element increases, which is in line with an observed weaker multiple bond. In addition there are multiple examples of ditetrelenes ($R_2E{=}ER_2$) known, which appear to be in an equilibrium in solution to their corresponding momomers, the tetrylenes ($:ER_2$).[17]

Selected examples of multiple bonded silicon compounds are given in *Figure 1.2*: The 1,2-dihalodisilenes **I-5** (X = Cl, Br; R^1 = silyl, aryl)[22–25] are promising building blocks in low valent silicon chemistry in the formal oxidation (+II). The silicon(I) compounds **I-6** (R^2 = silyl, aryl),[26–30] which feature a Si ≡ Si triple bond, were accessed either by $2e^-$ reduction of the diahlodisilenes **I-5** ($R^2 = R^1$) or by $4e^-$ reduction of the corresponding tetrahalodisilanes $[SiX_2(R^2)]_2$ (X = Cl, Br; $R^2 \neq R^1$).[31] The disilenyl-dianions **I-7**[32,33] (R^3 = aryl) in the formal oxidation state (0) were obtained straightforward upon $4e^-$ reduction of aryl-substituted dihalodisilenes **I-5** with KC_8. The lithiumdisilenide **I-8**[34,35] proved to be an exceptional starting material, enabling a rapid development of low valent silicon chemistry (for more details see *section 2.5.1*), which enabled the isolation of the hexasila-benzene-isomer **I-12**.[36] The trisilallene **I-9**,[37] features the first example of silicon with cumulated double bonds and was later on re-acknowledged as a monoatomic silicon(0) species stabilized by two coordinate silylene moieties (for more detail see *section 2.7.1*). The cyclo-tetrasilabutadiene derivatives **I-10**[38] can be formally seen as a dimer of a disilyne (**I-6**). The spirocyclic pentasilaspiropentadiene **I-11** was obtained upon reduction of the silane R^7–$SiBr_2Cl$ ($R^7 = Si(SiMe_2tBu)_3$) with KC_8 in THF.[39]

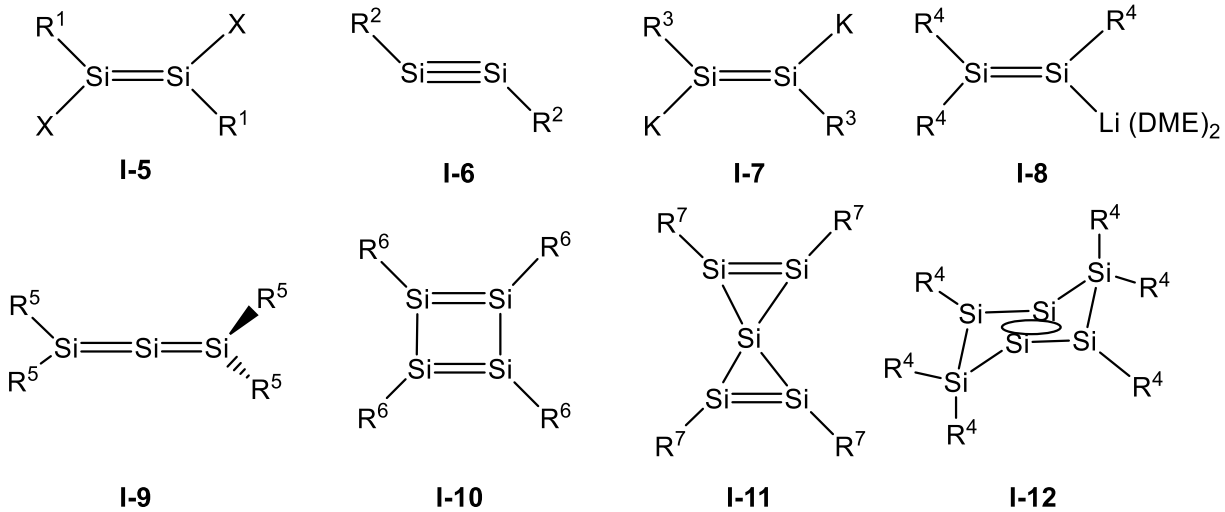

Figure 1.2. Selected examples of acyclic (**I-5** – **I-9**) and cyclic (**I-10** –**I-12**)silicon compounds with multiple bonds; R^1 = silyl ($SiMe\{SitBu_3\}_2$), aryl (Eind, EMind, Bbt, Tbb); R^2 = silyl ($SiMe\{SitBu_3\}_2$, $Si(iPr)(Dsi)_2$, $Si(Np)(Dsi)_2$), aryl (Bbt, Tbb); R^3 = aryl (Eind, Trp*), R^4 = Trip; $R^5 = SiMe(tBu)_2$, R^6 = EMind; $R^7 = Si(SiMe_2tBu)_3$; Abbreviations are given in *section 5.12*.

In the literature two major models are used in the description of the non-classical bonding situation of multiply bonded main group elements. a) The Carter–Goddard–Malrieu–Trinquier (CGMT) model[40–43] or b) Second-Order Jahn-Teller distortions (SOJT)[44]

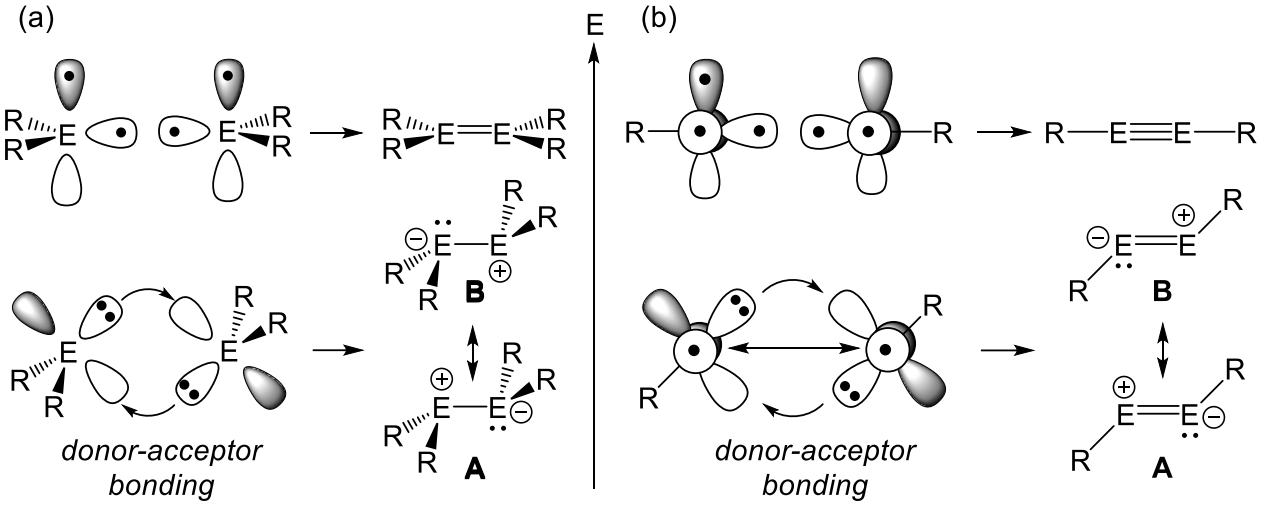

Figure 1.3. Bonding description of ditetrelenes (a) and ditetrelynes (b) according to the CGMT model. (Top) classical planar tetrel-tetrel double bond (a)/ tetrel-tetrel triple bond (b); (Bottom) double donor-acceptor bonding in pyramidalized ditetrelenes (a) and *trans*-bent ditetrelynes (b). For the heavier tetrelenes (Si – Pb) the singlet state is lower in energy and the singlet to triplet energy gap increases gradually from Si to Pb.

The CGMT-model provides a correlation between the singlet-triplet energy separation of the tetrel fragments (ER_2 or ER) and the electronic and structural characteristics of the molecule. For instance, if the two-fold singlet-triplet energy difference ($2{\cdot}\Delta E_{S-T}$) of the tetrel-fragments exceeds the total ditetrelene or ditetrelyne bond energy E_{s+p}, then the donor-acceptor model is used. In this case, the *trans*-bending of the E–E bond can simply be described by two donor-acceptor bonds of the two tetrel centers (*Figure 1.3*). In this case the tetrel-tetrel bond can be described by two resonance structures **A** and **B**, which contain a E-centered lone-pair and lone-vacancy leading to non-planar geometry with a slight degree of pyramidalization at E (*Figure 1.3* bottom). If the two-fold singlet-triplet energy difference ($2{\cdot}\Delta E_{S-T}$) is smaller than the total bond energy (E_{s+p}), then the tetrel bond can be viewed as triplet-fragments and as such a classical planar or linear structure is obtained (*Figure 1.3* top).

A more nuanced approach features the SJOT-model, which regards the structural distortions as a consequence of mixing of the highest occupied molecular orbital (HOMO, typically the π-bond) with an unoccupied orbital (LUMO+1, typically the σ*-orbital). The orbital mixing, which is an example of a second-order Jahn-Teller interaction (SOJT), produces nonbonding electron density, which causes the geometrical distortion through interelectronic repulsion.

This interaction is inversely correlated with the orbital energy difference and depends on the electronegativity of the substituents. [44]

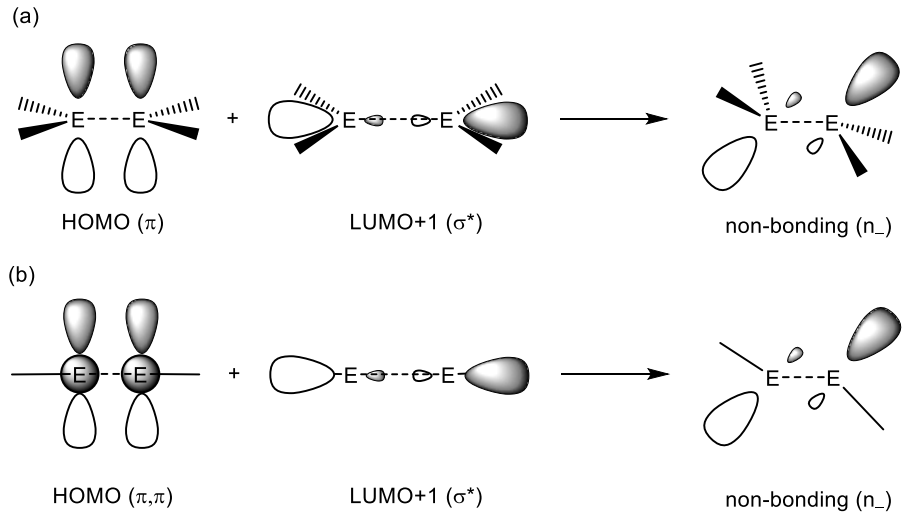

Figure 1.4. Orbital mixing in ditetrelenes (a) and ditetrelynes (b) as a result of the second-order Jahn-Teller interaction.[44]

1.1.2 Silylenes

Tetrylenes (ER_2, E = tetrel element, R = singly bonded substituent) are compounds that feature a divalent tetrel atom with a sextet electronic configuration. There are two electronic states of tetrylenes: a singlet state, in which they possess a lone pair of electrons and a vacant p-orbital and a triplet state, in which the two non-bonding orbitals are populated by a single electron each. In contrast to carbenes, which can be in a singlet (CR_2, R = π-donating substituent) or triplet ground state (CH_2), silylenes (SiR_2 = H, π-donating substituent, alkyl, aryl) have a singlet ground state, due to the unwillingness of the silicon atom to undergo high s,p-orbital hybridisation.[45] Their low coordination number and singlet-triplet energy difference ΔE_{ST} account for the very high reactivity. Therefore they were known to be laboratory curiosites for a long time and could be only studied in argon or hydrocarbon matrices at cryogenic temperatures.[46] Their reactivity can be significantly diminished upon coordination of a Lewis base to the empty p-orbital or by hyperconjugation with other filled orbitals.

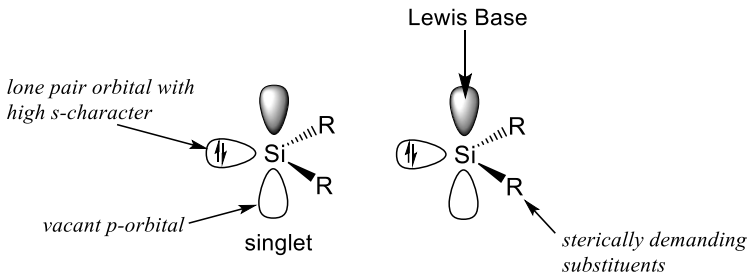

Figure 1.5. From left to right: silylene in the singlet-groundstate, Lewis base stabilized silylene.

The first monomeric silicon(II) compound, the decamethylsilicocene (**I-13**) was isolated in 1986 by Jutzi and co-workers, which allowed a versatile follow up chemistry (*Figure 1.6*).[47] 4 years later the spirocyclic bis(disphosphino)silicon(II) compound $Si[(PMe_2)_2C(SiMe_3)]_2$ (**I-14**)[48] was reported by Karsch et al. Reaction of **I-13** with $[C_5Me_5H_2][B(C_6F_5)_4]$ or $[H(EtO)_2][B(C_6F_5)_4]$ yielded the "silicocenium" cation $[Si(\eta^5\text{-}C_5Me_5)][B(C_6F_5)_4]$ (**1-15**)$[B(C_6F_5)_4]$,[49,50] which itself provided to be an essential building block in the generation of functionalized silicon(II) compounds upon reaction with nucleophiles.[51] The cation selectively reacted with the metallate $Na[Tp^{Me}Mo(CO)_2(PMe_3)]$ (Tp^{Me} = κ^3-N,N′,N″-hydridotris(3,5-dimethyl-1-pyrazolyl)-borate) directly affording the molybdenum-silylidyne **I-16**.[50]

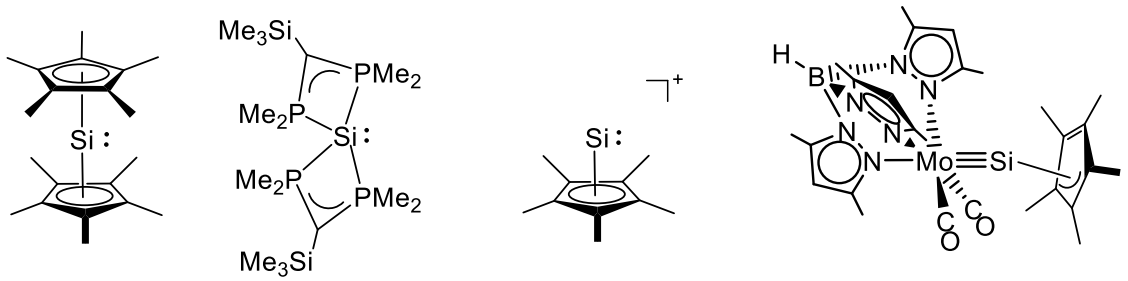

I-13 **I-14** **I-15** **I-16**

Figure 1.6. First isolable silicon(II) compounds decamethylsilicocene (**I-13**) and spirocyclic bis-phospino-silicon(II) compound **I-14**. Remarkable follow up products of **I-13** are the "silicocenium" cation **I-15** and molybdenum-silylidyne complex **I-16**. Formal charges are not given for the sake of simplicity.

The first silylene, the N-hererocyclic silylene (NHSi) $Si[N(tBu)CH]_2$ (**I-17**) (*Figure 1.7*), was isolated by M. Denk and R. West in 1994,[52] which can be considered as the heavier homologue to the first reported N-heterocyclic carbene by Arduengo et al. in 1991. [53] Since then the number of cyclic and acylic silylenes rapidly increased yielding a plethora of different silylenes, selected examples are given in *Figure 1.7*. The first dialkyl-substituted cyclic silylene **I-18**[54] was reported by Kira et al.

The NHSi **I-19** reported by the work group of Driess features an interesting ambivalent reactivity, due to the presence of an unsaturated backbone of the β-ketoiminato substituent and the electrophilic silylene silicon atom.[55] The first cyclic (alkyl)(amino) silylene (CAASi) (**I-20**) [56]was reported by Iwamoto et al. and can be viewed as the heavier analogue to the first reported CAAC by Bertrand et al. in 2005. [57]

The first acyclic silylenes **I-21**[58] and **I-22**[59] were isolated by the research groups of Aldrige and Power in 2012, respectively. The research group of Filippou enabled the isolation of the two-coordinated cationic chromiosilylene **I-23**, which was obtained via the carbonylation of the cationic silylidyne complex $[(\eta^5\text{-}C_5Me_5)(CO)_2Cr{\equiv}Si(SIDipp)]^+$ (SIDipp = $C[N(Dipp)CH_2]_2$, Dipp = C_6H_3-2,6-*i*Pr_2).[60] The first diboryloxysilylene **I-24**[61] was reported by Aldridge et al., which features the first example of a silylene connected to two oxygen centers.

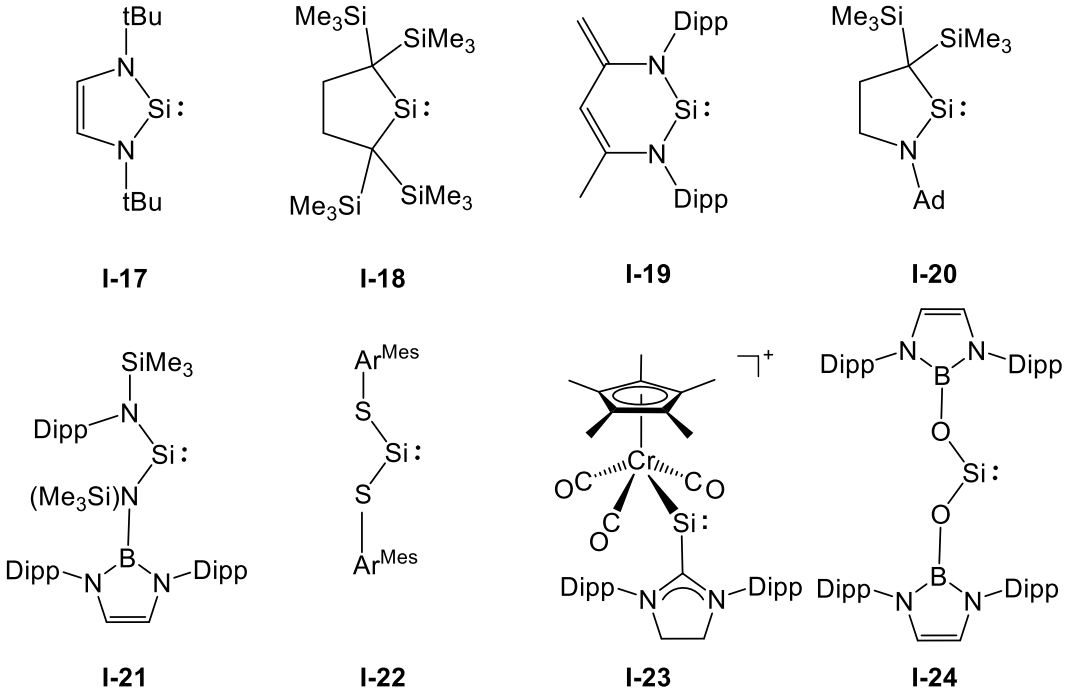

Figure 1.7. Selected examples of cyclic (**I-17** – **I-20**) and acyclic silylenes (**I-21** – **I-24**). Formal charges are not given for the sake of simplicity. Dipp = C_6H_3-2,6-iPr_2; Ad = Adamantyl, Ar^{Mes} = C_6H_3-2,6-Mes (Mes = C_6H_2-2,4,6-Me_3).

Synthetic access to the first acyclic bis(silyl)-silylene **I-25** has been reported by Inoue et al., which features an equilibrium at ambient temperature to the corresponding disilene **I-26**, upon migration of a TMS group.[62] In contrast to the acyclic silylenes mentioned above it features an even higher reactivity, due to the wider angle R-Si-R' and the smaller HOMO–LUMO gap.[62] The research group of A. Hinz, recently reported the first two-coordinate halosilylene **I-27** (X = Br, I), upon stabilization by a sterically high demanding carbazolyl substituent. Halide abstraction using Ag[Al(O{C(CF_3)$_3$}$_4$] led to the isolation of a mono-substituted silicon(II) cation.[63]

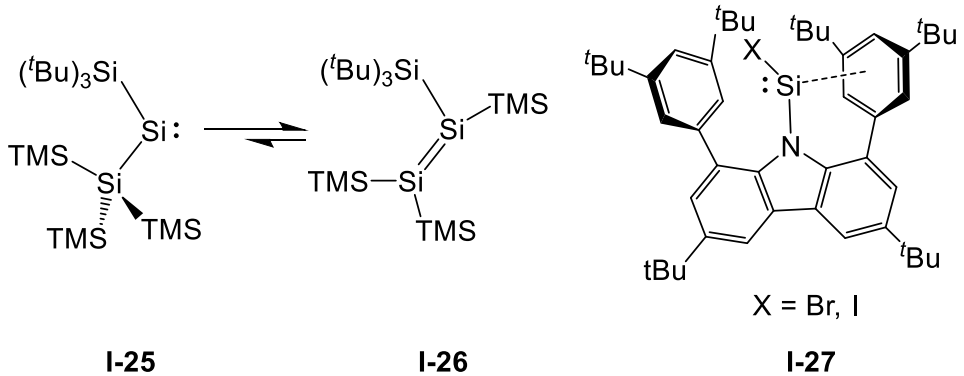

I-25 **I-26** **I-27**

Figure 1.8. Recentyl reported two-coordinated acyclic silylenes, bearing silyl-groups (**I-25**) and halogen substituents (**I-27**).

Functional silylenes, bearing one or more halogen substituent, are interesting starting materials in low valent silicon chemistry. However, due to their high reactivity they need additional kinetic and thermodynamic stabilization, by the use of sterically high demanding substituents and Lewis bases. The Lewis base can be provided intramolecularly in the form of a monoanionic bidentate ligand (*Figure 1.9* (a)) or intermolecularly typically by the use of N-heterocylcic carbenes (NHCs) (*Figure 1.9* (b)) or cyclic (alkyl)(amino)carbenes (CAACs) (*chapter 1.2* and *1.3*). Two-coordinate halosilylenes, if not trapped by a Lewis-base, are transient species in solution and are prown to dimerization yielding the corresponding dihalodisilenes (R)Si(X)=Si(X)(R).[64] The silicon(II) compounds **I-27** (X = Br, I) by A. Hinz are the only reported isolated two-coordinated halosilylenes, without the stabilization of a Lewis base, which are additionally stabilized by the π-interaction of a peripheral phenyl substituent of the sterically encumbered carbazolyl substituent (*Figure 1.8*).[63]
Entry into the chemistry was provided in 2006 by the N-heterocyclic silylene (NHSi) (**I-19**), which upon reaction with $SiMe_3OTf$ (OTf = OSO_2CF_3) afforded the first example of a functional silylene **I-28**.[55]

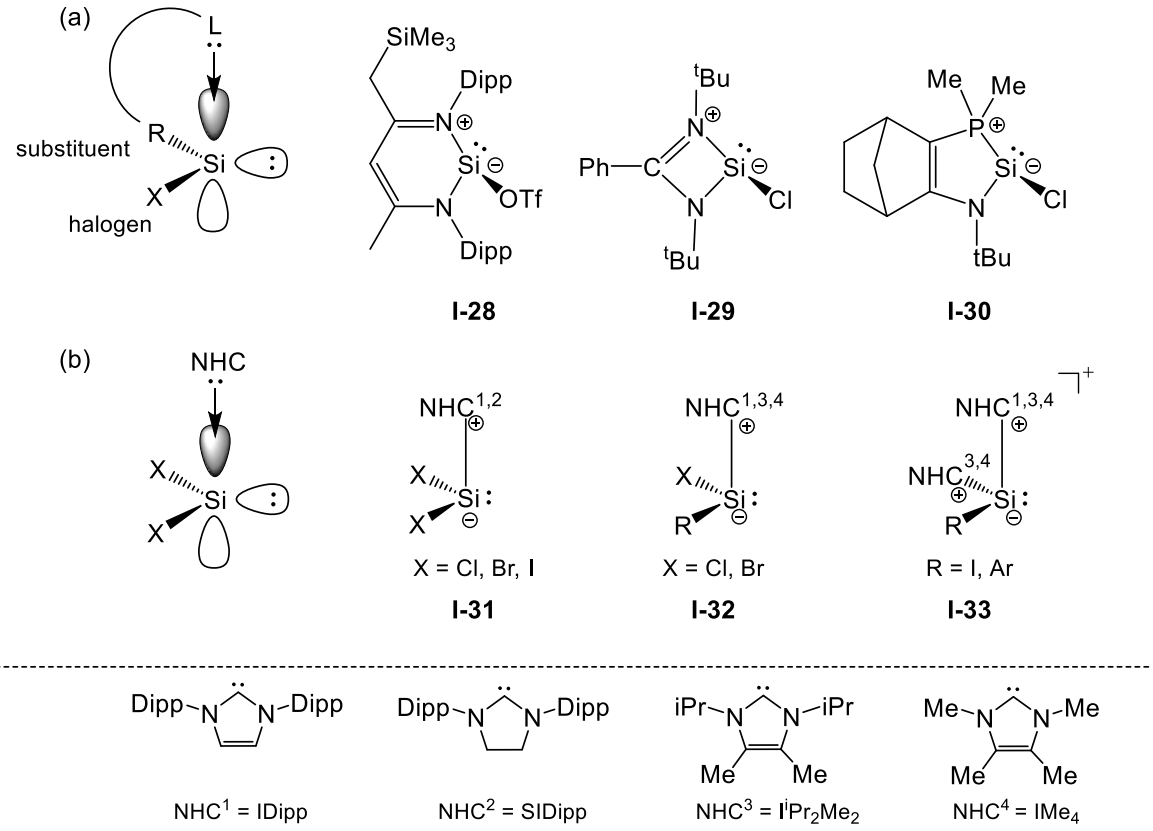

Figure 1.9. Stabilization of functionalized halosilylenes with an intramolecular Lewis base (a) yielding the three-coordinated silylenes **I-28** – **I-30** or by an external Lewis base (NHCs = $NHC^{1,2,3,4}$) affording the dihalo-(**I-31**) and monohalo (**I-32**) silylenes and the silylium-ylidenes **I-33**.

In the same year the first isolable base stabilized halosilylene, the amidinato stabilized chlorosilylene SiCl[(N(*t*Bu))$_2$CPh] (**I-26**) was reported by H. W. Roesky et al.[65]
Compound **I-29** proved to be a very suitable starting material in the isolation of a plethora of functionalized silicon(II) compounds of the type SiR[(N(t-Bu))$_2$CPh].[66]
The phosphinoenamido chlorosilylene **I-30**, reported by Baceiredo et al.,[67] features another example of a monoanionic bidentate stabilized halosilylene, which features the first example of a sila-Wittig reagent.
The stabilization of dihalosilylenes by the use of NHCs (*Figure 1.9* bottom) with sterically demanding substituents at the N-atom yielded the three coordinated dihalosilylenes **I-31** (NHC^1: X = Cl[68], Br[69], I[70]; NHC^2: X = Cl[71], Br[71], I[72]). These compounds led to a renessaince of the low valent silicon chemistry enabling the isolation of a multitude of different silicon compounds with intruging bonding features, which are the subject to several review articles.[73–79] Substantial examples of the follow up chemistry of **I-31** are given in *Figure 2.5* (*chapter 2.2*).
The NHC stabilized monohalosilylenes **I-32**, were either obtained upon dehydrohalogenation of substituted chlorosilanes of the type Si(R)HCl$_2$ (R = Ar^{Mes}, Ar^{Trip}, NH(Dipp)) using small N-heterocyclic carbenes (NHC^3: IMe$_4$, NHC^4: IiPr$_2$Me$_2$),[80,81] addition of small carbenes (NHC^3: IMe$_4$, NHC^4: IiPr$_2$Me$_2$) to dibromodisilenes (*E*)-[(Ar)(Br)Si=Si(Br)(Ar)] [25] or nucleophile substitution of carbene stabilized silicon(II)-dihalides SiCl$_2$(NHC^1) (NHC^1 = IDipp = C[N(Dipp)CH]$_2$) with suitable nucleophiles.[82] A more detailed introduction into the topic is given in *chapter 2.2*. Silylium-ylidenes **I-33** were either obtained upon reaction of dibromodisilenes (*E*)-[(Ar)(Br)Si=Si(Br)(Ar)] with 4 equivalents of carbenes NHC^{3,4} [25]or by reaction of dihalosilylene SiI$_2$(SIDipp) (**I-31**) with NHC^3 (I*i*Pr$_2$Me$_2$).[70] Furthermore reaction of dihalosilylene SiI$_2$(SIDipp) with three equivalents of carbene NHC^4 (IMe$_4$) afforded the dicationic NHC complex of silicon(II) [Si(NHC^4)$_3$]$^{2+}$.[70]

1.2 Cyclic (Alkyl)(Amino)Carbenes (CAACs)

Since of the isolation of the first singlet carbene **I-34**[83,84] in 1988 by Bertrand and co-workers and the first N-heterocylclic carbene (NHC) **I-35**[53] by the research group of Arduengo in 1991, the chemistry of isolable carbenes rapidly increased. Nowadays, stable carbenes are known to be the most powerful tools in organic, inorganic and organometallic chemistry[85] and they have even found medicinal[86,87] and material science[88] applications. Especially, in the field of low valent main group chemistry they allowed the isolation of main group elements in unusual low oxidation states and intriguing bonding motivs.[89,90,74,75,91,76–79]

In 2005 cyclic (alkyl)(amino)carbenes (CAACs) were synthesized by the research group of G. Bertrand.[57] Since then, a vast variety of derivatives with different ring size and different vicinal alkyl group have emerged. Selected examples of NHCs and CAACs are given in *Figure 1.10*. Up to date, CAACs are the most nucleophilic (σ-donating) and also electrophilic (π-accepting) stable carbenes. They are widley used in transition metal chemistry and catalysis[92–94] and enabled over the past decade the isolation of main group elements in unsual low oxidation states, in particular main group radicals.[95–98] In addition, CAACs were found to be useful in activation of small molecules such as CO, H_2 [99,100] and of strong bonds such as B-H and Si-H.[97]

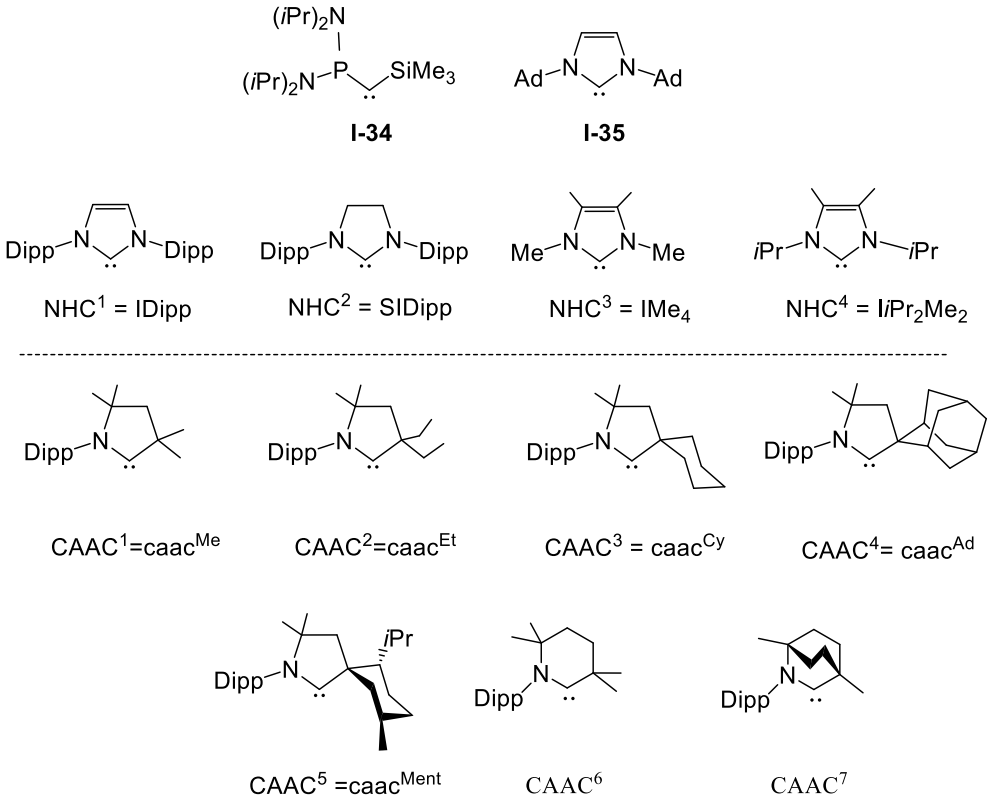

Figure 1.10. Selected examples of NHCs and CAACs; Dipp = C_6H_3-2,6-*i*Pr_2; Ad = adamantyl. The abbreviations IDipp, SIDipp, IMe_4, I*i*Pr_2Me_2 as well as $caac^{Me}$, $caac^{Et}$, $caac^{Cy}$ and $caac^{Ment}$ will be commonly used throughout this work.

More recently, also CAACs with a six membered skeleton have been synthesized (CAAC^{6,7}).[93] Preliminary results suggest, that these CAACs are even stronger σ-donors and π-acceptors, than the first reported CAACs (CAAC$^{1\text{-}3}$) by Bertrand and co-workers. In this work, however I will exclusively focus on the carbene CAAC^{1} = caac^{Me} and its properties in the stabilization of low valent silicon compounds in comparison to classical NHC-stabilized systems.

1.2.1 Electronic properties of CAACs

The electronic properties of CAACs differ drastically from those of NHCs. The substitution of one of the two π-donating nitrogen atoms by quaternary carbon atom makes CAACs slightly more nucleophilic (σ-donating) but also considerably more electrophilic (π-accepting) than NHCs. Quantum chemical studies of representative carbenes (*Figure 1.11*) clearly show a significant higher lying HOMO in CAACs (–5.35 eV (**CAAC-1**)) versus the classical NHCs (–5.63 (**NHC-1**), –5.82 eV (**NHC-2**), as well as a remarkably lowered LUMO (–0.06 eV (**CAAC-1**) in comparison to the NHC model compounds (0.83 eV (**NHC-1**), 1.00 eV (**NHC-2**)). The higher HOMO and lower LUMO energies of CAACs results in a lower singlet-triplet energy gap in CAACs (48.0 kcal/mol) compared to that of the NHCs (72 kcal/mol, 82 kcal/mol).[93]

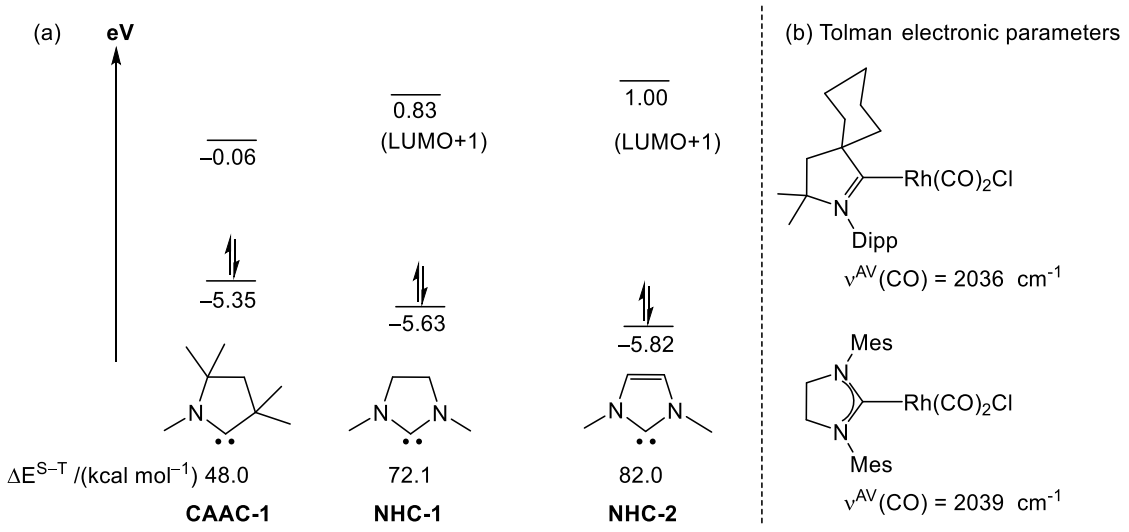

Figure 1.11. (a) Calculated HOMO-LUMO gap (eV) and $\Delta E^{S\text{-}T}$ (kcal/mol) of representative carbenes at the B3LYP/def2-TZVPP level of theory with ultrafine grid;[93] (b) Tolman electronic parameters of carbene stabilized rhodium complexes in comparison, formal charges not given for the sake of simplicity.[101,102]

The experimentally obtained Tolman electronic parameters[103] derived from (CAAC)Rh(CO)$_2$Cl and (NHC)Rh(CO)$_2$Cl and the analogous iridium complexes indicate that the donation of CAACs ((caac^{Cy})Rh(CO)$_2$Cl $\tilde{\nu}^{AV}$(CO)= 2036 cm^{-1})[101] is only slighty greater than that of NHCs ((SIMes)Rh(CO)$_2$Cl $\tilde{\nu}^{AV}$(CO)= 2039 cm^{-1}).[102]

In this context it is important to note that the TEP value gives the overall donation properties of the ligand, which are rationalized upon subtracting the π-acidity from the σ-donation.

So far, two methods have been developed to gain experimental access to the π-accepting properties of a given carbene ligand:
In 2013, Bertrand and co-workers could show, that the ^{31}P NMR chemical shift of carbene-phosphinidene adducts can be used as an indicator for the π-accepting properties of carbenes.[104,105] The carbene-phosphinidene aducts can be be represented by two canonical structures (*Figure 1.12*): a phoshpaalkene **A** with a typical P=C double bond and a carbene-phosphinidene aduct **B** with a dative P–C single bond. The more π-accepting the carbene, the more double bond character is observed in the ^{carb}C–P bond and the more downfield shifted is the observed ^{31}P resonance of the carbene phosphinidene aduct.[104] In the same year the research group of Ganter could show, that also the ^{77}Se NMR chemical shift of carbene-selenium adducts can be used in the determination for the π-accepting properties of carbenes.[106,107] Similar to the phosphinedene adducts mentioned above, the selenium adducts can be described by two extreme canonical structrues **A'** and **B'**. The more π-accepting the carbene, the more double bond character is observed in the ^{carb}C–Se bond and the more downfield shifted is the observed ^{77}Se resonance of the carbene selenium adduct.

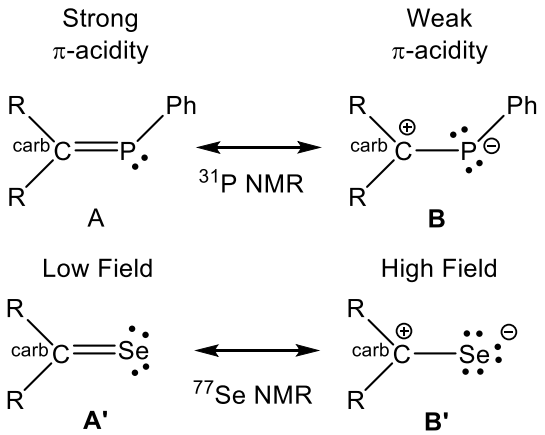

Figure 1.12. Possible resonance formulas of carbene-phosphinidene adducts and carbene-selene adducts for the determination of the π-acceptor properties of carbenes.

In comparison to the ^{31}P NMR scale of Bertrand, the ^{77}Se NMR scale has the advantage, that the selenium-adducts are more conveniently to prepare and that the ^{77}Se NMR scale features a much broader chemical shift range (>900 ppm). However, selenium is toxic and ^{77}Se NMR is not as routinely available as ^{31}P NMR. Both methods, reveal a remarkable difference in the π-acceptor acidity of CAAC carbenes with regard to NHCs. With exception of the dicarboxamido carbenes given in *Figure 1.13* it can be concluded, that in terms of the π-accepting capability the CAAC carbenes are among the strongest, which can be seen by a drastic downfield shift ($\delta(^{31}P)$ = 56 – 69 ppm, $\delta(^{77}Se)$ = 492 ppm), when compared to NHCs with a saturated ($\delta(^{31}P)$ = –10 ppm, $\delta(^{77}Se)$ = 181 ppm) and the NHCs with unsaturated backbones ($\delta(^{31}P)$ = (–18) – (–32) ppm, $\delta(^{77}Se)$ = 178 – 220 ppm).

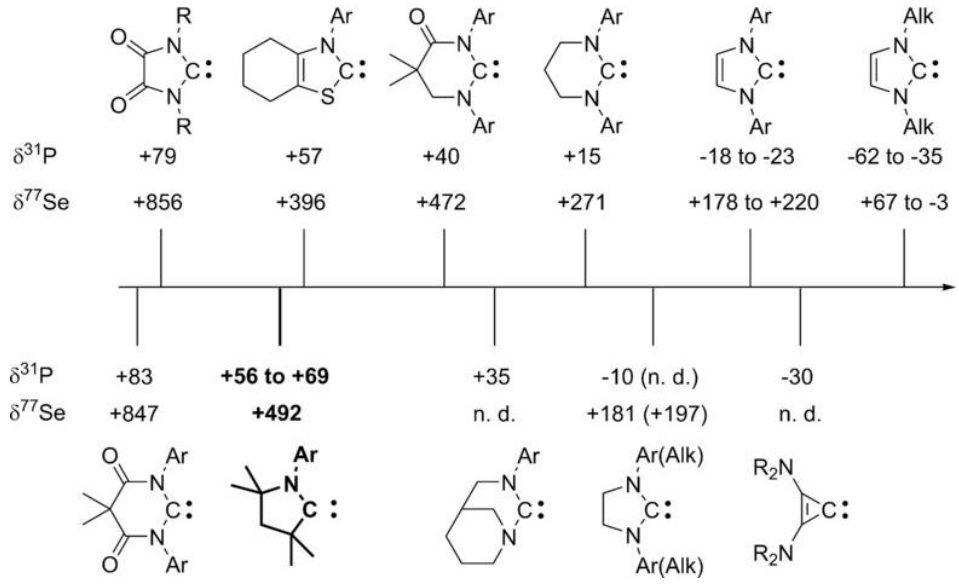

Figure 1.13. The π-accepting properties of carbenes based on ^{31}P and ^{77}Se NMR chemical shifts of carbene-phosphinidene and carbene-selenium adducts. n.d. = not determined.[97]

In 2015 Roesky *et al.* developed, by the use of ^{15}N NMR in a series of CAAC-E adducts, a general method for the reliable estimation of the extend of the π-backdonation ($C^{CAAC} \leftarrow E/M$) of the bonded element (main group E or metal M) to the carbene center in relation to the $C^{CAAC} \rightarrow E/M$ σ-donation.[108] By a combined experimental and theoretical study they showed whether the carbene σ-donation or the E/M π-backdonation is stronger, upon comparing the ^{15}N NMR shifts to certain threshholds (*Figure 1.14*). In contrast, to the methods mentioned above, this approach is limited to CAAC carbenes, since the $^{15}N\{^1H\}$ resonances in CAACs can differ drastically depending on the electronic structure of the used E/M, while NHCs feature only minor changes in the $^{15}N\{^1H\}$ resonances, due to the high delocalization of the $N=C^{carb}$ double bonds.[108] Despite this flaw, the ^{15}N NMR scale of H. Roesky is a powerful tool in analyzing the bonding mode of CAACs in low molecular silicon-chemistry. In fact, this scale can be applied to all diamagnetic compounds synthesized in this work and thus can be used to make a viable prognosis of the molecular structure of the silicon-compound together with other NMR spectroscopic methods.

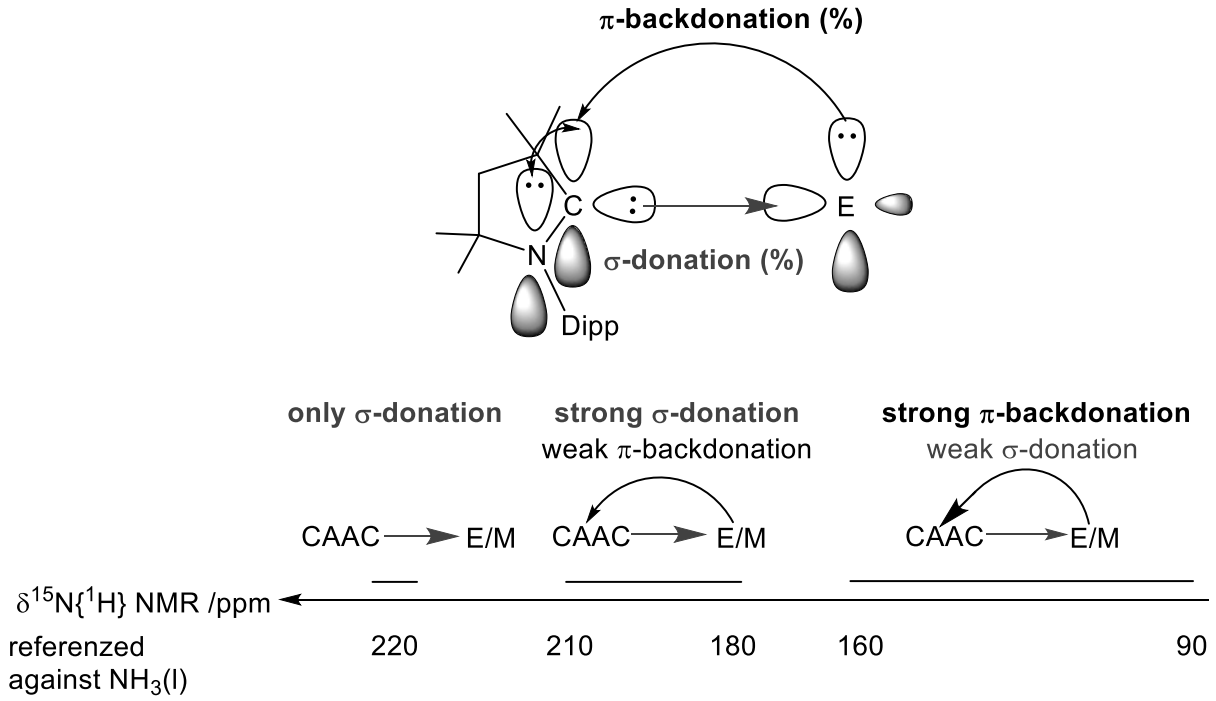

Figure 1.14. ^{15}N NMR scale to estimate the π-backdonation of a bonded fragment (E/M) to the carbene center and the σ-donation from the carbene center to E/M. ^{15}N NMR values given referenced versus liquid NH_3, in the original publication values are referenced versus CH_3NO_2.[108]
$\delta(^{15}N(CH_3NO_2)_{ref} = \delta(^{15}N(NH_3(l))_{ref} - 380.5$ ppm

The bonding situation in NHC and CAAC stabilized main group compounds, especially in low valent silicon compounds, is an ongoing controversial debate about the true nature of the C^{carb}–Si bond and their accurate schematic representation.[109–113]
A commonly used representation is the usage of the arrow notation, which emphasizes on the donor-acceptor aspect of the dative bond ($C^{carb} \rightarrow Si$) (*Figure 1.15,* (a)). In contrast, partial covalency is indicated by the zwitterionic representation (*Figure 1.15*, (b)). They both can be viewed as borderline cases and their use highly depends on the nature of the particular bond. In cyclic (alkyl)(amino)carbene (CAACs) stabilized systems the accurate representation of the C^{carb}–Si bond becomes even more complicated. Since CAACs feature superior π-accepting properties than NHCs the nature of the C^{carb}–Si bond can be described with an increased double bond character (*Figure 1.15,* (c) and (d)). Therefore, in order to properly describe the nature of the C^{carb}–Si bond in a particular compound, the compound needs to be fully characterized by X-ray diffraction, NMR spectroscopic methods and analyzed by quantum chemical calculations.
For the sake of simplicity, the arrow representation (a) will not be used throughout this work. Depending on the increased Si–C^{carb} double bond character of any particular compound, in correlation to the Si–C^{carb} bond length, sum of angles at the silicon center and $^{15}N\{^{1}H\}$ NMR resonance the formulas (b), (c) and (d) will be frequently used.

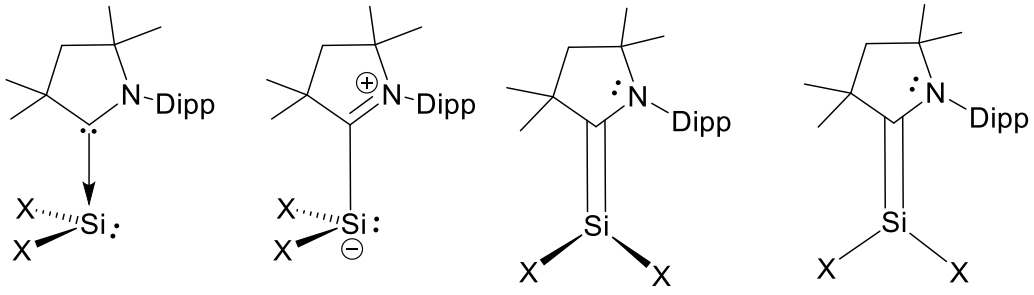

Figure 1.15. Different representations of the nature of the Si–C^{carb} bond in CAACs.

1.3 CAAC and NHC-stabilized low valent silicon compounds

The molecular chemsitry of silicon has witnessed a renaissance in recent years after the realization that N-heterocyclic carbenes (NHCs) as well as cylic (alkyl)(amino)carbenes (CAACs) are particularly useful Lewis bases for the thermodynamic and kinetic stabilization of highly reactive low-oxidation state molecular silicon species leading to a plethora of novel silicon compounds with intriguing bonding features and synthetic potential.[89,90,74,75,91,76–79]

Milestones in this field was provided by the pioneer work by Robinson et al., Filippou et al. and Roesky et al.[79] Especially the research groups of Roesky and So et al. focused on appending CAAC ligands to silicon centers in low oxidation states. [95–98]

In this section we will take a look at selected examples of $NHC^{1,2}$ (NHC^1 = IDipp ,NHC^2 = SIDipp) and $CAAC^{1\text{-}3}$ ($caac^{Me/Et/Cy}$) stabilized silicon compounds and will compare them to each other in order to highlight the remarkable difference of NHC and CAAC in the stabilization of low valent silicon compounds. Thus, the results will be not discussed in coherent historical but rather in a conceptual manner, whereas silicon compounds of same oxidation states stabilized by different carbenes are compared to each other.

1.3.1 CAAC and NHC-stabilized silicon(0) compounds

The chemistry of silicon(0) compounds started to flourish in 2008 with the isolation of the first disilicon(0) compound **I-36^{NHC}** stabilized by an N-heterocyclic carbene by Robinson et al.[114] In analogy, to the disilicon(0) compound **I-36^{NHC}** the research group of Roesky isolated the $caac^{Me/Cy}$ stabilized disilicon(0) compound **I-36^{CAAC}**.[115,116] At first glance both compounds appear remarkably similar: They both feature a planar C^{carb}-Si=Si-C^{carb} core with an almost trans bent skeletal configuration consistent with the predominantly 3p-character of the Si–Si π-bond and the 3s-character of the Si lone pair orbitals. However, major differences can be seen in the relative orientation of the carbene with respect to the Si=Si bond. In fact, in **I-36^{NHC}** the carbenes are orientated orthogonally (φ_{NHC} = 87.0(1)°) with respect to the planar core to the molecule, whereas in **I-36^{CAAC}** the CAAC carbenes are orientated more towards the Si=Si plane (φ_{CAAC} = 53.2(3)°). Another indication gives the $^{15}N\{^1H\}$ resonance of $Si_2(caac^{Me})_2$ (174.5 ppm)[this work], which according to the $^{15}N\{^1H\}$ NMR scale provided by Roesky[108] (*Figure 1.14*) suggests equal strong σ-donation, as well as π-acceptance of the CAAC carbene atom in the Si–C^{carb} bond in $Si_2(caac^{Me})_2$ (**I-36^{CAAC}**). These findings, suggest a partial delocalization of the Si–Si π-bond in **I-36^{CAAC}** over the C^{carb}-Si-Si moiety in comparison to **I-36^{NHC}**, which in sharp contrast features a localized Si=Si bond.

These electronic differences are also highlighted by the different colors of the compounds: crystals of **I-36^{NHC}** and **I-36^{CAAC}** are red and dark purple, respectively. The color change from red (**I-36^{NHC}**) to purple (**I-36^{CAAC}**) can be highly likely attributed to the difference in energy of the LUMO within the carbenes (CAAC/NHC), due to the lower lying LUMO of CAAC (*Figure 1.11*). In the same year by the research group of Filippou the NHC[1] stabilized phosphasilenylidene **I-37^{NHC}** [117] and the NHC[2] stabilized disilavinylidene **I-35^{NHC}** was isolated.[118] Entry to the chemistry was provided by the NHC stabilized silicon(II)-halides **I-31^{NHC}** [68–71](*Figure 1.18*), which were obtained by the respective two electron reduction of the corresponding tetrahalosilane carbene adducts.

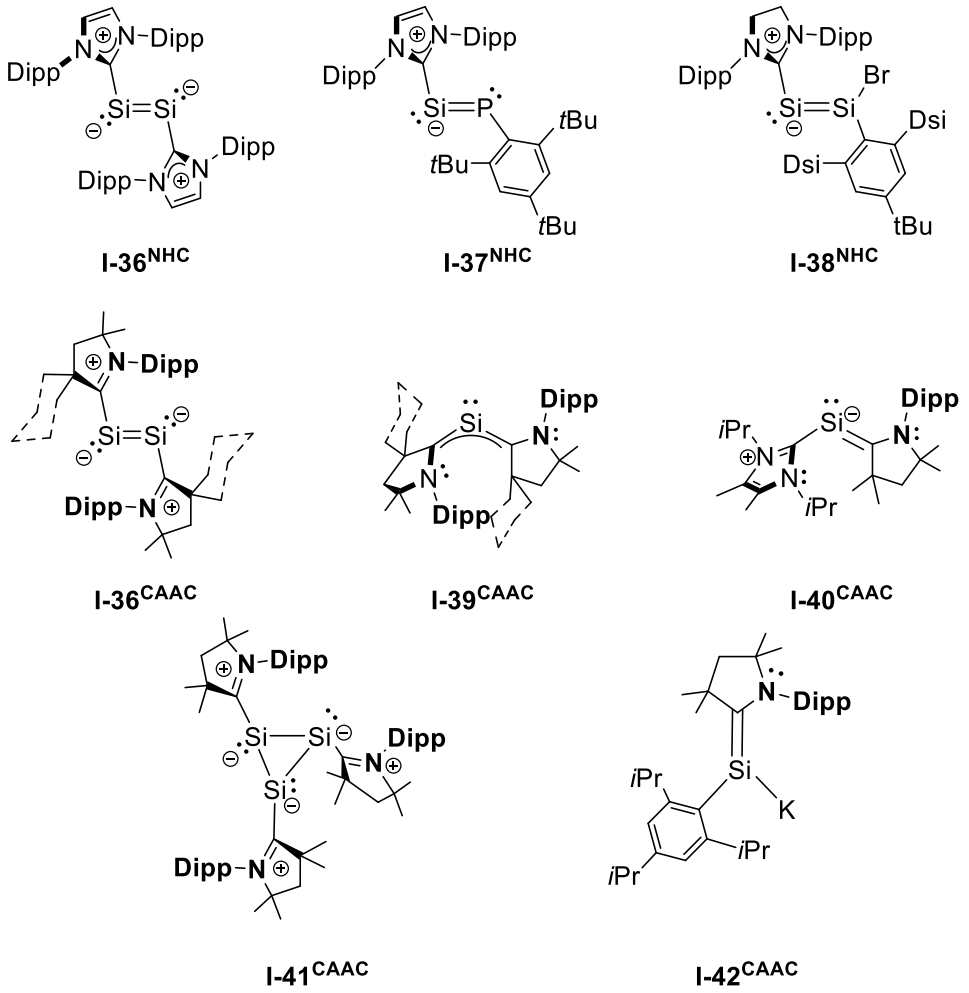

Figure 1.16. Literature known NHC and CAAC-stabilized silicon(0) compounds in comparison. For the sake of simplicity bidentate mono-atomic silicon(0) complexes are not listed here (for more detail see *chapter 2.7*).

In contrast to NHCs, CAACs enabled the isolation of the carbene stabilized mono-atomic silicon(0) complexes **I-39^{CAAC}** [119,120] and **I-40^{CAAC}** [121], respectively, which can be obtained straightforward upon reduction of the precursors **I-50^{CAAC}** (X = Cl)[122] (*Figure* **1.19**) and **I-48^{CAAC}** [121] (*Figure 1.18*).

Both mono-atomic silicon(0) complexes feature considerable amounts of double bond character in the Si–C^{carb} bond, which consequently leads to a delocalization of the π-bond over the C^{carb}–Si–C^{carb} moiety in **I-39^{CAAC}** and to a bent-silallene type of structure with localized Si=C^{carb} bond in **I-40^{CAAC}**.

The considerable double bond character in **I-39^{CAAC}** can also be shown by the $^{15}N\{^1H\}$ NMR resonance in Si($caac^{Me}$)$_2$ (153.1 ppm)[this work], which according to the $^{15}N\{^1H\}$ NMR scale by Roesky[108] features a stronger π-acceptance than σ-donation of the carbene carbon atom in the Si–C^{carb} bond in **I-39^{CAAC}**. In addition, straight-forward reduction of 3 equivalents of CAAC carbene aduct of $SiCl_4$ with 12 equiv. of KC_8 led to the formation of triatomic silicon(0) cluster **I-41^{CAAC}** [123]. The compound features three interconnected silicon(0) centers, each bearing a pair of electrons and a trigonal pyramidalized structure.

The one pot reduction of the silane $SiCl_3$(Trip) (Trip = C_6H_2-2,4,6-iPr_3) in the presence of $caac^{Me}$ carbene with 8 equiv. of KC_8 led to the formation of the unprecedent silicon(0) compound **I-42^{CAAC}**.[124] Originally described as silanylidene anion, the compound can be rather classified as a potassium-silenide with a strong Si=C^{carb} double bond and a covalently connected potassium ion. As such the compound compares rather well to literature known alkali-metal silenides[125,126] (a more detailed introduction into the topic is given in *chapter 2.5*).

1.3.2 CAAC and NHC-stabilized silicon(I) compounds

The silicon(I) chemistry started to flourish with the isolation of the disilicon(0) compound **I-36^{NHC}** and the isolation of the first dihalodisilicon(I) compound **I-43^{NHC}** (X = Cl)[114] by Robinson et al. in 2008. Selective oxidation of **I-36^{NHC}** with dihaloethane by the research group of Filippou helped to complete the homologue series of dihalodisilicon(I) compounds **I-43^{NHC}** (X = Cl, Br, I).[127] The compounds can be rationalized as formal bis NHC aducts of disilynes and are often described as interconnected bis-silylenes. In analogy to **I-43^{NHC}** the research groups of Roesky and So isolated a variety of different CAAC stabilized disilicon(I)-compounds upon one pot reduction of the corresponding halosilane precursors in the presence of CAAC carbene **I-43^{CAAC}** (X = Cl[128], I[121], H[129], Me[130], Ph[131]) (a more detailed introduction is given in *chapter 2.4*). In contrast to NHC-stabilized silicon(I) compounds, the CAAC-supported compounds feature significantly more planarized silicon ceneters. In fact, the compounds can be best described as 1,4-diamino-2,3-disilabutadiene type of derivatives.[128]

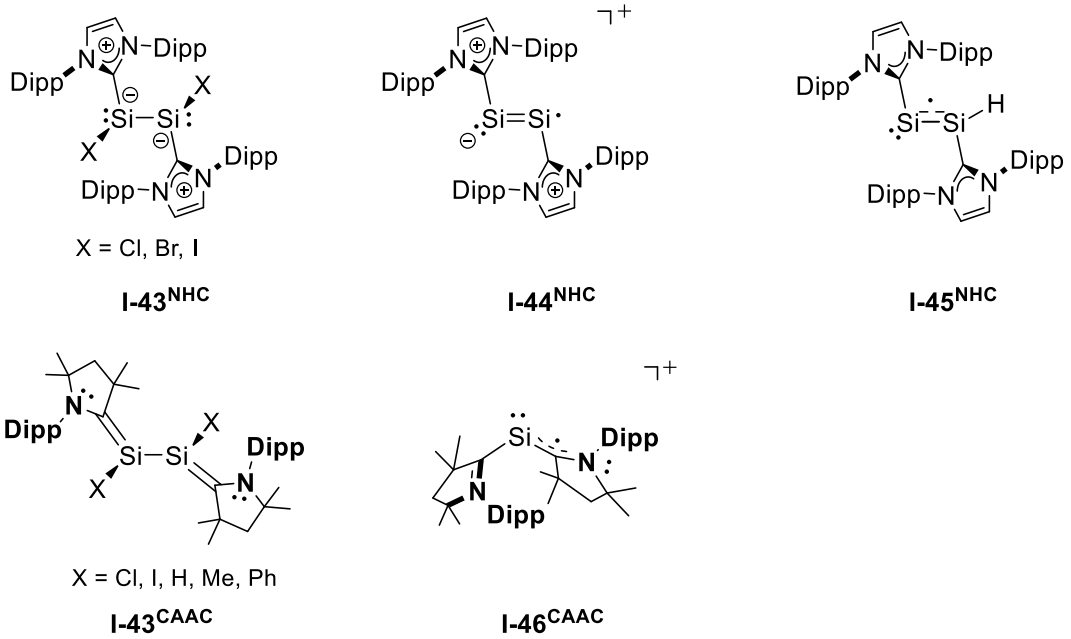

Figure 1.17. Literature known NHC and CAAC-stabilized silicon(I) compounds in comparison. No formal charges of **I-45**^{NHC} and **I-46**^{CAAC} are given for simplicity.

Open shell silicon(I) compounds could be accessed by selective 1e$^-$ oxidation of the disilicon(0) compound **I-36**^{NHC} to yield the radical cation **I-44**^{NHC} [132]or by the protonation and subsequent reduction of **I-36**^{NHC} yielding the neutral radical **I-45**^{NHC}.[133]

The first monoatomic silicon(I) radical, in contrast, could be trapped by two CAAC carbenes in the form of **I-46**^{CAAC} .[134] The compound can be rationalized as the formal 1e$^-$ oxidation product of the monoatomic silicon(0) compound **I-39**^{CAAC} and was originally obtained upon reaction of SiH_2I_2 with three equivalents of caac^{Me}.[134] In contrast to the NHC stabilized silicon-radicals (**I-44**^{NHC} and **I-45**^{NHC}) radical cation **I-46**^{CAAC} features considerable delocalization towards the carbene carbon atom, highlighting the superior π-accepting capabilities of CAAC versus NHC.

1.3.3 CAAC and NHC-stabilized silicon(II) compounds

The isolation of NHC-stabilized silicon(II) compounds bearing halogen atoms **I-31**^{NHC} (X = Cl – I, NHC^{1,2} = IDipp, SIDipp, see also *section 1.1.2*) provided essential starting materials for the further exploration of the silicon chemistry in low oxidation states (substantial examples of the follow up chemistry are given in *chapter 2.2*). In analogy, CAAC-stabilized dihalosilylenes **I-31**^{CAAC} (X = Br[135], I[121]) have been isolated. Structural and electronic structure of both NHC and CAAC-stabilized systems behave very similar: they feature a trigonal pyramidal silicon center with the electron pair located at the silicon center with an inversed polarized $Si^{\delta-}$–$C^{\delta+}$ donor-acceptor single bond.

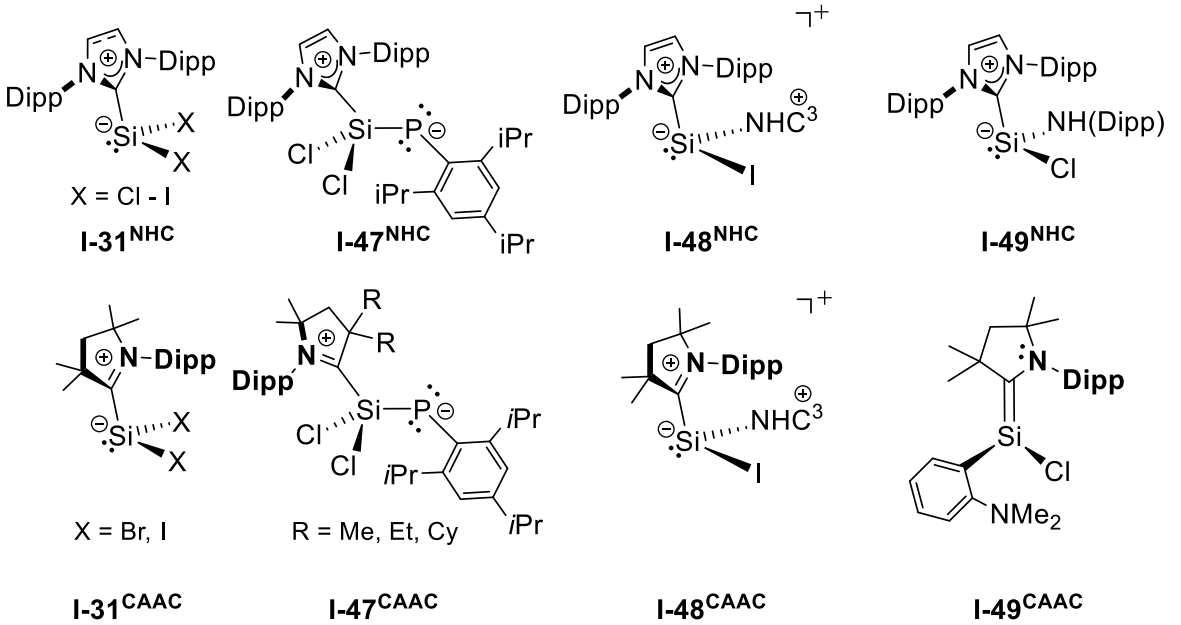

Figure 1.18. Literature known NHC and CAAC-stabilized silicon(II) compounds; NHC^3 = I*i*Pr$_2$Me$_2$ = :C[N(*i*Pr)C(Me)]$_2$.

CAAC-stabilized dihalosilylenes were isolated as red solids, whereas NHC-stabilized dihalosilylenes were obtained as yellow powders. This can be highly likely, attributed the smaller HOMO–LUMO gap in **I-31^{CAAC}** in comparison to **I-31^{NHC}** in analogy to the smaller HOMO–LUMO gap in CAAC with respect to NHC (the nature of the electronic structure is discussed in *chapter 2.1*).

Both carbene stabilized dichlorosilylenes (carbene)SiCl$_2$ (carbene = NHC or CAAC) can stabilize a phosphinidene (P–Ar) yielding the silylene phosphinidene adducts **I-47^{NHC}** and **I-47^{CAAC}**, respectively.[136] Structurally both compounds behave very similarly. However, crystals of **I-47^{NHC}** are red, whereas crystals of **I-47^{CAAC}** are blue. Theoretical calculations reveal a π(Si=P) bond in the HOMO of both compounds. The intense dark blue color of **I-47^{CAAC}** can be attributed to the lower lying LUMO, in comparison to **I-47^{NHC}** and arises due to the strong charge transfer transition from π(Si=P) to π*(CAAC).[136] In analogy to NHC-stabilized diodosilylenes, the CAAC stabilized diodosilylene selectively reacts with the carbene NHC^3 (NHC^3 = I*i*Pr$_2$Me$_2$ = :C[N(*i*Pr)C(Me)]$_2$), via the displacement of a iodide to the silylium-ylidenes **I-48^{NHC}** [70]and **I-48^{CAAC}** [121], respectively. In contrast to the precursors, the structural properties of **I-48^{NHC}** and **I-48^{CAAC}** differ significantly: overall **I-48^{CAAC}** (Σ°Si = 327.94°) is more planarized with respect to **I-48^{NHC}** (Σ°Si = 301.4°) and features a shorter Si–C^{carb} bond length (d(Si–C^{CAAC}) = 1.878(5) Å (**I-48^{CAAC}**), d(Si–C^{NHC}) = 1.947(2) Å (**I-48^{NHC}**). This is also reflected in the MO analysis of **I-48^{CAAC}**, which indicates that the HOMO is mainly localized at the Si atom with a slight back-donation to the C–N π*-MO of the caac^{Me} fragment, in contrast to the HOMO of **I-48^{NHC}** is exclusevly localized at the Si atom and does not feature any back-donation.[121]

In case of NHC and CAAC-stabilized monohalosilylenes major differences in the electronic structure are observed. Compound **I-49^{CAAC}** [137] is overall more planarized ($\Sigma°Si$ = 321.0 °) in comparison to silylene **I-49^{NHC}** [82] ($\Sigma°Si$ = 290.5°) and features much shorter Si–C^{carb} bond length's (d(Si–C^{CAAC}) = 1.853(1) Å (**I-49^{CAAC}**), d(Si–C^{NHC}) = 1.980(3) Å (**I-49^{NHC}**). In fact, compound **I-49^{CAAC}** features partial Si=C^{CAAC} double bond character and thus can be best described by both silene and silylene resonance structures (a more detailed explanation is given in *chapter 2.2*).

1.3.4 CAAC-stabilized silicon(IV) di-radicals

In contrast to NHCs, CAACs enabled the isolation of silicon(IV)-diradicals, such as the bis-CAAC compounds **I-50**$^{\mathbf{CAAC}}$ [122,138–141] and the dimers **I-51**$^{\mathbf{CAAC}}$.[140,142] The compounds can be best described as four coordinate silicon centers coordinated by neutral CAAC carbenes, each bearing an unpaired electron at the carbene carbon atom.

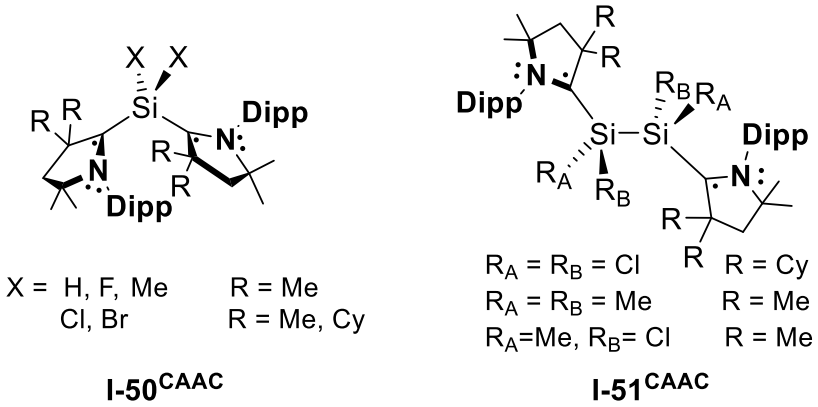

Figure 1.19. Literature known bis CAAC-stabilized silicon di-radicals.

Depending on the nature of the interaction of the two radical centers they can be distinguished between two main classes: disbiradical (no interaction) or biradical (interaction) (*Figure 1.20*).[98] If the two unpaired electrons in a single molecule are separated by a significant distance (r) or the spins orientated orthogonally to each other they show no exchange interaction (*J*) and as such they can be classified as dis-biradicals. They are like two doublets within the same molecule. If a strong interaction of the two radicals occurs the compound can be termed as biradical. This leads to two classical situations: (a) the two spins may align in the same direction (positive exchange interaction, triplet state) or (b) the two spins align in opposite direction to each other (negative exchange interaction, singlet state).

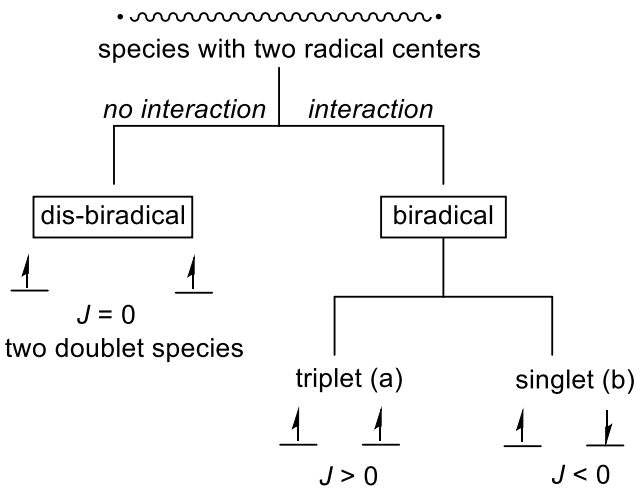

Figure 1.20. Definition of dis-biradical and biradicals reproduced from reference [143].

It should be noted that in both cases the two radicals occupy different orbitals. In case of a singlet biradical (b) the molecule does not contain a net magnetic moment and as such it is EPR silent and can be characterized by means of NMR spectroscopic methods. Triplet biradicals (a), contrary, are paramagnetic and typically two sets of EPR signals are observed.

Therefore the CAAC-stabilized silicon diradicals **I-50^{CAAC}** and **I-51^{CAAC}** can be sorted by the nature of the interaction of the two radical centers (*Table 1.1*). In case of $SiCl_2(caac^{Me})_2$ two different polymorphs were obtained and separated by fractional crystallization. Polymorph 2 appeared to be diamagnetic and was stable for at least one week in air, in contrast to polymorph 1 which appeared NMR silent and was characterized as dis-biradical.[122] Interestingly, no polymorphs were observed in the case of $SiBr_2(caac^{Me/Cy})_2$. According to the author the compound decomposed in solution at ambient temperature.[139]

Dr. U Das, later could show that $SiBr_2(caac^{Me})_2$, in fact, appears to be in a on- off equilibrium of free $caac^{Me}$ carbene to $SiBr_2(caac^{Me})$ (**I-31^{CAAC}**) (for more detail see *chapter 2.1*). Preliminary results by the research group of Filippou suggests that $SiMe_2(caac^{Me})_2$ can be isolated as well as singlet biradical, being diamagnetic and NMR spectroscopically characterized.[144]

Table 1.1. CAAC-stabilized silicon diradicals **I-50^{CAAC}** and **I-51^{CAAC}** sorted by the nature of the interaction of the two radical centers.

	nature of the unpaired e⁻	**electronic groundstate**	**characterization method**	**Ref.**
$SiF_2(caac^{Me})_2$	biradical	singlet	NMR / EPR-silent	[138]
$SiCl_2(caac^{Me})_2$ Polymorph-1	dis-biradical	two doublet species	EPR	[122]
$SiCl_2(caac^{Me})_2$ Polymorph-2	biradical	singlet	NMR/ EPR-silent	[122]
$SiCl_2(caac^{Cy})_2$	biradical	singlet	NMR	[139]
$SiBr_2(caac^{Me/Cy})_2$	biradical	singlet	NMR / no EPR charact. possible	[139]
$SiH_2(caac^{Me})_2$	biradical	triplet	EPR	[140]
$SiMe_2(caac^{Me})_2$	biradical	triplet	EPR	[141]
$[SiCl_2(caac^{Cy})]_2$	biradical	singlet	NMR	[142]
$[SiMeCl(caac^{Me})]_2$	dis-biradical	two doublet species	EPR	[140]
$[SiMe_2(caac^{Me})]_2$	dis-biradical	two doublet species	EPR	[140]

1.3.5 CAAC-stabilized silicon(IV) monoradicals

In contrast to NHCs, CAACs enabled the isolation of silicon(IV) monoradicals, such as **I-52^{CAAC}** and **I-53^{CAAC}**. [145] Major contribution was provided by the research group of Roesky, which enabled the isolation of silicon(IV) monoradicals, either upon reduction of the respective CAAC carbene adducts of silanes ((caac^{Me})SiF_4, (caac$^{Me/Cy}$)$SiCl_4$)[138,146] or the one pot reduction of the halosilanes in presence of CAAC carbene with KC_8.[141,145] The monoradical $SiPh_3$(caac^{Cy}) was obtained by nucleophilic substitution of the $SiCl_3$(caac^{Cy}) with phenyllithium.[147] Partial contribution was also provided by the research group of A. C. Filippou by Christoph Plett, which during the work of his bachelor thesis completed the homologue series of methyl chlorido substituted silicon(III)-radcials **I-52^{CAAC}** ((R_A)$_3$ = $MeCl_2$, Me_3 ; R = Me).[144] Similar, to the diradicals mentioned before, the compounds can be best described as four coordinate silicon centers coordinated by a neutral CAAC carbene, bearing an unpaired electron at the carbene center.

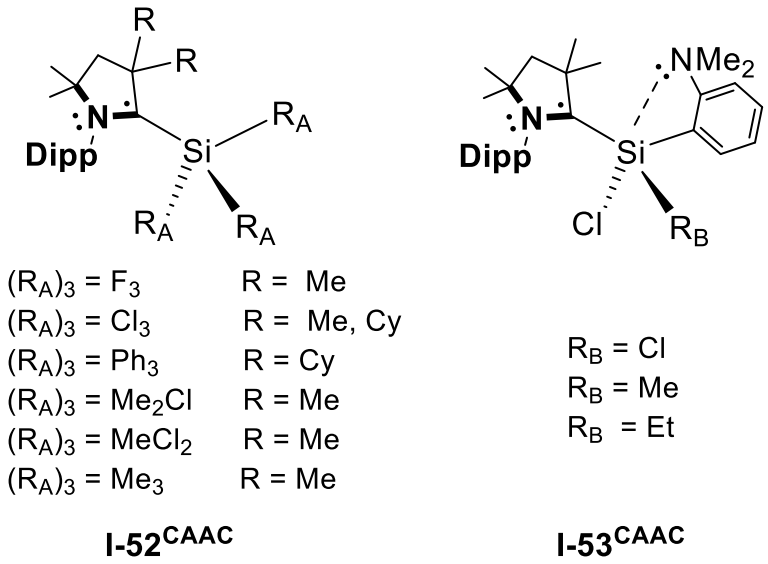

Figure 1.21. Literature known CAAC-stabilized silicon(IV) compounds.

1.4 Further CAAC-carbene stabilized main group compounds

Through the application of CAACs as σ-donors a variety of low valent main group compounds of the group 2 and 13–15 of the periodic table could be isolated next to the silicon compounds discussed in *chapter 1.3*.[95–98] In addition also a handful of saturated group 1 and 2 CAAC complexes have been explored.[148,149] In this section selected examples of CAAC stabilized main group compounds will be discussed.

1.4.1 Group 14 main group radicals

Since the discovery of the first CAAC carbene by Bertrand and co-workers in 2005,[57] the chemistry of main group radicals supported by cyclic (alkyl)(amino)carbenes developed rapidly and was subject of several review articles.[78,95,97,98] Selected examples of main group radicals in unusual low oxidation states are given in *Figure 1.22*: a two coordinate boryl-radical-cation **I-54**$^{\mathbf{CAAC}}$ [150], the bis-caac^{Me} stabilized aluminium(II)chloride **I-55**$^{\mathbf{CAAC}}$ [151], the allenyl/propagyl radicals **I-56**$^{\mathbf{CAAC}}$ [78], a two coordinate neutral germanium(I)-radical **I-57**$^{\mathbf{CAAC}}$ [152], a phosphanyl-radical cation **I-58**$^{\mathbf{CAAC}}$ [153] and a neutral stibanyl(II)-radical **I-59**$^{\mathbf{CAAC}}$ [154]. Notably, similar paramagnetic species could not be accessed with the corresponding NHC precursors.[150] This highlights the superiority of CAACs over NHCs for the stabilization of main group radicals.

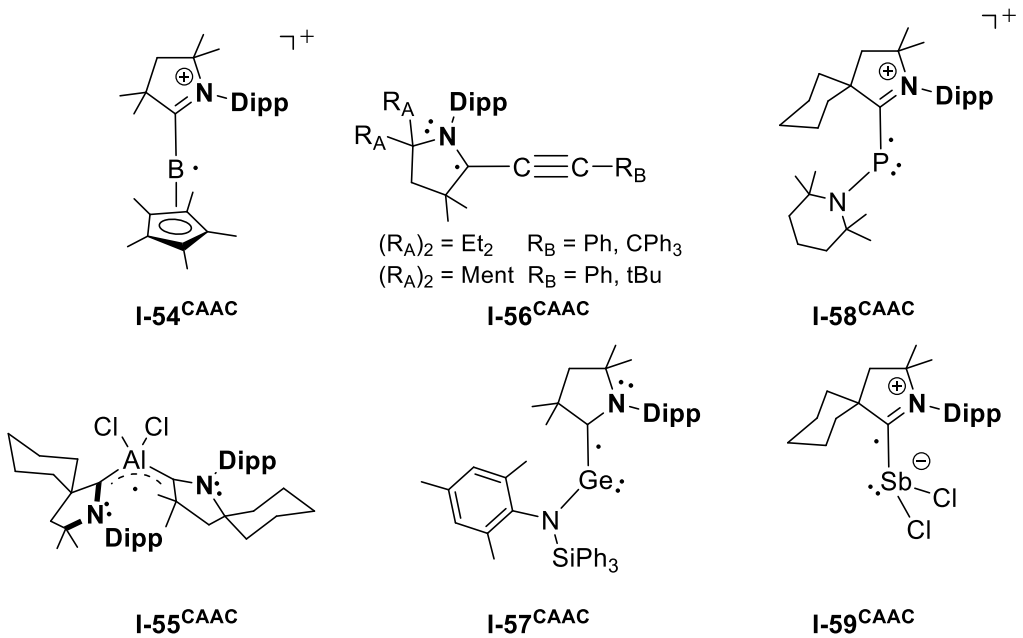

Figure 1.22. Selected examples of CAAC-stabilized main group radicals in unusual low oxidation states.

1.4.2 Group 14 main group compounds in zero oxidation state

CAAC carbenes expanded the range of zero valent main group compounds, which were accessible before only through the application of NHCs.[155] Although the heavier homologues of the ditetrel(0) compound could be isolated **I-60^{NHC}** (E^{14} = Ge[156], Sn[157]), via the applications of NHCs the isolation of the lighter carbon homologue remained elusive.[158] Through the application of CAACs, Roesky et al. and Bertrand et al. independently reported the experimental approach for isolating the dicarbene stabilized diatomic carbon C_2(caac$^{Me/Et}$)$_2$ (**I-61^{CAAC}**).[159,160] The neutral cumulene can be easily oxidized to the air stable radical cation $[C_2^{\bullet}]^+$ (**I-62^{CAAC}**) and di-cation $[C_2]^{2+}$ (**I-63^{CAAC}**).

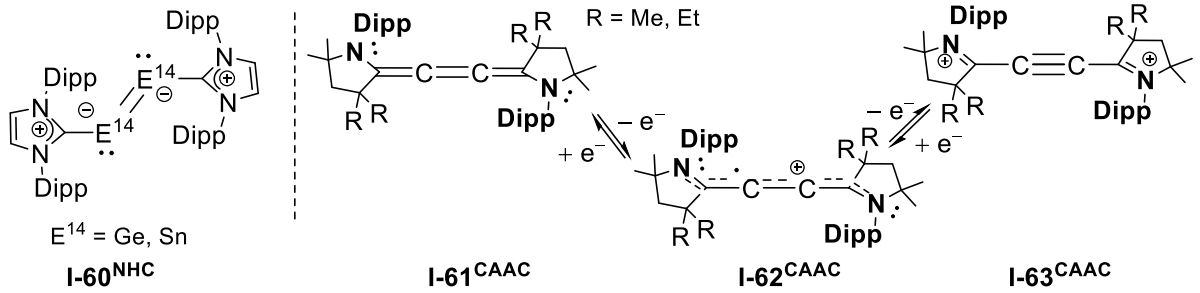

Figure 1.23. NHC -stabilized tetrel(0) complexes in comparison to the CAAC-stabilized diatomic carbon, in different oxidation states.

CAACs were also successfully used in the stabilization of monoatomic germanium(0)-compounds. **I-64^{CAAC}** was obtained by Roesky et al. upon one pot reduction of $GeCl_2$(dioxane) in presence of two equivalents caac^R carbene (R = Me, Cy) with two equivalents of KC_8.[161]

In addition one pot reduction of the germane $GeCl_3$(Trip) (Trip = C_6H_2-2,4,6-*i*Pr$_3$) in the presence of caac^{Me} carbene with 8 equiv. of KC_8 led to the formation of the unprecedent germanium(0) compound **I-65^{CAAC}**.[124] Originally described as germanylidene anion, the compound can be rather classified as a potassium-germenide with a strong Ge=C^{carb} double bond and a covalently connected potassium ion.

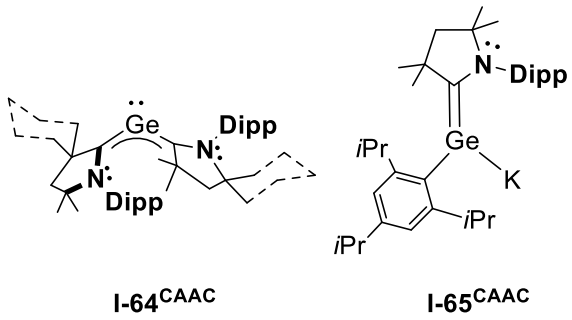

Figure 1.24. CAAC-stabilized monoatomic germanium(0) compounds.

1.4.3 Other main group compounds in zero oxidation state

The research group of Braunschweig could show that the reduction of the (caac^{Me})$BeCl_2$ complex in presence of caac^{Me} carbene yielded the bis-caac^{Me} stabilized monoatomic Be(0) compound **I-66^{CAAC}**, which is the first example of a neutral zero-valent s-block metal.[162] In analogy to the NHC-stabilized B≡B bond (**I-67^{NHC}**), reported by Braunschweig et al.,[163,164] the corresponding caac^{Me}-stabilized B_2-compound (**I-67^{CAAC}**), could be isolated,[165] which differs substantially from the parent NHC coordinated compound. In fact, compound **I-67^{CAAC}** features strong B–C^{carb} double bond character and as such it can be rather described as a an electro-deficient dibora-cumulene. Entry to the chemistry provided the bis carbene (NHC or CAAC) aduct of B_2Br_4 upon 4e$^-$ reduction by sodium-naphtanelide.[165] The nature of the different electronic structure of the NHC and caac^{Me}-stabilitzed B_2-compound could also be shown in terms of their reactivity.[166,167] Compound **I-67^{CAAC}** , for example, selectively reacts with dihydrogen (H_2) at ambient temperature yielding the caac^{Me} stabilized boron(I) compound (caac^{Me})BH=BH(caac^{Me}), whereas the NHC-stabilized compound **I-67^{NHC}** does not react even upon prolonged heating.[168]

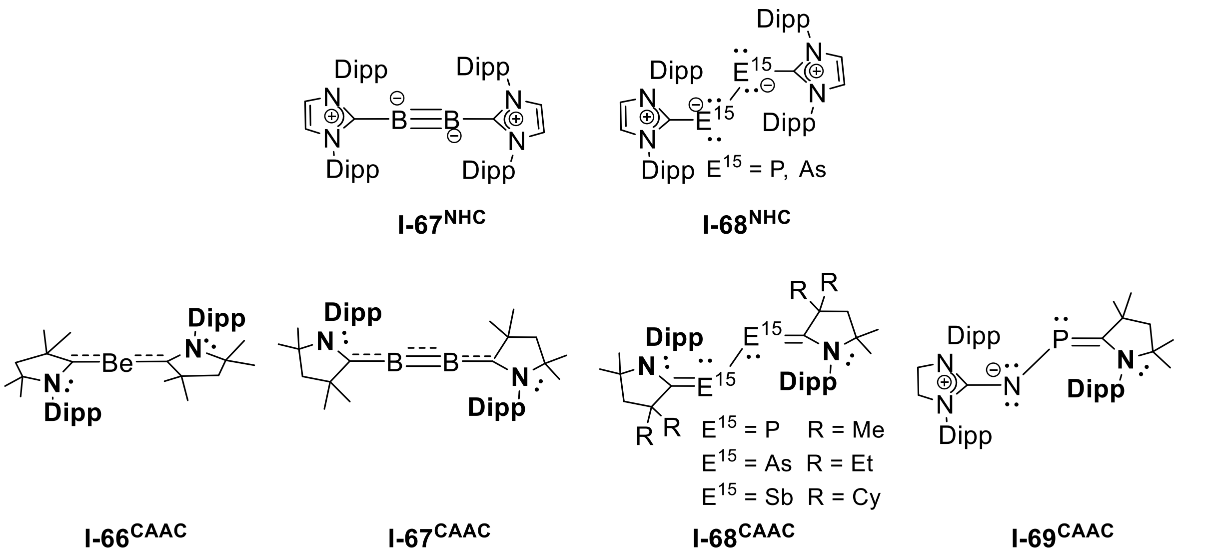

Figure 1.25. Selected examples of Literature known NHC and CAAC main group element compounds in the zero oxidation state.

Remarkably, the exact same phenomenon is observed for the bis (CAAC)-P_2 and bis (NHC)-P_2 adducts. The bis NHC adduct of P_2 (**I-68^{NHC}**) was isolated by Robinson et al., upon reduction of the carbene adduct (NHC)PCl_3 with three equivalents of KC_8.[169] The research group of Bertrand isolated the CAAC adduct **I-68^{CAAC}**, two years later in 2010, upon reaction of the caac^{Cy} carbene with white phosphorus (P_4).[170] Cyclovoltammetry of the two compounds revealed dramatic different redox properties.

Due to the superior π-accepting properties of the CAAC carbene compound **I-68^{CAAC}** featured only a single reversible one-electron oxidation ($E_{1/2}$ = 0.536 V *vs*. Fc+/Fc), whereas **I-68^{NHC}** featured two reversible one-electron oxidations ($E_{1/2}$ = –1.408 V; –0.178 V *vs*. Fc+/Fc). The corresponding radical cations, could be isolated upon one electron oxidation with $[Ph_3C][B(C_6F_5)_4]$. [170] Similarly to the NHC and CAAC adducts of B_2 (**I-67^{NHC}**, **I-67^{CAAC}**), compound **I-68^{CAAC}** is best described as a diphosphacumulene, whereas **I-68^{NHC}** can be rather described as an NHC stabilized diphosphinidene.

The heavier homologues to the bis (carbene)-P_2 adducts, have also been reported. In 2008 Robinson et al. isolated the NHC-stabilized diarsenic (As_2) molecule, upon reduction of the adduct (NHC)$AsCl_3$ with three equivalents of KC_8.[171] 10 years later, Hudnall et al., reported the isolation of $(caac^{Et})_2As_2$ (**I-68^{CAAC}**) by following the same synthetic protocol with minor modifications.[172] Both compounds are structural very similar. The As–C^{carb} bond in the CAAC supported case (1.837(5) Å) is significant shorter, compared to the parent NHC stabilized compound (1.881(2) Å), suggesting partial As–C^{CAAC} double bond character in $(caac^{Et})_2As_2$. Multiple attempts to isolate Sb(0) and Bi(0) species upon reduction of the adducts (NHC)$SbCl_3$ and (NHC)$BiCl_3$ were unsuccessful.[173] The only example of a diatomic antimony species in the zero oxidation state could be synthesized through application of CAAC carbene by the research group of Bertrand in 2014. [154] Thus far, no mono- or diatomic bismuth compounds in the zero oxidation state have been reported.

The isolation of a carbene stabilized phosphorus mononitride (PN) in **I-69^{CAAC}** highlights the ability of CAAC carbenes in stabilization of highly reactive species.[174] The compound was obtained upon one pot reduction of PCl_2(NHI) (NHI = N-heterocylcic imine, :N=C[N(Dipp)CH]$_2$) in the presence with $caac^{Me}$ carbene with magnesium.

1.5 Goals and objectives of this work

Silicon compounds in low oxidation states, especially dihalosilylenes (SiX_2), are highly unstable molecules, which are involved as fleeting intermediates in large scale industrial processes in the synthesis of alkyl(chloro)silanes[5,6] and highly pure polysilicon,[7] without which today's production of silicones and semiconductors would be inconceivable. Their high reactivity, which ultimately lead to either disproportionation or polymerization, could be tamed by the use of strong σ-donating N-heterocyclic carbene (NHC) ligands, which sequestered their electrophilicity through the reversed polarized ylidic $Si^{\delta-}$–$NHC^{\delta+}$ bond. This concept enabled the isolation of dihalosilylenes (SiX_2) as bottleable SiX_2(NHC) adducts, which had in recent years a major impact on the development of molecular silicon chemistry, leading to a plethora of novel compounds with intriguing bonding features and synthetic potential (see *chapter 1.3*).
It was anticipated that the ylidic character of the silicon-carbene bond could be tuned by using the cyclic (alkyl)(amino)carbene (CAAC) ligand, which in contrast to classical NHCs does not only provide stronger σ-donation properties, but also superior π-accepting capabilities (see *chapter 1.2*), leading to an unique reactivity pattern of the resulting adduct SiX_2(CAAC). For this sake, the CAAC stabilized dibromosilylene $SiBr_2(caac^{Me})$ (**1**) ($caac^{Me}$ (CAAC) = :C[N(Dipp)(CMe_2)(CH_2)(CR_2)], $R_2 = Me_2$) was prepared and a detailed synthetic and physiochemical study was planned.

The objectives of this work can be summarized with regard to the following points:

a) to synthesize **1** and to study its electronic structure by quantum chemical calculations.
b) to explore the reactivity of **1** and to develop access to synthetic equivalents of CAAC stabilized silylenes SiBr(R)
c) to synthesize the silicon(I) dimer $Si_2Br_2(caac^{Me})_2$ (**9-Br**) and to investigate its reactivity towards unsaturated nucleophiles
d) to find a selective pathway to a $caac^{Me}$-stabilized silagermenylidene ($caac^{Me}$)Ge=SiBr(Tbb) (**14-Ge**) and disilavinylidene ($caac^{Me}$)Si=SiBr(Tbb) (**14**)
e) to study the reactivity and electronic structure of **14** in comparison to the parent NHC stabilized disilavinylidene.

2 Results and Discussion

2.1 CAAC-Stabilized Dibromosilylene

2.1.1 Synthesis and properties of 1

The novel silicon(II) halide $SiBr_2(caac^{Me})$ (**1**), which was first prepared by Dr. U. Das,[175] is described. Compound **1** was synthesized via the $2e^-$-reduction of the tetrabromosilane-carbene adduct (CAAC)$SiBr_4$, which was prepared by reacting CAAC with $SiBr_4$ in a hydrocarbon solvent (*Scheme 2.1*) Although on the first glance its molecular properties ($d(Si–C^{carb})$ = 2.017(2) Å, $\Sigma\sphericalangle(Si)$ = 289.94°) are very similar to that of the NHC stabilized dibromosilylenes such as $SiBr_2(NHC^2)$ (NHC^2 = SIDipp = :C[N(Dipp)CH_2]$_2$) ($d(Si–C^{carb})$ = 2.012(2) Å, $\Sigma\sphericalangle(Si)$ = 289.7°)),[71] it features some noticeable electronic differences (*section 2.1.2*), which lead to remarkable differences in terms of its reactivity.

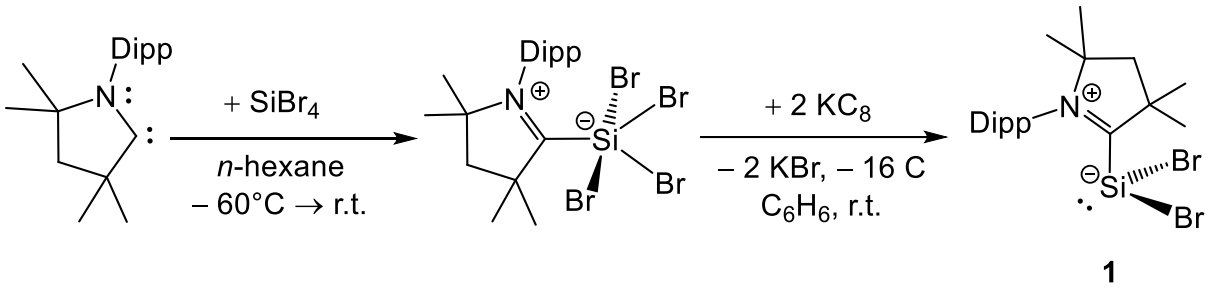

Scheme 2.1. Synthesis of $SiBr_2(caac^{Me})$ (**1**).

In analogy to the synthesis of NHC stabilized dihalosilylenes $SiX_2(NHC^{1,2})$ (**I-3l^{NHC}**) (X = Br, I) (NHC^1 = IDipp = :C[N(Dipp)CH]$_2$,), two electron reduction of a suitable silicon(IV) precursor was envisioned as a suitable approach to prepare $SiBr_2(caac^{Me})$ (**1**).[135] Reduction of $SiX_4(NHC^{1,2})$ with KC_8 in benzene, in fact, appeared to be a very effiecient method in the synthesis of NHC stabilized dihalosilylenes in high yields. The method was also recently employed in the synthesis of $SiI_2(caac^{Me})$ (**I-3l^{CAAC}**), starting from $SiI_4(caac^{Me})$.[121] Interestingly, reduction of $SiCl_4(caac^{Me})$ by two equivalents of KC_8 in benzene at ambient temperature did not lead to the desired dichlorosilylene $SiCl_2(caac^{Me})$. Monitoring of the reaction mixture by ^{1}H NMR spectroscopy in (D_6)benzene, instead, revealed the formation of a product mixture of the diradical $SiCl_2(caac^{Me})_2$[122] and the silicon(I)-dimer $Si_2Cl_2(caac^{Me})_2$,[128] which were synthesized independently by the research group of H. W. Roesky.

For the reduction approach $SiBr_4(caac^{Me})$ was prepared by reacting a suspension of $caac^{Me}$ carbene with $SiBr_4$ in *n*-hexane at –60°C. After workup, the carbene adduct ($caac^{Me}$)$SiBr_4$ could be isolated in high yield (> 95 %).

The adduct ($caac^{Me}$)$SiBr_4$ is insoluble in *n*-hexane, moderately soluble in benzene and highly soluble in dichloromethane. It is unstable in dichloromethane and in THF decomposing unselectively to unidentified products. Solutions of the compound are highly sensitive to hydrolysis leading to the formation of [$caac^{Me}$(H)]Br.

Similarly, like related carbene aducts $SiCl_4(NHC^{1,5})$ (NHC^1 = IDipp, NHC^5 = IMes = C[N(Mes)CH]$_2$, Mes = C_6H_2-2,4,6-Me_3)[68,114] and $SiCl_4(CAAC^{1,3})$ ($CAAC^1$ = $caac^{Me}$, $CAAC^3$ = $caac^{Cy}$),[146] the silicon center adopts a trigonal bipyramidal (TBP) geometry in which the $caac^{Me}$ occupies the equatorial site of the TBP. The compound was first isolated and fully characterized by Dr. U. Das. He could show, that the NMR spectroscopic properties of $SiBr_4(caac^{Me})$ are highly solvent dependent, suggesting a solvent dependent structural preference of the adduct. For example, the neutral adduct is observed in (D_6)benzene with a $^{29}Si\{^1H\}$ resonance at –90.8 ppm and dissociated ions of $[SiBr_3(caac^{Me})]^+$ Br^- in (D_2)dichloromethane with a signal at –54.9 ppm, respectively.[175]

Reduction of $SiBr_4(caac^{Me})$ with two equivalents of KC_8 in benzene at room temperature afforded after work up the silicon(II)bromide $SiBr_2(caac^{Me})$ (**1**) as a brick red solid in analytically pure form. The synthesis could be performed in high scale, allowing the isolation of 21 g of silylene adduct **1** (see *chapter 4.4*) in a single reduction in 68 % yield. Compound **1** is a thermally robust solid, which decomposes upon melting in a vacuum sealed capillary tube at 176 °C. It is is highly soluble in THF, well soluble in benzene and insoluble in *n*-hexane and diethylether. Remarkably, in contrast to $SiX_2(NHC^{1,2})$ and $SiI_2(caac^{Me})$ compound **1** is redox-unstable in benzene and THF solution at ambient temperature. Dark red solutions of **1** in (D_6)benzene turn red-purple after 0.5 h at ambient temperature, whereas solutions of **1** in (D_8)THF take atleast 24 hours to display the same color change. Monitoring of the decomposition by ^1H NMR spectroscopy in (D_6)benzene reveals the formation of the silicon(I) dimer $Si_2Br_2(caac^{Me})_2$ (**9-Br**). In addition an increasing broadening of the signals of **1** were observed, suggesting that also a paramagnetic compound (highly likely a silicon(III) species) is formed during the redox-disproportionation of **1**. Surprisingly, the decomposition of **1** in (D_6)benzene stops after 20 h at ambient temperature, leading to a mixture of ca. 20 mol% of **9-Br** with respect to **1**, suggesting an equilibrium between **1** and the products of the redox-disproportionation. The $caac^{Me}$-stabilized silicon(I) dimer **9-Br** was selectively prepared upon reduction of **1** with KC_8 in benzene and isolated as dark purple solid in 77 % yield (for more details see *chapter 2.4*). The paramagnetic silicon(III) compound, could be verified as $SiBr_3(caac^{Me})$-radical and was isolated by Dr. U. Das upon reduction of $SiBr_4(caac^{Me})$ with 1 equivalent of KC_8 in benzene as orange microcrystalline solid in 79 % yield.[175] The molecular structure of the compound features a tetragonal coordinated silicon center with the unpaired electron mainly localized at the C^{carb} atom. $SiBr_3(caac^{Me})$ compares well to the literature known $SiCl_3(caac^{Me})$ radical.[146]

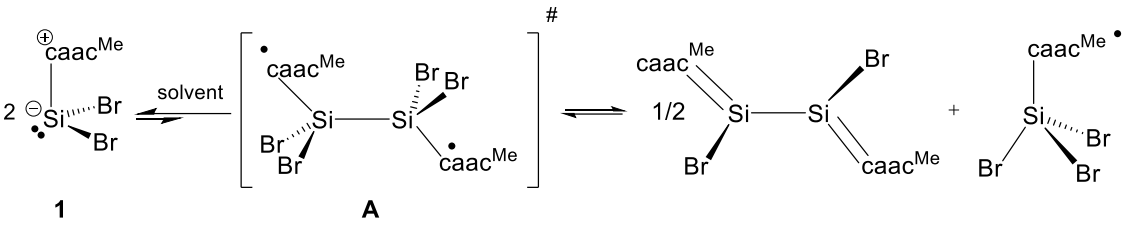

Scheme 2.2. Redox-disproportionation of $SiBr_2(caac^{Me})$ (**1**) via the presumed intermediate **A** to $Si_2Br_2(caac^{Me})_2$ (**9-Br**) and $SiBr_3(caac^{Me})$ radical.

The reversible character of the redox-disproportionation reaction, together with Dr. U. Das, could be shown upon dissolving a 2:1 mixture $SiBr_3(caac^{Me})$ and $Si_2Br_2(caac^{Me})_2$ (**9-Br**) in (D_6)benzene. ^{1}H-NMR spectroscopy of the solution undoubtly confirmed the formation of $SiBr_2(caac^{Me})$ (**1**) and displayed the same ratio of **9-Br** (20 mol%) to **1**, as observed in the ^{1}H NMR spectrum of pure compound **1** in (D_6)benzene after 20 h at ambient temperature. The decomposition of **1**, highly likely, proceeds via a presumed dimeric diradical **A**, as an intermediate, which upon Si–Si bond cleavage undergoes the redoxdisproportionation yielding **9-Br** and $SiBr_3(caac^{Me})$. The slower decomposition rate of **1** in (D_8)THF, compared to (D_6)benzene might be attributed to the coordinating effect of the solvent, which coordinates weakly to **1** and thus renders the dimerization of the molecule more difficult. In fact, adding 1-equivalent of $caac^{Me}$ carbene to a pure sample of **1** in (D_6)benzene reverts the redox-disproportionation reaction and leads via an reversible on-off equilibrium of the $caac^{Me}$ carbene to the literature known $SiBr_2(caac^{Me})_2$.[175]

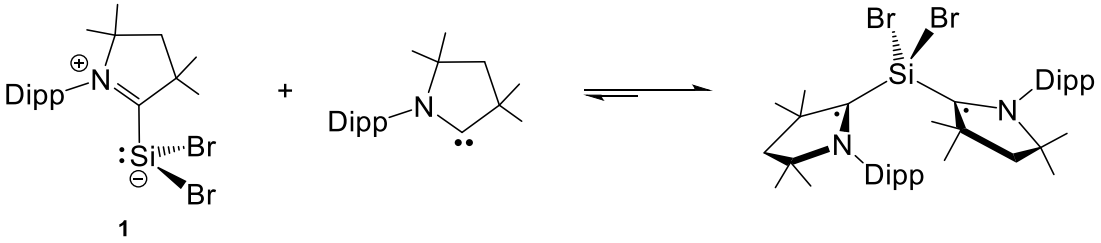

Scheme 2.3. Reversible on-off equilibrium of $caac^{Me}$ to **1**, yielding $SiBr_2(caac^{Me})_2$.

Calorimetric measurements, which were performed in collaboration with the group of Prof. Dr. Sven Schneider, upon titration of $caac^{Me}$ carbene to $SiBr_2(caac^{Me})$ (**1**) under inert atmosphere, gave direct access to the thermodynamic parameters of the reversible coordination of $caac^{Me}$ to **1**. A more detailed introduction in the method is given in *chapter 5.4*. Fitting the obtained curve Q (heat) against equivalents of added titrant (carbene $caac^{Me}$) gave the stoichiometry ($n = 1.017 \pm 0.015$)), the reaction enthalpy ($\Delta H° = -38.59 \pm 0.81$ kJ mol^{-1}) and the association constant ($K_B = (5.18 \pm 0.49) \times 10^2$ L mol^{-1}). Using the Gibb's Helmholtz relation and Van't Hoff relation the free reaction enthalpy ($\Delta G° = -15.5 \pm 0.2$ kJ mol^{-1}) and reaction entropy ($\Delta S° = -77.5 \pm 2$ J K^{-1} mol^{-1}) were calculated, respectively.

Table 2.1. Thermodynamic parameters for the reversible association of caac^{Me} to **1** obtained from the isothermal titration calorimetry and Van't Hoff analysis of recorded variable temperature ^{1}H NMR spectra in (D_8)THF.

Thermodynamic parameter	Calculated Value	
	Isothermal Titration Calorimetry[this work]	Van't Hoff analysis VT ^{1}H NMR[175]
K_{eq}^{298} (M)	$(5.18 \pm 0.49) \times 10^2$ L mol^{-1}	$(4.26 \pm 0.50) \times 10^2$ L mol^{-1}
ΔH^{298} (kJ·mol^{-1})	-38.6 ± 0.8 kJ mol^{-1}	-39 ± 3 kJ mol^{-1}
ΔG^{298} (kJ·mol^{-1})	-15.5 ± 0.2 kJ mol^{-1}	-15 ± 4 kJ mol^{-1}
ΔS^{298} (J·mol^{-1} K^{-1})	-77.5 ± 2 J K^{-1} mol^{-1}	-79 ± 10 J K^{-1} mol^{-1}

The thermodynamic parameters of the reversible association of caac^{Me} to **1** obtained from the isothermal titration calorimetry, do compare well with the values derived from the Van't Hoff Analysis of recorded VT ^{1}H NMR spectra of $SiBr_2$(caac^{Me})$_2$ in (D_8)THF, which was performed by Dr. U. Das.[175] Plotting ln(K) versus 1/T gave a linear correlation. The enthalpy of activation ($\Delta H^{\ddagger} = -39 \pm 3$ kJ mol^{-1}) and entropy of activation ($\Delta S^{\ddagger} = -79 \pm 10$) J K^{-1} mol^{-1}) were obtained from the slope and the intercept of the linear fit, respectively. The Gibbs free energy was calculated using the Gibb's Helmholtz equation and was shown to be $\Delta G^{\ddagger}(298K) = -15 \pm 4$ kJ mol^{-1}.[175]

Single crystals of **1** were obtained from a 1:5 v/v THF/Et_2O solvent mixture of **1** after storing for several days at –60 °C. The molecular structure (*Figure 2.1*) displays a three coordinated silicon center with trigonal pyramidal geometry ($\Sigma°Si = 289.94°$, DP(Si) = 78 %).

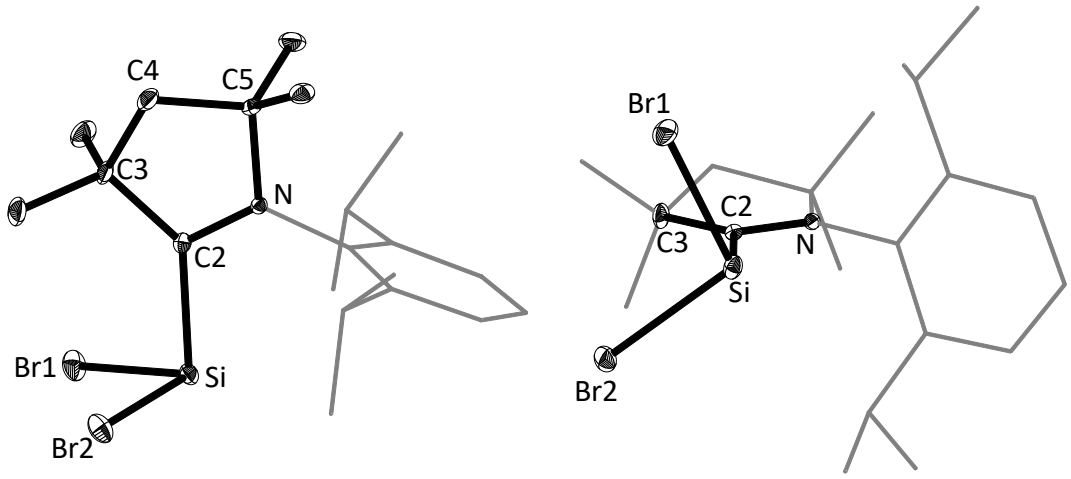

Figure 2.1. (Left) DIAMOND plot of the molecular structure of **1**; thermal ellipsoids are shown at 30 % probability level and the hydrogen atoms were omitted. In the depicted structure the Dipp-substituent of the caac^{Me} ligand is presented in the wire-frame for the sake of clarity. Selected bond lengths [Å] and angles [°]: Si–Br1 2.3591(7), Si–Br2 2.3542(7), Si–C2 2.017(2), N–C1 1.468(2), N–C2 1.301(3), N–C5 1.532(3), C2–C3 1.534(3); Br2–Si–Br1 99.26(2), C2–Si–Br1 93.72(6), C2–Si–Br2 96.96(6), C1–N–C5 119.7(2), C2–N–C1 124.7(2), C2–N–C5 115.4(2), C6–C1–N 119.3(2), C6–C1–C10 122.3(2), C10–C1–N 118.3(2), N–C2–Si 116.2(2), N–C2–C3 109.2(2), C3–C2–Si 134.5(2); (Right) view along the Si–C2 bond vector of the silylene-carbene core.

The Si–C^{carb} bond length (2.017(2) Å) of **1** is is remarkably elongated, when compared to $SiBr_2$(IDipp) (**1-NHC^1**) (1.989(2) Å),[69] but compares well to the diiodide analogue $SiI_2(caac^{Me})$ (2.013(5) Å)[121] and to $SiBr_2$(SIDipp) (**1-NHC^2**) (2.012(2) Å) [71] (*Table 2.2*). In addition, the degree of pyramidalization (DP), the Si–C^{carb} bond length, as well the twist angle τ of **1** are closely related to that of $SiBr_2$(SIDipp) (**1-NHC^2**) (*Table 2.2*).

Besides the strong similarities of $SiBr_2(caac^{Me})$ and $SiBr_2$(SIDipp) in terms of their molecular structure, they drastically differ in terms of the colors. Compound **1**, similarly as $SiI_2(caac^{Me})$, features a dark red color in the solid state and solution, whereas **1-NHC^2** displays a yellow color, similar like other NHC stabilized silylenes. This might be attributed due to differences of the electronic structure of **1** compared to **1-NHC^2**.

Another interesting structural feature of **1** is the twist of the silylene plane versus the carbene plane (*Figure 2.1*, left). Both bromine atoms Br1 and Br2 are pointing away from the N-Dipp moiety of the $caac^{Me}$ ligand (τ(Br1-Si-C2-N) = 114.8(2)°, τ(Br2-Si-C2-N) = –145.4(2)°, and are assymetrically exposed towards the C3-atom. Similar feature, is also observed in $SiI_2(caac^{Me})$, where the two iodine atoms I1 and I2 are pointing away from the N-Dipp moiety of the $caac^{Me}$ carbene (τ(I1-Si-C1-N) = –139.6(4)°, τ(I2-Si-C1-N) = 118.4(4)°).[121]

Table 2.2. Selected structural paramters of dibromosilylene $SiBr_2(caac^{Me})$ (**1**) in comparison to literature known NHC stabilized silylenes and $caac^{Me}$ diradicaloids .

Comp.	Si–C^{carb} / Å	N–C^{carb} / Å	Σ∢(Si) / (deg)	DP[a] / %	τ[b] / (deg)	Ref.
$SiBr_2(caac^{Me})$ **1**	2.017(2)	1.301(3)	289.9	78	79.1(1)	
$SiBr_2(caac^{Me})_2$	1.853(5)	1.405(6)	–	–	–	*U. Das*
	1.853(5)	1.389(6)				
$SiI_2(caac^{Me})$	2.013(5)	1.301(6)	299.7	67	97.5	[121]
$SiCl_2(caac^{Me})_2$	1.845(2)	1.399(2)	–	–	–	[122]
	1.848(2)	1.395(2)				
$SiBr_2$(IDipp)	1.989(3)	1.358(4)	292.7	75	50.4	[69]
(**1-NHC^1**)		1.363(3)				
$SiBr_2$(SIDipp)	2.012(2)[a]	1.337(2)	288.6	79	70.3	[71]
(**1-NHC^2**)	2.002(2)	1.343(2)	290.8	77	54.4	
$SiBr_2$(IDipp-Me_2)	2.007(8)	1.352(11)	297.2	70	41.1	[176]

[a]: The degree of pyramidalization (DP) value of 0 % describes a trigonal planar coordination of the silicon atom with the sum of bond angles equal to 360 °. A DP value of 100 % corresponds to a trigonal pyramidal coordination of the silicon atom with the sum of bond angles equal to 270 °.
DP (in %) = 100 % · [360 − Σ∢(Si) /(deg)]/90
[b]: The twist angle (τ) is defined as the angle between the silicon and Ccarbene coordination planes defined by the atoms X1-Si1-SX2 (X = Cl, Br, I) and C3-C2-N1 for CAAC (N1-C1-N2 for NHC), respectively.

^{1}H, $^{13}C\{^{1}H\}$ and $^{29}Si\{^{1}H\}$ NMR spectra of **1**, display an averaged C_S-symmetry in solution, which can be rationalized via fast rotation of the Si–C^{carb} bond at the prochiral silicon center. In order to avoid the redox-disproportionation of **1**, the compound was NMR spectroscopically characterized in (D_8)THF at 243 K. The $^{13}C^{CAAC}$ resonance appears as a broad signal at $\delta(^{13}C)$ = 231.2 ppm ($\Delta\nu_{1/2}$ = 23 Hz), which is comparable to that of the $SiI_2(caac^{Me})$ ($\delta(^{13}C)$ = 230.1 ppm)[121] but is significantly downfield shifted, when compared to $SiBr_2$(SIDipp) (**1-NHC²**) (188.7 ppm). The $^{29}Si\{^{1}H\}$ resonance of the three coordinated silicon center appears at 14.35 ppm and compares well to that of **1-NHC¹** (15.8 ppm) and **1-NHC²** (10.8 ppm) and is downfield shifted when compared to the diodosilylene $SiI_2(caac^{Me})$ (–2.1 ppm). The (^{1}H, ^{15}N) HMBC spectrum revealed a crosspeak at 231.3 ppm, which could be assigned to the nitrogen atom of the $caac^{Me}$ ligand, which is slightly downfield shifted when compared to free $caac^{Me}$ (220.6 ppm) and surprisingly identical to that of the pyrolidinium salt $[(caac^{Me})H]Cl$ (231.0 ppm).

Table 2.3. Selected multi-nuclear NMR chemical shift values (in ppm) of **1** and related NHC and $caac^{Me}$ supported silicon halides.

Comp	$\delta(^{13}C^{carb})$ / ppm	$\delta(^{29}Si)$ / ppm	$\delta(^{15}N^{carb})$[a] / ppm	Ref.
$SiBr_4(caac^{Me})$	197.7[b]	–54.9[b]	256.8[b]	
	–	–195.3[c]	213.1[c]	
$SiBr_2(caac^{Me})$ (**1**)	231.2[d] ($\Delta\nu_{1/2}$ = 23 Hz)	14.35[d] ($\Delta\nu_{1/2}$ = 17 Hz)	231.3[d]	*U. Das*
$SiBr_2(caac^{Me})_2$ [c]	141.2[d] ($\Delta\nu_{1/2}$ = 23 Hz)	–29.04[d] ($\Delta\nu_{1/2}$ = 3 Hz)	131.4[d]	
$SiI_2(caac^{Me})$	230.1[c]	-2.1[c]	–	[121]
$SiCl_2(caac^{Me})_2$	–[e]	–14.1[c] ($\Delta\nu_{1/2}\approx$ 60 Hz)	130.6[c]	[122]
$SiCl_2(caac^{Me})_2$	142.7[c] ($\Delta\nu_{1/2}\approx$ 25 Hz)	–14.1[c] ($\Delta\nu_{1/2}\approx$ 60 Hz)	131.3[c]	*U. Das*
$SiBr_2$(IDipp) (**1-NHC¹**)	164.5[c]	15.8[c]	–	[69]
SiI_2(IDipp)	158.4[c]	–9.7[c]	–	[70]
$SiBr_2$(SIDipp) (**1-NHC²**)	188.7[c]	10.8[c]	–	[71]
SiI_2(SIDipp)	–[e]	–11.2[c]		[72]
$SiCl_2$(IMes)	–[e]	17.8[f]	–	[68]
$SiBr_2$(IDipp-Me_2)	162.5[c]	14.0[c]	–	[176]

[a]: ^{15}N NMR resonance of the single nitrogen atom in the CAAC carbene-ring referenced against NH_3(l). [b]: (D_2)dichloromethane, 213 K, [c]: (D_6)benzene, 298 K, [d]: (D_8)THF, 243K; [e]: no signal was observed; [f]: measured in (D_8)THF at 298 K.

According to the structural and NMR spectroscopic data the cyclic (alkyl)(amino)carbene CAAC is connected via Si–C^{carb} single bond to the dibromosilylene ($SiBr_2$) in **1,** in analogy to NHC stabilized dibromosilylenes $SiBr_2$(NHC).

2.1.2 Electronic structure of 1

The electronic structure of $SiBr_2(caac^{Me})$ (**1**) and related NHC-stabilized dibromosilylenes $SiBr_2(NHC^{1,2})$ (NHC^1 = IDipp (**1-NHC¹**), NHC^2 = SIDipp (**1-NHC²**)) was investigated by quantum chemical calculations, which were performed at the B97-D3(BJ)-ATM/def2-TZVP level of theory by Jens Rump. More details on the computional calculations are given in *chapter 5.11*. The structural parameters of the calculated structures in the gas phase do compare well to the structures derived from single-crystal X-ray diffraction of **1** and literature known NHC stabilized dibromosilylenes **1-NHC¹** [57] and **1-NHC²** [71] (*Table 5.74* and *Table 5.75*).
Natural Bond Orbital analysis of the wave function of $\mathbf{1}_{calc}$ and dibromosilylenes $\mathbf{1\text{-}NHC^1}_{calc}$ and $\mathbf{1\text{-}NHC^2}_{calc}$ led to a leading natural Lewis structure (NLS) with localized bond pair electron NBOs for the Si–C^{carb} and Si–Br σ-bonds as well as a localized lone pair of electron pair at the silicon center featuring high Lewis occupancy above 1.93 e^- (Table 2.4).

Table 2.4. Selected results of the natural bond orbital (NBO), natural resonance theory (NRT) and natural population (NPA) analyses of carbene stabilized dibromosilylenes **1**, **1-NHC¹** and **1-NHC²** calculated by Jens Rump at the B97-D3(BJ)^{ATM}/def2-TZVP level of theory.

NBO A–B	occ.[a]	NHO (A,B)[b] hyb. (pol. in %)	WBI[c] A–B	NRT-BO[d] tot/cov/ion	Natural Lewis structure (NLS)
$SiBr_2(caac^{Me})$ (**1**)					
LP(Si)	1.95	$sp^{0.2}$			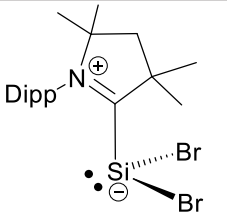
σ(Si–C^{carb})	1.93	$sp^{9.4}$ (20), $sp^{1.6}$ (80)	0.63	0.95/0.36/0.59	
σ(C^{carb}–N)	1.98	$sp^{2.5}$ (33), $sp^{1.5}$ (67)	1.51	1.83/1.10/0.73	
π(C^{carb}–N)	1.95	p (27), p (73)			
$SiBr_2$(IDipp) (**1-NHC¹**)					
LP(Si)	1.94	$sp^{0.2}$			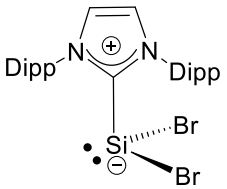
σ(Si–C^{carb})	1.95	$sp^{11.0}$ (20), $sp^{1.4}$ (79)	0.66	0.99/0.36/0.63	
σ(C^{carb}–N)	1.98	$sp^{2.4}$ (36), $sp^{1.8}$ (64)	1.25	1.42/0.91/0.51	
π(C^{carb}–N)	1.88	p (26), p (74)			
$SiBr_2$(SIDipp) (**1-NHC²**)					
LP(Si)	1.95	$sp^{0.2}$			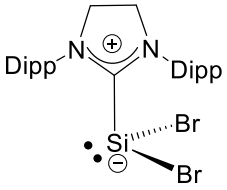
σ(Si–C^{carb})	1.93	$sp^{11.3}$ (20), $sp^{1.5}$ (80)	0.62	0.91/0.33/0.58	
σ(C^{carb}–N)	1.98	$sp^{2.2}$ (36), $sp^{1.6}$ (64)	1.29	1.47/0.90/0.57	
π(C^{carb}–N)	1.95	p (22), p (78)			

[a]: occ.= occupancy in e^-; [b]: NHO = Natural Hybrid Orbital, pol. (polarization) = $(C_i)^2 \cdot 100\%$, where C_i = coefficient of NHO; [c]: Wiberg bond index; [d]: total, covalent and ionic NRT bond order.

The Si–C^{carb} bonds are strongly polarized toward the carbon atoms. Compound **1** features a rather strong N=C^{carb} double bond (NRT-BO(tot): 1.83), whereas the other dibromosilylenes feature partial π-character in the N–C^{carb} bond (NRT-BO(tot): 1.47, 1.42), which can be attributed to the delocalization of the π-bond over the two nitrogen centers in the NHC stabilized dibromosilylenes. In terms of the NBO-NRT results compound **1** is remarkably similar to the NHC-stabilized dibromosilylenes.

The NBO results are reflected in the frontier orbitals of $\mathbf{1}_{calc}$, $\mathbf{1\text{-}NHC^1}_{calc}$ and $\mathbf{1\text{-}NHC^2}_{calc,}$ (*Figure 2.2*). The HOMO mainly contains the lone pair at the Si-center, whereas the LUMO corresponds to the empty p-orbital of the C^{carb} atom. However, the energy eigenvalues of the Kohn-Sham orbitals of **1**, reveal remarkable differences with respect to the NHC-stabilized dibromosilylenes. The HOMO of **1** (–4.51 eV) lies only slightly lower in comparison to **1-NHC^1** (–4.44 eV) and **1-NHC^2** (–4.47 eV), whereas the LUMO in **1** (–2.75 eV) is drastically decreased with respect to the IDipp (–1.94 eV) and SIDipp (–2.04 eV) stabilized dibromosilylenes. The results are in line with the theoretical calculations of the free $caac^{Me}$ carbene with respect to that of NHC (lower lying LUMO, drastically decreased singlet-triplet gap).[93] The small HOMO – LUMO gap in **1** ($E_{HOMO-LUMO}$ = 1.76 eV) might explain the intense red color of **1** in the solid state and solution in contrast to the NHC stabilized dibromosilylenes $SiBr_2(NHC^{1,2})$($E_{HOMO-LUMO}$ = 2.47 eV (NHC^1), 2.43 eV (NHC^2)) which appear yellow.

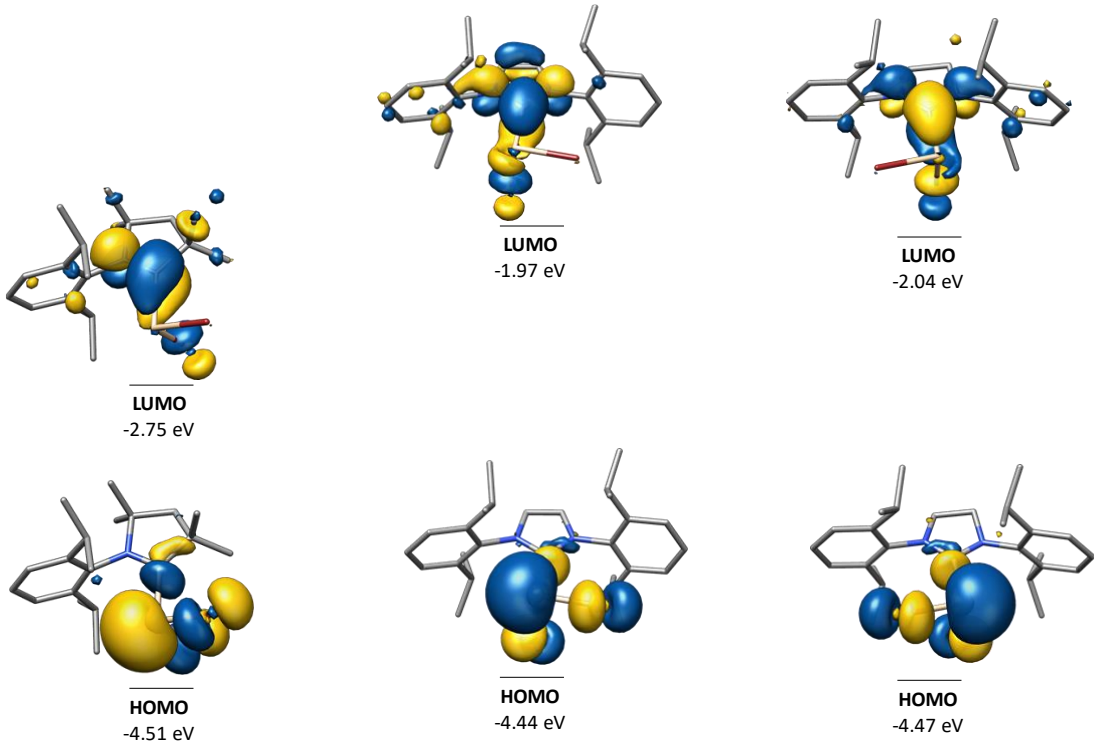

Figure 2.2. Selected Kohn-Sham molecular orbitals of $SiBr_2(caac^{Me})$ (**1**) (left), $SiBr_2$(IDipp) (**1-NHC^1**) (middle) and $SiBr_2$(SIDipp) (**1-NHC^2**) (right) and their energy eigenvalues in eV; calculated by Jens Rump at the B97-D3(BJ)^{ATM}/def2-TZVP level of theory.

The nature of Si–C^{carb} in NHC and CAAC stabilized dibromosilylenes $SiBr_2$(carbene) (carbene = $NHC^{1,2}$ (IDipp, SIDipp), CAAC ($caac^{Me}$)) was also studied by Natural Orbital of Chemical Valence in combination with Extended Transtion State theory analysis (NOCV-ETS).[177–179] Within the ETS scheme the energy of the formation of the Si–C^{carb} bond (ΔE_{int}) in **1**, **1-NHC¹** and **1-NHC²** was analyzed starting from the fragments (CAAC/NHC) and $SiBr_2$ in their equilibrium geometry and electronic ground state. ΔE_{int} = –BDE, where BDE is the Si–C^{carb} bond dissociation energy and is composed of the bond cleavage energy (BCE) and ΔE_{prep}, see (eq. 2.1). The ETS scheme decomposes BCE into a number of chemically meainingful components given in (eq. 2.2).

$$\Delta E_{intern} = -\mathrm{BDE} = -\mathrm{BCE} + \Delta \mathrm{E}_{prep} \qquad \text{(eq. 2.1)}$$

$$\mathrm{BCE} = \Delta \mathrm{E}_{\mathrm{orb}} + \Delta \mathrm{E}_{\mathrm{Pauli}} + \Delta \mathrm{E}_{\mathrm{elstat}} \qquad \text{(eq. 2.2)}$$

ΔE_{prep} is the sum of the preparation energies of the fragments; ΔE_{orb} is the total orbital interaction energy, ΔE_{Pauli} is the Pauli repulsion energy, ΔE_{elstat} is the electrostatic interaction energy.

Although the overall interaction energies ($\Delta E_{int} = -BDE$) of the compounds do not differ significantly (*Table 2.5*) the bond cleavage energy of **1** (237.9 kJ mol^{-1}) lies 13 and 11 kJ mol^{-1} higher in energy with respect to the Dipp and SIDipp stabilized dibromosilylenes. This can mostly attributed to the dramatic lowered orbital interaction energy in **1** ($\Delta E_{orb,1}$ = –390.3 kJ mol^{-1}) which lies 33.8 kJ mol^{-1} and 40.5 kJ mol^{-1} lower in energy with respect to **1-NHC¹** and **1-NHC²**. The orbital interaction energy ($\Delta E_{orb,1,}$ see also *Figure 2.3*)describes the LP(C^{carb}) → p(Si) σ-donation. Remarkably, no significant difference in the Br_2Si(LP) → C^{carb} π-backdonation ($\Delta E_{orb,2}$) is observed. In addition, considerable amounts of an orbital interaction energy of the Si(LP) to the Si–C^{carb} σ-bond ($\Delta E_{orb,3}$) is observed, which in terms of its values almost equals the Br_2Si(LP) → C^{carb} π-backdonation ($\Delta E_{orb,2}$). The NOCV-ETS analysis, clearly shows that the CAAC carbene provides a greater σ-donation strength in dibromosilylenes in comparison to NHCs. This is in line with experimental observations, which reveal the carbene exchange reactions of $SiBr_2$(NHC^2) and SiX_2(NHC^1) (X =Cl, Br) with one and two equivalents of $CAAC^{1,2}$ leading to the formation of **1**[175] and diradicals SiX_2($CAAC^{1,2}$) (**I-50^{CAAC}**) next to the free NHCs, respectively.[139]

Table 2.5. Results of the energy decomposition analysis of carbene stabilized dibromosilylenes **1**, **1-NHC¹** and **1-NHC²** (energies in kJ mol^{-1}).

compound	$\Delta E_{orb,1}$	$\Delta E_{orb,2}$	$\Delta E_{orb,3}$	ΔE_{orb}	BCE	ΔE_{prep}	BDE	ΔE_{int}
1	–390.3	–23.8	–32.8	–497.6	237.9	36.5	201.4	–201.4
1-NHC¹	–357.1	–32.8	–28.4	–462.9	224.9	26.0	198.9	–198.9
1-NHC²	–349.8	–24.3	–29.6	–447.1	226.5	35.9	190.6	–190.6

LP(C^{carb}) → p(Si) σ-donation		
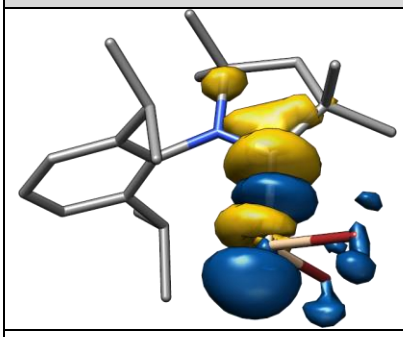	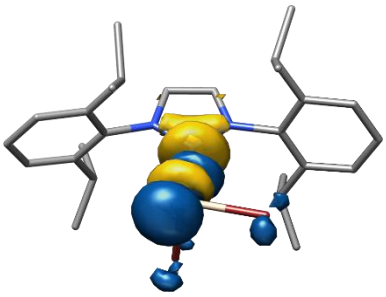	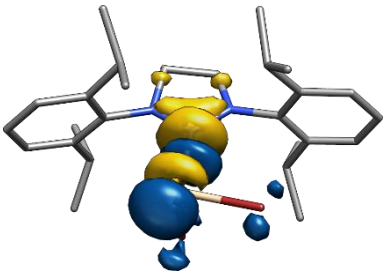
1 $\Delta\rho_1 = -0.91\psi^2_{-1} + 0.91\psi^2_{+1}$ iso = 0.004 e·Bohr^{-3}	**1-NHC^1** $\Delta\rho_1 = -0.87\psi^2_{-1} + 0.87\psi^2_{+1}$ iso = 0.004 e·Bohr^{-3}	**1-NHC^2** $\Delta\rho_1 = -0.87\psi^2_{-1} + 0.87\psi^2_{+1}$ iso = 0.004 e·Bohr^{-3-3}
Br_2Si(LP) → p(C^{carb}) π-backdonation		
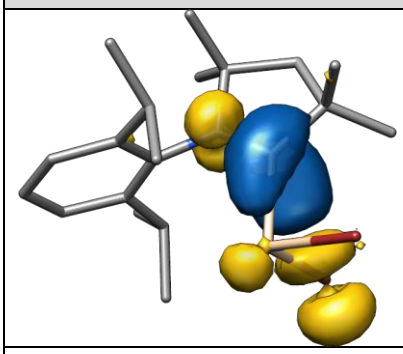	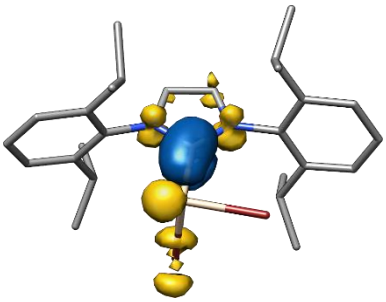	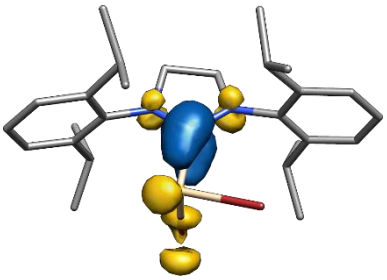
1 $\Delta\rho_2 = -0.33\psi^2_{-2} + 0.33\psi^2_{+2}$ iso = 0.001 e·Bohr^{-3}	**1-NHC^1** $\Delta\rho_2 = -0.32\psi^2_{-2} + 0.32\psi^2_{+2}$ iso = 0.002 e·Bohr^{-3}	**1-NHC^2** $\Delta\rho_2 = -0.29\psi^2_{-2} + 0.29\psi^2_{+2}$ iso = 0.002 e·Bohr^{-3}
Br_2Si(LP) → σ(Si–C^{carb}) interaction		
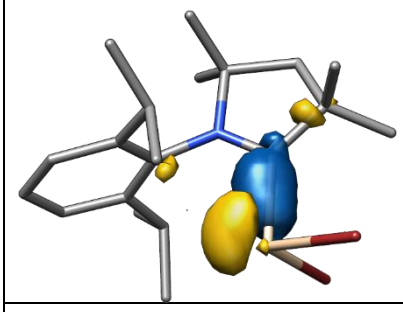	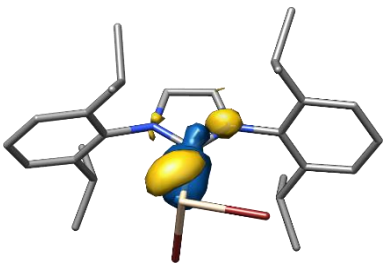	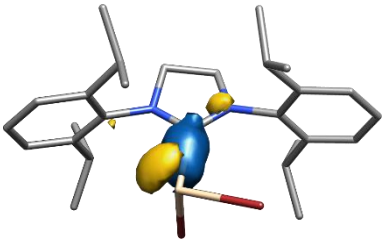
1 $\Delta\rho_3 = -0.22\psi^2_{-3} + 0.22\psi^2_{+3}$ iso = 0.0017 e·Bohr^{-3}	**1-NHC^1** $\Delta\rho_3 = -0.21\psi^2_{-3} + 0.21\psi^2_{+3}$ iso = 0.0015 e·Bohr^{-3}	**1-NHC^2** $\Delta\rho_3 = -0.21\psi^2_{-3} + 0.21\psi^2_{+3}$ iso = 0.0015 e·Bohr^{-3}

Figure 2.3. Isosurface plots of deformation densities ($\Delta\rho_n$) of complementary NOCVs (ψ^2_{-n} and ψ^2_{+n})of $SiBr_2$($caac^{Me}$) (**1**)(left columm), $SiBr_2$(IDipp) (**1-NHC^1**)(middle column) and $SiBr_2$(SIDipp) (**1-NHC^2**) (right column).

2.2 CAAC-Supported Silicon(II) Bromides

2.2.1 Introduction

The synthesis of N-heterocyclic carbene stabilized functional halosilylenes SiX(R)(NHC) remains a challenging task, since they are extremely air sensitive and often decompose in solution at ambient temperature. There are four synthetic approaches in the synthesis of functionalized halosilylenes known: a) dehydrohalogenation of substituted chlorosilanes of the type $Si(R)HCl_2$ ($R = Ar^{Mes}$, Ar^{Trip}, $N(SiMe_3)(Dipp)$) using small N-heterocyclic carbenes (NHC^3: IMe_4, NHC^4: $IiPr_2Me_2$)[80,81], b) reduction of substituted trihalosilane $Si(R)Cl_3$ ($R = o\text{-}C_6H_4\text{-}NMe_2$) in presence of a carbene ($caac^{Me}$)[137], c) addition of small carbenes (NHC^3: IMe_4, NHC^4: $IiPr_2Me_2$) to dibromodisilenes (*E*)-[(Ar)(Br)Si=Si(Br)(Ar)] (Ar = Bbt, EMind, Tbb)[25] or d) nucleophile substitution of carbene stabilized silicon(II)-dihalides $SiCl_2(NHC^1)$ (NHC^1 = IDipp = $:C[N(Dipp)CH]_2$) with suitable nucleophiles.[82]

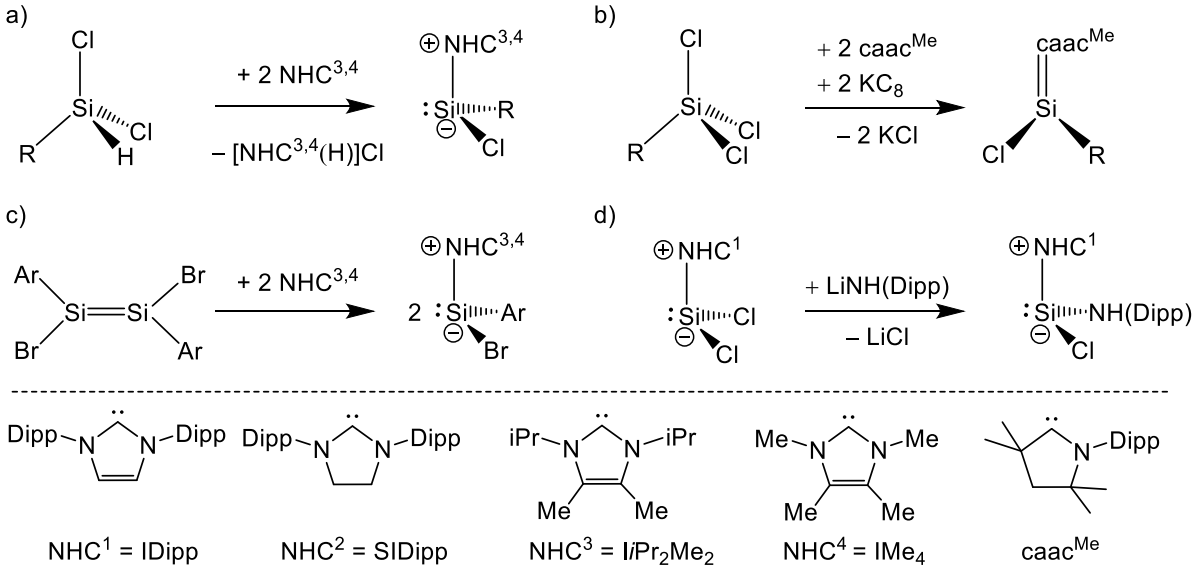

Figure 2.4. Literature known synthetic approaches to carbene stabilized functionalized halosilylenes SiX(R)(NHC).

Methods a) and b) provide a straight-forward approach starting from silicon(IV) precursors, but they have the disadvantage that they are limited to certain types of substituents ($R = Ar^{Mes}$, Ar^{Trip}, $N(SiMe_3)Dipp$). Similarly method c) is limited to the amount of substituents of literature known dihalodisilenes and can lead as well to bis NHC adducts of silyliumylidene cations $[Si(R)(NHC^{3,4})_2]Br$ (R = EMind with $NHC^3 = IMe_4$ or $NHC^4 = IiPr_2Me_2$; R = Tbb with $NHC^3 = IMe_4$), thus rendering the isolation of carbene-stabilized monohalosilylenes difficult.[25] In fact, the monobromosilylenes $SiBr(Bbt)(NHC^3)$ and $SiBr(EMind)(NHC^4)$ were only characterized by means of NMR spectroscopic methods.[25]

Method d) provides the most versatility of installing different nucleophiles at the low valent silicon center. However, the only literature known example of a straightforward nucleophilic substitution at a carbene stabilized silicon(II)-dihalide yielding a functionalized halosilylene is the reaction of $SiCl_2(NHC^1)$ (NHC^1 = IDipp) with Li[NH(Dipp)], affording the monochlorosilylene SiCl(NHDipp)(NHC^1).[82]

Other attempts of substitution reactions at silicon(II)-dihalides $SiX_2(NHC^{1,2})$ (X = Cl, Br, I) (NHC^1 = IDipp, NHC^2 = SIDipp) with KCp*,[50] Li[TBoN] (TBoN = N(SiMe$_3$){B(DAB)}; DAB = [N-(Dipp)CH]$_2$, Dipp = C_6H_3-2,6-*i*Pr),[180] LiN(Me)(Ar^{Mes})[181] and NaOAr^{Mes} ,[181] led to the formation of two coordinated acylic silylenes **II-1** . In comparison, reaction of the dilithiosilane (tBu$_2$MeSi)$_2$SiLi$_2$ with $SiCl_2(NHC^1)$ gives the trisilaallene **II-2**.[37] Reaction of the silylene $SiCl_2(NHC^1)$ with LiP(Mes*)(TMS) let to the formation of the substituted halosilylene SiCl{P(SiMe$_3$)(Mes*)(NHC^1) at temperatures below 243 K, which upon reaching ambient temperature upon elimination of TMSCl generated the carbene stabilized phosphasilenyliden **II-3**.[117] Interestingly, reaction of $SiBr_2(NHC^2)$ with TbbLi, did not afford the expected monobromosilylene SiBr(Tbb)(NHC^2). Instead, the formation of the silyl-silylene SiBr(SiBr$_2$Tbb)(NHC^2) was observed, which was used as starting material in the synthesis of the NHC stabilized disilavinylidene **II-4**.[118]

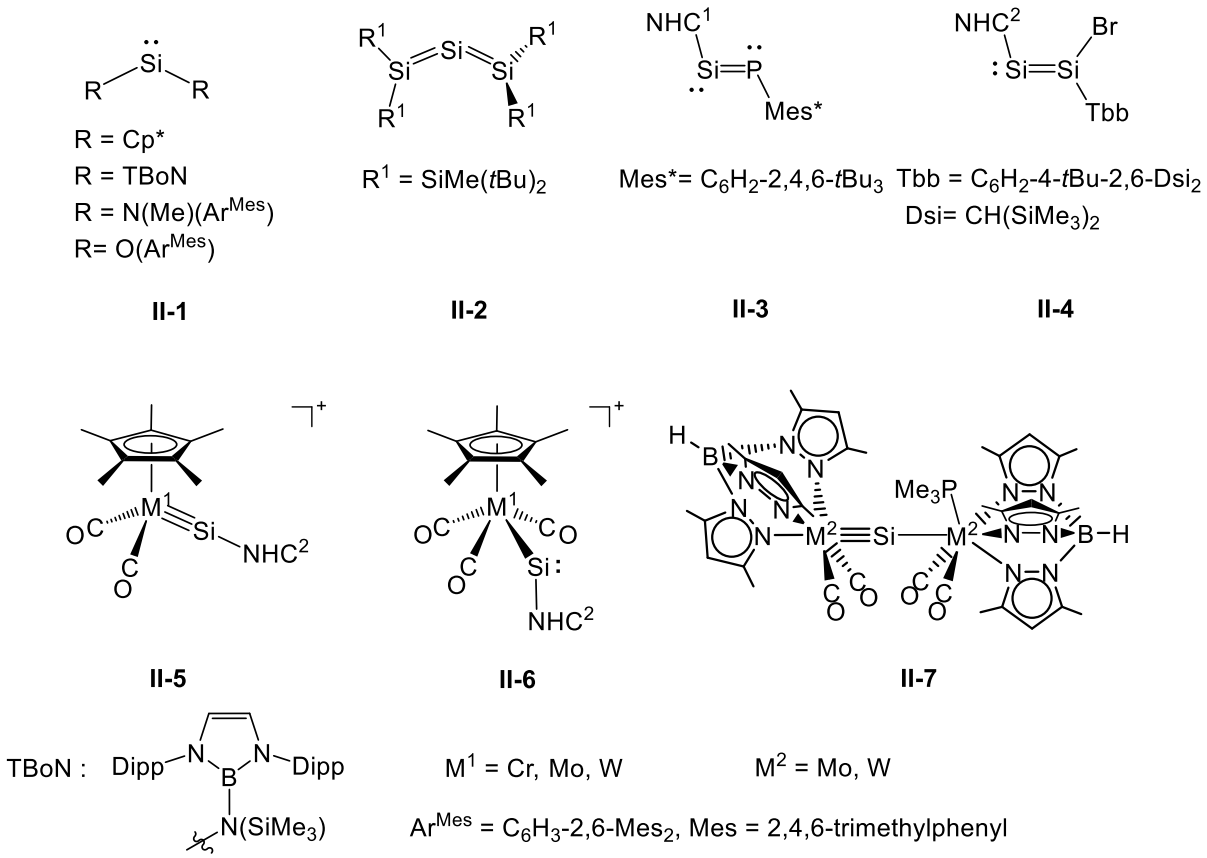

Figure 2.5. Novel two coordinate silicon compounds obtained from the silicon(II)-dihalides $SiX_2(NHC^{1,2})$; formal charges were not included for simplicity.

Reaction of $SiBr_2(NHC^2)$ with the metallates $Li[CpM(CO)_3]$ (M = Cr, Mo, W) led via elimination of CO to the silylidene complexes $(Cp)M(CO)_2$=SiBr(SIDipp) (M = Cr, Mo, W), which enabled the isolation of the silylidyne complexes **II-5**, and metallosilylenes **II-6**.[182] Similar like the nucleophiles mentioned in case of **II-1,** the metallates $Li[Tp'M(CO)_2(PMe_3)]$ (M = Mo, W) reacted with $SiBr_2(NHC^2)$ in 2:1 fashion and enabled access to the unprecedented metallasilylidynes **II-7**.[183]

In contrast, the chemistry of cyclic alkyl(amino)carbene stabilized silicon(II) dihalides $SiX_2(CAAC)$ (CAAC = $caac^{Me}$; X = Br, I) is still at its infancy.[121,135] In this work the high synthetic potential of the silicon(II) dibromide $SiBr_2(caac^{Me})$ (**1**) in substitution with a wide variety of different nucleophiles will be shown leading to silicon(II)bromides of the type $SiBr(Nu)(caac^{Me})$, which were not accessible before with corresponding NHC compounds, highlighting the major differences of CAACs versus NHCs in the stabilization of low valent silicon compounds.

Notably reaction of **1** with 1 equivalent of nucleophiles such as MeLi or $LiN(iPr)_2$, NaCp, NaCp* as well as larger nucleophiles such as EindLi or $Ar^{Mes}Li$ in THF solution at ambient temperature were not successful. Monitoring of the reaction mixture by ^1H NMR spectroscopy in (D_6)benzene revealed the selective formation of $Si_2Br_2(caac^{Me})_2$ (**9-Br**).

2.2.2 Synthesis and properties of SiBr(R)(caac^{Me})

Treatment of a red THF solution of $SiBr_2$(caac^{Me}) (**1**) with either a solution of $Li(THF)_3[Si(SiMe_3)_3]$ or LiMes in THF afforded an orange-brown suspension, which after work-up afforded SiBr($SiTMS_3$)(caac^{Me}) (**2-Si**) and SiBr(Mes)(caac^{Me}) (**2-Mes**) as a yellow/orange solids in 65 % and 55 % yield, respectively.
Treatment of a suspension of **1** in *n*-hexane with either $LiPMes_2$ or $NaN(TMS)_2$ afforded after sonication an orange-brown suspension, which after work-up afforded SiBr($PMes_2$)(caac^{Me}) (**2-P**) and SiBr($NTMS_2$)(caac^{Me}) (**2-N**), as bright orange and yellow powders in 55 % and 50 % yield, respectively. Treatment of a red solution of **1** in DME with a solution of NaOMes*, similarly afforded an orange-brown suspension, which after work up afforded SiBr(OMes*)(caac^{Me}) (**2-O**) as a bright orange powder with 18 % yield. All compounds are stable for months at ambient temperature under argon atmosphere and are thermally robust solids, decomposing unselectively upon melting in the temperature range of 179°C (**2-P**) – 199°C (**2-Mes**). The color of the compounds varies between yellow (**2-Mes**, **2-N**) and orange (**2-Si**, **2-P**, **2-O**). The compounds are moderately soluble in *n*-hexane and highly soluble in benzene and THF affording yellow-orange solutions.

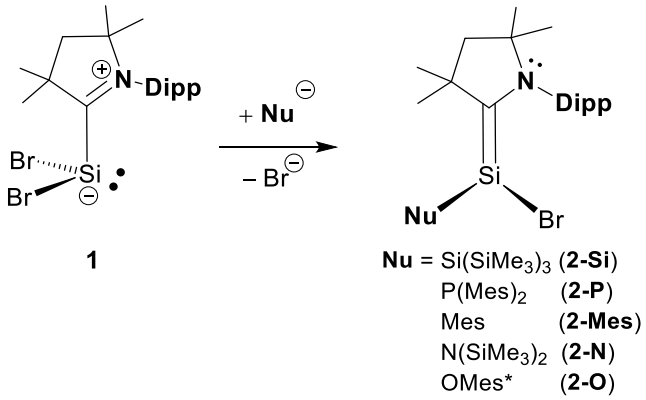

Scheme 2.4. Synthesis of pyramidal 2-(amino)silenes SiBr(Nu)(caac^{Me}) upon reaction of **1** with nucleophiles.

The molecular structures of the functionalized monobromo-silenes (**2-Si** – **2-O**) (*Figure* 2.6 and *Figure 2.7*) feature a stereogenic slightly trigonal pyramidalized silicon(II) center. The sum of angles at the Si-center ranges from 321.6°(**2-O**) to 336.5°(**2-Si**) and lies in between of that of **1** (Σ∢(Si) = 289.94°) and a classical trigonal planar silicon in planar silenes (Σ∢(Si)= 360.0°). In the same fashion, the Si–C^{carb} bond lengths ranging from 1.836(2) Å (**2-Si**) to 1.897(3) Å (**2-O**) are significantly shorter compared to that of **1** (2.017(2) Å) and lie in between that of a typical Si=C double bond (1.702 – 1.764 Å)[184] and a classical Si–C^{carb} single-bond (1.963(2) Å),[80] indicating a significant degree of π-character in the Si–C^{carb} bond in this class of compounds.

This trend is further supported by the N–C^{carb} bond lengths (1.353(2) Å (**2-Si**) – 1.342(4) Å (**2-O**)) which are elongated compared to that of **1** (1.301(3) Å). The Si–Br bond lengths (2.2921(4) Å (**2-Si**) – 2.3107(4) Å (**2-N**)) are notably shorter than that of **1** (2.3591(7) Å and 2.3542(7) Å) but still longer than that of $SiBr_2$ (2.245(3) Å).[185] All compounds feature Si–Nu single bonds **2-Si** (d(Si–Si) = 2.3655(6) Å), **2-Mes** (d(Si–C^{Ar}) = 1.907(1) Å), **2-P** (d(Si–P) = 2.237(3) [2.240(3)] Å), **2-N** (d(Si–N) = 1.758(1) Å) and **2-O** (d(Si–O) = 1.686(2) Å), which are comparable to those of related silanes.

The pyramidalization of the silicon centers, renders the molecules chiral, according to the Cahn-Ingold-Prelog priority rules the stereodescriptor *R* can be assigned in the molecular structures depicted in *Figure 2.6* and *Figure 2.7*. The other enantiomer is also found in the crystal-lattice, the compounds crystallizing in the achiral space groups P-1 (**3-Mes**, **3-P**, **3-N**) and $P2_1/n$ (**2-Si**, **2-O**), respectively. Interestingly, the N-Dipp moiety in all five cases is orientated towards the bromine substituent (τ(N-C^{carb}-Si-Br) = 39.6(1)°(**2-Si**) –54.4(1)°(**2-O**)), thus according to the priority roules in the *E*–*Z* system of alkenes, defined by IUPAC, the stereodescriptor ***Z*** can be used and they can be described as (Z)-2-(amino)silenes.

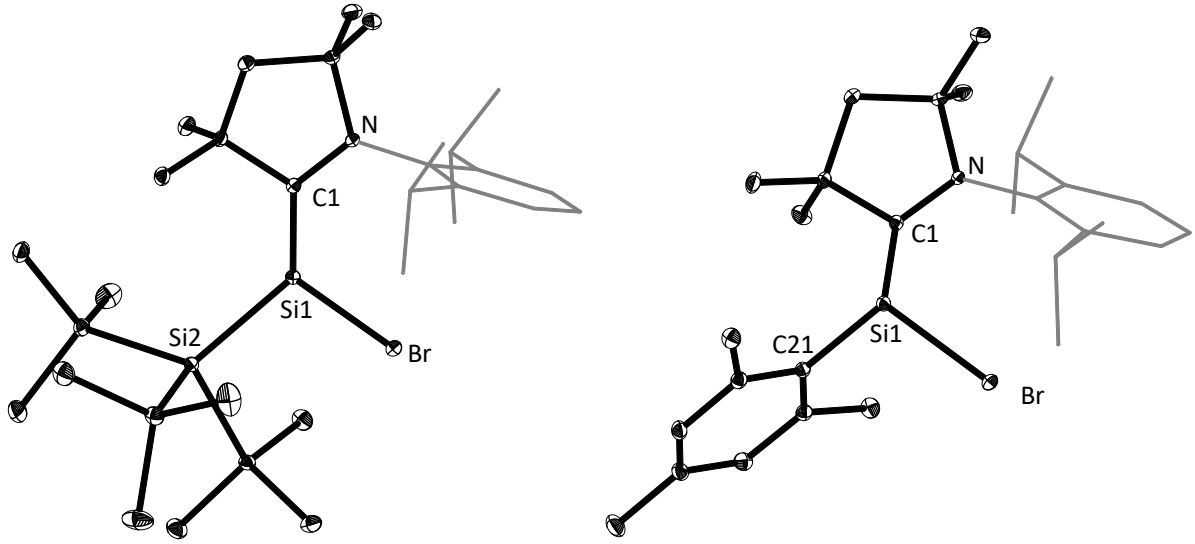

Figure 2.6. DIAMOND plot of the molecular structures of the pyramidal silenes **2-Si** (left) and **2-Mes** (right). Thermal ellipsoids are set at 30 % propability level and hydrogen atoms are omitted. In the depicted structures the Dipp-substituent of the $caac^{Me}$ ligand is presented in the wire-frame for the sake of clarity. Selected bond lengths [Å], bond angles [°] and torsion angles [°]:
2-Si: Si1–Si2 2.3655(6), Si1–C1 1.836(2), Si1–Br 2.2921(4), C1–N 1.353(2), Si2–Si3 2.3656(6),Br–Si1–Si2 102.69(2), C1–Si1–Br 109.69(5), C1–Si1–Si2 124.14(5), Br–Si1–C1–N 39.6(2).
2-Mes: Si–C1 1.842(1), Si–C21 1.907(1), N–C1 1.350(2), Si1–Br 2.2952(4), C1–Si–Br 111.94(4), C1–Si1–C21 110.45(5), C21–Si–Br 103.94(4), Br–Si–C1–N –40.6(2). In both cases the *R*-enantiomer is shown, the crystallographic unit contains both enantiomers.

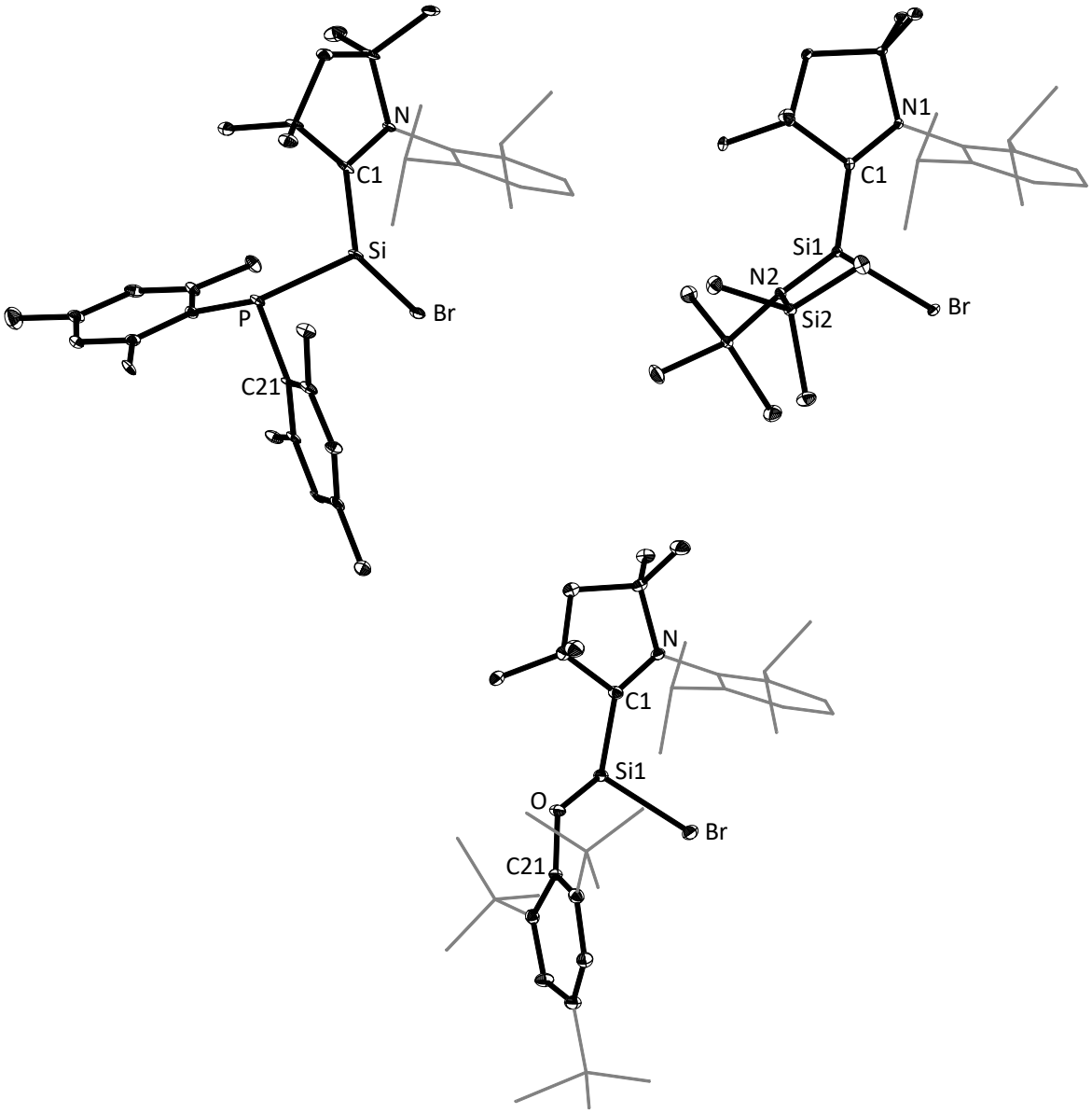

Figure 2.7. DIAMOND plot of the molecular structures of the pyramidal silenes **2-P** (left), **2-N** (right) and **2-O** (bottom). Thermal ellipsoids are set at 30 % propability level and hydrogen atoms are omitted. In the depicted structures the Dipp-substituent of the caac^{Me} ligand and the tBu-groups of the Mes* substituent in **2-O** are presented in the wire-frame for the sake of clarity. Selected bond lengths [Å], bond angles [°] and torsion angles [°]:

2-P: Si1–C1 1.850(8)[1.862(8)], Si1–P 2.237(3) [2.240(3)], Si1–Br 2.273(2) [2.286(2)], P–C21 1.847(8) [1.840(8)], C1–N 1.362(10) [1.337(10)], P–Si–Br 112.8(1) [113.1(1)], C1–Si–Br 113.73(3) [112.1(3)], C1–Si–P 109.9(3) [108.3(3)], Br–Si–C1–N -33.0(4) [-32.9(5)]. The unit cell features two independent molecules.

2-N: Si1–C1 1.866(2), Si1–N2 1.758(1), Si1–Br 2.3107(4), C1–N1 1.349(2), N2–Si2 1.763(1), N2–Si1–Br 104.69(4), N2–Si1–C1 113.66(6), C1–Si1–Br 110.45(5), Br–Si1–C1–N1 46.9(2).

2-O: Si1–C1 1.897(3), Si–O 1.686(2), Si–Br 2.276(1), O–C21 1.395(3), C1–N 1.342(4), O–Si–Br 102.9(1), O–Si–C1 107.4(1), C1–Si–Br 111.3(1), C21–O–Si 125.5(2), Br–Si1–C1–N 54.4(2). In all three cases the *R*-enantiomer is shown, the crystallographic unit contains both enantiomers.

In terms of their structural features as the low degree of pyramidalization, rather short Si–C^{carb} bond lengths and small twist angles, functionalized monobromo-silenes (**2-Si** – **2-O**) differ drastically from related NHC stabilized halosilylenes (*Table 2.6*) but compare well to the recently reported chlorosilene $SiCl(C_6H_4\text{-}6\text{-}NMe_2)(caac^{Me})$.[137] In case of silyl and aryl substituted silenes the degree of pyramidailization (DP: 26 % (**2-Si**) < 37 % (**2-Mes**)) increases with the electronegativity of the substituent (Si < C). In case of π-donating substituents the degree of pyramidalization (DP: 28 % (**2-P**) < 35 % (**2-N**) < 43 % (**2-O**)) increases with increasing electronegativity of the substituent (P < N < O). In the same fashion, the Si–C^{carb} bond lengths increase 1.850(8) Å (**2-P**) < 1.866(2) Å (**2-N**) < 1.897(3) Å (**2-O**). This trend is in line with a decrease of the N–C^{carb} bond lengths 1.36(1) Å(**2-P**) < 1.349(2) Å(**2-N**) < 1.342(4) Å (**2-O**), suggesting a significant increase of the silylene character with higher electronegativity of the introduced substituent at the silene moiety.

Table 2.6. Selected structural paramters of dihalosilylene **1** and pyramidal silenes **2-Si** – **2-O** in comparison to literature known compounds.

Comp.	Si–C^{carb} / Å	N–C^{carb} / Å	Σ∢(Si) / (deg)	DP[a] / %	τ[b] / (deg)	Ref.
$SiBr_2(caac^{Me})$ **1**	2.017(2)	1.301(3)	289.9	78	79.1	
$SiBr(SiTMS_3)(caac^{Me})$ **2-Si**	1.836(2)	1.353(2)	336.5	26	5.4	
$SiBr(Mes)(caac^{Me})$ **2-Mes**	1.842(1)	1.350(2)	326.3	37	8.6	*this*
$SiBr(PMes_2)(caac^{Me})$ **2-P**	1.856(4)[c]	1.349(2)[c]	334.9[c]	28[c]	9.2[c]	*work*
$SiBr(NTMS_2)(caac^{Me})$ **2-N**	1.866(2)	1.349(2)	328.8	35	0.6	
$SiBr(OMes^*)(caac^{Me})$ **2-O**	1.897(3)	1.342(4)	321.6	43	2.5	
$SiCl(C_6H_4\text{-}6\text{-}NMe_2)(caac^{Me})$	1.853(1)	1.345(2)	321.0	43	9.1	[137]
$SiMe(C_6H_4\text{-}6\text{-}NMe_2)(caac^{Me})$	1.809(1)	1.374(1)	335.4	27	4.5	[137]
$SiCl(Ar^{Trip})(IMe_4)$	1.937(2)	1.355(2) 1.386(3)	299.2	68	72.4	[80]
$SiCl\{N(Dipp)(TMS)\}(I^iPr_2Me_2)$	2.002(2)	1.369(2) 1.358(2)	305.2	61	78.9	[81]
SiCl{NH(Dipp)}(IDipp)	1.980(3)	1.358(2) 1.362(2)	290.5	77	118.5	[82]

[a]: The degree of pyramidalization (DP) value of 0 % describes a trigonal planar coordination of the silicon atom with the sum of bond angles equal to 360°. A DP value of 100 % corresponds to a trigonal pyramidal coordination of the silicon atom with the sum of bond angles equal to 270°.
DP (in %) = 100 % · [360 − Σ∢(Si) /(deg)]/90
[b]: The twist angle (τ) is defined as the angle between the silicon and Ccarbene coordination planes defined by the atoms X1-Si1-R (X = Br, Cl).
(R = Si2, CAr, P, N2; O)and C2-C1-N1 for CAAC (N1-C1-N2 for NHC), respectively.
[c]: mean values of two independent molecules are given.

Even though all caac^{Me}-stabilized silicon(II) bromides (**2-Nu**) featue a C_1-symmetry in the solid state, ^{1}H-NMR spectra reveal an averaged C_s-symmetry in (D_6)benzene at ambient temperature (**2-Si** and **2-Mes** see *Figure 2.8*; **2-N**, **2-P** and **2-O** see *chapter 4.4*), even in (D_8)toluene at –80 °C (see for example in *Figure* 5.8), indicating a dynamic behavior.

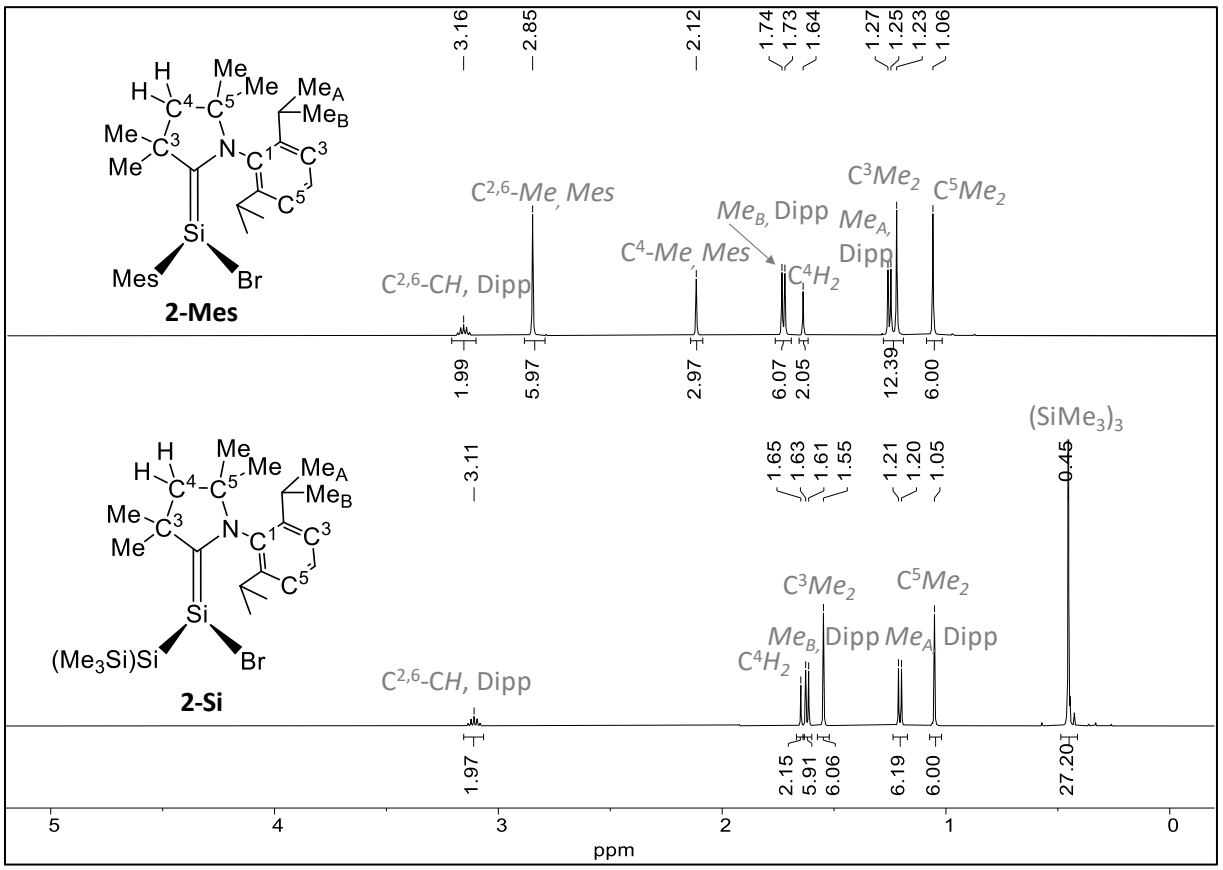

Figure 2.8. Aliphatic region of the ^{1}H NMR spectra (500.17 MHz) of pure samples of **2-Mes** (top) and **2-Si**) (bottom) in (D_6)benzene at ambient temperature, showing an averaged C_S-symmetry. All signals were assigned by correlation spectroscopy (see *section 4.4*.).

Quantum chemical calculations at the RI-B97D3/def2-TZVPP level of theory revealed a low barrier for the enantiomerization process that proceeds by a pyramidal inversion of the trigonal pyramidal silicon center via a trigonal planar transition state (15.3 kJ mol^{-1} (**2-P**), 24.7 kJ mol^{-1} (**2-Mes**), 26.8 kJ mol^{-1} (**2-N**))) suggesting a fast isomerization between the *S*- and *R*- enantionsmers in solution (*Figure 2.9*).

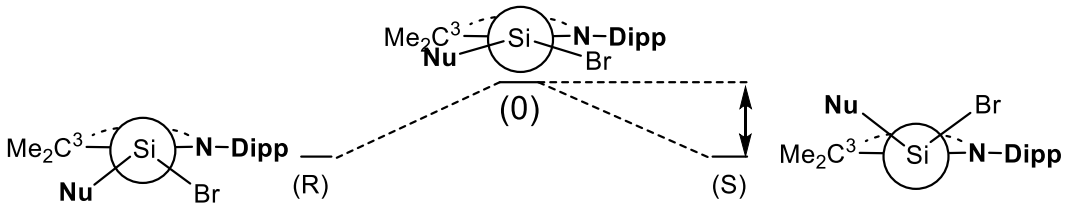

Figure 2.9. Enantiomerization of silicon(II) bromides SiBr(Nu)(caac^{Me}) (**2-Nu**) upon pyramidal inversion of the silicon center. Newman projection alongside the Si–C^{carb} bond in **2-Nu**.

The caac^{Me}-stabilized Si(II) bromides **2-Nu** do not show any trend regarding the $^{13}C^{CAAC}$ resonances (*Table 2.7*). One might expect an increasing upfield shift of the $^{13}C^{CAAC}$ resonance with increasing Si–C^{carb} double bond character and increasing planarization of the silicon center ($\Sigma\measuredangle$(Si) → 360°). However, this trend is not observed in all the examples of **2-Nu**, since the different substituents can have a significant effect on the electronic structure of the corresponding silicon(II) bromide (see *section 2.3.4*). The ^{29}Si NMR resonance of of the silenic silicon center in **2-Mes** (10.5 ppm) is upfield shifted compared to **2-Si** (24.69 ppm), in analogy to the reported upfield shift of the ^{29}Si resonance in disilenes ($R_2Si{=}SiR_2$) with aryl ($\delta(^{29}Si)$ = 63.3 –90.3 ppm) and silyl substituents ($\delta(^{29}Si)$ = 132.4 –156.6 ppm).[24,186] In case of the π-donating substituted silenes the ^{29}Si NMR resonance of the silenic silicon center increases with increasing electronegativity of the substituent (7.0 ppm (**2-P**) < 18.5 ppm (**2-N**) < 26.4 ppm (**2-O**)). The $^{15}N^{CAAC}$ resonances of the compounds lie in the range of 170.8 ppm (**2-P**) – 151.8 ppm (**2-N**) and are drastically upfield shifted compared to **1** (231.3ppm) indicating less π-character in the N–C^{carb} bond.

Table 2.7. Selected multi-nuclear NMR chemical shift values of pyramidal silenes **2-Si** – **2-O**, and their comparison with literature known caac^{Me} and NHC stabilized monohalosilylenes. NMR spectroscopic data is given in (D_6)benzene, if not mentioned otherwise in the legend.

Comp	$\delta(^{13}C^{carb})$ / ppm	$\delta(^{29}Si^{II})$[a] / ppm	$\delta(^{15}N^{CAAC})$[b] / ppm	Ref.
$SiBr_2$(caac^{Me}) **1**	231.2[c] ($\Delta\nu_{1/2}$ = 23 Hz)	14.35[c] ($\Delta\nu_{1/2}$ = 17 Hz)	231.3[c]	
SiBr($SiTMS_3$)(caac^{Me}) **2-Si**	204.9	24.69	162.95	
SiBr(Mes)(caac^{Me}) **2-Mes**	194.7	10.5	158.8	*this work*
SiBr($PMes_2$)(caac^{Me}) **2-P**	204.3 (d,22Hz)	7.0 (d, 185 Hz)	170.8	
SiBr($NTMS_2$)(caac^{Me}) **2-N**	190.3	18.5	151.8	
SiBr{OMes*}(caac^{Me}) **2-O**	200.0	26.4	164.9	
SiCl(C_6H_4-6-NMe_2)(caac^{Me})	198.9[c]	27.3[c]	–	[137]
SiMe(C_6H_4-6-NMe_2)(caac^{Me})	176.4	21.1	–	[137]
SiCl(Ar^{Trip})(IMe_4)	166.7	0.7	–	[80]
SiCl{N(Dipp)(TMS)}(IPr_2Me_2)	164.1	3.1	–	[81]
SiCl{NH(Dipp)}(IDipp)	171.7	–6.0	–	[82]

[a]: ^{29}Si resonance of the three coordinated silicon(II)-center. [b]: ^{15}N NMR resonance of the single nitrogen atom in the CAAC carbene-ring referenced against NH_3(l). [c]: measured in (D_8)THF at 243 K.

The amount of σ-donation and π-backdonation of the Si–C^{CAAC} bond can be estimated, uppon comparing the ^{15}N NMR resonances to certain threshholds, which was shown by experiment and theory.[108]

Compound **1**, for instance, has a ^{15}N NMR shift of 231.3 ppm and lies above the threshhold of 220.5 ppm, which is indicative for a pure caac^{Me} → Si σ-donation.
In comparison, the $^{15}N^{CAAC}$ resonances of the caac^{Me}-supported silicon(II) bromides lie in the range of 170.8 ppm (**2-P**) – 151.8 ppm (**2-N**) and thus lie in-between the treshholds of strong caac^{Me} → Si σ-donation (210 – 180 ppm) and strong Si → caac^{Me} π-backdonation (160 – 90 ppm), suggesting equal amounts of σ-donation and π-backdonation in the Si–C^{CAAC} bond in **2-Nu**.[3]

It appears that the caac^{Me}-stabilized silicon(II) bromides show to be the borderline case between a trigonal pyramidal, NHC-stabilized silylene and a trigonal planar, Brook type silene (*Figure 2.10*). This phenomenon is already extensively studied by theory in the case of silenes of the type $Z_2Si=(X)C(Y)$ (Z = H, Me, $SiMe_3$) with strongly-electrondonating X and Y groups (X, Y = NH_2, O), which are completely described by zwitterionic (reverse-polarized) resonance structures. Such zwitterionic silenes are singly (Si–C) rather than doubly bonded (Si=C), and have a distinctly pyramidalized slicion atom due to negative charge acumulation at the silicon center. Substituents at the silicon center (Z = H, Me, $SiMe_3$) appeared to have only minor influences on the structural parameters.[187,188]
The silicon(II) bromides are best described with two resonance formulas, which are contributing equally: an ylidic (reverse-polarized) form and a silene form (*Figure 2.10*).
In order to describe this phenomenon, this class of compounds is termed as "pyramidal 2-(amino)silenes" or "zwitterionic 2-(amino)silenes". The structural and electronic similarities between **2-Mes** (Σ∢(Si) = 326.3°, d(Si–C^{carb}) = 1.836(2) Å) and the recently reported CAAC-supported Si(II)-halide SiCl(C_6H_4-2-NMe_2)(caac^{Me}) (Σ∢(Si) = 320.9°, d(Si–C^{carb}) = 1.853 (1) Å)[137], prompted us to classify this compound as well as a "pyramidal 2-aminosilene" rather than a CAAC-stabilized silylene.

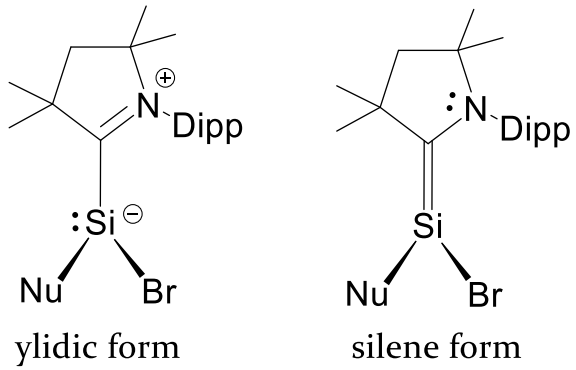

Figure 2.10. Resonance structures of caac^{Me}-stabilized Si(II)-bromides.

3 In the publication given in reference [108] the $^{15}N\{^1H\}$ resonances are referenced against CH_3NO_2. $\delta(^{15}N(CH_3NO_2)_{ref} = \delta(^{15}N(NH_3(l))_{ref} - 380.5$ ppm.

2.2.3 Electronic structure of SiBr(R)(caac^{Me})

The nature of the electronic structure of the silicon(II) bromides **2-Nu** was investigated by quantum chemical calculations, which were performed at the B97-D3(BJ)-ATM/def2-TZVP level of theory by Jens Rump. More details on the computional calculations are given in *chapter 5.11*. The structural parameters of the calculated structures in the gas phase do compare well to the structures derived from single-crystal X-ray diffraction (*Table 5.76* and *Table 5.77*).

Natural Bond Orbital (NBO) analysis of the wave function of **2-Si**$_{calc}$, **2-Mes**$_{calc}$, **2-P**$_{calc}$ and **2-N**$_{calc}$ led to a leading natural Lewis structure (NLS) with localized bond pair NBOs for the Si–C^{carb}, Si–Br and Si–Nu σ-bonds as well as one π(Si–C^{carb}) bond featuring a high Lewis occupancy above 1.84 e^- (*Table 2.8*). The Si–C^{carb} σ-bonds are strongly polarized toward the carbene carbon atoms (66 – 74 %), whereas the C^{carb}–N σ-bond is strongly polarized towards the nitrogen atom (64 %). The π(Si–C^{carb}) bond is equally polarized between the silicon and carbon centers (C^{carb} = 42 – 50 %), similar to that of alkenes and silenes. Considerable delocalization is evidenced by the low Lewis occupancy of the electron pair at the nitrogen center (1.60 e^-) of pure p-character. In addition, the NRT bond orders of the Si–C^{carb} (1.26 – 1.42) and C^{carb}–N bonds (1.37 – 1.44) further supports considerable amounts of double bond characters of these two bonds.

The NRT analysis reveals a silene type structure with the highest contribution in silicon(II)-bromides **2-Nu** with a Si=C^{carb} double bond (*Figure 2.11*). Remarkably, the zwitterionic structure appeared to be drastically less populated and instead CAAC carbene dissoziated resonance structures are observed, which feature a two-coordinated bromosilylene SiBr(R). Contributions of an allenic structure were observed in case of π-donating substituents in **2-P** and **2-N**.

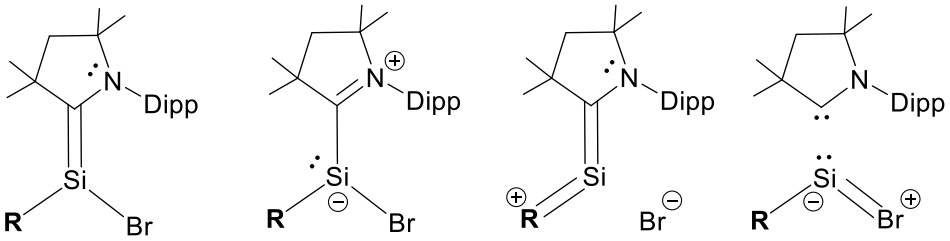

R = $SiTMS_3$	53.8 %	7.3 %	0 %	17.5%
R = Mes	52.5 %	0 %	0 %	20.4 %
R = $PMes_2$	35.0 %	11.7 %	16.2 %	7.5%
R = $NTMS_2$	46.4 %	0 %	6.1 %	20.5 %

Figure 2.11. NRT resonance structures and their respective percentage values for **2-Si**, **2-Mes**, **2-P** and **2-N**. All contributions above 1.0 % are considered and contributions with dissociated substituent R (< 2 %) were neglected.

Table 2.8. Selected results of the natural bond orbital (NBO), natural resonance theory (NRT) and natural population (NPA) analyses of silicon(II)-bromides **2-Si**, **2-Mes**, **2-P**, **2-N** at the B97-D3(BJ)^{ATM}/def2-TZVP level of theory calculated by Jens Rump. The graphical inlets depict the Natural Lewis structure of the NBO analysis and its NRT contribution.

NBO A–B	occ.[a]	NHO (A,B)[b] hyb. (pol. in %)	WBI[c] A–B	NRT-BO[d] tot/cov/ion	Natural Lewis structure (NLS)
		2-Si			
LP(N)	1.60	p			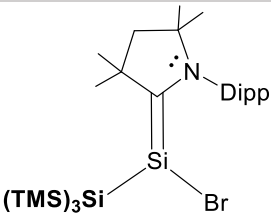
σ(Si1–C^{carb})	1.90	sp$^{1.3}$ (31), sp$^{2.2}$ (69)	1.20	1.36/1.05/0.31	
π(Si1–C^{carb})	1.86	p (50), sp$^{9.6}$ (50)			
σ(Si1–Br)	1.97	sp$^{5.5}$ (25), sp$^{4.3}$ (75)	0.81	1.19/0.51/0.68	
σ(C^{carb}–N)	1.98	sp$^{2.3}$ (36), sp$^{1.7}$ (64)	1.24	1.37/0.91/0.46	53.8 %
		2-Mes			
LP(N)	1.60	p			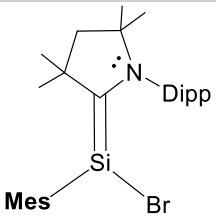
σ(Si–C^{carb})	1.88	sp$^{1.2}$ (34), sp$^{2.7}$ (66)	1.16	1.35/1.02/0.33	
π(Si–C^{carb})	1.85	P (46), sp$^{6.2}$ (53)			
σ(Si–Br)	1.96	sp$^{4.6}$ (25), sp$^{4.3}$ (75)	0.82	1.30/0.48/0.82	
σ(C^{carb}–N)	1.98	sp$^{2.4}$ (36), sp$^{1.6}$ (64)	1.25	1.44/0.94/0.50	52.5 %
		2-P			
LP(N)	1.59	p			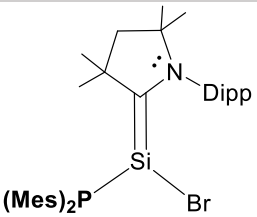
σ(Si–C^{carb})	1.91	sp$^{1.9}$ (26), sp$^{1.8}$ (74)	1.12	1.42/0.93/0.49	
π(Si–C^{carb})	1.84	sp$^{7.5}$ (58), p (42)			
σ(Si–Br)	1.96	sp$^{4.4}$ (26), sp$^{4.3}$ (74)	0.80	0.95/0.45/0.51	
σ(C^{carb}–N)	1.98	sp$^{2.4}$ (36), sp$^{1.6}$ (64)	1.27	1.43/0.93/0.51	35 %
		2-N			
LP(N1)	1.59	p			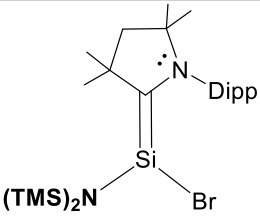
σ(Si–C^{carb})	1.89	sp$^{0.9}$ (30), sp$^{2.2}$ (70)	1.13	1.26/0.96/0.30	
π(Si–C^{carb})	1.86	sp$^{7.9}$ (51), sp$^{9.2}$ (49)			
σ(Si–Br)	1.96	sp$^{3.1}$ (25), sp$^{4.2}$ (75)	0.80	1.12/0.42/0.70	
σ(C^{carb}–N1)	1.98	sp$^{2.4}$ (36), sp$^{1.6}$ (64)	1.26	1.43/0.94/0.49	46.4 %

[a]: occ.= occupancy in e^-. [b]: NHO = Natural Hybrid Orbital, pol. (polarization) = $(C_i)^2 \cdot 100\%$, where C_i = coefficient of NHO. [c]: Wiberg bond index. [d]: total, covalent and ionic NRT bond order.

2-Si

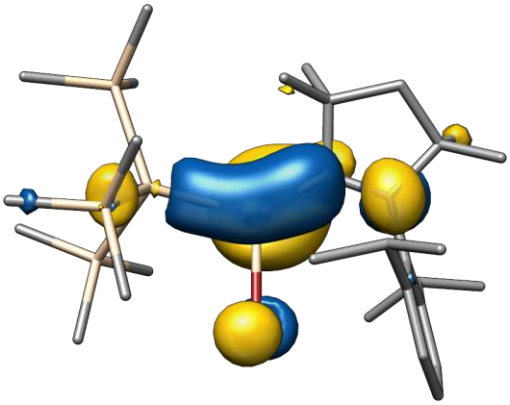

HOMO [–3.93]

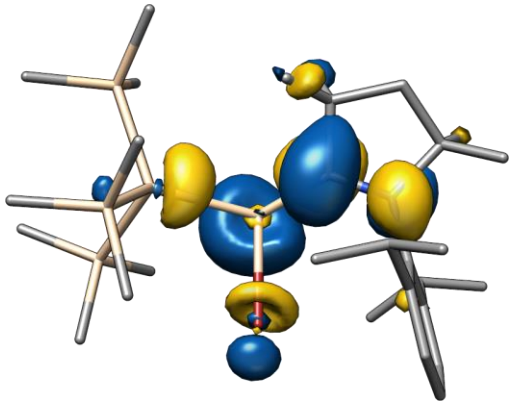

LUMO [–1.99]

2-Mes

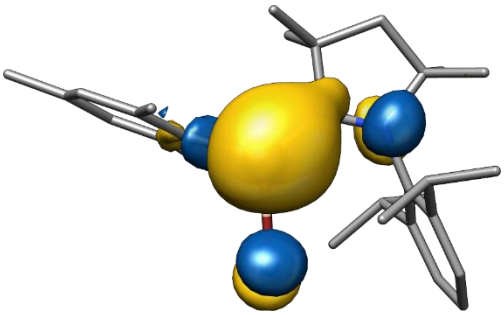

HOMO [–3.92]

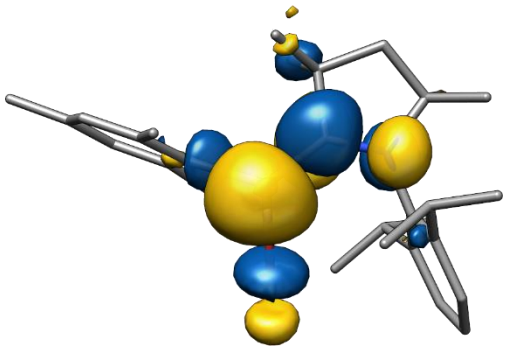

LUMO [–1.88]

2-P

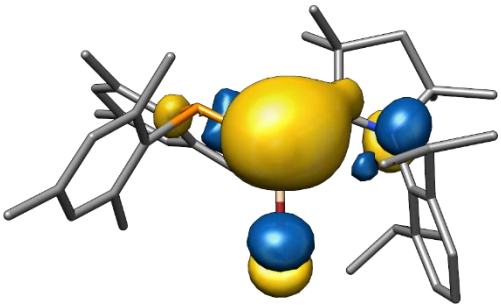

HOMO [–4.05]

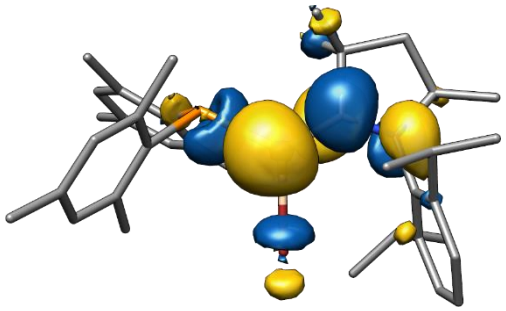

LUMO [–2.16]

2-N

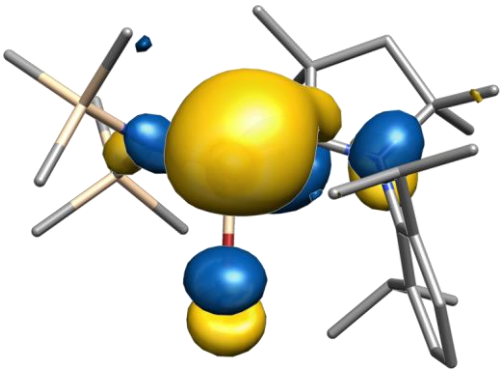

HOMO [–3.92]

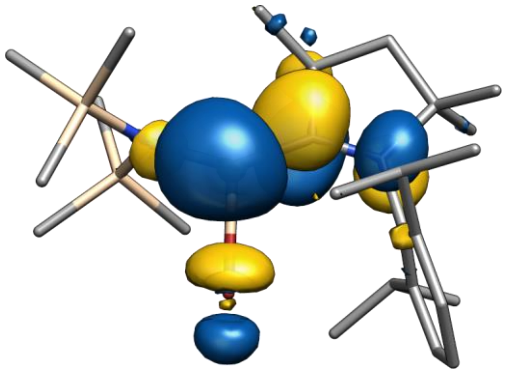

LUMO [–2.02]

Figure 2.12. Selected Kohn-Sham molecular orbitals of **2-Si**, **2-Mes**, **2-P** and **2-N** with their energy eigenvalues in eV.

The NBO results are reflected in the frontier orbitals of **2-Si**$_{calc}$, **2-Mes**$_{calc}$, **2-P**$_{calc}$ and **2-N**$_{calc}$ (*Figure 2.12*). The HOMO mainly contains the Si–C^{carb} π-bond and the LUMO corresponds to the antibonding π-combination of the Si–C^{carb}–N moiety. The HOMO–LUMO gap in **2-Si** (1.94 eV), **2-P** (1.89 eV) and **2-N** (1.90 eV) is significantly increased with respect to SiBr$_2$(caac^{Me}) (**1**) (1.76 eV) and might be responsible for their orange color in the solid state and solution, where as **2-Mes** (2.04 eV) appears as a yellow solid.

In summary, silicon(II)-bromides **2-Nu** can be best described as pyramidal or zwitterionic 2-(amino)silenes, which feature the borderline case between a trigonal pyramidal, NHC-stabilized silylene and a trigonal planar, Brook type silene (*Figure* 2.13). Their molecular structures feature C_1-symmetry, where the stereodescriptors (R and S) can be clearly assigned at the chiral silicon(II) center. Their low inversion barriers ($\Delta G^{\ddagger}_{calc}$ = 15 – 27 kJ mol^{-1}) enable a fast *R*-/*S*-enantionemerization in solution, which leads to NMR spectra with averaged C_S-symmetry. Given their silenic nature (partial Si=C^{carb} double bond character), no rotation of the Si–C^{carb} bond is observed in solution nor in the solid state, which consistently leads to E/Z-stereoisomers. Interestingly though, compounds **2-Si**, **2-Mes**, **2-P**, **2-N** and **2-O** could be only isolated as (***Z***)-isomers (with the N-Dipp moiety of the carbene orientated towards the bromine substituent), thus they can be termed as pyramidal (***Z***)-2-(amino)silenes.

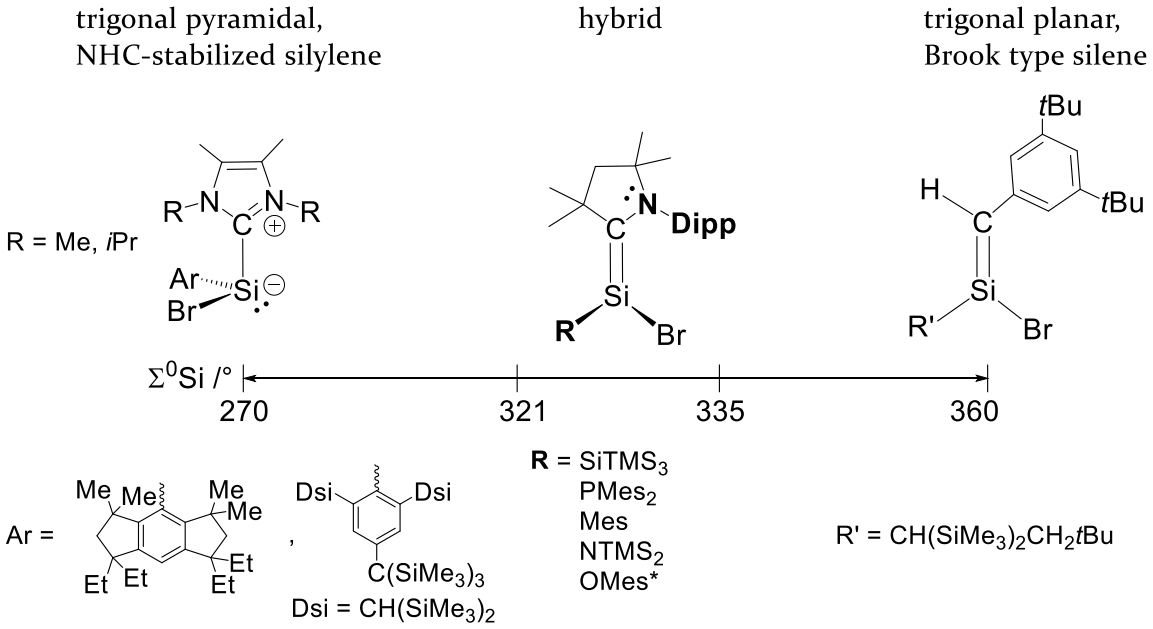

Figure 2.13. Compounds **2-Nu** as borderline case of a NHC-stabilized bromosilylene, such as SiBr(Ar)(NHC^{3,4}) (Ar = EMind, Tbb) (NHC^3 = I*i*Pr$_2$Me$_2$; NHC^4 = IMe$_4$),[25] and the recently reported trigonal planar coordinated bromosilene (R')SiBr=C(H)(R), reported by Iwamoto et al.[189]

2.2.4 Isolation and thermal E→ Z isomerization of SiBr(Eind)(caac^{Me})

The *Z* → *E* (or cis – trans) isomerization of alkenes has been extensively studied and is widely used in organic syntheses and is also involved in biological reactions.[190] The isomerization of alkenes usually proceeds via rotation of the C=C double bond via a diradical intermediate.[190] The rotation of the C=C double bond in ethylene has a high activation barrier of 272 kJ mol^{-1} and thus can be only induced photochemically. Stabilization of the diradical intermediate with aryl or silyl substituents leads to significant lower rotational barriers of 188 kJ mol^{-1} in stilbene or 126 kJ mol^{-1} in $R_1(R_2)C=C(R_1)R_2$ (R_1 = $SiMe_3$, R_2 = $SiMe_2Ph$), allowing a thermal induced isomerization at ambient temperature.[191,192]

The isomerization of the heavier ditetrelenes has been barely studied so far. Experimental studies of the isomerization barriers of aryl substituted disilenes of the type Mes(R)Si=Si(R)Mes (R = tBu, $N(TMS)_2$, 1-adamantyl, C_6H_3-2,6-Et_2) vary from 106 to 131 kJ mol^{-1},[193,194] in case of tetrasilyl substituted disilenes they are only 63 kJ mol^{-1}.[195]

The are at least three distinct pathways known for the *E*,*Z*-isomerization of heavier alkenes as shown in *Figure 2.14*: rotation around the Si–E (E = C, Si) bond (path 1), dissociation-recombination (path 2) and silene-alkylsilylene for E=C or disilene-silylsilylene for E= Si interconversion (path 3).[24]

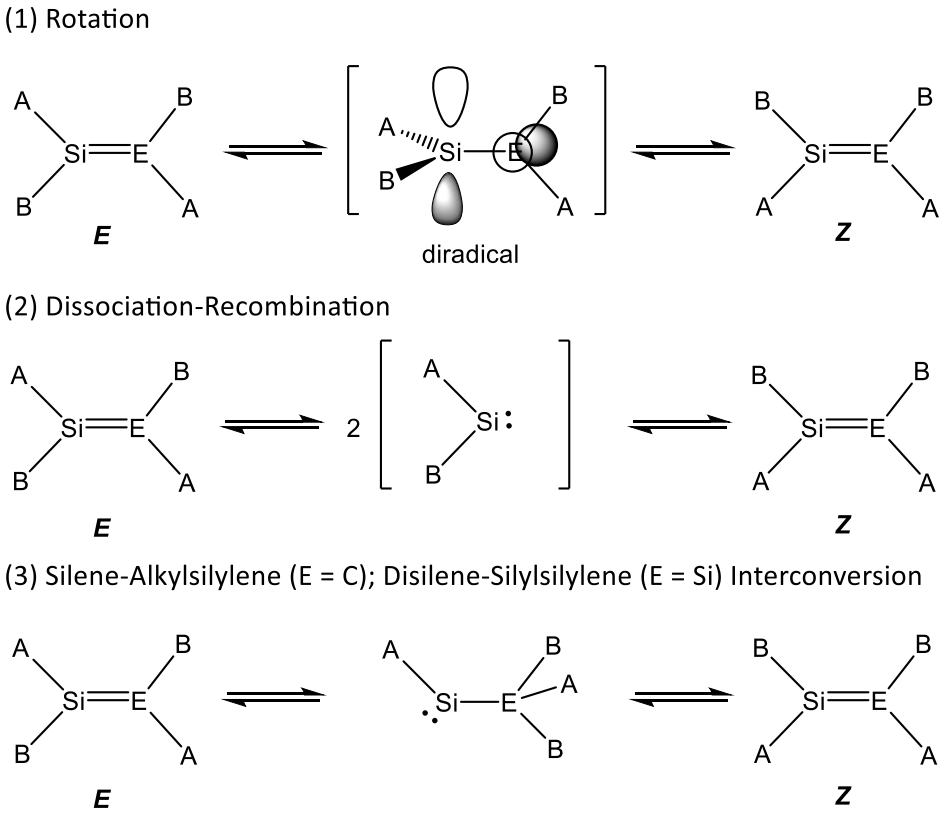

Figure 2.14. Three possible pathways of E,Z-isomerization of disilenes (E = Si) and silenes (E = C).

The *E*-,*Z*-isomerization of a stable silyl substituted silene ((tBu$_2$MeSi)(tBuMe$_2$Si)Si=CH(1-Ad)) was investigated very recently by the Y. Apeloig et al.[196] In their case the isomerization proceeded via an unusual silyl migration (path 3) leading to a silylene intermediate where the rotation of the Si–C bond occurred easily and the *E*-isomer was formed selectively upon backmigration of the silyl group to the silicon center (*Figure 2.14*).

Herein the synthesis of an unsymmetrically substituted 2-aminosilene SiBr(Eind)(caac^{Me}) (**2-Eind**) is reported. Detailed kinetic studies show that 2-aminosilene **2-Eind-*E*** undergoes an irreversible *E* to *Z* isomerization at 90 – 110 °C with an activation barrier of 115.1 (± 1.7) kJ mol^{-1}, $\Delta H^{\ddagger}$ = 112.6 (± 1.7) kJ mol^{-1}, $\Delta S^{\ddagger}$ = –8.3 (± 0.2) J K^{-1} mol^{-1}. The process highly likely occurs via the rotation of the Si–C^{carb} bond. Both compounds **2-Eind-*E*** and ***2-Eind-Z*** were fully characterized and differ substantially in their electronic structure.

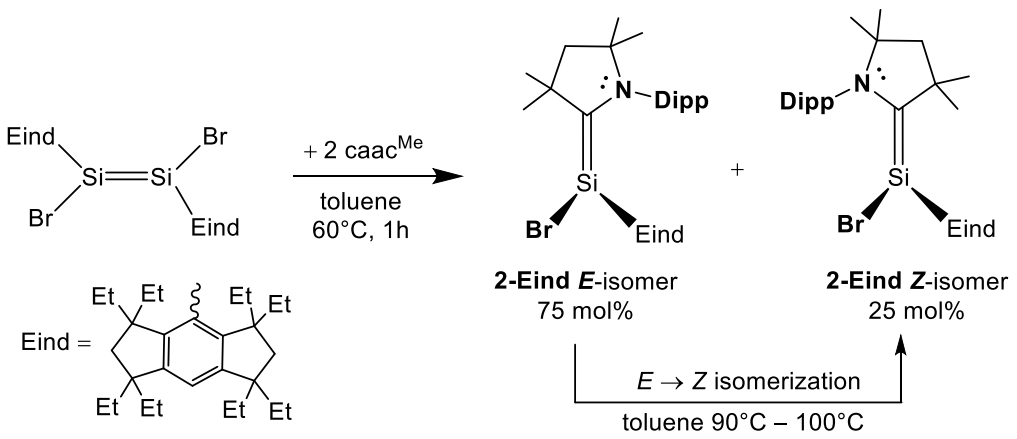

Scheme 2.5. Reaction of Eind-Disilene (E)-[Eind(Br)Si=Si(Br)Eind] with two equivalents of caac^{Me} carbene in toluene at 60 °C.

2.2.4.1 Synthesis and properties of 2-Eind-*E* and 2-Eind-*Z*

2-Aminosilene **2-Eind-*E*** was synthesized upon reaction of (*E*)-[Eind(Br)Si=Si(Br)Eind] with 2 eqivalents of caac^{Me} carbene in toluene solution at 60 °C for 1 h. Monitoring the reaction progress by ^{1}H NMR spectroscopy in (D_6)benzene revealed the complete consumption of the starting materials and the selective formation of **2-Eind-*E***, alongside with 22 mol% of **2-Eind-*Z***. Fractional crystallization from *n*-pentane at –60 °C (**2-Eind-*Z*** appears to be less soluble in aliphatic solvents) afforded **2-Eind-*E*** as an orange, air sensitive, powder in 27 % yield. The compound is stable for months at ambient temperature under argon atmosphere in the solid state. Heating of the compound in a vacuum-sealed capillary-tube to 153 °C, results in a color change from orange to yellow and the complete conversion from the *E*-isomer to the *Z*-isomer. **2-Eind-*E*** is very well soluble in aliphatic and aromatic solvents, affording orange-yellow solutions.

The compound is thermolabile and slowly deteriorates in solution to the yellow ***Z***-isomer. At ambient temperature the conversion is extremely slow, it takes more than two weeks to form at least 10 mol% of the ***Z***-isomer of a pure sample of **2-Eind-*E*** in (D_6)benzene. Heating a pure sample of **2-Eind-*E*** in toluene at 100 °C for 20 h was accompanied by a color change from orange to yellow. Monitoring of the reaction progress by ^{1}H NMR spectroscopy in (D_6)benzene revealed the selective formation of the *Z*-isomer **2-Eind-*Z***. After work up the compound could be obtained as a yellow, highly air sensitive, powder in 38 % yield. **2-Eind-*Z*** decomposes unselectively upon melting at 185 °C in a sealed vacuum capillary. The compound is moderately soluble in aliphatic solvents and well soluble in aromatic solvents affording clear yellow solutions.

Orange single crystals of **2-Eind-*E*** and clear yellow blocks of **2-Eind-*Z*** were obtained from *n*-hexane and Et_2O solutions at –30 °C, respectively. The molecular structure of **2-Eind-*E*** (*Figure 2.15* (left)) and **2-Eind-*Z*** (*Figure 2.15* (right)) feature a three-coordinated silicon center, with a trigonal planar structure in **2-Eind-*E*** ($\Sigma\measuredangle$(Si) = 356.9°) and a slightly pyramidalized structure in **2-Eind-*Z*** ($\Sigma\measuredangle$(Si) = 346.1°).

The N-Dipp moiety of the caac^{Me} ligand in **2-Eind-*E*** is orientated trans with respect to the bromine substituent (*Figure 2.15* (left)), thus according to the priority rules of *Z*/*E* alkenes, defined by IUPAC, the stereodescriptor ***E*** can be assigned.

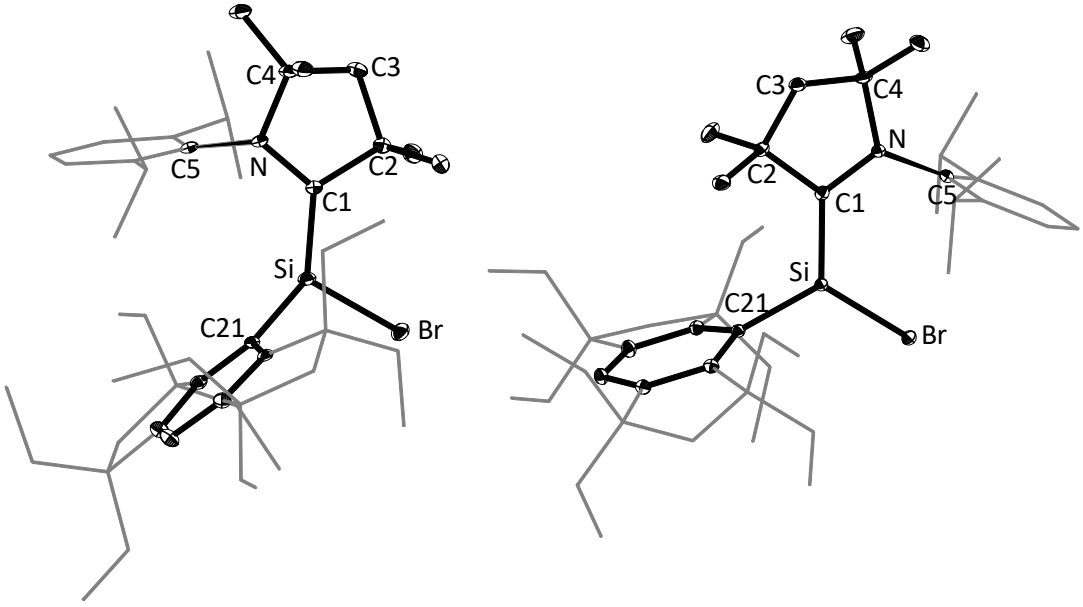

Figure 2.15. Diamond plot of the molecular structure of **2-Eind-*E*** (left) and **2-Eind-*Z*** (right), thermal ellipsoids are set at 30 % probability, and hydrogen atoms were omitted. In the depicted structures the Dipp-substituent of the caac^{Me} ligand and the aliphatic framework of the Eind-substituent are presented in the wire-frame for the sake of clarity. Selected bond lengths [Å], bond angles [°] and torsion angles [°]:
2-Eind-*E*: Si–C1 1.768(3), Si–Br 2.250(1), Si–C21 1.904(3), N–C1 1.421(4), C1–Si–Br 113.5(1), C1–Si–C21 132.5(1), C21–Si–Br 110.9(1), C1–N–C4 110.3(2), C1–N–C5 124.3(2), C5–N–C4 120.8(2), Br–Si–C1–N 17.0(2), C21–Si–C1–N –30.2(4), Br–Si–C1–C2 –11.4(3).
2-Eind-*Z*: Si–C1 1.796(2), Si–Br 2.2472(6), Si–C21 1.892(2), N–C1 1.385(3), C1–Si–Br 116.1(1), C1–Si–C21 118.8(1), C21–Si–Br 111.8(1), C1–N–C4 113.8(2), C1–N–C5 123.0(2), C5–N–C4 122.6(2) Br–Sil–C1–N –27.6(2), C21–Si–C1–N –165.4(2), Br–Si–C1–C2 173.8(2).

Conversely, the N-Dipp moiety of the caac^{Me} ligand in **2-Eind-*Z*** (*Figure 2.15* (right)) is orientated, towards the bromine atom thus the stereodescriptor ***Z*** can be assigned.
In analogy, the Eind substituent in **2-Eind-*E*/*Z*** is orientated cis ($\tau(C^{Ar}\text{-Si-}C^{carb}\text{-N}) = -30.2(4)°$) and trans ($\tau(C^{Ar}\text{-Si-}C^{carb}\text{-N}) = -165.4(2)°$) with respect to the N-Dipp moiety in **2-Eind-*E*** and **2-Eind-*Z***, respectively, and orthogonally with respect to the planar core in both the molecules. The single nitrogen atom in the caac^{Me} ligand in **2-Eind-*E*** ($\sum°N = 355.4°$) is slightly more pyramidalized than in **2-Eind-*Z*** ($\Sigma\measuredangle(N^{CAAC}) = 359.3°$).
The Si–C^{Ar} bond lengths in **2-Eind-*E*** (1.904(3) Å) and **2-Eind-*Z*** (1.892(2) Å) compare well to that of the starting material *E*-[Eind(Br)Si=Si(Br)Eind] (1.888(2) Å)[23] and lie in the typical range of Si–C^{Ar} single bonds (1.879 – 1.894 Å).[34,197]
Major differences in the structures can be seen by a noticeable twist of the N-C^{carb}-C2 and C^{Ar}-Si-Br planes in **2-Eind-*E*** ($\tau = 18.0°$) in comparison to **2-Eind-*Z*** ($\tau = 5.2°$), which can be attributed to the high steric repulsion of the Eind-substituent to the Dipp-substituent in **2-Eind-*E***. The Si–C^{carb} bond length in **2-Eind-*E*** (1.768(3) Å) is significantly shorter when compared to pyramidal bromo-silenes **2-Nu** (1.836(2) – 1.897(3) Å) and compares well to that of typical Si=C double bonds (1.702 – 1.764 Å) reported in trigonal planar silenes.[184] This observation stays in line with the N–C^{carb} bond length of 1.421(4) Å (**2-Eind-*E***), which is dramatically elongated compared to that of **2-Nu** (1.342(4) – 1.353(2) Å) and $SiBr_2$(caac^{Me}) (**1**) (1.301(3) Å). The strong Si=C^{carb} bond character and the noticeable twist angle ($\tau = 18.0°$) of the C^{Ar}–Si–Br moiety with respect to the N–C^{carb}-C2 moiety in **2-Eind-*E*** leads to an overall chiral structure. Applying the priority rules for axial chirality, according to IUPAC, the stereo-descriptor R_a with the chirality axis passing through the Si–C^{carb} bond can be assigned in the molecular structure of **2-Eind-*E*** depicted in *Figure 2.15* (left).
The Si–C^{carb} bond length in **2-Eind-*Z*** (1.796(2) Å) is slightly elongated compared to the ***E***-isomer (1.768(3) Å) and similar like the pyramidal silenes **2-Nu** it lies in between to that of a classical Si=C double bond (1.702 – 1.764 Å)[184] and a typical Si–C^{carb} single-bond (1.963(2) Å),[80] indicating considerable π-character in the Si–C^{carb} bond in **2-Eind-*Z***. The N–C^{carb} bond length in **2-Eind-*Z*** (1.385(3) Å) by the same token is significantly shorter compared to **2-Eind-*E*** (1.421(4) Å), indicating a higher degree of π-character in the N–C^{carb} bond and thus a smaller degree of π-character in the Si–C^{carb} in the *Z*-isomer compared to the *E*-isomer. The pyramidalization of the silicon center in **2-Eind-*Z***, renders the molecules chiral, according to the Cahn-Ingold-Prelog priority rules the stereodescriptor *R* can be assigned in the molecular structure of **2-Eind-*Z*** depicted in *Figure 2.15* (right). The other enantiomer is also found in the crystal-lattice the space group of the crystal being achiral (P-1).

In terms of its structural properties **2-Eind-*Z*** compares well to pyramidal 2-(amino)silenes **2-Nu** discussed in section *section 2.2.2*, whereas **2-Eind-*E*** features the characteristics of a trigonal planar silene, similar to the recently reported bromosilene (R)Si(Br)=CH(Ar) (R = $CH(SiMe_3)_2CH_2tBu$, Ar = C_6H_3-3,5-tBu_2) by Iwamoto et al. (*Figure 2.13*).[189]

Table 2.9. Selected structural paramters of **2-Eind-*E*** and **2-Eind-*Z*** in comparison to literature known compounds.

Comp.	Si–$C^{carb/sp2}$ / Å	N–C^{carb} / Å	Σ∢(Si) / (deg)	θ(Si)[a] / (deg)	τ[b] / (deg)	Ref.
SiBr(Eind)($caac^{Me}$) **2-Eind-*E***	1.768(3)	1.421(4)	356.9	23.1	18.0	
SiBr(Eind)($caac^{Me}$) **2-Eind-Z**	1.796(2)	1.385(3)	346.1	35.7	5.2	*this*
SiBr(Mes)($caac^{Me}$) **2-Mes**	1.842(1)	1.350(2)	326.3	54.2	8	*work*
SiCl(C_6H_4-6-NMe_2)($caac^{Me}$)	1.853(1)	1.345(2)	321.0	57.5	9.1	[137]
(R)Si(Br)=CH(Ar)[c]	1.716(2)	–	360.0	13.4	4.6	[189]

[a]: The bent angle (θ) in deg is defined as the angle between Si–C^{carb} and the Br–Si–R plane.
[b]: The twist angle (τ) is defined as the angle between the silicon and Ccarbene coordination planes defined by the atoms Xl–Sil–R (X = Br, Cl) (R = C^{Ar}, C^{Alk})and C2–Cl–Nl for CAAC (Hl–Cl–C^{Ar} for the sp^2 carbon atom in the silene), respectively.
[c]: R = $CH(SiMe_3)_2CH_2tBu$, Ar = C_6H_3-3,5-tBu_2

The ^1H, $^{13}C\{^1H\}$ as well as $^{29}Si\{^1H\}$ NMR spectra of **3-Eind-*E*** at ambient temperature in (D_6)benzene feature C_1-symmetry, reflecting the axial chirality of the molecule observed in the molecular structure. Recorded NMR spectra of **3-Eind-*Z***, in contrast, reveal an averaged C_S-symmetry at ambient temperature in (D_6)benzene solution, indicating a dynamic behavior in solution. This can be rationalized upon an pyramidal inversion of the silicon center in solution via a planar transition state, which proceeds via a rather low inversion barrier similar to that of the 2-(amino)silenes **2-Nu** (*Figure 2.9* in *section 2.2.2*).

The ^1H NMR spectrum of **2-Eind-*E*** (*Figure 2.16* (bottom)) displays four singlets for the methyl groups of ($C^3Me_AMe_B$, $C^5Me_AMe_B$), as well as two doublets for the hydrogen atoms ($C^4H_AH_B$) for the backbone of the $caac^{Me}$ carbene moiety. In total four doublets of the methyl groups of the isopropyl groups ($C^2CH_AMe_AMe_B$ and $C^6CH_BMe_CMe_D$) as well as two septets for the methine protons of the isopropyl groups ($C^2CH_AMe_AMe_B$ and $C^6CH_BMe_CMe_D$) are observed in the aliphatic region for the Dipp substituent. In case of the Eind substituent 8 triplets for the methyl groups (CH_AH_BMe), 16 multiplets were observed for the diastereotopic methylene groups (CH_AH_BMe) as well as 4 doublets for the backbone hydrogen atoms could be assigned in the aliphatic region of the ^1H NMR spectrum.

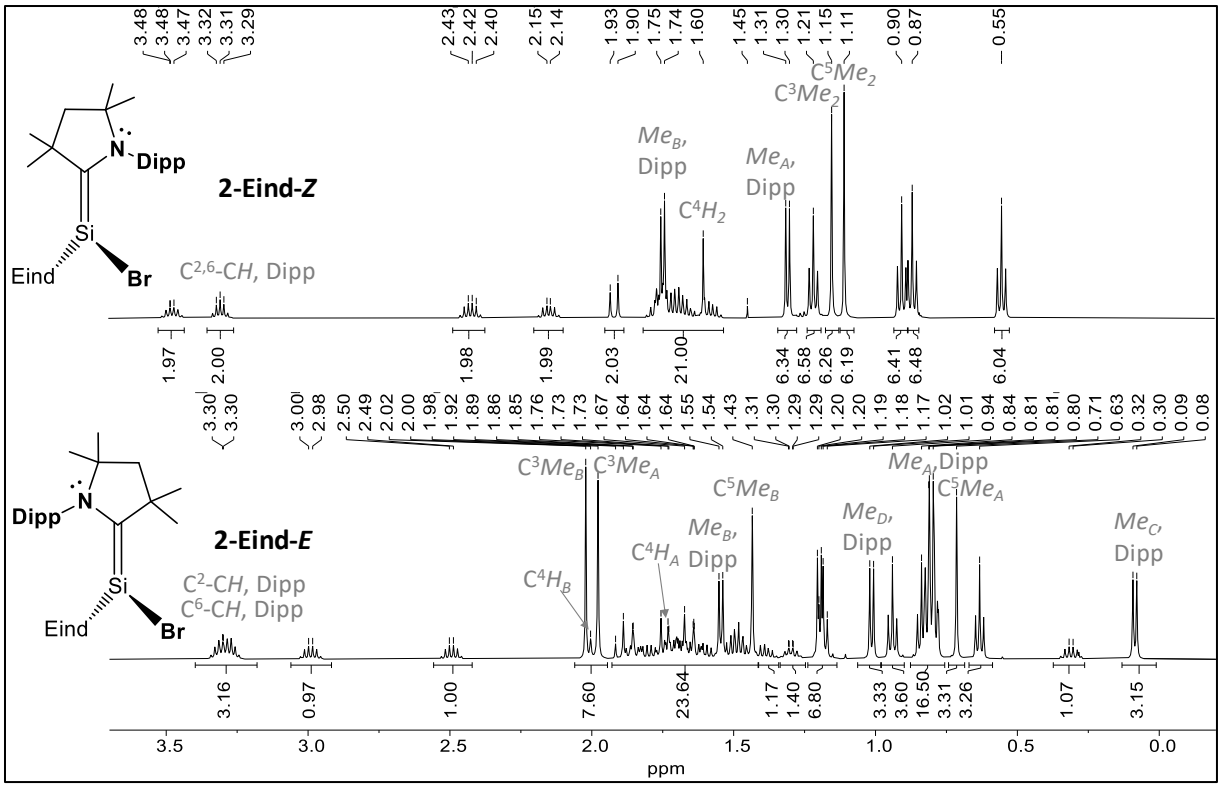

Figure 2.16. Comparison of the aliphatic region of ^{1}H NMR spectra (500.14 MHz) of pure samples of **2-Eind-*Z*** (top) and **2-Eind-*E*** (bottom) in (D_6)benzene at ambient temperature, showing the averaged C_S-symmetry in **2-Eind-Z** and the found C_1-symmetry in **2-Eind-E**, respectively. All signals were assigned via high resolution correlation spectroscopy (see *section 4.4*).

The ^{1}H NMR spectrum of **2-Eind-*Z*** (*Figure 2.16* (top)) displays two singlets for the methyl groups of (C^3Me_2, C^5Me_2), as well as one singlet for the hydrogen atoms (C^4H_2) for the backbone of the caac^{Me} carbene moiety. In total two doublets of the methyl groups of the isopropyl groups ($C^{2,6}$-CHMe_AMe_B) as well as one septet for the methine protons of the isopropyl groups ($C^{2,6}$-CHMe$_A$Me$_B$) are observed in the aliphatic region for the Dipp substituent. In case of the Eind substituent 4 triplets for the methyl groups (CH$_A$H$_B$*Me*), 8 multiplets were observed for the diastereotopic methylene groups (CH_AH_BMe) as well as 2 doublets for the backbone hydrogen atoms could be assigned in the aliphatic region of the ^{1}H NMR spectrum. The full NMR assignment of **2-Eind-*E*** and **2-Eind-*Z*** was made possible through high-resolution correlation spectroscopy.

The ^{29}Si{^{1}H} NMR spectra of **2-Eind-*E*** and **2-Eind-*Z*** display resonances at 31.1 ppm and 1.85 ppm, respectively, which are significantly downfield and upfield shifted, when compared to SiBr(Mes)(caac^{Me}) (**2-Mes**) (10.5 ppm), respectively.

The $^{13}C^{CAAC}$ NMR resonance in **2-Eind-*E*** is with 165.2 ppm drastically upfield shifted when compared to **2-Eind-*Z*** (175.9 ppm) and **2-Mes** (195.0 ppm), indicating a strong Si=C^{carb} π-bond in **2-Eind-*E***. The ^{1}H ^{15}N HMBC spectrum displays a crosspeak at 104.3 ppm (**3-Eind-*E***), which is drastically upfield shifted when compared to that of the dibromosilylene $SiBr_2(caac^{Me})$ (**1**) (231.3 ppm), as well as significanty upfield shifted when compared to **2-Eind-*Z*** (135.1 ppm) and **2-Mes** (158.8 ppm), suggesting a C^{carb}–N single bond, which is in line with the C^{carb}–N bond length of 1.421(4) Å.
The $^{15}N^{CAAC}$ NMR resonance of **3-Eind-*E*** (104.3 ppm) and **3-Eind-*Z*** lie (135.1 ppm) in the range of 160 – 90 ppm of the ^{15}N NMR scale by H. Roesky and co-workers[108] and thus suggests a strong Si–C^{carb} π-backdonation.

Table 2.10. Selected multi-nuclear NMR chemical shift values of **2-Eind-*E*** and **2-Eind-*Z*** and their comparison with literature known pyramidal 2-(amino)silenes.

Comp	δ($^{13}C^{carb}$) / ppm	δ(^{29}Si) / ppm	δ($^{15}N^{CAAC}$) / ppm	Ref.
SiBr{Eind}($caac^{Me}$) **2-Eind-*E***	165.2[b]	31.1	104.3	
SiBr{Eind}($caac^{Me}$) **2-Eind-Z**	175.9[b]	1.8	135.1	*this*
SiBr{Mes}($caac^{Me}$) **2-Mes**	194.7[b]	10.5	158.8	*work*
SiCl{C_6H_4-6-NMe_2}($caac^{Me}$)	198.9[a]	27.3	–	[137]
SiMe{C_6H_4-6-NMe_2}($caac^{Me}$)	176.4[b]	21.1	–	[137]

[a]: (D_8)THF, 243 K; [b]: (D_6)benzene, 298 K

NMR spectroscopic properties, as well as bonding parameters of the molecular structure suggest pure silene type character in **2-Eind-*E*** with a rather strong Si=C^{carb} bond and an axial chirality observed in solid state and solution. As such compound **2-Eind-*E*** can be rather termed as twisted bromo-silene.
The NMR spectroscopic results, as well as the structural parameters of **2-Eind-*Z*** suggest a pyramidalized silene type structure in the ***Z***-isomer, in contrast to the ***E***-isomer. In terms of its bonding parameters (Σ∢(Si) = 346.1°), d(Si–C^{carb}) = 1.796(2) Å) as well as NMR resonances (δ(^{15}N) = 135.1 ppm) **2-Eind-*Z*** seems to have the strongest π-contribution in the Si–C^{carb} bond compared to the other pyramidal *Z*-bromo-silenes **2-Nu** (Σ∢(Si) = 321.6 – 334.9(1)°).

2.2.4.2 Kinetic study of the thermal *E* → *Z* isomerization of 2-Eind

The kineitics of the ***E*** → ***Z*** thermal isomerization was studied at 90 °C, 100 °C and 110 °C. Pure sample of **2-Eind-*E*** was dissolved in (D_8)toluene and distributed into three young-NMR samples. The change in the *E* : *Z* ratio was monitored by ^{1}H NMR, by integration of the C^3-{CH_AH_BMe}$_x$, Eind Signal of the ***E***-isomer (at 0.57 ppm, signal A) and the $C^{3,5}$-$CH_AH_BMe_A$, Eind resonance of the ***Z*** isomer (at 0.49 ppm, signal B). The kinetic constants of the irreversible ***E*** → ***Z*** isomerization were derived from the Arrhenius equation

$$[A] = [A_0] \cdot e^{(-k \cdot t)} \qquad \text{(eq. 2.3)}$$

Details to the kinetic measurements are given in the experimental part (see *chapter 5.7*). The thermodynamic parameters of the activation barrier of the thermal induced ***E*** → ***Z*** isomerization are obtained from the Eyring-Polanyi equation plot of ln(k/T) vs 1/T: The enthalpy of activation ($\Delta H^{\ddagger}$ = 112.6 ± 1.7 kJ mol^{-1}) and entropy of activation ($\Delta S^{\ddagger}$ = –8.3 ± 0.2 J K^{-1} mol^{-1}) were obtained from the slope and the intercept of the linear fit, respectively.

The Gibbs free activation energy can be calculated using the Gibb's Helmholtz equation, which gives $\Delta G^{\ddagger}$(298K) = 115.1 ± 1.7 kJ mol^{-1}.

The isomerization of SiBr(Eind)(caac^{Me}) from the ***E*** isomer into the ***Z***-isomer can be rationalized by the rotation of the Si–C^{carb} bond. Rotation of the Si–C^{carb} bond by 90° leads to a pyramidal transition state (the silicon center is much stronger pyramidalized), which could not be observed by ^{1}H NMR spectroscopy, which upon rotation transforms itself into the thermodynamically favored ***Z***-isomer. However further theoretical investigations are needed to get a better insight into the nature of the irreversible isomerization of **2-Eind**.

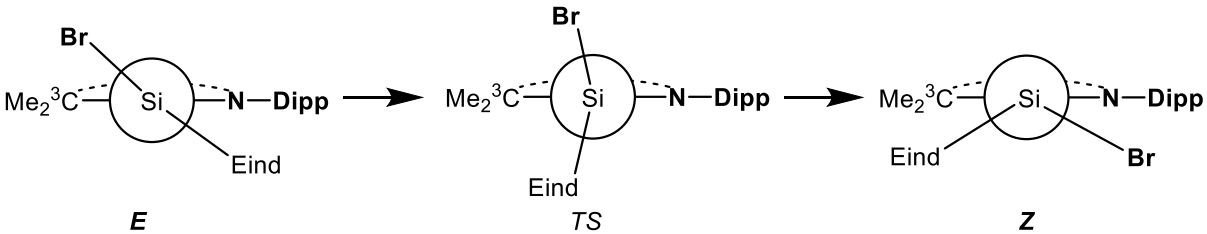

Figure 2.17. Newman projection of SiBr(Eind)(caac^{Me}) **2-Eind**, showing the stepwise rotation of the Si–C^{carb} bond which results in the irreversible ***E*** → ***Z*** isomerization. The rotation undergoes highly likely via a transition state (TS), in which the N-Dipp is orientated orthogonal with respect to the SiBr(Eind) moiety. The transition state should feature a more pyramidalized silicon center and an elongated Si–C^{carb} bond. Upon further rotation of the Si–C^{carb} bond the thermodynamically favored ***Z***-isomer is formed.

2.2.5 Reactivity of pyramidal 2-(amino)silenes

2.2.5.1 Bromide abstraction of SiBr(R)(caac^{Me})

Abstraction of the bromide in pyramidal 2-(amino)silenes with Na[B{C_6H_2-3,5-$(CF_3)_2$}$_4$] or Li$(Et_2O)_{2.5}$[B$(C_6F_5)_4$] appeared to be unsuccessfull. Silenes **2-Si** and **2-N** did not show any reaction with 1.0 equiv. of these reagents mentioned above in fluorobenzene at ambient temperature. Upon heating to 60 °C for several hours a slow reaction progress happened but the reactions were unselective. Monitoring of the reaction mixture by ^{1}H no D NMR in fluorobenzene revealed the formation of the hydridosilenes **5-Si** and **5-N** among other unknown reaction products. Hydridosilenes **5-Si** and **5-N** were independently synthesized upon reaction of the two -coordinated silicon(I) radicals **3-Si** and **3-N** with 1,4-cyclohexadiene (see *section 2.3.5*).

The reaction of **2-O** with 1.0 equiv. of Na[B{C_6H_2-3,5-$(CF_3)_2$}$_4$] in fluorobenzene at ambient temperature resulted in a decolorization of the orange solution into a yellowish solution, alongside the formation of a voluminous white precipitate. ^{1}H no D-NMR spectroscopy of the supernatant solution revealed a rather unselecetive decomposition. ^{1}H NMR spectroscopy in (D_8)THF of the white precipitate revealed the formation of NaOMes*.

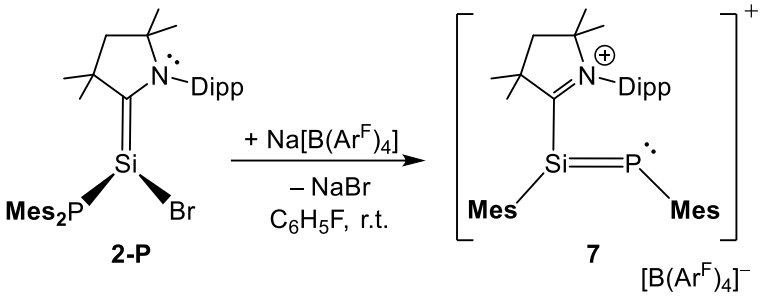

Scheme 2.6. NMR spectroscopic evidence for the formation of cation **7**, upon halide abstraction of **2-P** with Na[B$(Ar^F)_4$] ([B$(Ar^F)_4]^-$ = [B{C_6H_2-3,5-$(CF_3)_2$}$_4$]).

The reaction of **2-P** with 1.0 equiv. of Na[B{C_6H_2-3,5-$(CF_3)_2$}$_4$] in fluorobenzene appeared to be particulary interesting. At ambient temperature a slow conversion was observed. Upon heating of the reaction mixture for 2 h at 60 °C resulted in a color change from orange to dark red. ^{1}H no D NMR spectroscopy of an aliquote of the reaction mixture in fluorobenzene revealed the formation of the cation [(Mes)P=Si(Mes)(caac^{Me})][B$(Ar^F)_4$] (**7**) next to 18 mol% of [caac^{Me}(H)][B$(Ar^F)_4$]. The ^{31}P{^{1}H} NMR spectrum revealed several signals of unknown side products. Different attempts to isolate the compound upon crystallization from fluorobenzene/*n*-hexane mixtures failed and resulted in the formation of a red oil. The compound slowly decomposes in THF or Et_2O, showing the increased formation of [caac^{Me}(H)][B$(Ar^F)_4$]. Nevertheless, the compound was characterized by NMR spectroscopy.

The $^{29}Si\{^{1}H\}$ spectrum of the crude product **7** displays a doublet at 148.0 ppm ($^{1}J(^{29}Si,^{31}P)$ = 166.7 Hz) and the $^{31}P\{^{1}H\}$ spectrum a broad signal at 255.3 ppm ($\Delta\nu_{1/2}$ = 177 Hz). The $^{13}C^{CAAC}$ and $^{15}N^{CAAC}$ resonances of **7** (210.1 ppm, 209.95 ppm) are considerably upfield shifted when compared to the starting material **2-P** (204.3 ppm, 170.8 ppm) and suggest a Si–C^{CAAC} single bond. NMR spectroscopic features of **7** suggest a phosphasilene type of structure with a singly bonded $caac^{Me}$ carbene. Compound **7** can be rationalized as the formal 1e⁻ oxidation product of the silenyl-phosphanyl radical **6** (see *section 2.3.6*).

2.2.5.2 Reactivity of SiBr(R)($caac^{Me}$) towards nucleophiles

The bromine atom in pyramidal 2-(amino)silenes, indeed can be further substituted with smaller nucleophiles. NMR spectroscopic evidence for the formation of hydridosilenes SiH(R)($caac^{Me}$) (R = $SiTMS_3$ (**5-Si**), $NTMS_2$ (**5-N**)) was shown upon reaction of SiBr(R)($caac^{Me}$) (R = $SiTMS_3$ (**2-Si**), $NTMS_2$ (**2-N**)) with $NaBEt_3H$ at ambient temperature in toluene and (D_6)benzene solution, respectively. Compound **5-Si** was isolated and fully characterized upon reaction of silicon(I) radical **3-Si** with 1,4-cyclohexadiene, whereas **5-N** was characterized by NMR spectroscopy. The isolation and characterization of the compounds is described in *section 2.3.5*.

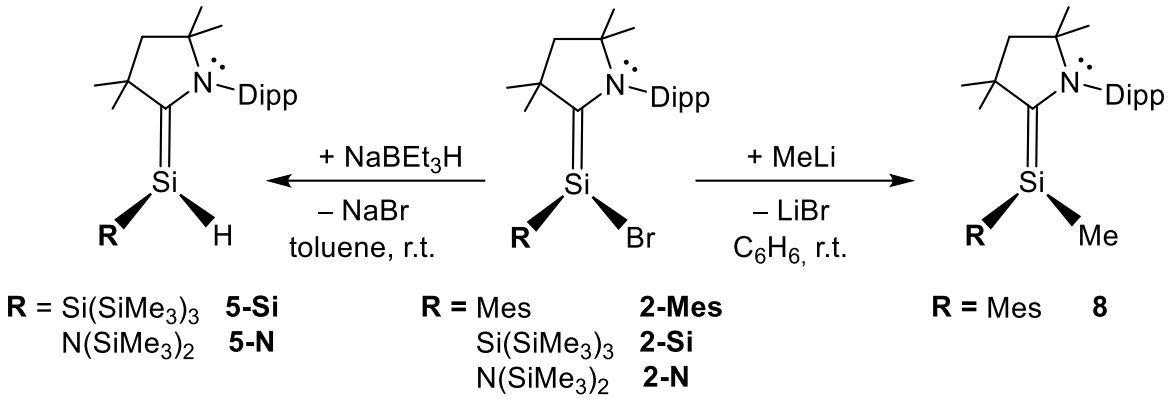

Scheme 2.7. Reaction of **2-Mes**, **2-Si** and **2-N** with MeLi and $NaBEt_3H$ yielding the corresponding functionalized silicon(II) compounds.

Reaction of a solution SiBr(Mes)($caac^{Me}$) (**2-Mes**) in benzene with 1.0 equiv. of MeLi selectively afforded the substituted silene SiMe(Mes)($caac^{Me}$) (**8**). After crystallization, compound **8** could be obtained as orange powder in NMR spectroscopically pure form in 28 % yield. The compound is extremely air sensitive, quickly decolorizing upon contact with air. It is highly soluble in aromatic and aliphatic solvents, giving intense orange solutions.

^{1}H, $^{13}C\{^{1}H\}$ and $^{29}Si\{^{1}H\}$ NMR spectra reveal an averaged *Cs*-symmetry of the molecule in solution. The $^{29}Si\{^{1}H\}$ resonance of **8** (–8.60 ppm) is significantly upfield shifted when compared to the starting material **2-Mes** (10.5 ppm).

Similarly, the $^{13}C^{CAAC}$ and $^{15}N^{CAAC}$ resonances in **8** (171.96 ppm, 111.9 ppm) are drastically upfield shifted when compared to **2-Mes** (195 ppm, 158.8 ppm), but compare rather well to the resonances of the bromosilene **2-Eind-*E*** and the silene SiMe(C_6H_4-6-NMe_2)($caac^{Me}$) (*Table 2.11*).

The NMR spectroscopic features of the compound (e. g. similar to **2-Eind-*E***), suggest a silene type of structure in **8** with a trigonal planar coordinated silicon atom ($\Sigma\measuredangle$(Si) = 360°). Likewise, the $^{29}Si\{^1H\}$ resonances of **5-Si** (–47.6 ppm) and **5-N** (–5.43 ppm) are significantly upfield shifted to their respective starting materials **2-Si** (24.69 ppm) and **2-N** (18.5 ppm). The upfield shifted $^{15}N^{CAAC}$ resonances in **5-Si** (147.1 ppm) and **5-N** (126.7 ppm) with respect to **2-Si** (162.95 ppm) and **2-N** (151.8 ppm) suggest the presence of a strong π(Si–C^{CAAC}) bond in **5-Si** and **5-N** in analogy to compound **8**. In fact, the $^{15}N^{CAAC}$ resonances of substituted silicon(II) compounds **5-Si** (147.1 ppm), **5-N** (126.7 ppm) and **8** (111.9 ppm) fall in the range of 160 –90 ppm and thus according to the ^{15}N NMR scale by Roesky et al. they feature a strong Si → $caac^{Me}$ π-backdonation accompanied by a weak $caac^{Me}$ → Si σ-donation.[108]

Table 2.11. Selected multi-nuclear NMR chemical shifts of silenes **5-Si**, **5-N** and **8** compared to their starting materials and literature known pyramidal 2-(amino)silenes. NMR spectroscopic data is given in (D_6)benzene, if not mentioned otherwise in the legend.

Comp	δ($^{13}C^{carb}$) / ppm	δ($^{29}Si^{II}$)[a] / ppm	δ($^{15}N^{CAAC}$)[b] / ppm	Ref.
$SiBr_2(caac^{Me})$ **1**	231.2[c] ($\Delta\nu_{1/2}$= 23 Hz)	14.35 ($\Delta\nu_{1/2}$= 17 Hz)	231.3	
$SiBr(SiTMS_3)(caac^{Me})$ **2-Si**	204.9	24.69	162.95	
$SiBr(NTMS_2)(caac^{Me})$ **2-N**	190.3	18.5	151.8	*this*
$SiBr(Eind)(caac^{Me})$ **2-Eind-*E***	165.2	31.1	104.3	*work*
$SiBr(Mes)(caac^{Me})$ **2-Mes**	194.7	10.5	158.8	
$SiH(SiTMS_3)(caac^{Me})$ **5-Si**	208.9	–47.6	147.1	
$SiH(NTMS_2)(caac^{Me})$ **5-N**	193.2	–5.43	126.7	
$SiMe(Mes)(caac^{Me})$ **8**	171.96[b]	–8.60	111.9	
$SiCl(C_6H_4$-6-$NMe_2)(caac^{Me})$	198.9[a]	27.3	–	[137]
$SiMe(C_6H_4$-6-$NMe_2)(caac^{Me})$	176.4	21.1	–	[137]

[a]: ^{29}Si resonance of the three coordinated silicon(II)-center. [b]: ^{15}N NMR resonance of the single nitrogen atom in the CAAC carbene-ring referenced against NH_3(l). [c]: (D_8)THF, 243 K.

2.3 Access to the first Neutral Silicon(I) Radicals

2.3.1 Introduction

The molecular chemistry of silicon in oxidation state +1 has witnessed a remarkable upswing over the past two decades through the application of N-heterocyclic carbenes (NHCs) or cyclic (alkyl)(amino)carbenes (CAACs) leading to a plethora of novel compounds with intriguing bonding features and synthetic potential.[76,77,79,95–98,198] Closed shell silicon(I) compounds have been widely studied, there are four classes of neutral silicon(I) compounds known: disilynes **II-8** (R = Alkyl, Aryl, Silyl)[26–30] (*Figure 2.18*), which feature a silicon-silicon triple bond, NHC-stabilized Si(I) dimers **II-9** (X = Cl, Br, I),[127] which can be seen as NHC adducts of the corresponding disilynes, caac^{Me}-stabilized Si(I) dimers **II-10** (R^2 = Cl, Br, I, H, Me), [121,128–130] which can be rather described as 1,4-diamino-2,3-disila-1,3-butadiene derivatives, and Si(I) dimers, which feature bidentate ligands, such as amidinato (**II-11**) or phosphinoenamido (**II-12**) type of compounds.[199,200]

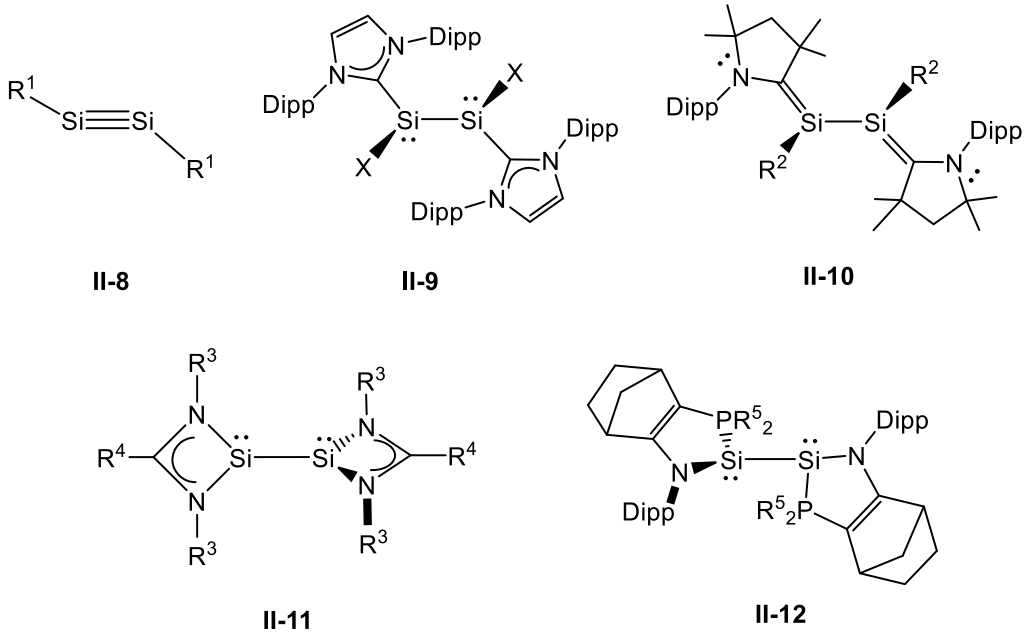

Figure 2.18. Important classes of neutral dimeric silicon(I) compounds (X = Cl, Br, I), R^1 = alkyl, aryl, silyl; R^2 = Cl, Br, I, H, Me, Ph; R^3 = *t*Bu, R^4 = Ph or R^3 = Dipp, R^4 = C_6H_4-4-*t*Bu; R^5 = *t*Bu). Formal charges are not included for simplicity.

Open shell two-coordinate silicon(I) compounds, in contrast, are especially challenging, due to their high reactivity and susceptibility for dimerization.[121,127–130,199,200] Only a handful of stable hypovalent charged silicon radicals have been reported thus far, which were stabilized either by the use of NHCs ($[Si_2(NHC)_2]^+$) and CAACs ($[Si(CAAC)_2]^+$) or bulky organosilyl groups (M[SiR_2], R = SiMe(^{t}Bu)$_2$, M = Li, Na, K).

Radical cations, such as **II-13**[134] and **II-14**[132](*Figure 2.19*), which can be formally seen as 1e⁻-oxidation products of the corresponding neutral silicon(0) compounds, were obtained by the reaction of SiI_2H_2 with three equivalents of $caac^{Me}$ carbene and the oxidation of $Si_2(IDipp)_2$ with $[Fe(C_5Me_5)_2][BAr^F{}_4]$ ($Ar^F = C_6H_3$-3,5-$(CF_3)_2$), respectively. In contrast, radical anions, such as **II-15**[201], **II-16**[202,203], and **II-17**[204] are obtained via the reduction of their corresponding silylenes, disilenes and disilynes with alkali metals.

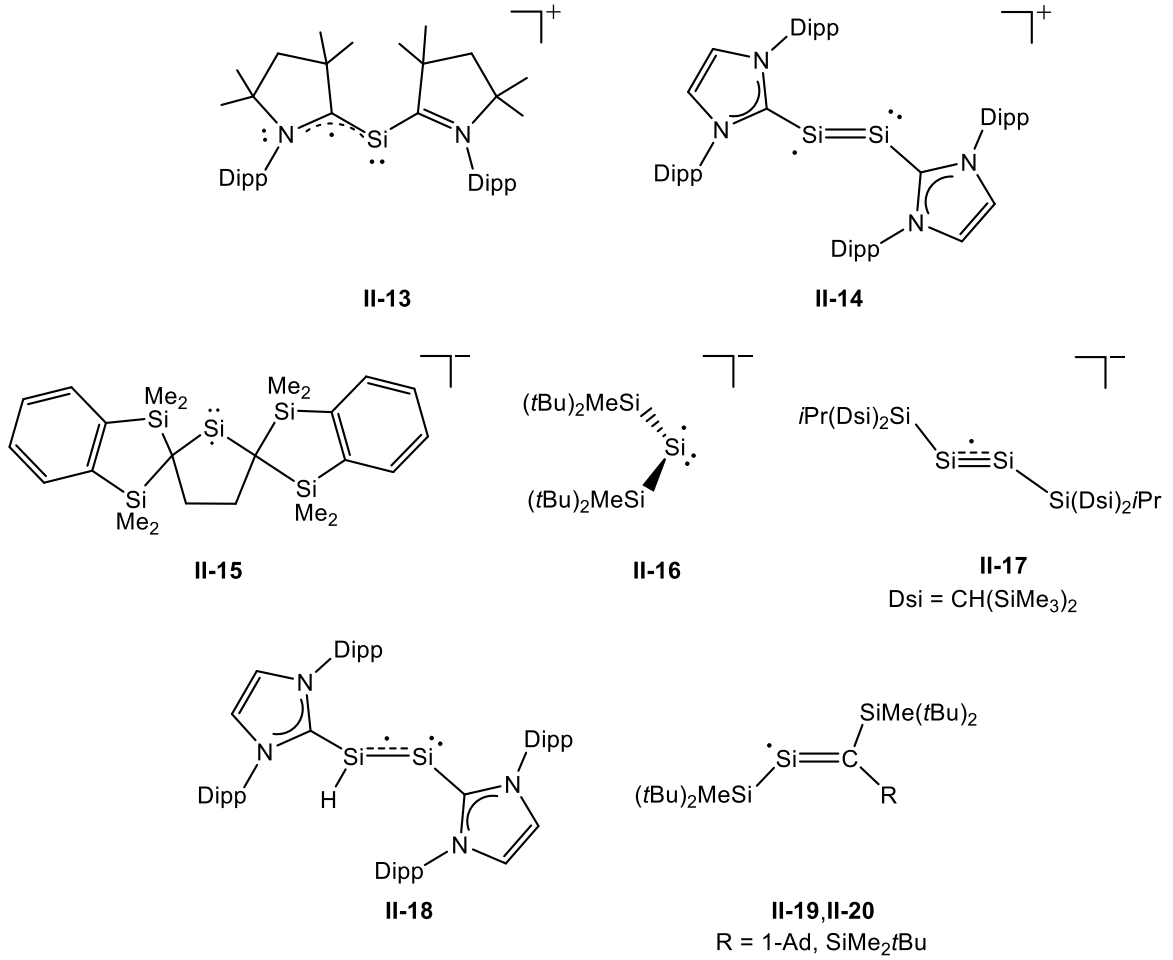

Figure 2.19. Literature known isolated cationic (**II-13**, **II-14**), anionic (**II-15**, **II-16** and **II-17**) and neutral (**II-18, II-19** and **II-20**) silicon(I) radicals. Neutral silenyl radicals **II-19** and **II-20** are persistent ($t_{1/2}$ = 0.5 h) and could be only analyzed by EPR spectroscopy. Formal charges are not included for simplicity.

Isolated neutral two-coordinate silicon(I) radicals, however, are exceptionally rare. The only known silicon example is compound **II-18**[133] (*Figure 2.19*), a π-type monoradical with a formal bond order of 1.5 between the two low valent silicon centers, obtained via the 1e⁻-reduction of $[Si_2(IDipp)_2H][BAr^F{}_4]$.[205] Besides the spectroscopic evidence of a persistent ($t_{1/2}$ = 0.5 h) silenyl radicals **II-19** and **II-20**[206] (*Figure 2.19*), which was determined to be an s-type radical with a formal Si=C double bond, no two-coordinated neutral Si(I)-radical of the type $[:Si^I(R)L]^\bullet$ (R = single bonded substiuent, L = Lewis Base, *Figure 2.20*) has been isolated thus far.

However, the heavier homologue [Ge{N(SiR$_3$)Ar}(caac^{Me})]$^{\bullet}$ (**I-57^{CAAC}**) (R = Ph, Me; Ar = Mes, Dipp), a π-type monoradical with the spin density mainly localized at the Ge and C^{carb}–centers, has been reported, obtained by the reduction of [Ar(SiR$_3$)NGeCl$_3$] with KC$_8$ in the presence of caac^{Me}.[152]

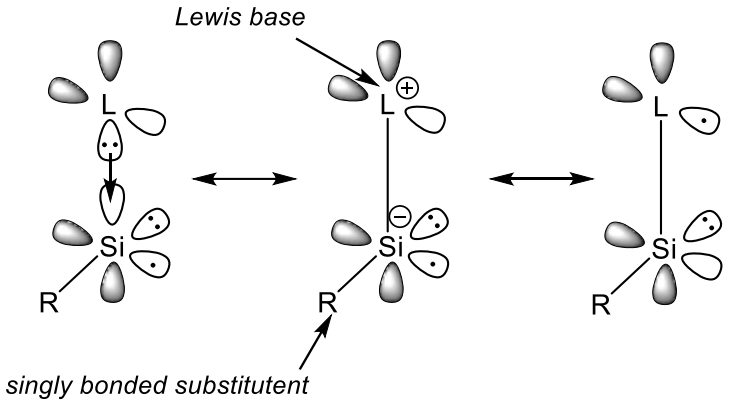

Figure 2.20. Possible resonance formulas of a Lewis base supported silicon(I)-radical.

The main challenge in isolating these compounds is their high reactivity, which ultimately leads either to their decomposition via abstraction of a hydrogen atom from a common organic solvent, or by dimerization leading to [RSi(L)–Si(L)R] species. The reduction of NHC-tetrahalosilane complexes [(IDipp)SiX$_4$] (X = Cl, Br, I) or [(caac^{Me})SiX$_4$], for example, did not afford any carbene stabilized silicon(I) radical; instead only the NHC-stabilized Si(I) dimers **II-9** (X = Cl, Br, I) and the corresponding caac^{Me}-stabilized Si(I) dimers **II-10** (R = Cl[128], Br[this work], I[121]) were formed. Similarly, reduction of the arylchlorosilylene SiCl(Ar^{Mes})(IMe$_4$) (Ar^{Mes} = C$_6$H$_3$-2,6-Mes, Mes = C$_6$H$_2$-2,4,6-Me$_3$) with KC$_8$ in THF led to the formation of the silicon(I)-dimer Si$_2$(Ar^{Mes})$_2$(IMe$_4$)$_2$.[72]

On the other hand, reduction of the NHC-stabilized arylchlorosilylene SiCl(Ar^{Trip})(IMe$_4$) (Ar^{Trip} = C$_6$H$_3$-2,6-Trip, Trip = C$_6$H$_2$-2,4,6-*i*Pr$_3$) by one equivalent of KC$_8$ in THF led to a purple colored solution.[72] EPR spectroscopy of the dark purple solution inTHF suggested the presence of a silicon centered radical, which may be attributed to the neutral silicon(I) radical [:Si(Ar^{Trip})(IMe$_4$)]$^{\bullet}$. The extremely air sensitive compound could not be isolated, due rather fast decomposition in solution and low selectivity of the reaction.[72] Likewise, silenyl radicals **II-19** and **II-20**, could only be proven in solution by EPR-spectroscopy, since it were shown to decompose to the hydrosilenes (R$_A$)HSi=C(R$_A$)(R) (R$_A$ = SiMe(*t*Bu)$_2$, R = 1-Ad, SiMe$_2$*t*Bu) at ambient temperature in solution ($t_{1/2}$ = 0.5 h), respectively.[206] In order to circumvent these side-reactions it was decided to use the caac^{Me}-carbene, which has already shown synthetic potential in the stabilization of low valent silicon radicals,[98] in conjunction with sterically highly demanding substituents, which have been shown to have a significant stabilization effect on silicon centered radicals.[96]

Indeed, neutral two-coordinate silicon(I) radicals of the type Si(R)(caac^{Me}) (R = $SiTMS_3$ (**3-Si**), $NTMS_2$ (**3-N**), OMes* (**3-O**) were synthetically accessible by the simple 1e$^-$-reduction of the corresponding 2-aminobromosilene SiBr(R)(caac^{Me}) (**2**) with KC_8. The reactivity of **3-Si** towards KC_8 and 1,4-cyclohexadiene afforded 2-aminopotassiumsilenide SiK($SiTMS_3$)(caac^{Me}) (**4-Si**) and 2-aminohydridosilene SiH($SiTMS_3$)(caac^{Me}) (**5-Si**), respectively.

2.3.2 Synthesis and properties of neutral two-coordinated silicon(I) radicals

Neutral two-coordinated silicon(I) radicals Si(R)(caac^{Me}) (R = $SiTMS_3$ (**3-Si**), $NTMS_2$ (**3-N**), OMes* (**3-O**)) were obtained upon one electron reduction of their respective 2-aminobromosilenes SiBr(R)(caac^{Me}) (**2-Si**, **2-N**, **2-O**) with 1.1 equiv. of KC_8 in benzene after stirring at ambient temperature for at least 16 h. Dark purple crystals of **3-Si**, red-purple crystals of **3-N** were obtained from *n*-pentane at 0°C in 77 % and 83 % yield, respectively. Radical **3-O** was obtained as an orange-brown-microcrystalline solid upon recrystallizing from toluene/*n*-pentane mixture 1:5 with 59 % yield. All compounds are highly pyrophoric, decomposing immediately upon contact with air. Thermal decomposition of the silicon(I) radicals in vacuum sealed glass capillaries were detected upon melting at 134 °C (**3-Si**), 145 °C (**3-N**) and 214 °C (**3-O**). ^{1}H NMR spectroscopy of the molten mass of the radicals **3-Si** and **3-N** in (D_6)benzene, revealed the presence of hydridosilene SiH($SiTMS_3$)(caac^{Me}) (**5-Si**) and SiH($NTMS_2$)(caac^{Me}) (**5-N**) as major decomposition product ,respectively.

Compounds **3-Si** and **3-N** are well soluble in *n*-hexane, benzene or THF, affording dark purple (**3-Si**) and red-purple (**3-N**) solutions, even at low concentrations (100 µM). Radical **3-O**, in contrast, is moderately soluble in *n*-hexane but well soluble in benzene and toluene, affording orange solutions.

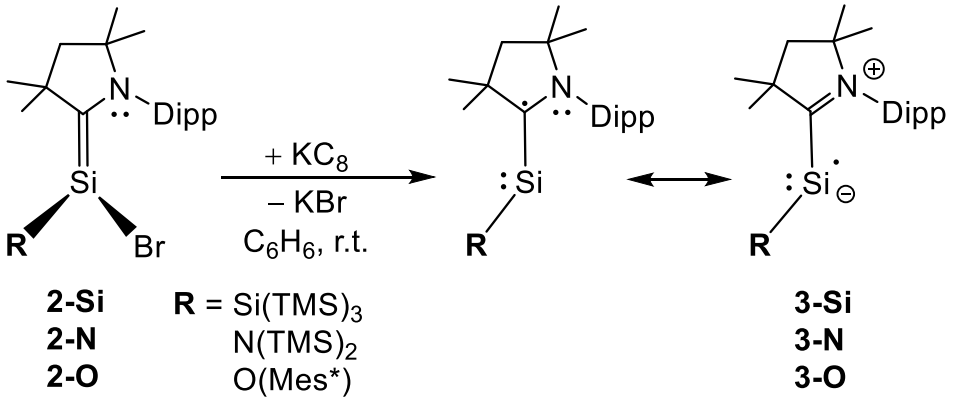

Figure 2.21. Synthesis of the silicon(I) radicals **3-Si, 3-N, 3-O** upon 1e$^-$ reduction of pyramidal 2-(amino)silenes.

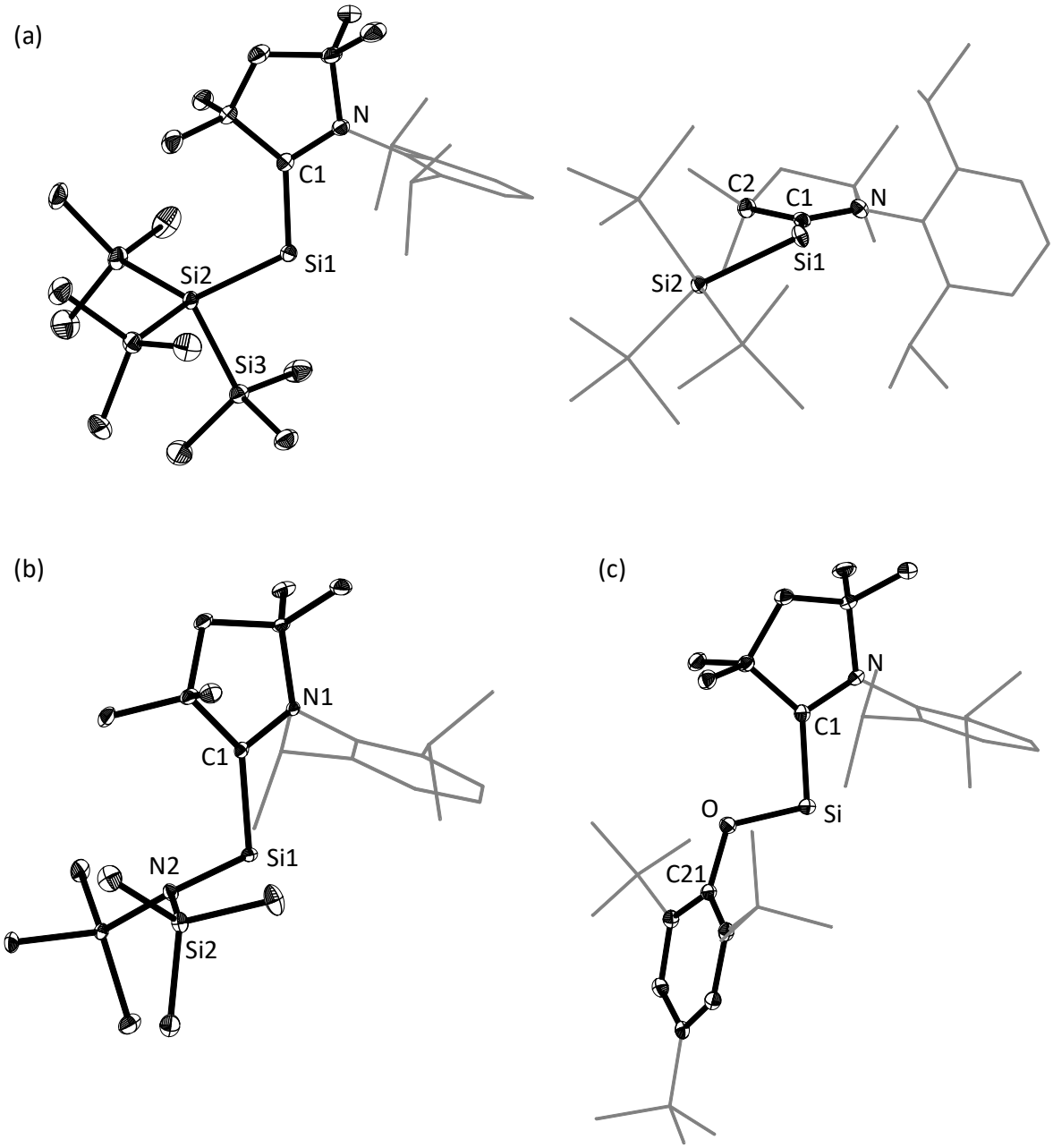

Figure 2.22. DIAMOND plot of the molecular structures of silicon(I) radicals (S_a)-**3-Si** (a), **3-N** (b) and **3-O** (c). Thermal ellipsoids are set at 30 % propability level and hydrogen atoms were omitted. In the depicted structures the Dipp-substituent of the caac^{Me} ligand and the *t*Bu-groups of the Mes* substituent in **3-O** are presented in the wire-frame for the sake of clarity. (Top right) different view of (S_a)-**3-Si** along the Si–C1 bond, showing the bent structure in silicon(I) radical (S_a)-**3-Si**. Selected bond lengths [Å], bond angles [°] and torsion angles [°]:

3-Si: Si1–C1 1.870(2), Si1–Si2 2.3992(5), C1–N 1.349(2), C1–Si1–Si2 112.93(5), Si3–Si2–Si1 97.26(2), N–C1–Si1–Si2 –163.1(2). Depicted in (S_a) configuration. The other enantiomer is also found in the crystal-lattice, the compound crystallizing in the achiral space group ($P2_1/n$).

3-N: Si1–C1 1.895(4), Si1–N2 1.804(3), Si2–N2 1.757(3), N1–C1 1.361(4), N2–Si1–C1 106.6(2), Si2–N2–Si1 115.4(2), N1–Si1–C1–N2 –176.9(3).

3-O: Si–C1 1.865(2), Si–O 1.713(2), O–C21 1.395(2), N–C1 1.363(3), O–Si–C1 100.1(1), C21–O–Si 118.8(1), N–C1–Si–O –178.5(2).

The molecular structures of the silicon radicals **3-Si**, **3-N** and **3-O** were determined by single crystal X-ray diffraction analysis (*Figure 2.22*). The radicals feature a V-shaped geometry at the divalent Si(I)-center. The R–Si–C^{carb} angles (∡ =112.93(5)° (**3-Si**), 106.6(2)° (**3-N**), 100.1(1)° (**3-O**)) decrease with increasing electronegativity of the substituents (Si < N < O). The N-Dipp moiety of the $caac^{Me}$ ligand is orientated trans with respect to the substituents retaining the orientation found in their respective starting materials. The dihedral angle N–C^{carb}–Si–R of **3-Si** (–163.1(2)°) suggest a slightly twisted structure in radical **3-Si** and an almost coplanar structure in **3-N** (–176.9(3)°) and **3-O** (–178.5(2)°), respectively.

The conformation of the $caac^{Me}$ and the $SiTMS_3$ substituents in **3-Si** leads to axial chirality (*Figure 2.22*, top right). In fact, the $caac^{Me}$ and $SiTMS_3$ substituents adopt an *antiperiplanar* conformation, leading to axial chirality with the chirality axis passing through the Si1–C^{carb} bond. The two enantiomers, which are characterized with the stereo descriptors (S_a)-**3-Si** and (R_a)-**3-Si**, differ in the sign of the torsion angle Si2–Si1–C^{carb}–N (S_a)-**1**: –163.1°, R_a-**1**: +163.1° and were both observed in the crystal-lattice, the compound crystallizing in an achiral space group ($P2_1/c$). In contrast, silicon(I) radicals **3-N** and **3-O** feature a planar N-C^{carb}-Si–R (R = N2, O2) core with an almost trans bent skeletal configuration, which renders the molecules achiral with the mirror plane passing through the N–C^{carb}–Si moiety.

The Si–C^{carb} bond lengths (1.870(2) Å (**3-Si**), 1.895(4) Å (**3-N**), 1.865(2) Å (**3-O**)) lie in between that of a typical Si=C double bonds (1.702 – 1.764 Å)[184] and a classical Si–C^{carb} single-bond (1.963(2) Å), [80] indicating a significant degree of π-character in the Si–C^{carb} bond in the silicon(I) radicals (**3-Si** – **3-O**). The Si–C^{carb} bond lengths of **3-Si** (1.870(2) Å) and **3-N** (1.895(4) Å) are significantly elongated with respect to their starting materials the pyramidal 2-(amino)silenes **2-Si** (1.836(2) Å) and **2-N** (1.866(2) Å). In contrast, the Si–C^{carb} bond length of **3-O** (1.856(4) Å), featuring the lowest bond length among the silicon(I) radicals, is significantly shortened compared to its starting material **2-O** (1.897(3) Å).

In terms of its structural features radical **3-Si**, differs quite remarkably from silicon(I) radicals **3-N** and **3-O**, suggesting a different delocalization of the unpaired electron.

This stays in agreement with quantum chemical calculations (see section 2.3.4) which indicate that **3-Si**, **3-N** and **3-O** are π-type monoradicals in which the unpaired electron occupies a π(Si–C^{carb})-orbital leading to a high spin density at the Si (52 % (**3-Si**), 41 % (**3-N**), 32 % (**3-O**) and C^{carb} (36 % (**3-Si**), 33 % (**3-N**), 37 % (**3-O**)) atoms and a formal Si–C bond order of 1.48 (**3-Si**), 1.34 (**3-N**) and 1.38 (**3-O**), respectively.

^{1}H NMR spectroscopy of the silicon(I) radicals **3-Si**, **3-N** and **3-O** in (D_6)benzene showed the presence of broad signals (*Figure 2.23*), originating from the paramagnetic species. The ^{1}H NMR spectra of **3-Si** (*Figure 2.23*, bottom) and **3-N** (*Figure* 5.5, middle) in addition featured sharp signals, which originate from tiny amounts (less than 1 mol%) of hydridosilenes SiH(R)(caac^{Me}) (R = $SiTMS_3$ (**5-Si**), $NTMS_2$ (**5-N**)), respectively.

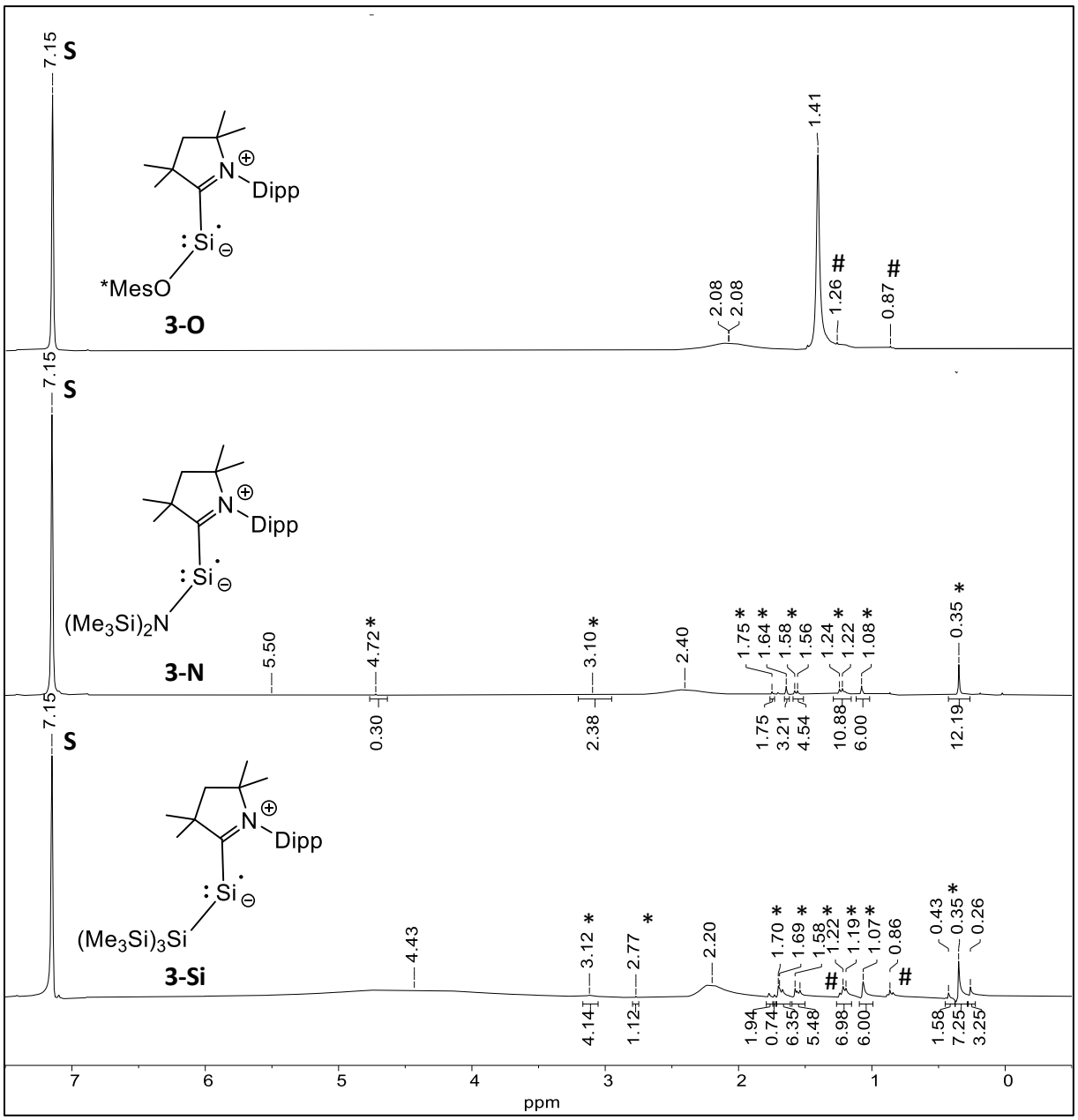

Figure 2.23. ^{1}H NMR spectra (300.14 MHz) of pure samples of **3-Si** (bottom), **3-N** (middle) and **3-O** (top) in (D_6)benzene at ambient temperature. The signal of the deuterated solvent is marked with the character **S** and residual solvent peaks of *n*-pentane are marked with the character #. The symbol (*) marks the ^{1}H NMR resonances of the corresponding hydridosilenes SiH($SiTMS_3$)(caac^{Me}) (**5-Si**) and SiH($NTMS_2$)(caac^{Me}) (**5-N**) present in the compounds **3-Si** and **3-N**, respectively.

Recorded ^{1}H NMR spectra of a 60 mM solution of **3-Si** and **3-N** in a time interval of 0.5 h over the course of 4 h did not show any significant change (*Figure* 5.15 and *Figure 5.17*). These results are in line with UV/Vis measurements of **3-Si** and **3-N** in *n*-hexane, which did not reveal any sign of major decomposition of the radicals after 4 h at ambient temperature in solution (*Figure 5.92* and *Figure 5.95*).

Recorded ^{1}H NMR spectra of **3-Si** and **3-N** over the course of 2 days revealed a rather slow unselective decomposition in solution (*Figure 5.16* and *Figure 5.18*) with the formation of ca. 4 mol% hydridosilene **5-Si** and 2 mol% hydridosilene **5-N** with respect to the signal of the deuterated solvent, respectively.[4] Furthermore, a detailed cw-X-band-EPR-spectroscopic study **5-Si** and **5-N** in *n*-pentane and benzene at ambient temperature for 10 days (*Figure* 5.74), did not show any formation of paramagnetic decompositon products and revealed only a rather slow decomposition of the radicals, which is in line with the ^{1}H NMR spectroscopic measurements.

In order to determine the kinetics of the decomposition of **3-Si** at reasonable concentrations (ca. 50 mM), the Evans method was used. Therefore the ^{1}H NMR spectrum of three NMR samples of radical **3-Si** with different concentrations in (D_6)benzene solution and coinserted glass-capillaries filled with pure (D_6)benzene were measured at ambient temperature. The frequency shifts of the deuterated solvent signals were determined and correlated with the known concentrations of the radical. Since the frequency shift correlates in linear fashion with the concentration of the radical in solution it can be used to calculate the concentration of the radical at any given time in solution. In order to study the decompositon ^{1}H NMR spectra of the three Evan's method samples of radical **3-Si** were recorded atleast twice a day over the course of two weeks. The plot of the calculated concentration of radical **3-Si** against the time (*Figure 5.69*), clearly showed a decomposition pseudo first order. Subsequent, linear regression of the plot of ln[R] against the time, gave a reaction rate constant of 3.6 h^{-1} and a half life of 8 days.

Silicon(I) radical **3-O**, in contrast, did not show any signs of decompositon, even upon heating the ^{1}H NMR sample in (D_6)benzene to 60 °C for 4 h. However, the EPR spectrum of **3-O** in toluene showed a slow decomposition at ambient temperature, which might be attributed to the solvent and the strong diluted conditions. The high thermal stability of **3-O** in (D_6)benzene, as well as the higher lying melting point of **3-O** (221 °C) compared to **3-Si** (134 °C(dec)) and **3-N** (145 °C(dec)) may be attributed to the higher spin density in **3-O** at the C^{carb} atom.

---

[4] The mol% of hydridosilene **5-Si** present in a concentrated solution of **3-Si** in (D_6)benzene was determined by quantitative ^{1}H NMR spectroscopy using isolated **5-Si** as external standard (more details are given in *section 5.5.1*).

UV-Vis-NiR spectroscopy of **3-Si** in *n*-hexane (*Figure 2.24*) revealed four absorbtion maxima located at 258, 335, 410 and 529 nm, of which the intense absorptions at 403, 529 nm and an underlying absorption maximum of 620 nm (which can be reasoned by the deconvolution band see *Figure* 5.91) are responsible for the purple color of **3-Si**.

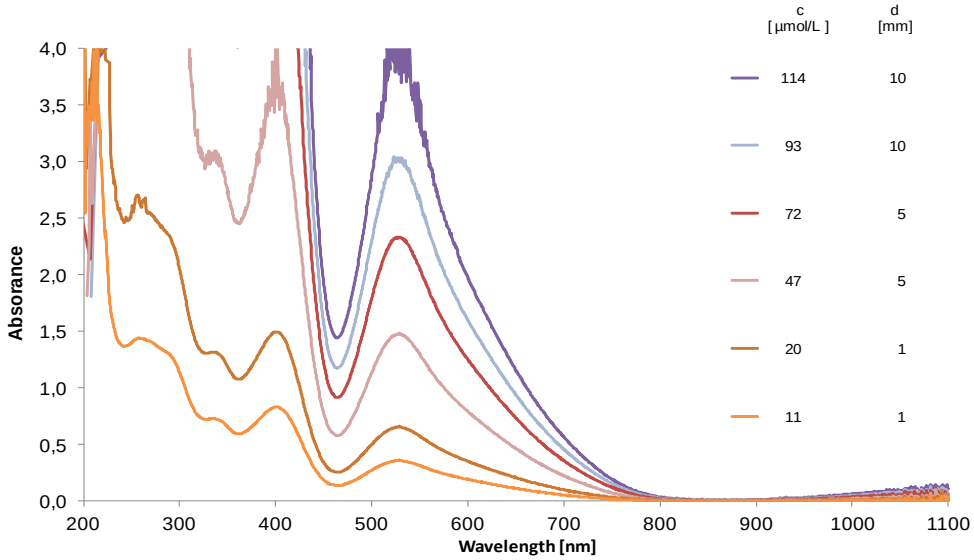

Figure 2.24. UV/Vis-NIR spectra of **3-Si** in n-hexane from 200 – 1100 nm at different concentrations (c) and path lengths (d).

UV-Vis-NiR spectroscopy of **3-N** (*Figure 2.25*), in contrast revealed absorption maxima located at 287, 313, 410 and 495 nm, of which the intense absorption bands at 495 nm and 410 nm, and underlying absorption maxima at 355 and 313 nm (which can be reasoned by the deconvolution band (*Figure 5.94*) are responsible for the red color of **3-N**.

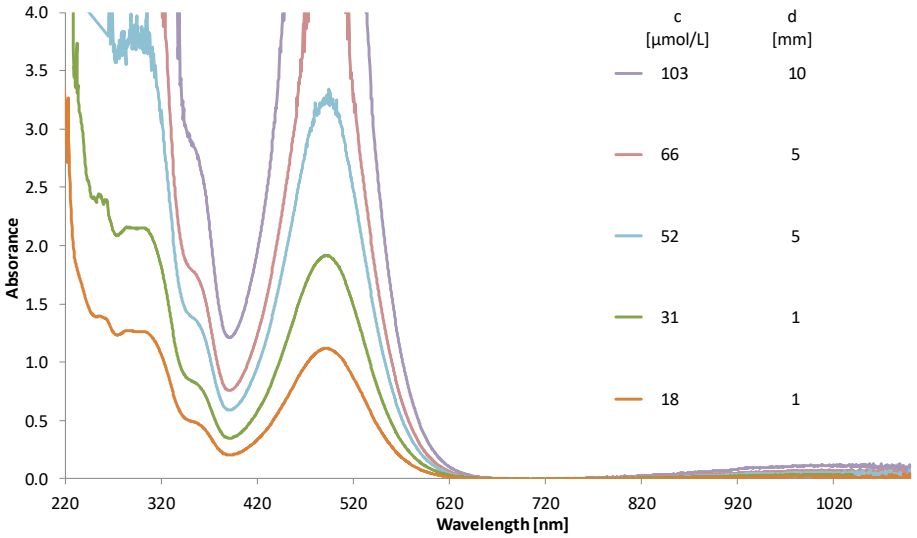

Figure 2.25. UV/Vis-NIR spectra of **3-N** in n-hexane from 200 – 1100 nm at different concentrations (c) and path lengths (d).

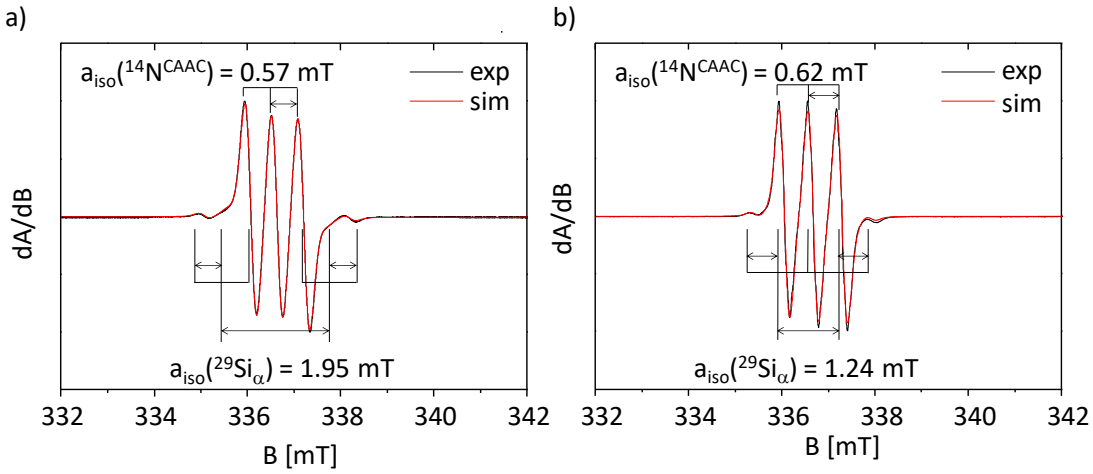

Figure 2.26. Experimental (-) and simulated (-) cw X-band EPR spectra of **3-N** (left) in *n*-pentane at 293 K (g_{iso} = 2.0044, $A_{iso}(^{29}Si)$ = 1.95 mT, $a_{iso}(^{14}N)$ = 0.57 mT) and **3-O** (right) in toluene at 293 K (g_{iso} = 2.0038, $a_{iso}(^{29}Si)$ = 1.24 mT, $a_{iso}(^{14}N)$ = 0.62 mT).

Further insight into the structure of the neutral two-coordinated silicon(I) radicals was provided by continuous wave (cw) EPR spectroscopy at X-band frequency (B_0 = 9.35 GHz). EPR spectra of pure samples of **3-Si**, **3-N** in *n*-pentane and **3-O** in toluene at ambient temperature featured the typical coupling pattern observed in previously reported caac^{Me}-stabilized silicon-radicals. The g_{iso} values (2.0065 (**3-Si**), 2.0044 (**3-N**), 2.0038 (**3-O**)), are significantly greater than that of the free electron value of 2.0023, compare well to to the recently reported heavier homologue Ge{NMes(SiPh$_3$)}(caac^{Me}) (g_{iso} = 2.0075) and the radical cation [Si(caac^{Me})$_2$]$^+$ (**II-13**) (g_{iso} = 2.0037).[134] The values lie in the typical range of caac^{Me}-stabilized three coordinated silicon-radicals (g_{iso} = 2.0019 – 2.0052).[98]

The hyperfine coupling pattern of **3-N** and **3-O** can be described as a triplet, superimposed on a weaker doublet of triplets, which is poorly resolved due to strong overlap. The triplet results from the coupling of the unpaired electron to the single nitrogen with hyperfine coupling constants of $a_{iso}(^{14}N)$ = 0.57 mT (**3-N**) and 0.62 mT (**3-O**), respectively. The signal of weaker intensity can be attributed to the ^{29}Si-isotopologues of **3-N** and **3-O** (natural abundance 4.67 %), most likely of the silenic silicon-center, so that the unpaired electron couples to this silicon yielding a doublet with hyperfine coupling constants of $a_{iso}(^{29}Si)$ = 1.95 mT (**3-N**) and 1.24 mT(**3-O**), respectively and additionally to the single nitrogen with the same hyperfine coupling constants as for ^{28}Si-isotopologue of **3-N** and **3-O**. The at the B97-D3(BJ)^{ATM}/def2-TZVP level of theory calculated ^{14}N and ^{29}Si hyperfine-coupling constants in **3-N$_{calc}$** (0.19 mT, –2.76 mT) and **3-O$_{calc}$** (0.19 mT, –1.93 mT) deviate slightly from the experimentally obtained values in **3-N** (0.57 mT, 1.95 mT) and **3-O** (0.61 mT, 1.24 mT) but are within the limit of deviation of the used method. Further hfcc's to $^{14}N_{\beta}$ are not observed, which fits to the calculated weak hyperfine coupling constant of $a_{iso}(^{14}N_{ß})$ = 0.06 mT.

Table 2.12. Comparison of EPR-spectroscopic features of silicon(I) radicals **3-Si**, **3-N** and **3-O** with literature known two-coordinate Si-radicals.

Comp.	**EPR cond.**	g_{iso}	**M**[a]	$a_{iso}(^{29}Si_{\alpha})$ / mT	$a_{iso}(^{14}N)$ / mT	$a_{iso}(^{1}H)$ / mT	**Ref.**
$Si(SiTMS_3)(caac^{Me})$	*n*-pent.	2.0065	t	3.81	0.44	–	
(**3-Si**)	293K						
$Si(SiTMS_3)(caac^{Me})$	*n*-pent.	2.0065	t	3.73	0.44	0.09	
(**3-Si**)	173K						*this*
$Si(NTMS_2)(caac^{Me})$	*n*-pent.	2.0044	t	1.95	0.57	–	*work*
(**3-N**)	293K						
$Si(OMes^*)(caac^{Me})$	tol.	2.0038	t	1.24	0.62	–	
(**3-O**)	293K						
(IDipp)Si(H)Si(IDipp)	*n*-hex.	2.0056	17	1.73	0.10	0.61	[133]
(**II-18**)	336 K			0.43	0.25		
$(R_A)Si=C(R_A)(R_B)$ [b]	tol.	2.001	m	13.75	–	–	[206]
(**II-19**)	300 K			3.23			
$[Si(caac^{Me})_2]^{+\cdot}\ I^-$	tol./THF	2.0037	t	7.54[d]	0.66	–	[134]
(**II-13**)	298 K						
$[Si_2(IDipp)_2]^{+\cdot}\ [BAr_4^F]^-$	Et_2O	1.9979	m	5.99	–	–	[132]
(**II-14**)	220 K						
$[Li(12\text{-crown-}4)_2]$	DME	2.0074	m	2.91	–	–	[202]
$[(R_A)_2Si]$ (**II-16**)	298 K						
$[K(DME)_4]$	4-Me-	1.9996	m	3.92	–	–	[204]
$[Si_2(R_C)_2]$(**II-17**) [c]	THF						
	298 K						

[a]: Multiplicity (M) of the EPR signal. [b]: R_A = $SiMe(tBu)_2$, R_B = $SiMe_2(tBu)$. [c]: R_C = $Si(iPr)(Dsi)_2$ (Dsi = $CH(SiMe_3)_2$)[d]: The ^{29}Si hfcc was not visible at ambient temperature and could only be assigned at 115 K in tol./THF.

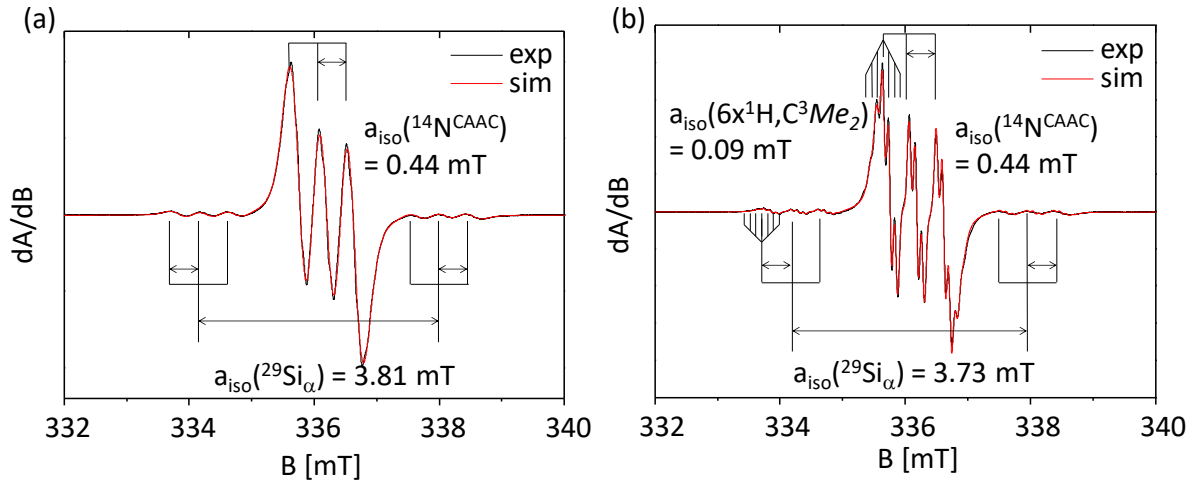

Figure 2.27. Experimental (-) and simulated (-) cw X-band EPR spectra of **3-Si** in *n*-pentane at a) 293 K (g_{iso} = 2.0065, $a_{iso}(^{29}Si)$ = 3.81 mT, $a_{iso}(^{14}N)$ = 0.44 mT); b) 173 K (g_{iso} = 2.0065, $a_{iso}(^{29}Si)$ = 3.73 mT, $a_{iso}(^{14}N)$ = 0.44 mT, 6 x H: $a_{iso}(^{1}H)$ = 0.09 mT).

The EPR spectrum of **3-Si** at 173 K (*Figure 2.27* b), in contrast, features a much more nuanced hyperfine coupling pattern. The multiplett at g_{iso} value of 2.0065 can be best described as a triplet of heptets superimposed on a weaker doublet of triplets of heptets. The first signal originated from the coupling of the unpaired electron to the single nitrogen and the six hydrogen atoms of the two $C^{3}Me_2$ with hyperfine coupling constants of $a_{iso}(^{14}N)$ = 0.44 mT and $a_{iso}(^{1}H)$ = 0.09 mT, respectively. The signal of weaker intensity is a doublet of triplets of heptets and can be assigned to the ^{29}Si-isotopologue of **3-Si** (natural abundance 4.67 %), in which the unpaired electron couples to this silicon yielding a doublet with a hyperfine coupling constant $a_{iso}(^{29}Si)$ = 3.73 mT and couples additionally to the single nitrogen and the six hydrogens with the same hyperfine coupling constants as for ^{28}Si-isotopologue of **3-Si**. The at the B97-D3(BJ)^{ATM}/def2-TZVP level of theory calculated ^{29}Si, ^{14}N and ^{1}H hyperfine coupling constants of −4.67 mT, 0.18 mT and 0.09 mT in **3-Si$_{calc}$** deviate slightly from the experimentally obtained values of 3.73 mT, 0.44 mT and 0.09 mT of **3-Si**, but are within the limit of deviation of the used method. In addition the ^{29}Si hfcc in **3-Si** (3.73 mT) compares remarkably well to that reported of the disilyne radical-anion $[Si_2(Si(iPr)(Dsi)_2]^-$ (Dsi = $CH(SiMe_3)_2$) (**II-17**)[204] ($a_{iso}(^{29}Si)$ = 3.92 mT). Further hfcc's to ^{29}Siβ and ^{29}Siγ could not be resolved, which fits to the calculated weak hyperfine coupling constants of $a_{iso}(^{29}Si_{ß})$ = 0.45 mT and $a_{iso}(^{29}Si_{\gamma})$ = 0.23 mT and the very low probability of having two ^{29}Si atoms in **3-Si**. Interestingly, increasing the temperature of the *n*-pentane solution of **3-Si** in the range from 173 K to 298 K showed a gradual broadening of the lines and ultimately vanishing of the ^{1}H hyperfine coupling pattern under the line-width (see *Figure 2.27* a and *Figure 5.72*). Intuitively, one would have expected the opposite behavior, i. e. an increasing line width with decreasing temperature because the anisotropic contributions are less averaged at lower temperature.

Thus, this behavior indicates, that higher temperature a dynamic process is operative, which probably involves a hindered rotation around the Si–C^{carb} bond. Indeed, quantum chemical calculations suggest that radical **3-Si** has a hindered rotation of the Si–C^{carb} bond in solution with an energy barrier of 41 kJ mol^{-1}, which leads to a well resolved ^{1}H hyperfine splitting at lower temperature. At higher temperature the onset of rotation leads to EPR line broadening and a smearing of the hyperfine coupling constants.
Notably, a solution of **3-Si** in benzene yields even at 298 K a cw EPR spectrum with well-resolved ^{1}H hyperfine coupling that resembles the spectrum of **3-Si** in *n*-pentane but at 173 K (*Figure* 5.73). This behavior can be rationalized via the viscosities of both solvents, η = 0.603 mPa/sec for benzene and η = 0.214 mPa/sec for *n*-pentane, both at 298 K. In the solvent of higher viscosity, benzene, the dynamics sets on at a higher temperature than for the solvent of lower viscosity, pentane. Indeed, the viscosity of pentane at 173 K η_{173K} = 0.515 mPa/sec)[207] becomes very similar to the viscosity of benzene at 298 K.

The molecular and electronic structure of neutral two-coordinated silicon(I) radicals **3-Si**, **3-N** and **3-O** clearly differ to the recently reported, in solution generated, silenyl radicals $[(R_A)Si{=}C(R_A)(R)]^{\bullet}$ (R_A = SiMe(*t*Bu)$_2$, R = $SiMe_2$*t*Bu (**II-19**), 1-adamantyl (**II-20**),[206] which were identified as s-type radicals by (a) elongated Si–C^{carb} bonds compared to calculated Si=C^{sp2} double bonds, (b) decreased angles at the dicoordinated silicon center and (c) dramatic decreased $^{29}Si_{\alpha}$ hyperfine coupling constants (*Table 2.13*).

Table 2.13. Selected structural parameters and EPR spectrosocopic features of **3-Si**, **3-N** and **3-O** in comparison to literature known silenyl-radicals and CAAC-supported germanium(I) radicals.

Compound	E–$C^{carb/sp2}$ [a] / Å	$C^{carb/sp2}$–E–R[b] / (deg)	g_{iso} / (deg)	$a_{iso}(^{29}Si_{\alpha})$ / (mT)	$a_{iso}(^{14}N)$ / (mT)	Ref.
Si{Si(TMS)$_3$}(caac^{Me}) (**3-Si**)	1.870(2)	112.9(1)	2.0065[f]	3.81	0.44	*this*
Si{N(TMS)$_2$}(caac^{Me}) (**3-N**)	1.895(4)	106.6(2)	2.0044[f]	1.95	0.57	*work*
Si{OMes*}(caac^{Me}) (**3-O**)	1.865(2)	100.1(1)	2.0038[g]	1.24	0.62	
$(R_A)Si{=}C(R_A)(R_B)$[c]	1.744[e]	140.7[e]	2.001[h]	13.75	–	[206]
$(R_A)Si{=}C(R_A)(R_C)$[c]	1.761[e]	134.7[e]	2.001[h]	14.80	–	[206]
Ge{N(Mes)(R_D)}(caac^{Me})[d]	1.980(3)	110.2(1)	2.0075[i]	–	0.50	[152]
Ge{N(Dipp)(R_E)}(caac^{Cy})[d]	1.987(2)	114.9(1)	2.007[i]	–	0.53	[152]

[a]: E =Si, Ge. [b]: R = Si, N or O. [c]: R_A = SiMe(*t*Bu)$_2$; R_B = $SiMe_2$(*t*Bu); R_C = 1-adamantyl; [d]: Mes = C_6H_2-2,4,6-Me_3; R_D = $SiPh_3$; R_E = $SiMe_3$. [e] structural parameters calculated at the UPBE0/def2-TZVPP//UB97D/6–311+G(d,p) level of theory. [f]: *n*-pentane 293 K. [g]: toluene 293 K. [h] toluene 300 K. [i]: toluene 298 K.

Structural and electronic properties of the silicon(I) radicals **3-Si**, **3-N** and **3-O**, however, compare extremely well to recently reported CAAC-stabilized germanium(I) radicals [Ge{N(SiR$_3$)Ar}(caac$^{Me/Cy}$)]$^{\bullet}$ (caac^{Me}: Ar = Mes R = Ph; caac^{Cy}: Ar = Dipp, R = Me; (**I-57^{CAAC}**),[152] by similar angles of the C^{carb}–Si1–Si2 and C^{carb}–Ge–N2 skeleton, similar g_{iso} values and similar ^{14}N hfcc's, respectively (*Table 2.13*).

2.3.3 Comparative studies of the dynamics in silicon(I) radical 3-Si

Analysis of the potential energy hypersurface (PES) at the B97-D3(BJ)-ATM/def2-TZVP level of theory by Jens Rump revealed two dynamic processes of silicon-radical **3-Si**, rationalizing the line broadening of EPR spectrum of **3-Si** at ambient temperature (*Figure 2.27* a). The first process involves a rotation of the Si(TMS)$_3$-substituent at the Si1–Si2 bond, which proceeds via a rather low energy barrier of 19 kJ mol^{-1} and has no influence on the hfcc's of **3-Si**. The second process including the rotation of the caac^{Me} substituent about the Si1–C1 bond, proceeds via an unusual mechanism. In fact, the caac^{Me} carbene ligand does not rotate in this process but rather the two-coordinated Si1 atom about the Si2–C1 rotation axis (*Figure 2.28*).

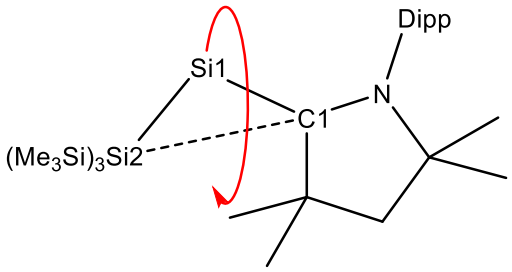

Figure 2.28. Dynamics of silicon(I) radical **3-Si** upon rotation of the dicoordinate silicon atom about the Si2–C1 rotational axis.

During this process the caac^{Me} carbene wobbles constantly, in order to keep the sum of angle at the C1 atom (355.7 – 360.0°) to the greatest possible extend unchanged. Rotation of the dicoordinated Si1 atom about the Si2–C1 rotation axis in **3-Si** via the *antiperiplanar* structure **3-Si-TS**(anti) (τ = 180.0°)[5] (*Figure 2.29*) leads to a fast inversion of the two enantiomers (S_a)-**3-Si** (τ = –165.0°) and (R_a)-**3-Si$_{calc}$** (τ = 165.0°) respectively, which proceeds via a low energy barrier of 4.9 kJ mol^{-1} and leads to enantiotopic C^3*Me$_2$* methylgroups, resulting in a well resolved ^{1}H hyperfine splitting into septets at 173 K (*Figure 2.27* b).

[5] The torsion angle (τ) is defined by the atoms Si2–Si1–C1–N. The clockwise angle ranges from 0° to 180°, whereas the anticlockwise angle ranges from 0° to –180°.

At higher temperatures, however, the larger barrier of 21.9 kJ mol^{-1} via (S_a)-**3-Si-TS$_{rot}$** (τ = −95.0°) might be overcome leading to the local minimum structure (S_a)-**3-Si*** (τ = −65.0°) which can be directly interconverted to the (R_a)-**3-Si*** enantiomer with a rather high lying energy barrier of 39.6 kJ mol^{-1} via **3-Si-TS**(syn) (τ = 0.0°) (*Figure 2.29*). During this process the Si2–Si1–C1 angle (α) undergoes a significant change, which is accompanied by a dramatic change of the Si1–C1–N angle (β). It is safe to assume that the change of the angle α has a significant effect on the spin-density of radical **3-Si**, which results in a significant effect on the observed hffc's, resulting in the line-broadening observed in the EPR spectrum of **3-Si** at ambient temperature (*Figure 2.27*, (a)).
The rotation of the Si–C^{CAAC} bond via the larger barrier proceeds via three transition states: two in *synclinal* ((*S$_a$*)-**3-Si-TS$_{rot}$** and (*R$_a$*)-**3-Si-TS$_{rot}$**) and one in *synperiplanar* conformation (**3-Si-TS**(syn)), whereas the rotation via the lower energy barrier proceeds via an *antiperiplanar* conformer (**3-Si-TS**(anti)), which lies 4.9 kJ mol^{-1} higher in energy than (*R$_a$*)-**3-Si$_{calc}$**, interconverting the two enantiomers.

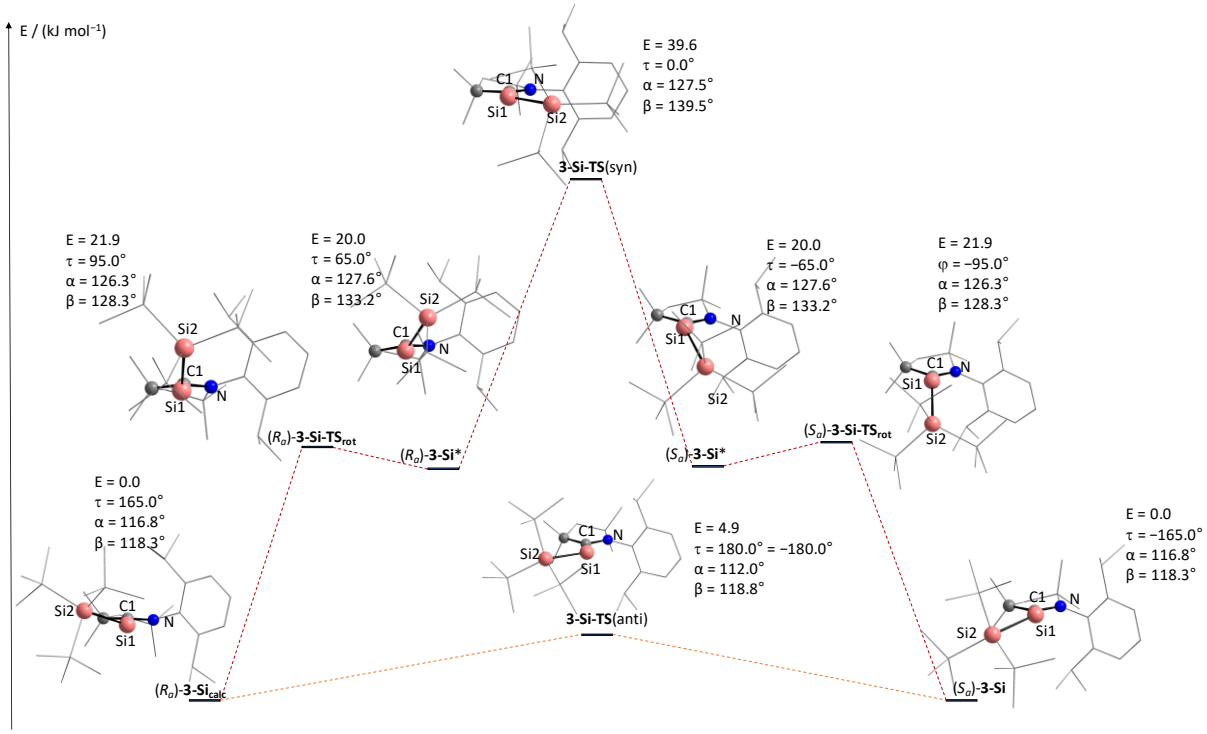

Figure 2.29. Proposed mechanism for the stereodynamics of **3-Si$_{calc}$**, *E* = energy versus (*S$_a$*)-**3-Si**$_{calc}$ in kJ mol^{-1}, τ: torsion angle N–C1–Si1–Si2, α: angle Si2–Si1–C1, β: angle Si1–C1–N.

2.3.4 Electronic structure of neutral two coordinated silicon(I) radicals

The electronic structure of the neutral two coordinated silicon(I) radicals **3-Si**, **3-N** and **3-O** was investigated by quantum chemical calculations, which were performed at the B97-D3(BJ)-ATM/def2-TZVP level of theory by Jens Rump. More details on the computional calculations are given in *chapter 5.11*. The structural parameters of the calculated structures in the gas phase do compare well to the structures derived from single-crystal X-ray diffraction (*Table 5.78* and *Table 5.79*).

The plot of the spin densities of the silicon(I) radicals (*Figure 2.30*) clearly reveals a π-type radical character in compounds **3-Si**, **3-N** and **3-O**. The spin density is mostly distributed among the Si, C^{carb} and N atoms. Overall the spin density at the silicon center decreases with increasing electronegativity of the substituents 53 > 41 > 32 % in the series **3-Si** < **3-N** < **3-O**, whereas the spin-density at the respective C^{carb} and N atom increases in **3-Si** (C^{carb} = 23 %, N = 16 %) < **3-N** (C^{carb}= 33 %, N = 21 %) < **3-O** (C^{carb} = 37 %, N = 22 %). Similarly, the partial charge at the silicon center increases with increasing electronegatvity of the substituents in **3-Si** (+0.40) < **3-N** (+0.88) < **3-O**(+0.93).

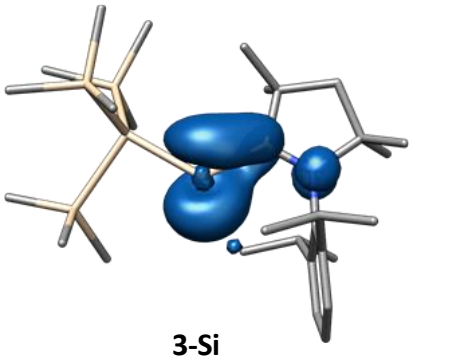

3-Si

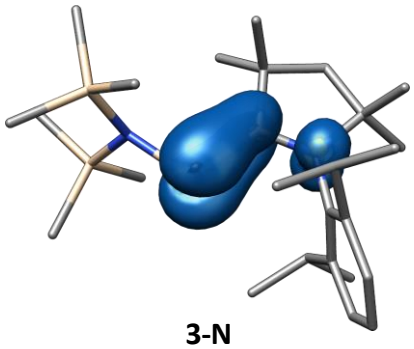

3-N

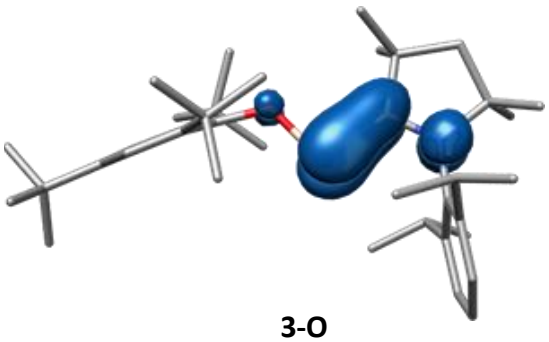

3-O

	3-Si	**3-N**	**3-O**
Si	+0.40 / 53	+0.80 / 41	+0.93 / 32
C^{carb}	−0.20 / 23	−0.22 / 33	−0.27 / 37
N	−0.40 / 16	−0.39 / 21	−0.39 / 22

natural charges (q) / natural spin density (%)

Figure 2.30. Plot of the spin densities of neutral two coordinated silicon(I) radicals **3-Si**, **3-N** and **3-O**, calculated at the B97-D3(BJ)^{ATM}/def2-TZVP level of theory by Jens Rump. Natural charges (q) and contributions of natural spin density (%) are given in the table.

The observed spin densities are in line with the experimental obtained ^{29}Si hyperfine coupling constants, which decrease 3.81 mT (**3-Si**) > 3.11 mT (**3-N**) >1.24 mT (**3-O**), whereas the ^{14}N hyperfine coupling constants increase 0.44 mT (**3-Si**) > 0.57 mT (**3-N**) > 0.62 mT (**3-O**). These findings suggest that the unpaired electron is distributed over the Si and C^{carb} centers with the spin density at the C^{carb} and N increasing with increasing electronegativty of the substituent.

Natural bond analysis of the wave function of **3-Si**$_{calc}$, **3-N**$_{calc}$ and **3-O**$_{calc}$ led to a leading natural Lewis α-spin- as well as a β-spin state structure (NLS). Combining both spin state structures resulted in a representative Lewis formula (α+β) for the electronic structure of the neutral two-coordinated silicon(I) radicals (*Figure 2.31*).

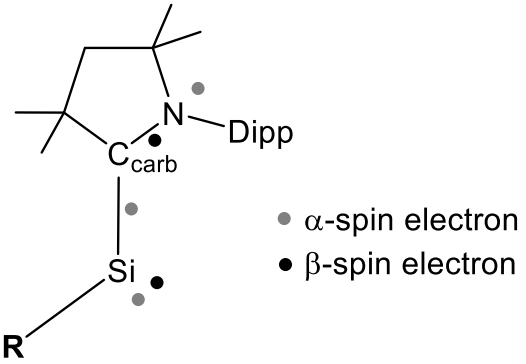

R = Si(SiMe$_3$)$_3$ (**3-Si**), N(SiMe$_3$)$_2$ (**3-N**), OMes* (**3-O**)

Figure 2.31. Combined α+β-spin state Lewis formula for neutral two coordinated silicon(I) radicals **3-Si**, **3-N** and **3-O**. Electrons placed in the middle of a bond represent π-bonding NBO's in only one spin set.

The representative Lewis formula (α+β) in silicon(I) radicals **3-R** features Si–C^{carb} and Si–R (R = Si, N, O) σ-bonds, as well as a lone pair at the silicon center with high Lewis occupancy above 1.84 e^- (*Table 2.14*). The spin density of the radicals can be mostly attributed to the α-spin NBO in the Si–C^{carb} π-bond, which features a high Lewis occupancy above 0.95 e^-. Additionally, two more spin centers are found, which due to the opposite direction of the spin states are canceling each other out: the α-spin NBO of pure p-character at the nitrogen atom and the β-spin NBO in the C^{carb}–N π-bond.
The π(Si–C^{carb}) α-NBO shows less polarization towards the C^{carb} atom in **3-Si** (57 %) but significant more polarization in **3-N** (62 %) and **3-O** (66 %), which results in a significant decrease in the spin density at the silicon centers in **3-N** and **3-O** (*Figure 2.30*). The π(C^{carb}–N) β-NBO is strongly polarized towards the N atom (71 %(**3-Si**), 70 % (**3-N**), 70 % (**3-O**)), and therefore compensating the α-spin NBO of pure p-character at the nitrogen atom, leading to the small spin density at this nitrogen atom as calculated (*Figure 2.30*).

The NRT-BO's of the Si–C^{carb} (1.34 – 1.48) and C^{carb}–N bond (1.49 – 1.59) in the silicon(I) radicals feature partial double bond character, reflecting the nature of the respective π-bonds occupied by a single electron.

Table 2.14. Selected results of the natural bond orbital (NBO), natural resonance theory (NRT) and natural population (NPA) analyses of neutral two-coordinated silicon(I) radicals calculated by Jens Rump at the B97-D3(BJ)^{ATM}/def2-TZVP level of theory.

NBO A–B	spin	occ.[a]	NHO (A,B)[b] hyb. (pol. in %)	WBI[c] A–B	NRT-BO[d] tot/cov/ion
3-Si					
LP(Sil)	α+β	1.84	$sp^{0.39}$		
LP(N)	α	0.86	p		
σ(Sil–C^{carb})	α+β	1.94	$sp^{5.54}$ (21), $sp^{1.44}$ (79)	1.07	1.48/0.86/0.62
π(Sil–C^{carb})	α	0.95	p (43), p (57)		
σ(C^{carb}–N)	α+β	1.98	$sp^{2.58}$ (35), $sp^{1.62}$ (65)	1.29	1.49/0.95/0.54
π(C^{carb}–N)	β	0.96	p (29), p (71)		
3-N					
LP(Sil)	α+β	1.92	$sp^{0.30}$		
LP(N)	α	0.88	p		
σ(Sil–C^{carb})	α+β	1.96	$sp^{5.48}$ (20), $sp^{1.43}$ (80)	0.96	1.34/0.65/0.69
π(Sil–C^{carb})	α	0.96	p (38), p (62)		
σ(C^{carb}–N)	α+β	1.98	$sp^{2.61}$ (35), $sp^{1.61}$ (65)	1.34	1.59/1.01/0.58
π(C^{carb}–N)	β	0.96	p (30), p (70)		
3-O					
LP(Sil)	α+β	1.94	$sp^{0.26}$		
LP(N)	α	0.89	p		
σ(Sil–C^{carb})	α+β	1.96	$sp^{5.66}$ (20), $sp^{1.45}$ (80)	0.93	1.38/0.63/0.76
π(Sil–C^{carb})	α	0.96	p (34), p (66)		
σ(C^{carb}–N)	α+β	1.98	$sp^{2.59}$ (35), $sp^{1.65}$ (65)	1.32	1.59/1.02/0.57
π(C^{carb}–N)	β	0.96	p (30), p (70)		

[a]: occ. = occupancy in e^-. [b]: NHO = Natural Hybrid Orbital, pol. (polarization) = $(C_i)^2$ 100%, where C_i = coefficient of NHO. [c]: Wiberg bond index. [d]: total, covalent and ionic NRT bond order.

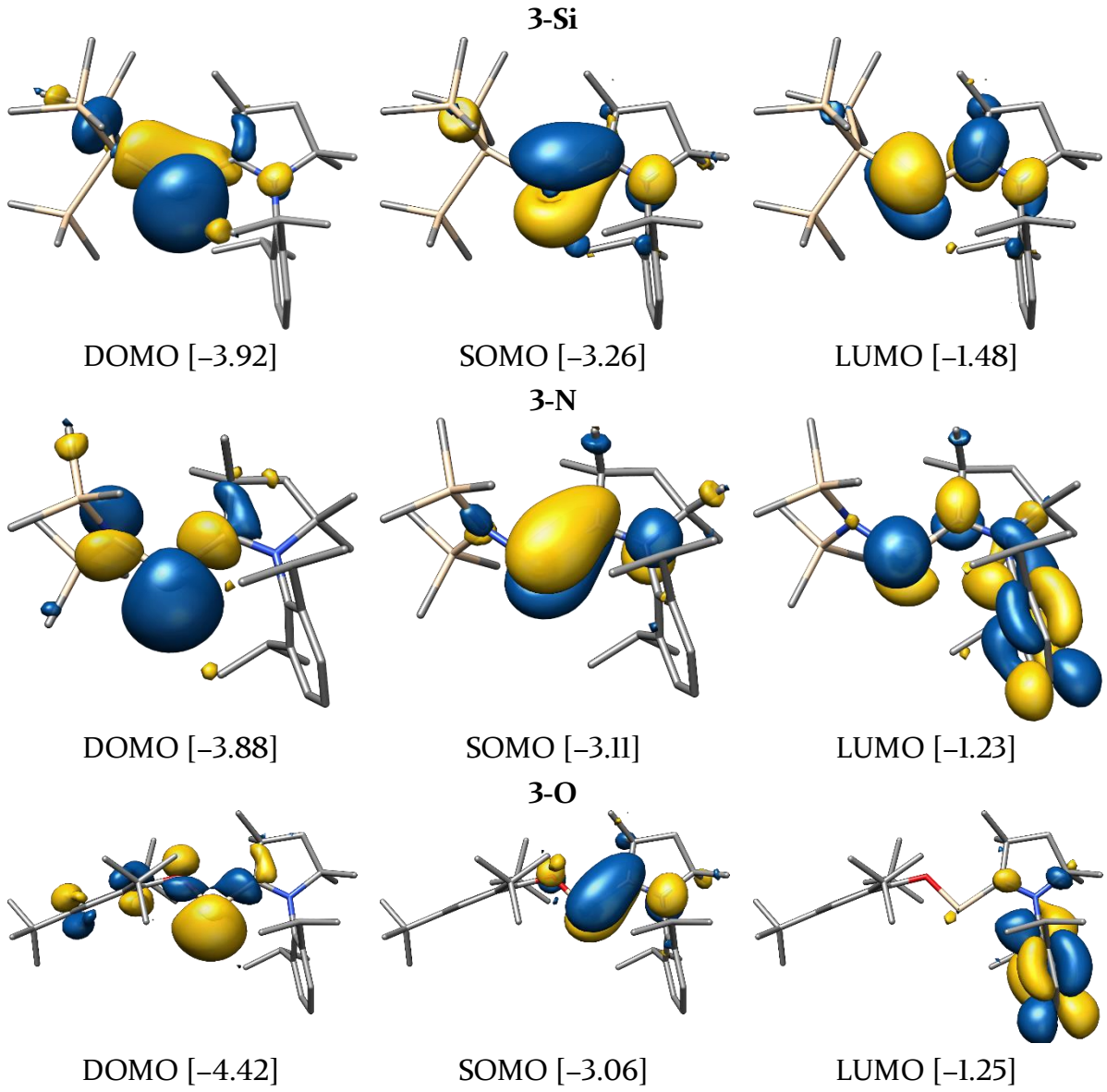

Figure 2.32. Selected Kohn-Sham molecular orbitals of **3-Si**, **3-N** and **3-O**. Their energy eigenvalues are given in eV; isosurface value = 0.04 $e^{1/2}$·$Bohr^{-3/2}$.

The NBO results are reflected in the frontier orbitals of **3-Si**$_{calc}$, **3-N**$_{calc}$ and **3-O**$_{calc}$ (*Figure 2.32*). The DOMO mainly contains the lone pair at the Si atom, the SOMO corresponds to Si–C^{carb} π-bond occupied by a single electron and the LUMO with exception of **3-O** corresponds to the antibonding π-combination of the Si–C^{carb}–N moiety.

2.3.5 Reactivity of neutral two-coordinated silicon(I) radicals

Preliminary reactivity studies of the neutral silicon(I) radicals **3-Si** and **3-N** towards KC_8 and 1,4-cyclohexadiene revealed the formation of potassium-silenides $SiK(R)(caac^{Me})$ (R = $SiTMS_3$ (**4-Si**), $NTMS_2$ (**4-N**)) and hydridosilenes $SiH(R)(caac^{Me})$ (R = $SiTMS_3$ (**5-Si**), $NTMS_2$ (**5-N**)), respectively. Compound **4-Si** and **5-Si** were isolated and fully characterized, also by X-ray diffraction analysis, whereas **4-N** and **5-N** were characterized by NMR spectroscopic methods. The isolation and characterization of potassium-silenides is described in *chapter 2.5*.

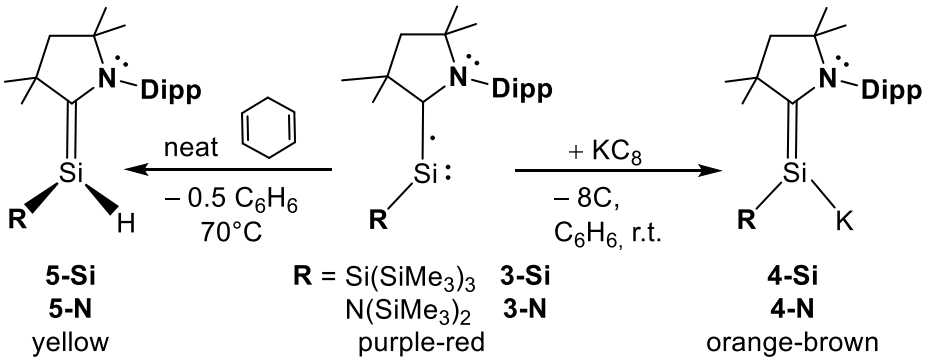

Scheme 2.8. Reactivity of silicon(I) radicals **3-Si** and **3-N** towards KC_8 and 1,4-cyclohexadiene, yielding potassium silenides **4-Si**, **4-N** and hydridosilenes **5-Si**, **5-N**.

2.3.5.1 Reactivity of silicon(I) radicals 3-Si and 3-N towards KC_8

The cyclic voltammogram of the neutral two-coordinated silicon(I) radicals $Si(SiTMS_3)(caac^{Me})$ (**3-Si**) (*Figure 2.33* (a)) and $Si(NTMS_2)(caac^{Me})$ (**3-N**) (*Figure 2.33* (b)) measured at ambient temperature in THF revealed a reversible $1e^-$ electron reduction with a half-wave potential at E_{pa} = –1.501 V (**3-Si**) and E_{pa} = –1.673 V (**3-N**) vs. $DMFc^{+/0}$, respectively.

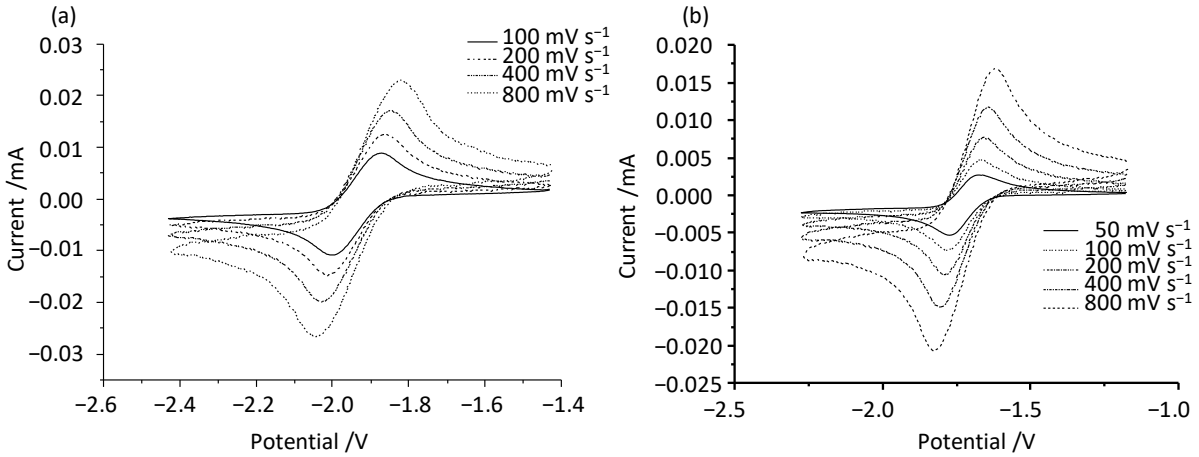

Figure 2.33. Single scan cyclic voltammogramms of (a): **3-Si** from (–2.5) to (–1.4) V and (b): **3-N** from (–2.5) to (–1.0) V at different scan rates at ambient temperature in fluorobenzene; electrolyte: 60 mM $(nBu_4N)[Al\{OC(CF_3)_3\}_4]$; reference electrode: decamethylferrocene $(DMFc)^{+1/0}$.

The observed reversible 1e⁻-reduction of **3-Si** and **3-N** was encouraging to reduce the compounds chemically. Indeed, reduction of radicals **3-Si** and **3-N** with 1.1 equivalents of KC_8 in benzene at ambient temperarture afforded the potassium-silenides $SiK(R)(caac^{Me})$ (R = $SiTMS_3$ (**4-Si**), $NTMS_2$ (**4-N**)), respectively. Compounds **4-Si** and **4-N**, also could be obtained upon direct reduction of the bromosilenes $SiBr(R)(caac^{Me})$ (R = $SiTMS_3$ (**2-Si**), $NTMS_2$ (**2-N**)) with three equivalents of KC_8. Both compounds will be discussed in depth in *chapter 2.5*.

2.3.5.2 Reactivity of silicon(I) radicals 3-Si and 3-N towards 1,4-cyclohexadiene

Heating of the silicon(I) radicals **3-Si** and **3-N** in neat 1,4-cyclohexadiene for 4 h at 70 °C, resulted in a color change from red-purple to yellow. Monitoring of the reaction mixture by ^1H NMR spectroscopy in (D_6)benzene revealed the quantitative formation of the hydridosilenes $SiH(R)(caac^{Me})$ (R = $SiTMS_3$ (**5-Si**), $NTMS_2$ (**5-N**)), respectively. Compound **5-Si** was isolated and fully characterized, while analogus compound **5-N** was characterized by NMR spectroscopy. After solvent evaporation the hydridosilene **5-Si** could be quantitatively obtained as a brick yellow solid. The compound is stable for months under argon atmosphere and slowly decomposes upon contact with air. It reversibly melts in a vacuum sealed capillary tube at 172 °C with only minor signs of decompositon, according to ^1H NMR spectroscopy in (D_6)benzene.The hydridosilene is highly soluble in *n*-hexane, benzene and THF, affording clear yellow solutions.

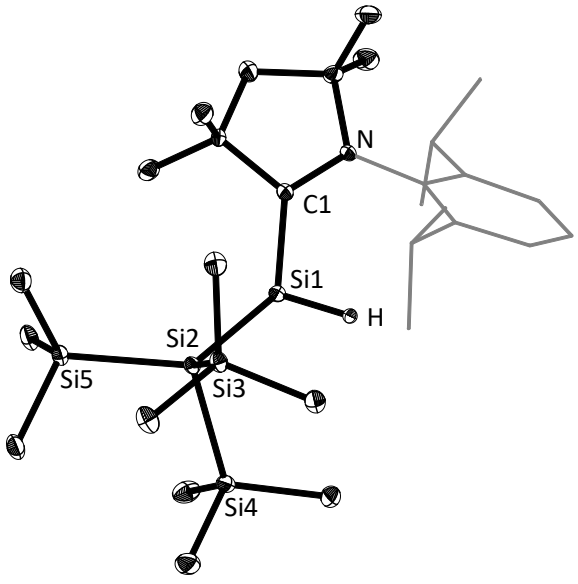

Figure 2.34. DIAMOND plot of the molecular structure of **5-Si** at 100 K. Thermal ellipsoids are set at 30 % propability and hydrogen atoms were omitted. In the depicted structure the Dipp-substituent of the $caac^{Me}$ ligand is presented in the wire-frame for the sake of clarity. Selected bond lengths [Å] and bond angles [°]: Si1–C1 1.811(1) [1.805(6), 1.811(5)], C1–N 1.372(6) [1.381(6), 1.362(6)], Si1–Si2 2.335(1) [2.341(1), 2.333(1)] C1–Si1–Si2 127.4(2) [127.3(2), 126.2(2)]. Values are given for three independent molecules in the unit cell.

Suitable single crystals of **5-Si** were grown from *n*-hexane after one week at –24 °C. The molecular structure of **5-Si** (*Figure 2.34*) features C_1-symmetry and a slightly trigonal pyramidalized silicon(II) center. The sum of angels at the Si-center of 339° (**5-Si**) ($\Sigma\measuredangle(Si)_{calc}$ = 339.5°) lies inbetween of that of the SiH(R)(NHC^4) (NHC^4 = IMe$_4$ = :C[N(Me)C(Me)]$_2$, R = Si*t*Bu$_3$) ($\Sigma\measuredangle(Si)$ = 290.84°)[208] and typical silenes ($\Sigma\measuredangle(Si)$ = 360.0°).[184] The Si–C^{carb} bond length of 1.809(2) Å is significantly shorter compared to that of SiH(R)(IMe$_4$) (1.942(3) Å)[208] and longer compared to the Si=C bonds of silenes (d(Si–C) = 1.702 – 1.764 Å).[184] The Si1–Si2 bond length 2.336(1) Å (**5-Si**) is slightly shorter than that of the silicon(I) radical **3-Si** (2.3992(5) Å) and that of the potassiumsilenide **4-Si** (2.397(3) Å), but comparable to 2-aminobromosilene **2-Si** (2.3655(6) Å) and the Si–Si single bond of SiH(R)(NHC^4) (2.4151(8) Å).[208] In terms of its structural parameters **5-Si** compares rather well to the caac^{Me}-stabilized silicon(I) dimer Si$_2$H$_2$(caac^{Me})$_2$ (*Table 2.15*).[129]

Table 2.15. Selected structural paramters of hydridosilene **5-Si** in comparison to related compounds.

Comp.	Si–Si / Å	Si–C^{carb} / Å	N–C^{carb} / Å	$\Sigma\measuredangle(Si)$ / (deg)	DP[a] / %	Ref.
SiBr(SiTMS$_3$)(caac^{Me}) **2-Si**	2.3655(6)	1.836(2)	1.353(2)	336.5	26	
Si(SiTMS$_3$)(caac^{Me}) **3-Si**	2.3992(5)	1.869(2)	1.349(2)	–	–	*this*
SiK(SiTMS$_3$)(caac^{Me}) **4-Si**	2.397(3)	1.813(9)	1.42(1)	352.9	8	*work*
SiH(SiTMS$_3$)(caac^{Me}) **5-Si**	2.336(1)[b]	1.809(2)[b]	1.372(6)[b]	339[c]	23	
				339.5[d]		
SiH(Si*t*Bu$_3$)(IMe$_4$)	2.4151(8)	1.942(3)	1.358(4)	291	77	[208]
Si$_2$H$_2$(caac^{Me})$_2$	2.334(1)	1.817(2)	1.362(2)	327.4	36	[129]

[a]: The degree of pyramidalization (DP) value of 0% describes a trigonal planar coordination of the silicon atom with the sum of bond angles equal to 360°. A DP value of 100% corresponds to a trigonal pyramidal coordination of the silicon atom with the sum of bond angles equal to 270°.
DP (in %) = 100 % · [360 − $\Sigma\measuredangle(Si)$ /(deg)]/90
[b]: Mean values of three independent molecules in the unit cell given. For the discussion the mean values x_u were used. Standard deviations were calculated using the following formula $\sigma^2 = \Sigma (x_i - x_u)^2/(n^2-n)$, x_i equals the invidual value and n equals the total number of invidual values.
[c]: The position of the silicon bonded hydrogen atom was localized and refined.
[d]: Calculated at the B97-D3(BJ)-ATM/def2-TZVP level of theory by Jens Rump.

The ^{29}Si{^{1}H} NMR spectrum of **5-Si** in (D$_6$)benzene displays resonances at –10.03 (TMS), –125.84 (*Si*(TMS)$_3$) and –47.7 ppm (*Si*=caac^{Me}), respectively. The ^{29}Si-resonance at the silenic Si-center (–47.7 ppm) is downfield shifted compared to that of the NHC-stabilized hydridosilylene SiH(R)(NHC^4) (δ = –137.8 ppm)[208] and upfield shifted compared to classical hydridosilenes, such as (SiMe^{t}Bu$_2$)HSi=C(SiMe^{t}Bu$_2$)(SiMe$_2^t$Bu) (δ = 134.0 ppm)[206] and (Dsi$_2$*i*PrSi)HSi=CH(SiMe$_3$) (δ = 116.1 ppm),[209] but appears remarkably close to that of Si$_2$H$_2$(caac^{Me})$_2$ ($\delta(^{29}Si)$ = –45.5 ppm).[129]

^{1}H NMR spectroscopy in (D_6)benzene reveals an averaged *Cs*-symmetry in solution for **5-Si**, even in (D_8)toluene at –80 °C (*Figure 5.9*). Quantum chemical calculations at the B97-D3(BJ)-ATM/def2-TZVP level of theory reveal an enantiomerization, which proceeds via a planar transition state and a rather low inversion barrier of 6.7 kJ mol^{-1}, suggesting a fast isomerization between the *S*- and *R*- enantiomers in solution.

The ^{1}H NMR resonance of (H)Si=C^{carb} in **5-Si** ($\delta(^{1}H)$ = 2.77 ppm, $^{1}J(^{29}Si,^{1}H)$ = 188.4 Hz) is drastically upfield shifted compared to that of hydridosilenes, such as (SiMe^{t}Bu$_2$)HSi=C(SiMe^{t}Bu$_2$)(SiMe$_2$^{t}Bu) ($\delta(^{1}H)$ = 6.67 ppm, $^{1}J(^{29}Si,^{1}H)$ = 173.73 Hz)[206] and (Dsi$_2$iPrSi)HSi=CH(SiMe$_3$) ($\delta(^{1}H)$ = 6.28 ppm, $^{1}J(^{29}Si,^{1}H)$ = 189.0Hz),[209] but compares well to that of Si_2H_2(caac^{Me})$_2$ ($\delta(^{1}H)$ = 3.59 ppm, $^{1}J(^{29}Si,^{1}H)$ = 163 Hz).[129]

The ν(Si-H) band for **5-Si** (2120 cm^{-1}) in the solid state lies in-between that of the hydridosilylene SiH(R)(IMe$_4$) (1984 cm^{-1}) [208] and the hydridosilene (Tbt)HSi=C(Ar)$_2$ (Tbt = C$_6$H$_2$-2,4,6-Dsi$_3$, Dsi = CH(SiMe$_3$)$_2$;(Ar)$_2$ = xanthenyl-group) (2280 cm^{-1}).[210]

The compound **5-Si** can be described as a pyramidal 2-aminosilene similar to the pyramidal 2-aminobromosilenes SiBr(R)(caac^{Me}) (R = SiTMS$_3$ (**2-Si**), Mes (**2-Mes**), PMes$_2$ (**2-P**), NTMS$_2$ (**2-N**) and OMes* (**2-O**)) discussed in this work (*chapter 2.2*). It features similar structural and spectroscopic parameters (d(Si–C^{carb}) = 1.809(2) Å, Σ^{0}Si = 339°, $\delta(^{29}Si)$ = –47.7 ppm) with those of Si_2H_2(caac^{Me})$_2$ (d(Si–C^{carb}) = 1.817(2) Å, Σ^{0}Si = 327.5°, $\delta(^{29}Si)$ = –45.5 ppm).[129]

2.3.6 Synthesis and properties of a (silenyl)phosphanyl radical (6)

The isolation of neutral two-coordinated phosphanyl-radicals remains especially challenging, due to their high proclivity to dimerize, even in the solid state.[211] Despite many efforts, only a few two coordinated phosphanyl radicals have been isolated and characterized by X-ray diffraction analysis (*Figure 2.35*). Most of them are resonance stabilized by either CAAC carbenes (**II-21**)[153] , NHI's (N-heterocylcic-imine, NHI = :N=C[N(Dipp)CH]$_2$) (**II-24** and **II-25**)[212] or by the redox couple of nitridovanadium trisanilide (IV/V) complexes (**II-23**)[213]. Due to their high degree of delocalization they can be rather described as π-type radicals, whereas dialkylphosphanyl-radical **II-22**[214], features a p-type radical, with the spin density mainly localized at the phosphorus center.

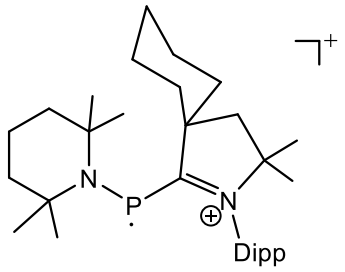

II-21

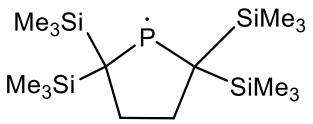

II-22

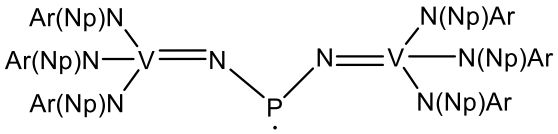

II-23

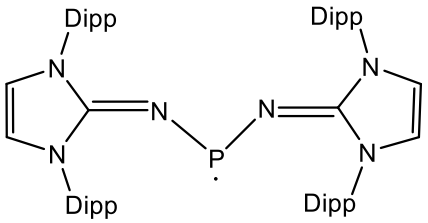

II-24

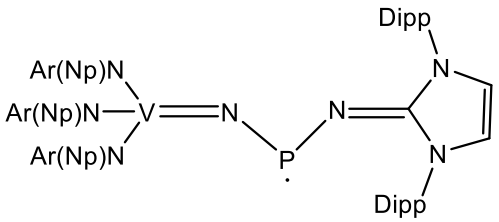

II-25

Figure 2.35. Literature known two-coordinated phosphanyl-radicals. Dipp = C_6H_3-2,6-*i*Pr_2; Np = neopentyl (CH_2–CMe_3); Ar = C_6H_3-3,5-Me_2).

On the other hand, the chemistry of phospha-silenes has flourished over the past two decades, enabling a multitude of interesting compounds with intruiging bonding features.[215] Examples substantiating this development are the stable 1,3-diphospha-2-silaallyl lithium Li[(Mes*)P=Si(ᵗBu)-P(Mes*)][216,217], a variety of phospha-sila-heterobutadiene systems,[215] carbene-stabilized dihalophosphasilenes (Trip)P=$SiCl_2$(carbene) (carbene = $CAAC^{1-3}$, NHC^{1})[136] (**I-47**$^{NHC/CAAC}$: see *Figure 1.18*) and the NHC-stabilized phosphasilenylidene (Mes*)P=Si(IDipp) (**I-37**^{NHC}: see *Figure 1.16*).[117] To the best of our knowledge, no two-coordinated neutral (silenyl)phosphanyl radical has been reported thus far.

Pyramidal 2-aminosilene **2-P**, indeed, upon one electron reduction with KC_8 provided a convenient access to the (silenyl)phosphanyl radical **6** (*Figure 2.36*), which provides the first example of a neutral two-coordinated phosphanyl-radical stabilized by a 2-aminosilenyl group, where the unpaired electron is fully delocalized over the P–Si–C^{CAAC} moiety.

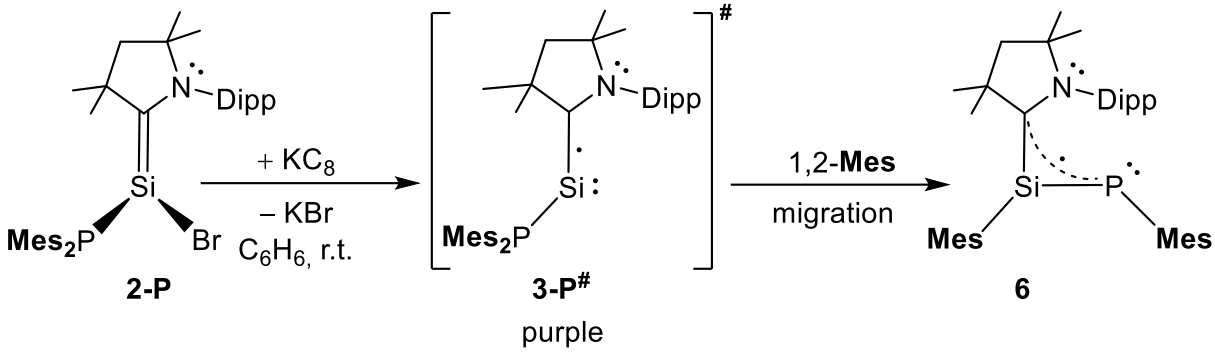

Figure 2.36. Synthesis of the silicon(I) radical **6** upon reduction of pyramidal 2-aminosilene **3-P**.

Reduction of $SiBr(PMes_2)(caac^{Me})$ (**2-P**) with 1.1 equiv. of KC_8 in benzene at ambient temperature was accompanied by an immediate color change to dark purple. Upon stirring of the reaction mixture for 0.5 h at ambient temperature the dark purple color vanished and the suspension slowly turned orange-brown. Monitoring of the reaction mixture by ^{1}H NMR spectroscopy in (D_6)benzene revealed the selective formation of a paramagnetic compound with small amounts of unknown impurities (below the threshold of the ^{13}C satellites of the deuterated solvent). Red single crystals of **6** were obtained from *n*-pentane at –24 °C in 33 % yield. The compound is highly pyrophoric, decomposing immediately upon contact with air. Radical **6** decomposes unselectively upon melting at 172 °C. The compound is well soluble in *n*-pentane, benzene and THF, affording orange-brown solutions.

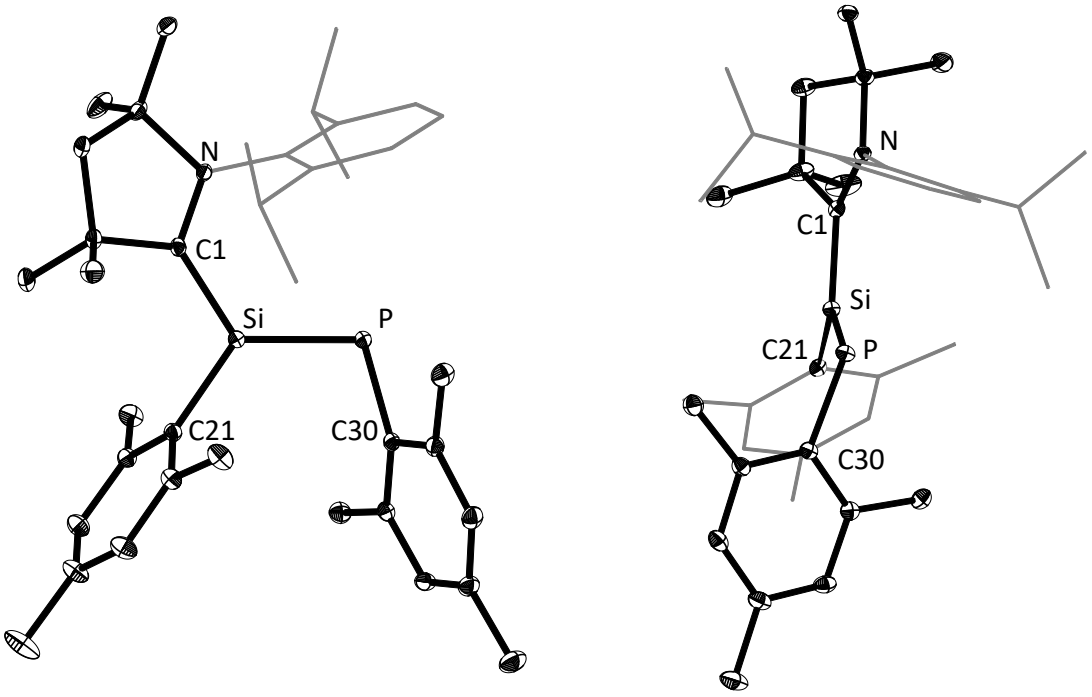

Figure 2.37. (Left) DIAMOND plot of the molecular structure of radical **6**. Thermal ellipsoids are set at 30 % propability level and hydrogen atoms were omitted. In the depicted structure the Dipp-substituent of the caac^{Me} ligand is presented in the wire-frame for the sake of clarity. Selected bond lengths [Å], bond angles [°] and torsion angles [°]: Si–P 2.1080(8), P–C30 1.855(2), Si–C1 1.813(2), Si–C21 1.877(2), N–C1 1.369(3), C30–P–Si 103.11(7), C1–Si–P 122.29(7), C1–Si1–C21 113.19(9) C21–Si–P 124.45(7), N–C1–Si–P 12.7(2), C1–Si–P–C30 164.7(2), C21–Si–P–C30 –18.7(2). (Right) Different view of **6** illustrating the relative orientation of the caac^{Me} carbene with respect to the Si=P bond.

The solid-state structure of **6** was determined by sc-XRD analysis (*Figure 2.37*). The planar core of the structure consists of the atoms C1, Si, P, C30, in which the trigonal planar coordinated silicon center ($\Sigma\sphericalangle$(Si) = 359.9°) is connected to a V-shape dicoordinated P atom (C30-P-Si1 = 103.11(7)°) via a Si=P bond (2.108(1) Å). The P-Mes and caac^{Me} groups are orientated trans to each other (τ(C1-Si-P-C30) = 164.7(2)°) and the Mes substituents are orientated orthogonal with respect to the planar core of the molecule. The caac^{Me} ligand (τ(N-C1-Si-P) = 12.7(2)°), in contrast, is orientated in plane to the Si=P bond (*Figure 2.37* right), suggesting a delocalization of the unpaired electron along the atoms Si, P and C^{carb} in **6**. The Si=P bond length in **6** (2.1080(8) Å) compares well to literature known phosphasilenes (2.062(1) – 2.1585(9) Å)[215] and the isolobal NHC-supported heterocumulene (Mes*)P=Si(NMes)(IDipp) (2.094(1) Å).[218]

The Si–C^{carb} bond length in **6** (1.813(2) Å), is signifcantly shortened compared to its starting material SiBr(PMes$_2$)(caac^{Me}) (**2-P**) (1.850(8) Å), which is in line with a significant elongation of the N–C^{carb} bond in **7** (1.369(3) Å) compared to **2-P** (1.33(1) Å), indicating strong π-character in the Si–C^{carb} bond.

Radical **6** clearly differs from (Mes*)P=Si(NMes)(IDipp) and the NHC-stabilized phosphasilenylidene ((Mes*)P=Si(IDipp)) by a significant decrease of the Si–C^{carb} bond length, which is in line with the more co-planar orientation of the carbene with respect to the Si=P moiety (*Table 2.16*). This can be attributed to the delocalization of the unpaired electron in **6** over the P–Si–C^{carb} moiety.

Table 2.16. Selected structural parameters of radical **7** and related literature known compounds.

Comp.	Si–P / Å	Si–C^{carb} / Å	Si-P-R / (deg)	φ_{carb} [a] / (deg)	Ref.
$SiBr(PMes_2)(caac^{Me})$ (**3-P**)	2.237(3)	1.850(8)	–	–	
	2.240(3)	1.862(8)			*this*
(Mes)P=Si(Mes)($caac^{Me}$) (**6**)	2.108(1)	1.813(2)	103.1(1)	21.5(1)	*work*
(Mes*)P=Si(NMes)(IDipp)[b]	2.094(1)	1.936(2)	102.6(1)	117.4(6)	[218]
(Mes*)P=Si(IDipp)	2.118(1)	1.960(2)	102.6(1)	95.9(1)	[117]
(Trip)P=$SiCl_2$($caac^{Me}$)[c]	2.121(1)	1.944(2)	105.6(1)	–	[136]
(Trip)P=$SiCl_2$(IDipp)	2.121(1)	1.928(3)	95.0(1)	–	[136]

[a]: φ_{carb} the angle between the least-squares plane of the NHC or CAAC five-membered ring and the plane defined by the P=Si–C^{carb} atoms. [b]: Mes*= C_6H_2-2,4,6-*t*Bu_3, [c]: Trip = C_6H_2-2,4,6-*i*Pr_3

The ^{1}H-NMR spectrum of radical **6** in (D_6)benzene (*Figure 5.7*) at ambient temperature featured broad signals, as expected for a paramagnetic compound. In comparison to the two coordinated neutral silicon(I) radicals **3-Si** and **3-N**, the compound appeared to be stable in solution and did not show any diamagnetic decomposition products in the ^{1}H NMR spectrum after one week at ambient temperature.

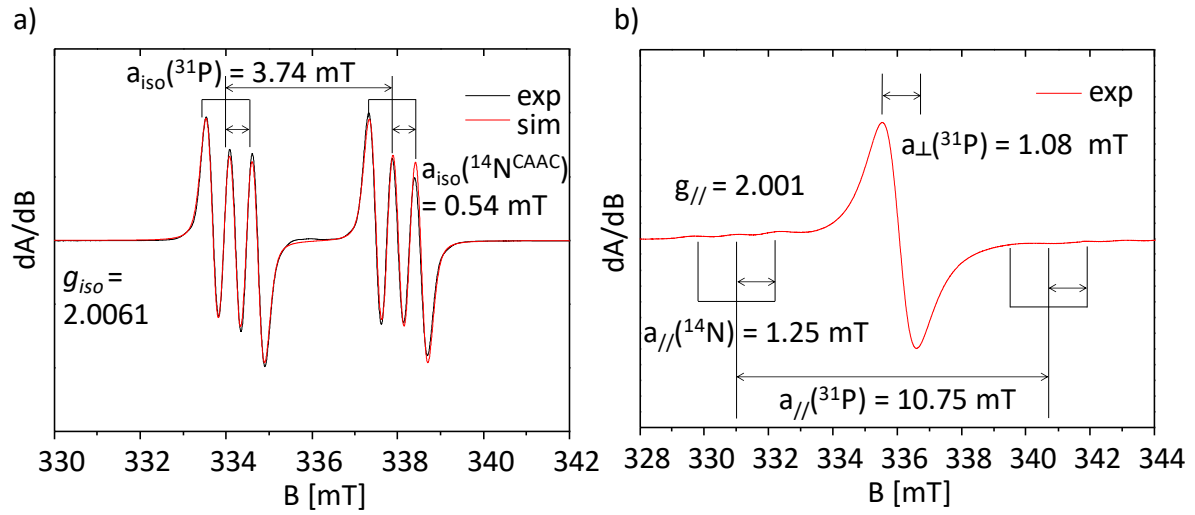

Figure 2.38. Experimental (–) and simulated (–) cw X-band EPR spectra of **6** in *n*-pentane at a) 293 K (g_{iso} = 2.00611, $a_{iso}(^{31}P)$ = 3.74 mT, $a_{iso}(^{14}N)$ = 0.54 mT); b) EPR spectrum of **6** in *n*-pentane at 100 K (frozen solution) with assigned hfcc constants of **6**, featuring axial symmetry: $g_{//}$ = 2.0010, $a_{//}(^{31}P)$ = 10.75 mT, $a_{//}(^{14}N)$ = 1.25 mT, $a_{\perp}(^{31}P)$ = 1.08 mT.

Further insight into the structure of the neutral two coordinated phosphanyl-radical **6** was provided by continuous wave (cw) EPR spectroscopy at X-band frequency (B_0 = 9.35 GHz).

EPR spectra with resolved hyperfine coupling pattern could be obtained from samples of **6** in *n*-pentane solution at 293 K (*Figure 2.38* a). The spectrum displays a multiplet with a g_{iso} value of 2.0061, which is greater than that of the free electron value of 2.0023 and compares well to the radical cation **II-21** (g_{iso} = 2.007).[153] The hyperfine pattern can be described as a doublet of triplets, due to the coupling of the unpaired electron to the phosphorus and the single nitrogen in the $caac^{Me}$ moiety with hyperfine coupling constants of $a_{iso}(^{31}P)$ = 3.74 mT and $a_{iso}(^{14}N)$ = 0.57 mT, respectively. In the temperature range 173 K – 293 K in *n*-pentane no signal of weaker intensity of the ^{29}Si-isotopologue of **6** (natural abundance 4.67 %) could be observed. Recorded EPR spectra in the frozen solution at 100 K (*Figure 2.38* b) displayed typical axial symmetry. The g-factors and hfc tensors were determined as follows: $g_{//}$ = 2.0010, $a_{//}(^{31}P)$ = 10.75 mT, $a_{//}(^{14}N)$ = 1.25 mT, $a_{\perp}(^{31}P)$ = 1.08 mT. The at the B97-D3(BJ)^{ATM}/def2-TZVP level of theory calculated isotropic ^{31}P and ^{14}N hyperfine coupling constants of 4.31 mT and 0.15 mT deviate slightly from the experimentally obtained values in **6** (3.74 mT, 0.57 mT) but are within the limit of deviation of the used method. In addition, the ^{14}N hyperfine coupling constant in **6** (0.57 mT) agrees well with that of the radical cation **II-21** (g_{iso} = 2.007, $a_{iso}(^{14}N)$ = 0.4 mT).[153] The ^{31}P hyperfine coupling constant in **6** (3.74 mT) is much smaller compared to literature known isolated two-coordinate phosphanyl radicals (*Table 2.17*) and s-type phosphanyl radicals (6.5 – 10 mT), which were generated in solution,[219,220] suggesting a high degree of delocalization of the unpaired electron at the P, Si and C^{carb} centers.

Table 2.17. Comparison of EPR spectroscopic features of phosphanyl radical **6**, compared to silicon(I) radicals **3-Si**, **3-N**, **3-O** and literature known two-coordinated phosphanyl radicals.

Comp.	**EPR cond.**	**g_{iso}**	**M[a]**	**$a_{iso}(^{31}P)$ [mT]**	**$a_{iso}(^{29}Si\alpha)$ [mT]**	**$a_{iso}(^{14}N)$ [mT]**	**Ref.**
$Si(SiTMS_3)(caac^{Me})$ (**3-Si**)	*n*-pent., 293K	2.0065	t	–	3.81	0.44	
$Si(NTMS_2)(caac^{Me})$ (**3-N**)	*n*-pent., 293K	2.0044	t	–	3.11	0.57	*this*
$Si(OMes^*)(caac^{Me})$ (**3-O**)	tol., 293K	2.0038	t	–	1.24	0.62	*work*
$(Mes)P{=}Si(Mes)(caac^{Me})$ (**6**)	*n*-pent., 293K	2.0061	dt	3.74	–	0.54	
$[P(R)(caac^{Cy})]^+ [BAr_4^F]^-$ (**II-21**) [b]	C_6H_5F, 298 K	2.007	dt	9.9	–	0.40	[153]
$P(Alkyl)_2$ [c] (**II-22**)	3-MP[d], 298 K	2.0086	d	9.63	1.73	–	[214]
$P(NV\{NNp(Ar)\}_3)_2$ [d] (**II-23**)	toluene, 298 K	1.984	m	4.25 2.38(^{51}V)	–	–	[213]
$P(NV\{NNp(Ar)\}_3)(NHI)$ (**II-25**) [d]	THF, 298 K	1.981	oct.	weak 5.8(^{51}V)	–	–	[212]
$P(NHI)_2$ [e] (**II-24**)	THF, 298 K	2.005	d	7.8	–	–	[212]

[a] Multiplicity (M) of the EPR signal.
[b]: R = 2,2,6,6-tetramethylpiperidin-1-yl, $caac^{Cy}$ = $C[N(Dipp)CH_2CR_2]$, (R_2 = $(CH_2)_5$, Dipp = C_6H_3-2,6-*i*Pr_2).
[c]: $P(Alkyl)_2$ = 2,2,5,5-tetrakis-(trimethylsilyl)-1-phosphacyclopentane-1-yl.
[d]: Np = neopentyl, Ar = C_6H_3-3,5-Me_2
[e]: NHI = :N=C[N(Dipp)CH]$_2$. [d]: 3-methyl-pentane.

2.3.7 Electronic structure of (silenyl)phosphanyl radical 6

The electronic structure of the (silenyl)phosphanyl radical **6** was investigated by quantum chemical calculations, which were performed at the B97-D3(BJ)-ATM/def2-TZVP level of theory by Jens Rump. More details on the computional calculations are given in *chapter 5.11*. The structural parameters of the calculated structure in the gas phase do compare well to the structure derived from single-crystal X-ray diffraction of **6** (*Table 5.79*).

The plot of the spin density of the phosphanyl-radical **6** (*Figure 2.39*) reveals π-type radical with the spin density mainly distributed over the P, C^{carb} and N atoms. Remarkably, no spin density at the silicon center is found, which is in line with the observations of the EPR spectrum of **6**, that does not show any ^{29}Si hyperfine coupling. The high population of the spin density at the P atom (39 %) and the C^{carb} atom (38 %), suggests that the unpaired electron at the phosphorus atom is stabilized by the delocalization to the carbene center. Thus, the compound can be seen as the borderline case between a phosphanyl radical connected to a 2-aminosilenyl-substituent or a $caac^{Me}$ stabilized phosphasilenyl radical.

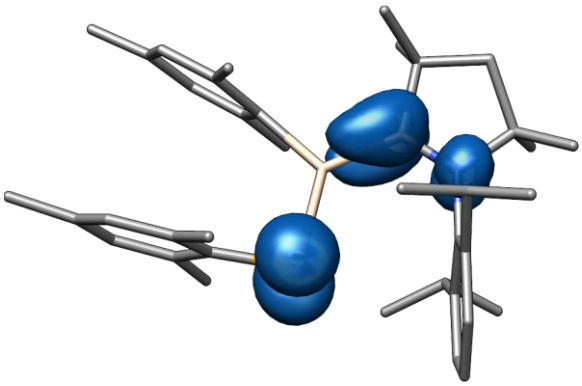

6

	natural charges (q)	natural spin density (%)
Si	+1.10	−1
C^{carb}	−0.30	38
N	−0.40	20
P	−0.09	39

Figure 2.39. Plot of the spin density of (silenyl)phosphanyl-radical **6**, calculated at the B97-D3(BJ)^{ATM}/def2-TZVP level of theory by Jens Rump. Natural charge(q) and contributions of natural spin density (%) of atoms are given in the table.

Natural bond analysis of the wave function of $\mathbf{6}_{calc}$ led to a leading natural Lewis α-spin- as well as a β-spin state structure (NLS). Combining both spin state structures resulted in a representative Lewis formula (α+β) for the electronic structure of the (silenyl)phosphanyl radical (*Figure 2.40*).

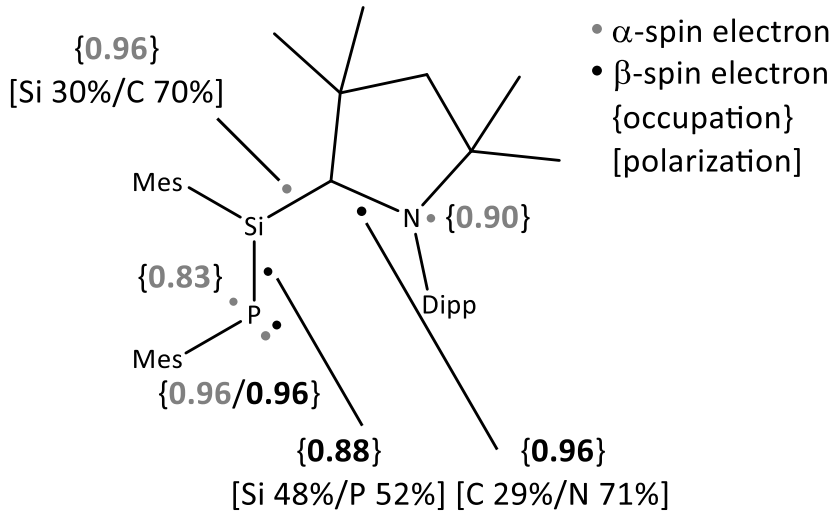

Figure 2.40. Combined α+β-spin state Lewis formula for phosphanyl radical **6**. Electrons placed in the middle of a bond represent π-bonding NBO's in only one spin set.

The representative Lewis formula (α+β) of the phosphanyl radical features P–Si, Si–C^{carb} and C^{carb}–N σ-bonds, as well as a lone pair at the phosphorus center with high Lewis occupancy above 1.92 e^- (*Table 2.18*). The spin density of the phosphanyl radical **6** can be mostly attributed to three NBOs occupied by a single electron, an α-spin NBO at the phosphorus atom with pure p-character, a β-spin NBO in the Si–P π-bond and an α-spin NBO in the Si–C^{carb} π-bond. Additionally, two more spin centers are found, which do to the opposite direction of the spin states are canceling each other out: the α-spin NBO of pure p-character at the nitrogen atom and the β-spin NBO in the C^{carb}–N π-bond.

Table 2.18. Selected results of the natural bond orbital (NBO), natural resonance theory (NRT) and natural population (NPA) analyses of the phosphanyl radical **6** at the B97-D3(BJ)^{ATM}/def2-TZVP level of theory calculated by Jens Rump.

NBO A–B	spin	occ.[a]	NHO (A,B)[b] hyb. (pol. in %)	WBI[c] A–B	NRT-BO[d] tot/cov/ion
			6		
$LP_1(P)$	α+β	1.92	$sp^{0.5}$		1.36/-/-
$LP_2(P)$	α	0.83	p		
LP(N)	α	0.90	p		0.43/-/-
σ(Si–P)	α+β	1.92	$sp^{1.6}$ (43), $sp^{4.5}$ (57)	1.45	1.50/1.26/0.24
π (Si–P)	β	0.88	p (48), p (52)		
σ(Sil–C^{carb})	α+β	1.96	$sp^{2.3}$ (25), $sp^{1.5}$ (75)	1.01	1.31/0.72/0.59
π(Sil–C^{carb})	α	0.96	p (30), p (70)		
σ(C^{carb}–N)	α+β	1.98	$sp^{2.4}$ (37), $sp^{1.7}$(63)	1.25	1.52/1.01/0.51
π(C^{carb}–N)	β	0.96	p (29), p (71)		

[a]: occ.= occupancy in e^-. [b]: NHO = Natural Hybrid Orbital, pol. (polarization) = $(C_i)^2 \cdot 100\%$, where C_i = coefficient of NHO. [c]:Wiberg bond index. [d]: total, covalent and ionic NRT bond order.

The high spin density at the phosphorus center can be attributed to the α-spin NRT-BO in the p-orbital of this phosphorus atom. The π(Si–P) β-NBO does not show significant polarization and thus is equally shared between the phosphorus- and the silicon atom, whereas the π(Si–C^{carb}) α-NBO is strongly polarized to the carbene atom (70 %), leading to a significant spin density at the carbene center as calculated (*Figure 2.39*). On the other hand, the π(C^{carb}–N) β-NBO is strongly polarized towards the N atom (71 %), and therefore compensates the α-spin NBO of pure p-charcter at the nitrogen atom, leading to a smaller spin density at this nitrogen atom as calculated (*Figure 2.39*).

The NBO results are reflected in the frontier orbitals of $\mathbf{6}_{calc}$ (*Figure 2.41*). The DOMO corresponds mainly to a P–Si π-bond, the SOMO contains the unpaired electron in a π-type orbital that is the bonding combination of the π*(C^{carb}–N) with the π*(P=Si) orbital. The LUMO, features a π*-orbital in the Mes substituent, whereas the LUMO+5 features the antibonding π*-combination of the P–Si–C^{carb}–N moiety.

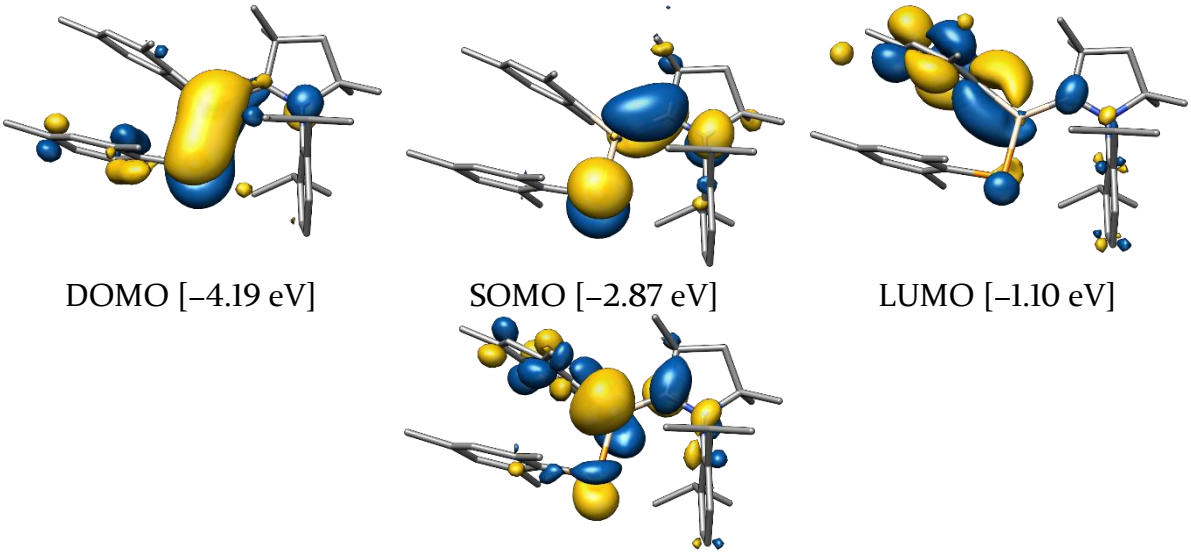

Figure 2.41. Selected Kohn-Sham quasi-restricted molecular orbitals of the phosphanyl radical **6**. Their energy eigenvalues are given in eV; isosurface value = 0.04 $e^{1/2}$·$Bohr^{-3/2}$.

2.4 CAAC-Stabilized Disilicon(I) Compounds

2.4.1 Introduction

NHC and CAAC-stabilized disilicon(I) compounds, especially halogen-disilicon(I) compounds are promising starting materials in low molecular silicon chemistry.[79] The first NHC-stabilized disilicon(I) compound was observed upon reduction of $SiCl_4(NHC^I)$ (NHC^I = IDipp = :C[N(Dipp)CH]$_2$) with 6-equivalents of KC_8 next to the NHC-stabilized disilicon(0) compound $Si_2(NHC^I)_2$ by Robinson et al. in 2008 and could be isolated in a rather low yield of 6.1 %.[114] A more elegant way to access NHC-stabilized dihalodisilicon(I) compounds was described by the research group of Filippou, upon selective oxidation of $Si_2(NHC^I)_2$[114] with 1,2-dihaloethane (*Scheme 2.9*). [127] The compounds can be strikingly viewed as bis NHC adducts of dihalodisilynes

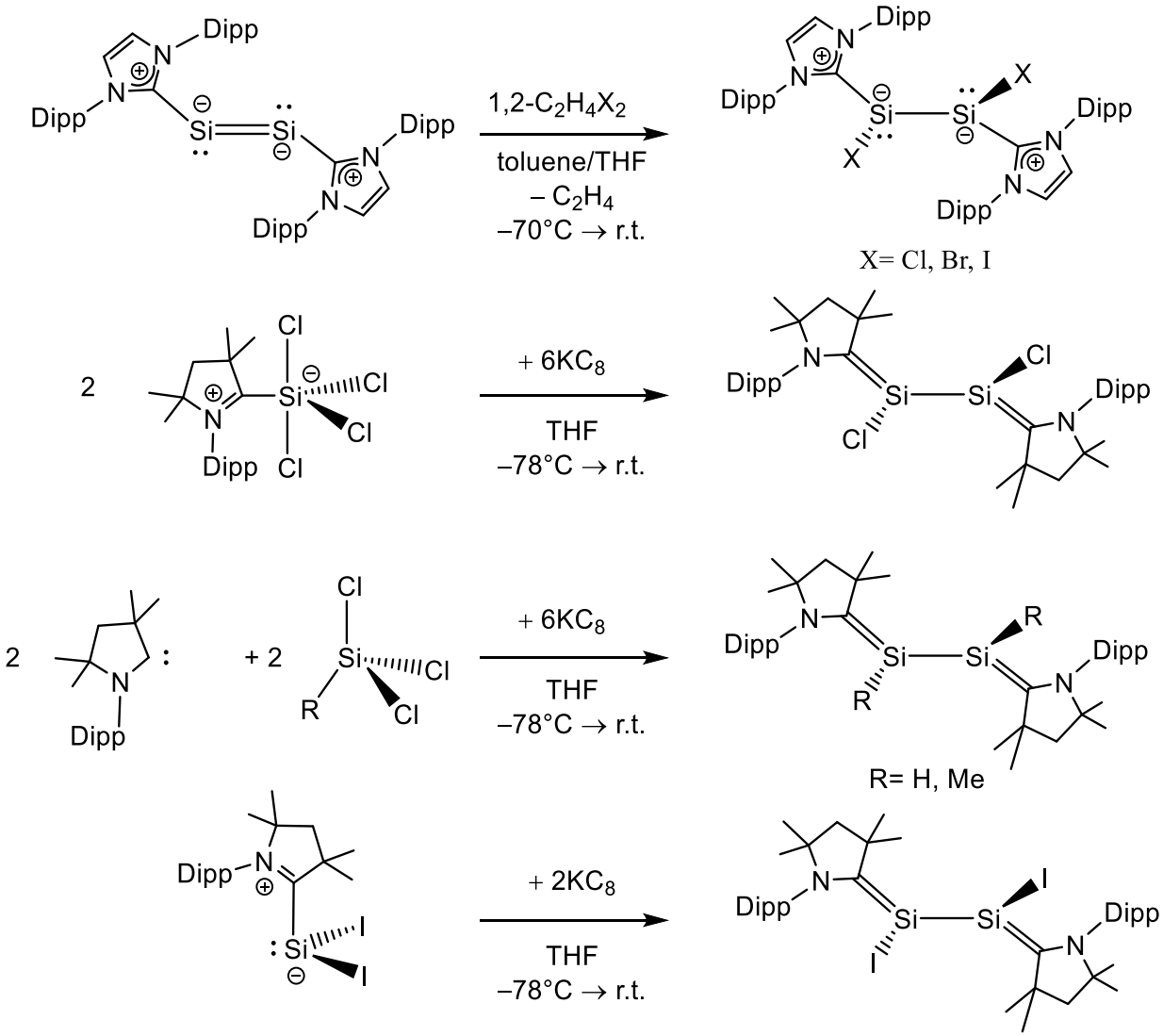

Scheme 2.9. Different synthetic approaches to NHC and CAAC-stabilized disilicon(I) compounds.

In 2013, the first CAAC-stabilized disilicon(I) compound was isolated, upon reduction of $(caac^{Me})SiCl_4$ with 6 equivalents of KC_8 in THF by Roesky et al.[128] In contrast to NHC-stabilized silicon(I) compounds, the CAAC-supported compounds feature significantly more planarized silicon centers.

In fact, the compounds can be best described as 1,4-diamino-2,3-disilabutadienes.[128] In the following years by the research group of H. Roesky, utilizing the one pot approach of reducing silanes $SiRCl_3$ (R = H, Me) in presence of CAAC carbenes with 6 equivalents of KC_8 led to the formation of functionalized disilicon(I) compounds $Si_2R_2(caac^{Me})_2$ (R = H, Me).[129,130]

An alternative route to CAAC-stabilized disilicon(I) compounds was provided by the research group of So. Reduction of the dihalosilylene $SiI_2(caac^{Me})$ with 1 equivalent of KC_8 led to the formation of the diiodide-disilicon(I) compound $Si_2I_2(caac^{Me})_2$.[121]

Recently, the aryl substituted disilicon(I) compound $Si_2Ph_2(caac^{Me})_2$ [6] has been reported and was obtained as a byproduct via the one pot reduction of a phosphenylsilane with KC_8 in presence of $caac^{Me}$ carbene (*Scheme 2.10*).[131]

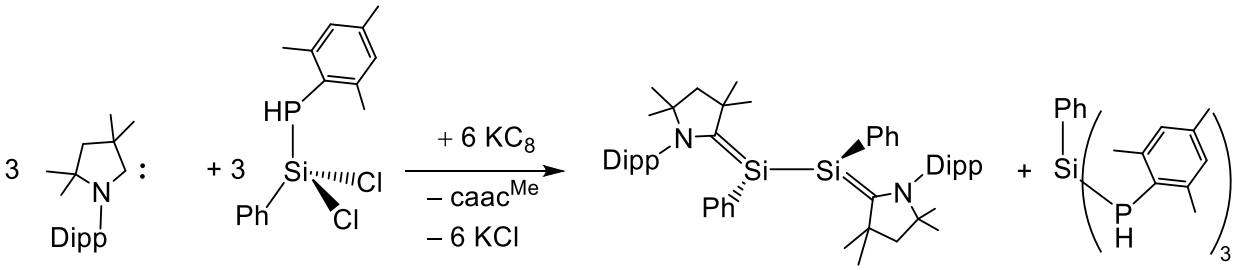

Scheme 2.10. Serendipitous synthesis of $Si_2Ph_2(caac^{Me})_2$.

Besides the tremendous efforts in isolating $caac^{Me}$-stabilized disilicon(I) compounds, no reactivity of these compounds have been reported thus far.

[6] The compound could be only charactized by X-ray diffraction, no NMR spectroscopic data is given in the reference [131].

2.4.2 Synthesis and properties of $Si_2Br_2(caac^{Me})_2$

The Si(I) compound $Si_2Br_2(caac^{Me})_2$ (**9-Br**) can be obtained either upon reduction of $SiBr_2(caac^{Me})$ with 1 equiv. of KC_8 or directly upon reduction of $SiBr_4(caac^{Me})$ with 3 equiv. of KC_8. In the latter case the compound can be isolated as dark purple solid in 50 % overall yield after work up, in comparison to the direct approach with a yield of 36 %. The compound is highly air sensitive and decomposes upon melting at 173 °C in a vacuum sealed capillary. It is moderately soluble in aliphatic solvents and well soluble in aromatic solvents and THF, affording deep red-purple colored solutions.

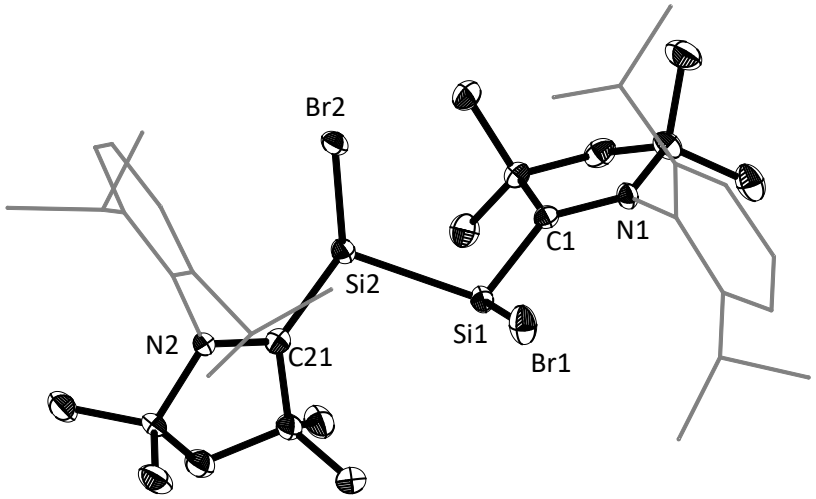

Figure 2.42. DIAMOND plot of the molecular structure of **9-Br**, thermal ellipsoids are set at 30 % probability, and hydrogen atoms were omitted. The Dipp substituent of the $caac^{Me}$ ligand is presented in the wire frame for the sake of clarity. Selected bond lengths [Å], bond angles [°] and torsion angles [°]: Si–C1 1.844(4), Si2–C21 1.844(4), Si1–Si2 2.341(2), Si1–Br1 2.294(1), Si2–Br 2.297(1), N1–C1 1.347(5), N2–C21 1.348(5), Br1–Si1–Si2 108.5(1), C1–Si1–Br 112.0(1), C1–Si1–Si2 107.1(1), Br2–Si2–Si1 108.0(1), C21–Si2–Br2 111.8(1), C21–Si2–Si1 106.3(1), C21–Si2–Si1–C1 169.5(2), N1–C1–Si1–Si2 150.5(3), N2–C21–Si2–Si1 150.1(3), Br1–Si1–Si2–Br2 50.7(1).

The molecular structure of **9-Br** was determined by single X-ray diffraction (*Figure 2.42*). The compound features two stereogenic slightly trigonal pyramidalized silicon centers ($\Sigma\measuredangle$(Si1) = 327.6°, $\Sigma\measuredangle$(Si2) = 326.1°) of the same configuration (*R*,*R*). The bromine substituents of **9-Br** adopt a synclinal conformation (τ(Br2–Si2–Si1–Br1) = 50.7(1)°) and the sterically more demanding $caac^{Me}$ groups an antiperiplanar conformation (τ(C21–Si2–Si1–C1) = 169.5(2)°). The two carbene groups are orientated orthogonal with respect to each other (carbene to carbene plane twist angle = 76.3(2)°).

The silicon centers in **9-Br** are drastically less pyramidalized (DP(Si1) = 36 %, DP(Si2) = 38 %) in comparison to the NHC-stabilized $Si_2Br_2(IDipp)_2$ (DP(Si1) = 62 %, DP(Si2) = 64 %),[127] which can be seen by a dramatic decrease of the $Si–C^{carb}$ bond length in **9-Br** (1.844(4) Å) compared to the NHC compound (1.940(3) Å).[127]

Compound **9-Br** completes the homologue series of the caac^{Me}-stabilized silicon(I) dimers $Si_2X_2(caac^{Me})_2$ (X = Cl[128], Br[this work], I[121], H[129], Me[130], Ph[131]). Their low degree of silicon pyramidalization (DP: 16 – 38) and the rather short Si–C^{carb} bond lengths (1.798(1) – 1.846(3) Å), suggest pronounced silene type of character of this class of compounds, which can be better described as 1,4-diamino-2,3-disila-1,3-butadienes.

Table 2.19. Selected structural paramters of the Si(I) compound **9-Br** in comparison to **1**, **2-Si** and literature known compounds.

Comp.	Si–Si / Å	Si–C^{carb} / Å	N–C^{carb} / Å	Σ∢(Si) / (deg)	DP[a] / %	τ[b] / (deg)	Ref.
$SiBr_2(caac^{Me})$ **1**	–	2.017(2)	1.301(3)	289.9	78	79.1	
$Si_2Br_2(caac^{Me})_2$	2.341(2)	1.844(4)	1.347(5)	327.6	36	13.0	this
9-Br		1.844(4)	1.348(5)	326.1	38	14.9	work
$Si_2Br_2(IDipp)_2$	2.385(1)	1.940(3)	1.373(5)[e]	303.9	62	24.2	[127]
		1.936(3)	1.375(4)[e]	302.3	64	23.8	
$Si_2Cl_2(caac^{Me})_2$	2.306(1)[c]	1.823(3)	1.336(3)	328.0	36	5.4	[128]
		1.826(3)	1.337(2)	329.0	34	7.3	
$Si_2I_2(caac^{Me})_2$	2.337(1)	1.846(3)	1.343(3)	328.3	35	11.5	[121]
		1.841(3)	1.345(3)	330.6	33	11.0	
$Si_2H_2(caac^{Me})_2$	2.334(1)[d]	1.817(2)	1.362(2)	327.4	36	1.3	[129]
$Si_2Me_2(caac^{Me})_2$	2.314(1)	1.798(1)	1.384(1)	345.2	16	2.1	[130]
		1.804(1)	1.383(1)	344.0	16		
$Si_2Ph_2(caac^{Me})_2$	2.306(1)	1.805(2)	1.381(3)	343.3	19	9.1	[131]
		1.803(2)	1.377(3)	345.8	16	9.9	

[a]: The degree of pyramidalization (DP) value of 0 % describes a trigonal planar coordination of the silicon atom with the sum of bond angles equal to 360°. A DP value of 100 % corresponds to a trigonal pyramidal coordination of the silicon atom with the sum of bond angles equal to 270°.

DP (in %) = 100 % · [360 − Σ∢(Si) / (deg)]/90

[b]: The twist angle (τ) is defined as the angle between the silicon and Ccarbene coordination planes defined by the atoms X1–Si1–Si2 (X2–Si2–Si1) and C2–C1–N1 (C22–C21–N2), respectively. Likewise for NHC-stabilized compounds the twist angle (τ) is defined as the angle between the X1–Si1–Si2 (X2–Si2–Si1) and the N1–C1–N2 (N3–C28–N4) coordination planes.

[c]: mean value of two independent molecules are given.

[d]: compound contains a crystallographic inversion center at the Si–Si midpoint.

[e]: averaged value of two bond lengths of the same carbene.

2.4.3 Stereodynamics in $Si_2Br_2(caac^{Me})_2$ (9-Br) and related compounds

Even though **9-Br** featues a C_2-symmetry in the solid state, ^{1}H-NMR spectra of **9-Br** reveal an averaged C_s-symmetry in (D_6)benzene and (D_8)toluene at ambient temperature in solution (*Figure 2.43*, middle spectrum), indicating a dynamic behavior. Upon cooling of the NMR sample to 213 K the C_2-symmetry can be frozen out (*Figure 2.43*, bottom spectrum) thus reflecting the symmetry observed in the solid state. In contrast, in the high temperature limit spectrum (*Figure 2.43*, top spectrum) one set of sharp signals for the caac^{Me} substituents in **9-Br** with a C_S-symmetry is observed, suggesting the presence of a transition state in which a mirror plane bisects both caac^{Me} substituents in **9-Br.** In order to rationalize the stereodynamics in **9-Br** and related literature known compounds $Si_2X_2(caac^{Me})_2$ (X = Cl[128], I[121], H[129], Me[130], Ph[131]) quantum chemical calculations at the B97-D3/def2-TZVP level of theory were performed by Ruben Fleischer in his Bachelor thesis.[221]

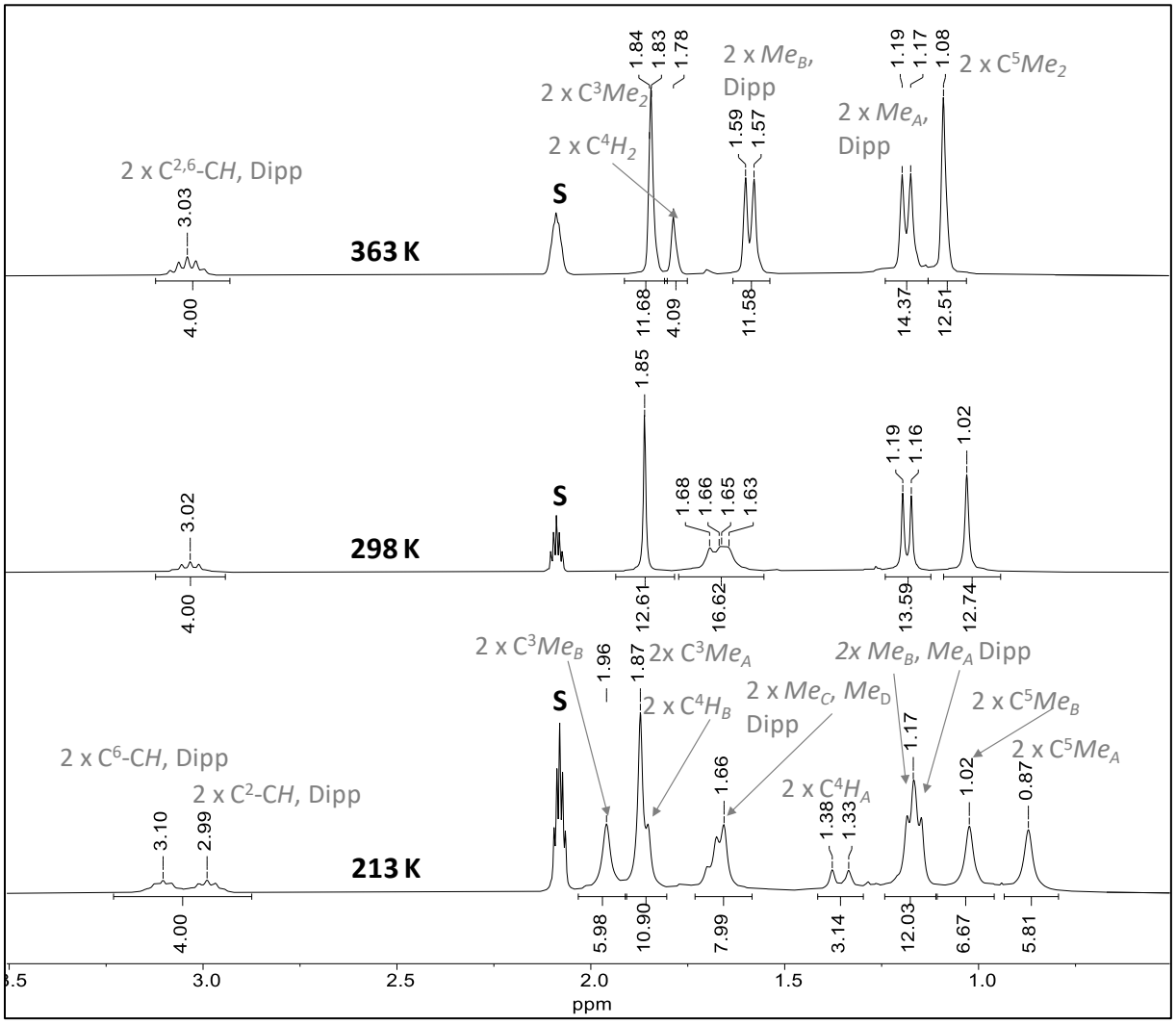

Figure 2.43. Excerpt of the ^{1}H NMR spectra (300.14 MHz) of **9-Br** in (D_8)toluene at 213 K (bottom), 298 K (middle), 363 K (top); signals of the deuterated solvent are marked with the character **S**.

The fast enantiomerization of **9-Br** can be rationalized by two pathways: a direct pathway (a) upon a concerted pyramidal inversion of the two chiral silicon centers in **9-Br** (*Figure 2.44*, (a)) or an indirect pathway (b) upon a stepwise consecutive pyramidal inversion of the two silicon centers in **9-Br** (*Figure 2.44*, (b)).

Pathway (a) proceeds via a co-planar transition state (0,0)-**9-Br**, which features C_S-symmetry with the mirror plane bisecting both caac^{Me} substituents and thus explains the simple ^{1}H NMR spectrum of **9-Br** at ambient temperature (*Figure 2.43*, middle spectrum). However, theoretical calculations by Ruben Fleischer revealed, that this process undergoes via rather high calculated activation barrier of 138.1 kJ mol^{-1}. [7]

The indirect pathway (b) proceds via transition states which feature a trigonal planar coordinated silicon center next to a chiral trigonal pyramidalized silicon center in (0,*S*) and (*S*,0)-**9-Br** and proceeds with a calcualted inversion barrier of 39.7 kJ mol^{-1} (**9-Br**) to the meso-form (*R*,S) and (*S*,*R*) of **9-Br**, which transform themselves upon pyramidal inversion of the second silicon center to the corresponding *R*,*R* and *S*,*S* enantiomers, respectively.[7] However, none of these transition states feature a C_S-symmetry with a mirror plane bisecting both caac^{Me} substituents, thus they do not provide a sufficient explanation for the simple ^{1}H NMR spectrum of **9-Br** at ambient temperature.

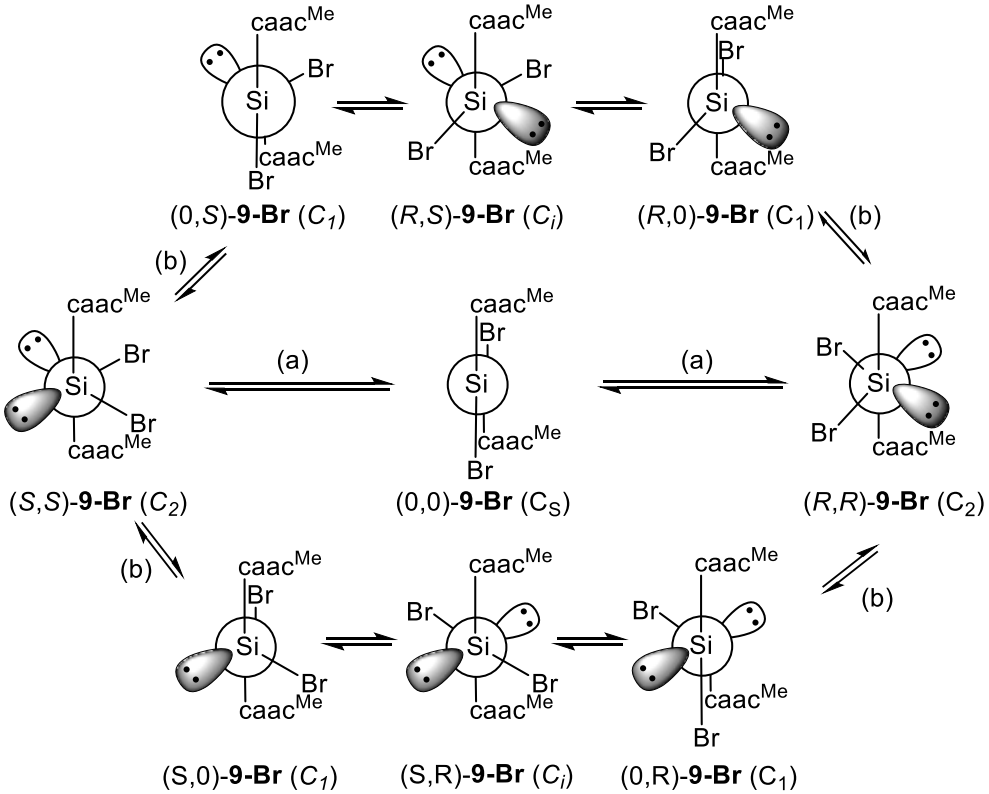

Figure 2.44. Newman projection of $Si_2Br_2(caac^{Me})_2$ (**9-Br**), along the Si–Si bond, showing the enantiomerization via (a) a single pathway through a concerted pyramidal inversion of both silicon centers or (b) via two enantiomeric pathways through a stepwise consecutive pyramidal inversion of each silicon center in **9-Br**.

[7] calculated at the B97-D3/def2-TZVP level of theory by Ruben Fleischer, see reference [221].

The stereodynamics in **9-Br** can be related to spontaneous racemization reactions observed in chiral organic molecules.[222,223] These type of reactions are defined as narcissistic reactions, in which the reactand and product are mirror images with respect to a fixed plane and are interconverting into each other.[222,223]

Depending on the conditions two types of reactions are distinguished: Synchronous narcissistic reactions feature an unique path, which passes through the midpoint of the two enantiomers with relfection symmetry, as resempled by pathway (a) in **9-Br**. In contrast, nonsynchronous narcissistic reactions proceed via two enantiomeric pathways, neither of which passes through the point with reflection symmetry, as resembled by pathway (b) in **9-Br**. The intermediates in the two enantiomeric pathways may appear chiral, but relate to each other by a center of symmetry.[222,223]

The synchronous pathway (a) in **9-Br** which proceeds via the midpoint (0,0) (*Figure* **2.45**, red) lies to high in energy, whereas the nonsynchronous pathway (b) in **9-Br** proceeds via two enantiomeric pathways through the intermediates (*S*,*R*) and (*R*,*S*) (*Figure 2.45*, blue) with a calculated energy barrier of 39.7 kJ mol^{-1} .

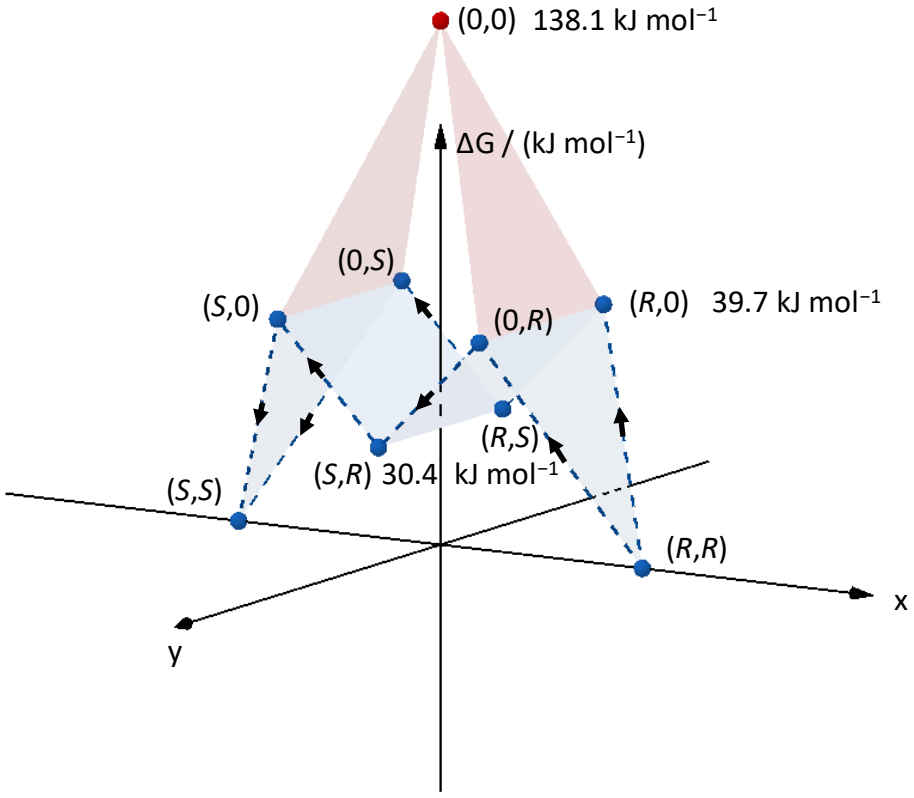

Figure 2.45. 3D plot of the enantiomerization of $Si_2Br_2(caac^{Me})_2$ (**9-Br**). The z-axis gives values of the calculated free activation energy ($\Delta G^{\#}_{calc}$) at the B97-D3/def2-TZVP level of theory by Ruben Fleischer, see reference [221]. The single path through the midpoint of the two enantiomers *R*,*R* and *S*,*S* via transition state (0,0) is shown in red (synchronous enantiomerization, pathway (a)). The two enantiomeric pathways, upon stepwise pyramidal inversion of the two chiral silicon centers in **9-Br** via the transition states (0,*R*) and (*R*,0) are shown in blue (nonsynchronous enantiomerization, pathway (b)).

It is safe to assume, that on the NMR time scale a molecule takes on all chiral structures of the two nonsynchronous enantiomeric paths (*Figure 2.45*, blue) and changes so quickly so that resonances for a time averaged C_S-symmetric structure are observed, thus explaining the simple ^{1}H NMR spectrum of **9-Br** at ambient temperature in solution (*Figure 2.43*, middle spectrum).[8] Indeed, the experimental result of a full line shape analysis (55.3 ± 3.4 kJ mol^{-1}) of recorded VT ^{1}H NMR spectra of **9-Br** in (D_8)toluene spectra (see *section 5.6.4*) does compare remarkably well to the calculated inversion barrier of 39.7 kJ mol^{-1} for the nonsyncrhonous enantiomerization in **9-Br** (*Figure 2.45*). The structural as well as NMR spectroscopic (*vide infra*) similarities of **9-Br** to the literature known caac^{Me}-stabilized silicon(I) dimers $Si_2X_2(caac^{Me})_2$ (X = Cl[128], I[121], H[129], Me[130], Ph[131]) highly suggest that the averaged C_S-symmetry of these compounds can be rationalized as well by a nonsynchronous enantiomerization (*Table 2.20*).

Table 2.20. NMR spectroscopic data (given in (D_6)benzene at 298 K, if not mentioned otherwise in the legend) of Si(I) compound **9-Br**, compared to **1** and literature known disilicon(I) compounds.

Comp.	Sym[a]	δ(^{29}Si) / ppm	δ($^{13}C^{carb}$) / ppm	δ(^{15}N) / ppm	Ref.
$SiBr_2(caac^{Me})$ (**1**)	C_S	14.35[b] ($\Delta\nu_{1/2}$ = 17 Hz)	231.2[b] ($\Delta\nu_{1/2}$ = 23 Hz)	231.3[b]	*this work*
$Si_2Br_2(caac^{Me})_2$ **9-Br**	C_S	19.84	208.3	174.3	
$Si_2Br_2(IDipp)_2$	C_2	34.9	177.1	–	[127]
$Si_2Cl_2(caac^{Me})_2$	C_S	25.62	–[c]	–	[128]
$Si_2I_2(caac^{Me})_2$	C_2[d]	–0.5	207.2	–	[121]
$Si_2H_2(caac^{Me})_2$	C_S	–45.5	211.8	–	[129]
$Si_2Me_2(caac^{Me})_2$	C_S	0.72	191.3	–	[130]

[a]: averaged symmetry found by NMR spectroscopy in solution at ambient temperature. [b]: measured in (D_8)THF at 243 K. [c]: signal was not given in the literature. [d]: $Si_2I_2(caac^{Me})_2$ featured a C_2-symmetry with broad resonances in the recorded ^{1}H NMR spectrum in (D_6)benzene at ambient temperature. It is safe to assume that the signals coalesces at higher temperatures.

The ^{29}Si{^{1}H} NMR spectrum of **9-Br** displays a resonance of 19.84 ppm, which is slightly downfield shifted compared to the starting material 14.4 ppm (**1**) and lies in between that of $Si_2Cl_2(caac^{Me})_2$ (25.6 ppm)[128] and $Si_2I_2(caac^{Me})_2$ (–0.5 ppm).[121] The drastic upfield shift of the $^{15}N^{CAAC}$ resonance of 174.3 ppm in **9-Br** compared to that of **1** (231.3 ppm) as well the significant upfield shift of the $^{13}C^{carb}$ resonance at 207.9 ppm compared to that of **1** (231.2 ppm) are in line with the increased Si–C^{carb} double bond character observed in the molecular structure (d(Si–C^{carb}) = 1.844(4) Å, Σ∢(Si1) = 327.6°, Σ∢(Si2) = 326.1°).

[8] S. Nozinovic, U. Das, F. Gstrein, personal communication, july **2022**.

2.4.4 Reactivity of $Si_2Br_2(caac^{Me})_2$

Besides the isolation of 1,4-diamino-2,3-disila-1,3-butadienes $Si_2R_2(caac^{Me})_2$ (R = Cl, I, H, Me) via either $3e^-$ -reduction of $caac^{Me}$-stabilized tetrachlorosilane, $1e^-$ -reduction of $caac^{Me}$-stabilized diodosilylene $SiI_2(caac^{Me})$ or one pot reduction of $SiHCl_3$ and $SiMeCl_3$ in the presence of $caac^{Me}$ carbene with KC_8 no reactivity of $caac^{Me}$-stabilized silicon(I) dimers have been reported thus far.[121,128–130]

On the contrast the reactivity of the NHC-stabilized halo-silicon(I) dimers $Si_2X_2(NHC^1)_2$ (X = Cl, Br, I) (NHC^1 = IDipp = :C[N(Dipp)CH]$_2$) has been tremendously studied by the research group of Filippou (*Figure 2.46*).[224] Major contribution to this research gave Dr. Marius Arz, who enabled the isolation of the highly air sensitive disilicon(I) salts $[Si_2(X)(NHC^1)][B(C_6F_5)_4]$ upon halide abstraction of the respective silicon(I)dimers with $[Li(Et_2O)_2][B(C_6F_5)_4]$. He could also show that the NHC-stabilized halo-silicon(I) dimers can be selectively oxidized to the corresponding NHC-supported dihalosilylenes, using dihaloethane as oxidation reagent. The weak bonding of the NHC in these dimers could be exploited upon a carbene exchange reaction with the small carbene IMe_4, which led to the formation of the salt $[Si_2(NHC^4)_4]Br_2$ (NHC^4 = IMe_4). [224]

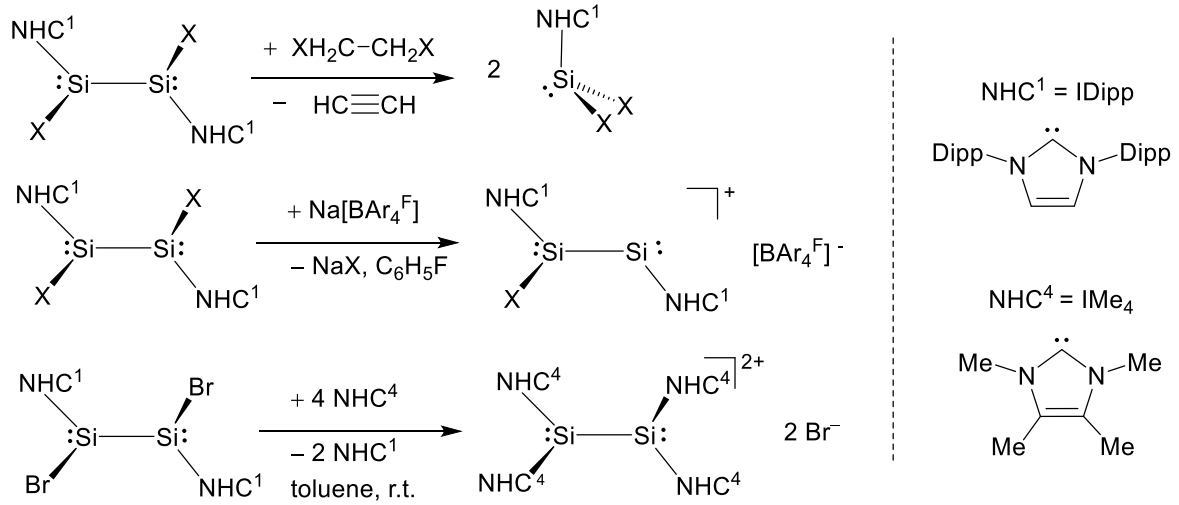

Figure 2.46. Reactivity of NHC-stabilized halo-silicon(I) dimers $Si_2X_2(IDipp)_2$ (X = Cl, Br, I). Formal charges are not given for the sake of simplicity.

Substitution reactions of NHC-stabilized silicon(I)halides with nucleophiles such as $LiSi(SiMe_3)_3{\cdot}2(THF)$, $Li[(C_5H_5)Mo(CO)_2(PMe_3)]$, $LiP(SiMe_3)_2{\cdot}2(THF)$, LiMes·2(THF), NaOPh and $Tip_2Si{=}Si(Tip)Li(DME)_2$ appeared to be unsuccesfull. Monitoring of the reaction mixtures by ^1H NMR spectroscopy in (D_6)benzene revealed the selective formation of the disilicon(0) compound $Si_2(NHC^1)_2$.[224]

Since cyclic (alkyl)(amino)carbenes are much stronger π-acceptors than typical pure σ-donating NHCs, a higher electrophilicity at the silicon-centers was envisioned in caac^{Me}-stabilized halosilicon(I) dimers towards nucleophiles.

The steric bulk of the used nucleophile in the substitution reactions appeared to be particularly important. Reaction of $Si_2Br_2(caac^{Me})_2$ (**9-Br**) with two equivalents of sterically high demanding nucleophiles such as $LiSi(SiMe_3)_3{\cdot}2(THF)$ or $LiPMes_2$ in THF solution at ambient temperature were not successful. Monitoring the reaction mixture by ^1H NMR spectroscopy in (D_6)benzene revealed the selective formation of the disilicon(0) compound $Si_2(caac^{Me})_2$.[115] Similarly, $Si_2Br_2(caac^{Me})_2$ did not react with two equivalents of MesLi in THF solution either at ambient temperature nor upon heating for several hours at 60 °C. The substituted silicon(I) compound $Si_2Mes_2(caac^{Me})_2$ (**9-Mes**) was only accessible upon 1e$^-$-reduction from SiBr(Mes)(caac^{Me}) (**2-Mes**) (see *section 2.4.5*).

2.4.4.1 Reactivity of $Si_2Br_2(caac^{Me})_2$ towards NaCp

Heating a red-purple solution of $Si_2Br_2(caac^{Me})_2$ (**9-Br**) in THF with 4 equiv. of NaCp for 23 h at 50 °C let to a color change from red-purple to orange-brown. Monitoring of the reaction mixture by ^1H NMR spectroscopy in (D_6)benzene revealed the formation of $Si_2Cp'_2(caac^{Me})_2$ (**9-Cp'**) with moderate selectivity. After extraction from formed salts with toluene, and multiple washing attempts with THF and *n*-pentane the compound could be isolated as a bright orange powder with 22 % yield. ^1H NMR spectroscopy in (D_6)benzene revealed the presence of an impurity of 20 mol% which can be highly likely attributed to the *E,Z* -stereoisomer of **9-Cp'** (*Scheme 2.11*). Multiple crystallization and washing steps could not lower the amount of the *E,Z*-diasteromer present in the sample **9-Cp'**. In contrast to $Si_2Mes_2(caac^{Me})_2$ (**9-Mes**) (see *section 2.4.5*) the *E,Z*-diasteromer could not be formed upon heating of the *E,E* isomer in (D_6)benzene or (D_8)THF. Instead the decomposition of $Si_2Cp'_2(caac^{Me})_2$ was observed. The *E,E*-isomer could be fully characterized, whereas the *E,Z*-isomer could be only characterized partially via multinuclear NMR spectroscopy, due to the low intensity of the respective signals in the corresponding ^1H, $^{13}C\{^1H\}$ and $^{29}Si\{^1H\}$ NMR spectra.

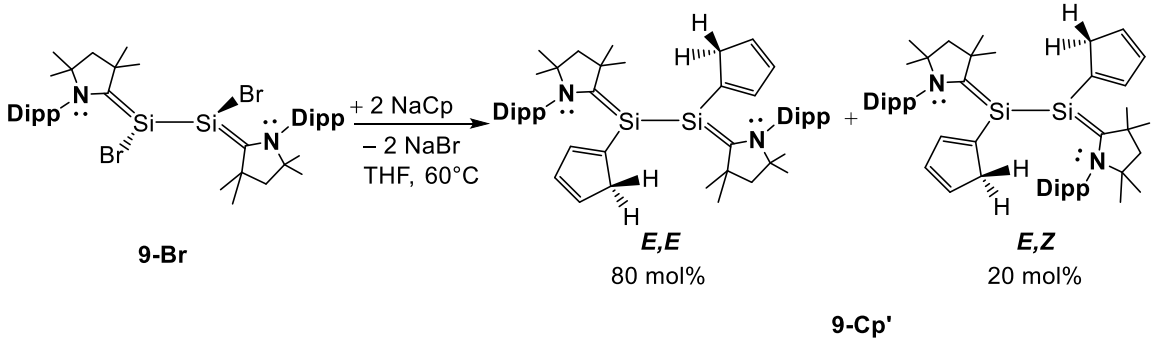

Scheme 2.11. Synthesis of $Si_2Cp'_2(caac^{Me})_2$ **9-Cp'** upon substitution reaction from $Si_2Br_2(caac^{Me})_2$ (**9-Br**).

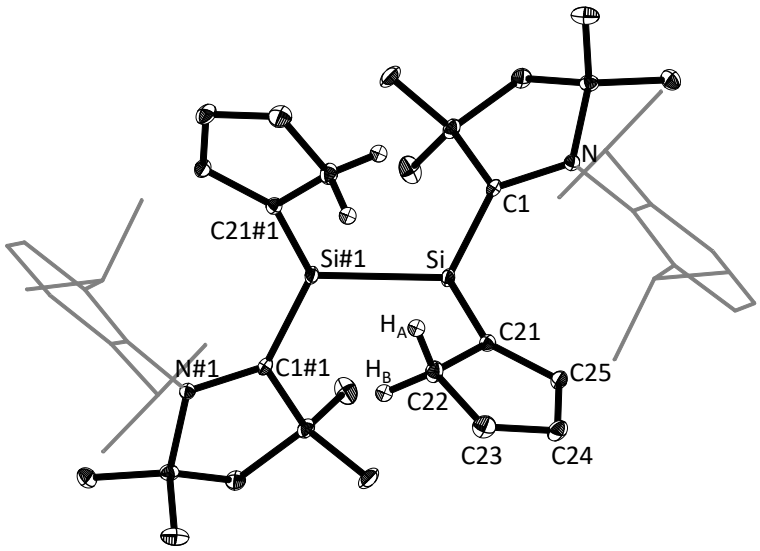

Figure 2.47. DIAMOND plot of the molecular structure of **9-Cp'**. Thermal ellipsoids are set at 30 % propability level and hydrogen atoms were omitted. In the depicted structure the Dipp-substituent of the caac^{Me} ligand is presented in the wire-frame for the sake of clarity. Selected bond lengths [Å], bond angles [°] and torsion angles [°]:
Si–Si#1 2.2884(6), Si–C1 1.789(1), Si–C21 1.863(1), C1–N 1.383(2), C21–C22 1.505(2), C21–C25 1.364(2), C22–C23 1.480(2), C23–C24 1.350(2), C24–C25 1.457(2), C1–Si–Si#1 114.80(4), C1–Si–C21 125.23(6), C21–Si–Si#1 111.03(4), C#1–Si#1–Si–C1 141.7(1), Si#1–Si–C1–N 163.6(1), C21#1–Si#1–Si–C21 80.0(2).

The molecular structure of **9-Cp'** features a C_2-symmetry, which renders the two almost planar coordinated silicon centers (Σ∢(Si) = 351.1(1)°) equally. The Cp-substituents of **9-Cp'** (τ(C21#1–Si#1–Si–C21 = 80.0(2)°) as well the sterically more demanding caac^{Me} groups (τ(C1#1–Si#1–Si1–C1) = 141.7(1)°) adopt a gauche conformation. The two carbene centers are orientated almost orthogonal with respect to each other (carbene to carbene plane twist angle = 81.8(1)°) and the N-Dipp moiety of the caac^{Me} ligand is orientated trans with respect to the Si(Cp')(caac^{Me}) group (τ(Si#1–Si–C1–N) = 163.6(1)°). The skeleton of the structure can be thus best described as a *E*,*E*-1,4-diamino-2,3-disila-1,3-butadiene**.** The Cp' as well SiCp'(caac^{Me}) substituents of both silicon centers are considerably bent with respect to the Si–C1^{carb} bond (bent angle 31.1(1)°) thus leading to an overall chiral structure. Applying the priority rules for axial chirality, according to IUPAC, the stereo descriptors R_a whith the chirality axis passing through the Si–Si bond can be assigned in the molecular structure of **9-Cp'** depicted in *Figure 2.47*.
The most interesting feature of the compound are the Cp-substituents, which in fact happened to be isomerized into a cyclopenta-1,3-dien-1-ide substituent with localized double bonds at the C21–C25 (1.364(2) Å) and C23–C24 (1.350(2) Å) atoms and classical C–C single bonds in the rest of the Cp' backbone C22–C23 (1.480(2) Å), C22–C21 (1.505(2) Å), C24–C25 (1.457(2) Å). The Si–C^{carb} bond length in **9-Cp'** (1.789(1) Å) is drastically shortened compared to Si_2Br_2(caac^{Me})$_2$ **9-Br** (1.844(4) Å), which is reflected by a significant elongation of the N–C^{carb} bond in **9-Cp'** (1.383(2) Å) compared to that of **9-Br** (1.347(5) Å).

These findings are in line with the low degree of pyramidalization of **9-Cp'** (DP = 10 %) compared to **9-Br** (DP = 36, 38 %) indicating a stronger π-bond in **9-Cp'** compared to that of **9-Br**. The Si–Si bond length (2.288(1) Å) in **9-Cp'** is significantly shorter in comparison to **9-Br** (2.341(2) Å) and the caac^{Me}-stabilized silicon(I) dimer $Si_2Me_2(caac^{Me})_2$ (2.314(1) Å)[130] and lies exactly in-between that of a typical Si–Si single bond of tetrakis(trimethylsilyl)-silane (2.369(3) Å)[225] and a typical Si=Si double bond given in reported disilenes (2.143 – 2.260(2) Å).[24] This may be attributed to a strong conjugation of the 2-aminosilene moieties via the Si–Si backbone of the molecule.
The low degree of pyramidalization of **9-Cp'** (DP = 10 %) aswell the high bent angle of the substituents with respect to the Si–C^{carb} bond (bent angle 31.1 °) suggest that compound **9-Cp'** can be best described as a bent *E,E*-1,4-diamino-2,3-disila-1,3-butadiene. The compound compares well in terms of its structural features to the *Z,Z*-isomer of $Si_2Mes_2(caac^{Me})_2$ (**9-Mes-Z,Z**) (see *section 2.4.5*), and seems to be significantly less pyramidalized (DP = 10%) compared to **9-Br** (DP = 36, 38 %), **9-Mes-*E,E*** (DP = 19 %) and $Si_2Me_2(caac^{Me})_2$ (DP = 16 %)[130] (*Table 2.21*).

Table 2.21. Selected structural paramters of the Si(I) compound **9-Cp'** in comparison to literature known alkyl substituted caac^{Me} stabilized silicon(I) dimers.

Comp.	Si–Si / Å	Si–C^{carb} / Å	N–C^{carb} / Å	Σ∢(Si) / (deg)	DP[a] / %	τ[b] / (deg)	Ref.
$Si_2Br_2(caac^{Me})_2$ **9-Br**	2.341(2)	1.844(4)	1.347(5)	327.6	36	13.0	
		1.844(4)	1.348(5)	326.1	38	14.9	
$Si_2Cp'_2(caac^{Me})_2$ **9-Cp'**	2.288(1)	1.789(1)	1.383(2)	351.1	10	6.4	*this*
$Si_2Mes_2(caac^{Me})_2$ **9-Mes *Z,Z***	2.336(3)	1.79(1)	1.40(1)	353.4	7	6.6	*work*
$Si_2Mes_2(caac^{Me})_2$ **9-Mes *E,E***	2.329(3)	1.793(7)	1.406(8)	342.8	19	18.7	
		1.796(8)	1.409(8)	340.5	22	19.6	
$Si_2Me_2(caac^{Me})_2$	2.314(1)	1.798(1)	1.384(1)	345.2	16	2.1	[130]
		1.804(1)	1.383(1)	344.0	16	1.4	
$Si_2Ph_2(caac^{Me})_2$	2.306(1)	1.805(2)	1.381(3)	343.3	19	9.1	[131]
		1.803(2)	1.377(3)	345.8	16	9.9	

[a]: The degree of pyramidalization (DP) value of 0 % describes a trigonal planar coordination of the silicon atom with the sum of bond angles equal to 360°. A DP value of 100 % corresponds to a trigonal pyramidal coordination of the silicon atom with the sum of bond angles equal to 270°.
DP (in %) = 100 % · [360 − Σ∢(Si) /(deg)]/90
[b]: The twist angle (τ) is defined as the angle between the silicon and Ccarbene coordination planes defined by the atoms X1-Si1-Si2 (X2-Si2-Si1) and C2-C1-N1 (C22-C21-N2), respectively.

The ^{1}H, $^{13}C\{^{1}H\}$ as well as $^{29}Si\{^{1}H\}$ NMR spectra in (D_8)THF (the compound is barely soluble in benzene) feature C_2-symmetry, reflecting the axial chirality of the molecule observed in the molecular structure.

The ^{1}H NMR spectrum of **9-Cp'** (*Figure 2.48*) displays four singlets for the methyl groups of ($C^{3}Me_{A}Me_{B}$, $C^{5}Me_{A}Me_{B}$), as well as two doublets for the hydrogen atoms ($C^{4}H_{A}H_{B}$) for the backbone of the caac^{Me} carbene moiety. In total four doublets of the methyl grupps of the isopropyl groups ($C^{2}CH_{A}Me_{A}Me_{B}$ and $C^{6}CH_{B}Me_{C}Me_{D}$) as well as two septets for the methine protons of the isopropyl groups are observed in the aliphatic region for the Dipp substituent. In case of the Cp' two doublets for the diastereotopic protons of of the methylene-group ($C^{5}H_{A}H_{B}$, Cp'), as well as in total three multiplets of the Cp'-backbone ($C^{2,3,4}$-*H*, Cp') are observed. The full NMR assignment of **9-Cp'** was made possible through high-resolution correlation spectroscopy.

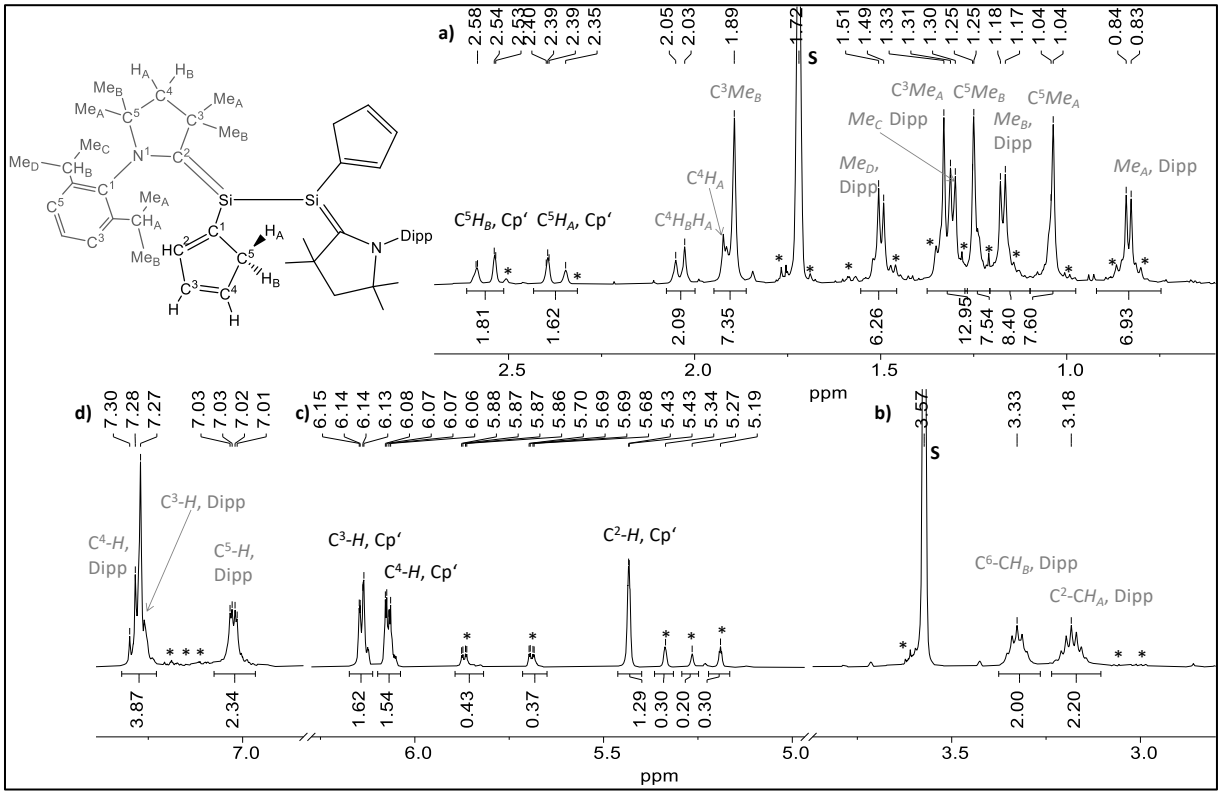

Figure 2.48. Four excerpts (a – d) of the ^{1}H NMR spectrum of $Si_2(Cp')_2(caac^{Me})_2$ (**9-Cp'**) in (D_8)THF at 298 K; the signal of the deuterated solvent is marked with **S**; the symbol (*) marks tiny amounts of the *E,Z* diastereomer.

The ^{29}Si{^{1}H} NMR spectrum of **9-Cp'** displays a resonance at –5.65 ppm, which is significantly upfield shifted when compared to $Si_2Br_2(caac^{Me})_2$ **9-Br** (19.8 ppm) but compares well to $Si_2Mes_2(caac^{Me})_2$ *E,E* (–2.7 ppm). The $^{13}C^{carb}$ -resonance in **9-Cp'** is with 180.9 ppm drastically upfield shifted when compared to **9-Br** (208.3 ppm) and significantly upfield shifted when compared to **9-Mes-*E,E*** (196.9 ppm), indicating a strong Si=C^{carb} π-bond. The ^{1}H ^{15}N HMBC spectrum displays a crosspeak at 132.9 ppm (**9-Cp'**), which is drastically upfield shifted when compared to the silicon(I) dimer **9-Br** (174.3 ppm) and compares well to **9-Mes-*E,E*** (134.6 ppm), suggesting a N–C^{carb} single bond, which is in line with the N–C^{carb} bond length of 1.383(2) Å.

NMR spectroscopic properties, as well as bonding parameters of the molecular structure suggest a disilabutadiene type of character in **9-Cp'** with a rather strong Si=C^{carb} double bond. In terms of the NMR spectroscopic properties **9-Cp'** compares well to the Mes substituted disilicon(I) compound **9-Mes-*Z,Z*** (*Table 2.22*) isolated in this work (see *section 2.4.5*).

Table 2.22. NMR spectroscopic data (given in (D_6)benzene at 298 K, if not mentioned otherwise in the legend) of isolated caac^{Me}-stabilized Si(I)-dimers, compared to literature known compounds

Comp.	Diast.[a]	Sym[b]	δ(^{29}Si) / ppm	δ(^{13}C^{carb}) / ppm	δ(^{15}N) / ppm	Ref.
$Si_2Cp'_2(caac^{Me})_2$ **9-Cp'-*E,E***	E,E	C_2	–5.65	180.9	132.9	
$Si_2Br_2(caac^{Me})_2$ **9-Br**	Z,Z	C_S	19.84	208.3	174.3	*this*
$Si_2Mes_2(caac^{Me})_2$ **9-Mes-*Z,Z***	Z,Z	C_2	10.1[c]	185.8	120.9	*work*
$Si_2Mes_2(caac^{Me})_2$ **9-Mes-*E,E***	E,E	C_S	–0.21[c]	196.9	133.7	
$Si_2Br_2(IDipp)_2$	–	C_2	34.9	177.1	–	[127]
$Si_2Cl_2(caac^{Me})_2$	Z,Z	C_S	25.62	–[d]	–	[128]
$Si_2I_2(caac^{Me})_2$	Z,Z	C_2[e]	–0.5	207.2	–	[121]
$Si_2H_2(caac^{Me})_2$	E,E	C_S	–45.5	211.8	–	[129]
$Si_2Me_2(caac^{Me})_2$	E,E	C_S	0.72	191.3	–	[130]

[a]: Determined orientation of the N-Dipp moiety in the soid state (orientated cis (Z) or trans (E) to the high priority group at the silenic silicon-center). [b]: averaged symmetry found by NMR spectroscopy in solution at ambient temperature. [c]: measured in (D_6)benzene at 343 K. [d]: signal was not given in the literature. [e]: $Si_2I_2(caac^{Me})_2$ featured a *C_2*-symmetry with broad resonances in the recorded ^{1}H NMR spectrum in (D_6)benzene at ambient temperature. It is safe to assume, that the signals coalesces at higher temperatures.

The impurity of 20 mol% observed in **9-Cp'** was of considerable interest and was investigated by NMR correlation spectroscopy: Revealing the identity of a *E,Z*-distereoisomer of **9-Cp'** which bears two different silicon resonances (–6.31 and –8.51 ppm) as well as two different $^{13}C^{CAAC}$ resonances at 182.9 and 182.2 ppm, respectively. The impurity could not be removed neither upon multiple washing steps with THF nor crystallization from the THF filtrate. Heating a pure sample of **9-Cp'** in (D_6)benzene at 80 °C for 20 h led to the complete decomposition of **9-Cp'**. Alkene **X**, was identified as major decomposition product next to tiny amounts of byproduct **Y**. Both compounds were characterized by multinuclear NMR correlation spectroscopy.

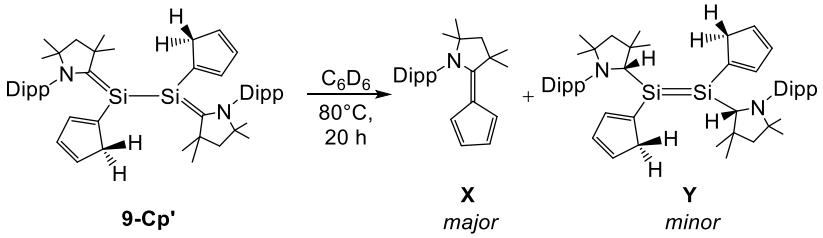

Scheme 2.12. Decomposition of **9-Cp'** upon heating in (D_6)benzene.

2.4.4.2 Reactivity of $Si_2Br_2(caac^{Me})_2$ towards alkynyl-lithium reagents

Addition of LiC≡CR (R = $SiMe_3$, Mes) to a red-purple solution of $Si_2Br_2(caac^{Me})_2$ **9-Br** in THF led after stirring for 19 h to a color change to yellow-brown. Monitoring of the reaction mixture by ^1H NMR spectroscopy in (D_6)benzene revealed the selective formation of $Si_2(C{\equiv}CR)_2(caac^{Me})_2$ (R = $SiMe_3$, Mes) (**9-C_2TMS** and **9-C_2Mes**), respectively. After work up both compounds could be isolated as orange powders in moderate yields (39 % (**9-C_2Mes**), 54 % (**9-C_2TMS**)). Both compounds immediately decolorize upon contact with air and decompose unselectively at 215 °C (**9-C_2Mes**) and 221 °C (**9-C_2TMS**), respectively. The compounds are well soluble in aliphatic and aromatic solvents affording orange solutions.

Orange-brown single crystals of **9-C_2TMS** and **9-Mes** were obtained from *n*-hexane solutions at –30 °C. The molecular structures of **9-C_2TMS** (*Figure 2.49* (left)) and **9-C_2Mes** (*Figure 2.49* (right)) feature a C_2-symmetry, leading to two homotopic trigonal pyramidalized silicon centers (Σ∢(Si) = 335.6° (**9-C_2TMS**), 342.4° (**9-C_2Mes**)).

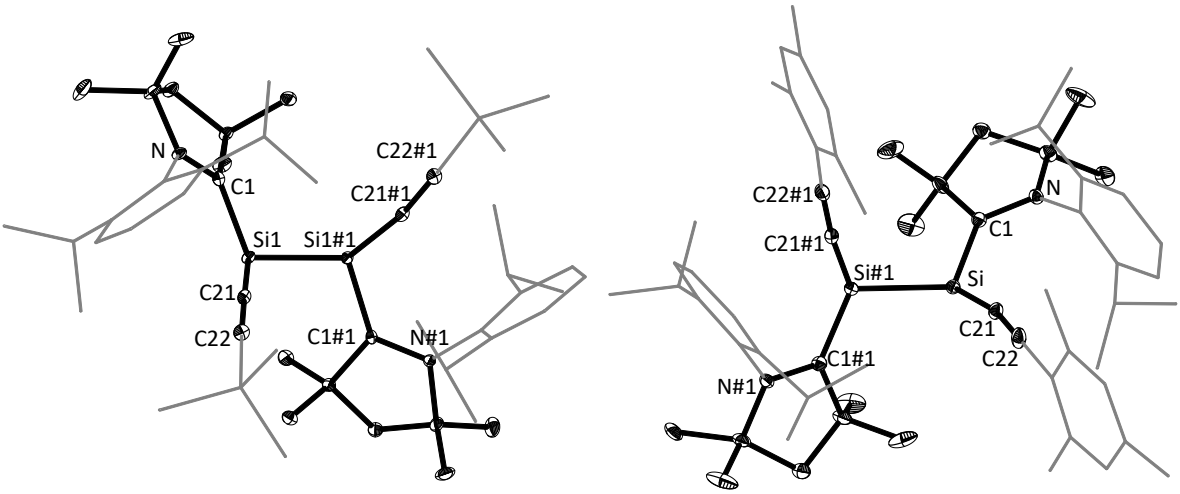

Figure 2.49. DIAMOND plot of the molecular structures of acetylide substituted $caac^{Me}$-stabilized silicon(I) dimers **9-C_2TMS** (left) and **9-C_2Mes** (right). Thermal ellipsoids are set at 30 % propability level and hydrogen atoms were omitted. In the depicted structures the Dipp-substituent of the $caac^{Me}$ ligands and the $SiMe_3$ group and the Mes-substituent are presented in the wire-frame for the sake of clarity. Selected bond lengths [Å], bond angles [°] and torsion angles [°]:

9-C_2TMS: Si1–Si1#1 2.313(1), Si1–C1 1.821(3), Si1–C21 1.836(3), N–C1 1.353(3), C21–C22 1.212(4), C22–$Si2^{TMS}$ 1.830(3), C1–Si1–Si1#1 109.8(1), C1–Si1–C21 113.3(1), C21–Si1–Si1#1 112.5(1), C1–Si1–Si1#1–C1#1 –169.8(2), Si1#1–Si1–C1–N –148.2(2), C21–Si1–Si1#1–C21#1 –64.1(2). Depicted in (*S*,*S*) configuration. The other enantiomer is also found in the crystal-lattice, the compound crystallizing in the achiral space group (C2/c).

9-C_2Mes: Si–Si#1 2.291(2), Si1–C1 1.804(3), Si1–C21 1.810(3), N–C1 1.365(4), C21–C22 1.215(5), C22–$C23^{Mes}$ 1.50(1), C21–Si–Si#1 111.1(1), C1–Si1–Si#1 114.4(1), C1–Si1–C21 116.9(2), C1–Si1–Si1#1–C1#1 152.8(2), Si1#1–Si1–C1–N 158.9(3), C21–Si–Si#1–C21#1 63.0(2). Depicted in (*R*,*R*) configuration. The other enantiomer is also found in the crystal-lattice, the compound crystallizing in the achiral space group (P-4).

The alkinyl substituents are in gauche conformation ($\tau(C^{C\equiv C}–Si–Si–C^{C\equiv C})$ = –64.1(2)° (**9-C$_2$TMS**), 63.0(2)° (**9-C$_2$Mes**)) and the sterically more demanding caac^{Me} groups adopt an antiperiplanar conformation ($\tau(C^{carb}–Si–Si–C^{carb})$ = –169.8(2)° (**9-C$_2$TMS**), 152.8(2)° (**9-C$_2$Mes**)). The two caac^{Me} carbenes are orientated almost orthogonal with respect to each other (twist angle = 96.4(2)° (**9-C$_2$TMS**), 114.9(4)° (**9-C$_2$Mes**)). The N-Dipp moieties of the caac^{Me} ligand are orientated trans with respect to the SiSi(C$_2$R)(caac^{Me}) group ($\tau(N–C^{carb}–Si–Si)$ = –148.2(2) (**9-C$_2$TMS**), 158.9(3) (**9-C$_2$Mes**)). Thus, according to the priority rules for E/Z alkenes, defined by IUPAC, the stereodescriptor ***E,E*** can be assigned.

The silicon centers in **9-C$_2$TMS** and **9-C$_2$Mes** are less pyramidalized (DP(Si) = 27 % (**9-C$_2$TMS**), 20 % (**9-C$_2$Mes**)) than in Si$_2$Br$_2$(caac^{Me})$_2$ **9-Br** (DP(Si1,Si2) = 36°, 38°), leading to a decrease of the Si–C^{carb} bond length (1.821(3) Å (**9-C$_2$TMS**), 1.804(3) Å (**9-C$_2$Mes**)) compared to the bromo-silicon(I)-dimer (1.844(4) Å (**9-Br**)). These results are in line with a slight elongation of the N–C^{carb} bond length in **9-C$_2$TMS** (1.353(3) Å) and **9-C$_2$Mes** (1.365(4) Å) compared to that of **9-Br** (1.347(5) Å).

The Si–Si bond length of 2.313(1) Å (**9-C$_2$TMS**) and 2.291(1) Å (**9-C$_2$Mes**) are significantly shortened compared to that of the starting material with 2.341(2) Å (**9-Br**).

The Si–C$^{C\equiv C}$ bond lengths in **9-C$_2$TMS** (1.836(3) Å) and **9-C$_2$Mes** (1.810(3) Å) compare well to the Me$_3$Si–C$^{C\equiv C}$ bond in **9-C$_2$TMS** (1.830(2) Å), suggesting significant amounts of hyperconjugation of the silicon carbon bonds in the silenic silicon center. The Si–C$^{C\equiv C}$ bond lengths (1.836(3) Å (**9-C$_2$TMS**), 1.810(3) Å (**9-C$_2$Mes**)) overall compare well to the recently reported alkinyl substituted disilene Si$_2$(C$_2$-TMS)$_2$(Bbt)$_2$ (Bbt = C$_6$H$_2$-2,4,6-Dsi$_3$, Dsi = CH(SiMe$_3$)$_2$) (1.811(4) Å).[226] The alkynyl (C≡C) bond lengths in **9-C$_2$TMS** (1.212(4) Å) and **9-C$_2$Mes** (1.215(5) Å) are almost equal to that of the C(sp)-C(sp) bond in bis(trimethylsilyl)-acetylene (1.208(3) Å).[227]

Similar to **9-Br**, the ^{1}H-NMR spectra of **9-C$_2$TMS** and **9-C$_2$Mes** reveal an averaged C_S-symmetry in (D$_6$)benzene at ambient temperature, in contrast to the C_2-symmetry observed in the solid state. No change of the NMR spectra was observed at lower temperatures, even in (D$_8$)toluene at –80 °C, suggesting a fast enantiomerization (*Figure 2.50*) at the NMR time scale, which proceeds via a rather low inversion barrier.

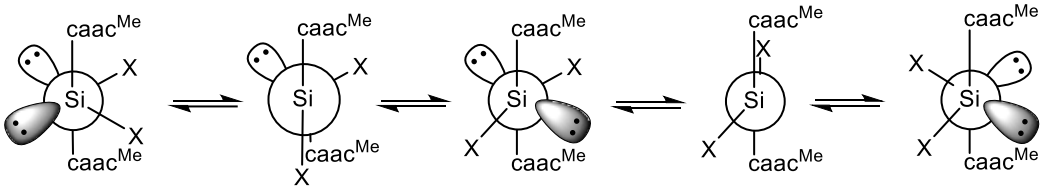

Figure 2.50. Enantiomerisation of caac^{Me}-stabilized silicon(I) dimers Si$_2$(X)$_2$(caac^{Me})$_2$ (X = Cl[128], I[121], H[129], Me[130], Ph[131] and X [*this work*]= Br, C ≡C-R; R = TMS, Mes) via a nonsynchronous enantiomerization (more details are given in *section 2.4.3*).

The structural as well as NMR spectroscopic (*vide infra*) similarities of **9-C_2TMS** and **9-C_2Mes** to **9-Br** and the literature known caac^{Me}-stabilized silicon(I) dimers Si_2X_2(caac^{Me})$_2$ (X = Cl[128], I[121], H[129], Me[130], Ph[131]) highly suggest that the averaged C_S-symmetry (*Table 2.23*) of these compounds can be rationalized as well by a nonsynchronous enantiomerization (see *section 2.4.3*).

Table 2.23. NMR spectroscopic data (given in (D_6)benzene at 298 K, if not mentioned otherwise in the legend) of isolated caac^{Me}-stabilized Si(I)-dimers, compared to literature known compounds

Comp.	Diast.[a]	Sym[b]	δ(^{29}Si) / ppm	δ($^{13}C^{carb}$) / ppm	δ(^{15}N) / ppm	Ref.
Si_2Br_2(caac^{Me})$_2$ **9-Br**	Z,Z	C_S	19.84	208.3	174.3	
Si_2(C≡CTMS)$_2$(caac^{Me})$_2$ **9-C_2TMS**	E,E	C_S	–42.2	203.4	157.7	*this*
Si_2(C≡CMes)$_2$(caac^{Me})$_2$ **9-C_2Mes**	E,E	C_S	–36.5	197.3	150.9	*work*
Si_2Cl_2(caac^{Me})$_2$	Z,Z	C_S	25.62	–[c]	–	[128]
Si_2I_2(caac^{Me})$_2$	Z,Z	C_2[d]	–0.5	207.2	–	[121]
Si_2H_2(caac^{Me})$_2$	E,E	C_S	–45.5	211.8	–	[129]
Si_2Me_2(caac^{Me})$_2$	E,E	C_S	0.72	191.3	–	[130]

[a]: Determined orientation of the N-Dipp moiety in the soid state (orientated cis (Z) or trans (E) to the high priority group of the silenic silicon-center). [b]: averaged symmetry found by NMR spectroscopy in solution at ambient temperature. [c]: signal was not given in the literature. [d]: Si_2I_2(caac^{Me})$_2$ featured a C_2-symmetry with broad resonances in the recorded ^{1}H NMR spectrum in (D_6)benzene at ambient temperature. It is safe to assume that the signals coalesces at higher temperatures.

The ^{29}Si{^{1}H} NMR spectra of **9-C_2TMS** and **9-C_2Mes** display resonances at –42.2 and –36.5 ppm, respectively, that are drastically upfield shifted when compared to **9-Br** (19.84 ppm). The $^{15}N^{CAAC}$ resonances at 157.7 ppm (**9-C_2TMS**) and 150.9 ppm (**9-C_2Mes**) are significantly upfield shifted, when compared to **9-Br** (174.3 ppm) and are in line with the increased π-character of the Si–C^{carb} bond observed in their molecular structures. The $^{13}C^{carb}$ resonances of **9-C_2TMS** (203.4 ppm) and **9-C_2Mes** (197.3 ppm) are only slightly upfield shifted when compared to **9-Br** (207.9 ppm).

The stretching vibration of the alkinyl group (ν(C≡C) in **9-C_2TMS** (2057 cm^{-1}) and **9-C_2Mes** (2143 cm^{-1}) are significantly shifted to higher wave numbers in comparison to the lithium-acetylides Li-C_2-R (R = $SiMe_3$, 1981 cm^{-1}; R = Mes, 2023 cm^{-1}).

2.4.5 Isolation and thermal *Z,Z* → *E,E* isomerization of $Si_2Mes_2(caac^{Me})_2$

The novel 1,4-diamino-2,3-disila-1,3-butadiene $Si_2(Mes)_2(caacMe)_2$ (**9-Mes**) features the first example of a thermal induced *Z,Z* → *E,E* isomerization of a disilabutadiene. Entry to the chemistry provided 2-aminosilene $SiBr(Mes)(caac^{Me})$ (**2-Mes**), which upon $1e^-$ -reduction with KC_8 selectively afforded 1:1 diasteromeric mixture of **9-Mes-*Z,Z*** and **9-Mes-*E,E*** (*Scheme 2.13*). Heating of the mixture in *m*-xylene at 130 °C for 4 h led to the selective formation of the *E,E* isomer. Both compounds were fully characterized, also by X-ray diffraction analysis and the kinetics of the process studied by time resolved variable temperature ^1H NMR spectroscopy.

Detailed kinetic studies show that **9-Mes** undergoes an irreversible *Z,Z* to *E,E* isomerization at 90 – 110 °C with an activation barrier of 120.2 ± 2.3 kJ mol^{-1}, $\Delta H^{\ddagger} = 126.3 \pm 2.3$ kJ mol^{-1}, $\Delta S^{\ddagger} = 20.4 \pm 0.6$ J K^{-1} mol^{-1}. Experimental results suggest that the isomerization process occurs highly likely by a stepwise consecutive rotation of the two $Si–C^{carb}$ bonds in **9-Mes-*Z,Z***.

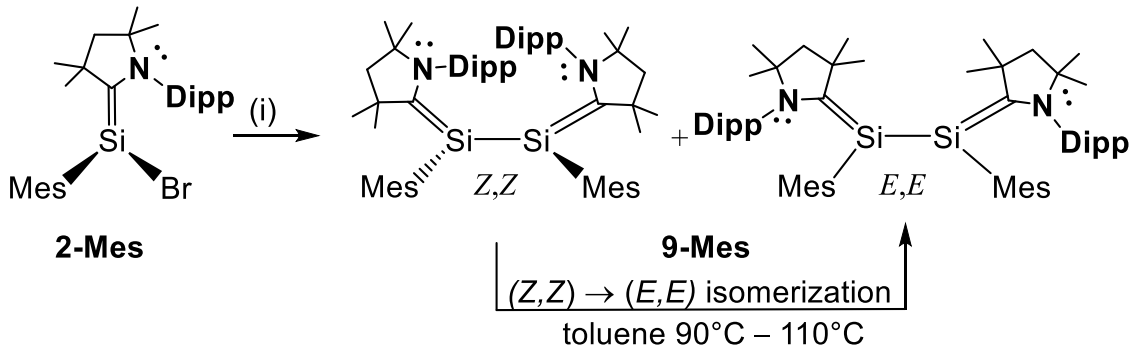

Scheme 2.13. Synthesis of the silicon(I) dimer **9-Mes**, upon $1e^-$ -reduction of **2-Mes**; (i) 1 equiv. of KC_8 in C_6H_6 at r.t., 7 d.

2.4.5.1 Synthesis and properties of 9-Mes-*Z,Z* and 9-Mes-*E,E*

Reduction of 2-aminosilene **2-Mes** with 1.2 equiv. of KC_8 in benzene at ambient temperature was accompanied by a color change form orange-yellow to dark purple. Monitoring of the reaction mixture by ^1H NMR spectroscopy in (D_6)benzene revealed the rather slow conversion of **2-Mes** in the respective $caac^{Me}$ silicon(I) dimer **9-Mes**. Full conversion and selective formation of **9-Mes** as a 1:1 diastereomeric mixture (*Z,Z* : *E,E*) was achieved after stirring of the reaction mixture for 7 d. After extraction from the black graphite residue with benzene and crystallization from *n*-pentane at 4 °C **9-Mes** could be obtained as ***Z,Z*** : ***E,E*** mixture with ratio of 1 : 1 in 72 % yield as an orange powder in analytically pure form. The amounts of the *Z,Z*-isomer can be increased upon repeated washing steps with *n*-pentane at –30 °C, upon which the intensity of the orange color (**9-Mes-*Z,Z***) of the solid increases, however with severe loss of yield.

The diastereomeric mixture of **9-Mes** (***Z,Z*** : ***E,E*** = 1: 1*)* slowly decolorizes upon contact with air. Prolonged heating (1 h) of the orange solid (***Z,Z*** : ***E,E*** = 1: 1*)* at 60 °C, already leads to color change to brown, which can be originated to the increased formation of the thermodynamically favored dark purple ***E,E*** isomer. The transformation can be completed in a sealed vacuum glass capillary upon heating to 171 °C, resulting in the formation of a dark purple powder. ^{1}H NMR spectroscopy of the dark purple mass in (D_6)benzene revealed the quantitative formation of the ***E,E***-isomer. The diastereomeric mixture (orange-powder) is well soluble in benzene, toluene and THF and moderately soluble in *n*-pentane and *n*-hexane, affording dark purple solutions (the color can be attributed to the ***E,E***-isomer).
Heating of the isolated diastereomeric mixture of **9-Mes** (***Z,Z*** : ***E,E*** = 1: 1*)* in *m*-xylene at 130 C for 3 h resulted in the selective formation of **9-Mes-*E,E***, according to an aliquot analyzed by ^{1}H NMR-spectroscopy in (D_6)benzene. After work up, **9-Mes-*E,E*** could be isolated as dark purple microcrystalline solid in 79 % yield in analytically pure form. The compound slowly decolorizes to a white solid upon exposure to air and reversibly melts at 216 °C. Upon reaching 220 °C the dark purple mass changes to a yellow colored melt. ^{1}H NMR spectroscopy of the yellow mass revealed a rather unselective decomposition. The compound is well soluble in aliphatic and aromatic solvents, affording dark purple solutions.

Orange single crystals of **9-Mes-*Z,Z*** were grown from the diastereomeric mixture of **9-Mes** (***Z,Z*** : ***E,E*** = 1: 1*)* in a saturated *n*-pentane solution 4 °C. Dark purple blocks of **9-Mes-*E,E*** were obtained upon crystallization of the isolated ***E,E***-isomer in *n*-pentane at –30 °C. The molecular structure of **9-Mes-*Z,Z*** (*Figure 2.51* a) and **9-Mes-*E,E*** (*Figure **2.51*** (b)) feature two three-coordinated silicon centers, which are interconnected via a Si–Si single bond (2.336(3) Å (***Z,Z***), 2.329(3) Å (***E,E***)). In **9-Mes-*Z,Z*** the two silicon-centers display a trigonal planar structure (Σ∢(Si1) = 353.4° (***Z,Z***), Σ∢(Si2) = 353.2° (***Z,Z***)), whereas in **9-Mes-*E*,E** the silicon centers are significantly pryamidalized (Σ∢(Si1) = 342.8° (***E,E***), Σ∢(Si2) = 340.5° (***E,E***)). In both cases the silenyl (Si=C^{carb}) moieties are orientated orthogonally with respect to each other, as evidenced by the torsion angles of τ(C^{carb}-Si-Si-C^{carb}) = 125.5(6)° (***Z,Z***))) and τ(C^{carb}-Si-Si-C^{carb}) = 107.8(4)°(***E,E***)).
Both N-Dipp moieties of the $caac^{Me}$ ligands in **9-Mes-*Z,Z*** are orientated cis with respect to the Si–Si moiety (*Figure 2.51* a (right)), thus according to the priority rules of *E*/*Z* alkenes, defined by IUPAC, the stereodescriptor ***Z,Z*** can be assigned. Conversely, both N-Dipp moieties of the $caac^{Me}$ ligands in **9-Mes-*E,E*** are orientated trans with respect to the Si–Si moiety (*Figure 2.51* b (right)) and thus the stereodescriptors ***E,E*** can be assigned.

The Mes substituents are in gauche ($\tau(C^{Mes}\text{-Si-Si-}C^{Mes}) = 63.8(5)°$) in **9-Mes-*Z,Z*** and in synclinal conformation in **9-Mes-*E,E*** ($\tau(C^{Mes}\text{-Si-Si-}C^{Mes}) = 12.3(4)°$) and are orientated orthogonally with respect to the Si–Si bond in both molecules. Given the gauche and synclinal conformation of the Mes substituents in **9-Mes-*Z,Z*** and **9-Mes-*E,E*** the two solid state structures almost feature C_2-symmetry, respectively.

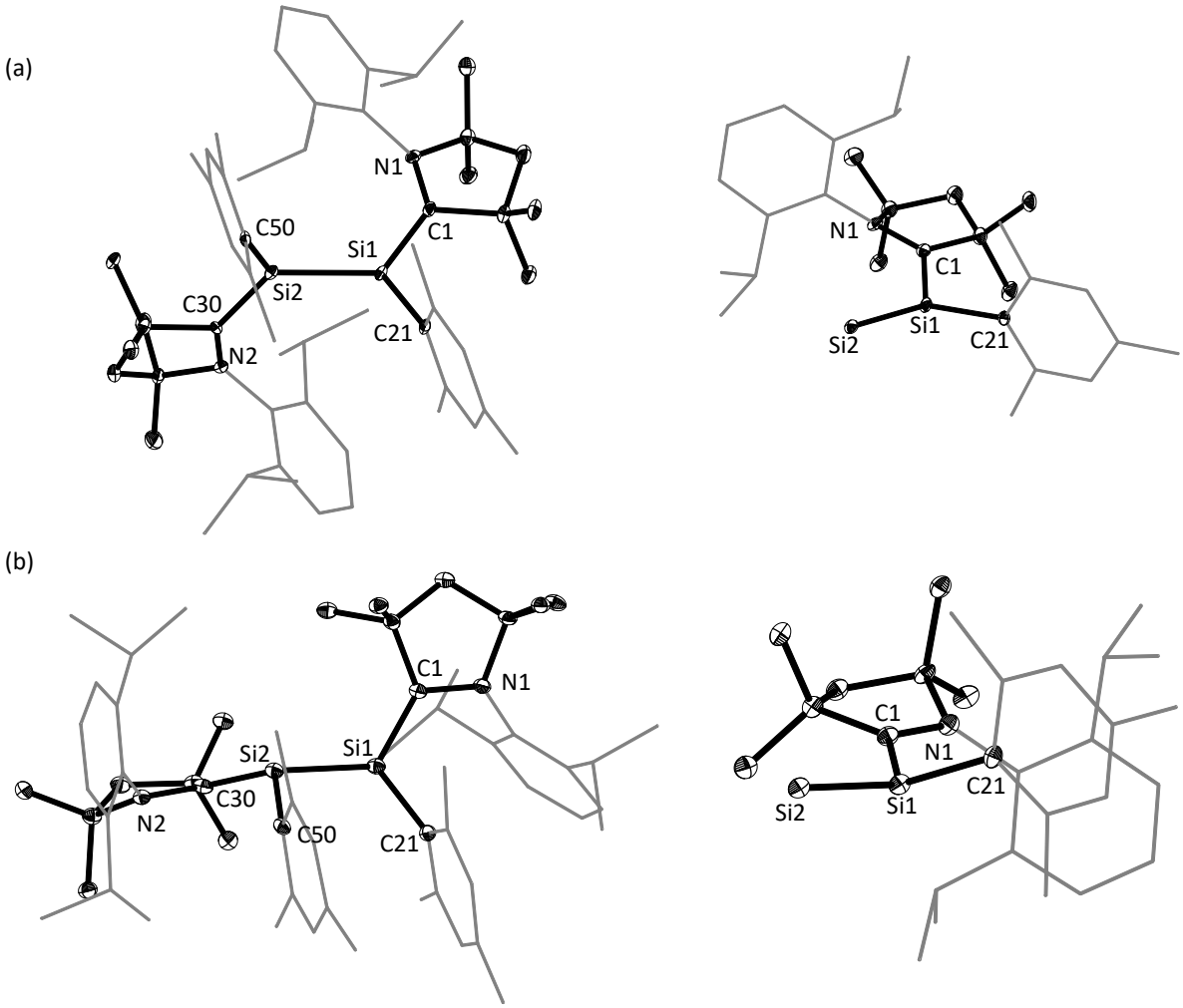

Figure 2.51. Diamond plot of the molecular structure of **9-Mes-*Z,Z*** (a) and **9-Mes-*E,E*** (b) and depicted conformation of one pyramidal 2-aminosilene moiety(right), respectively. Thermal ellipsoids are set at 30 % probability, and hydrogen atoms were omitted. In the depicted structures the Dipp-substituent of the caac^{Me} ligand and the Mes-substituent are presented in the wire-frame for the sake of clarity. Selected bond lengths [Å], bond angles [°] and torsion angles [°]:

9-Mes-*Z,Z*: Si1–Si2 2.336(3), Si–C1 1.79(1), Si1–C21 1.92(1), Si2–C30 1.79(1), Si2–C50 1.90(1), N1–C1 1.40(1), N2–C30 1.40(1), C1–Si1–Si2 127.1(3), C1–Si1–C21 112.8(5), C21–Si1–Si2 113.5(3), C30–Si2–Si1 126.4(3), C30–Si2–C50 113.3(4), C50–Si2–Si1 113.5(3), C30–Si2–Si1–C1 125.5(6), N1–C1–Si1–Si2 -22.7(2), N2–C30–Si2–Si1 -23.7(2), C21–Si1–Si2–C50 63.8(5).

9-Mes-*E,E*: Si1–Si2 2.329(3), Si1–C1 1.793(7), Si1–C21 1.904(7), Si2–C30 1.796(8), Si2–C50 1.899(7), N1–C1 1.406(8), N2–C30 1.409(8), C1–Si1–Si2 121.3(3), C1–Si1–C21 113.8(3), C21–Si1–Si2 107.7(2), C30–Si2–Si1 120.8(2), C30–Si2–C50 113.0(3), C50–Si2–Si1 106.7(2), C1–Si1–Si2–C30 107.8(4), N1–C1–Si1–Si2 173.0(5), N2–C30–Si2–Si1 172.2(4), C21–Si1–Si2–C50 12.3(4).

The Si–C^{carb} bond lengths in **9-Mes-*Z,Z*** (1.79(1) Å, 1.79(1) Å) and **9-Mes-*E,E*** (1.793(7) Å, 1.796(8) Å) are on the shorter end of literature reported Si–C^{carb} bond lengths in caac^{Me}-stabilized silicon(I) dimers (*Table 2.24*) and are only slightly increased compared to typical Si=C double bonds reported in silenes (1.702 – 1.764 Å).[184] The dramatic shortening of the Si–C^{carb} bond is in line with a significant elongation of the N–C^{carb} bond in **9-Mes-*Z,Z*** (1.40(1) Å, 1.40(1) Å) and **9-Mes-*E,E*** (1.406(8) Å, 1.409(8) Å) compared to that observed in the starting material **2-Mes** (1.350(2) Å).

Applying the priority rules for axial chirality, according to IUPAC, the stereo descriptor R_a whith the chirality axis passing through the Si–Si bond can be assigned in the molecular structure of **9-Mes-*Z,Z*** depicted in *Figure 2.51* a.

The significant pyramidalization of the two silicon centers in **9-Mes-*E,E***, renders the molecules chiral, according to the Cahn-Ingold-Prelog priorities rules the stereodescriptor *R,R* can be assigned in the molecular structure of **9-Mes-*E,E*** depicted in *Figure 2.51* (b). The other enantiomer is also found in the crystal-lattice, the compound crystallizing in the achiral space group ($P2_1/c$).

Table 2.24. Crystallographic data of **9-Mes** and its isomers, compared to literature known compounds.

Comp.	Si–Si / Å	Si–C^{carb} / Å	N–C^{carb} / Å	Σ∢(Si) / (deg)	DP[a] / %	Ref.
SiBr(Mes)(caac^{Me}) (**2-Mes**)	–	1.842(1)	1.350(2)	326.3	37	
Si_2Mes_2(caac^{Me})$_2$	2.336(3)	1.79(1)	1.40(1)	353.4	7	*this*
orange (**9-Mes-*Z,Z***)		1.79(1)	1.40(1)	353.2	8	*work*
Si_2Mes_2(caac^{Me})$_2$	2.329(3)	1.793(7)	1.406(8)	342.8	19	
dark purple (**9-Mes-*E,E***)		1.796(8)	1.409(8)	340.5	22	
$Si_2Cp'_2$(caac^{Me})$_2$ **9-Cp'**	2.288(1)	1.789(1)	1.383(2)	351.1	10	
Si_2Cl_2(caac^{Me})$_2$	2.306(1)[b]	1.823(3)	1.336(3)	328.0	36	[128]
		1.826(3)	1.337(2)	329.0	34	
Si_2I_2(caac^{Me})$_2$	2.337(1)	1.846(3)	1.343(3)	328.3	35	[121]
		1.841(3)	1.345(3)	330.6	33	
Si_2H_2(caac^{Me})$_2$	2.334(1)[c]	1.817(2)	1.362(2)	327.4	36	[129]
Si_2Me_2(caac^{Me})$_2$	2.314(1)	1.798(1)	1.384(1)	345.2	16	[130]
		1.804(1)	1.383(1)	344.0	16	
Si_2Ph_2(caac^{Me})$_2$	2.306(1)	1.805(2)	1.381(3)	343.3	19	[131]
		1.803(2)	1.377(3)	345.8	16	

[a]: DP the degree of pyramidalization (DP) value of 0 % describes a trigonal planar coordination of the silicon atom with the sum of bond angles equal to 360°. A DP value of 100 % corresponds to a trigonal pyramidal coordination of the silicon atom with the sum of bond angles equal to 270°.

DP (in %) = 100 % · [360 − Σ∢(Si) / (deg)]/90

[b]: mean value of two independent molecules are given.

[c]: compound contains a crystallographic inversion center at the mid point of the Si–Si bond.

In terms of structural parameters **9-Mes-*Z,Z*** remarkably differs from the reported caac^{Me}-stabilized silicon(I) dimers, by containing trigonal planar coordinated silicon centers (DP(Si1, Si2) = 7, 8) and the sterically highly unfavorable Z,Z conformation (*Table 2.24*). However, the compound compares remarkably well to the cyclopentadienyl substituted dislicon(I) compound **9-Cp'**, isolated in this work. The thermodynamically favored ***E,E***-isomer, in contrast, compares well to the reported caac^{Me} stabilized silicon(I) compounds by containing significant pyramidalized silicon centers (DP(Si1, Si2) = 19, 22) and a highly dynamic structure in solution (*Table 2.24*).

The full NMR assignment of both isomers **9-Mes-*Z,Z*** and **9-Mes-*E,E*** present in the diastereromeric mixture was made possible in (D_6)benzene at 343 K through high-resolution correlation spectroscopy.
The ^{1}H, $^{13}C\{^{1}H\}$ as well as $^{29}Si\{^{1}H\}$ NMR spectra of **9-Mes-*Z,Z*** in (D_6)benzene can be rationalized by a C_2-symmetry, which renders the two Si(Mes)(caac^{Me}) moieties equally. NMR spectra of **9-Mes-*E,E*** in the same diastereomeric mixture reveal an averaged C_S-symmetry at elevated temperatures with broad signals stil appearing at 343 K (*Figure* 2.52).

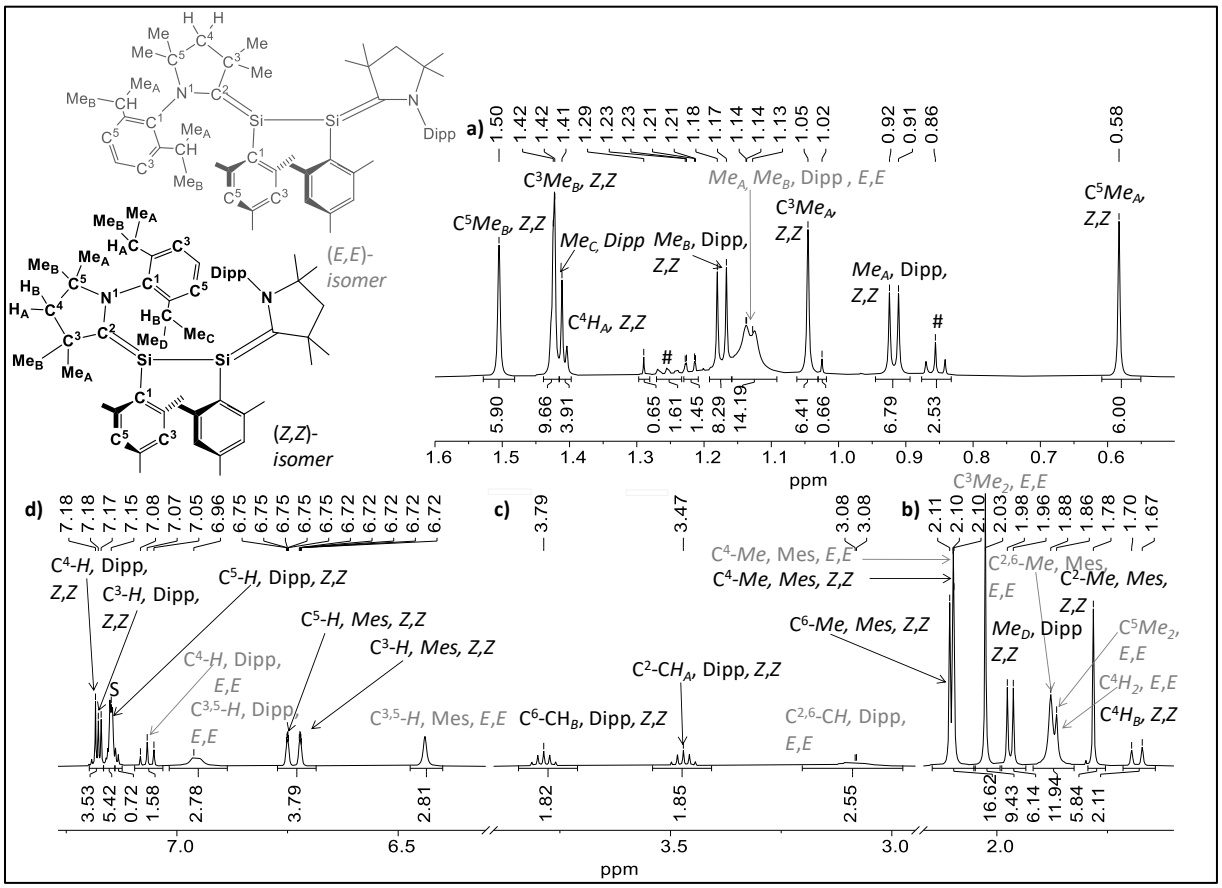

Figure 2.52. Signal assignment of the ^{1}H NMR spectrum (500.17 MHz) of the diastereomeric mixture of **9-Mes** in (D_6)benzene at 343 K; signals of the deuterated solvent and *n*-pentane are marked with the character S and an asterisk (#), respectively.

The ^{1}H NMR spectrum of **9-Mes-*Z,Z*** (*Figure 2.52*) displays four singlets for the methyl groups of (C^{3}*Me$_A$Me$_B$*, C^{5}*Me$_A$Me$_B$*), as well as two doublets for the hydrogen atoms (C^{4}*H$_A$H$_B$*) for the backbone of the caac^{Me} carbene moiety. In total four doublets of the methyl grupps of the isopropylgroups (C^{2}CH$_A$*Me$_A$Me$_B$* and C^{6}CH$_B$*Me$_C$Me$_D$*) as well as two septets for the methine protons of the isopropyl groups are observed in the aliphatic region for the Dipp substituent. In case of the Mes substituent three signals of the Me-groups (C^{2,4,6}-*Me*, Mes), as well as two resonances for the C^{3,5}-*H* protons in the aromatic region are observed, suggesting a rigid structure in solution. The Mes substituent does not rotate even at elevated temperatures (*Figure 2.52*).
In contrast, the ^{1}H NMR resonances of **9-Mes-*E,E*** present in the diasteromeric mixture (*Figure 2.52*) display two singlets for the methyl groups of (C^{3}*Me$_2$*, C^{5}*Me$_2$*) and a singlet for the hydrogen atoms (C^{4}*H$_2$*) for the backbone of the caac^{Me} carbene moiety. Two broad resonances were observed for the methyl groups of the isopropylgroups (C^{2,6}CH*Me$_A$*Me$_B$ and C^{2,6}CHMe$_A$*Me$_B$*), as well as one broad signal for the methine protons of the isopropyl groups (C^{2,6}C*H*Me$_A$Me$_B$). Similarly, the Mes-substituent featured broad resonances: two signals for the Me group (C^{2,6}-*Me* and C^{4}-*Me*) and one resonance for the aromatic C^{3,5}-*H* protons are observed. These findings suggest a highly fluctional behavior for **9-Mes-*E,E*** in solution, which was investigated by VT ^{1}H NMR spectroscopy (see *section 2.4.5.2*).

Table 2.25. Crystallographic and NMR spectroscopic data (given in (D$_6$)benzene 298 K) of isolated caac^{Me}-stabilized silicon(I)-dimers, compared to literature known compounds.

Comp.	Diast.[a]	Sym[b]	δ(^{29}Si) / ppm	δ(^{13}C^{carb}) / ppm	δ(^{15}N) / ppm	Ref.
SiBr(Eind)(caac^{Me}) **2-Eind-*E***	*E*	C_1	31.1	165.2	104.3	
SiBr(Eind)(caac^{Me}) **2-Eind-Z**	*Z*	C_S	1.8	175.9	135.1	*this*
Si$_2$Mes$_2$(caac^{Me})$_2$ **9-Mes-*Z,Z***	*Z,Z*	C_2	10.1[c]	185.8	120.9	*work*
Si$_2$Mes$_2$(caac^{Me})$_2$ **9-Mes-*E,E***	*E,E*	C_S	–0.21[c]	195.9	133.7	
Si$_2$Cl$_2$(caac^{Me})$_2$	*Z,Z*	C_S	25.62	–[d]	–	[128]
Si$_2$I$_2$(caac^{Me})$_2$	*Z,Z*	C_2[e]	–0.5	207.2	–	[121]
Si$_2$H$_2$(caac^{Me})$_2$	*E,E*	C_S	–45.5	211.8	–	[129]
Si$_2$Me$_2$(caac^{Me})$_2$	*E,E*	C_S	0.72[d]	191.3	–	[130]

[a]: Determined orientation of the N-Dipp moiety in the soid state (orientated cis (*Z*) or trans (*E*) to the high priority group of the silenic silicon-center in the solid state. [b] averaged symmetry found by NMR spectroscopy in solution at ambient temperature. [c]: measured in (D$_6$)benzene at 343 K. [d]:signal was not given in the literature. [e]: Si$_2$I$_2$(caac^{Me})$_2$ featured a C_2-symmetry with broad resonances in the recorded ^{1}H NMR spectrum in (D$_6$)benzene at ambient temperature. It is safe to assume that the signals coalesces at higher temperatures.

The $^{29}Si\{^{1}H\}$-NMR spectrum of the diastereromeric mixture of **9-Mes** in (D_6)benzene at 343 K displays two signals at –0.21 (***E,E***) and 10.1 ppm (***Z,Z***), respectively. The significant upfield shift of the silenic Si-resonance of ***Z,Z***-isomer (10.1 ppm) towards the ***E,E***-isomer (–0.21 ppm) can be rationalized by the stronger π-character of the $Si=C^{carb}$ double bond observed in ***Z,Z***-isomer compared to the ***E,E***-isomer. Further evidence for the increased Si=C π-character in the ***Z,Z***-isomer are given by the $^{13}C^{CAAC}$ and $^{15}N^{CAAC}$ resonances in **9-Mes-*Z,Z*** (185.8 ppm, 120 ppm), which are significantly upfield shifted compared to **9-Mes-*E,E*** (195.9 ppm, 133.7 ppm).

In terms of structural and NMR spectroscopic features **9-Mes-*Z,Z***, differs substantially of literature known $caac^{Me}$–stabilized silicon(I)-dimers, which can be attributed to the rather strong $Si=C^{carb}$ silene character and the rigid structure observed in solution (*Table* 2.19 and *Table 2.21*). The dark purple isomer **9-Mes-*E,E***, on the other hand, in terms of its structural and NMR spectroscopic features compares well to $Si_2Me_2(caac^{Me})_2$[130] and the typical reported pyramidalized 1,4-diamino,2,3-disilabutadienes. Overall the system is strongly related to the SiBr(Eind)($caac^{Me}$) (**2-Eind**) compound, which featured an irreversible *E* → *Z* isomerization (see *section 2.2.4*).

2.4.5.2 Study of the dynamics in 9-Mes-*E,E* by VT-NMR spectroscopy

The NMR spectroscopic characterization of **9-Mes-*E,E*** after isolation as dark purple solid, gave a much clearer picture in the nature of the dynamic processes, which were observed in (D_6)benzene (*Figure 2.53*) and in (D_8)toluene solution (*Figure 2.54*).

The ^{1}H NMR of **9-Mes-*E,E*** in (D_8)toluene at 298 K (*Figure 2.54*, middle) displayed broad signals with exception of the C^3-*Me*$_A$Me$_B$, C^4-*Me*, Mes and C^4-*H*, Dipp resonances which were observed as sharp signals, indicating a dynamic process with rather high activation barrier at ambient temperature in solution. At 243 K (*Figure 2.54*, bottom) a C_2-symmetry could be frozen out, whereas at 373 K (*Figure 2.54*, top) an averaged C_S-symmetry was observed for the caac^{Me} and Mes substituents in **9-Mes-*E,E***, respectively.

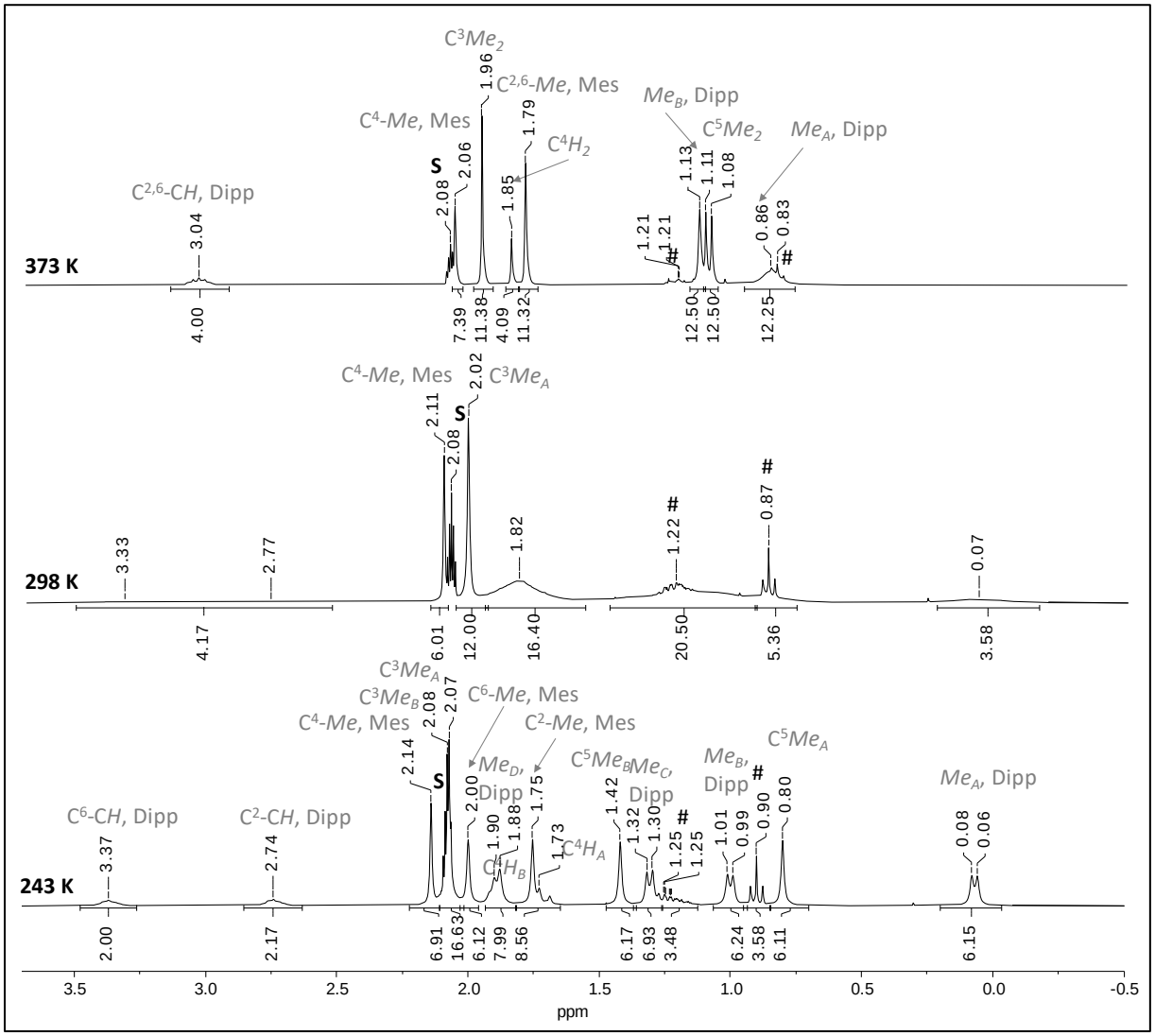

Figure 2.54. Excerpt of the ^{1}H NMR spectra (300.14 MHz) of **9-Mes-E,E** in (D_8)toluene at 243 K (bottom), 298 K (middle), 373 K (top); signals of the deuterated solvent and *n*-pentane are marked with the character **S** and an asterisk (#), respectively. The compound was characterized by high resolution correlation NMR spectroscopy in (D_8)toluene at 243 K and 343 K, respectively (for more information see *chapter 4.4*)

This can be highly likely attributed to two dynamic processes in **9-Mes-*E,E*** at ambient temperature in solution (*Figure 2.55*): an enantiomerisation of the two chiral silicon centers in **9-Mes-*E,E*** (*Figure 2.55*, (a)), via a nonsynchronous narcissistic reaction as described for **9-Br** (see *section 2.4.3*), as well as a hindered rotation of the Mes substituents about their respective Si–C^{Mes} bonds (*Figure 2.55*, (b)). At 243 K both dynamic processes can be frozen out resulting in an observed C_2-symmetry for **9-Mes-*E,E*** with two homotopic Si(Mes)($caac^{Me}$) moieties and rigid Mes substituents (*Figure 2.54*, bottom), respectively. At 373 K the fast enantiomerization of the chiral silicon centers in **9-Mes-*E,E*** lead to a time averaged achiral structure with the mirror plane bisecting both $caac^{Me}$ substituents accompanied by a fast rotation of the Si–C^{Mes} bonds, thus explaining the simple ^{1}H NMR spectrum of **9-Mes-*E,E*** at that temperature (*Figure 2.54*, top).

A full line shape analysis of recorded variable temperature ^{1}H NMR spectra of **9-Mes-*E,E*** (see *section 5.6.5*) in (D_8)toluene was performed. The enantiomerization was studied upon simulation of the two septets C^2-CH_AMe$_A$Me$_B$ and C^6-CH_BMe$_B$Me$_C$ of the *i*Pr groups of the Dipp substituents, which featured a coalescence temperature at 293 K. The hindered rotation of the Mes substituent was studied upon simulation of the two aromatic resonances C^3-*H* and C^5-*H* of the Mes group, which featured coalescence temperature at 283 K. The Gibb's free energy of activation gave 58.6 ± 2.0 kJ mol^{-1} and 59.4 ± 3.1 kJ mol^{-1} for the enantiomerisation and hindered rotation, respectively.

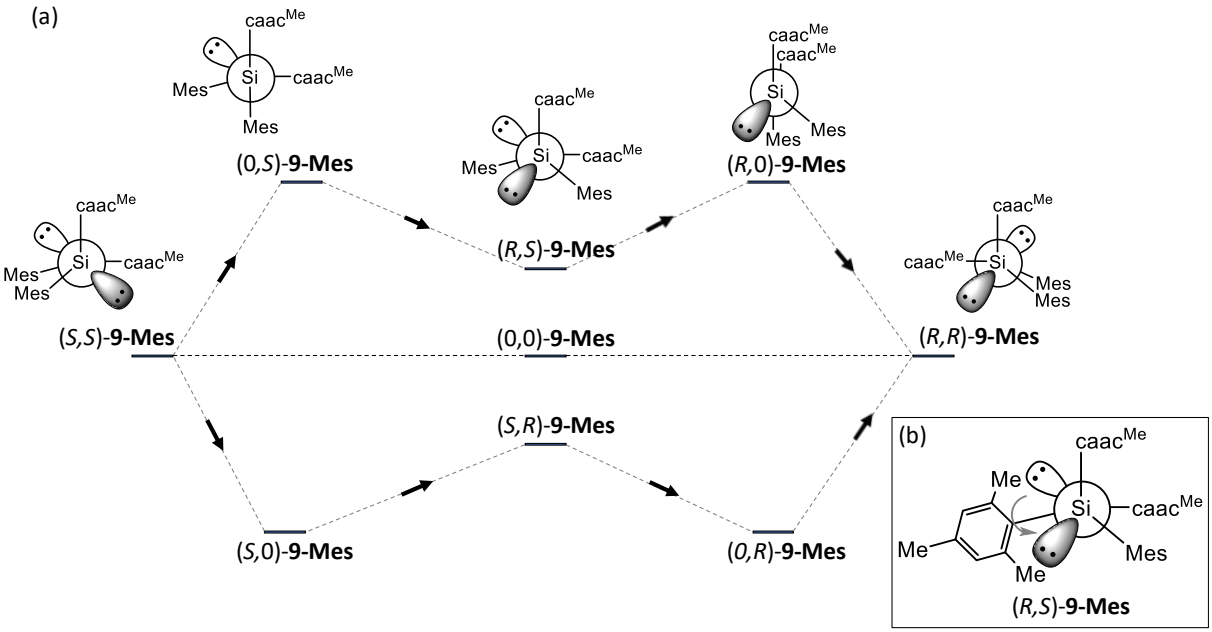

Figure 2.55. (a): 2D plot of the two enantiomeric pathways, leading to the enantiomerization of the two chiral silicon centers in **9-Mes-*E,E***. Newman projection of $Si_2Mes_2(caac^{Me})_2$ (**9-Mes-*E,E***) along the Si–Si bond showing the stepwise pyramidal inversion of the two chiral silicon centers along one of the two pathways. In analogy to **9-Br** it is safe to assume, that the direct pathway via the transition state (0,0)-**9-Mes** lies to high in energy (for more details see *section 2.4.3*). (b): Rotation of the Mes substituent about the Si–C^{Mes} bond in the (*R*,*S*) diastereomer of **9-Mes-*E,E***.

It might be that both dynamic processes (a) and (b) are interconnected with each other. Due to the synclinal orientation of the Mes substituents in **9-Mes-*E,E*** in the molecular structure the rotation of the Mes-groups seems to be impossible. Upon enantiomerization of one chiral silicon center the (*S,R*) diastereomer is formed, which in terms of sterical demands might allow the rotation of the Si–C^{Mes} bond at elevated temperatures (*Figure 2.55*, (b)). However, further theoretical calculations are necessary to get a better insight into the nature of the dynamic processes in **9-Mes-*E,E***.

2.4.5.3 Kinetic study of the thermal *Z,Z* → *E,E* isomerization in 9-Mes

The kinetics of the *E,E* → *Z,Z* thermal isomerization was studied at 90 °C, 100 °C and 110 °C (see also *section 5.7.2*). A 1:1 diastereomeric mixture of **9-Mes** (*Z,Z* : *E,E*) was dissolved in (D_8)toluene and distributed into three young-NMR samples. The change in the *Z,Z* to *E,E* ratio was monitored by ^{1}H NMR spectroscopy, by integration of the $C^{3,5}$–*H*, Mes resonances of the ***E,E*** and the ***Z,Z*** isomer, respectively. The kinetic constants of the irreversible ***Z,Z*** → ***E,E*** isomerization were derived from the Arrhenius equation. The thermodynamic parameters of the activation barrier of the thermal induced ***Z,Z*** → ***E,E*** isomerization are obtained from the Eyring-Polanyi equation plot of ln(k/T) vs 1/T: The enthalpy of activation ($\Delta H^{\ddagger}$ = 126.3 ± 2.3 kJ mol^{-1}) and entropy of activation ($\Delta S^{\ddagger}$ = 20.4 ± 0.6 J K^{-1} mol^{-1}) were obtained from the slope and the intercept of the linear fit, respectively. The Gibbs free activation energy can be calculated using the Gibb's Helmholtz equation, which gives $\Delta G^{\ddagger}$(298 K) = 120.2 ± 2.3 kJ mol^{-1}.

The ***Z,Z*** → ***E,E*** isomerization in $Si_2Mes_2(caac^{Me})_2$ (**9-Mes**) can be rationalized by two pathways: a concerted rotation of the $caac^{Me}$ substituents about their Si–C^{carb} bonds (*Figure 2.56*) or a stepwise consecutive rotation of the Si–C^{carb} bonds bonds in both 2-(amino)silenyl-moieties (*Figure 2.57*), which proceeds via an ***E,Z*** diastereomer.

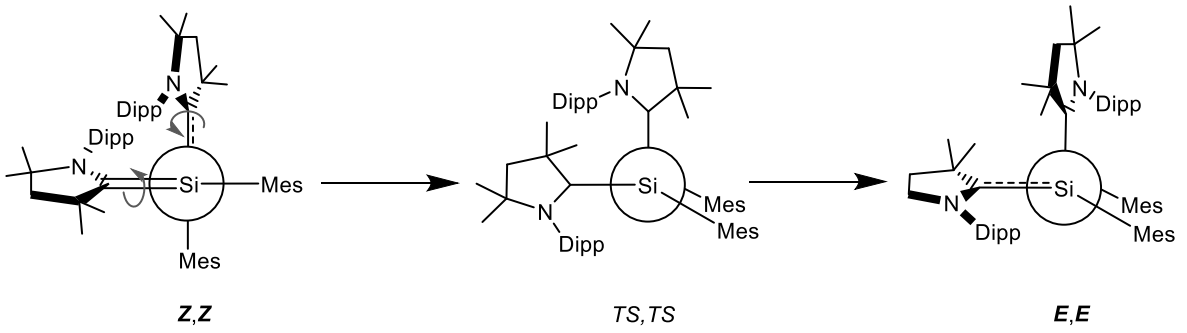

Figure 2.56. Newman projection of $Si_2Mes_2(caac^{Me})_2$ (**9-Mes**), along the Si–Si bond, showing the concerted rotation of the Si–C^{carb} bonds, which results in the irreversible ***Z,Z*** → ***E,E*** isomerization. The concerted rotation undergoes highly likely via a transition state (*TS*, *TS*) in which both N-Dipp groups are orientated orthogonal with respect to the Si(Mes)Si(Mes)($caac^{Me}$) moiety. The transition state should feature more pyramidalized silicon centers and elongated Si–C^{carb} bonds. Upon further rotation of both Si–C^{carb} bonds the thermodynamically favored ***E,E***-isomer is formed.

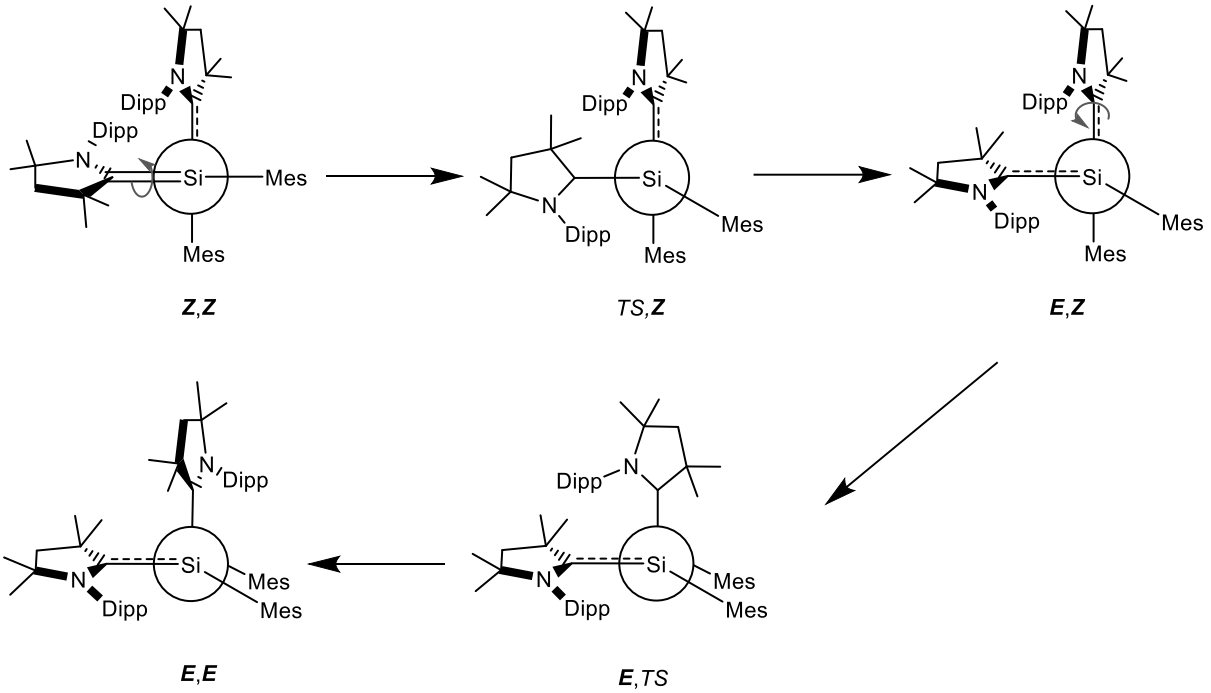

Figure 2.57. Newman projection of $Si_2Mes_2(caac^{Me})_2$ (**9-Mes**), along the Si–Si bond, showing the stepwise consecutive rotation of the $Si–C^{carb}$ bonds, which results in the irreversible ***Z,Z*** → ***E,E*** isomerization. The stepwise consecutive rotation undergoes highly likely via transition state (*TS*,**Z**) to an intermediate ***E,Z*** diastereomer. The rotation of the second $Si–C^{carb}$ bond proceeds via the transition state (***E***,*TS*) to the thermodynamically favored ***E,E***-isomer. The transition states should feature more pyramidalized silicon centers and elongated $Si–C^{carb}$ bonds.

The experimentally obtained activation barrier of $\Delta G^{‡}(298K) = 120.2 \pm 2.3$ kJ mol^{-1} for the irreversible ***Z,Z*** → ***E,E*** isomerization in **9-Mes** compares rather well to activation barrier of $G^{‡}(298K) = 115.1 \pm 1.7$ kJ mol^{-1} for the irreversible ***E*** → ***Z*** isomerization in **3-Eind**, which features the rotation of a single $Si–C^{carb}$ bond. This highly suggests, that the isomerization in **9-Mes** undergoes by a stepwise consecutive rotation of the $caac^{Me}$ substituents about their respective $Si–C^{carb}$ bonds via the transient ***E***,**Z** diastereomer of **9-Mes**, which could not be detected by ^{1}H NMR spectroscopy during the kinetic study. However, further theoretical calculations are necessary in order to give an accurate description of the irreversible isomerization in **9-Mes**.

2.5 Chemistry of Potassium-Silenides

2.5.1 Introduction

Over the last two decades the chemistry of alkalimetal substituted silenes (R_2C=SiR(M), R = singly bonded substitutent, M = metal) and disilenes (R_2Si=SiR(M)) developed rapidly, enabling the isolation of novel silicon compounds with intriguing bonding features and unique reactivities.[184,228,229,19] Examples substantiating this development include a large number of disilenyl-anions, such as the aryl substituted lithiumdisilenide **II-26**,[34] which was first observed by Weidenbruch et al. and later isolated by Scheschkewitz upon reduction of Tip_2SiCl_2 with lithium in DME at elevated temperatures in 51 % yield.[35] The research group of Sekiguchi, synthesized independently the disilenide **II-27**,[230,231] upon reduction of the tetrasilabutadiene R_2Si=Si(Mes)-Si(Mes)=SiR_2 (R = SiMe(*t*Bu)$_2$) by reaction with either tBuLi or KC_8. Similarly, the silyl substitued disilenide **II-28**[232], was obtained upon reductive cleavage of Si–Si bond of the tetrasilylsilene $Si_2(SiMe^tBu_2)_4$. Alkyl-disilenide **II-29**[233], was obtained from Kira's first isolable cycilic dialkylsilylene (**I-18**)[54] upon oxidative addition of *t*BuSiCl_3, followed by reduction with an excess of KC_8. Disilenides **II-30**[234] and **II-31**[204] were obtained upon reaction of Sekiguchi's disilyne (Si(*i*Pr)(Dsi)$_2$)Si ≡ Si(Si(*i*Pr)(Dsi)$_2$)[26] (Dsi = CH($SiMe_3$)$_2$) with MeLi, and KC_8, respectively. The disilenyl-dianion **II-32**[32] (Ar = Eind = 1,1,3,3,5,5,7,7-Octaethyl-s-hydrindacene) and **II-33**[33] (Ar = Trp* = aliphatic substituent in a rigid triptcyclic framework), could be directly obtained upon 2e$^-$ -reduction from the respective dibromodisilene (Ar)SiBr=SiBr(Ar) (Ar = Eind, Trp*) with KC_8.

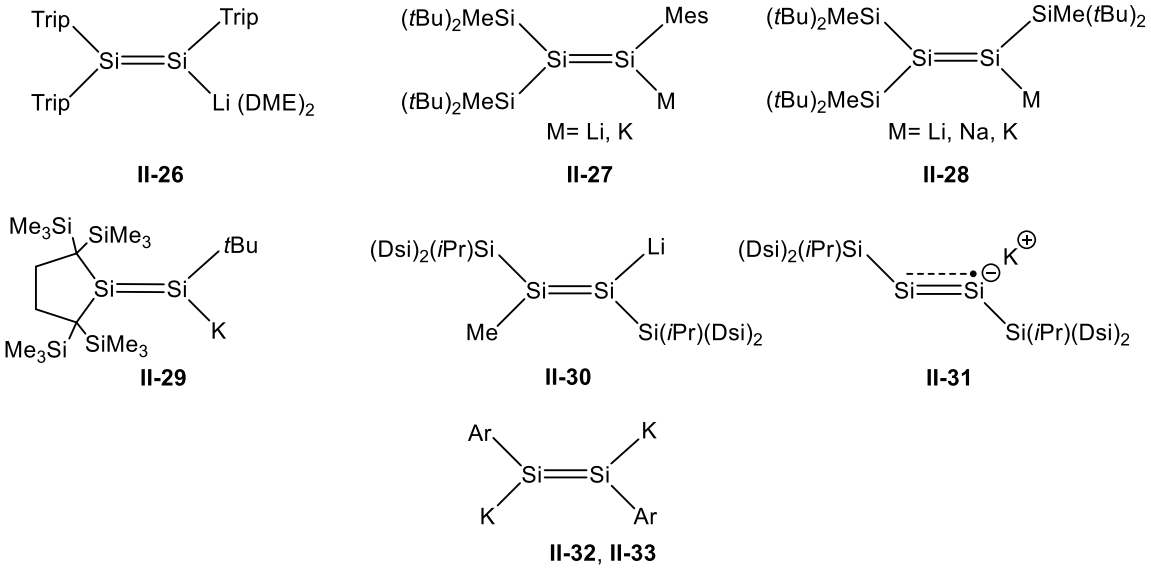

Figure 2.58. Literature known alkalimetal disilenides; Trip = C_6H_2-2,4,6-*i*Pr$_3$, Dsi = CH($SiMe_3$)$_2$.

In the sharp contrast to the wide variety of disilenyl-anions (R_2Si=SiRM) only four examples of silenyl-anions (R_2C=SiRM) with coordinated alkali-metal ions are known: The lithiumsilenides **II-34**[125] (SiR_3 = Si(*t*Bu)$_2$Me), **II-35**[125] (SiR_3 = Si(*t*Bu)Me$_2$) and **II-36**[126] were reported by Apeloig et al. The 1-adamantyl substituted silenides **II-34** and **II-35** were synthesized upon addition of THF to the aggregates of lithium silenolate with silanides [(*t*Bu$_2$MeSi)$_2$Si=C(OLi)(1-Ad)]·R_3SiLi (R_3S = (*t*Bu)$_2$MeSi (**II-34**), (*t*Bu)Me$_2$Si (**II-35**)), respectively.[125] Lithiumsilenide **II-36**, was obtained in a similar way, where the aggregate was generated in situ at low temperatures upon addition of 3.5 equiv. of LiSiMe(*t*Bu)$_2$ to the bromosilane ((*t*Bu)Me$_2$Si)$_2$Si(Br)–C(=O)(SiMe(*t*Bu)$_2$) and consecutive elimination of lithiumsilanolate LiOSiMe(tBu)$_2$ upon warming up to ambient temperatures. Silenide **II-36** could be isolated and fully characterized as contact ion pair and as well as separated solvated ion pair, which differ in terms of their colors, NMR spectroscopy and strurtural properties. [126]

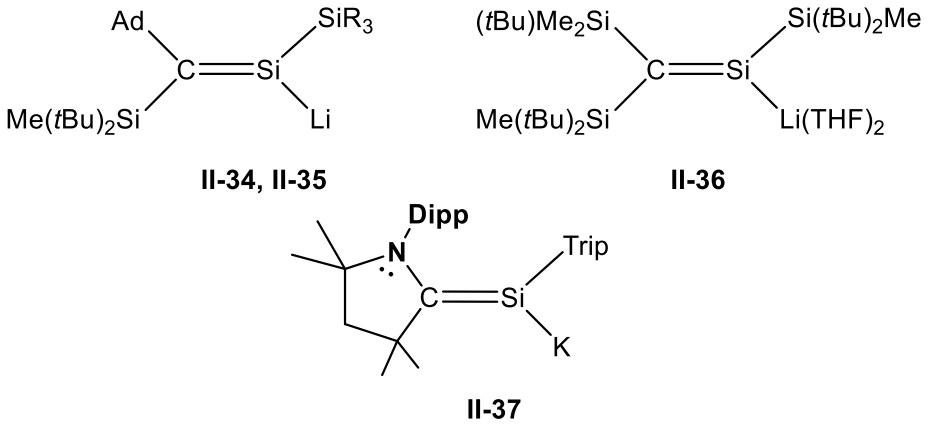

II-34, II-35 **II-36**

II-37

Figure 2.59. Literature known, silenyl anions with a coordinated alkali metal ion; SiR_3 = SiMe(*t*Bu)$_2$ (**II-34**), SiMe$_2$(*t*Bu) (**II-35**), Trip = C_6H_2-2,4,6-*i*Pr$_3$; Ad = adamantyl.

The potassium-silenide **II-37**[124] was reported recently by H. Roesky et al. and was obtained upon one pot reduction of the trichlorosilane TripSiCl$_3$ in precence of caac^{Me} carbene with 8.5 equiv. of KC_8 in THF starting at lower temperatures. In contrast to lithiumsilenides **II-34 – II-36**, the sp^2 hyrbridized carbon in **II-37** is not originated from a singly or doubly bonded substituent, but rather to the carbene carbon center of the neutral cyclic alkyl(amino)carbene ligand.

2.5.1.1 Reactivty of Silenides

Over the last two decades the chemistry of alkalimetal substituted silenes (R_2C=SiR(M), R = singly bonded substitutent, M = metal) and disilenes (R_2Si=SiR(M)) developed rapidly, leading to a plethora of novel silicon compounds with intriguing bonding features and synthetic potential.[184,228,229,19] Since of the isolation of the first lithiumdisilenide $Trip_2Si$=Si(Trip)Li (**II-26**) in 2004 by Scheschkewitz et al. the number of disilenides expanded rapidly (*Figure 2.58*) enabling the exploration of their chemistry. Selected examples substantiating this development include the isolation of functionalized disilenes[228], phosphasilenes[235], tetrasilabutadienes[236], trans-metallated disilenides[237], disilabicyclopentan-4-ones[238],cyclotrisilanes,[228] a tricyclic aromtic isomer to hexasilabenzene,[36] a trisilaallylchloride,[239] an unprecedent reduction product of CO,[240] as well as a mixed heavier Si=Ge analogue of a vinyl anion.[241]

In the sharp contrast to the wide variety of disilenyl-anions (R_2Si=SiRM) only four examples of silenyl-anions (R_2C=SiRM) are known (*Figure 2.59*). Especially scarce is the reactivity of silenides. Major contribution in studying the reactivity of lithium-silenides was provided by the research group of Apeloig. Reaction of lithium silenides **II-35** and **II-36** (*Scheme 2.14*) with a variety of halogen containing electrophiles led via oxidation of the silicon center to the formation of persistent silenyl radicals **II-19** and **II-20**, which can be described as s-type radicals with the spin density mainly localized at the silicon center.[206] Similarly, reaction of silenide **II-36** with (*t*Bu)HgCl led to the formation of the transmetallated silenide **II-40**, which upon irradiation in toluene solution selectively transformed into the silenyl radical **II-20**.[206] The silenyl radicals could be only characterized by EPR spectroscopy in solution, since they decompose rather fast ($t_{1/2}$ = 0.5 h) to the respective hydridosilenes (**II-38**, **II-39**). The observed silenyl radicals by Apeloig et al. clearly differ to the isolated two-coordinated neutral silicon(I) radicals discussed in this work (see *section 2.3.2*).

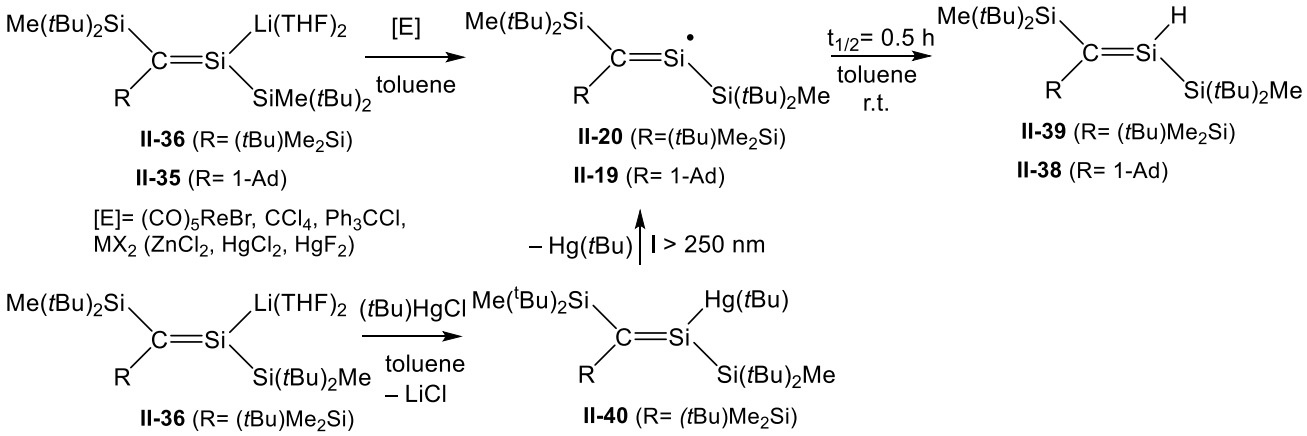

Scheme 2.14. Literature known reactivity of lithium-silenides **II-35** and **II-36** with selected electrophiles.[206]

Very recently Apeloig could also show the unprecedent reaction of silenyllithium **II-36** with CO (*Scheme 2.15*), which can be rationalized by the reductive insertion of CO into the Si=C bond, yielding the lithium 1-silaallenolate **II-41**, which appears as a dimer in the solid state. Reaction of lithium 1-silaallenonlate **II-41** with $SiMe_3Cl$ led to the formation of a silaallene **II-42**.[242]

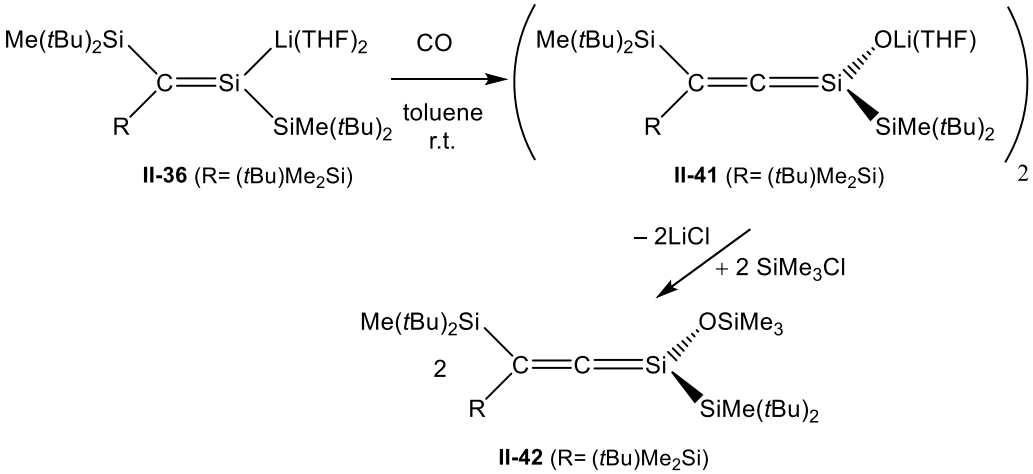

Scheme 2.15. Literature known reaction of silenyllithium **II-36** with CO at ambient temperature.

2.5.2 Synthesis and Properties of Potassium-Silenides

2.5.2.1 Synthesis and properties of SiK(R)(caac^{Me})

Potassium-silenides **4-Si** and **4-N** were obtained via the 1e$^-$-reduction of the radical **3-Si** and **3-N** with KC_8 or by the direct reduction of 2-aminobromosilenes SiBr(R)(caac^{Me}) (R = Si(SiMe$_3$)$_3$ (**2-Si**), N(SiMe$_3$)$_2$ (**2-N**)) with 3 equivalents of KC_8 in benzene, respectively. Similarly, potassium-silenide **4-P**, could be obtained upon reduction of SiBr(PMes$_2$)(caac^{Me}) (**3-P**) with 3 equivalents of KC_8 in benzene. Monitoring of the reaction mixture by ^{1}H NMR spectroscopy in (D_6)benzene revealed the quantitative formation of potassium-silenides SiK(R)(caac^{Me}) (R = Si(SiMe$_3$)$_3$ (**4-Si**), N(SiMe$_3$)$_2$ (**4-N**), PMes$_2$ (**4-P**)). After work up, **4-Si** was obtained in analytically pure form as orange-brown solid in 84 % yield. The isolation of potassium-silenides **4-N** and **4-P** appeared to be particulary challenging, since as soon as separated from KC_8, the compounds decomposed unselectively upon evaporation of the solvent. Nevertheless silenides **4-N** and **4-P** were characterized in solution of an reaction aliquot by multinuclear NMR correlation spectroscopy.

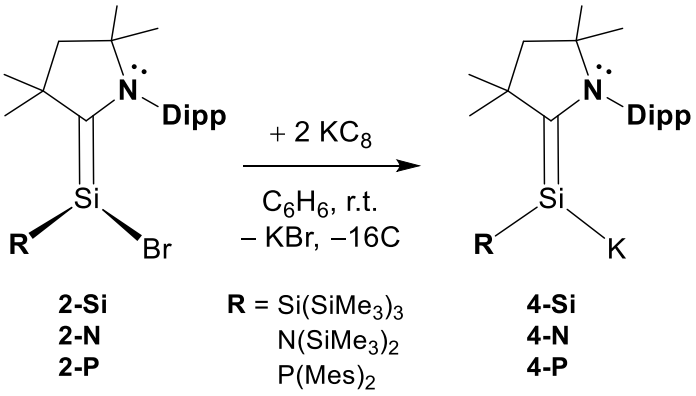

Scheme 2.16. Synthesis of potassium-silenides upon reduction of pyramidal 2-(amino)silenes

The silenides are highly pyrohphoric and immediately decomposes upon contact with air, but can be stored under argon atmosphere for months. Analytically pure **4-Si** decomposes upon melting in a vacuum sealed capillary tube at 178 °C. Silenide **4-Si** is sparingly soluble in *n*-hexane but well soluble in benzene, affording dark brown solutions.

Suitable single crystals of **4-Si·(Et$_2$O)** were grown from Et$_2$O at –24 °C as orange-blocks.The molecular structre of **4-Si·(Et$_2$O)** (*Figure 2.60*) features C_1-symmetry and a trigonal planar coordinated silicon(0) center. The sum of angles in **4-Si·(Et$_2$O)** ($\Sigma\sphericalangle$(Si) = 352.8°) is closely related to the trigonal planar lithium silenides ($\Sigma\sphericalangle$(Si) = 359.6°–360.0° (**II-34** – **II-36**)).[125,126]

The Si–C^{carb} bond length in **4-Si·(Et_2O)** (1.809(2) Å) is only slightly shorter compared to that of the pyramidal 2-aminosilene **2-Si** (1.836(2) Å) but still longer than that of the lithium-silenides (**II-34** – **II-36**: d(Si–C^{carb}) = 1.762(3) – 1.778(3) Å).[125,126]
Besides the monomeric character of **4-Si·(Et_2O)**, it compares well to the 2-aminosilenide SiK(Trip)($caac^{Me}$) (Trip = C_6H_2-2,4,6-*i*Pr_3) (**II-37**), which appears as dimer in the solid state.[124] This can be seen by the similarities of the Si–C^{carb} and N–C^{carb} bond lengths of **4-Si·(Et_2O)** (1.813(9) Å, 1.422(10) Å) to those observed in **II-37** (d(Si–C^{carb}) = 1.793(2) Å, d(N–C^{carb}) = 1.424(3) Å). [124] Similarly, the potassium ion is covalently bonded to the Si-center in **4-Si·(Et_2O)** (d(Si–K) = 3.298(3) Å) like reported for the 2-aminosilenide **II-37** (d(Si–K) = 3.284(1) Å) [124] and lies in the typical range of potassium silanides (d(Si–K) = 3.37 – 3.42 Å).[243] In addition, the covalently bonded potassium ion is further supported by the π-interaction of the aromatic Dipp-supstituent d(C_{ring}–K) = 3.167(2) – 3.368(6) Å of the $caac^{Me}$-ligand, as described in the case of **II-37** (d(C_{ring}–K) = 3.044(2) – 3.510(2) Å). [124] The Si–Si bond length in **4-Si·(Et_2O)** (2.397(3) Å) is shorter than in the contact ion pair in **II-36** (2.486(2) Å) but compares well to the free silenide $[Li(THF)_4]^+$ $[(R_A)Si{=}C(R_A)(R_B)]^-$ (2.41(1) Å).[126]

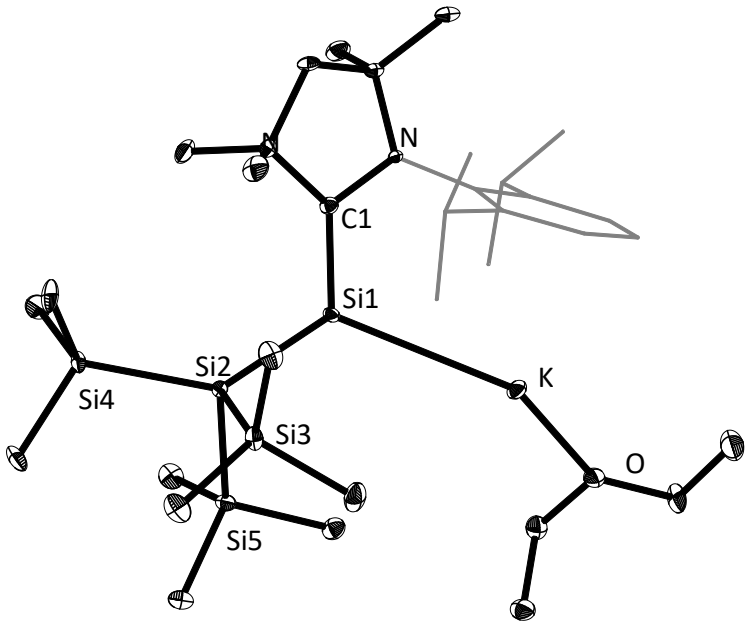

Figure 2.60. DIAMOND plot of the molecular structure of **4-Si·(Et_2O)** at 100 K. Thermal ellipsoids are set at 30 % propability and hydrogen atoms were omitted. In the depicted structure the Dipp substituent of the $caac^{Me}$ ligand is presented in the wire-frame for the sake of clarity. Selected bond lengths [Å], bond angles [°] and torsion angles [°]: Si1–Si2 2.397(3), Si1–C1 1.813(9), Si1–K 3.298(3), C1–N 1.422(10), Si2–Si3 2.3583(3),K–Si1–Si2 123.96(11), C1–Si1–K 113.93(3), C1–Si1–Si2 115.0(3).

The $^{29}Si\{^{1}H\}$ NMR spectrum of **4-Si** in (D_6)benzene displays resonances at –10.38 ppm(*TMS*), –132.09 ppm (*Si*(TMS)$_3$) and 14.34 ppm (*Si*=caac^{Me}). The ^{29}Si NMR resonance for the silenic silicon center in **4-Si** (14.35 ppm) is slightly upfield shifted when compared to the bromosilene **2-Si** (δ = 24.69 ppm) and to the recently reported 2-aminosilenide **II-37** (δ = 26.63 ppm).[124] Furthermore, this resonance is drastically upfield shifted when compared to the lithium silenides ($\delta(^{29}Si)$ = 243.87 ppm (**II-34**), 405.5 ppm (**II-36**)),[125,126]] and downfield shifted when compared to the potassium silanide KSi(SiMe$_3$)$_3$ ($\delta(^{29}Si)$ = –185.7 ppm).[243] These findings suggest, that potassium-silenide **4-Si** has considerable amount of a zwitterionic silene type of structure with a singly bonded silicion center (Si–C), which is further supported by the Si–C^{carb} bond distance of 1.809(2) Å, which is still significantly elongated in comparison to the lithiumsilenide **II-36** (1.762(3) Å).[126] The $^{13}C^{CAAC}$ resonance of **4-Si** (212.7 ppm) in (D_6)benzene is downfield shifted to that in **II-36** ($\delta(^{13}C(sp^2)$ = 143.5 ppm)[126] but compares well to silenes such as (Me$_3$Si)$_2$Si=C(OSiMe$_3$)R$_C$ (R$_C$ = *t*Bu, bicycle[2.2.2]octyl) ($\delta(^{13}C(sp^2)$ = 212.7 ppm),[244,245] showing the strong dependency on the $^{13}C(sp^2)$ signal of the substituents at the carbon center.

Structural and spectroscopic properties suggest a silenide structure with a covalently bonded potassium cation, which is further supported by the π-interaction of the aromatic Dipp substituent. The structural and electronic similarities between **4-Si** (d(Si–C^{carb}) = 1.813(9) Å, d(N–C^{carb}) = 1.42(1) Å) and the recently reported silicon(0) compound **II-37** (d(Si–C^{carb}) = 1.793(2) Å, d(N–C^{carb}) = 1.424(3) Å)[124] prompted us to classify this compound as well as potassium-silenide.

2.5.2.2 Synthesis and properties of potassium-silenides SiK(C≡CR)(caac^{Me})

After stirring a mixture of 2,3-disilabutadienes Si$_2$(C≡CR)$_2$(caac^{Me})$_2$ (R = SiMe$_3$ (**9-C$_2$TMS**), Mes (**9-C$_2$Mes**)) and 3 equivalents of KC$_8$ in benzene at ambient temperature for 3 h the supernatant solution turned dark red. Monitoring of the reaction mixture by ^{1}H NMR spectroscopy in (D_6)benzene revealed the quantitative formation of the potassiumsilenides SiK(C≡CR)(caac^{Me}) (R = SiMe$_3$ (**10-C$_2$TMS**), Mes (**10-C$_2$Mes**)), respectively.

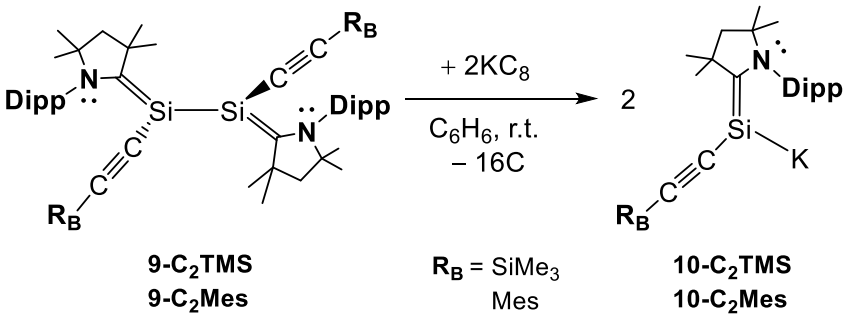

Scheme 2.17. Synthesis of potassium-silenides upon reduction of pyramidal 1,4-diamino-2,3-disilabutadienes.

After work up, potassium-silenide **10-C$_2$TMS** could be isolated as dark red highly pyrophoric powder in 79 % yield, whereas **10-C$_2$Mes** could be obtained only as crude red powder with purity of 92 % according to ^{1}H NMR spectroscopy in (D_6)benzene. Attempts to purify compound **10-C$_2$Mes** upon washing with superdried *n*-pentane (dried additionally over KC_8) at ambient temperature or crystallization from Et_2O resulted in the formation of considerably amounts of decomposition products. Similar behavior was not observed in case of **10-C$_2$TMS**, the compound could be obtained in analytically pure form after washing with superdried *n*-pentane at ambient temperature and was isolated as an orange-brown solid. The compound decomposes upon melting at 182 °C. ^{1}H NMR spectroscopy of the molten mass in (D_6)benzene revealed a rather unselective decomposition.

Similar like the literature reported potassium-silenide SiK(Trip)(caac^{Me}) (Trip = C_6H_2-2,4,6-*i*Pr$_3$) (**II-37**)[124] the silenide **10-C$_2$TMS** appears as a dimer in the solid state (*Figure* 2.61 (left)). The crystallographic inversion center (i) is located at the mid-point of the four-membered Si_2K_2 ring. The structure can be rationalized as a dimer between two trigonal planar coordinated potassium-silenides ($\Sigma\measuredangle$(Si) = 357.1°), which are twisted by 180° to each other and are coordinated via their respective K–Si bonds.

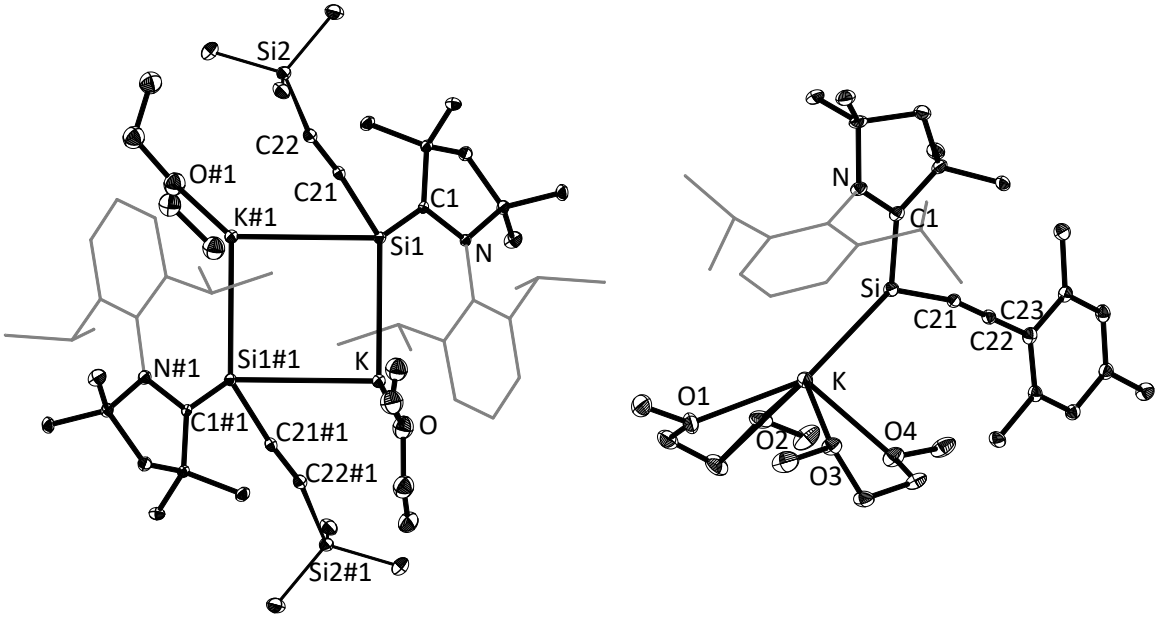

Figure 2.61. DIAMOND plot of the molecular structures of potassium-silenides (**10-C$_2$TMS**)$_2$ **x** (**Et$_2$O**)$_2$ (left) and **10-C$_2$Mes** x (**DME**)$_2$ (right). Thermal ellipsoids are set at 30 % propability level and hydrogen atoms were omitted. In the depicted structures the Dipp-substituent of the caac^{Me} ligand is presented in the wire-frame for the sake of clarity. Selected bond lengths [Å], bond angles [°] and torsion angles [°]:
(**10-C$_2$TMS**)$_2$ **x** (**Et$_2$O**)$_2$: Si1–C1^{carb} 1.790(3), N–C1^{carb} 1.408(4), Si1–C21 1.876(4), C21–C22 1.231(5), C22–Si2 1.823(4), Si1–K 3.316(1), Si1#1–K1 3.282(1), Si1–K1#1 3.282(1), C1–Si–K 119.3(1); C1–Si1–C21 102.8(2), C21–Si1–K 135.0(1), C1–Si1–K#1 139.5(1), K–Si–K#1 86.52.
10-C$_2$Mes x (**DME**)$_2$: structure is shown for the illustration purpose, crystallographic parameters are not given, due to the poor quality of the crystal.

The molecular structure of the analogous potassium-silenide **10-C_2Mes** depicted in *Figure 2.61* (right) reveals the coordinating effect of DME to the potassium cation, enabling the isolation of the corresponding monomer. The rather short Si–C^{carb} bond in **10-C_2TMS** (1.790(3) Å) is slightly elongated compared to the lithium-silenides (*Table 2.26*), but still significantly shorter compared to that of the starting material **9-C_2TMS** (1.821(3) Å) and the silenide **4-Si** (1.813(9) Å), indicating a strong Si=C^{carb} double bond at the trigonal planar coordinated silicon center. The Si–C^{carb} bond shortening is in line with a dramatic increase of the N–C^{carb} bond length in **10-C_2TMS** (1.408(4) Å) compared to that of the starting material **9-C_2TMS** (1.353(3) Å). Both Si–C^{carb} and N–C^{carb} bond-lengths of **10-C_2TMS** (1.790(3) Å, 1.408(4) Å) are remarkably similar to potassium-silenide **II-37** (d(Si–C^{carb}) = 1.793(2) Å, d(N–C^{carb}) = 1.424(3) Å).[124]
In analogy to potassium silenide **II-37** the potassium ion is covalently bonded to the Si-center (d(Si–K) = 3.316(1) Å (**10-C_2TMS**)) and is slightly elongated compared to **II-37** (d(Si–K) = 3.284(1) Å) [124] and **4-Si** (d(Si–K) = 3.298(3) Å) and lies in the typical range of potassium silanides (d(Si–K) = 3.37 – 3.42 Å).[243] In addition to the π-interaction of the aromatic Dipp-supstituent d(K–C^{Dipp}) = 3.252(1) – 3.563(4) Å), the potassium ion is stabilized by the π-interaction of the alkynyl-group (d(K–$C^{C\equiv C}$) = 3.000(1) – 3.257(1) Å), which is reflected in the slight elongation of the C ≡ C bond in **10-C_2TMS** (1.231(5) Å), when compared to **9-C_2TMS** (1.212(4) Å). Similarly, the Si1–$C^{C\equiv C}$ bond distance in **10-C_2TMS** (1.876(4) Å) is significantly elongated when compared to **9-C_2TMS** (1.836(3) Å) and the Me_3Si–$C^{C\equiv C}$ bond in **10-C_2TMS** (1.823(4) Å).

Table 2.26. Selected structural parameters of structurally characterized potassium-silenides **4-Si** and **10-C_2TMS** in comparison to literature known lithium- and potassium-silenides.

Comp.	Si–$C^{carb/sp2}$ / Å	N–C^{carb} / Å	Σ∢(Si) / (deg)	Σ°$C^{carb/sp2}$ / (deg)	τ[a] / (deg)	Ref.
SiK($SiTMS_3$)($caac^{Me}$)(**4-Si**)	1.813(9)	1.42(1)	352.8	360.0	8.1	*this*
SiK{C_2TMS}($caac^{Me}$) (**10-C_2TMS**)	1.790(3)	1.408(4)	357.1	360.0	3.7	*work*
SiK(Trip)($caac^{Me}$) (**II-37**)	1.793(2)	1.424(3)	359.7	359.9	1.8	[124]
Li(R_A)Si=C(Ad)(R_A) (**II-34**)	1.773(3)	–	359.7	359.9	13.1	[125]
Li(R_B)Si=C(Ad)(R_A) (**II-35**)	1.778(3)	–	359.6	359.9	10.2	[125]
$(THF)_2$·Li(R_A)Si=C(R_B)(R_A)[b] (**II-36**)	1.762(3)	–	359.8	359.8	4.4	[126]
Li$(THF)_4$ [(R_A)Si=C(R_B)(R_A)][b] (**II-36**)	1.766(3)	–	–	–	–	[126]

[a]: The twist angle (τ) is defined as the angle between the silicon and $C^{carb/sp2}$ coordination planes defined by the atoms X–Si–R (X = K, Li; R = Si_2, C^{Ar}, $C^{C\equiv C}$) and C_2–C_1^{CAAC}–N_1 (R–C^{sp2}–Si_2; R = C^{alk}, Si) coordination planes. [b]: R_A = Si(*t*Bu)$_2$Me, R_B = Si(*t*Bu)Me_2.

^{1}H, ^{13}C{^{1}H} and ^{29}Si{^{1}H} NMR spectra of **10-C$_2$TMS** and **10-C$_2$Mes** feature C_i-and C_S-symmetry reflecting the observed symmetry in the solid state, respectively. The ^{29}Si NMR resonances of the silenic silicon(0) centers in **10-C$_2$TMS** (–19.4 ppm) and **10-C$_2$Mes** (–15.5 ppm) are downfield shifted with respect to their dimeric silicon(I) starting materials $Si_2(C_2\text{-}R)_2(caac^{Me})_2$ (R = SiMe$_3$: –23.2 ppm (**9-C$_2$TMS**); R = Mes: –36.5 ppm(**9-C$_2$Mes**)) but drastically upfield shifted when compared to **II-37** ($\delta(^{29}Si)$ = 26.63 ppm)[124] and **4-Si** ($\delta(^{29}Si)$ = 14.34 ppm). The strong upfield shift of the $^{15}N^{CAAC}$ resonances in **10-C$_2$TMS** (119.95 ppm) and **10-C$_2$Mes** (117.3 ppm) compared to the pyramidalized disilabutadienes **9-C$_2$TMS** (157.7 ppm) and **9-C$_2$Mes** (150.9 ppm) suggest a rather strong Si=C^{carb} bond in the potassium-silenides, compared to their starting materials, which feature partial silicon-carbene double bond character.

The solid-state ATR-IR spectra of **10-C$_2$TMS** and **10-C$_2$Mes** display ν(C ≡ C) values of 1982 cm^{-1} and 2042 cm^{-1}, respectively, which are drastically shifted to lower wavenumbers compared to the disilabutadienes **9-C$_2$TMS** (2057 cm^{-1}) and **9-C$_2$Mes** (2143 cm^{-1}). Structural and spectroscopic properties of **10-C$_2$TMS** and **10-C$_2$Mes** suggest a 2-aminosilenide structure with a covalently bonded potassium cation, which is further supported by the π-interaction of the aromatic Dipp and alkinyl group.

Table 2.27. Selected multi-nuclear NMR chemical shifts of silenides **4-Si**, **4-N**, **4-P**, **10-C$_2$TMS** and **10-C$_2$Mes** and their comparison to literature known lithium silenides and potassium silenides. NMR spectroscopic data given in (D$_6$)benzene at 298 K, if not given otherwise in the legend.

Comp	$\delta(^{29}Si)$[a] / ppm	$\delta(^{13}C^{carb/sp2})$ / ppm	$\delta(^{15}N^{CAAC})$[b] / ppm	Ref.
SiK(SiTMS$_3$)(caac^{Me})(**4-Si**)	14.4	213.0	117.6	
SiK(NTMS$_2$)(caac^{Me})(**4-N**)	86.5	200.7	90.5	*this*
SiK(P(Mes)$_2$)(caac^{Me}) (**4-P**)	–[c]	210.3	114.9	*work*
SiK(C$_2$TMS)(caac^{Me})(**10-C$_2$TMS**)	–19.4	220.0	119.9	
SiK(C$_2$Mes)(caac^{Me})(**10-C$_2$Mes**)	–15.5	217.2	117.3	
SiK(Trip)(caac^{Me}) (**II-37**)	26.6	195.1	–	[124]
Li(R$_A$)Si=C(Ad)(R$_A$) (**II-35**)	243.9	174.9	–	[125]
(THF)$_2$·Li(R$_A$)Si=C(R$_B$)(R$_A$) (**II-36**)	347.8	143.5	–	[126]
[Li(THF)$_4$]$^+$ [(R$_A$)Si=C(R$_B$)(R$_A$)]$^-$ (**II-36**)	405.5[d]	134.2[d]	–	[126]

[a]: ^{29}Si NMR resonance of the three-coordinated silicon center. [b]: ^{15}N NMR resonance of the single nitrogen atom in the CAAC carbene-ring referenced against NH$_3$(l). [c]: No ^{29}Si NMR resonance could be detected in the 1D and 2D ^{29}Si NMR spectra of an aliquot of the reaction mixture of **4-P**. [d]: Measured in (D$_8$)THF at 298 K.

2.5.3 Reactivity of an alkynyl functionalized silenide

Remarkably, no reactivity of the potassium-silenide SiK(Trip)(caac^{Me}) (Trip = C_6H_2-2,4,6-iPr_3) (**II-37**)[124] has been reported thus far. Herein the reactivity of the alkynyl substituted potassium-silenide SiK(C_2-TMS)(caac^{Me}) (**10-C_2TMS**) with low valent silicon and germanium compounds is reported, showing the high potential of silenide **10-C_2TMS** as a versatile building block in low valent silicon chemistry.

Interestingly, a concentrated solution of **10-C_2TMS** in (D_6)benzene did not react with excess of CO in a high-pressure young NMR tube at ambient temperature or upon heating to 80 °C for 3 h. The $^{13}C\{^1H\}$-NMR spectrum in (D_6)benzene of the reaction mixture revealed the presence of free CO with a $^{13}C\{^1H\}$ resonance of 184.1 ppm.

Reaction of **10-C_2TMS** with 0.5 equiv. of disilene (*E*)-[Tbb(Br)Si=Si(Br)Tbb] (Tbb = C_6H_2-2,6-Dsi_2-4-*t*Bu, Dsi = $CH(SiMe_3)_2$) in (D_6)benzene at ambient temperature was not successful. Monitoring of the reaction mixture by ^1H NMR spectroscopy revealed a redox-reaction with the rather selective formation of disilabutadiene $Si_2(C_2TMS)_2$(caac^{Me}) (**9-C_2TMS**). Similarly, reaction of **9-C_2TMS** with 1.0 equiv. of $SiBr_2$(SIDipp) in benzene at ambient temperature led according to ^1H NMR spectrospy in (D_6)benzene via a redox reaction to the formation of the silicon(I) compounds $Si_2(C_2TMS)_2$(caac^{Me})$_2$ (**9-C_2TMS**) and Si_2Br_2(SIDipp)$_2$, respectively.

Reaction of silenide **10-C_2TMS** with 1.0 equiv. of [SiCp*][B(Ar^F)$_4$][246] in fluorobenzene at ambient temperature led to the formation of a dark brown solution. ^1H NMR spectroscopy of an aliquote of the reaction mixture in (D_6)benzene, revealed the formation of disilabutadiene **9-C_2TMS** next to $SiCp^*_2$ in a ratio 2:1. These results are in line with the observation of Jutzi et al., which suggest that upon reduction of the [SiCp*] the silicon(I)-compound $Si_2Cp^*_2$ is formed, which decomposes via redox disproportionation into $SiCp^*_2$ and elemental silicon.[246]

2.5.3.1 Reaction of 10-C_2TMS with $SiBr_2$(caac^{Me})

In situ generated SiK(C≡CTMS)(caac^{Me}) (**10-C_2TMS**), upon reduction of the caac^{Me}-stabilized silicon(I) dimer Si_2(C≡CTMS)$_2$(caac^{Me})$_2$ (**9-C_2TMS**) with three equivalents of KC_8 in benzene at ambient temperature was added dropwise via a filter-syringe to a clear red solution of $SiBr_2$(caac^{Me}) (**1**). Thereby a color change to dark red was observed. Monitoring of the reaction mixture by ^1H NMR spectroscopy in (D_6)benzene after stirring for 2 h at ambient temperature revealed the formation of SiBr(caac^{Me})Si(C≡CTMS)(caac^{Me}) (**11-Br**) with moderate selectivity, along side the formation of the disilicon(I) compounds Si_2Br_2(caac^{Me})$_2$ (**9-Br**: 16 mol%) and Si_2(C≡CTMS)$_2$(caac^{Me})$_2$ (**9-C_2TMS**: 20 mol%).

After separation from KBr several recrystallizations were necessary in order to obtain **11-Br** as red powder in analytically pure form with rather low yield of 5 % (*chapter 4.4*).

The compound immediately decomposes upon contact with air and shows a melting point of 185.5 °C. ^{1}H NMR spectroscopy of the molten mass in (D_6)benzene revealed only minor decomposition.

The molecular structure of **11-Br** was determined by single X-ray diffraction (*Figure* 2.62). The compound features two stereogenic trigonal pyramidalized silicon centers (Σ∢(Si1) = 338.8 °, Σ∢(Si2) = 324.6°) of the same configuration (R,R). The bromine and acetylido-substituents of **11-Br** adopt a synclinal conformation (τ(Br–Si2–Si1–C21) = 62.5(1)°) and the sterically more demanding caac^{Me} groups adopt an antiperiplanar conformation (τ(C1–Si1–Si2–C26) = 173.0(1)°). The two carbene centers are orientated orthogonal with respect to each other (carbene to carbene plane twist angle: 78.6(1)°). As expected, the silicon center containing the bromine substituent is significantly more pyramidalized (DP(Si2) = 39 %) compared to the TMS-acetylide substituted silicon center (DP(Si1) = 23 %). This trend is further supported by a significantly longer Si–C^{carb} bond (1.855(2) Å) at the Si2 center compared to the Si1-center (1.819(2) Å). The Si2–Si1 bond length (2.324(7) Å) lies in the typical range for Si–Si single bonds observed for the caac^{Me}-stabilized silicon(I) dimers (2.306(1) – 2.337(1) Å).[121,128–130]

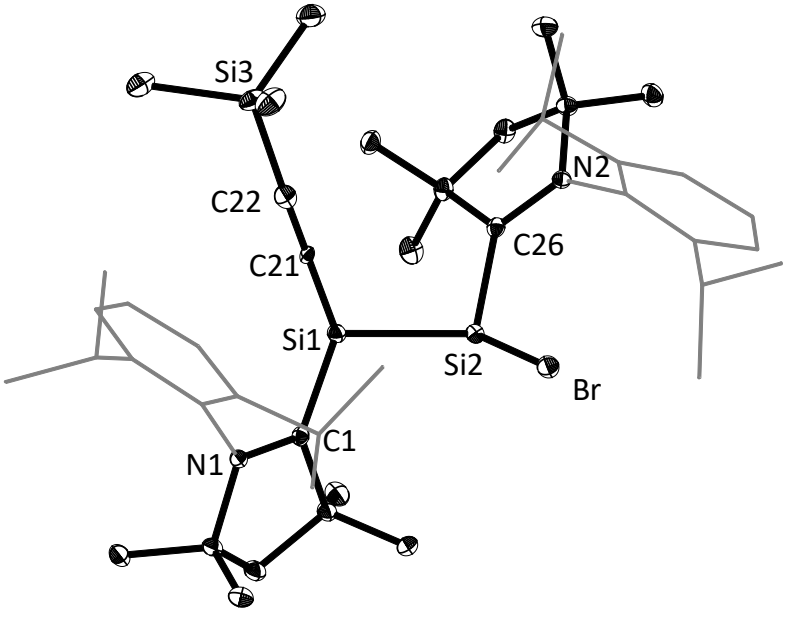

Figure 2.62. DIAMOND plot of the molecular structures of the silicon(I) compound **11-Br**. Thermal ellipsoids are set at 30 % propability level and hydrogen atoms were omitted. In the depicted structure the Dipp substituent of the caac^{Me} ligand is presented in the wire-frame for the sake of clarity. Selected bond lengths [Å], bond angles [°] and torsion angles [°]: Si1–Si2 2.3243(7), Si1–C1^{carb} 1.819(2), Si1–C21 1.885(2), Si2–C26^{carb} 1.855(2), Si2–Br 2.308(1), N1–C1 1.353(2), N2–C26 1.343(2), C21–C22 1.151(3), Si3–C22 1.841(2), C1–Si1–Si2 111.1(1), C1–Si1–C21 113.9(1), C21–Si1–Si2 113.8(1), Br–Si2–Si1 108.6(2), C26–Si2–Br 111.8(1), C26–Si2–Si1 104.2(6), C1–Si1–Si2–C26 173.0(1), N1–C1–Si1–Si2 151.0(2), N2–C26–Si2–Si1 143.4(2), Br–Si2–Si1–C21 62.5(1).

Compound **11-Br** can be seen as an asymmetric recombination of the two silicon(I) compounds $Si_2Br_2(caac^{Me})_2$ (**9-Br**) and $Si_2(C_2\text{-TMS})_2(caac^{Me})_2$ (**9-C_2TMS**). The Si–C^{carb} and C^{carb}–N bond lengths, as well the sum of angles of the silicon center of the $SiBr(caac^{Me})$ moiety in **11-Br**, do compare well to those of **9-Br** (*Table 2.28*). Similarly, the structural features of the $Si(C_2TMS)(caac^{Me})$ moiety in **11-Br** do compare well to those of **9-C_2TMS** (*Table 2.28*).

Table 2.28. Selected structural paramters of the asymmetric Si(I) compound **11-Br** in comparison to related symmetric silicon(I) compounds synthesized throughout this work.

Comp.	Si–Si / Å	Si–C^{carb} / Å	N–C^{carb} / Å	Σ∢(Si) / (deg)	DP[a] / %	τ[b] / (deg)	Ref.
$Si(C{\equiv}CTMS)(caac^{Me})$	2.324(7)	1.819(2)	1.353(2)	338.9	23	11.4	*this*
$SiBr(caac^{Me})$ **11-Br**		1.855(2)	1.343(2)	324.5	39	21.5	*work*
$Si_2Br_2(caac^{Me})_2$	2.341(2)	1.844(4)	1.347(5)	327.6	36	13.0	
9-Br		1.844(4)	1.348(5)	326.1	38	14.9	*this*
$Si_2(C{\equiv}CTMS)_2(caac^{Me})_2$	2.313(1)						*work*
9-C_2TMS		1.821(3)	1.353(3)	335.6	27	12.5	

[a]: The degree of pyramidalization (DP) value of 0 % describes a trigonal planar coordination of the silicon atom with the sum of bond angles equal to 360°. A DP value of 100 % corresponds to trigonal pyramidal coordination of the silicon atom with the sum of bond angles equal to 270°.
DP (in %) = 100 % · [360 − Σ∢(Si) / (deg)]/90
[b]: The twist angle (τ) is defined as the angle between the silicon and Ccarbene coordination planes defined by the atoms X1–Si1–Si2 (X2–Si2–Si1) and C2–C1–N1 (C22–C21–N2), respectively.

Although the molecular structure of **11-Br** features C_1-symmetry, ^{1}H NMR spectra at ambient temperature in (D_6)benzene solution clearly reveal two different $caac^{Me}$ ligands with an averaged C_S-symmetry. Thus, two singlets for the C^3Me_2 and C^5Me_2 resonances, a singlet for the C^4H_2 protons and a septet ($C^{2,6}$-$CHMe_AMe_B$, Dipp) and two doublets ($C^{2,6}$-$CHMe_AMe_B$, Dipp) in the aliphatic region of the ^{1}H NMR spectrum (*Figure 2.63*) are observed for each $caac^{Me}$ substituent. The full NMR assignment of **11-Br** was made possible through high-resolution correlation spectroscopy. No change of the NMR spectra was observed at lower temperatures, even in (D_8)toluene at –80°C, suggesting a fast enantiomerisation at the NMR time scale, which proceeds via a rather low inversion barrier. It can be highly likely assumed that the enantiomerization undergoes via a nonsynchronous narcissistic reaction in analogy to **9-Br** (see *section 2.4.3*). Whereby two enantiomeric paths, each via stepwise consecutive pyramidal inversion of the silicon centers, lead to a time averaged achiral structure wich the mirror plane bisecting the $caac^{Me}$ substituents, thus explaining the simple ^{1}H NMR spectrum of **11-Br**.

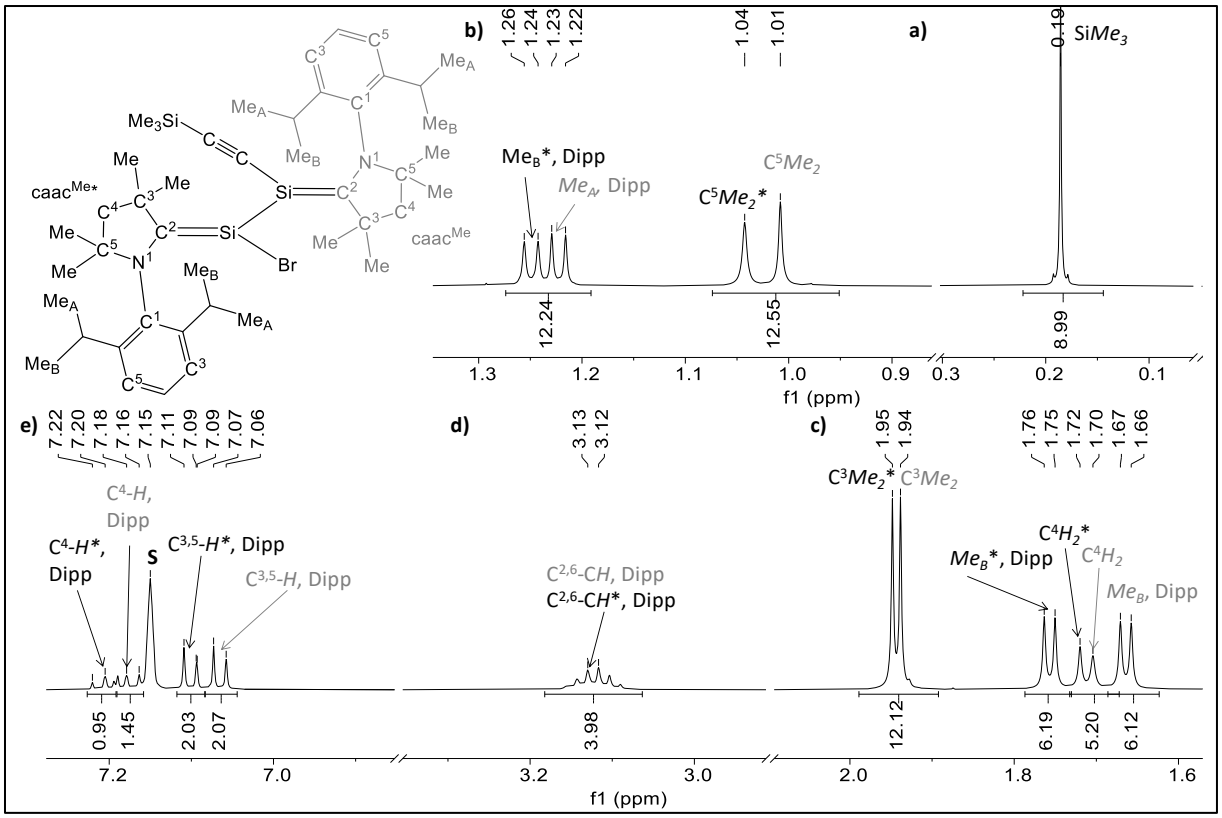

Figure 2.63. ^{1}H NMR spectrum (500.13 MHz) of a pure sample of SiBr(caac^{Me})Si{C$_2$-TMS}(caac^{Me}) (**11-Br**) in (D$_6$)benzene at 298 K, the signal of the deuterated solvent is marked with **S**.

The ^{29}Si{^{1}H} NMR spectrum of **11-Br** displays three resonances at –25.56 ppm (*Si*(C≡CTMS)(caac^{Me})), –23.07 (*Si*Me$_3$) and 9.10 ppm (*Si*Br(caac^{Me}). Compared to the symmetric silicon(I) counterparts Si$_2$Br$_2$(caac^{Me})$_2$ (19.84 ppm (**9-Br**)) and Si$_2$(C≡CTMS)$_2$(caac^{Me})$_2$ (–42.2 ppm (**9-C$_2$TMS**) the silenic center bearing the bromine substituent (9.10 ppm) is significantly upfield shifted while the alkynyl bearing silicon center (–25.56 ppm) is significantly downfield shifted. The ^{13}C^{CAAC} as well as ^{15}N^{CAAC} resonances of the SiBr(caac^{Me}) (208.5 ppm, 173.9 ppm) and Si(C≡CTMS)(caac^{Me}) (203.3 ppm, 158.8 ppm) moieties compare well to the symmetric silicon(I) dimers **9-Br** (207.9 ppm, 174.3 ppm) and **9-C$_2$TMS** (203.4 ppm, 157.7 ppm) reflecting the similar electronic structures, which is also supported by the similarities in terms of their molecular structures.

The stretching vibration of the C ≡ C bond in **11-Br** ($\tilde{\nu}$ = 2057 (m) cm^{-1}) is identical when compared to the symmetric silicon(I) counterpart **9-C$_2$TMS** ($\tilde{\nu}$ = 2057 (m) cm^{-1}), thus highlighting the strong similarities of the electronic structures of both compounds.

Compound **11-Br** can be best described as an asymmetric version of a pyramidal 1,4-diamino-2,3-disila-1,3-butadiene. The bromine substituent bears room for further functionalization, thus making it a promising building block in low molecular silicon chemistry.

2.5.3.2 Reactivity of an asymmetric caac^{Me}-stabilized silicon(I) compound

Preliminary reactivity studies of SiBr(caac^{Me})-Si(C≡CTMS)(caac^{Me}) (**11-Br**) appeared to be rather promising although the compound could be only obtained in extremely low yields (5 %), since in the reaction the two symmetric disilicon(I) compounds **9-Br** and **9-C$_2$TMS** are formed as well in considerable amounts and multiple recrystallization steps were necessary in order to remove them.

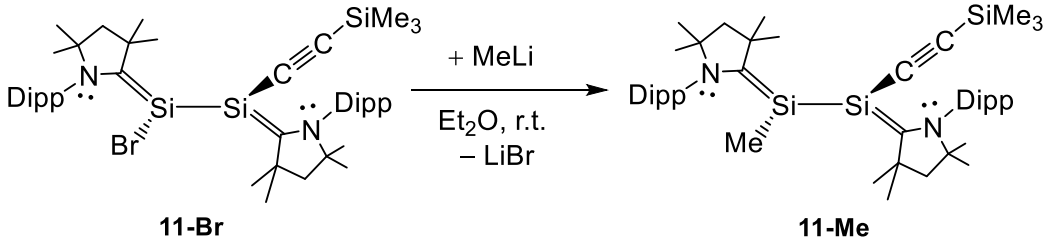

Scheme 2.18. Reaction of asymmetric silicon(I) compound **11-Br** with MeLi.

Addition of 1.1 equiv. MeLi to a dark red solution of **11-Br** in Et_2O led to color change to orange-brown after stirring at ambient temperature for 1 h. Monitoring of the reaction mixture by ^{1}H NMR spectroscopy in (D_6)benzene revealed the selective formation of SiMe(caac^{Me})Si(C≡CTMS)(caac^{Me}) (**11-Me**). Interestingly reaction of **9-Br** with 2 equivalents of MeLi in THF at ambient temperature did not selectively afford the literature known Si_2Me_2(caac^{Me})$_2$.[118] Monitoring of the reaction mixture in (D_6)benzene revealed instead the formation of $SiMe_2$(caac^{Me})$_2$ [141] as major product. After extraction from LiBr, and crystallization from *n*-pentane at –60 °C compound **11-Me** could be obtained as an orange powder with a purity of 95 % according to ^{1}H NMR spectroscopy in (D_6)benzene in 5 % yield. The impurity could be attributed to tiny amounts of **9-C$_2$TMS**, which was present in the starting material**.** The compound is extremely well soluble in aliphatic solvents, such as *n*-pentane and *n*-hexane, affording orange-brown solutions. Unfortunately, no suitable single crystals of the compound could be obtained. Nevertheless, the compound was characterized throughout NMR spectroscopy. Similar, like in case of **11-Br**, ^{1}H NMR spectra display two caac^{Me} ligands with C_S-symmetry. This can be attributed upon a fast consecutive inversion of the two chiral silicon(I) centers in **11-Me**. The silicon atom bearing the methyl group (Si*Me*) appears at 0.02 ppm in the ^{1}H NMR spectrum in (D_6)benzene and is downfield shifted compared to the symmetric caac^{Me} stabilized silicon(I) compound Si_2Me_2(caac^{Me})$_2$ (–0.48 ppm).[130] Overall the compound can be seen as asymmetric recombination of the two silicon(I) compounds Si_2Me_2(caac^{Me})$_2$[118] and Si_2(C_2TMS)$_2$(caac^{Me})$_2$ (**9-C$_2$TMS**). Thus the ^{29}Si{^{1}H} and $^{13}C^{CAAC}$ resonances of the SiMe(caac^{Me}) (–1.01 ppm, 192.6 ppm,) and Si(C_2TMS)(caac^{Me}) (–39.44 ppm, 201.4 ppm) moieties of **11-Me** are remarkably similar to the symmetric silico(I) dimers Si_2Me_2(caac^{Me})$_2$ (0.723 ppm, 191.3 ppm) and **9-C$_2$TMS** (–42.2 ppm, 203.4 ppm) reflecting the similar electronic structures observed in these compounds.

Compound **11-Me**, could clearly show, that **11-Br** can be further functionalized with small nucleophiles under retention of the 1,4-diamino-2,3-disila-1,3-butadiene backbone. Upon substitution the π-bond character of the Si–C^{carb} bond significantly increases, which can be seen by the notable decrease of the $^{15}N^{CAAC}$ resonance of the SiBr($caac^{Me}$) moiety in **11-Br** (173.9 ppm) compared to that of the SiMe($caac^{Me}$) moiety in **11-Me** (152.7 ppm).

Reduction of **11-Br** with 1.1 equivalents of KC_8 in benzene at ambient temperature resulted in a color change to dark purple. Monitoring of the reaction mixture by ^1H NMR spectroscopy in (D_6)benzene after 17 h at ambient temperature, revealed the presence of broad signals, which may be attributed to a silicon centered radical. Unfortunately, the compound could not be crystallized from *n*-hexane at –30 °C or –60 °C respectively (given the low amounts (200 mg) of used starting material **11-Br**). Given the similarties of the observed structure of **11-Br** with pyramidal 2-(amino)silenes SiBr(R)($caac^{Me}$) (R = $SiTMS_3$ (**2-Si**), $NTMS_2$ (**2-N**), OMes* (**2-O**)) it is assumed that the analogous silicon(I) radical is formed upon $1e^-$ reduction, like it is observed in the case of the isolated silicon(I) radicals Si(R)($caac^{Me}$) (R = $SiTMS_3$ (**3-Si**), $NTMS_2$(**3-N**), OMes*(**3-O**)).

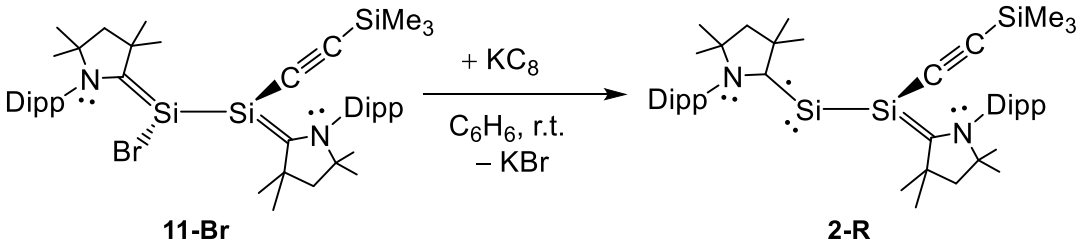

11-Br **2-R**

Scheme 2.19. Assumed formation of a two-coordinated neutral silicon(I) radical **2-R**, upon reduction of **11-Br** with KC_8.

2.5.3.3 Reaction of **11-C_2TMS** with GeCl(Ar^{Mes})

In situ generated SiK(C≡CTMS)($caac^{Me}$) (**11-C_2TMS**) in benzene was added dropwise via a filter-syringe to a clear orange solution of GeCl(Ar^{Mes}) in benzene. The solution directly turned blue-turquiose. Monitoring of the reaction mixture by NMR spectroscopy in (D_6)benzene after stirring for 2 h at ambient temperature revealed the selective formation of ($caac^{Me}$)Si(C≡CTMS)($GeAr^{Mes}$) (**12**), alongside tiny amounts of **9-C_2TMS**. After separation of KBr, upon twofold extraction with benzene and *n*-hexane, **12** could be obtained as dark purple single crystals in 22 % yield upon crystallization from *n*-hexane at 4 °C. The compound decomposes upon melting at 165 °C and immediately decolorizes upon contact with air. **12** is very well soluble in aromatic and aliphatic solvents affording intense blue-turquiose colored solutions.

The solid-state structure of **12-*E*** was determined by sc-XRD analysis of purple single crystals, which were grown from a saturated solution in *n*-hexane at 4 °C (*Figure 2.64* left). The planar core of the structure consists of the atoms C25, Si1, Ge, C1, in which the trigonal planar coordinated silicon center (Σ∢(Si) = 358.1°) is connected to a V-shape dicoordinated Ge atom (C1-Ge-Si1 101.0(3)°) via a Si=Ge bond (2.300(3) Å).

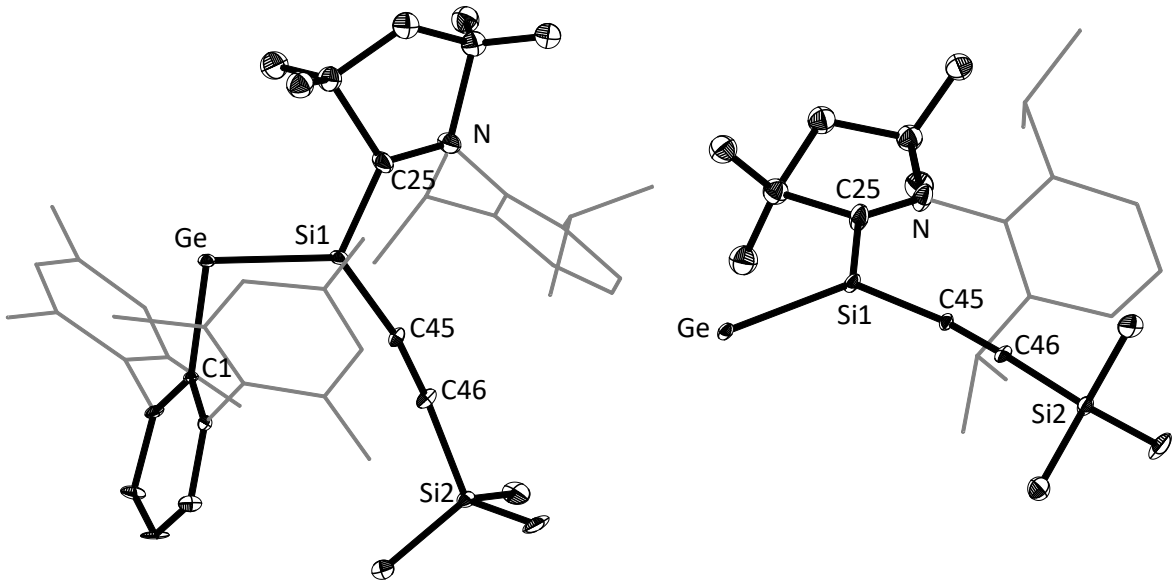

Figure 2.64. Diamond plot of the molecular structure of **12-*E*** (left) and depicted conformation of the 2-aminosilene moiety(right). Thermal ellipsoids are set at 30 % probability, and hydrogen atoms were omitted. In the depicted structures the Dipp-substituent of the $caac^{Me}$ ligand and the Mes-substituent are presented in the wire-frame for the sake of clarity. Selected bond lengths [Å], bond angles [°] and torsion angles [°]: Ge–Si1 2.301(3) [2.303(3)], Ge–C1 2.015(9) [2.010(9)], Si1–C25 1.840(10) [1.804(14)], Si1–C45 1.837(9) [1.776(10)], N–C25 1.287(11) [1.303(7)], C45–C46 1.194(11) [1.215(12)], C46–Si2 1.845(10) [1.890(10)], C1-Ge-Si1 101.0(3) [99.0(3)], C25–Si1–Ge 117.8(3) [116.9(5)], C45–Si1–Ge 127.8(3) [126.2(4)], C45–Si1–C25 112.5(5) [115.0(6)], C25–Si1–Ge–C1 –179.7(4) [177.3(6)], N–C25–Si–Ge –161.5(7) [–161.6(2)], C1–Ge–Si1–C45 17.1(5) [13.7(5)]. Two independent molecules were found in the unit cell.

The N-Dipp moiety of the caac^{Me} ligand of **12-*E*** is orientated trans with respect to the (Ar^{Mes})Ge moiety (τ(N-C25-Si-Ge) = 161.5(2) °) (*Figure 2.64* (right))., thus according to the priority rules of *Z*/*E* alkenes the stereodescriptor ***E*** can be assigned.

The bulky Ar^{Mes} and caac^{Me} groups are orientated in trans-position to each other (τ(C25-Si1-Ge-C1) = –179.7(4)°) and the Ar^{Mes} substituent is orientated orthogonal with respect to the planar core of the molecule. The caac^{Me} ligand (τ(N-C25-Si-Ge) = –161.5(7)°), in contrast, is orientated in plane to the Si=Ge bond, suggesting a conjugation of the Si–Ge π-bond with the C^{carb} centered empty p-orbital and the formation of a 3c-2e π_{oop} bond leading to an elongation of the Si=Ge bond and a shortening of the Si–C^{carb} bond in **12-*E***. In fact, the Si=Ge bond length of **12-*E*** (2.300(3) Å) is significantly elongated compared to literature known silagermenylidenes (I*i*Pr$_2$Me$_2$)Ge=Si(R$_1$)(R$_2$) (2.252(1) Å (R$_1$ =R$_2$ = Trip)[247],and 2.276(1) Å (R$_1$ = Trip, R$_2$ = SiCl(Trip)$_2$) [248] and lies exactly in between that of typical Si=Ge double bonds present in silagermene (tBu$_3$)$_2$Si=Ge(Mes)$_2$ (2.2769(8) Å)[249] and Si–Ge single bonds 2.383 – 2.416 Å in silylgermanes.[250] The Si–C^{carb} bond length in **12-*E*** (1.84(1) Å)) is significantly elongated when compared to the former silenide (1.790(3) Å) and compares well to Si–C^{carb} bond lengths reported in caac^{Me}-stabilized silicon(I) dimers (1.798(1) – 1.846(3) Å), which are rather described as 2,3-disilabutadienes.[121,128–130]

The compound compares well to the very recently reported NHC-supported heteroditetrylyne (Ar^{Mes})Ge=SiCl(SIDipp) (**II-43 = 12-NHC**)[253] (*Table 2.29*) and in terms of its Si–C^{carb} bonding nature it compares well to the (silenyl)phosphanyl radical (**6**). Compounds **12** and **12-NHC** clearly differ to NHC-stabilized disilynes and digermynes by a drastic increase of the Si=Ge bond length and significantly decrease of the Si–C^{carb} bond lengths , which is line with the more co-planar orientation of the carbene with respect to the Si–Ge moiety (*Table 2.29*).

Table 2.29. Selected structural paramters of the (silenyl)germylene **12-*E*** in comparison to related literature known compounds.

Comp.	E–E / Å	Si–C^{carb} / Å	E-E-R / (deg)	φ_{carb} [a] / (deg)	Ref.
(caac^{Me})Si(C≡CTMS)(GeAr^{Mes})	2.300(3)	1.840(10)	101.0(3)	24.7(4)	this
(**12-*E***)	2.302(4)	1.804(14)	99.0(3)	13.6(6)	work
(Mes)P=Si(Mes)(caac^{Me}) **6**	2.108(1)	1.813(2)	103.1(1)	21.5(1)	
(Ar^{Mes})Ge=Si(Cl)(SIDipp)	2.2841(5)	1.877(2)	100.87(5)	3.9(1)	[138]
(**12-NHC**)		1.878(2)	98.91(5)	7.9(1)	
(SiR$_3$)Si=Si(SiR$_3$)(IMe$_4$)[b]	2.199(1)	1.922(2)	120.35(2)	98.0(1)	[251]
(BR$_2$)Ge=Ge(BR$_2$)(I*i*Pr$_2$Me$_2$)[c]	2.279(1)	2.003(5)	111.6(1)	86.2(2)	[252]

[a]: φ_{carb} the angle between the least-squares plane of the CAAC or NHC five-membered ring and the plane defined by the C^{carb} and the doubly-bonded tetrel atoms. [b]: SiR$_3$ = Si(*i*Pr)(CH(SiMe$_3$)$_2$)$_2$, IMe$_4$ = C[N(Me)C(Me)]$_2$. [c]: BR$_2$ = B[N(Dipp)CH]$_2$. I*i*Pr$_2$Me$_2$ = C[N(*i*Pr)C(Me)]$_2$.

^{1}H NMR spectra of **12** in (D_8)toluene at ambient temperature (*Figure 2.65,* middle spectrum) display two sets of broad signals of the caac^{Me}, Ar^{Mes} and TMS-groups, showing a dynamic behavior in solution. Recorded ^{1}H NMR spectra at variable temperatures in (D_8)toluene, in fact, reveal a reversible cis to trans (*Z* to *E*) isomerization, which highly likely proceeds via rotation of the Si–C^{carb} bond. Resulting in a equilibrium mixture of 28.5 mol% ***Z***-isomer to 71.5 mol% ***E***-isomer in (D_8)toluene at 243 K (*Figure 2.65,* bottom spectrum). At this temperature both isomers feature caac^{Me} substituents with C_S-symmetry, accompanied by a hindered rotation of the Mes groups at the Ar^{Mes} substituent. In the high temperature limit spectrum at 373 K (*Figure 2.65,* top spectrum) only one set of signals are observed for the caac^{Me} and Ar^{Mes} substituents, respectively, suggesting a fast interconversion of the two isomers via the rapid rotation of the Si–C^{carb} bond on the NMR timescale. Both isomers have been fully chraracterized by HR correlation spectroscopy in (D_8)toluene at 243 K (see *chapter 4.4*) and were identified by 1D and 2D NOE NMR experiments (*Figure 2.66*), respectively.

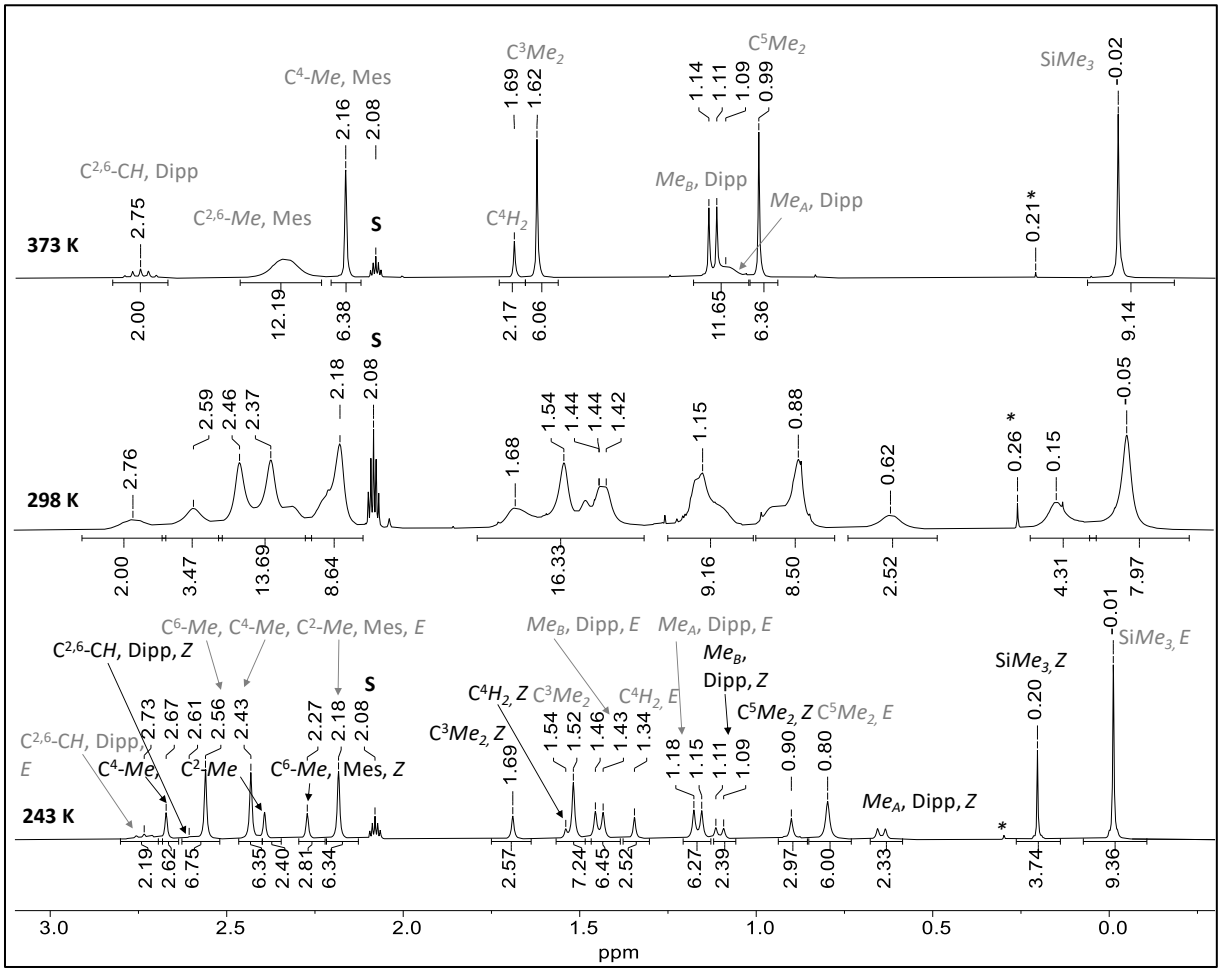

Figure 2.65. Excerpt of the ^{1}H NMR spectra (300.13 MHz) of (caac^{Me})Si(C ≡ CTMS)(GeAr^{Mes}) (**12**) in (D_8)toluene at 243 K (bottom), 298 K (middle) and 373 K (top); the residual proton signal of the deuterated solvent is marked with the character **S**. The signal marked with the character (*) attributes to the TMS-signal of tiny amounts of **9-C$_2$TMS** (<2 mol%) present in compound **12**.

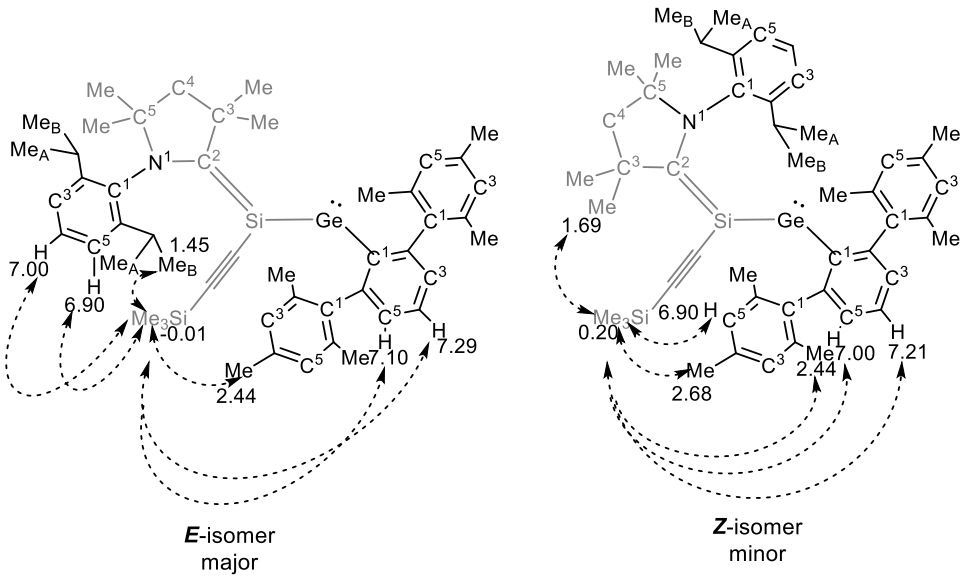

Figure 2.66. Depicted 1D and 2D NOE correlations in **12** order to assign the two isomers. The chemical shifts of the interacting proton resonances are given in ppm.

The $^{29}Si\{^{1}H\}$ NMR spectrum of **12** at 243 K displays two signals of the TMS groups (–22.2 ppm ***E***, –21.6 ppm ***Z***) aswell of the silenic silicon centers (72.2 ppm **Z**, 73.7 ppm ***E***) of the two isomers, respectively. The $^{29}Si\{^{1}H\}$ resonances of the silenic silicon center in **12** (72.2 ppm ***Z***, 73.7 ppm ***E***) are slightly upfield shifted, when compared to $Ar^{Mes}Ge{=}SiCl(SDipp)$ **12-NHC** (81.8 ppm) and appear at lower field, when compared to (R)*Si*=SiR(IMe$_4$) (R = Si(*i*Pr)(CH(SiMe$_3$)$_2$)$_2$, δ (^{29}Si) = 28.7 ppm).

The $^{13}C^{CAAC}$ resonances of **12** (208.0 ppm ***Z***, 210.8 ppm ***E***) are significantly upfield shifted compared to **12-NHC** (185.4 ppm), reflecting the different electronic nature of CAAC versus NHC. Both $^{13}C^{CAAC}$ and $^{15}N^{CAAC}$ resonances in **12** compare rather well to previously synthesized pyramidal 2-(amino)silenes SiBr(R)(caac^{Me}) with π-donor substituents (R = PMes$_2$ (**2-P**), OMes* (**2-O**)) in this work (*Table 2.30*).

Table 2.30. Comparison of NMR spectroscopic parameters of **12** with related literature known compounds. NMR spectroscopic data are given in (D$_6$)benzene, if not mentioned otherwise in the legend.

Comp	δ($^{13}C^{carb}$) / ppm	δ(^{29}Si)[a] / ppm	δ(^{15}N)[b] / ppm	Ref.
(caaac^{Me})Si(C≡CTMS)(GeAr^{Mes}) (**12**)				
Z-isomer	208.0[d]	72.2[d]	175.6[d]	
E-isomer	210.8[d]	73.7[d]	169.5[d]	*this*
SiBr(PMes$_2$)(caac^{Me}) (**3-P**)	204.3 (d,22Hz)	7.0 (d, 185 Hz)	170.8	*work*
SiBr(OMes*)(caac^{Me}) (**3-O**)	200.0	26.4	164.9	
(Ar^{Mes})Ge=Si(Cl)(SIDipp) (**12-NHC**)	185.4	81.8	114.5	[253]
(SiR$_3$)Si=Si(SiR$_3$)(IMe$_4$)[c]	160.9	28.7	–	[251]

[a]: ^{29}Si resonance of the three-coordinated silicon(II) center. [b]: ^{15}N NMR resonance of the nitrogen atom(s) in the CAAC (NHC) carbene-ring referenced against NH$_3$(l). [c]: SiR$_3$ = Si(*i*Pr)(CH(SiMe$_3$)$_2$)$_2$. [d]: measured in (D$_8$)toluene at 243 K.

2.5.3.4 Study of the dynamics of the reversible E→Z isomerization in 12

The dynamics of the reversible *Z* → *E* isomerization in **12** was studied via recorded ^{1}H NMR spectra of **12** at variable temperatures in (D_8)toluene (see also *section 5.6.9*). ^{1}H NMR spectra in (D_8)toluene below the coalescence temperature (203 – 293 K) were used for a Van't Hoff Analysis. The change of the *E* : *Z* ratio upon increasing temperature was monitored by ^{1}H NMR, by integration of the Si*Me*$_3$-resonance of the ***Z***-isomer (at 0.26 ppm, signal A) and the ***E***-isomer (at 0.049 ppm, signal B), respectively. The thermodynamic parameters for the reversible isomerization were obtained from the Van't Hoff equation.

$$\ln(K_{eq}) = -\frac{\Delta H}{R} \cdot \frac{1}{T} + \frac{\Delta S}{R} \qquad \text{(eq. 2.4)}$$

Details on the Van't Hoff analysis of the variable temperature ^{1}H NMR spectra are given in the experimental part (see *section 5.6.9*). The thermodynamic parameters of the reversible *Z* → *E* isomerization were obtained form the plot of ln(A/B) versus 1/T. The enthalpy ($\Delta H^{\ddagger}$ = 2.22 ± 0.1 kJ mol^{-1}) and entropy ($\Delta S^{\ddagger}$ = –1.6 ± 0.2 J K^{-1} mol^{-1}) were obtained from the slope and the y-intercept of the linear fit, respectively. The Gibbs free energy ($\Delta G^{\ddagger}$(298K) = 1.8 ± 0.1 kJ mol^{-1}), which can be calculated using the Gibb's Helmholtz equation, can be seen as relative energy difference between the two isomers, suggesting that the ***E***-isomer lies 1.8 ± 0.1 kJ mol^{-1} lower in energy than the ***Z***-isomer.
In order to study the kinetics of the reversible *E* → *Z* isomerization ^{1}H NMR spectra of **12** in (D_8)toluene in the temperature range 273 – 373 K were recorded. A full line shape analysis was performed in order to obtain the thermodynamic parameters of activation of the process. Therefore, the two Si*Me*$_3$-resonances were simulated using the gNMR software. The process was treated as interaction of two hydrogen atoms of two different molecules with two different concentrations, where the concentration of the two signals were constrained by the relation $c_2 = 1 - c_1$. During the simulation the exchange rate constant (k_1), as well as the concentration c_1 (Si*Me*$_3$-Group of the ***E***-isomer) were optimized. Details on the line shape analysis are given in the experimental part (see *section 5.6.9*). The exchange rate constants (k_{-1}) for the back-isomerization (*Z* → *E*) were obtained by $k_{-1} = k_1/K_{eq}$, whereas K_{eq} was calculated at each temperature using the Van't Hoff Equation and the thermodynamic parameters ($\Delta H^{\ddagger}$ = 2.22 ± 0.1 kJ mol^{-1}; $\Delta S^{\ddagger}$ = –1.6 ± 0.2 J K^{-1} mol^{-1}). The thermodynamic parameters of activation for the *E* → *Z* and back-isomerization were obtained by the plot ln(k_1/T) versus 1/T and ln(k_{-1}/T) versus 1/T, respectively. The enthalpy of activation ($\Delta H^{\ddagger}_{(E\rightarrow Z)}$ = 60.4 ± 1.0 kJ mol^{-1} and $\Delta H^{\ddagger}_{(Z\rightarrow E)}$ = 58.2 ± 1.0 kJ mol^{-1}) and entropy of activation ($\Delta S^{\ddagger}_{(E\rightarrow Z)}$ = –16.9 ± 2.8 J K^{-1} mol^{-1}, $\Delta S^{\ddagger}_{(Z\rightarrow E)}$ = –18.5 ± 2.8 J K^{-1} mol^{-1}) of the cis-trans isomerization were extracted from the slope and the y-intercept of the linear fit, respectively applying the linearized form of the Eyring equation.

$$\ln\left(\frac{k}{T}\right) = \ln\left(\frac{k_B}{h}\right) + \left(\frac{\Delta S^{\ddagger}}{R}\right) + \left(-\frac{\Delta H^{\ddagger}}{R}\right) \cdot \frac{1}{T} \qquad \text{(eq. 2.5)}$$

The Gibbs free activation energy can be calculated using the Gibb's Helmholtz equation, which gives $\Delta G^{\ddagger}(298\ K) = 65.4 \pm 1.1\ kJ\ mol^{-1}$ for the $E \rightarrow Z$ isomerization and $\Delta G^{\ddagger}(298\ K) = 63.7 \pm 1.1\ kJ\ mol^{-1}$ for the back-isomerization ($Z \rightarrow E$).

The reversible $E \rightarrow Z$ isomerization of (caac^{Me})Si(C≡CTMS)(Ar^{Mes}) (**12**) can be rationalized by the rotation of the Si–C^{carb} bond, which proceeds via an activation barrier of $65.4 \pm 1.1\ kJ\ mol^{-1}$ (*Figure 2.67*). Rotation of the Si–C^{carb} bond by 90° leads highly likely to the transition state **TS**, which presumably should feature a longer Si–C^{carb} bond and much more wider Si-Ge-R angle likewise observed in the isolated NHC-stabilized disilyne (R)*Si*=SiR(IMe$_4$) (R = Si^{i}Pr(CH(SiMe$_3$)$_2$)$_2$, d(Si–C^{carb}) = 2.199(1), Si-Si-R = 120.35(2) °)[251] compared to **12-*E*** (d(Si–C^{carb})= 1.841(1), Si-Ge-R = 101.0(3) °). Upon further rotation the **TS** transform itself to the *Z*-isomer which lies by $1.8 \pm 0.1\ kJ\ mol^{-1}$ higher in energy.

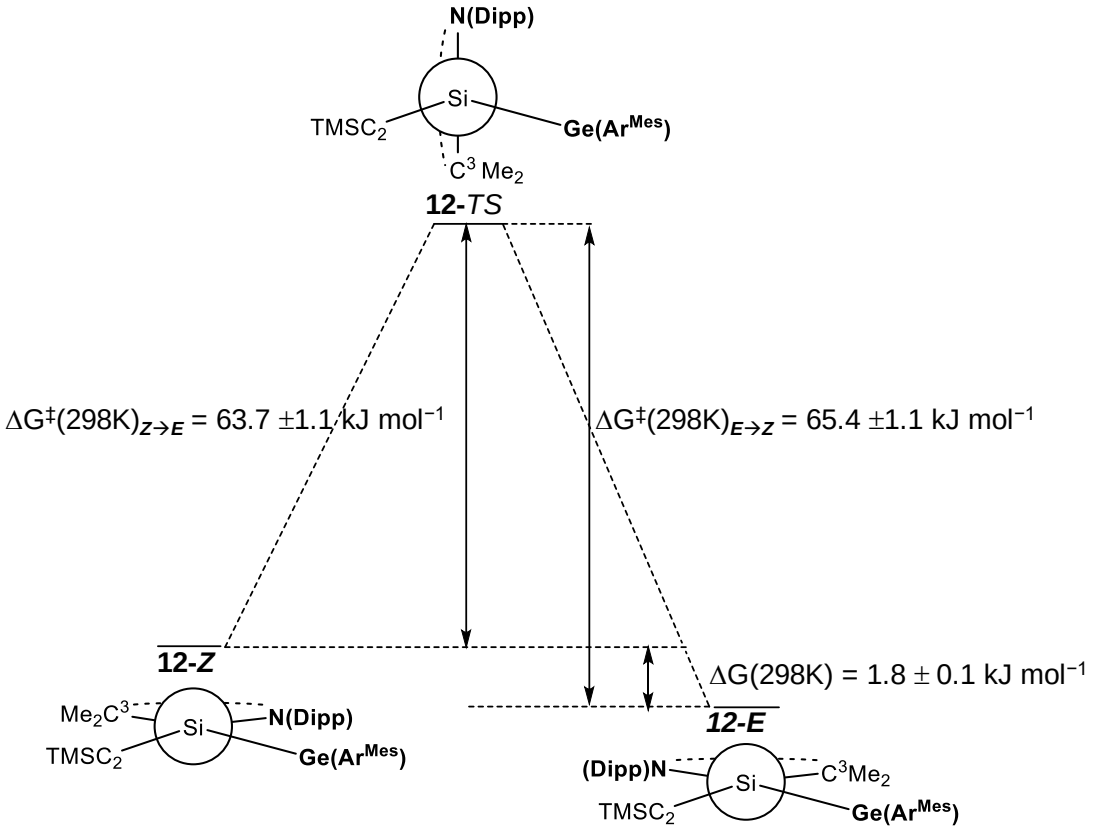

Figure 2.67. Energy profile for the reversible E → Z isomerization in Ar^{Mes}GeSi(C≡CTMS)(caac^{Me}) (**12**) with the depicted structures in the Newman projection along the Si–Ge bond. The thermodynamic activation parameters and thermodynamic parameters for the isomerization were obtained from a full line shape analysis and Van't Hof plot, respectively. The transition state (**12-*TS***) can be rationalized upon rotation of the Si–C^{carb} bond by 90°.

2.5.3.5 Electronic structure of (silenyl)germylene 12

The electronic structure of the (silenyl)germylene **12-*E*** was investigated by quantum chemical calculations, which were performed at the B97-D3(BJ)-ATM/def2-TZVP level of theory by Leonard R. Maurer. More details on the computional calculations are given in *chapter 5.11*. The structural parameters of the calculated structure in the gas phase do compare well to the structure derived from single-crystal X-ray diffraction of **12-*E*** (*Table* 5.81). Herein, the electronic structure of **12-*E*** is discussed in comparison to the NHC-stabilized germasilyne (Ar^{Mes})Ge=Si(Cl)(SIDipp) (**12-NHC**), which has been reported very recently by the research group of A. C. Filippou.[253]

Natural bond orbital analysis of the wave function of **12-*E*$_{calc}$**, led to a leading natural Lewis structure (NLS) with localized bond pair NBOs for the Si–C^{carb}, Si–Ge, Si–$C^{C\equiv C}$ and Ge–CAr^{Mes} σ-bonds and one lone pair NBO at the two-coordinate germanium center with high Lewis occupancies above 1.90 e^-. The Si–Ge σ-bond is polarized towards the silicon atom (60 %) and is formed by a $sp^{1.33}$ Si-NHO and an orbital of the germanium atom with high p-character ($sp^{9.12}$). The Si–$C^{C\equiv C}$ σ-bond is polarized towards the carbon center (72 %) and formed by the $sp^{2.57}$ Si-NHO and the $sp^{1.04}$ C-NHO. Considerable delocalization is evidenced by the low Lewis occupancy of the Si–C^{carb} π-bond (1.63 e^-), which features next to no polarization of the silicon and the carbon atom. In addition, the NRT-bond orders in **12-*E*$_{calc}$** show considerable amount of double bond character in the Si–C^{carb} (1.4) and Si–Ge bond (1.3). The NBO results clearly show C ≡ C bond character (NRT-BO 2.8) in the alkynyl substituent with only minor delocalization of the two C–C π-bonds of pure p-character to the silicon center (NRT-BO ($C^{C\equiv C}$–Si)= 1.1).

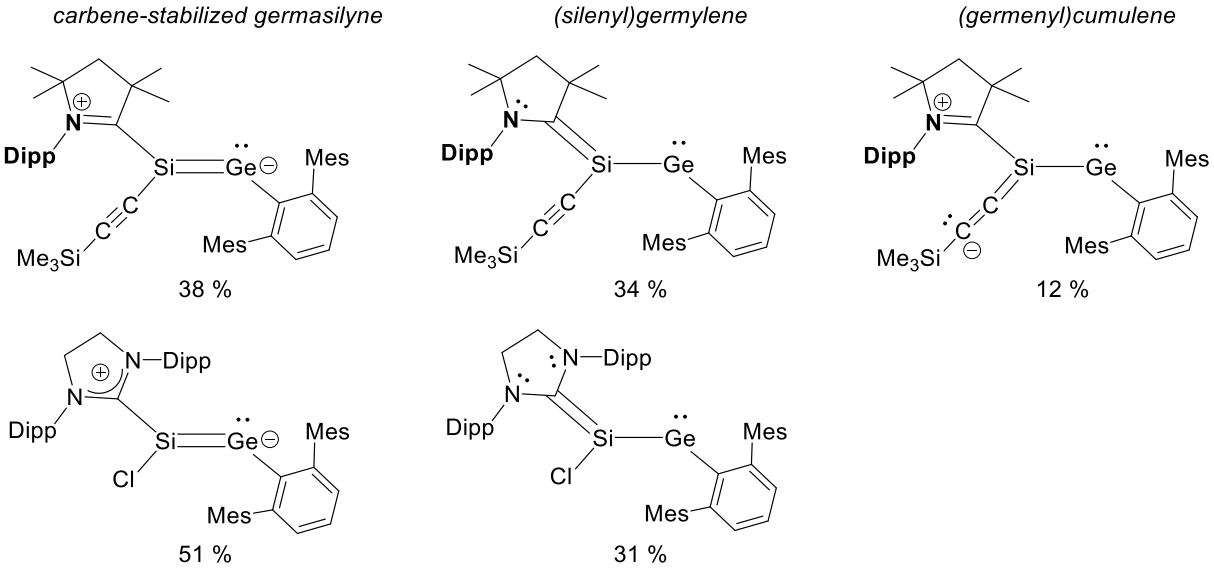

Figure 2.68. Most dominant NRT resonance structures for **12-*E*** in comparison to the parent NHC-stabilized compound **12-NHC**.[253]

The dominant NRT resonance structures of **12** give a much clearer picture of the nature of the electronic structure (*Figure 2.68*). In fact, **12** can be best described as hybrid of a cyclic (alkyl)(amino)carbene stabilized germasilyne (38 %) and a (silenyl)germylene (34 %) (*Figure 2.68*). Small amounts of a (germenyl)cumulene (12 %), upon delocalization of electron density to the alkinyl moiety, is observed as well.

Although the electronic structure on the first glance strongly resembles the structure of the SIDipp-stabilized silagermyne (Ar^{Mes})Ge=SiCl(SIDipp) (**12-NHC**) major differences can be seen in the results of the NRT-BO analysis. Overall the Si–C^{carb} σ-bond of the three-cooridinated silicon center in **12-*E*** features more sp^2-character ($sp^{2.51}$), similar to that of silenes, whereas in the NHC analogous compound the silicon center features more sp^3-character ($sp^{2.9}$). In addition, the bond order of the Si–C^{carb} bond in **12-*E*$_{calc}$** (1.4) is higher with respect to the bond order of the Si–Ge bond (1.3) **12-*E*$_{calc}$**, in contrast to the NHC stabilized silagermyne **12-NHC** where more double dond character is observed in the Si–Ge bond (1.5) with respect to the Si–C^{carb} bond (1.3).

Table 2.31. Selected results of the natural bond orbital (NBO), natural resonance theory (NRT) and natural population (NPA) analysis of **12-*E*$_{calc}$**, performed by Leonard Maurer. The graphical inlet depicts the Natural Lewis structure of the NBO analysis and its NRT contribution.

NBO A–B	occ.[a]	NHO (A,B)[b] hyb. (pol. in %)	WBI[c] A–B	NRT-BO[d] tot/cov/ion	atom/ group	q/Σq[e]
(Ar^{Mes})Ge–Si(C_2TMS)($caac^{Me}$) (**12-*E***)						
LP(Ge)	1.91	$sp^{0.25}$			$caac^{Me}$	–0.07
σ(Si–C^{carb})	1.95	$sp^{2.51}$(26), $sp^{1.51}$(74)	1.1	1.4/0.9/0.5	Si	+0.37
π(Si–C^{carb})	1.63	p(51), p(49)			Ge	+0.67
σ (Si–Ge)	1.90	$sp^{1.33}$(60), $sp^{9.12}$(40)	1.2		C ≡ CTMS	–0.53
σ(Si–$C^{C\equiv C}$)	1.97	$sp^{2.57}$(28), $sp^{1.04}$(72)	0.9	1.1/0.7/0.4	Ar^{Mes}	–0.43
σ(C–C)$^{C\equiv C}$	1.99	$sp^{0.97}$(49), $sp^{0.90}$(51)	2.7	2.8/2.8/ –	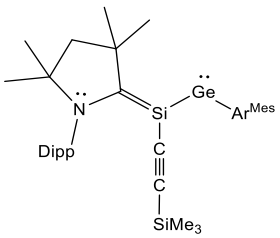	
π1(C–C)$^{C\equiv C}$	1.95	p(51), p(49)				
π2(C–C)$^{C\equiv C}$	1.95	p(50), p(50)				
σ (Ge–CAr^{Mes})	1.93	$sp^{8.43}$(27), $sp^{2.46}$(73)	0.8	1.0/0.5/0.4	34 %	

[a]: occ.= occupancy in e^-; [b]: NHO = Natural Hybrid Orbital, pol. (polarization) = $(C_i)^2 \cdot 100\%$, where C_i = coefficient of NHO; [c]: Wiberg bond index; [d]: total, covalent and ionic NRT bond order; [e]: q = NPA charge of the atom, ∑q = total NPA charge of the group.

The change in the NRT bond orders is in line with the contribution percentage of the most dominant NRT-resonance structures (*Figure 2.68*): in **12-*E*$_{calc}$** both the silagermyne (38 %) and the (silenyl)germylene (34 %) resonance structures contribute almost equally, whereas in **12-NHC** the contribution of the total amount of carbene-stabilized germasilyne (51 %) is greater with respect to the silenyl)germylene (31 %) resonance structure.[253]

The silene resonance structure is responsible for the formation of two diastereomers, **12-*E*** and **12-*Z***, which are equilibrating with each other at ambient temperature in solution. Due to the superior π-accepting capability of the CAAC carbene in **12**, the contribution of the silene resonance structure in **12** is higher, in comparison to the parent NHC compound **12-NHC,** which manifests itself in a rather high activation barrier of 65.4 ± 1.1 kJ mol^{-1} for the Si–C^{carb} rotation in **12**, in contrast to **12-NHC** where the rotation of the Si–C^{carb} bond proceeds via a calculated small activation barrier of ca. 18 kJ mol^{-1}.[253]

The NBO results are reflected in the frontier orbitals of **12-*E*$_{calc}$**. The HOMO-1 contains mainly the lone pair at the Ge atom, the HOMO corresponds to the 3c-2e π_{oop}(C^{carb}–Si–Ge)-bond and the LUMO corresponds to the empty p orbital at the Ge atom with some antibonding π_{oop}(Si–C^{carb}) contribution.

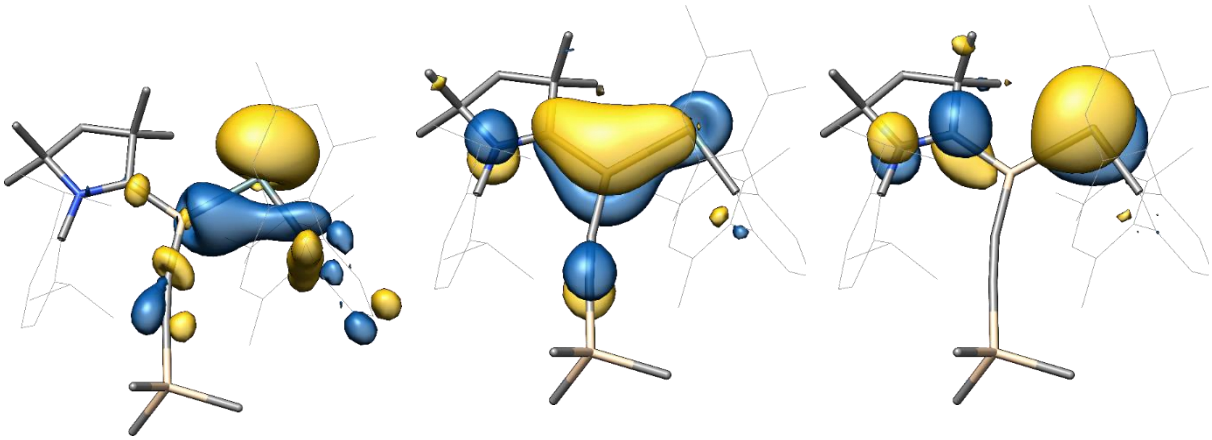

HOMO–1 [–4.51] HOMO [–3.84] LUMO [–2.37]

Figure 2.69. Selected molecular orbitals of **12-*E*$_{calc}$** and their orbital energies in eV. Hydrogen atoms are omitted for clarity. The isosurface value is set to 0.04 e$^{1/2}$·Bohr$^{-3/2}$.

2.6 CAAC-Stabilized Disilavinylidene and Silagermenylidene

2.6.1 Introduction

The heavier group 14 homologues of alkynes RE≡ER (E = Si, Ge, Sn, Pb, R = singly bonded substituent) and their valence-isomerization to vinylidenes :E=ER$_2$ are of considerable interest in theoretical and experimental chemistry.[17,254]
Calculations of the potential energy surface (PES) reveal a dramatic difference between C_2H_2 and its heavier congeners: In case of carbon the vinylidene H_2C=C: is the only higher energy minimum structure, which rapidly isomerizes via a 1,2 hydrogen migration to acetylene with a very low energetic barrier (10.40 ± 0.04 kJ mol^{-1}).[255,256]

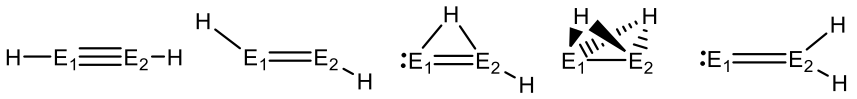

	A	B	C	D	E
$E_1 = E_2 = Si$	0.0	−79.5	−95.0	−157.7	−98.7
$E_1 = E_2 = Ge$	0.0	−107.9	−131.0	−192.5	−132.2
$E_1 = Ge$; $E_2 = Si$	0.0	−94.1	−142.5	−167.5	−132.3
$E_1 = Si$; $E_2 = Ge$	0.0	−94.1	−119.4	−167.5	−86.7

Figure 2.70. Calculated minimum structures of E_2H_2. Depicted are linear **A**, trans-bent **B**, monohydrid bridged **C**, bishydrid bridged **D** and vinylidene **E** isomers and calculated energies in kJ mol^{-1} for Si and Ge from the literature.[257,258]

In contrast, the linear alkyne like structure **A** in the case of heavier analogues E_2H_2 (E = Si – Pb) lies relatively high in energy, reflecting the reduced E–E bond order of the heavier congeners which can be attributed to a mixing of the σ* and π-orbitals as a consequence of their greatly increased core-core repulsion.[259] However, other isomers are predicted to be closer at the energetic minimum: a *trans*-bent structure **B**, a structure bridged by one hydrogen **C** and two hydrogen atoms **D** and the vinylidene isomer **E**.[254,260,261] Experimental evidence for the exotic chemical structures **C** and **D** was provided by Si_2H_2, via rotational spectroscopy in low-temperature matrices.[262,263] Isomer **E** could be experimentally probed in the case of vinylidene H_2C=C: and disilavinylidene H_2Si=Si:, which were generated as transient species in the gas phase. Vinylidene was generated upon collision of in *situ*-generated vinylidene anions with xenon atoms and features a lifetime of 0.4 μsec.[264–266]

The heavier analogous disilavinylidene was produced recently in the gas phase reaction of atomic silicon (Si) with silane (SiH_4), under single–collision conditions in molecular beam experiments and was shown to be in a equilibrium with the monobridged and dibridged isomers **C** and **D**.[267]

Out of the 4 isomers of the heavier analogues E_2R_2 (E = Si – Pb), only the *trans*-bent structures of type **B**, as well as vinylidenes **E** could be isolated in the solid state thus far. *Trans*-bent structures have been realized using sterically very demanding substituents, enabling the isolation and exploration of the chemistry of *trans*-bent ditretylynes E_2R_2 (E = Si[26–30], Ge[268–272], Sn[273], Pb[274], R = silyl, aryl, alkyl). The recently reported digermavinylidene **II-47**[252] (*Figure 2.7l*) by the research group of Aldridge features the first example of an isolated heavier analogue of vinylidene, which was enabled by the stabilization of the stericallly encumbered boryl ligand B[N(Dipp)CH]$_2$ (Dipp = C_6H_3-2,6-*i*Pr$_2$).

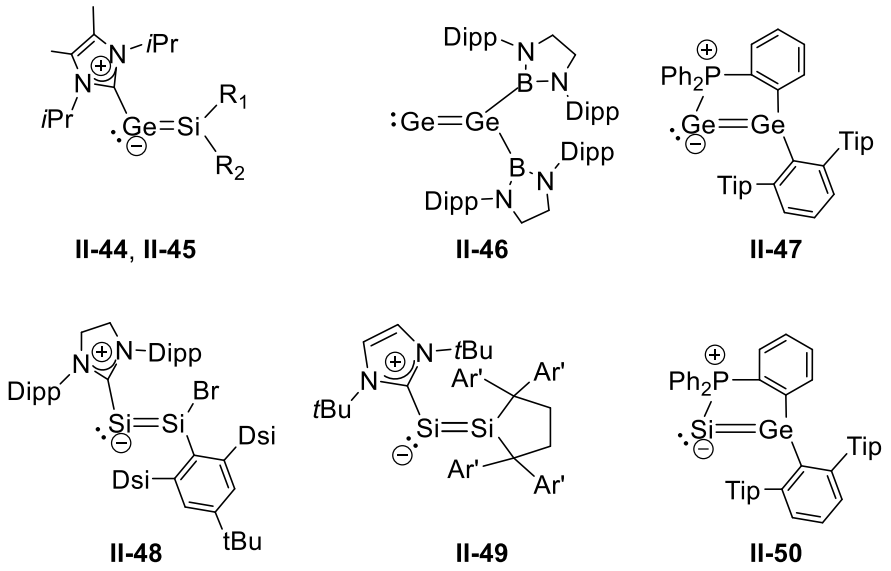

Figure 2.7l. Literature known heavier congeners of vinylidenes with **II-44** (R_1 = $R_{2=}$ Trip) and **II-45** (R_1 = Trip, R_2 = Si(Trip)$_2$Cl).; Ar' = C_6H_2-3,5-*t*Bu$_2$-4-OMe. For comparison reasons to related CAAC-stabilized compounds isolated in this work compound **II-48** will also be termed as **I4-NHC**.

The high reactivity of the heavier vinylidenes could be tamed by the use of Lewis Bases, such as phosphanes, which enabled the isolation of the phosphine stabilized digermavinylidene **II-47**[275] and germasilenylidene **II-50**[276] and N-heterocyclic carbenes (NHCs). This concept enabled the isolation of the I*i*Pr$_2$Me$_2$-stabilized silagermenylidenes **II-44**[247]and **II-45**[248]and the isolation of the SIDipp-stabilized disilavinylidene **II-48**[118] , as well as the NHC stabilized dialkyl-disilavinylidene **II-49**.[277] NHC-stabilized disilavinylidenes **II-48** and **II-49**, notably, are the only reported disilicon-analoga of vinylidenes thus far.

Remarkably, cyclic (alkyl)(amino)carbenes (CAACs) were not used so far in the stabilization of heavier vinylidenes, even though they differ quite remarkably from the parent NHCs, providing much stronger π-acceptor properties.[76,95,97,98]

2.6.1.1 Reactivity of literature reported heavier vinylidenes

Since the isolation of NHC-coordinated silagermenylidenes (R_2Si = Ge) **II-44**[247]and **II-45**[248] by Scheschkewitz in 2013 and 2014 the chemistry of heavier vinylidenes has flourished, leading to cycloaddition reactions at Si=Ge bond and coordination of the electron pair at the zero-valent germanium center to transition metal complexes. Reaction of base-free digermavinylidene **II-46**[252] with dihydrogen (H_2), led via the migration of the sterically stericallly encumbered boryl ligand $B[N(Dipp)CH]_2$ (Dipp = C_6H_3-2,6-*i*Pr_2) to the tetrahydridodigermene. Phosphane-stabilized digermavinylidene **II-47**[275] gave a [2+2] cycloaddition reaction with adamantylphosphaalkyne (Ad–C ≡ P) and upon reaction with adamantylazide (Ad–N_3) the tetrameric cluster $[(GeN\text{-}Ad)_4]$ was obtained, essentially revealing the transfer of the zero-valent germanium atom. On the other hand, the synthesis of vinylidenes with a terminal zero-valent silicon atom appeared especially challenging. The NHC stabilized disilavinylidene **II-48**[118], reported by the research group of A. C. Filippou in 2015 layed the foundation in this field. The NHC-stabilized dialkyldisilavinylidne **II-49**[277] and the phosphane stabilized germasilyenilidene **II-50**[276] were reported very recently. Besides of the oxidation of disilavinylidene **II-49** with N_2O no reactivity of disilavinylidenes have been reported thus far in the literature. [277]

The reactivity of the NHC-stabilized disilavinylidene **II-48** has been studied by the research group of A. C. Filippou over the last 6 years. Major contribution to this research gave Simon Schwarzwald, which discovered a versatile reactivity of disilavinylidene **II-48** (*Figure 2.72*). The reaction of disilavinylidene **II-48** with electrophiles afforded the addition products (**II-51**), σ-type complexes (**II-52**) and π-complexes (**II-56**). Reaction of **II-48** with nucleophiles led to various products: Reaction of the disilavinylidene with lithiumorganyles LiR (R = Me, CH_2Ph) afforded the substituted products (SIDipp)Si=Si(R)(Tbb) (R = Me (**II-58**), CH_2Ph (**II-59**)). Reaction of **II-48** with NaPCO gave the disiladiphospha cyclopentadiene **II-60**. The weak bonding of the NHC in the disilavinylidene could be exploited upon a carbene exchange reaction with the small carbene IMe_4, which led to the formation of the salt $[(IMe_4)_2Si\text{-}Si(IMe_4)Tbb]Br$ (**II-57**).[181]

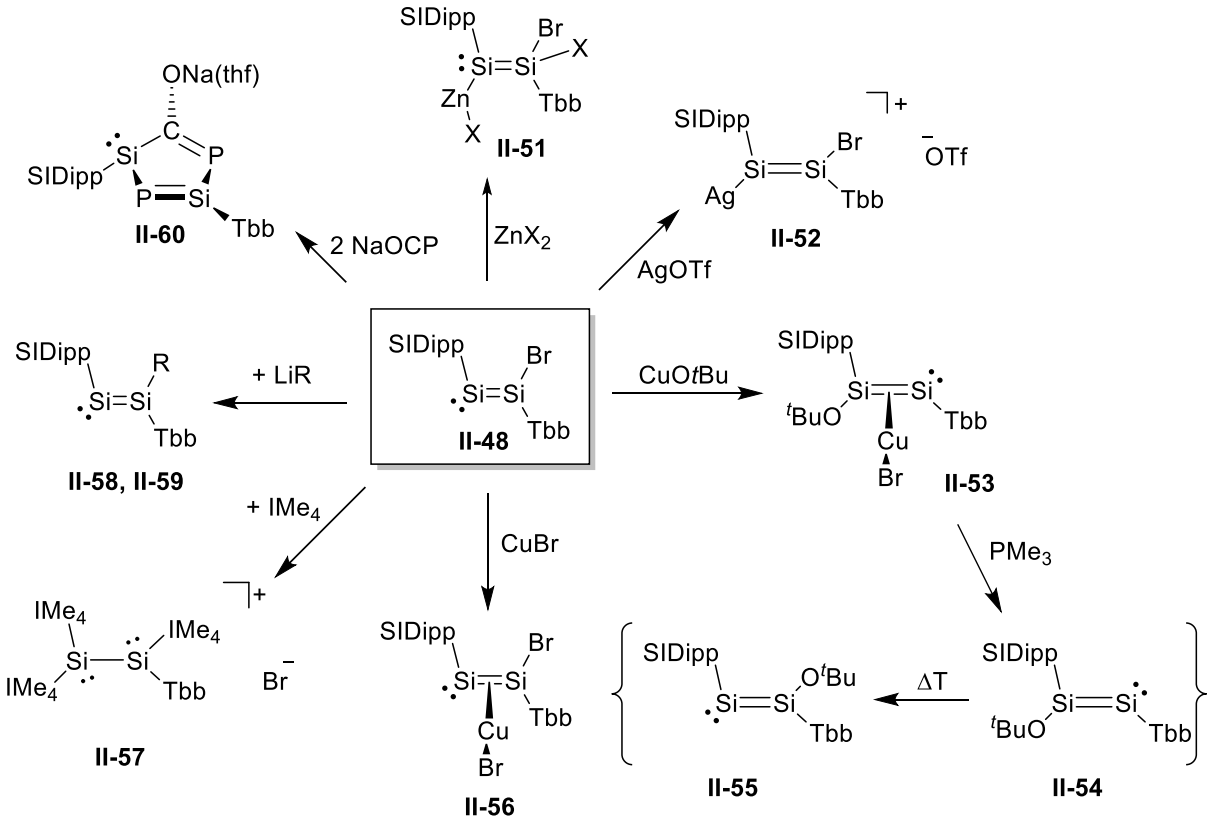

Figure 2.72. Overview of the versatile reactivty of the NHC-stabilized disilavinylidene **II-48** reported by Simon Schwarzwald.[181] Formal charges are not given for the sake of simplicity.

Remarkably, reaction of the disilavinylidene **II-48** with the Cu(I)-alkoxide (CuOtBu) led to the formation of a push-pull complex of a carbene stabilized disilyne CuBr{(SIDipp)(*t*BuO)Si=SiTbb)} (**II-53**). By subsequently abstracting CuBr with PMe_3, the NHC-stabilized alkoxydisilyne (SIDipp)(*t*BuO)Si=SiTbb) (**II-54**) was liberated and found to isomerize to the NHC-stabilized alkoxydisilavinylidene (SIDipp)Si=Si(O*t*Bu)Tbb (**II-55**) at elevated temperatures. [181]

.

2.6.2 Synthesis and properties of (caac^{Me})E=SiBr(Tbb) (E = Si, Ge)

2.6.2.1 Synthesis and properties of EBr(SiBr$_2$Tbb)(caac^{Me}) E = Si (13),Ge (13-Ge)

Adding 2 equiv. of a clear red solution of SiBr$_2$(caac^{Me}) (**1**) in benzene to a 2:1 mixture of 4-dmap and (*E*)-Tbb(Br)Si=Si(Br)Tbb in benzene at ambient temperature afforded a dark blue solution (see *section 4.4.32*), which slowly changed its color to yellow-brown over the course of 19 h. Monitoring the reaction progress by ^{1}H-NMR spectroscopy in (D$_6$)benzene revealed a selective conversion to the caac^{Me}-stabilized bromosilylsilylene **13,** which was isolated as a yellow, air sensitive solid in 77 % yield after work-up. Compound **13** is stable for months at ambient temperature under argon atmosphere and is a thermally robust solid, decomposing upon melting at 199 °C in a vacuum-sealed capillary tube. The reaction pathway can be rationalized by the following way: 4-dmap acts as a lewis base and activates the 1,2-dibromidisilene (*E*)-Tbb(Br)Si=Si(Br)Tbb yielding *in situ* the 4-dmap stabilized bromosilylene (Br)(Tbb)Si(4-dmap).[9,10] SiBr$_2$(caac^{Me}) (**1**) as a stronger lewis-base replaces 4-dmap and leads to a Lewis base-stabilized intermediate which then rapidly rearranges via a 1,2-migration of bromine from the four-coordinated to the three-coordinated silicon center to give the final product **13**.

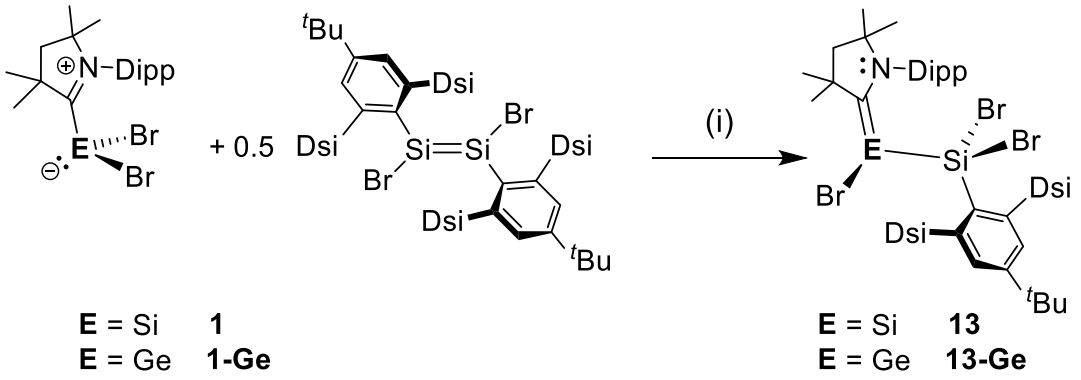

Scheme 2.20. Synthesis of silylsilylene **13** and silylgermylene **13-Ge**, starting from SiBr$_2$(caac^{Me}) and GeBr$_2$(caac^{Me}), respectively. (i) Si: 4-dmap, benzene, r.t.; Ge: toluene, 100°C.

---

[9] The analogous Lewis-base adduct of 4-pyrrolidinopyridine (PPy) to the 1,2 dibromodisilene (*E*)-EMind(Br)Si=Si(Br)EMind has been reported, see reference [23].

[10] Reaction of (*E*)-Tbb(Br)Si=Si(Br)Tbb with 2 equivalents of 4-dmap, led according to ^{1}H NMR spectroscopy in (D$_6$)benzene to the complete consumtion of the disilene and the the formation of a mixture of different products, from which the formal [2+2] cycloaddition product of 1 equiv. 4-dmap to (*E*)-Tbb(Br)Si=Si(Br)Tbb could be crystallized, see reference [278].

In a similar way, the heavier homologue **13-Ge** was synthesized. Heating a 2:1 mixture of $GeBr_2(caac^{Me})$ (**1-Ge**) and (E)-[Tbb(Br)Si=Si(Br)Tbb] in toluene at 100 °C for 2 h afforded a dark red solution. Monitoring the reaction progress by ^1H NMR spectroscopy in (D_6)benzene revealed the selective conversion to the $caac^{Me}$-stabilized bromogermylene **13-Ge**, which was isolated as a red, air sensitive powder in 77 % yield after work up.
Also **13-Ge** is stable for months at ambient temperature under argon atmosphere and is a thermally robust solid, decomposing upon melting at 194 °C, respectively. ^1H NMR spectroscopy of the molten mass in (D_6)benzene revealed a rather unsective decomposition in **13** and the selective formation of $GeBr_2(caac^{Me})$ (**1-Ge**) and $TbbSiBr_3$ in **13-Ge**, after cleavage of the Ge–Si single bond. One might expect the formation of disilene of (E)-[Tbb(Br)Si=Si(Br)Tbb] next to **1-Ge** upon cleavage of the Ge–Si bond of **13-Ge**. However, this was not observed in the ^1H NMR spectrum of the molten mass of **13-Ge**, suggesting that the disilene was further oxidized to $TbbSiBr_3$. In comparison, thermal decomposition of **13** is unselective.

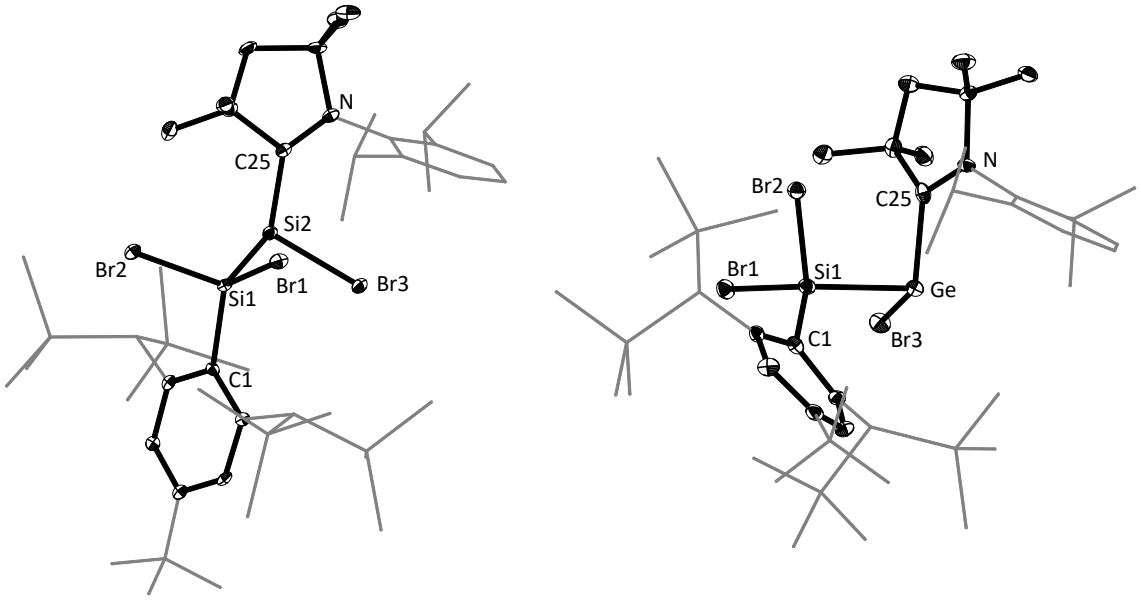

Figure 2.73. Diamond plot of the Molecular structure of **13** (left) and **13-Ge** (right), thermal ellipsoids are set at 30 % probability, and hydrogen atoms were omitted. In the depicted structures the Dipp-substituent of the $caac^{Me}$ ligand and the disyl-groups $(CH(SiMe_3)_2)$ and *t*Bu-group of the Tbb substituent are presented in the wire-frame for the sake of clarity. Selected bond lengths [Å], bond angles [°] and torsion angles [°]:
13: Si1–Si2 2.369(3), Si1–C1 1.903 (8), Si2–C25 1.879(8),C25–N 1.331(10), Si1–Br1 2.263(2) , Si1–Br2 2.262(2), Si2–Br3 2.303(2), C1–Si1–Si2 111.7(3), C1–Si1–Br1 118.0(3), C1–Si1–Br2 104.7(2), C25–Si2–Si1 112.7(3), C25–Si2–Br3 109.3(3), Si1–Si2–Br3 91.6(1), Si2–Si1–Br1 106.9(2), Si2–Si1–Br2 117.0(1), C1–Si1–Si2–C25 –179.1(3), C1–Si1–Si2–Br3 –67.4(2), C25–Si2–Si1–Br1 -48.6(3), C25–Si2–Si1–Br2 60.3(3), Br1–Si1–Si2–Br3 63.1(1);
13-Ge: Ge1–Si1 2.510(2), Si1–C1 1.888 (5), Ge–C25 2.094(5),C25–N 1.297(6), Si1–Br1 2.285(2), Si1–Br2 2.242(2), Ge–Br3 2.4529(7), C1–Si1–Ge 113.2(2), C1–Si1–Br1 106.4(2), C1–Si1–Br2 110.2(2), C25–Ge–Si1 97.9(2), C25–Ge–Br3 98.8(2), Si1–Ge–Br3 94.7(4), Ge–Si1–Br1 105.5(1), Ge–Si1–Br2 117.5(1), C1–Si1–Ge–C25 –145.7(4), C1–Si1–Ge–Br3 114.9(3), C25–Ge–Si1–Br1 –29.3(2), C25–Ge–Si1–Br2 84.1(2), Br1–Si1–Ge–Br3 –128.7(1).

Yellow single crystals of **13**, as well as clear red blocks of **13-Ge** were obtained from *n*-hexane solution at –30 °C. The molecular structures of both compounds can be compared to the NHC stabilized bromosilylene SiBr(SiBr$_2$Tbb)(SIDipp) (**13-NHC**).[118] The three coordinated tetrel(II) center is trigonal pyramidal coordinated (Σ∢(Si2) = 313.6° (**13**), Σ∢(Ge) = 291.4° (**13-Ge**)). The sum of angle a the silicon center in **13** (Σ∢(Si) = 313.6°) is drastically increased compared to that of **13-NHC** (Σ∢(Si) = 287.4°) and lies in-between that of SiBr$_2$(caac^{Me}) (Σ∢(Si) = 289.94 °) and a classical trigonal planar silene (Σ∢(Si) = 360.0 °).[184] In fact, the Si–C^{carb} bond length (1.879(8) Å) in **13** is significantly shortented, when compared to **13-NHC** (1.978(3) Å), and lies in the upper limit of previously reported pyramidal 2-(amino)silenes SiBr(R)(caac^{Me}) reported in this work (1.836(2) Å (**2-Si**) – 1.897(3) Å (**2-O**)) (see *section 2.2.2*), suggesting some π(Si–C^{carb}) bonding in **13**. The Ge–C^{carb} bond in **13-Ge** (2.094(5) Å), in contrast, is only slightly shorter than that of GeBr$_2$(caac^{Me}) (2.128(3) Å), which is in line with the retained strong pyramidalization at the Ge-center in **13-Ge** (Σ°Ge = 291.4°) in comparison to GeBr$_2$(caac^{Me}) (**1-Ge**)(Σ∢(Ge) = 288.5°).

The bulky caac^{Me} and Tbb substituents adopt an antiperiplanar conformation in **13** (τ(C^{Ar}–Si1–Si2–C^{carb}) = 179.1(1)°) and an anticlinal conformation in **13-Ge** (τ(C^{Ar}–Si1–Ge–C^{carb}) = 145.0(1)°) and the caac^{Me} and Tbb-aryl-plane are orientated almost orthogonally with respect to each other. The bromine atoms Br1 and Br3 adopt a synclinal conformation along the Si1–Si2 (2.369(3) Å (**13**)) and an anticlinal conformation along the Si–Ge (2.510(2) Å (**13-Ge**) single bonds as evidenced by the torsion angles of τ(Br1–Si1–Si2–Br3) = 63.1(1)° (**13**) and τ(Br1–Si–Ge–Br3) = –128.7(1)° (**13-Ge**),respectively.

The Si1–Si2 bond distance of **13** (2.369(3) Å) is slightly shorter than that in **13-NHC** (2.391(1) Å) and compares well with that of the amidinato-stabilized silylsilylene Si[SiX{(N*t*Bu)$_2$CHPh}][(N*t*Bu)$_2$CPh] (X = H: d(Si–Si) = 2.377(5) Å; X = Cl: d(Si–Si) = 2.381(7) Å).[279] The Si–Ge bond length in **13-Ge** compares well to the IMe$_4$-stabilized (chlorosilyl)chlorogermylene (2.497(1) Å).[280] The Ge–Br3 bond lengh in **13-Ge** (2.453(1) Å), does not change significantly compared to the starting material GeBr$_2$(caac^{Me}) (**1-Ge**) (2.4533(4), 2.4589(3) Å) and the Si–Br bond lengths of the SiBr$_2$(Tbb) moiety in **13** (2.263(3) Å, 2.262(2) Å) and **13-Ge** (2.285(1) Å, 2.242(1) Å) are comparable to those of **13-NHC** (2.263(1) Å, 2.2861(1) Å).

^{1}H, ^{13}C{^{1}H} and ^{29}Si{^{1}H} NMR spectra of **13** feature an averaged *Cs*-symmetry (*Figure 2.74* bottom), indicating a dynamic behavior in solution, whereas the ^{1}H NMR spectra of **13-Ge** (*Figure 2.74* top) suggest the presence of a C_1-symmetric structure in solution.

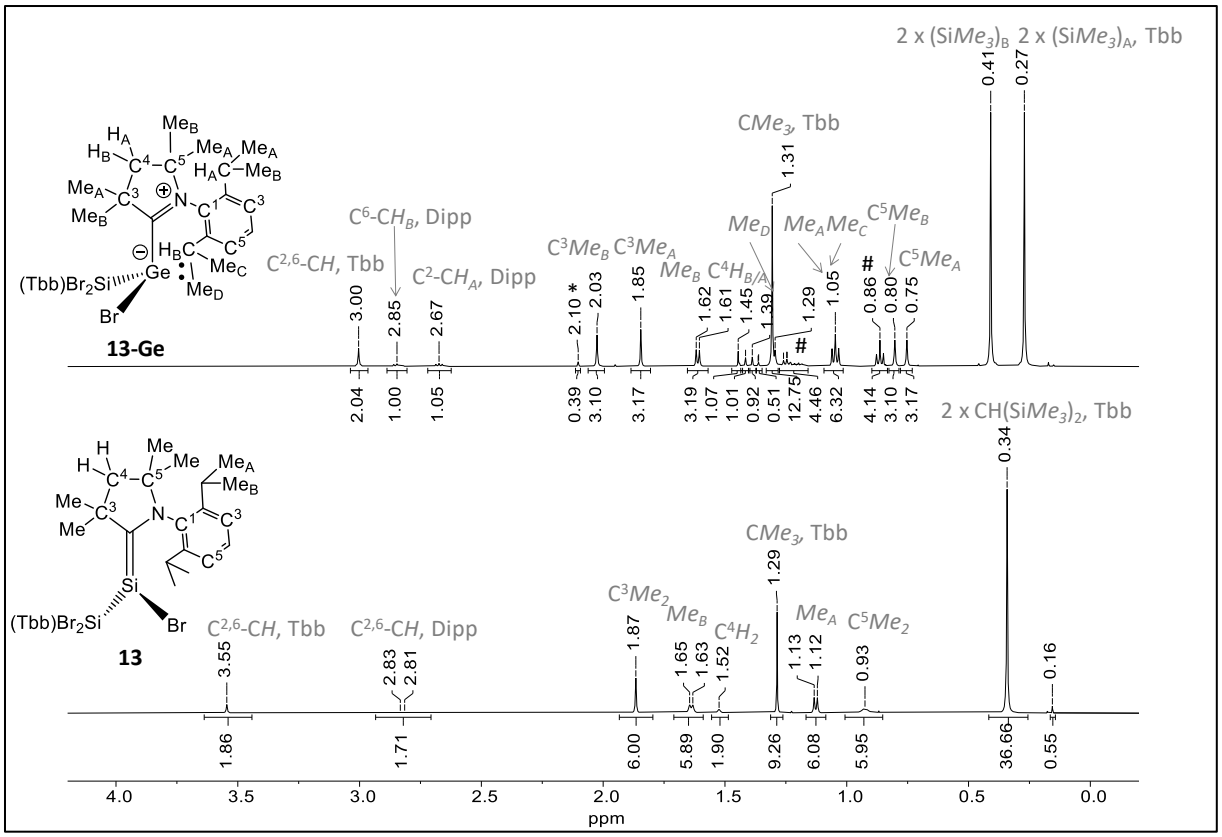

Figure 2.74. Excerpt of the aliphatic region of the ^{1}H-NMR spectra of pure samples of **13** (bottom) and **13-Ge** (top) in (D_6)benzene at 298 K. The symbol # and (*) marks residual solvent peaks of *n*-pentane and toluene, respectively. All signals were assigned via high resolution correlation spectroscopy (*chapter 4.4*).

VT ^{1}H NMR spectra of **13** at 193 – 298 K in (D_8)toluene revealed a hindered rotation of the Tbb substituent at lower temperatures and a pyramidal inversion of the silenic silicon center, leading to C_1 symmetry at 193 K. Lineshape analysis of these two processes, gave a Gibbs free activation enhalpy of 54.2 ± 2.4 kJ mol^{-1} for the pyramidal inversion and 41.1 ± 1.9 kJ mol^{-1} for the hindered Tbb rotation at 298 K, respectively. The low temperature limit spectrum of **13** (*Figure* 5.40), in fact, is almost identical to the ^{1}H NMR spectrum of **13-Ge** measured in (D_6)benzene (*Figure 2.74* top).

The ^{29}Si{^{1}H} NMR spectrum of **13** in (D_6)benzne displays resonances at –10.6 (*Si*Br_2(Tbb)), 3.3 (4x(*Si*Me_3)) and 8.5 ppm ((caac^{Me})*Si*). The ^{29}Si-resonance for the silenic Si center (8.5 ppm) in **13** is upfield shifted when compared to $SiBr_2$(caac^{Me}) (δ = 14.4 ppm) and downfield shifted, when compared to **13-NHC** (–1.9 ppm). The ^{29}Si-resonance of the *Si*Br_2Tbb substituent is comparable to that of **13-NHC** (–11.3 ppm). The ^{29}Si{^{1}H} NMR spectrum of **13-Ge** in (D_6)benzene displays resonances at 2.7 (*Si*Me_3)$_A$, 3.37 ($SiMe_3$)$_B$ and 10.29 ppm (*Si*Br_2Tbb). The tetrahedral silicon center in **13-Ge** (10.29 ppm) is downfield shifted to that of the lighter homologue **13** (–10.6 ppm (*Si*Br_2(Tbb)).

The remarkable upfield shift of the $^{13}C^{CAAC}$ resonance in **13** (217.4 ppm) compared to **13-Ge** (244.7 ppm), $SiBr_2(caac^{Me})$ (**1**) (231.2 ppm) and $GeBr_2(caac^{Me})$ (**1-Ge**) (241.6 ppm) indicates the higher $Si{=}C^{carb}$ double bond character in **13**.

According to structural and NMR spectroscopic features compound **13** can be rather classified as a pyramidal 2-aminosilene, similar to the pyramidal 2-(amino)silenes $SiBr(R)(caac^{Me})$ (**2-Nu**) discussed in *chapter 2.2*. In comparison, **13-Ge** is better described as a carbene stabilized (silyl)germylene with an inverted polarization of the $Ge^{\delta-}{-}(C^{carb})^{\delta+}$ bond. In terms of its structural properties **13-Ge** ($d(Ge{-}C^{carb}) = 2.094(5)$ Å, $\Sigma\measuredangle(Ge) = 291.4$ °) compares well to the recently reported NHC-stabilized (chlorosilyl)chlorogermylene $GeCl(SiClR_2)(IMe_4)$ ($R_2 = [N\text{-}(t\text{Bu})CH]_2$) ($d(Ge{-}C^{carb}) = 2.081(2)$ Å, $\Sigma\measuredangle(Ge) = 296.9$ °).[280]

2.6.2.2 Synthesis and properties of $(caac^{Me})E{=}SiBr(Tbb)$ E = Si (14), Ge (14-Ge)

Reduction of **13** and **13-Ge** with two equivalents of KC_8 in DME was accompanied by a color change from yellow to green (**14**) and red to blue (**14-Ge**), respectively. Monitoring of the two reaction mixtures via ^1H NMR spectroscopy in (D_6)benzene, revealed the quantitative formation of the $caac^{Me}$-stabilized disilavinylidene **14** and silagermenylidene **14-Ge**, respectively.

Both compounds were isolated upon crystallizuation from *n*-pentane at –30 °C, yielding **14** and **14-Ge** as dark green and dark blue microcrystalline solids in 50 % (**14**) and 73 % (**14-Ge**) yield, respectively. Both compounds are extremly air sensitive, immediatley decolorizing upon exposure to air. Under argon atmosphere, however, they are stable for months at ambient temperature, decomposing in a sealed vacuum capliallary upon melting at 195 °C (**14**) and 182 °C (**14-Ge**), respectively.

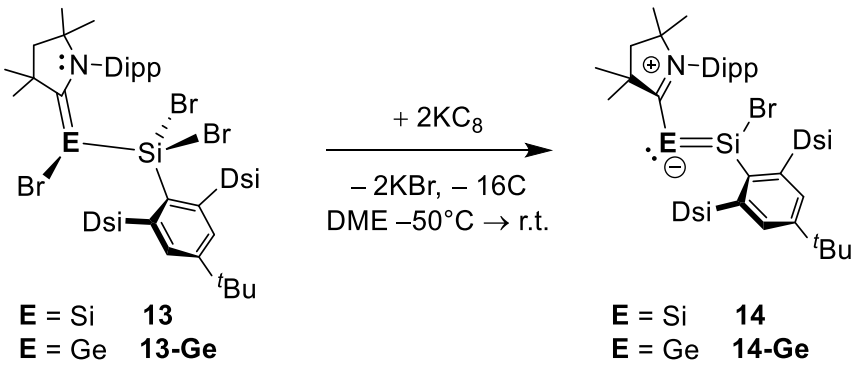

Scheme 2.21. Synthesis of the $caac^{Me}$-stabilized disilavinyldene **14** and silagermavinylidene **14-Ge**, upon reduction of the silylsilylene **13** and silylgermylene **13-Ge**, respectively.

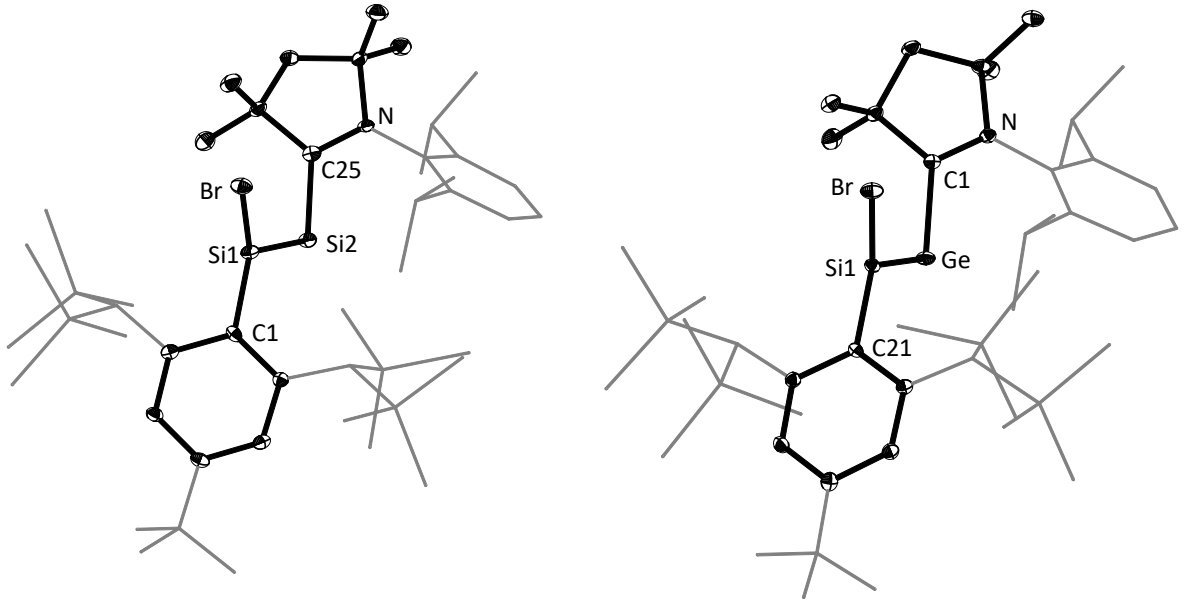

Figure 2.75. Diamond plot of the Molecular structure of **14** (left) and **14-Ge** (right), thermal ellipsoids are set at 30 % probability, and hydrogen atoms were omitted. In the depicted structures the Dipp-substituent of the caac^{Me} ligand and the disyl-groups (CH(SiMe$_3$)$_2$) and *t*Bu-group of the Tbb substituent are presented in the wire-frame for the sake of clarity. Selected bond lengths [Å], bond angles [°] and torsion angles [°]: **14**: Si1–Si2 2.194(2) [2.181(2)], Si1–C1 1.874(5) [1.879(5)], Si2–C25 1.878(5) [1.868(6)], N–C25 1.338(6) [1.325(6)], Si1–Br 2.278(2) [2.273(2)], C1–Si1–Si2 118.2(2) [119.9(2)], C1–Si1–Br 108.2(2) [106.9(2)], C25–Si2–Si1 106.8(2) [105.6(2)], Si2–Si1–Br 127.8(7) [128.0(1)], C1–Si1–Si2–C25 178.2(3) [176.9(2)], C25–Si2–Si1–Br –32.1(2) [–32.1(2)], N–C25–Si2–Si1 135.6(3) [137.9(4)] Values are given for two independent molecules in the unit cell, for simplicity the first set of values is discussed in the main text. **14-Ge**: Si1–Ge 2.249(1), Si1–C21 1.890(2), Ge–C1 1.987(2), N–C1 1.318(3), Si1–Br 2.281(1), C1–Ge–Si1 105.5(1), C21–Si1–Ge 119.3(1), C21–Si1–Br 107.5(1), Ge–Si1–Br 128.1(3), C21–Si1–Ge–C1 180.0(2), C1–Ge–Si1–Br –28.7(1), N–C1–Ge–Si1 136.4(2).

Dark green single crystalls of **14** and clear blue blocks of **14-Ge** were obtained from saturated *n*-pentane solutions at –30 °C. The molecular structure of both compounds (*Figure 2.75*) on the first glance are remarkably similar to the NHC-stabilized disilavinylidene (SIDipp)Si=SiBr(Tbb) (**II-48** = **14-NHC**).[118] The planar core of the structure consists of the atoms C^{Ar}, Si1, E, C^{carb} (E = Si2 (**14**), Ge (**14-Ge**)). The three coordinated silicon center in **14** (Σ∢(Si1) = 354.2°)and **14-Ge** (Σ∢(Si1) = 354.9°) deviate slightly from the trigonal planar coordination observed in **14-NHC** (Σ∢(Si1) = 360.1°). The bulky Tbb and caac^{Me} groups are orientated in trans-position to each other as evidenced by the torsion angles τ(C^{Ar}–Si1–Si2–C^{carb}) = 178.2(3)° (**14**) and τ(C^{Ar}–Si1–Ge–C^{carb}) = 180.0(2)° (**14-Ge**) and the Tbb substituent is orientated orthogonal with respect to the planar core of the molecule in analogy to **14-NHC** (τ(C^{Ar}–Si1–Si2–C^{carb}) = 177.3(2)°).

Interestingly, the relative orientation of the carbene with respect to the Si=E (E = Si, Ge) moiety in **14** (φ_{CAAC} = 57.8(2)° [51.9(3)°]) and **14-Ge** (φ_{CAAC} = 49.7(1)°) is remarkably different compared to **14-NHC** (φ_{NHC} = 94.8(2)°), suggesting some delocalisation of the tetrel-silicon π-bond over the C^{carb}–Si2–Si1 moiety in **14** and the C^{carb}–Ge–Si1 moiety in **14-Ge**. In addition the bromine subsituents in **14** (τ(C^{carb}–Si2–Si1–Br) = –32.1(2)°) and **14-Ge** (τ(C^{carb}–Ge–Si1–Br) = –28.7(1)°) are considerably bent, compared to **14-NHC** (τ(C^{carb}–Si2–Si1–Br) = –4.0(1)°), leading to a slightly pyramidalized silicon center of SiBr(Tbb) in **14** (Σ°Si2 = 354.2 °) and **14-Ge** (Σ°Si2 = 354.9 °). These structural features lead to C_1-symmetric solid state structures of **14** and **14-Ge**, whereas **14-NHC** features C_S-symmetry with the mirror plane passing through the planar core of the molecule.

The Si–C^{carb} bond length in **14** (1.878(5) Å) and the Ge–C^{carb} bond length in **14-Ge** (1.9872(2) Å) are considerably shorter with respect to their parent dibromotetrylenes $SiBr_2(caac^{Me})$ (**1**) (2.017(2) Å) and $GeBr_2(caac^{Me})$ (**1-Ge**) (2.128(3) Å) and lie in the typical range of Si–C^{Ar} single bonds (1.879 – 1.894 Å).[34,197] This trend is in line with a significant elongation of the N–C^{carb} bonds in **14** (1.338(6) Å) and **14-Ge** (1.318(3) Å), compared to their dibromotetrylenes **1** (1.301(3) Å) and **1-Ge** (1.297(6) Å), suggesting an increased π-character in the tetrel-carbene bond, respectively. The Si=Si bond (2.194(2) Å) in **14** is slightly longer compared to **14-NHC** (2.167(2) Å)[118] but still significantly shorter than that of $Si_2(caac^{Me})_2$ (2.254(1) Å)[115] and (E)-Tbb(Br)Si=Si(Br)Tbb (2.216 Å).[25] The Ge=Si bond in **14-Ge** (2.249(1) Å), compares well to that of the NHC-stabilized silagermenylidenes **II-44** (R_1 = R_2 = Trip; 2.252(1) Å)[247] and **II-45** (R_1 = Trip, R_2 = $SiCl(Trip)_2$; 2.276(1) Å)[248] and to the silagermene $(tBu_3)_2Si{=}Ge(Mes)_2$ (2.2769(8) Å).[249]

Table 2.32. Structural parameters of **14** and **14-Ge** in comparison to literature known NHC-stabilized disilavinylidenes and silagermenylidenes.

Comp.	E–E / Å	E–C^{carb} / Å	C^{carb}-E-E / (deg)	φ_{carb} [a] / (deg)	Ref.
($caac^{Me}$)Si=SiBr(Tbb) (**14**)	2.194(2)	1.878(5)	105.5(1)	57.8(2)	
	2.181(2)	1.868(6)	105.6(2)	51.9(3)	*this*
($caac^{Me}$)Ge=SiBr(Tbb) (**14-Ge**)	2.249(1)	1.9872(2)	106.8(2)	49.7(1)	*work*
(SIDipp)Si=SiBr(Tbb) (**14-NHC**)	2.167(2)	1.937(4)	97.6(1)	94.8(2)	[118]
(I*t*Bu)Si=Si(R_1)$_2$ (**II-49**)[b]	2.179(1)	1.962(2)	105.4(1)	89.6(1)	[277]
(I*i*Pr_2Me_2)Ge=Si(R_2)$_2$ (**II-44**)[c]	2.252(1)	2.047(2)	98.90(5)	63.8(1)	[247]
(I*i*Pr_2Me_2)Ge=Si(R_2)($SiCl(R_2)_2$)[c] (**II-45**)	2.276(1)	2.061(4)	101.9(1)	61.1(2)	[248]

[a]: φ_{carb} the angle between the least-squares plane of the CAAC/NHC five-membered ring and the plane defined by the C^{CAAC}/C^{NHC} and the doubly-bonded tetrel atoms.

[b]: (R_1)$_2$ = [C(Ar)$_2$-(CH_2)$_2$-C(Ar)$_2$] (Ar = C_6H_2-3,5-*t*Bu_2-4-OMe). [c]: R_2 = Trip = C_6H_2-2,4,6-*i*Pr_3.

Compounds **14** and **14-Ge** clearly differ from the NHC-stabilized disilavinylidenes and silagermenylidenes by a drastic decrease of the E–C^{carb} bond lengths and the more co-planar orientation of the carbene with respect to the Si=Si and Si=Ge moiety (*Table* 2.32), suggesting a weak delocalization of the tetrel-tetrel π-bond via the C^{carb}-Si2-Si1 moiety in **14** and the C^{carb}–Ge–Si1 moiety in **14-Ge**.

^{1}H, $^{13}C\{^{1}H\}$ and $^{29}Si\{^{1}H\}$ NMR spectra of **14** and **14-Ge** indicate an averaged C_s-symmetric structure in solution, in contrast to the C_1 symmetry in the solid state, which can be rationalized by the rapid rotation of the Tbb and $caac^{Me}$ groups about their respective Si–C bonds (*Figure 2.76* (a) and (b)). Recorded ^{1}H NMR spectra of **14** and **14-Ge** at variable temperatures in (D_8)toluene (193 – 298 K) reveal only the hindered rotation of the Tbb substituent (*Figure 2.76* (b)), which is evidenced by splitting of the signal of the TMS groups into two signals at temperatures below 253 K (see *section 5.6.7* and *5.6.8.*).

(a) Enantiomerization upon rotation of the E–C^{CAAC} bond

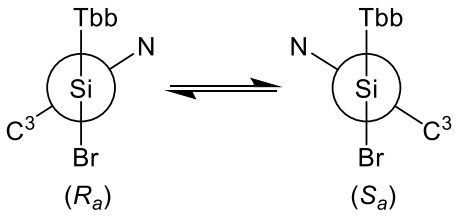

Newman projection Si_{Tbb} to C^{CAAC} center

(b) Hindered rotation of the Si-C^{Tbb} bond

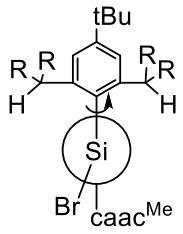

Newman projection along the Si=E bond

Figure 2.76. Dynamic processes of **14** and **14-Ge** at ambient temperature in solution, which can be rationalized upon rotation of the tetrel-carbene carbon bond (a) and the rotation of the Tbb substituent (b).

Full line shape analysis of the recorded variable temperature ^{1}H NMR spectra gave the Gibb's energy of activation of $\Delta G^{\ddagger}(298K) = 53.3 \pm 1.7$ kJ mol^{-1} (**14**) and $\Delta G^{\ddagger}(298K) = 51.6 \pm 3.8$ kJ mol^{-1} (**14-Ge**) for the hindered rotation of the Si–C^{Tbb} bond, respectively. In comparison the rotation of the $caac^{Me}$ carbene occurs rapidly, even at 193 K in (D_8)toluene solution. This observation is in line with the results of the analysis of the potential energy hypersurface scan (PES) at the B97-D3(BJ)-ATM/def2-TZVP level of theory (*section 5.11.8*), which suggest that **14** and **14-Ge** are quite flexible, undergoing a rotation of the $caac^{Me}$ substituents about their respective Si–C^{carb} and Ge–C^{carb} bonds (*Figure 2.76* (a)), with low barriers of 14 kJ mol^{-1} (**14**) and 9 kJ mol^{-1} (**14-Ge**), respectively, rationalizing the simple ^{1}H NMR spectrum of **14** and **14-Ge** (*Figure 2.77*).

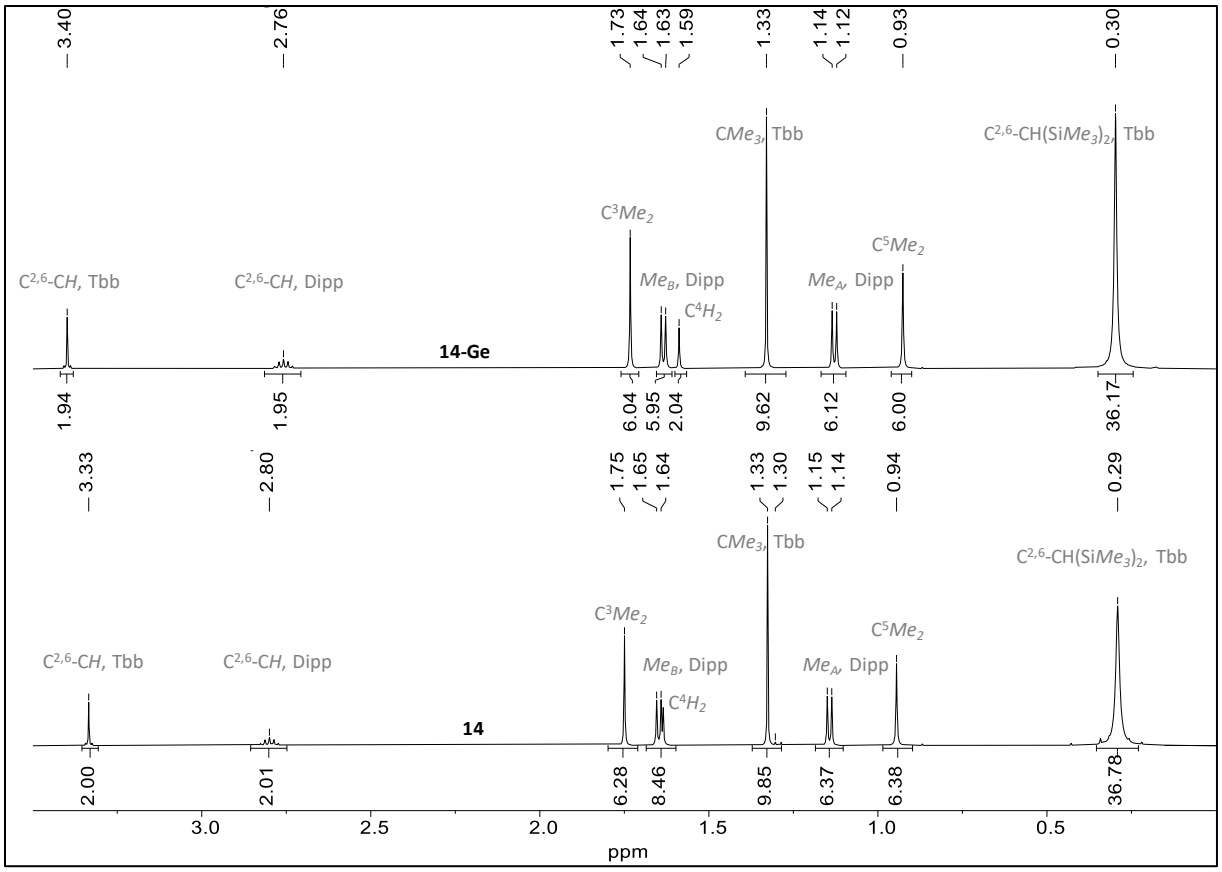

Figure 2.77. Excerpt of the ^{1}H-NMR spectra (500.14 MHz) of pure samples of **14** (bottom) and **14-Ge** (top) in (D_6)benzene at 298 K.

The ^{29}Si{^{1}H} NMR spectrum of **14** in (D_6)benzene displays resonances at 2.44 (4x*Si*Me$_3$), 73.1 ppm (*Si*(caac^{Me})) and 96.2 ppm (*Si*(Br)Tbb). These signals were assigned by ^{1}H, ^{29}Si correlation spectroscopy. The chemical shift of the threefold coordinated Si atom (δ(Si1) = 96.2 ppm) is comparable to that of (*E*)-Tbb(Br)Si=Si(Br)Tbb (84.12 ppm in (D_6)benzene)[25] and that of the threefold coordinated Si atom in **14-NHC** (86.0 ppm).[118] The ^{29}Si NMR resonance for the two coordinate Si atom in **14** (δ(Si2) = 73.1 ppm) is significantly downfield shifted compared to **14-NHC** (34.6 ppm)[118] but appears at much higher field when compared to Si$_2$(caac^{Me})$_2$ (253.3 ppm in (D_6)benzene).[115] The ^{29}Si{^{1}H} NMR spectrum of **14-Ge** in (D_6)benzene, similarly, displays resonances at 2.3 (4x*Si*Me$_3$) and 120.4 ppm (*Si*(Br)Tbb).

The chemical shift of the threefold coordinated Si atom in **14-Ge** (δ(Si1) = 120.4 ppm) is downfield shifted compared to **14** (96.2 ppm) and **14-NHC** (86.0 ppm). In terms of their ^{29}Si{^{1}H}-resonances vinylidenes **14** and **14-Ge** appear more upfield shifted compared to the NHC stabilized systems (*Table 2.33*).

The $^{13}C^{CAAC}$ and $^{15}N^{CAAC}$ resonances of **14** and **14-Ge**, which were assigned by NMR correlation spectroscopy, gave a better insight into the nature of the tetrel-carbene bond: The $^{13}C^{CAAC}$ resonances in **14** (241.4 ppm) and **14-Ge** (255.4 ppm) are only slightly downfield shifted when compared to the dibromotetrylenes $SiBr_2(caac^{Me})$ (**1**) (231.2 ppm) and $GeBr_2(caac^{Me})$ (**1-Ge**) (241.6 ppm).

In contrast, the $^{15}N^{CAAC}$ resonances in **14** (197.4 ppm) and **14-Ge** (205.5 ppm) are remarkably upfield shifted compared to **1** (231.3 ppm) and **1-Ge** (234.2 ppm). These findings suggest a significant decrease of the π-character of the N–C^{carb} bond, which consequently leads to an increase of the π-character of the tetrel-carbene bond in **14** and **14-Ge**, which is in line with the tetrel-carbene bond shortening and N–C^{carb} elongation observed in the solid state structures. This observation is in line with the ^{15}N NMR scale reported by Roesky et al.:[108] The $^{15}N^{CAAC}$ resonances in **14** (197.4 ppm) and **14-Ge** (205.5 ppm) lie in the range of 210 – 180 ppm, which is indicative for a strong $C^{carb} \rightarrow E$ (E = Si, Ge) σ–donation, accompanied by a weak $E \rightarrow C^{carb}$ π–backdonation in **14** and **14-Ge**, respectively.

Table 2.33. NMR spectroscopic features of $caac^{Me}$-stabilized disilavinylidene **14** and silagermenylidene **14-Ge**, compared to their respective starting matierials and NHC-stabilized tetrelvinylidenes. Chemical shifts are given in (D_6)benzene at 298 K, if not mentioned otherwise in the legend.

Comp	$\delta(^{29}Si^{carb})$[a] / ppm	$\delta(^{29}Si^{R2/R3})$[b] / ppm	$\delta(^{13}C^{carb})$ / ppm	$\delta(^{15}N)$[c] / ppm	Ref.
$SiBr_2(caac^{Me})$ **1**	14.35[a]	–	231.2[f]	231.3[f]	
$GeBr_2(caac^{Me})$ 1-**Ge**	–	–	241.6	234.2	
$SiBr\{SiBr_2(Tbb)\}(caac^{Me})$ (**13**)	–1.9	–10.6	217.4	195.2[g]	*this*
$GeBr\{SiBr_2(Tbb)\}(caac^{Me})$ (**13-Ge**)	–	10.3	244.7	236.9	*work*
$(caac^{Me})Si{=}SiBr(Tbb)$ (**14**)	73.1	96.2	241.4	197.4	
$(caac^{Me})Ge{=}SiBr(Tbb)$ (**14-Ge**)	–	120.4	255.4	205.5	
$SiBr\{SiBr_2(Tbb)\}(SIDipp)$(**13-NHC**)	–1.9	–11.3	190.9	–	[118]
$(SIDipp)Si{=}SiBr(Tbb)$ (**14-NHC**)	34.6	86.0	204.6	133.8	[118]
$(I\textit{t}Bu)Si{=}Si(R_1)_2$ (**II-49**) [d]	129.4	221.8	158.2	–	[277]
$(I\textit{i}Pr_2Me_2)Ge{=}Si(R_2)_2$ (**II-44**)[e]	–	158.9	177.9	–	[247]
$(I\textit{i}Pr_2Me_2)Ge{=}Si(R_2)(SiCl(R_2)_2)$[e] (**II-45**)	–	162.5	178.5	–	[248]

[a]: ^{29}Si resonance of the CAAC/NHC carbene coordinated silicon atom. [b]: ^{29}Si NMR resonance of the three-coordinated or four-coordinated silicon atom bearing the sterically demanding Tbb, $(R_1)_2$, $(R_2)_2$ substituents. [c]: ^{15}N NMR resonance of the nitrogen atom(s) in the CAAC (NHC) carbene ring referenced against $NH_3(l)$. [d]: $(R_1)_2 = [C(Ar)_2\text{-}(CH_2)_2\text{-}C(Ar)_2]$ (Ar = C_6H_2-3,5-*t*Bu_2-4-OMe). [e]: R_2 = Trip= C_6H_2-2,4,6-*i*Pr_3. [f]: Measured in (D_8)THF, 243 K. [g]: Measured in (D_8)toluene, 243 K.

2.6.2.3 Electronic structure of (caac^{Me})E=SiBr(Tbb) E = Si (14), Ge (14-Ge)

The electronic structure of the CAAC-stabilized disilavinylidene **14** and silagermenylidene **14-Ge** was investigated by quantum chemical calculations and compared with that of the NHC-stabilized disilavinylidene (SIDipp)Si=SiBr(Tbb) (**14-NHC**).[118] The calculations were performed at the B97-D3(BJ)-ATM/def2-TZVP level of theory by Leonard R. Maurer. More details on the computional calculations are given in *chapter 5.11*. The structural parameters of the calculated structures in the gas phase do compare well to the structures derived from single-crystal X-ray diffraction of **14**, **14-Ge** (*Table 5.82*) and **14-NHC** (*Table 5.83*).

Natural bond orbital analysis of the wave function of **14**$_{calc}$, **14-Ge**$_{calc}$ and **14-NHC**$_{calc}$ led to a leading natural Lewis structure (NLS) with localized bond pair NBOs for the Si–C^{carb}, Si–Si and Si–C^{Tbb} σ-bonds, one π(Si–Si) bond and lone pair at the carbene stabilized silicon center. In case of the NHC-stabilized disilavinylidene **14-NHC** all σ-bonds and the π(Si–Si) bond feature a high Lewis occupancy above 1.83 e^- (*Table 2.34)*.

CAAC-stabilized ditetrelavinylidenes **14**$_{calc}$, **14-Ge**$_{calc}$ in sharp contrast feature a much lower Lewis occupancy for the Si–E (E= Si, Ge) π-bond (1.63 e^- (**14**$_{calc}$), 1.64 e^- (**14-Ge**$_{calc}$), suggesting significant amount of delocalization of the π–electrons over the C^{carb}–Si–Si moiety. In addition, the NRT bond orders show considerable amounts of double bond character in the Si–C^{carb} bond in **14** (1.5) and **14-Ge** (1.3) in comparison to **14-NHC** (1.1), which features a Si–C^{carb} single bond. This trend is in line with the experimentally observed decreased Si–C^{carb} bond lengths of **14** and **14-Ge** in comparison to **14-NHC**. Interestingly, the Lewis occupancy of the electron pair at the silicon center in **14** (1.69 e^-) is slightly lower than that of **14-NHC** (1.77 e^-), whereas the occupancy of the elenctron pair at the germanium center in **14-Ge** (1.76 e^-) is comparable to that of **14-NHC** (1.77 e^-). The remaining electron density can be found in the π*(N–C^{carb}) NBO (0.50 e^- (**14**), 0.45 e^- (**14-Ge**)), suggesting an increased delocalization of the electron pair of the tetrel atom in **14** in comparison to **14-Ge**.

The dominant NRT resonance structures of **14** and **14-Ge** give a much clearer picture of the nature of their electronic structure (*Figure 2.78*). In fact, **14** can be rather described as a hybrid of a disilavinylidene (47 %) and a disilaallene (31 %), mostly due to the delocalization of the electron pair at the silicon center to the Si–C^{carb} π-bond. Only a minor part (9 %) can be attributed to the delocalization of the Si–Si π-bond in the formation of a silylium-silenylidene resonance structure. Whereas **14-Ge** can be best rationalized as a hybrid of silagermenylidene (43 %) and a silagermabutadiene (26 %) type of compound, due to the delocalization of the Si–Ge π-bond with a minor contribution of a silagermynium bromide structure (20 %). Remarkably, no such resonance fromulas are found in case of the NHC-stabilized disilavinylidene **14-NHC**, highlighting the remarkable difference of the electronic structures of these compounds.

Table 2.34. Selected results of the natural bond orbital (NBO), natural resonance theory (NRT) and natural population (NPA) analyses of **14-NHC**, **14** and **14-Ge**. The graphical inlets depict the Natural Lewis structure of the NBO analysis and its NRT contribution.

NBO A–B	occ.[a]	NHO (A,B)[b] hyb. (pol. in %)	WBI[c] A–B	NRT-BO[d] tot/cov/ion	atom/ group	q/Σq[e]
(SIDipp)Si=SiBr(Tbb) (**14-NHC**)						
LP(Si)	1.77	$sp^{0.3}$			Si^{NHC}	0.00
σ(Si–C^{carb})	1.93	$sp^{7.7}$(22), $sp^{1.3}$(78)	0.8	1.1/0.6/0.5	Si^{Tbb}	+0.61
σ(Si–Si')	1.91	$sp^{8.7}$(41), $sp^{1.2}$(59)	1.8	1.9/1.7/1.2	Br	–0.36
π(Si–Si')	1.83	p(50), p(50)			SIdipp	+0.01
σ(Si'–Br)	1.97	$sp^{4.8}$(26), $sp^{3.9}$(74)	0.8	0.8/0.4/0.4	Tbb	–0.26
σ(Si'–C^{Tbb})	1.94	$sp^{2.3}$(28), $sp^{2.3}$(72)	0.8	1.0/0.6/0.4	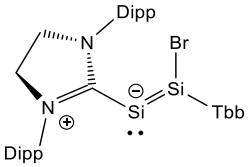	
σ*(Si'–Br)	0.16	$sp^{4.8}$(74), $sp^{3.9}$(26)				
π*(Si–Si')	0.09	p(50), p(50)				
($caac^{Me}$)Si=SiBr(Tbb) (**14**)						
LP(Si)	1.69	$sp^{0.4}$			Si^{CAAC}	+0.14
σ(Si–C^{carb})	1.94	$sp^{5.8}$(23), $sp^{1.4}$ (77)	1.1	1.5/0.9/0.6	Si^{Tbb}	+0.67
σ(Si–Si')	1.92	$sp^{8.9}$ (39), $sp^{0.9}$ (62)	1.6	1.7/1.5/0.2	Br	–0.36
π(Si–Si')	1.63	p (52), p (48)			$caac^{Me}$	–0.04
σ(Si'–Br)	1.97	$sp^{5.0}$ (25), $sp^{3.9}$ (75)	0.8	1.1/0.5/0.6	Tbb	–0.41
σ(Si'–C^{Tbb})	1.94	$sp^{2.4}$ (28), $sp^{2.5}$ (72)	0.8	0.9/0.5/0.4	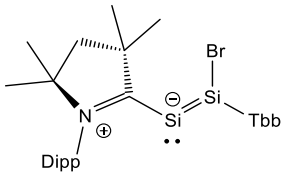	
π*(N–C^{carb})	0.50	p (27), p (73)			(47 %)	
($caac^{Me}$)Ge=SiBr(Tbb) (**14-Ge**)						
LP(Ge)	1.76	$sp^{0.24}$			Ge	+0.06
σ(Ge–C^{carb})	1.93	$sp^{8.1}$ (24), $sp^{1.5}$ (76)	1.0	1.3/0.8/0.5	Si^{Tbb}	+0.67
σ(Ge–Si)	1.91	p (38), $sp^{0.9}$ (62)	1.6	1.8/1.5/0.3	Br	–0.36
π(Ge–Si)	1.64	p (52), p (48)			$caac^{Me}$	+0.05
σ(Si–Br)	1.97	$sp^{4.8}$ (25), $sp^{3.9}$ (75)	0.8	1.0/0.4/0.6	Tbb	–0.42
σ(Si–C^{Tbb})	1.94	$sp^{2.4}$ (28), $sp^{2.5}$ (72)	0.8	0.9/0.5/0.4	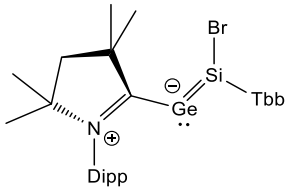	
σ*(Si–Br)	0.16	$sp^{4.8}$ (75), $sp^{3.9}$ (25)				
π*(N–C^{carb})	0.45	p (26), p (74)			(43 %)	

[a]: occ. = occupancy in e^-; [b]: NHO = Natural Hybrid Orbital, pol. (polarization) = $(C_i)^2 \cdot 100\%$, where C_i = coefficient of NHO; [c]: Wiberg bond index; [d]: total, covalent and ionic NRT bond order;
[e]: q = NPA charge of the atom, ∑q = total NPA charge of the group.

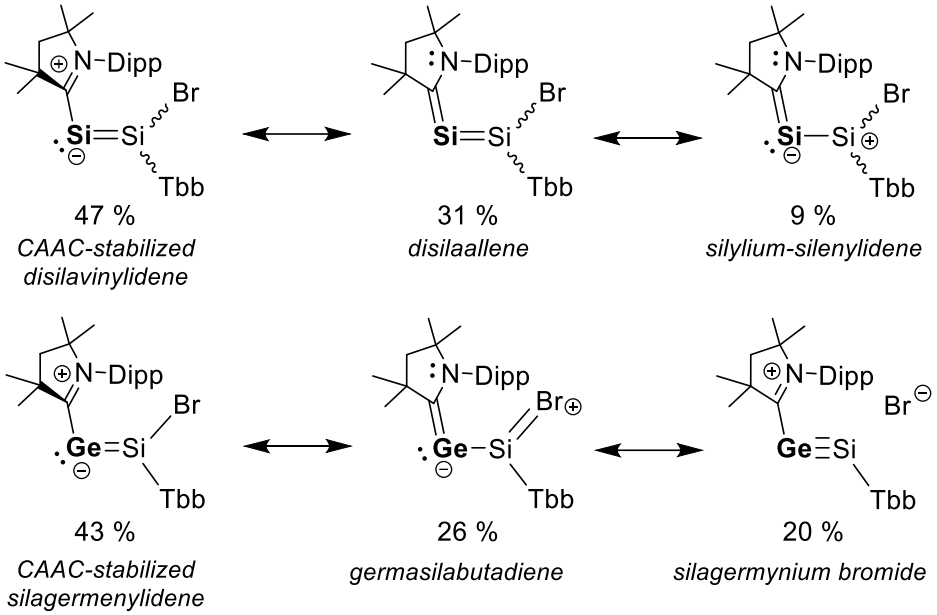

Figure 2.78. Most dominant NRT resonance structures for **14** and **14-Ge;** a wavy bond means that it can be anything and is not constrained for this bond motif search. All contributions above 1.0 % are considered.

The NBO results are reflected in the frontier orbitals of **14** and **14-Ge** (*Figure 2.80*). The HOMO-1 contains mainly the lone pair at the terminal Si atom, the HOMO corresponds to the 3c-2e $\pi_{oop}(C^{carb}–E–Si)$-bond (E = Si, Ge) with the major contribution of the Si=E bond and the LUMO corresponds to the empty p-orbital at the three-coordinated silicon center and some antibonding $\pi_{oop}(E–C^{carb})$ (E = Si, Ge) contribution.

The HOMO in **14** and **14-Ge** clearly differs from that of the NHC-stabilized disilavinylidene **14-NHC**, which in sharp contrast features a localized Si–Si π-bond (*Figure 2.79*).

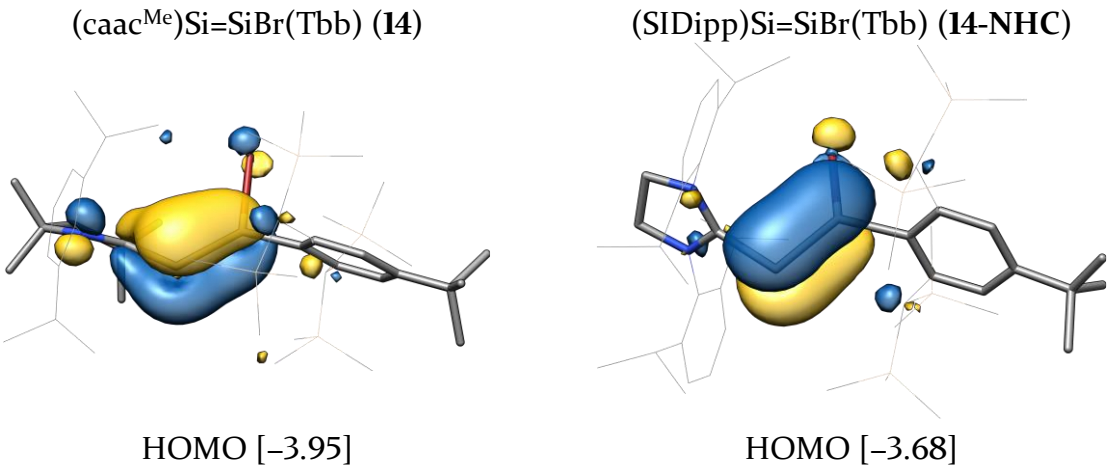

Figure 2.79. Selected Kohn-Sham molecular orbitals of disilavinylidenes **14** (left) and **14-NHC** (right) and their orbital energies in eV. Hydrogen atoms are omitted for clarity. The isosurface value is set to 0.04 $e^{1/2}$ $Bohr^{-3/2}$.

(caac^{Me})Si=SiBr(Tbb) (**14**)

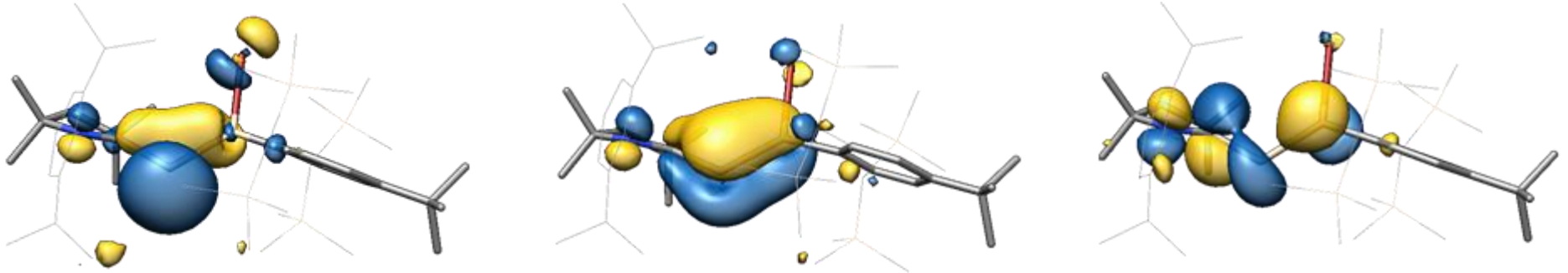

HOMO–1 [–4.70] HOMO [–3.95] LUMO [–2.29]

(caac^{Me})Ge=SiBr(Tbb) (**14-Ge**)

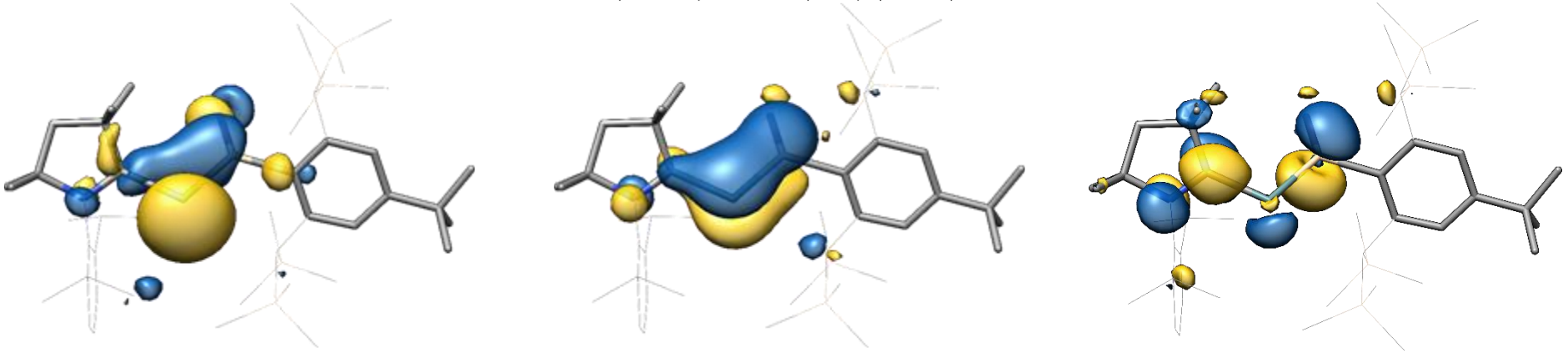

HOMO–1 [–4.82] HOMO [–3.83] LUMO [–2.24]

Figure 2.80. Selected Kohn-Sham molecular orbitals of **14** and **14-Ge** and their orbital energies in eV. Hydrogen atoms are omitted for clarity. The isosurface value is set to 0.04 $e^{1/2}$·$Bohr^{-3/2}$.

2.6.2.4 Comparative Studies of the UV/Vis spectra of 14, 14-Ge and 14-NHC

The electronic structure of the caac^{Me}-stabilized disilavinylidne **14**, silagermenylidene **14-Ge** and NHC-stabilized disilavinylidene **14-NHC** was also investigated by UV/Vis spectroscopy. Already strong diluted solutions of **14** and **14-Ge** in *n*-hexane reveal a dark green and dark blue color, respectively. In contrast, the NHC-stabilized disilavinylidene **14-NHC** features a dark red colored solution (*Figure 2.81*, bottom right).

The UV/Vis spectrum of **14** and **14-Ge** reveal an additional absorption band at 588 nm and 597 nm, respectively, in contrast to the NHC-stabilized disilavinylidene **14-NHC**, where the first absorption band appears at 515 nm (*Figure 2.81*). Simulation of the UV/Vis spectra by quantum chemical calculations at the RI-B97-D3/def2-TZVP(CPCM/hexane) level of theory performed by Dr. Gregor Schnakenburg reveal that the additional absorption bands in **14** (λ_1(exp) = 588 nm, λ_1(calc) = 557.9 nm) and **14-Ge** (λ_1(exp) = 597 nm, λ_1(calc) = 558.0 nm) can be mostly attributeted to the excitation of the 3c-2e π_{oop}(C^{carb}–E–Si)-bond (E = Si, Ge) in the HOMO to the respective anti-bonding LUMO (**14**: 62.6 %, **14-Ge**: 61.6 %), as well by a minor excitation of the lone pair at the dicoordinated tetrel center (HOMO–1) to the corresponding LUMO (**14**: 16.0 %, **14-Ge**: 11.8%) (*Table 2.35*). In contrast, the first absorption maximum of the disilavinylidene **14-NHC** occurs at much higher energy (λ_1(exp) = 515 nm, λ_1(calc) = 568.8 nm) and can be mostly attributed to the excitation of the localized π(Si–Si) bond in the HOMO in **14-NHC** to the anti-bonding LUMO with 87.1 % contribution (*Table 2.35*). These observations are in line with the calculated small HOMO–LUMO gap in **14** (1.66 eV) and **14-Ge** (1.59 eV), when compared to **14-NHC** (1.93 eV).

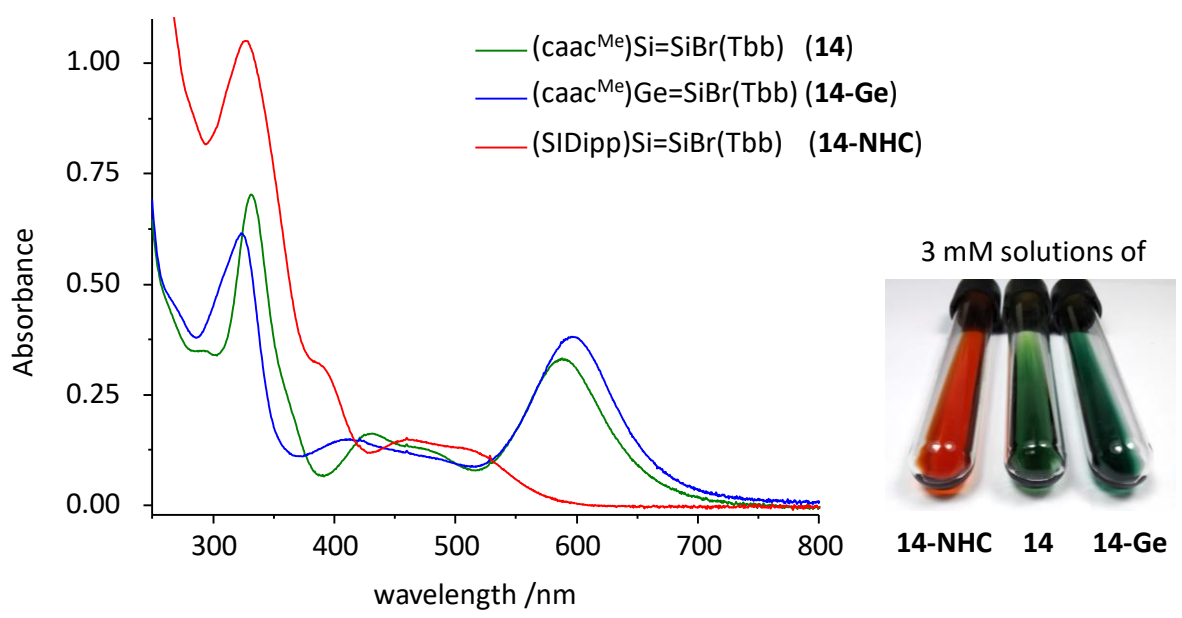

Figure 2.81. UV/Vis spectra of caac^{Me}-stabilized tetrelavinylidenes **14** and **14-Ge** in comparison to the NHC-stabilized disilavinylidene **14-NHC** in *n*-hexane at ambient temperature.

Table 2.35. Experimental and calculated first two absorption maxima of the of the UV/Vis spectra of **14**, **14-Ge** and **14-NHC** in *n*-hexane at ambient temperature. Contributions with less than 5 % are not listed. Calculations were performed at the RI-B97-D3/def2-TZVP(CPCM/hexane) level of theory by Dr. G. Schnakenburg.

λ(exp) /nm	λ(calc) /nm	excitation	contribution /%	Kohn-Sham orbital	energy /eV[a]
		(caac^{Me})Si=SiBr(Tbb) (**14**)			
588	557.9	HOMO → LUMO	62.6	HOMO-1	–4.70
		HOMO–1 → LUMO	16.0	HOMO	–3.95
		HOMO → LUMO+1	9.8	LUMO	–2.29
		HOMO–1 → LUMO+1	8.9	LUMO+1	–1.75
476	508.0	HOMO → LUMO+1	66.1	LUMO+4	–1.11
		HOMO → LUMO	10.1		
		HOMO → LUMO+4	8.1		
		HOMO–1 → LUMO	6.3		
		HOMO–1 → LUMO+1	6.8		
		(caac^{Me})Ge=SiBr(Tbb) (**14-Ge**)			
597	558.0	HOMO → LUMO	61.6	HOMO-1	–4.82
		HOMO → LUMO+1	17.1	HOMO	–3.83
		HOMO–1 → LUMO	11.8	LUMO	–2.24
		HOMO–1 → LUMO+1	5.8	LUMO+1	–1.74
526	516.3	HOMO → LUMO+1	59.6	LUMO+4	–1.10
		HOMO → LUMO	13.7		
		HOMO → LUMO+4	13.3		
		HOMO–1 → LUMO+1	6.0		
		(SIDipp)Si=SiBr(Tbb) (**14-NHC**)			
515	568.8	HOMO → LUMO	87.1	HOMO-1	–4.77
		HOMO → LUMO+1	7.4	HOMO	–3.68
455	515.5	HOMO → LUMO+1	62.0	LUMO	–1.75
		HOMO → LUMO+3	13.8	LUMO+1	–1.56
		HOMO → LUMO+4	12.1	LUMO+3	–1.22

[a]: Orbital energies of the Kohn-Sham orbitals of **14-NHC**, **14** and **14-Ge** in the ground-state calculated at the B97-D3(BJ)-ATM/def2-TZVP level of theory by Leonard R. Maurer.

The RI-B97-D3/def2-TZVP(CPCM/hexane) calculated wavelengths for the absorption maxima (*Table 2.35*), deviate slightly from the experimentally obtained values but lie within the limit of deviation of the used method.

The smaller HOMO–LUMO gap, which results in the first absorption band in **14** (λ_1(exp) = 588 nm, HOMO–LUMO = 1.66 eV) and **14-Ge** (λ_1(exp) = 597 nm, HOMO–LUMO = 1.59 eV) compared to **14-NHC** (λ_1(exp) = 515 nm, HOMO–LUMO = = 1.93 eV) can mostly be attributed the lower lying LUMO in **14** (–2.29 eV)and **14-Ge** (–2.24 eV) with respect to that of **14-NHC** (–1.75 eV).

The second maximum of **14** (λ_2(exp) = 476 nm, λ_2(calc) = 508 nm) and **14-Ge** (λ_2(exp) = 526 nm, λ_2(calc) = 516 nm) can be mostly attributed to the excitation of the HOMO to the corresponding LUMO+1 with contributions of 66.1 % (**14**) and 59.6 % (**14-Ge**), respectively. Similar in disilavinylidene **14-NHC** the second maximum (λ_2(exp) = 455 nm, λ_2(calc) = 515 nm) could be assigned to the excitation of the π(Si–Si) bond in the HOMO to the corresponding LUMO+1 with 62.0 % contribution. Further experimentally observed low-lying maxima could not be assigned to the calculated values, since the simulation leads to many overlapping bands. A summary of the calculated values in relation to the experimental obtained absorption maxima is given in *section 5.11.10*.

Remarkably, the CAAC-stabilized compounds **14** and **14-Ge**, feature significant amount of excitation of the lone pair of the dicoordinated tetrel(0) atom (HOMO-1) in the first two absorption bands of the calculated UV/Vis spectra with contributions of 24.9 % (**14**) and 17.1 % (**14-Ge**) for λ_1(calc) and 13.1 % (**14**) and 6.0 % (**14-Ge**) for λ_2(calc), respectively. Whereas in the parent NHC-compound **14-NHC** no excitation of the HOMO-1 is observed in the first two absorption maxima (*Figure 2.82*). This may be attributed to the signifantly lower lying HOMO in **14** (–3.95 eV)and **14-Ge** (–3.83 eV)with respect to **14-NHC** (–3.68 eV), as well by the lower lying LUMO in **14** (–2.29 eV) and **14-Ge** (–2.24 eV) compared to **14-NHC** (–1.75 eV), which result in smaller energy gaps for the HOMO–1 → LUMO (2.41 eV (**14**), 2.58 eV (**14-Ge**)) and HOMO–1 → LUMO+1 (2.95 eV (**14**), 3.08 eV (**14-Ge**)) transitions compared to that of **14-NHC** (HOMO–1 → LUMO: 3.02 eV; HOMO–1 → LUMO+1: 3.21 eV). In fact, the excitation of the HOMO–1 in **14-NHC** occurs at much higher energy i. e. lower lying maxima (λ(calc) = 402.3 nm, HOMO–1 → LUMO 15.2 %, see *Table 5.87*).

Overall CAAC-stabilized disilavinylidene **14** and silagermenylidene **14-Ge** clearly differ from the NHC-supported disilavinylidene **14-NHC** by a more co-planar orientated caac^{Me} carbene ligands, shortened E–C^{carb} (E = Si, Ge) bond lengths and slightly more pyramidalized SiBr(Tbb) moieties. These small structural changes lead to significant differences in their electronic structures, which is reflected by a delocalization of the Si–Si and Si–Ge π-bond, lower lying LUMOs, smaller HOMO–LUMO gaps and the excitation of the lone pair in the HOMO–1 as well as the 3c-2e π_{oop}(C^{carb}–E–Si)-bond (E = Si, Ge) in the HOMO to their respective antibonding LUMO and LUMO+1 in the first two absorption maxima of their calculated UV/Vis spectra, resulting in their dark green and blue colors, respectively.

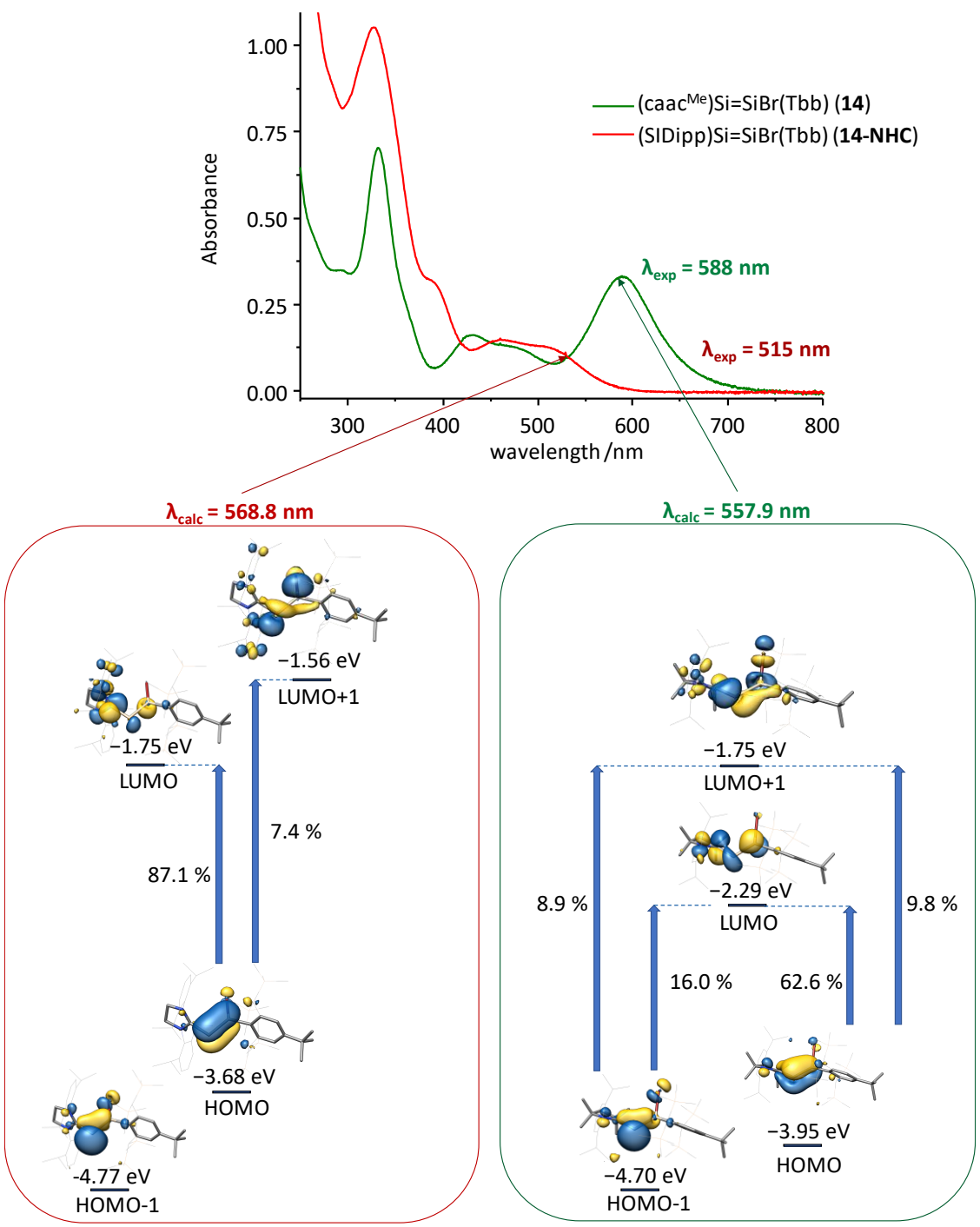

Figure 2.82. UV/Vis spectrum of (caac^{Me})Si=SiBr(Tbb) (**14**) and (SIDipp)Si=SiBr(Tbb) (**14-NHC**) in *n*-hexane at ambient temperature with the assignment of the excitations of the corresponding molecular orbitals for the first absorption bands. In **14** the excitation occurs from HOMO and HOMO–1 to the corresponding LUMO and LUMO+1, whereas in **14-NHC** only the excitation of the HOMO is observed in the first maximum (λ_1).

2.6.3 Reactivity of CAAC-stabilized disilavinylidene (caac^{Me})Si=SiBr(Tbb) (14)

In the following the reactivity of the cyclic (alkyl)(amino)carbene-stabilized disilavinylidene **14** is reported. Since CAACs are much stronger π-acceptors than typical pure σ-donating NHCs, a higher electrophilicity at the silenic silicon center (SiBr(Tbb)) is envisioned in **14** than in **14-NHC**.

Multiple attempts to remove the bromine atom in **14**, in order to yield a cationic disilyne failed. Disilavinylidene did not react with $Na[B\{C_6H_2\text{-}3,5\text{-}(CF_3)_2\}_4]$ or $Li(Et_2O)_{2.5}[B(C_6F_5)_4]$ in fluorobenzene at ambient temperature. Heating of the reaction mixtures to 60 °C, revealed a rather slow but unselective consumption of the disilavinylidene, according to ^{1}H no D NMR spectroscopy of an aliquote in fluorobenzene. Reaction of **14** with 0.5 equiv. $Ag_2B_{12}Cl_{12}$ in fluorobenzene at ambient temperature led to a color change form dark green to red. Monitoring of the reaction mixture by ^{1}H no D NMR spectroscopy of an aliquot in fluorobenzene, revealed the selective formation of a Ag-adduct next to tiny amounts of an unknown impurity. Multiple attempts to crystallize the compound from fluorobenzene, *n*-hexane mixtures and 1,2-diflorobenzene *n*-hexane mixtures, as well as toluene failed.

Addition of precooled 1,2-difluorobenzene to a solid mixture of **14** and $Al(C_6F_5)_3$ at –60 °C led to a color change from dark green to purple. Monitoring of the reaction mixture by ^{1}H no D NMR spectroscopy revealed no change in the ^{1}H NMR resonances of the disilavinylidene. The ^{29}Si{^{1}H} NMR revealed only minor changes, as evidenced by the ^{29}Si resonances of 95.2 (Si(Br)Tbb) and 72.0 ppm ((caac^{Me})Si) in fluorobenzene compared to that of 96.2 (Si(Br)Tbb) and 73.1 ppm ((caac^{Me})Si) in **14**. Similarly,the ^{19}F{^{1}H}-NMR of an aliqoute of the reaction mixture in (D_6)benzene revealed only small changes, as evidenced by the ^{19}F resonances of –121.1 (3 x $C^{2,6}$-*F*), –153.7 (3 x C^4-F) and –162.3 ppm (3 x $C^{3,5}$-F) when compared to that of –124.9 (3 x $C^{2,6}$-*F*), –146.7 (3 x C^4-F) and –157.6 ppm (3 x $C^{3,5}$-F) in the starting material.[281,282] These findings suggest, that the disilavinylidene features a weak coordination, presumably via the lone pair of the two-coordinated silicon center to the alane.

Reaction of **14** with one equivalent of $LiNMe_2$ or LiMes in THF at ambient temperature, resulted in a fast color change from dark green to yellow brown. Monitoring of the reaction progress by ^{1}H NMR spectroscopy in (D_6)benzene revealed a rather unselective conversion of the disilavinylidene.

2.6.3.1 Reaction of 14 with Li(C≡C–TMS)

Addition of a slightly yellow solution of Li(C≡C–TMS) in THF to a dark green solution of disilavinylidene **14** at ambient temperature resulted in a color change from dark green to tuirquiose-green. Monitoring of the reaction mixture by ^{1}H NMR spectroscopy in (D_6)benzene revealed the selective formation of (caac^{Me})Si=Si(C_2–TMS)(Tbb) (**14-C_2TMS**). After work up, the compound could be isolated with a purity of ca. 95 %, according to ^{1}H NMR spectroscopy in (D_6)benzene. Due to the high liphophilicity of the compound, it could not be crystallized from *n*-hexane or diethylether. In highly polar solvents such as $CHCl_3$ and CH_3CN the compound decomposed very quickly to a yellow brown solution. Nevertheless, the compound could be characterized by NMR-correlation spectroscopy and ATR-IR spectroscopy. The isolated dark green solid is highly air sensitive and quickly decolorizes upon contact with air.

The stretching vibration of the C≡C bond in **14-C_2TMS** ($\tilde{\nu}$ = 2059 (vw) cm^{-1}) is shifted to higher wavenumbers compared to the starting matieral Li(C≡C–TMS) ($\tilde{\nu}$ = 1986 (vw) cm^{-1}) and compares well to that of (caac^{Me})Si(C_2-TMS)(GeAr^{Mes}) (**12**) ($\tilde{\nu}$ = 2063 (w) cm^{-1}).

Similar to **14**, the ^{1}H NMR spectrum of **14-C_2TMS** in (D_6)benzene at ambient temperature displays an averaged C_S-symmetry. The ^{29}Si{^{1}H}-NMR spectrum displays displays four signals: two resonances at –20.7 (C_2TMS) and 2.2 (4 x TMS of Tbb) ppm for the TMS-groups, as well as two resonances at 83.9 ppm (*Si*(C_2-TMS)Tbb) and 110.6 ppm (caac^{Me})*Si*) for the two doubly bonded silicon-centers, respectively.

The ^{29}Si{^{1}H} resonance of two-coordinated silicon center in **14-C_2TMS** (110.6 ppm) is significantly downfield shifted compared to that of disilavinylidene **14** (73.1 ppm). The silenic silicon-center in **14-C_2TMS** (83.9 ppm), on the other hand, is significantly upfield shifted compared to **14** (96.2 ppm) and downfield shifted, when compared to the alkynyl substituted disilene $Si_2(C_2TMS)_2(Bbt)_2$ (Bbt = C_6H_2-2,4,6-Dsi_3, Dsi = $CH(SiMe_3)_2$) (δ(^{29}Si) = 44.6 ppm (*Si*(C_2-TMS)Bbt).[226]

The similarities of the $^{13}C^{CAAC}$ and $^{15}N^{CAAC}$ resonances in **14-C_2TMS** (243.9 ppm, 201.3 ppm) compared to **14** (241.1 ppm, 197.4 ppm) suggest, that the nature of the Si–C^{carb} bond and thus the overall electronic structure of the disilavinylidene did not change significantly upon substitution with Li(C≡C–TMS).

2.6.3.2 Reaction of 14 with LiMe

Addition of 1 equiv. of a LiMe-solution in *n*-pentane/Et_2O (1:1) to a dark green solution of ($caac^{Me}$)Si=SiBr(Tbb) (**14**) in *n*-pentane at –30 °C, resulted in a color change to yellow-green. Monitoring of the reaction mixture by ^1H NMR spectroscopy in (D_6)benzene after warming up to ambient temperature revealed the selective formation of ($caac^{Me}$)Si=Si(Me)Tbb (**14-Me**) alongside with tiny amounts of the starting material **14** and the follow up product **15** (*Scheme 2.22*). After work up, **14-Me** could be obtained as a dark green microcrystalline solid 39 % yield in analytically pure form. The compound quickly decolorizes upon contact with air and is well soluble in benzene, *n*-pentane and diethylether.

Remarkably, isolated compound **14-Me** reacted in *n*-pentane with another equivalent of LiMe in *n*-pentane/Et_2O (1:1) at –30 °. Upon warming up to ambient temperature the color changed from green to dark red. Monitoring of the reaction mixture by ^1H NMR spectroscopy in (D_6)benzene revealed the selective formation of lithium-silenide **15**. After work up, **15** could be isolated as a red powder with 17 % yield in analytically pure form. The compound is highly pyrophoric and is well soluble in *n*-pentane, Et_2O and benzene.

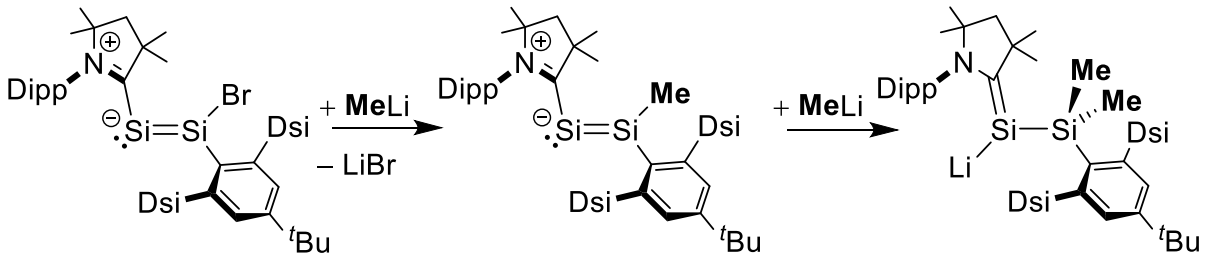

Scheme 2.22. Reaction of $caac^{Me}$-stabilized disilavinylidene **14** with MeLi.

Green single crystals of **14-Me** and clear red blocks of **15·(Et_2O)** were obtained from saturated *n*-pentane solutions at –30 °C, respectively. The molecular structure of **14-Me** (*Figure 2.83* left), compares well to that of the starting material **14** (*Table 2.36*). As in **14**, also the methyl-substituent in **14-Me** is significantly bent with respect to the planar core consisting of the atoms C^{Ar}, Si1, Si2, C^{carb} which can be evidenced by the torsion angles τ(C^{carb}–Si2–Si1–Br) = –32.1(2)°(**14**) and τ(C^{carb}–Si2–Si1–Me) = –25.1(2)°(**14-Me**), respectively. In contrast to literature known NHC-stabilized disilavinylidenes the $caac^{Me}$ carbene plane in **14** (φ_{CAAC} = 57.8(2) ° [51.9(3) °]) and **14-Me** (φ_{CAAC} = 57.2(1) °) is orientated more towards the Si=Si bond, suggesting some delocatization of the silicon-silicon π-bond over the C^{carb}–Si2–Si1 moiety in **14** and **14-Me**.

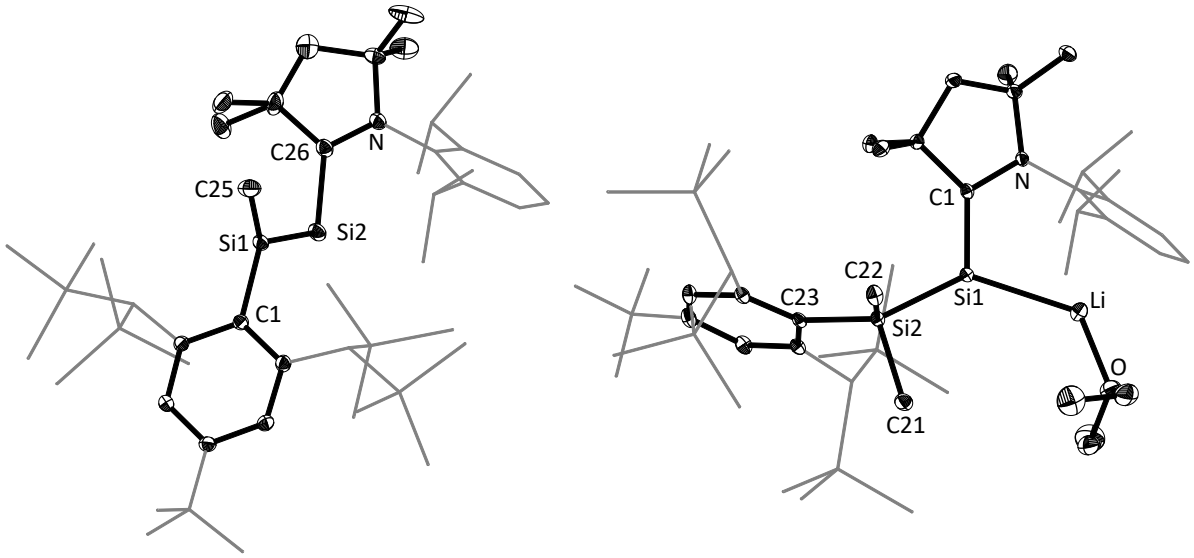

Figure 2.83. Diamond plot of the molecular structure of **14-Me** (left) and **15·(Et₂O)** (right), thermal ellipsoids are set at 30 % probability, and hydrogen atoms were omitted. In the depicted structures the Dipp substituent of the caac^{Me} ligand and the disyl groups (CH(SiMe$_3$)$_2$) and *t*Bu group of the Tbb substituent are presented in the wire-frame for the sake of clarity. Selected bond lengths [Å], bond angles [°] and torsion angles [°]:
14-Me: Si1–Si2 2.1918(8), Si1–C1 1.895(2), Si1–C25 1.902(3), Si2–C26 1.880(2), N–C26 1.336(3), C1–Si1–Si2 117.07(7), C1–Si1–C25 110.31(10), C25–Si1–Si2 129.19(8), C26–Si2–Si1 104.58(7), C1–Si1–Si2–C26 178.1(1), C25–Si1–Si2–C26 –25.1(2), N–C26–Si2–Si1 131.0(2).
15·(Et₂O): Si1–Si2 2.3646(5), Si1–C1 1.8068(14), Si1–Li 2.547(3), Si2–C21 1.9015(16), Si2–C22 1.9089(14), Si2–C23 1.9434(14), N–C1 1.4184(16), Si2–Si1–Li 128.91(6), C1–Si1–Si2 115.25(5), C1–Si1–Li 108.27(7), C23–Si2–Si1–C1 73.2(1), N–C1–Si1–Si2 168.6(1).

Table 2.36. Structural properties of **14** and **14-Me** in comparison to literature known NHC stabilized disilavinylidenes and silagermenylidenes.

Comp.	E–E / Å	E–C^{carb} / Å	C^{carb}-E-E / (deg)	φ_{carb} [a] / (deg)	Ref.
(caac^{Me})Si=Si(Br)(Tbb) (**14**)	2.194(2)	1.878(5)	105.5(1)	57.8(2)	
	2.181(2)	1.868(6)	105.6(2)	51.9(3)	*this*
(caac^{Me})Si=Si(Me)(Tbb) (**14-Me**)	2.192(1)	1.880(2)	104.6(1)	57.2(1)	*work*
(SIDipp)Si=SiBr(Tbb) (**14-NHC**)	2.167(2)	1.937(4)	97.6(1)	94.8(2)	[118]
(ItBu)Si=Si(R$_1$)$_2$ (**II-49**) [b]	2.179(1)	1.962(2)	105.4(1)	89.6(1)	[277]
(IPr$_2$Me$_2$)Ge=Si(R$_2$)$_2$ (**II-44**)[c]	2.252(1)	2.047(2)	98.90(5)	63.8(1)	[247]
(IPr$_2$Me$_2$)Ge=Si(R$_2$)(SiCl(R$_2$)$_2$)[c] (**II-45**)	2.276(1)	2.061(4)	101.9(1)	61.1(2)	[248]

[a]: φ_{carb} the angle between the least-squares plane of the CAAC/NHC carbene five-membered ring and the plane defined by the C^{CAAC}/C^{NHC} atom and the doubly-bonded tetrel atoms.
[b]: (R$_1$)$_2$ = [C(Ar)$_2$-(CH$_2$)$_2$-C(Ar)$_2$] (Ar = C$_6$H$_2$-3,5-*t*Bu$_2$-4-OMe).
[c]: R$_2$ = Trip = C$_6$H$_2$-2,4,6-*i*Pr$_3$.

In comparison to **14-Me**, compound **15** (*Figure 2.83* right) features a completly different structure. The molecular structure of **15** compares well to the potassium-silenide SiK(SiTMS$_3$)(caac^{Me}) (**4-Si**) (see *section 2.5.2*) and literature known lithium-silenides (*Table 2.37*). Compound **15** features C_S-symmetry and a trigonal planar coordinated silicon(0) center ($\Sigma°$Sil = 352.4°). The Si–C^{carb} bond length in **15** (1.807(2) Å) is significantly elongated when compared to lithium-silenides (1.762(3) Å – 1.778(3) Å)[125,126] but compares rather well to the potassium-silenides synthesized in this work. The lithium ion is covalently bound to the Si-center in **15** (2.547(3) Å) and further stabilized by π-interaction of the aromatic Dipp substituent (d(C$_{ring}$-Li) = 2.226(3) Å) and coordination of a diethylether molecule. In contrast, to literature known lithium-silenides (2.613(6) Å – 2.722(3) Å)[125,126] and lithium-silanides (2.59 – 2.64 Å)[283], the Si–Li bond length in **15** (2.547(3) Å) is significantly shorter, suggesting an even stronger coordination of the alkali-metal ion to the low valent silicon center.

Table 2.37. Selected structural parameters of **15** in comparison to structurally characterized silenides **4-Si** and **10-C$_2$TMS** in this work and literature known lithium- and potassium-silenides.

Comp.	Si–C^{carb} / Å	N–C^{carb} / Å	Σ∢(Si) / (deg)	Σ∢(C$^{carb/sp2}$) / (deg)	τ[a] / (deg)	Ref.
SiK(SiTMS$_3$)(caac^{Me})(**4-Si**)	1.813(9)	1.42(1)	352.8	360.0	8.1	
SiK(C$_2$TMS)(caac^{Me}) (**10-C$_2$TMS**)	1.790(3)	1.408(4)	357.1	360.0	3.7	*this work*
SiLi{SiMe$_2$(Tbb)}(caac^{Me}) (**15**)	1.807(2)	1.418(2)	352.4	359.9	2.9(1)	
SiK(Trip)(caac^{Me}) (**II-37**)	1.793(2)	1.424(3)	359.7	359.9	1.8	[124]
Li(R$_A$)Si=C(Ad)(R$_A$) (**II-34**)[b]	1.773(3)	–	359.7	359.9	13.1	[125]
Li(R$_B$)Si=C(Ad)(R$_A$) (**II-35**)[b]	1.778(3)	–	359.6	359.9	10.2	[125]
(THF)$_2$·Li(R$_A$)Si=C(R$_B$)(R$_A$) [b] (**II-36**)	1.762(3)	–	359.8	359.8	4.4	[126]
Li(THF)$_4$ [(R$_A$)Si=C(R$_B$)(R$_A$)][b] (**II-36**)	1.766(3)	–	–	–	–	[126]

[a]: The twist angle (τ) is defined as the angle between the silicon and C^{CAAC} (C^{sp2}) coordination planes defined by the atoms M–Si–R (M = K, Li; R = Si, C) and C2–C^{CAAC}–N (R–C^{sp2}–Si; R = C, Si), respectively.
[b]: R$_A$ = Si(*t*Bu)$_2$Me, R$_B$ = Si(*t*Bu)Me$_2$.

Similar to **14**, the ^{1}H NMR spectrum of **14-Me** in (D$_6$)benzene at ambient temperature displays an averaged C_S-symmetry, suggesting a fast rotation of the caac^{Me} carbene and Tbb substituent at the NMR time scale. The ^{29}Si{^{1}H}-NMR spectrum displays three signals: one resonance at 1.9 ppm for the TMS-groups of the Tbb-substituent and two resonances at 99.5 (*Si*(caac^{Me})) and 140.8 ppm (*Si*Me(Tbb)) for the double bonded silicon-centers, respectively.

The $^{29}Si\{^{1}H\}$ resonance of the two-coordinated silicon center in **14-Me** (99.5 ppm) is significantly downfield shifted compared to that of disilavinylidene **14** (73.1 ppm). Similarly, the silenic silicon-center in **14-Me** (140.8 ppm) is significantly downfield shifted compared to **14** (96.2 ppm).

The similar $^{13}C^{CAAC}$ and $^{15}N^{CAAC}$ chemical shifts in **14-Me** (241.5 ppm, 190.1 ppm) compared to **14** (241.1 ppm, 197.4 ppm) suggest a similar electronic structure of **14** and its substitution product **14-Me**. These findinds are in line with the observed bonding paremeters of **14** ($d(Si–C^{carb})$ = 1.878(5) Å, $d(N–C^{carb})$ = 1.338(6) Å) and **14-Me** ($d(Si–C^{carb})$ = 1.880(2) Å, $d(N–C^{carb})$ = 1.336(3) Å). Thus compound **14-Me** can be described as a $caac^{Me}$-stabilized disilavinylidene.

^{1}H, $^{13}C\{^{1}H\}$ and $^{29}Si\{^{1}H\}$ NMR spectra of **15**, reflect the observed C_S-symmetry in the solid state. The $^{29}Si\{^{1}H\}$ spectrum displays a quadruplet at 44.6 ppm ($^{1}J(^{29}Si,^{7}Li)$ = 65 Hz) for the silenic silicon-center, a singlet 2.1 ppm for the TMS-groups of the Tbb substituent and a triplet at –20.8 ppm ($^{2}J(^{29}Si,^{7}Li)$ = 4 Hz) for the $SiMe_2$(Tbb) moiety. The $^{29}Si\{^{1}H\}$ resonance of the silenic silicon center (44.6 ppm) is drastically upfield shifted when compared to **14-Me** (96.5 ppm) and literature known lithium-silenides (243.9 – 405.5 ppm).[125,126] The $^{13}C^{CAAC}$ and $^{15}N^{CAAC}$ signals of **15** (213.0 ppm, 117.6 ppm) are drastically upfield shifted when compared to **14-Me**, revealing the considerable increase of the $Si=C^{carb}$ double bond character. They appear at similar positions to those of charactized potassium-silenides described in this work (*Table 2.38*).

Table 2.38. NMR spectroscopic features of **14-Me** and **15** in comparison to related literature known compounds, given in (D_6)benzene at 298 K.

Comp	$\delta(^{29}Si^{carb})$[a] / ppm	$\delta(^{29}Si^{R2/R3})$[b] / ppm	$\delta(^{13}C^{carb})$ / ppm	$\delta(^{15}N)$[c] / ppm	Ref.
($caac^{Me}$)Si=SiBr(Tbb) (**14**)	73.1	96.2	241.4	197.4	
($caac^{Me}$)Si=Si(C_2TMS)(Tbb) (**14-C_2TMS**)	110.7	83.8	243.9	201.3	*this work*
($caac^{Me}$)Si=Si(Me)(Tbb) (**14-Me**)	96.5	140.7	241.5	190.1	
($caac^{Me}$)Si(Li)–$SiMe_2$(Tbb) (**15**)	44.6	–20.8	210.3	117.3	
($caac^{Me}$)Si(K)–Si($SiMe_3$)$_3$ (**4-Si**)	14.4	–132.1	213.0	117.6	
(SIDipp)Si=SiBr(Tbb) (**14-NHC**)	34.6	86.0	204.6	133.8	[118]
(I*t*Bu)Si=Si(R_1)$_2$ (**II-49**) [d]	129.4	221.8	158.2	–	[277]
(I*i*Pr$_2$Me$_2$)Ge=Si(R_2)$_2$ (**II-44**)[e]	–	158.9	177.9	–	[247]
(I*i*Pr$_2$Me$_2$)Ge=Si(R_2)(SiCl(R_2)$_2$)[e] (**II-45**)	–	162.5	178.5	–	[248]

[a]: ^{29}Si NMR resonance of the CAAC/NHC carbene-coordinated silicon(0) center. [b]: ^{29}Si NMR resonance of the three- and four-coordinated silicon center bearing the sterically demanding Tbb, $SiMe_3$, (R_1)$_2$ and (R_2) substituents. [c]: ^{15}N NMR resonance of the nitrogen atom(s) in the CAAC (NHC) carbene ring referenced against NH_3(l). [d]: (R_1)$_2$ = [C(Ar)$_2$-(CH$_2$)$_2$-C(Ar)$_2$] (Ar = C_6H_2-3,5-*t*Bu$_2$-4-OMe).
[e]: R_2 = Trip = C_6H_2-2,4,6-*i*Pr$_3$.

2.6.3.3 Synthesis and properties of the unprecedent potassium silenide 16

Addition of DME to a mixture of **14** and 2 equiv. of KC_8 at –50 °C resulted into the formation of a dark green suspension. Upon reaching ambient temperature the color of the reaction mixture changed to dark red. Monitoring of the reaction progress via ^{1}H NMR spectroscopy in (D_6)benzene at ambient temperature revealed the selective formation of the C-H activated product **16·DME** (*Scheme 2.23*)

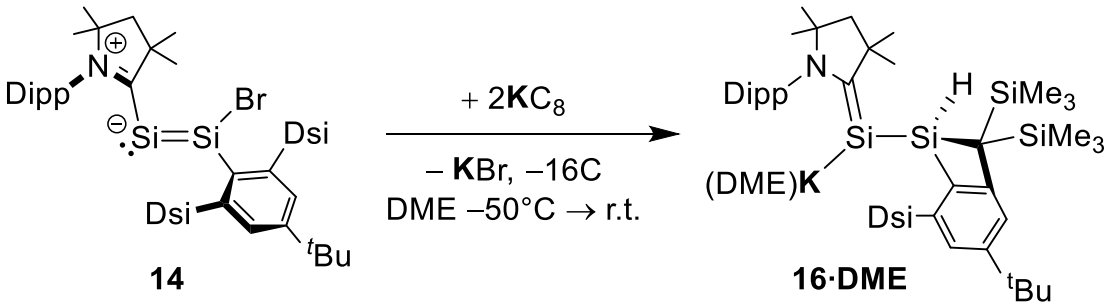

Scheme 2.23. Reduction of **14** with KC_8 in DME.

After work up, the potassium silenide **16·DME** could be isolated in analytically pure form as red microcrystalline solid in 21 % yield. The compound is highly pyrophoric, immediately decomposing upon contact with air. It decomposes upon melting at 187 °C in sealed vacumm glass capillary to a dark brown mass. ^{1}H NMR spectroscopy in (D_6)benzene of the molten mass revealed a rather unselective decomposition.

The isolation of the potassium silenide **16** appeared to be especially challenging. Attempts to isolate the compound, upon reduction of **14** with 2 equiv. of KC_8 in THF, followed by crystallization from *n*-pentane, resulted in the isolation of the caac^{Me} adduct **16·caac^{Me}** (*Figure 2.84* right), even though ^{1}H NMR spectroscopy in (D_6)benzene revealed no presence of free carbene in the reaction solution. These findings suggest, that the potassium-silenide, without the coordination of DME, decomposes in *n*-pentane solution upon loss of free caac^{Me} carbene.

Suitable single crystals of **16·DME** coulde be grown from 1:5 v/v DME/*n*-hexane mixtures at 4 °C. The molecular structure of **16·DME** (*Figure 2.84* left) features C_1-symmetry and a trigonal planar coordinated silicon center ($\Sigma\measuredangle$(Si) = 359.7(2)°) as the hypersilyl potassium-silenide SiK(SiTMS$_3$)(caac^{Me}) (**4-Si**) (see *section 2.5.2*). The Si–C^{carb} bond length (1.834(7) Å) is significantly shortened compared to that of the starting material **14** (1.878(5) Å), indicating considerable π(Si–C^{carb}) bonding, but is still longer than that of the literature known lithium-silenide Li(R_A)Si=C(R_A)(R_B) (R_A = SiMe(tBu)$_2$ R_B = SiMe$_2$(*t*Bu)) (1.762(3) Å).[126]

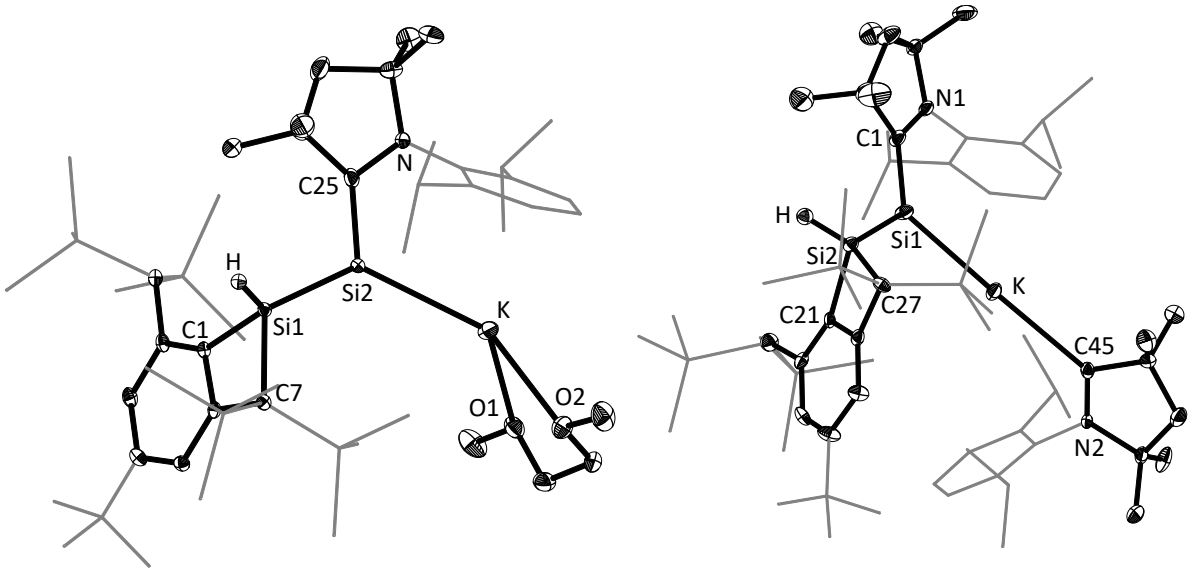

Figure 2.84. Diamond plot of the molecular structure of **16·DME** (left) and **16·caac^{Me}** (right), thermal ellipsoids are set at 30 % probability, and hydrogen atoms were omitted. In the depicted structures the Dipp-substituent of the caac^{Me} ligand and the $SiMe_3$-groups and *t*Bu-group of the Tbb-substituent are presented in the wire-frame for the sake of clarity. Selected bond lengths [Å], bond angles [°] and torsion angles [°]: **16·DME:** Si2–K 3.179(3), Si2–Si1 2.351(2), Si2–C25 1.834(7), Si1–C1 1.889(6), Si1–C7 2.020(6), N–C25 1.415(8), Si1–Si2–K 131.4(1), C25–Si2–K 119.0(2), C25–Si2–SI1 109.3(2), C1–Si1–Si2 119.0(2), C1–Si1–C7 75.0(2); C7–Si1–Si2 120.0(2). The structure features a side occupancy of 12 % alongside the Si1–Si2 bond. For the sake of simplicity, the atomic parameters of the main occupancy are given.
16·caac^{Me}: Si1–K 3.266(3) [3.274(3)], Si1–Si2 2.345(3) [2.336(3)], Si1–C1 1.770(8) [1.796(9)], Si2–C21 1.874(7) [1.882(8)], Si2–C27 2.020(8) [1.980(8)], C1–N1 1.413(8) [1.376(9)], K–C45 2.918(8) [2.938(9)], C45–N2 1.315(9) [1.332(10)], Si2–Si1–K 123.41(11) [123.87(12)], C1–Si1–K 124.9(3) [124.2(3)], C1–Si1–Si2 111.0(3) [111.3(3)], C21–Si2–Si1 111.0(2) [112.5(2)], C21–Si2–C27 75.2(3) [75.3(3)], C27–Si2–Si1 125.6(3) [124.8(2)]. The unit cell features two independent molecules.

The structure of **16·DME** can be compared to the literature known potassium silenide SiK(Trip)(caac^{Me}) (**II-37**) (Trip = C_6H_2-2,4,6-*i*Pr_3), which appears as dimer in the solid state.[124] The Si–C^{carb} and N–C^{carb} bond-lengths of **16·DME** (1.834(7) Å, 1.415(8) Å) are remarkably similar to those in SiK(Trip)(caac^{Me}) ((d(Si–C^{carb}) = 1.793(2) Å, d(N–C^{carb}) = 1.424(3) Å). [124] Similarly, the potassium ion is covalently bonded to the Si-center (d(Si–K) = 3.179(3) Å (**16-DME**). The Si–K distance is shorter than in **II-37** (d(Si–K) = 3.284(1) Å)[124] and typical potassium silanides (d(Si–K) = 3.37 – 3.42 Å).[243] In addition, the covalently bonded potassium ion is further supported by the π-interaction of the aromatic Dipp substituent of the caac^{Me} ligand (d(C_{ring}–K) = 3.167(2) – 3.368(6) Å), as described in the case of **II-37** (d(C_{ring}–K) = 3.044(2) – 3.510(2) Å).[124] The Si–Si single bond in **16·DME** (2.351(2) Å) is significantly shorter compared to that of the lithium silenide Li(R_A)Si=C(R_A)(R_B) (2.486(2) Å) but compares well to the free silenide $[Li(THF)_4]^+$ $[(R_A)Si=C(R_A)(R_B)]^-$ (2.41(1) Å).[126]

^{1}H, ^{13}C{^{1}H} and ^{29}Si{^{1}H} NMR spectra at ambient temperature in (D_6)benzene solution reflect the C_1-symmetry observed in the solid state. The ^{29}Si{^{1}H} NMR spectrum displays 4 resonances for the diastereotopic $SiMe_3$ groups of the Tbb substituent at –0.68, 0.08, 0.50 and 2.0 ppm, a resonance for the tetrahedrally coordinated silicon center at –15.5 ppm and a resonance of the silenic silicon center at –0.30 ppm. Compared to the disilavinylidene **14** ($\delta(^{29}Si(caac^{Me})$ = 73.1 ppm) the ^{29}Si-resonance of the $caac^{Me}$ bonded silicon center in **16·DME** ($\delta(^{29}Si(caac^{Me})$ = –0.30 ppm) is drastically upfield shifted and lies in the typical range of potassium-silenieds $SiK(R)(caac^{Me})$ synthesized in this work (*Table 2.39*). The strong $Si{=}C^{carb}$ double bond character is reflected by the drastic upfield shift of the $^{13}C^{CAAC}$ and $^{15}N^{CAAC}$ resonances in **16·DME** (217.9 ppm, 124.7 ppm) compared to the starting material **14** (241.4 ppm, 197.4 ppm).

Interestingly, the ^{29}Si–^{1}H coupling constant of **16·DME** ($\delta(^{1}H)$ = 6.56 ppm, $^{1}J(^{29}Si, ^{1}H)$ = 155.8 Hz), differs drastically from other silanes, such as $TbbSiH(OEt)_2$ ($\delta(^{1}H)$ = 5.25 ppm, $^{1}J(^{29}Si, ^{1}H)$ = 227 Hz) and $TbbSiH_3$ ($\delta(^{1}H)$ = 4.16 ppm, $^{1}J(^{29}Si, ^{1}H)$ = 196 Hz).[25] The ^{29}Si–^{1}H coupling constant in **16·DME** (155.8 Hz) is also significantly smaller than those of some C–H activation products of $Si_2(Tbt)_2$ ($\delta(^{1}H)$ = 5.93 ppm) and $Si_2(Tbb)_2$ ($\delta(^{1}H)$ = 5.85 ppm, $^{1}J(^{29}Si, ^{1}H)$ = 181.6 Hz).[284,285] Similarly, the observed ν(Si-H) value for **16·DME** (2037 cm^{-1}) in the solid state is drastically shifted to lower wavenumbers compared to $TbbSiH_3$ (2138 cm^{-1}). These findings suggest a lower degree of sp-hybridization in the Si–H bond in **16·DME**, when compared to the sp^3 hybridization in related hydridosilanes.

Table 2.39. NMR spectroscopic features of potassium-silenide **16·DME** and **16·caac^{Me}** compared to literature known potassium and lithium-silenides. The NMR spectroscopic data is given in (D_6)benzene at 298 K, if not mentioned otherwise in the legend.

Comp	$\delta(^{29}Si^{M})$[a] / ppm	$\delta(^{29}Si^{R3})$[b] / ppm	$\delta(^{13}C^{carb/sp2})$ / ppm	$\delta(^{15}N)$[c] / ppm	Ref.
$(caac^{Me})SiK–Si(SiMe_3)_3$ (**4-Si**)	14.4	–132.1	213.0	117.6	
$(caac^{Me})Si(Li)–SiMe_2(Tbb)$ (**15**)	44.6	–20.8	210.3	117.3	
$(caac^{Me})Si(K)–SiH(Tbb')\cdot caac^{Me}$ [d] (**16·caac^{Me}**)	–0.50	–15.5	217.6	125.0	*this work*
$(caac^{Me})SiK–\{SiH(Tbb')\}\cdot DME$ [d] (**16·DME**)[a]	–0.30	–15.5	217.9	124.7	
$SiK(Trip)(caac^{Me})$ (**II-37**)[e]	26.63	–	195.1	–	[124]
$Li(R_A)Si{=}C(R_A)(R_B)\cdot(THF)_2$ (**II-36**)[f]	405.5	–7.2	134.2	–	[126]
$[Li(THF)_4][(R_A)Si{=}C(R_A)(R_B)]$ (**II-36**)[f]	347.8[g]	–4.6[g]	143.5[g]	–	[126]

[a]: ^{29}Si NMR resonance of the three-coordinated silicon center bearing the alkali metal. [b]: ^{29}Si NMR resonance of the silyl substituent bonded to the low valent silicon center. [c]: ^{15}N NMR resonance of the single nitrogen atom in the CAAC carbene ring. [d]: {SiH(Tbb'} = Si(H){C($SiMe_3$)$_2$-C_6H_2-3-*t*Bu-5-(CH)($SiMe_3$)$_2$; [e]: Trip = C_6H_2-2,4,6-*i*Pr$_3$. [f]: R_A = SiMe(*t*Bu)$_2$ R_B = $SiMe_2$(*t*Bu)); [g] (D_8)THF at 298 K.

2.6.3.4 Reaction of 14 with IMe_4

Addition of IMe_4 to a dark green colored solution of (caac^{Me})Si=SiBr(Tbb) (**14**) afforded a dark red solution. Monitoring of the reaction by ^{1}H NMR spectroscopy in (D_6)benzene revealed the selective formation of the IMe_4 adduct **17**, which was isolated as a orange-red powder in 53 % yield. The compound immediatelty decomposes upon contact with air and decomposes upon melting at 175 °C unselectively. Compound **17** is insoluble in aliphatic solvents, moderately soluble in benzene and toluene and well soluble in fluorobenzene and THF, affording intense dark red solutions. Unfortunately, no single crystals of the compound could be obtained, after different crystallization attempts from toluene, THF, DME or Et_2O. Compound **17** slowly decomposes in benzene solution at ambient temperature. Heating of an NMR sample in (D_6)benzene for 2 h drastically increases the decomposition rate, upon which free IMe_4 carbene is formed and a complex mixture of different decomposition products, which feature atleast three different Tbb-substituents with C_1-symmetry. Interestingly no free (caac^{Me})Si=SiBr(Tbb) (**14**) is formed during this process.

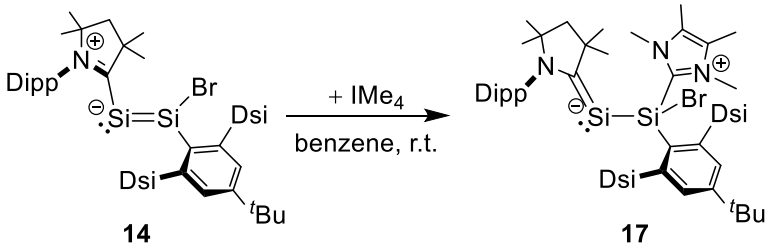

14 **17**

Scheme 2.24. Reactivity of caac^{Me}-stabilized disilavinylidene **14** towards the carbene IMe_4.

The ^{1}H NMR spectrum of **17** reflects the C_1-symmetry of the compound resulting from the presence of a stereogenic silicon center in which both the IMe_4 and Tbb substituent are rotating rapidly around the respective Si–C bonds (*Figure 2.85*).

The connectivity of the molecule could be proven by (^{1}H ^{29}Si) HMBC spectroscopy, which clearly shows the IMe_4 coordination to the Tbb coordinating silicon center. The ^{29}Si{^{1}H} NMR spectrum of **17** in (D_6)benzene displays resonances at –57.2 (*Si*Br(IMe_4)(Tbb), 1.9 (*Si*Me$_3$)$_A$, 2.0 (*Si*Me$_3$)$_B$ and 28.1 ppm (Si(caac^{Me})), respectively. The ^{29}Si resonance of the tetracoordinated silicon center in **17** (–57.2 ppm) is drastically upfield shifted compared to that of the starting material (96.2 ppm (**14**)) and the bromo(silyl)silene **13** (–10.6 ppm). Similarly the ^{29}Si resonance of the dicoordinated silicon center in **17** (28.1 ppm) is significantly upfield shifted relative to that of the starting material (73.1 ppm (**14**)), but downfield shifted compared to **13** (8.46 ppm). The $^{13}C^{CAAC}$ (191.3 ppm) and $^{15}N^{CAAC}$ resonances (141.2 ppm) in **17** are drastically upfield shiftet compared to those of **14** ($\delta(^{13}C^{CAAC})$ = 241.4 ppm, $\delta(^{15}N^{CAAC})$ = 197.4 ppm), suggesting considerable π-character in the Si–C^{carb} bond in **17**.

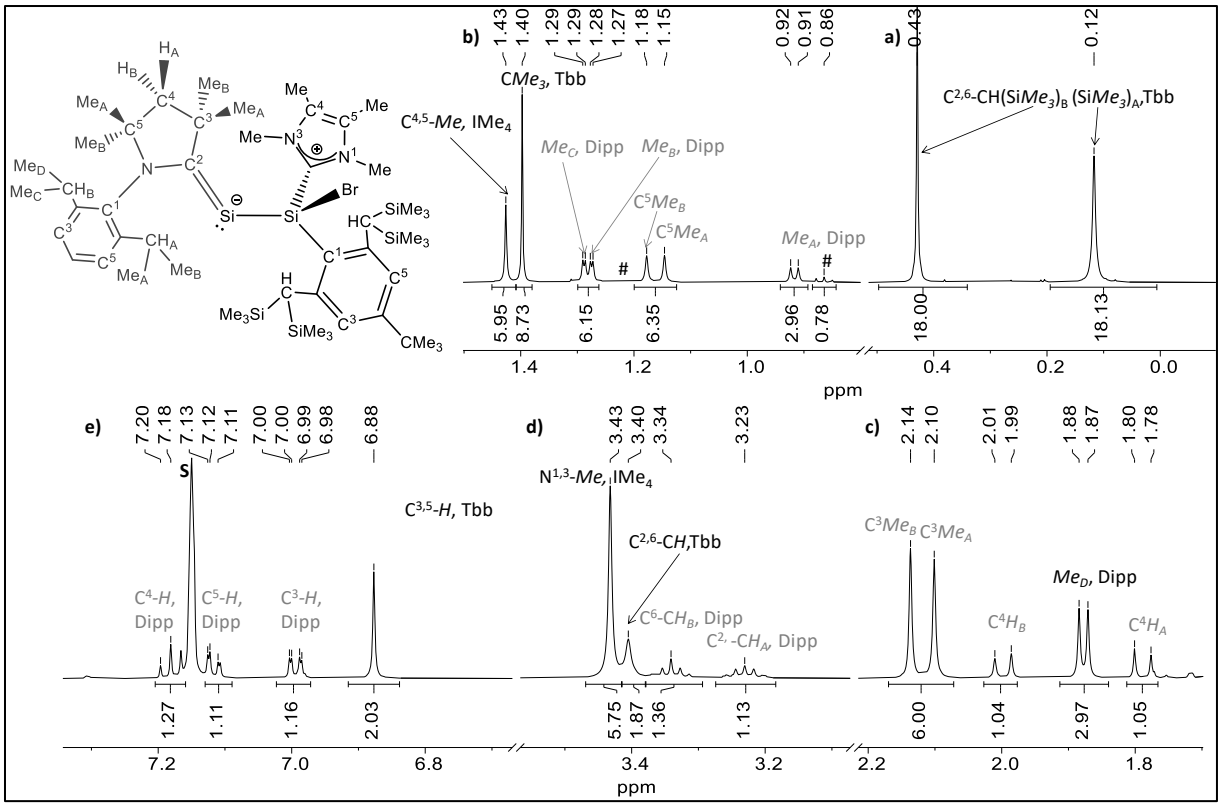

Figure 2.85. ^{1}H NMR spectrum (500.14 MHz) of a pure sample of (caac^{Me})=Si–SiBr(IMe$_4$)(Tbb) (**17**) in (D$_6$)benzene at 298 K. The residual proton signal of the deuterated solvent is marked with the character **S**, tiny amounts of *n*-pentane are marked with the character #.

According to the NMR spectroscopic features **17** can be best described as a zwitterionic silylium-silenide. In terms of ^{29}Si NMR resonances it compares rather well to IMe$_4$-stabilized silyliumylidenes (*Table 2.40*).

Table 2.40. NMR spectroscopic features of the IMe$_4$ adduct of disilavinylidene **17** compared to literature known IMe$_4$ containing low valent silicon compounds; NMR spectroscopic data are given in (D$_6$)benzene, if not mentioned otherwise in the legend.

Comp	δ(^{29}Si^{carb}) / ppm	δ(^{29}Si$^{R2/R3}$) / ppm	δ(^{13}C^{carb}) / ppm	δ(^{15}N) / ppm	Ref.
(caac^{Me})SiBr–SiBr$_2$(Tbb) (**13**)	8.46	–10.6	217.4	–	
(caac^{Me})Si=SiBr(Tbb) (**14**)	73.1	96.2	241.4	197.4	*this*
(caac^{Me})Si–SiBr(IMe$_4$)(Tbb)(**17**)	28.1	–57.2	191.3 169.5[a]	141.2 174.7[a]	*work*
[(IMe$_4$)$_2$Si–Si(IMe$_4$)(Tbb)]Br [b] (**II-57**)	–69.5[c] or –57.2	–69.5[c] or –57.2	166.8[c] 172.2[a]	–	[286]
[Si$_2$(IMe$_4$)$_2$]Br$_2$		–79.3[c]	164.9[c]	–	[224]
[Si(IMe$_4$)$_2$(Tbb)]Br		–70.9	160.4	–	[25]
SiBr(IMe$_4$)(Bbt)		–10.9	167.5	–	[25]

[a]: ^{13}C^{carb} and ^{15}N NMR resonances of the carbene (NHC) connected to the three coordinated silicon(II)-center.
[b]: The assignment of the two resonances δ(^{29}Si^{carb}) and δ(^{29}Si^{R2}) was not possible due to missing cross peaks in the corresponding ^{1}H ^{29}Si HMBC spectrum.[286] [c]: (D$_8$)THF, 298 K.

2.6.3.5 Synthesis and Properties of a carbene-stabilized disilynylium salt

Upon addition of Na[B{C_6H_2-3,5-$(CF_3)_2$}$_4$] (NaB(Ar^F)$_4$) to a dark red solution of **17** in fluorobenzene the color of the reaction mixture rapidly changed from red to dark blue. Monitoring of the reaction mixture by ^{1}H no D NMR spectroscopy of an aliquot in fluorobenzene revealed the quantitative formation of the salt **18**, which was isolated as dark blue, highly air sensitive, solid in 85 % yield. The compound reversibly melts at 175 °C with only minor decomposition. It is insoluble in aliphatic solvents and benzene, but well soluble in fluorobenzene, chlorobenzene and THF, affording dark blue solutions. In contrast to the starting material **17**, the compound is stable at ambient temperature in solution and does not even decompose upon heating in THF solution.

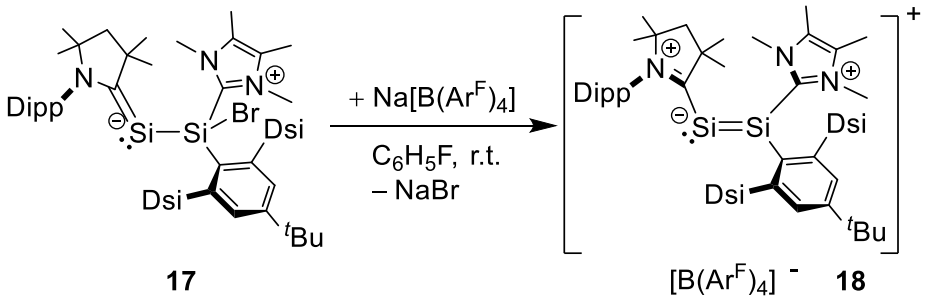

17 **18**

Scheme 2.25. Bromide abstraction of the zwitterionic silylium-silenide **17**, yielding the disilynylium salt **18**.

Suitable single crystals could be grown from fluorobenzene/*n*-hexane mixtures (1:2) or bromobenzene. The structure of the salt **18** (*Figure 2.86* left) compares well to the caac^{Me}-supported disilavinylidene **14** (see *chapter 2.6.2*). The planar core of the structure consists of the atoms Cl^{Tbb}, Si1, C25^{NHC}, Si2 and C35^{CAAC} ($\Sigma°$Si1 = 358.9(1)° (**18**), 354.2(1)° (**14**)). The bulky Tbb and caac^{Me} groups are orientated in trans-position to each other as evidenced by the torsion angles (τ(Cl^{Tbb}–Si1–Si2–C35^{CAAC}) = –168.5 (2)° (**18**); 178.2(3)° (**14**)) and the Tbb substituent is orientated orthogonal with respect to the planar core of the molecule. Similar to **14**, the caac^{Me} carbene in **18** is orientated towards the planar core of the molecule (φ_{CAAC} = 38.1(1)°), suggesting some delocalisation of the π(Si–Si) bond over the C^{CAAC}–Si2–Si1 moiety in **18**. In addition, the C^{NHC} carbon atom of the IMe_4 ligand in **18** (τ(C^{CAAC}–Si2–Si1–C^{NHC}) = 24.9(2) °) is considerably bent, in analogy to the bromine substituent in **14** (τ(C^{CAAC}–Si2–Si1–Br) = –32.1(2) °). Both structural features lead to a C_1-symmetric solid state structure. The Si=Si bond in **18** (2.203(1) Å) compares well to the disilavinylidene **14** (2.194(2) Å) and to the cation [(IDipp)Si=Si(IDipp)Me]$^+$ (2.191(1) Å)[205] and is significantly shorted when compared to the caac^{Me}-stabilized disilicon(0) compound (caac^{Me})Si=Si(caac^{Me}) (2.254(2) Å).[115] The Si–C^{CAAC} bond length in **18** (1.896(3) Å) is slighty elongated compared to **14** (1.878(5) Å) and lies in the typical range of Si–C^{Ar} single bonds (1.879 – 1.894 Å).[34,197]

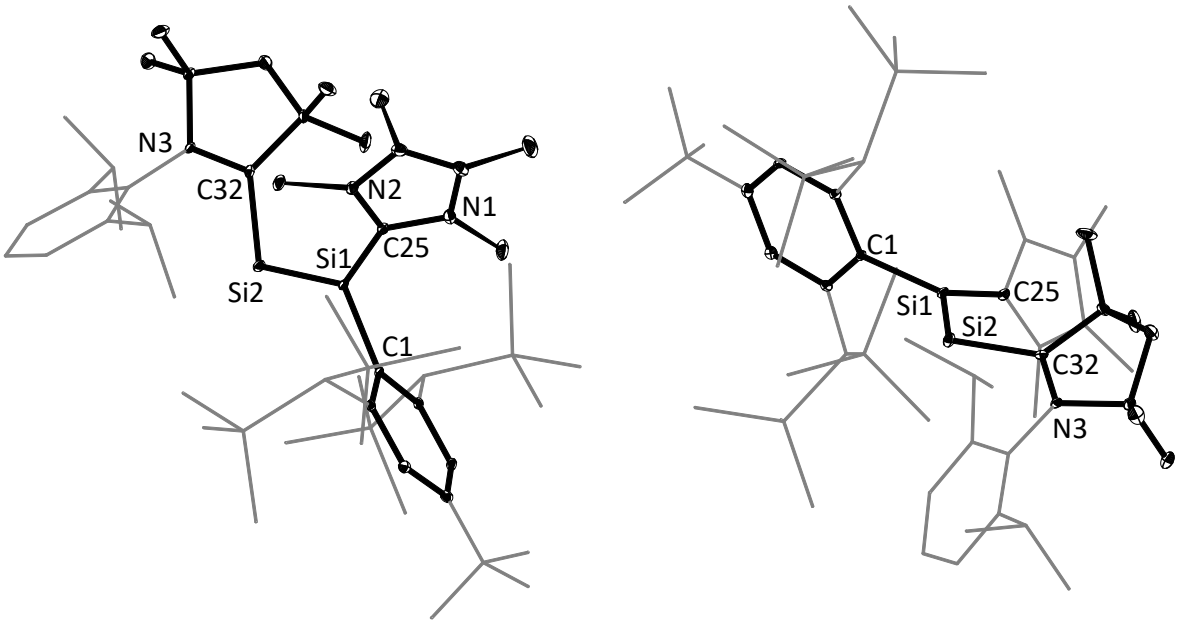

Figure 2.86. (Left) DIAMOND plot of the molecular structure of **18**, thermal ellipsoids are set at 30 % probability level and hydrogen atoms were omitted. In the depicted structure the Dipp substituent of the caac^{Me} ligand and the disyl groups (CH(SiMe$_3$)$_2$) and *t*Bu group of the Tbb substituent are presented in the wire-frame for the sake of clarity. Selected bond lengths [Å], bond angles [°] and torsion angles [°]: Si1–Si2 2.203(1), Si1–C1 1.886(3), Si1–C25 1.919(3), Si2–C32 1.896(3), C25–N1 1.346(4), C25–N2 1.345(4), C32–N3 1.316(4), C1–Si1–Si2 121.3(1), C1–Si1–C25 106.5(1), C25–Si1–Si2 131.2(1), C32–Si2–Si1 109.0(1), C32–Si2–Si1–C1 -168.5(2), C32–Si2–Si1–C25 24.9(2). (Right) Different view of **18** illustrating the different orientation of the Si-bonded caac^{Me} and Tbb rings; hydrogen atoms were omitted, the Dipp-substituent of the caac^{Me} ligand and the disyl groups (CH(SiMe$_3$)$_2$) and *t*Bu group of the Tbb substituent as well as the IMe$_4$ ligand are presented in the wire-frame for the sake of clarity.

The N–C^{CAAC} bond length (1.316(4) Å) of the cationic compound is slightly shortened, compared to that of the disilavinylidene **14** (1.338(6) Å). These findings suggest a slightly lower π-contribution in the Si–C^{CAAC} bond in the disylinium salt **18**, compared to that of **14**. In terms of the Si–C^{CAAC} bond length and relative orientation of the CAAC carbene (*Figure 2.86* right) compound **18** (d(Si–C^{CAAC}) = 1.896(3) Å, $\varphi_{carbene}$ = 38.1(1)°) compares well to Si$_2$(caac^{Me})$_2$ (d(Si–C^{CAAC}) = 1.887(4) Å, $\varphi_{carbene}$ = 53.2(3)°),[115] but differs drastically from the cations [(IDipp)Si=Si(IDipp)R]$^+$ (R = H, Me, Et) (*Table 2.41*). In the NHC-stabilized systems the NHC bonded to the dicoordinated Si atom is orientated almost orthogonally (*Table* 2.41) with respect to the planar core of the molecule and features a typical Si–C^{carb} single bond. In comparison, in the caac^{Me}-stabilized compounds the Si–C^{CAAC} bond length is significantly shortened and the angle $\varphi_{carbene}$ (38.1(1) – 57.8(2)°) indicates some π(Si–C^{CAAC}) bond character.

The Si–C^{NHC} bond length and angle φ_{NHC} of the IMe_4 bonded to the three-coordinate silicon(II)-center in **18** *(Table 2.41* → [c]), are increased compared to [(IDipp)Si=Si(R)(IDipp)]$^+$ (R = H, Me), but compare well to that reported for [(IDipp)Si=Si(Et)(IDipp)]$^+$, indicating an influence of the steric bulk of the used substituent at the three-coordinated silicon(II)-center on the bonding parameters.

Table 2.41. Selected structural parameters of the carbene stabilized disilynium cation **18**, compared to related NHC and CAAC-stabilized silicon(0) compounds and disilynium cations.

Comp.	Si–Si / Å	Si–C^{carb} / Å	C^{carb}-Si-Si / (deg)	φ_{carb} [a] / (deg)	Ref.
($caac^{Me}$)Si=SiBr(Tbb) (**14**)	2.194(2) [2.181(2)][b]	1.878(5) [1.868(6)][b]	105.5(1) [105.6(2)][b]	57.8(2) [51.9(3)][b]	*this work*
[($caac^{Me}$)Si=Si(IMe_4)(Tbb)] [$B(Ar^F)_4$] (**18**)	2.203(1)	1.896(3) 1.919(3)[c]	109.0(1) 131.2(1) [c]	38.1(1) 43.8(2) [c]	
($caac^{Me}$)Si=Si($caac^{Me}$)	2.254(2)	1.887(4)	103.7(1)	53.2(3)	[115]
(IDipp)Si=Si(IDipp)	2.229(1)	1.927(2)	93.4(1)	87.0(1)	[114]
[(IDipp)Si=Si(IDipp)H)] [$B(Ar^F)_4$]	2.187(1)	1.940(2) 1.882(2)[c]	95.3(1) 116.7(1)[c]	70.6(1) 9.2(1)[c]	[205]
[(IDipp)Si=Si(IDipp)Me)] [$B(Ar^F)_4$]	2.191(1)	1.947(2) 1.901(2)[c]	95.1(1) 114.6(1)[c]	78.7(1) 13.2(1)[c]	[205]
[(IDipp)Si=Si(IDipp)Et] [$B(Ar^F)_4$]	2.173(1)	1.941(2) 1.912(2)[c]	100.1(1) 108.4(1)[c]	87.7(1) 52.3(1)[c]	[205]

[a]: φ_{carb} the angle between the least-squares plane of the CAAC/NHC carbene five-membered ring and the plane defined by the C^{CAAC}/C^{NHC} atom and the doubly-bonded tetrel atoms.
[b]: values given of two independent molecules in the unit cell.
[c]: values of the carbene bonded to the three coordinated silicon(II)-center.

As **14**, the salt **18** features an averaged C_S-symmetry in fluorobenzene and (D_8)THF solution. VT ^{1}H NMR spectra of **18** at variable temperatures temperatures (193 – 298 K) did not show any significant change, suggesting a fast rotation of the $caac^{Me}$, IMe_4 and Tbb-ligands in solution at the NMR timescale, about the respective Si–C bonds.
The ^{29}Si{^{1}H} NMR spectrum of **18** in (D_8)THF displays resonances at 3.1 (4x*Si*Me_3), 83.6 (*Si*(IMe_4)(Tbb) and 118.1 ppm (Si($caac^{Me}$)), respectively. Compared to the starting material **17** (28.1 ppm ((Si($caac^{Me}$)), –57.2 ppm (*Si*Br(IMe_4)(Tbb)) the silicon resonances of **18** are drastically downfield shifted (118.1 ppm (*Si*($caac^{Me}$), 83.6 ppm (*Si*(Tbb)). The resonance of the dicoordinated Si atom in **18** (118.1 ppm) is significantly downfield shifted compared to that of the disilavinylidene **14** (73.1 ppm).

The $^{13}C^{CAAC}$ and $^{15}N^{CAAC}$ resonances in **18** (239.1 ppm, 215.9 ppm) are drastically downfield shifted when compared to starting material **17** (191.3, 141.2 ppm), reflecting the nature of the Si–C^{CAAC} single bond in **18** in contrast to the Si=C^{CAAC} double bond observed in **17** (*Table 2.42*).

The $^{15}N^{CAAC}$ resonance in **18** (215.9 ppm) is also slightly downfield shifted, when compared to disilavinylidene **14** (197.4 ppm) and the disilicon(0)-compound $Si_2(caac^{Me})_2$ (174.5 ppm),[115] but more upfield shifted compared to $SiBr_2(caac^{Me})$ (**1**) (231.3 ppm). These findings suggest, a significant less π-character in the Si–C^{CAAC} bond in **18**, when compared to **14** and $Si_2(caac^{Me})_2$, but still slightly more π-charcter when compared to **1**.

Table 2.42. NMR spectroscopic features of carbene-stabilized dislinylium salt **18**, compared to **14**, **17** and related NHC-stabilized compounds. The NMR spectroscopic data has been obtained in (D_8)THF at 298 K, if not given otherwise in the legend.

Comp	δ($^{29}Si^{carb}$) / ppm	δ($^{29}Si^{R2}$) / ppm	δ($^{13}C^{carb}$) / ppm	δ(^{15}N) / ppm	Ref.
$SiBr_2(caac^{Me})$ **1**	14.35[a]	–	231.2[a]	231.3[a]	
($caac^{Me}$)Si=SiBr(Tbb) (**14**)	73.1[b]	96.2[b]	241.4[b]	197.4[b]	
($caac^{Me}$)Si–SiBr(IMe_4)(Tbb) (**17**)	28.1[b]	–57.2[b]	191.3[c]	141.2[c]	*this work*
			169.5[d]	174.7[d]	
[($caac^{Me}$)Si=Si(IMe_4)(Tbb)] $[B(Ar^F)_4]$ (**18**)	118.1	83.6	239.1[c]	215.9[c]	
			153.3[d]	175.4[d]	
($caac^{Me}$)Si=Si($caac^{Me}$)	252.3[b]	252.3[b]	236.3[b]	174.5[b]	[115]
(IDipp)Si=Si(IDipp)	223.9[b]	223.9[b]	195.9[b]		[114]
[(IDipp)Si=Si(IDipp)H)] $[B(Ar^F)_4]$	125.4[e]	69.4[e]	174.5[c]	–	[205]
			161.8[d]		
[(IDipp)Si=Si(IDipp)Me)] $[B(Ar^F)_4]$	115.2	102.8	177.1[c]	–	[205]
			162.9[d]		
[(IDipp)Si=Si(IDipp)Et] $[B(Ar^F)_4]$	87.2	111.6	176.1[c]	–	[205]
			164.2[d]		

[a]: measrued in (D_8)THF, 243 K. [b]: measured in (D_6)benzene, 298 K. [c]: $^{13}C^{carb}$ and ^{15}N NMR resonances of the carbene (NHC or CAAC) connected to the di-coordinated silicon(0) center. [d]: $^{13}C^{carb}$ and ^{15}N NMR resonances of the carbene (NHC) bonded to the three-coordinated silicon(II)-center.
[e]: measrued in (D_8)THF, 213 K.

2.6.3.6 Electronic structure of disilynylium cation 18$^+$

The electronic structure of the the cation in **18** (**18**$^+_{calc}$) was investigated by quantum chemical calculations, which were performed at the B97-D3(BJ)-ATM/def2-TZVP level of theory by Leonard R. Maurer. More details on the computional calculations are given in *chapter 5.11*. The structural parameters of the calculated structure in the gas phase do compare well to the structure derived from the single-crystal X-ray diffraction of **18** (*Table 5.84*).

Natural bond analysis of the wave function of **18**$^+_{calc}$ led to a leading natural Lewis structure (NLS) with localized bond pair NBOs for the Si–C^{CAAC}, Si–Si and Si–C^{Tbb}, Si–C^{NHC} σ-bonds, one π(Si–Si) bond and one lone pair at the dicoordinated silicon center (*Table 2.34*). With exception of the π(Si–Si) bond (1.64 e^-) all NBOs feature a high Lewis occupancy above 1.77 e^-. The Si–Si σ-bond is polarized to the dicoordinated silicon atom (62 %) and is formed by a sp$^{1.0}$ Si-NHO and an NHO with high p-character of the three coordinated silicon center. The Si–C^{CAAC} σ-bond is strongly polarized to the carbene center (77 %) and is formed by a Si-NHO of high p-character with a sp$^{1.4}$ C^{CAAC}-NHO. Considerable delocalization is evidenced by the low Lewis occupancy of the Si–Si π-bond (1.64 e^-), which shows little polarization. In addition, the NRT bond orders show considerable amounts of double bond character in the Si–C^{CAAC} (1.3) and the Si–Si bond (1.6) in **18**$^+_{calc}$. Loewdin-population analysis reveals a 3c-2e π_{oop}(C^{CAAC}–Si1–Si2)-bond for the HOMO, where the electron density is shared between the C^{CAAC} (6.1 %), Si1 (29.4 %) and Si2 (32.3 %) atoms.

Table 2.43. Selected results of the natural bond orbital (NBO), natural resonance theory (NRT) and natural population (NPA) analysis of **18**$^+_{calc}$.

NBO A–B	occ.[a]	NHO (A,B)[b] hyb. (pol. in %)	WBI[c] A–B	NRT-BO[d] tot/cov/ion
LP(Si)	1.71	sp$^{0.35}$		
σ(Si–Si')	1.90	sp$^{1.04}$ (62), sp$^{7.80}$(38)	1.6	1.6/1.3/0.3
π(Si–Si')	1.64	p (55), p (45)		
σ(Si–C^{CAAC})	1.94	sp$^{6.01}$ (23), sp$^{1.44}$ (77)	1.0	1.3/0.8/0.6
σ(Si'–C^{NHC})	1.95	sp$^{3.64}$ (25), sp$^{1.40}$ (75)	0.7	1.0/0.5/0.5
σ(Si'–C^{Tbb})	1.94	sp$^{2.40}$ (29), sp$^{2.43}$ (71)	0.8	1.0/0.6/0.4

[a]: occ. = occupancy in e^-. [b]: NHO = Natural Hybrid Orbital, pol. (polarization) = $(C_i)^2$·100%, where C_i = coefficient of NHO. [c]: Wiberg bond index. [d]: total, covalent and ionic NRT bond order.

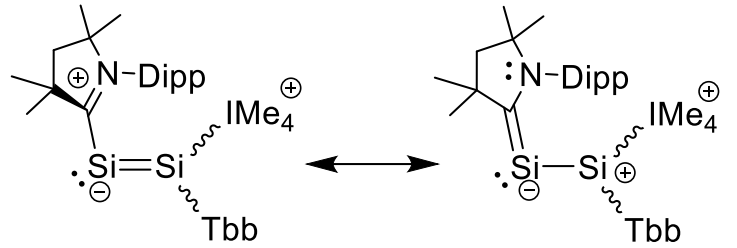

Figure 2.87. Most dominant NRT resonance structures for **18**$^{+}_{calc}$; a wavy bond means that it can be anything and is not constrained for this bond motif search. All contributions above 1.0 % are considered. 10 % was attributed to structures, where the Si–Si bond was cleaved.

The dominant NRT resonance structures of **18**$^{+}$ are depicted in *Figure 2.78*. In fact, **18**$^{+}$ can be rather described as a hybrid of a disilavinyliumylidene (60.9 %) and a silyliumylidenyl-silenide (18.6 %), mostly due to the delocalization of the Si–Si π-bond. The NBO results are reflected in the frontier orbitals of **18**$^{+}$. The HOMO–1 contains mainly the lone pair at the Si atom, the HOMO corresponds to the 3c-2e $\pi_{oop}(C^{CAAC}–Si–Si)$-bond with the major contribution of the π-bond of the silicon centers and the LUMO corresponds to the antibonding combination of $\pi(Si–C^{CAAC})$ and $\pi(Si–C^{NHC})$.

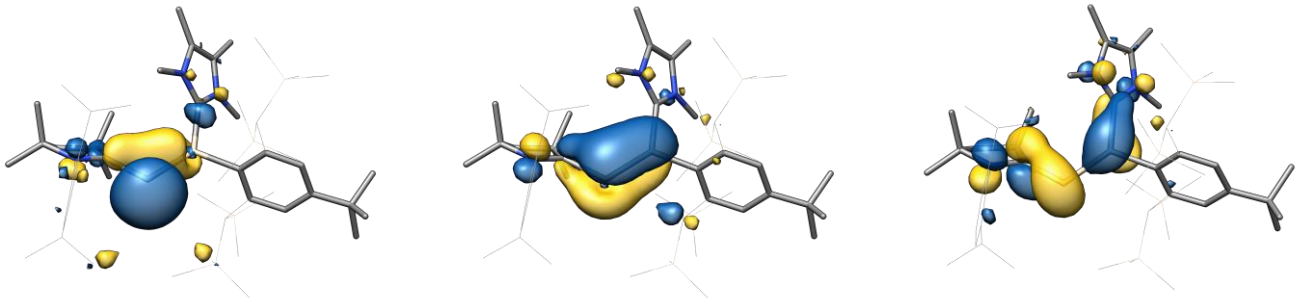

HOMO-1 [–6.97] HOMO [–6.51] LUMO [–5.06]

Figure 2.88. Selected Kohn-Sham molecular orbitals of **18**$^{+}_{calc}$ and their orbital energies in eV. Hydrogen atoms are omitted for clarity. The isosurface value is set to 0.04 $e^{1/2}$·$Bohr^{-3/2}$.

2.7 Reactivity of a CAAC-stabilized Silylone

2.7.1 Introduction

Silylones is called a class of compounds, in which a formally Si(0) atom is stabilized by two neutral ligands. They feature four valence electrons in form of two lone pairs at the silicon(0) center. One lone pair is orientated in the plane of the molecule, whereas the second lone pair is orientated perpendicular to the plane and delocalized in a π-type orbital over the neutral ligands (*Figure 2.89*).[287,288]

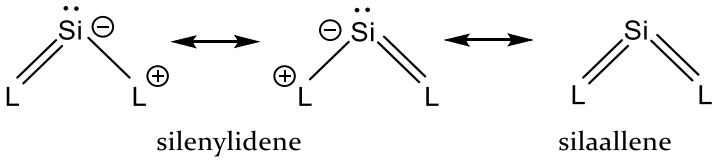

Figure 2.89. Resonance structure of silylones.

Since of the discovery of the first trisilaallene **II-61**[289] by Kira et al. in 2003, which was later described as a silylone bearing two silylene ligands,[290] the number of silylones expanded rapidly (*Figure 2.90*). Examples substantiating this development are the bis(NHC)-supported silylone **II-62**[291], the CAAC-stabilized silylones (CAAC = :C[N(Dipp)CMe$_2$CH$_2$CR$_2$], Dipp = C$_6$H$_3$-2,6-*i*Pr$_2$) **II-63** (R$_2$ = Me$_2$ = caac^{Me})[119] and **II-64** (R$_2$ = [(CH$_2$)$_5$] = caac^{Cy}),[120] the germylene stabilized silylone **II-65**[292] and the cyclic bis(NHSi) supported silylones **II-66,**[293] **II-67**[294] and **II-68.**[295] Very recently the (CAASi)-stabilized silylone **II-69** was reported by Iwamoto et al. The latter case appeared to be particulary interesting, since it featured two different electronic structures: a π-localized silenylidene structure in the solid state **II-69** and a π-delocalized silenylidene structure in solution **II-70**.[296]

The isolation of variety of different silylones (**II-61** – **II-70**) over the past ten years enabled the exploration of their chemistry (*Figure 2.90*). The reaction of the bis(NHC) silylone **II-62** with lewis acids, such as GaCl$_3$ and ZnCl$_2$, afforded mono and bis acid-base adducts, respectively.[287,297]

Oxidation of silylones **II-62** and **II-67** with chalcogens (S, Se, Te) yielded base-stabilized SiX$_2$ (X = S, Se, Te), which can be seen as heavy homologues of CO$_2$.[297,298] Reaction of silylone **II-62** with CO$_2$ resulted into the formation of the dicarbonato complex (bis-NHC)Si(CO$_3$)$_2$.[299] In contrast, reaction of **II-62** with N$_2$O remained uncontrollable, resulting into the formation of different dimeric silicon-oxo-species, depending on the reaction conditions.[293]

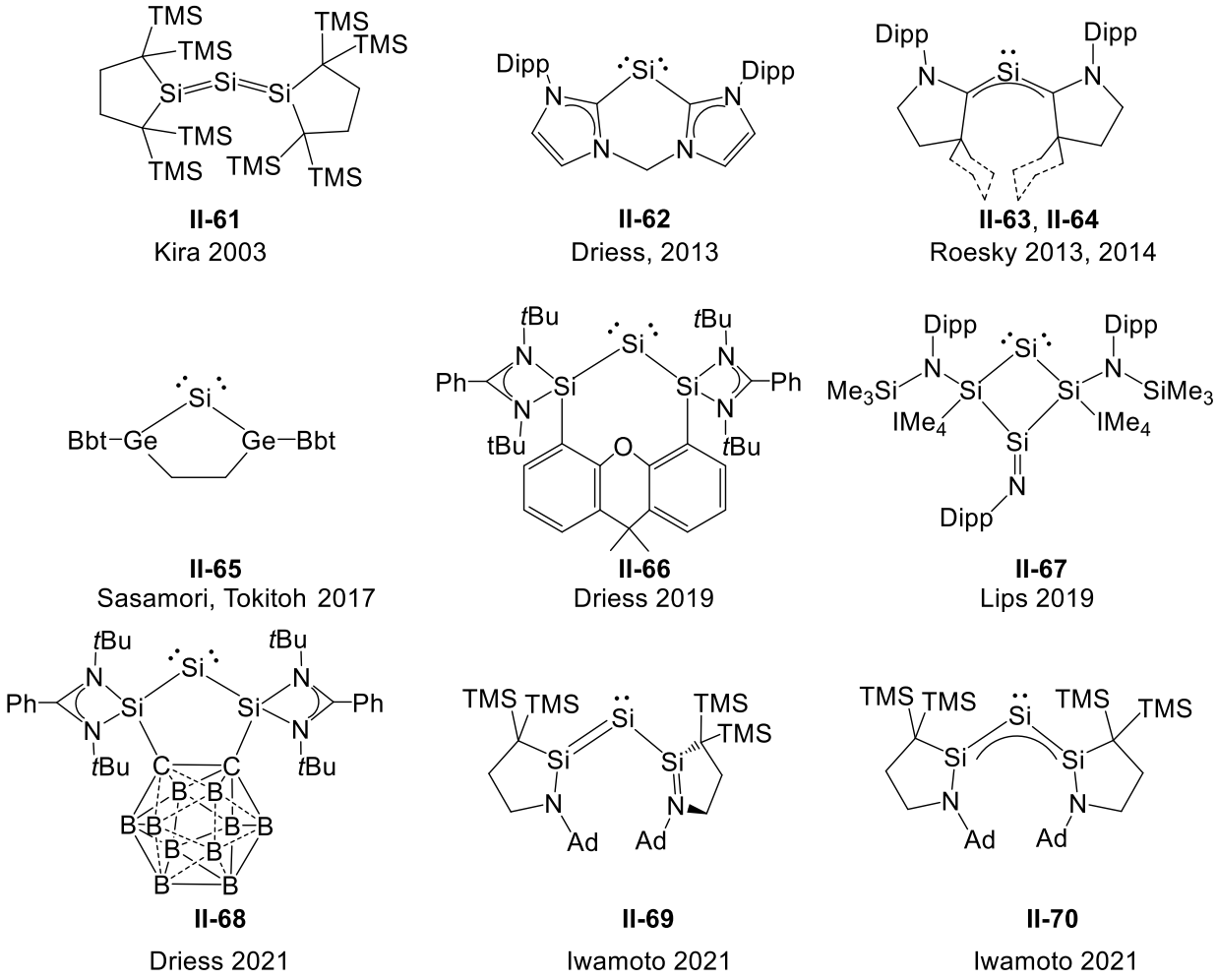

II-61
Kira 2003

II-62
Driess, 2013

II-63, **II-64**
Roesky 2013, 2014

II-65
Sasamori, Tokitoh 2017

II-66
Driess 2019

II-67
Lips 2019

II-68
Driess 2021

II-69
Iwamoto 2021

II-70
Iwamoto 2021

Figure 2.90. Literature known monoatomic silicon(0) complexes **II-61** – **II-70**. Formal charges are not given for the sake of simplicity.

The bis(NHSi) stabilized silylone **II-66** reacted with NH_3, yielding a 1,3-diaminotrisilane, in which all the silicon centers were fully oxidized to +IV.[293]

Interestingly, the bis(NHSi)-stabilized silylone **II-66** did not react with H_2 or ethylene. However upon activation of **II-66** by BPh_3, which afforded a frustrated Lewis-base-acid pair, it selectively reacted with dihydrogen resulting in the formation of the hyrdido sillylium-ylidene salt [SiH{bis(NHSi}][$HBPh_3$].[293]

Similarly, upon activation of **II-66** with BPh_3 a reaction with ethylene occurred, which led to the formation of a zwitterionic silylene SiR{bis(NHSi)} with an ethenylido substituent (R = CH_2-CH_2-BPh_3). [293] Very recently, Driess et al. could also show the $1e^-$-reduction of silylone **II-68** with potassiumnaphtanelide, which resulted in the unprecedent formation of a dimeric bis(NHSi) supported silicon(I) dication $[Si^I–Si^I]^{+2}$. The oxidation of the silylone from oxidation state 0 to +1 upon $1e^-$ reduction can be rationalized by the net movement of two electrons into the carborane cage with the loss of one electron at Si^0 to give Si^I. [295]

Roesky et al. described the reduction of the bis CAAC-stabilized silylones Si(caac^{Me})$_2$ (**II-63**)[119] and Si(caac^{Cy})$_2$ (**II-64**)[119] with potassium, resulting in the insertion of the Dipp C–H bonds of the supporting CAAC ligands, yielding the CAAC-stabilized Si(II) compounds **II-71** and **II-72**, respectively.[120] In terms of their structural features (d(Si–C^{CAAC}) = 1.821(2) Å (**II-71**), 1.824(2) Å (**II-72**), d(N–C^{CAAC}) = 1.383(3) Å (**II-71**), 1.383(3) Å (**II-72**) Σ∢(Si) = 338.8° (**II-71**), 340.9° (**II-72**)) as well as NMR spectroscopic features (δ(^{13}C^{CAAC}) = 171.10 ppm (**II-71**), 173.50 ppm (**II-72**); δ(^{29}Si^{II}) = 54.6 pm (**II-71**), 55.98 ppm (**II-72**)), compounds **II-71** and **II-72** compare rather well to the 2-aminosilene SiBr(Eind)(caac^{Me})-*Z* (**2-Eind-*Z***) (see *section 2.2.4*), suggesting that compounds **II-71** and **II-72** can be classified as pyramidal 2-(amino)silenes aswell.

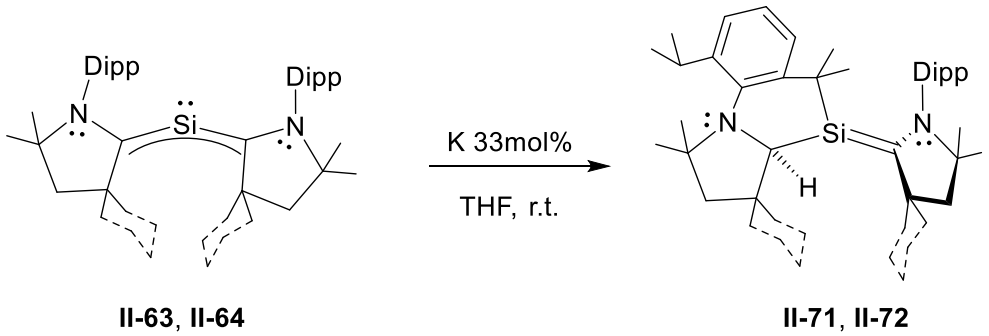

II-63, **II-64** **II-71**, **II-72**

Scheme 2.26. Reduction of CAAC stabilized silylones **II-62** and **II-63** with potassium yielding cyclic pyramidal 2-(amino)silenes **II-70** and **II-71**. Formal charges are not given for the sake of simplicity.

These results highlight the rapid exploration of the chemistry of silylones. Remarkably, besides the isolation and reduction of the bis caac^{Me}-stabilized silylone **II-63**, no further reactivity of this compound has been reported thus far.

2.7.2 Reactivity of Si(caac^{Me})$_2$

The reactivity of Si(caac^{Me})$_2$ (**II-63**) was studied by the research group of A. C. Filippou. Major contribution to this research gave Dr. Billa Prashant, who succeeded in the isolation of [SiH(caac^{Me})$_2$][B(Ar^F)$_4$] (**II-73**) upon protonation of the silylone **II-63** with Brookhart's acid [H(Et$_2$O)$_2$] [B(Ar^F)$_4$] (*Scheme 2.27*).[300] He could show that **II-73** can be selectively reduced with 1 equivalent of KC$_8$ to the neutral silicon radical SiH(caac^{Me})$_2$ (**II-73**), which can be described as π-type radical with the spin density delocalized over the C^{CAAC}–Si–C^{CAAC} moiety. On the other hand silylone **II-63**, could be selectively oxidized with [FeCp$_2$][B(Ar^F)$_4$] to the corresponding literature known radical cation **II-13**.[134]

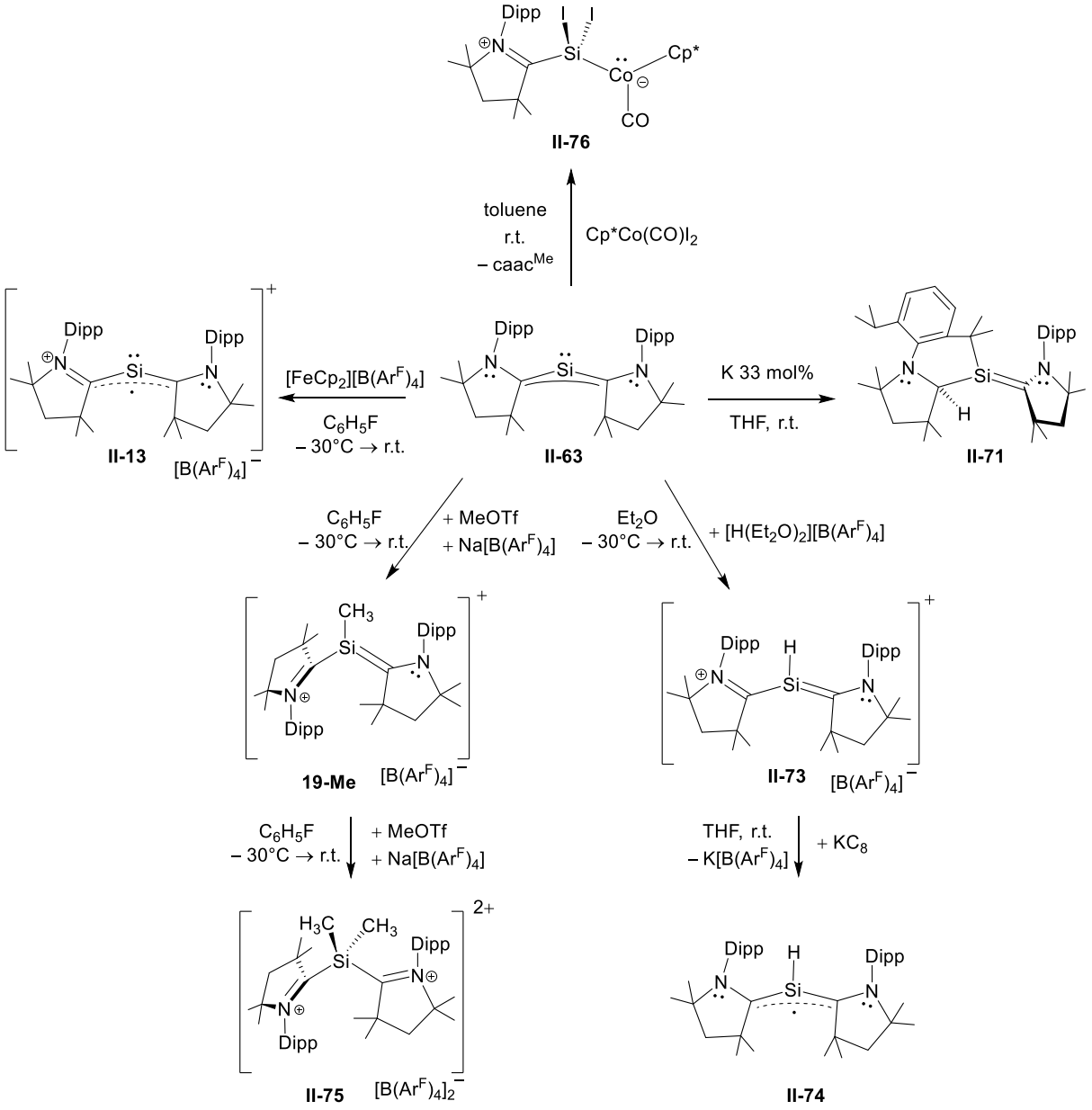

Scheme 2.27. Overview of the reactivity of the caac^{Me}-stabilized silylone **II-63** reported by Billa Prashant in his lab report and Christoph Plett in his bachelor thesis. The isolation and characterization of compound **19-Me** will be discussed in this work.

Major contribution to the investigation of the reactivity of **II-63** was also provided by Christoph Plett, who investigated the reactivity of the silylone **II-63** towards transition metal complexes.[I44] He could show that the silylone selectively reacts with Cp*Co(CO)I_2 upon oxidative addition yielding the diodosilylene aduct **II-76**, upon loss of one equivalent of caac^{Me} carbene.[I44] The compound compares well to the analogous compound **20** (see *chapter 2.8*), synthesized in this work. In addition, he could show that the silylium-ylidene **I9-Me**, described in this work, reacts with a second equivalent of MeOTf resulting in the formation of the salt **II-75**, containing the Si(IV) dication $[SiMe_2(caac^{Me})_2]^{2+}$.[I44]

2.7.3 Improved synthesis of Si(caac^{Me})$_2$

The synthesis of Si(caac^{Me})$_2$ was improved: The procedure described in the literature involves a reduction of $SiCl_2(caac^{Me})_2$ with 2.0 equiv. of KC_8 in THF at –78 °C followed by warming up to ambient temperature.[II9] This leads, however, to the concomitant formation of **II-71** (atleast 20 mol%), according to ^{1}H NMR spectroscopy in (D_6)benzene of an aliquot of the reaction mixture after stirring for 4 h at ambient temperature. The impurity could be only removed upon repeated washing with a THF/*n*-pentane 1/5 mixture upon which dramatically decreased the yield 2.5 %.

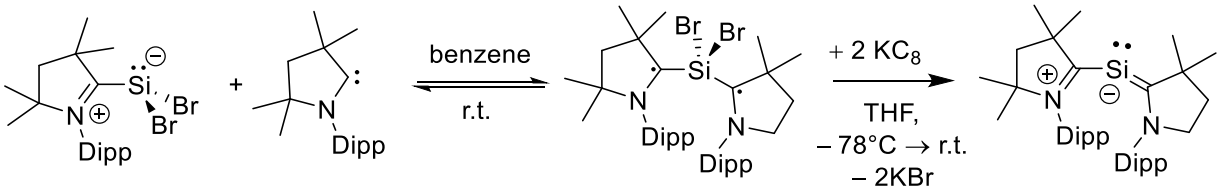

Scheme 2.28. Improved synthesis of silylone Si(caac^{Me}) upon reduction of $SiBr_2(caac^{Me})$ in the presence of caac^{Me} carbene.

The improved synthetic protocol proceeds via $SiBr_2(caac^{Me})_2$, which is formed upon addition of caac^{Me} carbene to a red solution of $SiBr_2(caac^{Me})$ in benzene. After evaporation of the solvent the dark blue $SiBr_2(caac^{Me})_2$ is mixed with 2.2 equiv. of KC_8. After condensation of THF to the solid mixture and subsequent stirring at –78 °C for 0.5 h the reaction mixture was brought to ambient temperature. Monitoring of the reaction mixture by ^{1}H NMR spectroscopy in (D_6)benzene revealed the selective formation of Si(caac^{Me})$_2$ alongside with only tiny amounts of (caac^{Me}H)$_2$O (4 mol%) and **II-71** (2 mol%). After work up the literature known compound could be isolated in 81 % yield in analytically pure form upon crystallization from *n*-hexane.

In the following the reaction of Si(caac^{Me})$_2$ (**II-63**) with methyltriflate is described, which resulted in the isolation of the silylium-ylidene salt [SiMe(caac^{Me})$_2$][B(Ar^F)$_4$] (**19-Me**). Notably reaction of **II-63** with 2 equivalents of methyliodide at ambient temperature led to a color change of royal-blue to red and to the formation of the silicon(IV) compound (caac^{Me})SiMe$_2$I$_2$ next to free caac^{Me}. The identity of the caac^{Me} stabilized diiodosilane was verified by X-ray diffraction analysis (*Figure 5.2*).

2.7.4 Synthesis and properties of [Si(Me)(caac^{Me})$_2$][B(Ar^F)$_4$]

After addition of 1.0 equiv. of methyltriflate to a 1:1 mixture of Si(caac^{Me})$_2$ and NaB(Ar^F)$_4$ (B(Ar^F)$_4$ = B{C$_6$H$_3$-3,5-(CF$_3$)$_2$}$_4$) in fluorobenzene at –30 °C the reaction mixture turned dark green. Monitoring of the reaction mixture, after reaching ambient temperature, via ^{1}H NMR spectroscopy in (D$_8$)THF revealed the selective formation of [Si(Me)(caac^{Me})$_2$][B(Ar^F)$_4$] (**19-Me**), alongside with small amounts (10 mol%) of [caac^{Me}(H)][B(Ar^F)$_4$]. After work up, compound **19-Me** could be isolated in analytically pure form as green microcrystalline solid in 53 % yield.

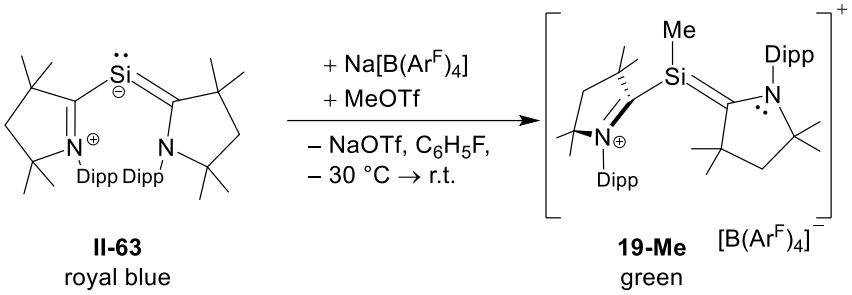

II-63
royal blue

19-Me
green

Scheme 2.29. Synthesis of silyliumylidene salt **19-Me** upon oxidativte addition of MeOTf to Si(caac^{Me})$_2$.

The compound is extremely oxygen sensitive and quickly decolorizes upon contact with air. It decomposes upon melting at 255 °C. Compound **19-Me** is insoluble in *n*-hexane and benzene but well soluble in flurobenzene, THF and Et$_2$O, affording intense dark green solutions.

The origin of the dark green color was analyzed by UV-Vis-NiR spectroscopy of **19-Me** in in Et$_2$O solution at ambient temperature, revealing two absorption maxima at 399 (ε = 5137.9 L mol^{-1} cm^{-1}) and 631 nm (ε = 8854.7 L mol^{-1} cm^{-1}) (*Figure 5.102*). Underlying absorption maxima at 720, 602 nm and 418 nm, 388 nm, respectively were identified upon deconvolution of the absorption bands (*Figure 5.103*).

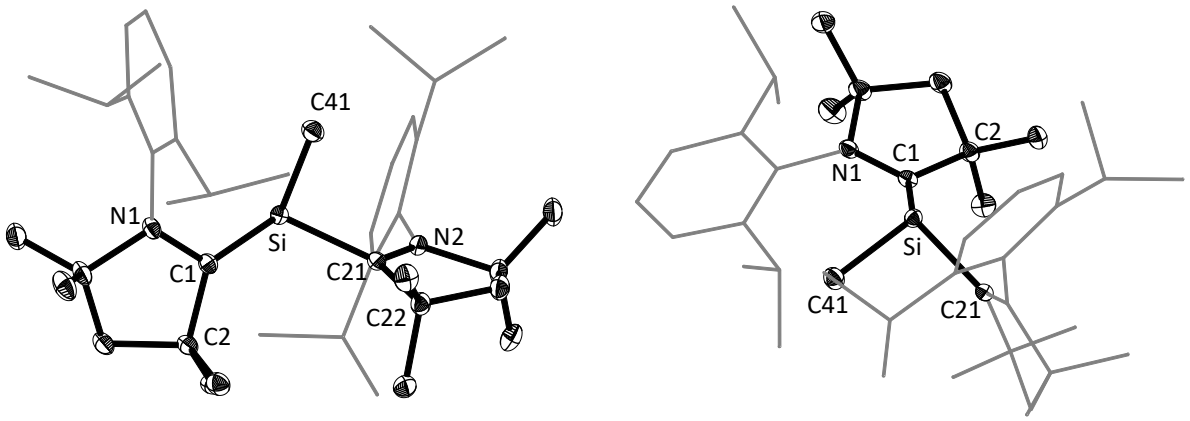

Figure 2.91. (Left) DIAMOND plot of the molecular structure of the cation of **19-Me**, thermal ellipsoids are set at 30 % probability level and hydrogen atoms were omitted. In the depicted structure the Dipp substituent of the caac^{Me} ligand is presented in the wire-frame for the sake of clarity. Selected bond lengths [Å], bond angles [°] and torsion angles [°]: Si1–C1 1.890(2), Si1–C21 1.970(2), Si1–C41 1.907(2), N1–C1 1.339(2), N2–C21 1.308(2), C1–Si–C21 117.39(8), C1–Si–C41 108.91(9), C41–Si–C21 95.10(9), C41–Si–C1-N1 48.9(2), C41–Si–C21–N2 –89.1(2), C1–Si–C21–N2 156.5(2), C21–Si–C1–N1 155.3(2). (Right) Different view of **19-Me** illustrating the relative orientation of the Dipp substituents in the 2-aminosilene moiety; hydrogen atoms were omitted, the Dipp substituents of the caac^{Me} ligand and the orthogonal orientated caac^{Me} ligand are presented in the wire-frame for the sake of clarity.

Single crystals suitable for a X-ray diffraction analysis of **19-Me** were obtained from a mixture of Et_2O/*n*-hexane (1:2) at 4 °C. The molecular structure features a three coordinate slightly pyramidalized ($\Sigma\measuredangle$(Si) = 321.4°) silicon(II) center with a singly bonded methyl substituent (d(Si–C^{Me}) = 1.907(2) Å). The two carbene ligands are orientated orthogonal with respect to each other (carbene to carbene twist angle 68.2(1)°), leading to an overall C_1-symmetry of the cation. The carbene orientated in the plane of the SiMe moiety, features a significant shortened Si–C^{CAAC} bond length of 1.890(2) Å, compared to the out of plane lying carbene (1.970(3) Å), indicating a significant π-character in the Si–C^{CAAC} bond. The N-Dipp moiety of the in-plane lying caac^{Me} carbene is orientated towards the Me-group (*Figure 2.91* right). Thus, according to the priority rules applied for *E*/*Z* alkenes, according to IUPAC, the stereodescriptor ***E*** can be assigned. The Si–C^{CAAC} bond of 1.890 Å in **19-Me** lies in the upper limit of Si–C^{CAAC} bonds in pyramidal 2-(amino)silenes reported in this work (1.796(2) – 1.897(3) Å). The shortened Si–C^{CAAC} bond length of the caac^{Me} in the plane, which consists of the atoms C1-Si-C41, is connected to a N–C^{CAAC} (1.339(2) Å) bond that is longer than that of the other caac^{Me} group (1.308(2) Å). The compound can be strikingly viewed as caac^{Me}-stabilized 2-amino-silenylidene cation. In terms of its structural parameters compound **19-Me** clearly differs from [SiH(caac^{Me})$_2$][B(Ar^F)$_4$], which features a delocalized π-system over both Si–C^{CAAC} bonds, but compares rather well to [SiI(caac^{Me})$_2$]I and [SiI(I*i*Pr$_2$Me$_2$)(caac^{Me})]I (*Table 2.44*).

Table 2.44. Selected structural paramters of **19-Me** in comparison to literature known compounds

Comp.	Si–C^{CAAC} / Å	N–C^{CAAC} / Å	Σ∢(Si) / (deg)	DP[a] / %	$\tau_{carbene}$[b] / (deg)	Ref.
$SiBr_2(caac^{Me})$ **1**	2.017(2)	1.301(3)	289.9	78	–	
$SiBr\{OMes^*\}(caac^{Me})$ (**2-O**)	1.897(3)	1.342(4)	321.6	43	–	*this*
$[SiMe(caac^{Me})_2][B(Ar^F)_4]$	1.890(2)	1.339(2)	321.4	43	68.2(1)	*work*
(**19-Me**)	1.970(2)	1.308(2)				
$[SiH(caac^{Me})_2]I$ (**II-73**)	1.867(2)	1.331(2)	330.3	33	42.2(2)	[300]
	1.881(2)	1.316(2)				
$[SiI(caac^{Me})_2]I$	1.937(2)	1.323(3)	314.5	51	74.9(3)	[175]
	2.011(2)	1.311(3)				
$[SiI(IiPr_2Me_2)(caac^{Me})]I$	1.878(5)	1.332(6)	322.9	41	95.6(3)	[121]
	1.946(5)	1.360(6)				
$Si(caac^{Me})_2$ (**II-63**)	1.841(2)	1.378(2)	–	–	53.0(2)	[119]
	[1.842(2)]	[1.378(2)]				
	1.847(2)	1.374(2)				
	[1.848(2)]	[1.387(2)]				

[a]: DP the degree of pyramidalization (DP) value of 0 % describes a trigonal planar coordination of the silicon atom with the sum of bond angles equal to 360 °. A DP value of 100 % corresponds to a trigonal pyramidal coordination of the silicon atom with the sum of bond angles equal to 270 °. DP (in %) = 100 % · [360 − Σ∢(Si) / (deg)]/90

[b]: The carbene to carbene twist angle ($\tau_{carbene}$) is defined as the angle between the two carbene coordination planes defined by the atoms N1–C1–C2 for $caac^{Me}$-1 and N2–C21–C22 for $caac^{Me}$-2 (N2–C21–N3 for I*i*Pr_2Me_2), respectively.

The $^{29}Si\{^1H\}$-NMR spectrum of **19-Me** in (D_8)THF at ambient temperature displays a signal at 5.97 ppm, which is drastically upfield shifted compared to the silylone $Si(caac^{Me})_2$ (66.5 ppm)[119] and significantly downfield shifted, when compared to $[SiH(caac^{Me})_2][B(Ar^F)_4]$ (–24.4 ppm).[300] The ^{29}Si resonance of **19-Me** (5.97 ppm) compares well to the $caac^{Me}$-stabilized silicon(I) dimer $Si_2Me_2(caac^{Me})_2$ (0.72 ppm). The $^{13}C^{CAAC}$ and $^{15}N^{CAAC}$ resonances in **19-Me** (216.1 ppm, 201.8 ppm) are remarkably downfield shifted, when compared to $Si(caac^{Me})_2$ (210.9 ppm, 153.2 ppm),[119] suggesting a lower π-character in the Si–C^{CAAC} bond compared to $Si(caac^{Me})_2$, which features a delocalized π-system over the C^{CAAC}–Si–C^{CAAC} bonds. According to the ^{15}N NMR scale reported by Roesky et al.[108] the $^{15}N^{CAAC}$ resonance in **19-Me** (201.8 ppm) lies in the range of 210 – 180 ppm, which is indicative for a strong C^{carb} → Si σ-donation, accompanied by a weak Si → C^{carb} π-backdonation in **19-Me**.

2.7.4.1 Study of the dynamics in 19-Me by VT-NMR spectroscopy

^{1}H, ^{13}C{^{1}H} and ^{29}Si{^{1}H} NMR spectra in (D_8)THF at ambient temperature display an averaged C_S-symmetry (*Figure 2.92*, top spectrum), in contrast to the C_1-symmetry observed in the solid state. This can be highly likely attributed to two dynamic processes in **19-Me** at ambient temperature in solution: a pyramidal inversion of the trigonal pyramidalized silicon center via a trigonal planar transition state (*Figure 2.93*, top) and a rotation of the caac^{Me} substituents about their respective Si–C^{carb} bonds (*Figure 2.93*, bottom). The first process consequently leads to one set of homotopic resonances for the caac^{Me} substiuents, which probably proceeds via a low energy barrier and is still active in the recorded low temperature limit spectrum of **19-Me**, thus explaining the observed C_2-symmetry in the ^{1}H NMR spectrum of **19-Me** in (D_8)THF solution at –80 °C (*Figure 2.92*, bottom spectrum).

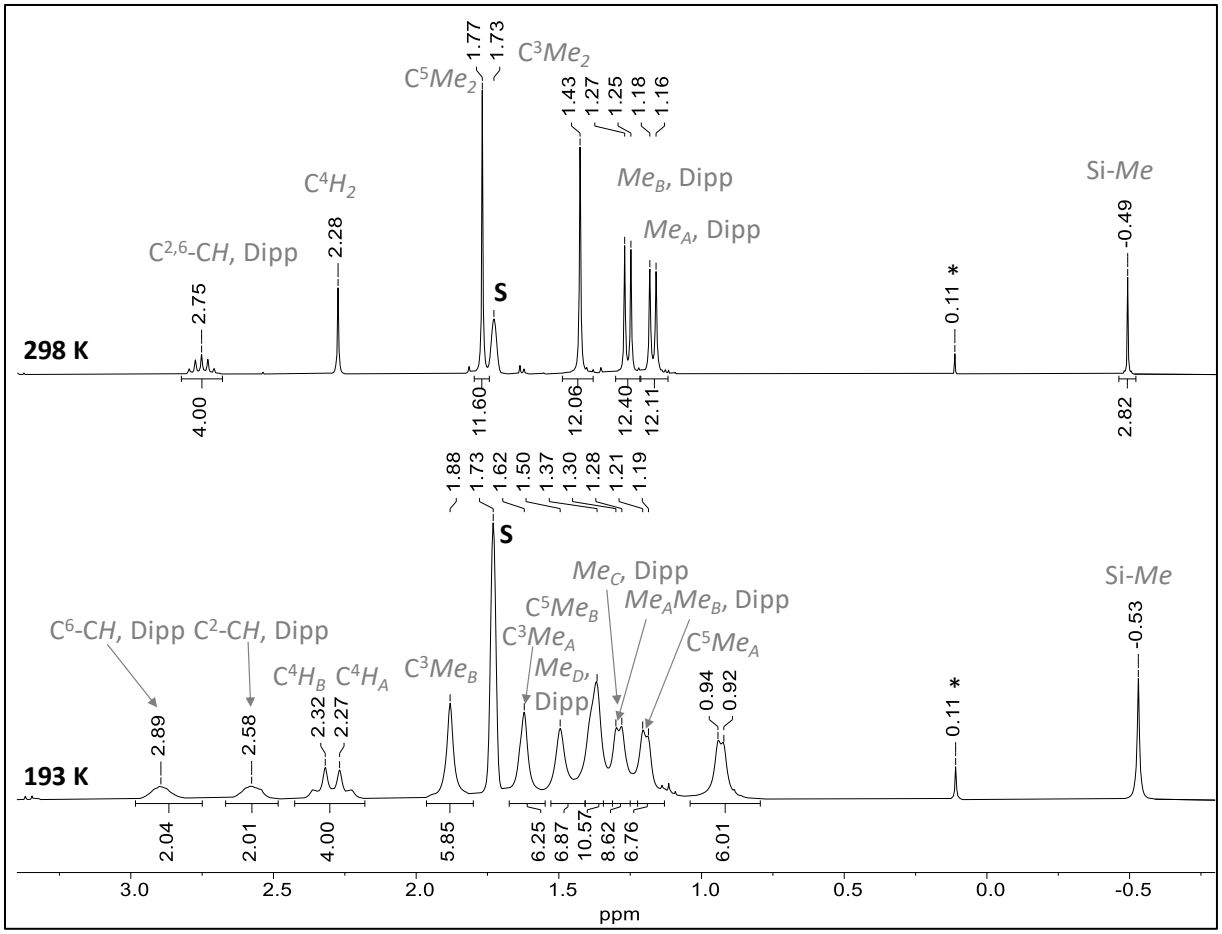

Figure 2.92. Excerpt of the ^{1}H NMR spectra (300.14 MHz) of **19-Me** in (D_8)THF at 243 K (bottom) and 298 K (top); signals of the deuterated solvent are marked with the character **S.** The signal marked with the symbol (*) corresponds to tiny amounts of silicon-grease originated from the used syringe.

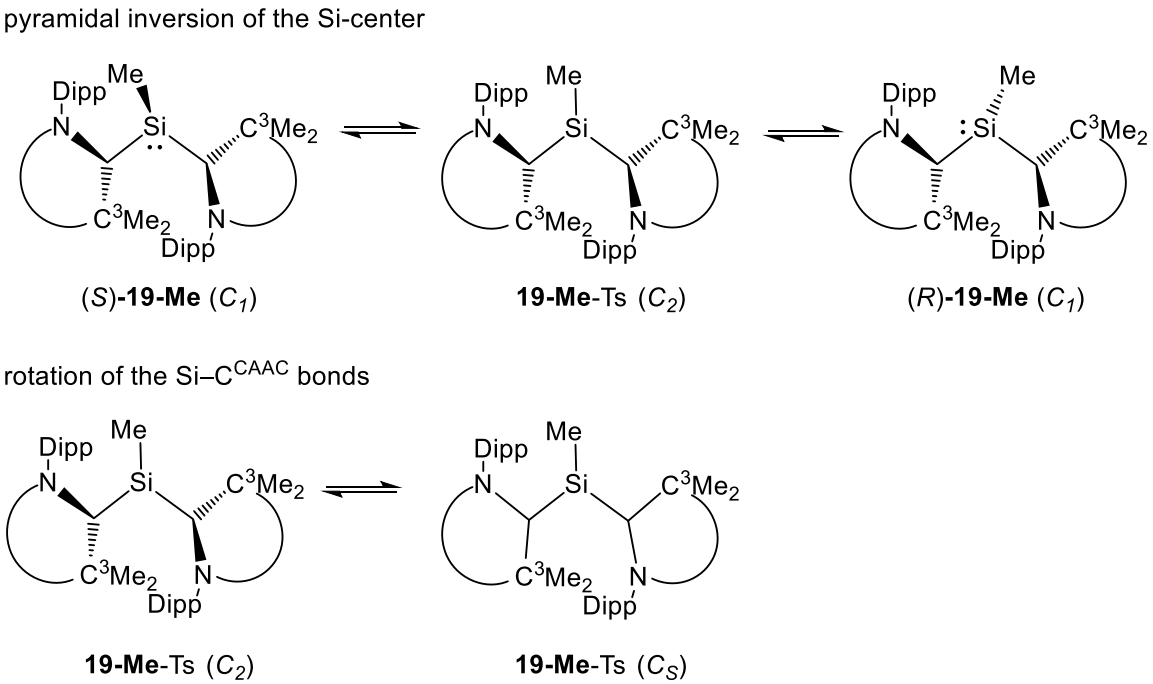

Figure 2.93. Dynamic processes of **19-Me** at ambient temperature in solution, which can be rationalized upon pyramidal inversion of the chiral silicon center via a planar transition state (top) and the rotation of the caac^{Me} substituents about their respective Si–C^{CAAC} bonds (bottom).

The second process, i. e. the rotation of the caac^{Me} substituents about their respective Si–C^{carb} bonds, enables the coplanar orientation of the caac^{Me} substituents in the trigonal planar transition state **19-Me**-TS and thus leads to a mirror plane bisecting the N–C^{carb}–C^{3}Me$_2$ carbene planes, enabling the observed C_S-symmetry and thus rationalizing the simple ^{1}H NMR spectrum of **19-Me** (*Figure 2.92*, top spectrum) at ambient temperature.

Line shape analysis of the recorded VT ^{1}H NMR spectra in (D$_8$)THF (for details see *section 5.6.3*) gave the activation parameters of the second dynamic process: $\Delta H^{\ddagger} = 30.8 \pm 0.5$ kJ mol^{-1} and $\Delta S^{\ddagger} = -58.4 \pm 2.3$ J K^{-1} mol^{-1}. Using the Gibb's Helmholtz equation the free enthalpy of activation was calculated and found to be $\Delta G^{\ddagger}(298K) = 48.2 \pm 0.8$ kJ mol^{-1} for the rotation of the Si–C^{carb} bond in **19-Me**.

2.8 Reactions of CAAC-Stabilized Dibromosilylene with Transition Metal Complexes

2.8.1 Introduction

Over the past two decades NHC-stabilized silicon(II) halides have received considerable attention as σ-donor ligands in transition metal chemistry.[90] $SiCl_2$(IDipp) for example, reacts with a variety of transition metal carbonyls to generate mono-and bis-substitution products (*Scheme 2.30*). Reaction of $SiCl_2$(IDipp) with $Fe_2(CO)_9$, $CpCo(CO)_2$ and $CpV(CO)_4$ led to the formation of transition metal complexes **II-77**, **II-78** and **II-79**.[301] Similarly reaction of $SiCl_2$(IDipp) with $Ni(CO)_4$, $Co_2(CO)_8$ and $Rh(CO)_2Cl_2$ led to the formation of the transition metal complexes **II-80**[302], **II-81**[303] and **II-82**.[304]

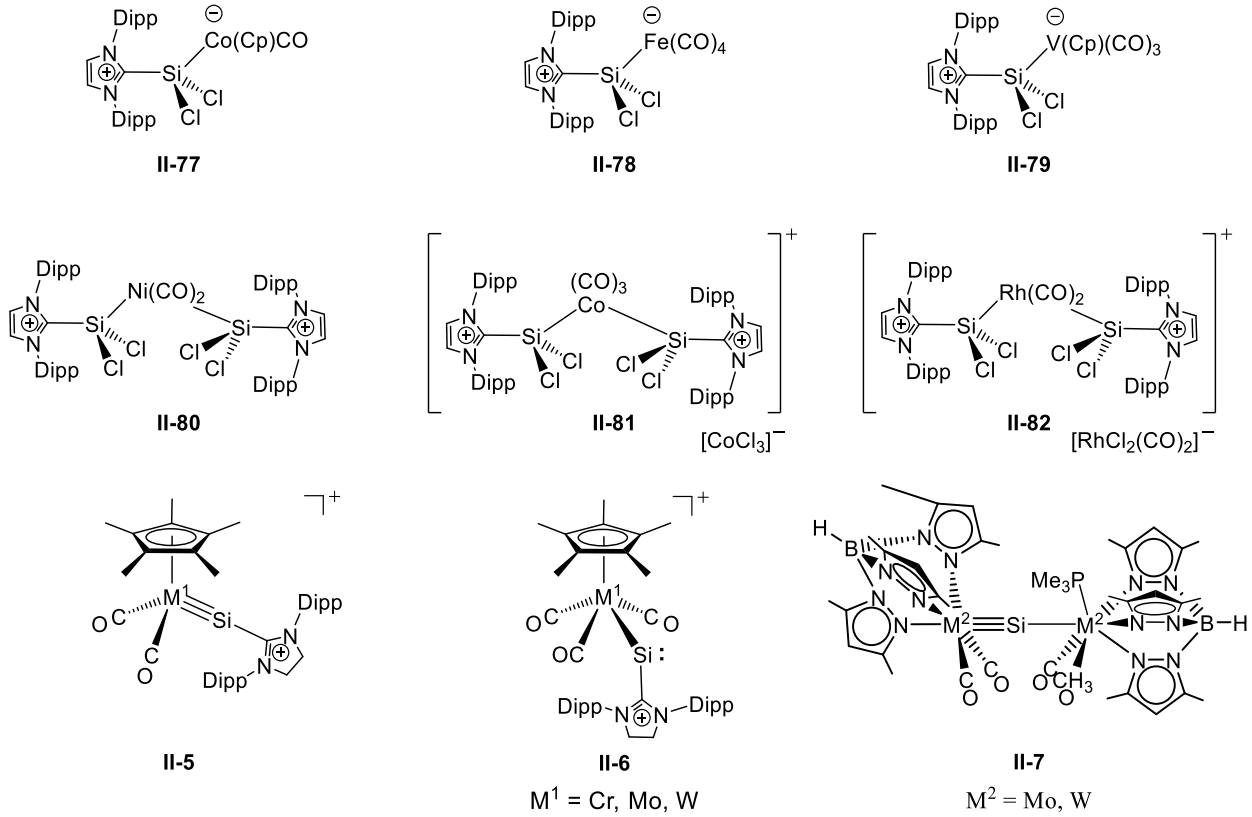

Scheme 2.30. Carbonyl substitution products (**II-76** – **II-78**) and (**II-79** – **II-81**), metalsilylidyne complexes **II-5**, metallosilylenes **II-6** and metallasilylidynes **II-6**.

Reaction of $SiBr_2$(SIDipp) with metallates $Li[Cp^*M(CO)_3]$ (M = Cr, Mo, W) led via elimination of CO to the metallo-silylidene complexes $(Cp^*)M(CO)_2$=SiBr(SIDipp) (M = Cr, Mo, W), which enabled the isolation of silylidynes **II-5**, and metallosilylenes **II-6**.[182] The metallates $Li[Tp'M(CO)_2(PMe_3)]$ (M = Mo, W) reacted with $SiBr_2$(SIDipp) in 2:1 fashion leading to the metallasilylidynes **II-7**.[183]

Remarkably, the reactivity of cyclic (alkyl)(amino)carbene-stabilized dihalosilylenes towards transition metals was not studied so far. This might be attributed to the fact that $SiI_2(caac^{Me})$ appeared to be the only example in the literature of a CAAC-stabilized dihalosilylene.[121]

Reaction of $SiBr_2(caac^{Me})$ (**1**) with one equivalent of $Na[CpCr(CO)_3]$, $Na[CpMo(CO)_3]$ as well as $Na[Tp'Mo(CO)_2(PMe_3)]$ in (D_6)benzene at ambient temperature, did not yield any of the Si-containing products. ^1H NMR spectrosocopy, instead, revealed the rather selective formation of $Si_2Br_2(caac^{Me})_2$ (**9-Br**), as evidenced by the distinct color change of the reaction solutions to red-purple.

2.8.2 Synthesis of $CpCo(CO)SiBr_2(caac^{Me})$ (20)

Stirring a dark red solution of $SiBr_2(caac^{Me})$ (**1**) with $CpCo(CO)_2$ in toluene at ambient temperature under partial vacuum for 24 h let to a color change to dark-green. Monitoring of the reaction mixture by ^1H NMR spectroscopy in (D_6)benzene revealed the quantitative formation of **20**. After work up **20** was isolated as dark green microcrystalline solid in 81 % yield. The compound slowly decolorizes upon contact with air and decomposes upon melting at 172 °C. The adduct is insoluble in *n*-hexane, moderately soluble in benzene and toluene and well soluble in THF and diethylether affording dark green solutions.

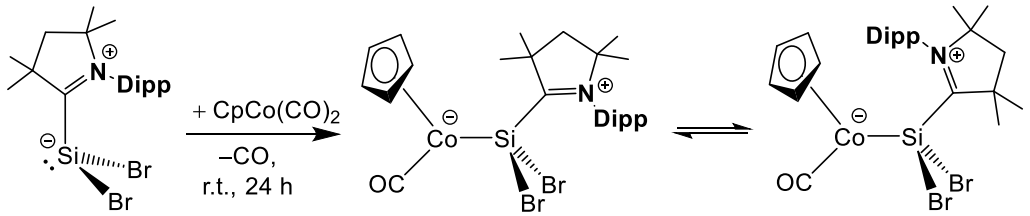

Figure 2.94. Synthesis of transition metal complex **20**, starting from dibromosilylene **1**.

Interestingly compound **20** features two very strong CO stretching vibrations in the solid state at 1889 cm^{-1} and 1868 (vs) cm^{-1}, suggesting the formation of two conformers. At ambient temperature in solution an averaged CO stretching vibration is observed (toluene: 1877 cm^{-1}, *n*-hexane: 1879 cm^{-1}), suggesting a fast interconversion of the two isomers in solution. The result is in line with ^1H NMR spectroscopy of **20** in (D_8)toluene, revealing broadened signals of the $caac^{Me}$ substituent at ambient temperature (*Figure 2.95*, middle), an observed C_1-symmetry at 243 K (*Figure 2.95*, bottom) and an averaged C_S-symmetry in the high temperature limit spectrum (*Figure 2.95*, top). Line shape analysis of the recorded VT ^1H NMR spectra of **20** (see *section 5.6.2*) gave the thermodynamic parameters for the activation process involving a hindered rotation of the $caac^{Me}$ around the $Si–C^{CAAC}$ bond: $\Delta H^{\ddagger} = 48.6 \pm 1.0$ kJ mol^{-1} and $\Delta S^{\ddagger} = -23.8 \pm 1.6$ J K^{-1} mol^{-1}. Using the Gibb's Helmholtz equation the free energy of activtation was calculated to be $\Delta G^{\ddagger}(298K) = 55.6 \pm 1.0$ kJ mol^{-1}.

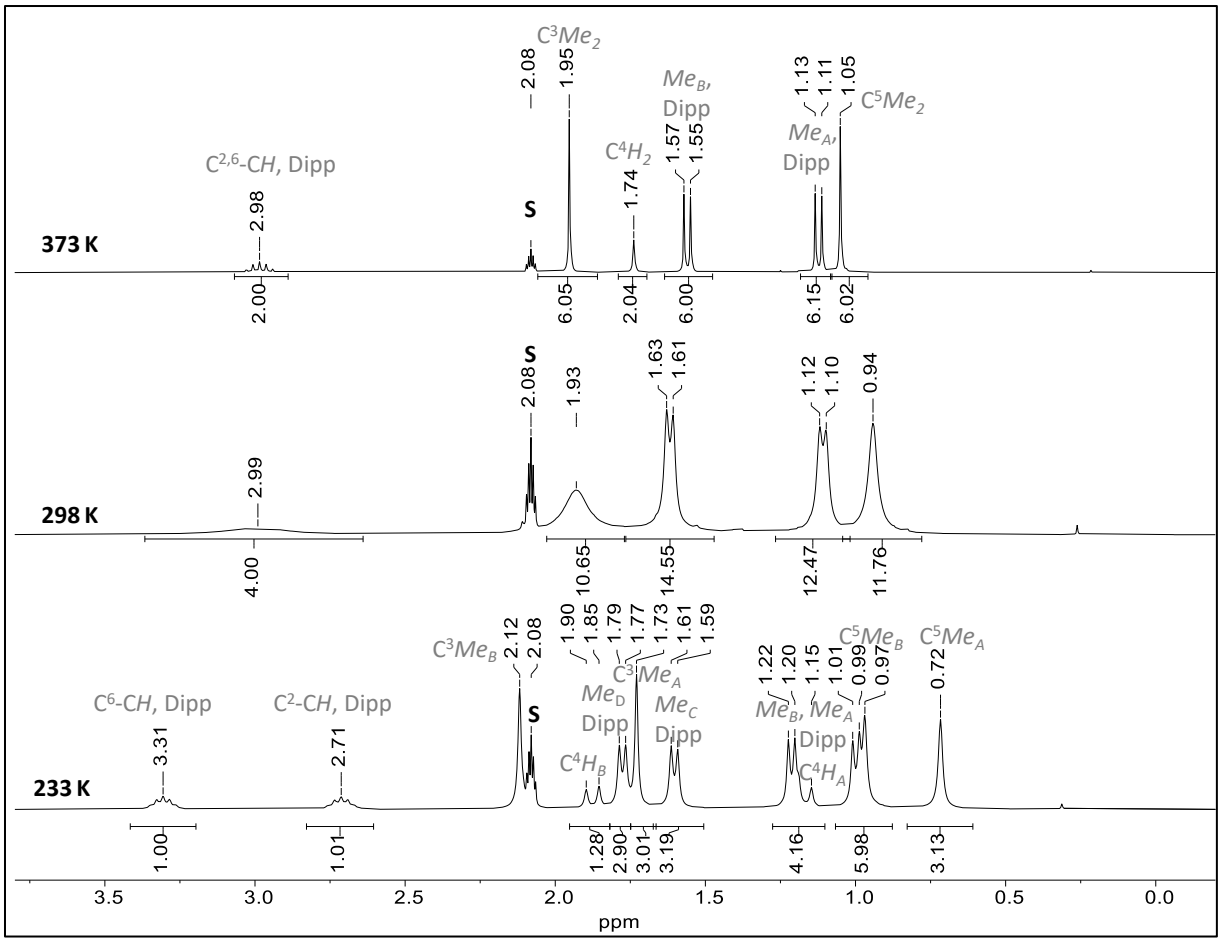

Figure 2.95. Excerpt of the ^{1}H NMR spectra (300.14 MHz) of **20** in (D$_8$)toluene at 233 K (bottom), 298 K (middle), 373 K (top); signals of the deuterated solvent are marked with the character **S**.

The ^{29}Si{^{1}H} NMR resonance of **20** (14.9 ppm) compares rather well to that of the starting material **1** (14.4 ppm) and lies in-between that of the dichlorosilylene (**II-77**) and diiodosilylene (**II-76**) cobaltcomplexes (*Table 2.45*). The $^{13}C^{CAAC}$ and $^{15}N^{CAAC}$ resonances of **20** (215.7 ppm, 228.7 ppm) are upfield shifted compared to **1** (231.2 ppm, 231.3 ppm).

Table 2.45. Selected multi-nuclear NMR chemical shift values of **20** compared to literature known carbonyl substitution products.

Comp	δ($^{13}C^{carb}$) / ppm	δ(^{29}Si) / ppm	δ(^{15}N)[a] / ppm	Ref.
$SiBr_2(caac^{Me})$ **1**	231.2[b] ($\Delta\nu_{1/2}$= 23 Hz)	14.35[b] ($\Delta\nu_{1/2}$= 17 Hz)	231.3[b]	*this work*
$CpCo(CO)SiBr_2(caac^{Me})$ **20**	215.7[c]	14.9[c]	228.7[c]	
$Cp^*Co(CO)SiI_2(caac^{Me})$ (**II-76**)	216.0[c]	–57.6[c]	225.8[c]	[144]
$Cp^*Co(CO)SiCl_2$(IDipp) (**II-77**)	155.0[d]	31.86[d]	–	[301]
$Fe(CO)_4SiCl_2$(IDipp) (**II-78**)	–[e]	59.20[d]	–	[301]
$Cp^*V(CO)_3SiCl_2$(IDipp) (**II-79**)	–[e]	88.70[d]	–	[301]

[a]: ^{15}N NMR resonance of the nitrogen atom(s) in the carbene ring referenced against NH_3(l). [a]: (D$_8$)THF, 243 K. [c]: (D$_6$)benzene, 298 K. [d]: (D$_2$)dichloromethane, 298 K. [e]: signal not assigned.

3 Summary and Outlook

3.1 Summary

The cyclic (alkyl)(amino)carbene-supported dibromosilylene $SiBr_2(caac^{Me})$ (**1**) was obtained via an optimized synthesis, which involves a reductive dehalogenation of $SiBr_4(caac^{Me})$ with two equivalents of KC_8 in benzene and was isolated in 68 % yield. The compound was characterized by NMR spectroscopy and X-ray diffraction analysis and was analyzed by quantum chemical calculations.

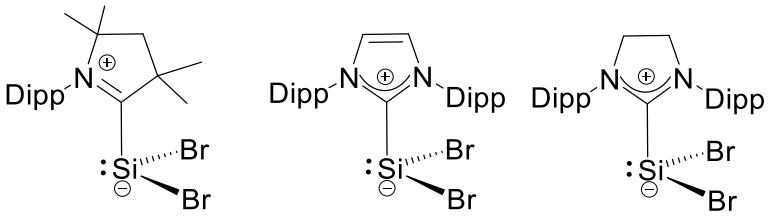

1 **1-NHC^1** **1-NHC^2**

Figure 3.1. Comparison of $SBr_2(caac^{Me})$ (**1**) to literature known NHC-stabilized dibromosilylenes $SiBr_2$(IDipp) (**1-NHC^1**)[69] and $SiBr_2$(SIDipp) (**1-NHC^2**).[71]

The key features of the $caac^{Me}$-stabilized dibromosilylene **1** are:

- a trigonal pyramidalized silicon(II) center ($\Sigma\measuredangle$(Si) = 289.9°)
- a Si–C^{carb} single bond (2.017(2) Å), which compares well to Si–C^{carb} single bonds of NHC-stabilized dibromosilylenes (1.989(3) Å (**1-NHC^1**)[69], 2.012(2) Å (**1-NHC^2**)[71]
- unlike the related NHC-supported silicon(II)dihalides, compound **1** undergoes a redox-disproportionation at ambient temperature in solution, leading to an equilibrium mixture of **1**, the radical $SiBr_3(caac^{Me})^{\bullet}$ and $Si_2Br_2(caac^{Me})_2$ (**9-Br**)

According to the structural and spectroscopic data the Si–C^{carb} bond in **1** can be best described as a polarized $Si^{\delta+}$–$C^{\delta-}$ donor-acceptor single bond. In terms of the structural properties compound **1** compares well to the NHC-supported silicon(II)-dihalide $SiBr_2$(SIDipp) (**1-NHC^2**). Quantum chemical calculations, at the B97-D3(BJ)-ATM/def2-TZVP level of theory, however, reveal a remarkably smaller HMO–LUMO gap in **1** ($E_{HOMO-LUMO}$ = 1.76 eV), in comparison to NHC-stabilized dibromosilylenes $SiBr_2(NHC^{1,2})$ ($E_{HOMO-LUMO}$ = 2.43 eV (NHC^1 = IDipp) 2.47 eV (NHC^2 = SIDipp)), as well as a significant increased Si–C^{carb} bond strength in **1** ($\Delta E_{int} = -BCE = -237.9$ kJ mol^{-1}), which can be attributed to a greater σ-donation strength of the CAAC carbene in dibrommosilylene $SiBr_2$(carbene) in comparison to NHCs.

Starting from **1**, an unique approach to caac^{Me}-supported silicon(II) compounds was achieved by metathetical exchange with C, Si, N, P and O-centered nucleophiles. Thus a series of novel Si(II) bromides of the general formula SiBr(Nu)(caac^{Me}) (Nu = $SiTMS_3$ (**2-Si**), $PMes_2$ (**2-P**), Mes (**2-Mes**), $NTMS_2$ (**2-N**), OMes* (**2-O**)) were obtained (*Scheme 3.1*). All compounds were isolated as crystalline thermally stable solids and were fully characterized, also by X-ray diffraction analysis. The key features of the silicon(II) bromides are:

- shortened Si–C^{carb} bonds (1.836(2) – 1.897(3) Å), which lie in between that of a typical Si=C double bond (1.702 – 1.764 Å)[184] and a classical Si–C^{carb} single-bond (1.963(2) Å)[80]
- sum of bond angles at the Si-center ranging from 321.6 – 336.5°, which lie in-between that of classical silenes ($\Sigma\measuredangle$(Si) = 360°) and pyramidalized silylenes ($\Sigma\measuredangle$(Si) = 289.9° (**1**))
- an observed C_1-symmetry in the solid state and a time averaged C_S-symmetry in solution at ambient temperature according to ^{1}H NMR spectroscopy in (D_6)benzene

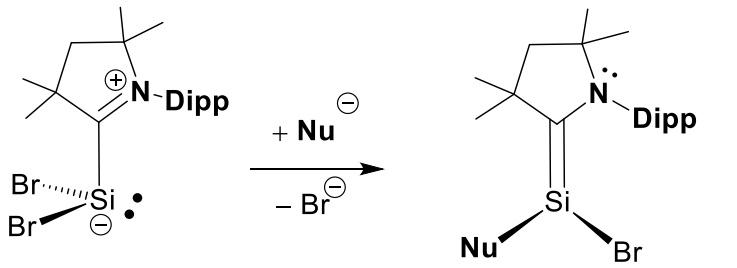

Scheme 3.1. Synthesis of pyramidal 2-(amino)silenes SiBr(Nu)(caac^{Me}) (**2-Nu**) upon reaction of **1** with nucleophiles.

In summary compounds **2-Si**, **2-Mes**, **2-P**, **2-N** and **2-O** can be best described as pyramidal or zwitterionic 2-(amino)silenes, which feature the borderline case between a trigonal pyramidailzed Lewis-base stabilized silylene and a trigonal planar silene. Their low inversion barriers ($\Delta G^{\ddagger}$ = 15 – 27 kJ mol^{-1}), calculated at the RI-B97D3/def2-TZVPP level of theory, enable a fast (*R*)-/(*S*)-enantionemerization in solution, which lead to NMR spectra with averaged C_S-symmetry. Given the silenic character of the Si=C^{CAAC} bond no *E*/*Z*-isomerization via the rotation about the Si–C^{CAAC} bond is observed in solution nor in the solid state. Interestingly though, all these compounds **2-Si** – **2-O** could be only isolated as *Z*-isomers, thus grants it their name as pyramidal (*Z*)-2-(amino)silenes.

The nature of different *E*,*Z*-diastereomers in pyramidal 2-(amino)silenes could be investigated, upon isolation of SiBr(Eind)(caac^{Me}) (**2-Eind**). Reaction of two equivalents of caac^{Me} carbene with Eind-disilene (*E*)-[Eind(Br)Si=Si(Br)Eind][23,25,305] in benzene at 60 °C led to the formation of **2-Eind-*E*** and **2-Eind-*Z*** as diastereomeric mixture. Interestingly, **2-Eind** featured a thermal induced ***E*** → ***Z*** isomerization. Both compounds were fully characterized, also by X-ray diffraction analysis and the kinetics of the process studied by variable temperature ^{1}H NMR experiments.

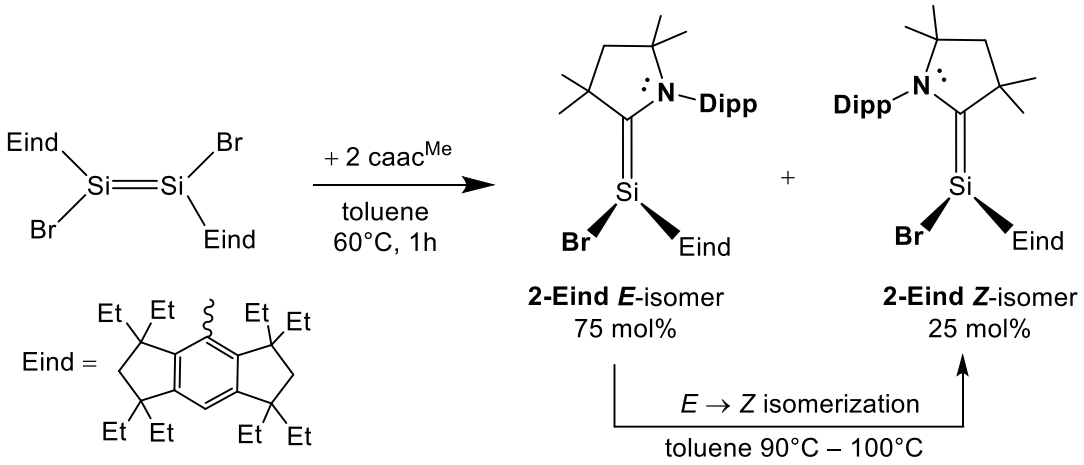

Scheme 3.2. Reaction of Eind-Disilene (*E*)-[Eind(Br)Si=Si(Br)Eind] with two equivalents of caac^{Me} carbene in toluene at 60 °C.

Compound **2-Eind-*Z***, compares well to the pyramidal 2-(amino)silenes mentioned above, whereas **2-Eind-*E***, differs remarkably, which can be shown by the following features:

- a rather short Si–C^{carb} bond (1.768(3) Å) which compares well to typical Si=C bonds reported in silenes (1.702 – 1.764 Å)[184]
- a trigonal planar coordinated silicon-center (Σ∢(Si) = 356.9°)
- the observed C_1-symmetry in the solid state is reflected in the ^{1}H-NMR spectrum at ambient temperature
- the ^{15}N^{CAAC} resonance (100.4 ppm) lies below the treshhold of 160 ppm, suggesting a much stronger the Si–C^{carb} π-acceptance than σ-donation

These findings suggest that **2-Eind-*E***, can be rather described as a twisted 2-(amino)silene with a rigid structure in solution. Detailed kinetic studies show that compound **2-Eind-*E*** undergoes an *E* → *Z* isomerization at 90 – 110 °C with an activation barrier of 115.1 ± 1.7 kJ mol^{-1}, $\Delta H^{\ddagger}$ = 112.6 ± 1.7 kJ mol^{-1}, $\Delta S^{\ddagger}$ = –8.3 ± 0.2 J K^{-1} mol^{-1}. The isomerization process occurs highly likely by the rotation of the Si–C^{carb} bond similar to that of alkenes.

Preliminary reactivity studies of pyramidal 2-(amino)silenes could clearly show, that the bromine substituent can be replaced with smaller nucleophiles. Reaction of SiBr(R)(caac^{Me}) (R = SiTMS$_3$ (**2-Si**), NTMS$_2$ (**2-N**)) with NaBEt$_3$H in toluene at ambient temperature selectively afforded the hydridosilenes SiH(R)(caac^{Me}) (R = SiTMS$_3$ (**5-Si**), NTMS$_2$ (**5-N**)), respectively. The compounds were independently synthesized upon reaction of the silicon(I) radicals Si(R)(caac^{Me}) (R = Si(SiMe$_3$)$_3$ (**3-Si**), N(SiMe$_3$)$_2$ (**3-N**)) with 1,4-cyclohexadiene. Compound **5-Si** was fully characterized, also by X-ray diffraction analysis, whereas compounds **5-N** and **8** were charactized by NMR spectroscopy.

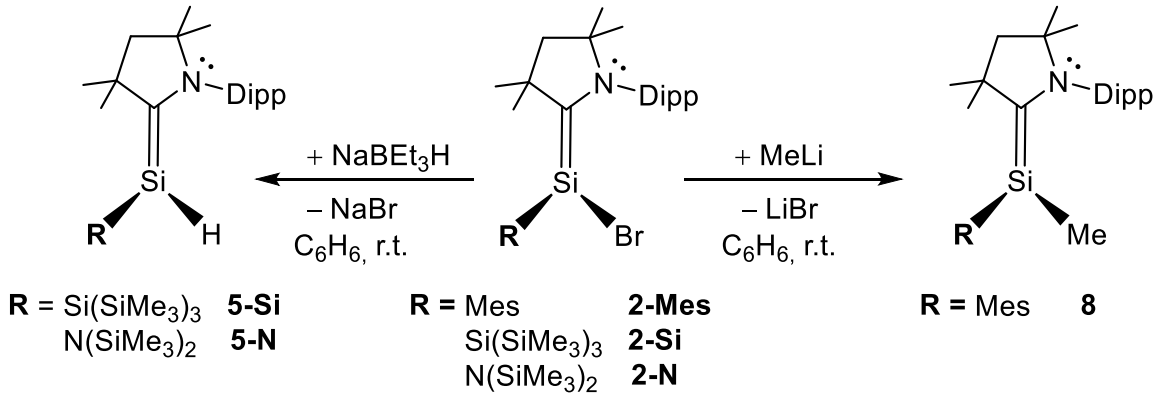

Scheme 3.3. Reaction of **2-Mes**, **2-Si** and **2-N** towards MeLi and NaBEt$_3$H yielding the corresponding functionalized silicon(II) compounds.

Reaction of a solution SiBr(Mes)(caac^{Me}) (**2-Mes**) in benzene with 1.0 equiv. of MeLi selectively afforded the substituted silene SiMe(Mes)(caac^{Me}) (**8**) which was isolated and characterized by NMR spectroscopy. NMR spectroscopic features of **8** suggest a much more planarized structure in comparison to the starting material **2-Mes**.

Reduction of novel pyramidal 2-(amino)silenes SiBr(R)(caac^{Me}) by 1e$^-$ with KC_8 in benzene provided to be particulary interesting, enabling the isolation of a plethora of unprecedent caac^{Me}-stabilized silicon(I) compounds with intriguing bonding features and synthetic potential. Depending on the substituent R of the used 2-(amino)silene a different outcome was observed: Sterical high demanding substituents enabled the isolation of neutral two-coordinated silicon(I) radicals Si(R)(caac^{Me}) (R = $SiTMS_3$ (**3-Si**), $NTMS_2$ (**3-N**), OMes* (**3-O**)), the isolation of which remained elusive thus far. All three compounds were isolated as crystalline thermolabile solids and were fully characterized, also by X-ray diffraction analysis. The key features of these silicon(I) radicals are

- a V shaped geometry at the divalent silicon-center (112.9(1)°(**3-Si**), 106.6(2)° (**3-N**), 100.1(1)° (**3-O**))
- the Si–C^{carb} bond lengths (1.870(2) Å (**3-Si**),1.895(4) Å (**3-N**), 1.865(2) Å (**3-O**)) feature partial double bond character
- with increase of electronegativity of the substituent (Si < N <O), the caac^{Me} carbene increasingly aligns with the substituent in co-planar fashion, the ^{29}Si hfcc's decrease: 3.73 mT (**3-Si**) > 1.95 mT (**3-N**) > 1.24 mT (**3-O**) and the ^{14}N hfcc's increase 0.44 mT (**3-Si**) < 0.57 mT (**3-N**) <0.62 mT (**3-O**)

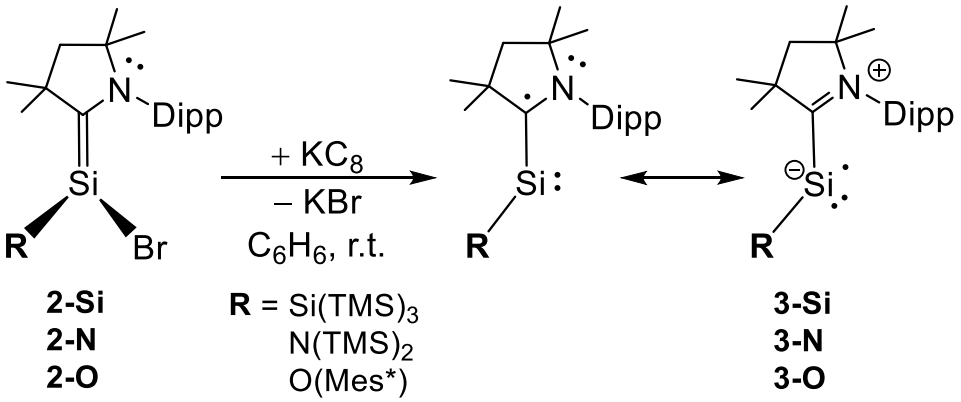

Figure 3.2. Synthesis of neutral two-coordinated silicon(I) radicals **3-Si, 3-N** and **3-O**.

The compounds can be best described as π-type radicals, in which the spin density of the unpaired electron is mainly distributed between the Si, C^{carb} and N^{CAAC} atoms. Quantum chemical calculations reveal a decrase of the spin density at the silicon atom with increasing electronegativity of the substituents (56 % (**3-Si**) > 49 % (**3-N**) > 32 % (**3-O**)), which consequently leads to an increase of the spin density at the C^{carb} and N^{CAAC} atoms (23 %,15 %(**3-Si**) < 29 %, 19 % (**3-O**) < 37 %, 22 % (**3-O**). These results are line with the experimental observations (decrease of the ^{29}Si hfcc's, increase of the ^{14}N hfcc's with increasing electronegativity of the substituents).

Reduction of the pyramidal 2-(amino)silene SiBr(PMes$_2$)(caac^{Me}) (**2-P**) by 1e$^-$, using KC_8 in benzene at ambient temperature led to the formation of an intermediate dark purple colored silicon(I) radical [Si(PMes$_2$)(caac^{Me})]$^{\#}$, which upon 1,2-Mes migration transformed itself to the unprecedent phosphanyl radical (Mes)P=Si(Mes)(caac^{Me}) (**6**). The compound could be isolated as orange-red microcrystalline solid and was fully characterized. The key features of radical **6** are

- a trigonal planar coordinated silicon center ($\Sigma\measuredangle$(Si) = 359.9°)
- a Si=P bond (2.108(1) Å), which compares well to that of literature known phosphasilenes (2.062(1) – 2.1585(9) Å)[215]
- the Si–C^{carb} bond length (1.813(2) Å)) is significantly shorter than the starting material and two-coordinated silicon(I)-radicals mentioned above
- ^{31}P hyperfine coupling constant (3.74 mT) is significantly smaller than that of literature known two-coordinate phosphanyl radicals (6.5 – 10mT),[219,220] suggesting a high degree of hyperconjugation of the unpaired electron among the P, Si and C^{carb} atoms

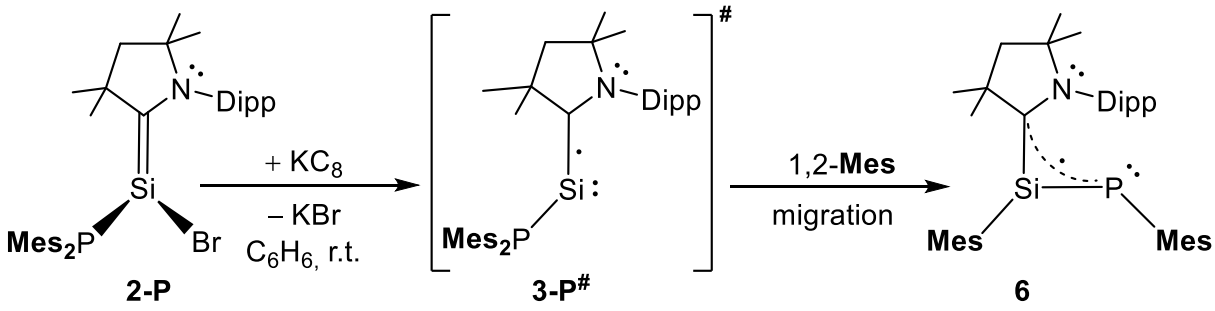

Figure 3.3. Synthesis of the phosphanyl radical **6** upon reduction of pyramidal 2-(amino)silene **2-P**.

Quantum chemical caluclations of **6** are in line with the experimental results and suggest a π-type of radical in **6** with the spin density mainly distributed between the P (43 %), Si (0 %), C^{carb} (38 %) and N (19 %) atoms. Thus **6**, can be best described as (silenyl)phosphanyl-radical.

Reduction of SiBr(Mes)(caac^{Me}) (**2-Mes**) by 1e$^-$ with KC_8 in benzene led to the formation of the neutral caac^{Me}-stabilized disilicon(I) compound Si_2Mes_2(caac^{Me})$_2$ (**9-Mes**), which was obtained as a mixture of two diastereomers *Z,Z* and *E,E*. Both compounds were fully characterized, also by X-ray diffraction analysis. Upon heating of the diastereromeric mixture an irreversible *Z,Z* → *E,E* isomerization was observed, the kinetics of which were studied by variable temperature ^{1}H NMR spectroscopy. The key features of both compounds are:

- trigonal planar coordinated silicon centers in **9-Mes-*Z,Z***($\Sigma\measuredangle$(Si) = 353.4°) and pyramidalized silicon centers in **9-Mes-*E,E***($\Sigma\measuredangle$(Si1,Si2) = 342.8°, 340.5°)
- Si–Si single bonds (2.336(3) Å (***Z,Z***), 2.329(3) Å (***E,E***)), comparable to reported 1,4-diamino-2,3-disilabutadienes (2.306(1) – 2.337(1) Å)[121,128–130]
- short Si–C^{carb} bond lengths (1.79(1) Å (***Z,Z***), 1.796(8) Å (***E,E***)), which feature a strong π-character
- ^{1}H ,^{13}C{^{1}H} and ^{29}Si{^{1}H} NMR specta reveal a rigid structure for the ***Z,Z*** isomer and a highly dynamic behavior for the ***E,E*** isomer at ambient temperature in solution

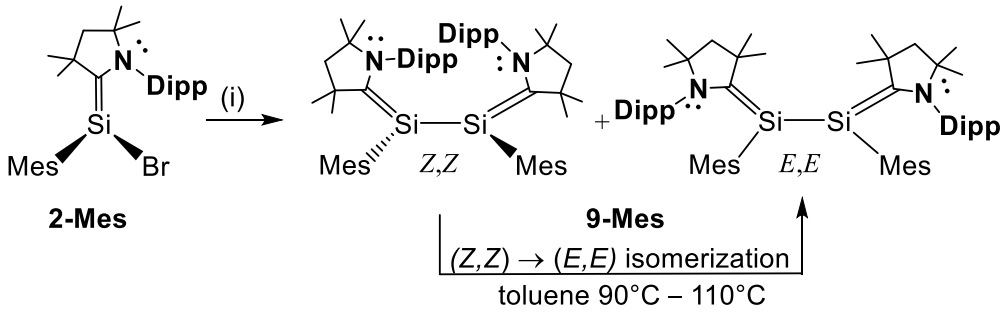

Scheme 3.4. Synthesis of **9-Mes**, upon 1e$^-$ -reduction of **2-Mes**; (i) 1 equiv. of KC_8 in C_6H_6 at r.t., 7 d.

According to the experimental results **9-Mes-*Z,Z*** can be best described as a 2,3-disilabutadiene with trigonal planar coordinated silene moieties, which are orientated almost perpendicular to each other. Compound **9-Mes-*Z,Z*** features axial chirality in the solid state (with the chirality axis passing through the Si–Si bond) and a rigid structure in solution. Compound **9-Mes-*E,E***, in contrast, can be best described as a pyramidalized disilabutadiene, which features an averaged C_S-symmetry at elevated temperature in solution, due to a stepwise pyramidal inversion of the two chiral silicon centers in **9-Mes-*E,E***. Detailed kinetic studies show that **9-Mes-*Z,Z*** undergoes an *Z,Z* → *E,E* isomerization at 90 – 110 °C with an activation barrier of $\Delta G^{\ddagger}(298K) = 120.2 \pm 2.3$ kJ mol^{-1}, $\Delta H^{\ddagger} = 126.3 \pm 2.3$ kJ mol^{-1}, $\Delta S^{\ddagger} = 20.4 \pm 0.6$ J K^{-1} mol^{-1}. It may be assumed that the isomerization proceeds via stepwise rotation of the caac^{Me} substituents about their Si–C^{carb} bonds. The system relates well to the 2-(amino)silene SiBr(Eind)(caac^{Me}) (**2-Eind**).

Reduction of $SiBr_2(caac^{Me})$ (**1**) by $1e^-$ with KC_8 in benzene led to the formation of $Si_2Br_2(caac^{Me})_2$ (**9-Br**). The compound completes the homologue series of the $caac^{Me}$-stabilized silicon(I) dimers $Si_2X_2(caac^{Me})_2$ (X = Cl[128], Br, I[121], H[129], Me[130], Ph[131]). Similar, like the other literature reported $caac^{Me}$-stabilized silicon(I) dimers, the compound can be best described as the borderline case of a co-planar disilabutadiene and a bis-carbene adduct of a disilyne which features trigonal pyramidalized silicon centers.

Salt metatheis reactions of **9-Br** with unsaturated nucleophiles led to the formation of functionalized disilicon(I) compounds of the type $Si_2R_2(caac^{Me})_2$ (R = Cp' (**9-Cp**), C≡CTMS (**9-C_2TMS**)), C≡CMes (**9-C_2Mes**)). All compounds were isolated as microcrystalline solids and fully characterized, also by X-ray diffraction analysis.

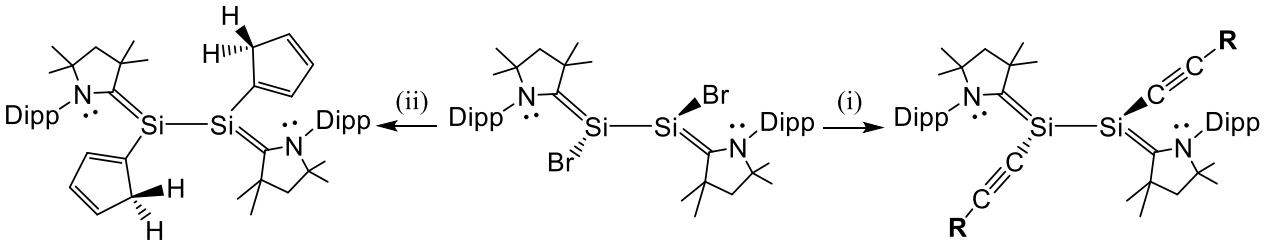

Scheme 3.5. Reactivity of **9-Br** towards unsaturated nucleophiles; (i) 2 equiv. of Li-C≡CSiMe$_3$ or Li-C≡CMes in THF, r.t.; (ii) 2 equiv. of NaCp, THF, 60 °C, 48 h.

Acetylide substituted silicon(I)-compounds **9-C_2TMS** and **9-C_2Mes** feature the typical structural and NMR spectroscopic features of $caac^{Me}$-stabilized silicon(I) dimers: substituents in gauche conformation, $caac^{Me}$ carbenes in anti-periplanar conformation, two pyramidailized silicon centers ($\Sigma\measuredangle$(Si) = 335.6 (**9-C_2TMS**), 342.4 (**9-C_2Mes**) interconnected via a Si–Si bond, shortened Si–C^{carb} bond lengths (1.821(3) Å (**9-C_2TMS**), 1.810(3) Å (**9-C_2TMS**), as well as an observed *C_2*-symmetry in the solid state and an averaged *Cs*-symmetry observed by ^{1}H NMR spectroscopy in solution.

The Cp substituted silicon(I) compound **9-Cp'** provided to be particulary interesting. Upon substituition of **9-Br** with NaCp, in fact, the Cp-substituents happened to be isomerized into a cylcopenta-1,3-dien-1-ide substituent with localized double bonds and single bonds (*Scheme 3.5*). According to structural and NMR spectroscopic features compound **9-Cp'** can be best described as a 2,3-disilabutadiene with trigonal planar coordinated silene moieties, which are orientated almost perpendicular to each other. Compound **9-Cp'** features axial chirality in the solid state (with the chirality axis passing through the Si–Si bond) and a rigid structure in solution.

Reduction of pyramidal 2-(amino)silenes $SiBr(R_A)(caac^{Me})$ (R_A = $SiTMS_3$ (**2-Si**), $NTMS_2$ (**2-N**), $PMes_2$ (**2-P**)) by $2e^-$ with KC_8, selectively afforded the potassium-silenides $SiK(R_A)(caac^{Me})$ (R_A = $Si(SiMe_3)_3$ (**4-Si**), $N(SiMe_3)_2$ (**4-N**), $P(Mes)_2$ (**4-P**)). Surprisingly, $2e^-$-reduction of the alkinyl substituted disilabutadienes $Si_2(C{\equiv}C\text{-}R_B)_2(caac^{Me})_2$ (R_B = $SiMe_3$ (**9-C_2TMS**), Mes (**9-C_2Mes**)) led, via cleavage of the Si–Si bond aswell to the formation of the potassium-silenides of the type $SiK(C{\equiv}C\text{-}R_B)(caac^{Me})$ (R_B = $SiMe_3$ (**10-C_2TMS**), Mes (**10-C_2Mes**)). Besides compounds **4-N** and **4-P**, which decomposed during work up, all compounds were fully characterized, also by X-ray diffraction analysis.

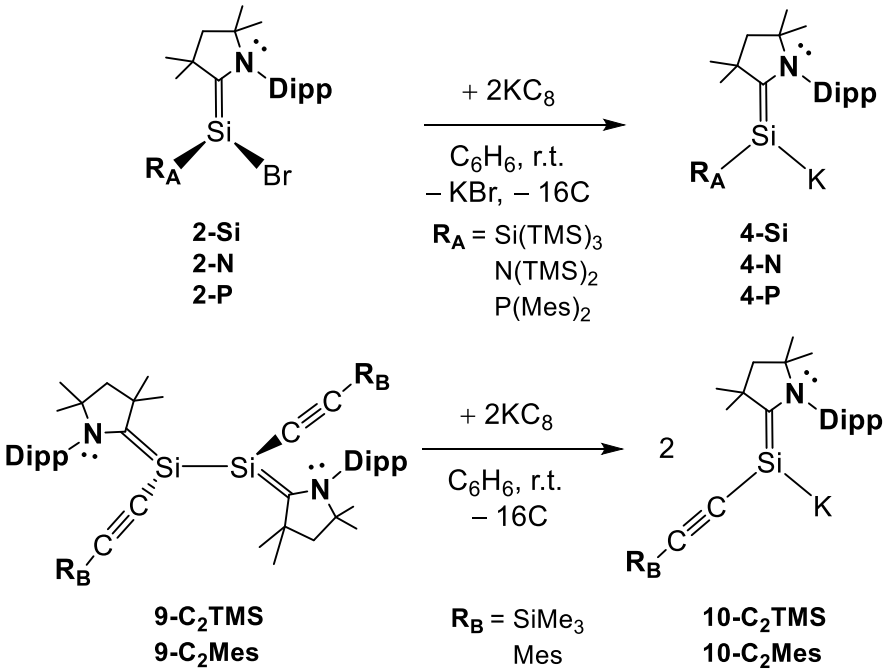

Scheme 3.6. Synthesis of potassium-silenides upon reduction of pyramidal 2-(amino)silenes or pyramidal 1,4-diamino-2,3-disilabutadienes.

The key features of both compounds are:

- trigonal planar coordinated silicon centers (352.8° (**4-Si**), 357.1° (**11-C_2TMS**)
- $Si{=}C^{carb}$ bonds (1.813(9) Å (**4-Si**), 1.790(3) Å (**10-C_2TMS**)) which are slightly elongated when compared to literature known lithium-silenides (1.766(3) – 1.778(3) Å).[125,126]
- covalently bonded potassium cations, which are stabilized by π-interaction of the aromatic Dipp substituents.

The potassium-silenides mentioned above appeared to be particulary interesting building blocks in low valent silicon chemistry. Reaction of silenide **10-C$_2$TMS** with SiBr$_2$(caac^{Me}) (**1**) and digermene [GeCl(Ar^{Mes})]$_2$ led to the formation of asymmetric silicon(I) compound (caac^{Me})SiBr-Si(C≡CTMS)(caac^{Me}) (**11-Br**) and (silenyl)germylene **12**, respectively. Both compounds were fully characterized, also by X-ray diffraction analysis. (Silenyl)germylene **12** appeared to be the first example of a silene, which features a reversible $Z \rightarrow E$ isomerization at ambient temperature. Thermodynamic parameters (ΔG, ΔH, ΔS), as well as the thermodynamic parameters of activation (ΔG$^{\#}$, ΔH$^{\#}$, ΔS$^{\#}$), for the isomerization were obtained from a Van't Hoff plot and a full line shape analysis of VT ^{1}H NMR spectra of **12**, respectively.

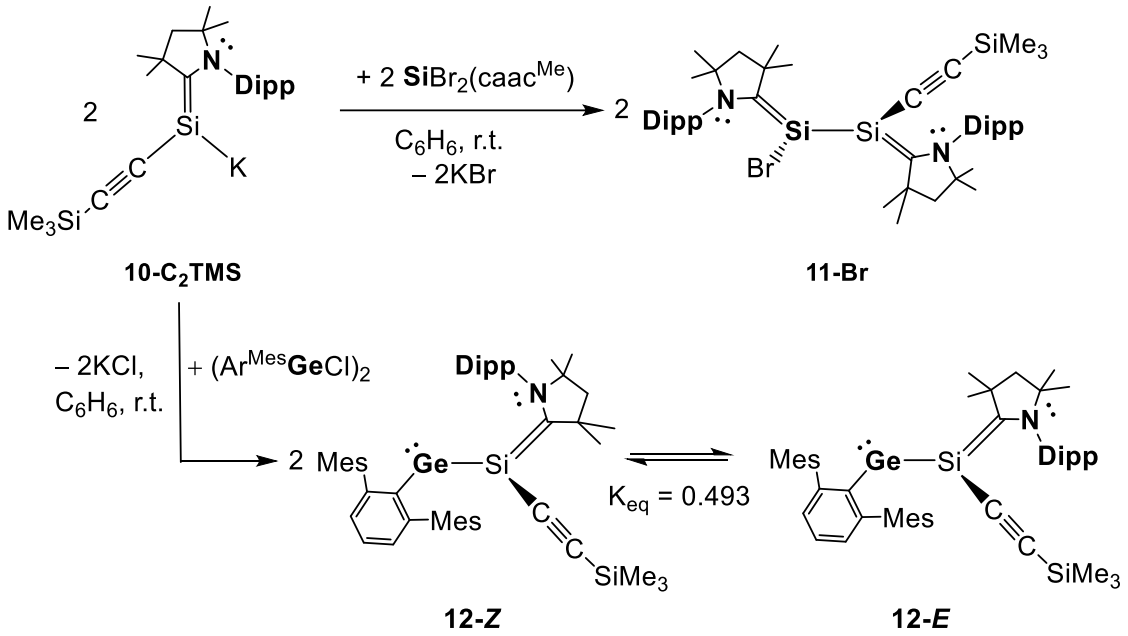

Figure 3.4. Reaction of potassium-silenide **10-C$_2$TMS** with SiBr$_2$(caac^{Me}) (**1**) and (Ar^{Mes}GeCl)$_2$.

Asymmetric silicon(I) compound **11-Br**, compares well to its symmetric congeners Si$_2$Br$_2$(caac^{Me})$_2$ (**9-Br**) and Si$_2$(C$_2$-TMS)$_2$(caac^{Me})$_2$ (**9-C$_2$TMS**). According to structural and NMR spectroscopic features it can be described as a pyramidalized 1,4-diamino-2,3-disilabutadiene. Although the compound appears to be in *C1*-symmetric in the solid state, the two caac^{Me} ligands each feature an averaged *Cs*-symmetry in solution, which can be attributed to a stepwise pyramidal inversion of the two chiral silicon centers in solution.

(Silenyl)germylene **12** provides a more elongated Ge–Si bond (2.300(3) [2.302(4)] Å) and more shortened Si–C^{carb} bond (1.84(1)[1.80(1)] Å) compared to the recently reported NHC-stabilized germasilyne Ar^{Mes}Ge=SiCl(SIDipp) (d(Ge=Si) = 2.2841(5) Å, d(Si–C^{carb}) = 1.877(2) [1.878(2)] Å) (**12-NHC**).[253] Both isomers (***E*** and ***Z***) in **12** are equilibrating at ambient temperature in solution (K$_{eq}$(298K) = 0.493 (± 0.001)).

The NMR assignment of *E* and *Z* isomers was made possible via high resolution correlation NMR spectroscopy at –30 °C and both isomers have been unevocually assigned via 1D NOE and 2D NOE NMR experiments.
According to Van't Hoff analysis the *E*-isomer lies 1.8 ± 0.1 kJ mol^{-1} lower in energy. The reversible $E \rightarrow Z$ isomerization can be rationalized by the rotation of the caac^{Me} substituent about the Si–C^{carb} bond, which proceeds via a rather high activation barrier of $\Delta G^{\ddagger}(298K)$ = 65.4 ± 1.1 kJ mol^{-1}, which was obtained from a full line shape analysis of VT ^{1}H NMR spectra in (D_8)toluene solution.

Since the caac^{Me}-stabilized germasilyne **12** can be seen as a formal constitution isomer to carbene-stabilized silagermenylidenes, the question arose if silagermenylidenes or disilavinylidenes are accessible via the stabilization of the cyclic (alkyl)(amino)carbene. Indeed, caac^{Me}-supported disilavinylidene **14** and silagermenylidene **14-Ge** could be isolated via an efficient two step synthesis. Entry to the chemistry provided $SiBr_2$(caac^{Me}) (**1**), which was reacted in 2:1 fashion with the 1,2-dibromodisilene (E)-Tbb(Br)Si=Si(Br)Tbb in the presence of two equivalents of 4-dmap to afford the bromo-silicon(II) compound SiBr($SiBr_2$Tbb)(caac^{Me}) (**13**). Compound **13** was then selectively reduced with KC_8 to give the caac^{Me}-stabilized disilavinylidene **14,** as a dark green solid. $GeBr_2$(caac^{Me}) (**1-Ge**) reacted in a similar way with the 1,2-dibromodisilene to the germanium analogous compound GeBr($SiBr_2$Tbb)(caac^{Me}) (**13-Ge**), which upon 2e$^-$ reduction with KC_8 yielded the caac^{Me}-stabilized silagermenylidene **14-Ge** as a dark blue solid. All four compounds were fully characterized, also by X-ray diffraction analysis.

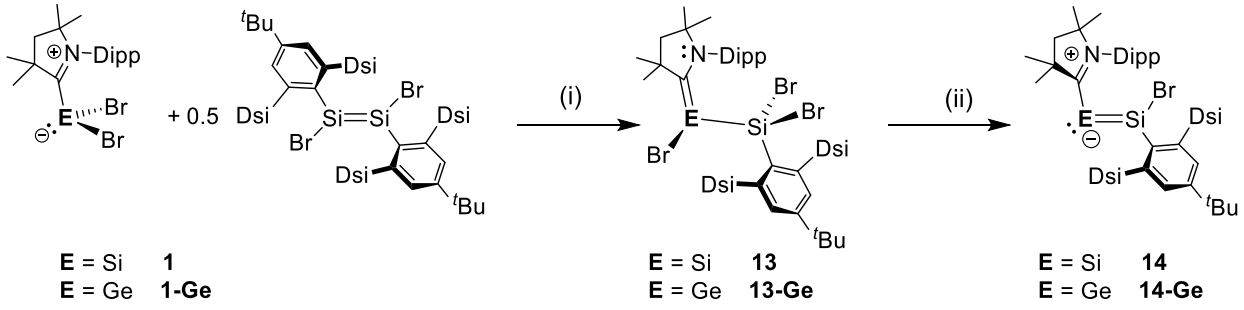

Scheme 3.7. Synthesis of caac^{Me}-stabilized disilavinyldene **14** and silagermenylidene **14-Ge**, starting from $SiBr_2$(caac^{Me}) and $GeBr_2$(caac^{Me}), respectively. (i) Si: 4-dmap, benzene, r.t.; Ge: toluene, 100 °C; (ii) 2KC_8, DME –50 °C → r.t.

In terms of structural and NMR spectroscopic properties compound **13**, differs drastically from the literature known (silyl)silylene SiBr(SiBr$_2$(Tbb)(SIDipp) (**13-NHC**)[118], but compares well to the pyramidal 2-(amino)silenes SiBr(Nu)(caac^{Me}) (**2-Nu**), mentioned above. The germanium(II) bromide **13-Ge**, in contrast, features the characteristics of an NHC-stabilized germylene with a polarized Ge$^{\delta+}$–C$^{\delta-}$ donor-acceptor single bond.
In terms of its structural properties compound **13-Ge** (d(Ge–C^{carb}) = 2.094(5) Å), Σ∢(Ge) = 291.4 °) compares well to the recently reported NHC-stabilized (chlorosilyl)chlorogermylene GeCl(SiClR$_2$)(NHC^4) (NHC^4 = IMe$_4$, R$_2$ = [N-(*t*Bu)CH]$_2$) (d(Ge–C^{carb}) = 2.081(2) Å), Σ∢(Ge) = 296.9 °).[280]
The key features of the caac^{Me}-stabilized disilavinylidene **14** and silagermenylidene **14-Ge** are:

- Si=Si (2.194(2) Å) and Si=Ge (2.249(1) Å) double bonds, which compare well to literature known disilavinylidenes and silagermenylidenes
- Shortened Si–C^{carb} (1.878(5) Å) and Ge–C^{carb} (1.9872(2) Å) single bonds, compared to NHC-supported heavier tetrelavinylidenes
- A more planar orientation of the caac^{Me} carbene moieties (φ_{CAAC} = 127.1° (**14**), 126.0° (**14-Ge**)) towards the Si=E (E = Si, Ge) bond, in comparison to the orthogonal orientation of the NHC in (SIDipp)Si=SiBr(Tbb) (**14-NHC**: φ_{NHC} = 95.8°)[118]
- Quantum chemical studies suggest an in-between behavior of disilavinylidene and silallene resonance structures in **14** and **14-Ge**.

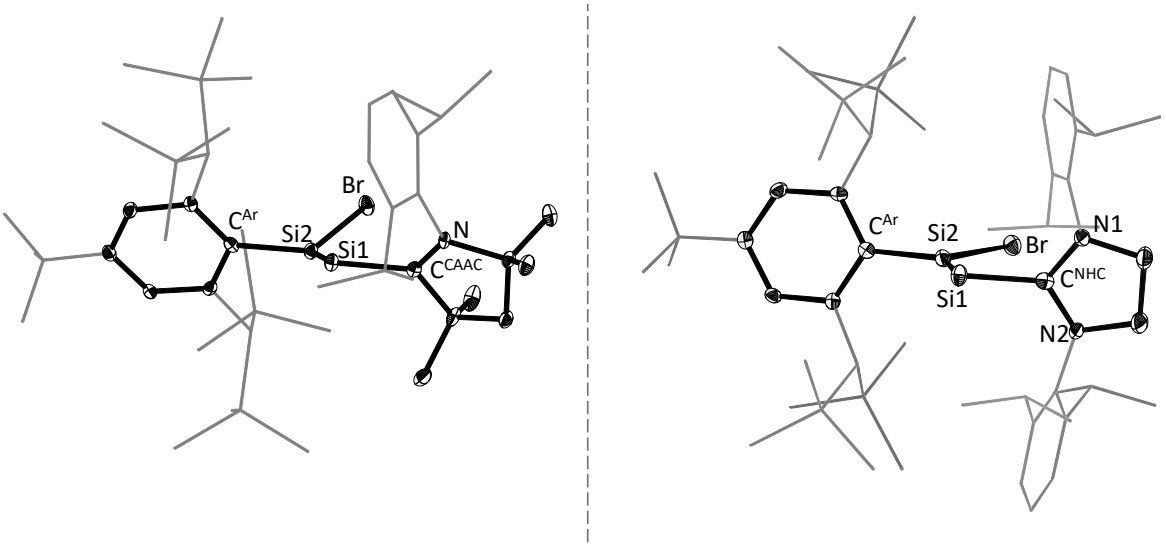

Figure 3.5. Diamond plot of the molecular structure of CAAC-supported disilavinylidene **14** (left) in comparison to the literature known NHC-stabilized disilavinylidene **14-NHC** (right), reported by Filippou et al.[118] Thermal ellipsoids are set at 30 % probability, and hydrogen atoms were omitted. In the depicted structures the Dipp-substituents of the caac^{Me} and SIDipp ligand, the disyl-groups (CH(SiMe$_3$)$_2$) and *t*Bu-group of the Tbb substituent are presented in the wire-frame for the sake of clarity.

Since the CAAC-stabilized disilavinylidene **14**, clearly differs in terms of its electronic structure to the parent NHC-stabilized disilavinylidene (SIDipp)Si=SiBr(Tbb) (**14-NHC**), the reactivity of compound **14** was of considerable interest.

Since cyclic (alkyl)(amino)carbenes are much stronger π-acceptors than typical pure σ-donating NHCs, a higher electrophilicity at the SiBr(Tbb) moiety in **14** was envisioned, compared to that of the NHC-stabilized disilavinylidene **14-NHC**. Indeed, the bromine atom could be easily substituted with nucleophiles such as Li-C≡CTMS and MeLi, leading to substituted disilavinylidenes of the type (caac^{Me})Si=Si(R)Tbb (R = C≡CTMS (**14-C$_2$TMS**), Me (**14-Me**)). The reaction of disilavinylidene **14** with MeLi, appeared to be particulary interesting. Substituted compound **14-Me** reacts with an additional equivalent of MeLi leading to the unprecedent lithium-silenide **15**. With exception of **14-C$_2$TMS**, which could not be crystallized, all three compounds were fully characterized, also by X-ray diffraction.

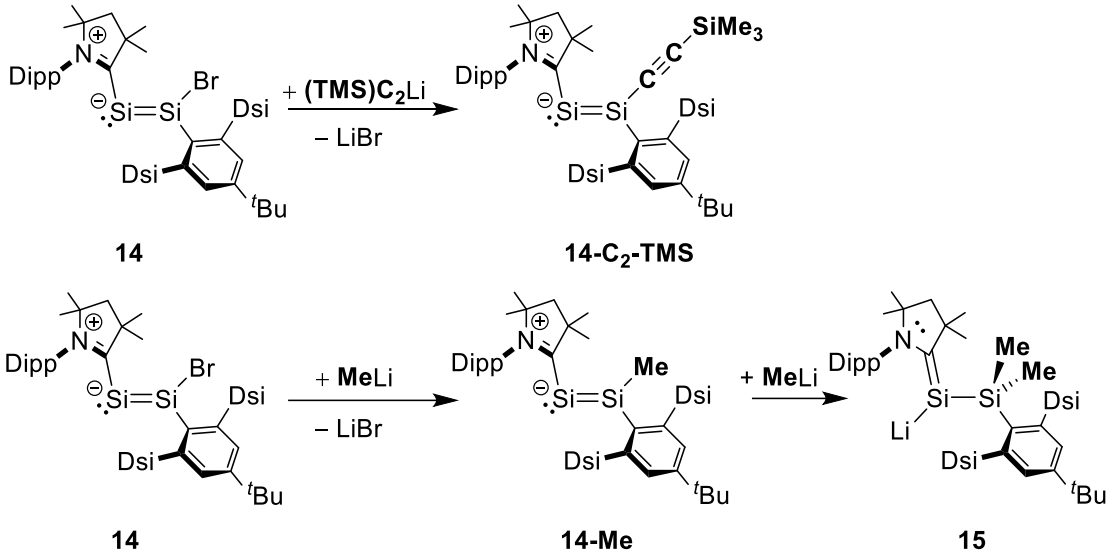

Scheme 3.8. Reactivity of disilavinylidene **14** towards nucleophiles.

In terms of the structural and NMR spectroscopic properties compounds **14-Me** and **14-C$_2$TMS**, compare well to the CAAC-stabilized disilavinylidene **14**. Compound **15**, in sharp contrast, can be rather described as a lithium-silenide. Thus **15** compares well to the potassium-silenide SiK(SiTMS$_3$)(caac^{Me}) (**4-Si**) and to the recently reported potassium-silenide SiK(Trip)(caac^{Me}) (Trip = C$_6$H$_2$-2,4,6-*i*Pr$_3$).[124]

Two e⁻-reduction of disilavinylidene **14** led to the formation of the unprecedent potassium-silenide **16**. Reaction of **14** with IMe_4 yielded the carbene adduct **17**, which can be rather described as a zwitterionic silylium-silenide. Subsequent halide abstraction from **17** with $Na[B(Ar^F)_4]$ ($[B\{C_6H_3\text{-}3,5\text{-}(CF_3)_2)_4\}]$)led to the formation of the disilynylium salt **18**. With exception of IMe_4 adduct **17**, which could not be crystallized, all compounds were fully characterized, also by X-ray diffraction analysis.

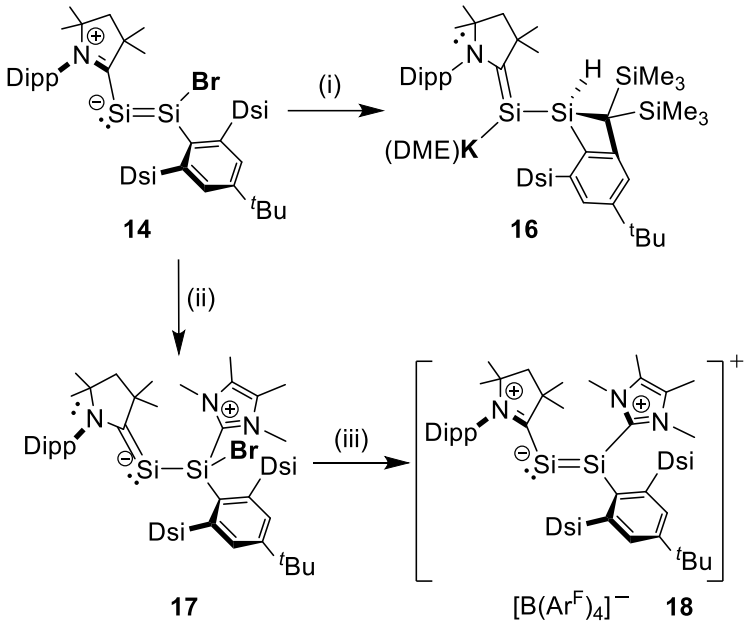

Scheme 3.9. Reactivity of $caac^{Me}$-stabilized disilavinylidene **14**; (i) $2KC_8$, DME, –50 °C → r.t.; (ii) IMe_4, benzene, r.t.; (iii) $Na[B(Ar^F)_4]$, C_6H_5F r.t.

Potassium-silenide **16**, does compare well to the silenides, mentioned above.

NMR spectroscopic properties of IMe_4 adduct **17** ($\delta(^{13}C^{CAAC})$ = 191.3 ppm, $\delta(^{15}N^{CAAC})$ = 141.2 ppm) compared to disilavinylidene **14** ($\delta(^{13}C^{CAAC})$ = 241.4 ppm, $\delta(^{15}N^{CAAC})$ = 197.4 ppm), suggest a strong π-character in the $Si{=}C^{CAAC}$ bond in **17**. According to the NMR spectroscopic features compound **17** can be best described as a zwitterionic silylium-silenide.

The key features of the carbene stabilized disilynylium salt **18** are:

- Si=Si (2.203(1) Å) double bonds, which are slightly elongated compared to the NHC-stabilized cations [(IDipp)Si=SiR(IDipp)]$^+$ (R = H, Me, Et) (2.173(1) – 2.191(1) Å)[205]
- significantly shortened Si–C^{CAAC} (1.896(3) Å) bonds compared to the Si–C^{NHC} bonds in [(IDipp)Si=SiR(IDipp)]$^+$ (1.940(2) Å – 1.947(2) Å)[205]
- a more planar orientation of the terminal caac^{Me} carbene (φ_{CAAC} = 35.5°) towards the Si=Si bond in comparision to the orthogonal orientation of the NHC in [(IDipp)Si=SiR(IDipp)]$^+$ (φ_{NHC} = 71.1 – 88.0°)[205]
- quantum chemical studies reveal a delocalization of the Si–Si π-bond over the C^{CAAC}–Si1–Si2 moiety in **18** compared to the localized Si=Si bond in cations [(IDipp)Si=SiR(IDipp)]$^+$

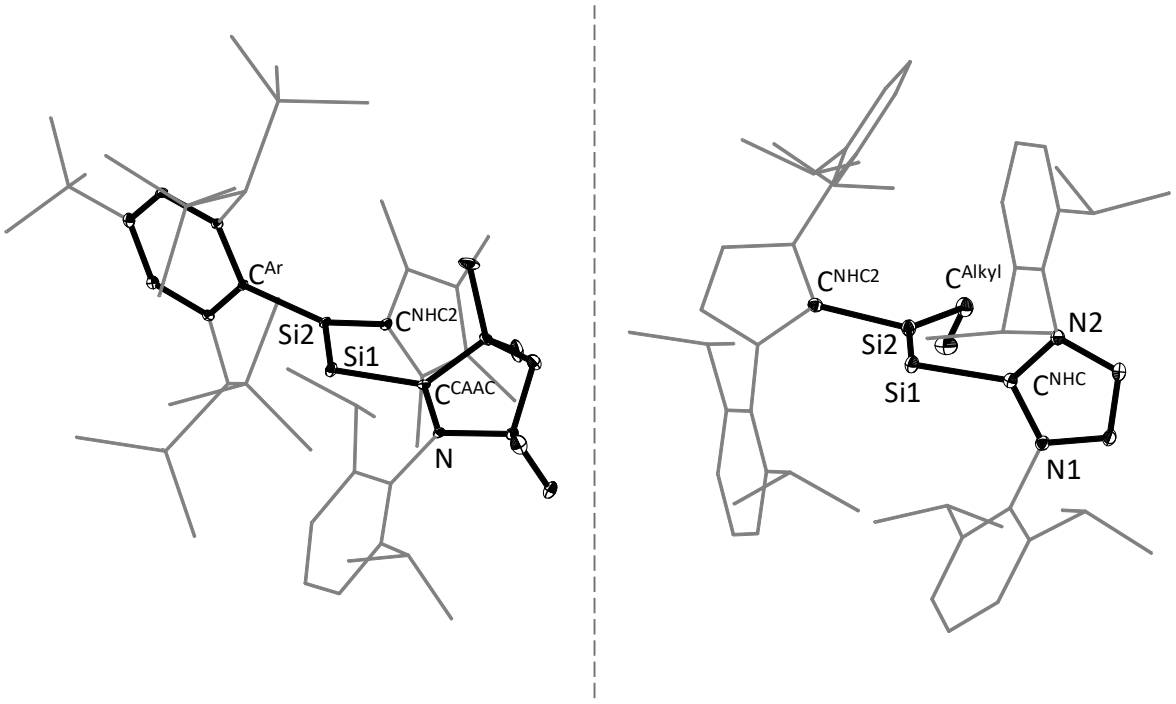

Figure 3.6. DIAMOND plot of the molecular structure of CAAC-supported cation [(caac^{Me})Si=Si(IMe$_4$)(Tbb)]$^+$ (**18**$^+$) (left) in comparison to the literature known NHC-stabilized cation [(IDipp)Si=Si(Et)(IDipp)]$^+$ (right), reported by Filippou et al.[205] Thermal ellipsoids are set at 30 % probability level and hydrogen atoms were omitted. In the depicted structures the Dipp-substituents of the caac^{Me} and IDipp ligands, the disyl-groups (CH(SiMe$_3$)$_2$) and *t*Bu-group of the Tbb-substituent as well as the backbone of the silicon(II) bonded NHC's are presented in the wire-frame for the sake of clarity.

Thus according to structural and NMR spectroscopic properties as well as quantum chemical calculations disilynylium cation **18**$^+$ can be best described as a hybrid of a disilavinyliumylidene and a silyliumylidenyl-silenide, mostly due to the delocalization of the Si–Si π-bond.

The reactivity of the bis caac^{Me}-stabilized silylone Si(caac^{Me})$_2$ was of considerable interest.[119] Therefore, the procedure described in the literature for the synthesis of Si(caac^{Me})$_2$ was improved. The improved synthetic protocol proceeds via SiBr$_2$(caac^{Me})$_2$, which is formed upon addition of caac^{Me} carbene to SiBr$_2$(caac^{Me}) (**1**). Two-electron reduction of SiBr$_2$(caac^{Me})$_2$ with KC_8 in THF at –78 °C selectively afforded silylone Si(caac^{Me})$_2$ which was isolated in 81 % yield.

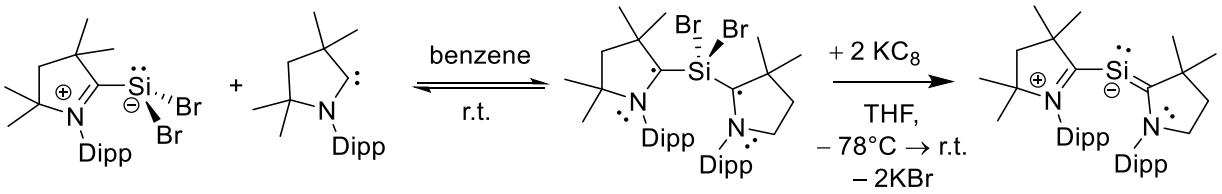

Scheme 3.10. Improved synthesis of silylone Si(caac^{Me})$_2$ upon reduction of SiBr$_2$(caac^{Me}) in the presence of caac^{Me} carbene.

In presence of Na[B(Ar^F)$_4$] ([B(Ar^F)$_4$] = [B{C$_6$H$_3$-3,5-(CF$_3$)$_2$}$_4$)]) the compound reacts selectively with methyltriflate yielding the silyliumylidene salt [SiMe(caac^{Me})$_2$][B(Ar^F)$_4$] (**19-Me**). The compound was fully characterized also by X-ray diffraction.

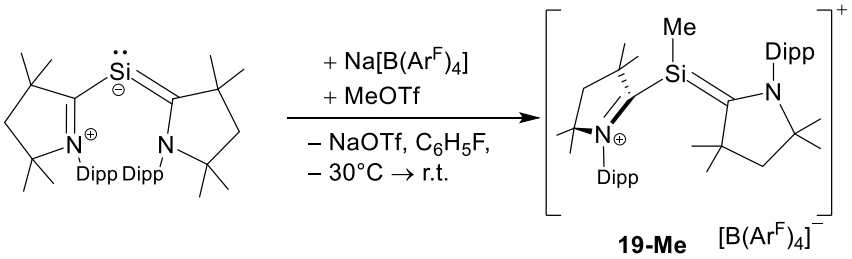

Scheme 3.11. Synthesis of silyliumylidene salt **19-Me** upon oxidativte addition of MeOTf to Si(caac^{Me})$_2$.

The key features of silyliumylidene salt **19-Me** are:

- a trigonal pryamidalized silicon(II) center ($\Sigma\measuredangle$(Si) = 321.4°)
- shortened Si–C^{carb} (1.890(2) Å) bond of the in plane lying caac^{Me} carbene, compared to the out of plane lying caac^{Me} carbene (1.970(2) Å)
- an observed C_1-symmetry in the solid state and an averaged C_S-symmetry found by NMR spectroscopy at ambient temperature in solution

In terms of its structural and NMR spectroscopic properties compound **19-Me**, compares well to pyramidal bromosilenes SiBr(Nu)(caac^{Me}) (**2-Nu**) and [SiI(caac^{Me})$_2$]I. The compound, thus can be best described as caac^{Me}-stabilized 2-(amino)silenylidene salt with considerable amounts of Si=C^{CAAC} double bond character.

Preliminary reactivity studies of $SiBr_2(caac^{Me})$ (**1**) towards transition metal complexes were carried out. In contrast to $SiBr_2$(SIDipp) (**1-NHC²**), which provided to be an exeptional starting material in the generation of metallo-silylidene complexes, silylidynes[182] and metallasilylidynes[50,183] compound **1** appeard to be to redox-active upon reaction with transition metallates such as $Na[CpCr(CO)_3]$, $Na[CpMo(CO)_3]$ and $Na[Tp'Mo(CO)_2(PMe_3)]$. Monitoring of the reaction mixtures by ^1H NMR spectroscopy in (D_6)benzene at ambient temperature revealed the rather selective formation of $Si_2Br_2(caac^{Me})_2$ (**9-Br**), accompanied with the distinct color change to red-purple.
Reaction of **1** with $CpCo(CO)_2$ in toluene at ambient temperature led to the selective formation of the silylene σ-adduct $CpCo(CO)SiBr_2(caac^{Me})$ (**20**). The compound was isolated as dark green microcrystalline solid in analytically pure form in 81 % yield. Compound **20** was characterized by elemental analysis and spectroscopic methods.

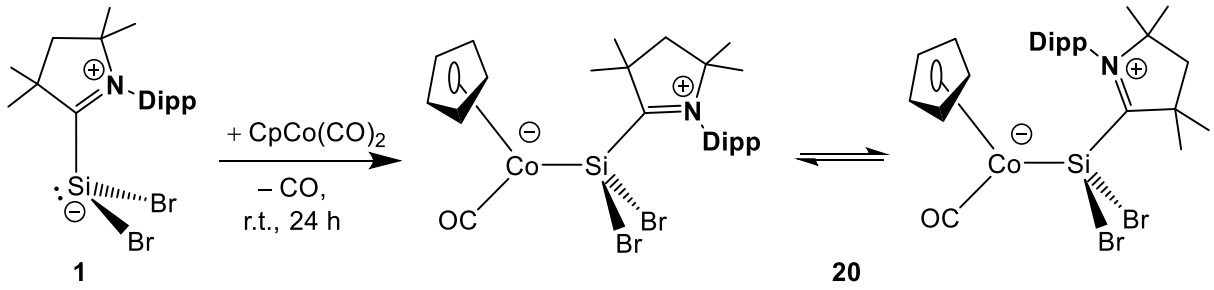

Scheme 3.12. Synthesis of transition metal complex **20**, starting from dibromosilylene **1**.

IR spectroscopy, as well as ^1H NMR spectroscopy at ambient temperature suggest a fast interconversion of two isomers in solution (*Scheme 3.12*). The nature of the dynamic process was studied by line shape analysis of recorded ^1H NMR spectra at variable temperatures in (D_8)toluene. The dynamic process can be attributed to a hindererd rotation of the $caac^{Me}$ ligand about the $Si–C^{carb}$ bond at the prochiral silicon center in **2**. Line shape analysis of recorded ^1H NMR spectra at variable temperatures gave the thermodynamic parameters of activation for this process: $\Delta H^{\ddagger} = 48.6 \pm 1.0$ kJ mol^{-1} and $\Delta S^{\ddagger} = -23.8 \pm 1.6$ J K^{-1} mol^{-1}. The negative entropy of activation, suggests a highly ordered transition state. Using the Gibb's Helmholtz equation the energy of activtation can be calculated $\Delta G^{\ddagger}(298K) = 55.6 \pm 1.0$ kJ mol^{-1}.

Table 3.1. Summary of bonding parameters and NMR spectroscopic data (given in (D_6)benzene at 298K, if not mentioned otherwise in the legend) of **1** and isolated pyramidal 2-(amino)silenes (**2-Nu**) compared to literature known compounds.

Comp.	Diast.[a]	Si–C^{carb} / Å	N–C^{carb} / Å	Σ∢(Si) / (deg)	DP[b] / %	θ[c] / (deg)	τ[d] / (deg)	Sym[e]	δ(^{29}Si)[f] / ppm	δ($^{13}C^{carb}$) / ppm	δ(^{15}N)[g] / ppm	Ref.
$SiBr_2(caac^{Me})$ (**1**)	–	2.017(2)	1.301(3)	289.9	78	81.7	100.8	C_S	14.4[h]	231.2[h]	231.3[h]	
$SiBr\{Si(TMS)_3\}(caac^{Me})$ (**2-Si**)	*Z*	1.836(2)	1.353(2)	336.5	26	43.8	5.4	C_S	24.7	204.9	162.9	
$SiBr\{Mes\}(caac^{Me})$ (**2-Mes**)	*Z*	1.842(1)	1.350(2)	326.3	37	54.2	8.6	C_S	10.5	194.7	158.8	
$SiBr\{P(Mes)_2\}(caac^{Me})$ (**2-P**)	*Z*	1.850(8)	1.36(1)	336.4	26	47.8	8.0	C_S	7.0	204.3	170.8	*this*
		1.862(8)	1.34(1)	335.1	28	51.2	10.3					*work*
$SiBr\{N(TMS)_2\}(caac^{Me})$ (**2-N**)	*Z*	1.866(2)	1.349(2)	328.8	35	53.2	0.6	C_S	18.5	190.3	151.8	
$SiBr\{OMes^*\}(caac^{Me})$ (**2-O**)	*Z*	1.897(3)	1.342(4)	321.6	43	58.0	2.5	C_S	26.4	200.0	164.9	
$SiBr\{Eind\}(caac^{Me})$ (**2-Eind-*E***)	*E*	1.768(3)	1.421(4)	356.9	3	23.1	18.0	C_1	31.1	165.2	104.3	
$SiBr\{Eind\}(caac^{Me})$ (**2-Eind-Z**)	*Z*	1.796(2)	1.385(3)	346.1	15	35.8	5.2	C_S	1.8	175.9	135.1	
$SiBr\{SiBr_2(Tbb)\}(caac^{Me})$ (**13**)	*Z*	1.879(8)	1.33(1)	313.6	51.6	59.1	9.2	C_S	8.5	217.4	–	
$SiCl\{C_6H_4\text{-}6\text{-}NMe_2\}(caac^{Me})$	*Z*	1.853(1)	1.345(2)	321.0	43	57.5	9.1	C_1[h]	27.3[h]	198.9[h]	–	[137]
$SiMe\{C_6H_4\text{-}6\text{-}NMe_2\}(caac^{Me})$	*E*	1.809(1)	1.374(1)	335.4	27	46.0	4.5	C_S	21.1	176.4	–	[137]
$SiCl\{Ar^{Trip}\}(IMe_4)$	–	1.937(2)	1.355(2)	299.2	68	97.0	72.4	C_2	0.7	166.7	–	[80]
			1.386(3)									
$SiCl\{N(Dipp)(TMS)(IiPr_2Me_2)$	–	2.002(2)	1.369(2)	305.2	61	74.7	101.1	C_2	3.1	164.1	–	[81]
			1.358(2)									
$SiCl\{NH(Dipp)\}(IDipp)$	–	1.980(3)	1.358(2)	290.5	77	84.3	118.5	C_2	–6.0	171.7	–	[82]
			1.362(2)									

[a]: Determined orientation of the N-Dipp moiety in the solid state (orientated cis (*Z*) or trans (*E*) to the high priority group of the silenic silicon center). [b]: Degree of pyramidalization = DP (in %) = 100 % · [360 − Σ∢(Si) / (deg)]/90. A DP value of 0 % describes a trigonal planar coordination of the silicon atom and a DP value of 100 % corresponds to a trigonal pyramidal coordination of the silicon atom. [c]: The bent angle (θ) is defined as the angle between the silylene coordination plane defined by the atoms X–Si–R (X = Br, Cl, C^{Me}; R = Si, C^{Ar}, P, N, O) and the Si–C^{carb} bond. [d]: The twist angle (τ) is defined as the angle between the silylene and the carbene coordination planes defined by the atoms X–Si–R (X = Br, Cl, C^{Me}; R = Si, C^{Ar}, P, N, O) and C2–Cl^{CAAC}–N1 (N1–Cl^{NHC}–N2), respectively. [e]: Sym = observed symmetry of the carbene (NHC or CAAC) in the ^{1}H NMR spectrum. [f]: ^{29}Si NMR resonance of the three-coordinated silicon center. [g]: ^{15}N NMR resonance of the N-atom(s) in the CAAC (NHC) carbene ring referenced against NH_3(l). [h]: Measured in (D_8)THF at 243 K.

Table 3.2. Summary of selected bonding parameters and X-band EPR spectroscopic data of isolated neutral two-coordinated silicon(I) radicals compared to literature known carbene-stabilized two-coordinated silicon(I)-radicals.

Comp.	Si–C^{carb} / Å	N–C^{carb} / Å	R-E-C^{carb} / deg)	φ_{carb}[a] / (deg)	EPR cond.	g_{iso}	M[b]	a(^{29}Siα) / mT	a(^{14}N) / mT	a(^{1}H) / mT	Ref.
Si{Si(TMS)$_3$}(caac^{Me}) (**3-Si**)	1.870(2)	134.9(2)	112.9(1)	26.1(1)	*n*-pentane, 293K	2.0065	t	3.81	0.44	-	
Si{Si(TMS)$_3$}(caac^{Me}) (**3-Si**)					*n*-pentane, 173K	2.0065		3.73	0.44	0.09	*this*
Si{N(TMS)$_2$}(caac^{Me}) (**3-N**)	1.895(4)	1.361(4)	106.6(2)	179.5(2)	*n*-pentane, 293K	2.0044	t	1.95	0.57	-	*work*
Si(OMes*)(caac^{Me}) (**3-O**)	1.865(2)	1.363(3)	100.1(1)	5.4(1)	Toluene 293K	2.0038	t	1.24	0.62		
(Mes)P=Si(Mes)(caac^{Me}) (**6**)	1.813(2)	1.369(3)	122.3(7)	21.5(1)	Toluene 293K	2.0038	dt	3.74 (^{31}P)	0.54		
[Si(caac^{Me})$_2$]$^{\cdot}$I	1.896(4) 1.867(3)	1.319(4) 1.332(4)	122.9(2)	2.7(2) 59.4(2)	Tol./THF 298 K	2.0037	t	7.54[c]	0.66	–	[134]
Ge{N(SiPh$_3$)Mes}(caac^{Me})	1.980(3)	1.369(3)	110.2(1)	19.7(2)	*n*-hexane 298K	2.0065	t	–	0.50		[152]
(IDipp)Si(H)Si(IDipp)	1.873(4)[d]	1.381(4)[d]	109.5(1)[d]	179.6(2)	*n*-hexane, 336 K	2.0056	m	1.73 0.43	0.10 0.25		[133]
[Si$_2$(IDipp)$_2$]$^{\cdot}$[BAr$_4^F$]	1.910(8) 1.899(7)	1.368(1) 1.377(1)	101.9(2) 109.9(2)	133.2(3) 177.3(3)	Et$_2$O 220 K	1.9979	m	5.99	–	–	[132]

[a]: φ_{carb} relative orientation of the carbene plane with respect to the plane formed by the atoms C^{carb}, Si, R (R = Si, N, O). [b] Multiplicity (M) of the EPR signal. [c]: This ^{29}Si hfcc was not visible at ambient temperature and could only be assigned at 115 K in Tol./THF. [d]: The compound contains a crystallographic inversion center in the middle of the Si–Si bond.

Table 3.3. Summary of selected bonding parameters and NMR spectroscopic data (given in (D_6)benzene at 298 K, if not mentioned otherwise in the legend) of **1** and isolated caac^{Me}-stabilized disilicon(I) compounds, compared to literature known caac^{Me}-stabilized silicon(I) compounds.

Comp.	Diast.[a]	Si–Si / Å	Si–C^{carb} / Å	N–C^{carb} / Å	Σ∢(Si) / deg)	DP[b] / %	θ[c] / deg)	τ[d] / (deg)	Sym[e]	δ(^{29}Si)[f] / ppm	δ(^{13}C^{carb}) / ppm	δ(^{15}N)[g] / ppm	Ref.
$SiBr_2$(caac^{Me}) (**1**)	–	–	2.017(2)	1.301(3)	289.9	78	81.7	100.8	C_S	14.4[h]	231.2[h]	231.3[h]	
Si_2Br_2(caac^{Me})$_2$ (**9-Br**)	*Z,Z*	2.341(2)	1.844(4)	1.347(5)	327.6	36	55.1	13.0	C_S	19.84	208.3	174.3	
			1.844(4)	1.348(5)	326.1	38	56.4	14.9					
Si_2Mes_2(caac^{Me})$_2$ (**9-Mes-*Z,Z***)	*Z,Z*	2.336(3)	1.79(1)	1.40(1)	353.4	7	24.1	6.6	C_2	10.1	185.8	120.9	
			1.79(1)	1.40(1)	353.2	8	24.5	5.9					*this*
Si_2Mes_2(caac^{Me})$_2$ (**9-Mes-*E,E***)	*E,E*	2.329(3)	1.793(7)	1.406(8)	342.8	19	51.8	18.7	C_S	–0.21	195.9	133.7	*work*
			1.796(8)	1.409(8)	340.5	22	40.6	19.6					
$Si_2Cp'_2$(caac^{Me})$_2$ (**9-Cp'**)	*E,E*	2.288(1)[f]	1.789(1)	1.384(2)	351.1	10	31.1	6.3	C_2	–5.65	180.9	132.9	
$Si_2(C_2TMS)_2$(caac^{Me})$_2$ (**9-C$_2$TMS**)	*E,E*	2.313(1)[f]	1.821(3)	1.353(3)	335.6	27	49.9	12.5	C_S	–42.2	203.4	157.7	
$Si_2(C_2Mes)_2$(caac^{Me})$_2$ (**9-C$_2$Mes**)	*E,E*	2.291(1)[f]	1.810(3)	1.365(4)	342.4	20	41.4	4.0	C_S	–36.5	197.3	150.9	
Si(C_2TMS)(caac^{Me})–	*E*	2.324(7)	1.819(2)	1.353(2)	338.9	23	46.5	11.4	C_S	–25.6	203.3	158.5	
–SiBr(caac^{Me}) (**11-Br**)	*Z*		1.855(2)	1.343(2)	324.5	39	58.2	21.5	C_S	9.10	208.5	173.9	
Si_2Cl_2(caac^{Me})$_2$	*Z,Z*	2.306(1)	1.823(3)	1.336(3)	328.0	36	53.9	4.0	C_S	25.62	–[j]	–	[128]
			1.826(3)	1.337(2)	329.0	34	54.0	6.4					
Si_2I_2(caac^{Me})$_2$	*Z,Z*	2.337(1)	1.846(3)	1.343(3)	328.3	35	51.6	11.0	C_2	–0.5	207.2	–	[121]
			1.841(3)	1.345(3)	330.6	33	53.5	11.5					
Si_2H_2(caac^{Me})$_2$	*E,E*	2.334(1)[i]	1.817(2)	1.362(2)	327.4	36	34	1.3	C_S	–45.5	211.8	–	[129]
Si_2Me_2(caac^{Me})$_2$	*E,E*	2.314(1)	1.798(1)	1.384(1)	345.2	16	38.9	2.1	C_S	0.72[k]	191.3[k]	–	[130]
			1.804(1)	1.383(1)	344.0	16	37.5	1.4					
Si_2Ph_2(caac^{Me})$_2$	*E,E*	2.306(1)	1.805(2)	1.381(3)	343.3	19	41.0	9.1	–[l]	–	–	–	[131]
			1.803(2)	1.377(3)	345.8	16	38.1	9.9					

[a] – [g]: See legend *Table 3.1*; [h]: Measured in (D_8)THF at 243 K. [i]: The compound contains an inversion center in the middle of the Si–Si bond. [j]: The signal was not reported in the literature. [k]: Measured in (D_8)THF at 298 K; [l]: The compound was not characterized by NMR spectroscopy.

Table 3.4. Summary of selected bonding parameters and NMR spectroscopic data (given in (D_6)benzene at 298 K, if not mentioned otherwise in the legend) of lithium and potassium-silenides isolated in this work, compared to literature known silenyl-anions.

Comp.	Si–C^{carb} / Å	N–C^{carb} / Å	Σ∢(Si) / (deg)	Σ∢($C^{carb/sp2}$) / (deg)	τ[a] / (deg)	δ(^{29}Si)[b] / ppm	δ($^{13}C^{carb/sp2}$)[c] / ppm	δ(^{15}N)[d] / ppm	Ref.
SiK{Si(TMS)$_3$}(caac^{Me}) (**4-Si**)	1.813(9)	1.42(1)	352.8	360.0	8.1	14.4	213.0	117.6	
SiK{N(TMS)$_2$}(caac^{Me}) (**4-N**)	–	–	–	–	–	86.5	200.7	90.5	
SiK{P(Mes)$_2$}(caac^{Me}) (**4-P**)	–	–	–	–	–	–[g]	210.3	114.9	
SiK(C$_2$-TMS)(caac^{Me}) (**10-C$_2$TMS**)	1.790(3)	1.408(4)	357.1	360.0	3.7	–19.4	220.0	119.9	*this*
SiK{C$_2$-Mes}(caac^{Me}) (**10-C$_2$Mes**)	–	–	–	–	–	–15.5	217.2	117.3	*work*
SiLi{SiMe$_2$(Tbb)}(caac^{Me}) (Et$_2$O) (**15·Et$_2$O**)	1.807(2)	1.418(2)	352.4	359.9	2.9(1)	44.6	210.4	117.3	
SiK{SiH(Tbb‘)}(caac^{Me})·(caac^{Me}) (**16·caac^{Me}**)	1.770(8)	1.413(8)	359.3	359.9	2.9	–0.50	217.6	125.0	
	1.796(9)	1.376(9)	359.4	360.0	1.6				
SiK{SiH(Tbb‘)}(caac^{Me})·(DME) (**16·DME**)	1.834(7)	1.415(8)	359.7	359.9	19.9	–0.30	217.9	124.7	
SiK(Trip)(caac^{Me})[e]	1.793(2)	1.424(3)	359.7	359.9	1.8	26.6	195.1	–	[124]
Li(R$_A$)Si=C(Ad)(R$_A$)[f]	1.773(3)	–	359.7	359.9	13.1	243.9	174.9	–	[125]
Li(R$_B$)Si=C(Ad)(R$_A$)[f]	1.778(3)	–	359.6	359.9	10.2	347.8	143.5	–	[125]
(THF)$_2$·Li(R$_A$)Si=C(R$_B$)(R$_A$)[f]	1.762(3)	–	359.8	359.8	4.4	405.5	134.2	–	[126]
Li(THF)$_4$ [(R$_A$)Si=C(R$_B$)(R$_A$)][f]	1.766(3)	–	–	–	–	26.6[h]	195.1[h]	–	[126]

[a]: The twist angle (τ) is defined as the angle between the silicon and $C^{carb/sp2}$ coordination planes defined by the atoms X–Si–R (X = K, Li; R = Si$_2$, C^{Ar}, $C^{C=C}$) and C$_2$–C_1^{CAAC}–N$_1$ (R–C^{sp2}–Si$_2$; R = C^{alk}, Si) coordination planes. [b]: ^{29}Si NMR resonance of the three-coordinated silicon center. [c]: ^{13}C NMR resonance of the doubly bonded CAAC carbene or sp^2 hybridized carbon atom. [d]: ^{15}N NMR resonance of the single nitrogen atom in the CAAC carbene ring referenced against NH_3(l). [e]: Trip = C_6H_2-2,4,6-*i*Pr$_3$, [f]: R$_A$ = Si(*t*Bu)$_2$Me, R$_B$ = Si(*t*Bu)Me$_2$. [g]: No ^{29}Si NMR resonance could be detected in the 1D and 2D ^{29}Si NMR spectra of an aliquot of the reaction mixture of **4-P**. [h]: Measured in (D_8)THF at 298 K.

Table 3.5. Summary of selected bonding parameters and NMR spectroscopic data (in (D_6)benzene at 298 K, if not mentioned otherwise in the legend) of caac^{Me}-stabilized disilavinylidenes, silagermenylidenes and silagermynes isolated in this work in comparison to the releated NHC-stabilized compounds.

Comp.	E–E / Å	E–C^{carb} / Å	C^{carb}–E–E / (deg)	φ_{carb} (deg)[a] / (deg)	$\delta(^{29}Si^{carb})$[b] / ppm	$\delta(^{29}Si^{R2})$[c] / ppm	$\delta(^{13}C^{carb})$ / ppm	$\delta(^{15}N)$[d] / ppm	Ref.
(caac^{Me})Si=SiBr(Tbb) (**14**)	2.194(2)	1.878(5)	105.5(1)	57.8(2)	73.1	96.2	241.4	197.4	
	[2.181(2)]	[1.868(6)]	[105.6(2)]	51.9(3)					
(caac^{Me})Si=SiC$_2$-TMS(Tbb)	–	–	–	–	110.7	83.8	243.9	201.3	
(**14-C$_2$TMS**)									
[(caac^{Me})Si=Si(IMe$_4$)(Tbb)]	2.203(1)	1.896(3)	109.0(1)	38.1(1)	118.1[i]	83.6	239.1	215.9	*this*
[B(Ar^F)$_4$] (**18**)		1.919(3)[j]	131.2(1)[j]	43.8(2)[j]			153.3[j]	175.4[j]	*work*
(caac^{Me})Si=SiMe(Tbb) (**14-Me**)	2.192(1)	1.880(2)	104.6(1)	57.2(1)	96.5	140.7	241.5	190.1	
(caac^{Me})Ge=SiBr(Tbb) (**14-Ge**)	2.249(1)	1.9872(2)	106.8(2)	49.7(1)	–	120.4	255.4	205.5	
(caac^{Me})Si(C$_2$-TMS)=Ge(Ar^{Mes})	2.300(3)[k]	1.84(1)	101.0(3)	24.7(4)	72.2(*Z*)[l]	–	208.0(*Z*)	175.6(*Z*)	
(**12**)	[2.302(4)][k]	[1.80(1)]	[99.0(3)]	[13.6(6)]	73.7(*E*)[l]	–	210.8(*E*)	169.5(*E*)	
(SIDipp)Si=SiBr(Tbb)	2.167(2)	1.937(4)	97.6(1)	94.8(2)	34.6	86.0	204.6	133.8	[118]
(I*t*Bu)Si=Si(R$_1$)$_2$ [e]	2.179(1)	1.962(2)	105.4(1)	89.6(1)	129.4	221.8	158.2	–	[277]
(I*i*Pr$_2$Me$_2$)Ge=Si(R$_2$)$_2$ [f]	2.252(1)	2.047(2)	98.90(5)	63.8(1)	–	158.9	177.9	–	[247]
(I*i*Pr$_2$Me$_2$)Ge=Si(R$_2$)(SiCl(R$_2$)$_2$)[f]	2.276(1)	2.061(4)	101.9(1)	61.1(2)	–	162.5	178.5	–	[248]
(SIDipp)Si(Cl)=Ge(Ar^{Mes})	2.2841(5)	1.877(2)	100.87(5)	3.9(1)	81.8	–	185.4	114.5	[253]
		1.878(2)	98.91(5)	7.9(1)					
(IMe$_4$)Si(SiR$_3$)=Si(SiR$_3$) [g]	2.199(1)	1.922(2)	120.35(2)	81.9(1)	28.7	–	160.9	–	[251]
(I*i*Pr$_2$Me$_2$)Ge(BR$_2$)=Ge(BR$_2$) [h]	2.279(1)	2.003(5)	111.6(1)	93.8(2)	–	–		–	[252]

[a]: φ_{carb} the angle between the least-squares plane of the carbene five-membered ring and the plane defined by the C^{carb} and the doubly-bonded tetrel atoms.
[b]: ^{29}Si NMR resonance of the CAAC/NHC coordinated silicon center. [c]: ^{29}Si NMR resonance of the three-coordinated silicon(II) center. [d]: ^{15}N NMR resonance of the N-atom(s) in the CAAC (NHC) carbene ring referenced against NH_3(l). [e]: $(R_1)_2$ = [C(Ar)$_2$-(CH$_2$)$_2$-C(Ar)$_2$] (Ar = C$_6$H$_2$-3,5-*t*Bu$_2$-4-OMe). [f]: R_2 = Trip= C$_6$H$_2$-2,4,6-*i*Pr$_3$. [g]: SiR$_3$ = Si(*i*Pr)(CH(SiMe$_3$)$_2$)$_2$. [h]: I*i*Pr$_2$Me$_2$ = C[N(*i*Pr)C(Me)]$_2$. BR$_2$ = B[N(Dipp)CH]$_2$. [i]: Measured in (D_8)THF, 298 K. [j]: Bonding parameters and spectroscopic data of the IMe$_4$ carbene in **18**. [k]: crystallographic properties of the *E*-isomer. [l] measured in (D_8)toluene, 243 K.

3.2 Outlook

In this work was shown that neutral two-coordinate silicon(I) radicals of the type Si(R)(caac^{Me}) (**3-R**) are accessible via the 1e$^-$ reduction of pyramidal 2-(amino)silenes. Besides their reduction to potassium-silenides SiK(R)(caac^{Me}) (**4-R**) and activation of cyclohexadiene in the formation of hydridosilenes SiH(R)(caac^{Me}) (**5-R**) no reactivity of these compounds has been studied thus far. This opens up a new field in studying their reactivity. In fact, the silicon(I) radicals might be valuable starting materials upon recombination with transition metal radicals [R'ML$_3$], which are generated in situ from the corresponding transition metal dimers [R'ML$_3$]$_2$ (for example [Cp*Cr(CO)$_3$]$_2$, [Tp'Cr(CO)$_3$]$_2$, [Tp'Mo(CO)$_2$PMe$_3$]$_2$), in the synthesis of metalla-silylidynes.

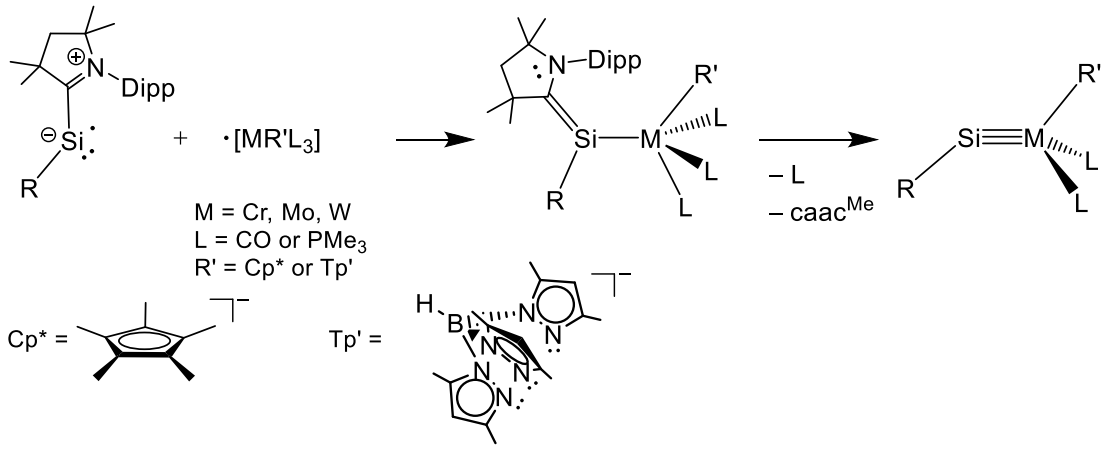

Figure 3.7. Possible reaction sequence to a group VI-metallasilylidyne.

The potassium-silenide SiK(C≡CTMS)(caac^{Me}) (**10-C$_2$TMS**), isolated in this work, provided to be a promising building block. The reactivity with organic electrophiles such as CO_2, ClC(O)Ph, PhC(O)Ph, as well as conjugated systems should be tested. Since the reactivity of silenyl-anions is recently a very fast developing field.

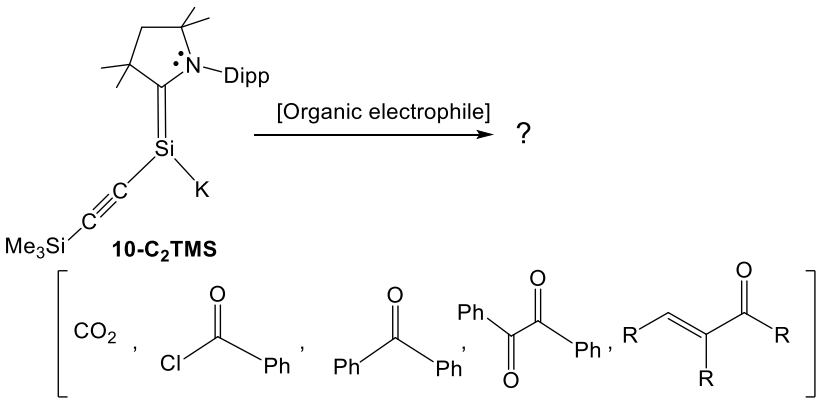

Scheme 3.13. Possible reactivity studies of silenide **10-C$_2$TMS** with organic electrophiles.

The CAAC-supported disilavinylidene (caac^{Me})Si=SiBr(Tbb) (**14**) described in this work appeared to have an enhanced electrophilicity at the SiBr(Tbb) moiety compared to the NHC-stabilized disilavinylidene. Also the high proclivity of the system to form Si=(caac^{Me}) double bonds, as well as the less sterical demand compared to SIDipp might facilitate the reactivity towards transition metals. In particular, the oxidative addition of transition metal centers bearing one or two halogen centers [MX_2L_n], for example [$X_2M(PMe_3)_4$] (M = Cr, Mo, W; X = Cl, Br) or [$TaX_2(PMe_3)_4$], [$TaX_2(dmpe)_2$] (X = Cl, Br) to the disilavinylidene should be tested. The dinitrogen-complexes [$Cl_2M(PMe_3)_3$=N–N=$MCl_2(PMe_3)_3$] (M = Mo, W) might be also useful reagents. In case the lewis basidity of **14** is not strong enough to foster a nucleophilic attack the reactivity of the IMe_4 aduct **17** should be tested towards halogen bearing transition metal complexes.

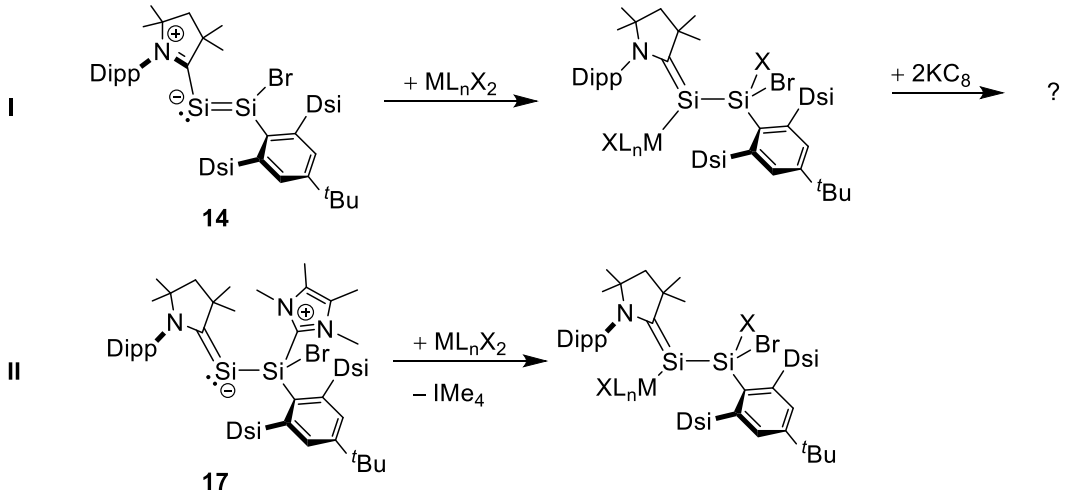

Scheme 3.14. Plausible synthetic route to silenyl-transition metal complexes, which upon reduction might lead to promising disilavinylidene transition metal complexes.

The CV of the disilynylium salt **18** features a reversible 1e$^-$-reduction $E_{1/2}$ = –1.388 V vs. $DMFc^{+/0}$, suggesting the formation of a silicon(I) radical. The compound should be isolated upon reduction of **18** with 1 equiv. of KC_8. The paramagnetic compound might feature an interesting electronic structure (*Scheme 3.15*).

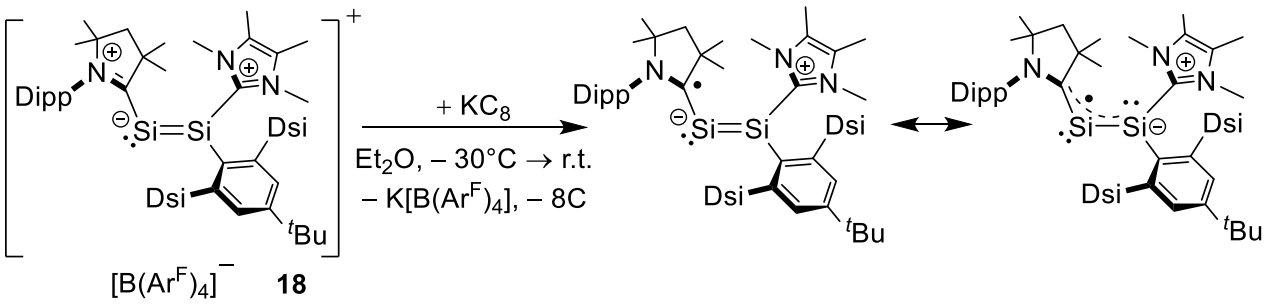

Scheme 3.15. Feasable synthetic approach to a silicon(I) radical, with an assumed delocalized spin density over the C^{carb}, Si1 and Si2 atoms.

4 Experimental Section

4.1 General part

All experiments were carried out under strict exclusion of air and moisture in an atmosphere of argon using Schlenk or glove box techniques. Argon was commercially received with a purity of ≥ 99.998 % and passed through a gas purification system composed of two consecutive columns to remove traces of oxygen and water. The first column was filled with the BTS catalyst Puristar® R3–11G operating at ca. 80 °C, whereas the second column was filled with 4 Å molecular sieves and kept at room temperature. All glassware was dried in a drying oven at approximately 110 °C and baked in fine vacuum (10^{-2} mbar) prior to use. Stainless steel transfer and filter cannulas (∅ = 1 or 2 mm) were used for the transfer of liquids and filtrations through Glass Microfiber filters (GF/B) from Whatman™, respectively. Fritted glass (porosity: *P3*) was used for the filtrations carried out inside the glove boxes.
All solvents were dried upon refluxing over suitable drying agents, were purged several times with argon during reflux and distilled under argon. The following drying agents were used for the solvents:

Solvent	**Prior storage over**	**Predrying agent**	**Drying agent**
n-hexane,*n*-pentane, PE		sodium-wire	sodium-wire/tetraglyme (0.5 vol%)
Tetrahydrofuran (THF)[a] Dimethoxyethane (DME)[a] diethyl ether (Et_2O)[a]	KOH	sodium-wire	sodium-wire/ benzophenone dianion ($Na_2[Ph_2CO]$)[a]
benzene, toluene			sodium-wire
Chloroform ($CHCl_3$)		Sicapent	CaH_2
Dichloromethane (CH_2Cl_2)[b]	$CaCl_2$	Sicapent(1) Sicapent(2)	CaH_2
Fluorobenzene[c]		CaH_2	$LiAlH_4$[c]

[a]: THF, DME and Et_2O are typically dried by distillation over Na/benzophenone ketyl ($Na[Ph_2CO]$), see references [306] and [307]. For the synthesis and characterization of $Na_2[Ph_2CO]$ see [308]. [b]: commercial available dichloromethane (CH_2Cl_2) depending on the supplier contained either traces of ethanol or amylenes, which were removed upon extraction of the solvent with sulphuric acid and water. Therefore a thoroughly drying procedure needed to be carried out, involving the destiliation from two sicapent predryer flasks. [c]: commercial available fluorobenzene contained traces of acetone, which were removed upon stirring the predryed solvent over $LiAlH_4$ for atleast 3 h and freshly recondensing it prior to use.

After distillation all solvents were degassed by freeze-pump-thaw cycles and stored in glove boxes in SCHOTT DURAN® laboratory glass bottles. For very sensitive compounds the solvents *n*-pentane and benzene were stirred over night over KC_8 and filtered inside the glovebox prior to use. For air-stable compounds commercially available solvents were used without purification.

4.2 Analytic methods

4.2.1 NMR spectroscopy

The NMR spectra were recorded either on a Bruker Avance 300 MHz or a Bruker Avance IIID 500 MHz NMR spectrometer in dry deoxygenated deuterated solvents, using Ø = 5 mm NMR tubes equipped with J. Young valves. The deuterated solvents were dried by stirring over sodium-potassium alloy ((D6)benzene, (D8)toluene and (D8)THF) or CaH_2 ((D2)dichloromethane and (D5)chlorobenzene) degassed and then trap-to-trap condensed and stored over molecular sieves (4 Å) in Schlenk flasks equipped with J. Young valves. The ^{1}H and $^{13}C\{^{1}H\}$ NMR spectra were calibrated against the residual proton and natural abundance ^{13}C resonances of the deuterated solvent relative to tetramethylsilane set at $\delta = 0$ ppm ((D6)benzene: $\delta_H = 7.15$ ppm and $\delta_C = 128.0$ ppm; (D8)toluene: $\delta_H = 2.08$ ppm and $\delta_C = 20.43$ ppm; (D5)chlorobenzene: $\delta_H = 7.14$ ppm and $\delta_C = 125.96$ ppm; (D8)THF: $\delta_H = 1.73$ ppm and $\delta_C = 25.3$ ppm; (D2)dichloromethane: $\delta_H = 5.32$ ppm and $\delta_C = 53.8$ ppm), respectively. The recently reported ^{1}H no D NMR method was employed at the Bruker Avance IIID 500 MHz NMR spectrometer and was used for monitoring reaction mixture solutions in benzene(C_6H_6), fluorobenzene (C_6H_5F) and *m*-difluorobenzene (C_6H_4-1,3-F_2).[309]

The ^{29}Si NMR spectra were calibrated using the ^{2}H frequency of the deuterated solvent (lock frequency) and the frequency ratio value $\Xi(^{29}Si) = 19.867187$ as recommended by IUPAC for $SiMe_4$ as external reference.[310] The ^{15}N NMR spectra were calibrated using the ^{2}H frequency of the deuterated solvent (lock frequency) and the frequency ratio value $\Xi(^{15}N) = 10.132912$ as recommended by IUPAC for neat liquid ammonia as external reference.[310] All lock frequencies were calibrated internally against the ^{1}H NMR signals of solutions of tetramethylsilane ($\delta_H = 0$ ppm) with a volume fraction of ≤ 1 % in the corresponding degassed deuterated solvent. The ^{15}N NMR signals of the compounds were obtained by inverse detected 2D NMR (^{1}H-^{15}N HMBC pulse sequence) experiments. The following abbreviations were used for the forms and multiplicities of the NMR signals: s – singlet, d – doublet, t – triplet, sept – septet, m – multiplet, br – broad. The full width at half maximum of broad signals was designated with $\Delta\nu_{1/2}$ and is given in Hz. All coupling constants are given in Hz as absolute values regardless of their signs. The ^{1}H and ^{13}C NMR signals of all compounds were assigned by a combination of ^{1}H-^{13}C HMQC and HMBC experiments.

The ^{1}H NMR signals of the C^{5} and C^{3}-bonded methyl groups of caac^{Me} were assigned by ^{1}H-^{15}N HMBC spectroscopy. This allowed in combination with the ^{1}H-^{13}C HMQC and HMBC experiments an unequivocal assignment of all proton and carbon resonances including those of the diastereotopic methyl groups of the $C^{2,6}$-bonded isopropyl groups of the 2,6-diisopropylphenyl (Dipp) substituent, which were labeled with the subscript letters A and B, respectively. The label A was arbitrarily used for the more shielded methyl protons of the isopropyl groups.

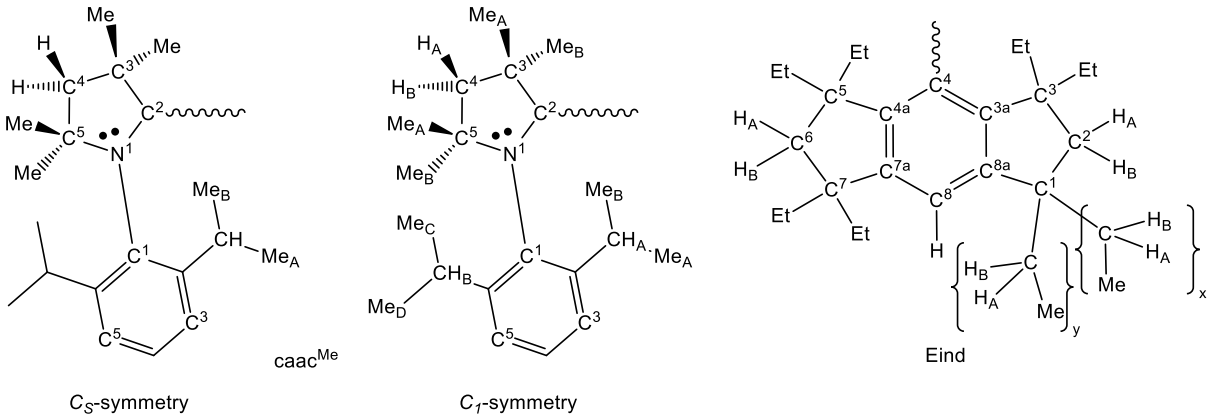

Figure 4.1. caac^{Me} and Eind ligand numbering scheme of the work group of A. C. Filippou.

4.2.2 X-ray crystallography

Typically, crystals for the X-ray diffraction analysis were filtered from their supernatant solution at the temperature of crystallization and covered with Fomblin Y® lubricant. A crystal suitable for the measurement was selected on a microscope and transferred to the y diffractometer. The data collection was performed on a Bruker D8-Venture diffractometer using graphite monochromated Mo-K_α radiation (ƛ= 0.7107 Å). The diffractometer was equipped with a low-temperature device (Oxford Cryostream 700er series, 100.0 K). Intensities were measured by fine-slicing ω and ϕ-scans and corrected for background, polarization and Lorentz effects. An absorption correction by integration was applied for all data sets.[11] The structures were solved by direct methods and refined anisotropically by the least-squares procedure implemented in the SHELX program system.[12] Hydrogen atoms except the silicon-bonded hydrogen atom were included using the riding model on the bound carbon atoms. The silicon-bonded hydrogen atom was found on the difference Fourier map and anisotropically refined. Selected crystallographic refinement data are listed in *section 5.1*.

11 SADABS, 2009/2, AXS, 2009.

12 G. M. Sheldrick, SHELXS97 and SHELXL97, University of Göttingen, Germany, 1997.

4.2.3 Elemental Analysis

The C, H, N analyses were carried out in quadruplicate for each sample using an Elementar Vario Micro elemental analyser. The individual C, H and N values did not differ by more than ±0.3 %, and the mean C, H, N values are given for each compound. The mean values of the measurements are given. The sample handling and measurement was done by the central EA facility of the Institute.

4.2.4 Melting points determination

The melting points were determined of analytically pure samples in duplicate using a Büchi melting point apparatus M-560, which was calibrated by using the following melting points standards: 4-nitrotoluene (52.5 +/– 0.2 °C at 0.5 °C/min), diphenylacetic acid (147.7 +/– 0.2 °C at 0.5 °C/min), caffeine (236.5 +/– 0.2 °C at 0.5 °C/min), and potassium nitrate (334.5 +/– 0.2 °C at 0.5 °C/min). The samples were sealed in glass capillaries under vacuum and heated once with a gradient of 5 °C/min for a rough determination of the melting point or temperature of starting decomposition. Heating of the second and third samples was then repeated with a gradient of 2 °C/min starting 20 °C below the temperature of melting or decomposition determined in the first experiment. The onset temperature of melting or decomposition of the samples is given without correction for the temperature gradient. The thermally treated samples were cooled to ambient temperature and analyzed by ^{1}H NMR spectroscopy in (D_6)benzene to elucidate whether decomposition had occurred.

4.2.5 CW-EPR spectroscopy

The samples used for the continuous-wave EPR (CW-EPR) experiments were prepared by dissolving small amounts of analytically pure compound (typically 1 mg, determined by fine balance) and dissolving it in 10 mL of solvent (*n*-pentane, benzene or toluene, which was additionally dried overnight over KC_8 and filtered prior to use) in the glove box in order to afford dilute solutions (c ≈ 200 µmol L^{-1}). The solution was transferred to a Wilmad® Suprasil EPR tube (Ø = 3.8 mm) tapped with a J. Young valve and diluted 1 : 1 with the corresponding solvent to obtain a concentration of c ≈ 100 µmol L^{-1}. The solution was immediately frozen in liquid nitrogen prior to the EPR measurements to ensure that the radical does not start to decompose prior to the EPR measurment. In case of *n*-pentane the CW-EPR experiments were performed at 100 K and from 173 K to 298 K in 5 K steps. In case of benzene the CW-EPR experiments were performed at 100 K, 200 K and from 273 K to 298 K in 5 K steps at X-band microwave (MW) frequencies on a Bruker EMXmicro EPR spectrometer with the EMXmicro standard resonator (E4119001). The sample temperature was adjusted using a liquid nitrogen evaporator and the ER 4131VT temperature control system.

A Super High-Q resonator (empty resonator frequency: 9.85 GHz) and an Oxford ESR900 helium gas-flow cryostat was employed. For each measurement it was validated neither that a saturation of the EPR signal occurred nor that the resolution could be further improved by varying the microwave power and the modulation amplitude. The spectra were simulated using the garlic routine of the EasySpin program package.[311]

4.2.6 Evan's method

The magnetic measurements of radical **3-Si** were carried out via the Evan's method with modification of Sur at ambient temperature in (D_6)benzene solution.[312,313] Therefore three coaxial NMR tubes were constructed by inserting a one-end-sealed glass capillary tube of 1.0 mm diameter and approximately 10 cm in length into each J-young NMR tube. The capillary tube can be easily prepared from the Pasture pipette.

Solutions of known concentration of analytically pure paramagnetic compounds were prepared in (D_6)benzene and each filled up to 5 cm height into the prepared capillary tubes. The tubes were inserted carefully into three J-Young NMR tubes containing 0.4 mL of (D_6)benzene each. ^{1}H NMR spectra were recorded under the standard conditions (300.13 MHz, Puls Sequence zg30, ns = 16, D1 = 1.000, Acq. Time = 5.4527).

4.2.7 Cyclic Voltammetry

The cyclic voltammetric studies were performed with an Autolab Eco electrochemical workstation composed of a Metrohm Autolab PGSTAT 100 potentiostat/galvanostat. The results were analyzed with the NOVA software version 2.1.4 (Metrohm Autolab). The experiments were carried out in a glove box under argon in a gas-tight specially designed full-glass three-electrode cell at ambient temperature. A glassy carbon electrode (GCE Ø = 2 mm) was used as working electrode, a Pt wire of 1 mm diameter as counter electrode and referenced against ferrocene $[Fe(C_5H_5)_2]^{+1/0}$ which was added after the measurement. The experiments were carried out in either THF or fluorobenzene and depending on the analyte [*n*Bu$_4$N][PF$_6$] or [*n*Bu$_4$N][Al(OC(CF$_3$)$_3$)$_4$] were used as supporting electrolytes, respectively. All potentials are reported relative to the reference electrode. For comparison reasons, the half-wave potential of the $[Fe(C_5H_5)_2]^{+1/0}$ versus the $[Fe(C_5Me_5)_2]^{+1/0}$ redox couple was determined under the same conditions by a separate cyclic voltammetric experiment and found to be $E_{1/2}$ = 520 mV.

4.2.8 UV/Vis NIR spectroscopy

The UV-Vis-NIR spectra of analytically pure compounds were recorded on a Thermo Scientific Evolution 300 spectrometer in a special designed quartz cuvette under inert conditions. The measurements were performed using three different path lengths (d = 1 mm, 5 mm and 10 mm) and four different concentrations (ranging from 400 µmol L^{-1} to 10 µmol L^{-1}) in *n*-hexane or Et_2O(which was additionally dried over KC_8 and filtered piror to use) at ambient temperature. The absorption bands were determined by means of band deconvolution assuming a Gaussian line profile.

4.3 List of isolated and spectroscopically characterized compounds

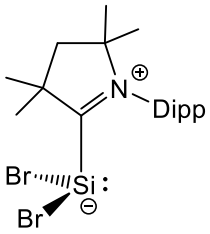

1

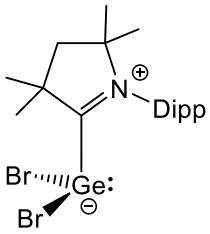

1-Ge

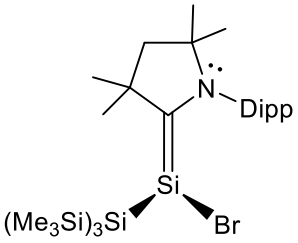

2-Si

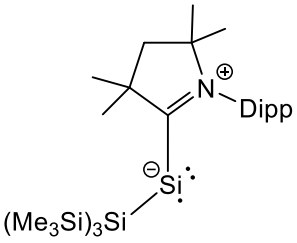

3-Si

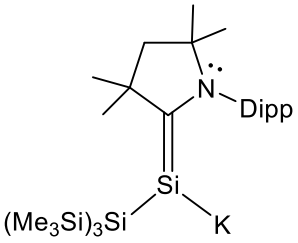

4-Si

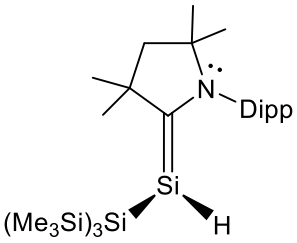

5-Si

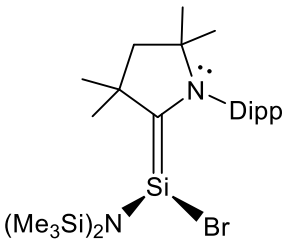

2-N

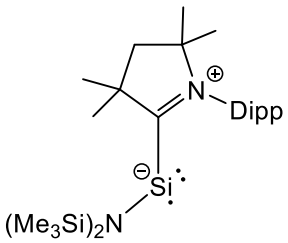

3-N

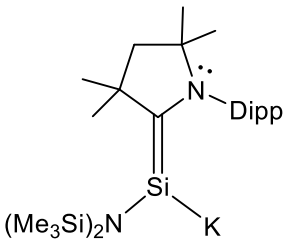

4-N

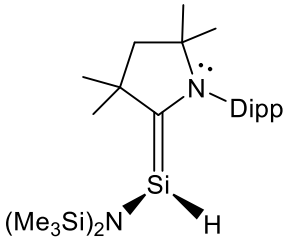

5-N

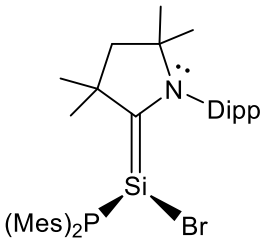

2-P

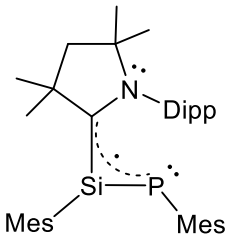

6

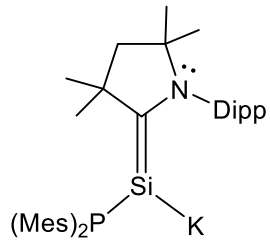

4-P

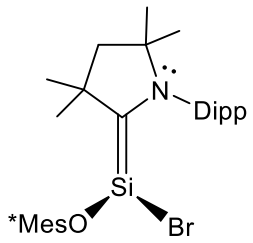

2-O

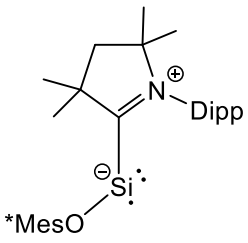

3-O

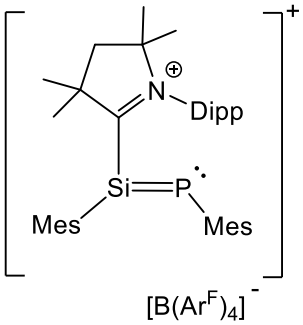

7

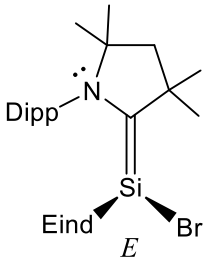

2-Eind-*E*

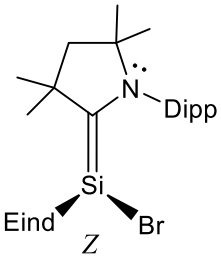

2-Eind-*Z*

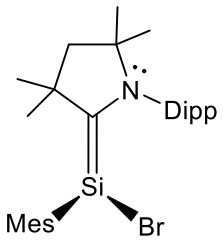

2-Mes

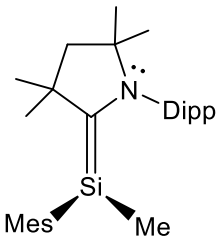

8

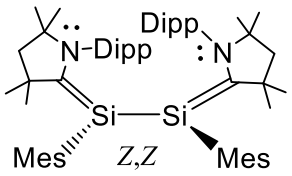

9-Mes-*Z,Z*

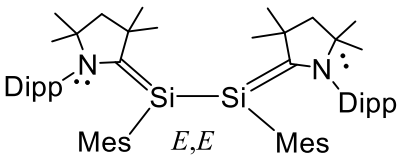

9-Mes-*E,E*

as diasteromeric mixture

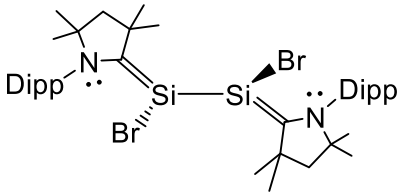

9-Br

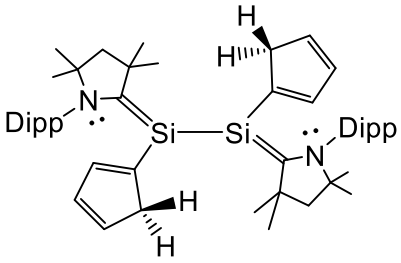

9-Cp‘

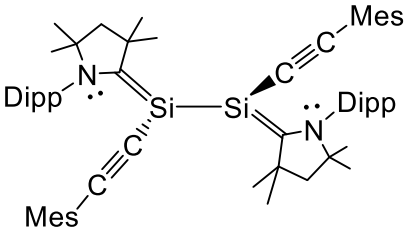

9-C$_2$Mes

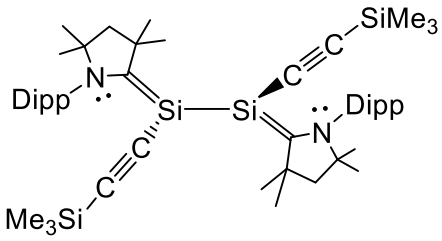

9-C$_2$TMS

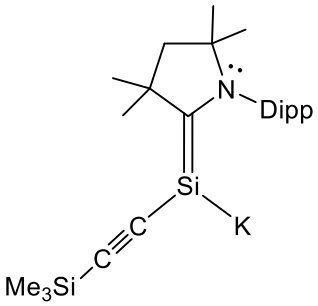

10-C$_2$TMS

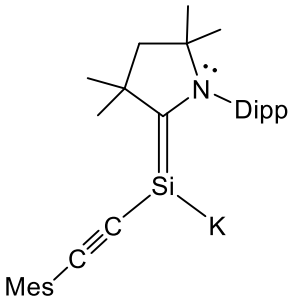

10-C$_2$Mes

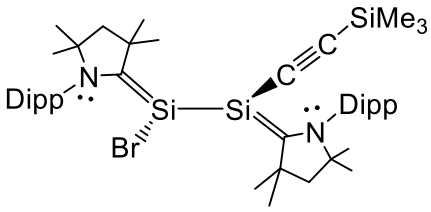

11-Br

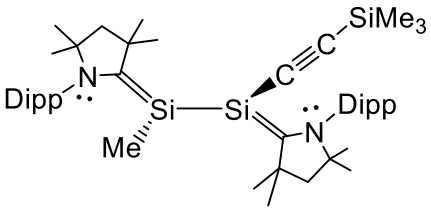

11-Me

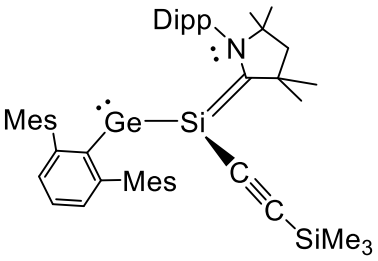

12

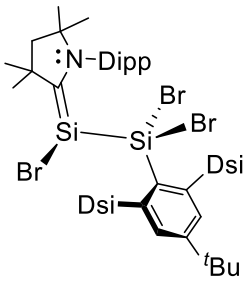

13

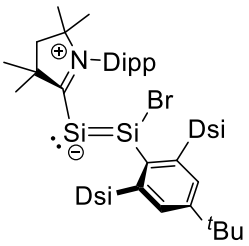

14

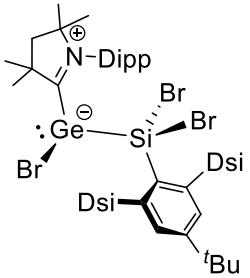

13-Ge

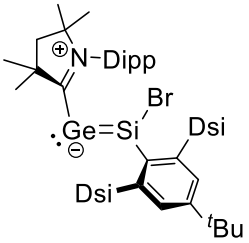

14-Ge

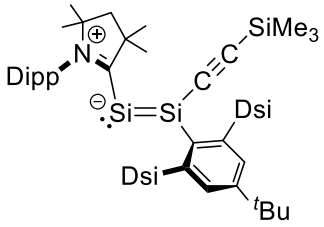

14-C_2TMS

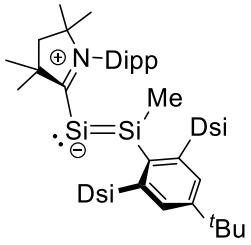

14-Me

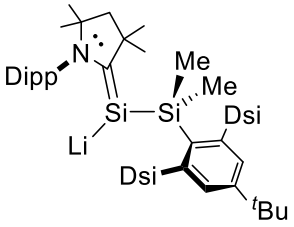

15

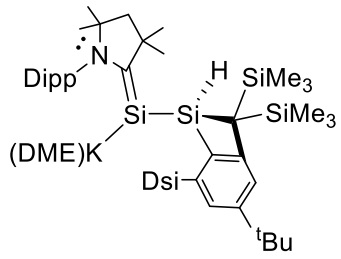

16

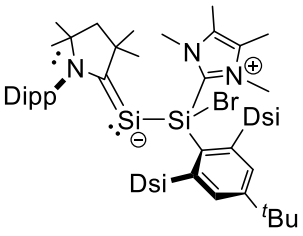

17

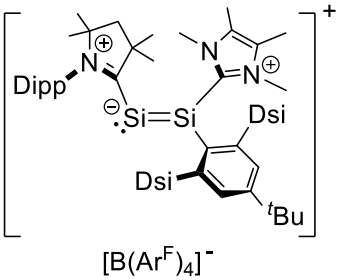

18

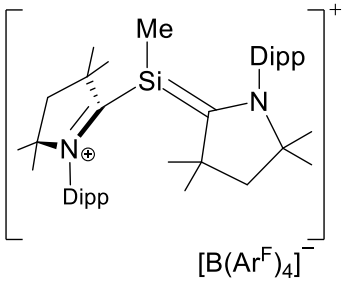

19

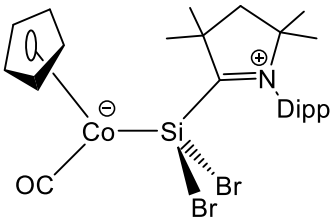

20

4.4 Syntheses and analytical/spectroscopic data of compounds

4.4.1 $SiBr_2(caac^{Me})$ (1)

A 1 L Schlenk tube was charged with $SiBr_4(caac^{Me})$ (41.5 g, 65.5 mmol, 1.0 equiv.), KC_8 (19.49 g, 144 mmol, 2.2 equiv.) and 500 mL of benzene at ambient temperature. The suspension was sonicated for 1 h, upon which the color of the solution changed from colorless to red-brown. After stirring at ambient temperature for 19 h the color of the superenatant solution changed to red-purple. An aliquot of the reaction mixture was taken and analyzed by ^{1}H NMR spectroscopy in (D_6)benzene, revealing the selective formation of $SiBr_2(caac^{Me})$ (**1**) alongside small amounts of $Si_2Br_2(caac^{Me})_2$ (**9-Br**) and small amounts of unknown ($caac^{Me}$)H containing product of unknown composition (ca. 5 mol%). The reaction mixture was filtered (p3 frit) and the black graphite residue extracted with 5 x 50 mL of benzene.[13] The combined red-purple filtrate was reduced to volume of approx. 40 mL, upon which a part of the product precipitated out as a brick-red solid. In order to complete the precipitation 200 mL of *n*-hexane was added. The brick-red precipitate was filtered (p3 frit), washed with 4 x 10 mL of benzene/*n*-hexane (1:5) followed by 3 x10 mL of *n*-pentane and finally dried in fine vacuum for 0.5 h at ambient temperature.[14] Yield: 21.23 g (44.8 mmol, 68%).

Properties: Dibromosilylene **1** is insoluble in *n*-hexane, moderately soluble in benzene and toluene, and well soluble in THF at ambient temperature. It disproportionates in benzene, toluene and THF solution at ambient temperature, its red colored solutions turning purple due to the formation of $Si_2Br_2(caac^{Me})_2$ (**9-Br**). The disproportionation is moderately fast in benzene and toluene, but slow in THF at ambient temperature and leads to an equilibrium between $SiBr_2(caac^{Me})$ (**1**), the radical $SiBr_3(caac^{Me})^{\bullet}$ and $Si_2Br_2(caac^{Me})_2$ (**9-Br**).

Elemental analysis: $C_{20}H_{31}Br_2NSi$ (473.36 g·mol^{-1}): calcd./%: C 50.75, H 6.60, N 2.96; found/%: C 50.80, H 6.65, N 2.84 . **Melting point:** 176 – 177 °C (dec).

^{1}H NMR (300.13 MHz, (D_6)benzene, 298 K): δ (ppm) = 0.74 (s, 6H, C^5Me_2), 1.02 (d, ^3J(H,H) = 6.7 Hz, 6H, $C^{2,6}$-CHMe_AMe$_B$, Dipp), 1.41 (s, 2H, C^4H_2), 1.44 (d, ^3J(H,H) = 6.7 Hz, 6H, $C^{2,6}$-CHMe$_A$$Me_B$, Dipp), 1.88 (s, 6H, C^3Me_2), 2.65 (sept, ^3J(H,H) = 6.7 Hz, 2H, $C^{2,6}$-C*H*Me$_A$Me$_B$, Dipp), 6.91 (m, 2H, $C^{3,5}$-*H*, Dipp), 7.04 (m, 1H, C^4-*H*, Dipp).

---

13 To reduce the volume of benzene a mixture of THF/benzene (1:10) can be used for the extraction $SiBr_2(caac^{Me})$.

14 The contact of the crude product with the solvents should be as short as possible in order to avoid the disproportionation reaction of the compound.

^{1}H NMR (500.17 MHz, (D_8)THF, 298 K): δ (ppm) = 1.32 (d, ^{3}J(H,H) = 6.7 Hz, 12H, $C^{2,6}$-CHMe_AMe_B, Dipp), 1.41 (s, 6H, $C^{5}Me_2$), 1.96 (s, 6H, $C^{3}Me_2$), 2.22 (s, 2H, $C^{4}H_2$), 2.81 (sept, ^{3}J(H,H) = 6.7 Hz, 2H, $C^{2,6}$-C*H*Me_AMe_B, Dipp), 7.33 (d, ^{3}J(H,H) = 7.8 Hz, 2H, $C^{3,5}$-*H*, Dipp), 7.43 (t, ^{3}J(H,H) = 7.8 Hz, 1H, C^{4}-*H*, Dipp).

^{1}H NMR (500.17 MHz, (D_8)THF, 243 K): δ (ppm) = 1.30 (d, ^{3}J(H,H) = 6.6 Hz, 6H, $C^{2,6}$-CH$Me_A$$Me_B$, Dipp), 1.32 (d, ^{3}J(H,H) = 6.6 Hz, 6H, $C^{2,6}$-CH$Me_A$$Me_B$, Dipp). 1.40 (s, 6H, $C^{5}Me_2$), 1.95 (s, 6H, $C^{3}Me_2$), 2.24 (s, 2H, $C^{4}H_2$), 2.78 (sept, ^{3}J(H,H) = 6.6 Hz, 2H, $C^{2,6}$-C*H*Me_AMe_B, Dipp), 7.37 (d, ^{3}J(H,H) = 7.7 Hz, 2H, $C^{3,5}$-*H*, Dipp), 7.47 (t, ^{3}J(H,H) = 7.7 Hz, 1H, C^{4}-*H*, Dipp).

^{13}C{^{1}H} NMR (125.77 MHz, (D_8)THF, 298 K): δ (ppm) = 24.2 (s, 2C, $C^{2,6}$-CH$Me_A$$Me_B$, Dipp), 27.1 (s, 2C, $C^{2,6}$-CH$Me_A$$Me_B$, Dipp), 28.7 (s, 2C, $C^{5}Me_2$), 29.7 (s, 2C, $C^{2,6}$-*C*HMe_AMe_B, Dipp), 31.1 (s, 2C, $C^{3}Me_2$), 52.8 (s, 1C, $C^{4}H_2$), 58.7 (s, 1C, $C^{3}Me_2$), 80.6 (s, 1C, $C^{5}Me_2$), 126.1 (s, 2C, $C^{3,5}$-H, Dipp), 131.2 (s, 1C, C^{4}-H, Dipp), 132.8 (s, 1C, C^{1}, Dipp), 146.3 (s, 2C, $C^{2,6}$, Dipp), 231.7 (br, $\Delta\nu_{1/2}$ = 30 Hz, NC^{2}).

^{13}C{^{1}H} NMR (125.77 MHz, (D_8)THF, 243 K): δ (ppm) = 24.0 (s, 2C, $C^{2,6}$-CH$Me_A$$Me_B$, Dipp), 27.2 (s, 2C, $C^{2,6}$-CH$Me_A$$Me_B$, Dipp), 28.5 (s, 2C, $C^{5}Me_2$), 29.7 (s, 2C, $C^{2,6}$-*C*HMe_AMe_B, Dipp), 30.9 (s, 2C, $C^{3}Me_2$), 51.9 (s, 1C, $C^{4}H_2$), 59.0 (s, 1C, $C^{3}Me_2$), 80.9 (s, 1C, $C^{5}Me_2$), 126.1 (s, 2C, $C^{3,5}$-H, Dipp), 131.3 (s, 1C, C^{4}-H, Dipp), 132.3 (s, 1C, C^{1}, Dipp), 145.9 (s, 2C, $C^{2,6}$, Dipp), 231.2 (br, $\Delta\nu_{1/2}$ = 23 Hz, NC^{2}).

^{29}Si{^{1}H} NMR (99.37 MHz, (D_8)THF, 243 K): δ (ppm) = 14.4 (s, 1Si).

^{1}H-^{15}N HMBC (500.17 MHz, 50.68 MHz, (D_8)THF, 243 K): δ_N (ppm) = 231.3 (s, 1N, *N*C^{2}).

4.4.2 $GeBr_2(caac^{Me})$ (1-Ge)

To a colorless suspension of 2.50 g of $GeBr_2$(1,4-dioxane) (7.80 mmol, 1.00 equiv.) in 100 mL of benzene a clear solution of 2.23 g $caac^{Me}$ (7.80 mmol, 1.00 equiv.) in 10 mL of benzene was added. Upon addition a yellow precipitate formed immediately. The reaction mixture was concentrated to a volume of approx. 10 mL. Then 50 mL of *n*-pentane was added and the yellow suspension filtered. The yellow solid was dried for 1 h at 60 °C.[15] Then the compound was washed with 50 mL of THF/*n*-pentane mixture (1:5) followed by 20 mL *n*-pentane. Drying at fine vacuum for 1 h at 60 °C afforded $GeBr_2(caac^{Me})$ (**1-Ge**)[16] in analytical pure form as a yellow powder. Yield: 3.90 g (7.53 mmol, 97 %).

Properties: Dibromogermylene **1-Ge** slowly decolorizes upon contact with air. It is insoluble in *n*-hexane and *n*-pentane, poor soluble in benzene and toluene, and well soluble in THF at ambient temperature. In contrast to $SiBr_2(caac^{Me})$ the compound is stable in solution and does not show any signs of decomposition.

Elemental analysis: $C_{20}H_{31}Br_2NGe$ (517.90 g·mol^{-1}): calcd./%: C 46.38, H 6.03, N 2.71; found/%: C 46.24, H 6.00, N 2.49. **Melting point:** 243 °C (partial dec).

^{1}H NMR (300.13 MHz, (D_6)benzene, 298 K): δ (ppm) = 0.71 (s, 6H, C^5Me_2), 0.98 (d, ^3J(H,H) = 6.6 Hz, 6H, $C^{2,6}$-CHMe_AMe$_B$, Dipp), 1.31 (d, ^3J(H,H) = 6.6 Hz, 6H, $C^{2,6}$-CHMe$_A$$Me_B$, Dipp), 1.41 (s, 2H, C^4H_2), 1.95 (s, 6H, C^3Me_2), 2.66 (sept, ^3J(H,H) = 6.6 Hz, 2H, $C^{2,6}$-CHMe$_A$Me$_B$, Dipp), 6.84 (m, 2H, $C^{3,5}$-*H*, Dipp), 6.99 (m, 1H, C^4-*H*, Dipp).

^{1}H NMR (500.17 MHz, (D_8)THF, 298 K): δ (ppm) = 1.28 (d, 6H, ^3J(H,H) = 6.6 Hz, $C^{2,6}$-CHMe_AMe$_B$, Dipp), 1.33 (d, ^3J(H,H) = 6.6 Hz, 6H, $C^{2,6}$-CHMe$_A$$Me_B$, Dipp), 1.43 (s, 6H, C^5Me_2), 1.96 (s, 6H, C^3Me_2), 2.21 (s, 2H, C^4H_2), 2.85 (sept, ^3J(H,H) = 6.6 Hz, 2H, $C^{2,6}$-CHMe$_A$Me$_B$, Dipp), 7.39 (d, ^3J(H,H) = 7.6 Hz, 2H, $C^{3,5}$-*H*, Dipp), 7.50 (t, ^3J(H,H) = 7.6 Hz, 1H, C^4-*H*, Dipp).

^{13}C{^{1}H} NMR (125.77 MHz, (D_8)THF, 298 K): δ (ppm) = 24.2 (s, 2C, $C^{2,6}$-CHMe$_A$$Me_B$, Dipp), 27.9 (s, 2C, $C^{2,6}$-CHMe_AMe$_B$, Dipp), 28.7 (s, 2C, C^5Me_2), 29.5 (s, 2C, $C^{2,6}$-CHMe$_A$Me$_B$, Dipp), 31.0 (s, 2C, C^3Me_2), 52.3 (s, 1C, C^4H_2), 60.3 (s, 1C, C^3Me_2), 81.8 (s, 1C, C^5Me_2), 126.5 (s, 2C, $C^{3,5}$-H, Dipp), 131.7 (s, 1C, C^4-H, Dipp), 132.1 (s, 1C, C^1, Dipp), 146.6 (s, 2C, $C^{2,6}$, Dipp), 241.6 (s, 1C, NC^2).

^{1}H-^{15}N HMBC (500.17 MHz, 50.68 MHz, (D_8)THF, 298 K): δ_N (ppm) = 234.2 (s, 1N, *N*C^2).

---

15 ^{1}H NMR spectroscopy in (D_6)benzene revealed the presence of 6 mol% of 1,4-dioxane.

16 The analogous compound $GeCl_2(caac^{Me})$ is reported by H. Roesky et al., see reference [161].

4.4.3 SiBr(SiTMS$_3$)(caac^{Me}) (2-Si)

To a red solution of SiBr$_2$(caac^{Me}) (**1**) (855 mg, 1.81 mmol, 1.00 equiv.) in 20 mL of THF was added dropwise a solution of Li(THF)$_3$[Si(SiMe$_3$)$_3$] (935 mg, 1.99 mmol, 1.10 equiv.) in 20 mL of THF at ambient temperature. An orange-brown solution was immediately formed. After stirring for 1 h at ambient temperature an aliquot was taken and analyzed by ^{1}H NMR spectroscopy in (D$_6$)benzene, which showed complete consumption of **1** and selective formation of SiBr(SiTMS$_3$)(caac^{Me}) (**2-Si**) alongside small amounts (ca. 6 mol%) of Si$_2$Br$_2$(caac^{Me})$_2$ (**9-Br**). The reaction mixture was worked-up by evaporating the solvent to dryness under fine-vacuum, drying the crude product at 40 °C under fine-vacuum for 1 h, and removing the LiBr from the crude product by extracting it with *n*-hexane (115 mL). The dark-brown *n*-hexane filtrate was evaporated to obtain an orange-brown solid, which was dried under fine-vacuum for 1 h at 40 °C. This solid was crystallized twice from *n*-hexane (10 mL) at 0 °C to afford, after filtering off the red mother liquor and drying the solid under fine-vacuum for 1 h at 40 °C, SiBr(SiTMS$_3$)(caac^{Me}) (**2-Si**) as analytically pure orange powder. Yield: 760 mg (1.19 mmol, 66 %).

Properties: Compound **2-Si** is well soluble in benzene, toluene or THF, but shows only a medium solubility in aliphatic solvents, such as *n*-pentane or *n*-hexane.

Elemental analysis: C$_{29}$H$_{58}$BrNSi$_5$ (641.11 g/mol): calcd./%: C 54.33, N 2.18, H 9.12; found/%: C 54.35, N 2.04, H 9.15. **Melting point:** 190 °C (dec).

^{1}H NMR (500.17 MHz, (D$_6$)benzene, 298 K): δ (ppm) = 0.45 (s, 27H, (Si*Me*$_3$)$_3$), 1.05 (s, 6H, C^5*Me*$_2$), 1.21 (d, ^{3}*J*(H,H)= 6.8 Hz, 6H, C^{2,6}-CH*Me*$_A$Me$_B$, Dipp), 1.55 (s, 6H, C^3*Me*$_2$), 1.62 (d, ^{3}*J*(H,H)= 6.7 Hz, 6H, C^{2,6}-CHMe$_A$*Me*$_B$, Dipp), 1.65 (s, 2H, C^4*H*$_2$), 3.11 (sept, ^{3}*J*(H,H)= 6.7 Hz, 2H, C^{2,6}-C*H*Me$_A$Me$_B$, Dipp), 7.04 (d, ^{3}*J*(H,H)= 7.8 Hz, 2H, C^{3,5}-*H*, Dipp), 7.18 (dd, ^{3}*J*(H,H)= 7.8 Hz, 1H, C^4-*H*, Dipp).

^{13}C{^{1}H} NMR (75.48 MHz, (D$_6$)benzene, 298 K): δ (ppm) = 3.9 (s, 9C, (Si*Me*$_3$)$_3$), 25.5 (s, 2C, C^{2,6}-CH*Me*$_A$Me$_B$, Dipp), 26.5 (s, 2C, C^{2,6}-CHMe$_A$*Me*$_B$, Dipp), 28.8 (s, 2C, C^5*Me*$_2$), 29.2 (s, 2C, C^{2,6}-*C*HMe$_A$Me$_B$, Dipp), 36.2 (s, 2C, C^3*Me*$_2$), 50.5 (s, 1C, *C*^{3}Me$_2$), 55.2 (s, 1C, *C*^{4}H$_2$), 72.4 (s, 1C, *C*^{5}Me$_2$), 124.9 (s, 2C, *C*^{3,5}-H, Dipp), 129.0 (s, 1C, *C*^{4}-H, Dipp), 135.9 (s, 1C, *C*^{1}, Dipp), 148.8 (s, 2C, *C*^{2,6}, Dipp), 205.2 (s, 1C, N*C*^{2}).

^{29}Si{^{1}H} NMR (99.36 MHz, (D$_6$)benzene, 298 K): δ (ppm) = 24.7 (s, 1Si, *Si*=caac^{Me}), 8.5 (s, 3Si, Si(*Si*Me$_3$)$_3$), –101.4 (s, 1Si, *Si*(SiMe$_3$)$_3$).

^{1}H-^{15}N HMBC (500.14 MHz, 50.69. MHz, (D$_6$)benzene, 298K): δ$_N$ (ppm) = 162.9 (1N, *N*C^2).

4.4.4 Si(SiTMS$_3$)(caac^{Me})• (3-Si)

A Schlenk tube was charged with SiBr(SiTMS$_3$)(caac^{Me}) (**2-Si**) (575 mg, 0.897 mmol, 1.0 eq.) and KC_8 (133 mg, 1.37 mmol, 1.1 eq.) and 20 mL benzene were added to it at ambient temperature. After stirring for 14 h at ambient temperature the reaction solution turned dark-purple. Monitoring of the reaction mixture after 15 h at ambient temperature by ^{1}H-NMR spectroscopy in (D_6)benzene revealed the presence of broad signals originating from a paramagnetic compound, next to tiny amounts of SiH(SiTMS$_3$)(caac^{Me}) (**5-Si**). The reaction mixture was filtered off and extracted with benzene (3 × 5 mL). The resulting combined dark-purple extracts were evaporated and dried under fine-vacuum for 0.5 h at 40 °C. The dark-brown residue was dissolved in 3 mL of boiling *n*-pentane. Dark purple crystals were obtained after storing the solution for 5 h at −24 °C. The crystals were isolated after separating the purple colored mother liquor by a filter cannula and the solid was dried under fine-vacuum for 1 h at 40 °C. Yield: 389 mg (0.693 mmol, 77 %).

Properties: Silicon(I) radical **3-Si** is well soluble in *n*-pentane, *n*-hexane, benzene and THF affording dark purple solutions, which slowly decompose over time. The major decomposition product appears to be the hydridosilene SiH(SiTMS$_3$)(caac^{Me}) (**5-Si**) (*section 5.5.2*).

Elemental Analysis: $C_{29}H_{58}NSi_5$ (561.21 g/mol): calcd./%: C 62.07, N 2.50, H 10.42; found/%: C 62.13, N 2.49, H 10.26 . **Melting Point:** 134 °C (dec).

X-band CW EPR (9.85 GHz, *n*-pentane, 293 K, 90 µmol L^{-1}): g_{iso}= 2.0065 (a_{iso}(^{14}N) = 0.44 mT, a_{iso}(^{29}Si$_\alpha$) = 3.81 mT).

X-band CW EPR (9.85 GHz, *n*-pentane, 173 K, 90 µmol L^{-1}): g_{iso}= 2.0065 (a_{iso}(^{14}N) = 0.44 mT, a_{iso}(6 x ^{1}H, C^3*Me*$_2$) = 0.09 mT, a_{iso}(^{29}Si$_\alpha$) = 3.73 mT).

4.4.5 SiK(SiTMS$_3$)(caac^{Me}) (4-Si)

SiBr(SiTMS$_3$)(caac^{Me}) (**2-Si**) (400 mg, 0.624 mmol, 1.0 equiv.) and KC_8 (253 mg, 1.872 mmol, 3.0 equiv.) were suspended in 20 mL of benzene. The reaction mixture was stirred for 16 h at ambient temperature and the suspension turned dark brown. NMR spectroscopy of an aliquot of the reaction mixture in (D_6)benzene revealed the quantitative formation of SiK(SiTMS$_3$)(caac^{Me}) (**4-Si**). The reaction mixture was filtered off via a filter cannula inside the glovebox and the graphite residue was extracted with benzene (3 × 4 mL). The combined dark brown filtrate was evaporated, re-suspended in pentane (5 mL) and dried at the high vacuum for 0.5 h at ambient temperature. The brown powder was washed with 4 mL of *n*-pentane via a 1 mm filter cannula inside the glovebox. Drying at high vacuum for 1 h at ambient temperature afforded analytically pure SiK(SiTMS$_3$)(caac^{Me}) (**4-Si**) as a brown powder. Yield: 314 mg (0.523 mmol, 84 %).
Properties: Silenide **4-Si** is highly pyrophoric and immediately decomposes upon contact with air. It is moderately soluble in *n*-hexane and well soluble in benzene. Its solution in Et_2O decomposes slowly at ambient temperature.
Elemental Analysis: $C_{29}H_{58}NKSi_5$ (600.30 g/mol): calcd./% : C 58.02, N 2.33, H 9.74; found/%: C 58.15, N 2.23, H 9.69. **Melting point:** 178 °C (dec).

^{1}H NMR (500.17 MHz, (D_6)benzene, 298 K): δ (ppm) = 0.55 (s, 27H, (Si*Me*$_3$)$_3$), 1.18 (d, ^3J(H,H)= 6.7 Hz, 6H, C^{2,6}-CH*Me*$_A$Me$_B$, Dipp), 1.23 (s, 6H, C^5*Me*$_2$), 1.36 (d, ^3J(H,H)= 6.7 Hz, 6H, C^{2,6}-CHMe$_A$*Me*$_B$, Dipp), 1.90 (s, 6H, C^3*Me*$_2$), 2.10 (s, 2H, C^4*H*$_2$), 3.45 (sept, ^3J(H,H)= 6.7 Hz, 2H, C^{2,6}-C*H*Me$_A$Me$_B$, Dipp), 6.64 – 6.67 (m, 1H, C^4-*H*, Dipp), 6.69 – 6.71 (m, 2H, C^{3,5}-*H*, Dipp).

^{13}C{^{1}H} NMR (75.48 MHz, (D_6)benzene, 298 K): δ (ppm) = 4.6 (s, 9C, (Si*Me*$_3$)$_3$), 24.7 (s, 2C, C^{2,6}-CH*Me*$_A$Me$_B$, Dipp), 27.7 (s, 2C, C^{2,6}-CHMe$_A$*Me*$_B$, Dipp), 28.3 (s, 2C, C^{2,6}-*C*HMe$_A$Me$_B$, Dipp), 29.2 (s, 2C, C^5*Me*$_2$), 37.2 (s, 2C, C^3*Me*$_2$), 48.3 (s, 1C, *C*^{3}Me$_2$), 58.7 (s, 1C, *C*^{4}H$_2$), 64.6 (s, 1C, *C*^{5}Me$_2$), 124.2 (s, 2C, *C*^{3,5}-H, Dipp), 125.1 (s, 1C, *C*^{4}-H, Dipp), 145.2 (s, 1C, *C*^{1}, Dipp) , 154.3 (s, 2C, *C*^{2,6}, Dipp), 213.0 (s, 1C, N*C*^{2}).

^{29}Si{^{1}H} NMR (99.36 MHz, (D_6)benzene, 298 K): δ (ppm) = 14.4 (s, 1Si, *Si*=caac^{Me}), –10.4 (s, 3Si, (*Si*Me$_3$)$_3$), –132.1 (s, 1Si, *Si*(SiMe$_3$)$_3$).

^{1}H-^{15}N HMBC (500.17 MHz, 50.69 MHz, (D_6)benzene, 298K): δ_N (ppm) = 117.6 (1N, *N*C^2).

4.4.6 SiH(SiTMS$_3$)(caac^{Me}) (5-Si)

NMR spectroscopic detection of 5-Si upon reaction of 2-Si with NaBEt$_3$H
To an orange solution of 20 mg of SiBr(SiTMS$_3$)(caac^{Me}) (**2-Si**) (0.032 mmol, 1.0 equiv.) in 0.5 mL of (D$_6$)benzene in a young NMR tube 32 mg of a 1 M solution of NaBEt$_3$H in toluene (0.886 g/mL, 0.036 mmol, 1.1 equiv) was added at ambient temperature. Upon shaking the color of the reaction mixture changed to yellow-brown. Monitoring of the reaction mixture by ^{1}H NMR spectroscopy revealed the selective formation of SiH(SiTMS$_3$)(caac^{Me}) (**5-Si**), alongside tiny impurities in the TMS region.

Synthesis of 5-Si from 3-Si
0.584 g Si(SiTMS$_3$)(caac^{Me}) (**3-Si**) (1.04 mmol, 1.0 equiv.) was dissolved in 1.0 mL of 1,4-cyclohexadiene (0.847 g, 10.57 mmol, 10.2 equiv.). The reaction mixture was stirred for 10 min at ambient temperature followed by stirring at 70 °C for 4 h. During the heating the reaction purple colored reaction solution turned yellow-orange. NMR spectroscopy of an aliquot of the reaction mixture in (D$_6$)benzene revealed the quantitative formation of hydridosilene **5-Si**.The solution was evaporated and dried at fine-vacuum for 0.5 h at 60 °C. The yellow-orange residue was redissolved in 6 mL of *n*-pentane and evaporated to dryness. Drying at fine-vacuum for another 0.5 h at 60 °C afforded analytically pure SiH(SiTMS$_3$)(caac^{Me}) (**5-Si**). Yield: 0.585 g (1.04 mmol, quantitative)
Properties: Hydridosilene **5-Si** decolorizes upon contact with air. It is well soluble in benzene, *n*-hexane and THF, affording yellow solutions.
Elemental Analysis: C$_{29}$H$_{59}$NSi$_5$ (562.21 g/mol): calcd./%: C 61.95, N 2.49, H 10.58; found/%: C 61.13, N 2.37, H 10.53. **Melting point**: 172 °C (partial dec).

ATR-IR (solid): $\tilde{\nu}$ (cm^{-1}) = 3056 (vw), 2963 (m), 2889 (w), 2865 (w), 2120 (w) [ν(Si-H)], 1866 (vw), 1581 (vw), 1440 (w), 1382 (w), 1364 (w), 1325 (s), 1314 (s), 1257 (s), 1240 (m), 1201 (s), 1140 (s), 1083 (vw), 1050 (m), 933 (vw), 861 (m), 827 (vs), 800 (s), 682 (s), 623 (s), 572 (m), 510 (vw), 480 (vw), 430 (vw), 408 (vw).

^{1}H NMR (500.17 MHz, (D$_6$)benzene, 298 K): δ = 0.35 (s, 27H, (Si(*Me*)$_3$)$_3$), 1.07 (s, 6H, C^5*Me*$_2$), 1.23 (d, ^3J(H,H)= 6.8 Hz, 6H, C^{2,6}-CH*Me*$_A$Me$_B$, Dipp), 1.55 (d, ^3J(H,H)= 6.7 Hz, 6H, C^{2,6}-CHMe$_A$*Me*$_B$, Dipp), 1.58 (s, 6H, C^3*Me*$_2$), 1.73 (s, 2H, C^4*H*$_2$), 2.77 (s, ^1J(Si,H)= 188.4 Hz, 1H, Si-*H*), 3.12 (sept, ^3J(H,H)= 6.7 Hz, 2H, C^{2,6}-C*H*Me$_A$Me$_B$, Dipp), 7.08 – 7.10 (m, 2H, C^{3,5}-*H*, Dipp), 7.12–7.14 (m, 1H, C^4-*H*, Dipp).

$^{13}C\{^1H\}$ NMR (125.78 MHz, (D_6)benzene, 298 K): δ (ppm) = 2.8 (s, 9C, $(SiMe_3)_3$), 24.6 (s, 2C, $C^{2,6}$-CH$Me_A$$Me_B$, Dipp), 28.1 (s, 2C, $C^{2,6}$-CH$Me_A$$Me_B$, Dipp), 28.8 (s, 2C, $C^{2,6}$-CH$Me_A$$Me_B$, Dipp), 29.2 (s, 2C, C^5Me_2), 35.5 (s, 2C, C^3Me_2), 48.3 (s, 1C, C^3Me_2), 54.8 (s, 1C, C^4H_2), 70.1 (s, 1C, C^5Me_2), 125.4 (s, 2C, $C^{3,5}$-H, Dipp), 128.7 (s, 1C, C^4-H, Dipp), 136.1 (s, 1C, C^1, Dipp), 148.8 (s, 2C, $C^{2,6}$-CH$Me_A$$Me_B$, Dipp), 208.9 (s, 1C, NC^2).

$^{29}Si\{^1H\}$ NMR (99.36 MHz, (D_6)benzene, 298 K): δ (ppm) = –10.0 (s, 3Si, $Si(SiMe_3)_3$), –47.6 (s, 1Si, $caac^{Me}$=*Si*), –125.8 (s, 1Si, $Si(SiMe_3)_3$).

^1H-^{15}N HMBC (500.17 MHz, 50.69 MHz, (D_6)benzene, 298 K): δ_N (ppm) = 147.08 (1N, NC^2).

4.4.7 $SiBr(NTMS_2)(caac^{Me})$ (2-N)

To a red suspension of $SiBr_2(caac^{Me})$ (**1**) (2.00 g, 4.23 mmol, 1.0 equiv.) in 100 mL of *n*-hexane was added $NaNTMS_2$ (0.930 g, 5.07 mmol, 1.2 equiv.) in portions of approximately 0.10 g over 10 min at ambient temperature. A dark brown suspension was formed immediately. After sonicating for 1.5 h the reaction mixture turned orange-brown. An aliquote of the reaction mixture was taken and analyzed by ^1H NMR spectroscopy in (D_6)benzene, revealing the selective formation of $SiBr(NTMS_2)(caac^{Me})$ (**2-N**), alongside tiny amounts of $Si_2Br_2(caac^{Me})_2$ (**9-Br**) (< 5 mol%). The orange brown suspension was filtered and the the resulting dark brown residue was reextracted with 50 mL and 2 x 10 mL of *n*-hexane. The combined organic phases were evaporated and dried on high vacuum for 1 h at 40 °C. The orange-brown residue was redesolved in 10 mL of boiling *n*-pentane. After storing for 19 h at –24 °C a yellow-orange precipitate was formed, which was separated from the brown motherliquor upon filtration. The solid was washed 5 x 10 mL of *n*-pentane at ambient temperature. After drying at fine vacuum for 2 h at 40 °C analytically pure **2-N** was obtained as an orange-yellow solid (0.878 g, 37 %). The washing solutions were combined and concentrated at high vacuum to a volume of approx. 10 mL. The solution was stored overnight at –24 °C to afford a second crop of **2-N** as brown yellow crystals which were filtered, washed 2 x 5 mL of *n*-pentane and dried under high vacuum for 1 h (0.312 g, 13 %). Total Yield: 1.19 g of $SiBr(NTMS_2)(caac^{Me})$ (**2-N**) (1.795 mmol, 50 %).

Properties: Compound **2-N** quickly decolorizes upon contact with air. It is moderately soluble in *n*-hexane and *n*-pentane and well soluble in benzene and THF.

Elemental Analysis: $C_{26}H_{49}BrN_2Si_3$ (553.84 g/mol): calcd./%: C 56.38, N 5.06, H 8.92; found/%: C 56.18, N 4.93, H 8.89. **Melting point:** 180 °C (dec).

^{1}H NMR (300.13 MHz, (D_6)benzene, 298 K): δ (ppm) = 0.45 (s, ^{2}J(H,Si) = 118.6 Hz, ^{1}J(H,C)= 6 Hz, 18H, (Si*Me*$_3$)$_2$), 1.04 (s, 6H, C^5*Me*$_2$), 1.21 (d, ^{3}J(H,H) = 6.6 Hz, 6H, C^{2,6}-CH*Me*$_A$Me$_B$, Dipp), 1.59 (s, 6H, C^3*Me*$_2$), 1.65 (s, 2H, C^4*H*$_2$), 1.66 (d, ^{3}J(H,H) = 6.6 Hz, 6H, C^{2,6}-CHMe$_A$*Me*$_B$, Dipp), 2.99 (sept, ^{3}J(H,H) = 6.6 Hz, 2H, C^{2,6}-C*H*Me$_A$Me$_B$, Dipp), 7.05-7.08 (m, 2H, C^{3,5}-*H*, Dipp), 7.15-7.20 (m, 1H, C^4-*H*, Dipp overlapping with the (D_6)benzene signal).

^{13}C{^{1}H} NMR (125.87 MHz, (D_6)benzene, 298 K): δ (ppm) = 5.10 (s, ^{1}J(C,Si)= 57 Hz, 6C, N(Si*Me*$_3$)$_2$), 26.0 (s, 2C, C^{2,6}-CH*Me*$_A$Me$_B$, Dipp), 27.0 (s, 2C, C^{2,6}-CHMe$_A$*Me*$_B$, Dipp), 28.9 (s, 2C, C^5*Me*$_2$), 29.4 (s, 2C, C^{2,6}-*C*HMe$_A$Me$_B$, Dipp), 33.2 (s, 2C, C^3*Me*$_2$), 50.1 (s, 1C, *C*^{3}),55.9 (s, 1C, *C*^{4}H$_2$), 71.2 (s, 1C, *C*^{5}), 125.4 (s, 2C, *C*^{3,5}-H, Dipp), 129.1 (s, 1C, *C*^{4}-H, Dipp), 135.0 (s, 1C, *C*^{1}, Dipp) , 148.7 (s, 2C, *C*^{2,6}, Dipp), 190.7 (s, 1C, N*C*^{2}).

^{29}Si{^{1}H}-NMR (99.36 MHz, (D_6)benzene, 298 K): δ (ppm) = 5.4 (s, 2Si, N(*Si*Me$_3$)$_2$), 18.4 (s, 1Si, *Si*(caac^{Me})).

^{15}N{^{1}H} NMR (50.69 MHz, (D_6)benzene, 298 K): δ_N (ppm) = 151.8 (s, 1N, *N*C^2), 299.9 (s, 1N, *N*(SiMe$_3$)$_2$).

4.4.8 Si(NTMS$_2$)(caac^{Me})• (3-N)

SiBr(NTMS$_2$)(caac^{Me}) (**3-N**) (0.877 g,1.58 mmol, 1.0 eq.) and KC_8 (0.235 g, 1.74 mmol, 1.1 eq.) were suspended in 20 mL of benzene. After stirring for 19 h at ambient temperature the reaction mixture turned dark red. An aliquote of the reaction mixture was taken and analyzed by ^{1}H NMR spectroscopy in (D_6)benzene, revealing the presence of broad signals originating from a paramagnetic compound, alongside tiny amounts of the hydridosilene SiH(NTMS$_2$)(caac^{Me}) (**5-N**). The reaction mixture was filtered and the resulting black graphite residue extracted with 3 x 5 mL of benzene. The resulting combined dark red filtrate was evaporated and dried under high vacuum for 0.5 h at 40 °C. The dark-red residue was redesolved in 4 mL of boiling *n*-pentane. Dark red crystals were obtained after storing the solution for 2 h at ambient temperature, which were separated from the dark red mother liquor upon filtration. Drying under fine vacuum for 1 h at 40 °C afforded analytically pure **3-N** as dark red solid. Yield: 0.619 g (1.306 mmol, 83 %).

Properties: Silicon(I) radical **3-N** is extremely pyrophoric and immediately decomposes upon contact with air. It is well soluble in benzene, *n*-pentane and THF, affording dark red solutions, which slowly decompose over time. The major decomposition product appears to be the hydridosilene SiH(NTMS$_2$)(caac^{Me}) (**5-N**) (see *section 5.5.3*).

Elemental Analysis: $C_{26}H_{49}N_2Si_3$ (473.94 g/mol): calcd./%: C 65.89, N 5.91, H 10.42; found/%: C 65.79, N 5.85, H 10.53 %. **Melting point:** 145 °C (dec)

X-band CW EPR (9.85 GHz, *n*-pentane, 293 K, 200 µmol L^{-1}): g_{iso}= 2.0044 ($a_{iso}(^{14}N)$ = 0.57 mT, $a_{iso}(^{29}Si_{\alpha})$ = 1.95 mT).

4.4.9 SiK(NTMS$_2$)(caac^{Me}) (4-N)

SiBr(NTMS$_2$)(caac^{Me}) (**2-N**) (0.400 g, 0.722 mmol, 1.0 equiv.) and KC_8 (0.293 g, 2.17 mmol, 3.0 equiv.) were suspended in 30 mL of benzene. The orange-brown suspension was sonicated for 0.5 h and stirred at ambient temperature. After stirring at ambient temperature for 18 h the reaction mixture turned dark brown. An aliquot of the reaction mixture was taken and analyzed by ^{1}H NMR specoscopy in (D_6)benzene revealing the selective formation of SiK(NTMS$_2$)(caac^{Me}) (**4-N**) alongside tiny amounts of SiH(NTMS$_2$)(caac^{Me}) (**6-N**) (< 5 mol%). The reaction mixture was filtered upon which the color of the dark brown supernatant solution turned to dark red. After evaporation of the solvent a dark red solid was obtained. ^{1}H NMR spectroscopy in (D_6)benzene revealed the complete decomposition of potassium-silenide **4-N** and the rather selective formation of hydridosilene **5-N** alongside broad signals which were attributed to the silicon(I)-radical **3-N**.

The compound was NMR spectroscopically characterized by the aliquot of the reaction mixture in (D_6)benzene:

^{1}H NMR (300.13 MHz, (D_6)benzene, 298 K): δ (ppm) = 0.61 (s, ^2J(H,Si) = 117.4 Hz, 18H, (Si*Me*$_3$)$_2$), 1.23 (d, ^3J(H,H) = 6.8 Hz, 6H, C^{2,6}-CH*Me*$_A$Me$_B$, Dipp), 1.26 (s, 6H, C^5*Me*$_2$), 1.52 (d, ^3J(H,H) = 6.7 Hz, 6H, C^{2,6}-CHMe$_A$*Me*$_B$, Dipp), 2.02 (s, 6H, C^3*Me*$_2$), 2.08 (s, 2H, C^4*H*$_2$), 3.60 (sept, ^3J(H,H) = 6.8 Hz, 2H, C^{2,6}-C*H*Me$_A$Me$_B$, Dipp), 6.63-6.66 (m, 1H, C^4-*H*, Dipp), 6.70 (d, ^3J(H,H) = 7.3 Hz, 2H, C^{3,5}-*H*, Dipp).

^{13}C{^{1}H} NMR (125.87 MHz, (D_6)benzene, 298 K): δ (ppm) = 6.07 (s, ^1J(C,Si)= 56 Hz, 6C, N(Si*Me*$_3$)$_2$), 25.0 (s, 2C, C^{2,6}-CH*Me*$_A$Me$_B$, Dipp), 28.0 (s, 2C, C^{2,6}-*C*HMe$_A$Me$_B$, Dipp), 28.6 (s, 2C, C^{2,6}-CHMe$_A$*Me*$_B$, Dipp), 29.6 (s, 2C, C^5*Me*$_2$), 34.6 (s, 2C, C^3*Me*$_2$), 48.3 (s, 1C, *C*^{3}), 61.2 (s, 1C, *C*^{4}H$_2$), 63.1 (s, 1C, *C*^{5}), 124.1 (s, 2C, *C*^{3,5}-H, Dipp), 125.0 (s, 1C, *C*^{4}-H, Dipp), 144.3 (s, 1C, *C*^{1}, Dipp), 154.7 (s, 2C, *C*^{2,6}, Dipp), 200.7 (s, 1C, N*C*^{2}).

^{29}Si{^{1}H}-NMR (99.36 MHz(D_6)benzene, 298 K): δ (ppm) = –5.5 (s, 2Si, N(*Si*Me$_3$)$_2$),86.5 (s, 1Si, *Si*(caac^{Me})),

^{1}H-^{15}N HMBC (500.17 MHz, 50.69 MHz, (D_6)benzene, 298 K): δ_N (ppm) = 90.5 (s, 1N, *N*C^2), 35.7 (s, 1N, *N*(SiMe$_3$)$_2$),

4.4.10 SiH(NTMS$_2$)(caac^{Me}) (5-N)

Attempted synthesis of 5-N from 2-N

To a solution of 554 mg SiBr(NTMS$_2$)(caac^{Me}) (**2-N**) (1.00 mmol, 1.0 equiv) in 20 mL of toluene at –30 °C 10 mL of a 0.1 M solution of NaBEt$_3$H solution in toluene was added dropwise in 10 min at –30 °C. Upon warming up to ambient temperature the color of the reaction mixture changed to yellow-brown. Monitoring of the reaction mixture after 1 h at ambient temperature by ^{1}H NMR spectroscopy in (D$_6$)benzene revealed the selective formation of **5-N**, alongside some tiny impurities in the TMS region. The yellow-brown suspension was filtered and evaporated to dryness. Compound **5-N** was obtained as crude yellow-brown powder (422 mg) with a purity of 90 %, according to ^{1}H NMR spectroscopy. The compound appeared to be extremely lipophilic and could not be crystallized from *n*-pentane or (SiMe$_3$)$_2$O at –60 °C.

NMR spectroscopic detection of 5-N upon reaction of 3-N with 1,4-CHD

A young NMR tube was charged with 10 mg of Si(NTMS$_2$)(caac^{Me})$^{\bullet}$ (**3-N**) (0.021 mmol, 1.0 equiv.), 0.5 mL of (D$_6$)benzene and 16 mg 1,4-cyclohexadiene (0.20 mmol, 9.5 equiv.). The red purple solution was heated at 50 °C for 2 h upon which the color changed to yellow-orange. Monitoring of the reaction mixture by ^{1}H NMR spectroscopy revealed the selective formation of SiH(NTMS$_2$)(caac^{Me}) (**5-N**). The compound appeared to be thermolabile, decomposing unselectively upon prolonged heating. Nevertheless, the compound was charactized by high resolution NMR correlation spectroscopy.
The compound was NMR spectroscopically characterized in the reaction mixture in (D$_6$)benzene:

^{1}H NMR (300.13 MHz, (D$_6$)benzene, 298 K): δ (ppm) = 0.35 (s, ^2J(H,Si) = 118.7 Hz, ^1J(H,C)= 6.4 Hz, 18H, (Si*Me*$_3$)$_2$), 1.08 (s, 6H, C^5*Me*$_2$), 1.23 (d, ^3J(H,H) = 6.7 Hz, 6H, C^{2,6}-CH*Me*$_A$Me$_B$, Dipp), 1.56 (d, ^3J(H,H) = 6.7 Hz, 6H, C^{2,6}-CHMe$_A$*Me*$_B$, Dipp), 1.64 (s, 6H, C^3*Me*$_2$), 1.76 (s, 2H, C^4*H*$_2$), 2.52 (s, 4H, 2 x C*H*$_2$, 1,4-CHD excess), 3.10 (sept, ^3J(H,H) = 6.7 Hz, 2H, C^{2,6}-C*H*Me$_A$Me$_B$, Dipp), 4.72 (s, 1H, ^1J(Si,H)= 198 Hz, Si-*H*), 5.60 (s, 4H, 4 x C*H*, 1,4-CHD excess), 7.10-7.12 (m, 2H, C^{3,5}-*H*, Dipp), 7.15-7.19(m, 1H, C^4-*H*, Dipp overlapping with the (D$_6$)benzene signal).

^{13}C{^{1}H} NMR (125.87 MHz, (D$_6$)benzene, 298 K): δ (ppm) = 4.49 (s, ^1J(C,Si)= 57 Hz, 6C, N(Si*Me*$_3$)$_2$), 25.3 (s, 2C, C^{2,6}-CH*Me*$_A$Me$_B$, Dipp), 26.1 (s, 2C, 2 x *C*H$_2$, 1,4-CHD excess), 28.4 (s, 2C, C^{2,6}-CHMe$_A$*Me*$_B$, Dipp), 28.5 (s, 2C, C^{2,6}-*C*HMe$_A$Me$_B$, Dipp), 29.5 (s, 2C, C^5*Me*$_2$), 33.5 (s, 2C, C^3*Me*$_2$), 48.3 (s, 1C, *C*^{3}), 56.3 (s, 1C, *C*^{4}H$_2$), 68.5 (s, 1C, *C*^{5}), 124.6 (s, 4C, 4 x *C*H, 1,4-CHD excess), 125.7 (s, 2C, *C*^{3,5}-H, Dipp), 128.5 (s, 1C, *C*^{4}-H, Dipp), 135.2 (s, 1C, *C*^{1}, Dipp), 148.8 (s, 2C, *C*^{2,6}, Dipp), 193.2 (s, 1C, N*C*^{2}).

^{29}Si{^{1}H}-NMR (99.36 MHz, (D_6)benzene, 298 K): δ (ppm) = –5.43 (s, 1Si, *Si*(caac^{Me})), 4.0 (s, 2Si, N(*Si*Me$_3$)$_2$),

^{1}H-^{15}N HMBC (500.17 MHz, 50.69 MHz, (D_6)benzene, 298 K): δ_N (ppm) = 22.9 (s, 1N, *N*(SiMe$_3$)$_2$), 126.7 (s, 1N, *N*C^2).

4.4.11SiBr(PMes$_2$)(caac^{Me}) (2-P)

To a red suspension of SiBr$_2$caac^{Me} (**1**) (2.00 g, 4.23 mmol, 1.0 equiv.) in 100 mL of hexane was added LiPMes$_2$(THF) (1.988 g, 5.71 mmol, 1.35 equiv.) in portions of approximately 0.20 g over 10 min at ambient temperature. A dark brown suspension was formed immediately. After sonicating at ambient temperature for 1 h the reaction mixture turned orange-brown. An aliquot of the reaction mixture was taken and analyzed by ^{1}H NMR spectroscopy in (D_6)benzene revealing the selective formation of SiBr(PMes$_2$)(caac^{Me}) (**2-P**), alongside tiny amounts of Si$_2$Br$_2$(caac^{Me})$_2$ (**9-Br**) (< 5 mol%). The orange brown suspension was filtered, the orange-brown filtrate was evaporated and dried under high vacuum for 0.5 h at 40 °C. The resulting brown-orange residue was washed with 10 mL of *n*-pentane and 3 x 10 mL benzene/*n*-pentane (1:1) followed by 10 mL of *n*-pentane. After drying for 1 h at 40 °C at high vacuum analytically pure **2-P** was obtained as a bright orange solid. (Yield: 0.946 g, 33 %). The orange-brown washing solutions were combined and were evaporated. The residue was dried for 0.5 h at 40 °C at high vacuum and redissolved in 10 mL *n*-pentane. After storing at 0 °C for 19 h a second crop of microcrystalline solid was obtained which was removed form the orange-red mother-liquor upon filtration, washed with 2 x 5 mL of benzne/*n*-pentane and 5 mL *n*-pentane and dried under high vacuum for 1 h (Yield: 0.592 g, 21 %). Total Yield: 1.538 g (2.23 mmol, 55 %).

Properties: Compound **2-P** rapidly decolorizes upon contact with air. It is moderately soluble in *n*-hexane and *n*-pentane and well soluble in benzene, toluene and THF, affording intense orange solutions.

Elemental Analysis: for $C_{38}H_{53}BrNPSi$ (662.8 g/mol): calcd./%: C 68.86, N 2.11, H 8.06; found/%: C 68.42, N 1.91, H 8.06. **Melting point:** 179 °C (dec).

^{1}H NMR (500.13 MHz, (D_6)benzene, 298 K): δ (ppm) = 1.01 (s, 6H, C^5*Me$_2$*), 1.18 (d, ^3J(H,H) = 6.6 Hz, 6H, C^{2,6}-CH*Me$_A$*Me$_B$, Dipp), 1.50 (d, ^3J(H,H) = 6.7 Hz, 6H, C^{2,6}-CHMe$_A$*Me$_B$*, Dipp), 1.67 (s, 2H, C^4*H$_2$*), 1.80 (s, 6H, C^3*Me$_2$*), 2.06 (s, 6H, 2 × C^4-*Me*, Mes), 2.65 (s, 12H, 2 × C^{2,6}-*Me*, Mes), 3.01 (sept, ^3J(H,H) = 6.7 Hz, 2H, C^{2,6}-C*H*Me$_A$Me$_B$, Dipp), 6.75 (d, ^4J(P,H) = 3.0 Hz, 4H, 2 × C^{3,5}-*H*, Mes), 6.97 (d, ^3J(H,H) = 7.7 Hz, 2H, C^{3,5}-*H*, Dipp), 7.08 (t, ^3J(H,H) = 7.7 Hz, 1H, C^4-*H*, Dipp).

$^{13}C\{^1H\}$ NMR (125.87 MHz, (D_6)benzene, 298 K): δ (ppm) = 20.9 (s, 2C, 2 × C^4-*Me*, Mes), 25.1 (d, ^3J(C,P) = 12 Hz, 4C, 2 × $C^{2,6}$-*Me*, Mes), 25.7 (s, 2C, $C^{2,6}$-CH*Me*$_A$Me$_B$, Dipp), 26.9 (s, 2C, $C^{2,6}$-CHMe$_A$*Me*$_B$, Dipp), 29.2 (s, 2C, $C^{2,6}$-*C*HMe$_A$Me$_B$, Dipp), 29.3 (s, 1C, C^5-*Me*$_2$), 31.9 (d, ^4J(C,P) = 17 Hz, 1C, C^3*Me*$_2$), 51.6 (d, ^3J(C,P) = 2 Hz, 1C, *C*^{3}), 55.8 (d, ^4J(C,P) = 2 Hz, 1C, *C*^{4}H$_2$), 72.4 (s, 1C, *C*^{5}), 125.2 (s, 2C, *C*^{3,5}-H, Dipp), 129.2 (s, 1C, *C*^{4}-H, Dipp), 130.1 (d, ^3J(C,P) = 4 Hz, 4C, 2 × *C*^{3,5}-H, Mes), 133.0 (d, ^1J(C,P) = 20 Hz, 2C, 2 × *C*^{1}, Mes), 134.7 (s, 1C, *C*^{1}, Dipp), 136.8 (s, 2C, 2 × *C*^{4}, Mes), 142.9 (d, ^2J(C,P) = 15 Hz, 4C, 2 × *C*^{2,6}, Mes), 148.2 (s, 2C, *C*^{2,6}, Dipp), 204.3 (d, ^2J(C,P) = 23 Hz, 1C, N*C*^{2}).

$^{31}P\{^1H\}$ NMR (202.48 MHz, (D_6)benzene, 298 K): δ (ppm) = –56.6 (t, ^1J(Si,P) = 185.2 Hz).

$^{29}Si\{^1H\}$ NMR (99.36 MHz, (D_6)benzene, 298 K): δ (ppm) = 6.99 (d, ^{1}J(Si,P) = 185.6 Hz).

^1H-^{15}N HMBC(500.17, 50.68 MHz, (D_6)benzene, 298 K): δ_N (ppm) = 170.8 (s, 1N, *N*C^2).

4.4.12 SiK(PMes$_2$)(caac^{Me}) (4-P)

SiBr(PMes$_2$)(caac^{Me}) (**2-P**) (0.100 g, 0.151 mmol, 1.0 equiv.) and KC_8 (0.061 g, 0.453 mmol, 3.0 equiv.) were mixed and suspendet in 10 mL of benzene at ambient temperature. The reaction mixture was sonicated for 0.5 h and stirred for 20 h at ambient temperature. An aliquote of the reaction mixture was taken and analyzed by ^{1}H NMR spectroscopy in (D_6)benzene revealing the selective formation of SiK(PMes$_2$)(caac^{Me}) (**4-P**). The black graphite residue was filtered off and the resulting clear red solution evapotared to dryness. ^{1}H NMR spectroscopy of the crude product in (D_6)benzene revealed the complete unselective decomposition of the silenide **4-P**.
NMR spectroscopic characterization of **4-P** by an aliquote of the reaction mixture:

^1H NMR (500.13 MHz, (D_6)benzene, 298 K): δ (ppm) = 1.24 (d, ^3J(H,H) = 6.6 Hz, 6H, $C^{2,6}$-CH*Me*$_A$Me$_B$, Dipp),1.25 (s, 6H, C^5*Me*$_2$), 1.39 (d, ^3J(H,H) = 6.6 Hz, 6H, $C^{2,6}$-CHMe$_A$*Me*$_B$, Dipp), 2.06 (s, 2H, C^4*H*$_2$),), 2.10 (s, 6H, 2 × C^4-*Me*, Mes), 2.19 (s, 6H, C^3*Me*$_2$), 2.70 (s, 12H, 2 × $C^{2,6}$-*Me*, Mes), 3.50 (sept, ^3J(H,H) = 6.6 Hz, 2H, $C^{2,6}$-C*H*Me$_A$Me$_B$, Dipp), 6.71 (br s, $\Delta\nu_{1/2}$ = 3.8 Hz, 4H, 2 × $C^{3,5}$-*H*, Mes), 6.85 (m, 3H, $C^{3,5}$-*H* and C^4-*H*, Dipp).

$^{13}C\{^1H\}$ NMR (125.87 MHz, (D_6)benzene, 298 K): δ (ppm) = 20.9 (s, 2C, 2 × C^4-*Me*, Mes), 25.1 (s, 2C, $C^{2,6}$-CH*Me*$_A$Me$_B$, Dipp), 25.2 (d, ^3J(C,P) = 11 Hz, 4C, 2 × $C^{2,6}$-*Me*, Mes), 28.0 (s, 2C, $C^{2,6}$-CHMe$_A$*Me*$_B$, Dipp), 28.3 (s, 2C, $C^{2,6}$-*C*HMe$_A$Me$_B$, Dipp), 29.1 (s, 1C, C^5-*Me*$_2$), 34.8 (d, ^4J(C,P) = 17 Hz, 1C, C^3*Me*$_2$), 50.3 (br s, $\Delta\nu_{1/2}$ = 4 Hz, 1C, *C*^{3}), 60.4 (br s, $\Delta\nu_{1/2}$ = 5 Hz, 1C, *C*^{4}H$_2$), 64.6 (s, 1C, *C*^{5}), 124.1 (s, 2C, *C*^{3,5}-H, Dipp), 125.8 (s, 1C, *C*^{4}-H, Dipp), 129.2 (d, ^3J(C,P) = 2 Hz, 4C, 2 × *C*^{3,5}-H, Mes), 133.3 (s, 2C, 2 × *C*^{4}, Mes), →

142.7 (d, ^2J(C,P) = 12 Hz, 4C, 2 × *C*^{2,6}, Mes), 143.0 (s, 1C, *C*^{1}, Dipp), 144.2* (br s, 2C, 2 × *C*^{1}, Mes), 152.5 (s, 2C, *C*^{2,6}, Dipp), 210.3* (br s, 1C, N*C*^{2}). [17]

^{31}P{^{1}H} NMR (202.48 MHz, (D_6)benzene, 298 K) δ (ppm) = –53.6 (br s, $\Delta\nu_{1/2}$ = 57 Hz, *P*(Mes)$_2$).

^{29}Si{^{1}H} NMR (99.36 MHz, (D_6)benzene, 298 K): δ (ppm) = –[18]

^{1}H-^{15}N HMBC (500.17, 50.68 MHz, (D_6)benzene, 298 K): δ_N (ppm) = 114.9 (s, 1N, *N*C^2).

4.4.13(Mes)P–Si(Mes)(caac^{Me})• (6)

SiBr(PMes$_2$)(caac^{Me}) (**3-P**) (0.950 g,1.43 mmol, 1.0 eq.) and KC_8 (0.213 g, 1.57 mmol, 1.1 eq.) were suspended in 20 mL of benzene. The reaction mixture immediately turned dark purple. After 0.5 h at ambient temperature the suspension turned dark brown. An aliquot of the reaction mixture was taken and analyzed by ^{1}H NMR spectroscopy in (D_6)benzene, revealing the presence of broad signals originating from a paramagnetic compound next to tiny amounts of diamagnetic impurities. The brown suspension was filtered and the resulting black graphite residue extracted with 3 x 5 mL of benzene. The combined dark brown filtrate was evaporated and dried under high vacuum for 0.5 h at 40 °C. The dark brown residue was redesolved in 4 mL of boiling *n*-pentane and stored at 0 °C for 3 d. Small dark red crystals were filtered off, dried for 0.5 h at high vacuum at 40 °C and extracted again with 2 x 2 mL of *n*-pentane at ambient temperature. Dark red single crystals were obtained after storing the solution at –24 °C overnight, which were filtered and dried under fine vacuum for 1 h at 40 °C to afford analytically pure **6**·. Yield: 0.274 g (0.470 mmol, 33 %).

Properties: Phosphanyl radical **6** is highly pryophoric and immediately decomposes upon contact with air. It is well soluble in *n*-pentane, benzene and THF, affording orange-red solution. In contrast to the other silicon(I) radicals (**3-R**) no decomposition is observed in the ^{1}H NMR spectra in (D_6)benzene at ambient temperature.

Elemental Analysis: $C_{38}H_{53}NPSi$ (582.89 g/mol): calcd./%: C 78.30, N 2.40, H 10.16; found/%: C 78.45, N 2.35, H 9.15. **Melting point:** 172°C(dec).

X-band CW EPR (9.85 GHz, *n*-pentane, 293 K, 400 µmol L^{-1}): g_{iso}= 2.0061 (a_{iso}(^{14}N) = 0.54 mT, a_{iso}(^{31}P) = 3.74 mT).

---

[17] Signals marked with the symbol (*) were not found in the ^{13}C{^{1}H} NMR spectrum, showed however crosspeaks with significant intensity in the ^{1}H,^{13}C HMBC spectrum, respectively.

[18] No silicon resonance could be observed, neither in the 1D nor in the 2D ^{29}Si{^{1}H} NMR spectra.

4.4.14 [(Mes)P=Si(Mes)(caac^{Me})][B(C$_6$H$_3$-3,5-(CF$_3$)$_2$)$_4$] (7)

Attempts to synthesize compound 7

To an orange solution of SiBr(PMes$_2$)(caac^{Me}) (**2-P**) (0.400 g, 0.604 mmol, 1.00 equiv.) in 20 mL of fluorobenzene a clear solution of Na[B(C$_6$H$_2$-3,5-(CF$_3$)$_2$}$_4$] (0.524 mg, 0.591 mmol, 0.98 equiv.) in 20 mL of fluorobenzene was added dropwise over the course of 15 min at ambient temperature. The reaction mixture was stirred for 10 min at ambient temperature and then stirred for 2 h at 60 °C upon which the color changed to dark red. An aliquote of the reaction mixture was taken and analyzed by ^{1}H no D NMR spectroscopy in fluorobenzene, revealing the selective formation of [(Mes)P=Si(Mes)(caac^{Me})][B(C$_6$H$_2$-3,5-(CF$_3$)$_2$}$_4$] (**7**) alongside 18 mol% of [(caac^{Me})H][B(C$_6$H$_2$-3,5-(CF$_3$)$_2$}$_4$]. 20 mL of *n*-hexane were added and tiny amounts of a white precipitate were filtered. The clear red solution was evaporated and freeze dryed. 842 mg of **7** was obtained as a crude red solid.

Properties: Crude compound **7** is very well soluble in toluene, fluorobenzene and forms a red oil upon contact with aliphatic solvents. In THF and Et$_2$O the compound slowly decomposes upon which the amounts of the caac^{Me}H salt increases. The compound does not crystallizes from fluorobenzene/*n*-hexane mixtures (1:1; 1:2) or toluene at 4 °C or –30 °C, instead a red oil is formed. Crystallization attempts from Et$_2$O/*n*-hexane mixtures resulted in the crystallization of [(caac^{Me})H][B(Ar^F)$_4$].[19]

Preliminary NMR spectroscopic characterization of **7** in fluorobenzene (C$_6$H$_5$F):

^{1}H no D NMR (500.13 MHz, fluorobenzene, 298 K): δ (ppm) = 0.35 (s, 6H, C^3*Me$_2$*), 0.46 (d, ^{3}*J*(H,H) = 6.6 Hz, 6H, C^{2,6}-CH*Me$_A$*Me$_B$, Dipp), 0.55 (s, 6H, C^5*Me$_2$*), 0.75 (d, ^{3}*J*(H,H) = 6.6 Hz, 6H, C^{2,6}-CHMe$_A$*Me$_B$*, Dipp), 1.10 (s, 3H, C^2-*Me*, Si-Mes), 1.13 (s, 3H, C^6-*Me*, Si-Mes), 1.16 (s, 6H, C^{2,6}-*Me*, P-Mes), 1.17 (s, 2H, C^4*H$_2$*), 1.39 (s, 6H, 2 × C^4-*Me*, Si-Mes and P-Mes), 1.81 (sept, ^{3}*J*(H,H) = 6.6 Hz, 2H, C^{2,6}-C*H*Me$_A$Me$_B$, Dipp), 5.73 (br s, Δν$_{1/2}$ = 3.9 Hz, 2H, C^{3,5}-*H*, Si-Mes), 5.73 (br s, Δν$_{1/2}$ = 3.7 Hz, 2H, C^{3,5}-*H*, P-Mes), 6.52 (d , ^{3}*J*(H,H) = 7.8 Hz, 2H, C^{3,5}-*H*, Dipp), 6.63 (t, ^{3}*J*(H,H) = 7.7 Hz, 1H, C^4-*H*, Dipp), 6.86 (br s, Δν$_{1/2}$ = 4.9 Hz, 4H, 4 × C^4-*H*, B(Ar^F)$_4$), 7.54* (m, 8H, 4 × C^{2,6}-*H*, B(Ar^F)$_4$*)*.

^{13}C{^{1}H} NMR (125.87 MHz, fluorobenzene, 298 K): δ (ppm) = 51.2 (br s, Δν$_{1/2}$ = 7 Hz, 1C, *C*^{4}H$_2$), 54.4 *(*d, Δν$_{1/2}$ = 7 Hz, 1C, *C*^{3}*)*, 84.6 (s, Δν$_{1/2}$ = 7 Hz, 1C, *C*^{5}), 142.9 (d, ^{2}*J*(C,P) = 11 Hz, 4C, *C*^{2,6}, Mes), 143.2 (s, 2C, *C*^{2,6}, Dipp), 210.1 (br s, Δν$_{1/2}$ = 10.6 Hz, 1C, N*C*^{2}).[20]

^{31}P{^{1}H} NMR (202.48 MHz, fluorobenzene, 298 K): δ (ppm) = 255.3 (br s, Δν$_{1/2}$ = 177 Hz).

---

[19] Direct synthetic access to salt **7** might be feasible via the 1e$^-$ oxiditation of phosphanyl-radical **6**. A solution of **6** (10 mg, 0.0172 mmol) and [FeCp*$_2$][B{C$_6$H$_3$-3,5-(CF$_3$)$_2$}$_4$] (20 mg, 0.0172 mmol) in fluorobenzene, however, according to ^{1}H no D NMR spectroscopy did not reveal any reaction, even upon prolonged heating at 60 °C.

[20] Not all of the carbon resonances could be assigned, since ^{1}H, ^{13}C HSQC measurement could not be performed in non deuterated fluorobenzene.

^{29}Si{^{1}H}-NMR (99.36 MHz, fluorobenzene, 298 K): δ (ppm) = 148.23 (d, ^{1}J(Si,P)= 166.7 Hz).

^{1}H-^{15}N HMBC (500.17, 50.68 MHz, fluorobenzene, 298 K): δ_N (ppm) = 249.94 (s, 1N, *N*C^{2}).

4.4.15 SiBr(OMes*)(caac^{Me}) (2-O)

To a red solution of 2.00 g of SiBr$_2$(caac^{Me}) (**1**) (4.225 mmol, 1.00 equiv.) in 40 mL of DME a clear yellow solution of 1.322 g NaOMes* (4.648 mmol, 1.10 equiv.) in 40 mL of DME was added dropwise during the course of 10 minutes. At the end of the alcoholate addition the reaction mixture changed to orange-brown. The reaction mixture was stirred for an additional hour at ambient temperature. An aliquote of the reaction mixture was taken and analyzed by ^{1}H NMR spectroscopy in (D_6)benzene, revealing the selective formation of **2-O**, alongside with tiny amounts of SiBr$_2$(caac^{Me})$_2$, which stayed in equilibrium with SiBr$_2$(caac^{Me}) and free caac^{Me} carbene. 50 mL of *n*-hexane were added and the brown suspension filtered. The orange-brown filtrate was evaporated and dried under fine vacuum for 0.5 h at ambient temperature upon which a dark black solid was obtained. Extracting with 5 x 10 mL of *n*-hexane, affored tiny amounts of a dark blue residue (ca. 100 mg) and an orange-brown extract. The orange-brown extract was concentrated to a volume of approx. 10 mL. After storing at –30 °C for 19 h an orange-brown microcrystalline solid was obtained, which was removed from the dark brown motherliquor upon filtration at –30 °C. The orange-brown microcrystalline solid was washed with 3 x 8 mL of precooled *n*-pentane at –30 °C, upon which the orange color of the solid intensified. The orange powder (540 mg) was dried for 1 h at ambient temperature. Additional drying for 4 h at 70 °C was required to remove considerable amounts of coordinated DME (16 mol%). The solid was extracted again with 4 x 10 mL of *n*-hexane and the resulting orange-red extract was concentrated to a volume of approx. 10 mL. After storing at –30 °C for 20 h a bright orange microcrystalline solid was obtained, which was separated from the orange-red motherliquor upon filtration at –30 °C. Drying at fine vacuum for 2 h at 50 °C afforded SiBr(OMes*)(caac^{Me}) (**2-O**) in analytical pure form as a bright orange powder. Yield: 416 mg (0.635 mmol, 15 %).

Properties: Bromo-silene **2-O** rapidly decolorizes upon contact with air. It is moderately soluble in *n*-hexane and *n*-pentane and well soluble in benzene, toluene, THF and DME, affording orange solutions.

Elemental Analysis: $C_{38}H_{60}BrNSiO$ (654.88 g/mol): calcd./%: C 69.69, N 2.14, H 9.23; found/%: C 69.40, N 1.95, H 9.44 . **Melting point:** 185 °C (dec).

^{1}H NMR (500.13 MHz, (D_6)benzene, 298 K): δ (ppm) = 1.02 (s, 6H, C^5Me_2), 1.15 (d, ^3J(H,H) = 6.7 Hz, 6H, $C^{2,6}$-CHMe_AMe$_B$, Dipp), 1.30 (s, 9H, C^4-CMe_3, Mes*), 1.52 (d, ^3J(H,H) = 6.7 Hz, 6H, $C^{2,6}$-CHMe$_A$$Me_B$, Dipp), 1.69 (s, 2H, C^4H_2), 1.76 (s, 18H, $C^{2,6}$-CMe_3, Mes*), 1.82 (s, 6H, C^3Me_2), 2.90 (sept, ^3J(H,H) = 6.7 Hz, 2H, $C^{2,6}$-C*H*Me$_A$Me$_B$, Dipp), 6.98-6.99 (m, 2H, $C^{3,5}$-*H*, Dipp), 7.04-7.07 (m, 1H, C^4-*H*, Dipp), 7.43 (s, 2H, $C^{3,5}$-*H*, Mes*).

^{13}C{^{1}H} NMR (125.87 MHz, (D_6)benzene, 298 K): δ (ppm) = 25.6 (s, 2C, $C^{2,6}$-CHMe_AMe$_B$, Dipp), 26.8 (s, 2C, $C^{2,6}$-CHMe$_A$$Me_B$, Dipp), 29.15 (s, 1C, C^5Me_2), 29.2 (s, 2C, $C^{2,6}$-*C*HMe$_A$Me$_B$, Dipp), 31.0 (s, 2C, C^3Me_2), 31.8 (s, 3C, C^4-CMe_3, Mes*), 33.1 (s, 6C, $C^{2,6}$-CMe_3, Mes*), 34.5 (s, 1C, C^4-*C*Me$_3$, Mes*), 36.5 (s, 2C, $C^{2,6}$-*C*Me$_3$), 51.9 (s, 1C, C^3), 54.8 (s, 1C, C^4H_2), 74.2 (s, 1C, C^5), 122.9 (s, 2C, $C^{3,5}$-H, Mes*), 125.3 (s, 2C, $C^{3,5}$-H, Dipp), 129.4 (s, 1C, C^4-H, Dipp), 133.8 (s, 1C, C^1, Dipp), 140.7 (s, 2C, 2 × $C^{2,6}$, Mes*), 142.5 (s, 1C, C^4, Mes*), 147.8 (s, 2C, $C^{2,6}$, Dipp), 151.1 (s, 1C, C^1, Mes*), 200.0 (s, 1C, NC^2).

^{29}Si{^{1}H} NMR (99.36 MHz, (D_6)benzene, 298 K): δ (ppm) = 26.4 (s, 1Si, *Si*(caac^{Me})).

^{1}H-^{15}N HMBC (500.17, 50.68 MHz, (D_6)benzene, 298 K): δ_N (ppm) = 164.9 (s, 1N, *N*C^2).

4.4.16Si(OMes*)(caac^{Me})$^{\bullet}$ (3-O)

SiBr(OMes*)(caac^{Me}) (**2-O**) (0.350 g,0.534 mmol, 1.0 eq.) and KC_8 (0.079 g, 0.588 mmol, 1.1 eq.) were suspended in 20 mL of benzene. After stirring for 23 h at ambient temperature the reaction mixture turned red-brown. An aliquote of the reaction mixture was taken and analyzed by ^{1}H NMR spectroscopy in (D_6)benzene, revealing broad signals originating from a paramagnetic compound, alongside with tiny amounts of unknown impurities. The reaction mixture was filtered and the resulting black graphite residue extracted with 3 x 5 mL of benzene. The resulting combined red-brown filtrate was evaporated and dried under high vacuum for 0.5 h at 40 °C. After extraction of the solid with 5 x 6 mL of *n*-pentane, the extract was concentrated to a volume approx. 5 mL. An orange-brown microcrystalline solid was obtained after storing for 2 h at –30 °C, which was separated from the red-brown motherliquor upon filtration. Drying under fine vacuum for 0.5 h at 40 °C afforded **3-O** (219 mg) as an orange-brown powder, which still contained tiny amounts of diamagnetic impurities according to ^{1}H NMR spectroscopy in (D_6)benzene. The compound was resuspendet in a mixture of 5 mL of toluene/*n*-hexane (1:5), after storing for 1.5 h at –30 °C the orange-brown precipitate was separated from the orange-brown motherliquor upon filtration. Drying under fine vacuum for 1 h at 40 °C afforded analytically pure **3-O** as a orange brown solid. Yield: 0.182 g (0.317 mmol, 59 %).

Properties: Silicon(I) radical **3-O** is extremely pyrophoric and immediately decomposes upon contact with air. It is well soluble in benzene and toluene and moderately soluble in aliphatic solvents.

In contrast to analogous silicon(I) radicals SiR(caac^{Me}) (R = SiTMS$_3$ (**3-Si**), NTMS$_2$ (**3-N**)) the compound does not decompose in (D_6)benzene solution at ambient temperature.
Elemental Analysis: $C_{38}H_{60}NSiO$ (574.97 g/mol): calcd./%: C 79.38, N 2.44, H 10.52; found/%: C 79.39, N 2.28, H 10.50. **Melting point:** 214 °C (dec at 221 °C).

X-band CW EPR (9.85 GHz, toluene, 293 K, 174 µmol L^{-1}): g_{iso}= 2.0038 ($a_{iso}(^{14}N)$ = 0.62 mT, $a_{iso}(^{29}Si_{\alpha})$ = 1.24 mT).

4.4.17SiBr(Eind)(caac^{Me}) E-(orange)-isomer (2-Eind-*E*)

To a yellow suspension of 454 mg (*E*)-[Eind(Br)Si=Si(Br)Eind] (0.464 mmol, 1.00 equiv.) in 20 mL of benzene a colorless solution of 265 mg caac^{Me} (0.928 mmol, 2.00 equiv.) in 15 mL of benzene was added dropwise in 12 minutes. An orange-yellow suspension was formed immediately, which was stirred for 1 h at ambient temperature. Upon heating to 60 °C for 1 h a clear orange-red solution was formed, which contained only a slight turbidity. An aliquot of the reaction solution was analyzed by ^{1}H NMR spectroscopy in (D_6)benzene revealing the complete consumption of the starting materials and the selective formation of SiBr(Eind)(caac^{Me}) (**2-Eind**) as a diastereomeric mixture of an ***Z***- (yellow) (22 mol%) and ***E***-(orange) (78 mol%) isomer. The reaction mixture was worked-up by removing the slight turbidty upon filtration, evaporating the solvent to dryness under fine-vacuum and drying the crude product at 60 °C under fine-vacuum for 0.5 h. The orange solid was dissolved in *n*-pentane (5 mL), stored for 1 d at –30 °C and for 1 d at –60 °C. After filtering off the orange mother liquor a first crop of crystalline orange-yellow material (247 mg) was isolated, which consisted of the ***Z***-(yellow) (32 mol%) and ***E***-(orange) (68 mol%) isomer, according to ^{1}H NMR spectroscopy in (D_6)benzene. The orange mother liquor was concentrated to a volume of 1 mL upon which an orange precipitate was formed, which was filtered at ambient temperature and dried at the fine vacuum for 1 h at 60 °C in order to give SiBr(Eind)(caac^{Me}) **2-Eind-*E*** as analytically pure orange powder. Yield: 191 mg (0.246 mmol, 27 %).
Properties: Compound **2-Eind-*E*** slowly decolorizes upon contact with air. Heating of the orange solid to 153 °C results in the formation of small red melt nuclei, which upon cooling down to ambient temperature change to a yellow solid. ^{1}H-NMR spectroscopy of the yellow solid in (D_6)benzene reveals the rather selective formation of the ***Z***-isomer (**2-Eind-*Z***). Compound **2-Eind-*E*** is well soluble in benzene and toluene, as well in aliphatic sovents, such as *n*-pentane or *n*-hexane, affording orange solutions.
The compound slowly decomposes in solution to the ***Z***-isomer, a respective ^{1}H NMR sample in (D_6)benzene after 18 days featured the formation of 9 mol% of the ***Z***-isomer. Upon heating for 2 days at 90 °C the conversion can be completed.

Elemental analysis: $C_{48}H_{76}BrSi$ (775.11 g/mol): calcd./%: C 74.38, N 1.80, H 9.88; found/%: C 74.74, N 1.66, H 9.89.

^{1}H NMR (500.17 MHz, (D_6)benzene, 298 K): δ (ppm) = 0.08 (d, ^3J(H,H)= 6.8 Hz, 3H, C^6-$CH_BMe_CMe_D$), 0.32 (dq, ^2J(H,H)= 14.4 Hz, ^3J(H,H)= 7.1 Hz, 1H, C^3-{CH_AH_BMe}$_x$, Eind), 0.63 (t, ^3J(H,H)= 6.9 Hz, 3H, C^3-{CH_AH_BMe}$_x$, Eind), 0.71 (s, 3H, $C^5Me_AMe_B$), 0.80 (t, ^3J(H,H)= 6.9 Hz, 6H, C^1-{CH_AH_BMe}$_x$ and C^1-{CH_AH_BMe}$_y$, Eind), 0.80 (t, ^3J(H,H)= 7.3 Hz, 3H, C^7-{CH_AH_BMe}$_x$, Eind), 0.81 (t, ^3J(H,H)= 7.2 Hz, 3H, C^3-{CH_AH_BMe}$_y$, Eind), 0.84 (t, ^3J(H,H)= 7.3 Hz, 3H, C^5-{CH_AH_BMe}$_x$, Eind), 0.94 (t, ^3J(H,H)= 7.4 Hz, 3H, C^7-{CH_AH_BMe}$_y$, Eind), 1.01 (d, ^3J(H,H)= 6.9 Hz, 3H, $CH_BMe_CMe_D$), 1.18 (t, ^3J(H,H)= 7.3 Hz, 3H, C^5-{CH_AH_BMe}$_y$, Eind), 1.19 (d, ^3J(H,H)= 7.0 Hz, 3H, C^2-$CH_AMe_AMe_B$, Dipp), 1.31 (dq, ^2J(H,H)= 14.3 Hz, ^3J(H,H)= 7.1 Hz, 1H, C^3-{CH_AH_BMe}$_y$, Eind), 1.39 (m, 1H, C^7-{CH_AH_BMe}$_x$, Eind),1.43 (s, 3H, $C^5Me_AMe_B$), 1.50 (m, 1H, C^7-{CH_AH_BMe}$_x$, Eind), 1.54 (d, ^3J(H,H)= 6.8 Hz, 3H, C^2-$CH_AMe_AMe_B$, Dipp), 1.60-1.80 (m, 4H, C^1-{CH_AH_BMe}$_{x/y}$ and C^1-{CH_AH_BMe}$_{x/y}$, Eind}, 1.61 (m, 1H, C^5-{CH_AH_BMe}$_x$, Eind), 1.63 (m, 1H, C^3-{CH_AH_BMe}$_x$, Eind), 1.65 (d, ^2J(H,H)= 16.3 Hz, 2H, $C^2H_AH_B$ and $C^2H_AH_B$, Eind), 1.72-1.73 (m, 2H, C^7-{CH_AH_BMe}$_y$, and C^7-{CH_AH_BMe}$_y$, Eind), 1.74 (d, ^2J(H,H)= 12.4 Hz, 1H, $C^4H_AH_B$), 1.87 (m, 1H, C^5-{CH_AH_BMe}$_y$, Eind), 1.88 (d, ^2J(H,H)= 16.5 Hz, 2H, $C^6H_AH_B$ and $C^6H_AH_B$, Eind), 1.98 (s, 3H, $C^3Me_AMe_B$), 2.00 (d, ^2J(H,H)= 12.5 Hz, 1H, $C^4H_AH_B$), 2.02 (s, 3H, $C^3Me_AMe_B$), 2.50 (dq, ^2J(H,H)= 14.4 Hz, ^3J(H,H)= 7.2 Hz, 1H, C^3-{CH_AH_BMe}$_x$, Eind), 2.99 (dq, ^2J(H,H)= 14.2 Hz, ^3J(H,H)= 7.1 Hz, 1H, C^5-{CH_AH_BMe}$_x$, Eind), 3.27 (m, 1H, C^2-$CH_AMe_AMe_B$, Dipp), 3.29 (m, 1H, C^6-$CH_BMe_CMe_D$, Dipp), 3.30 (m, 1H, C^5-{CH_AH_BMe}$_y$, Eind), 6.77 (dd, ^3J(H,H)= 7.6 Hz, ^4J(H,H)= 1.9 Hz, 1H, C^3-*H*, Dipp), 6.78 (s, 1H, C^8-*H*, Eind), 6.94 (t, ^3J(H,H)= 7.6 Hz, 1H, C^4-*H*, Dipp), 6.97 (dd, ^3J(H,H)= 7.6 Hz, ^4J(H,H)= 1.9 Hz, 1H, C^5-*H*, Dipp).

^{13}C{^{1}H} NMR (75.48 MHz, (D_6)benzene, 298 K): δ (ppm) = 9.15-9.27 (4·s, 4C, C^1-{CH_AH_BMe}$_{x/y}$ and C^7-{CH_AH_BMe}$_{x/y}$, Eind),[21] 10.15 (s, 1C, C^5-{CH_AH_BMe}$_y$, Eind), 11.06 (s, 1C, C^3-{CH_AH_BMe}$_x$, Eind), 11.43 (s, 1C, C^5-{CH_AH_BMe}$_x$, Eind), 11.69 (s, 1C, C^3-{CH_AH_BMe}$_y$, Eind), 24.04 (s, 1C, C^6-$CH_BMe_CMe_D$, Dipp), 24.53 (s, 2C, C^2-$CH_AMe_AMe_B$ and C^2-$CH_AMe_AMe_B$, Dipp), 26.54 (s, 1C, $C^5Me_AMe_B$), 26.60 (s, 1C, C^6-$CH_BMe_CMe_D$, Dipp), 27.9 (s, 2C, C^2-$CH_AMe_AMe_B$ and C^6-$CH_BMe_CMe_D$, Dipp), 31.13 (s, 1C, C^5-{CH_AH_BMe}$_x$, Eind), 31.15 (s, 1C, C^1-{CH_AH_BMe}$_x$, Eind), 31.18 (s, 1C, $C^5Me_AMe_B$), 31.25 (s, 1C, C^1-{CH_AH_BMe}$_y$, Eind), 32.22 (s, 1C, C^3-{CH_AH_BMe}$_x$, Eind), 32.81 (s, 1C, $C^3Me_AMe_B$), 33.42 (s, 1C, $C^3Me_AMe_B$), 33.68 (s, 1C, C^3-{CH_AH_BMe}$_y$, Eind), 34.75 (s, 1C, C^7-{CH_AH_BMe}$_x$, Eind), 35.35 (s, 1C, C^7-{CH_AH_BMe}$_y$, Eind), 36.4 (s, 1C, C^5-{CH_AH_BMe}$_y$, Eind), 41.8 (s, 1C, $C^2H_AH_B$, Eind), 42.9 (s, 1C, $C^6H_AH_B$, Eind), 47.4 (s, 1C, C^1, Eind), →

[21] The signals could not be clearly assignend, due to the strong overlap of the crosspeaks in the corresponding ^{1}H,^{13}C-HMBC and HSQC NMR spectra.

47.5 (s, 1C, *C*^{7}, Eind), 49.9 (s, 1C, *C*^{3}), 53.2 (s, 1C, *C*^{3}, Eind), 54.2 (s, 1C, *C*^{5}, Eind), 57.5 (s, 1C, *C*^{4}H_AH_B), 68.9 (s, 1C, *C*^{5}), 124.1 (s, 1C, *C*^{4}, Eind), 124.18 (s, 1C, *C*^{8}-H, Eind), 124.19 (s, 1C, *C*^{3}-H, Dipp), 126.2 (s, 1C, *C*^{5}-H, Dipp), 127.04 (s, 1C, *C*^{4}-H, Dipp), 143.3 (s, 1C, *C*^{1}, Dipp), 147.3 (s, 1C, *C*^{2}, Dipp), 149.1 (s, 1C, *C*^{6}, Dipp), 149.5 (s, 1C, *C*^{7a}, Eind), 149.7 (s, 1C, *C*^{8a}, Eind), 156.2 (s, 1C, *C*^{4a}, Eind), 156.5 (s, 1C, *C*^{3a}, Eind), 165.2 (s, 1C, N*C*^{2}).

^{29}Si{^{1}H} NMR (99.36 MHz, (D_6)benzene, 298 K): δ (ppm) = 31.1 (s, 1Si, *Si*=caac^{Me}).

^{1}H-^{15}N HMBC (500.14 MHz, 50.69. MHz, (D_6)benzene, 298 K): δ_N (ppm) = 104.25 (1N, *N*C^{2}).

4.4.18 SiBr(Eind)(caac^{Me}) Z-(yellow) isomer (2-Eind-*Z*)

To a yellow suspension of 450 mg (*E*)-[Eind(Br)Si=Si(Br)Eind] (0.460 mmol, 1.00 equiv.) in 20 mL of toluene a colorless solution of 262 mg caac^{Me} (0.919 mmol, 2.00 equiv.) in 20 mL of toluene was added dropwise in 15 minutes. An orange-yellow suspension was formed immediately, which was stirred for 10 min at ambient temperature. Upon heating to 60 °C for 1 h a clear orange-red solution was formed, which contained only a slight turbidity. An aliquot of the reaction solution was analyzed by ^{1}H NMR spectroscopy in (D_6)benzene, revealing the complete consumption of the starting materials and the selective formation of SiBr(Eind)(caac^{Me}) as a diastereomeric mixture of an **Z**- (yellow) (19 mol%) and ***E***-(orange) (81 mol%) isomers. The reaction mixture was filtered in order to remove the slight turbidity. The clear orange-red solution was stirred for 20 h at 100 °C, upon which the color changed to orange yellow. An aliquote of the reaction mixture in (D_6)benzene revealed the selective formation of the ***Z***-isomer next to 8 mol% of the ***E***-isomer. The product was extracted with *n*-pentane (20 mL), the volume of the yellow extract concentrated to 10 mL, recrystallized two times from *n*-pentane (10 mL) at –30 °C. After removing of the orange mother liquor by filtration and drying of the compound for 1 h at 60 °C **2-Eind-*Z*** was obtained as analytically pure yellow powder. Yield: 267 mg (0.345 mmol, 37.5%).

Propterties: Compound **2-Eind-*Z*** rapidly decomposes upon contact with air. It is moderately soluble in *n*-pentane and *n*-hexane and well soluble in benzene and toluene, affording orange-yellow solutions. The compound is stable at ambient temperature in solution.

Elemental analysis: $C_{48}H_{76}BrSi$ (775.11 g/mol): calcd./%: C 74.38, N 1.80, H 9.88; found/%: C 74.46, N 1.55, H 10.12. **Melting poin:** 185 °C (dec).

^{1}H NMR (500.17 MHz, (D_6)benzene, 298 K): δ (ppm) = 0.55 (t, ^{3}J(H,H)= 7.3 Hz, 6H, $C^{3,5}$-$CH_AH_BMe_A$, Eind), 0.87 (t, ^{3}J(H,H)= 7.4 Hz, 6H, $C^{1,7}$-$CH_AH_BMe_A$, Eind), 0.90 (t, ^{3}J(H,H)= 7.5 Hz, 6H, $C^{1,7}$-$CH_CH_DMe_B$, Eind), 1.11 (s, 6H, $C^{5}Me_2$), 1.15 (s, 6H, $C^{3}Me_2$), 1.21 (t, ^{3}J(H,H)= 7.4 Hz, 6H, $C^{3,5}$-$CH_CH_DMe_B$, Eind), 1.30 (d, ^{3}J(H,H)= 6.7 Hz, 6H, $C^{2,6}$-$CHMe_AMe_B$, Dipp), 1.58 (dq, ^{2}J(H,H)= 13.9 Hz, ^{3}J(H,H)= 7.5 Hz, 2H, $C^{1,7}$-$CH_AH_BMe_A$, Eind), 1.60 (s, 2H, $C^{4}H_2$), 1.69-1.66 (m, 4H, $C^{1,7}$-$CH_CH_DMe_B$ and $C^{1,7}$-$CH_CH_DMe_B$, Eind), 1.71 (d, ^{2}J(H,H)= 13.6 Hz, 2H, $C^{2,6}$-H_AH_B, Eind), 1.72 (m, 2H, $C^{3,5}$-$CH_AH_BMe_A$, Eind), 1.74 (d, 6H, $^{3}J_{H,H}$= 6.7 Hz, $C^{2,6}$-$CHMe_AMe_B$, Dipp),1.78 (m, 2H, $C^{1,7}$-$CH_AH_BMe_A$, Eind), 1.92 (d, ^{2}J(H,H)= 13.6 Hz, 2H, $C^{2,6}$-H_AH_B, Eind), 2.14 (dq, ^{2}J(H,H)= 13.5 Hz, ^{3}J(H,H)= 7.4 Hz, 2H, $C^{3,5}$-$CH_CH_DMe_B$, Eind), 2.42 (dq, ^{2}J(H,H)= 14.1 Hz, ^{3}J(H,H)= 7.2 Hz, 2H, $C^{3,5}$-$CH_AH_BMe_A$, Eind), 3.31 (sept, ^{3}J(H,H)= 6.8 Hz, 2H, $C^{2,6}$-$CHMe_AMe_B$, Dipp), 3.48 (dq, ^{2}J(H,H)= 13.8 Hz, ^{3}J(H,H)= 7.4 Hz, 2H, $C^{3,5}$-$CH_CH_DMe_B$, Eind), 6.81 (s, 1H, C^{8}-*H*, Eind), 7.14 (m overlapping with (D_6)benzene signal, 2H, $C^{3,5}$-*H*, Dipp), 7.23 (dd, ^{3}J(H,H)= 7.13 Hz, 1H, C^{4}-*H*, Dipp).

^{13}C{^{1}H} NMR (75.48 MHz, (D_6)benzene, 298 K): δ (ppm) = 9.35 (s, 2C, $C^{1,7}$-CH_AH_B-Me_A, Eind), 9.40 (s, 2C, $C^{1,7}$-CH_CH_D-Me_B, Eind), 9.97 (s, 2C, $C^{3,5}$-CH_AH_B-Me_A, Eind), 10.98 (s, 2C, $C^{3,5}$-CH_CH_D-Me_B, Eind), 26.34 (s, 2C, $C^{2,6}$-$CHMe_AMe_B$, Dipp), 26.36 (s, 2C, $C^{2,6}$-$CHMe_AMe_B$, Dipp), 28.6 (s, 2C, $C^{2,6}$-$CHMe_AMe_B$, Dipp), 29.6 (s, 2C, $C^{5}Me_2$), 31.28 (s, 2C, $C^{1,7}$-CH_AH_B-Me_A, Eind), 33.08 (s, 2C, $C^{3,5}$-$CH_AH_BMe_A$, Eind), 34.2 (s, 2C, $C^{3}Me_2$), 35.5 (s, 2C, $C^{1,7}$-$CH_CH_DMe_B$, Eind), 36.7 (s, 2C, $C^{3,5}$-$CH_CH_DMe_B$, Eind), 42.3 (s, 2C, $C^{2,6}$-H_AH_B, Eind), 47.9 (s, 2C, $C^{1,7}$, Eind), 48.75 (s, 1C, $C^{3}Me_2$),54.5 (s, 2C, $C^{3,5}$, Eind), 57.0 (s, 1C, $C^{4}H_2$), 68.5 (s, 1C, $C^{5}Me_2$), 122.6 (s, 1C, C^{8}-H, Eind), 125.3 (s, 2C, $C^{3,5}$-H, Dipp), 127.5 (s, 1C, C^{4}, Eind), 128.7 (s, 1C, C^{4}-H, Dipp), 137.1 (s, 1C, C^{1}, Dipp), 148.8 (s, 2C, $C^{8a,7a}$, Eind), 149.4 (s, 2C, $C^{2,6}$, Dipp),156.2 (s, 2C, $C^{4a,3a}$, Eind), 175.9 (s, 1C, NC^{2}).

^{29}Si{^{1}H} NMR (99.36 MHz, (D_6)benzene, 298 K): δ (ppm) = 1.85 (s, 1Si, *Si*=caac^{Me}).

^{1}H-^{15}N HMBC (500.14 MHz, 50.69 MHz, (D_6)benzene, 298 K): δ_N (ppm) = 135.1 (1N, NC^{2}).

4.4.19 SiBr(Mes)(caac^{Me}) (2-Mes)

To a red solution of $SiBr_2$(caac^{Me}) (**1**) (1.00 g, 2.11 mmol, 1.0 equiv.) in 20 mL of THF was added dropwise a clear solution of mesithyllithium (0.280 g, 2.22 mmol, 1.05 equiv.) in 20 mL of THF in 15 min at ambient temperature. The color of the reaction mixture changed to orange-brown immediately. After 0.5 h at ambient temperature an aliquote of the reaction mixture was taken and analyzed by ^{1}H NMR spectroscopy in (D_6)benzene revealing the selective formation of **2-Mes**. The solvent was removed under reduced pressure and the resulting dark-brown residue was dried for 0.5 h under fine vacuum at 40 °C. The crude orange-brown solid was extracted with 20 mL *n*-hexane and 3 x 5 mL *n*-hexane. The combined organic phases were evaporated and dried under fine vacuum for 0.5 h at 40 °C. The orange-brown residue was resuspended in 4 mL of *n*-hexane and stored for 17 h at –30 °C. The orange suspension was filtered at –30 °C. After drying under fine vacuum for 1 h at 60 °C SiBr(Mes)(caac^{Me}) (**2-Mes**) was obtained as a orange-yellow solid in analytically pure form. Yield: 0.600 g (1.17 mmol, 55 %).

Properties: Compound **2-Mes** quickly decolorizes upon contact with air. It is moderately soluble in *n*-hexane and well soluble in benzene and THF, affording orange-yellow solutions.

Elemental Analysis: $C_{29}H_{42}BrNSi$ (512.6 g/mol): calcd./%: C 67.94, N 2.73, H 8.26; found/%: C 68.09, N 2.64, H 8.34 %. **Melting point:** 199 °C (dec).

^{1}H NMR (500.17 MHz, (D_6)benzene, 298 K): δ = 1.06 (s, 6H, C^5*Me$_2$*), 1.23 (s, 6H, C^3*Me$_2$*), 1.26 (d, ^3J(H,H)= 6.7 Hz, 6H, C^{2,6}-CH*Me$_A$*Me$_B$, Dipp), 1.64 (s, 2H, C^4*H$_2$*), 1.73 (d, ^3J(H,H)= 6.7 Hz, 6H, C^{2,6}-CHMe$_A$*Me$_B$*, Dipp), 2.12 (s, 3H, C^4-*Me*, Mes), 2.85 (s, 6H, C^{2,6}-*Me*, Mes), 3.16 (sept, ^3J(H,H)= 6.7 Hz, 2H, C^{2,6}-C*H*Me$_A$Me$_B$, Dipp), 6.85 (s, 2H, C^{3,5}-*H*, Mes), 7.14 (d, ^3J(H,H)= 7.9 Hz, 2H, C^{3,5}-*H*, Dipp overlapping with the (D_6)benzene signal), 7.24 (t, ^3J(H,H)= 7.9 Hz, 1H, C^4-*H*, Dipp).

^{13}C{^{1}H} NMR (125.78 MHz, (D_6)benzene, 298 K): δ (ppm) = 21.2 (s, 1C, C^4-*Me*, Mes), 26.0 (s, 2C, C^{2,6}-CH*Me$_A$*Me$_B$, Dipp), 26.9 (s, 2C, C^{2,6}-CHMe$_A$*Me$_B$*, Dipp), 27.0 (s, 2C, C^{2,6}-*Me*, Mes), 29.0 (s, 2C, C^{2,6}-*C*HMe$_A$Me$_B$, Dipp), 29.4 (s, 2C, C^5*Me$_2$*), 31.0 (s, 2C, C^3*Me$_2$*), 50.3 (s, 1C, *C*^{3}) , 55.7 (s, 1C, *C*^{4}H$_2$), 71.3 (s, 1C, *C*^{5}), 125.4 (s, 2C, *C*^{3,5}-H, Dipp), 128.3 (s, 2C, *C*^{3,5}-H, Mes), 129.1 (s, 1C, *C*^{4}-H, Dipp), 135.0 (s, 1C, *C*^{1}, Dipp) , 137.9 (s, 1C, *C*^{1}, Mes), 139.5 (s, 1C, *C*^{4}, Mes) , 144.9 (s, 2C, *C*^{2,6}, Mes), 148.9 (s, 2C, *C*^{2,6}, Dipp), 195.0 (s, 1C, N*C*^{2}).

^{29}Si{^{1}H} NMR (99.36 MHz, (D_6)benzene, 298 K): δ (ppm) = 10.5 (s, 1Si, *Si*(caac^{Me})).

^{15}N{^{1}H} NMR (50.69 MHz, (D_6)benzene, 298 K): δ (ppm) = 158.8 (s, 1N, *N*C^2).

4.4.20 SiMe(Mes)(caac^{Me}) (8)

To a solution of 200 mg SiBr(Mes)(caac^{Me}) (**2-Mes**) (0.390 mmol, 1.0 equiv.) in 10 mL of benzene 2.5 mL of a solution of MeLi (0.16 mol/L, 0.390 mmol, 1.0 equiv., in Et_2O) was added dropwise in 5 min at ambient temperature. After stirring for 1 h at ambient temperature, another 2 mL of MeLi (0.16 mol/L, 0.32 mmol, 0.82 equiv.) were added, upon which the color of the reaction mixture changed to dark brown. An aliquot of the reaction mixture was taken and analyzed by ^{1}H NMR spectroscopy in (D_6)benzene, which revealed the quantitative formation of SiMe(Mes)(caac^{Me}) (**8**). The dark brown solution was evaporated and the residue extracted with 3 x 5 mL of *n*-hexane. The combined organic extracts were evaporated and dried under fine vacuum for 0.5 h at 40 °C. The orange-brown solid was redesolved in 1 mL of *n*-hexane and stored over night at –30 °C. An orange precipitate was removed from the dark brown mother liquor upon filtration at –30 °C. Drying under fine vacuum afforded SiMe(Mes)(caac^{Me}) (**8**) as orange powder in NMR spectroscopically pure form. Yield: 49 mg (0.11 mmol, 28 %).

Properties: Compound **8** slowly decolorizes to a white solid upon exposure to air. It is well soluble in benzene, *n*-hexane and Et_2O, affording orange solutions.

^{1}H NMR (500.14 MHz, (D_6)benzene, 298 K)**:** δ (ppm) = –0.14 (s, 3H, Si-*Me*), 1.20 (s, 6H, C^5*Me$_2$*), 1.28 (d, ^3J(H,H) = 6.7 Hz, 6H, C^{2,6}-CH*Me$_A$*Me$_B$, Dipp), 1.35 (s, 6H, C^3*Me$_2$*,), 1.51 (d, ^3J(H,H) = 6.7 Hz, 6H, C^{2,6}-CHMe$_A$*Me$_B$*, Dipp), 1.86 (s, 2H, 2 x C^4*H$_2$*), 2.13 (s, 3H, C^4-*Me*, Mes), 2.78 (s, 6H, C^{2,6}-*Me*, Mes), 3.46 (sept, ^3J(H,H) = 6.7 Hz, 2H, C^{2,6}-C*H*Me$_A$Me$_B$, Dipp), 6.87 (s, 2H, C^{3,5}-*H*, Mes), 7.12-7.13 (m, 2H, C^{3,5}-*H*, Dipp), 7.17-7.20 (m, 1H, C^4-*H*, Dipp).

^{13}C{^{1}H} NMR (125.78 MHz, (D_6)benzene, 298 K): δ (ppm) = –2.61 (s, 1C, Si-*Me*), 21.3 (s, 1C, C^4-*Me*, Mes), 25.56 (s, 2C, C^{2,6}-CH*Me$_A$*Me$_B$, Dipp), 26.56 (s, 2C, C^{2,6}-*Me*, Mes), 26.7 (s, 2C, C^{2,6}-CH$_A$Me$_A$*Me$_B$*, Dipp), 28.5 (s, 2C, C^{2,6}-*C*HMe$_A$Me$_B$, Dipp), 29.6 (s, 2C, C^5*Me$_2$*), 32.7 (s, 2C, C^3*Me$_2$*), 46.7 (s, 1C, *C^3*), 57.9 (s, 1C, *C^4*H$_2$), 66.4 (s, 1C, *C^5*), 125.4 (s, 2C, *C^{3,5}*-H, Dipp), 127.9 (s, 2C, *C^{3,5}*-H, Mes overlapping with the (D_6)benzene signal), 128.3 (s, 1C, C^4-H, Dipp), 135.9 (s, 1C, *C^1*, Mes), 137.9 (s, 1C, *C^1*, Dipp), 138.8 (s, 1C, *C^4*, Mes), 144.85 (s, 2C, *C^{2,6}*, Mes), 151.1 (s, 2C, *C^{2,6}*, Dipp), 171.96 (s, 1C, *C^2*).

^{29}Si{^{1}H} NMR (99.36 MHz, (D_6)benzene, 298 K): δ (ppm) = –8.60 (s, 1Si, *Si*(caac^{Me})).

^{1}H-^{15}N HMBC (500.14 MHz, 50.69. MHz, (D_6)benzene, 298 K): δ_N (ppm) = 111.9 (1N, *NC^2*).

4.4.21 $Si_2(Mes)_2(caac^{Me})_2$ as a mixture of Z,Z and *E,E* isomers (9-Mes)

800 mg of $SiBr(Mes)(caac^{Me})$ (**3-Mes**) (1.56 mmol, 1.0 equiv.) and 253 mg of KC_8 (1.873 mmol, 1.2 equiv.) were suspendet in 30 mL of benzene, sonicated for 0.5 h and stirred at ambient temperature. An aliquot of the reaction mixture in (D_6)benzene after 18 h revealed a rather slow conversion rate (23 mol%), with the selective formation of $Si_2(Mes)_2(caac^{Me})_2$ (**9-Mes**). Full conversion was achieved after stirring at ambient temperature for 7 d. The ^{1}H NMR spectrum of the reaction mixture in (D_6)benzene after 7 d revealed the selective formation of two isomers: a ***Z*,*Z***-isomer (which featured sharp resonances and a C_2-symmetry at ambient temperature) and a ***E*,*E***-Isomer (which featured broad resonances at ambient temperature and a C_S-symmetry at higher temperatures), which were formed in approx. ratio of 1:1. The reaction mixture was filtered, and the KC_8-residue was extracted with 3 x 10mL of benzene. The combined dark purple filtrates were evaporated and dried under fine vacuum for 1 h at 40 °C. The dark brown solid was redesolved in 8 mL of boiling *n*-pentane and stored at 4 °C for 2 d. A yellow-brown microcrystalline solid was separated from the dark purple mother liquor upon filtration at 4 °C. After drying at the fine vacuum for 1.5 h at 40 °C, $Si_2(Mes)_2(caac^{Me})_2$ (**9-Mes**) was obtained as a 1 : 1 mixture of an ***Z*,*Z*** (orange) and ***E*,*E*** (purple) isomer in analytical pure form. Yield: 489 mg (0.565 mmol, 72 %)[22]

Properties: The diasteromeric mixture slowly decolorizes to a white solid upon exposure to air. Upon heating of **9-Mes** in the solid state the ***Z*,*Z***-isomer in the diastereromeric mixture slowly converts into the ***E*,*E***-isomer. At 171 °C the compound changes its color from orange to purple, at 206°C dark purple melt nuclei are obtained, which completely melt at 216°C. ^{1}H NMR spectroscopy of the molten dark purple mass in (D_6)benzene reveal the selective formation of the ***E*,*E***-isomer. The yellow-brown isomeric mixture gives intense dark purple solutions (the color in solution can be attributed to the ***E*,*E***-isomer). Similar to the transformation in the solid state, the transformation of the ***Z*,*Z***-isomer into the ***E*,*E*** isomer occurs also in solution. A present sample of the 1:1 diastereomeric mixture takes atleast 9 h at 90°C in (D_8)toluene to fully convert into the ***E*,*E***-isomer. The kinetics of this process was analyzed by VT ^{1}H NMR (*section 5.7.2*). The diasteromeric mixture is well soluble in benzene, toluene and THF and moderately soluble in *n*-pentane and *n*-hexane.

Elemental analysis: $C_{58}H_{84}N_2Si_2$ (865.47 g/mol): calcd./%: C 80.49, H 9.78, N 3.24; found/%: C 80.15, H 9.57, N 3.10.

---

[22] The amount of the ***Z*,*Z***-isomer present in the diasteromeric mixture of **9-Mes** can be increased upon repeated washing steps with *n*-pentane at –30 °C, upon which the orange color of the solid intensifies, however with severe loss of yield.

^{1}H NMR (500.14 MHz, (D_6)benzene, 343 K)**:** δ (ppm) = 0.58 (s, 6H, 2 × $C^5Me_A$$Me_B$, ***Z,Z***), 0.86 (t, ^3J(H,H) = 6.9 Hz, CH_3 *n*-pentane), 0.92 (d, ^3J(H,H) = 6.7 Hz, 6H, 2 × C^2-$CH_A$$Me_A$$Me_B$, Dipp ***Z,Z***), 1.05 (s, 6H, 2 × $C^3Me_A$$Me_B$, ***Z,Z***), 1.14 (m, 24H, 2 × $C^{2,6}$-CH$Me_A$$Me_B$ and 2 × $C^{2,6}$-CH$Me_A$$Me_B$, Dipp, ***E,E***), 1.17 (d, ^3J(H,H) = 6.8 Hz, 6H, 2 × $C^{2,6}$-CH$Me_A$$Me_B$, Dipp, ***Z,Z***), 1.40 (d, ^2J(H,H) = 12.0 Hz, 2H, 2 × $C^4H_AH_B$, ***Z,Z***), 1.41 (d, ^3J(H,H) = 6.8 Hz, 6H, 2 × C^6-$CH_B$$Me_C$$Me_D$, Dipp ***Z,Z***),1.43 (s, 6H, $C^3Me_A$$Me_B$, ***Z,Z***), 1.51 (s, 6H, 2 × $C^5Me_A$$Me_B$, Z,Z), 1.67 (d, ^2J(H,H) = 12.0 Hz, 2H, 2 × $C^4H_AH_B$, Z,Z), 1.79 (s, 6H, 2 × C^2-*Me*, Mes, ***Z,Z***), 1.87 (br s, $\Delta\nu_{1/2}$ = 4.2 Hz, 14H, 2 × C^5Me_2 and 2 × C^4H_2, ***E,E***), 1.88 (br s, $\Delta\nu_{1/2}$ = 6.7 Hz, 12 H, 2 × $C^{2,6}$-*Me*, Mes, ***E,E***), 1.97 (d, ^3J(H,H) = 6.7 Hz, 6H, 2 × C^6-$CH_B$$Me_C$$Me_D$, Dipp ***Z,Z***), 2.03 (s, 12H, 2 × C^3Me_2, ***E,E***), 2.10 (s, 12H, 2 × C^4-*Me*, Mes, ***Z,Z*** and 2 × C^4-*Me*, Mes, ***E,E***), 2.10 (s, 6H, 2 x C^6-*Me*, Mes, ***Z,Z***), 3.08 (br s, $\Delta\nu_{1/2}$ = 42 Hz, 4H, 2 x $C^{2,6}$-C*H*$Me_A$$Me_B$, Dipp, ***E,E***), 3.47 (sept, ^3J(H,H) = 6.8 Hz, 2H, 2 × C^2-$CH_A$$Me_A$$Me_B$, Dipp, ***Z,Z***), 3.79 (sept, ^3J(H,H) = 6.8 Hz, 2H, 2 × C^6-$CH_B$$Me_C$$Me_D$, Dipp, ***Z,Z***), 6.44 (br s, $\Delta\nu_{1/2}$ = 4.9 Hz, 4H, 2 × $C^{3,5}$-*H*, Mes, ***E,E***), 6.73 (s, 2H, 2 × C^3-*H*, Mes, ***Z,Z***), 6.75 (s, 2H, 2 × C^5-*H*, Mes, ***Z,Z***), 6.95-6.97 (br m, 4H, 2 × $C^{3,5}$-*H*, Dipp, ***E,E***), 7.07 (t, ^3J(H,H) = 7.7 Hz, 2H, 2 × C^4-*H*, Dipp, ***E,E***), 7.14 (m, 2H, 2 × C^4-*H*, Dipp, ***Z,Z*** overlapping with the (D_6)benzene signal), 7.17-7.19 (m, 4H, 2 × C^3-*H*, Dipp, ***Z,Z*** and 2 × C^5-*H*, Dipp, ***Z,Z***).

^{13}C{^{1}H} NMR (125.78 MHz, (D_6)benzene, 343 K): δ (ppm) = 21.0 (s, 2C, 2 × C^4-*Me*, Mes, ***E,E***), 21.15 (s, 2C, 2 × C^4-*Me*, Mes, ***Z,Z***), 25.06 (s, 2C, 2 × C^2-$CH_A$$Me_A$$Me_B$, Dipp, ***Z,Z***), 26.1 (s, 2C, 2 × $C^5Me_A$$Me_B$, ***Z,Z***), 26.13 (s, 6C, 2 × C^2-*Me*, Mes, ***Z,Z*** and 2 × $C^{2,6}$-*Me*, Mes, ***E,E***), 26.39 (s, 2C, 2 × C^6-$CH_B$$Me_C$$Me_D$, Dipp, ***Z,Z***), 26.75 (s, 2C, 2 × C^2-*C*$H_A$$Me_A$$Me_B$, Dipp, ***Z,Z***), 26.80 (s, 2C, 2 × C^2-$CH_A$$Me_A$$Me_B$, Dipp, ***Z,Z***), 26.9 (br s, $\Delta\nu_{1/2}$ = 20 Hz, 8C, 2 × $C^{2,6}$-CH$Me_A$$Me_B$ and 2 × $C^{2,6}$-CH$Me_A$$Me_B$, Dipp, ***E,E***), 28.28 (s, 8C, 2 × C^5Me_2, ***E,E*** and 2 × $C^{2,6}$-*C*H$Me_A$$Me_B$,Dipp ***E,E***), 28.52 (s, 2C, 2 × C^6-*Me*, Mes, ***Z,Z***), 29.13 (s, 2C, 2 × C^6-$CH_B$$Me_C$$Me_D$, Dipp, ***Z,Z***), 29.36 (s, 2C, 2 × C^6-*C*$H_B$$Me_C$$Me_D$, Dipp, ***Z,Z***), 30.56 (s, 2C, 2 × $C^5Me_A$$Me_B$, ***Z,Z***), 32.99 (s, 2C, 2 × $C^3Me_A$$Me_B$, ***Z,Z***), 34.08 (s, 2C, 2 × $C^3Me_A$$Me_B$, ***Z,Z***), 36.9 (br s, $\Delta\nu_{1/2}$ = 37 Hz, 4C, 2 × C^3Me_2, ***E,E***), 49.3 (s, 2C, 2 × C^3, ***E,E***), 51.6 (s, 2C, 2 × C^3, ***Z,Z***), 58.1 (s, 2C, 2 × C^4H_2, ***E,E***), 58.8 (s, 2C, 2 × $C^4H_AH_B$, ***Z,Z***), 67.0 (s, 2C, 2 × C^5, ***E,E***), 67.2 (s, 2C, 2 × C^5, ***Z,Z***), 124.9 (s, 2C, 2 × C^3-H, Dipp, ***Z,Z***), 125.4 (br s, $\Delta\nu_{1/2}$ = 25 Hz, 4C, 2 × $C^{3,5}$-H, Dipp, ***E,E***), 125.9 (s, 2C, 2 × C^5-H, Dipp, ***Z,Z***), 127.06 (s, 2C, 2 × C^3-H, Mes, ***Z,Z***), 127.12 (s, 2C, 2 × C^5-H, Mes, ***Z,Z***), 127.4 (s, 2C, 2 × C^4-H, Dipp, Z,Z),127.47 (s, 2C, 2 × $C^{3,5}$-H, Mes, ***E,E***), 127.8 (s, 2C, 2 × C^4-H, Dipp, ***E,E*** overlapping with the (D_6)benzene signal), 134.9 (s, 2C, 2 × C^1, Mes, ***E,E***), 137.3 (s, 2C, 2 × C^4, Mes, ***Z,Z***), 138.2 (s, 2C, 2 × C^4, Mes, ***E,E***), 139.7 (s, 2C, 2 × C^1, Mes, ***Z,Z***), 142.9 (s, 2C, 2 × C^1, Dipp, ***E,E***), 143.8 (s, 2C, 2 × C^1, Dipp, ***Z,Z***), 145.5 (s, 2C, 2 × C^2, Mes, ***Z,Z***), 146.1 (br s, $\Delta\nu_{1/2}$ = 8.5 Hz, 4C, 2 × $C^{2,6}$, Mes, ***E,E***), 146.5 (s, 2C, 2 × C^6, Mes, ***Z,Z***), 148.1 (s, 2C, 2 × C^2, Dipp, ***Z,Z***), 148.9 (br s, $\Delta\nu_{1/2}$ = 13 Hz, 4C, 2 × $C^{2,6}$, Dipp, ***E,E***), 149.3 (s, 2C, 2 × C^6, Dipp, ***Z,Z***), 185.8 (s, 2C, 2 × NC^2, ***Z,Z***), 195.9 (br s, $\Delta\nu_{1/2}$ = 5 Hz, 2C, 2 × NC^2, ***E,E***).

^{29}Si{^{1}H} NMR (99.36 MHz, (D_6)benzene, 343 K): δ (ppm) = –0.21 (s, 2Si, 2 × *Si*(Mes)(caac^{Me}), ***E*,*E***), 10.1 (s, 2Si, 2 × *Si*(Mes)(caac^{Me}), ***Z*,*Z***).
^{1}H-^{15}N HMBC (500.14 MHz, 50.69. MHz, (D_6)benzene, 343 K): δ_N (ppm) = 120.9 (2N, 2 × *N*C^2, ***Z*,*Z***), 133.7 (1N, 2 × *N*C^2, ***E*,*E***).

4.4.22 $Si_2Mes_2(caac^{Me})_2$ *E,E* isomer (9-Mes-*E,E*)

300 mg of the diastereomeric mixture of $Si_2Mes_2(caac^{Me})_2$ (**9-Mes**) were dissolved in 10 mL of m-xylene. The dark purple solution was heated to 130 °C and stirred at this temperature for 3 h. An aliquot of the reaction mixture was taken and analyzed by ^{1}H NMR spectroscopy in (D_6)benzene, revealing the selective formation of the ***E*,*E*** isomer. The reaction mixture was evaporated and dried at fine vacuum for 0.5 h at 60 °C. The dark purple solid was extracted with 4 x 5 mL *n*-pentane and the resulting dark purple extract evaporated and dried at the fine vacuum for 0.5 h at 40 °C. The crude product was redesolved in 2 mL of *n*-pentane and stored at –30 °C overnight. A dark purple microcrystalline solid was separated from the dark purple mother liquor upon filtration at –30 °C and dried at the fine vacuum for 1 h, affording the ***E,E*** isomer of $Si_2Mes_2(caac^{Me})_2$ (**9-Mes-*E,E***) in analytically pure form. Yield: 237 mg (0.273 mmol, 79 %).
Proprerties: Compound **9-Mes-*E,E*** slowly decolorizes to a white solid upon exposure to air. It is well soluble in benzene, toluene and moderately soluble in *n*-pentane and *n*-hexane, affording dark purple solutions.
Elemental analysis: $C_{58}H_{84}N_2Si_2$ (865.47 g/mol): calcd./%: C 80.49, H 9.78, N 3.24; found/%: C 80.55, H 9.79, N 3.03. **Melting point:** 216 °C (dec at 220 °C).

^{1}H NMR (500.14 MHz, (D_6)benzene, 298 K)**:** δ (ppm) = 0.13-0.15 (br s, $\Delta\nu_{1/2}$ = 217 Hz, 6H, 2 × C^2-CH$_A$*Me$_A$*Me$_B$, Dipp, ***E*,*E***), 0.86 (br s, $\Delta\nu_{1/2}$ = 53 Hz, 6H, 2 × C^5*Me$_A$*Me$_B$, ***E*,*E***), 1.07 (br s, $\Delta\nu_{1/2}$ = 210 Hz, 6H, 2 × C^2-CH$_A$Me$_A$*Me$_B$*, Dipp, ***E*,*E***), 1.31 (br s, $\Delta\nu_{1/2}$ = 125 Hz, 6H, 2 × C^6-CH$_B$*Me$_C$*Me$_D$, Dipp ***E*,*E***), 1.40 (br s, $\Delta\nu_{1/2}$ = 78 Hz, 2 × C^{5}Me$_A$*Me$_B$*, ***E*,*E***), 1.84 (br s, $\Delta\nu_{1/2}$ = 126 Hz, 20H, 2 × C^4*H$_A$H$_B$*; 2 × C^2-*Me*, Mes; 2 × C^6-*Me*, Mes and 2 × C^6-CH$_B$Me$_C$*Me$_D$*, Dipp ***E*,*E*** overlapping with each other), 2.06 (br s, $\Delta\nu_{1/2}$ = 3 Hz, 6H, 2 × C^4-*Me*, Mes, ***E*,*E***), 2.11 (br s, $\Delta\nu_{1/2}$ = 3 Hz, 12H, 2 × C^3*Me$_A$*Me$_B$ and 2 × C^{3}Me$_A$*Me$_B$*, ***E*,*E***),2.80 (br s, $\Delta\nu_{1/2}$ = 127 Hz, 2H, 2 × C^2-C*H$_A$*Me$_A$*Me$_B$*, Dipp, ***E*,*E***), 3.38 (br s, $\Delta\nu_{1/2}$ = 93 Hz, 2H, 2 × C^6-C*H$_B$*Me$_C$*Me$_D$*, Dipp, ***E*,*E***), 6.47 (br s, $\Delta\nu_{1/2}$ = 42 Hz, 4H, 2 × C^{3,5}-*H*, Mes, ***E*,*E***), 6.75-7.05 (br s, $\Delta\nu_{1/2}$ = 210 Hz, 4H, 2 × C^3-*H* and 2 × C^5-*H*, Dipp, ***E*,*E***), 7.10 (t, ^{3}J(H,H) = 7.6 Hz, 2H, 2 × C^4-*H*, Dipp, ***E*,*E***).

NMR spectroscopic characterization of **9-Mes-*E,E*** in (D_8)toluene at 243 K:

^{1}H NMR (500.14 MHz, (D_8)toluene, 243 K)**:** δ (ppm) = 0.07 (d, ^3J(H,H) = 6.6 Hz, 6H, 2 × C^2-CH_A*Me_A*Me_B, Dipp, ***E,E***), 0.81 (s, 6H, 2 × C^5*Me_A*Me_B, ***E,E***), 1.00 (d, ^3J(H,H) = 6.6 Hz, 6H, 2 × C^2-$CH_A$$Me_A$*$Me_B$*, Dipp, ***E,E***), 1.31 (d, ^3J(H,H) = 6.7 Hz, 6H, 2 × C^6-CH_B*Me_C*Me_D, Dipp ***E,E***), 1.42 (s, 6H, 2 × $C^5$$Me_A$*$Me_B$*, ***E,E***), 1.70 (d, ^2J(H,H) = 12.0 Hz, 2H, 2 × C^4*H_A*H_B, ***E,E***), 1.76 (s, 6H, 2 × C^2-*Me*, Mes, ***E,E***), 1.89 (d, ^3J(H,H) = 6.7 Hz, 6H, 2 × C^6-$CH_B$$Me_C$*$Me_D$*, Dipp ***E,E***), 1.90 (d, ^2J(H,H) = 12.0 Hz, 2H, 2 × $C^4$$H_A$*$H_B$*, ***E,E***), 2.00 (s, 6H, 2 x C^6-*Me*, Mes, ***E,E***), 2.08 s, 12H, 2 × C^3*Me_A*Me_B and 2 × $C^3$$Me_A$*$Me_B$*, ***E,E*** overlapping with the (D_8)toluene signal), 2.15 (s, 6H, 2 × C^4-*Me*, Mes, ***E,E***), 2.74 (sept, ^3J(H,H) = 6.6 Hz, 2H, 2 × C^2-*C*$H_A$$Me_A$$Me_B$, Dipp, ***E,E***), 3.37 (sept, ^3J(H,H) = 6.7 Hz, 2H, 2 × C^6-*C*$H_B$$Me_C$$Me_D$, Dipp, ***E,E***), 6.35 (s, 2H, 2 × C^3-*H*, Mes, ***E,E***), 6.50 (s, 2H, 2 × C^5-*H*, Mes, ***E,E***), 6.77 (dd, ^3J(H,H) = 7.6 Hz, ^4J(H,H) = 2.0 Hz, 2H, 2 × C^3-*H*, Dipp, ***E,E***), 7.10-7.12 (m, 2H, 2 × C^5-*H*, Dipp, ***E,E*** overlapping with the (D_8)toluene signal), 7.14 (m, 2H, 2 × C^4-*H*, Dipp, ***E,E*** overlapping with the (D_8)toluene signal).

^{13}C{^{1}H} NMR (125.78 MHz, (D_8)toluene, 243 K)**:** δ (ppm) = 21.2 (s, 2C, 2 × C^4-*Me*, Mes, ***E,E***), 22.9 (s, 2C, 2 × C^2-CH_A*Me_A*Me_B, Dipp, ***E,E***), 25.6 (s, 6C, 2 × C^2-*Me*, Mes, ***E,E***), 25.7 (s, 2C, 2 × C^6-CH_B*Me_C*Me_D, Dipp, ***E,E***), 26.0 (s, 2C, 2 × C^5*Me_A*Me_B, ***E,E***), 26.3 (s, 2C, 2 × C^6-*Me*, Mes, ***E,E***), 26.7 (s, 2C, 2 × C^6-$CH_B$$Me_C$*$Me_D$*, Dipp, ***E,E***), 28.0 (s, 2C, 2 × C^6-*C*$H_B$$Me_C$$Me_D$, Dipp, ***E,E***), 28.2 (s, 2C, 2 × C^2-$CH_A$$Me_A$*$Me_B$*, Dipp, ***E,E***), 28.4 (s, 2C, 2 × C^2-*C*$H_A$$Me_A$$Me_B$, Dipp, ***E,E***), 31.1 (s, 2C, 2 × $C^5$$Me_A$*$Me_B$*, ***E,E***), 35.0 (s, 2C, 2 × C^3*Me_A*Me_B, ***E,E***), 38.4 (s, 2C, 2 × $C^3$$Me_A$*$Me_B$*, ***E,E***), 49.1 (s, 2C, 2 × *C*^{3}, ***E,E***), 57.1 (s, 2C, 2 × *C*^{4}$H_A$$H_B$, ***E,E***), 66.8 (s, 2C, 2 × *C*^{5}, ***E,E***), 124.0 (s, 2C, 2 × *C*^{3}-H, Dipp, ***E,E***), 126.5 (s, 2C, 2 × *C*^{5}-H, Dipp, ***E,E***), 126.7 (s, 2C, 2 × *C*^{5}-H, Mes, ***E,E***), 127.0 (s, 2C, 2 × *C*^{4}-H, Dipp, ***E,E***), 129.1 (s, 2C, 2 × *C*^{3}-H, Mes, ***E,E***), 134.2 (s, 2C, 2 × *C*^{1}, Mes, ***E,E***), 136.8 (s, 2C, 2 × *C*^{4}, Mes, ***E,E***), 142.3 (s, 2C, 2 × *C*^{1}, Dipp, ***E,E***), 145.2 (s, 2C, 2 × *C*^{6}, Mes, ***E,E***), 146.5 (s, 2C, 2 × *C*^{2}, Mes, ***E,E***), 147.4 (s, 2C, 2 × *C*^{6}, Dipp, ***E,E***), 149.1 (s, 2C, 2 × *C*^{2}, Dipp, ***E,E***), 196.9 (s, 2C, 2 × N*C*^{2}, ***E,E***).

^{29}Si{^{1}H} NMR (99.36 MHz, (D_8)toluene, 243 K)**:** δ (ppm) = –2.7 (s, 2Si, 2 × *Si*{Mes}(caac^{Me}), ***E,E***).

^{1}H-^{15}N HMBC (500.14 MHz, 50.69. MHz, (D_8)toluene, 243 K)**:** δ_N (ppm) = 134.6 (1N, 2 × *N*C^2, ***E,E***).

NMR spectroscopic characterization of **9-Mes-*E,E*** in (D_8)toluene at 343 K:

^{1}H NMR (500.14 MHz, (D_8)toluene, 343 K)**:** δ (ppm) = 1.10-1.11 (br m, $\Delta\nu_{1/2}$ = 17.4 Hz, 24H, 2 × C^5*Me*$_2$ and 2 × $C^{2,6}$-CH*Me*$_A$Me$_B$ as well as 2 × $C^{2,6}$-CHMe$_A$*Me*$_B$, Dipp, ***E,E***), 1.80 (br s, $\Delta\nu_{1/2}$ = 7.6 Hz, 12H, 2 × $C^{2,6}$-*Me*, Mes, ***E,E***), 1.84 (s, 4H, 2 × C^4*H*$_2$, ***E,E***), 1.98 (s, 12H, 2 × C^3*Me*$_2$ ***E,E***), 2.08 (s, 6H, 2 × C^4-*Me*, Mes, ***E,E*** overlapping with the (D_8)toluene signal), 3.03 ((br s, $\Delta\nu_{1/2}$ = 46.6 Hz, 4H, 2 × $C^{2,6}$-C*H*Me$_A$Me$_B$, Dipp, ***E,E***), 6.38 (br s, $\Delta\nu_{1/2}$ = 3.9 Hz, 4H, 2 × $C^{3,5}$-*H*, Mes, ***E,E***), 6.89-6.91 (br m, $\Delta\nu_{1/2}$ = 39 Hz, 2H, 2 × $C^{3,5}$-*H*, Dipp, ***E,E***), 7.02 (t, ^3J(H,H) = 7.5 Hz, 2H, 2 × C^4-*H*, Dipp, ***E,E***).

^{13}C{^{1}H} NMR (125.78 MHz, (D_8)toluene, 343 K)**:** δ (ppm) = 21.1 (s, 2C, 2 × C^4-*Me*, Mes, ***E,E***), 25.0 (br s, $\Delta\nu_{1/2}$ = 64 Hz, 4C, 2 × $C^{2,6}$-CH*Me*$_A$Me$_B$ and 2 × $C^{2,6}$-CHMe$_A$*Me*$_B$, Dipp, ***E,E***), 26.2 (s, 4C, 2 × $C^{2,6}$-*Me*, Mes, ***E,E***), 27.0 (s, $\Delta\nu_{1/2}$ = 27 Hz, 4C, 2 × C^5*Me*$_2$, ***E,E***), 28.4 (br s, 4C, 2 × $C^{2,6}$-*C*HMe$_A$Me$_B$, Dipp, ***E,E***), 37.1 (br s, $\Delta\nu_{1/2}$ = 49 Hz, 4C, 2 × C^3*Me*$_2$, ***E,E***), 49.4 (s, 2C, 2 × *C*^{3}, ***E,E***), 58.3 (s, 2C, 2 × *C*^{4}H$_2$, ***E,E***), 67.1 (s, 2C, 2 × *C*^{5}, ***E,E***), 125.6 (br s, 4C, 2 × *C*^{3,5}-H, Dipp, ***E,E*** overlapping with the (D_8)toluene signal), 127.2 (s, 2C, 2 × *C*^{4}-H, Dipp, ***E,E***), 128.0 (s, 2C, 2 × *C*^{3,5}-H, Mes, ***E,E*** overlapping with the (D_8)toluene signal), 134.9 (s, 2C, 2 × *C*^{1}, Mes, ***E,E***), 137.3 (s, 2C, 2 × *C*^{4}, Mes, ***E,E***), 142.9 (s, 2C, 2 × *C*^{1}, Dipp, ***E,E***), 146.2 (br s, $\Delta\nu_{1/2}$ = 10 Hz, 4C, 2 × *C*^{2,6}, Mes, ***E,E***), 148.9 (br s, $\Delta\nu_{1/2}$ = 16 Hz, 4C, 2 × *C*^{2,6}, Dipp, ***E,E***), 196.0 (s, 2C, 2 × N*C*^{2}, ***E,E***).

^{29}Si{^{1}H} NMR (99.36 MHz, (D_8)toluene, 343 K)**:** δ (ppm) = –0.32 (s, 2Si, 2 × *Si*{Mes}(caac^{Me}), ***E,E***).

^{1}H-^{15}N HMBC (500.14 MHz, 50.69. MHz, (D_8)toluene, 343 K)**:** δ_N (ppm) = 133.7 (2N, 2 × *N*C^2, ***E,E***).

4.4.23 $Si_2Br_2(caac^{Me})_2$ (9-Br)

Synthesis of 9-Br from $SiBr_2(caac^{Me})$

$SiBr_2(caac^{Me})$ (**1**) (5.00 g, 105.6 mmol, 1.0 equiv.) and KC_8 (1.93 g, 142.6 mmol, 1.35 equiv.) were suspended in 150 mL of benzene. After 0.5 h the suspension turned dark purple. The reaction mixture was stirred overnight at ambient temperature. An aliquot of the reaction mixture was taken after 19 h at ambient temperature and analyzed by ^{1}H NMR spectroscopy in (D_6)benzene, revealing the selective formation of **9-Br**. The dark purple suspension was filtered and the black residue extracted with 5 x 5 mL of benzene. The combined dark purple filtrate was evaporated and dried at fine vacuum for 1 h at ambient temperature. The dark purple solid was redesolved in 10 mL toluene/*n*-hexane mixture (1:10). After storing of the suspension for 19 h at –60 °C the dark purple precipitate was removed from the dark purple mother liquor upon filtration. Drying at fine vacuum for 1.5 h at ambient temperature afforded analytically pure **9-Br** as a dark purple solid. Yield: 3.183 g (77 %, overall yield from $SiBr_4(caac^{Me})$ 50 %).

Synthesis of 9-Br from $SiBr_4(caac^{Me})$

$SiBr_4(caac^{Me})$ (5.70 g, 9.00 mmol, 1.0 equiv.) was suspendet in 180 mL of benzene. KC_8 (3.772 g, 27.9 mmol, 3.1 equiv.) was added to the suspension in small portions over period of 0.5 h. Upon addition the reaction mixture turned reddish-brown. The reaction mixture was sonicated for 0.5 h and stirred at ambient temperature. After stirring for 19 h at ambient temperature the supernatant solution turned red-purple. After 46 h at ambient temperature the supernatant solution changed to dark purple. An aliquote of the reaction mixture was taken and analyzed by ^{1}H NMR spectrsocpy in (D_6)benzene, revealing the selective formation of $Si_2Br_2(caac^{Me})_2$ (**9-Br**). The black graphite was filtered, the product reextracted with 3 x 20 mL of benzene. The combined red-purple filtrates were evaporated and dried under fine vacuum for 0.5 h at 40 °C. The crude dark purple product was washed with 2 x 10 mL of *n*-pentane, followed by 3 x 5mL benzene/*n*-penate mixture (1:5) and another 2 x 10 mL *n*-pentane. Drying at the fine vacuum for 1 h at 40 °C afforded $Si_2Br_2(caac^{Me})_2$ (**9-Br**) as a purple powder in analytically pure form. Yield: 1.27 g (3.24 mmol, 36 %)

Properties: Disilicon(I) compound **9-Br** quickly decolorizes upon contact with air. It is moderately soluble in *n*-hexane and well soluble in benzene, toluene and THF, affording red-purple solutions.

Elemental analysis: $C_{40}H_{62}Br_2N_2Si_2$ (786.91 g/mol): calcd./%: C 61.05, N 3.56, H 7.94; found/%: C 61.31, N 3.19, H 8.11. **Melting point:** 173 °C (dec).

^{1}H NMR (500.17 MHz, (D_6)benzene, 298 K): δ (ppm) = 1.01 (s, 12H, 2 × C^5*Me*$_2$), 1.17 (d, ^3J(H,H) = 6.7 Hz, 12H, 2 × $C^{2,6}$-CH*Me*$_A$Me$_B$, Dipp), 1.69 (s, 4H, 2 × C^4*H*$_2$), 1.72 (br s, $\Delta\nu_{1/2}$ = ca. 21 Hz, 12H, 2 × $C^{2,6}$-CHMe$_A$*Me*$_B$, Dipp), 1.92 (s, 12H, 2 × C^3*Me*$_2$), 3.07 (sept, ^3J(H,H) = 6.7 Hz, 4H, 2 × $C^{2,6}$-C*H*Me$_A$Me$_B$, Dipp), 7.07 (d, ^3J(H,H) =7.7 Hz, 4H, 2 × $C^{3,5}$-*H*, Dipp), 7.18 (t, ^3J(H,H) =7.7 Hz, 2H, 2 × C^4-*H*, Dipp).

^{1}H NMR (300.13 MHz, (D_8)THF, 298 K): δ (ppm) = 1.22 (d, ^3J(H,H) = 6.7 Hz, 12H, 2 × $C^{2,6}$-CH*Me*$_A$Me$_B$, Dipp), 1.29 (s, 12H, 2 × C^5*Me*$_2$) 1.40 (br, $\Delta\nu_{1/2}$ = ca. 15 Hz, 12H, 2 × $C^{2,6}$-CHMe$_A$*Me*$_B$, Dipp), 1.78 (s, 12H, 2 × C^3*Me*$_2$), (s, 4H, 2 × C^4*H*$_2$), 3.07 (sept, ^3J(H,H) = 6.7 Hz, 4H, 2 × $C^{2,6}$-*CH*Me$_A$Me$_B$, Dipp), 7.07 – 7.10 (m, 4H, 2 × $C^{3,5}$-*H*, Dipp), 7.22 (dd, ^3J(H,H) = 8.4, 6.9 Hz, 2H, 2 × C^4-*H*, Dipp).

^{13}C{^{1}H} NMR (125.77 MHz, (D_6)benzene, 298 K): δ (ppm) = 25.5 (s, 4C, 2 × $C^{2,6}$-CH*Me*$_A$Me$_B$, Dipp), 27.2 (br s, $\Delta\nu_{1/2}$ = 27 Hz, 4C, 2 × $C^{2,6}$-CHMe$_A$*Me*$_B$, Dipp), 29.1 (br s, $\Delta\nu_{1/2}$ = 33 Hz, 2 × 4C, 2 × C^5*Me*$_2$ and 2 × $C^{2,6}$-*C*HMe$_A$Me$_B$, Dipp), 32.8 (br, $\Delta\nu_{1/2}$ = 65 Hz, 4C, 2 × C^3*Me*$_2$), 51.7 (s, 2C, 2 × *C*^{3}), 55.5 (s, 2C, 2 × *C*^{4}H$_2$), 72.4 (s, 2C, 2 × *C*^{5}), 125.0 (s, 4C, 2 × *C*^{3,5}-H, Dipp), 129.2 (s, 2C, 2 × *C*^{4}-H, Dipp), 134.9 (s, 2C, 2 × *C*^{1}, Dipp), 148.5 (s, 4C, 2 × *C*^{2,6}, Dipp), 208.3 (s, 2C, 2 × N*C*^{2}).

^{29}Si{^{1}H} NMR (99.36 MHz, (D_6)benzene, 298 K): δ (ppm) = 19.8 (s, 2Si).

^{1}H-^{15}N HMBC (500.17, 50.68 MHz, (D_6)benzene, 298K): δ_N (ppm) = 174.3 (s, 2N, 2 × *N*C^2).

4.4.24 $Si_2Cp'_2(caac^{Me})_2$ (9-Cp')

$Si_2Br_2(caac^{Me})_2$ (**9-Br**) (1.00 g, 1.27 mmol, 1.0 equiv.) and NaCp (0.448 g, 5.08 mmol, 4.0 equiv.) were dissolved in 30 mL of THF. The dark purple solution was stirred for 10 min at ambient temperature and then stirred at 50 °C. After stirring at 50 °C for 23 h the reaction mixture turned orange-brown. An aliquote of the reaction mixture was taken and analyzed by ^{1}H NMR spectroscopy in (D_6)benzene, which revealed the formation of $Si_2Cp'_2(caac^{Me})_2$ (**9-Cp'**) with a moderate selectivity. The reaction mixture was evaporated and dried under fine vaccum for 0.5 h at 40 °C. The orange-brown solid was extracted with 50 mL of toluene, followed by 3 x 20 mL of toluene. The combined organic extracts were evaporated and dried under fine vacuum. The orange-brown residue was washed with 2 x 20 mL of THF followed by 3 x 20 mL of *n*-pentane. After drying under fine vacuum for 1 h at 50 °C, **9-Cp'** was obtained as a bright orange powder. Yield: 207 mg (0.273 mmol, 22 %).[23]

Properties: Disilicon(I) compound **9-Cp'** slowly deocolorizes upon contact with air. It is moderately soluble in benzene, toluene, *n*-pentane and THF, affording orange solutions. The compound is thermolabile. Heating a (D_6)benzene sample of **9-Cp'** for 20 h at 80 °C leads to the complete decomposition and the rather selective formation of alkene **X** next to small amounts of the ($caac^{Me}H$)Si(Cp')=Si(Cp')($caac^{Me}H$)(**Y**).

Elemental Analysis: $C_{50}H_{72}N_2Si_2$ $(C_4H_8O)_{0,11}$ (765.22 g/mol): calcd./%: C 79.17, N 3.66, H 9.60; found/%: C 78.63, N 3.67, H 9.65.

NMR spectroscopic assignment of $Si_2Cp'_2(caac^{Me})_2$ (**9-Cp'**):

^{1}H NMR (500.17 MHz, (D_8)THF, 298 K): δ (ppm) = 0.83 (d, ^3J(H,H) = 6.7 Hz, 6H, 2 × C^2-$CH_AMe_AMe_B$, Dipp),1.04 (s, 6H, 2 × $C^5Me_AMe_B$), 1.17 (d, ^3J(H,H) = 6.7 Hz, 6H, 2 × C^2-$CH_AMe_AMe_B$, Dipp), 1.25 (s, 6H, 2 × $C^5Me_AMe_B$), 1.31 (d, ^3J(H,H) = 6.7 Hz, 6H, 2 × C^6-$CH_AMe_CMe_D$, Dipp), 1.33 (s, 6H, 2 × $C^3Me_AMe_B$), 1.50 (d, ^3J(H,H) = 6.7 Hz, 6H, 2 × C^6-$CH_AMe_CMe_D$, Dipp), 1.89 (s, 6H, 2 × $C^3Me_AMe_B$), 1.90 (d, ^2J(H,H) = 11.9 Hz, 2H, 2 × $C^4H_AH_B$), 2.04 (d, ^2J(H,H) = 11.9 Hz, 2H, 2 × $C^4H_AH_B$), 2.37 (d, ^2J(H,H) = 24.0 Hz, 2H, 2 × $C^5H_AH_B$, Cp'), 2.56 (d, ^2J(H,H) = 24.0 Hz, 2H, 2 × $C^5H_AH_B$, Cp'), 3.18 (sept, ^3J(H,H) = 6.7 Hz, 2H, 2 × C^2-$CH_AMe_AMe_B$, Dipp), 3.33 (sept, ^3J(H,H) = 6.7 Hz, 2H, 2 × C^6-$CH_BMe_CMe_D$, Dipp), 5.43 (m, 2H, 2 × C^2-*H*, Cp'), 6.06-6.08 (m, 2H, 2 × C^4-*H*, Cp'), 6.14 (dd, ^3J(H,H) = 5.0 Hz, ^3J(H,H) = 1.0 Hz, 2H, 2 × C^3-*H*, Cp'), 7.02 (dd, ^3J(H,H) =7.5 Hz, ^4J(H,H) = 2.8 Hz 2H, 2 × C^5-*H*, Dipp), 7.27 (m, 2H, 2 × C^3-*H*, Dipp overlapping with the C^4-*H*, Dipp signal), 7.28 (t, ^3J(H,H) =7.5 Hz, 2H, 2 × C^4-*H*, Dipp).

---

[23] The compound contained small amounts of an impurity, which can be highly likely attributed to a *E,Z* diastereromer of $Si_2Cp'_2(caac^{Me})_2$. It bears two different carbene resonances (at 182.9 and 182.2 ppm), as well as two different silicon resonances (–6.31 and -8.51 ppm). The impurity could not be removed nether upon multiple THF washing steps nor crystallization from the THF filtrate.

$^{13}C\{^1H\}$ NMR (125.77 MHz, (D_8)THF, 298 K): δ (ppm) = 24.7 (s, 2C, 2 × C^2-$CH_AMe_AMe_B$, Dipp), 25.0 (s, 2C, 2 × C^6-$CH_BMe_CMe_D$, Dipp overlapping with the (D_8)THF signal), 25.8 (s, 2C, 2 × C^2-$CH_AMe_AMe_B$, Dipp), 28.2 (s, 2C, 2 × C^6-$CH_BMe_CMe_D$), 28.5 (s, 2C, 2 × $C^5Me_AMe_B$), 29.1 (s, 2C, 2 × C^2-$CH_AMe_AMe_B$, Dipp), 29.6 (s, 2C, 2 × C^6-$CH_BMe_CMe_D$, Dipp), 30.2 (s, 2C, 2 × $C^5Me_AMe_B$), 34.3 (s, 2C, 2 × $C^3Me_AMe_B$), 36.6 (s, 2C, 2 × $C^3Me_AMe_B$), 48.6 (s, 2C, $C^5H_AH_B$, Cp'), 48.8 (s, 2C, 2 × C^3), 58.8 (s, 2C, 2 × $C^4H_AH_B$), 67.8 (s, 2C, 2 × C^5 overlapping with the (D_8)THF signal), 125.2 (s, 2C, 2 × C^5-H, Dipp), 126.2 (s, 2C, 2 × C^3-H, Dipp), 128.8 (s, 2C, 2 × C^4-H, Dipp), 133.8 (s, 2C, 2 × C^4-H, Cp'), 136.2 (s, 2C, 2 × C^3-H, Cp'), 139.7 (s, 2C, 2 × C^1, Dipp), 143.7 (s, 2C, 2 × C^2-H, Cp'), 146.5 (s, 2C, 2 × C^1, Cp'), 150.6 (s, 2C, 2 × C^6, Dipp), 152.1 (s, 2C, 2 × C^2, Dipp), 180.9 (s, 2C, 2 × NC^2).

$^{29}Si\{^1H\}$ NMR (99.36 MHz, (D_8)THF, 298 K): δ (ppm) = –5.65 (s, 2Si, 2 × $Si(caac^{Me})$).

^1H-^{15}N HMBC (500.17, 50.68 MHz, (D_8)THF, 298 K): δ_N (ppm) = 132.9 (s, 2N, 2 × NC^2).

Thermal Decomposition of $Si_2Cp'_2(caac^{Me})_2$ (9-Cp')

A pure NMR sample of **9-Cp'** in (D_6)benzene was heated at 80 °C for 20 h upon which the color of the solution changed from orange to yellow-brown. Monitoring of the reaction mixture by ^1H NMR spectroscopy revealed the complete decomposition of **9-Cp'** and the selective formation of alkene **X**, alongside of tiny amounts of the byproduct **Y**.

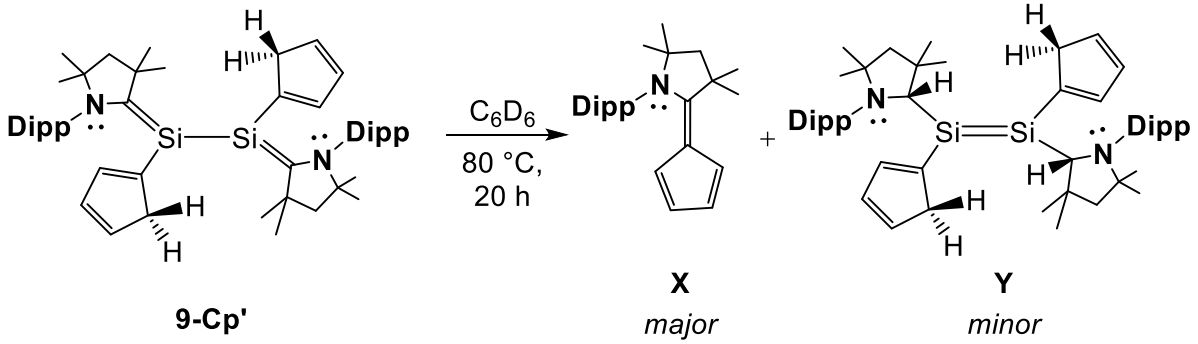

Scheme 4.1. Decomposition of **9-Cp'** upon heating in (D_6)benzene.

NMR spectroscopic characterization of alkene **X**:

^1H NMR (500.17 MHz, (D_6)benzene, 298 K): δ (ppm) = 1.01 (s, 6H, C^5Me_2), 1.11 (d, ^3J(H,H) = 6.9 Hz, 6H, $C^{2,6}$-$CH_AMe_AMe_B$, Dipp), 1.15 (d, ^3J(H,H) = 6.9 Hz, 6H, 2 × C2,^{6}-$CHMe_AMe_B$, Dipp), 1.63 (s, 6H, C^3Me_2), 1.72 (s, 2H, C^4H_2), 3.00 (sept, ^3J(H,H) = 6.8 Hz, 2H, $C^{2,6}$-$CHMe_AMe_B$, Dipp), 5.16 (m, 1H, C^2-*H*, Cp'), 6.28 (m, 1H, C^3-*H*, Cp'), 6.53 (m, 1H, C^5-*H*, Cp'), 6.99 (m, 1H, C^4-*H*, Cp'), 7.11 (d, 2H, ^3J(H,H) = 7.6 Hz, $C^{3,5}$-*H*, Dipp), 7.21 (t, ^3J(H,H) =7.6 Hz, 1H, C^4-*H*, Dipp).

^{13}C{^{1}H} NMR (125.77 MHz, (D_6)benzene, 298 K): δ (ppm) = 24.4 (s, 2C, $C^{2,6}$-$CHMe_A$*Me_B*, Dipp), 25.6 (s, 2C, $C^{2,6}$-CH*Me_A*Me_B, Dipp), 29.15 (s, 2C, 2 × C^5*Me_2*), 29.17 (s, 2C, $C^{2,6}$-*C*HMe_AMe_B, Dipp), 33.4 (s, 2C, C^3*Me_2*), 45.0 (s, 1C, *C*^{3}), 55.6 (s, 1C, *C*$^4H_2$), 67.1 (s, 1C, *C*^{5}), 113.5 (s, 1C, *C*^{1}, Cp'), 118.7 (s, 1C, *C*^{2}-H, Cp'), 120.1 (s, 1C, *C*^{4}-H, Cp'), 120.7 (s, 1C, *C*^{5}-H, Cp'), 121.7 (s, 1C, *C*^{5}-H, Cp'), 125.9 (s, 2C, *C*^{3,5}-H, Dipp), 129.4 (s, 1C, *C*^{4}-H, Dipp), 135.9 (s, 1C, *C*^{1}, Dipp), 148.3 (s, 2C, *C*^{2,6}, Dipp), 166.9 (s, 1C, N*C*^{2}).

^{1}H-^{15}N HMBC NMR (500.17, 50.68 MHz, (D_6)benzene, 298 K): δ_N (ppm) = 134.45 (s, 1N, *N*C^2).

Tentative NMR assignment of minor decomposition product **Y**:

^{1}H NMR (500.17 MHz, (D_6)benzene, 298 K): δ (ppm) = 1.02 (s, 6H, 2 × C^5*Me_A*Me_B), 1.13 (s, 6H, 2 × C^5Me_A*Me_B*), 1.14 (d, ^{3}*J*(H,H) = 6.7 Hz, 6H, 2 × C^6-CH_A*Me_C*Me_D, Dipp), 1.17 (s, 6H, 2 × C^3*Me_A*Me_B), 1.27 (d, ^{3}*J*(H,H) = 6.7 Hz, 6H, 2 × C^2-CH_A*Me_A*Me_B, Dipp), 1.28 (d, ^{3}*J*(H,H) = 6.7 Hz, 6H, 2 × C^6-CH_AMe_C*Me_D*, Dipp), 1.31 (d, ^{3}*J*(H,H) = 6.7 Hz, 6H, 2 × C^2-CH_AMe_A*Me_B*, Dipp), 1.47 (s, 6H, 2 × C^3Me_A*Me_B*), 1.86 (d, ^{2}*J*(H,H) = 11.9 Hz, 2H, 2 × C^4*H_A*H_B), 2.03 (d, ^{2}*J*(H,H) = 11.9 Hz, 2H, 2 × C^4H_A*H_B*), 2.46 (d, ^{2}*J*(H,H) = 24.2 Hz, 2H, 2 × C^5*H_A*H_B, Cp'), 2.54 (d, ^{2}*J*(H,H) = 24.2 Hz, 2H, 2 × C^5H_A*H_B*, Cp'), 3.37 (sept, ^{3}*J*(H,H) = 6.7 Hz, 2H, 2 × C^2-*C*$H_AMe_AMe_B$, Dipp), 4.00 (sept, ^{3}*J*(H,H) = 6.8 Hz, 2H, 2 × C^6-*C*$H_BMe_CMe_D$, Dipp), 4.61 (s, 2H, 2 × C^2-*H*), 5.86 (m, 2H, 2 × C^2-*H*, Cp'), 6.16-6.17 (m, 2H, 2 × C^3-*H*, Cp'), 6.77 (dd, ^{3}*J*(H,H) = 5.4 Hz, ^{3}*J*(H,H) = 1.5 Hz, 2H, 2 × C^4-*H*, Cp'), 7.03 (dd, ^{3}*J*(H,H) =6.9 Hz, ^{4}*J*(H,H) = 2.8 Hz 2H, 2 × C^5-*H*, Dipp), 7.06-7.08 (m, 2H, 2 × C^3-*H*, Dipp overlapping with the C^4-*H*, Dipp signal), 7.08 (m, 2H, 2 × C^4-*H*, Dipp).

^{13}C{^{1}H} NMR (125.77 MHz, (D_6)benzene, 298 K): δ (ppm) = 24.6 (s, 2C, 2 × C^2-CH_A*Me_A*Me_B, Dipp), 25.8 (s, 2C, 2 × C^2-CH_AMe_A*Me_B*, Dipp), 26.0 (s, 2C, 2 × C^6-CH_B*Me_C*Me_D, Dipp), 26.1 (s, 2C, 2 × C^6-CH_BMe_C*Me_D*), 27.35 (s, 2C, 2 × C^2-*C*$H_AMe_AMe_B$, Dipp), 27.43 (s, 2C, 2 × C^6-*C*$H_BMe_CMe_D$, Dipp), 28.8 (s, 2C, 2 × C^5*Me_A*Me_B), 29.3 (s, 2C, 2 × C^5Me_A*Me_B*), 30.9 (s, 2C, 2 × C^3*Me_A*Me_B), 33.0 (s, 2C, 2 × C^3Me_A*Me_B*), 40.5 (s, 2C, *C*$^5H_AH_B$, Cp'), 41.2 (s, 2C, 2 × *C*^{3}), 57.4 (s, 2C, 2 × *C*$^4H_AH_B$), 62.6 (s, 2C, 2 × *C*^{5}), 75.8 (s, 2C, 2 × C^2-H), 124.6 (s, 2C, 2 × *C*^{5}-H, Dipp), 125.0 (s, 2C, 2 × *C*^{3}-H, Dipp), 126.7 (s, 2C, 2 × *C*^{4}-H, Dipp), 130.2 (s, 2C, 2 × *C*^{2}-H, Cp'), 131.8 (s, 2C, 2 × *C*^{3}-H, Cp'), 135.6 (s, 2C, 2 × *C*^{4}-H, Cp'), 140.5 (s, 2C, 2 × *C*^{1}, Dipp), 148.2 (s, 2C, 2 × *C*^{1}, Cp'), 150.0 (s, 2C, 2 × *C*^{6}, Dipp), 151.9 (s, 2C, 2 × N*C*^{2}, Dipp).

^{29}Si{^{1}H} NMR (99.36 MHz, (D_6)benzene, 298 K): δ (ppm) = –5.46 (s, 2Si, 2 × *Si*(caac^{Me})).

4.4.25 $Si_2(C{\equiv}CMes)_2(caac^{Me})_2$ (9-C_2Mes)

To a purple solution of $Si_2Br_2(caac^{Me})_2$ (**9-Br**) (0.70 g, 0.889 mmol, 1.0 equiv.) in 15 mL THF was added dropwise a clear solution of LiC≡CMes (0.350 g, 1.957 mmol, 2.2 equiv.) in 15 mL THF in 10 min at ambient temperature. After stirring for 18 h at ambient temperature the color changed to orange-brown. An aliquote of the reaction mixture was taken and analyzed by ^{1}H NMR spectroscopy in (D_6)benzene revealing the selective formation of $Si_2(C{\equiv}CMes)_2(caac^{Me})_2$ (**9-C_2Mes**). The reaction mixture was evaporated and the resulting orange-brown residue was dried at high vacuum for 0.5 h at 40 °C. The product was extracted with 3 x 20 mL of *n*-pentane. The combined organic phases were evaporated and dried at high vacuum for 1.5 h at 40 °C. The orange-brown residue was redesolved in 2 mL of *n*-pentane. After storing at –60 °C for 19 h orange crystals were obtained which were removed from the brown motherliquor upon filtration at –60 °C. Drying under fine vacuum for 1 h at 40 °C afforded NMR spectroscopically pure **9-C_2Mes** as an orange powder. Yield: 0.320 g (0.350 mmol, 39 %).

Properties: Disilicon(I) compound **9-C_2Mes** immediately decolorizes upon contact with air. It is well soluble in *n*-pentane, benzene, toluene and THF, affording orange brown solutions.

Elemental Analysis: $C_{62}H_{84}N_2Si_2$ (913.51 g/mol): calcd./%: C 81.52, N 3.07, H 9.27; found/%: C 79.91, N 2.87, H 9.01.[24]

ATR-IR (solid): $\tilde{\nu}$ (cm^{-1}) = 2964 (m), 2924 (m), 2865 (w), 2143 (vw) [[ν(C ≡ C)],, 1610 (vw), 1463 (m), 1441 (m), 1382 (w), 1363 (w), 1329 (vs), 1254 (w), 1235 (w), 1220 (m), 1197 (s), 1179 (m), 1137 (m), 1044 (m), 1026 (m), 936 (vw), 905 (w), 852 (m), 808 (m), 798 (m), 783 (m), 729 (w), 696 (vw), 612 (w), 577 (m), 457 (w), 418 (w).

^{1}H NMR (500.17 MHz, (D_6)benzene, 298 K): δ (ppm) = 1.08 (s, 12H, 2 × C^5Me_2), 1.12 (d, ^3J(H,H) = 6.6 Hz, 12H, 2 × $C^{2,6}$-CH$Me_A$$Me_B$, Dipp), 1.63 (d, ^3J(H,H) = 6.7 Hz, 12H, 2 × $C^{2,6}$-CH$Me_A$$Me_B$, Dipp), 1.82 (s, 4H, 2 × C^4H_2), 2.06 (s, 12H, 2 × C^3Me_2), 2.09 (s, 6H, 2 × C^4-*Me*, Mes), 2.45 (s, 12H, 2 × $C^{2,6}$-*Me*, Mes) 3.19 (sept, ^3J(H,H) = 6.7 Hz, 4H, 2 × $C^{2,6}$-C*H*$Me_A$$Me_B$, Dipp), 6.76 (s, 4H, 2 × $C^{3,5}$-*H*, Mes), 6.90 (t, ^3J(H,H) = 7.8 Hz, 2H, 2 × C^4-*H*, Dipp) 6.95 (d, ^3J(H,H) = 7.8 Hz, 4H, 2 × $C^{3,5}$-*H*, Dipp).

[24] According to the elemental analysis the compound still contains 21 mol% of LiBr. In order to obtain the analytically pure compound the compound need to be extracted again with *n*-hexane.

$^{13}C\{^{1}H\}$ NMR (125.77 MHz, (D_6)benzene, 298 K): δ (ppm) = 21.3 (s, 2C, 2 × C^4-*Me*, Mes), 22.1 (s, 4C, 2 × $C^{2,6}$-*Me*, Mes*)*, 25.0 (s, 4C, 2 × $C^{2,6}$-CH*Me*$_A$Me$_B$, Dipp), 27.2 (s, 4C, 2 × $C^{2,6}$-CHMe$_A$*Me*$_B$, Dipp), 29.0 (s, 4C, 2 × $C^{2,6}$-*C*HMe$_A$Me$_B$, Dipp), 29.1 (s, 4C, 2 × C^5*Me*$_2$), 35.1 (s, 4C, 2 × C^3*Me*$_2$), 49.4 (s, 2C, 2 × *C*^{3}), 56.5 (s, 2C, 2 × *C*^{4}H$_2$), 69.3 (s, 2C, 2 × *C*^{5}), 101.4 (s, 2C, 2 × *C* ≡ C-Mes), 110.5 (s, 2C, 2 × C ≡ *C*-Mes), 123.2 (s, 4C, 122.9, 2 × *C*^{1}, Mes), 124.9 (s, 4C, 2 × *C*^{3,5}-H, Dipp), 127.6 (s, 4C, 2 × *C*^{3,5}-H, Mes),

128.6 (s, 2C, 2 × *C*^{4}-H, Dipp), 136.1 (s, 2C, 2 × *C*^{4}, Mes), 136.3 (s, 2C, 2 × *C*^{1}, Dipp), 140.4 (s, 4C, 2 × *C*^{2,6}, Mes), 148.8 (s, 4C, 2 × *C*^{2,6}, Dipp), 197.3 (s, 2C, 2 × NC^2).

$^{29}Si\{^{1}H\}$ NMR (99.36 MHz, (D_6)benzene, 298 K): δ (ppm) = –36.5 (s, 2Si, 2 × *Si*(caac^{Me})).

^{1}H-^{15}N HMBC (500.17, 50.68 MHz, (D_6)benzene, 298 K): δ_N (ppm) =150.90 (s, 2N, 2 × *N*C^2).

4.4.26 SiK(C≡CMes)(caac^{Me}) (10-C_2Mes)

0.236 g of $Si_2(C{\equiv}CMes)_2(caac^{Me})_2$ (**9-C_2Mes**) (0.258 mmol, 1.0 equiv.) and 0.105 g KC_8 (0.775 mmol, 3.0 equiv.) were suspended in 10 mL of benzene. After 1 h at ambient temperature the reaction mixture turned dark red. After stirring at ambient temperature for 18 h an aliquote was taken and analyzed by ^{1}H NMR spectroscopy in (D_6)benzene, revealing the quantitative formation of SiK(C≡CMes)(caac^{Me}) (**10-C_2Mes**). The reaction mixture was filtered and the black graphite residue extracted with 3 x 2 mL of benzene. The combined dark red filtrate was evaporated and freeze dried. Drying at high vacuum for 3 h at ambient temperature afforded SiK(C≡CMes)(caac^{Me}) (**10-C_2Mes**) as a dark-red powder. Yield: 0.250 g (0.504 mmol, 98 %).[25]

Propreties: Silenide **10-C_2Mes** is highly pyrophoric and quickly decomposes upon contact with air. It is moderately soluble in *n*-hexane and *n*-pentane and well soluble in benzene and THF, affording dark red solutions.

ATR-IR (solid): $\tilde{\nu}$ (cm^{-1}) = 2922 (m), 2856 (m), 2042 (m) [[ν(C ≡ C)], 1466 (m), 1434 (m), 1377 (w), 1359 (w), 1320 (m), 1283 (m), 1247 (m), 1212 (w), 1191 (w), 1171 (s), 1142 (vs), 1034 (m), 929 (m), 901 (m), 856 (m), 814 (w), 788 (w), 742 (m), 729 (s), 700 (w), 611 (w), 582 (w), 564 (w), 539 (m), 514 (w), 492 (w), 468 (w), 434 (w), 419 (w).

^{1}H NMR (500.17 MHz, (D_6)benzene, 298 K): δ (ppm) = 1.20 (s, 6H, C^5Me_2), 1.21 (d, ^3J(H,H) = 6.6 Hz, 6H, $C^{2,6}$-CHMe_AMe$_B$, Dipp), 1.55 (d, ^3J(H,H) = 6.6 Hz, 6H, $C^{2,6}$-CHMe$_A$$Me_B$, Dipp), 2.06 (s, 2H, C^4H_2), 2.15 (s, 3H, C^4-*Me*, Mes)), 2.17 (s, 6H, C^3Me_2), 2.48 (s, 6H, $C^{2,6}$-*Me*, Mes) 3.42 (sept, ^3J(H,H) = 6.6 Hz, 4H, $C^{2,6}$-C*H*Me$_A$Me$_B$, Dipp), 6.70-6.75 (m, 1H, C^4-*H*, Dipp), 6.78 (s, 2H, $C^{3,5}$-*H*, Mes), 6.84-6.85 (m, 2H, $C^{3,5}$-*H*, Dipp).

^{13}C{^{1}H} NMR (125.77 MHz, (D_6)benzene, 298 K): δ (ppm) = 21.2 (s, 2C, $C^{2,6}$-*Me*, Mes), 22.0 (s, 1C, C^4-*Me*, Mes), 24.8 (s, 2C, $C^{2,6}$-CHMe_AMe$_B$, Dipp), 28.2 (s, 2C, $C^{2,6}$-CHMe$_A$$Me_B$, Dipp), 28.5 (s, 2C, $C^{2,6}$-*C*HMe$_A$Me$_B$, Dipp), 29.0 (s, 2C, C^5Me_2), 34.6 (s, 2C, C^3Me_2), 49.8 (s, 1C, C^3), 59.0 (s, 1C, C^4H_2), 65.3 (s, 1C, C^5), 116.7 (s, 1C, *C* ≡ C-Mes), 124.1 (s, 1C, C^1, Mes), 124.8 (s, 2C, $C^{3,5}$-H, Dipp), 125.1 (s, C, C ≡ *C*-Mes), 126.7 (s, 2C, C^4-H, Dipp), 128.3 (s, 2C, $C^{3,5}$-H, Mes overlapping with the (D_6)benzene signal), 134.7 (s, 1C, C^4, Mes), 138.2 (s, 2C, $C^{2,6}$, Mes), 142.4 (s, 1C, C^1, Dipp), 152.6 (s, 2C, $C^{2,6}$, Dipp), 217.2 (s, 1C, NC^2).

^{29}Si{^{1}H} NMR (99.36 MHz, (D_6)benzene, 298 K): δ (ppm) = –15.5 (s, 1Si, *Si*(caac^{Me})).

^{1}H-^{15}N HMBC (500.17, 50.68 MHz, (D_6)benzene, 298 K): δ_N (ppm) = 117.3 (s, 1N, *N*C^2).

---

25 Washing with *n*-pentane at ambient temperature inside the glovebox led to unselective decomposition of the compound. Even though *n*-pentane was further dried over KC_8 the same result was obtained.

4.4.27 $Si_2(C{\equiv}CTMS)_2(caac^{Me})_2$ (9-C_2TMS)

To a purple solution of $Si_2Br_2(caac^{Me})_2$ (**9-Br**) (1.00 g, 1.27 mmol, 1.0 equiv.) in 25 mL THF was added dropwise a clear solution of LiC≡CTMS (0.280 g, 2.68 mmol, 2.10 equiv.) in 25 mL THF. The reaction mixture was stirred over night at ambient temperature. After stirring for 19 hours at ambient temperature the color of the reaction mixture changed to orange-brown. An aliquote of the reaction mixture was taken and analyzed by ^{1}H NMR spectroscopy in (D_6)benzene revealing the selective formation of $Si_2(C \equiv CTMS)_2(caac^{Me})_2$ (**9-C_2TMS**). The reaction mixture was evaporated and the resulting orange-brown residue dried under fine vacuum for 0.5 h at 40 °C. The product was extracted with 25 mL of benzene and 4 x 5 mL of benzene. The combined organic phases were evaporated and dried under fine vacuum for 1.5 h at 40 °C. The orange-brown residue was redesolved in 4 mL of *n*-pentane and stored for 4 d at –60 °C. Orange crystals were removed from the orange-brown mother liquor upon filtration at –60 °C. Drying under fine vacuum for 1 h at 40 °C afforded analytically pure **9-C_2TMS** as an orange powder. Yield: 0.560 g (0.682 mmol, 54 %).

Properties: Disilicon(I) compound **9-C_2TMS** immediately decolorizes upon contact with air. It is well soluble in *n*-pentane, benzene and THF, affording orange-brown solutions.

Elemental Analysis: $C_{50}H_{80}N_2Si_4$ (821.53 g/mol): calcd./%: C 73.10, N 3.41, H 9.82; found/%: C 73.19, N 3.38, H 9.87 %. **Melting point:** 221 °C (dec).

ATR-IR (solid): $\tilde{\nu}$ (cm^{-1}) = 2997 (m), 2960 (m), 2864 (w), 2057 (m) [[ν(C ≡ C)], 1464 (w), 1439 (w), 1383 (w), 1347 (s), 1243 (m), 1197 (m), 1177 (m), 1135 (m), 1051 (w), 1026 (w), 931 (vw), 914 (vw), 851 (vs), 837 (vs), 807 (s), 788 (m), 767 (m), 757 (m), 705 (w), 694 (w), 697 (s), 626 (vw), 611 (vw), 576 (m), 483 (vw), 430 (w).

^{1}H NMR (500.17 MHz, (D_6)benzene, 298 K): δ (ppm) = 0.17 (s, 18H, 2 × (Si*Me*$_3$)$_2$), 1.04 (s, 12H, 2 × C^5*Me*$_2$), 1.30 (d, ^{3}*J*(H,H) = 6.7 Hz, 12H, 2 × C^{2,6}-CH*Me*$_A$Me$_B$, Dipp), 1.68 (d, ^{3}*J*(H,H) = 6.6 Hz, 12H, 2 × C^{2,6}-CHMe$_A$*Me*$_B$, Dipp), 1.73 (s, 4H, 2 × C^4*H*$_2$), 1.92 (s, 12H, 2 × C^3*Me*$_2$), 3.16 (sept, ^{3}*J*(H,H) = 6.6 Hz, 4H, 2 × C^{2,6}-C*H*Me$_A$Me$_B$, Dipp), 7.08 (d, ^{3}*J*(H,H) = 7.6 Hz, 4H, 2 × C^{3,5}-*H*, Dipp), 7.20 (t, ^{3}*J*(H,H) = 7.6 Hz, 2H, 2 × C^4-*H*, Dipp).

^{13}C{^{1}H} NMR (125.77 MHz, (D_6)benzene, 298 K): δ (ppm) = 0.39 (s, 6C, 2 × Si*Me*$_3$), 25.0 (s, 4C, 2 × C^{2,6}-CH*Me*$_A$Me$_B$, Dipp), 27.7 (s, 4C, 2 × C^{2,6}-CHMe$_A$*Me*$_B$, Dipp), 29.0 (s, 4C, 2 × C^{2,6}-*C*HMe$_A$Me$_B$, Dipp), 29.2 (s, 4C, 2 × C^5*Me*$_2$), 34.0 (s, 4C, 2 × C^3*Me*$_2$), 49.4 (s, 2C, 2 × *C*^{3}), 55.8 (s, 2C, 2 × *C*^{4}H$_2$), 70.2 (s, 2C, 2 × *C*^{5}), 116.2 (s, 2C, 2 × *C* ≡ C-SiMe$_3$), 119.5 (s, 2C, 2 × C ≡ *C*-SiMe$_3$), 124.8 (s, 4C, 2 × *C*^{3,5}, Dipp), 128.9 (s, 2C, 2 × *C*^{4}, Dipp), 135.7 (s, 2C, 2 × *C*^{1}, Dipp), 149.7 (s, 4C, 2 × *C*^{2,6}, Dipp), 203.4 (s, 2C, 2 × NC^2).

^{29}Si{^{1}H} NMR (99.36 MHz, (D_6)benzene, 298 K): δ (ppm) = –42.2 (s, 2Si, 2 × *Si*(caac^{Me})), -23.2 (s, 2Si, 2 × *Si*Me$_3$).

^{1}H-^{15}N HMBC (500.17, 50.68 MHz, (D_6)benzene, 298 K): δ_N (ppm) = 157.7 (s, 2N, 2 × *N*C^{2}).

4.4.28 SiK(C≡CTMS)(caac^{Me}) (10-C_2TMS)

Si_2(C≡CTMS)$_2$(caac^{Me})$_2$ (**9-C_2TMS**) (1.281 g, 1.559 mmol, 1.0 equiv.) and KC_8 (0.632 g, 4.677 mmol, 3.0 equiv.) were suspended in 10 mL of benzene. The reaction mixture was stirred for 2 h at ambient temperature upon which the supernatant solution turned dark red. An aliquote of the reaction mixture was taken and analyzed by ^{1}H NMR spectroscopy in (D_6)benzene, revealing the quantitative formation of SiK(C≡CTMS)(caac^{Me}) (**10-C_2TMS**). The reaction mixture was filtered and the black graphite residue extracted with 4 x 10 mL of benzene. The combined dark red filtrate was evaporated and dried under fine vacuum for 0.5 h at 40 °C. The red powder was washed with 5 mL of *n*-pentane. Drying at fine vacuum for 1 h at 40 °C afforded analytically pure **10-C_2TMS** as a red powder. Yield: 1.028 g (2.285 mmol, 79 %).

Properties: Potassium-silenide **10-C_2TMS** is highly pyrophoric and quickly decomposes upon contact with air. It is moderately soluble in *n*-pentane and well soluble in benzene, affording dark red solutions. Compound **10-C_2TMS** slowly decomposes in Et_2O solution. **Elemental Analysis:** $C_{25}H_{40}NKSi_2$ (449.86 g/mol): calcd./%: C 66.75, N 3.11, H 8.96; found/%: C 66.45, N 2.97, H 8.92. **Melting point:** 182 °C (dec).

ATR-IR (solid): $\tilde{\nu}$ (cm^{-1}) = 2944 (m), 2861 (m), 1982 (s) [ν(C ≡ C)], 1466 (m), 1436 (m), 1380 (m), 1361 (w), 1323 (m), 1286 (m), 1246 (m), 1191 (s), 1172 (s), 1143 (m), 1110 (w), 1048 (m), 1032 (w), 929 (w), 839 (vs), 813 (vs), 788 (m), 760 (s), 740 (s), 692 (m), 613 (w), 584 (m), 525 (w), 493 (w), 470 (w), 436 (w).

^{1}H NMR (500.17 MHz, (D_6)benzene, 298 K): δ (ppm) = 0.29 (s, 9H, (Si*Me*$_3$)$_2$), 1.17 (s, 6H, C^{5}*Me*$_2$), 1.22 (d, ^{3}*J*(H,H) = 6.7 Hz, 6H, C^{2,6}-CH*Me*$_A$Me$_B$, Dipp), 1.51 (d, ^{3}*J*(H,H) = 6.6 Hz, 6H, C^{2,6}-CHMe$_A$*Me*$_B$, Dipp), 2.05 (s, 2H, C^{4}*H*$_2$), 2.13 (s, 6H, C^{3}*Me*$_2$), 3.37 (sept, ^{3}*J*(H,H) = 6.6 Hz, 2H, C^{2,6}-C*H*Me$_A$Me$_B$, Dipp), 6.92 (d, ^{3}*J*(H,H) = 7.5 Hz, 2H, C^{3,5}-*H*, Dipp), 7.00 (t, ^{3}*J*(H,H) = 7.5 Hz, 1H, C^{4}-*H*, Dipp).

^{13}C{^{1}H} NMR (125.77 MHz, (D_6)benzene, 298 K): δ (ppm) = 1.14 (s, 3C, Si*Me*$_3$), 24.9 (s, 2C, C^{2,6}-CH*Me*$_A$Me$_B$, Dipp), 28.3 (s, 2C, C^{2,6}-CHMe$_A$*Me*$_B$, Dipp), 28.5 (s, 2C, C^{2,6}-*C*HMe$_A$Me$_B$, Dipp), 29.2 (s, 2C, C^{5}*Me*$_2$), 34.0 (s, 2C, C^{3}*Me*$_2$), 49.9 (s, C, *C*^{3}), 59.1 (s, C, *C*^{4}H$_2$), 65.2 (s, 2C, *C*^{5}), 123.3 (s, C, C ≡ *C*-SiMe$_3$), 124.7 (s, 2C, *C*^{3,5}-H, Dipp), 126.6 (s, C, *C*^{4}-H, Dipp), 142.1 (s, C, *C*^{1}, Dipp), 143.7 (s, C, *C* ≡ C-SiMe$_3$), 152.6 (s, 2C, *C*^{2,6}, Dipp), 220.0 (s, C, N*C*^{2}).

^{29}Si{^{1}H} NMR (99.36 MHz, (D_6)benzene, 298 K): δ (ppm) = –25.6 (s, 2Si, *Si*Me$_3$), –19.4 (s, Si, *Si*(caac^{Me})).

^{1}H-^{15}N HMBC (500.17, 50.68 MHz, (D_6)benzene, 298 K): δ_N (ppm) = 119.95 (s, 1N, *N*C^{2}).

4.4.29 SiBr(caac^{Me})Si(C≡C-TMS)(caac^{Me}) (11-Br)

0.400 g of $Si_2(C{\equiv}CTMS)_2(caac^{Me})_2$ (**9-C_2TMS**)(0.409 mmol, 1.0 equiv.) and 0.264 g KC_8 (1.951 mmol, 4.77 equiv.) were suspended in 20 mL of benzene. The reaction mixture was stirred for 17 h at ambient temperature and the suspension turned dark red. An aliquote of the reaction mixture was taken and analyzed by ^{1}H NMR spectroscopy in (D_6)benzene revealing the quantitative formation of SiK(C≡CTMS)(caac^{Me}) (**10-C_2TMS**). The reaction mixture was added dropwise via filter syringe to a solution of 383 mg $SiBr_{2(}caac^{Me}$) (**1**) (0.810 mmol, 2.0 equiv.) in 20 mL of benzene inside the glovebox, thereby the solution turned directly dark red. The reaction mixture was stirred for another 2 h at ambient temperature. An aliquot of the reaction mixture in (D_6)benzene revealed the selective formation of **11-Br**, alongside 16 mol% of $Si_2Br_2(caac^{Me})_2$ (**9-Br**) and 20 mol% of $Si_2(C{\equiv}CTMS)_2(caac^{Me})_2$ (**9-C_2TMS**). The dark red suspension was filtered and the residue extracted with 3 x 10 mL of benzene. The combined organic phases were evaporated and dried at high vacuum for 0.5 h at 40 °C. The black-red residue was redesolved in 4 mL of boiling pentane, cooled to ambient temperature and stored overnight at –30 °C. Dark red crystals were separated from the dark red mother liquor at –30 °C. Drying at high vacuum for 1 h at 30 °C afforded **11-Br** as a dark red powder. Yield: 0.415 g (64 %).[26]

After 3 times recrystallizing from toluene (5 mL each) at –30 °C and an additional recrystallization step from *n*-pentane (2 mL) at –30 °C the compound could be isolated in analytically pure form. Yield: 0.030 g (5 %).

Properties: Assymetric silicon(I) compound **11-Br** immediately decolorizes upon contact with air. It is moderately soluble in *n*-pentane and *n*-hexane and well soluble in benzene, toluene, THF and Et_2O, affording orange-red solutions.

Elemental Analysis: $C_{45}H_{71}BrN_2Si_3$ (804.22 g/mol): calcd./%: C 67.21, N 3.48, H 8.90; found/%: C 67.36, N 3.33 , H 9.01. **Melting point:** 185.5 °C.

ATR-IR (solid): $\tilde{\nu}$ (cm^{-1}) = 3057 (vw), 2962 (m), 2925 (m), 2865 (m), 2057 (m) [[ν(C ≡ C)], 1583 (vw), 1464 (m), 1440 (m), 1384 (m), 1339 (vs), 1272 (vw), 1244 (m), 1195 (s), 1177 (s), 1133 (s), 1083 (vw), 1050 (vw), 1027 (vw), 1008 (m), 931 (vw), 913 (vw), 853 (s), 838 (s), 807 (s), 771 (s), 758 (m), 704 (m), 678 (m), 626 (vw), 611 (m), 574 (m), 548 (w), 476 (w), 423 (m).

NMR-assignment of SiBr(caac^{Me}*)-Si(C≡CTMS)(caac^{Me}) (**11-Br**): The signals of the cyclic (alkyl)(amino)carbene (caac^{Me}) coordinated to the bromine bonded silicon center are marked with the symbol (*).

---

[26] According to ^{1}H NMR spectroscopy in (D_6)benzene the compound still contained 14 mol% of $Si_2Br_2(caac^{Me})_2$ (**9-Br**) and 8 mol% of $Si_2(C{\equiv}CTMS)_2(caac^{Me})_2$ (**9-C_2TMS**).

^{1}H NMR (500.14 MHz, (D_6)benzene, 298 K)**:** δ (ppm) = 0.18 (s, 9H, Si*Me*$_3$), 1.01 (s, 6H, C^5Me_2), 1.04 (s, 6H, C^5Me_2*), 1.22 (d, ^3J(H,H) = 6.6 Hz, 6H, $C^{2,6}$-CH*Me*$_A$Me$_B$, Dipp), 1.24 (d, ^3J(H,H) = 6.7 Hz, 6H, $C^{2,6}$-CH*Me*$_A$Me$_B$*, Dipp), 1.66 (d, ^3J(H,H) = 6.7 Hz, 6H, $C^{2,6}$-CHMe$_A$*Me*$_B$, Dipp), 1.70 (s, 2H, C^4H_2), 1.72 (s, 2H, C^4H_2*),), 1.75 (d, ^3J(H,H) = 6.7 Hz, 6H, $C^{2,6}$-CHMe$_A$*Me*$_B$*, Dipp), 1.94 (s, 6H, C^3Me_2), 1.95 (s, 6H, C^3Me_2*), 3.12 (sept, ^3J(H,H) = 6.7 Hz, 2H, $C^{2,6}$-C*H*Me$_A$Me$_B$, Dipp), 3.12 (sept, ^3J(H,H) = 6.6 Hz, 2H, $C^{2,6}$-C*H*Me$_A$Me$_B$*, Dipp), 7.06 (d, ^3J(H,H) = 7.7 Hz, 2H, $C^{3,5}$-*H*, Dipp), 7.10 (d, ^3J(H,H) = 7.7 Hz, 2H, $C^{3,5}$-*H**, Dipp) 7.18 (t, ^3J(H,H) = 7.6 Hz, 1H, C^4-*H*, Dipp), 7.20 (t, ^3J(H,H) = 7.7 Hz, 1H, C^4-*H**, Dipp).

^{13}C{^{1}H} NMR (125.78 MHz, (D_6)benzene, 298 K): δ (ppm) = 0.56 (s, 3C, Si*Me*$_3$), 25.0 (s, 2C, $C^{2,6}$-CH*Me*$_A$Me$_B$*, Dipp), 25.5 (s, 2C, $C^{2,6}$-CH*Me*$_A$Me$_B$, Dipp), 27.3 (s, 2C, $C^{2,6}$-CHMe$_A$*Me*$_B$*, Dipp), 27.8 (s, 2C, $C^{2,6}$-CHMe$_A$*Me*$_B$, Dipp), 28.9 (s, 2C, C^5-Me_2*), 29.0 (s, 2C, $C^{2,6}$-*C*HMe$_A$Me$_B$*, Dipp), 29.12 (s, 2C, $C^{2,6}$-*C*HMe$_A$Me$_B$, Dipp), 29.24 (s, 2C, C^5Me_2), 33.1 (s, 2C, C^3Me_2), 34.3 (s, 2C, C^3Me_2*), 49.8 (s, 1C, C^3), 51.5 (s, 1C, C^{3*}), 55.4 (s, 1C, C^4H_2*), 55.9 (s, 1C, C^4H_2), 70.5 (s, 1C, C^5), 72.2 (s, 1C, C^5*), 115.8 (s, 1C, Si-*C* ≡ C), 120.1 (s, 1C, C ≡ *C*-TMS), 124.8 (s, 2C, $C^{3,5}$-H, Dipp), 125.0 (s, 2C, $C^{3,5}$-H*, Dipp), 128.9 (s, 1C, C^4-H, Dipp), 129.2 (s, 1C, C^4-H*, Dipp), 134.8 (s, 1C, C^1*, Dipp), 135.6 (s, 1C, C^1, Dipp), 148.6 (s, 2C, $C^{2,6}$*, Dipp), 149.5 (s, 2C, $C^{2,6}$, Dipp), 203.3 (s, C, C^2), 208.5 (s, C, C^2*).

^{29}Si{^{1}H} NMR (99.36 MHz, (D_6)benzene, 298 K): δ (ppm) = –25.56 (s, 1Si, *Si*(C_2TMS)(caac^{Me})), –23.07 (s, 1Si, *Si*Me$_3$), 9.10 (s, 1Si, *Si*Br(caac^{Me}*).

^{1}H-^{15}N HMBC (500.14 MHz, 50.69. MHz, (D_6)benzene, 298K): δ_N (ppm) = 158.5 (1N, *N*C^2), 173.7 (1N, *N*C^2*).

4.4.30SiMe(caac^{Me})Si(C≡CTMS)(caac^{Me}) (11-Me)

To a red solution of 0.400 g of SiBr(caac^{Me})Si(C≡CTMS)(caac^{Me}) (**11-Br**)[27] (0.497 mmol, 1.0 equiv.) in 10 mL of Et_2O a MeLi solution (2 mL, 0.274 mol L^{-1}, 0.548 mmol, 1.1 equiv.) was added dropwise in 2 min at ambient temperature. After stirring for 1 h at ambient temperature the reaction mixture turned orange-brown. An aliquote of the rection mixture was taken and analyzed by ^{1}H NMR spectroscopy in (D_6)benzene revealing the selective formation of SiMe(caac^{Me})Si(C≡CTMS)(caac^{Me}) (**11-Me**). The solvent was evaporated and dried at high vacuum for 0.5 h at 40 °C. The dark brown residue was extracted with 3 x 10 mL of *n*-pentane. The combined extracts were evaporated and dried at high vacuum for 0.5 h at 40 °C. The dark brown residue was redesolved in 1 mL *n*-pentane and stored for 2 d at –60 °C.

---

[27] The used starting material contained 14 mol% of Si_2Br_2(caac^{Me})$_2$ (**9-Br**) and 8 mol% of Si_2(C≡CTMS)$_2$(caac^{Me})$_2$ (**9-C_2TMS**).

After removing of the dark brown mother liquor upon filtration at –60 °C and drying at high vacuum for 1 h at 40 °C silicon(I) compound **11-Me** was obtained as an orange microcrystalline solid. Yield: 0.020 g (5 %).[28]

Properties: Assymetric silicon(I) compound **11-Me** immediately decolorizes upon contact with air. It is very well soluble in *n*-pentane, benzene and Et_2O, affording orange solutions.

NMR-assignment of SiMe(caac^{Me}*)-Si(C≡CTMS)(caac^{Me}) (**11-Me**): The signals of the cyclic (alkyl)(amino) carbene (caac^{Me}) bonded to the methyl substituted silicon center are marked with the symbol (*).

^{1}H NMR (500.14 MHz, (D_6)benzene, 298 K)**:** δ (ppm) = 0.02 (s, 3H, Si-*Me*), 0.14 (s, 9H, Si*Me*$_3$), 1.03 (s, 6H, C^5*Me*$_2$*), 1.13 (s, 6H, C^5*Me*$_2$), 1.22 (d, ^3J(H,H) = 6.8 Hz, 6H, C^{2,6}-CH*Me*$_A$Me$_B$, Dipp), 1.24 (d, ^3J(H,H) = 6.8 Hz, 6H, C^{2,6}-CH*Me*$_A$Me$_B$*, Dipp), 1.53 (d, ^3J(H,H) = 6.7 Hz, 6H, C^{2,6}-CHMe$_A$*Me*$_B$, Dipp), 1.60 (d, ^3J(H,H) = 6.7 Hz, 6H, C^{2,6}-CHMe$_A$*Me*$_B$*, Dipp), 1.74 (s, 2H, C^4*H*$_2$*), 1.83 (s, 6H, C^3*Me*$_2$), 1.87 (s, 2H, C^4*H*$_2$), 1.99 (s, 6H, C^3*Me*$_2$*), 3.13 (sept, ^3J(H,H) = 6.8 Hz, 2H, C^{2,6}-C*H*Me$_A$Me$_B$*, Dipp), 3.35 (sept, ^3J(H,H) = 6.8 Hz, 2H, C^{2,6}-C*H*Me$_A$Me$_B$, Dipp), 7.05 (d, ^3J(H,H) = 7.7 Hz, 2H, C^{3,5}-*H**, Dipp), 7.08 (d, ^3J(H,H) = 7.7 Hz, 2H, C^{3,5}-*H*, Dipp), 7.16 (m, 1H, C^4-*H*, Dipp overlapping with the (D_6)benzene signal), 7.20 (t, ^3J(H,H) = 7.7 Hz, 1H, C^4-*H**, Dipp).

^{13}C{^{1}H} NMR (125.78 MHz, (D_6)benzene, 298 K): δ (ppm) = 0.66 (s, 3C, Si*Me*$_3$), 1.69 (s, 1C, Si-*Me*), 25.0 (s, 2C, C^{2,6}-CH*Me*$_A$Me$_B$*, Dipp), 25.3 (s, 2C, C^{2,6}-CH*Me*$_A$Me$_B$, Dipp), 26.6 (s, 2C, C^{2,6}-CHMe$_A$*Me*$_B$, Dipp), 27.3 (s, 2C, C^{2,6}-CHMe$_A$*Me*$_B$*, Dipp), 28.8 (s, 2C, C^{2,6}-*C*HMe$_A$Me$_B$, Dipp), 29.0 (s, 2C, C^{2,6}-*C*HMe$_A$Me$_B$*, Dipp), 29.06 (s, 2C, C^5*Me*$_2$), 29.25 (s, 2C, C^5*Me*$_2$*), 34.6 (s, C, C^3*Me*$_2$), 35.4 (s, C, C^3*Me*$_2$*), 48.8 (s, C, *C*^{3*}), 49.2 (s, C, *C*^{3}), 55.9 (s, C, *C*^{4}H$_2$*), 57.4 (s, C, *C*^{4}H$_2$), 67.7 (s, C, *C*^{5}), 69.6 (s, C, *C*^{5}*), 115.5 (s, C, Si-*C* ≡ C), 119.3 (s, C, C ≡ *C*-TMS), 124.7 (s, 2C, *C*^{3,5}-H*, Dipp), 125.2 (s, 2C, *C*^{3,5}-H, Dipp), 128.5 (s, 1C, *C*^{4}-H, Dipp), 128.8 (s, 1C, *C*^{4}-H*, Dipp), 135.9 (s, 1C, *C*^{1*}, Dipp), 137.6 (s, 1C, *C*^{1}, Dipp), 149.6 (s, 2C, *C*^{2,6*}, Dipp), 150.4 (s, 2C, *C*^{2,6}, Dipp), 192.6 (s, C, *C*^{2*}), 201.36 (s, C, C^2).

^{29}Si{^{1}H} NMR (99.36 MHz, (D_6)benzene, 298 K): δ (ppm) = –39.44 (s, 1Si, *Si*(C$_2$TMS)(caac^{Me})), –23.15 (s, 1Si, *Si*Me$_3$), –1.01(s, 1Si, *Si*{Me}(caac^{Me}*).

^{1}H-^{15}N HMBC (500.14 MHz, 50.69. MHz, (D_6)benzene, 298 K): δ_N (ppm) = 137.1 (1N, *N*C^2), 152.7 (1N, *N*C^{2*}).

---

[28] The compound is extremely lipophylic and crystallizes out porly from aliphatic sovents, thus explaining the low yield of the isolated compound. The compound contains tiny amounts of **9-C$_2$TMS** (< 5 mol%).

4.4.31 (caac^{Me})Si(C≡CTMS)(GeAr^{Mes}) (12)

0.800 g of $Si_2(C{\equiv}CTMS)_2(caac^{Me})_2$ (**9-C_2TMS**) (0.974 mmol, 1.0 equiv.) and 0.527 g KC_8 (3.895 mmol, 4.0 equiv.) were suspended in 40 mL of benzene. The reaction mixture was stirred for 15 h at ambient temperature and the suspension turned dark red. An aliquote of the reaction mixture was taken and analyzed by ^{1}H NMR spectroscopy in (D_6)benzene revealing the quantitative formation of SiK(C≡CTMS)(caac^{Me}) (**10-C_2TMS**). The reaction mixture was added dropwise in 45 min via filter syringe to a solution of 821 mg of $[GeCl(Ar^{Mes})]_2$ (0.974 mmol, 1.0 equiv.) in 40 mL of benzene inside the glovebox, thereby the solution turned directly blue-turquoise. The reaction mixture was stirred for another 2 h at ambient temperature. An aliquot of the reaction mixture in (D_6)benzene revealed the selective formation of **12**, alongside with tiny amounts of **9-C_2TMS**. The reaction mixture was filtered and the residue was extracted with 2 x 5 mL of benzene. The combined organic phases were evaporated and dried at high vacuum for 0.5 h at 40 °C. The residue was redesolved in 4 mL of boiling *n*-pentane, cooled to ambient temperature and stored for 2 d at –60 °C. The blue-turquoise colored mother liquor was removed by filtration at –60 °C. After drying at the fine vacuum for 1 h at 40 °C, 0.837 g of **12** was obtained as a dark purple microcrystalline solid.[29] The dark purple solid was extracted again with 5 x 10 mL of *n*-hexane, the blue-turquoise solution was evaporated and dried at high vacuum for 0.5 h at 60 °C. The resulting dark blue foam was extracted again with 4 x 5 mL of *n*-hexane and the extract evaporated to dryness. The compound was redessolved in 1.4 mL of *n*-pentane. After storing at 4 °C for two days, dark purple single crystals were separated from the blue-turquoise mother liquor and dried at the fine vacuum for 2 h at 60 °C, affording (caac^{Me})Si(C≡CTMS)(GeAr^{Mes}) (**12**) in analytical pure form. Yield: 0.344 g (0.432 mmol, 22 %).

Properties: Compound **12** immediately decolorizes upon contact with air. It is very well soluble in *n*-pentane, *n*-hexane and benzene, affording blue-truquiouse solutions.

Elemental analysis: $C_{49}H_{65}NSi_2Ge$ (796.8 g/mol): calcd./%: C 73.86, N 1.76, H 8.22; found/%: C 73.65, N 1.69, H 8.38. **Melting point:** 160 °C (dec at 165 °C).

ATR-IR (solid): $\tilde{\nu}$ (cm^{-1}) = 2960 (w), 2918 (w), 2864 (w), 2063 (w) [[ν(C ≡ C)], 1610 (vw), 1573 (vw),1439 (m), 1354 (s), 1245 (m), 1193 (m), 1176 (m), 1133 (m), 1083 (m), 1041 (vw), 1020 (vw), 934 (m), 909 (vw), 839 (vw), 807 (s), 797 (m), 778 (m), 758 (m), 736 (m), 701 (w), 629 (vw), 608 (w), 573 (w), 548 (vw), 484 (w), 466 (w), 431 (vw).

---

[29] According to the elemental analysis (found: C 73.06, N 1.63, H 8.28 %) the compound still contained 12 mol% of KCl. In addition ^{1}H NMR spectroscopy revealed the presence of tiny amounts of $Si_2(C{\equiv}CTMS)_2(caac^{Me})_2$ (**9-C_2TMS**)(< 2mol%).

NMR spectroscopic characterization of the diastereromeric mixture in **12** (71 mol% ***E***, 29 mol% ***Z***) at –30 °C in (D_8)toluene:

^{1}H NMR (500.14 MHz, (D_8)toluene, 243 K)**:** δ (ppm) = –0.01 (s, 9H, Si*Me*$_3$,***E***), 0.20 (s, 9H, Si*Me*$_3$,***Z***), 0.64 (d, ^3J(H,H) = 6.6 Hz, 6H, C^{2,6}-CH*Me*$_A$Me$_B$, Dipp, ***Z***), 0.80 (s, 6H, C^{5}Me$_2$, ***E***),), 0.90 (s, 6H, C^5*Me*$_2$, ***Z***), 1.10 (d, ^3J(H,H) = 6.7 Hz, 6H, C^{2,6}-CHMe$_A$*Me*$_B$, Dipp, ***Z***), 1.16 (d, ^3J(H,H) = 6.7 Hz, 6H, C^{2,6}-CH*Me*$_A$Me$_B$, Dipp, ***E***), 1.34 (s, 2H, C^4*H*$_2$, ***E***), 1.44 (d, ^3J(H,H) = 6.6 Hz, 6H, C^{2,6}-CHMe$_A$*Me*$_B$, Dipp, ***E***), 1.52 (s, 6H, C^3*Me*$_2$, ***E***), 1.54 (s, 2H, C^4*H*$_2$, ***Z***), 1.69 (s, 6H, C^3*Me*$_2$, ***Z***), 2.18 (s, 6H, 2 x C^2-*Me*, Mes, ***E***), 2.27 (s, 6H, 2 x C^6-*Me*, Mes, ***Z***), 2.39 (s, 6H, 2 x C^2-*Me*, Mes, ***Z***), 2.43 (s, 6H, 2 x C^4-*Me*, Mes, ***E***), 2.56 (s, 6H, 2 x C^6-*Me*, Mes, ***E***), 2.61 (sept, ^3J(H,H) = 6.7 Hz, 2H, C^{2,6}-C*H*Me$_A$Me$_B$, Dipp, ***Z***), 2.67 (s, 6H, 2 x C^4-*Me*, Mes, ***Z***), 2.73 (sept, ^3J(H,H) = 6.7 Hz, 2H, C^{2,6}-C*H*Me$_A$Me$_B$, Dipp, ***E***), 6.74 (br s, $\Delta\nu_{1/2}$ = 4 Hz, 2H, C^5-*H*, Mes, ***Z***), 6.76 (br s, $\Delta\nu_{1/2}$ = 4 Hz, 2H, 2 x C^5-*H*, Mes, ***E***), 6.86 br s, $\Delta\nu_{1/2}$ = 4 Hz, 2H, 2 x C^3-*H*, Mes, ***Z***), 6.89 (d, ^3J(H,H) = 7.8 Hz, 2H, C^{3,5}-*H*, Dipp, ***E***), 6.93 (br s, $\Delta\nu_{1/2}$ = 4 Hz, 2H, 2 x C^3-*H*, Mes, ***E***), 6.94 (m, 2H, C^{3,5}-*H*, Dipp, ***Z***) 6.99 (d, ^3J(H,H) = 7.5 Hz, 2H, C^{3,5}-*H*, C_6H_3, ***Z*** overlapping with the (D_8)toluene signal), 7.00 (t, ^3J(H,H) = 8.2 Hz, 1H, C^4-*H*, Dipp, ***Z***), 7.05 (t, ^3J(H,H) = 7.7 Hz, 1H, C^4-*H*, Dipp, ***Z*** overlapping with the (D_8)toluene signal), 7.09 (d, ^3J(H,H) = 7.5 Hz, 2H, C^{3,5}-*H*, C_6H_3, ***E***), 7.20 (t, ^3J(H,H) = 7.5 Hz, 1H, C^4-*H*, C_6H_3, ***Z***), 7.29 (t, ^3J(H,H) = 7.5 Hz, 1H, C^4-*H*, C_6H_3, ***E***).

^{13}C{^{1}H} NMR (125.78 MHz, (D_8)toluene, 243 K): δ (ppm) = –0.40 (s, 3C, Si*Me*$_3$, ***E***), –0.18 (s, 3C, Si*Me*$_3$, ***Z***), 21.26 (s, 8C, C^{2,6}-*Me*, Mes ***Z*** and C^{2,6}-*Me*, Mes, ***E***), 22.89 (s, 4C, 2 x C^4-*Me*, Mes ***Z*** and 2 x C^4-*Me*, Mes, ***E***), 24.55 (s, 2C, C^{2,6}-CH*Me*$_A$Me$_B$, Dipp, ***E***), 25.45 (s, 2C, C^{2,6}-CH*Me*$_A$Me$_B$, Dipp, ***Z***), 27.06 (s, 2C, C^{2,6}-CHMe$_A$*Me*$_B$, Dipp, ***E***), 28.35 (s, 2C, C^5*Me*$_2$, ***E***), 28.44 (s, 2C, C^5*Me*$_2$, ***Z***), 28.50 (s, 2C, C^{2,6}-CH*Me*$_A$Me$_B$, Dipp, ***Z***), 28.87 (s, 2C, C^{2,6}-*C*HMe$_A$Me$_B$, Dipp, ***Z***), 29.05 (s, 2C, C^{2,6}-*C*HMe$_A$Me$_B$, Dipp, ***E***), 30.85 (s, 2C, C^3*Me*$_2$, ***Z***), 38.20 (s, 2C, C^3*Me*$_2$, ***E***), 49.78 (s, 1C, *C*^{3}, ***Z***), 51.64 (s, 1C, *C*^{3}, ***E***), 54.0 (s, 1C, *C*^{4}H$_2$, ***E***), 54.74 (s, 1C, *C*^{4}H$_2$, ***Z***), 72.2 (s, 1C, *C*^{5}, ***Z***), 72.9 (s, 1C, *C*^{5}, ***E***), 111.3 (s, 1C, *C*≡C-SiMe$_3$, ***E***), 117.7 (s, 1C, *C*≡C-SiMe$_3$, ***Z***), 124.85 (s, 2C, *C*^{3,5}-*H*, Dipp, ***E*** overlapping with the (D_8)toluene signal),, 125.3 (s, 2C, *C*^{3,5}-*H*, Dipp, ***Z***), 126.9 (s, 1C, *C*^{4}-H, C_6H_3, ***Z***), 127.2 (s, 2C, *C*^{3,5}-H, C_6H_3, ***E***), 127.35 (s, 2C, *C*^{4}-H, C_6H_3, ***E***), 127.7 (s, 1C, C≡*C*-SiMe$_3$, ***E*** overlapping with (D_8)toluene signal), 128.2 (s, 2C, *C*^{3,5}-H, C_6H_3, ***Z***), 128.7 (s, 1C, C≡*C*-SiMe$_3$, ***Z*** overlapping with (D_8)toluene signal), 128.75 (s, 4C, *C*^{3}-H and *C*^{5}-H, Mes, ***E***), 129.1 (s, 4C, *C*^{3}-H and *C*^{5}-H, Mes, ***Z***), 129.4 (s, 1C, *C*^{4}-H, Dipp, ***E***), 129.9 (s, 1C, *C*^{4}-H, Dipp, ***Z***), 134.9 (s, 1C, *C*^{1}, Dipp, ***E***), 135.0 9 (s, 1C, *C*^{1}, Dipp, ***Z***), 135.2 (s, 2C, 2 x *C*^{6}, Mes, ***E***), 135.6 (s, 2C, 2 x *C*^{6}, Mes, ***Z***), 135.8 (s, 4C, 2 x *C*^{2}, Mes, ***Z*** and 2 x *C*^{2}, Mes, ***E***), 137.95 (s, 2C, 2 x *C*^{4}, Mes, ***E***), 138.05 (s, 2C, 2 x *C*^{4}, Mes, ***Z***), 139.3 (s, 2C, 2 x *C*^{1}, Mes, ***Z***), 139.5 (s, 2C, 2 x *C*^{1}, Mes, ***E***), 144.8 (s, 2C, *C*^{2,6}, C_6H_3, ***Z***), 145.0 (s, 4C, *C*^{2,6}, C_6H_3 ***E*** and *C*^{2,6}, Dipp, ***Z***), 147.9 (s, 2C, *C*^{2,6}, Dipp, ***E***), 160.3 (s, 1C, *C*^{1}, C_6H_3, ***E***), 162.9 (s, 1C, *C*^{1}, C_6H_3, ***Z***), 208.0 (s, 1C, N*C*^{2}, ***Z***), 210.8 (s, 1C, N*C*^{2}, ***E***).

^{29}Si{^{1}H} NMR (99.36 MHz, (D_8)toluene, 243 K): δ (ppm) = −22.2 (s, 1Si, *Si*Me$_3$, ***E***), −21.6 (s, 1Si, *Si*Me$_3$, ***Z***), 72.2 (s, 1Si, *Si*(caac^{Me}), ***Z***), 73.7 (s, 1Si, *Si*(caac^{Me}), ***E***).

^{1}H-^{15}N HMBC (500.14 MHz, 50.69. MHz, (D_8)toluene, 243 K): δ_N (ppm) = 169.5 (1N, *N*C^2, ***E***), 175.6 (1N, *N*C^2, **Z**).

NMR spectroscopic characterization of **12** at 75 °C in (D_8)toluene, which features the fast interconversion of the two isomers, via the rapid rotation of the Si–C^{carb} bond on the NMR time scale:

^{1}H NMR (500.14 MHz, (D_8)toluene, 347 K)**:** δ (ppm) = −0.01 (br s, $\Delta\nu_{1/2}$ = 8.7 Hz, 9H, Si*Me*$_3$), 0.96 (s, 6H, C^{5}Me$_2$), 1.12 (d, ^3J(H,H) = 6.9 Hz, 6H, C^{2,6}-CH*Me$_A$*Me$_B$, Dipp), 1.24 (br m, 6H, C^{2,6}-CHMe$_A$*Me$_B$*, Dipp), 1.61 (br s, $\Delta\nu_{1/2}$ = 5.5 Hz, 6H, C^3*Me$_2$*), 1.64 (br s, $\Delta\nu_{1/2}$ = 8.4 Hz, 2H, C^4*H$_2$*), 2.17 (s, 6H, 2 x C^4-*Me*, Mes), 2.33 (br s, $\Delta\nu_{1/2}$ = 12.0 Hz, 6H, 2 x C^6-*Me*, Mes), 2.40 (br s, $\Delta\nu_{1/2}$ = 16.5 Hz, 6H, 2 x C^6-*Me*, Mes), 2.77 (br m, $\Delta\nu_{1/2}$ = 12.9 Hz, 2H, C^{2,6}-C*H*Me$_A$Me$_B$, Dipp), 6.70 (br s, $\Delta\nu_{1/2}$ = 6.0 Hz, 2H, 2 x C^3-*H*, Mes), 6.82 (br s, $\Delta\nu_{1/2}$ = 7.5 Hz, 2H, 2 x C^5-*H*, Mes), 6.94 (d, ^3J(H,H) = 8.3 Hz, 2H, C^{3,5}-*H*, C$_6$H$_3$), 6.96 (m, 2H, C^{3,5}-*H*, Dipp overlapping with (D_8)toluene signal), 7.06 (m, 1H, C^4-*H*, Dipp, overlapping with (D_8)toluene signal), 7.20 (t, ^3J(H,H) = 8.3 Hz, 1H, C^4-*H*, C$_6$H$_3$).[30]

^{13}C{^{1}H} NMR (125.78 MHz, (D_8)toluene, 347 K): δ (ppm) = −0.06 (s, 3C, Si*Me$_3$*), 21.2 (s, 3C, 2 x C^4-*Me* and 2 x C^2-*Me*, Mes), 22.9 (s, 2C, 2 x C^6-*Me*, Mes), 25.2 (s, 2C, C^{2,6}-CH*Me$_A$*Me$_B$, Dipp), 27.9 (br s, $\Delta\nu_{1/2}$ = 35.5 Hz, 2C, C^{2,6}-CHMe$_A$*Me$_B$*, Dipp), 29.0 (s, 2C, C^5*Me$_2$*), 29.25 (s, 2C, C^{2,6}-*C*HMe$_A$Me$_B$, Dipp), 38.0 (br s, weak, C^3*Me$_2$*), 51.5 (br s, $\Delta\nu_{1/2}$ = 44.2 Hz, C, *C*^{3}), 56.1 (s, 1C, *C*^{4}H$_2$), 72.8 (s, 1C, *C*^{5}), 125.5 (s, 4C, *C*^{3,5}-H, Dipp), 127.3 (s, 1C, *C*^{4}-H, C$_6$H$_3$), 127.9 (s, 2C, *C*^{3,5}-H, C$_6$H$_3$), 128.6 (s, 2C, 2 x *C*^{5}-H, Mes), 128.9 (s, 2C, 2 x *C*^{3}-H, Mes), 129.8 (s, 1C, *C*^{4}-H, Dipp), 135.9 (s, 2C, 2 x *C*^{4}, Mes), 136.0 (s, 4C, 2 x *C*^{2}, Mes and 2 x *C*^{6}, Mes), 138.3 (s, 1C, *C*^{1}, Dipp), 139.7 (s, 2C, 2 x *C*^{1}, Mes), 145.3 (s, 2C, *C*^{2,6}, C$_6$H$_3$), 147.8 (br s, $\Delta\nu_{1/2}$ = 78.1 Hz, 2C, *C*^{2,6}, Dipp), 161.9 (br s, $\Delta\nu_{1/2}$ = 32 Hz, 1C, *C*^{1}, C$_6$H$_3$), 210.6 (br s, $\Delta\nu_{1/2}$ = 23 Hz, 1C, *C*^{2}).[31]

^{29}Si{^{1}H} NMR (99.36 MHz, (D_8)toluene, 347 K): δ (ppm) = −22.0 (s, 1Si, *Si*Me$_3$), 72.3 (s, 1Si, *Si*(caac^{Me}))

^{1}H-^{15}N HMBC (500.14 MHz, 50.69. MHz, (D_8)toluene, 347 K): δ (ppm) = 170.1 (1N, *N*C^2).

---

30 At 75 °C the C^{2,6}-CHMe$_A$Me$_B$ group features two signals for the methylgroups Me$_A$ (a well resolved doublet) and Me$_B$ (a rather broad signal with weak signal intensiy). The Mes substituent starts to rotate, which can be seen by the C^2-*Me* and C^6-*Me* resonances which are broad and start to merge with each other.

31 The ^{13}C{^{1}H} resonance of the alkinyl group, C≡*C*-SiMe$_3$ and C≡*C*-SiMe$_3$, could not be found, neither in the 1D nor the 2D NMR spectra. This might be due to the low signal intensity of those groups, the low scan number (1k) of the recorded ^{13}C{^{1}H} NMR spectrum and the dynamics of the molecule. The chemical shift of those signals should not differ significantly from the assigned resonances in the ^{13}C{^{1}H} NMR spectrum at –30 °C.

4.4.32 SiBr(SiBr$_2$Tbb)(caac^{Me}) (13)

A solution of 4-dmap (1.023 g, 8.38 mmol, 2.01 equiv.) in 20 mL of benzene was added dropwise to a suspension of lemon-yellow (*E*)-[Tbb(Br)Si=Si(Br)Tbb] (4.650 g, 4.167 mmol, 1.00 equiv.) in 100 mL of benzene at ambient temperature. The disilene rapidly dissolved to give an orange-yellow solution, which was stirred for 0.5 h and then treated with a dark red suspension of SiBr$_2$(caac^{Me}) (**1**)(3.960 g, 8.38 mmol, 2.01 equiv.) in 100 mL of benzene. During the addition of SiBr$_2$(caac^{Me}) (**1**) the color of the reaction solution turned dark blue.[32] Stirring was continued for 19 h. During this time the color of the solution changed from dark blue over green (ca. after 4 h) to yellow-brown (after 19 h). An aliquot of the reaction solution was analyzed by ^{1}H NMR spectroscopy in (D$_6$)benzene revealing a complete conversion to give SiBr(SiBr$_2$Tbb)(caac^{Me}) (**13**) and few byproducts in low concentration.[33] Small amounts of a black residue (50 mg) were filtered off, all volatiles of the filtrate were removed under vacuum and the crude product dried at 60 °C under vacuum for 0.5 h. The product was shortly stirred in 40 mL of *n*-pentane and after solvent evaporation dried again at 60 °C for 1 h under vacuum. The major portion of 4-dmap was removed by sublimation at 90°C under static vacuum and afterwards the yellow solid was washed with 40 mL of *n*-pentane at ambient temperature to afford **13** in analytically pure form. Yield: 7.840 g (7.60 mmol, 91 %).

Properties: Compound **13** slowly decolorizes to a white solid upon exposure to air. It is moderately soluble in *n*-pentane and *n*-hexane and well soluble in benzene, toluene and THF, affording yellow solutions. Compound **13** decomposes unselectively upon melting at 199 °C to a dark red colored melt.

Elemental analysis: C$_{44}$H$_{80}$Br$_3$NSi$_6$ (1031.34 g/mol): calcd./%: C 51.24, H 7.82, N 1.36; found/%: C 51.42, H 8.03, N 1.33. **Melting point:** 199 °C (dec).

^{1}H NMR (500.14 MHz, (D$_6$)benzene, 298 K)**:** δ (ppm) = 0.34 (s, 36H, C^{2,6}-CH(Si*Me*$_3$)$_2$, Tbb), 0.93 (br s, $\Delta\nu_{1/2}$ = 15 Hz, 6H, C^5*Me*$_2$), 1.12 (d, ^3J(H,H) = 6.6 Hz, 6H, C^{2,6}-CH*Me*$_A$Me$_B$, Dipp), 1.29 (s, 9H, C*Me*$_3$, Tbb), 1.52 (s, $\Delta\nu_{1/2}$ = 6 Hz, 2H, C^4*H*$_2$), 1.64 (d, ^3J(H,H) = 6.6 Hz, 6H, C^{2,6}-CHMe$_A$*Me*$_B$, Dipp), 1.87 (s, 6H, C^3*Me*$_2$), 2.82 (br s, $\Delta\nu_{1/2}$ = 26 Hz, 2H, C^{2,6}-*CH*Me$_A$Me$_B$, Dipp), 3.55 (s, 2H, C^{2,6}-C*H*(SiMe$_3$)$_2$, Tbb), 6.86 (s, 2H, C^{3,5}-*H*, Tbb), 6.99 (d, ^3J(H,H) = 8.1 Hz, 2H, C^{3,5}-*H*, Dipp), 7.09 (t, ^3J(H,H) = 8.1 Hz, 1H, C^4-*H*, Dipp).

---

32 ^{1}H NMR spectroscopy of the reaction mixture in (D$_6$)benzene after 1.5 h at ambient temperature reveals the presence of small amounts of the dark blue biradical SiBr$_2$(caac^{Me})$_2$ (11 mol%) and tiny amounts of caac^{Me} carbene (< 5 mol%) next to 14 mol% of **1** and 70 mol % **13**.

33 ^{1}H NMR spectroscopy of the reaction mixture in (D$_6$)benzene after 19 h at ambient temperature reveals the complete consumption of the by-products mentioned above and the selective formation of **13**, suggesting that the by-products were formed in the course of an equilibrium reaction.

$^{13}C\{^1H\}$ NMR (125.78 MHz, (D_6)benzene, 298 K): δ (ppm) = 2.12 (s, 12C, $C^{2,6}$-CH(Si*Me*$_3$)$_2$, Tbb), 25.7 (s, 2C, $C^{2,6}$-CH*Me*$_A$Me$_B$, Dipp), 27.2 (s, 2C, $C^{2,6}$-CHMe$_A$*Me*$_B$, Dipp), 28.8 (s, 2C, $C^{2,6}$-*C*H(SiMe$_3$)$_2$, Tbb), 29.2 (s, 2C, $C^{2,6}$-*C*HMe$_A$Me$_B$, Dipp), 29.3 (s, 2C, C^5*Me*$_2$), 31.0 (s, 3C, C*Me*$_3$, Tbb), 34.3 (s, 2C (*C*^{3}*Me*$_2$) and 1C (*C*Me$_3$, Tbb)), 53.2 (s, 1C, *C*^{3}), 54.6 (s, 1C, *C*^{4}H$_2$), 76.9 (s, 1C, *C*^{5}), 123.5 (s, 2C, *C*^{3,5}-H, Tbb), 124.9 (s, 1C, *C*^{1}, Tbb), 125.3 (s, 2C, *C*^{3,5}-H, Dipp), 129.9 (s, 1C, *C*^{4}-H, Dipp), 133.6 (s, 1C, *C*^{1}, Dipp), 147.1 (s, 2C, *C*^{2,6}, Dipp), 151.7 (s, 1C, *C*^{4}, Tbb), 152.7 (s, 2C, *C*^{2,6}, Tbb), 217.4 (s, 1C, N*C*^{2}).

$^{29}Si\{^1H\}$ NMR (99.36 MHz, (D_6)benzene, 298 K): δ (ppm) = –10.6 (s, 1Si, *Si*Br$_2$Tbb), 3.3 (s, 4Si, $C^{2,6}$-CH(*Si*Me$_3$)$_2$, Tbb), 8.5 (s, 1Si, (caac^{Me})*Si*).

^1H-^{15}N HMBC (500.14 MHz, 50.69. MHz, (D_8)toluene, 243 K): δ_N (ppm) = 195.2 (1N, *N*C^2).[34]

4.4.33 (caac^{Me})Si=Si(Br)Tbb (14)

1.865 g of SiBr(SiBr$_2$Tbb)(caac^{Me}) (**13**) (1.81 mmol, 1.0 equiv.) and 0.562 g of KC_8 (4.159 mmol, 2.3 equiv.) were mixed in a Schlenk tube. The Schlenk tube was cooled to –60 °C and 100 mL of DME was added. The suspension immediately turned dark purple and was stirred for 0.5 h at –60 °C. The cooling bath was exchanged against a –30 °C cooling bath and the reaction mixture stirred for 2 h at this temperature. During 1 h the reaction mixture was allowed to warm up to –10 °C upon which the color changed to dark blue. The cooling bath was then exchanged against an ice bath and the reaction mixture stirred for 1 h at this temperature. After stirring for 1 h at ambient temperature an aliquot of the reaction solution was taken and analyzed by ^{1}H NMR spectroscopy in (D_6)benzene showing a quantitative formation of (caac^{Me})Si=Si(Br)(Tbb) (**14**). The reaction solution was separated by filtration from the black insoluble part and the product extracted with *n*-pentane (2 × 20 mL). The combined dark green filtrates were evaporated to dryness and the obtained solid dried for 0.5 h at 60 °C under vacuum. The crude product was extracted with *n*-pentane (2 × 30 mL) and all volatiles were removed upon drying at the fine vacuum for 1 h at 60°C. The dark green residue was redissolved in 5 mL of *n*-pentane. Dark green crystals of (caac^{Me})Si=Si(Br)(Tbb) (**14**) were obtained after storing the solution for 1 d at –60 °C. The crystals were separated from the dark green colored mother liquor using a filter cannula and dried under fine-vacuum for 1 h at 60 °C. Yield: 1.187 g (1.36 mmol, 75 %).

Properties: Disilavinylidene **14** is a pyrophoric solid, which quickly decomposes upon contact with air. It is well soluble in toluene, benzene and *n*-pentane, affording dark green solutions.

---

[34] Due to the dynamics of **13** (see *section 5.6.6*) no cross peak could be observed in the ^{1}H- ^{15}N HMBC spectrum at ambient temperature. At 243 K the ^{15}N NMR resonance could be resolved.

Elemental analysis: $C_{44}H_{80}BrNSi_6$ (871.53 g/mol): calcd./%: C 60.64, H 9.25, N 1.61; found/%: C 60.83, H 9.27, N 1.49. **Melting point:** 195 °C; (dec at 210 – 215°C).

^{1}H NMR (500.14 MHz, (D_6)benzene, 298 K): δ (ppm) = 0.29 (s, 36H, $C^{2,6}$-CH(Si*Me*$_3$)$_2$, Tbb), 0.94 (s, 6H, C^5*Me*$_2$), 1.14 (d, ^3J(H,H) = 6.6 Hz, 6H, $C^{2,6}$-CH*Me*$_A$Me$_B$, Dipp), 1.33 (s, 9H, C*Me*$_3$, Tbb), 1.64 (s, 2H, C^4*H*$_2$), 1.65 (d, ^3J(H,H) = 6.6 Hz, 6H, $C^{2,6}$-CHMe$_A$*Me*$_B$, Dipp), 1.75 (s, 6H, C^3*Me*$_2$), 2.80 (sept, ^3J(H,H) = 6.6 Hz, 2H, $C^{2,6}$-*CH*Me$_A$Me$_B$, Dipp), 3.33 (s, ^2J(Si,H) = 10 Hz, 2H, $C^{2,6}$-C*H*(SiMe$_3$)$_2$, Tbb), 6.97 (s, 2H, $C^{3,5}$-*H*, Tbb), 7.06 (d, ^3J(H,H)= 7.8 Hz, 2H, $C^{3,5}$-*H*, Dipp), 7.16* (m, 1H, C^4-*H*, Dipp) (this signal overlaps with the residual proton signal of the deuterated solvent).

^{13}C{^{1}H} NMR (125.78 MHz, (D_6)benzene, 298 K): δ (ppm) = 1.36 (s, 12C, $C^{2,6}$-CH(Si*Me*$_3$)$_2$, Tbb), 24.5 (s, 2C, $C^{2,6}$-CH*Me*$_A$Me$_B$, Dipp), 28.3 (s, 2C, $C^{2,6}$-CHMe$_A$*Me*$_B$, Dipp), 28.9 (s, 2C, C^5*Me*$_2$), 29.2 (s, 2C, $C^{2,6}$-*C*HMe$_A$Me$_B$, Dipp), 31.3 (s, 3C, C^4-C*Me*$_3$, Tbb), 33.1 (s, 2C, C^3*Me*$_2$), 34.2 (s, 2C, $C^{2,6}$-*C*H(SiMe$_3$)$_2$, Tbb), 34.5 (s, 1C, *C*Me$_3$, Tbb), 52.4 (s, 1C, C^4H$_2$), 52.8 (s, 1C, C^3), 74.6 (s, 1C, C^5), 120.5 (s, 2C, $C^{3,5}$-H, Tbb), 125.9 (s, 2C, $C^{3,5}$-H, Dipp), 129.9 (s, 1C, C^4-H, Dipp), 134.0 (s, 1C, C^1, Dipp), 138.9 (s, 1C, C^1, Tbb), 146.7 (s, 2C, $C^{2,6}$, Dipp), 150.3 (s, 2C, $C^{2,6}$, Tbb), 151.8 (s, 1C, C^4, Tbb), 241.4 (s, 1C, N*C*^{2}).

^{29}Si{^{1}H} NMR (99.36 MHz, (D_6)benzene, 298 K): δ (ppm) = 2.4 (s, 4Si, $C^{2,6}$-CH(*Si*Me$_3$)$_2$, Tbb), 73.1 (s, 1Si, (caac^{Me})*Si*), 96.2 (s, 1Si, *Si*(Br)Tbb).

^{1}H-^{15}N HMBC (500.14 MHz, 50.69. MHz, (D_6)benzene, 298K): δ_N (ppm) = 197.4 (1N, *N*C^2).

4.4.34 GeBr(SiBr$_2$Tbb)(caac^{Me}) (13-Ge)

1.231 g of lemon-yellow (*E*)-[Tbb(Br)Si=Si(Br)Tbb] (1.103 mmol, 1.00 equiv.) and 1.00 g of GeBr$_2$(caac^{Me}) (1.93 mmol, 1.75 equiv.) were suspendet 150 mL in toluene at ambient temperature. The yellow suspension was slowly heated to 105 °C. Upon heating a clear orange solution was formed (at 60 °C) which upon reaching 105 °C slowly changed to dark red. Stirring of the reaction mixture at this temperature was continued for 2 h. An aliquot of the reaction solution was analyzed by ^{1}H NMR spectroscopy in (D_6)benzene revealing a selective formation of GeBr(SiBr$_2$Tbb)(caac^{Me}) (**13-Ge**) alongside of 5 mol% of GeBr$_2$(caac^{Me}).[35] The dark red solution was filtered, all volatiles of the filtrate were removed under vacuum and the crude product dried at 60 °C under vacuum for 0.5 h. The product was shortly stirred in 40 mL of *n*-hexane and after solvent evaporation dried again at 60 °C for 1 h under vacuum. The red solid was extracted with 5 x 10 mL of a mixture of *n*-pentane/toluene 1:5. The red extract was evaporated to dryness and

[35] Further heating and/or addition of more equivalents of (*E*)-[Tbb(Br)Si=Si(Br)Tbb] did not lower the concentration of remaining GeBr$_2$(caac^{Me}). The use of an excess of (*E*)-[Tbb(Br)Si=Si(Br)Tbb] is still advised since it reassures conversion rate of 95%. Excess of (*E*)-[Tbb(Br)Si=Si(Br)Tbb] can be easily removed upon washing with aliphatic solvents.

washed 4 x 10 mL with *n*-pentane and dried under fine vacuum at 60 °C for 2 h to yield GeBr(SiBr$_2$Tbb)(caac^{Me})·(***n*-pentane**)$_{0,5}$·(**toluene**)$_{0,06}$ [36] as a red powder. Yield: 1.664 g (1.547 mmol, 77 %).

Properties: Compound **13-Ge** slowly decolorizes to a white solid upon exposure to air. It is moderately soluble in *n*-pentane and *n*-hexane and well soluble in benzene, toluene and THF, affording red solutions.

Elemental analysis: $C_{44}H_{80}Br_3GeNSi_5(C_5H_{12})_{0,5}(C_7H_8)_{0,06}$ (1117.47 g/mol): calcd./%: C 50.43, H 7.80, N 1.25; found/%: C 50.42, H 8.09, N 1.10. **Melting point:** 194 °C (dec). ^{1}H NMR spectroscopy of the molten mass in (D_6)benzene reveals the rather selective formation of GeBr$_2$(caac^{Me}) and TbbSiBr$_3$.

^{1}H NMR (500.14 MHz, (D_6)benzene, 298 K)**:** δ (ppm) = 0.27 (s, 18H, C^{2,6}-CH(Si*Me*$_3$)$_A$(SiMe$_3$)$_B$, Tbb), 0.41 (s, 18H, C^{2,6}-CH(SiMe$_3$)$_A$(Si*Me*$_3$)$_B$, Tbb) 0.75 (s, 3H, C^5*Me$_A$*Me$_B$), 0.80 (s, 3H, C^{5}Me$_A$*Me$_B$*), 0.86 (t, ^3J(H,H) = 7.2 Hz, 6H, 2 x *Me*, *n*-pentane), 1.04 (d, ^3J(H,H) = 6.9 Hz, 3H, C^{2,6}-CH$_B$*Me$_C$*Me$_D$, Dipp), 1.06 (d, ^3J(H,H) = 6.9 Hz, 3H, C^{2,6}-CH$_A$*Me$_A$*Me$_B$, Dipp), 1.25 (m, 6H, 3 x C*H$_2$*, *n*-pentane), 1.30 (d, ^3J(H,H) = 6.9 Hz, 3H, C^{2,6}-CH$_A$Me$_A$*Me$_B$*, Dipp), 1.31 (s, 9H, C*Me$_3$*, Tbb), 1.40 (d, ^2J(H,H)= 12.9 Hz, 1H, C^4*H$_A$*H$_B$), 1.43 (d, ^2J(H,H)= 12.9 Hz, 1H, C^{4}H$_A$*H$_B$*),1.61 (d, ^3J(H,H) = 6.6 Hz, 3H, C^{2,6}-CH$_A$Me$_A$*Me$_B$*, Dipp), 1.85 (s, 3H, C^3*Me$_A$*Me$_B$), 2.03 (s, 3H, C^{3}Me$_A$*Me$_B$*), 2.67 (sept, ^3J(H,H) = 6.5 Hz, 1H, C^{2,6}-C*H$_A$*Me$_A$Me$_B$, Dipp), 2.85 (sept, ^3J(H,H) = 6.6 Hz, 1H, C^{2,6}-C*H$_B$*Me$_C$Me$_D$, Dipp), 3.00 (s, 2H, C^{2,6}-C*H*(SiMe$_3$)$_A$(SiMe$_3$)$_B$, Tbb), 6.93 (dd, ^3J(H,H) = 7.8 Hz, ^5J(H,H) =1.6 Hz,1H, C^3-*H*, Dipp), 6.94 (s, 2H, C^{3,5}-*H*, Tbb), 7.01 (dd, ^3J(H,H) = 7.8 Hz, ^5J(H,H) =1.6 Hz, 1H, C^5-*H*, Dipp), 7.07 (m, 1H, C^4-*H*, Dipp).

^{13}C{^{1}H} NMR (125.78 MHz, (D_6)benzene, 298 K): δ (ppm) = 2.07 (s, 6C, C^{2,6}-CH(SiMe$_3$)$_A$(Si*Me*$_3$)$_B$, Tbb), 2.09 (s, 6C, C^{2,6}-CH(Si*Me*$_3$)$_A$(SiMe$_3$)$_B$, Tbb), 14.24 (s, 2C, 2 x *Me*, *n*-pentane), 22.68 (s, 2C, 2 x *C*H$_2$, *n*-pentane), 24.31 (s, 1C, C^{2,6}-CH$_B$*Me$_C$*Me$_D$, Dipp), 24.67 (s, 1C, C^{2,6}-CH$_A$*Me$_A$*Me$_B$, Dipp), 27.32 (s, 1C, C^5*Me$_A$*Me$_B$), 27.43 (s, 1C, C^{2,6}-CH$_A$Me$_A$*Me$_B$*, Dipp), 28.74 (s, 1C, C^{2,6}-*C*H$_A$Me$_A$Me$_B$, Dipp), 29.26 (s, 1C, C^{2,6}-*C*H$_B$Me$_C$Me$_D$, Dipp), 29.29 (s, 1C, C^{2,6}-CH$_B$Me$_C$*Me$_D$*, Dipp), 29.79 (s, 1C, C^{5}Me$_A$*Me$_B$*), 30.19 (s, 1C, C^3 Me$_A$*Me$_B$*), 30.51 (s, 2C, C^{2,6}-*C*H(SiMe$_3$)$_A$(SiMe$_3$)$_B$, Tbb, 31.14 (s, 3C, C*Me$_3$*, Tbb), 32.44 (s, 1C, C^3*Me$_A$*Me$_B$), 34.36 (s, 1C, *C*Me$_3$, Tbb), 34.40 (s, 1C, CH$_2$, *n*-pentane), 51.98 (s, 1C, *C*^{4}H$_A$H$_B$), 58.68 (s, 1C, *C*^{3}), 81.13 (s, 1C, *C*^{5}), 123.0 (s, 2C, *C*^{3,5}-H, Tbb), 125.58 (s, 2C, *C*^{3}-H, Dipp), 125.64 (s, 2C,*C*^{5}-H, Dipp), 130.18 (s, 1C, *C*^{4}-H, Dipp), 130.46 (s, 1C, *C*^{1}, Tbb), 133.24 (s, 1C, *C*^{1}, Dipp), 145.24 (s, 1C, *C*^{6}, Dipp), 145.77 (s, 1C, *C*^{2}, Dipp), 151.56 (s, 1C, *C*^{4}, Tbb), 152.1 (s, 2C, *C*^{2,6}, Tbb), 244.72 (s, 1C, N*C*^{2}).

---

[36] Next to 0.5 equiv. of *n*-pentane 0.06 equiv. of toluene were present in the sample. Further drying of the compound for 4 h at 60°C and 4 h at 100°C did not lead to significant change of the molar ratio of the solvent molecules.

^{29}Si{^{1}H} NMR (99.36 MHz, (D_6)benzene, 298 K): δ (ppm) = 2.7 (s, 2Si, $C^{2,6}$-CH(*Si*Me$_3$)$_A$(SiMe$_3$)$_B$, Tbb), 3.37 (s, 2Si, $C^{2,6}$-CH(SiMe$_3$)$_A$(*Si*Me$_3$)$_B$, Tbb), 10.29 (s, 1Si, *Si*Br$_2$Tbb),

^{1}H-^{15}N HMBC (500.14 MHz, 50.69. MHz, (D_6)benzene, 298 K): δ_N (ppm) = 236.9 (1N, *N*C^2).

4.4.35 (caac^{Me})Ge=Si(Br)Tbb (14-Ge)

800 mg of GeBr(SiBr$_2$Tbb)(caac^{Me}) (**13-Ge**) (0.706 mmol, 1.0 equiv.) and 219 mg of KC_8 (1.623 mmol, 2.3 equiv.) were mixed in a Schlenk tube. The Schlenk tube was cooled to –60 °C and 40 mL of DME was added. The suspension immediately turned dark purple and was stirred for 1 h at –60 °C. The cooling bath was exchanged against a –30 °C cooling bath and the reaction mixture stirred for 2 h at this temperature. During 1 h the reaction mixture was allowed to warm up to –10 °C upon which the color changed to dark blue. The cooling bath was then exchanged against an ice bath and the reaction mixture stirred for 1 h at this temperature. After stirring for 1 h at ambient temperature an aliquot of the reaction solution was taken and analyzed by ^{1}H NMR spectroscopy in (D_6)benzene showing a quantitative formation of (caac^{Me})Ge=Si(Br)(Tbb) (**14-Ge**). The reaction solution was separated by filtration from the black insoluble part and the product extracted with *n*-hexane (2 × 20 mL). The combined dark blue filtrates were evaporated to dryness and the obtained solid dried for 0.5 h at 60 °C under vacuum. The crude product was extracted with *n*-pentane (3 × 20 mL) and all volatiles were removed upon drying at the fine vacuum for 1 h at 60 °C. The dark blue residue was redissolved in 1.5 mL of *n*-pentane. Dark blue crystals of (caac^{Me})Ge=Si(Br)(Tbb) (**14-Ge**) were obtained after storing the solution for 1 d at –30 °C. The crystals were separated from the dark blue colored mother liquor using a filter cannula and dried under fine-vacuum for 1 h at 60 °C. Yield: 474 mg (0.517 mmol, 73 %).

Properties: Silagermenylidene **14-Ge** is a pyrophoric solid, which quickly decomposes upon contact with air. It is well soluble in *n*-pentane, benzene/toluene and THF, affording dark blue solutions.

Elemental analysis: $C_{44}H_{80}BrNSi_5Ge$ (916.05 g/mol): calcd./%: C 57.69, H 8.80, N 1.53; found/%: C 58.03, H 8.99, N 1.40 %. **Melting point:** 182 °C (dec).

^{1}H NMR (500.14 MHz, (D_6)benzene, 298 K): δ (ppm) = 0.30 (s, 36H, $C^{2,6}$-CH(Si*Me$_3$*)$_2$, Tbb), 0.93 (s, 6H, C^5*Me$_2$*), 1.13 (d, ^3J(H,H) = 6.6 Hz, 6H, $C^{2,6}$-CH*Me$_A$*Me$_B$, Dipp), 1.33 (s, 9H, C*Me$_3$*, Tbb), 1.59 (s, 2H, C^4*H$_2$*), 1.64 (d, ^3J(H,H) = 6.6 Hz, 6H, $C^{2,6}$-CHMe$_A$*Me$_B$*, Dipp), 1.73 (s, 6H, C^3*Me$_2$*), 2.76 (sept, ^3J(H,H) = 6.5 Hz, 2H, $C^{2,6}$-C*H*Me$_A$Me$_B$, Dipp), 3.40 (s, ^2J(Si,H) = 9.6 Hz, 2H, $C^{2,6}$-C*H*(SiMe$_3$)$_2$, Tbb), 6.96 (s, 2H, $C^{3,5}$-*H*, Tbb), 7.04 (d, ^3J(H,H)= 7.7 Hz, 2H, $C^{3,5}$-*H*, Dipp), 7.15* (m, 1H, C^4-*H*, Dipp) (this signal overlaps with the residual proton signal of the deuterated solvent).

$^{13}C\{^1H\}$ NMR (125.78 MHz, (D_6)benzene, 298 K): δ (ppm) = 1.39 (s, 12C, $C^{2,6}$-CH(Si*Me*$_3$)$_2$, Tbb), 24.5 (s, 2C, $C^{2,6}$-CH*Me*$_A$Me$_B$, Dipp), 28.2 (s, 2C, $C^{2,6}$-CHMe$_A$*Me*$_B$, Dipp), 28.8 (s, 2C, C^5*Me*$_2$), 29.2 (s, 2C, $C^{2,6}$-*C*HMe$_A$Me$_B$, Dipp), 31.4 (s, 3C, C^4-*CMe*$_3$, Tbb), 32.6 (s, 2C, C^3*Me*$_2$), 33.7 (s, 2C, $C^{2,6}$-*C*H(SiMe$_3$)$_2$, Tbb), 34.5 (s, 1C, *C*Me$_3$, Tbb), 51.7 (s, 1C, *C*^{4}H$_2$), 54.2 (s, 1C, *C*^{3}), 76.6 (s, 1C, *C*^{5}), 120.6 (s, 2C, *C*^{3,5}-H, Tbb), 125.8 (s, 2C, *C*^{3,5}-H, Dipp), 129.9 (s, 1C, *C*^{4}-H, Dipp), 134.0 (s, 1C, *C*^{1}, Dipp), 139.9 (s, 1C, *C*^{1}, Tbb), 146.3 (s, 2C, *C*^{2,6}, Dipp), 150.1 (s, 2C, *C*^{2,6}, Tbb), 151.7 (s, 1C, *C*^{4}, Tbb), 255.4 (s, 1C, N*C*^{2}).

$^{29}Si\{^1H\}$ NMR (99.36 MHz, (D_6)benzene, 298 K): δ (ppm) = 2.3 (s, 4Si, $C^{2,6}$-CH(*Si*Me$_3$)$_2$, Tbb), 120.4 (s, 1Si, *Si*(Br)Tbb).

^1H-^{15}N HMBC (500.14 MHz, 50.69. MHz, (D_6)benzene, 298K): δ_N (ppm) = 205.5 (1N, *N*C^2).

4.4.36(caac^{Me})Si=Si(C≡CTMS)Tbb (14-C$_2$TMS)

To a green solution of 0.800 g of (caac^{Me})Si=Si(Br)Tbb (**14**) (0.918 mmol, 1.0 equiv.) in 20 mL THF a slightly yellow solution of 0.105 g LiC≡CTMS (1.010 mmol, 1.1 equiv.) in 20 mL THF was added at ambient temperature. Upon addition the dark green solution changed to a turquoise-green solution. After stirring for 1 h at ambient temperature an aliquot of the reaction solution was taken and analyzed by ^{1}H NMR spectroscopy in (D_6)benzene showing the selective formation of (caac^{Me})Si=Si(C≡CTMS)Tbb (**14-C$_2$TMS**). The reaction mixture was evaporated to dryness and the obtained solid dried for 0.5 h at 60 °C under vacuum. The crude product was extracted with *n*-hexane (4 × 10 mL) and all volatiles were removed upon drying at the fine vacuum for 1 h at 60 °C. In order ensure the complete revomal of LiBr, the compound was extracted again with *n*-pentane (4 × 2 mL) and the green turquoise filtrate removed under vacuum. After drying at fince vacuum for 2 h at 60 °C (caac^{Me})Si=Si(C≡CTMS)Tbb (**14-C$_2$TMS**) was obtained in NMR-spectroscopic pure form. Yield: 816 mg (0.918 mmol, 100 %).[37]

Properties: Compound **14-C$_2$TMS** is a pyrophoric solid, which quickly decomposes upon contact with air. It is extremely well soluble in benzene, *n*-pentane and diethylether, affording intense turquoise-green solutions. Compound **14-C$_2$TMS** quickly decomposes upon contact with CH_2Cl_2 and CH_3CN, affording a yellow solution and yellow-brown suspension, respectively.

ATR-IR (solid): $\tilde{\nu}$ (cm^{-1}) = 2953 (w), 2890 (w), 2869 (vw), 2059 (vw) [[ν(C≡C)], 1590 (vw), 1530 (vw), 1464 (vw), 1439 (vw), 1392 (m), 1363 (m), 1246 (m), 1201 (vw), 1176 (vw), 1162 (vw), 1135 (vw), 1011 (vw), 957 (vw), 940 (vw), 886 (w), 836 (vs), 804 (m), 760 (m), 685 (w), 664 (w), 645 (vw), 608 (vw), 562 (vw), 540 (vw), 469 (vw), 446 (w), 422 (w).

---

[37] The ^{1}H NMR spectrum reveals small amounts of a broadened signal, which can be attributed to a paramagnetic impurity. The compound is extremely lipophilic and could not be crystallized from *n*-pentane or (SiMe$_3$)$_2$O at –60 °C.

^{1}H NMR (500.14 MHz, (D_6)benzene, 298 K): δ (ppm) = 0.25 (s, 9H, C ≡ C-SiMe_3), 0.28 (s, 36H, $C^{2,6}$-CH(SiMe_3)$_2$, Tbb), 0.87 (s, 6H, C^5Me_2), 1.21 (d, ^3J(H,H) = 6.6 Hz, 6H, $C^{2,6}$-CH$Me_A$$Me_B$, Dipp), 1.35 (s, 9H, C$Me_3$, Tbb), 1.69 (d, ^3J(H,H) = 6.6 Hz, 6H, $C^{2,6}$-CH$Me_A$$Me_B$, Dipp), 1.74 (s, 2H, C^4H_2), 1.81 (s, 6H, C^3Me_2), 2.91 (sept, ^3J(H,H) = 6.6 Hz, 2H, $C^{2,6}$-C$H$$Me_A$$Me_B$, Dipp), 3.33 (s, ^2J(Si,H) = 9.7 Hz, 2H, $C^{2,6}$-CH(SiMe_3)$_2$, Tbb), 6.99 (s, 2H, $C^{3,5}$-H, Tbb), 7.09 (d, ^3J(H,H)= 7.6 Hz, 2H, $C^{3,5}$-H, Dipp), 7.18* (t, ^3J(H,H)= 7.6 Hz, 1H, C^4-H, Dipp) (this signal overlaps with the residual proton signal of the deuterated solvent).

^{13}C{^{1}H} NMR (125.78 MHz, (D_6)benzene, 298 K): δ (ppm) = 0.07 (s, 3C, C≡C-SiMe_3), 1.22 (s, 12C, $C^{2,6}$-CH(SiMe_3)$_2$, Tbb), 24.8 (s, 2C, $C^{2,6}$-CH$Me_A$$Me_B$, Dipp), 28.5 (s, 2C, $C^{2,6}$-CH$Me_A$$Me_B$, Dipp), 29.17 (s, 2C, $C^{2,6}$-CH$Me_A$$Me_B$, Dipp), 29.23 (s, 2C, C^5Me_2), 31.4 (s, 3C, C^4-CMe_3, Tbb), 32.8 (s, 2C, C^3Me_2), 34.37 (s, 2C, $C^{2,6}$-CH(SiMe_3)$_2$, Tbb), 34.44 (s, 1C, CMe$_3$, Tbb), 52.7 (s, 1C, C^4H$_2$), 53.6 (s, 1C, C^3), 74.6 (s, 1C, C^5), 118.4 (s, 1C, C ≡ C-SiMe$_3$), 120.3 (s, 2C, $C^{3,5}$-H, Tbb), 123.5 (s, 1C, C≡C-SiMe$_3$), 125.7 (s, 2C, $C^{3,5}$-H, Dipp), 129.7 (s, 1C, C^4-H, Dipp), 134.2 (s, 1C, C^1, Dipp), 135.6 (s, 1C, C^1, Tbb), 146.7 (s, 2C, $C^{2,6}$, Dipp), 150.2 (s, 2C, $C^{2,6}$, Tbb), 150.8 (s, 1C, C^4, Tbb), 243.9 (s, 1C, NC^2).

^{29}Si{^{1}H} NMR (99.36 MHz, (D_6)benzene, 298 K): δ (ppm) = –20.7 (s, 1Si, C≡C-SiMe$_3$), 2.2 (s, 4Si, $C^{2,6}$-CH(SiMe$_3$)$_2$, Tbb), 83.9 (s, 1Si, Si{C_2-SiMe$_3$}(Tbb)), 110.6 (s, 1Si, (caac^{Me})Si).

^{1}H-^{15}N HMBC (500.14 MHz, 50.69. MHz, (D_6)benzene, 298K): δ_N (ppm) = 201.3 (1N, NC^2).

4.4.37 (caac^{Me})Si=Si(Me)Tbb (14-Me)

To a cooled (–30 °C) dark green-blue solution of 1.000 g of (caac^{Me})Si=Si(Br)Tbb (**14**) (1.147 mmol, 1.00 equiv.) in 15 mL of *n*-pentane a precooled solution of MeLi (10.0 mL, 1.143 mmol, 0.996 equiv., 0.114 mol L^{-1}) in a solvent mixture of *n*-pentane/Et_2O (1:1) was added in 7 min upon which a colorless white precipitate was formed. The reaction mixture was stirred for 10 min at –30 °C and then allowed to warm up to ambient temperature. After 1 h at ambient temperature, 5 mL of Et_2O was added upon which the white solid redesolved (precipitated MeLi). During the course of 3 h at ambient temperature the color of the reaction mixture changed to green. An aliquot of the reaction mixture was taken and analyzed by ^{1}H NMR spectroscopy in (D_6)benzene, revealing the formation of 88 mol% (caac^{Me})Si=Si(Me)Tbb (**14-Me**) next to 8 mol% (caac^{Me})Si=Si(Br)Tbb (**15**) and 4 mol% of (caac^{Me})Si(Li)–Si(Me)$_2$Tbb (**15**). The reaction mixture was filtered and evaporated to dryness. The obtained green solid was dried for 1 h at 60 °C under vacuum. The crude product was extracted with *n*-pentane (3 × 10 mL) and all volatiles were removed upon drying at the fine vacuum for 1 h at 60 °C. The solid was dissolved in 4 mL of *n*-pentane. After storing at –30 °C for 2 d a black microcrystalline solid (566 mg) was obtained, which according to ^{1}H NMR spectroscopy in (D_6)benzene still contained 8 mol% of **15**. The solid was redesolved and extracted with 15 mL of *n*-pentane and the resulting clear solution was concentrated to a volume of approx. 4 mL. After storing at –30 °C for 2 d black single crystals were obtained, which after separation of the dark-green motherliquor at –30 °C, were dried for 1 h at 50 °C, affording (caac^{Me})Si=Si(Me)Tbb (**14-Me**) in analytically pure form. Yield: 363 mg (0.450 mmol, 39 %).

Properties: Disilavinylidene **14-Me** is a pyrophoric solid, which quickly decomposes upon contact with air. It is well soluble in benzene, *n*-pentane and diethylether, affording intense green solutions.

Elemental analysis: $C_{45}H_{83}NSi_6$ (806.66 g/mol): calcd./%: C 67.00, H 10.37, N 1.74; found/%: C 66.79, H 10.53, N 1.80. **Melting point:** 196 °C (dec).

^{1}H NMR (500.14 MHz, (D_6)benzene, 298 K): δ (ppm) = 0.24 (s, 36H, C^{2,6}-CH(Si*Me*$_3$)$_2$, Tbb), 1.01 (s, 6H, C^5*Me*$_2$), 1.18 (d, ^3J(H,H) = 6.6 Hz, 6H, C^{2,6}-CH*Me*$_A$Me$_B$, Dipp), 1.30 (s, 3H, Si*Me*(Tbb)), 1.35 (s, 9H, C*Me*$_3$, Tbb), 1.59 (d, ^3J(H,H) = 6.6 Hz, 6H, C^{2,6}-CHMe$_A$*Me*$_B$, Dipp), 1.65 (s, 6H, C^3*Me*$_2$), 1.73 (s, 2H, C^4*H*$_2$), 2.84 (sept, ^3J(H,H) = 6.6 Hz, 2H, C^{2,6}-C*H*Me$_A$Me$_B$, Dipp), 3.23 (s, ^2J(Si,H) = 9.7 Hz, 2H, C^{2,6}-C*H*(SiMe$_3$)$_2$, Tbb), 6.95 (s, 2H, C^{3,5}-*H*, Tbb), 7.07 (d, ^3J(H,H)= 7.8 Hz, 2H, C^{3,5}-*H*, Dipp), 7.18* (t, ^3J(H,H)= 7.8 Hz, 1H, C^4-*H*, Dipp) (this signal overlaps with the residual proton signal of the deuterated solvent).

$^{13}C\{^1H\}$ NMR (125.78 MHz, (D_6)benzene, 298 K): δ (ppm) = 1.27 (s, 12C, $C^{2,6}$-CH(Si*Me*$_3$)$_2$, Tbb), 12.35 (s, 1C, Si*Me*(Tbb)), 24.6 (s, 2C, $C^{2,6}$-CH*Me*$_A$Me$_B$, Dipp), 28.0 (s, 2C, $C^{2,6}$-CHMe$_A$*Me*$_B$, Dipp), 29.1 (s, 2C, C^5*Me*$_2$), 29.3 (s, 2C, $C^{2,6}$-*C*HMe$_A$Me$_B$, Dipp), 31.5 (s, 3C, C^4-C*Me*$_3$, Tbb), 33.2 (s, 2C, C^3*Me*$_2$), 33.6 (s, 2C, $C^{2,6}$-*C*H(SiMe$_3$)$_2$, Tbb), 34.4 (s, 1C, *C*Me$_3$, Tbb), 51.6 (s, 1C, *C*^{3}), 52.8 (s, 1C, *C*^{4}H$_2$), 73.0 (s, 1C, *C*^{5}), 120.2 (s, 2C, *C*^{3,5}-H, Tbb), 125.7 (s, 2C, *C*^{3,5}-H, Dipp), 129.4 (s, 1C, *C*^{4}-H, Dipp), 134.8 (s, 1C, *C*^{1}, Dipp), 140.1 (s, 1C, *C*^{1}, Tbb), 146.9 (s, 2C, *C*^{2,6}, Dipp), 149.3 (s, 2C, *C*^{2,6}, Tbb), 150.2 (s, 1C, *C*^{4}, Tbb), 241.5 (s, 1C, N*C*^{2}).

$^{29}Si\{^1H\}$ NMR (99.36 MHz, (D_6)benzene, 298 K): δ (ppm) = 1.9 (s, 4Si, $C^{2,6}$-CH(*Si*Me$_3$)$_2$, Tbb), 96.5 (s, 1Si, (caac^{Me})*Si*), 140.8 (s, 1Si, *Si*(Me)Tbb).

^1H-^{15}N HMBC (500.14 MHz, 50.69. MHz, (D_6)benzene, 298K): δ_N (ppm) = 190.3 (1N, *N*C^2).

4.4.38(caac^{Me})Si(Li)–Si(Me)$_2$Tbb (15)

To a solution of 0.200 g (caac^{Me})Si=SiMe(Tbb) (**14-Me**) (0.248 mmol, 1.00 equiv.) in a solvent mixture of 4 mL *n*-pentane and 4 mL Et$_2$O at –30 °C a solution of MeLi in Et$_2$O/*n*-pentane (1:1) (2.17 mL, 0.248 mmol, 1.0 equiv., 0.114 mol L^{-1}) was added. The reaction mixture was stirred for 10 min at –30 °C and then warmed to ambient temperature, upon which the color changed from green to dark red. An aliquote of the reaction mixture was taken after 1 h at ambitent temperature and analyzed by ^{1}H NMR spectroscopy in (D_6)benzene, revealing the complete consumption of the starting material and the selective formation of (caac^{Me})=Si(Li)–SiMe$_2$(Tbb) (**15**) alongside 3 mol% of a side product, which can be attributed highly likely to the corresponding hydridosilene (caac^{Me})=SiH–SiMe$_2$(Tbb). The reaction mixture was evaporated and dried under fine vacuum for 0.5 h at ambient temperature. Upon redesolving in 4 mL of *n*-pentane at ambient temperature a red precipitate was obtained, which was filtered and dried under fine vacuum for 1 h at ambient temperature. Yield: 40 mg (0.041 mmol, 16.5 %).

Properties: Silenide **15** is highly pyrophoric and immedieately decomposes upon contact with air. It is moderately soluble in *n*-pentane and well soluble in benzene and Et$_2$O, affording red solutions. The compound does not decompose over time at ambient temperature in solution, however upon addition of fresh solvents small amounts of decomposition is observed, which can be highly likely attributed to the corresponding hydridosilene.

Elemental analysis: $C_{46}H_{86}NSi_6Li(C_4H_{10}O)$ (902.77 g/mol): calcd./%: C 66.52, H 10.72, N 1.55; found/%: C 66.11, H 10.82, N 1.65 %. **Melting point:** 178 °C (partial dec).

^{1}H NMR (500.14 MHz, (D_6)benzene, 298 K): δ (ppm) = 0.34 (s, 36H, $C^{2,6}$-CH(Si*Me*$_3$)$_2$, Tbb), 0.82 (t, 6H, ^3J(H,H)= 7.1 Hz, 2 x *Me*, Et_2O), 0.97 (s, 6H, Si*Me*$_2$(Tbb)), 1.16 (d, ^3J(H,H) = 6.8 Hz, 6H, $C^{2,6}$-CH*Me*$_A$Me$_B$, Dipp), 1.28 (s, 6H, C^5*Me*$_2$), 1.40 (s, 9H, C*Me*$_3$, Tbb), 1.48 (d, ^3J(H,H) = 6.7 Hz, 6H, $C^{2,6}$-CHMe$_A$*Me*$_B$, Dipp), 1.85 (s, 6H, C^3*Me*$_2$), 2.06 (s, 2H, C^4*H*$_2$), 3.01 (s, 2H, $C^{2,6}$-C*H*(SiMe$_3$)$_2$, Tbb), 3.01 (q, 4H, ^{3}J(H,H)= 7.1 Hz, 2 x C*H*$_2$, Et_2O), 3.46 (sept, ^3J(H,H) = 6.7 Hz, 2H, $C^{2,6}$-C*H*Me$_A$Me$_B$, Dipp), 6.74 (t, ^3J(H,H)= 7.8 Hz, 1H, C^4-*H*, Dipp), 6.88 (d, ^3J(H,H)= 7.8 Hz, 2H, $C^{3,5}$-*H*, Dipp), 6.90 (s, 2H, $C^{3,5}$-*H*, Tbb).

^{13}C{^{1}H} NMR (125.78 MHz, (D_6)benzene, 298 K): δ (ppm) = 2.23 (s, 12C, $C^{2,6}$-CH(Si*Me*$_3$)$_2$, Tbb), 12.7 (s, 2C, Si*Me*$_2$(Tbb)), 14.6 (s, 2C, 2 x *Me*, Et_2O), 25.2 (s, 2C, $C^{2,6}$-CH*Me*$_A$Me$_B$, Dipp), 27.3 (s, 2C, $C^{2,6}$-CHMe$_A$*Me*$_B$, Dipp), 27.7 (s, 2C, $C^{2,6}$-*C*H(SiMe$_3$)$_2$, Tbb), 28.1 (s, 2C, $C^{2,6}$-*C*HMe$_A$Me$_B$, Dipp), 29.3 (s, 2C, C^5*Me*$_2$), 31.5 (s, 3C, C^4-C*Me*$_3$, Tbb), 34.1 (s, 1C, *C*Me$_3$, Tbb), 36.2 (s, 2C, C^3*Me*$_2$), 49.2 (s, 1C, C^3), 59.3 (s, 1C, C^4H_2), 64.9 (s, 1C, C^5), 65.5 (s, 2C, 2 x *C*H$_2$, Et_2O), 122.2 (s, 2C, $C^{3,5}$-H, Tbb), 125.4 (s, 2C, $C^{3,5}$-H, Dipp), 126.5 (s, 1C, C^4-H, Dipp), 137.7 (s, 1C, C^1, Dipp), 144.4 (s, 1C, C^1, Tbb), 148.0 (s, 1C, C^4, Tbb), 150.5 (s, 2C, $C^{2,6}$, Tbb), 151.7 (s, 2C, $C^{2,6}$, Dipp), 210.3 (s, 1C, NC^2).

^{29}Si{^{1}H} NMR (99.36 MHz, (D_6)benzene, 298 K): δ (ppm) = –20.8 (t, $^3J(^{29}Si,^7Li)$ = 4 Hz, 1Si, *Si*Me$_2$(Tbb)), 2.1 (s, 4Si, $C^{2,6}$-CH(*Si*Me$_3$)$_2$, Tbb), 44.6 (q, $^3J(^{29}Si,^7Li)$ = 65 Hz, 1Si, (caac^{Me})=*Si*(Li)).

^{1}H-^{15}N HMBC (500.14 MHz, 50.69. MHz, (D_6)benzene, 298K): δ_N (ppm) = 117.3 (1N, *N*C^2).

^{7}Li{^{1}H} NMR (194.33 MHz, (D_6)benzene, 298K): δ (ppm) = –1.82 (s, 1Li, (caac^{Me})=Si*Li*).

4.4.39SiK{Si(H)Tbb'}(caac^{Me}) (16)

480 mg of (caac^{Me})Si=SiBr(Tbb) (**14**) (0.551 mmol, 1.0 equiv.) and 171 mg of KC_8 (1.27 mmol, 2.3 equiv.) were mixed in a Schlenk tube. The Schlenk tube was cooled to –60 °C and 30 mL of DME were added. The suspension immediately turned dark purple and already after 10 min at –60 °C the color changed to dark green. The suspension was stirred for 1 h at –60 °C. The cooling bath was exchanged against a –30 °C cooling bath and the reaction mixture stirred for 2 h at this temperature. During 1 h the reaction mixture was allowed to warm up to –10 °C. The cooling bath was then exchanged against an ice bath and the reaction mixture stirred for 1 h at this temperature. After removal of the cooling bath the color of the reaction mixture changed from green to yellow to red-brown during stirring at ambient temperature for 1 h. An aliquote of the reaction mixture was taken and analyzed by ^{1}H NMR spectroscopy in (D_6)benzene, revealing the selective formation of potassium silenide **16**. The reaction solution was separated by filtration from the black insoluble part and the product extracted with *n*-pentane (2 × 10 mL). The combined dark red filtrates were evaporated to dryness and the

obtained solid dried for 0.5 h at 60 °C under vacuum. The crude product was extracted with *n*-pentane (5 × 10 mL) and the dark red extract concentrated to a volume of approx. 4 mL. Dark red crystals were already formed out of the solution at ambient temperature. The crystallization was completed upon storing the solution for 1 d at –30 °C. The crystals were separated from the red-brown colored mother liquor using a filter cannula, washed with 2 x 2°mL of *n*-pentane and dried under fine-vacuum for 2 h at ambient temperature affording the DME adduct SiK{Si(H)Tbb'}(caac^{Me})·DME (**16·DME**)[38,39] as a red solid in analytically pure form. Yield: 104 mg (0.113 mmol, 21 %).

Properties: Silenide **16·DME** is a pyrophoric solid, which quickly decomposes upon contact with air. It is well soluble in toluene, benzene and partially soluble in *n*-pentane, affording red solutions.

Elemental analysis: $C_{44}H_{80}BrNSi_6K\cdot(C_4H_{10}O_2)$ (920.85 g/mol): calcd./%: C 62.61, H 9.85, N 1.52; found/%: C 62.37, H 10.10, N 1.44. **Melting point:** 187 °C (dec).

ATR-IR (solid): $\tilde{\nu}$ (cm^{-1}) = 2947 (m), 2898 (w), 2859 (w), 2037 (w) [ν(Si-H)], 1570 (w), 1549 (w), 1449 (w), 1434 (w), 1381 (w), 1358 (w), 1322 (w), 1242 (s), 1190 (w), 1154 (s), 1126 (m), 1085 (s), 1049 (w), 1031 (w), 990 (m), 921 (w), 887 (m), 836 (vs), 811 (m), 779 (m), 762 (m), 737 (w), 721 (w), 685 (m), 669 (m), 636 (w), 609 (vw), 586 (w), 562 (w), 500 (w), 462 (vw), 429 (w).

NMR spectroscopic characterization of SiK{SiH(Tbb')}(caac^{Me})·DME (**16·DME**):

^{1}H NMR (500.14 MHz, (D_6)benzene, 298 K): δ (ppm) = 0.25 (s, 9H, C^6-CH(Si*Me$_3$*)$_C$(SiMe$_3$)$_D$, Tbb), 0.30 (s, 9H, C^6-CH(SiMe$_3$)$_C$(Si*Me$_3$*)$_D$, Tbb), 0.44 (s, 9H, C^2-C(Si*Me$_3$*)$_A$(SiMe$_3$)$_B$, Tbb), 0.48 (s, 9H, C^2-C(SiMe$_3$)$_A$(Si*Me$_3$*)$_B$, Tbb), 1.20 (s, 3H, C^5*Me$_A$*Me$_B$), 1.22 (d, ^3J(H,H) = 6.9 Hz, 3H, C^2-CH$_A$*Me$_A$*Me$_B$, Dipp), 1.25 (d, ^3J(H,H) = 6.9 Hz, 3H, C^6-CH$_B$*Me$_C$*Me$_D$, Dipp), 1.26 (s, 3H, C^{5}Me$_A$*Me$_B$*), 1.41 (s, 9H, C*Me$_3$*, Tbb), 1.50 (d, ^3J(H,H) = 6.9 Hz, 3H, C^2-CH$_A$Me$_A$*Me$_B$*, Dipp), 1.60 (d, ^3J(H,H) = 6.9 Hz, 3H, C^6-CH$_B$Me$_C$*Me$_D$*, Dipp), 2.08 (s, 3H, C^3*Me$_A$*Me$_B$), 2.11 (s, 2H, C^4*H$_A$*H$_B$ and C^{4}H$_A$*H$_B$*), 2.13 (s, 3H, C^{3}Me$_A$*Me$_B$*), 2.19 (s, ^2J(Si,H) = 10.1 Hz, 2H, C^6-C*H*(SiMe$_3$)$_C$(SiMe$_3$)$_D$, Tbb), 2.86 (s, 6H, 2 x *Me*, DME), 2.88 (s, 4H, 2 x C*H$_2$*, DME), 3.48 (sept, ^3J(H,H) = 6.9 Hz, 2H, C^2-C*H$_A$*Me$_A$Me$_B$, Dipp), 3.53 (sept, ^3J(H,H) = 6.9 Hz, 2H, C^6-C*H$_B$*Me$_C$Me$_D$, Dipp), 6.57 (s, ^1J(Si,H) = 155.8 Hz, 1H, Si-*H*), 6.80 (m, 1H, C^5-*H*, Dipp), 6.83 (m, 1H, C^4-*H*, Dipp), 6.85 (m, 1H, C^3-*H*, Dipp), 6.955 (s, 1H, C^5-*H*, Tbb), 6.965 (s, 1H, C^3-*H*, Tbb).

---

38 The compound is extremely sensitive: Upon crystallization from *n*-pentane inside the glovebox the formation of approx. 10 mol% of SiH{SiH(Tbb')}(caac^{Me}) was observed, according to ^{1}H NMR spectroscopy in (D_6)benzene. This impurity could be reduced to 2 mol% after washing with *n*-pentane at ambient temperature.

39 The coordination of DME to the potassium cation seems to be important in the stabilization of the compound. Reaction mixtures in THF, instead of DME, let upon isolation and crystallization from *n*-pentane to the caac^{Me}-coordinated compound SiK{SiH(Tbb')}(caac^{Me})·(caac^{Me}), although no free caac^{Me} carbene was observed in the reaction mixture.

$^{13}C\{^1H\}$ NMR (125.78 MHz, (D_6)benzene, 298 K): δ (ppm) = 0.73 (s, 3C, C^6-CH$(SiMe_3)_C(Si\mathit{Me_3})_D$, Tbb), 1.46 (s, 3C, C^2-C$(SiMe_3)_A(Si\mathit{Me_3})_B$, Tbb), 2.01 (s, 3C, C^6-CH$(Si\mathit{Me_3})_C(SiMe_3)_D$, Tbb), 3.38 (s, 3C, C^2-C$(Si\mathit{Me_3})_A(SiMe_3)_B$, Tbb), 23.57 (s, 1C, C^2-*C*$(SiMe_3)_A(SiMe_3)_B$, Tbb), 24.7 (s, 1C, C^2-$CH_A\mathit{Me_A}Me_B$, Dipp), 24.9 (s, 1C, C^6-$CH_B\mathit{Me_C}Me_D$, Dipp), 27.88 (s, 1C, C^2-$CH_AMe_A\mathit{Me_B}$, Dipp), 27.95 (s, 1C, C^6-*C*H$(SiMe_3)_C(SiMe_3)_D$, Tbb), 28.43 (s, 1C, C^2-*C*$H_AMe_AMe_B$, Dipp), 28.58 (s, 1C, C^6-*C*$H_BMe_CMe_D$, Dipp), 28.83 (s, 1C, C^6-$CH_BMe_C\mathit{Me_D}$, Dipp), 29.4 (s, 1C, $C^5\mathit{Me_A}Me_B$), 29.5 (s, 1C, $C^5Me_A\mathit{Me_B}$), 31.95 (s, 3C, C*Me*$_3$, Tbb), 34.75 (s, 1C, *C*Me_3, Tbb), 36.7 (s, 1C, $C^3\mathit{Me_A}Me_B$), 37.0 (s, 1C, $C^3Me_A\mathit{Me_B}$), 50.3 (s, 1C, *C*^{3}), 58.5 (s, 2C, 2 x *Me*, DME), 59.6 (s, 1C, $C^4H_AH_B$), 65.5 (s, 1C, *C*^{5}), 71.3 (s, 2C, 2 x *C*H_2, DME), 117.1 (s, 1C, *C*^{3}-H, Tbb), 119.9 (s, 1C, *C*^{5}-H, Tbb), 124.1 (s, 1C, *C*^{3}-H, Dipp), 124.3 (s, 1C, *C*^{5}-H, Dipp), 125.7 (s, 1C, *C*^{4}-H, Dipp), 144.0 (s, 1C, *C*^{2}, Tbb), 144.4 (s, 1C, *C*^{1}, Tbb), 144.9 (s, 1C, *C*^{6}, Tbb), 151.4 (s, 1C, *C*^{4}, Tbb), 153.53 (s, 1C, *C*^{2}, Dipp), 153.8 (s, 1C, *C*^{6}, Dipp), 157.9 (s, 1C, *C*^{1}, Dipp), 217.9 (s, 1C, N*C*^{2}).

$^{29}Si\{^1H\}$ NMR (99.36 MHz, (D_6)benzene, 298 K): δ (ppm) = –15.5 (s, 1Si, SiH(Tbb')), –0.68 (s, 1Si, C^2-C$(SiMe_3)_A(\mathit{Si}Me_3)_B$, Tbb), –0.30 (s, 1Si, (caac^{Me})*Si*), 0.08 (s, 1Si, C^2-C$(\mathit{Si}Me_3)_A(SiMe_3)_B$, Tbb), 0.50 (s, 1Si, C^6-CH$(\mathit{Si}Me_3)_C(SiMe_3)_D$, Tbb), 2.04 (s, 1Si, C^6-CH$(SiMe_3)_C(\mathit{Si}Me_3)_D$, Tbb),

^1H-^{15}N HMBC (500.14 MHz, 50.69. MHz, (D_6)benzene, 298K): δ_N (ppm) = 124.7 (1N, *N*C^2).

NMR spectroscopic characterization of SiK{SiH(Tbb')}(caac^{Me})·(caac^{Me}*) (**16·caac^{Me}**): Single crystals of the compound (see *footnote 39*) were dissolved in (D_6)benzene and characterized by NMR spectroscopy. Signals corresponding to the free caac^{Me} carbene, which is weakly coordinated to the potassium ion are marked with the symbol (*).

^1H NMR (500.14 MHz, (D_6)benzene, 298 K): δ (ppm) = 0.21 (s, 9H, C^6-CH$(Si\mathit{Me_3})_C(SiMe_3)_D$, Tbb), 0.28 (s, 9H, C^6-CH$(SiMe_3)_C(Si\mathit{Me_3})_D$, Tbb), 0.41 (s, 9H, C^2-C$(Si\mathit{Me_3})_A(SiMe_3)_B$, Tbb), 0.47 (s, 9H, C^2-C$(SiMe_3)_A(Si\mathit{Me_3})_B$, Tbb), 0.96 (s, 6H, $C^5\mathit{Me_2}$*), 1.05 (d, ^3J(H,H) = 6.8 Hz, 6H, $C^{2,6}$-$CH\mathit{Me_A}Me_B$*, Dipp), 1.15 (d, ^3J(H,H) = 6.8 Hz, 6H, $C^{2,6}$-$CHMe_A\mathit{Me_B}$*, Dipp), 1.18 (s, 3H, $C^5\mathit{Me_A}Me_B$), 1.21 (d, ^3J(H,H) = 6.9 Hz, 3H, C^2-$CH_A\mathit{Me_A}Me_B$, Dipp), 1.23 (d, ^3J(H,H) = 6.9 Hz, 3H, C^6-$CH_B\mathit{Me_C}Me_D$, Dipp), 1.24 (s, 3H, $C^5Me_A\mathit{Me_B}$), 1.25 (s, 6H, $C^3\mathit{Me_2}$*), 1.41 (s, 6H, $C^4\mathit{H_2}$*), 1.43 (s, 9H, C*Me*$_3$, Tbb), 1.46 (d, ^3J(H,H) = 6.9 Hz, 3H, C^2-$CH_AMe_A\mathit{Me_B}$, Dipp), 1.55 (d, ^3J(H,H) = 6.9 Hz, 3H, C^6-$CH_BMe_C\mathit{Me_D}$, Dipp), 2.06 (s, 3H, $C^3\mathit{Me_A}Me_B$), 2.09 (s, 2H, $C^4\mathit{H_A}H_B$ and $C^4H_A\mathit{H_B}$), 2.11 (s, 3H, $C^3Me_A\mathit{Me_B}$), 2.12 (s, 2H, C^6-C*H*$(SiMe_3)_C(SiMe_3)_D$, Tbb), 2.92 (sept, ^3J(H,H) = 6.9 Hz, 2H, $C^{2,6}$-*CH*Me_AMe_B, Dipp), 3.43 (sept, ^3J(H,H) = 6.9 Hz, 2H, C^2-C$H_AMe_AMe_B$, Dipp), 3.49 (sept, ^3J(H,H) = 6.9 Hz, 2H, C^6-C$H_BMe_CMe_D$, Dipp), 6.55 (s, ^1J(Si,H) = 156.8 Hz, 1H, Si-*H*), 6.67 (t, ^3J(H,H) = 7.5 Hz, 1H, C^4-*H**, Dipp), 6.79–6.83 (m, 3H, $C^{3,4,5}$-*H*, Dipp), 6.95 (s, 1H, C^5-*H*, Tbb), 6.96 (s, 1H, C^3-*H*, Tbb), 7.05 (d, ^3J(H,H) = 7.6 Hz, 2H, $C^{3,5}$-*H**, Dipp).

$^{13}C\{^1H\}$ NMR (125.78 MHz, (D_6)benzene, 298 K): δ (ppm) = 0.77 (s, 3C, C^6-$CH(SiMe_3)_C(SiMe_3)_D$, Tbb), 1.53 (s, 3C, C^2-$C(SiMe_3)_A(SiMe_3)_B$, Tbb), 2.01 (s, 3C, C^6-$CH(SiMe_3)_C(SiMe_3)_D$, Tbb), 3.50 (s, 3C, C^2-$C(SiMe_3)_A(SiMe_3)_B$, Tbb), 23.58 (s, 1C, C^2-$C(SiMe_3)_A(SiMe_3)_B$, Tbb), 24.8 (s, 1C, C^2-$CH_AMe_AMe_B$, Dipp), 25.0 (s, 1C, C^6-$CH_BMe_CMe_D$, Dipp), 26.6 (s, 2C, $C^{2,6}$-$CHMe_AMe_B$*, Dipp), 27.9 (s, 1C, C^2-$CH_AMe_AMe_B$, Dipp), 27.96 (s, 2C, C^3Me_2*), 27.98 (s, 1C, C^6-$CH(SiMe_3)_C(SiMe_3)_D$, Tbb), 28.4 (s, 1C, C^2-$CH_AMe_AMe_B$, Dipp), 28.5 (s, 1C, C^6-$CH_BMe_CMe_D$, Dipp), 28.8 (s, 1C, C^6-$CH_BMe_CMe_D$, Dipp), 29.0 (s, 2C, $C^{2,6}$-$CHMe_AMe_B$*, Dipp), 29.15 (s, 2C, C^5Me_2*), 29.4 (s, 1C, $C^5Me_AMe_B$), 29.5 (s, 1C, $C^5Me_AMe_B$), 31.97 (s, 3C, CMe_3, Tbb), 34.77 (s, 1C, CMe_3, Tbb), 36.8 (s, 1C, $C^3Me_AMe_B$), 36.9 (s, 1C, $C^3Me_AMe_B$), 50.2 (s, 1C, C^4H_2*), 50.3 (s, 1C, C^3), 57.6 (s, 1C, C^3*), 59.6 (s, 1C, $C^4H_AH_B$), 65.5 (s, 1C, C^5), 82.6 (s, 1C, C^5), 117.1 (s, 1C, C^3-H, Tbb), 119.9 (s, 1C, C^5-H, Tbb), 124.15 (s, 2C, $C^{3,5}$-H*, Dipp), 124.2 (s, 1C, C^3-H, Dipp), 124.3 (s, 1C, C^5-H, Dipp), 125.6 (s, 2C, C^4-H and C^4-H*, Dipp), 137.4 (s, 1C, C^1*, Dipp), 143.9 (s, 1C, C^2, Tbb), 144.4 (s, 1C, C^1, Tbb), 144.9 (s, 1C, C^6, Tbb), 145.7 (s, 2C, $C^{2,6}$*, Dipp), 151.4 (s, 1C, C^4, Tbb), 153.5 (s, 1C, C^2, Dipp), 153.9 (s, 1C, C^6, Dipp), 157.9 (s, 1C, C^1, Dipp), 217.9 (s, 1C, NC^2), 306.1 (s, 1C, NC^2*).

$^{29}Si\{^1H\}$ NMR (99.36 MHz, (D_6)benzene, 298 K): δ (ppm) = –5.5 (s, 1Si, SiH(Tbb')), –0.56 (s, 1Si, C^2-$C(SiMe_3)_A(SiMe_3)_B$, Tbb), 0.01 (s, 1Si, C^6- C^2-$C(SiMe_3)_A(SiMe_3)_B$, Tbb), 0.36 (s, 1Si, C^6-$CH(SiMe_3)_C(SiMe_3)_D$, Tbb), 2.05 (s, 1Si, C^6-$CH(SiMe_3)_C(SiMe_3)_D$, Tbb), 3.81 (s, 1Si, $(caac^{Me})Si$).

^1H-^{15}N HMBC (500.14 MHz, 50.69. MHz, (D_6)benzene, 298K,): δ_N (ppm) = 125.0 (1N, NC^2), 223.1 (1N, NC^2*).

4.4.40($caac^{Me}$)=Si–SiBr(IMe_4)(Tbb) (17)

To a green solution of 1.00 g of ($caac^{Me}$)Si=Si(Br)Tbb (**14**) (1.147 mmol, 1.0 equiv.) in 20 mL of benzene a slightly yellow solution of 0.143 g IMe_4 (1.152 mmol, 1.0 equiv.) in 10 mL benzene was added at ambient temperature. Upon addition the color of the solution changed from dark green to a dark red. After stirring for 1 h at ambient temperature an aliquot of the reaction solution was taken and analyzed by ^1H NMR spectroscopy in (D_6)benzene showing the selective formation of ($caac^{Me}$)=Si–SiBr(IMe_4)(Tbb) (**17**), alongside 14 mol% of free IMe_4. 60 mL of *n*-hexane was added and the reaction mixture was filtered. The clear red filtrate was evaporated to dryness and the obtained orange-brown solid dried for 1 h at 40 °C under vacuum. The crude product was washed with toluene (4 × 4 mL) and *n*-pentane (3 × 10 mL). After drying at fine vacuum for 1 h at 40 °C ($caac^{Me}$)=Si–SiBr(IMe_4)(Tbb) (**17**) was obtained in analytically pure form. Yield: 607 mg (0.610 mmol, 53 %).

Properties: Compound **17** is a pyrophoric solid, which quickly decomposes upon contact with air. It is insoluble in aliphatic solvents such as *n*-hexane, *n*-pentane, moderately soluble in benzene/toluene and well soluble in flurobenzene and THF affording red solutions. Compound **17** slowly decomposes in solution at ambient temperature in benzene. Heating of a NMR sample in (D_6)benzene for 2 h at 80 °C drastically increases the decomposition rate, upon which free IMe_4 is formed and a complex mixture of different decomposition products, which feature atleast three different Tbb substituents with C_1-symmetry. Interestingly no free (caac^{Me})Si=Si(Br)(Tbb) (**14**) is formed in this process.
Elemental analysis: $C_{51}H_{92}N_3Si_6Br$ (995.71 g/mol): calcd./%: C 61.52, H 9.31, N 4.22; found/%: C 61.28, H 9.48, N 4.15. **Melting point:** 175 °C (dec).

^{1}H NMR (500.14 MHz, (D_6)benzene, 298 K): δ (ppm) = 0.12 (s, 18H, $C^{2,6}$-CH(Si*Me*$_3$)$_A$(SiMe$_3$)$_B$, Tbb), 0.43 (s, 18H, $C^{2,6}$-CH(SiMe$_3$)$_A$(Si*Me*$_3$)$_B$, Tbb), 0.91 (d, ^3J(H,H) = 6.8 Hz, 3H, C^2-CH$_A$*Me*$_A$Me$_B$, Dipp), 1.15 (s, 3H, C^5*Me*$_A$Me$_B$), 1.18 (s, 3H, C^5Me$_A$*Me*$_B$), 1.28 (d, ^3J(H,H) = 6.8 Hz, 3H, C^6-CH$_B$*Me*$_C$Me$_D$, Dipp), 1.29 (d, ^3J(H,H) = 6.8 Hz, 3H, C^2-CH$_A$Me$_A$*Me*$_B$, Dipp), 1.40 (s, 9H, C*Me*$_3$, Tbb), 1.42 (s, 6H, $C^{4,5}$-*Me*, IMe_4), 1.79 (d, ^2J(H,H) = 12.4 Hz, 1H, C^4*H*$_A$H$_B$), 1.87 (d, ^3J(H,H) = 6.8 Hz, 3H, C^6-CH$_B$Me$_C$*Me*$_D$, Dipp), 2.00 (d, ^2J(H,H) = 12.4 Hz, 1H, C^4H$_A$*H*$_B$), 2.10 (s, 3H, C^3*Me*$_A$Me$_B$), 2.14 (s, 3H, C^3Me$_A$*Me*$_B$), 3.23 (sept, ^3J(H,H) = 6.7 Hz, 2H, C^2-C*H*$_A$Me$_A$Me$_B$, Dipp), 3.34 (sept, ^3J(H,H) = 6.8 Hz, 2H, C^6-C*H*$_B$Me$_C$Me$_D$, Dipp), 3.40 (br s, $\Delta\nu_{1/2}$ = 4.8 Hz, 2H, $C^{2,6}$-C*H*(SiMe$_3$)$_A$(SiMe$_3$)$_B$, Tbb), 3.43 (s, 6H, $N^{1,3}$-*Me*, IMe_4), 6.88 (s, 2H, $C^{3,5}$-*H*, Tbb), 6.99 (dd, ^3J(H,H) = 7.6 Hz, ^4J(H,H) = 1.6 Hz, 1H, C^3-*H*, Dipp), 7.11 (dd, ^3J(H,H) = 7.8 Hz, ^4J(H,H) = 1.6 Hz, 1H, C^5-*H*, Dipp), 7.18 (t, ^3J(H,H) = 7.8 Hz, 1H, C^4-*H*, Dipp).

^{13}C{^{1}H} NMR (125.78 MHz, (D_6)benzene, 298 K): δ (ppm) = 1.62 (s, 6C, $C^{2,6}$-CH(Si*Me*$_3$)$_A$(SiMe$_3$)$_B$, Tbb), 2.33 (s, 6C, $C^{2,6}$-C(SiMe$_3$)$_A$(Si*Me*$_3$)$_B$, Tbb), 8.6 (s, 2C, $C^{4,5}$-*Me*, IMe_4), 24.9 (s, 1C, C^2-CH$_A$*Me*$_A$Me$_B$, Dipp), 25.5 (s, 1C, C^2-CH$_A$Me$_A$*Me*$_B$, Dipp), 25.75 (s, 1C, C^6-CH$_B$*Me*$_C$Me$_D$, Dipp), 28.1 (s, 1C, C^2-*C*H$_A$Me$_A$Me$_B$, Dipp), 28.4 (s, 1C, C^6-CH$_B$Me$_C$*Me*$_D$, Dipp), 28.95 (s, 1C, C^5Me$_A$*Me*$_B$), 29.5 (s, 1C, C^5*Me*$_A$Me$_B$), 29.9 (s, 1C, C^6-*C*H$_B$Me$_C$Me$_D$, Dipp), 30.1 (s, 2C, $C^{2,6}$-*C*H(SiMe$_3$)$_A$(SiMe$_3$)$_B$, Tbb), 31.6 (s, 4C, C*Me*$_3$, Tbb and C^3Me$_A$*Me*$_B$), 34.1 (s, 1C, *C*Me$_3$, Tbb), 35.6 (s, 2C, $N^{1,3}$-*Me*, IMe_4), 37.3 (s, 1C, C^3*Me*$_A$Me$_B$), 49.5 (s, 1C, *C*^{3}), 57.5 (s, 1C, *C*^{4}H$_A$H$_B$), 68.7 (s, 1C, *C*^{5}), 122.3 (s, 2C, *C*^{3,5}-H, Tbb), 123.9 (s, 1C, *C*^{3}-H, Dipp), 125.0 (s, 1C, *C*^{5}-H, Dipp), 125.3 (s, 2C, *C*^{4,5}, IMe_4), 127.8 (s, 1C, *C*^{4}-H, Dipp overlapping with the (D_6)benzene signal), 137.4 (s, 1C, *C*^{1}, Dipp), 141.6 (s, 1C, *C*^{1}, Tbb), 146.2 (s, 1C, *C*^{4}, Tbb), 148.6 (s, 1C, *C*^{2}, Dipp), 148.7 (s, 2C, *C*^{2,6}, Tbb), 150.7 (s, 1C, *C*^{6}, Dipp), 169.5 (s, 1C, N*C*^{2}, IMe_4), 191.3 (s, 1C, N*C*^{2}).

^{29}Si{^{1}H} NMR (99.36 MHz, (D_6)benzene, 298 K): δ (ppm) = –57.2 (s, 1Si, SiBr(IMe_4)(Tbb)), 1.9 (s, 2Si, $C^{2,6}$-C(SiMe$_3$)$_A$(*Si*Me$_3$)$_B$, Tbb), 2.0 (s, 2Si, $C^{2,6}$-C(*Si*Me$_3$)$_A$(SiMe$_3$)$_B$, Tbb), 28.1 (s, 1Si, (caac^{Me})*Si*),

^{1}H-^{15}N HMBC (500.14 MHz, 50.69. MHz, (D_6)benzene, 298K): δ_N (ppm) = 141.2 (1N, *N*C^2), 174.7 (2N, *N*^{1,3}, IMe$_4$)

4.4.41[(caac^{Me})Si=Si(IMe$_4$)(Tbb)][B(C$_6$H$_3$-3,5-(CF$_3$)$_2$)$_4$)] (18)

To a red solution of 400 mg of (caac^{Me})=Si–SiBr(IMe$_4$)(Tbb) (**17**) (0.399 mmol, 1.0 equiv.) in 20 mL of fluorobenzene a colorless solution of 346 mg Na[B(C$_6$H$_3$-3,5-(CF$_3$)$_2$)$_4$)] (0,391 mmol, 0.98 equiv.) in 10 mL of fluorbenzene was added dropwise in 10 min at ambient temperature. The color of the reaction mixture immediately changed to dark blue. An aliquot of the reaction mixture was taken after 1 h at ambient temperature and analyzed by ^{1}H no D NMR in fluorobenzene, revealing the selective formation of [(caac^{Me})Si=Si(IMe$_4$)(Tbb)][B(C$_6$H$_3$-3,5-(CF$_3$)$_2$)$_4$)] (**18**) alongside 2 mol% of the starting material.[40] 10 mL of *n*-hexane was added and the reaction mixture stirred for another 1 h. Formed NaBr was filtered off and the dark blue filtrate was evaporated and dried at the fine vacuum for 0.5 h at 50 °C. The dark blue solid was washed with *n*-hexane (3 × 5 mL) and *n*-pentane (2 × 5 mL), upon which the starting material was recovered as red wash-solution. After drying at fine vacuum for 1.5 h at 60 °C [(caac^{Me})Si=Si(IMe$_4$)(Tbb)] [B(C$_6$H$_3$-3,5-(CF$_3$)$_2$)$_4$)] (**18**) was obtained as a dark blue solid in analytically pure form. Yield: 595 mg (0.334 mmol, 85%).

Properties: Disilynium salt **18** is a highly pyrophoric solid, which quickly decomposes upon contact with air. It is insoluble in aliphatic solvents and benzene, but well soluble in fluorobenzene, chlorobenzene and THF,[41] affording dark blue solutions. Compound **18** immediately decomposes unselectively upon contact with dichloromethane forming an orange-yellow solution.

Elemental analysis: $C_{83}H_{104}N_3Si_6BF_{24}$ (1779.02 g/mol): calcd./%: C 56.04, H 5.89, N 2.36; found/%: C 55.96, H 5.94, N 2.29. **Melting point:** 175 °C (minor dec).

^{1}H NMR (500.14 MHz, (D_8)THF, 298 K): δ (ppm) = 0.01 (s, 32H, C^{2,6}-CH(Si*Me$_3$*)$_2$, Tbb), 1.29 (s, 9H, C*Me$_3$*, Tbb), 1.33 (s, 6H, C^3*Me$_2$*), 1.37 (d, ^3J(H,H) = 6.7 Hz, 6H, C^{2,6}-CH*Me$_A$*Me$_B$, Dipp), 1.42 (s, 6H, C^5*Me$_2$*), 1.47 (d, ^3J(H,H) = 6.7 Hz, 6H, C^{2,6}-CHMe$_A$*Me$_B$*, Dipp), 2.26 (s, 2H, C^4*H$_2$*), 2.28 (s, 6H, C^{4,5}-*Me*, IMe$_4$), 2.79 (br s, $\Delta\nu_{1/2}$ = 4.8 Hz, 2H, C^{2,6}-C*H*(SiMe$_3$)$_2$, Tbb), 2.82 (sept, ^3J(H,H) = 6.7 Hz, 2H, C^{2,6}-C*H*Me$_A$Me$_B$, Dipp), 3.81 (s, 6H, N^{1,3}-*Me*, IMe$_4$), 6.79 (s, 2H, C^{3,5}-*H*, Tbb), 7.39 (d, ^3J(H,H) = 7.5 Hz, 2H, C^{3,5}-*H*, Dipp), 7.48 (t, ^3J(H,H) = 7.5 Hz, 1H, C^4-*H*, Dipp), 7.58 (br s, $\Delta\nu_{1/2}$ = 4.6 Hz, 4H, 4 × C^4-*H*, B(Ar^F)$_4$), 7.79* (m, 8H, 4 × C^{2,6}-*H*, B(Ar^F)$_4$). the signal marked with an asterisk is a slightly broadened multiplet with an unresolved fine structure.

---

40 This result was intendet. Previous test reactions revealed a quantitative formation of the cation. The 0.98 equiv. of NaB(Ar^F)$_4$ should ensure, that no excess of NaB(Ar^F)$_4$ is present in the reaction mixture in order to simplify the work up, since the starting material can be easily removed upon washing with *n*-hexane at ambient temperature.

41 The compound is stable in THF at ambient temperature and also stable upon heating in the same solvent for 4 h at 60 °C.

^{13}C{^{1}H} NMR (125.78 MHz, (D_8)THF, 298 K): δ (ppm) = 1.5 (s, 12C, $C^{2,6}$-CH(Si*Me*$_3$)$_2$, Tbb), 8.5 (s, 2C, $C^{4,5}$-*Me*, IMe$_4$), 24.5 (s, 2C, $C^{2,6}$-CH*Me*$_A$Me$_B$, Dipp), 28.7 (s, 2C, $C^{2,6}$-CHMe$_A$*Me*$_B$, Dipp), 29.4 (s, 2C, C^5*Me*$_2$), 30.1 (s, 2C, $C^{2,6}$-*C*HMe$_A$Me$_B$, Dipp), 31.3 (s, 3C, C*Me*$_3$, Tbb), 31.6 (s, 2C, C^3*Me*$_2$), 33.9 (s, 2C, $C^{2,6}$-*C*H(SiMe$_3$)$_2$, Tbb), 35.1 (s, 1C, *C*Me$_3$, Tbb), 36.1 (s, 2C, N^{1,3}-*Me*, IMe$_4$), 51.7 (s, 1C, *C*^{4}H$_2$), 53.8 (s, 1C, *C*^{3}), 78.7 (s, 1C, *C*^{5}), 118.2 (sept, ^3J(F,C) = 4 Hz, 4 × *C*^{4}-H, B(Ar^F)$_4$), 122.9 (s, 2C, *C*^{3,5}-H, Tbb), 125.5 (q, ^1J(F,C) = 272 Hz, 8C, 4 × C^{3,5}-*C*F$_3$, B(Ar^F)$_4$), 126.8 (s, 2C, *C*^{3,5}-H, Dipp), 130.0 (qq, ^2J(F,C) = 32 Hz, ^3J(B,C) = 3 Hz, 8C, 4 × *C*^{3,5}-CF$_3$, B(Ar^F)$_4$), 130.1 (s, 2C, *C*^{4,5}, IMe$_4$), 131.4 (s, 1C, *C*^{4}-H, Dipp), 132.2 (s, 1C, *C*^{1}, Tbb), 134.1 (s, 1C, *C*^{1}, Dipp), 135.6 (br s, $\Delta\nu_{1/2}$ = 3 Hz, 8C, 4 × *C*^{2,6}-H, B(Ar^F)$_4$), 146.6 (s, 2C, *C*^{2,6}, Dipp), 152.5 (s, 2C, *C*^{2,6}, Tbb), 152.8 (s, 1C, *C*^{4}, Tbb), 153.2 (s, 1C, *C*^{2}N, IMe$_4$), 162.7 (q, ^1J(C,B) = 50 Hz, 4C, 4 × *C*^{1}, B(Ar^F)$_4$), 240.5 (s, 1C, *C*^{2}N).

^{29}Si{^{1}H} NMR (99.36 MHz, (D_8)THF, 298 K): δ (ppm) = 3.1 (s, 4Si, C^{2,6}-C(S*i*Me$_3$)$_2$, Tbb), 84.5 (s, 1Si, *Si*(IMe$_4$)(Tbb)), 116.7(s, 1Si, (caac^{Me})*Si*).

^{1}H-^{15}N HMBC (500.14 MHz, 50.69. MHz, (D_8)THF, 298K): δ_N (ppm) = 176.6 (2N, *N*^{1,3}, IMe$_4$), 216.2 (1N, *N*C^2),

^{11}B{^{1}H} NMR (160.43 MHz, (D_8)THF, 298 K): δ (ppm) = –6.53 (1B, B(Ar^F)$_4$).

^{19}F{^{1}H} NMR (470.44 MHz, (D_8)THF, 298 K): δ (ppm) = –63.4 (12F, B(Ar^F)$_4$).

^{1}H NMR (500.04 MHz, (D_5)chlorobenzene, 298 K): δ (ppm) = -0.02 (s, 32H, C^{2,6}-CH(Si*Me*$_3$)$_2$, Tbb), 1.08 (s, 6H, C^5*Me*$_2$), 1.11 (s, 6H, C^3*Me*$_2$), 1.20 (d, ^3J(H,H) = 6.5 Hz, 6H, C^{2,6}-CH*Me*$_A$Me$_B$, Dipp), 1.24 (s, 9H, C*Me*$_3$, Tbb), 1.40 (d, ^3J(H,H) = 6.5 Hz, 6H, C^{2,6}-CHMe$_A$*Me*$_B$, Dipp), 1.77 (s, 6H, C^{4,5}-*Me*, IMe$_4$), 1.82 (s, 2H, C^4*H*$_2$), 2.60 (sept, ^3J(H,H) = 6.5 Hz, 2H, C^{2,6}-C*H*Me$_A$Me$_B$, Dipp), 2.62 (s, 2H, C^{2,6}-C*H*(SiMe$_3$)$_2$, Tbb), 3.50 (s, 6H, N^{1,3}-*Me*, IMe$_4$), 6.76 (s, 2H, C^{3,5}-*H*, Tbb), 7.06 (d, ^3J(H,H) = 7.5 Hz, 2H, C^{3,5}-*H*, Dipp), 7.07 (t, ^3J(H,H) = 7.5 Hz, 1H, C^4-*H*, Dipp), 7.61 (br s, $\Delta\nu_{1/2}$ = 4.4 Hz, 4H, 4 × C^4-*H*, B(Ar^F)$_4$), 8.24* (m, 8H, 4 × C^{2,6}-*H*, B(Ar^F)$_4$*)*. the signal marked with an asterisk is a slightly broadened multiplet with an unresolved fine structure.

^{13}C{^{1}H} NMR (125.75 MHz, (D_5)chlorobenzene, 298 K): δ (ppm) = 1.24 (s, 12C, C^{2,6}-CH(Si*Me*$_3$)$_2$, Tbb), 8.1 (s, 2C, C^{4,5}-*Me*, IMe$_4$), 24.2 (s, 2C, C^{2,6}-CH*Me*$_A$Me$_B$, Dipp), 28.1 (s, 2C, C^2-CHMe$_A$*Me*$_B$, Dipp), 28.8 (s, 1C, C^5*Me*$_2$), 29.3 (s, 1C, C^{2,6}-*C*HMe$_A$Me$_B$, Dipp), 30.9 (s, 3C, C*Me*$_3$, Tbb), 31.0 (s, 1C, C^3*Me*$_2$), 33.3 (s, 2C, C^{2,6}-*C*H(SiMe$_3$)$_2$, Tbb), 34.4 (s, 1C, *C*Me$_3$, Tbb), 35.2 (s, 2C, N^{1,3}-*Me*, IMe$_4$), 50.96 (s, 1C, *C*^{4}H$_2$), 52.6 (s, 1C, *C*^{3}), 77.5 (s, 1C, *C*^{5}), 117.8 (sept, ^3J(F,C) = 4 Hz, 4 x *C*^{4}-H, B(Ar^F)$_4$), 122.2 (s, 2C, *C*^{3,5}-H, Tbb), 124.9 (q, ^1J(F,C) = 272 Hz, 8C, 4 × C^{3,5}-*C*F$_3$, B(Ar^F)$_4$), 125.9 (s, 1C, *C*^{3,5}-H, Dipp), 128.5 (s, 2C, *C*^{4,5}, IMe$_4$), 130.0 (qq, ^2J(F,C) = 32 Hz, ^3J(B,C) = 3 Hz, 8C, 4 × *C*^{3,5}-CF$_3$, B(Ar^F)$_4$), 130.5 (s, 1C, *C*^{1}, Tbb), 130.8 (s, 1C, *C*^{4}-H, Dipp), 132.9 (s, 1C, *C*^{1}, Dipp), 135.2 (br s, $\Delta\nu_{1/2}$ = 10 Hz, 8C, 4 × *C*^{2,6}-H, B(Ar^F)$_4$), 145.4 (s, 2C, *C*^{2,6}, Dipp), 151.7 (s, 2C, *C*^{2,6}, Tbb), 152.6 (s, 1C, *C*^{4}, Tbb), 153.3 (s, 1C, *C*^{2}N, IMe$_4$), 162.4 (q, ^1J(C,B) = 50 Hz, 4C, 4 × *C*^{1}, B(Ar^F)$_4$), 239.1 (s, 1C, N*C*^{2}).

^{29}Si{^{1}H} NMR (99.36 MHz, (D_5)chlorobenzene, 298 K): δ (ppm) = 3.1 (s, 4Si, $C^{2,6}$-C(S*i*Me_3)$_2$, Tbb), 83.6 (s, 1Si, *Si*(IMe_4)(Tbb)), 118.1(s, 1Si, ($caac^{Me}$)*Si*).

^{1}H-^{15}N HMBC (500.14 MHz, 50.69. MHz, (D_5)chlorobenzene, 298K): δ_N (ppm) = 175.4 (2N, $N^{1,3}$, IMe_4), 215.9 (1N, NC^2).

^{11}B{^{1}H} NMR (160.43 MHz, (D_5)chlorobenzene, 298 K): δ (ppm) = –5.94 (1B, $B(Ar^F)_4$).

^{19}F{^{1}H} NMR (470.44 MHz, (D_5)chlorobenzene, 298 K): δ (ppm) = –61.9 (12F, $B(Ar^F)_4$).

4.4.42 [Si(Me)($caac^{Me}$)$_2$][B(C_6H_3-3,5-(CF_3)$_2$)$_4$)] (19-Me)

In a small Schlenk tube 0.300 g Si($caac^{Me}$)$_2$ (0.501 mmol, 1.00 equiv.) and 0.444 g Na[B(C_6H_3-3,5-(CF_3)$_2$)$_4$)] were dissolved in 10 mL of fluorobenzene. The dark blue solution was cooled to –30 °C and a precooled solution of MeOTf (0.1355 mol L^{-1}, 3.70 mL, 0.501 mmol, 1.00 equiv.) in 10 mL of fluorobenzene was added dropwise in 10 min at –30 °C. During the addition the color of the reaction mixture changed from dark blue to dark green. The green solution was brought to ambient temperature. An aliquote of the reaction mixture was taken and analyzed by ^{1}H NMR spectroscopy in (D_8)THF, revealing the selective formation of [Si(Me)($caac^{Me}$)$_2$][B(C_6H_3-3,5-(CF_3)$_2$)$_4$)] (**19-Me**), alongside small amounts of [$caac^{Me}$H][B(C_6H_3-3,5-(CF_3)$_2$)$_4$)] (10 mol%).[42] 3 mL of *n*-hexane was added, the suspension stirred for 0.5 h at ambient temperature, upon which a slight turbidity was observed. The resulting off-white precipitate (0.096 g, NaOTf) was filtered and the clear dark green filtrate evaporated to dryness. The green residue was washed with 3 x 5 mL of *n*-hexane and 5 mL of *n*-pentane and dried under fine vacuum for 2.5 h at 40 °C. The green powdery solid was redesolved in 3 mL of Et_2O, 6 mL of *n*-hexane was added during stirring of the solution and kept for 1 h at ambient temperature.[43] After storing at 4 °C for 20 h green single crystals were obtained, which were removed from the dark green mother liquor upon filtration at 4 °C. Drying at the fine vacuum for 1.5 h at 40 °C afforded [Si(Me)($caac^{Me}$)$_2$][B(C_6H_3-3,5-(CF_3)$_2$)$_4$)] (**19-Me**) as a green solid in analytically pure form. Yield: 0.395 g (0.267 mmol, 53 %).[44]

---

42 Selected NMR spectroscopic data of [$caac^{Me}$H][B(C_6H_3-3,5-(CF_3)$_2$)$_4$)]: **^{1}H NMR** (300.13 MHz, (D_8)THF, 298 K): δ (ppm) = 1.14 (d, ^{3}J(H,H) = 6.7 Hz, 6H, $C^{2,6}$-CH*Me*$_A$Me$_B$, Dipp), 1.39 (d, ^{3}J(H,H) = 6.7 Hz, 6H, $C^{2,6}$-CHMe$_A$*Me*$_B$, Dipp), 1.63 (s, 6H, C^5*Me*$_2$), 1.64 (s, 6H, C^3*Me*$_2$), 2.54 (s, 2H, C^4*H*$_2$), 2.78 (sept, ^{3}J(H,H) = 6.7 Hz, 2H, $C^{2,6}$-C*H*Me$_A$Me$_B$, Dipp), 7.52-7,55 (m, 2H, $C^{3,5}$-*H*, Dipp), 7.58 (br s, $\Delta\nu_{1/2}$ = 4 Hz, 4H, 4 × C^4-*H*, $B(Ar^F)_4$), 7.61-7.66 (m, 1H, C^4-*H*, Dipp), 7.79* (m, 8H, 4 × $C^{2,6}$-*H*, $B(Ar^F)_4$), 9.19 (s, 1H, NC^2-*H*).

43 The compound can also be precipitated from Et_2O using an excess of *n*-hexane. Fluorobenzene/*n*-hexane mixtures in contrast always let to the formation of an oily residue.

44 ^{1}H NMR spectroscopy in (D_8)THF still revealed the presence of 2 mol% of [$caac^{Me}$H][B(C_6H_3-3,5-(CF_3)$_2$)$_4$)], which could not be lowered, even with multiple crystallization attempts.

Properties: Silylium-ylidene **19-Me** quickly decolorizes upon contact with air. It is insoluble in *n*-hexane, *n*-pentane and benzene and well soluble in flourobenzene, THF and Et_2O, affording dark green solutions.
Elemental analysis: $C_{73}H_{77}N_2SiBF_{24}$ (1477.26 g/mol): calcd./%: C 59.35, H 5.25, N 1.90; found/%: C 59.35, H 5.28, N 1.83. **Melting point:** 255 °C (dec).

^{1}H NMR (500.14 MHz, (D_8)THF, 298 K): δ (ppm) = −0.49 (s, 3H, Si-*Me*), 1.17 (d, ^3J(H,H) = 6.6 Hz, 12H, 2 × $C^{2,6}$-CH*Me*$_A$Me$_B$, Dipp), 1.26 (d, ^3J(H,H) = 6.6 Hz, 12H, 2 × $C^{2,6}$-CHMe$_A$*Me*$_B$, Dipp), 1.43 (s, 12H, 2 × C^5*Me*$_2$), 1.77 (s, 12H, 2 × C^3*Me*$_2$), 2.27 (s, 4H, 2 × C^4*H*$_2$), 2.75 (sept, ^3J(H,H) = 6.6 Hz, 4H, 2 × $C^{2,6}$-C*H*Me$_A$Me$_B$, Dipp), 7.32 (d, ^3J(H,H) = 7.8 Hz, 4H, 2 × $C^{3,5}$-*H*, Dipp), 7.42 (t, ^3J(H,H) = 7.8 Hz, 2H, 2 × C^4-*H*, Dipp), 7.58 (br s, $\Delta\nu_{1/2}$ = 3 Hz, 4H, 4 × C^4-*H*, B(Ar^F)$_4$), 7.79* (m, 8H, 4 × $C^{2,6}$-*H*, B(Ar^F)$_4$). the signal marked with an asterisk is a slightly broadened multiplet with an unresolved fine structure.

^{13}C{^{1}H} NMR (125.78 MHz, (D_8)THF, 298 K): δ (ppm) = 0.33 (s, 1C, Si-*Me*), 25.7 (s, 4C, 2 x $C^{2,6}$-CHMe$_A$*Me*$_B$, Dipp), 26.9 (s, 4C, 2 × $C^{2,6}$-CH*Me*$_A$Me$_B$, Dipp), 29.8 (s, 2C, 2 × $C^{2,6}$-*C*HMe$_A$Me$_B$, Dipp), 30.0 (s, 4C, 2 × C^5*Me*$_2$), 31.7 (s, 4C, 2 × C^3*Me*$_2$), 53.7 (s, 2C, 2 × C^3), 54.1 (s, 2C, 2 x C^4H_2), 80.0 (s, 2C, 2 × C^5), 118.2 (sept, ^3J(F,C) = 4 Hz, 4 x C^4-H, B(Ar^F)$_4$), 125.5 (q, ^1J(F,C) = 273 Hz, 8C, 4 × $C^{3,5}$-CF_3, B(Ar^F)$_4$), 127.2 (s, 4C, 2 × $C^{3,5}$-H, Dipp), 130.0 (qq, ^2J(F,C) = 32 Hz, ^3J(B,C) = 3 Hz, 8C, 4 × $C^{3,5}$-CF_3, B(Ar^F)$_4$), 131.4 (s, 2C, 2 × C^4-H, Dipp), 134.4 (s, 2C, 2 × C^1, Dipp), 135.6 (br s, $\Delta\nu_{1/2}$ = 7 Hz, 8C, 4 × $C^{2,6}$-H, B(Ar^F)$_4$), 147.6 (s, 2C, $C^{2,6}$, Dipp), 162.7 (q, ^1J(C,B) = 50 Hz, 4C, 4 × C^1, B(Ar^F)$_4$), 216.1 (s, 1C, NC^2).

^{29}Si{^{1}H} NMR (99.36 MHz, (D_8)THF, 298 K): δ (ppm) = 5.97 (s, 1Si, (caac^{Me})*Si*).

^{1}H-^{15}N HMBC (500.14 MHz, 50.69. MHz, (D_8)THF, 298 K): δ_N (ppm) = 201.8 (2N, 2 × *N*C^2),

^{11}B{^{1}H} NMR (160.43 MHz, (D_8)THF, 298 K): δ (ppm) = −6.49 (1B, B(Ar^F)$_4$).

^{19}F{^{1}H} NMR (470.44 MHz, (D_8)THF, 298 K): δ (ppm) = −63.4 (12F, B(Ar^F)$_4$).

4.4.43 (Cp)(CO)Co–$SiBr_2(caac^{Me})$ (20)

To a dark red solution of 0.826 g of $SiBr_2(caac^{Me})$ (**1**) (1.75 mmol, 1.00 equiv.) in 20 mL of toluene a solution of 0.330 g of $CpCo(CO)_2$ (1.83 mmol, 1.05 equiv.) in 15 mL of toluene was added dropwise in 15 min at ambient temperature. The reaction mixture was stirred at ambient temperature under partial vacuum. After 1 h the dark red solution changed to purple, after 4 h it changed to dark brown and finally after 24 h it changed to dark green. An aliquot of the reaction mixture was taken and analyzed by ^{1}H NMR spectroscopy in (D_6)benzene revealing the quantitative formation of **20**. The dark green solution was evaporated and dried under fine vacuum for 0.5 h at 60 °C.

The green oily residue was extracted with 100 mL of *n*-pentane/toluene (95:5) and separated from the grew-white solid (0.060 g). The green extract was evaporated and dried at fine vacuum for 0.5 h at 60 °C. The compound was redessolved in 10 mL of boiling *n*-pentane/tolune (9:1) and stored overnight at 4 °C. A dark green microcrystalline solid was separated from the dark green mother liquor upon filtration at 0 °C. Drying at the fine vacuum for 2 h at 50 °C afforded Cp(CO)Co-$SiBr_2(caac^{Me})$ (**20**) as a dark green powder in analytically pure form. Yield: 879 mg (1.41 mmol, 81 %).

Properties: Silylene complex **20** quickly decolorizes upon contact with air. It is insoluble in *n*-hexane, moderately soluble in benzene/toluene and Et_2O and well soluble in THF at ambient temperature, affording green solutions.

Elemental analysis: $C_{26}H_{36}Br_2CoNOSi$ (625.40 g·mol^{-1}): calcd./%: C 49.93, H 5.80, N 2.25; found/%: C 49.85, H 5.94, N 2.25 %. **Melting point:** 172 °C (dec).

ATR-IR (solid): $\tilde{\nu}$ (cm^{-1}) = 2971 (w), 2953 (w), 2930 (w), 2868 (w), 1960 (vw), 1889 (vs) [ν(C ≡ O)], 1868 (vs) [ν(C ≡ O)], 1589 (vw), 1514 (w), 1503 (w), 1459 (m), 1405 (w), 1390 (w), 1370 (w), 1343 (m), 1328 (w), 1315 (w), 1265 (w), 1193 (w), 1179 (w), 1161 (w), 1124 (w), 1107 (w), 1052 (w), 1013 (w), 991 (w), 934 (w), 893 (w), 869 (w), 850 (w), 805 (w), 796 (s), 776 (m), 698 (w), 684 (w), 607 (m), 602 (m), 569 (m), 553 (vs), 507 (s), 472 (w), 446 (vs), 418 (m), 408 (m).

Solution cell IR (toluene, 298 K): $\tilde{\nu}$ (cm^{-1}) = 1877 [ν(C ≡ O)].

Solution cell IR (*n*-hexane, 298 K): $\tilde{\nu}$ (cm^{-1}) = 1879 [ν(C ≡ O)].

^{1}H NMR (500.14 MHz, (D_6)benzene, 298 K): δ (ppm) = 0.93 (br s, $\Delta\nu_{1/2}$ = 39.9 Hz, 6H, C^5Me_2), 1.11 (br s, $\Delta\nu_{1/2}$ = 27.5 Hz, 6H, $C^{2,6}$-CHMe_AMe$_B$, Dipp), 1.67 (br s, $\Delta\nu_{1/2}$ = 28.9 Hz, 6H, $C^{2,6}$-CHMe$_A$$Me_B$, Dipp), 1.96 (br s, $\Delta\nu_{1/2}$ = 73.2 Hz, 8H, C^3Me_2 and C^4H_2), 3.01 (br s, $\Delta\nu_{1/2}$ = 38.4 Hz, 2H, $C^{2,6}$-C*H*Me$_A$Me$_B$, Dipp), 4.91 (br s, $\Delta\nu_{1/2}$ = 13.7 Hz, 5H, Cp), 7.02 (br s, $\Delta\nu_{1/2}$ = 26.5 Hz, 2H, $C^{3,5}$-*H*, Dipp), 7.11 (br s, $\Delta\nu_{1/2}$ = 74.0 Hz, 1H, C^4-*H*, Dipp).

$^{13}C\{^1H\}$ NMR (125.77 MHz, (D_6)benzene, 298 K): δ (ppm) = 25.1 (s, 2C, $C^{2,6}$-CH*Me*$_A$Me$_B$, Dipp), 27.3 (br s, $\Delta\nu_{1/2}$ = 190 Hz, 4C, C^5*Me*$_2$ and $C^{2,6}$-CH*M*e$_A$Me$_B$ as well as $C^{2,6}$-CHMe$_A$*Me*$_B$, Dipp), 28.9 (s, 2C, $C^{2,6}$-*C*HMe$_A$Me$_B$, Dipp), 31.6 (br s, $\Delta\nu_{1/2}$ = 70 Hz, 2C, C^3*Me*$_2$), 49.8 (s, 1C, C^4H_2), 55.9 (s, 1C, C^3), 81.5 (s, 1C, C^5), 84. (s, 5C, *C*-H, Cp), 125.9 (br s, $\Delta\nu_{1/2}$ = 48 Hz, 2C, $C^{3,5}$-H, Dipp), 130.8 (s, 1C, C^4-H, Dipp), 132.6 (s, 1C, C^1, Dipp), 146.6 (s, 2C, $C^{2,6}$, Dipp), 211.5 (br, $\Delta\nu_{1/2}$ = 33 Hz, *C*O), 216.1 (s, 1C, NC^2).

$^{29}Si\{^1H\}$ NMR (99.37 MHz, (D_6)benzene, 298 K): δ (ppm) = 14.4 (s, 1Si).

NMR spectroscopic characterization of **20** in (D_8)toluene at 243 K:

^1H NMR (500.17 MHz, (D_8)toluene, 243 K): δ (ppm) = 0.74 (s, 3H, C^5*Me*$_A$Me$_B$), 0.98 (s, 3H, C^5Me$_A$*Me*$_B$), 1.00 (d, ^3J(H,H) = 6.4 Hz, 3H, C^2-CH$_A$*Me*$_A$Me$_B$, Dipp), 1.20 (d, ^2J(H,H) = 12.7 Hz, 1H, $C^4H_AH_B$), 1.21 (d, ^3J(H,H) = 6.4 Hz, 3H, C^6-CH$_A$*Me*$_C$Me$_D$, Dipp), 1.59 (d, ^3J(H,H) = 6.4 Hz, 3H, C^2-CH$_A$Me$_A$*Me*$_B$, Dipp), 1.74 (s, 3H, C^3*Me*$_A$Me$_B$), 1.76 (d, ^3J(H,H) = 6.4 Hz, 3H, C^6-CH$_A$Me$_C$*Me*$_D$, Dipp), 1.88 (d, ^2J(H,H) = 12.7 Hz, 1H, $C^4H_AH_B$), 2.12 (s, 3H, C^3Me$_A$*Me*$_B$), 2.72 (sept, ^3J(H,H) = 6.4 Hz, 1H, C^2-C*H*$_A$Me$_A$Me$_B$, Dipp), 3.30 (sept, ^3J(H,H) = 6.4 Hz, 2H, C^6-C*H*$_B$Me$_C$Me$_D$, Dipp), 4.92 (s, 5H, 5 x C-*H*, Cp), 6.88 (d, ^3J(H,H) = 7.6 Hz, 1H, C^3-*H*, Dipp), 6.98 (d, ^3J(H,H) = 7.6 Hz, 1H, C^5-*H*, Dipp overlapping with the signal of the deuterated solvent), 7.07 (t, ^3J(H,H) = 7.7 Hz, 1H, C^4-*H*, Dipp overlapping with the signal of the deuterated solvent).

$^{13}C\{^1H\}$ NMR (125.77 MHz (D_8)toluene, 243 K): δ (ppm) = 24.6 (s, 1C, C^2-CH$_A$*Me*$_A$Me$_B$, Dipp), 25.1 (s, 1C, C^6-CH$_B$*Me*$_C$Me$_D$, Dipp), 25.9 (s, 1C, C^2-CH$_A$Me$_A$*Me*$_B$, Dipp), 26.1 (s, 1C, C^5*Me*$_A$Me$_B$), 28.4 (s, 1C, C^6-CH$_B$Me$_C$*Me*$_D$), 28.6 (s, 1C, C^2-*C*H$_A$Me$_A$Me$_B$, Dipp), 28.9 (s, 1C, C^6-*C*H$_B$Me$_C$Me$_D$, Dipp), 30.2 (s, 1C, C^3Me$_A$*Me*$_B$), 30.6 (s, 1C, C^5Me$_A$*Me*$_B$), 32.1 (s, 1C, C^3*Me*$_A$Me$_B$), 48.9 (s, 1C, $C^4H_AH_B$), 55.7 (s, 1C, C^3), 81.3 (s, 1C, C^5), 84.0 (s, 5C, 5 x *C*-H, Cp), 125.1 (s, 2C, 2 × C^3-H, Dipp), 126.4 (s, 1C, C^5-H, Dipp), 130.7 (s, 1C, C^4-H, Dipp), 132.2 (s, 1C, C^1, Dipp), 146.0 (s, 1C, C^2, Dipp), 146.5 (s, 1C, C^6, Dipp), 211.4 (br s, $\Delta\nu_{1/2}$ = 9 Hz, 1C, CO), 215.7 (s, 1C, NC^2).

$^{29}Si\{^1H\}$-NMR (99.36 MHz, (D_8)toluene, 243 K): δ (ppm) = 14.9 (s, 1Si, *Si*(caac^{Me})).

^1H-^{15}N HMBC (500.17, 50.68 MHz, (D_8)toluene, 243 K): δ_N (ppm) = 228.7 (s, 1N, *N*C^2).

4.5 Modified syntheses of literature known compounds

4.5.1 *N*-(Dipp)-2-methylpropan-1-imine

A 2 L three-neck round-bottom flask equipped with a mechanical stirrer (KPG), a 250 mL dropping funnel and an argon inlet was charged with *para*-toluenesulfonic acid monohydrate (7.564 g, 39.8 mmol, 0.075 equiv.) and magnesiumsulphate (127.64 g, 1.06 mol, 2.00 equiv.). The apparatus was spilled multiple times with argon (atleast 3x) and 370 mL of dry dichloromethane was added. The suspension was stirred for 10 min at ambient temperature and 100.0 mL of red diisopropylaniline (ρ = 0.94 g/mL, 94 g, 530 mmol, 1.0 equiv.) was added dropwise over 1 h at ambient temperature. Upon addition the color of the supernatant solution changed to pale pink. After stirring for additional 10 min at ambient temperature 100.2 mL of isobutrylaldehyde (ρ = 0.79 g/mL, 79.2 g, 1.098 mol, 2.07 equiv.) was added dropwise for 1.5 h to the suspension. The reaction mixture was stirred for 20 h at ambient temperature. An aliquote of the reaction mixture was taken and analyzed by ^{1}H NMR spectroscopy in (D)chloroform, revealing the selective formation of the imine.[45] The white suspension was filtered with two filtercanulas under argon atmosphere and the product reextracted with 2 x 100 mL of dry dichloromethane. The combined organic extracts were concentrated under vacuum (0.1 mbar) for 1 h at 60 °C. The obtained pale yellow solution was destilled under dynamic vacuum (< 0.1 mbar) at an oil bath temperature of 120 –140°C using a Vigreux column. Fractions of the analytically pure product (101.2 g) were collected at a head temperature of 110°C as a colorless moderately viscos liquid. Using the heat gun (180°C) a second crop (4.30 g) of the product could be obtained at a head temperature of 125°C (< 0.1 mbar).[46] Yield: 101.02 g (475 mmol, 77 %).

^{1}H NMR (300.13 MHz, (D)chloroform, 298 K): δ (ppm) = 1.16 (d, ^{3}J(H,H) = 6,9 Hz, 12H, C^{2,6}-CH*Me*$_2$, Dipp), 1.24 (d, ^{3}J(H,H) = 6,9 Hz, 6H, C^{2}H(C*H*$_3$)$_2$), 2.71 (sept, ^{3}J(H,H) = 6,9 Hz, ^{3}J(H,H) = 4,8 Hz, 1H, C^{2}*H*Me$_2$), 2.92 (sept, ^{3}J(H,H) = 6,9 Hz, 2H, C^{2,6}-C*H*Me$_2$, Dipp), 7.13–3.83 (m, 3H, C^{3,4,5}-*H*, Dipp), 7.52 (d, ^{3}J(H,H) = 4.8 Hz, 1H, NC^{1}*H*).

^{15}N{^{1}H} NMR (50.69 MHz, (D)chloroform, 298 K): δ_N (ppm) = 328,2 (s, 1N, *N*C^{1}H).

---

45 The reaction is already complete after 2.5 h at ambient temperature. Longer stirring is not necessary for the completion of the reaction.

46 The second crop provided a purity of 88%, according ^{1}H NMR spectroscopy in (D)chloroform and was stored separately. It was combined with second crops of previous syntheses and redistilled at a later point.

4.5.2 *N*-(Dipp)-2,2,4-trimethylpent-4-en-1-imine

Lithiumdiisopropylamide was prepared in *situ*. In a 1 L Schlenk flask diisopropylamine (ρ = 0.72 g/mL, 30.67 g, 478.3 mmol, 1.00 Äq.) was dissolved in 660 mL of diethylether and cooled to –78 °C. 197.4 mL *n*-butyllithium in *n*-hexane (2,5 M, 493.5 mmol, 1,03 Äq.) was added dropwise over the course of 1 h to the reaction mixture at –78 °C. Stirring at this temperature was continued for another 0.5 h, the cooling bath was removed and the reaction mixture brought to ambient temperature. The reaction mixture was stirred for 1 h at ambient temperature before it was used for the following reaction step.

In a 1 L Schlenk flask 110.0 g of *N*-(Dipp)-2-methylpropanimine (475.4 mmol, 1.0 equiv.) was dissolved in 330 mL of diethylether and cooled to –78 °C. The prepared LDA solution mentioned above was cooled again to –78 °C and added dropwise over 2 h to the N-(Dipp)-2-methylproanimine solution at –78 °C. In the course of the addition of the LDA solution white precipitate was observed, which redesolved at the end of the addition. The reaction mixture was stirred for 0.5 h at –30 °C, then the cooling bath was removed and the reaction mixture brought to ambient temperature. After stirring at ambient temperature for 3 h the reaction mixture was evaporated and dried under high vacuum for 1 h at 50 °C. The yellow sticky crude material was redesolved in 660 mL of diethylether and cooled to –20 °C. A solution of 51.2 mL 3-chlor-2-methylpropene (57.35 g, ρ = 0,920 g/mL, 523 mmol, 1.10 equiv.) in 367 mL of diethylether was added dropwise for 2 h at –20 °C. The reaction mixture was stirred for 0.5 h at –20 °C. The cooling bath was removed and the reaction mixture brought to ambient temperature. After 22 h stirring at ambient temperature a pale yellow suspension formed. An aliquote of the reaction mixture was taken and analyzed by ^{1}H NMR spectroscopy in (D_6)benzene, revealing the quantitative formation of the en-imine. The reaction mixture was evaporated and dried under fine vacuum of 0.5 h at 30 °C. The yellow residue was extracted with 730 mL of petrolether. The yellowish extract was evaporated. After drying under fine vacuum for 1 h at 40 °C the *N*(Dipp)-2,2,4-trimethylpent-4-en-1-imine was obtained as a pale yellow oily liquid in NMR spectroscopic pure form. Yield : 135.72 g (475.4 mmol, quantitative).

^{1}H NMR (500.17 MHz, (D_6)benzene, 298 K): δ (ppm) = 1.16 (s, 6H, $C^{2}Me_2$), 1,18 (d, ^{3}J(H,H) = 6.9 Hz, 12H, $C^{2,6}$-CHMe_2, Dipp), 2.18 (d, ^{4}J(H,H) = 0.5 Hz, 2H, $C^{3}H_2$), 1,67 (dd, ^{4}J(H,H) = 0.9 Hz, ^{4}J(H,H) = 0.5 Hz, 3H, C^{4}-*Me*), 3.07 (sept, ^{3}J(H,H) = 6,9 Hz, 2H, $C^{2,6}$-C*H*Me_2, Dipp), 4.88 – 4.72 (m, 2H, $C^{5}H_2$), 7.14 – 7.07 (m, 3H, $C^{3,4,5}$-*H*, Dipp), 7.37 (s, 1H, NC^{1}*H*).

^{1}H NMR (500.17 MHz, (D)chloroform, 298 K): δ (ppm) = 1.21 (d, ^{3}J(H,H) = 6.9 Hz, 12H, $C^{2,6}$-CH*Me*$_2$, Dipp), 1.31 (s, 6H, C^{2}*Me*$_2$), 1.87 (s, 3H, C^{4}-*Me*), 2.36 (s, 2H, $C^{3}H_2$), 2.97 (sept, ^{3}J(H,H) = 6.9 Hz, 2H, $C^{2,6}$-C*H*Me$_2$, Dipp), 4.81 (m, 1H, $C^{5}H_AH_B$), 4.95 (m, 1H, $C^{5}H_AH_B$), 7.06 – 7.17 (m, 3H, C^{4}-*H* + $C^{3,5}$-*H*, Dipp), 7.62 (s, 1H, *C*^{1}-H, N=CH).

^{13}C{^{1}H} NMR (125.77 MHz, (D$_6$)benzene, 298 K): δ (ppm) = 23.6 (s, 4C, $C^{2,6}$-CH*Me*$_2$, Dipp), 25.05 (s, 1C, C^{4}-*Me*), 25,12 (s, 2C, C^{2}*Me*$_2$), 27.9 (s, 2C, *C*^{2,6}-*C*HMe$_2$, Dipp), 40,8 (s, 1C, *C*^{2}Me$_2$), 47.7 (s, 1C, *C*^{3}H$_2$), 115.2 (s, 1C, *C*^{5}H$_2$), 123.2 (s, 2C, *C*^{3,5}-H, Dipp), 124.2 (s, 1C, *C*^{4}-H, Dipp), 137.4 (s, 2C, *C*^{2,6}, Dipp), 142.5 (s, 1C, *C*^{4}), 149.5 (s, 1C, *C*^{1}, Dipp), 172.8 (s, 1C, N*C*^{1}H).

^{1}H-^{15}N HMBC (500.17 MHz, 50.68 MHz, (D$_6$)benzene, 298 K): δ_N (ppm) = 330.5 (s, 1N, *N*C^{1}H).

4.5.3 *N*-(Dipp)-2,2,4-trimethylpent-4-en-1-iminiumchloride

A 2 L three-neck round-bottom flask equipped with a mechanical stirrer (KPG), a 250 mL dropping funnel and an argon inlet was charged with *N*-(Dipp)-2,2,4-trimethylpent-4-en-1-imine (135.715 g, 475.4 mmol, 1.00 equiv.) and 375 mL petrolether and cooled to –78 °C. 110 mL of a HCl-solution in diethylether (30.7 w%, 722.6 mmol, 1.52 equiv.) was added dropwise to the reaction mixture at –78 °C for 1 h. During the HCl-addition the formation of a colorless precipitate was observed. The reaction mixture was stirred for 0.5 h at –78°C. The cooling bath was removed and the reaction mixture brought to ambient temperature. After 1.5 h stirring at ambient temperature the white suspension was evaporated. Drying at fine vacuum for 1 h at 30 °C afforded the iminiumchloride as a white solid in analytically pure form. Yield: 153.1 g (475.4 mmol, quantitative).

Properties: Airstable colorless solid. Insoluble in aliphatic solvents, well soluble in $CHCl_3$ and CH_2Cl_2.

Elemental analysis: $C_{20}H_{32}NCl$ (321.93 g·mol^{-1}): calcd./%: C 74.62; H 10.02; N 4.35; found/%: C 74.30; H 9.96; N 4.22.

^{1}H NMR (300.13 MHz, (D)chloroform, 298 K): δ (ppm) = 1.22 (d, ^{3}J(H,H) = 6.9 Hz, 12H, $C^{2,6}$-CH*Me*$_2$, Dipp), 1.67 (s, 6H, C^{2}*Me*$_2$), 1.82 (s, 3H, C^{4}-*Me*), 2.52 (s, 2H, $C^{3}H_2$), 2.93 (sept, ^{3}J(H,H) = 6.9 Hz, 2H, $C^{2,6}$-C*H*Me$_2$, Dipp), 4.77 (s, 1H, $C^{5}H_AH_B$), 4,98 – 4,97 (m, 1H, $C^{5}H_AH_B$), 7.20 (d, ^{3}J(H,H) = 7,8 Hz, 2H, $C^{3,5}$-*H*, Dipp), 7.35 (t, ^{3}J(H,H) = 7,8 Hz, 1H, C^{4}-*H*, Dipp), 7.97 (s, 1H, NC^{1}*H*), 16.70 (s, 1H, N*H*).

$^{13}C\{^1H\}$ NMR (125.78 MHz, (D)chloroform, 298 K): δ (ppm) = 23.5 (s, 4C, $C^{2,6}$-CHMe_2, Dipp), 24.6 (s, 1C, C^4-*Me*), 25.9 (s, 2C, C^2Me_2), 28.5 (s, 2C, $C^{2,6}$-*C*HMe_2, Dipp), 42.5 (s, 1C, $C^2(CH_3)_2$), 48.1 (s, 1C, C^3H_2), 116.5 (s, 1C, $C^5H_AH_B$), 124.2 (s, 2C, $C^{3,5}$-H, Dipp), 125.2 (s, 1C, C^1, Dipp), 130.2 (s, 1C, C^4-H, Dipp), 140.5 (s, 1C, C^4), 142.6 (s, 2C, $C^{2,6}$, Dipp), 188.5 (s, 1C, NC^1H).

4.5.4 N-(Dipp)-2,2,4,4-tetramethyl-3,4-dihydro-pyrrol-1-ium-chlorid ([caac^{Me}H]Cl)

N-(Dipp)-2,2,4-trimethylpent-4-en-1-iminiumchlorid (153.1 g, 475.4 mmol, 1.00 equiv.) was dissolved in 700 mL of chloroform. The white suspension was stirred for 22 h at 55 °C. An aliquote of the reaction mixture was analyzed by ^{1}H NMR spectroscopy in (D)chloroform, revealing the selective formation of [caac^{Me}H]Cl. The suspension was filtered. The yellowish filtrate was concentrated under vacuum to a volume approx. 250 mL, upon which a colorless white solid started to precipitate. 300 mL of diethylether was added and the resulting suspension filtered. The crude product was washed with 3 x 100 mL of chloroform/Et_2O (1:1) mixture. Drying under fine vacuum at 60 °C for 62 h, afforded [caac^{Me}H]Cl as coloroless white solid in analytically pure form. Yield: 126.7 g (393.5 mmol, 82.8 %).

Properties: Airstable colorless solid.

Elemental analysis: $C_{20}H_{32}NCl$ (321.93 g·mol^{-1}): calcd./%: C 74.62; H 10.02; N 4.35; found/%: C 74.72; H 10.00; N 4.25 %. **Melting point:** 198 °C(dec).

^{1}H NMR (300.13 MHz, (D)chloroform, 298 K): δ (ppm) = 1.10 (d, ^3J(H,H) = 6.8 Hz, 6H, $C^{2,6}$-CHMe_AMe$_B$, Dipp), 1.22 (d, ^3J(H,H) = 6.8 Hz, 6H, $C^{2,6}$-CHMe$_A$$Me_B$, Dipp), 1.43 (s, 6H, C^5Me_2), 1.60 (s, 6H, C^3Me_2), 2.31 (s, 2H, C^4H_2), 2.53 (sept, ^3J(H,H) = 6,8 Hz, 2H, $C^{2,6}$-C*H*$(CH_3)^A(CH_3)^B$, Dipp), 7,20 (d, ^3J(H,H) = 7,8 Hz, 2H, $C^{3,5}$-*H*, Dipp), 7,38 (t, ^3J(H,H) = 7.8 Hz, 1H, C^4-*H*, dipp), 11.00 (s, 1H, C^2-*H*).

^{1}H NMR (300.13 MHz, (D_3)acetonitrile, 298 K): δ (ppm) = 1.13 (d, ^3J(H,H) = 6.7 Hz, 6H, $C^{2,6}$-CHMe_AMe$_B$, Dipp), 1.33 (d, ^3J(H,H) = 6.7 Hz, 6H, $C^{2,6}$-CHMe$_A$$Me_B$, Dipp), 1.49 (s, 6H, C^5Me_2), 1.61 (s, 6H, C^3Me_2), 2.41 (s, 2H, C^4H_2), 2.73 (sept, ^3J(H,H) = 6.7 Hz, 2H, $C^{2,6}$-C*H*Me$_A$Me$_B$, Dipp), 7.43-7.45 (m, 2H, $C^{3,5}$-*H*, Dipp), 7.55-7.62 (m, 1H, C^4-*H*, dipp), 10.51 (s, 1H, C^2-*H*).

$^{13}C\{^1H\}$ NMR (125.78 MHz, (D)chloroform, 298 K): δ (ppm) = 21.8 (s, 2C, $C^{2,6}$-CHMe_AMe$_B$, Dipp), 26.46 (s, 2C, $C^{2,6}$-CHMe$_A$$Me_B$, Dipp), 26.48 (s, 2C, C^3Me_2), 28.2 (s, 2C, C^5Me_2), 29.7 (s, 2C, $C^{2,6}$-*C*HMe$_A$Me$_B$, Dipp), 48.2 (s, 1C, C^3), 49.1 (s, 1C, C^4H_2), 82.9 (s, 1C, C^5), 124,9 (s, 2C, $C^{3,5}$-H, Dipp), 128.7 (s, 1C, C^1, Dipp), 131.5 (s, 1C, C^4-H, Dipp), 144,2 (s, 2C, $C^{2,6}$, Dipp), 194.3 (s, 1C, NC^2H).

$^{15}N\{^1H\}$ NMR (50.69 MHz, (D)chloroform, 298 K): δ (ppm) = 231.0 (s, 1N, *N*C^2H).

4.5.5 caac^{Me} carbene

30.0 g of [caac^{Me}H]Cl salt (93.2 mmol, 1.0 equiv.) and 10.08 g of lithiumdiisopropylamide (94.1 mmol, 1.01 equiv.) were mixed in a 500 mL Schlenk tube. 350 mL of precooled THF (–78 °C) was added at –78 °C. The white suspension was stirred for 0.5 h at –78 °C. The cooling bath was removed and the reaction mixture brought to ambient temperature, upon which a yellowish milky suspension formed. An aliquote of the reaction mixture was taken and analyzed by ^{1}H NMR spectroscopy in (D_6)benzene, revealing the quantitative formation of caac^{Me} carbene. The reaction mixture was evaporated and dried for 1 h at 40 °C under fine vacuum. The yellowisch residue was extracted with 300 mL of *n*-hexane and 2 x 50 mL of *n*-hexane. The combined organic phases were evaporated and dried under fine vacuum for 0.5 h at 50 °C. The crude product was redesolved in 40 mL of *n*-hexane. After storing at –60 °C for 20 h a colorless microcrystalline solid was obtained, which was removed from the yellowish liquor upon filtration at –60 °C. Drying at the fine vacuum for 1 h at 40 °C afforded caac^{Me} carbene as a colorless solid in analytically pure form. Yield: 19.82 g (69.4 mmol, 75 %).

Properties: Colorless air and moisture sensitive solid. Well soluble in *n*-hexane, benzene and THF.

Elemental analysis: $C_{20}H_{31}N$ (285.47 g·mol^{-1}): calcd./%: C 84.15; H 10.95; N 4.91; found/%: C 83.61; H 10.99; N 4.74 %. **Melting point:** 86 °C (partial dec).

^{1}H NMR (500.17 MHz, (D_6)benzene, 298 K): δ (ppm) = 1.07 (s, 6H, C^{5}*Me$_2$*), 1.20 (d, 6H, ^{3}J(H,H) = 6.8 Hz, C^{2,6}-CH*Me$_A$*Me$_B$, Dipp), 1.23 (d, 6H, ^{3}J(H,H) = 6.8 Hz, C^{2,6}-CHMe$_A$*Me$_B$*, Dipp), 1.43 (s, 6H, C^{3}*Me$_2$*), 1.53 (s, 2H, C^{4}*H$_2$*), 3.13 (sept, 2H, ^{3}J(H,H) = 6.8 Hz, C^{2,6}-C*H*Me$_A$Me$_B$, Dipp), 7.13 (m, 2H, C^{3,5}-*H*, Dipp), 7.21 (m, 1H, C^{4}-*H*, Dipp).

^{1}H NMR (500.17 MHz, (D_8)THF, 298 K): δ (ppm) = 1.03 (d, 6H, ^{3}J(H,H) = 6.8 Hz, C^{2,6}-CH*Me$_A$*Me$_B$, Dipp), 1.28 (s, 6H, C^{5}*Me$_2$*), 1.29 (d, 6H, ^{3}J(H,H) = 6.8 Hz, C^{2,6}-CHMe$_A$*Me$_B$*, Dipp), 1.31 (s, 6H, C^{3}*Me$_2$*), 1.77 (s, 2H, C^{4}*H$_2$*), 3.08 (sept, 2H, ^{3}J(H,H) = 6.8 Hz, C^{2,6}-C*H*Me$_A$Me$_B$, Dipp), 7.20-7.22 (m, 2H, C^{3,5}-*H*, Dipp), 7.25-7.28 (m, 1H, C^{4}-*H*, Dipp).

^{13}C{^{1}H} NMR (125.77 MHz, (D_6)benzene, 298 K): δ (ppm) 21.8 (s, 2C, C^{2,6}-CHMe$_A$*Me$_B$*, Dipp), 26.1 (s, 2C, C^{2,6}-CH*Me$_A$*Me$_B$, Dipp), 28.1 (s, 2C, C^{3}*Me$_2$*), 29.1 (s, 2C, C^{5}*Me$_2$*), 29.4 (s, 2C, C^{2,6}-*C*HMe$_A$Me$_B$, Dipp), 50.6 (s, 1C, *C*^{4}H$_2$), 58.1 (s, 1C, *C*^{3}Me$_2$), 82.5 (s, 1C, *C*^{5}Me$_2$), 123.8 (s, 2C, *C*^{3,5}-H, Dipp), 128.1 (s, 1C, *C*^{4}-H, Dipp), 137.9 (s, 1C, *C*^{1}, Dipp), 146.1 (s, 2C, *C*^{2,6}-CHMe$_A$Me$_B$, Dipp), 313.5 (s, 1C, N*C*^{2}); The ^{13}C NMR chemical shifts of caac^{Me} given in (D_6)benzene compare well with those reported in ref. [57]

$^{13}C\{^1H\}$ NMR (125.77 MHz, (D_8)THF, 298 K): δ (ppm) = 21.9 (s, 2C, $C^{2,6}$-$CHMe_AMe_B$, Dipp), 26.2 (s, 2C, $C^{2,6}$-$CHMe_AMe_B$, Dipp), 28.2 (s, 2C, C^3Me_2), 29.6 (s, 2C, C^5Me_2), 29.9 (s, 2C, $C^{2,6}$-$CHMe_AMe_B$, Dipp), 51.1 (s, 1C, C^4H_2), 58.5 (s, 1C, C^3Me_2), 83.4 (s, 1C, C^5Me_2), 124.1 (s, 2C, $C^{3,5}$-H, Dipp), 128.4 (s, 1C, C^4-H, Dipp), 138.4 (s, 1C, C^1, Dipp), 146.6 (s, 2C, $C^{2,6}$-$CHMe_AMe_B$, Dipp), 314.2 (s, 1C, NC^2).

^1H-^{15}N HMBC (500.17 MHz, 50.68 MHz, (D_6)benzene, 298 K): δ_N (ppm) = 220.6 (s, 1N, NC^2).

4.5.6 $SiBr_4(caac^{Me})$

In a 1 L Schlenk tube 19.8 g $caac^{Me}$ carbene (69.4 mmol, 1.00 equiv.) were dissolved in 300 mL of *n*-hexane and cooled to –78 °C. A solution of 8.7 mL $SiBr_4$ (d = 2.80 g/mL, 70.1 mmol, 1.01 equiv.) in 200 mL of *n*-hexane was added dropwise over the course of 3 h at –78 °C. During the addition a voluminous, white solid precipitated. The reaction mixture was then allowed to warm to ambient temperature, the precipitate was filtered off using a filter-cannula (∅ = 2 mm) and dried under fine vacuum for 5 h at 40 °C to obtain $SiBr_4(caac^{Me})$ as white powder. Yield: 41.36 g (65.3 mmol, 94%).

Properties: Air and highly moisture sensitive white powder. The compound is sparingly soluble in benzene and well soluble in CH_2Cl_2. However, in CH_2Cl_2 solution the compound decomposes gradually at ambient temperature, its colorless solution turning yellow. Therefore, the NMR spectroscopic characterization of $SiBr_4(caac^{Me})$ in (D_2)dichloromethane was carried out at low temperature to slow down the decomposition.

^1H NMR (500.17 MHz, (D_6)benzene, 298 K): δ (ppm) = 0.97 (s, 6H, C^5Me_2), 1.00 (d, 6H, ^3J(H,H) = 6.5 Hz, $C^{2,6}$-$CHMe_AMe_B$, Dipp), 1.42 (s, 2H, C^4H_2), 1.58 (d, 6H, ^3J(H,H) = 6.5 Hz, $C^{2,6}$-$CHMe_AMe_B$, Dipp), 2.05 (s, 6H, C^3Me_2), 3.06 (sept, 2H, ^3J(H,H) = 6.5 Hz, $C^{2,6}$-$CHMe_AMe_B$, Dipp), 7.01 – 7.03 (m, 2H, $C^{3,5}$-H, Dipp), 7.05 – 7.08 (m, 1H, C^4-H, Dipp).

^1H NMR (500.17 MHz, (D_2)dichloromethane, 243 K): δ (ppm) = 1.31 (br d, 6H, ^3J(H,H) = 6.5 Hz, $C^{2,6}$-$CHMe_AMe_B$, Dipp), 1.32 (br d, 6H, ^3J(H,H) = 6.5 Hz, $C^{2,6}$-$CHMe_AMe_B$, Dipp), 1.67 (s, 6H, C^5Me_2), 1.99 (s, 6H, C^3Me_2), 2.61 (br, 2H, $C^{2,6}$-$CHMe_AMe_B$, Dipp), 2.67 (s, 2H, C^4H_2), 7.39 (br d, 2H, $C^{3,5}$-H, Dipp), 7.61 (br t, 1H, C^4-H, Dipp).

$^{13}C\{^1H\}$ NMR (75.48 MHz, (D_2)dichloromethane, 213 K): δ (ppm) = 24.5 (s, 2C, $C^{2,6}$-$CHMe_AMe_B$, Dipp), 25.9 (s, 2C, $C^{2,6}$-$CHMe_AMe_B$, Dipp), 28.4 (s, 2C, C^5Me_2), 28.9 (s, 2C, $C^{2,6}$-$CHMe_AMe_B$, Dipp), 29.8 (s, 2C, C^3Me_2), 49.2 (s, 1C, C^4H_2), 56.7 (s, 1C, C^3Me_2), 87.7 (s, 1C, C^5Me_2), 126.6 (s, 2C, $C^{3,5}$-H, Dipp), 129.2 (s, 1C, C^1, Dipp), 132.5 (s, 1C, C^4-H, Dipp), 144.2 (s, 2C, $C^{2,6}$-$CHMe_AMe_B$, Dipp), 197.7 (s, 1C, NC^2).

$^{29}Si\{^1H\}$ NMR (59.63 MHz, (D_6)benzene, 298 K): δ (ppm) = –195.3 (s, 1Si).

$^{29}Si\{^1H\}$ NMR (59.63 MHz, (D_2)dichloromethane, 213 K): δ (ppm) = –54.9 (s, 1Si).

^{1}H-^{15}N HMBC (500.17 MHz, 50.68 MHz, (D_6)benzene, 298 K): δ_N (ppm) = 213.1 (s, 1N, *N*C^2).

^{1}H-^{15}N HMBC (500.17 MHz, 50.68 MHz, (D_2)dichloromethane, 243 K): δ_N (ppm) = 256.8 (s, 1N, *N*C^2).

4.5.7 Si(caac^{Me})$_2$

To a red solution of 0.700 g of $SiBr_2$(caac^{Me}) (**1**) (1.479 mmol, 1.00 equiv.) in 10 mL of benzene a colorless solution of 0.422 g caac^{Me} carbene (1.479 mmol, 1.00 equiv.) in 10 mL benzene was added dropwise in 10 min at ambient temperature. A dark blue solution formed immediately. An aliquot of the reaction mixture was taken and analyzed by ^{1}H NMR spectroscopy in (D_6)benzene, revealing the selective formation of $SiBr_2$(caac^{Me})$_2$ alongside 25 mol% of caac^{Me} and 25 mol% $SiBr_2$(caac^{Me}).[47] After 10 min at ambient temperature the reaction mixture was evaporated and dried under fine vacuum for 1 h at 40 °C. To the dark blue solid 0.440 g of KC_8 was added (3.25 mmol, 2.2 equiv.) and the two solids mixed vigorously. 40 mL of THF was condensed via condensation bridge to the solid mixture. The reaction mixture was brought to –78 °C and stirred for 0.5 h at that temperature. The cooling bath was removed and the reaction mixture brought to ambient temperature. 5 h at ambient temperature an aliquote was taken and analyzed by ^{1}H NMR spectroscopy in (D_6)benzene, revealing the selective formation of Si(caac^{Me})$_2$, alongside tiny amounts of (caac^{Me}H)$_2$O and the literature known over-reduction product **II-71**.[120] The reaction mixture was evaporated and dried under fine vacuum for 0.5 h at 40 °C. The black residue was extracted with 60 mL of *n*-hexane and 5 x 5 mL of benzene. The combined dark blue extracts were evaporated and dried under fine vacuum for 0.5 h at 40 °C. The crude product was dissolved in 6 mL of *n*-hexane. After storing at –60 °C for 19 h dark blue crystals were obtained, which were removed from the dark blue mother liquor upon filtration at –60 °C. Drying at fine vacuum for 1 h at 40 °C afforded Si(caac^{Me})$_2$ in anaylitcal pure form. Yield: 0.722 g (1.21 mmol, 81 %). **Elemental analysis:** $C_{40}H_{62}N_2Si$ (599.0 g·mol^{-1}): calcd./%: C 80.20, H 10.44, N 4.68; found/%: 79.59, H 10.37, N 4.51 %.

^{1}H NMR (500.17 MHz, (D_6)benzene, 298 K): δ (ppm) = 0.99 (s, 6H, 2 × C^5*Me$_A$*Me$_B$), 1.06 (broad d, 6H, 2 × C^2-CH$_A$*Me$_A$*Me$_B$, Dipp), 1.19 (overlapped doublet and singlet, 12 H, 2 × C^2-CH$_A$Me$_A$*Me$_B$*, Dipp + 2 × C^{5}Me$_A$*Me$_B$*), 1.29 (broad d, 6H, 2 × C^6-CH$_B$*Me$_C$*Me$_D$, Dipp), 1.48 (broad d, 6H, 2 × C^6-CH$_B$Me$_C$*Me$_D$*, Dipp), 1.73 (s, 6H, 2 × C^3*Me$_A$*Me$_B$), 1.76 (s, 6H, 2 × C^{3}Me$_A$*Me$_B$*), 1.87 (m, 4H, 2 × C^4*H$_2$*), 2.67 (broad sept, 2H, 2 × C^2-C*H$_A$*Me$_A$Me$_B$,

[47] The compounds are in a dynamic equilibrium with each other. The equilibrium constant could be obtained from Isothermal Titration Calorimetry (*section 5.4.4*), as well Van't Hoff analysis of recored VT ^{1}H NMR spectra, see reference [175].

Dipp), 3.16 (broad sept, 2H, 2 × C^6-$CH_B$$Me_C$$Me_D$, Dipp), 7.07 (broad d, 2 H, 2 × C^5-*H*, Dipp), 7.13 (broad d, 2 H, 2 × C^3-*H*, Dipp), 7.17 (t, 2 H, ^3J(H,H) = 7.5 Hz, 2 × C^4-*H*, Dipp).

^{1}H NMR (500.17 MHz, (D_8)THF, 298 K): δ (ppm) = 0.73* (d, ^3J(H,H) = 6.4 Hz, 6H,2 × C^2-$CH_A$$Me_A$$Me_B$, Dipp), 1.08* (overlapped doublet and signlet, 12H, 2 × C^2-$CH_A$$Me_A$$Me_B$, Dipp and 2 × C^5-$Me_A$$Me_B$), 1.21* (d, ^3J(H,H) = 6.5 Hz, 6H, 2 × C^6-$CH_B$$Me_C$$Me_D$, Dipp),1.24 (d, 6H, ^3J(H,H) = 6.6 Hz, 2 x C^6-$CH_B$$Me_C$$Me_D$, Dipp), 1.29* (s, 6H, 2 × $C^5$$Me_A$$Me_B$), 1.60* (s, 6H, 2 × $C^3$$Me_A$$Me_B$), 1.74* (s, 6H, 2 × $C^3$$Me_A$$Me_B$ overlapping with the signal of the deuterated solvent), 1.98* (d, ^2J(H,H) = 12.0 Hz, 2H, 2 × $C^4$$H_A$$H_B$), 2.08* (d, ^2J(H,H) = 12.0 Hz, 2H, 2 × C^4-$H_A$$H_B$), 2.53* (sept, ^3J(H,H) = 6.4 Hz, 2H, 2 × C^2-$CH_A$$Me_A$$Me_B$, Dipp) 3.05* (sept, ^3J(H,H) = 6.5 Hz, 2H, 2 × C^6-$CH_B$$Me_C$$Me_D$, Dipp), 6.91-6.92* (m, 2H, 2 × C^3-*H*, Dipp), 7.04-7.07* (m, 4H, 2 × C^5-*H*, 2 × C^4-*H*, Dipp).

^{13}C{^{1}H} NMR (125.77 MHz, (D_6)benzene, 298 K, ppm): δ = 24.4** (s, 2C, 2 × C^2-CH$Me_A$$Me_B$, Dipp), 25.2** (s, 2C, 2 × C^6-CH$Me_C$$Me_D$, Dipp), 27.8** (s, 2C, 2 × C^2-CH$Me_A$$Me_B$, Dipp), 27.9** (s, 2C, 2 × C^6-CH$Me_C$$Me_D$, Dipp), 28.3** (s, 2C, 2 × C^2-*C*H$Me_A$$Me_B$, Dipp), 29.5** (s, 2C, 2 × $C^5$$Me_A$$Me_B$), 29.9** (s, 2C, 2 × C^6-*C*H$Me_C$$Me_D$, Dipp), 31.4** (s, 2C, 2 × $C^3$$Me_A$$Me_B$), 36.1 (s, 2C, 2 × $C^3$$Me_A$$Me_B$), 48.5** (s, 2C, 2 × $C^3$$Me_A$$Me_B$), 57.7** (s, 2C, 2 × C^4H_2), 68.8** (s, 2C, 2 × $C^5$$Me_A$$Me_B$), 124.9** (s, 2C, 2 × C^5-H, Dipp), 125.4** (s, 2C, 2 × C^3-H, Dipp), 136.2** (s, 2C, 2 × C^1, Dipp), 148.5** (s, 2C, 2 × C^6, Dipp), 148.9** (s, 2C, 2 × C^2, Dipp), 210.9 (s, 2C, 2 × NC^2).

^{13}C{^{1}H} NMR (125.77 MHz, (D_8)THF, 298 K): δ (ppm) = 24.5 (s, 2C, 2 × C^6-$CH_B$$Me_C$$Me_B$,Dipp), 25.1 (s, 2C, 2 × C^2-$CH_A$$Me_A$$Me_B$, Dipp overlapping with the signal of the deuterated solvent), 28.0 (s, 2C, 2 × C^6-$CH_B$$Me_C$$Me_D$, Dipp), 28.1 (s, 2C, 2 × C^2-$CH_A$$Me_A$$Me_B$, Dipp), 28.8 (s, 2C, 2 × C^6-*C*H$_B$Me$_C$Me$_D$, Dipp), 29.9 (s,4C, 2 × C^2-*C*$H_A$$Me_A$$Me_B$, Dipp and 2 × $C^5$$Me_A$$Me_B$), 30.3 (s, 2C, $C^5$$Me_A$$Me_B$), 31.6 (s, 2C, 2 × $C^3$$Me_A$$Me_B$), 36.4 (s, 2C, 2 × $C^3$$Me_A$$Me_B$), 49.1 (s, 2C, 2 × C^3), 58.3 (s, 2C, 2 × $C^4$$H_A$$H_B$), 69.4 (s, 2C, 2 × C^5), 125.1 (s, 2C, 2 × C^5–H, Dipp), 125.5 (s,2C, 2 × C^3-H, Dipp), 128.0 (s, 2C, 2 × C^4–H, Dipp), 136.7 (s, 2C, C^1, Dipp), 149.0 (s, 2C, 2 × C^6, Dipp), 149.3 (s, 2C, 2 × C^2, Dipp), 211.5 (s, 2C, 2 × NC^2).

^{29}Si{^{1}H} NMR (99.37 MHz, (D_6)benzene, 243 K): δ (ppm) = 66.5 (s, 1Si, *Si*(caac^{Me})).

^{1}H-^{15}N HMBC (500.17 MHz, 50.68 MHz, (D_6)benzene, 243 K): $δ_N$ (ppm) = 153.2* (2N, 2 × *N*C^2).

The ^{1}H, ^{13}C{^{1}H} and ^{29}Si{^{1}H} NMR spectroscopic data of Si(caac^{Me})$_2$ in (D_6)benzene compares well to that given in the reference [119]. Signals marked with asterisk (*) were not reported in the reference and signals marked with double asterisk (**) were not assigned.

4.5.8 $Si_2(caac^{Me})_2$

500 mg of $SiBr_2(caac^{Me})$ (**1**) (1.056 mmol, 1.00 equiv.) and 336 mg of KC_8 (2.48 mmol, 2.35 equiv.) were suspended in 20 mL of benzene. After 0.5 h at ambient temperature the reaction mixture changed red-purple. The reaction mixture was stirred overnight at ambient temperature. After 24 h at ambient temperature an aliquot was taken and analyzed by ^{1}H NMR spectroscopy in (D_6)benzene revealing the selective formation of $Si_2(caac^{Me})_2$. The reaction mixture was filtered and the black graphite residue extracted with 3 x 10 mL of benzene. The combined dark purple filtrates were evaporated and dried at the fine vacuum for 1 h at 40 °C. The dark purple residue was redesolved in 3 mL of *n*-pentane. After storing for 19 h at –60 °C the microcrystalline product was separated from the dark purple mother liquor upon filtration at –60 °C. Dryring at fine vacuum for 1 h at 40 °C afforded $Si_2(caac^{Me})_2$ in analytically pure form. Yield: 198 mg (0.316 mmol, 60 %).

^{1}H NMR (500.17 MHz, (D_6)benzene, 298 K): δ (ppm) = 1.07 (s, 12H, 2 × C^5-*Me*$_2$), 1.20 (d, ^3J(H,H) = 6.7 Hz, 12H,2 × $C^{2,6}$-CH*Me*$_A$Me$_B$, Dipp), 1.68 (d, 12H, ^3J(H,H) = 6.7 Hz, 2 × $C^{2,6}$-CHMe$_A$*Me*$_B$, Dipp), 1.71 (s, 12H, 2 × C^3*Me*$_2$), 1.77 (s, 4H, 2 × C^4*H*$_2$), 3.12 (sept, ^3J(H,H) = 6.7 Hz, 4H, 2 × $C^{2,6}$-C*H*Me$_A$Me$_B$, Dipp), 7.08-7.09 (m, 4H, 2 × $C^{3,5}$-*H,* Dipp), 7.11-7.13 (m, 2H, 2 × C^4-*H*, Dipp).

^{13}C{^{1}H} NMR (125.77 MHz, (D_6)benzene, 298 K): δ (ppm) = 24.8** (s, 4C, 2 × $C^{2,6}$-CH$_A$*Me*$_A$Me$_B$, Dipp), 28.4** (s, 4C, 2 × $C^{2,6}$-CHMe$_A$*Me*$_B$, Dipp), 29.1** (s, 4C, 2 × $C^{2,6}$-*C*HMe$_A$Me$_B$, Dipp), 29.5** (s, 4C, C^5*Me*$_2$), 31.8** (s, 4C, 2 × C^3*Me*$_2$), 49.9** (s, 2C, 2 × *C*^{3}), 54.4** (s, 2C, 2 × *C*^{4}H$_2$), 71.2** (s, 2C, 2 × *C*^{5}), 125.3** (s, 4C, 2 × *C*^{3,5}–H, Dipp), 128.9** (s, 2C, 2 × *C*^{4}–H, Dipp), 134.9** (s, 2C, *C*^{1}, Dipp), 148.2** (s, 4C, 2 × *C*^{2,6}, Dipp), 236.3 (s, 2C, 2 × N*C*^{2}).

^{29}Si{^{1}H} NMR (99.37 MHz, (D_6)benzene, 298 K): δ (ppm) = 252.3 (s, 1Si, *Si*($caac^{Me}$)).

^{1}H-^{15}N HMBC (500.17 MHz, 50.68 MHz, (D_6)benzene, 298 K): δ_N (ppm) = 174.5* (2N, 2 × N*C*^{2}).

The ^{1}H, ^{13}C{^{1}H} and ^{29}Si{^{1}H} NMR spectroscopic data of $Si_2(caac^{Me})_2$ compares well to that given in the reference [116]. Signals marked with asterisk (*) were not reported in the reference and signals marked with double asterisk (**) were not assigned.

4.5.9 (caac^{Me}H)$_2$O

To a clear solution of 0.300 g of caac^{Me} carbene (1.05 mmol, 1.0 equiv.) in 5 mL of THF a solution of degassed water in THF (1.9 mL, 0.277 mol L^{-1}, 0.526 mmol, 0.50 equiv.) was added dropwise at ambient temperature. After stirring for 0.5 h at ambient temperature an aliquot of the reaction mixture was taken and analyzed by ^{1}H NMR spectrosocopy in (D$_6$)benzene, revealing the selective formation of (caac^{Me}H)$_2$O. After evaporation of the solvent the crude solid was redesolved in 6 mL of boiling *n*-pentane. After slowly cooling to ambient temperature, colorless single crystals were obtained, which were removed from the yellowish mother-liquor upon filtration. Drying at fine vacuum for 1 h at 40 °C afforded (caac^{Me}H)$_2$O in analytically pure form as a colorless powder. Yield: 0.120 g (0.173 mmol, 33 %).

^{1}H NMR (300.13 MHz, (D$_6$)benzene, 298 K): δ (ppm) = 0.73 (s, 6H, 2 x C^5*Me$_A$*Me$_B$), 0.83 (s, 6H, 2 x C^{5}Me$_A$*Me$_B$*), 1.21 (d, 6H, ^{3}*J*(H,H) = 6.8 Hz, C^2-CH$_A$*Me$_A$*Me$_B$, Dipp), 1.30 (s, 6H, 2 x C^3*Me$_A$*Me$_B$), 1.30 (d, 6H, ^{3}*J*(H,H) = 6.8 Hz, C^6-CH$_B$*Me$_C$*Me$_D$, Dipp), 1.40 (d, 6H, ^{3}*J*(H,H) = 6.8 Hz, 2 x C^2-CH$_A$Me$_A$*Me$_B$*, Dipp), 1.54 (s, 6H, 2 x C^{3}Me$_A$*Me$_B$*), 1.59 (d, ^{2}*J*(H,H) = 12.4 Hz, 2H, 2 x C^4*H$_A$*H$_B$), 1.62 (d, 6H, ^{3}*J*(H,H) = 6.8 Hz, 2 x C^6-CH$_B$Me$_C$*Me$_D$*, Dipp), 1.90 (d, ^{2}*J*(H,H) = 12.4 Hz, 2H, 2 x C^{4}H$_A$*H$_B$*), 3.15 (sept, 2H, ^{3}*J*(H,H) = 6.6 Hz, 2 x C^2-C*H$_A$*Me$_A$Me$_B$, Dipp), 4.19 (sept, 2H, ^{3}*J*(H,H) = 6.9 Hz, 2 x C^2-C*H$_B$*Me$_C$Me$_D$, Dipp), 4.84 (s, 2H, 2 x C^2*H*), 7.08-7.10 (m, 2H, 2 x C^4-*H*, Dipp), 7.19-7.22 (m, 4H, 2 x C^{3,5}-*H*, Dipp).

^{13}C{^{1}H} NMR (125.77 MHz, (D$_6$)benzene, 298 K): δ (ppm) = 24.9** (s, 2C, 2 x C^5*Me$_A$*Me$_B$), 25.20** (s, 2C, 2 x C^2-CH$_A$Me$_A$*Me$_B$*, Dipp), 25.4** (s, 2C, 2 x C^6-*C*H$_B$Me$_C$*Me$_D$*, Dipp), 25.6** (s, 2C, 2 x C^2-CH$_A$*Me$_A$*Me$_B$, Dipp), 26.9** (s, 2C, 2 x C^6-*C*H$_B$*Me$_C$*Me$_D$, Dipp), 27.8** (s, 2C, 2 x C^6-*C*H$_B$Me$_C$Me$_D$, Dipp), 28.1** (s, 2C, 2 x C^2-*C*H$_A$Me$_A$Me$_B$, Dipp), 28.4** (s, 2C, 2 x C^{5}Me$_A$*Me$_B$*), 32.3** (s, 2C, 2 x C^{3}Me$_A$*Me$_B$*), 33.8** (s, 2C, 2 x C^3*Me$_A$*Me$_B$), 42.4** (s, 2C, 2 x *C^3*), 61.4** (s, 2C, 2 x *C^5*), 61.6** (s, 1C, *C^4*H$_A$H$_B$), 101.5** (s, 2C, 2 x *C^2*-H), 124.3** (s, 2C, 2 x *C^3*-H, Dipp), 124.8** (s, 2C, 2 x *C^5*-H, Dipp), 127.2** (s, 2C, 2 x *C^4*-H, Dipp), 141.4** (s, 2C, 2 x *C^1*, Dipp), 148.8** (s, 2C, 2 X *C^2*, Dipp), 152.7** (s, 2C, 2 X *C^6*, Dipp).

^{1}H-^{15}N HMBC (500.17 MHz, 50.68 MHz, (D$_6$)benzene, 298 K): δ$_N$ (ppm) = 73.9* (s, 1N, *N*C^{2}H).

The ^{1}H and ^{13}C{^{1}H} NMR spectroscopic data of (caac^{Me}H)$_2$O compares well to that reported in the reference [124]. Signals marked with asterisk (*) were not reported in the reference and signals marked with double asterisk (**) were not assigned.

4.6 List of compounds prepared according to established procedures

Compound	Experimenter	Reference
$SiBr_4$	Gstrein	[314]
KC_8	Gstrein	[315,316]
$Na[B(C_6H_3\text{-}3,5\text{-}(CF_3)_2)_4]$	J. Tewes	[317,318]
$Li(EtO)_2[B(C_6F_5)_4]$	C. Lindlahr	[319]
$Ag_2B_{12}Cl_{12}$	C. Lindlahr	[320]
$Al(C_6F_5)_3$	J. Tewes	[281,282]
$LiSiTMS_3$	Gstrein	[321,322]
$LiPMes_2$	Gstrein	[323]
MesLi	Gstrein	[324]
EindLi	J. Tewes	[32]
$NaNTMS_2$	Filippou group members	[325]
NaOMes*	C. Lippmann	[326–328]
NaC_5H_5	D. Kühlmorgen	[329]
LiC≡CTMS	Gstrein	[330,331]
LiC≡CMes	Gstrein	[331]
IMe_4	Filippou group members	[332]
$[Ge(Ar^{Mes})Cl]_2$	I. Papazoglou	[333]
$[Si(Tbb)Br]_2$	Gstrein	[25]
$[Si(Eind)Br]_2$	Gstrein	[23,25,305]

4.7 List of commercially available reagents

Compound	Supplier	Purification
n-butyl lithium (1.6 M in *n*-hexane)	Chemetall	used as received
tert.-butyl lithium (1.9 M in *n*-pentane)	Acros	used as received
MeLi (1.6 M in Et_2O)	Alfa Aesar	used as received
chlortrimethylislane	Alfa Aesar	Stirred over predried K_2CO_3, distilled under argon
1,4-cyclohexadiene	Alfa Aesar	Stirred over predried K_2CO_3 and recondensed
$CpCo(CO)_2$	ABCR	used as received
4-dmap	Fluka	sublimed at 60 °C
MeOTf	Fluorchem	used as reveived
CO (99.9997 %)	Air Liquide	
naphtaline	Across Organics	Sublimation at 70 °C

5 Appendix

5.1 Crystallographic data of synthesized compounds

Table 5.1. Crystal data and structure refinement parameters of $SiBr_2(caac^{Me})$(**1**) and $GeBr_2(caac^{Me})$ (**1-Ge**).

	1	**1-Ge**
Empirical formula	$C_{20}H_{31}Br_2NSi$	$C_{20}H_{31}NGeBr_2$
Moiety formula	C_{20} H_{31} Br_2 N Si	C_{20} H_{31} Br_2 Ge N
Formula weight	473.37	517.87
Temperature/K	123	100
Crystal system	monoclinic	monoclinic
Space group	$P2_1/n$	$P2_1/n$
a/Å	9.5712(7)	9.5971(4)
b/Å	17.9799(12)	17.6889(8)
c/Å	12.7369(9)	12.9441(6)
α/°	90	90
β/°	101.454(3)	102.862(2)
γ/°	90	90
Volume/Å^3	2148.2(3)	2142.28(17)
Z	4	4
ρ_{calc}g/cm^3	1.464	1.606
μ/mm^{-1}	3.832	5.163
F(000)	968.0	1040.0
Crystal size/mm^3	0.4 × 0.3 × 0.15	0.3 × 0.18 × 0.18
Absorption correction	empirical	empirical
Tmin; Tmax	0.2935; 0.7465	0.2668; 0.7461
Radiation	MoKα (λ = 0.71073)	MoKα (λ = 0.71073)
2Θ range for data collection/°	4.886 to 55.994°	3.964 to 55.996°
Completeness to theta	1.000	0.999
Index ranges	-12 ≤ h ≤ 12, -23 ≤ k ≤ 23, -16 ≤ l ≤ 16	-12 ≤ h ≤ 12, -23 ≤ k ≤ 23, -17 ≤ l ≤ 17
Reflections collected	70453	61374
Independent reflections	5179 [R_{int} = 0.0978, R_{sigma} = 0.0370]	5167 [R_{int} = 0.0787, R_{sigma} = 0.0370]
Data/restraints/parameters	5179/0/225	5167/0/225
Goodness-of-fit on F^2	1.026	1.109
Final R indexes [I>=2σ (I)]	R_1 = 0.0317, wR_2 = 0.0621	R_1 = 0.0357, wR_2 = 0.0887
Final R indexes [all data]	R_1 = 0.0474, wR_2 = 0.0665	R_1 = 0.0403, wR_2 = 0.0908
Largest diff. peak/hole / e Å^{-3}	1.18/-0.65	0.96/-0.89

Table 5.2. Crystal data and structure refinement parameters of $SiBr(SiTMS_3)(caac^{Me})$ (**2-Si**) and $SiBr(Mes)(caac^{Me})$ (**2-Mes**).

	2-Si	**2-Mes**
Empirical formula	$C_{29}H_{58}NSi_5Br$	$C_{29}H_{42}BrNSi$
Moiety formula	C_{29} H_{58} Br N Si_5	C_{29} H_{42} Br N Si
Formula weight	641.12	512.63
Temperature/K	100	99.99
Crystal system	monoclinic	triclinic
Space group	$P2_1/n$	P-1
a/Å	13.1794(6)	9.7863(9)
b/Å	16.3209(8)	10.2527(11)
c/Å	17.7547(8)	14.0965(13)
α/°	90	103.847(4)
β/°	109.5170(10)	93.866(4)
γ/°	90	101.541(4)
Volume/$Å^3$	3599.6(3)	1335.6(2)
Z	4	2
$\rho_{calc}g/cm^3$	1.183	1.275
μ/mm^{-1}	1.327	1.601
F(000)	1376.0	544.0
Crystal size/mm^3	0.18 × 0.14 × 0.04	0.14 × 0.12 × 0.11
Absorption correction	empirical	empirical
Tmin; Tmax	0.6387; 0.7462	0.6768; 0.7461
Radiation	MoKα (λ = 0.71073)	MoKα (λ = 0.71073)
2Θ range for data collection/°	5.48 to 55.998°	4.28 to 56°
Completeness to theta	0.998	0.999
Index ranges	-17 ≤ h ≤ 17, -21 ≤ k ≤ 21, -23 ≤ l ≤ 23	-12 ≤ h ≤ 12, -13 ≤ k ≤ 13, -18 ≤ l ≤ 18
Reflections collected	81721	65136
Independent reflections	8680 [R_{int} = 0.0585, R_{sigma} = 0.0296]	6453 [R_{int} = 0.0369, R_{sigma} = 0.0167]
Data/restraints/parameters	8680/0/342	6453/0/300
Goodness-of-fit on F^2	1.015	1.052
Final R indexes [I>=2σ (I)]	R_1 = 0.0257, wR_2 = 0.0560	R_1 = 0.0214, wR_2 = 0.0519
Final R indexes [all data]	R_1 = 0.0396, wR_2 = 0.0606	R_1 = 0.0240, wR_2 = 0.0530
Largest diff. peak/hole / e $Å^{-3}$	0.37/-0.27	0.53/-0.39

Table 5.3. Crystal data and structure refinement parameters of $SiBr(PMes_2)(caac^{Me})$ (**2-P**) and $SiBr(NTMS_2)(caac^{Me})$ (**2-N**).

	2-P	**2-N**
Empirical formula	$C_{80}H_{116}Br_2N_2OP_2Si_2$	$C_{26}H_{49}N_2Si_3Br$
Moiety formula	$2(C_{38}H_{53}BrNPSi)$, $C_4H_{10}O$	$C_{26}H_{49}BrN_2Si_3$
Formula weight	1399.68	553.85
Temperature/K	100.01	100
Crystal system	triclinic	triclinic
Space group	P-1	P-1
a/Å	9.4473(14)	9.1123(6)
b/Å	21.344(4)	9.5908(7)
c/Å	21.529(4)	20.0344(14)
α/°	117.632(6)	93.472(3)
β/°	90.046(6)	99.979(3)
γ/°	100.135(6)	118.334(2)
Volume/Å^3	3769.0(11)	1497.07(18)
Z	2	2
ρ_{calc}g/cm^3	1.233	1.229
μ/mm^{-1}	1.194	1.509
F(000)	1492.0	592.0
Crystal size/mm^3	0.24 × 0.12 × 0.03	0.14 × 0.11 × 0.06
Absorption correction	empirical	empirical
Tmin; Tmax	0.6087; 0.7461	0.6301; 0.7460
Radiation	MoKα (λ = 0.71073)	MoKα (λ = 0.71073)
2Θ range for data collection/°	4.396 to 50.5°	4.892 to 56°
Completeness to theta	0.999	1.000
Index ranges	-11 ≤ h ≤ 11, -25 ≤ k ≤ 25, -25 ≤ l ≤ 25	-12 ≤ h ≤ 12, -12 ≤ k ≤ 12, -26 ≤ l ≤ 26
Reflections collected	75227	76089
Independent reflections	13620 [R_{int} = 0.0932, R_{sigma} = 0.0658]	7216 [R_{int} = 0.0622, R_{sigma} = 0.0274]
Data/restraints/parameters	13620/24/833	7216/0/303
Goodness-of-fit on F^2	1.084	1.046
Final R indexes [I>=2σ (I)]	R_1 = 0.0845, wR_2 = 0.2341	R_1 = 0.0252, wR_2 = 0.0566
Final R indexes [all data]	R_1 = 0.1012, wR_2 = 0.2553	R_1 = 0.0347, wR_2 = 0.0604
Largest diff. peak/hole / e Å^{-3}	2.72/-1.34	0.41/-0.42

Table 5.4. Crystal data and structure refinement parameters of SiBr(OMes*)(caac^{Me}) (**2-O**).

	2-O
Empirical formula	$C_{38}H_{60}BrNOSi$
Moiety formula	C_{38} H_{60} Br N O Si
Formula weight	654.87
Temperature/K	123
Crystal system	monoclinic
Space group	$P2_1/n$
a/Å	16.0569(6)
b/Å	11.3630(5)
c/Å	20.7053(8)
α/°	90
β/°	96.361(3)
γ/°	90
Volume/Å^3	3754.5(3)
Z	4
ρ_{calc}g/cm^3	1.159
μ/mm^{-1}	1.155
F(000)	1408.0
Crystal size/mm^3	0.12 × 0.05 × 0.03
Absorption correction	integration
Tmin; Tmax	0.6703; 0.9018
Radiation	MoKα (λ = 0.71073)
2Θ range for data collection/°	5.342 to 55.998°
Completeness to theta	0.994
Index ranges	-15 ≤ h ≤ 21, -15 ≤ k ≤ 15, -27 ≤ l ≤ 27
Reflections collected	24923
Independent reflections	9012 [R_{int} = 0.1209, R_{sigma} = 0.1525]
Data/restraints/parameters	9012/18/407
Goodness-of-fit on F^2	0.859
Final R indexes [I>=2σ (I)]	R_1 = 0.0545, wR_2 = 0.0780
Final R indexes [all data]	R_1 = 0.1210, wR_2 = 0.0918
Largest diff. peak/hole / e Å^{-3}	0.86/-0.46

Table 5.5. Crystal data and structure refinement parameters of SiBr(Eind)(caac^{Me}) (**2-Eind-*E***) and (**2-Eind-Z**).

	2-Eind-*E*	**2-Eind-*Z***
Empirical formula	$C_{48}H_{76}NSiBr$	$C_{100}H_{162}Br_2N_2OSi_2$
Moiety formula	C_{48} H_{76} Br N Si	2(C_{48} H_{76} Br N Si), C_4 H_{10} O
Formula weight	775.09	1624.31
Temperature/K	100	100
Crystal system	monoclinic	triclinic
Space group	$P2_1/n$	P-1
a/Å	10.901(4)	8.8048(5)
b/Å	20.167(9)	13.9661(8)
c/Å	20.629(8)	20.4479(13)
α/°	90	75.498(2)
β/°	100.165(12)	81.088(2)
γ/°	90	74.503(2)
Volume/Å^3	4464(3)	2335.4(2)
Z	4	1
ρ_{calc}g/cm^3	1.153	1.155
μ/mm^{-1}	0.979	0.940
F(000)	1680.0	882.0
Crystal size/mm^3	0.22 × 0.16 × 0.09	0.33 × 0.08 × 0.05
Absorption correction	empirical	empirical
Tmin; Tmax	0.5563; 0.7460	0.5932; 0.7459
Radiation	MoKα (λ = 0.71073)	MoKα (λ = 0.71073)
2Θ range for data collection/°	4.012 to 55.994°	2.066 to 56°
Completeness to theta	0.998	0.998
Index ranges	-14 ≤ h ≤ 14, -26 ≤ k ≤ 26, -27 ≤ l ≤ 27	-11 ≤ h ≤ 11, -18 ≤ k ≤ 18, -27 ≤ l ≤ 27
Reflections collected	60953	90366
Independent reflections	10766 [R_{int} = 0.1050, R_{sigma} = 0.0758]	11277 [R_{int} = 0.0623, R_{sigma} = 0.0387]
Data/restraints/parameters	10766/0/482	11277/41/511
Goodness-of-fit on F^2	1.039	1.029
Final R indexes [I>=2σ (I)]	R_1 = 0.0587, wR_2 = 0.1396	R_1 = 0.0470, wR_2 = 0.1172
Final R indexes [all data]	R_1 = 0.0915, wR_2 = 0.1566	R_1 = 0.0621, wR_2 = 0.1265
Largest diff. peak/hole / e Å^{-3}	2.12/-0.58	1.69/-1.31

Table 5.6. Crystal data and structure refinement parameters of $Si(SiTMS_3)(caac^{Me})$ (**3-Si**) and $Si(NTMS_2)(caac^{Me})$ (**3-N**).

	3-Si	**3-N**
Empirical formula	$C_{29}H_{58}NSi_5$	$C_{26}H_{49}N_2Si_3$
Moiety formula	$C_{29}H_{58}NSi_5$	$C_{26}H_{49}N_2Si_3$
Formula weight	561.21	473.94
Temperature/K	150.01	100
Crystal system	monoclinic	monoclinic
Space group	$P2_1/c$	Cc
a/Å	9.8468(3)	9.7274(18)
b/Å	29.3237(9)	21.109(4)
c/Å	13.1377(4)	14.697(3)
α/°	90	90
β/°	108.9258(13)	98.490(4)
γ/°	90	90
Volume/Å^3	3588.36(19)	2984.7(10)
Z	4	4
ρ_{calc}g/cm^3	1.039	1.055
μ/mm^{-1}	1.969	0.174
F(000)	1236.0	1044.0
Crystal size/mm^3	0.34 × 0.16 × 0.1	0.3 × 0.28 × 0.06
Absorption correction	empirical	empirical
Tmin; Tmax	0.3980; 0.7536	0.5319; 0.7462
Radiation	CuKα (λ = 1.54178)	MoKα (λ = 0.71073)
2Θ range for data collection/°	6.028 to 135.484°	4.652 to 51.998°
Completeness to theta	1.000	0.997
Index ranges	-11 ≤ h ≤ 11, -34 ≤ k ≤ 35, -15 ≤ l ≤ 15	-11 ≤ h ≤ 11, -26 ≤ k ≤ 26, -18 ≤ l ≤ 18
Reflections collected	82854	15787
Independent reflections	6497 [R_{int} = 0.0615, R_{sigma} = 0.0263]	5755 [R_{int} = 0.0378, R_{sigma} = 0.0477]
Data/restraints/parameters	6497/7/333	5755/56/294
Goodness-of-fit on F^2	1.052	1.093
Final R indexes [I>=2σ (I)]	R_1 = 0.0354, wR_2 = 0.0892	R_1 = 0.0421, wR_2 = 0.0952
Final R indexes [all data]	R_1 = 0.0391, wR_2 = 0.0916	R_1 = 0.0454, wR_2 = 0.0965
Largest diff. peak/hole / e Å^{-3}	0.29/-0.30	0.43/-0.25

Table 5.7. Crystal data and structure refinement parameters of Si(OMes*)(caac^{Me}) (**3-O**) and (Mes)P=Si(Mes)(caac^{Me}) (**6**).

	3-O	**6**
Empirical formula	$C_{38}H_{60}NOSi$	$C_{38}H_{53}NSiP$
Moiety formula	C_{38} H_{60} N O Si	C_{38} H_{53} N P Si
Formula weight	574.96	582.87
Temperature/K	123	123
Crystal system	monoclinic	monoclinic
Space group	$P2_1/n$	$P2_1/n$
a/Å	10.1335(6)	9.1025(11)
b/Å	27.7473(12)	37.389(2)
c/Å	13.9191(7)	10.2961(8)
α/°	90	90
β/°	100.133(4)	102.547(8)
γ/°	90	90
Volume/Å^3	3852.7(3)	3420.4(5)
Z	4	4
ρ_{calc}g/cm^3	0.991	1.132
μ/mm^{-1}	0.087	0.141
F(000)	1268.0	1268.0
Crystal size/mm^3	0.28 × 0.2 × 0.01	0.3 × 0.2 × 0.18
Absorption correction	integration	integration
Tmin; Tmax	0.8859; 0.9826	0.6109; 0.9663
Radiation	MoKα (λ = 0.71073)	MoKα (λ = 0.71073)
2Θ range for data collection/°	5.03 to 51.294°	5.076 to 50.498°
Completeness to theta	0.998	0.961
Index ranges	-12 ≤ h ≤ 12, -33 ≤ k ≤ 30, -16 ≤ l ≤ 16	-10 ≤ h ≤ 10, -44 ≤ k ≤ 44, -11 ≤ l ≤ 12
Reflections collected	19582	18421
Independent reflections	7238 [R_{int} = 0.0754, R_{sigma} = 0.1274]	5966 [R_{int} = 0.0530, R_{sigma} = 0.0398]
Data/restraints/parameters	7238/0/387	5966/0/384
Goodness-of-fit on F^2	0.808	1.091
Final R indexes [I>=2σ (I)]	R_1 = 0.0488, wR_2 = 0.0750	R_1 = 0.0556, wR_2 = 0.1159
Final R indexes [all data]	R_1 = 0.1050, wR_2 = 0.0860	R_1 = 0.0682, wR_2 = 0.1212
Largest diff. peak/hole / e Å^{-3}	0.25/-0.20	0.51/-0.22

Table 5.8. Crystal data and structure refinement parameters of $SiK(SiTMS_3)(caac^{Me})$ (**4-Si**) and $SiH(SiTMS_3)(caac^{Me})$ (**5-Si**).

	4-Si	**5-Si**
Empirical formula	$C_{33}H_{68}KNOSi_5$	$C_{29}H_{59}NSi_5$
Moiety formula	C_{33} H_{68} K N O Si_5	C_{29} H_{59} N Si_5
Formula weight	674.43	562.22
Temperature/K	100	100
Crystal system	monoclinic	monoclinic
Space group	$P2_1/c$	Cc
a/Å	9.8025(7)	19.8686(8)
b/Å	9.8326(7)	45.4939(18)
c/Å	43.334(3)	12.2153(5)
α/°	90	90
β/°	94.491(4)	102.8390(15)
γ/°	90	90
Volume/$Å^3$	4163.9(5)	10765.4(8)
Z	4	12
$\rho_{calc}g/cm^3$	1.076	1.041
μ/mm^{-1}	0.295	0.216
F(000)	1480.0	3720.0
Crystal size/mm^3	0.24 × 0.21 × 0.06	0.18 × 0.17 × 0.02
Absorption correction	empirical	empirical
Tmin; Tmax	0.6417; 0.7459	0.6047; 0.7462
Radiation	MoKα (λ = 0.71073)	MoKα (λ = 0.71073)
2Θ range for data collection/°	1.886 to 56°	1.79 to 55.998°
Completeness to theta	0.998	0.998
Index ranges	-12 ≤ h ≤ 12, -12 ≤ k ≤ 12, -57 ≤ l ≤ 57	-26 ≤ h ≤ 26, -59 ≤ k ≤ 60, -16 ≤ l ≤ 16
Reflections collected	167188	125003
Independent reflections	10008 [R_{int} = 0.0807, R_{sigma} = 0.0356]	25856 [R_{int} = 0.1269, R_{sigma} = 0.1199]
Data/restraints/parameters	10008/12/371	25856/2/1006
Goodness-of-fit on F^2	1.329	0.985
Final R indexes [I>=2σ (I)]	R_1 = 0.1835, wR_2 = 0.3830	R_1 = 0.0518, wR_2 = 0.1106
Final R indexes [all data]	R_1 = 0.1839, wR_2 = 0.3833	R_1 = 0.1034, wR_2 = 0.1336
Largest diff. peak/hole / e $Å^{-3}$	0.76/-1.03	0.66/-0.39

Table 5.9. Crystal data and structure refinement parameters of $Si_2Br_2(caac^{Me})_2$ (**9-Br**) and $Si_2Cp'_2(caac^{Me})_2$ (**9-Cp'**).

	9-Br	**9-Cp'**
Empirical formula	$C_{40}H_{62}Br_2N_2Si_2$	$C_{50}H_{72}N_2Si_2$
Moiety formula	C_{40} H_{62} Br_2 N_2 Si_2	C_{50} H_{72} N_2 Si_2
Formula weight	786.91	757.27
Temperature/K	101.83	150.0
Crystal system	monoclinic	monoclinic
Space group	$P2_1/c$	C2/c
a/Å	16.160(2)	22.0636(4)
b/Å	14.482(2)	9.2937(2)
c/Å	17.749(2)	22.1043(4)
α/°	90	90
β/°	95.845(3)	98.3673(8)
γ/°	90	90
Volume/Å^3	4132.0(10)	4484.29(15)
Z	4	4
ρ_{calc}g/cm^3	1.265	1.122
μ/mm^{-1}	2.048	0.966
F(000)	1656.0	1656.0
Crystal size/mm^3	0.28 × 0.1 × 0.03	0.22 × 0.12 × 0.1
Absorption correction	multi-scan	empirical
Tmin; Tmax	0.576; 0.746	0.4077; 0.7536
Radiation	MoKα (λ = 0.71073)	CuKα (λ = 1.54178)
2Θ range for data collection/°	4.296 to 54°	8.086 to 135.496°
Completeness to theta	1.000	0.997
Index ranges	-20 ≤ h ≤ 20, 0 ≤ k ≤ 18, 0 ≤ l ≤ 22	-26 ≤ h ≤ 26, -11 ≤ k ≤ 11, -26 ≤ l ≤ 26
Reflections collected	9024	39560
Independent reflections	9024 [R_{int} = 0.1464, R_{sigma} = 0.0681]	4056 [R_{int} = 0.0629, R_{sigma} = 0.0374]
Data/restraints/parameters	9024/2/439	4056/3/258
Goodness-of-fit on F^2	1.120	1.051
Final R indexes [I>=2σ (I)]	R_1 = 0.0634, wR_2 = 0.1134	R_1 = 0.0410, wR_2 = 0.1051
Final R indexes [all data]	R_1 = 0.1002, wR_2 = 0.1225	R_1 = 0.0438, wR_2 = 0.1077
Largest diff. peak/hole / e Å^{-3}	1.14/-0.58	0.23/-0.43

Table 5.10. Crystal data and structure refinement parameters of $Si_2(C{\equiv}CTMS)_2(caac^{Me})_2$ (**9-C₂TMS**) and $Si_2(C{\equiv}CMes)_2(caac^{Me})_2$ (**9-C₂Mes**).

	9-C₂TMS	**9-C₂Mes**
Empirical formula	$C_{50}H_{80}N_2Si_4$	$C_{62}H_{84}N_2Si_2$
Moiety formula	$C_{50}\,H_{80}\,N_2\,Si_4$	$C_{62}\,H_{84}\,N_2\,Si_2$
Formula weight	821.52	913.49
Temperature/K	100	99.99
Crystal system	monoclinic	tetragonal
Space group	C2/c	P-4
a/Å	18.3848(10)	16.7526(11)
b/Å	16.6663(9)	16.7526(11)
c/Å	18.7419(10)	10.0619(10)
α/°	90	90
β/°	95.074(2)	90
γ/°	90	90
Volume/Å^3	5720.1(5)	2823.9(5)
Z	4	2
ρ_{calc}g/cm^3	0.954	1.074
μ/mm^{-1}	0.133	0.101
F(000)	1800.0	996.0
Crystal size/mm^3	0.3 × 0.12 × 0.1	0.15 × 0.15 × 0.14
Absorption correction	empirical	empirical
Tmin; Tmax	0.6413; 0.7461	0.6606; 0.7380
Radiation	MoKα (λ = 0.71073)	MoKα (λ = 0.71073)
2Θ range for data collection/°	6.504 to 55.998°	4.722 to 55.982°
Completeness to theta	0.996	0.923
Index ranges	-23 ≤ h ≤ 24, -22 ≤ k ≤ 22, -24 ≤ l ≤ 19	-22 ≤ h ≤ 22, -22 ≤ k ≤ 22, -13 ≤ l ≤ 13
Reflections collected	43079	60868
Independent reflections	6866 [R_{int} = 0.0729, R_{sigma} = 0.0594]	6456 [R_{int} = 0.1240, R_{sigma} = 0.0764]
Data/restraints/parameters	6866/0/264	6456/12/414
Goodness-of-fit on F^2	1.106	0.992
Final R indexes [I>=2σ (I)]	R_1 = 0.0767, wR_2 = 0.1718	R_1 = 0.0512, wR_2 = 0.1149
Final R indexes [all data]	R_1 = 0.0966, wR_2 = 0.1810	R_1 = 0.0828, wR_2 = 0.1296
Largest diff. peak/hole / e Å^{-3}	0.66/-0.34	0.21/-0.28

Table 5.11. Crystal data and structure refinement parameters of $Si_2Mes_2(caac^{Me})_2$ (**9-Mes-*Z,Z***) and $Si_2Mes_2(caac^{Me})_2$ (**9-Mes-*E,E***).

	9-Mes *Z,Z*	**9-Mes *E,E***
Empirical formula	$C_{68}H_{108}N_2Si_2$	$C_{121}H_{180}N_4Si_4$
Moiety formula	$C_{58}H_{84}N_2Si_2$, $2(C_5H_{12})$	$2(C_{58}H_{84}N_2Si_2)$, C_5H_{12}
Formula weight	1009.74	1803.04
Temperature/K	100	100
Crystal system	monoclinic	monoclinic
Space group	$P2_1$	$P2_1/c$
a/Å	11.7963(7)	13.732(2)
b/Å	18.9282(10)	22.982(4)
c/Å	14.0017(7)	17.598(3)
α/°	90	90
β/°	92.790(2)	101.071(4)
γ/°	90	90
Volume/Å^3	3122.6(3)	5450.2(15)
Z	2	2
ρ_{calc}g/cm^3	1.074	1.099
μ/mm^{-1}	0.097	0.104
F(000)	1116.0	1980.0
Crystal size/mm^3	0.28 × 0.26 × 0.18	0.18 × 0.09 × 0.05
Absorption correction	empirical	empirical
Tmin; Tmax	0.444209; 0.746070	0.5683; 0.7460
Radiation	MoKα (λ = 0.71073)	MoKα (λ = 0.71073)
2Θ range for data collection/°	2.912 to 52°	3.544 to 56°
Completeness to theta	1.000	0.999
Index ranges	-14 ≤ h ≤ 14, 0 ≤ k ≤ 23, 0 ≤ l ≤ 17	-18 ≤ h ≤ 18, -28 ≤ k ≤ 30, -23 ≤ l ≤ 23
Reflections collected	32447	99726
Independent reflections	32447 [R_{int} = 0.2007, R_{sigma} = 0.0949]	13064 [R_{int} = 0.5491, R_{sigma} = 0.4372]
Data/restraints/parameters	32447/1/679	13064/16/628
Goodness-of-fit on F^2	1.331	0.944
Final R indexes [I>=2σ (I)]	R_1 = 0.1156, wR_2 = 0.3055	R_1 = 0.1187, wR_2 = 0.2485
Final R indexes [all data]	R_1 = 0.1397, wR_2 = 0.3293	R_1 = 0.3715, wR_2 = 0.3592
Largest diff. peak/hole / e Å^{-3}	0.83/-0.74	0.38/-0.52

Table 5.12. Crystal data and structure refinement parameters of SiK(C≡CTMS)(caac^{Me}) (**10-C$_2$TMS**) and SiK(C≡CMes)(caac^{Me})·DME (**10-C$_2$Mes·DME**).

	10-C$_2$TMS	**10-C$_2$Mes·DME**
Empirical formula	$C_{62}H_{110}K_2N_2O_3Si_4$	$C_{39}H_{62}NO_4SiK$
Moiety formula	$2(C_{29}H_{50}KNOSi_2)$, $C_4H_{10}O$	$C_{39}H_{62}KNO_4Si$
Formula weight	1122.07	676.08
Temperature/K	100.0	123
Crystal system	triclinic	triclinic
Space group	P-1	P-1
a/Å	12.3764(7)	17.3481(8)
b/Å	16.4874(8)	23.7623(11)
c/Å	18.3964(9)	23.6953(11)
α/°	101.478(3)	96.641(4)
β/°	96.495(3)	110.018(4)
γ/°	107.946(3)	111.101(4)
Volume/Å^3	3438.0(3)	8238.3(7)
Z	2	8
ρ_{calc}g/cm^3	1.084	1.090
μ/mm^{-1}	0.248	0.194
F(000)	1228.0	2944.0
Crystal size/mm^3	0.16 × 0.06 × 0.05	0.48 × 0.29 × 0.28
Absorption correction	empirical	integration
Tmin; Tmax	0.6480; 0.7459	0.4621; 0.9365
Radiation	MoKα (λ = 0.71073)	MoKα (λ = 0.71073)
2Θ range for data collection/°	4.552 to 53.998°	5.38 to 50.5°
Completeness to theta	0.997	0.972
Index ranges	-15 ≤ h ≤ 15, -21 ≤ k ≤ 21, -23 ≤ l ≤ 23	-20 ≤ h ≤ 20, -28 ≤ k ≤ 27, -28 ≤ l ≤ 24
Reflections collected	87173	56932
Independent reflections	14828 [R_{int} = 0.0863, R_{sigma} = 0.0751]	29013 [R_{int} = 0.1232, R_{sigma} = 0.1401]
Data/restraints/parameters	14828/152/735	29013/121/1657
Goodness-of-fit on F^2	1.034	1.523
Final R indexes [I>=2σ (I)]	R_1 = 0.0704, wR_2 = 0.1795	R_1 = 0.1819, wR_2 = 0.4764
Final R indexes [all data]	R_1 = 0.1193, wR_2 = 0.2100	R_1 = 0.2409, wR_2 = 0.4984
Largest diff. peak/hole / e Å^{-3}	1.94/-1.37	1.59/-0.79

Table 5.13. Crystal data and structure refinement parameters of SiBr(caac^{Me})–Si(C≡CTMS)(caac^{Me}) (**11-Br**) and (caac^{Me})Si(C≡CTMS)(GeAr^{Mes}) (**12**).

	11-Br	**12**
Empirical formula	$C_{45}H_{71}N_2Si_3Br$	$C_{49}H_{65}GeNSi_2$
Moiety formula	C_{45} H_{71} Br N_2 Si_3	C_{49} H_{65} Ge N Si_2
Formula weight	804.21	796.79
Temperature/K	100	123
Crystal system	triclinic	orthorhombic
Space group	P-1	Pbca
a/Å	12.6731(5)	20.576(4)
b/Å	13.4162(6)	22.941(4)
c/Å	14.9142(6)	40.179(6)
α/°	67.326(2)	90
β/°	84.700(2)	90
γ/°	86.076(2)	90
Volume/Å^3	2328.31(17)	18966(6)
Z	2	16
ρ_{calc}g/cm^3	1.147	1.116
μ/mm^{-1}	0.991	0.727
F(000)	864.0	6816.0
Crystal size/mm^3	0.18 × 0.08 × 0.06	0.12 × 0.06 × 0.04
Absorption correction	empirical	integration
Tmin; Tmax	0.6665; 0.7462	0.6034; 0.8541
Radiation	MoKα (λ = 0.71073)	MoKα (λ = 0.71073)
2Θ range for data collection/°	5.936 to 51.992°	5.078 to 51.998°
Completeness to theta	0.998	0.860
Index ranges	-15 ≤ h ≤ 15, -16 ≤ k ≤ 16, -18 ≤ l ≤ 18	0 ≤ h ≤ 21, 0 ≤ k ≤ 28, 0 ≤ l ≤ 49
Reflections collected	66678	15901
Independent reflections	9151 [R_{int} = 0.0473, R_{sigma} = 0.0288]	15901 [R_{int} = ?, R_{sigma} = 0.5450]
Data/restraints/parameters	9151/13/479	15901/924/989
Goodness-of-fit on F^2	1.030	0.623
Final R indexes [I>=2σ (I)]	R_1 = 0.0302, wR_2 = 0.0709	R_1 = 0.0747, wR_2 = 0.1096
Final R indexes [all data]	R_1 = 0.0413, wR_2 = 0.0757	R_1 = 0.2528, wR_2 = 0.1515
Largest diff. peak/hole / e Å^{-3}	0.68/-0.28	0.57/-0.39

Table 5.14. Crystal data and structure refinement parameters of $SiBr(SiBr_2Tbb)(caac^{Me})$ (**13**) and $GeBr(SiBr_2Tbb)(caac^{Me})$ (**13-Ge**).

	13	**13-Ge**
Empirical formula	$C_{47}H_{87}Br_3NSi_6$	$C_{49}H_{92}Br_3GeNSi_5$
Moiety formula	$C_{44}H_{80}Br_3NSi_6$, C_3H_7	$C_{44}H_{80}Br_3GeNSi_5$, C_5H_{12}
Formula weight	1074.44	1148.00
Temperature/K	100	100
Crystal system	monoclinic	tetragonal
Space group	C2/c	$P4_12_12$
a/Å	46.231(4)	17.5503(11)
b/Å	10.2107(8)	17.5503(11)
c/Å	24.0938(19)	37.910(4)
α/°	90	90
β/°	99.693(3)	90
γ/°	90	90
Volume/Å^3	11211.1(15)	11676.7(19)
Z	8	8
ρ_{calc}g/cm^3	1.273	1.306
μ/mm^{-1}	2.317	2.711
F(000)	4520.0	4800.0
Crystal size/mm^3	0.14 × 0.11 × 0.04	0.16 × 0.08 × 0.02
Absorption correction	empirical	empirical
Tmin; Tmax	0.5781; 0.7459	0.5687; 0.7460
Radiation	MoKα (λ = 0.71073)	MoKα (λ = 0.71073)
2Θ range for data collection/°	1.788 to 55.998°	4.6 to 55.992°
Completeness to theta	0.995	0.997
Index ranges	-60 ≤ h ≤ 41, -13 ≤ k ≤ 13, -30 ≤ l ≤ 31	-23 ≤ h ≤ 23, -23 ≤ k ≤ 23, -50 ≤ l ≤ 50
Reflections collected	62436	215134
Independent reflections	13492 [R_{int} = 0.1118, R_{sigma} = 0.1110]	14069 [R_{int} = 0.3234, R_{sigma} = 0.1528]
Data/restraints/parameters	13492/10/538	14069/48/558
Goodness-of-fit on F^2	1.182	1.008
Final R indexes [I>=2σ (I)]	R_1 = 0.0954, wR_2 = 0.1978	R_1 = 0.0648, wR_2 = 0.1108
Final R indexes [all data]	R_1 = 0.1399, wR_2 = 0.2099	R_1 = 0.1404, wR_2 = 0.1327
Largest diff. peak/hole / e Å^{-3}	1.30/-2.30	0.68/-1.09

Table 5.15. Crystal data and structure refinement parameters of (caac^{Me})Si=SiBr(Tbb) (**14**) and (caac^{Me})Ge=SiBr(Tbb) (**14-Ge**).

	14	**14-Ge**
Empirical formula	$C_{44}H_{80}NSi_6Br$	$C_{44}H_{80}NSi_5GeBr$
Moiety formula	C_{44} H_{80} Br N Si_6	C_{44} H_{80} Br Ge N Si_5
Formula weight	871.54	916.04
Temperature/K	100	100
Crystal system	monoclinic	triclinic
Space group	$P2_1$	P-1
a/Å	15.1911(17)	12.6121(15)
b/Å	18.633(2)	14.5784(18)
c/Å	19.124(2)	16.349(2)
α/°	90	72.731(4)
β/°	103.794(3)	79.467(4)
γ/°	90	68.359(4)
Volume/Å^3	5257.2(10)	2659.0(6)
Z	4	2
ρ_{calc}g/cm^3	1.101	1.144
μ/mm^{-1}	0.946	1.467
F(000)	1880.0	976.0
Crystal size/mm^3	0.18 × 0.12 × 0.06	0.18 × 0.14 × 0.11
Absorption correction	empirical	empirical
Tmin; Tmax	0.5533; 0.7460	0.5967; 0.7459
Radiation	MoKα (λ = 0.71073)	MoKα (λ = 0.71073)
2Θ range for data collection/°	5.354 to 56°	5.196 to 55.998°
Completeness to theta	0.997	0.999
Index ranges	-20 ≤ h ≤ 20, -24 ≤ k ≤ 24, -25 ≤ l ≤ 25	-16 ≤ h ≤ 16, -19 ≤ k ≤ 19, -21 ≤ l ≤ 21
Reflections collected	89099	142059
Independent reflections	25349 [R_{int} = 0.1144, R_{sigma} = 0.1473]	12834 [R_{int} = 0.0981, R_{sigma} = 0.0495]
Data/restraints/parameters	25349/38/1003	12834/115/523
Goodness-of-fit on F^2	0.942	1.033
Final R indexes [I>=2σ (I)]	R_1 = 0.0496, wR_2 = 0.0812	R_1 = 0.0402, wR_2 = 0.0851
Final R indexes [all data]	R_1 = 0.1094, wR_2 = 0.0954	R_1 = 0.0644, wR_2 = 0.0946
Largest diff. peak/hole / e Å^{-3}	0.62/-0.65	1.22/-1.05

Table 5.16. Crystal data and structure refinement parameters of ($caac^{Me}$)Si=SiMe(Tbb) (**14-Me**) and SiLi{$SiMe_2$(Tbb)}($caac^{Me}$)·(Et_2O) (**15·(Et_2O)**).

	14-Me	**15·(Et_2O)**
Empirical formula	$C_{48}H_{90}NSi_6$	$C_{50}H_{96}LiNOSi_6$
Moiety formula	$C_{45}H_{83}NSi_6$, 0.5(C_6H_{14})	$C_{50}H_{96}LiNOSi_6$
Formula weight	849.74	902.75
Temperature/K	123	123
Crystal system	monoclinic	monoclinic
Space group	$P2_1/n$	$P2_1/n$
a/Å	15.4094(4)	14.8076(5)
b/Å	21.5668(8)	20.0960(5)
c/Å	17.2391(5)	19.7338(7)
α/°	90	90
β/°	107.496(2)	95.322(3)
γ/°	90	90
Volume/Å^3	5464.1(3)	5846.9(3)
Z	4	4
ρ_{calc}g/cm^3	1.033	1.026
μ/mm^{-1}	0.182	0.174
F(000)	1876.0	1992.0
Crystal size/mm^3	0.18 × 0.16 × 0.14	0.33 × 0.3 × 0.28
Absorption correction	integration	integration
Tmin; Tmax	0.8921; 0.9815	0.9718; 0.9953
Radiation	MoKα (λ = 0.71073)	MoKα (λ = 0.71073)
2Θ range for data collection/°	5.248 to 56°	5.426 to 54°
Completeness to theta	0.999	0.999
Index ranges	-20 ≤ h ≤ 19, -28 ≤ k ≤ 28, -22 ≤ l ≤ 22	-18 ≤ h ≤ 18, -25 ≤ k ≤ 25, -25 ≤ l ≤ 25
Reflections collected	58165	89317
Independent reflections	13191 [R_{int} = 0.0368, R_{sigma} = 0.0484]	12741 [R_{int} = 0.0602, R_{sigma} = 0.0498]
Data/restraints/parameters	13191/102/570	12741/74/590
Goodness-of-fit on F^2	0.985	0.887
Final R indexes [I>=2σ (I)]	R_1 = 0.0540, wR_2 = 0.1452	R_1 = 0.0336, wR_2 = 0.0763
Final R indexes [all data]	R_1 = 0.0837, wR_2 = 0.1571	R_1 = 0.0547, wR_2 = 0.0801
Largest diff. peak/hole / e Å^{-3}	0.94/-1.51	0.46/-0.30

Table 5.17. Crystal data and structure refinement parameters of SiK{Si(H)Tbb'}(caac^{Me}) x DME (**16·DME**) and SiK{Si(H)Tbb'}(caac^{Me}) x (caac^{Me}) (**16·caac^{Me}**).

	16·DME	**16·caac^{Me}**
Empirical formula	$C_{48}H_{89}KNO_2Si_6$	$C_{64}H_{111}KN_2Si_6$
Moiety formula	C_{48} H_{89} K N O_2 Si_6	C_{64} H_{111} K N_2 Si_6
Formula weight	919.84	1116.18
Temperature/K	100.0	100
Crystal system	monoclinic	triclinic
Space group	$P2_1/c$	P-1
a/Å	9.7162(4)	15.6605(19)
b/Å	43.956(2)	18.991(2)
c/Å	13.9149(6)	26.455(3)
α/°	90	97.015(6)
β/°	105.611(2)	104.373(6)
γ/°	90	105.817(6)
Volume/Å^3	5723.6(4)	7179.5(15)
Z	4	4
ρ_{calc}g/cm^3	1.067	1.033
μ/mm^{-1}	2.263	0.209
F(000)	2012.0	2448.0
Crystal size/mm^3	0.2 × 0.2 × 0.02	0.24 × 0.18 × 0.02
Absorption correction	empirical	empirical
Tmin; Tmax	0.3950; 0.7536	0.6329; 0.7460
Radiation	CuKα (λ = 1.54178)	MoKα (λ = 0.71073)
2Θ range for data collection/°	4.02 to 135.5°	2.276 to 52°
Completeness to theta	0.997	0.985
Index ranges	-11 ≤ h ≤ 11, -52 ≤ k ≤ 50, -16 ≤ l ≤ 16	-19 ≤ h ≤ 19, -23 ≤ k ≤ 23, -32 ≤ l ≤ 31
Reflections collected	63337	92887
Independent reflections	10359 [R_{int} = 0.0915, R_{sigma} = 0.0555]	27717 [R_{int} = 0.2884, R_{sigma} = 0.4376]
Data/restraints/parameters	10359/34/573	27717/151/1409
Goodness-of-fit on F^2	1.243	0.959
Final R indexes [I>=2σ (I)]	R_1 = 0.1093, wR_2 = 0.2446	R_1 = 0.1036, wR_2 = 0.2120
Final R indexes [all data]	R_1 = 0.1218, wR_2 = 0.2496	R_1 = 0.3250, wR_2 = 0.3072
Largest diff. peak/hole / e Å^{-3}	0.77/-0.62	0.84/-0.59

Table 5.18. Crystal data and structure refinement parameters of [(caac^{Me})Si=Si(IMe$_4$)(Tbb)][B(C$_6$H$_3$-3,5-(CF$_3$)$_2$)$_4$)] (**18**) and [Si(Me)(caac^{Me})$_2$][B(C$_6$H$_3$-3,5-(CF$_3$)$_2$)$_4$)] (**19-Me**).

	18	**19-Me**
Empirical formula	$C_{196}H_{233}B_2Br_5F_{48}N_6Si_{12}$	$C_{73}H_{77}N_2SiBF_{24}$
Moiety formula	5(C_6 H_5 Br), 2(C_{51} H_{92} N_3 Si_6), 2(C_{32} H_{12} B F_{24})	C_{41} H_{65} N_2 Si, C_{32} H_{12} B F_{24}
Formula weight	4343.12	1477.26
Temperature/K	100.0(1)	123
Crystal system	monoclinic	triclinic
Space group	C2/c	P-1
a/Å	27.1057(2)	12.8488(4)
b/Å	17.62210(10)	15.3071(5)
c/Å	44.2237(3)	20.1257(6)
α/°	90	69.523(2)
β/°	95.2590(10)	76.474(3)
γ/°	90	79.565(3)
Volume/Å^3	21034.9(2)	3583.8(2)
Z	4	2
ρ_{calc}g/cm^3	1.371	1.369
μ/mm^{-1}	2.614	0.138
F(000)	8944.0	1528.0
Crystal size/mm^3	0.5 × 0.5 × 0.3	0.26 × 0.19 × 0.1
Absorption correction	multi-scan	integration
Tmin; Tmax	0.38100; 1.00000	0.8677; 0.9843
Radiation	CuKα (λ = 1.54184)	MoKα (λ = 0.71073)
2Θ range for data collection/°	4.012 to 135.498°	5.332 to 55.998°
Completeness to theta	1.000	0.991
Index ranges	-32 ≤ h ≤ 32, -21 ≤ k ≤ 20, -53 ≤ l ≤ 53	-16 ≤ h ≤ 16, -20 ≤ k ≤ 20, -26 ≤ l ≤ 26
Reflections collected	300115	34355
Independent reflections	19071 [R_{int} = 0.3922, R_{sigma} = 0.0996]	17001 [R_{int} = 0.0585, R_{sigma} = 0.0745]
Data/restraints/parameters	19071/105/1314	17001/91/1012
Goodness-of-fit on F^2	1.047	0.911
Final R indexes [I>=2σ (I)]	R_1 = 0.0778, wR_2 = 0.1862	R_1 = 0.0567, wR_2 = 0.1401
Final R indexes [all data]	R_1 = 0.0844, wR_2 = 0.1920	R_1 = 0.0880, wR_2 = 0.1515
Largest diff. peak/hole / e Å^{-3}	1.74/-0.71	0.54/-0.48

Table5.19. Crystal data and structure refinement parameters of $(caac^{Me}H)_2O$ and $[(caac^{Me})SiMe_2I]I$.

	$(caac^{Me}H)_2O$	$[(caac^{Me})SiMe_2I]I$
Empirical formula	$C_{40}H_{64}N_2O$	$C_{34}H_{47}F_2I_2NSi$
Moiety formula	C_{40} H_{64} N_2 O	C_{22} H_{37} I N Si, I, 2(C_6 H_5 F)
Formula weight	588.93	789.61
Temperature/K	170	123(2)
Crystal system	triclinic	monoclinic
Space group	P-1	$P2_1/n$
a/Å	10.8343(4)	15.3622(3)
b/Å	11.9165(5)	10.8487(2)
c/Å	14.6816(6)	22.5660(5)
α/°	79.6716(17)	90
β/°	86.5542(18)	109.683(2)
γ/°	77.9840(17)	90
Volume/Å^3	1823.41(13)	3541.10(13)
Z	2	4
ρ_{calc}g/cm^3	1.073	1.481
μ/mm^{-1}	0.470	1.843
F(000)	652.0	1584.0
Crystal size/mm^3	0.25 × 0.16 × 0.11	0.26 × 0.24 × 0.16
Absorption correction	empirical	integration
Tmin; Tmax	0.2476; 0.7536	0.6404; 0.7932
Radiation	CuKα (λ = 1.54178)	MoKα (λ = 0.71073)
2Θ range for data collection/°	6.12 to 135.496°	5.366 to 55.996°
Completeness to theta	0.999	0.999
Index ranges	-13 ≤ h ≤ 12, -14 ≤ k ≤ 14, -17 ≤ l ≤ 17	-20 ≤ h ≤ 20, -14 ≤ k ≤ 14, -29 ≤ l ≤ 29
Reflections collected	46821	61266
Independent reflections	6610 [R_{int} = 0.0789, R_{sigma} = 0.0459]	8552 [R_{int} = 0.0408, R_{sigma} = 0.0355]
Data/restraints/parameters	6610/42/404	8552/6/347
Goodness-of-fit on F^2	1.052	0.929
Final R indexes [I>=2σ (I)]	R_1 = 0.0857, wR_2 = 0.2281	R_1 = 0.0292, wR_2 = 0.0682
Final R indexes [all data]	R_1 = 0.0911, wR_2 = 0.2380	R_1 = 0.0454, wR_2 = 0.0710
Largest diff. peak/hole / e Å^{-3}	0.45/-0.72	1.74/-0.70

5.2 Supplemental molecular structures

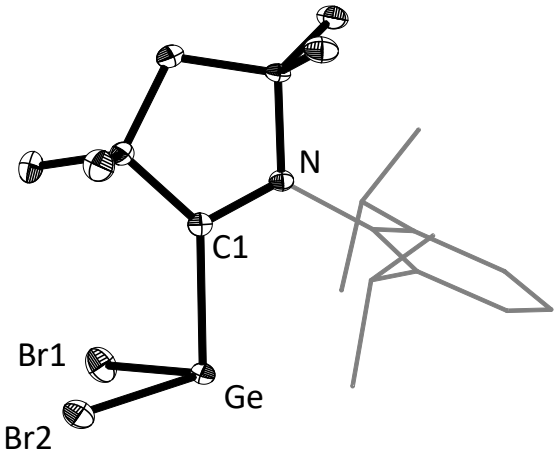

Figure 5.1. DIAMOND plot of the molecular structure of $GeBr_2(caac^{Me})$ (**1-Ge**), thermal ellipsoids are shown at 30% probability level and the hydrogen atoms are omitted. In the depicted structure the Dipp-substituent of the $caac^{Me}$ ligand is presented in the wire-frame for the sake of clarity. Selected bond lengths [Å], angles [°] and torsion angles [°]: Ge–Br1 2.4533(4), Ge–Br2 2.4589(4), Ge–C1 2.128(3), N–C1 1.299(3), N–C2 1.533(3), N–C5 1.463(3), Br1–Ge–Br2 97.998(14), C1–Ge–Br1 95.66(7), C1–Ge–Br2 94.83(7), N–C1–Ge–Br1 144.8(2), N–C1–Ge–Br2 –116.6(2).

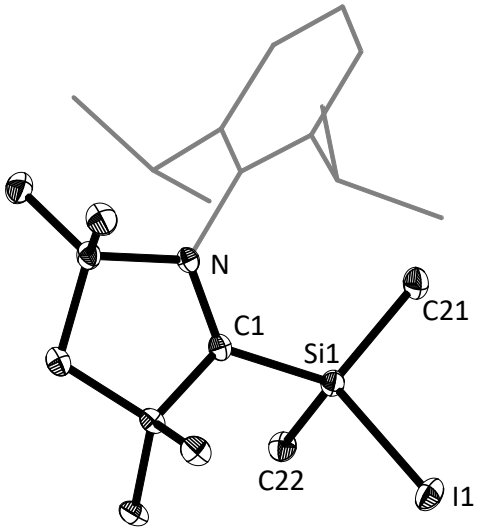

Figure 5.2. DIAMOND plot of the molecular structure of $[SiMe_2I(caac^{Me})]I$, thermal ellipsoids are shown at 30% probability level and the hydrogen atoms are omitted. In the depicted structure the Dipp-substituent of the $caac^{Me}$ ligand is presented in the wire-frame for the sake of clarity. Selected bond lengths [Å] and angles [°]: Si1–I1 2.4484(8), Si1–C1 1.948(3), Si1–C21 1.855(3), Si1–C22 1.852(3), N–C1 1.294(3), N–C4 1.552(3), N–C9 1.465(3), C1–Si1–I1 106.25(8), C21–Si1–I1 110.77(10), C21–Si1–C1 105.51(12), C22–Si1–I1 105.89(11), C22–Si1–C1 116.40(13), C22–Si1–C21 111.90(14).

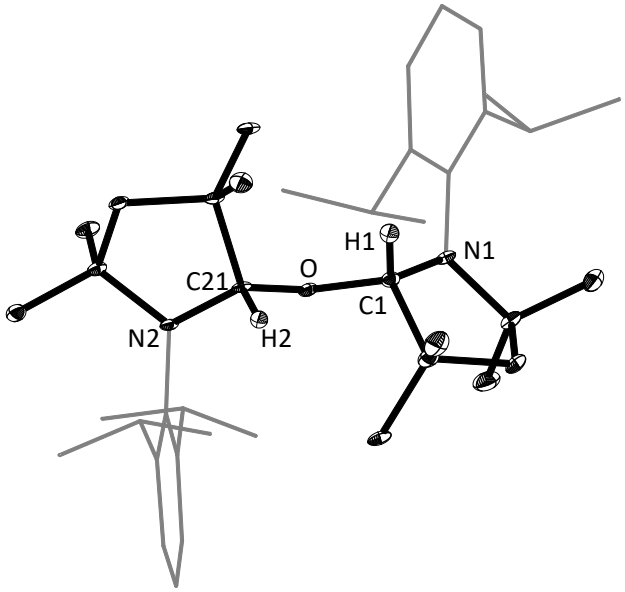

Figure 5.3. DIAMOND plot of the molecular structure of (caac^{Me}H)$_2$O, thermal ellipsoids are shown at 30% probability level and the hydrogen atoms are omitted. In the depicted structure the Dipp-substituent of the caac^{Me} ligand is presented in the wire-frame for the sake of clarity. Selected bond lengths [Å], angles [°] and torsion angles [°]: O–C1 1.453(2), O–C21 1.447(2), N1–C1 1.428(2), N1–C2, 1.487(2), N1–C5 1.431(2), N2–C21 1.433(2), N2–C22 1.480(2), N2–C25 1.433(2), C21–O–C1 115.13(12), O–C1–C4 115.33(13), N1–C1–O 109.18(13), N1–C1–C4 106.12(14), O–C21–C24 115.65(12), N2–C21–O 109.20(13), N2–C21–C24 105.73(13), N2–C21–O–C1 –160.8(2), N1–C1–O–C21 –162.0(2).

5.3 Supplemental ^{1}H NMR spectra of compounds

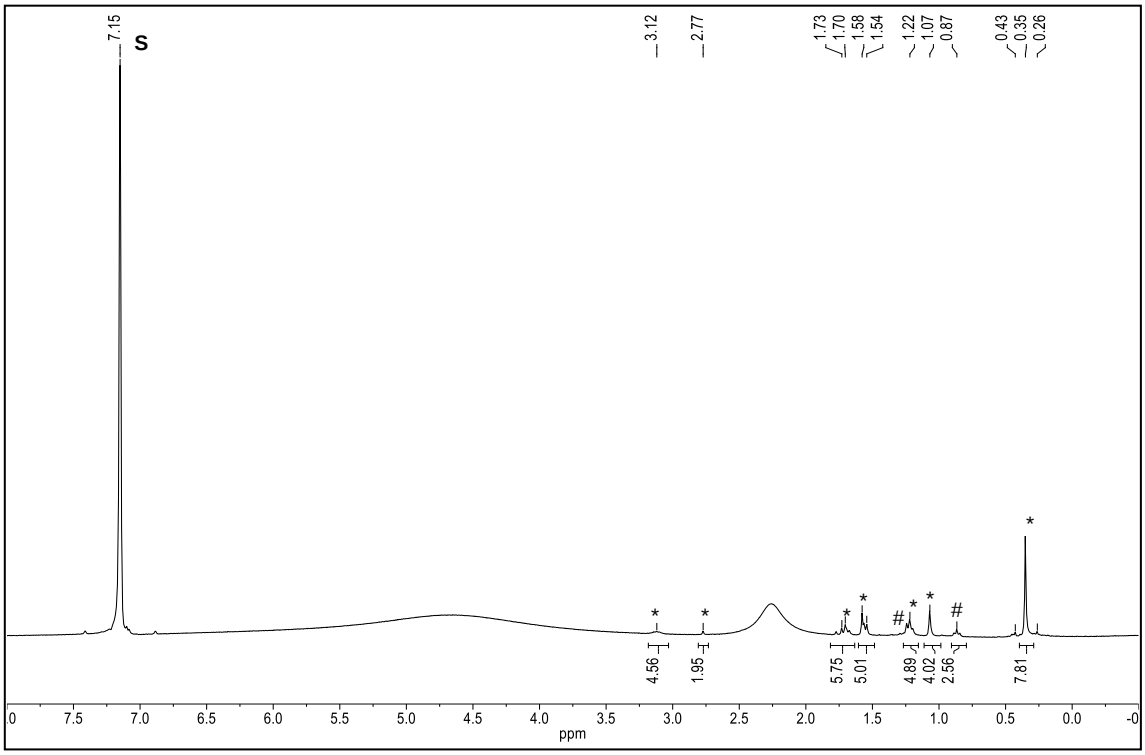

Figure 5.4. ^{1}H-NMR spectrum (300.13 MHz) of a 53 mM solution of Si(SiTMS$_3$)(caac^{Me}) (**3-Si**) in (D_6)benzene at 298 K. The signal of the deuterated solvent is marked with the character **S**, (*) marks the ^{1}H NMR resonances of the corresponding hydridosilene SiH(SiTMS$_3$)(caac^{Me}) (**5-Si**); # marks residual solvent signal of *n*-pentane.

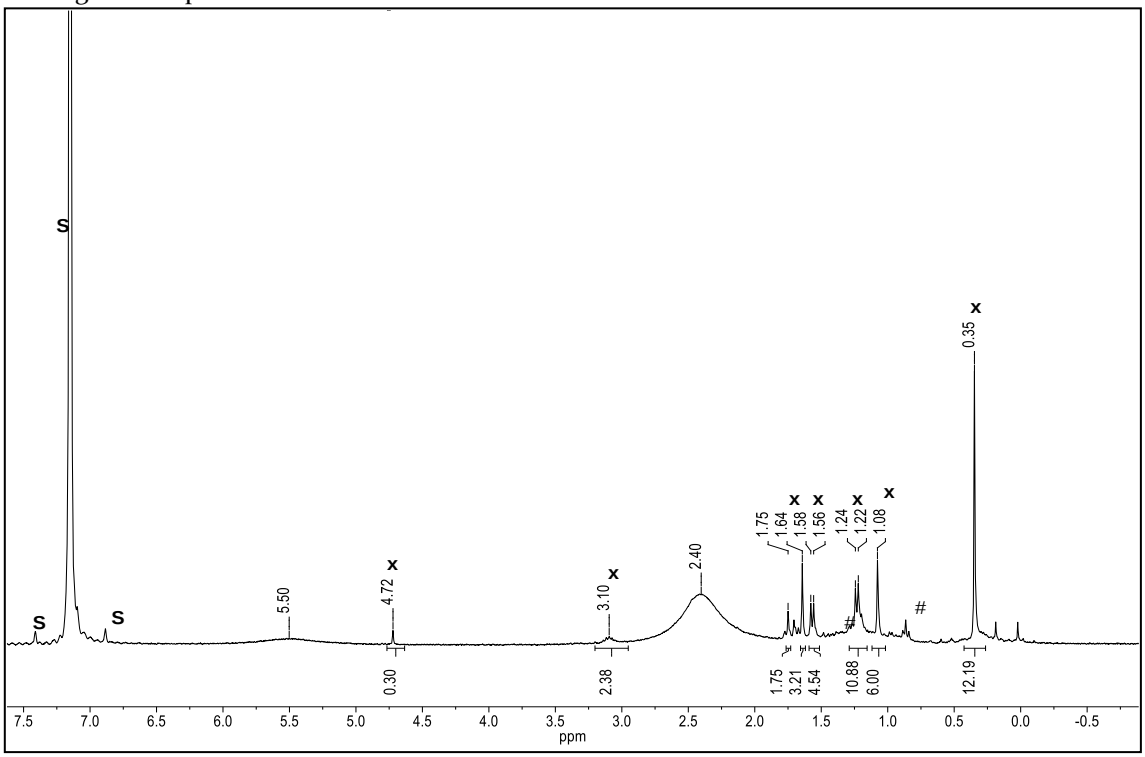

Figure 5.5. ^{1}H NMR spectrum (300.13 MHz) of a ca. 30 mM solution of Si(NTMS$_2$)(caac^{Me}) (**3-N**) in (D_6)benzene at 298 K. Tiny amounts of *n*-pentane are marked with the symbol #, as well as tiny amounts of hydridosilene SiH(NTMS$_2$)(caac^{Me}) (**5-N**) are marked with the symbol **x**, which is formed upon decomposition of the radical in solution.

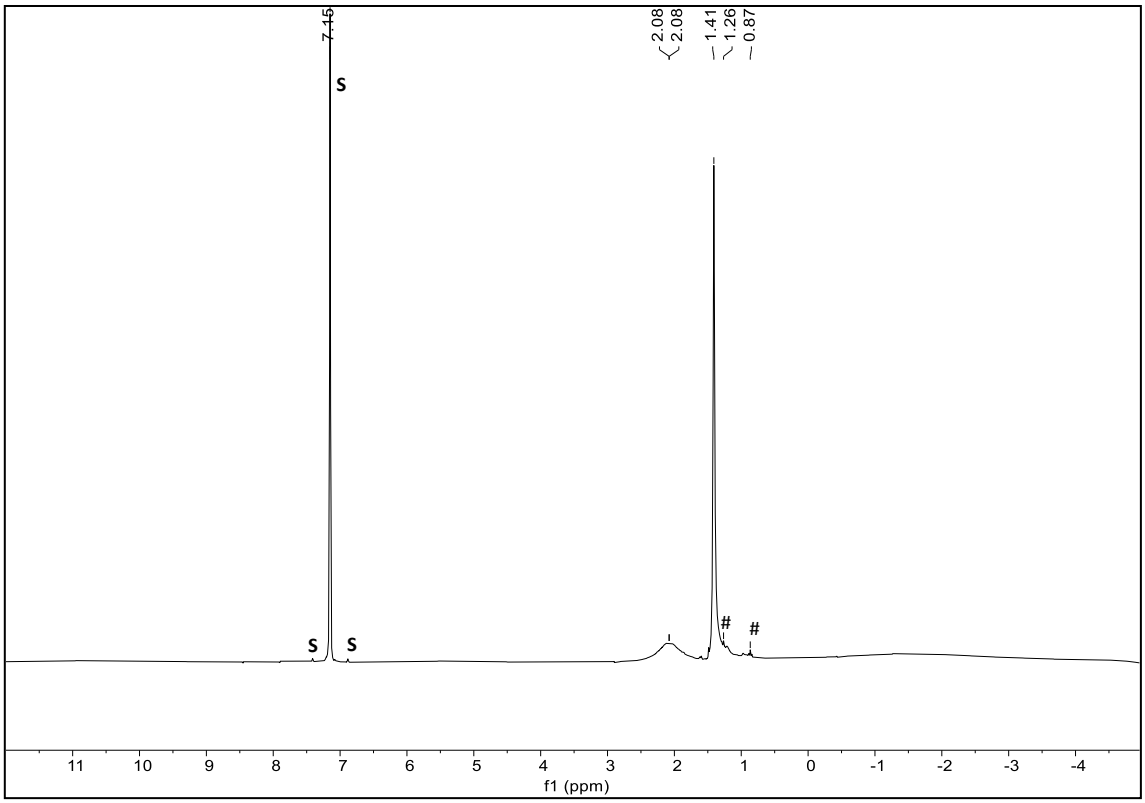

Figure 5.6. ^{1}H NMR spectrum (300.13 MHz) of a ca. 30 mM solution of Si(OMes*)(caac^{Me}) (**3-O**) in (D_6)benzene at 298 K showing a sharp signal at 1.41 ppm and a broadened signal at 2.08 ppm. The residual proton signal of the deuterated solvent and its ^{13}C satellites are marked with the character **S**. Tiny amounts of *n*-pentane are marked with the symbol #.

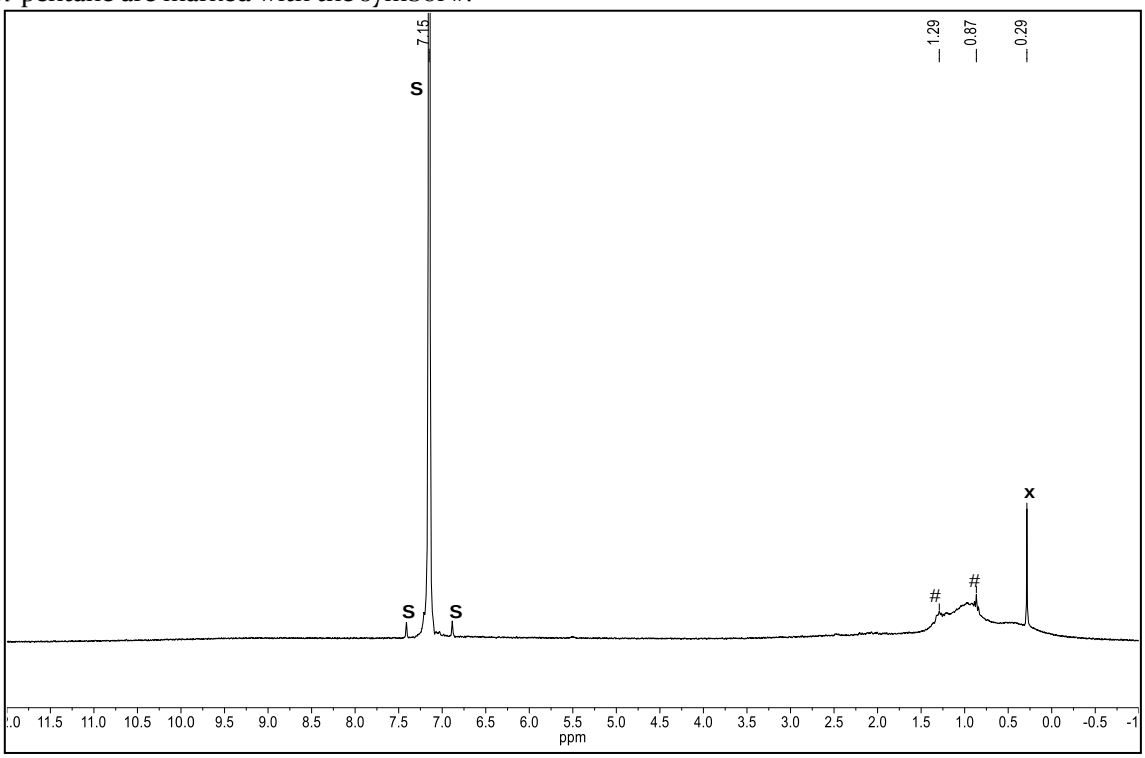

Figure 5.7. ^{1}H NMR spectrum (300.13 MHz) of a ca. 30 mM solution of (Mes)P-Si(Mes)(caac^{Me}) (**6**) in (D_6)benzene at 298 K showing very broad signals in the range 0.0 – 2.00 ppm. The residual proton signal of the deuterated solvent and its ^{13}C satellites are marked with the character **S**. Tiny amounts of *n*-pentane are marked with the symbol #, as well as tiny amounts of silicon grease (originated from the syringe) are marked with the symbol **x**.

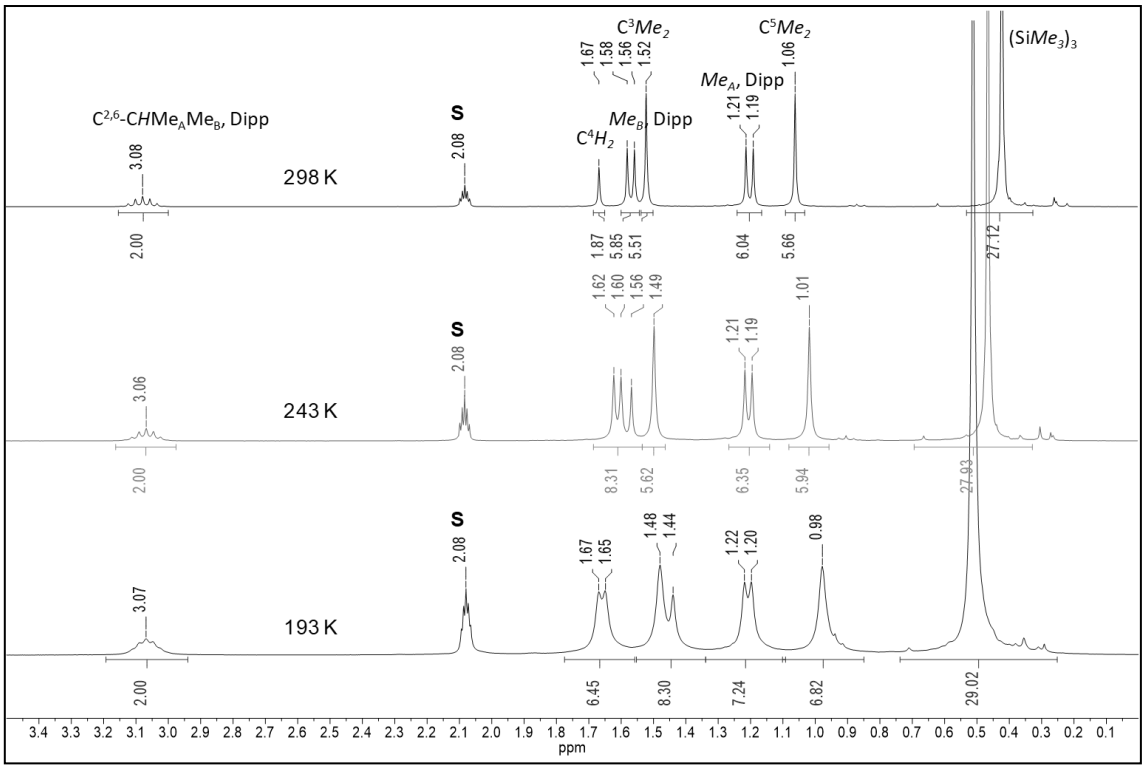

Figure 5.8. Stack plot of an excerpt (0.1 – 3.4 ppm) of ^{1}H NMR spectra of SiBr(SiTMS$_3$)(caac^{Me}) (**2-Si**) in (D$_8$)toluene at different temperatures (298 K (top), 243 K (middle), 193 K (bottom). The residual proton signal of the deuterated solvent is marked with **S**. The line-broadening at 193 K probably results from the higher viscosity of the solvent at lower temperature.

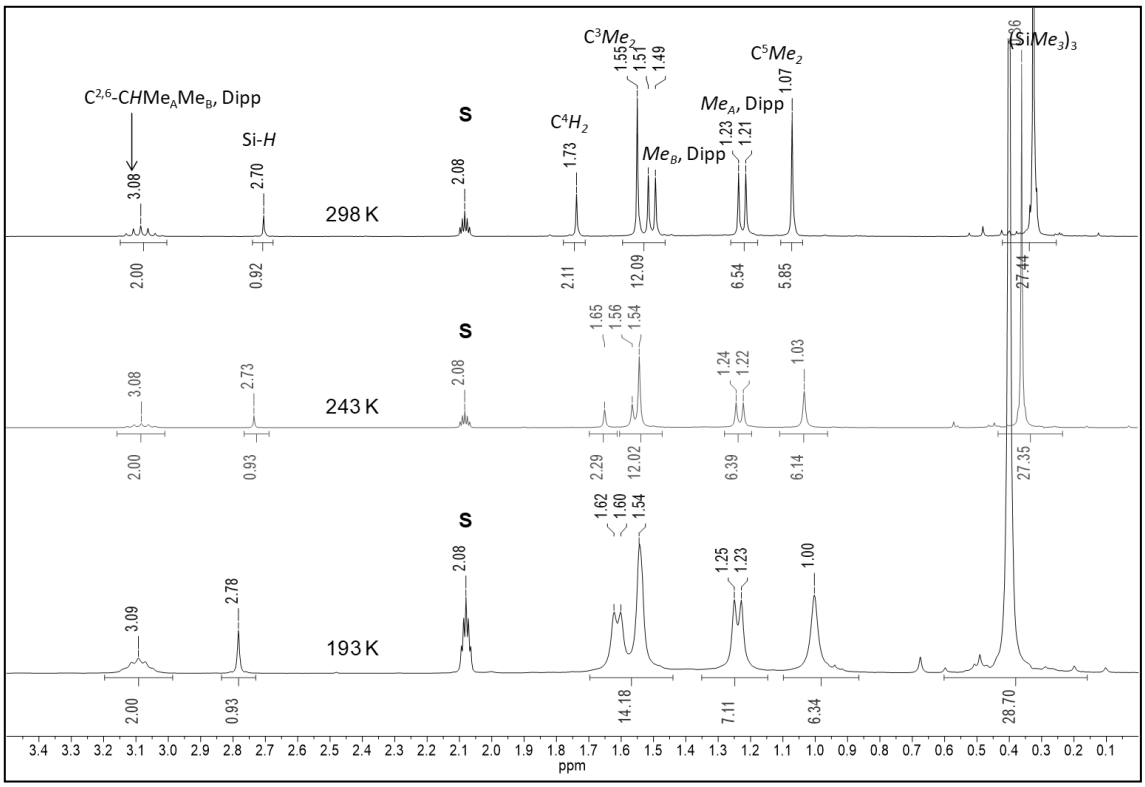

Figure 5.9. ^{1}H NMR spectra of SiH(SiTMS$_3$)(caac^{Me}) (**5-Si**) in (D$_8$)toluene at different temperatures (298 K (top), 243 K (middle), 193 K (bottom)). The residual proton signal of the deuterated solvent is marked with the character **S**. The line broadening at 193 K can be originated due to the higher viscosity of the solvent at lower temperatures.

5.4 Isothermal Titration Calorimetry of air sensitive compounds

5.4.1 Introduction

Isothermal Titration Calorimetry (ITC) is an useful analytical instrument to directly determine the equilibrium constant (K) and reaction enthalpy (ΔH) of a given reaction. By the use of the Gibb's Helmholtz equation ΔG can be calculated from K and the reaction entropy (ΔS) from the known ΔG and ΔH, respectively.

$$\Delta G = \Delta H - T\Delta S = -RT\ln(K) \qquad \text{(eq. 5.1)}$$

The method is originated from the biochemistry to determine the thermodynamic parameters of binding reactions by the detection of the heat change during the binding interaction.[334] The research group of A. K. Schneider could show in their recent publications that the method is also applicable to air sensitive chemistry.[335,336] Therefore the calorimeter has to be used inside the glovebox, which was special designed with a lower bottom plate, in order to perform the measurements. It has to be noted that during the calorimetric measurement the glovebox should not be used, since fluctuation of the argon pressure might influence the measured heat inside the mess cell.

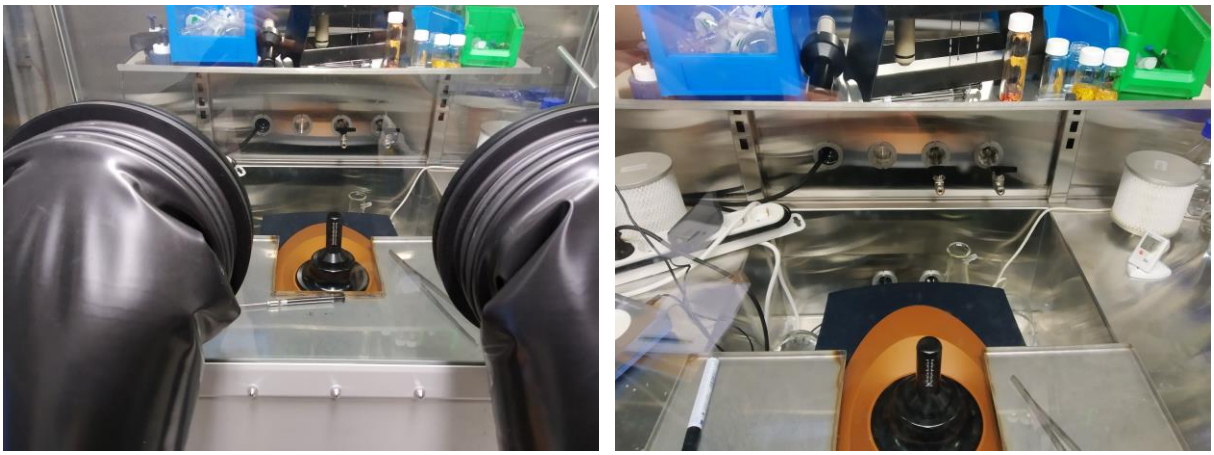

Figure 5.10. System of IT-Carlorimeter of AK Schneider inside the glovebox. TA Instruments NanoITC equipped with a 24 K gold cell with a sample volume of 1 mL operated in overfill mode and controlled by the ITCRun software version 3.4.6.0.

The ITC method is an extremely sensitive, rapid and direct method. It allows the direct measurement of the equilibrium constant (K), stoichiometry (n) and reaction enthalpy (ΔH).

The stoichiometry (n) is a useful value for the criteria of the reliability of the experiment: ideally it should give a value of 1, experimental values in the range of 1.05 – 0.95 are acceptable for a scientific result. Each studied reaction needs to be optimized in terms of formed heat (maximum upper limit 150 kJ mol^{-1}), curve form of the studied heat (Q) vs equivalent of added titrant and stoichiometry (n) by means of changing the concentration of the reactants (usually in the range of mM) or the temperature of the measurement (limits of the device 2 °C – 80 °C).
The method is however limited to 1:1 reactions of the type:

$$A + B \rightarrow C \qquad\qquad A + B \rightarrow C + D$$

Technically the heat of reactions higher order can be measured, the interpretation of the results is however much more complicated, since therefore polynomials of third order or higher need to be solved and applied to the measured data.

In order to perform the ITC measurements the desired reaction needs to fulfill the following criteria:[337]

a) The starting material has to be absolutely clean (impurities can have over proportional side heats and complicate the analysis)
b) Starting material and products need to be totally soluble in the selected solvent (the heat of the crystallization can be even higher than the heat of the desired reaction)
c) The heat of the reaction is high enough (at least +/- 0.1 µW per injection, otherwise the signal to noise ratio is to low)
d) The reaction equilibrates fast enough (at least 300 – 500 sec per injection, otherwise the uncontrollable diffusion from the injection syringe to the solution becomes dominant to the measured peak)
e) The product does not react with another equivalent of the starting material (chosen titrant). In order to obtain a full titration curve the reaction has to be performed with 2 equivalents of the titrant. However ΔH can still be obtained from the mean of the first peaks.
f) The reaction has to be selective (ITC measures the mean of all reaction heats in a present sample)

5.4.2 Principle of the measurement

The sample cell is filled with 950 µL of the analyte solution (mM solution) and the reference cell is filled with 1.3 mL of the corresponding solvent. The titrant (mM solution), should contain at least 2 equivalents compared to the analyte (in order to achieve a full titration curve) and is filled in a special injection syringe (volume 250 µL), which is a precision bore glass with a long stainless needle having a stir paddle attached to the extreme end (*Figure 5.11*), and inserted into the sample cell. Similarly the reference cell is filled with a syringe needle with a stirrer blave in order to simulate the same environment as in the sample cell.

The analyte solution is stirred throughout the whole experiment (usually with 350 rpm) in order to produce complete mixing in the cell within a few seconds after each injection. During an experiment, a small, constant power of less than a milliwatt is dissipated in the heater of the reference cell, which activates the cell feedback circuit to drive ΔT back to 0, which holds the temperature of the sample cell constant up to six digits after the decimal point.

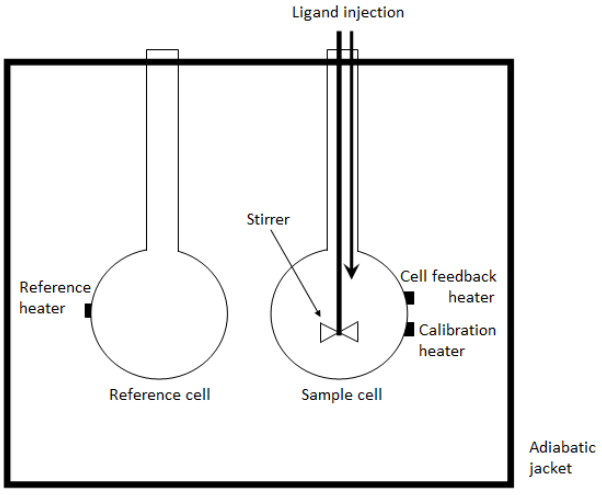

Figure 5.11. Schematic of an ITC instrument.

In the absence of a reaction, the feedback power will be constant at the resting baseline value. Usually the solution will be calibrated for 0.5 h in order to get a resting baseline, this is further checked by the software which starts the measurement when the regression line fits the set criteria (usually a slope of 0.3 µW/h with a standard deviation of 0.03). The Titration is set up in time intervals, which can be controlled via an injection schedule via the interactive software, with up to 300 – 500 sec (dependening on how fast the formed heat turns back to baseline), usually longer time intervals are not recommended due to the stronger effect of uncontrollable diffusion of the titrant into the analyte solution. The volume of the titrant should be added in 2.5 – 5 µL steps in order to get enough points for a graphical representation of the titration curve. After each addition of the titrant solution the reaction heats (exothermic reactions will temporarily decrease and endothermic reactions temporarily increase feedback power) are readily obtained by computer integration of these deflections (observed peaks of the plot of the registered µW against time in sec) from the resting baseline.

The Areas for all injections are determined by peak-by-peak computer integration and the resulting area table is then typically edited for heats of dilution. Therefore, the resulting heats Q (of each determined peak-area) are subtracted by a constant factor of the dilution enthalpy (which is usually in the range of 10 µJ per measured peak), which is done via the interactive software. This factor has to be determined in a separate measurement were the sample cell is filled with the pure solvent and the titrant is added with the same injection schedule as the measurement of the sample. The dilution of the analyte (from 950 µL to 1200 µL) is usually neglected. The processed data (differential heats, integral heats, and total titrant and analyte concentrations) are determined after corrections for the volumedisplacement in the total fill cell. The obtained curve Q against equivalents of added titrant is then deconvoluted using interactive nonlinear least squares, were the fitting parameters n, ΔH and K are automatically generated. The parameters can also be manually fixed in order to find the best fit. However it is better to not fix the parameter of stoichiometry (n), since it can give valuable information about the purity of the used analyte solution and the reliability of the experiment.

5.4.3 Thermodynamics of ITC Analysis

The during the measurement registered heat power ($P_s(t)$), which is applied to keep the temperature of the analyte cell against the reference cell constant, is a direct observable of the experiment:

$$P_s(t) = \frac{dQ}{dt} \qquad \text{(eq. 5.2)}$$

The formed or applied heat(Q) is the reaction enthalpy times the differential product concentration at a given volume.

$$P_s(t) = V_{cell}\Delta H \frac{d[C]}{dt} \qquad \text{(eq. 5.3)}$$

During the processing of the data the peaks of the heat power ($P_s(t)$) are integrated in certain time intervals (injection intervals) which leads to:

$$Q = V_{cell}\Delta H\,[C] \qquad \text{(eq. 5.4)}$$

In the ITC analysis the following reactions can be studied:

A + B → C A + B → C + D

$$K = \frac{[C]}{[A]\,[B]} \qquad \text{(eq. 5.5)} \qquad\qquad K = \frac{[C]\,[D]}{[A]\,[B]} \qquad \text{(eq. 5.6)}$$

Because the equilibrium concentrations [A] and [B] are not known during the titration, but the total (start)concentrations are

$$A_T = [A] + [C] \qquad \text{(eq. 5.7)} \qquad\qquad B_T = [B] + [C] \qquad \text{(eq. 5.8)}$$

The equations (eq. 5.7) and (eq. 5.8) can be inserted into the equations of the respective equilibrium constants (eq. 5.5) and (eq. 5.6):

$$K = \frac{[C]}{[A_T - C]\,[B_T - C]} \quad \text{(eq. 5.9)} \qquad\qquad K = \frac{[C]^2}{[A_T - C]\,[B_T - C]} \quad \text{(eq. 5.10)}$$

solving equations (eq. 5.9) and (eq. 5.10) for [C], which is essentially the calculation of the zero points of a quadratic equation leads to:

$$[C] = \frac{A_T + B_T + \frac{1}{K} - \left(\left(-A_T - B_T - \frac{1}{K}\right)^2 - 4\,A_T\,B_T\right)^{\frac{1}{2}}}{2} \qquad [C] = \frac{K(A_T + B_T) - \left(K(A_T - B_T)^2 - 4\,A_T\,B_T\right)^{\frac{1}{2}}}{2(K-1)}$$

(eq. 5.11) (eq. 5.12)

Inserting equations (eq. 5.11) and (eq. 5.12) into equation (eq. 5.4) leads to the equation for the fitting curve for the measurement in the both cases:

$$Q = V_{cell}\Delta H\,\frac{A_T + B_T + \frac{1}{K} - \left(\left(-A_T - B_T - \frac{1}{K}\right)^2 - 4\,A_T\,B_T\right)^{\frac{1}{2}}}{2} \qquad Q = V_{cell}\Delta H\,\frac{K(A_T + B_T) - \left(K(A_T - B_T)^2 - 4\,A_T\,B_T\right)^{\frac{1}{2}}}{2(K-1)}$$

(eq. 5.13) (eq. 5.14)

Equations (eq. 5.13) and (eq. 5.14) describe the fitting curves for the titration (plot of the integrated heat against aliquots of added titrant), were the reaction enthalpy (ΔH) and the equilibrium constant (K) are the direct observable fitting parameters of the curve.[48]

[48] The source of the derivation of the above mentioned formulas were taken from reference [338].

5.4.4 ITC Analysis of the reversible coordination of caac^{Me} to SiBr$_2$(caac^{Me})

Performed in collaboration with the Research Group of Sven Schneider (university of Göttingen), under the guidance of Daniel Delony 16-20.09.2019

Isothermal Titration Calorimetry was performed with a NanoITC device by TA INSTRUMENTS (24K gold cell and a sample volume of 1 mL) operated in overfill mode. Measurment by ITCRun Version 3.4.6.0, TA Instruments, 2017 and Evaluation by NanoAnalyze Version 3.7.5 TA Instruments, 2015. If not otherwise noted, room temperature (25 °C) was used as the operating temperature. Interpretation of the titration curves was performed using an independent model. The association reaction 1) was directly fitted with the model of Wiseman et al.[334], while the ligand exchange reaction was fitted with an adapted Wiseman model, taking the different form of the equilibrium constant of such reactions into account. [336]

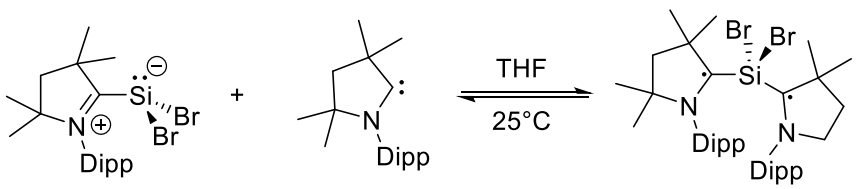

$C_{20}H_{31}NBr_2Si$ 473.37 g/mol

$C_{20}H_{31}N$ 285.48 g/mol

$C_{40}H_{62}N_2Br_2Si$ 758.84 g/mol

The experimental conditions were the following:

Internal Code	K-DD-63
Concentration and volume of SiBr$_2$(caac^{Me})	8.54 mM/950 µL
Concentration and volume of caac^{Me}	68.8 mM/250 µL
Injection Steps/Injected Volume	83 @ 3 µL
Waiting time between two additions	500 s
Stirring rate	350 rpm
Equilibration Time before experiment start	3131 s

The following graphs show the thermogram of the reaction mentoned above at 25°C. As background 20 µW Injection heat were subtracted.

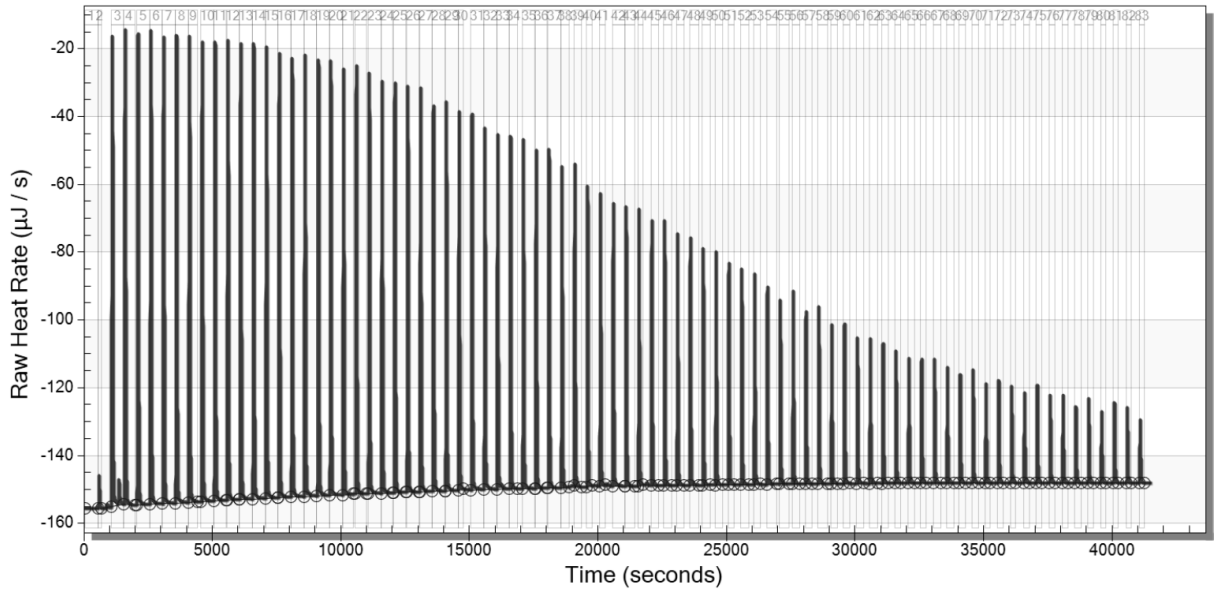

Figure 5.12. Thermodiagramm (raw heat rate in µJ s^{-1} against the time in s) of the 8.53 mM $SiBr_2(caac^{Me})$ solution during the addition of the 69.1 mM $caac^{Me}$ solution in THF at ambient temperature.

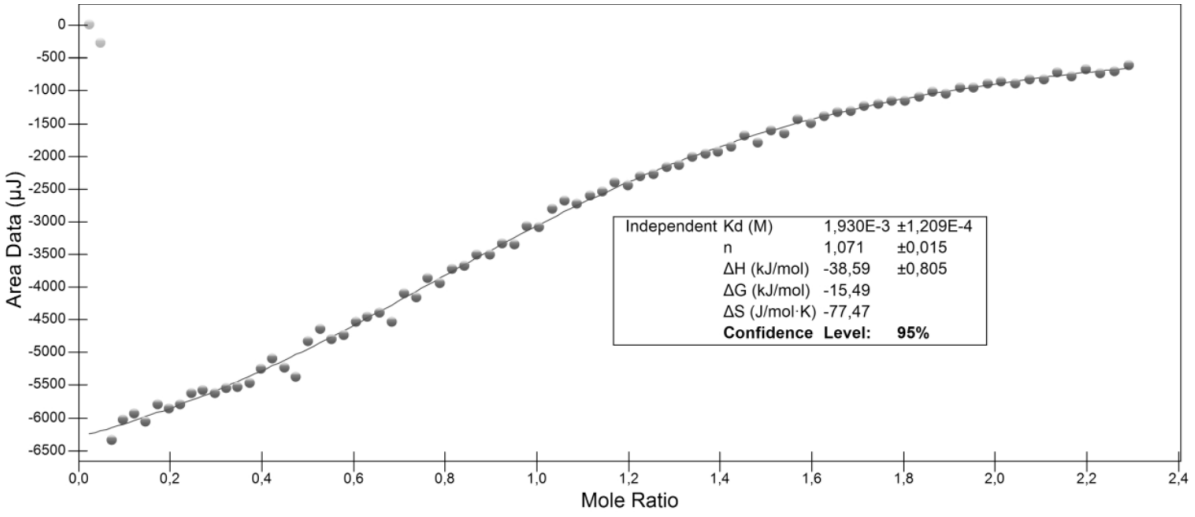

Figure 5.13. (Integrated) heat (Q) against added molar ratio of titrant $caac^{Me}$ carbene solution in THF at ambient temperature. The first data point was not taken into account.

Table 5.20. Results of the ITC analysis of the reversible association of $caac^{Me}$ carbene to $SiBr_2(caac^{Me})$ (**1**) at ambient temperature in THF.

Thermodynamic Parameter	Isothermal Titration Calorimetry
K_{eq}^{298} (M)	$(5.18 \pm 0.49) \times 10^2$ mol L^{-1}
ΔH^{298} (kJ·mol^{-1})	-38.6 ± 0.8 kJ mol^{-1}
ΔG^{298} (kJ·mol^{-1})	-15.5 ± 0.2 kJ mol^{-1}
ΔS^{298} (J·mol^{-1} K^{-1})	-77.5 ± 2 J K^{-1} mol^{-1}
Stoichiometry	1.071

5.5 ^{1}H NMR spectroscopic decomposition study of silicon(I) radicals

5.5.1 Determination of the amounts of 5-Si present in radical 2-Si

Using pure SiH(SiTMS$_3$)(caac^{Me}) (**5-Si**) as external standard the amount of hydridosilene **5-Si** present in the radical **2-Si** was estimated via quantitative ^{1}H NMR spectroscopy in(D_6)benzene.

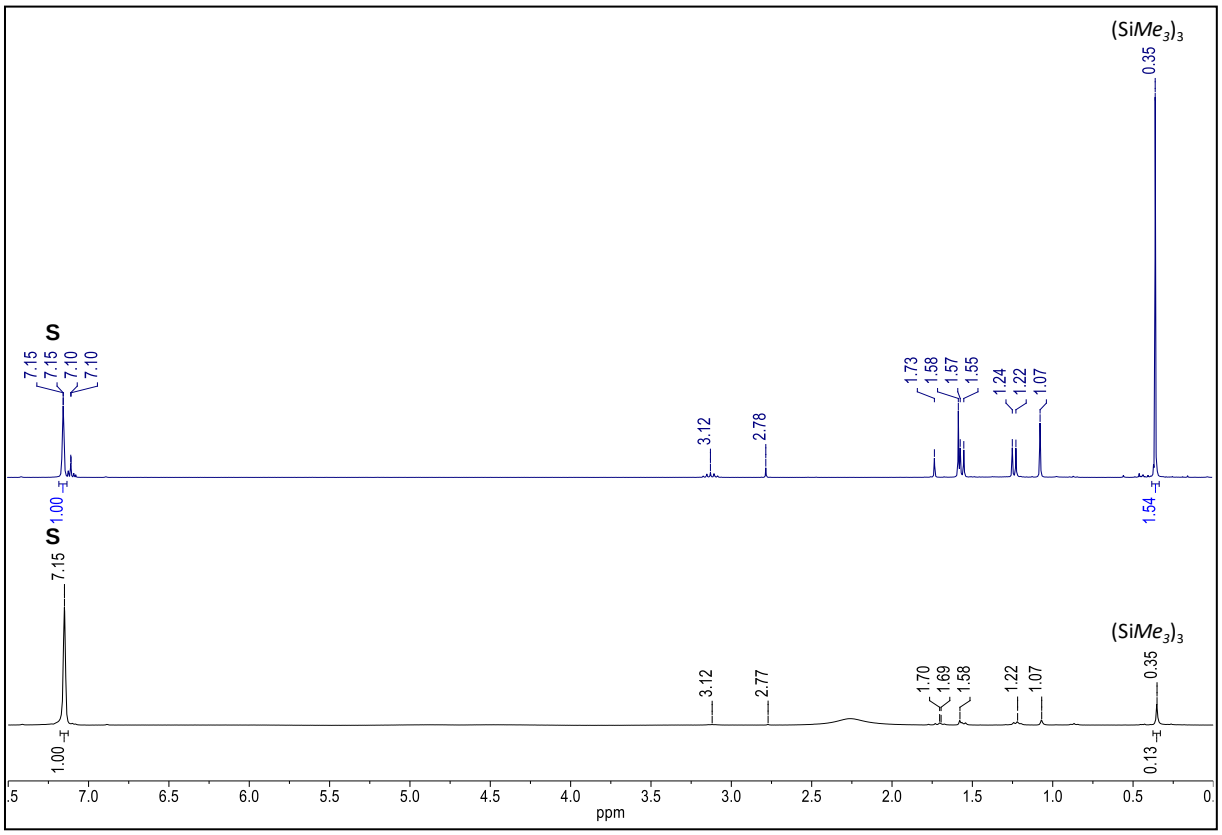

Figure 5.14. ^{1}H-NMR spectrum of pure hydridosilene **5-Si** (2.4 mg in 477.4 mg (D_6)benzene, measurement I, top) in comparison to silicon(I) radical **2-Si** (17.0 mg in 472.1 mg (D_6)benzene, measurement II, bottom) after 5 minutes at ambient temperature.

In quantitative ^{1}H NMR spectroscopy the most fundamental relationship is that the signal intensity in the NMR spectrum is directly proportional to the number of nuclei responsible for that particular resonance.[49]

$$I_x = K_{s(x)} * N_x \qquad \text{(eq. 5.15)}$$

I_x ... signal intensity of compound x; N_x ... number of nuclei responsible for that particular resonance;
$K_{S(x)}$ ... spectrometer constant, which is dependent of the puls excitation, the repetition time (relaxation delay) and broad band decoupling.

49 For more details see reference: S. K. Bharti, R. Roy, *Trends Anal. Chem.* **2012**, *35*, 5-26.

In order to quantify the hydridosilene **5-Si** present in radical **2-Si** (eq. 5.15) was used.[49]

$$\frac{m_x}{m_{Std}} = \frac{N_{std}}{N_x} * \frac{I_x}{I_{std}} * \frac{M_x}{M_{std}} \qquad \text{(eq. 5.16)}$$

and modified it with the constant K_S*:

$$\frac{m_x}{m_{Std}} = K_S{}^* * \frac{N_{std}}{N_x} * \frac{I_x}{I_{std}} * \frac{M_x}{M_{std}} \qquad \text{(eq. 5.17)}$$

m... mass of the compound, N ... number of nuclei, I... integral area, M ... molecular weight, K_S* ... equals to the quotient of spectrometer constants $K_{S(x)}/K_{S(std)}$, which ideally should give 1, when a 90° pulse is used and a relaxation delay of 5 times the relaxation time T1 is used.

In order to determine the constant K_S* we used the ^{1}H NMR spectrum of a known concentration of SiH(Tts)(caac^{Me}) (2.4 mg) (**5-Si**) in (D_6)benzene (477.4 mg) was measured under standard conditions: 300.13 MHz, puls sequence zg30, ns = 16, D = 1 sec, acquisition time = 4.2075 sec, 298 K . Therefore the relative integrals of the solvent peak C_6D_5H (7.15 ppm, 1H) and the peak for the silyl-groups in **5-Si** (0.35 ppm, (SiMe_3)$_3$, 27H) were used, which leads to the following equation (measurement I, see *Figure 5.14*):

$$\frac{m_{\mathbf{5-Si}}{}^I}{m_{C6D5H}{}^I} = K_S{}^* * \frac{1}{27} * \frac{I_{\mathbf{5-Si}}{}^I}{I_{C6D5H}{}^I} * \frac{M_{C6D5H}}{M_{\mathbf{5-Si}}} \qquad \text{(eq. 5.18)}$$

m_5 ... mass of compound **5-Si**, m_{C6D5H} ... mass of (D_6)benzene;

I_5 ... relative integral of the ($SiMe_3$)$_3$-group of **5-Si**, I_{C6D5H} ... relative integral of the solvent peak C_6D_5H;

M_5 molecular weight of **5-Si**, M_{C6D5H} ... molecular weight of (D_6)benzene.

Which leads to a constant of K_S* of:

$$K_S{}^* = \frac{m_{\mathbf{5-Si}}{}^I}{m_{C6D5H}{}^I} * 27 * \frac{I_{\mathbf{C6D5H}}{}^I}{I_{5-Si}{}^I} * \frac{M_{\mathbf{5-Si}}}{M_{\mathbf{C6D5H}}} \qquad \text{(eq. 5.19)}$$

Similarly, equation (eq. 5.18) was used for the calculation of the amount of hydridosilene **5-Si** in the given sample of radical **2-Si** (17.0 mg) in (D_6)benzene (472.1 mg) (measurement II, see *Figure 5.14*):

$$\frac{m_{\mathbf{5-Si}}{}^{II}}{m_{C6D5H}{}^{II}} = K_s{}^* * \frac{1}{27} * \frac{I_{\mathbf{5-Si}}{}^{II}}{I_{C6D5H}{}^{II}} * \frac{M_{C6D5H}}{M_{\mathbf{5-Si}}} \qquad \text{(eq. 5.20)}$$

which gives

$$m_{\mathbf{5-Si}}{}^{II} = K_s{}^* * \frac{1}{27} * \frac{I_{\mathbf{5-Si}}{}^{II}}{I_{C6D5H}{}^{II}} * \frac{M_{C6D5H}}{M_{\mathbf{5-Si}}} * m_{C6D5H}{}^{II} \qquad \text{(eq. 5.21)}$$

The molar ratio of hydridosilene **5-Si** with respect to radical **2-Si** can be calculated the following way:

$$X = \frac{m_{\mathbf{5-Si}}{}^{II}}{m_{\mathbf{2-Si}}} * \frac{M_{\mathbf{2-Si}}}{M_{\mathbf{5-Si}}} \qquad \text{(eq. 5.22)}$$

$m_{\mathbf{5\text{-}Si}}{}^{II}$ ... calculated mass of hydrosilene **5-Si** in radical **2-Si**, $m_{\mathbf{2\text{-}Si}}$ ... mass of radical **2-Si**

$M_{\mathbf{2\text{-}Si}}$ ... molecular weight of radical **2-Si**, $M_{\mathbf{5\text{-}Si}}$ ... molecular weight of hydrosilene **5-Si**

Inserting of (eq. 5.19) and (eq. 5.21) in (eq. 5.22) leads to the following result:

$$X = \frac{m_{\mathbf{5-Si}}{}^{I}}{m_{\mathbf{2-Si}}} * \frac{I_{C6D5H}{}^{I}}{I_{C6D5H}{}^{II}} * \frac{I_{\mathbf{5-Si}}{}^{II}}{I_{\mathbf{5-Si}}{}^{I}} * \frac{m_{C6D5H}{}^{II}}{m_{C6D5H}{}^{I}} * \frac{M_{\mathbf{2-Si}}}{M_{\mathbf{5-Si}}} \qquad \text{(eq. 5.23)}$$

Even though we can not determine exactly the mass of the benzene C_6D_5H, we can assume that the total mass of (D_6)benzene, which was determined by the fine balance, is direct proportional to the mass of C_6D_5H present in (D_6)benzene:

$$m((D_6)\text{benzene})_{total} = const * m_{C6D5H} \qquad \text{(eq. 5.24)}$$

Since equation (eq. 5.23) shows the quotient of $m_{C6D5H}{}^{II}/m_{C6D5H}{}^{I}$ we can insert the measured total mass of (D_6)benzene of the respective experiment (I and II), instead of the mass of C_6D_5H, since the (D_6)benzene solution was taken from the same batch and contained the same degree of deuteration and the constants are cancelling each other out.
Inserting of (eq. 5.24) in (eq. 5.23) and inserting the respective values lead to the following result:

$$X = \frac{2.4\ mg}{17.0\ mg} * \frac{0.13}{1.54} * \frac{472.1\ mg}{477.4\ mg} * \frac{561{,}21\ g/mol}{562{,}21\ g/mol} \qquad \text{(eq. 5.25)}$$
$$= 0.012$$

Finally the mol% of hydridosilene **5-Si** in radical **2-Si**, can be determined the following way:

$$P = \frac{X}{1 + X} * 100\ \% \qquad \text{(eq. 5.26)}$$

$$P = \frac{0.012}{1 + 0.012} * 100\ \% = 1.2\ \% \qquad \text{(eq. 5.27)}$$

5.5.2 Decomposition study of 3-Si

A present sample of 17.0 mg of Si(SiTMS$_3$)(caac^{Me}) (**3-Si**) in 0.5 ml (D_6)benzene, reveals the presence of 1.2 mol% SiH(Tts)(caac^{Me}) (**5-Si**), after 5 min in solution at ambient temperature.

Recorded ^{1}H NMR spectra in an interval of 0.5 h over a period of 4 h did not reveal any significant change of the NMR, which is in agreement with UV/Vis measurements, which did not show any sign of decomposition during 4 h in *n*-hexane solution (*section 5.10.1*).

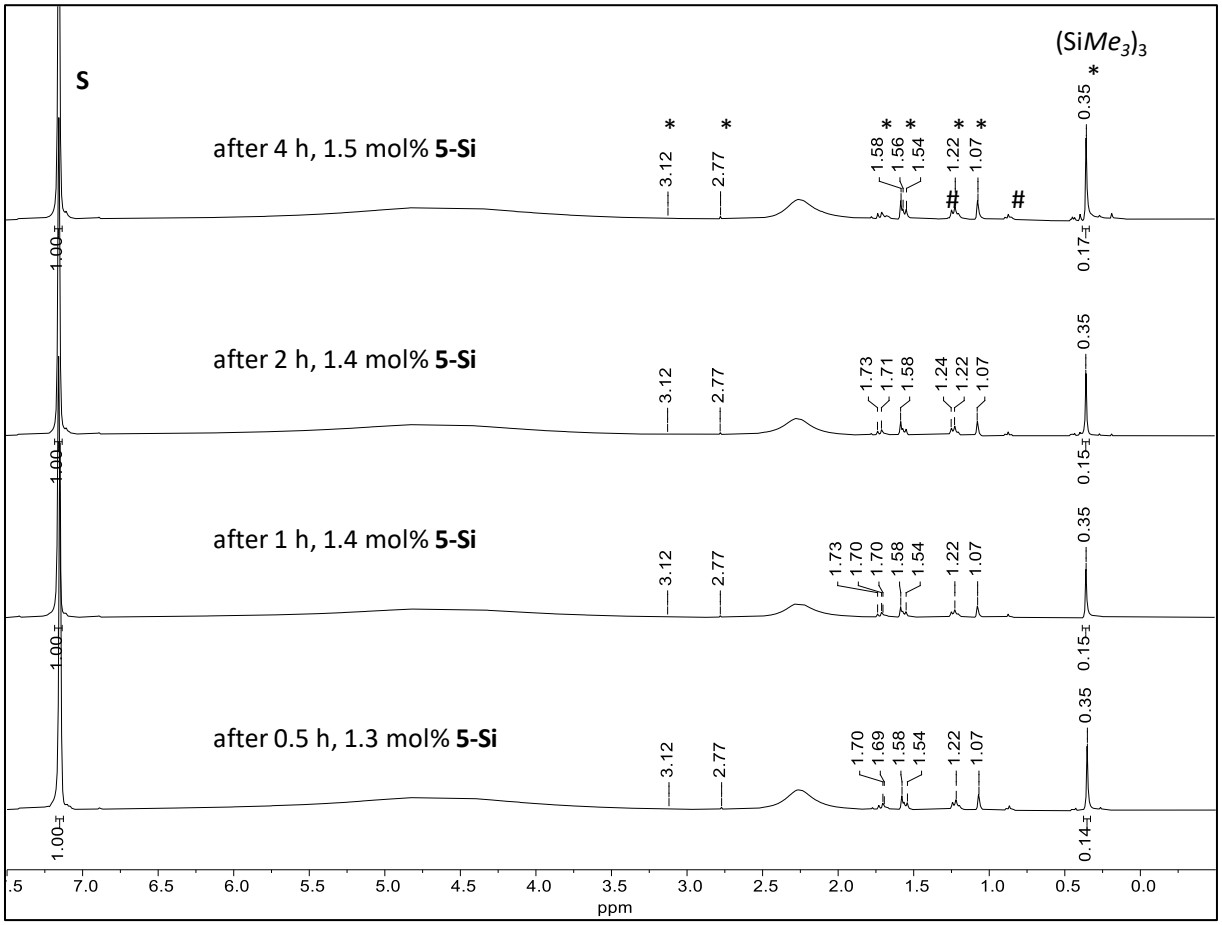

Figure 5.15. ^{1}H NMR spectra of Si(SiTMS$_3$)caac^{Me}) (**3-Si**) in (D_6)benzene at ambient temperature from bottom to top after 0.5, 1, 2 and 4 hours. The signals marked with (*) are assigned to the hydridosilene SiH(SiTMS$_3$)(caac^{Me}) (**5-Si**) which is the major decomposition product of the radical; the residual proton signal of the deuterated solvent is marked with the character **S**. The given mol% of hydridosilene **5-Si** was calculated using equations (eq. 5.25) and (eq. 5.26), applying the integral ratio of the SiMe$_3$-resonance with respect to the signal of the deuterated solvent in the depicted ^{1}H NMR spectra.

Recorded ^{1}H NMR spectra in an interval of 1 hour over a period of 3 days revealed a rather slow decomposition with the formation of 5 mol% hydrosilene **5-Si** after 3 days, hereby also other unknown decomposition products are formed.

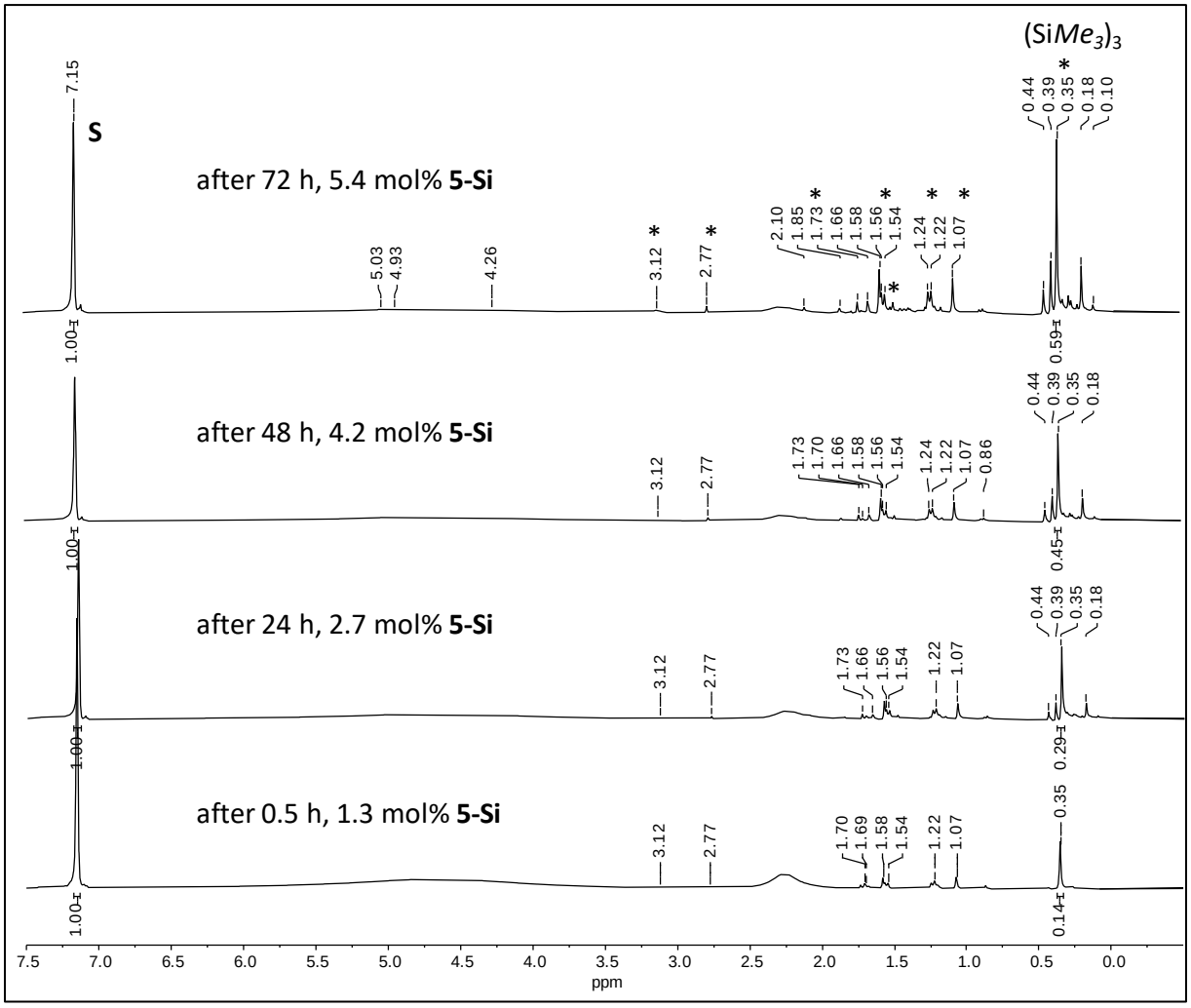

Figure 5.16. ^{1}H NMR spectra of Si(SiTMS$_3$)caac^{Me}) (**3-Si**) in (D_6)benzene at ambient temperature from bottom to top after 5 minutes, 24 hours, 48 hours and 72 hours. The signals marked with (*) are assigned to the hydridosilene SiH(SiTMS$_3$)(caac^{Me}) (**5-Si**) which is the major decomposition product of the radical; the residual proton signal of the deuterated solvent is marked with the character **S**. The given mol% of hydridosilene **5-Si** was calculated using equations (eq. 5.25) and (eq. 5.26), applying the integral ratio of the SiMe$_3$-resonance with respect to the signal of the deuterated solvent in the depicted ^{1}H NMR spectra.

5.5.3 Decomposition study of 3-N

A present sample of 14.5 mg of $Si(NTMS_2)(caac^{Me})$ radical (**3-N**) in 0.5 mL (D_6)benzene, reveals the presence of tiny amounts of $SiH(NTMS_2)(caac^{Me})$ (**5-N**), after 5 minutes in solution at ambient temperature. In analogy to the determined amounts of hydridosilene **5-Si** present in radical **3-Si**, it is safe to assume that roughly 1 mol% of **5-N** is present in the given (D_6)benzene solution of radical **3-N** (*Figure 5.17* bottom).
Recorded ^{1}H NMR spectra in an interval 0.5 h over a period of 4 h did not reveal any significant change of the NMR, which is in agreement with UV/Vis measurements, which did not show any sign of decomposition during 4 h in *n*-hexane solution (see *section 5.10.2*).

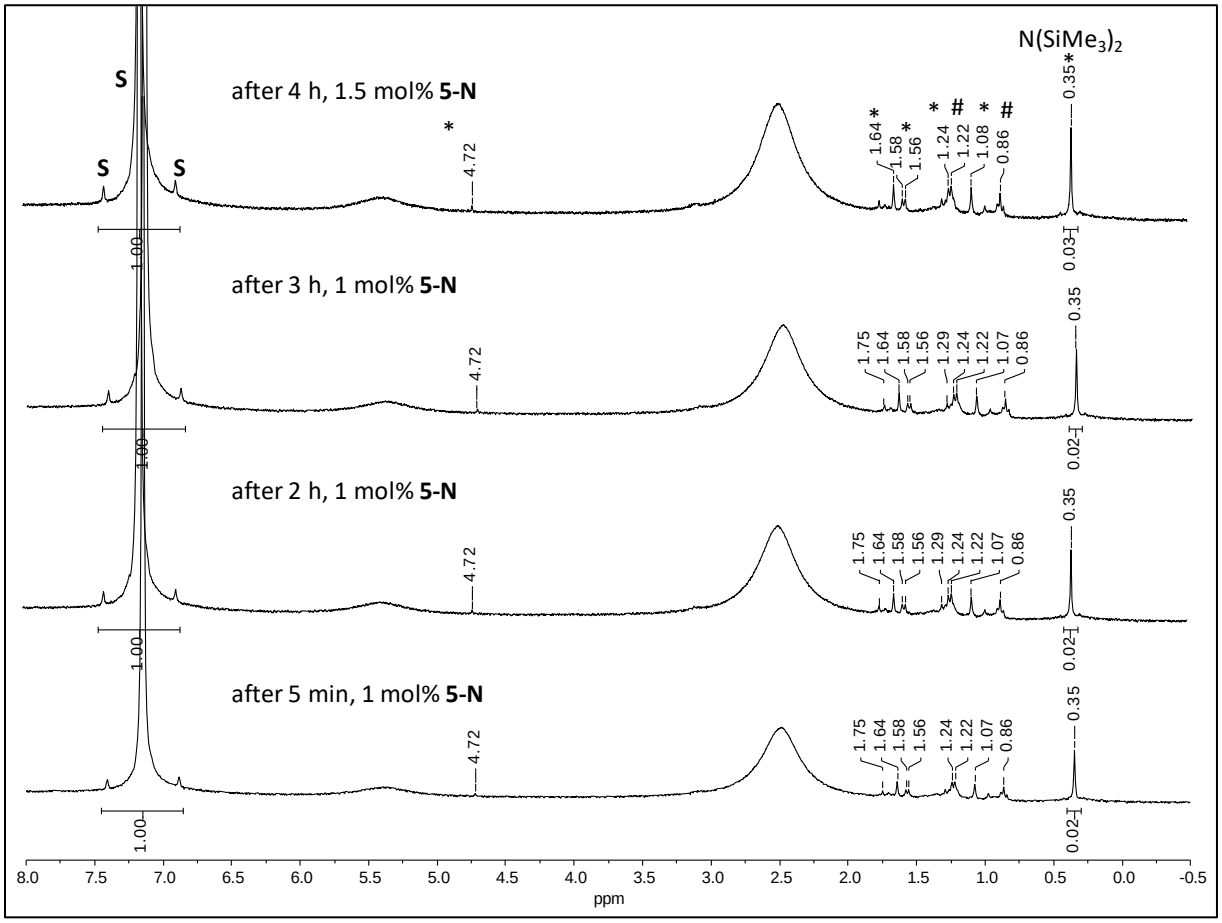

Figure 5.17. ^{1}H NMR spectra of $Si(NTMS_2)(caac^{Me})$ (**3-N**) in (D_6)benzene at ambient temperature from bottom to top after 1 h, 2 h, 3 h and 4 h. The signals marked with (*) are assigned to the hydridosilene $SiH(NTMS_2)(caac^{Me})$ (**5-N**) which is the major decomposition product of the radical; # marks tiny amounts of *n*-pentane present in the sample, the residual proton signal of the deuterated solvent as well as the ^{13}C satelites are marked with the character **S**. The given mol% of hydridosilene **5-N** was estimated to be 1 mol% in the first recorded ^{1}H NMR spectrum after 5 min at ambient temperature. Applying the integral ratio of the $SiMe_3$-resonance with respect to the signal of the deuterated solvent in the depicted ^{1}H NMR spectra was then used to estimate the mol% of **5-N** after any given time interval.

Recorded ^{1}H NMR spectra in an interval of 1 hour over a period of 2 days revealed a rather slow decomposition with the formation of roughly 2 mol% hydrosilene **5-N** after 2 days.

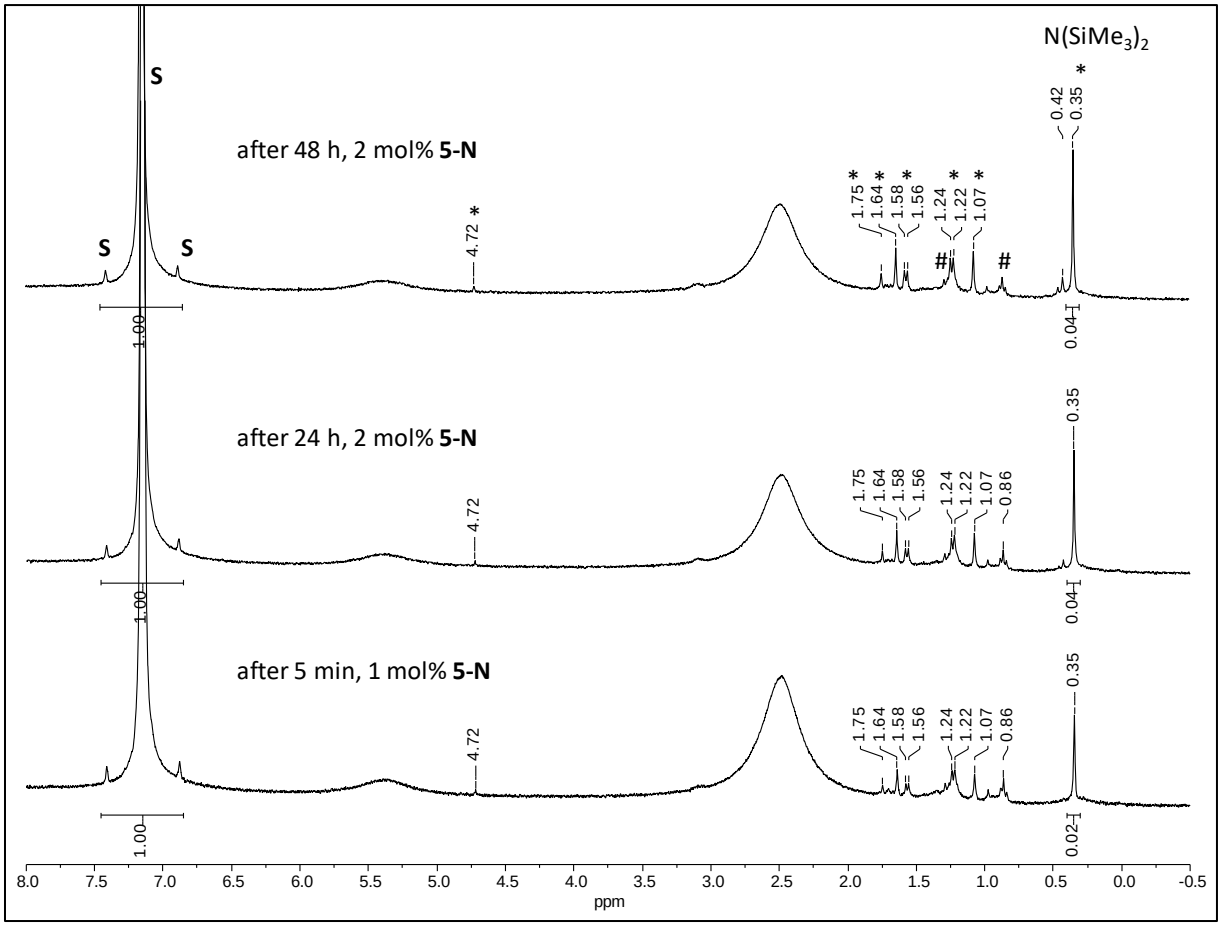

Figure 5.18. ^{1}H NMR spectra of Si(NTMS$_2$)(caac^{Me}) (**3-N**) in (D_6)benzene at ambient temperature from bottom to top after 5 minutes, 24 hours and 48 hours. The signals marked with (*) are assigned to the hydridosilene SiH(NTMS$_2$)(caac^{Me}) (**5-N**) which is the major decomposition product of the radical; # marks tiny amounts of *n*-pentane present in the sample; the residual proton signal of the deuterated solvent as well as the ^{13}C satelites are marked with the character **S**. The given mol% of hydridosilene **5-N** was estimated to be 1 mol% in the first recorded ^{1}H NMR spectrum after 5 min at ambient temperature. Applying the integral ratio of the SiMe$_3$-resonance with respect to the signal of the deuterated solvent in the depicted ^{1}H NMR spectra was then used to estimate the mol% of **5-N** after any given time interval.

5.6 Study of the dynamics of compounds by VT ^{1}H NMR spectrsocopy

5.6.1 General Part

In order to study dynamic processes, which were observed in serveral of isolated compounds ^{1}H NMR spectra were recorded at variable temperatures in the temperature range of (–90) – (100) °C (usually in (D_8)toluene). Full line-shape analysis was carried out using selected ^{1}H NMR resonances, which featured a coalescence. In order to obtain the first order exchange rate constants (k), the resonances were simulated using the software gNMR. [50]

The temperature dependence of the exchange rate constants was derived from a modified form of the linearized Eyring equation (eq. 1, k_B = Boltzmann constant, h = Planck´s constant, R = gas constant) assuming that the transmission coefficient κ is equal 1 and that the activation enthalpy ($\Delta H^{\ddagger}$) is constant over the temperature interval of the experiment ($\Delta C_p^{\ddagger} = d(\Delta H^{\ddagger})/dT = 0$, $\Delta C_p^{\ddagger}$ = heat capacity of activation).

$$\ln\left(\frac{k}{T}\right) = \ln\left(\frac{k_B}{h}\right) + \left(\frac{\Delta S^{\ddagger}}{R}\right) + \left(-\frac{\Delta H^{\ddagger}}{R}\right) \cdot \frac{1}{T} \qquad \text{(eq. 5.28)}$$

$$\Delta H^{\ddagger} = -R \cdot \text{slope} \; [\text{J} \cdot \text{mol}^{-1}] \qquad \text{(eq. 5.29)}$$

$$\Delta S^{\ddagger} = R \cdot \left(\text{Intercept} - \ln\left(\frac{k_B}{h}\right)\right) \; [\text{J} \cdot \text{K}^{-1} \cdot \text{mol}^{-1}] \qquad \text{(eq. 5.30)}$$

$$\Delta G^{\ddagger} = \Delta H^{\ddagger} - T \cdot \Delta S^{\ddagger} \qquad \text{(eq. 5.31)}$$

The enthalpy of activation ($\Delta H^{\ddagger}$) and entropy of activation ($\Delta S^{\ddagger}$) were obtained from the slope and the intercept of the linear fit using (eq. 5.29) and (eq. 5.30), respectively. $\Delta G^{\ddagger}$ was calculated from equation (eq. 5.31).

[50] gNMR, Version 5.0.6.0, P.H.M. Budzelaar, Ivorysoft, Centennial, USA, **2006**.

Using (eq. 5.32) the Gibbs energy of activation ($\Delta G^{\ddagger}$) can be estimated at the coalescence temperature (T_C):

$$\Delta G^{\ddagger} = 0.0191 \cdot T_c \cdot \left[9.97 + \log\left(\frac{T_c}{\Delta\nu}\right)\right] [\mathrm{kJ \cdot mol^{-1}}] \qquad \text{(eq. 5.32)}$$

where, $\Delta\nu$ is the separation of the exchanging signals in Hz in the low temperature limit spectrum where no exchange occurs (k = 0) and $\Delta\nu/J > 3$. (eq. 5.32) can be obtained form (eq. 2.5), assuming $k = 2.22(\Delta\nu)^{1/2}$. [339,340]

5.6.2 VT ^{1}H NMR spectra and line shape analysis of 20

The ^{1}H NMR spectrum of CpCo(CO)SiBr$_2$(caac^{Me}) (**20**) displays a broad signal for the C^{2,6}-C*H*Me$_2$ Dipp resonance at 3.02 ppm as well as a broad signal for the C^3*Me$_2$* group at 1.97 ppm in (D_8)toluene at ambient temperature in solution (*Figure 5.20*, top spectrum). Recording the ^{1}H NMR spectrum at 243 K led to the decoalescence of the C^{2,6}-C*H*Me$_2$ septet into two septets appearing at $\delta = 2.76$ and 3.34 ppm, which were assigned abritratrily as as C^2-C*H* and C^6-C*H*, respectively (*Figure 5.20*, bottom spectrum). The variable temperature ^{1}H NMR studies showed that the two septets coalesces at the coalescences temperature (T_c) of 283 K where also clearly the coalescence of the C^3*Me$_2$* and C^5*Me$_2$* resonances are observed. The dynamic process can be attributed to a hindered rotation of the caac^{Me} ligand about the Si–C^{carb} bond at the prochiral silicon(II) center in **20** (*Figure 5.19*).

Full line shape analysis of the septets was carried out using the g-NMR software, in order to obtain the exchange rate konstants (k) for the hindered Si–C^{carb} rotation in CpCo(CO)SiBr$_2$(caac^{Me}) (**20**) (*Figure 5.22*). The rate constants are listed in *Table 5.21*.

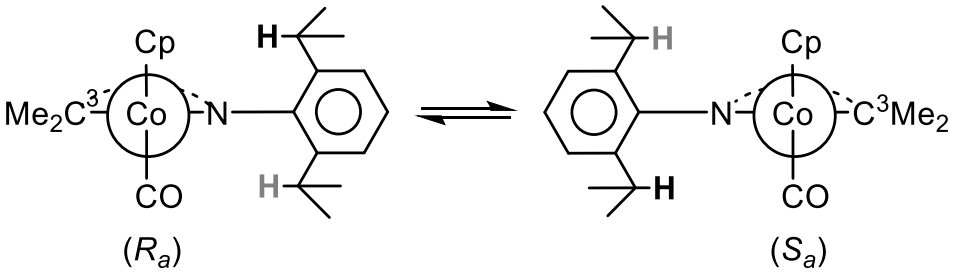

Figure 5.19. The relative orientation of the caac^{Me} carbene to the CpCo(CO) moiety leads to a form of axial chirality in the molecule with the chirality axis passing through the Co and C^{carb} atoms. Upon rotation of the Si–C^{carb} bond, the respective other enantiomer can be obtained in solution.

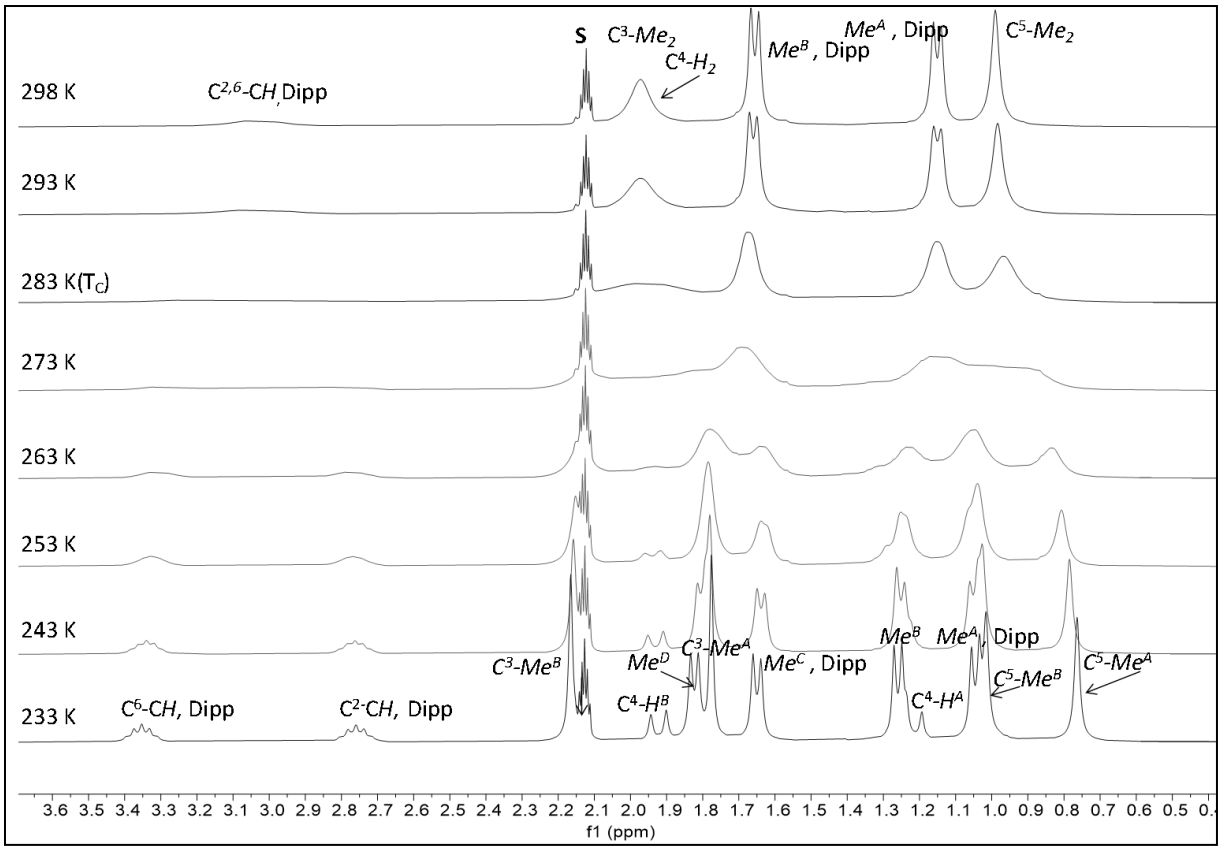

Figure 5.20. Excerpt of the ^{1}H NMR spectra (300.13 MHz) of CpCo(CO)SiBr$_2$(caac^{Me}) (**20**) in (D$_8$)toluene in the temperature range 233 – 298 K; the signal of the deuterated solvent is marked with the character **S**.

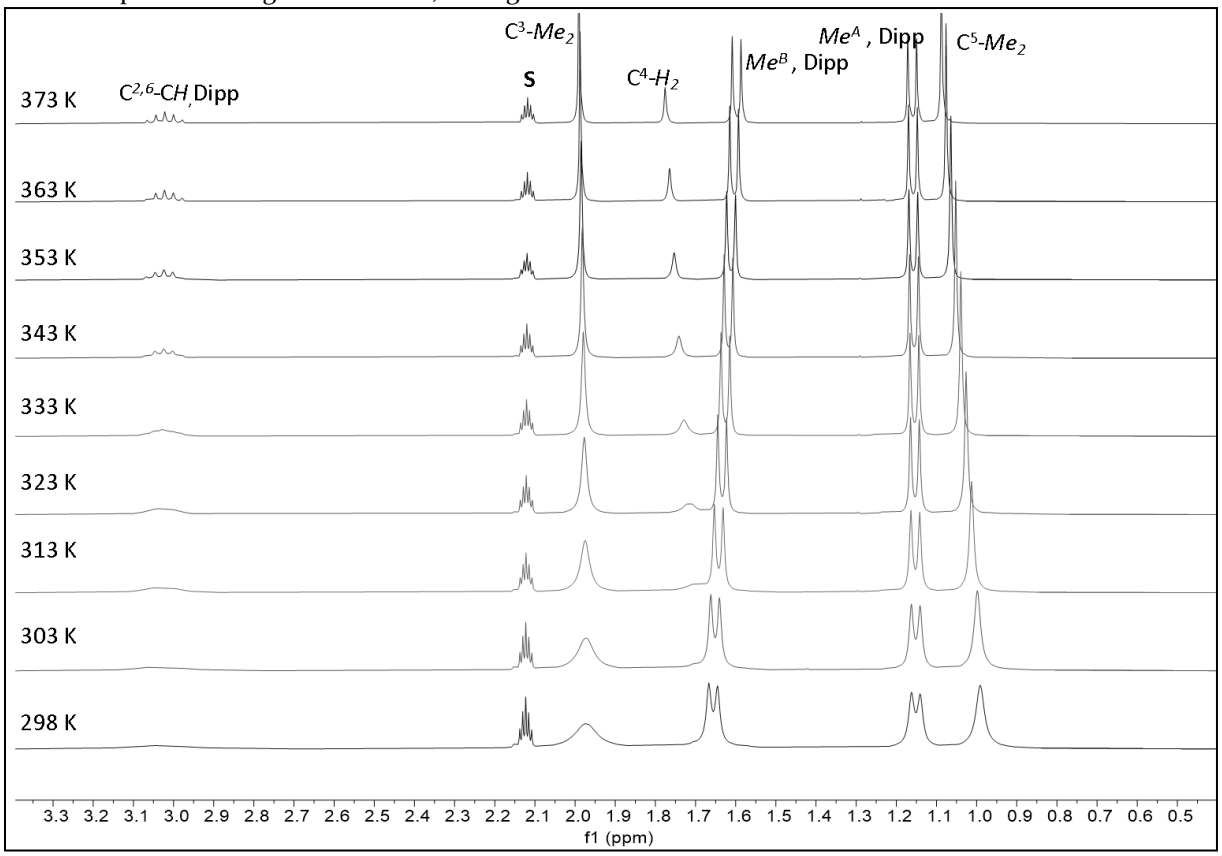

Figure 5.21. Excerpt of the ^{1}H NMR spectra (300.13 MHz) of CpCo(CO)SiBr$_2$(caac^{Me}) (**20**) in (D$_8$)toluene in the temperature range 298 – 373 K; the signal of the deuterated solvent is marked with the character **S**.

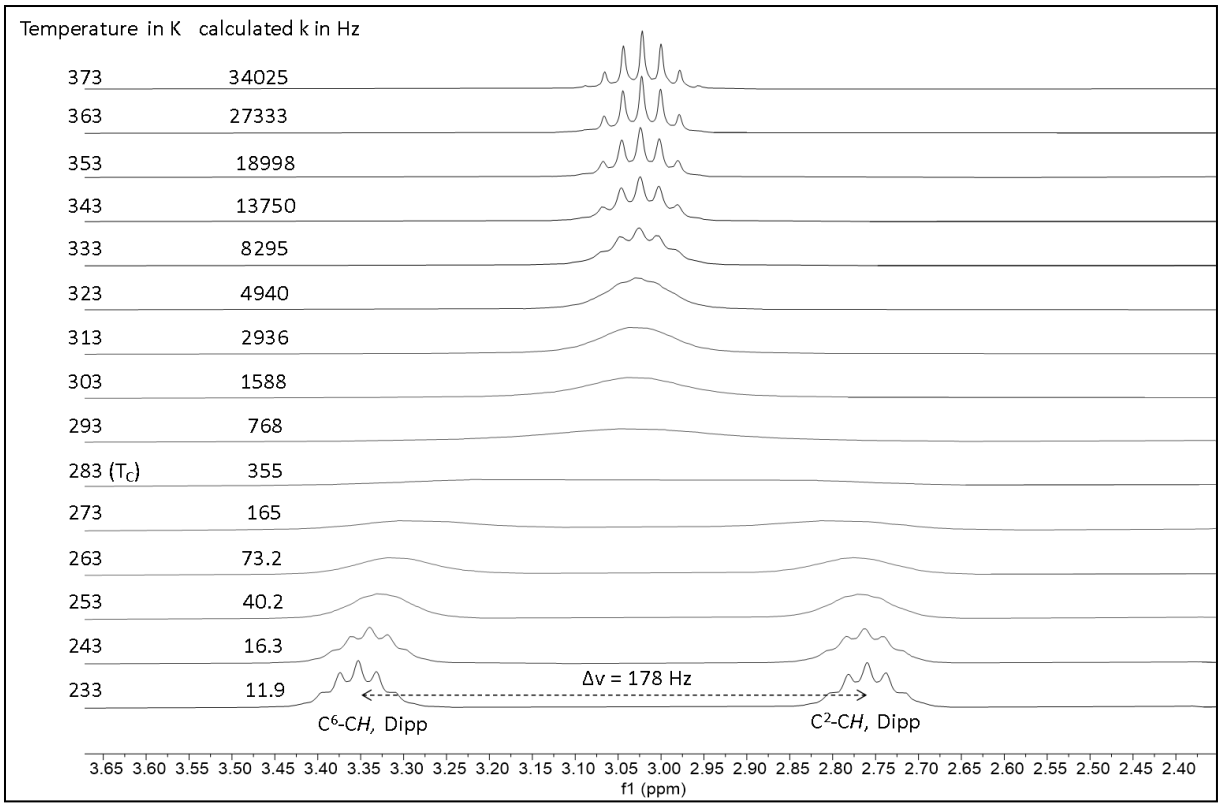

Figure 5.22. Excerpt of the ^{1}H NMR (300.13 MHz) spectra of CpCo(CO)SiBr$_2$(caac^{Me}) (**20**) in (D$_8$)toluene from 233 K – 373 K showing the exchange process involving the C^{2,6}-C*H*Me$_2$ resonances.

Table 5.21. Rate constants (k in Hz) for the hindered Si–C^{carb} rotation in **20** at different temperatures.

T /K	k_1 /Hz	$\sigma(k_1)$ /Hz	$\ln(k_1/T)$	1/T /K^{-1}
243	16.3	1.03	–2.70	0.004115
253	40.2	1.19	–1.84	0.003953
263	73.15	1.27	–1.28	0.003802
273	165.0	1.07	–0.50	0.003663
283	355.1	1.01	0.23	0.003534
293	768.2	1.01	0.96	0.003413
303	1588.2	1	1.66	0.003300
313	2937	1.01	2.24	0.003195
323	4940	1.01	2.73	0.003096
333	8295	1.05	3.22	0.003003
343	13750	1.05	3.69	0.002915
353	18998	1.07	3.99	0.002833
363	27334	1.1	4.32	0.002755
373	34025	1.16	4.51	0.002681

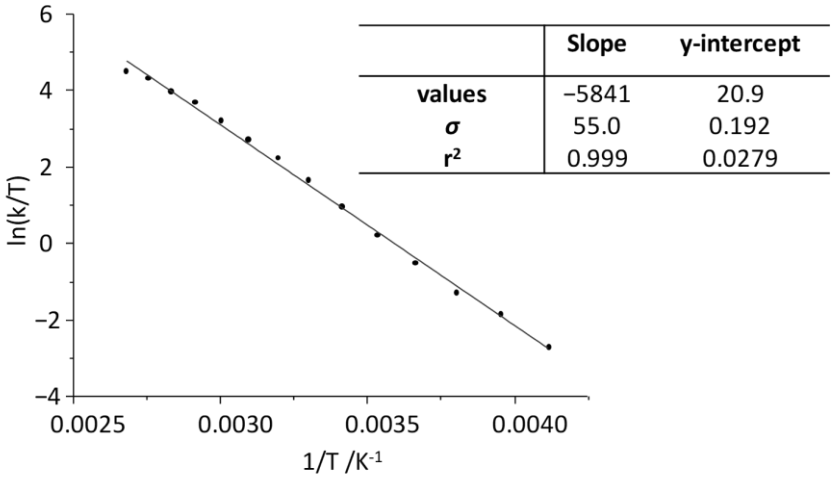

Figure 5.23. Eyring Plot of ln(k/T) versus 1/T for hindered rotation of the Si–C^{carb} bond in CpCo(CO)$SiBr_2$($caac^{Me}$) (**20**).

Table 5.22. Activation parameters for the Si–C^{carb} rotation in **20** obtained from full-line shape iteration.

Thermodynamic activation parameter	Calculated values[a] for the Si–C^{carb} rotation
$\Delta G^{\ddagger}$(298K)	55.6 ± 1.0 kJ mol^{-1}
$\Delta G^{\ddagger}(T_c)$	55.3 ± 1.0 kJ mol^{-1} (283 K)
$\Delta H^{\ddagger}$	48.6 ± 1.0 kJ mol^{-1}
$\Delta S^{\ddagger}$	−23.8 ± 1.6 J K^{-1} mol^{-1}

[a]: The error was calculated using the variance formula given in reference [341]. The average error of the temperature (σ(T)) was estimated to be 0.2 K.

Using (eq. 5.32) the Gibbs energy of activation ($\Delta G^{\ddagger}$) can be estimated at the coalescence temperature (T_C). The $\Delta G^{\ddagger}(T_C)$ values are listed in the table below.

Table 5.23. Estimated free Gibbs energy of activation using (eq. 5.32)at Tc ($\Delta G^{\ddagger}(T_c)$) for the Si–C^{carb} bond rotation in CpCo(CO)$SiBr_2$($caac^{Me}$) (**20**).

Dynamic process	T_c/K	Δν/Hz	$\Delta G^{\ddagger}(T_c)$/kJ·mol^{-1}
Si–C^{carb} rotation	283	178 Hz[a]	55.0

[a]: The distance between the signals of C^2-C*H* and C^6-C*H* of the Dipp substituent in the slow exchange limit spectrum at 233 K (*Figure* 5.22).

5.6.3 VT ^{1}H NMR spectra and line shape analysis of 19-Me

The ^{1}H NMR spectrum of [SiMe(caac^{Me})$_2$][B(Ar^F)$_4$] (**19-Me**) in (D$_8$)THF at ambient temperature features an averaged C_S-symmetry, displaying a sharp septet for the C^{2,6}-C*H*Me$_2$ Dipp resonance at 2.75 ppm (*Figure 5.45*, top spectrum). Recording the ^{1}H NMR spectrum at 193 K led to the decoalescence of the C^{2,6}-C*H*Me$_2$ septet into two septets appearing at δ = 2.61 and 2.93 ppm, which were assigned abritratrily as as C^2-C*H* and C^6-C*H*, respectively (*Figure 5.45*, bottom spectrum). The variable temperature ^{1}H NMR studies showed that the two septets coalesces at the coalescences temperature (T$_c$) of 223 K where also clearly the coalescence of the C^4-H_A and C^4-H_B resonances are observed. However, the C$_1$-symmetry of **19** observed in the solid state could not be frozen out, suggesting that an additional process is active, which leads to homotopic resonances for the caac^{Me} substituents in the ^{1}H NMR spectrum of **19** at 193 K and an observed averaged C_2-symmetry at that temperature. This can be highly likely attributed to a pyramidal inversion of the trigonal pyramidalized silicon center in **19** via a trigonal planar transition state, which is still active at 193 K. The dynamic process which could be frozen out by VT ^{1}H NMR spectroscopy can be attributed to a hindered rotation of the caac^{Me} substituents about their Si–C^{carb} bond (*Figure 5.24*).

Full line shape analysis of the septets was carried out using the g-NMR software, in order to obtain the exchange rate konstants (k) for the hindered Si–C^{carb} rotation of [SiMe(caac^{Me})$_2$][B(Ar^F)$_4$] (**19-Me**) (*Figure 5.26*). The rate constants are listed in the *Table* 5.27.

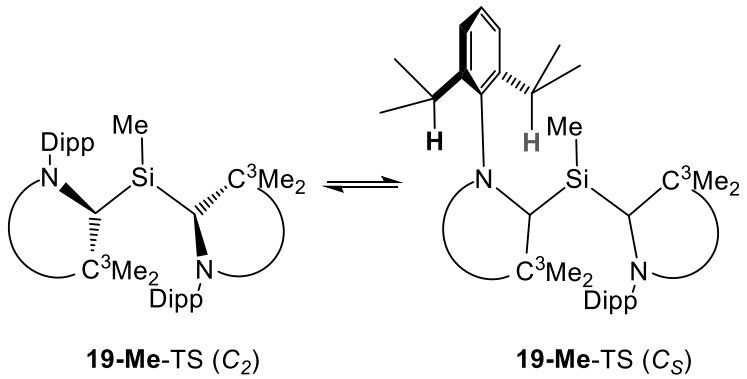

Figure 5.24. Rotation of caac^{Me} substituents about their respective Si–C^{carb} bonds in the trigonal planar transition state of **19-Me**-TS. Upon rotaton of the Si–C^{carb} bonds a *Cs*-symmetric transition state **19-Mes**-TS (C$_S$) is obtained with the mirror plane passing through the Si, C^{carb}, N and C3 atoms, leading to enantiotopic C^{2,6}-C*H*Me$_2$ Dipp resonances, respectively. Both caac^{Me} substituents are rendered equally by a C_2-symmetry.

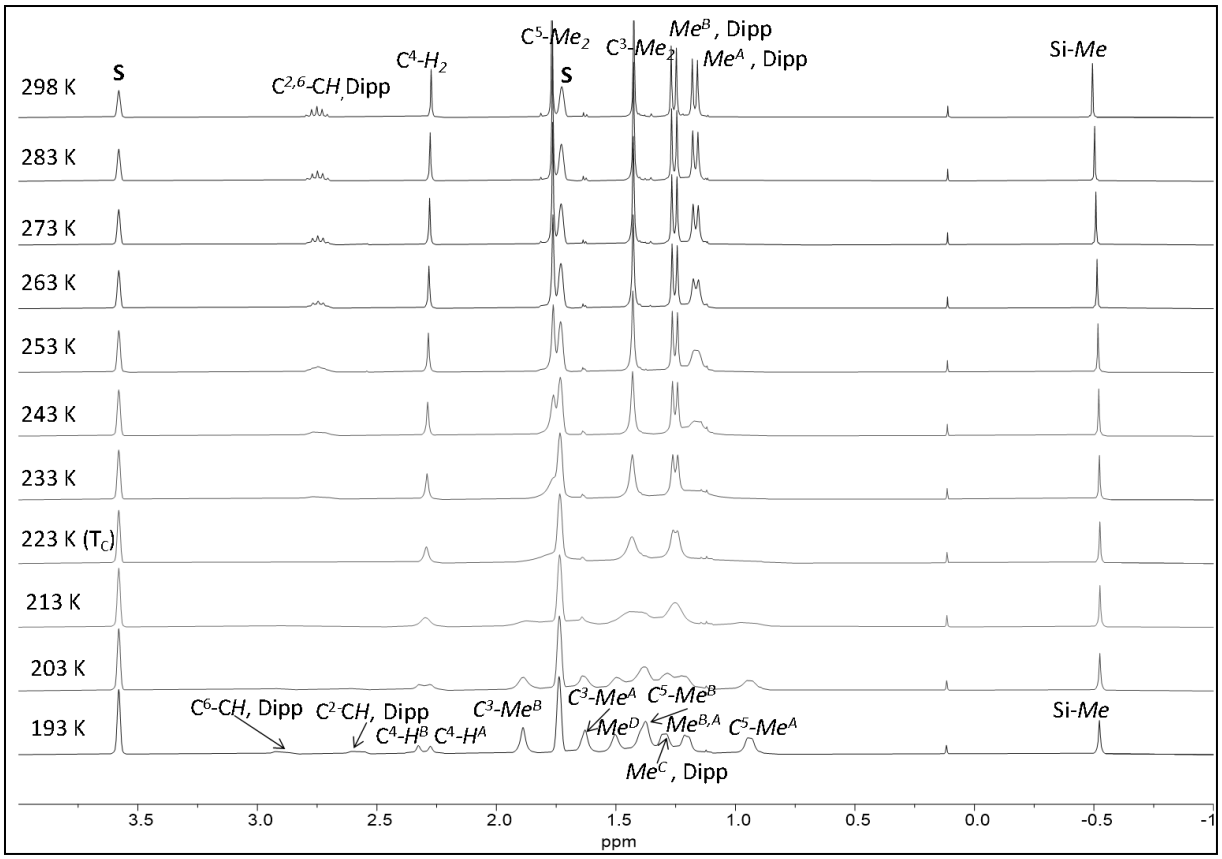

Figure 5.25. Excerpt of the ^{1}H NMR spectra (300.13 MHz) of [SiMe(caac^{Me})$_2$][B(Ar^F)$_4$] (**19-Me**) in (D$_8$)THF in the temperature range 193 K – 298 K; the signal of the deuterated solvent is marked with the character **S**.

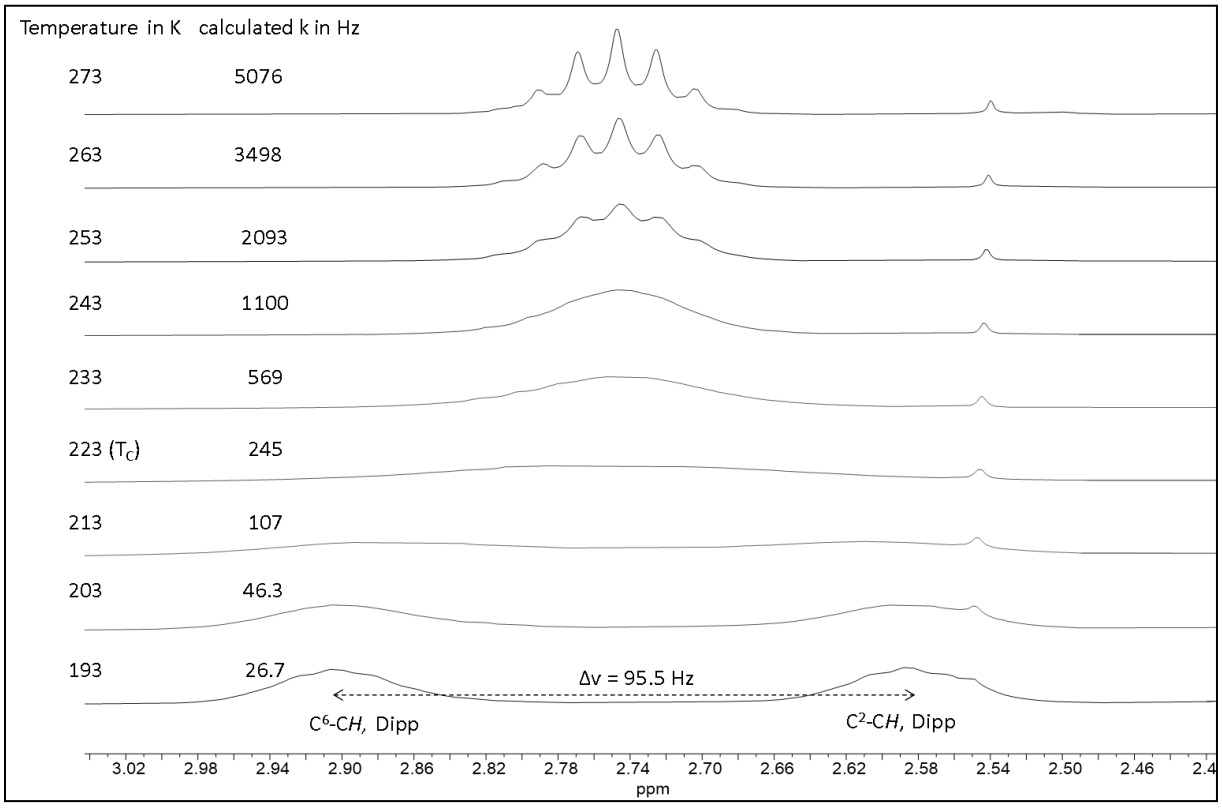

Figure 5.26. Excerpt of the ^{1}H NMR (300.13 MHz) spectra of of [SiMe(caac^{Me})$_2$][B(Ar^F)$_4$] (**19-Me**) in (D$_8$)THF from 193 K – 273 K showing the exchange process involving the C^{2,6}-CHMe$_2$ resonances.

Table5.24. Rate constants (k in Hz) for the Si–C^{carb} rotation in **19-Me** at different temperatures.

T /K	k_1 /Hz	$\sigma(k_1)$ /Hz	$\ln(k_1/T)$	1/T /K^{-1}
193	26.742	1.34	-1.98	0.005181
203	46.33	1.22	-1.48	0.004926
213	106.93	1.12	-0.69	0.004695
223	245.3	1.09	0.10	0.004484
233	569.38	1.11	0.89	0.004292
243	1100.27	1.23	1.51	0.004115
253	2093.15	1.44	2.11	0.003953
263	3497.84	1.26	2.59	0.003802
273	5075.75	1.16	2.92	0.003663

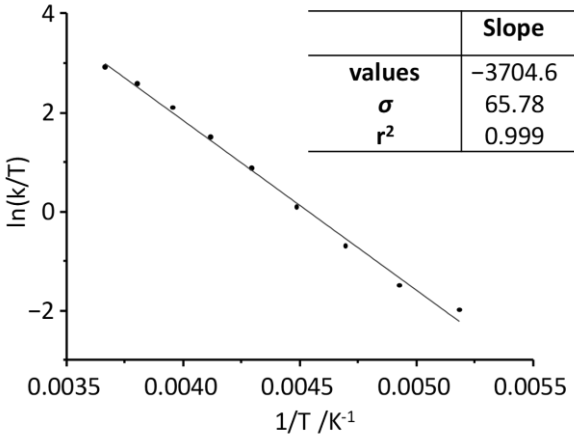

Figure 5.27. Eyring Plot of ln(k/T) versus 1/T for the Si–C^{carb} rotation in [SiMe(caac^{Me})$_2$][B(Ar^F)$_4$] (**19**).

Table 5.25. Activation parameters for the Si–C^{carb} rotation in **19-Me** obtained from full-line shape iteration.

Thermodynamic activation parameter	Calculated values[a] for the Si–C^{carb} rotation
$\Delta G^{\ddagger}$(298K)	48.2 ± 0.8 kJ mol^{-1}
$\Delta G^{\ddagger}(T_c)$	43.8 ± 0.8 kJ mol^{-1} (223 K)
$\Delta H^{\ddagger}$	30.8 ± 0.5 kJ mol^{-1}
$\Delta S^{\ddagger}$	-58.4 ± 2.3 J K^{-1} mol^{-1}

[a]: The error was calculated using the variance formula given in reference [341]. The average error of the temperature (σ(T)) was estimated to be 0.2 K.

Using (eq. 5.32) the Gibbs energy of activation ($\Delta G^{\ddagger}$) can be estimated at the coalescence temperature (T_C). The $\Delta G^{\ddagger}(T_C)$ values are listed in the table below.

Table 5.26. Estimated free Gibbs energy of activation using (eq. 5.32)at Tc ($\Delta G^{\ddagger}(T_c)$) for the for the Si–C^{carb} rotation in [SiMe($caac^{Me}$)$_2$][$B(Ar^F)_4$] (**19**).

Dynamic process	T_c/K	Δv/Hz	$\Delta G^{\ddagger}(T_c)$/kJ·mol^{-1}
Enantiomerization	223	95.5 Hz[a]	44.0

[a]: The distance between the signals of C^2-C*H* and C^6-C*H* of the Dipp substituent in the slow exchange limit spectrum at 193 K (see *Figure 5.26*).

5.6.4 VT ^{1}H NMR spectra and line shape analysis of 9-Br

The ^{1}H NMR of $Si_2Br_2(caac^{Me})_2$ (**9-Br**) in (D_8)toluene at 298 K displayed only one set of signals for the $caac^{Me}$ ligand. For example, one septet at δ = 3.02 ppm was observed for methine protons of the two $C^{2,6}$-C*H*Me_2 groups of the Dipp substituent (*Figure 5.29*). In addition the doublet of the Methyl-group Me_B of the Dipp substituent appears as a broad signal, which upon reaching higher temperatures resolves in a sharp doublet (*Figure* 5.30).Recording the ^{1}H NMR spectrum at 223 K led to the decoalescence of the $C^{2,6}$-C*H*Me_2 septet into two septets appearing at δ = 2.93 and 3.09 ppm, which were assigned abritratrily as as C^2-C*H* and C^6-C*H*, respectively (*Figure* 5.41, bottom spectrum). The variable temperature ^{1}H NMR studies showed that two septets coalesces at the coalescences temperature (T_c) of 263 K where also clearly the coalescence of the C^3-*Me*$_2$ and C^5-*Me*$_2$ resonances are observed. The dynamic process can be attributed to an enantiomerization proceeding via a stepwise consecutive pyramidal inversion of the two chiral silicon centers in **9-Br** (*Figure 5.28*).

Full line shape analysis of the septets was carried out using the g-NMR software, in order to obtain the exchange rate konstants (k) for the enenatiomeriziation of $Si_2Br_2(caac^{Me})_2$ (**9-Br**) (*Figure 5.31*). The rate constants are listed in the table below. The dynamic process can be attributed to an enantiomerization which proceeds via pyramidal inversion of the chiral silicon center via a planar transition state.

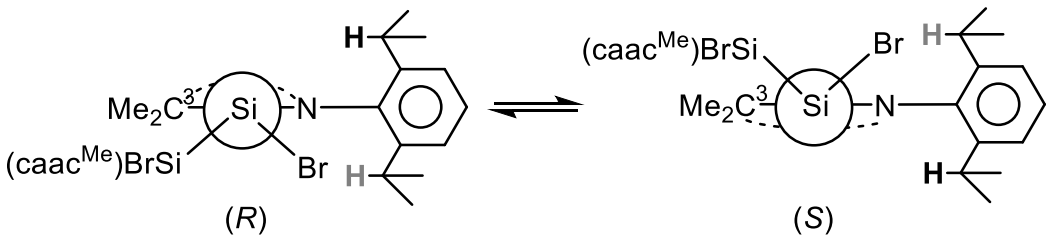

Figure 5.28. Enantiomerization of $Si_2Br_2(caac^{Me})_2$ (**9-Br**) via pyramidal inversion at the silicon center.

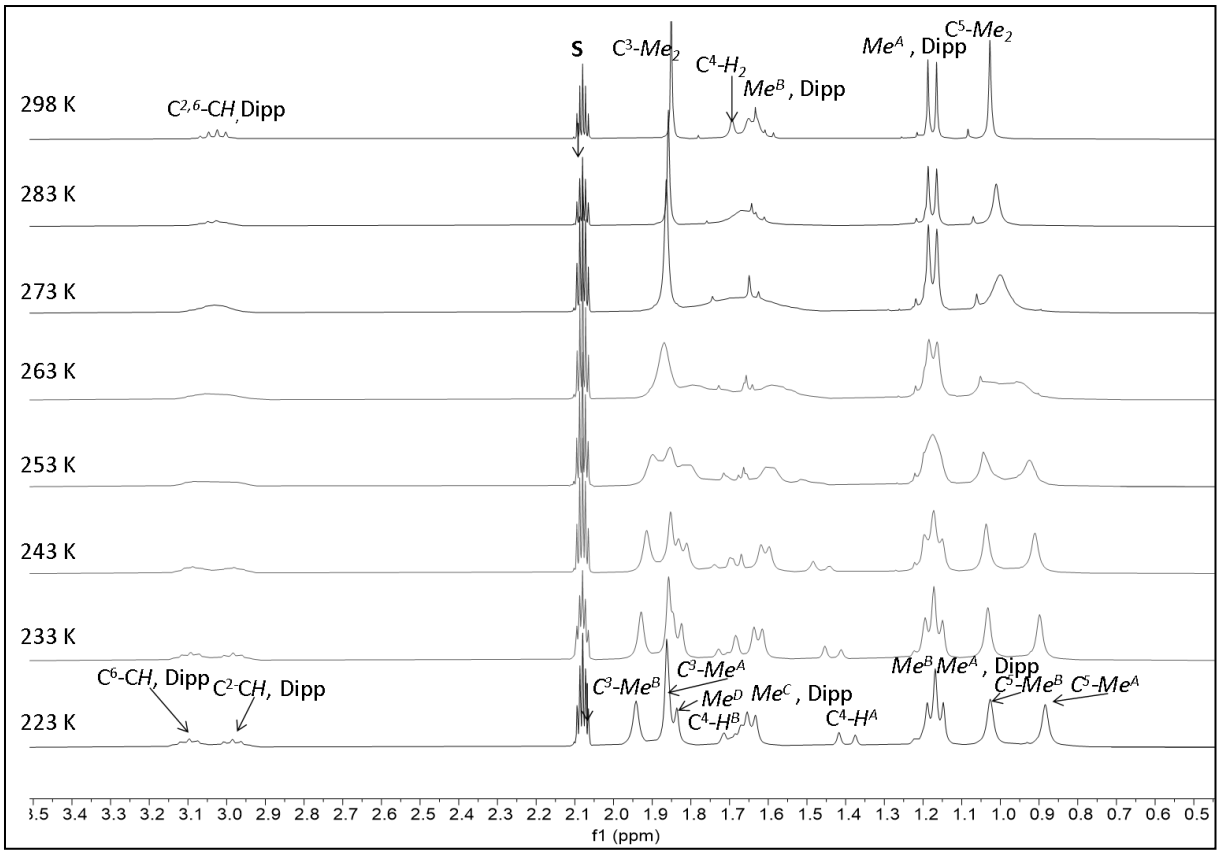

Figure 5.29. Excerpt of the ^{1}H NMR spectra (300.13 MHz) of $Si_2Br_2(caac^{Me})_2$ (**9-Br**) in (D_8)toluene in the temperature range 223 K – 298 K; the signal of the deuterated solvent is marked with the character **S**.

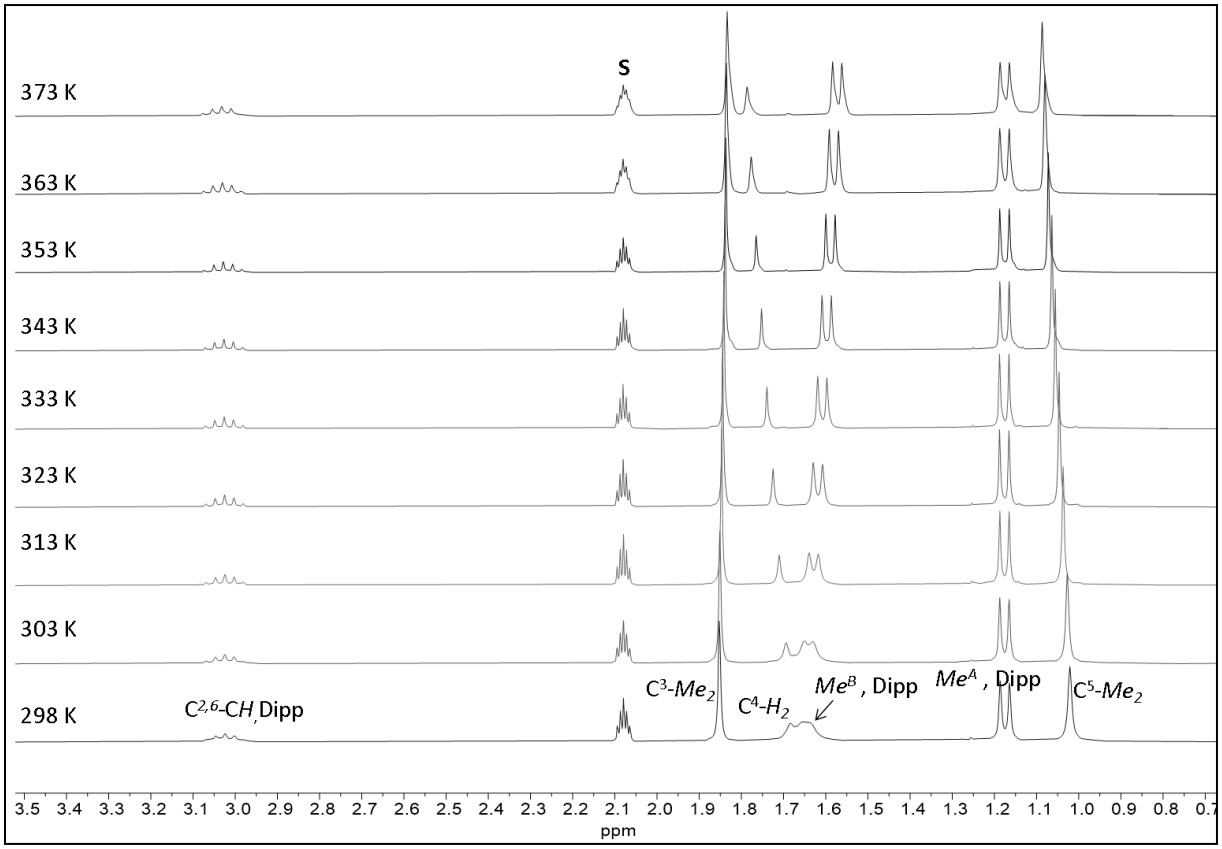

Figure 5.30. Excerpt of the ^{1}H NMR spectra (300.13 MHz) of $Si_2Br_2(caac^{Me})_2$ (**9-Br**) in (D_8)toluene in the temperature range 298 K – 373 K; the signal of the deuterated solvent is marked with the character **S**.

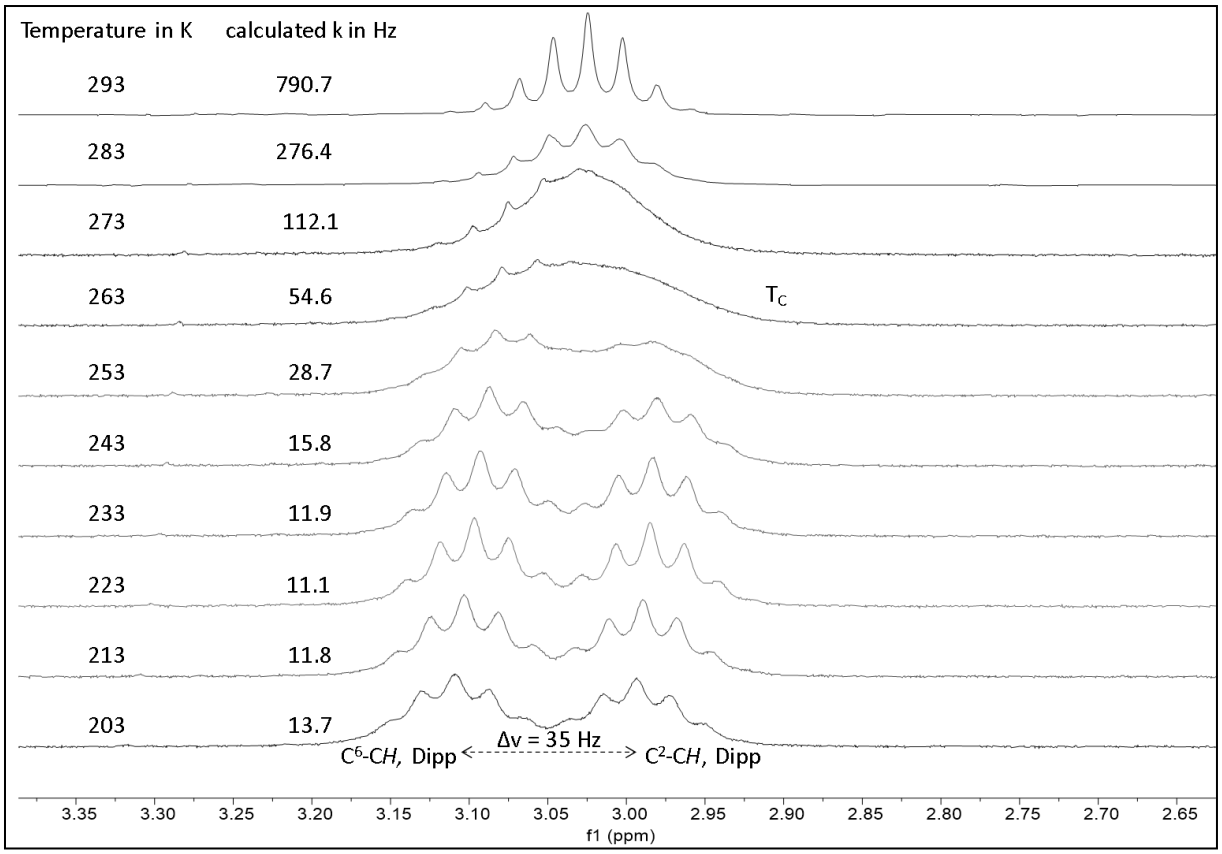

Figure 5.31. Excerpt of the ^{1}H NMR (300.13 MHz) spectra of $Si_2Br_2(caac^{Me})_2$ (**9-Br**) in (D_8)toluene from 203 K – 293 K showing the exchange process involving the $C^{2,6}$-C*H*Me_2 resonances.

Table 5.27. Rate constants (k in Hz) for the enatiomerization process in **9-Br** at different temperatures.

T /K	k /Hz	σ(k) /Hz	ln(k/T)	1/T /K^{-1}
243	17.7	1.41	–2.62	0.004115
253	31.8	1.14	–2.07	0.003953
263	60.2	1.07	–1.48	0.003802
273	126.9	1.10	–0.77	0.003663
283	299.7	1.65	0.06	0.003534
293	840.0	2.09	1.04	0.003356

The enthalpy of activation ($\Delta H^{\ddagger}$) and entropy of activation ($\Delta S^{\ddagger}$) were obtained from the slope and the intercept of the linear fit (*Figure 5.32)* using (eq. 5.29) and (eq. 5.30) and $\Delta G^{\ddagger}$ was calculated from (eq. 5.31).The activation parameters are summarized in *Table 5.28*.

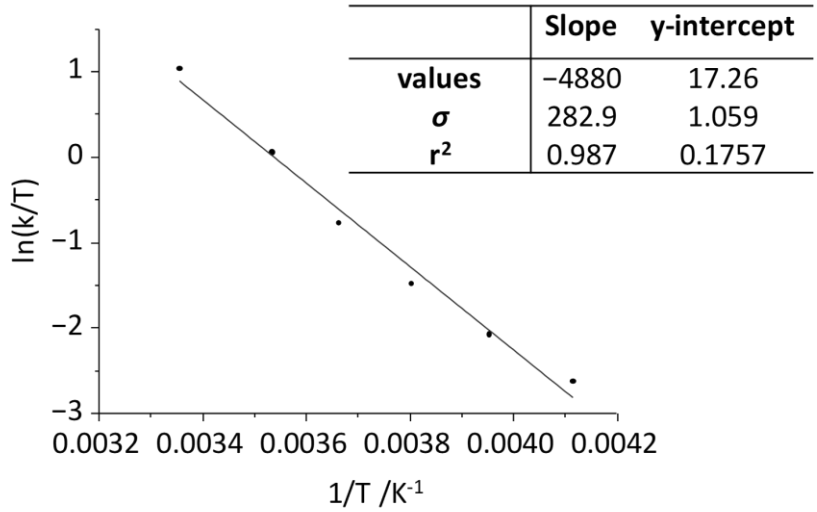

Figure 5.32. Eyring Plot of ln(k/T) versus 1/T for the enantiomerization process in $Si_2Br_2(caac^{Me})_2$ (**9-Br**).

Table 5.28. Activation parameters for the enantiomerization of **9-Br** obtained from full-line shape iteration.

Thermodynamic activation parameter	Calculated values[a] for the enantiomerization
$\Delta G^{\ddagger}$(298K)	55.3 ± 3.4 kJ mol^{-1}
$\Delta G^{\ddagger}(T_c)$	54.8 ± 3.4 kJ mol^{-1} (263 K)
$\Delta H^{\ddagger}$	40.6 ± 2.4 kJ mol^{-1}
$\Delta S^{\ddagger}$	-54.0 ± 8.8 J K^{-1} mol^{-1}

[a]: The error was calculated using the variance formula given in reference [341]. The average error of the temperature (σ(T)) was estimated to be 0.2 K.

Using (eq. 5.32) the Gibbs energy of activation ($\Delta G^{\ddagger}$) can be estimated at the coalescence temperature (T_C). The $\Delta G^{\ddagger}(T_C)$ values are listed in the table below.

Table 5.29. Estimated free Gibbs energy of activation using equation (5) at Tc ($\Delta G^{\ddagger}(T_c)$) for the enantiomerization in $Si_2Br_2(caac^{Me})_2$ (**9-Br**).

Dynamic process	T_c/K	Δν/Hz	$\Delta G^{\ddagger}(T_c)$/kJ·mol^{-1}
enantiomerisation	263	35 Hz[a]	54.5

[a] The distance between the signals of C^2-C*H* and C^6-C*H* of the Dipp substituent in the slow exchange limit spectrum at 213 K (*Figure* 5.31).

5.6.5 VT ^{1}H NMR spectra and line shape analysis of 9-Mes-*E,E*

The ^{1}H NMR of $Si_2Mes_2(caac^{Me})_2$ (**9-Mes-*E,E***) in (D_8)toluene at 298 K displayed broad signals with exception of the C^3-Me_AMe_B, C^4-*Me*, Mes and C^4-*H*, Dipp resonances which were observed as sharp signals, indicating a dynamic process with rather high activation barrier at ambient temperature in solution. The ^{1}H NMR of **9-Mes-*E,E*** in (D_8)toluene at 298 K featured the characteristics of a C_2-symmetric compound reaching the coalescence temperature. Upon recording a ^{1}H NMR spectrum at 100 °C sharp signals and NMR pattern of an averaged C_S-symmetry was observed, displaying one septet for the $C^{2,6}$-C*H*Me_2 group of the Dipp moiety at 3.04 ppm. Recording the ^{1}H NMR spectrum at 233 K led to the decoalescence of the $C^{2,6}$-C*H*Me_2 septet into two septets appearing at δ = 2.75 and 3.37 ppm, which were assigned arbitrarily as C^2-C*H* and C^6-C*H*, respectively. Similar temperature behavior of the $C^{3,5}$-*H*, Mes singlet signal was observed. The variable temperature ^{1}H NMR studies showed that the two septets merge at the coalescence temperature (T_C) of 303 K and the two singlets at 283 K, respectively. Two dynamic processes were attributed to the observed temperature dependent ^{1}H NMR spectrum: a) enantiomerization of the two chiral silicon centers in **9-Mes-*E,E***, via a pyramidal inversion, as well as b) hindered rotation of the Mes substituents at the chiral silicon centers. Both processes were described in a non-concerted fashion.

Full line shape analysis of the septets and the $C^{3,5}$-H, Mes singulets was carried out using the g-NMR software, in order to obtain the exchange rate konstants (k_1 and k_2) for the enenatiomerization and hindered Si–Mes rotation of $Si_2Mes_2(caac^{Me})_2$ (**9-Mes-*E,E***) (*Figure 5.37*). The rate constants are listed in *Table 5.30* and *Table 5.31*, respectively.

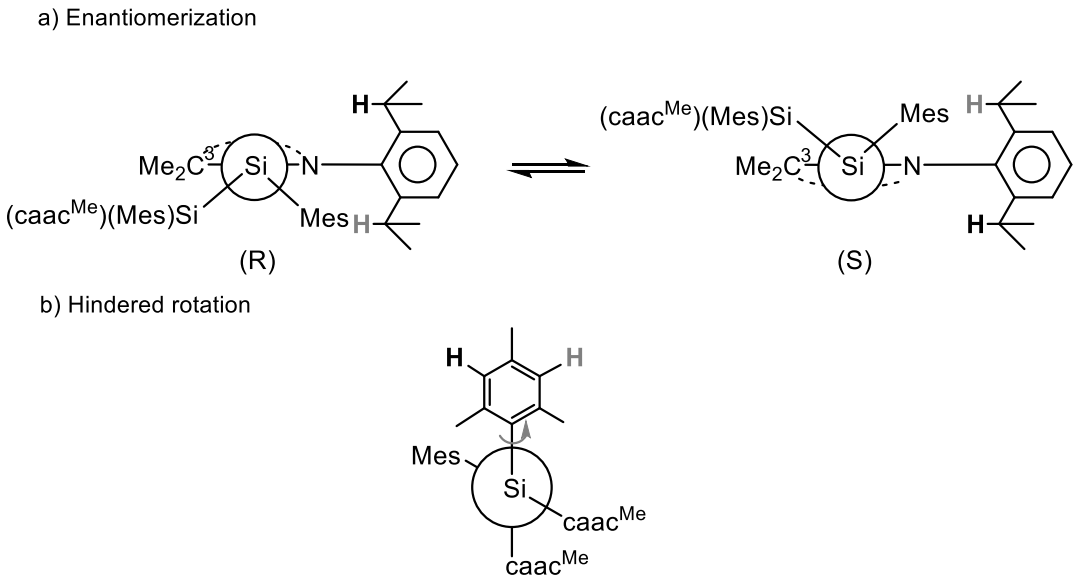

Figure 5.33. a) Enantiomerization of $Si_2Mes_2(caac^{Me})$ (**9-Mes**) via pyramidal inversion at the silicon center, b) Hindered rotation of the Mes-substituent bonded at the chiral silicon center.

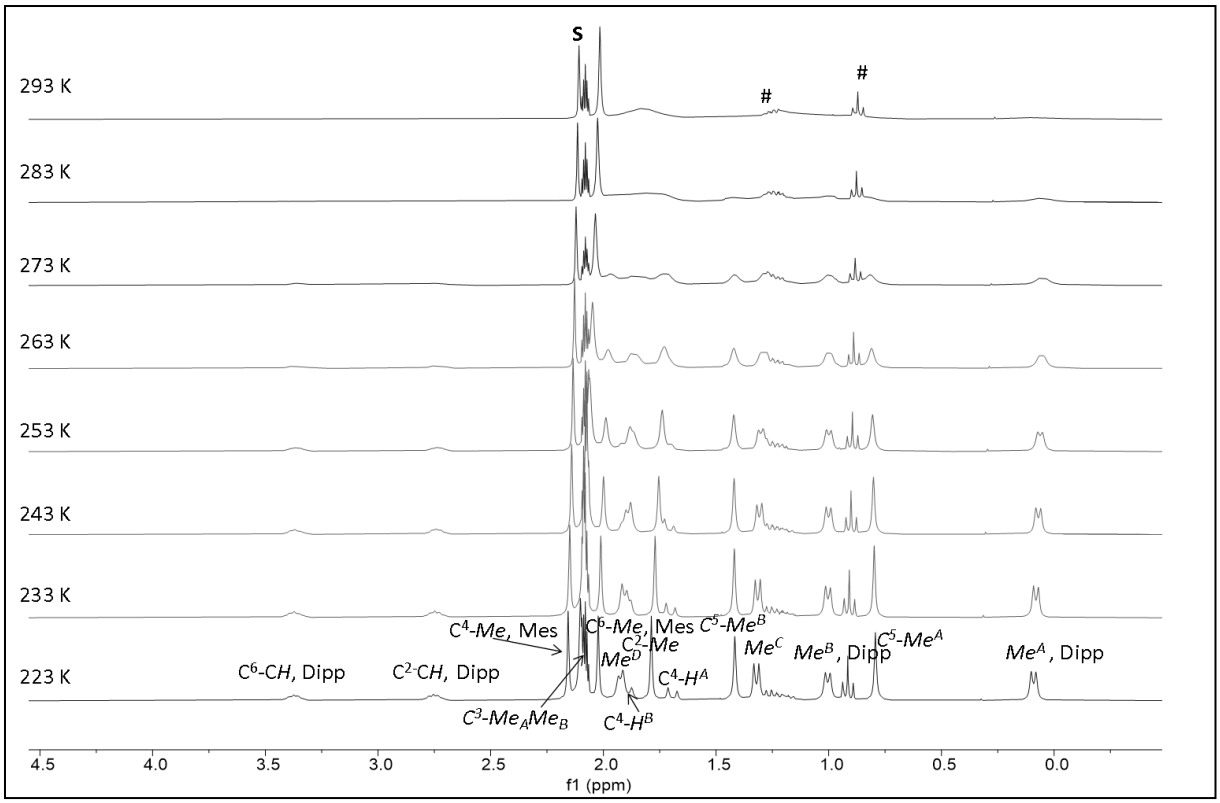

Figure 5.34. Excerpt of the ^{1}H NMR spectra (300.13 MHz) of $Si_2Mes_2(caac^{Me})_2$ (**9-Mes-*E,E***) in (D_8)toluene in the temperature range 223 – 293 K; the signal of the deuterated solvent is marked with the character **S**.

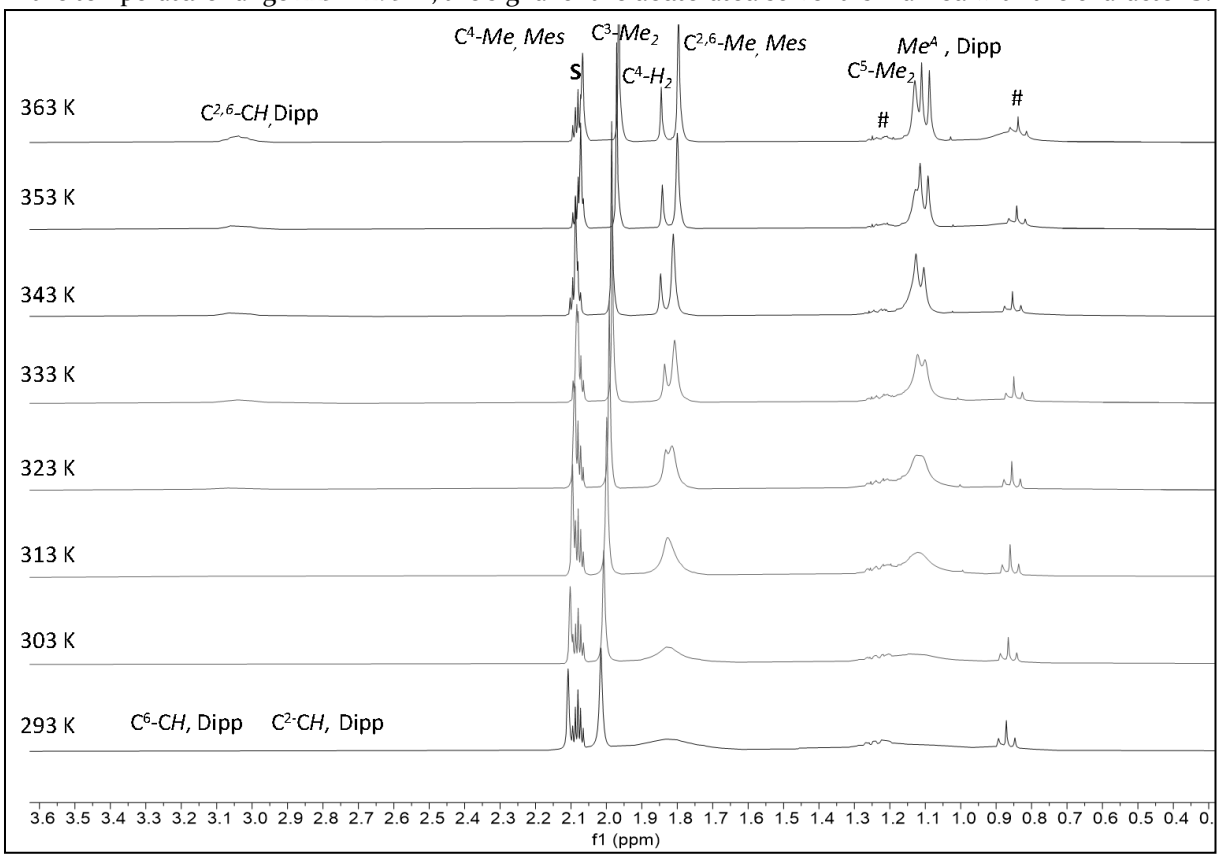

Figure 5.35. Excerpt of the ^{1}H NMR spectra (300.13 MHz) of $Si_2Mes_2(caac^{Me})_2$ (**9-Mes-*E,E***) in (D_8)toluene in the temperature range 293 – 363 K; the signal of the deuterated solvent is marked with the character **S**. Residual solvent peaks of *n*-pentane are marked with the character #.

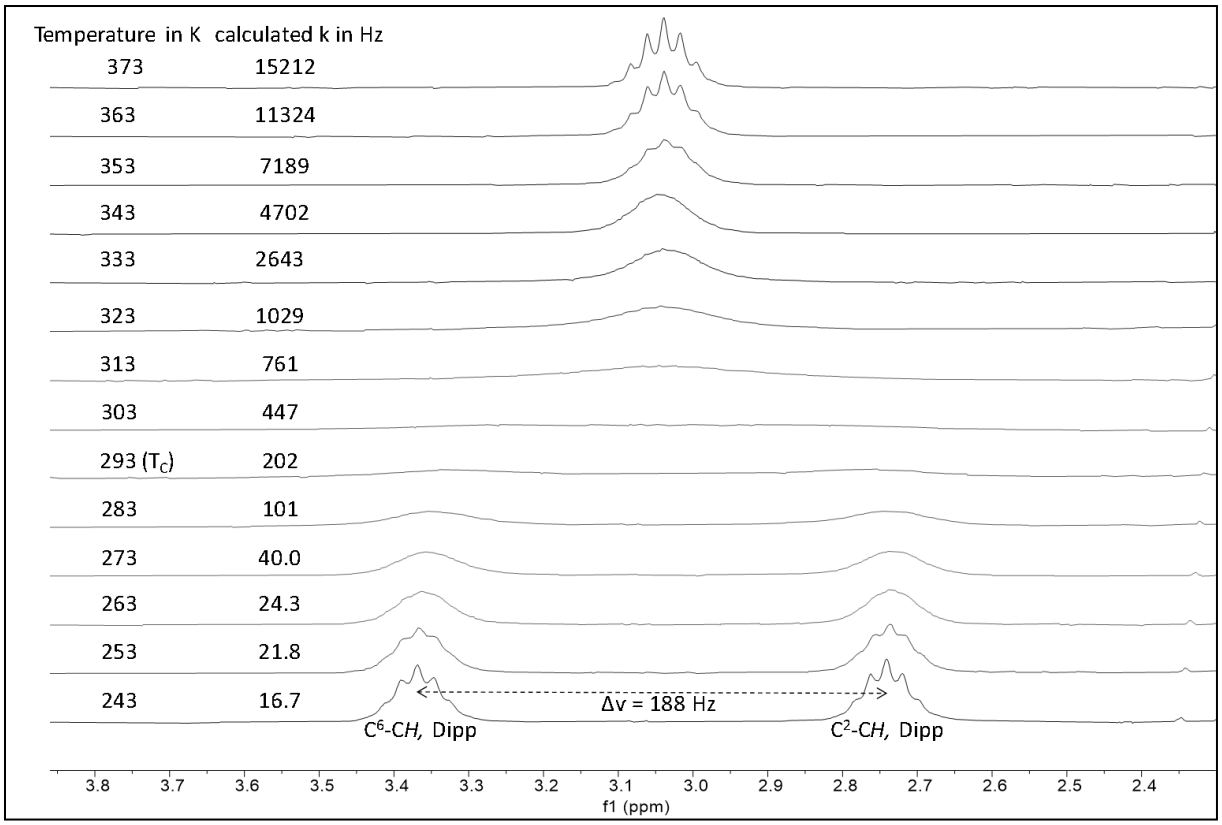

Figure 5.36. Excerpt of the ^{1}H NMR (300.13 MHz) spectra of $Si_2Mes_2(caac^{Me})_2$ (**9-Mes-*E,E***) in (D_8)toluene from 243 K – 373 K showing the exchange process involving the $C^{2,6}$-C*H*Me_2 group of the Dipp substituent.

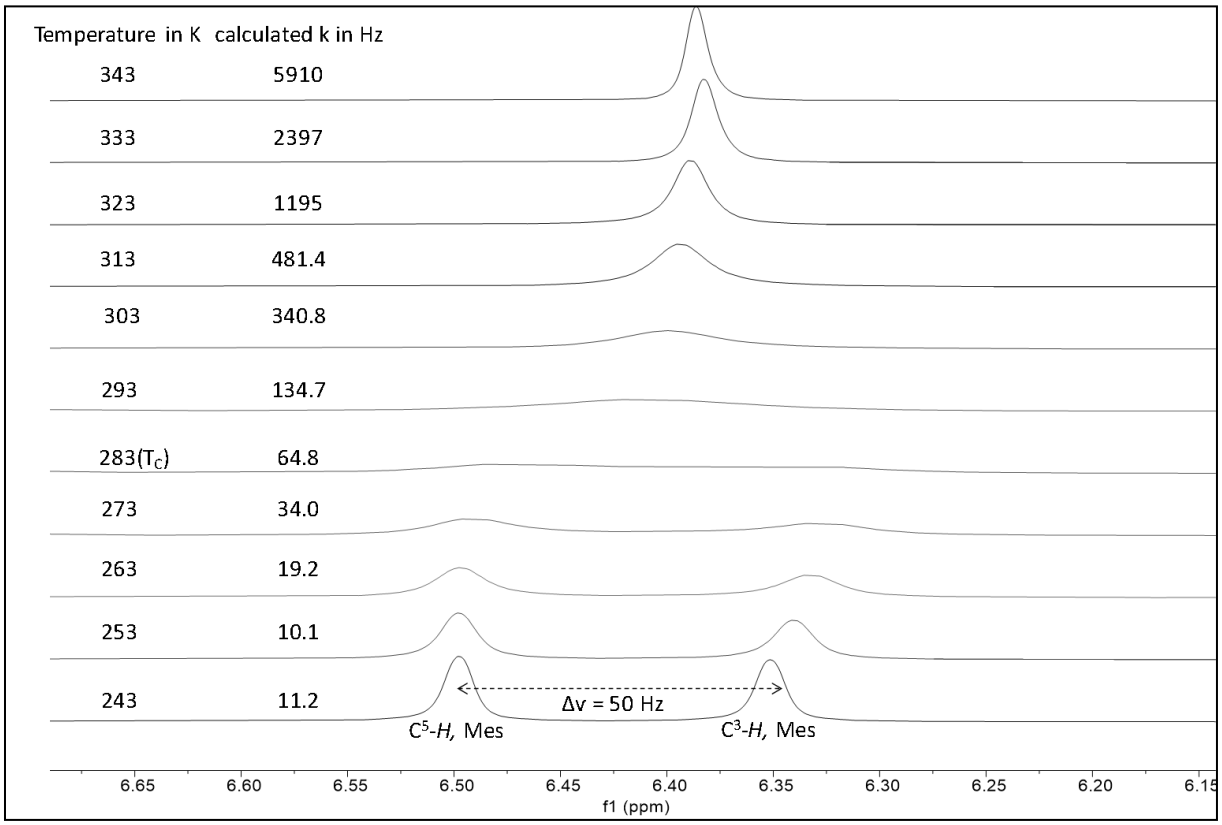

Figure 5.37. Excerpt of the ^{1}H NMR (300.13 MHz) spectra of $Si_2Mes_2(caac^{Me})_2$ (**9-Mes-*E,E***) in (D_8)toluene from 243 K – 343 K showing the exchange process involving the $C^{3,5}$-*H* resonances of the Mes substituent.

Table 5.30. Rate constants (k_1 in Hz) for the enatiomerization process in **9-Mes-*E,E*** at different temperatures.

T /K	k_1 /Hz	$\sigma(k_1)$ /Hz	$\ln(k_1/T)$	1/T /K^{-1}
253	21.8	1.38	–2.45	0.00395
263	24.3	1.19	-2.38	0.00380
273	40.0	1.07	-1.92	0.00366
283	100.7	1.08	-1.033	0.00353
293	201.6	1.09	-0.374	0.00341
303	447.4	1.13	0.390	0.00330
313	760.5	1.02	0.888	0.00319
323	1029	1.12	1.158	0.00310
333	2643	1.02	2.07	0.00300
343	4702	1.03	2.62	0.00292
353	7190	1.04	3.01	0.00283
363	11324	1.03	3.44	0.00276
373	15213	1.04	3.71	0.00268

Table 5.31. Rate constants (k_2 in Hz) for the hindered rotation of Si–Mes bond in **9-Mes-*E,E*** at different temperatures.

T /K	k_2 /Hz	$\sigma(k_2)$ /Hz	$\ln(k_2/T)$	1/T /K^{-1}
253	10.1	1.22	-3.22	0.00395
263	19.2	2.34	-2.62	0.00380
273	34.0	1.78	-2.08	0.00366
283	64.8	1.23	-1.48	0.00353
293	134.7	1.04	-0.777	0.00341
303	340.8	1.10	0.118	0.00330
313	481.4	1.03	0.43	0.00319
323	1195	1.03	1.31	0.00310
333	2397	1.10	1.97	0.00300
343	5910	2.03	2.85	0.00292

The enthalpy of activation ($\Delta H^{\ddagger}$) and entropy of activation ($\Delta S^{\ddagger}$) were obtained from the slope and the intercept of the linear fit (*Figure* 5.38 a and b) using (eq. 5.29) and (eq. 5.30) and $\Delta G^{\ddagger}$ was calculated from (eq. 5.31).The activation parameters are summarized in *Table 5.32*.

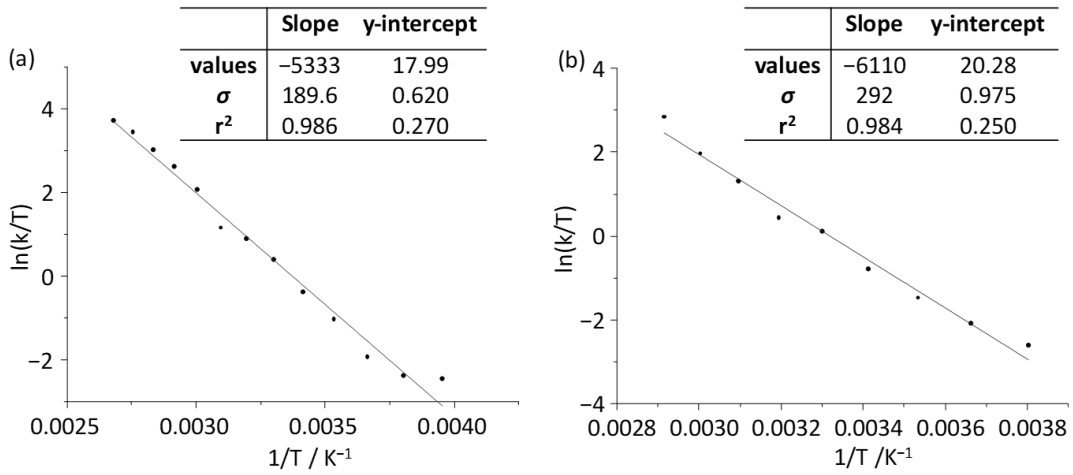

Figure 5.38. Eyring Plot of $\ln(k_1/T)$ versus 1/T for the enantiomerization process (a) and the hindered rotation of the Mes substituent (b) in $Si_2Mes_2(caac^{Me})_2$ (**9-Mes-*E,E***).

Table 5.32. Activation parameters for the enantiomerization and Mes-rotation processes of **9-Mes-*E,E*** obtained from full-line shape iteration.

Thermodynamic activation parameter	Calculated value[a]	
	Enantiomerization	Si–C^{Mes} rotation
$\Delta G^{‡}$(298K)	58.6 ± 2.0 kJ mol^{-1}	59.4 ± 3.1 kJ mol^{-1}
$\Delta G^{‡}(T_c)$	58.4 ± 2.0 kJ mol^{-1} (293 K)	59.0 ± 3.1 kJ mol^{-1} (283 K)
$\Delta H^{‡}$	44.3 ± 1.6 kJ mol^{-1}	50.8 ± 2.4 kJ mol^{-1}
$\Delta S^{‡}$	−48 ± 5.2 J K^{-1} mol^{-1}	−28.9 ± 8.1 J K^{-1} mol^{-1}

[a]: The error was calculated using the variance formula given in reference [341]. The average error of the temperature (σ(T)) was estimated to be 0.2 K.

Using (eq. 5.32) the Gibbs energy of activation ($\Delta G^{‡}$) can be estimated at the coalescence temperature (T_C). The $\Delta G^{‡}(T_C)$ values are listed in the table below.

Table 5.33. Estimated free Gibbs energy of activation using equation (5) at Tc ($\Delta G^{‡}(T_c)$) for the two dynamic processes of **9-Mes-*E,E***.

Dynamic process	T_c/K	Δv/Hz	$\Delta G^{‡}(T_c)$/kJ·mol^{-1}
enantiomerization	293	188 Hz[a]	56.9
Si–C^{Mes} rotation	283	50 Hz[b]	58.0

[a]: The distance between the signals of C^2-C*H* and C^6-C*H* of the Dipp substituent in the slow exchange limit spectrum at 243 K (*Figure* 5.36). [b] The distance between the signals of C^3-*H* and C^5-*H* of the Mes substituent in the slow exchange limit spectrum at 243 K (*Figure* 5.37).

5.6.6 VT ^{1}H NMR spectra and line shape analysis of 13

The ^{1}H NMR of SiBr(SiBr$_2$Tbb)(caac^{Me}) (**13**) in (D_8)toluene at 298 K displayed only one set of signals for the caac^{Me} and SiBr$_2$Tbb ligands bonded to the stereogenic silicon center. For example, one septet at δ = 2.80 ppm was observed for methine protons of the two C^{2,6}-C*H*Me$_2$ groups of the Dipp substituent and one sharp singlet was found at δ = 3.48 ppm for the methine protons of the two C^{2,6}-C*H*(SiMe$_3$)$_2$ groups of the SiBr$_2$Tbb substituent (*Figure* 5.40, top spectrum). Recording the ^{1}H NMR spectrum at 193 K led to the decoalesence of the C^{2,6}-C*H*Me$_2$ septet into two septets appearing at δ = 2.57 and 2.91 ppm, which were assigned arbitrarily as C^2-C*H* and C^6-C*H*, respectively (*Figure* 5.41, bottom spectrum). Similar temperature dependent behaviour of the C^{2,6}-C*H*(SiMe$_3$)$_2$ singlet signal was also observed. The variable temperature ^{1}H NMR studies showed that two septets coalesces at the coalescences temperature (T_c) of 273 K and the two singlets coalesces at 213 K.

Two dynamic processes were attributed to the observed temperature dependent ^{1}H NMR spectrum. These two dynamic processes are: enantiomerization proceeding via the pyramidal inversion at the stereogenic silicon center (*Figure 5.39* a) and the hindered rotation of the Tbb-ligand bonded to the prochiral tetrahedral silicon center (*Figure 5.39* b).

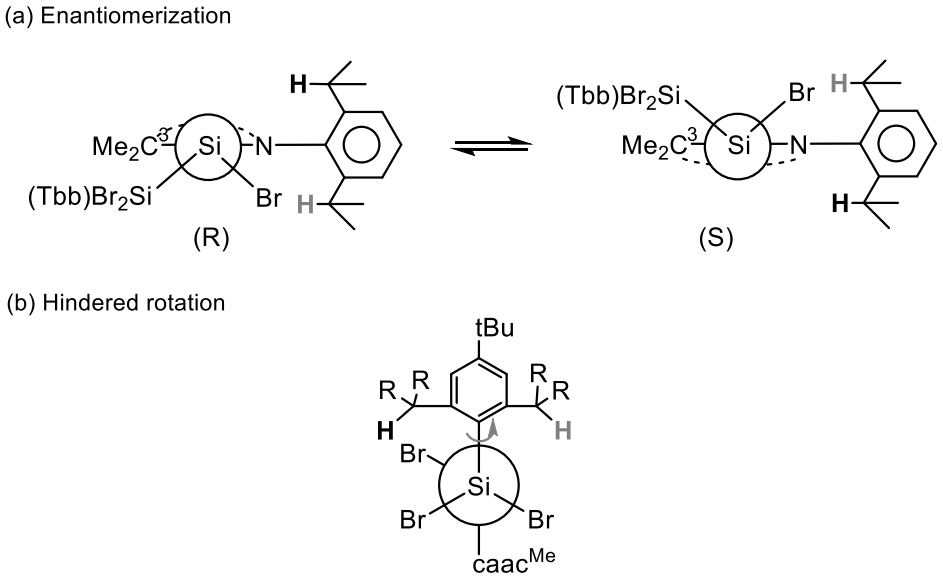

Figure 5.39. a) Enantiomerization of SiBr(SiBr$_2$Tbb)(caac^{Me}) (**13**) via pyramidal inversion at the silicon center, b) Hindered rotation of the Tbb-ligand bonded to the prochiral Si-center; R = SiMe$_3$.

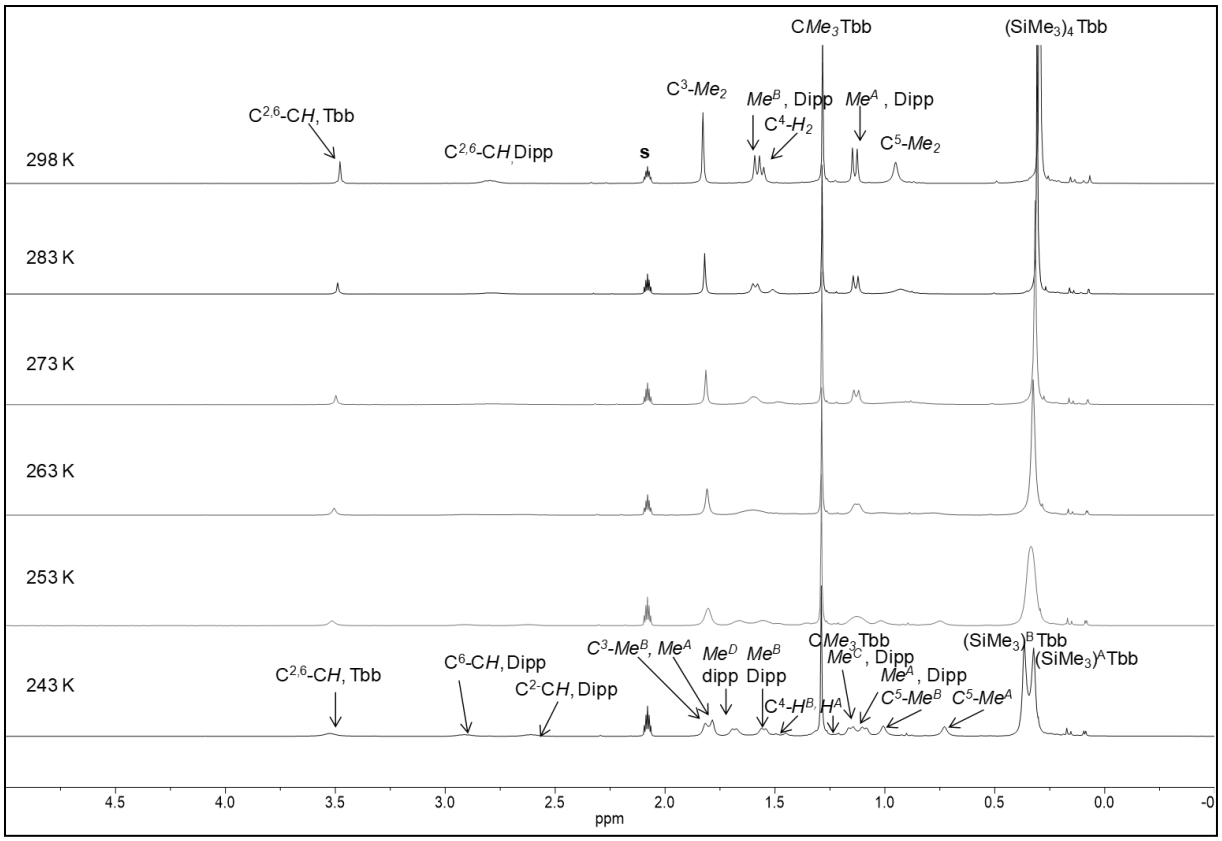

Figure 5.40. Excerpt of the ^{1}H NMR spectra (300.13 MHz) of SiBr(SiBr$_2$Tbb)(caac^{Me}) (**13**) in (D$_8$)toluene in the temperature range 243 – 298 K; the signal of the deuterated solvent is marked with the character **S**.

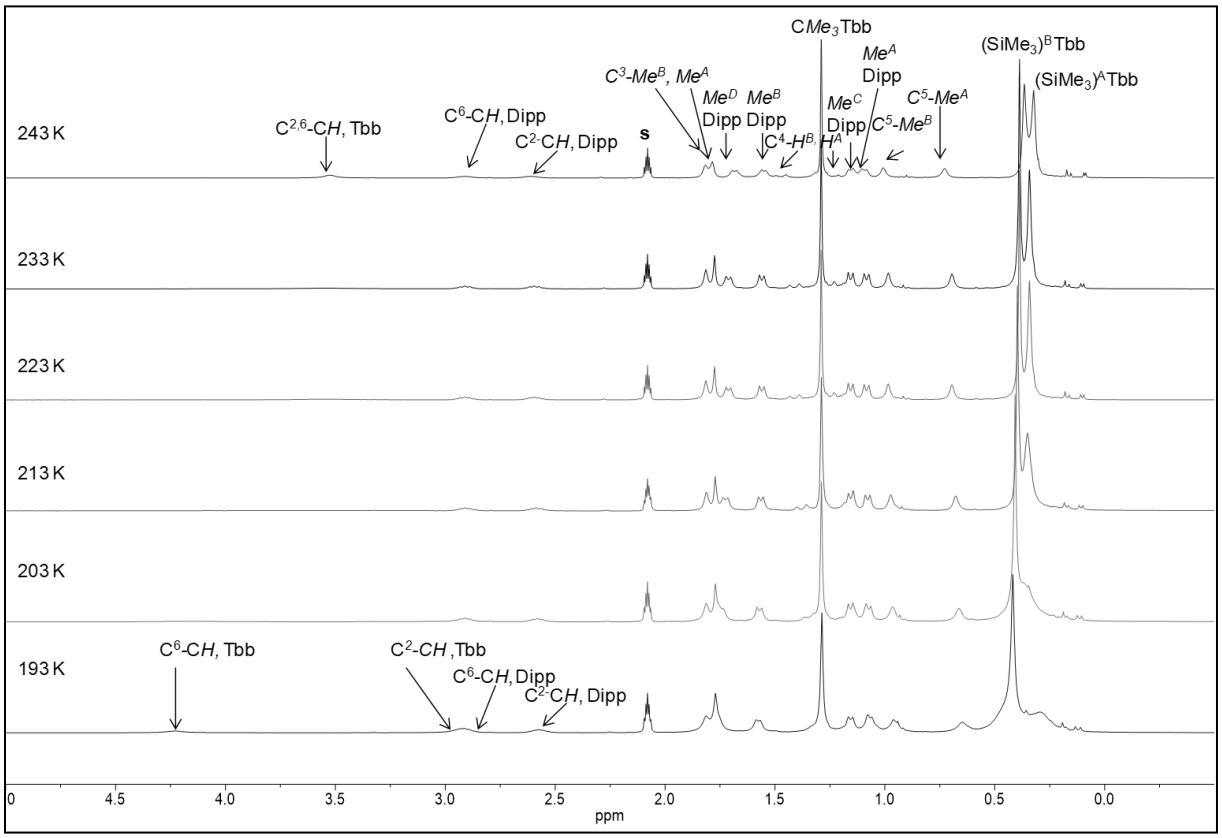

Figure 5.41. Excerpt of the ^{1}H NMR spectra (300.13 MHz) of SiBr(SiBr$_2$Tbb)(caac^{Me}) (**13**) in (D$_8$)toluene in the temperature range 193 – 243 K; the signal of the deuterated solvent is marked with the character **S**.

These dynamic processes are an example of an equally populated two-site chemical exchange process. Full line-shape analysis of the septet and the singlet signals (*Figure* 5.42) using the NMR simulation program gNMR was carried out to obtain the first order exchange rate constants k_1 and k_2 for the enantiomerization and the hindered Si–C^{Tbb} rotation process, respectively. The rate constants k_1 and k_2 are listed in *Table* 5.34 and *Table* 5.35, respectively.

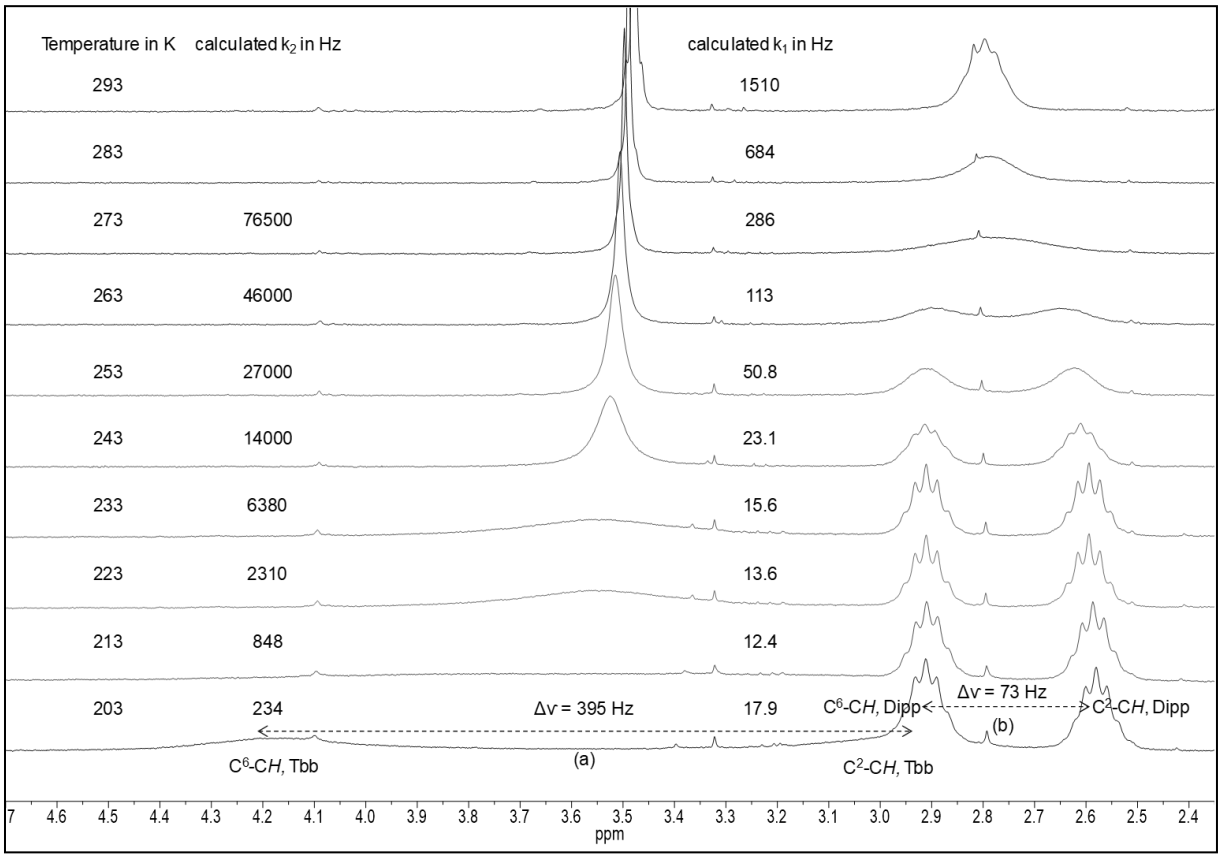

Figure 5.42. Excerpt of the ^{1}H NMR (300.13 MHz) spectra of SiBr(SiBr$_2$Tbb)(caac^{Me}) (**13**) in (D_8)toluene from 203 K – 293 K showing the exchange process involving the $C^{2,6}$-C*H*Me$_2$ and $C^{2,6}$-C*H*(SiMe$_3$)$_2$ groups. The rate constants k_1 and k_2 were obtained from full line-shape analysis using gNMR.

Table 5.34. Rate constants (k_1 in Hz) for the enatiomerization process in **13** at different temperatures.

T /K	k_1 /Hz	$\sigma(k_1)$ /Hz	$\ln(k_1/T)$	1/T /K^{-1}
243	23.1	1.70	–2.35	0.004115
253	50.8	1.25	–1.61	0.003953
263	113	1.14	–0.84	0.003802
273	286	1.29	0.05	0.003663
283	684	1.04	0.88	0.003534
293	1510	1.18	1.64	0.003413

Table 5.35. Rate constants (k_2 in Hz) for the hindered rotation of Si–C^{Tbb} bond in **13** at different temperatures**.**

T /K	k_2 /Hz	$\sigma(k_2)$ /Hz	$\ln(k_2/T)$	1/T /K^{-1}
203	234	5.64	0.14	0.004926
213	848	11.6	1.38	0.004695
223	2310	1.15	2.34	0.004484
233	6380	1.12	3.31	0.004292
243	14000	1.07	4.05	0.004115
253	27000	1.02	4.67	0.003953
263	46000	1.02	5.16	0.003802
273	76500	1.03	5.64	0.003663

The enthalpy of activation ($\Delta H^{‡}$) and entropy of activation ($\Delta S^{‡}$) were obtained from the slope and the intercept of the linear fit (*Figure* 5.43*)* using (eq. 5.29) and (eq. 5.30) and $\Delta G^{‡}$ was calculated from (eq. 5.31).The activation parameters are summarized in *Table* 5.36.

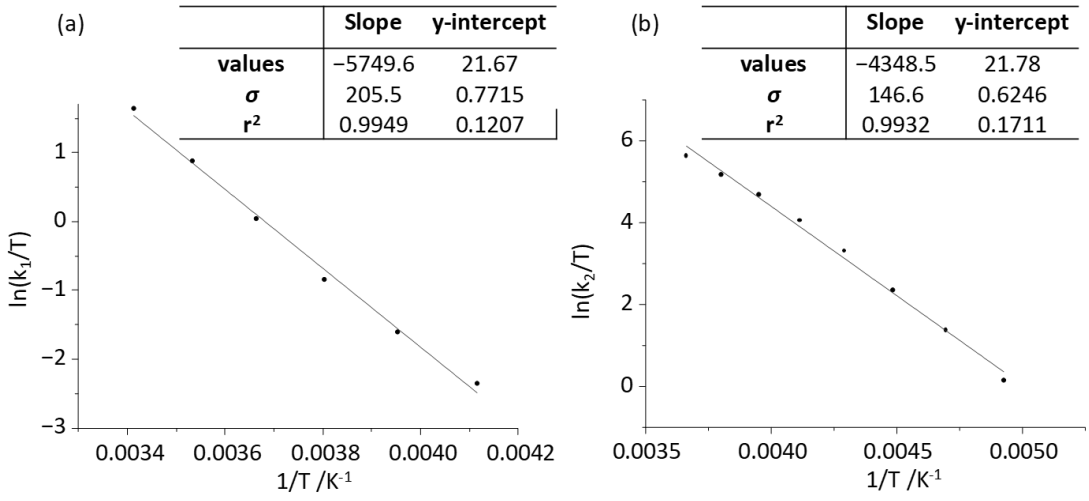

Figure 5.43. Eyring Plot of $\ln(k_1/T)$ versus 1/T for the enantiomerization process (a) and the Si–C^{Tbb} bond rotation (b) in $SiBr(SiBr_2Tbb)(caac^{Me})$ (**13**).

Table 5.36. Activation parameters for the enantiomerization and Tbb-rotation processes of **13** obtained from full-line shape iteration.

Thermodynamic activation parameter	Calculated value[a]	
	Enantiomerization	Si–C^{Tbb} rotation
$\Delta G^{\ddagger}$(298K)	54.2 ± 2.4 kJ mol^{-1}	41.1 ± 1.9 kJ mol^{-1}
$\Delta G^{\ddagger}(T_c)$	53.7 ± 2.4 kJ mol^{-1} (273 K)	39.7 ± 1.9 kJ mol^{-1} (213 K)
$\Delta H^{\ddagger}$	47.8 ± 1.7 kJ mol^{-1}	36.2 ± 1.2 kJ mol^{-1}
$\Delta S^{\ddagger}$	21 ± 6.4 J K^{-1} mol^{-1}	–17 ± 5.2 J K^{-1} mol^{-1}

[a]: The error was calculated using the variance formula given in reference [341]. The average error of the temperature (σ(T)) was estimated to be 0.2 K.

Using (eq. 5.32) the Gibbs energy of activation ($\Delta G^{\ddagger}$) can be estimated at the coalescence temperature (T_C). The $\Delta G^{\ddagger}(T_C)$ values are listed in the table below.

Table 5.37. Estimated free Gibbs energy of activation using equation (5) at Tc ($\Delta G^{\ddagger}(T_c)$) for the two dynamic processes of **13**.

Dynamic process	T_c/K	Δv/Hz	$\Delta G^{\ddagger}(T_c)$/kJ·mol^{-1}
enantiomerisation	273	73 Hz[a]	55.1
Si–C^{Tbb} rotation	213	395 Hz[b]	39.6

[a]: The distance between the signals of C^2-C*H* and C^6-C*H* of the Dipp substituent in the slow exchange limit spectrum at 213 K (*Figure* 5.42). [b]: The distance between the signals of C^2-C*H* and C^6-C*H* of the Tbb substituent in the slow exchange limit spectrum at 203 K (*Figure* 5.42).

5.6.7 VT ^{1}H NMR spectra and line shape analysis of 14

The dynamic process in (caac^{Me})Si=SiBr(Tbb) (**14**) involving the hindered rotation of the Si–C^{Tbb} bond was resolved in the variable temperature ^{1}H NMR spectra (*Figure* 5.44 and *Figure* 5.45). This dynamic process led to the mutual chemical exchange of the $SiMe_3$ groups of the C^{2}-and C^{6}-bonded disyl-groups of the Tbb substituent. Thus the slow exchange limit spectrum at 193 K showed two singlet signals for the $SiMe_3$ groups at δ = 0.28 and 0.42 ppm, which are arbitrarily labeled as $(SiMe_3)^A$ and $(SiMe_3)^B$. Coalescence of these two singlets was observed at 263 K leading to a time averaged singlet signal at temperatures above 263 K. This dynamic process is an example of an equally populated two site chemical exchange process. Full line-shape analysis of the singlet signals (*Figure* 5.46) using the NMR simulation program gNMR was carried out to obtain the first order exchange rate constants. The exchange rate constants (k) at different temperatures are listed in *Table* 5.38. The low temperature limit spectrum of **14** (*Figure* 5.45, bottom spectrum) displays only one set of signals for the caac^{Me} ligand. This observation and the C_1-symmetric molecular structure of **14** suggest that an enantiomerization process is occurring much faster than the ^{1}H NMR time scale leading to a time averaged signals for the caac^{Me} ligand. Free Gibbs energy of activation of this process was investigated computationally which reveal a low energy barrier of the Si–C^{carb} bond rotation.

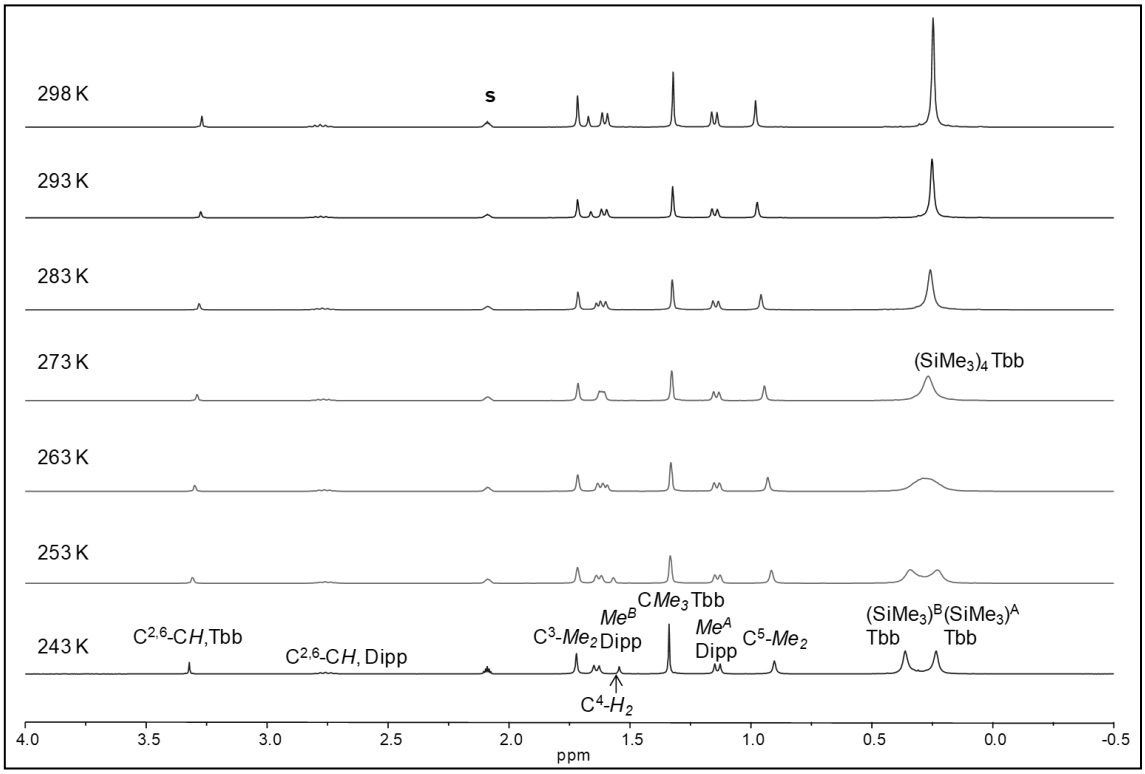

Figure 5.44. Excerpt of the variable temperature ^{1}H NMR spectra (300.13 MHz) of (caac^{Me})Si=SiBr(Tbb) (14) in (D_8)toluene in the temperature range 298 – 243 K; the residual proton signal of the deuterated solvent is marked with the character **s**.

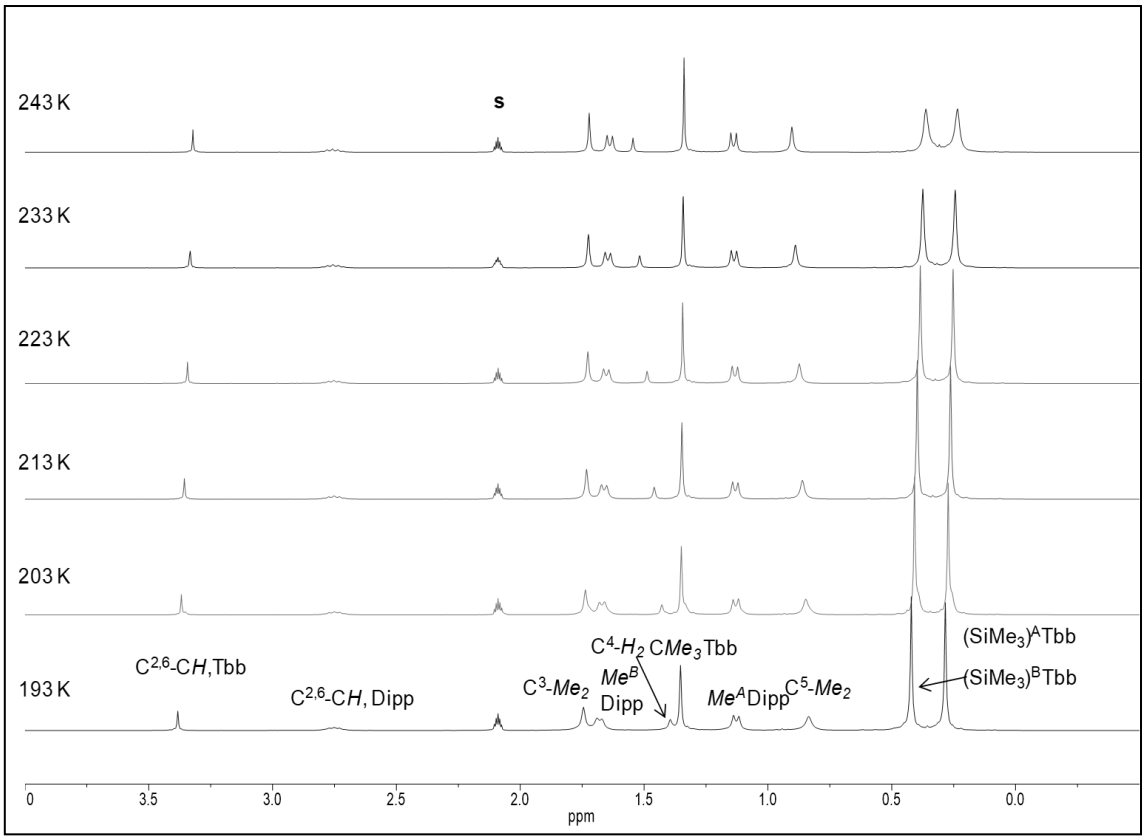

Figure 5.45. Excerpt of the variable temperature ^{1}H NMR spectra (300.13 MHz) of (caac^{Me})Si=SiBr(Tbb) (**14**) in (D_8)toluene in the temperature range 243 – 193 K; the residual proton signal of the deuterated solvent is marked with the character **s**.

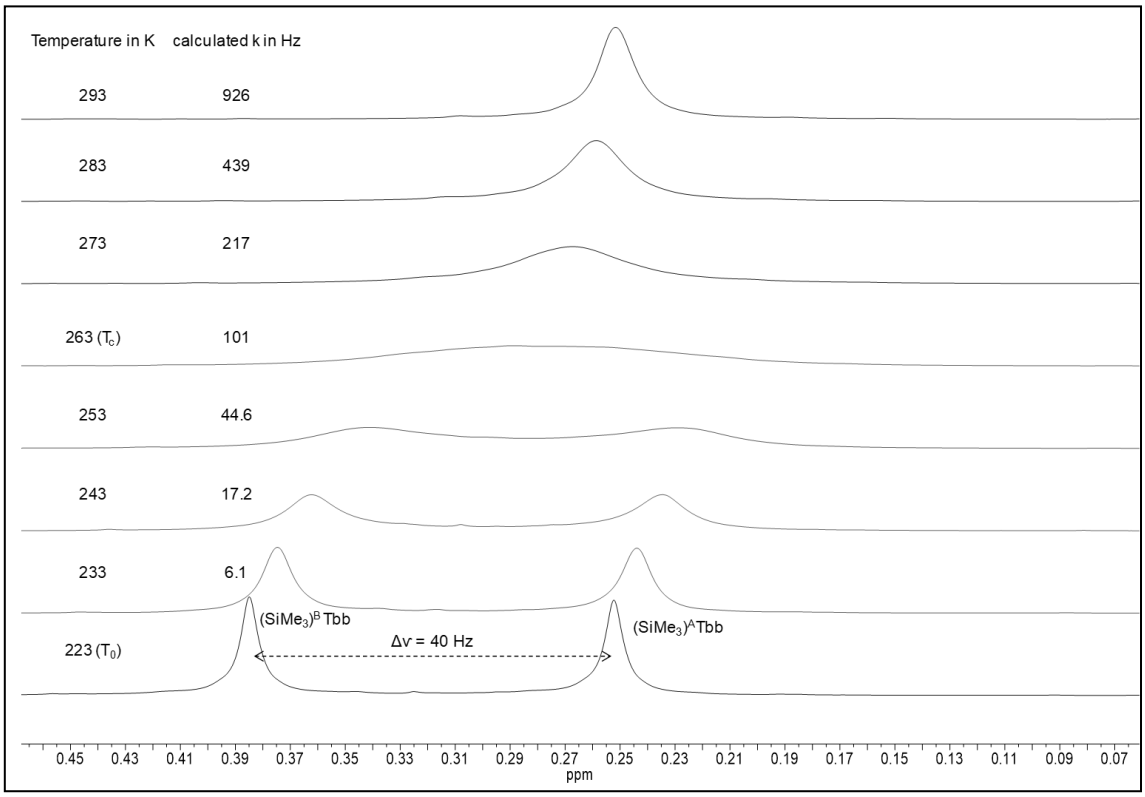

Figure 5.46. Excerpt of the variable temperature ^{1}H NMR (300.13 MHz) spectra of **14** in (D_8)toluene from 223 K – 273 K showing the exchange process involving $SiMe_3$ groups of the Tbb substituents. The rate constants (k) were obtained from full line-shape analysis using gNMR.

Table 5.38. Rate constants (k in Hz) for the hindered rotation of Si–C^{Tbb} bond in **14** at different temperatures.

T/K	k /Hz	σ(k) /Hz	ln(k/T)	1/T /K^{-1}
233	6.1	1.20	–3.64	0.004292
243	17.2	1.07	–2.65	0.004115
253	44.6	1.01	–1.74	0.003953
263	101	1.00	–0.96	0.003802
273	217	1.00	–0.23	0.003663
283	439	1.02	0.44	0.003534
293	926	1.05	1.15	0.003413

The enthalpy of activation ($\Delta H^{\ddagger}$) and entropy of activation ($\Delta S^{\ddagger}$) were obtained from the slope and the intercept of the linear fit (*Figure* 5.47*)* using (eq. 5.30) and (eq. 5.31) and $\Delta G^{\ddagger}$ was calculated from (eq. 5.32).

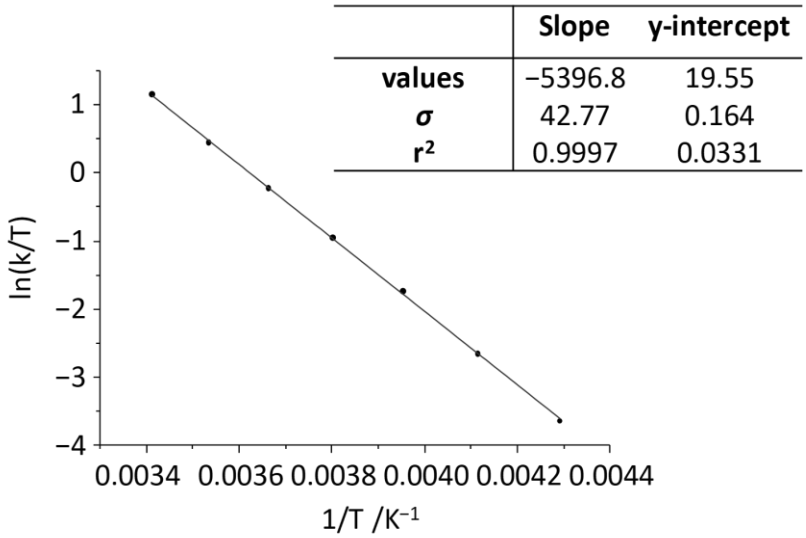

Figure 5.47. Eyring Plot of ln(k/T) versus 1/T for the Si–C^{Tbb} bond rotation process in (caac^{Me})Si=Si(Br)Tbb (**14**).

Table 5.39. Activation parameters for the Si–C^{Tbb} bond rotation process of **14** obtained from full-line shape iteration.

Activation parameter	Calculated value[a]
$\Delta G^{\ddagger}$(298K)	53.3 ± 1.7 kJ mol^{-1}
$\Delta G^{\ddagger}(T_c)$	54.1 ± 1.7 kJ mol^{-1} (263 K)
$\Delta H^{\ddagger}$	44.9 ± 1.1 kJ mol^{-1}
$\Delta S^{\ddagger}$	–35.0 ± 4.5 J K^{-1} mol^{-1}

[a]: The error was calculated using the variance formula given in reference [341]. The average error of the temperature (σ(T)) was estimated to be 0.2 K.

5.6.8 VT ^{1}H NMR spectra and line shape analysis of 14-Ge

The dynamic process in (caac^{Me})Ge=SiBr(Tbb) (**14-Ge**) involving the hindered rotation of the Si–C^{Tbb} bond was resolved in the variable temperature ^{1}H NMR spectra (*Figure* 5.44). This dynamic process led to the mutual chemical exchange of the $SiMe_3$ groups of the C^{2}-and C^{6}-bonded disyl-groups of the Tbb substituent. Thus the slow exchange limit spectrum at 233 K showed two singlet signals for the $SiMe_3$ groups at $\delta = 0.25$ and 0.38 ppm, which are arbitrarily labeled as $(SiMe_3)^A$ and $(SiMe_3)^B$. Coalescence of these two singlets was observed at 253 K leading to a time averaged singlet signal at temperatures above 263 K. This dynamic process is an example of an equally populated two site chemical exchange process. Full line-shape analysis of the singlet signals (*Figure* 5.46) using the NMR simulation program gNMR was carried out to obtain the first order exchange rate constants. The exchange rate constants (k) at different temperatures are listed in *Table* 5.38.

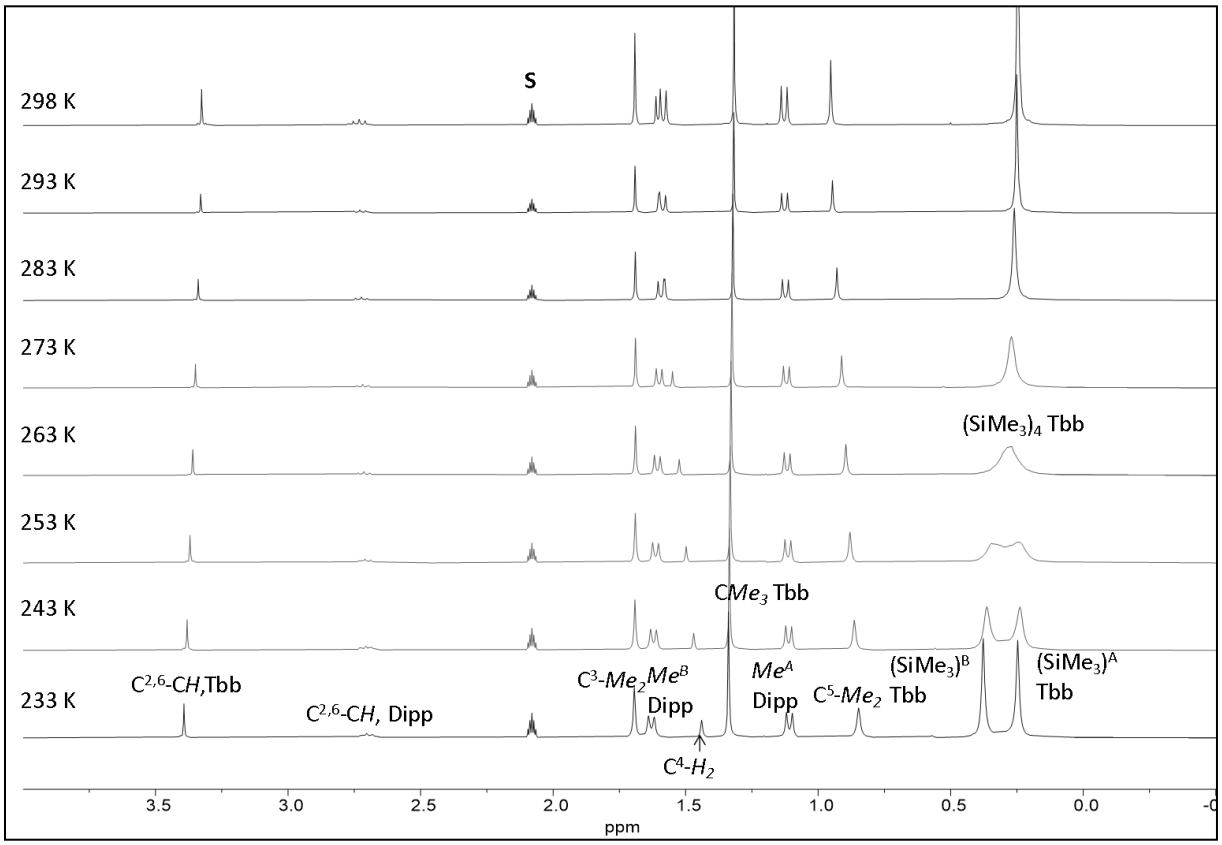

Figure 5.48. Excerpt of the variable temperature ^{1}H NMR spectra (300.13 MHz) of (caac^{Me})Ge=SiBr(Tbb) (**15-Ge**) in (D_8)toluene in the temperature range 298 – 233 K; the residual proton signal of the deuterated solvent is marked with the character **S**.

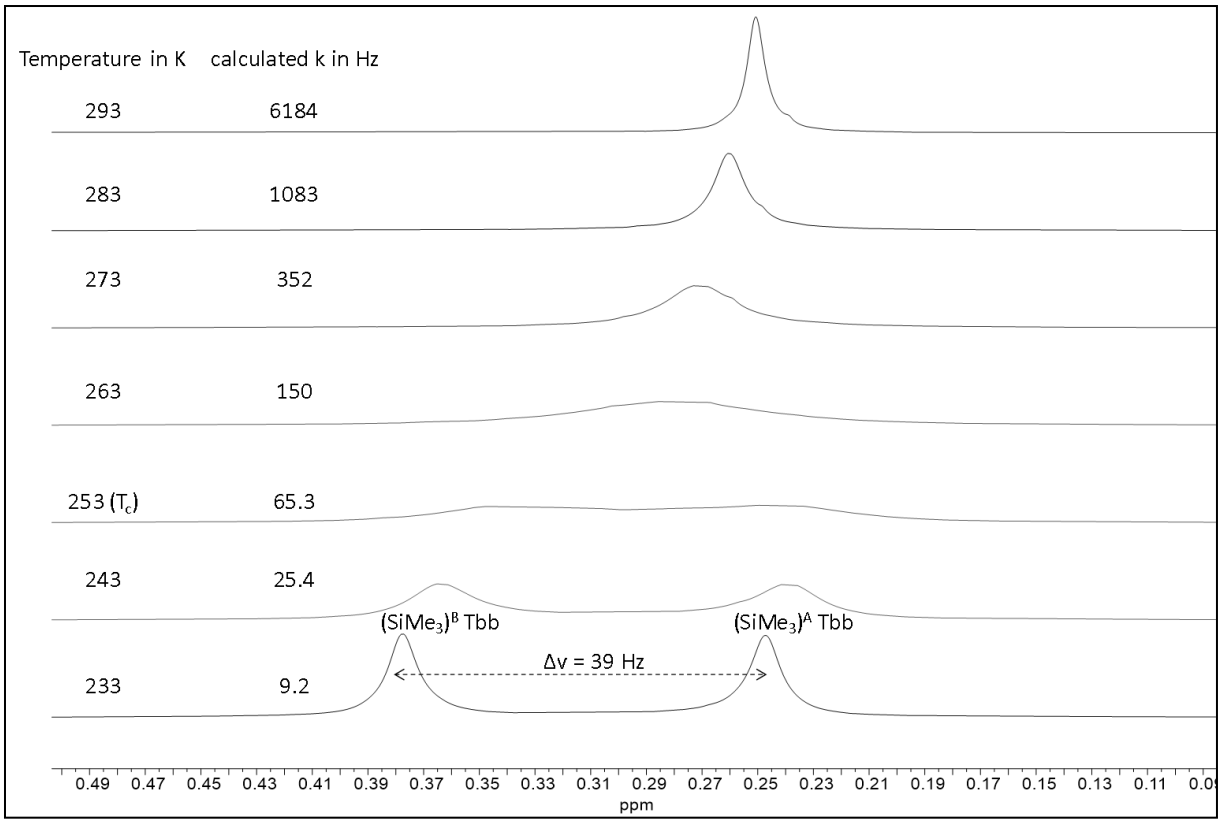

Figure 5.49. Excerpt of the variable temperature ^{1}H NMR (300.13 MHz) spectra of **14-Ge** in (D_8)toluene from 233 K – 293 K showing the exchange process involving $SiMe_3$ groups of the Tbb substituents. The rate constants (k) were obtained from full line-shape analysis using gNMR.

Table5.40. Rate constants (k in Hz) for the hindered rotation of Si–C^{Tbb} bond in **14-Ge** at different temperatures.

T/K	k /Hz	σ(k) /Hz	ln(k/T)	1/T /K^{-1}
233	9.179	2.948	–3.23	0.004292
243	25.41	1.227	–2.22	0.004292
253	65.29	1.03	–1.31	0.004115
263	149.66	1.01	–0.53	0.003953
273	351.72	1.02	0.29	0.003802
283	1083.43	1.11	1.38	0.003663
293	6184.43	8.776	3.08	0.003534

The enthalpy of activation ($\Delta H^{\ddagger}$) and entropy of activation ($\Delta S^{\ddagger}$) were obtained from the slope and the intercept of the linear fit (*Figure 5.47)* using (eq. 5.30) and (eq. 5.31) and $\Delta G^{\ddagger}$ was calculated from (eq. 5.32).

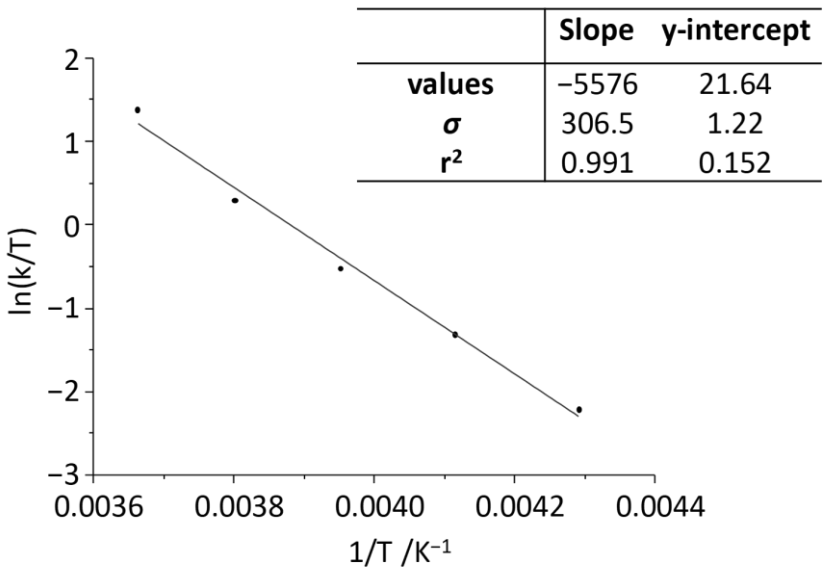

Figure 5.50. Eyring Plot of ln(k/T) versus 1/T for the Si–C^{Tbb} bond rotation process in ($caac^{Me}$)Ge=Si(Br)Tbb (**14-Ge**).

Table 5.41. Activation parameters for the Si–C^{Tbb} bond rotation process of **15-Ge** obtained from full-line shape iteration.

Activation parameter	Calculated value[a]
$\Delta G^{\ddagger}$(298K)	51.6 ± 3.8 kJ mol^{-1}
$\Delta G^{\ddagger}(T_c)$	50.8 ± 3.8 kJ mol^{-1} (253 K)
$\Delta H^{\ddagger}$	46.4 ± 2.5 kJ mol^{-1}
$\Delta S^{\ddagger}$	–17.7 ± 10.1 J K^{-1} mol^{-1}

[a]: The error was calculated using the variance formula given in reference [341]. The average error of the temperature (σ(T)) was estimated to be 0.2 K.

5.6.9 VT ^{1}H NMR spectra, Van't Hoff and line shape analysis of 12

The ^{1}H NMR spectrum of (caac^{Me})Si(C≡CTMS)(GeAr^{Mes}) (**12**) in (D_8)toluene at ambient temperature displays broad resonances (*Figure 5.51*, top spectrum). The dynamics can be traced back to a reversible ***E*** to ***Z*** isomerization, which proceeds via a rotation of the Si–C^{carb} bond. Both isomers, in addition feature hindered rotation of the Mes substituents of the Ar^{Mes} unit, which can be frozen out in both cases at 233 K (*Figure 5.51*, bottom spectrum). Both isomers have been fully chraracterized by high resolution correlation spectroscopy in (D_8)toluene at 243 K and were identified by 1D and 2D NOE NMR experiments respectively.

^{1}H NMR spectra in (D_8)toluene below the coalescence temperature (203 – 293K) were used for a Van't Hoff Analysis. Therefore the $SiMe_3$ resonances of the ***Z***-Isomer (0.26 ppm) and ***E***-Isomer (0.049 ppm) (*Figure 5.51*, bottom spectrum) were integrated in a defined integration interval and the change of the relative integrals (A/B) were analyzed with increasing temperature.

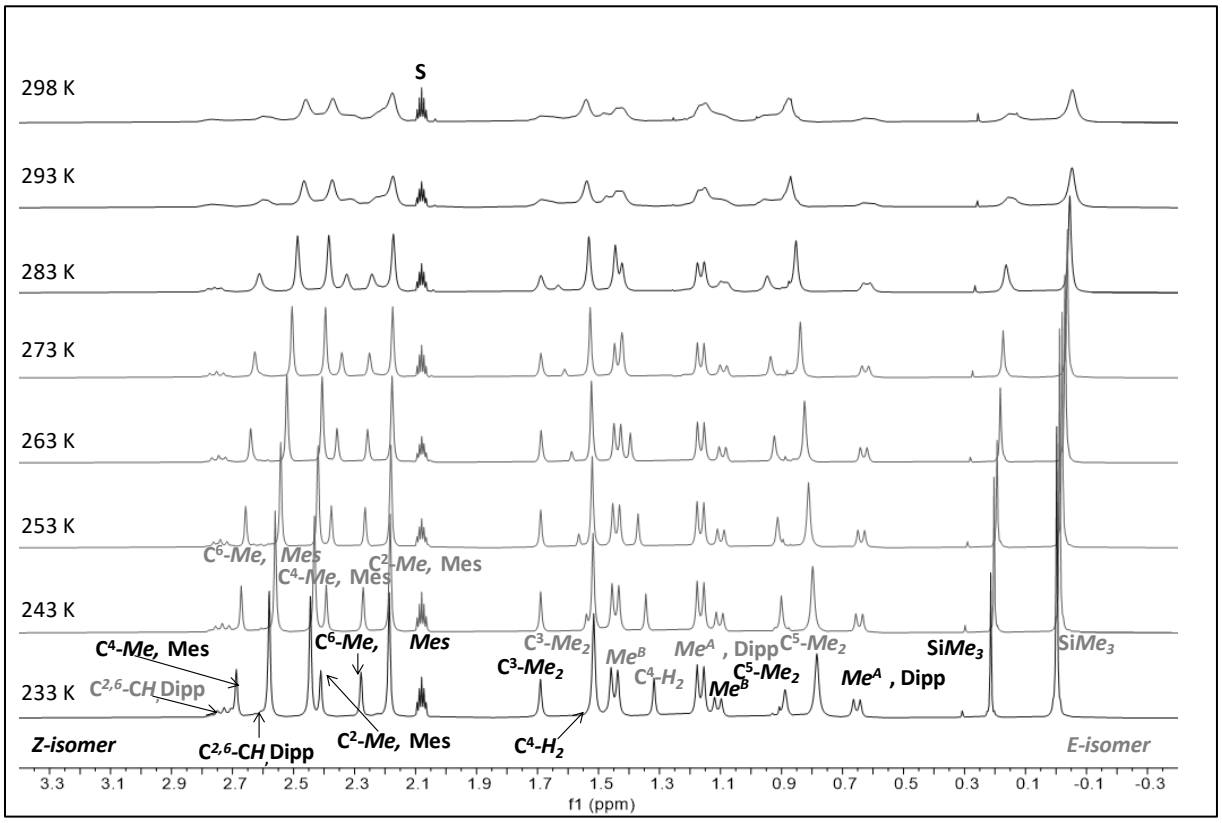

Figure 5.51. Excerpt of the variable temperature ^{1}H NMR spectra (300.13 MHz) of (caac^{Me})Si(C≡CTMS)(GeAr^{Mes}) (**12**) in (D_8)toluene in the temperature range 233 – 298 K; the residual proton signal of the deuterated solvent is marked with the character **S**.

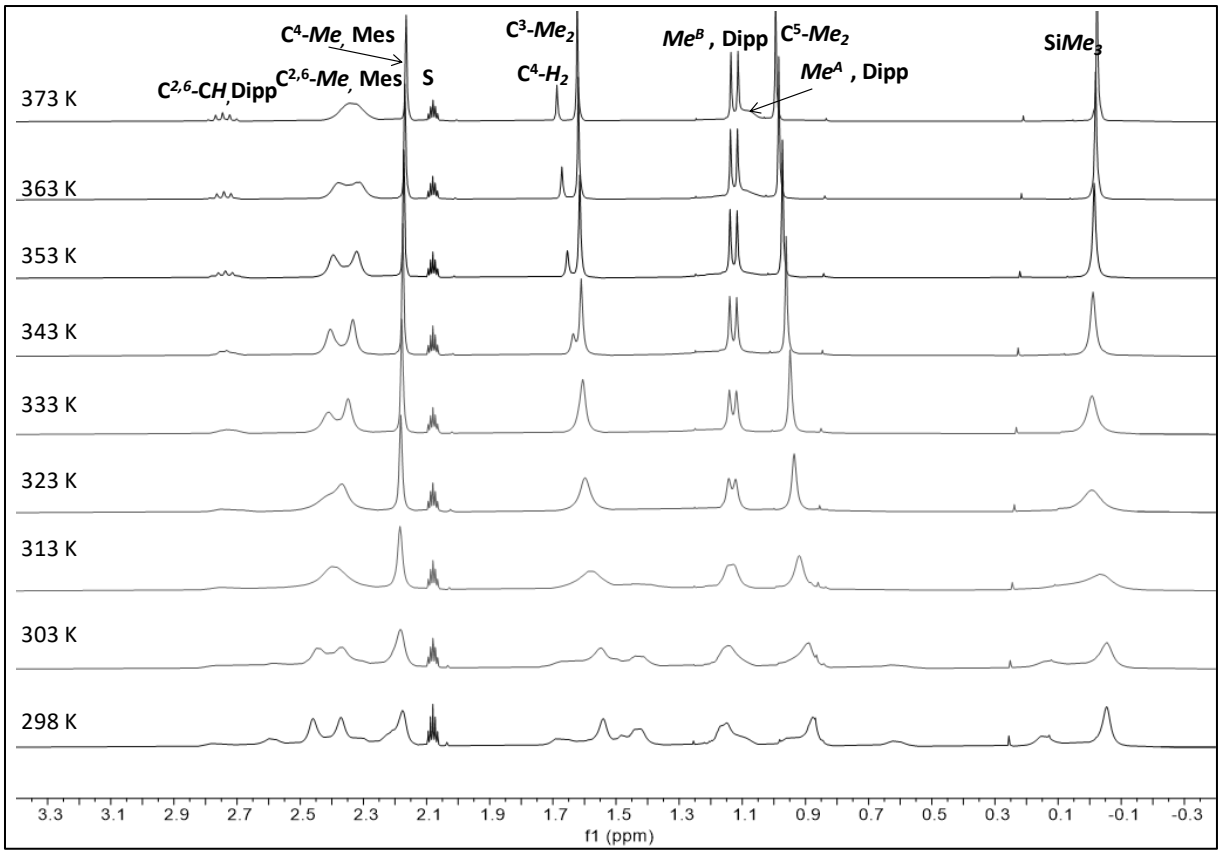

Figure 5.52. Excerpt of the variable temperature ^{1}H NMR spectra (300.13 MHz) of (caac^{Me})Si(C≡CTMS)(GeAr^{Mes}) (**12**) in (D$_8$)toluene in the temperature range 233 – 298 K.

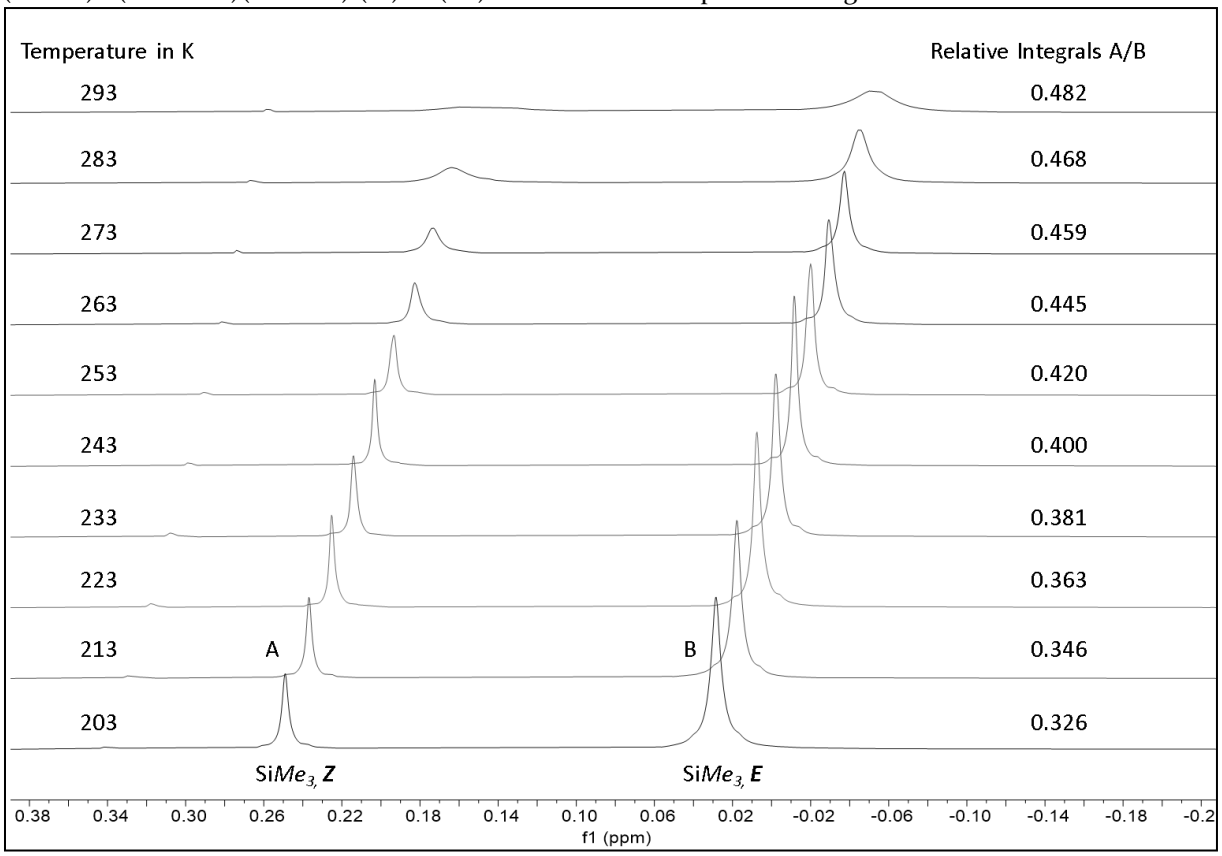

Figure 5.53. Excerpt of the variable temperature ^{1}H NMR (300.13 MHz) spectra of **12** in (D$_8$)toluene from 203 K – 293 K showing the exchange process involving SiMe$_3$ groups of the the two isomers and their relative integrals.

The equilibrium constant of the reversible (*E*)/(*Z*) isomerization was calculated according to the expression:

$$K_{eq} = \frac{[Z\ \text{isomer}]}{[E\ \text{isomer}]} = \frac{A}{B} \qquad \text{(eq. 5.33)}$$

Whereas K_{eq} is unitless. Since the concentration of the two isomers is directly proportional to their respective integral of their signals, the integral ratio of signal A (Si*Me*$_3$-resonance of the ***Z***-isomer) to B (Si*Me*$_3$-resonance isomer of the ***E***-isomer) can be used instead.

Using the Van't Hoff equation (eq. 5.34) the thermodynamic parameters of the isomerization can be calculated.

$$\ln(K_{eq}) = -\frac{\Delta H}{R} \cdot \frac{1}{T} + \frac{\Delta S}{R} \qquad \text{(eq. 5.34)}$$

A plot of ln(A/B) versus 1/T should give a linear correlation. The reaction enthalpy and entropy were extracted from the slope and y-intercept, respectively.

Table 5.42. Relative Integrals of the two Si*Me*$_3$-groups A (***Z***-Isomer) and B (***E***-isomer), as well as parameters for the Van't Hoff Plot.

T/K	K_{eq} = A/B	ln(A/B)	1/T /K^{-1}
203	0.3259	–1.121	0.00493
213	0.3456	–1.062	0.00469
223	0.3634	–1.012	0.00448
233	0.3813	–0.964	0.00429
243	0.3995	–0.918	0.00412
253	0.4200	–0.868	0.00395
263	0.4451	–0.810	0.00380
273	0.4593	–0.778	0.00366
283	0.4684	–0.758	0.00353
293	0.4823	–0.729	0.00341

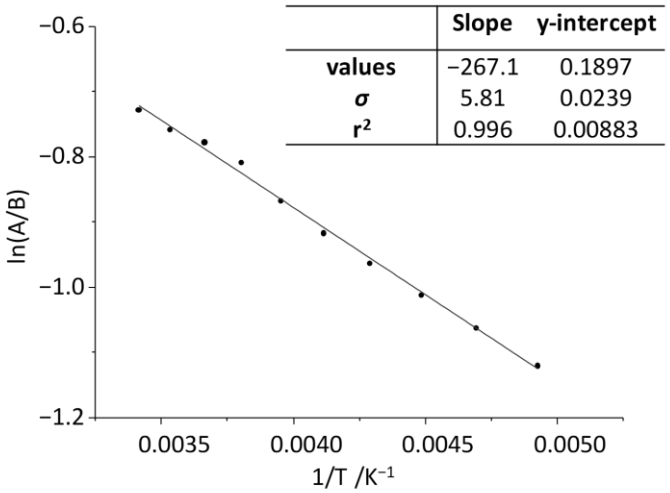

Figure 5.54. Van't Hof plot of ln(A/B) versus 1/T for the reversible (*E*)/(*Z*) isomerization in (caac^{Me})Si(C≡CTMS)(GeAr^{Mes}) (**12**).

Table 5.43. Thermodynamic paramters of the reversible (*E*)/(*Z*) isomerization in **12**.

Thermodynamic parameter	Calculated value[a]
ΔG(298K)	1.8 ± 0.1 kJ mol^{-1}
K_{eq}(298K)[b]	0.493 ± 0.001
ΔH	2.22 ± 0.1 kJ mol^{-1}
ΔS	1.6 ± 0.2 J K^{-1} mol^{-1}

[a]: The error was calculated using the variance formula given in reference [341]. The average error of the temperature (σ(T)) was estimated to be 0.2 K.
[b]: calculated equilibrium constant according to K = exp(slope·1/T + y-intercept), according to the parameters of the linear regression (*Figure 5.54*).

The obtained Gibbs Helmholtz energy at 298K (ΔG = 1.8 ± 0.1 kJ mol^{-1}) gives the relative energy of the two isomers, indicating that the ***E***-isomer is energetically favored by 1.8 kJ mol^{-1} in comparison to the **Z**-isomer.

Lineshape analysis of compound 12

^{1}H NMR spectra in the temperature range 273 – 373 K were used for a line shape analysis in order to obtain the thermodynamic parameters of activation of the process. Therefore the two Si*Me*$_3$-signals were simulated using the gNMR software. The process was treated as interaction of two hydrogen atoms of two different moleclues with two different concentrations, where the concentration of the two signals were constrained by the relation $c_2 = 1 - c_1$. During the simulation the exchange rate constant (k), as well as the concentration c_1 (Si*Me*$_3$-Group of the ***E***-Isomer) were optimized.

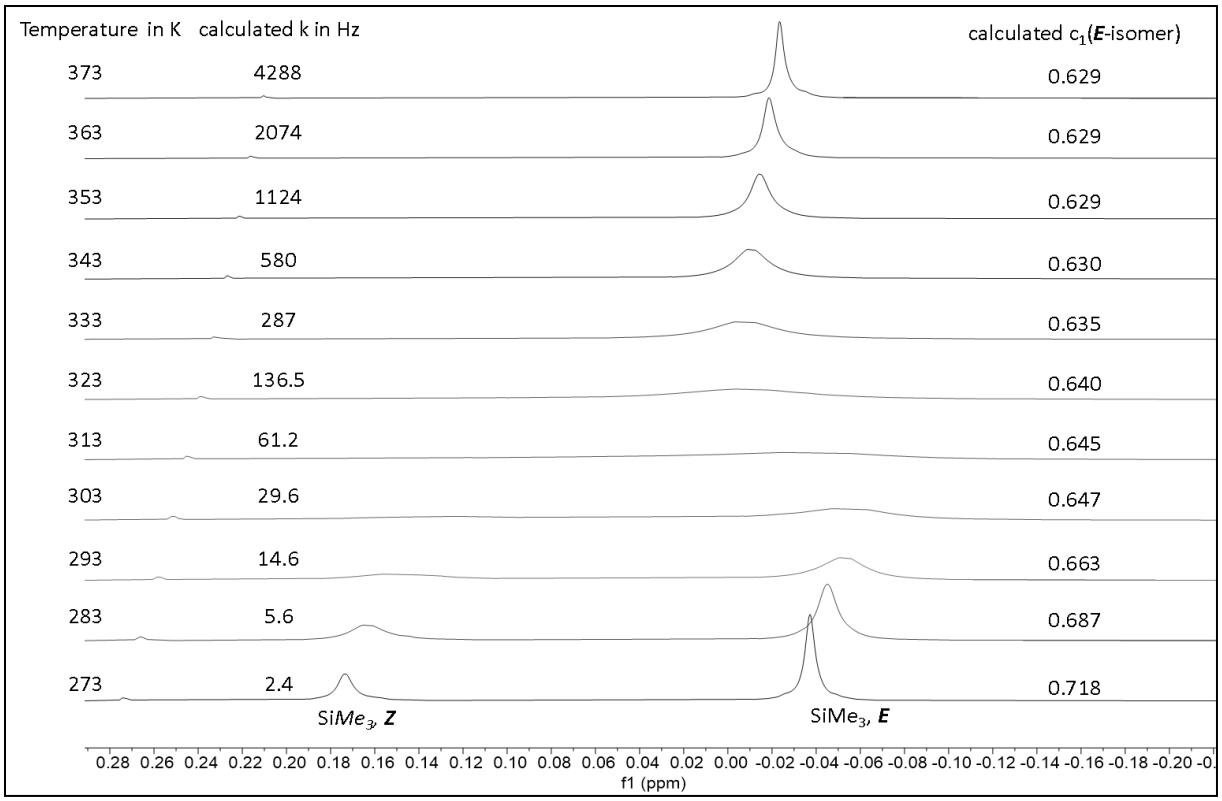

Figure 5.55. Excerpt of the variable temperature ^{1}H NMR (300.13 MHz) spectra of **12** in (D_8)toluene from 203 – 293 K showing the exchange process involving Si*Me*$_3$ groups of the the two isomers . The obtained exchange rate constants k, as well as the relative concentration of the ***E***-isomer c_1 are given.

Table 5.44. Rate constants (k_1 in Hz) and relative concentrations for the reversible ***E*** → ***Z*** isomerization in **12** at different temperatures.

T/K	k_1 /Hz	$\sigma(k_1)$ /Hz	c_1[a]	ln(k/T)	1/T /K^{-1}
273	2.4	5.09	0.718	–4.734	0.00366
283	5.6	1.54	0.687	–3.916	0.00353
293	14.6	1.16	0.663	–3.002	0.00341
303	29.6	1.1	0.647	–2.326	0.00330
313	61.2	1.01	0.645	–1.632	0.00319
323	136.5	1.01	0.640	–0.861	0.00310
333	287.0	1.01	0.635	–0.149	0.00300
343	579.8	1.02	0.630	0.525	0.00292
353	1124.0	1.04	0.629	1.158	0.00283
363	2074.0	1.19	0.629	1.743	0.00275
373	4288.0	1.79	0.629	2.442	0.00268

[a]: relative concentration of the ***E***-isomer obtained from the full line shape analysis. The concentration of the ***Z***-isomer can be calculated using the relation $c_2 = 1 - c_1$.

Applying the results from the Van't Hoff equation (*Table 5.43*) the equilibrium constant of the isomerization can be calculated at each temperature, using the relation:

$$K_{eq} = e^{\{-\frac{\Delta H}{R} \cdot \frac{1}{T} + \frac{\Delta S}{R}\}} \qquad \text{(eq. 5.35)}$$

From the calculated equilibrium constant at each temperature, the exchange rate constant for the back reaction (k_{-1}) (the ***Z*** → ***E*** isomerization) can be calculated:

$$k_{-1} = \frac{k_1}{K_{eq}} \qquad \text{(eq. 5.36)}$$

Table 5.45. Rate constants (k_1 in Hz) for the ***E*** → ***Z*** and ***Z*** → ***E*** (k_{-1} in Hz) isomerization in **12** at different temperatures.

T/K	k_1 /Hz	K_{eq}[a]	k_{-1}[b]	ln(k/T)	1/T /K^{-1}
273	2.4	0.454	5.3	-3.945	0.00366
283	5.6	0.470	12.0	-3.162	0.00353
293	14.6	0.486	30.0	-2.280	0.00341
303	29.6	0.501	59.1	-1.634	0.00330
313	61.2	0.515	118.8	-0.968	0.00319
323	136.5	0.529	258.1	-0.224	0.00310
333	287.0	0.542	529.4	0.464	0.00300
343	579.8	0.555	1044.9	1.114	0.00292
353	1124.0	0.567	1981.4	1.725	0.00283
363	2074.0	0.579	3580.6	2.289	0.00275
373	4288.0	0.591	7258.4	2.968	0.00268

[a]: calculated equilibrium constant at each temperature using the Van't Hoff equation $K_{eq} = \exp(-2.22 \cdot 10^3/R \cdot (1/T) + 1.577/R)$.

[b]: calculated exchange rate constants for the back reaction (k_{-1}) i. e. the ***Z*** → ***E*** isomerization, obtained from $k_{-1} = k_1/K$.

The plot $\ln(k_1/T)$ and $\ln(k_{-1}/T)$ versus 1/T gives a linear correlation.The enthalpy of activation ($\Delta H^{\ddagger}$) and entropy of activation ($\Delta S^{\ddagger}$) of the two processes were obtained from the slope and the intercept of the linear fit (*Figure 5.56)* using (eq. 5.29) and (eq. 5.30) and $\Delta G^{\ddagger}$ was calculated from (eq. 5.31).The activation parameters are summarized in *Table 5.46*.

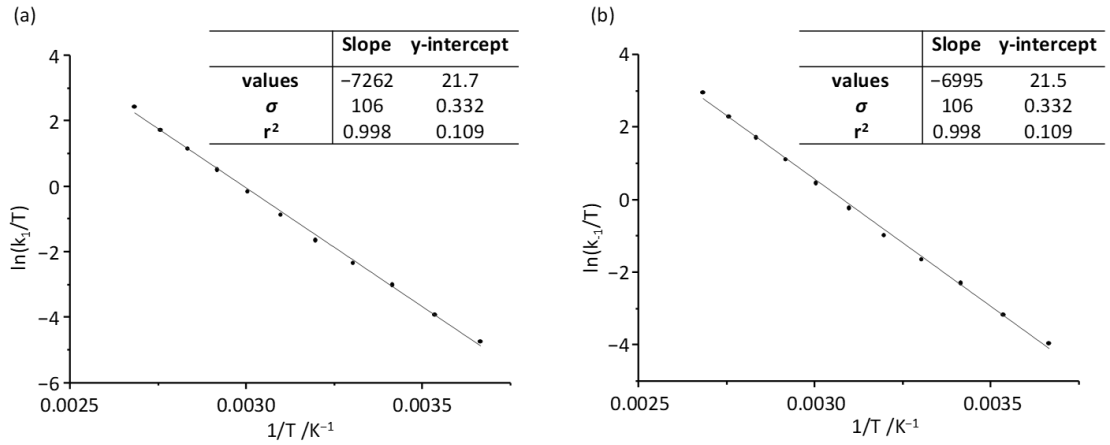

Figure 5.56. Eyring Plot of ln(k/T) versus 1/T for the ***E*** → ***Z*** isomerization (a) and for the ***Z*** → ***E*** isomerization (b) in (caac^{Me})Si(C≡CTMS)(GeAr^{Mes}) (**12**).

Table 5.46. Activation parameters for the ***E*** → ***Z*** as well the ***Z*** → ***E*** isomerization obtained from the full line shape analysis of **12**.

Thermodynamic activation parameter	Calculated value[a]	
	E → ***Z*** isomerization	***Z*** → ***E*** isomerization
$\Delta G^{\ddagger}$(298K)	65.4 ± 1.1 kJ mol^{-1}	63.7 ± 1.1 kJ mol^{-1}
$\Delta G^{\ddagger}(T_c)$	65.7 ± 1.1 kJ mol^{-1} (313 K)	63.9 ± 1.1 kJ mol^{-1} (313 K)
$\Delta H^{\ddagger}$	60.4 ± 1.0 kJ mol^{-1}	58.2 ± 1.0 kJ mol^{-1}
$\Delta S^{\ddagger}$	–16.9 ± 2.8 J K^{-1} mol^{-1}	–18.5 ± 2.8 J K^{-1} mol^{-1}

[a]: The error was calculated using the variance formula given in reference [341]. The average error of the temperature (σ(T)) was estimated to σ (T) = 0.2 K.

The dynamic process in the silenyl germylene (caac^{Me})Si(C≡CTMS)(GeAr^{Mes}) (**12**) can be attributed to a reversible ***Z*** to ***E*** -isomerization, which proceeds via rather high activation barrier. The Gibb's free energy difference of the two isomers could be obtained from a Van't Hoff plot, indicating that the ***E***-isomer lies 1.8 ± 0.1 kJ mol^{-1} lower in energy than the ***Z***-isomer. Full line shape analysis could give the thermodynamic activation parameters with a rather high free enthalpy of activation for the ***E*** → ***Z*** isomerization of $\Delta G^{\ddagger}$(298K) = 65.4 ± 1.1 kJ mol^{-1}. The calculated free enthalpy of activation of the back-isomerization (***Z*** → ***E***) of $\Delta G^{\ddagger}$(298K) = 63.7 ± 1.1 kJ mol^{-1} is exactly 1.7 kJ mol^{-1} lower, perfectly fitting the Gibb's free energy difference of 1.8 kJ mol^{-1}.

5.7 Kinetic study of compounds by time resolved VT ^{1}H NMR spectroscopy

5.7.1 Kinetic study of the irreversible *E* → *Z* isomierziation in 2-Eind

In case of SiBr(Eind)(caac^{Me}) two isomers have been observed: an orange ***E***-isomer (N-Dipp orientated trans with respect to the bromine substituent) with C_1-symmetry in (D_6)benzene solution at ambient temperature and the yellow ***Z***-isomer (N-Dipp orientated cis with respect to the bromine substituent) with an averaged C_S-symmetry in (D_6)benzene solution at ambient temperature. Both isomers were obtained in a ratio of 0.75 / 0.25 (***E*** / ***Z***) after reaction of 2 equivalents of caac^{Me} carbene with (*E*)-[Eind(Br)Si=Si(Br)Eind]. Interestingly the ***E***-isomer seems to be thermolabile and slowly transforms into the ***Z***-isomer at higher temperature in solution and in the solid state. The process is irreversible. In order to analyze the kinetics of the reaction and to determine the activation energy for the irreversible ***Z*** → ***E*** isomerization the following experiment was carried out:

26.9 mg of the analytically pure ***E***-isomer of SiBr(Eind)(caac^{Me}) (contained less than 5 mol% of the ***Z***-isomer, according to ^{1}H NMR spectroscopy in (D_6)benzene) were weighted in small Schlenk tube, using the fine balance. The compound was dissolved in 1.848 g of (D_8)toluene (density = 0.943 g/mL, 1.960 mL) yielding an orange solution of 0.0177 mmol mL^{-1}. The solution was divided into three Young-NMR tubes (0.5 mL each), ^{1}H NMR spectra in (D_8)toluene revealed the presence of ca. 3 mol% of **3-Eind-*Z***, present in the solution of **3-Eind-*E*** (*Figure 5.57*). The samples were stored overnight in a Schlenk tube at –30°C.

The next day, one Young-NMR tube was used at a time for a variable temperature NMR measurement. The first sample was measured at 110°C for 1.5 h. ^{1}H NMR spectra were recorded every two minutes using the automation of the Bruker Software at 110 °C for 1.5 h. After the measurement was completed the NMR machine was cooled to 100 °C. The next sample was added, ^{1}H NMR spectra were recorded every two minutes at 100 °C for 3 h. Then the device was cooled to 90 °C, the third and final sample was inserted and ^{1}H NMR spectra were recorded every two minutes at 90 °C for 6 h.

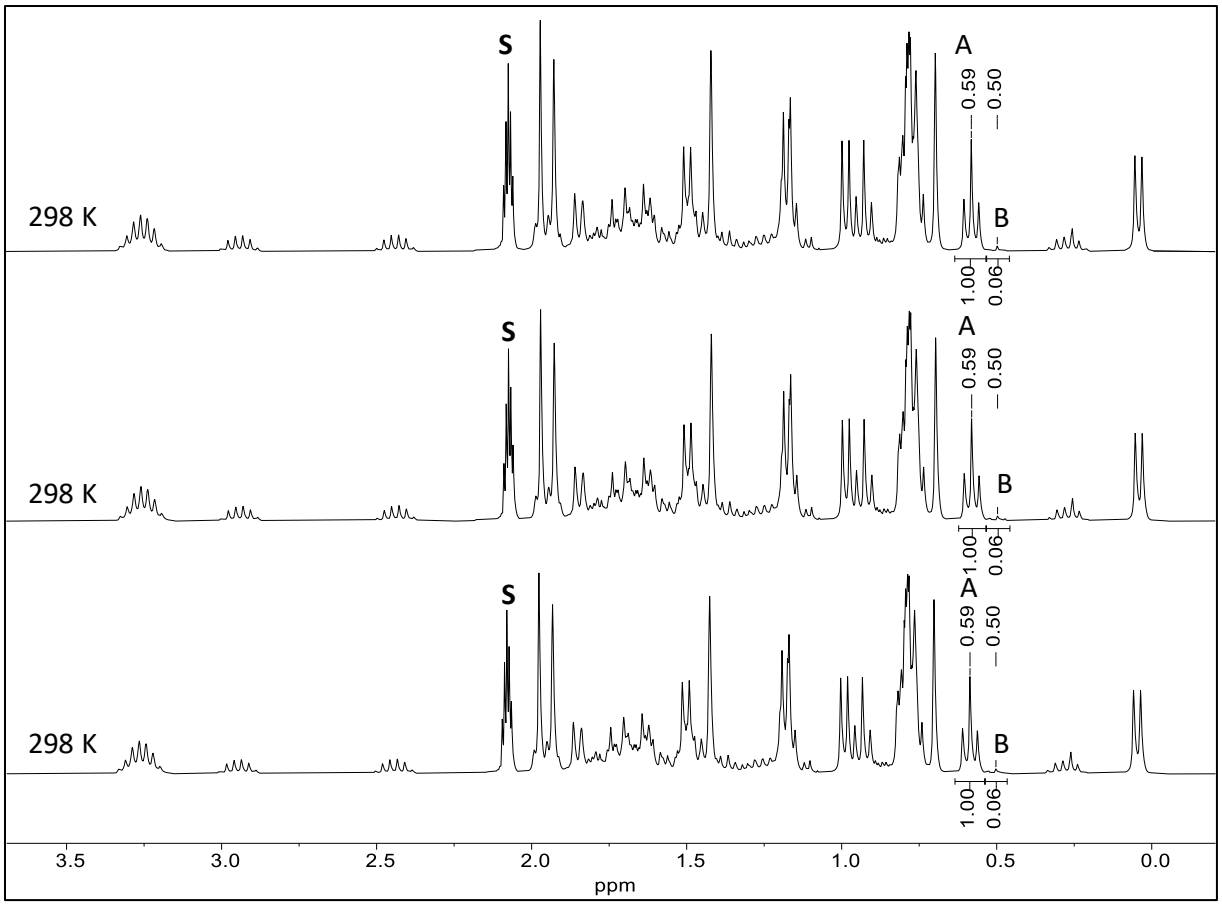

Figure 5.57. Excerpt of the ^{1}H NMR spectra (300.13 MHz) of **2-Eind-*E*** in (D_8)toluene solution at ambient temperature before heating. The C^{3}-{CH_AH_BMe}$_x$, Eind of the ***E***-isomer is marked with the letter A, the $C^{3,5}$-$CH_AH_BMe_A$, Eind resonance of the ***Z***-isomer is marked with the letter B. The signal of the deuterated solvent is marked with the character **S**. As evidenced by the relative integrals A(3H):B(6H) the samples contained ca. 3 mol% of the ***Z***-isomer prior to the kinetic study.

The conversion rate was followed by the C^{3}-{CH_AH_BMe}$_x$, Eind signal of the ***E***-isomer (at 0.57 ppm, signal A) and the $C^{3,5}$-$CH_AH_BMe_A$ resonance of the ***Z***-isomer (at 0.49 ppm, signal B) (*Figure 5.58*). Prior to the integration, phase correction and baseline correction were performed. All spectra were integrated using the following integration limits: [0.603 – 0.523 ppm] (signal A, 3H), [0.519 – 0.398 ppm] (signal B, 6H). The absolute values of the integration of signal A and B were collected and the absolute values of the integration of signal B divided by 2. The molar ratio [A]/([A]+[B]) was calculated multiplied with the concentration of the solution (0.0177 mmol mL^{-1}) in the Young-NMR tube and plotted against the time of the recorded respective ^{1}H NMR spectrum.

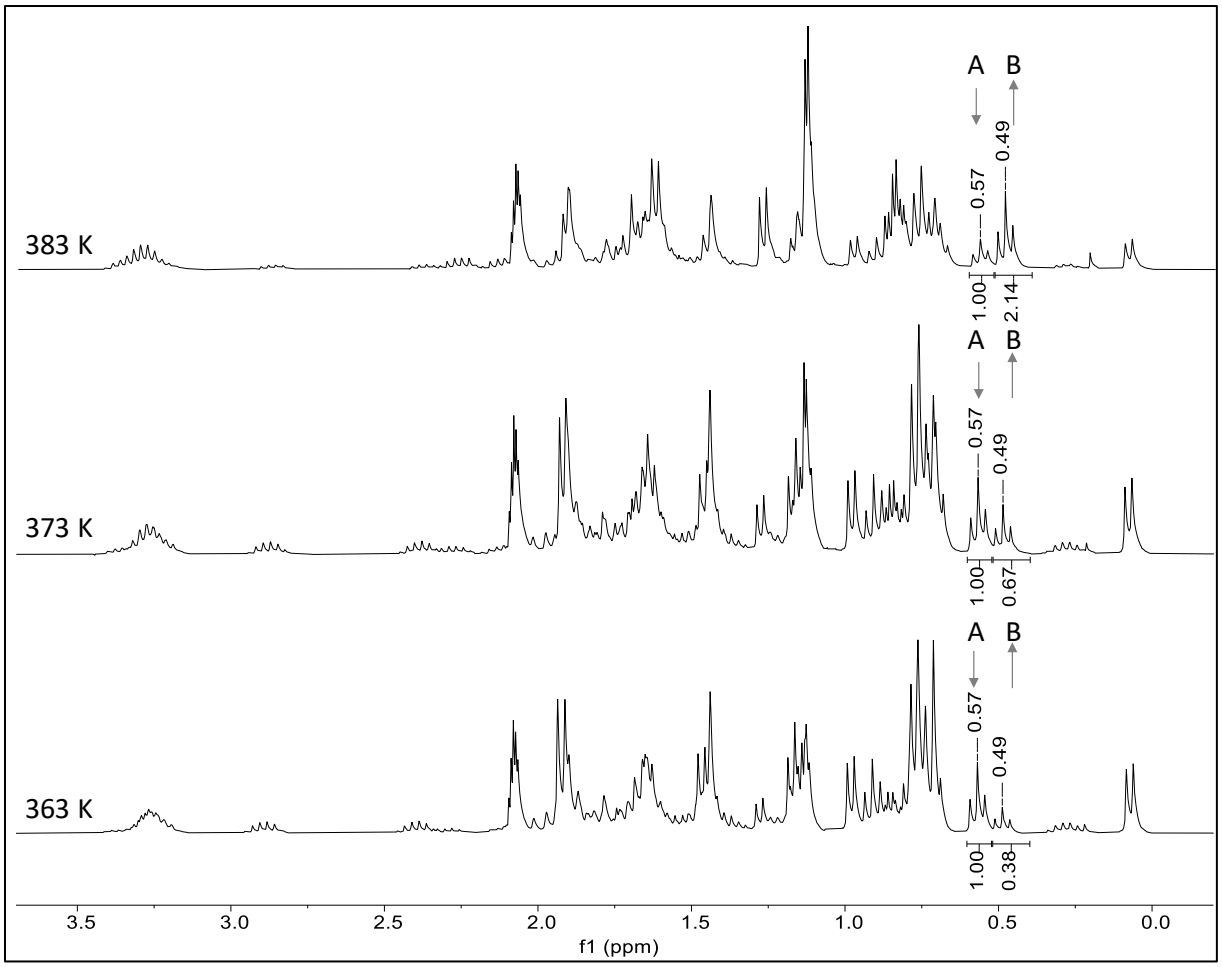

Figure 5.58. Exerpt of the first recorded ^{1}H NMR spectra (300.13 MHz) of SiBr(Eind)(caac^{Me}) (**2-Eind**) in (D_8)toluene at the beginning of the kinetic study at the different temperatures 383 K, 373 K and 363 K. The C^3-{CH_AH_BMe}$_x$, Eind of the ***E***-isomer is marked with the letter A, the $C^{3,5}$-$CH_AH_BMe_A$, Eind resonance of the ***Z***-isomer is marked with the letter B.

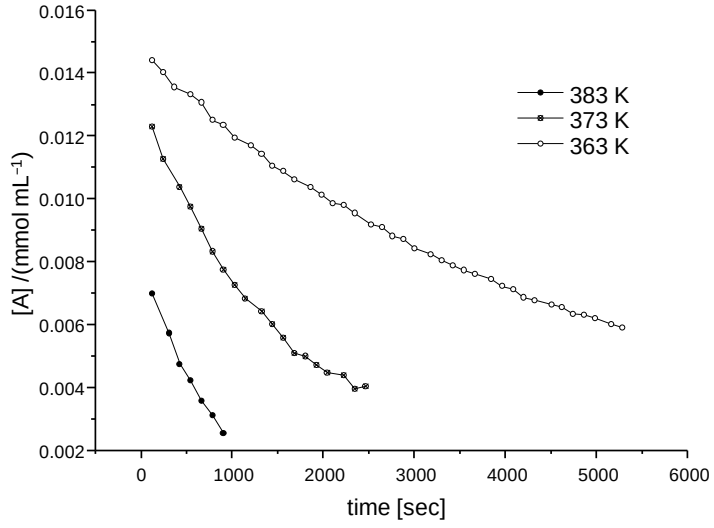

Figure 5.59. Determined concentration of the ***E***-isomer [A] in mmol mL^{-1} plotted against the time at different temperatures 363 K, 373 K and 383 K.

The thermally induced isomerization of the ***E*** isomer into the ***Z***-isomer can be described using the kinetics of a reaction first order (eq. 5.37):

$$[A] = [A_0] \cdot e^{(-k \cdot t)} \quad \text{(eq. 5.37)}$$

$$\ln[A] = -k \cdot t + \ln[A_0] \quad \text{(eq. 5.38)}$$

$$k = -\text{slope} \quad \text{(eq. 5.39)}$$

$$[A_0] = e^{\text{intercept}} \quad \text{(eq. 5.40)}$$

The reaction rate constants (k) and concentration of the ***E*** -isomer at the beginning of the experiment [A_0] were obtained from the slope and the intercept of the linear fit (see *Figure* 5.60 and Table 5.47) using (eq. 5.39) and (eq. 5.40). The results are summarized in *Table* 5.48.

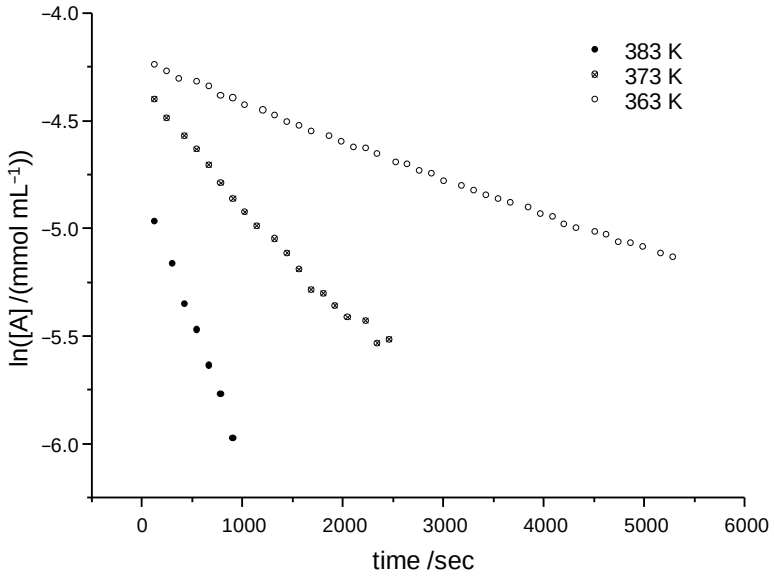

Figure 5.60. Plot of ln([A] /(mmol mL^{-1})) vs time, showing a linear correlation.

Table 5.47. Parameters of the linear regression of the plot ln([A]) versus t at different temperatures 363 K, 373 K, 383 K.

	383 K		**373 K**		**363 K**	
	slope	intercept	slope	intercept	slope	intercept
value	$-1.27 \cdot 10^{-3}$	−4.80	$-4.93 \cdot 10^{-4}$	−4.39	$-1.72 \cdot 10^{-4}$	−4.24
σ	$3.28 \cdot 10^{-5}$	$1.93 \cdot 10^{-2}$	$1.26 \cdot 10^{-5}$	$1.85 \cdot 10^{-2}$	$1.23 \cdot 10^{-6}$	$3.81 \cdot 10^{-3}$
r^2	0.997	0.0220	0.989	0.0387	0.998	0.0119

Table 5.48. Calculated reaction rate constants (k), concentration of SiBr(Eind)(caac^{Me}) ***E*** isomer [A_0] at the start of the experiment and mol% of the ***E***-isomer A_0 at different temperatures.

T /K	**k /sec^{-1}**	**σ(k) /sec^{-1} [a]**	**[A_0] /(mmol mL^{-1})**	**σ([A_0]) [b] /(mmol mL^{-1})**	**mol% of A_0 [c]**
383	$1.27 \cdot 10^{-3}$	$3.28 \cdot 10^{-5}$	$8.26 \cdot 10^{-3}$	$3.32 \cdot 10^{-5}$	46.7
373	$4.93 \cdot 10^{-4}$	$1.26 \cdot 10^{-5}$	$1.24 \cdot 10^{-2}$	$5.25 \cdot 10^{-5}$	70.2
363	$1.72 \cdot 10^{-4}$	$1.23 \cdot 10^{-6}$	$1.44 \cdot 10^{-2}$	$1.29 \cdot 10^{-5}$	81.1

[a]: Standard deviation of the reaction rate konstants σ(k), which was obtained from the standard deviation of the slope of the linear regression by σ(k) = –σ(slope) (*Table 5.47*).
[b]: Standard deviation of the concentration of **2-Eind-*E*** at the start of the experiment, which was obtained form the standard deviation of the y-intercept of the linear regression by σ([A_0]) = σ(y-intercept)/(y-intercept)·[A_0] (*Table 5.47*).
[c]: mol% of A_0= [A_0]/ (0.0177 mmol mL^{-1}) · 100 mol%. The obtained mol% perfectly fits with the corresponding relative integral A_0 of the first recorded ^{1}H NMR spectrum at the respective temperature (*Figure 5.58*).

The temperature dependence of the reaction rate constants was derived from a modified form of the linearized Eyring equation (eq. 2.5) (k_B = Boltzmann constant, h = Planck´s constant, R = gas constant) assuming that the transmission coefficient κ is equal 1 and that the activation enthalpy ($\Delta H^{\ddagger}$) is constant over the temperature interval of the experiment ($\Delta C_p^{\ddagger} = d(\Delta H^{\ddagger})/dT = 0$, $\Delta C_p^{\ddagger}$ = heat capacity of activation).

$$\ln\left(\frac{k}{T}\right) = \ln\left(\frac{k_B}{h}\right) + \left(\frac{\Delta S^{\ddagger}}{R}\right) + \left(-\frac{\Delta H^{\ddagger}}{R}\right) \cdot \frac{1}{T} \qquad \text{(eq. 2.5)}$$

$$\Delta H^{\ddagger} = -R \cdot \text{slope}\ [J \cdot mol^{-1}] \qquad \text{(eq. 5.29)}$$

$$\Delta S^{\ddagger} = R \cdot \left(\text{Intercept} - \ln\left(\frac{k_B}{h}\right)\right)\ [J \cdot K^{-1} \cdot mol^{-1}] \qquad \text{(eq. 5.30)}$$

$$\Delta G^{\ddagger} = \Delta H^{\ddagger} - T \cdot \Delta S^{\ddagger} \qquad \text{(eq. 5.31)}$$

The enthalpy of activation ($\Delta H^{\ddagger}$) and entropy of activation ($\Delta S^{\ddagger}$) were obtained from the slope and the intercept of the linear fit (*Figure 5.61)* using equations (eq. 5.29) and (eq. 5.30) and $\Delta G^{\ddagger}$ was calculated from equation (eq. 5.31). The activation parameters are summarized in *Table 5.50*.

Table 5.49. Reaction rate constants (k in sec^{-1}) for the ***E*** → ***Z*** isomerization of SiBr(Eind)($caac^{Me}$) (**2-Eind**) at different temperatures.

T /K	k /sec^{-1}	σ(k) /sec^{-1}	ln(k/T)	1/T /K^{-1}
383	$1.27 \cdot 10^{-3}$	$3.28 \cdot 10^{-5}$	–12.61	$2.61 \cdot 10^{-3}$
373	$4.93 \cdot 10^{-4}$	$1.26 \cdot 10^{-5}$	–13.54	$2.68 \cdot 10^{-3}$
363	$1.72 \cdot 10^{-4}$	$1.23 \cdot 10^{-6}$	–14.56	$2.75 \cdot 10^{-3}$

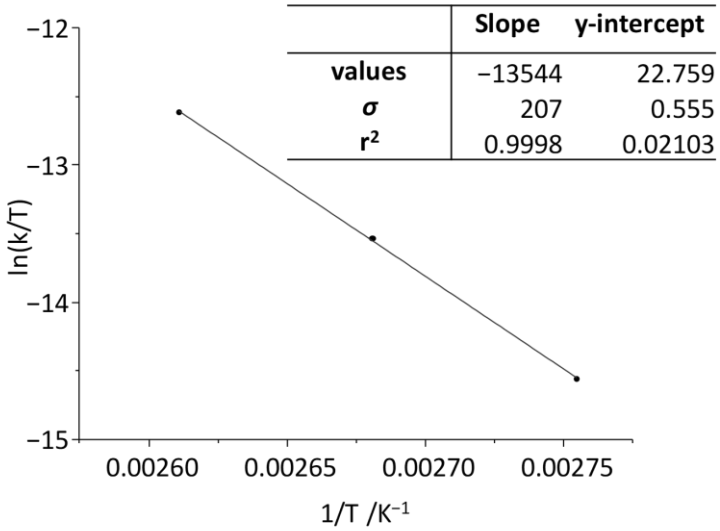

Figure 5.61. Eyring Plot of ln(k/T) versus 1/T for the ***E*** → ***Z*** isomerization process in SiBr(Eind)($caac^{Me}$) (**2-Eind**).

Table 5.50. Activation paramters of the irreversible ***E*** → ***Z*** isomerization in SiBr(Eind)($caac^{Me}$) (**2-Eind**)

Thermodynamic activation parameter	Calculated value[a] for the ***E*** → ***Z*** isomerization
$\Delta G^{\ddagger}$(298K)	115.1 ± 1.7 kJ mol^{-1}
$\Delta G^{\ddagger}$(383K)	115.8 ± 1.7 kJ mol^{-1} (383 K)
$\Delta H^{\ddagger}$	112.6 ± 1.7 kJ mol^{-1}
$\Delta S^{\ddagger}$	–8.3 ± 0.2 J K^{-1} mol^{-1}

[a]: The error was calculated using the variance formula given in reference [341]. The average error of the temperature (σ(T)) was estimated to be 0.2 K.

5.7.2 Kinetic study of the irreversible *Z,Z* → *E,E*-isomierziation in 9-Mes

In case of $Si_2(Mes)_2(caac^{Me})_2$ two isomers have been observed: an orange ***Z,Z*** isomer (N-Dipp orientated cis with respect to the Si-Si(Mes)($caac^{Me}$) moiety, in case of both silicon centers, with C_2-symmetry in (D_6)benzene solution at ambient temperature) and the dark purple ***E,E***-isomer (N-Dipp orientated trans with respect to the Si-Si(Mes)($caac^{Me}$) moiety, in case of both silicon centers, which features an averaged C_S-symmetry at higher temperatures in (D_8)toluene solution). Both isomers were obtained in a ratio approx. 1:1 after $1e^-$-reduction of SiBr(Mes)($caac^{Me}$) (**3-Mes**) with KC_8. Interestingly the **Z,Z**-isomer seems to be thermolabile and slowly transforms into the ***E,E*** isomer at higher temperature in solution and in the solid state. The process is irreversible. In order to analyze the kinetics of the reaction and to determine the activation energy for the irreversible (**Z,Z**) → (***E,E***) isomerization the following experiment was carried out:

25.7 mg of the diastereomeric mixture of **Z,Z** and ***E,E*** -isomer of $Si_2Mes_2(caac^{Me})_2$ were weighted in small Schlenk tube, using the fine balance. The compound was dissolved in 1.840 g of (D_8)toluene (density = 0.943 g/mL, 1.951 mL) yielding a dark purple solution of 0.01522 mmol mL^{-1}. The solution was divided into three Young-NMR tubes (0.5 mL each), ^{1}H NMR spectra in (D_8)toluene revealed the presence of 64.2 mol% of **9-Mes-*Z,Z*** and 35.8 mol% **9-Mes-*E,E*** in the diasteromeric mixture of **9-Mes** (*Figure 5.62*). The samples were stored overnight in a Schlenk tube at –30°C.

The next day, one Young-NMR tube was used at a time for a variable temperature NMR measurement. The first sample was measured at 110°C for 1.5 h. ^{1}H NMR spectra were recorded every two minutes using the automation of the Bruker Software at 110 °C for 1.5 h. After the measurement was completed the device was cooled to 100 °C. The next sample was added, ^{1}H NMR spectra were recorded every two minutes at 100 °C for 3 h. Then the device was cooled to 90 °C, the third and final sample was inserted and ^{1}H NMR spectra were recorded every two minutes at 90 °C for 6 h.

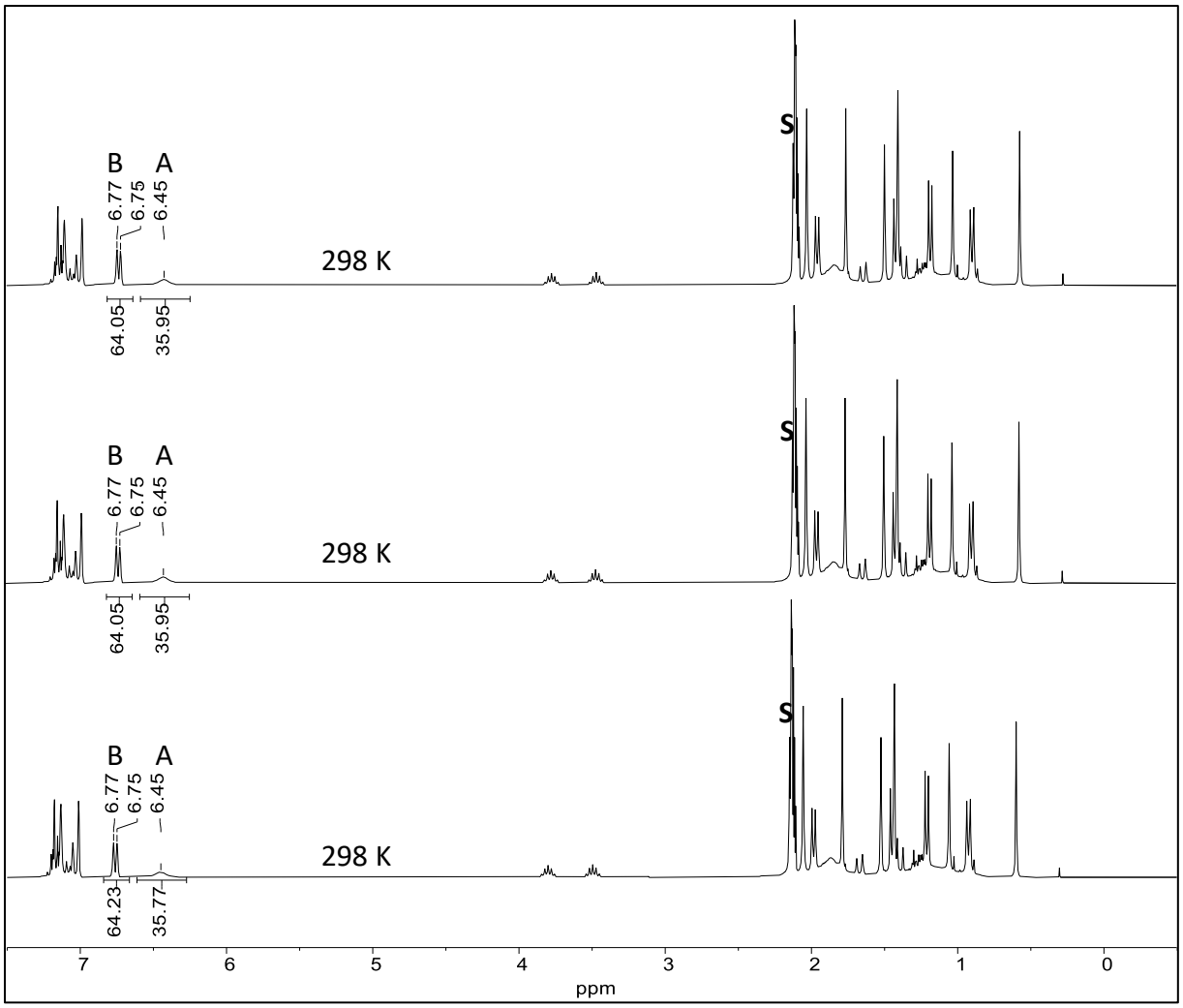

Figure 5.62. ^{1}H NMR spectra (300.13 MHz) of the diastereomeric mixture of **9-Mes** in (D_8)toluene solution at ambient temperature before heating. The $C^{3,5}$-*H*, Mes signal of the ***E,E***-isomer is marked with the letter A, the $C^{3,5}$-*H*, Mes resonance of the ***Z,Z***-isomer is marked with the letter B. The signal of the deuterated solvent is marked with the character **S**. As evidenced by the relative integrals A:B the samples contained ca. 35 mol% of the ***E,E***-isomer prior to the kinetic study.

The conversion rate was followed by the $C^{3,5}$-*H*, Mes Signal of the ***E,E***-isomer (at 6.40 ppm, signal A) and the $C^{3,5}$-*H*, Mes resonance of the **Z,Z** isomer (at 6.69 ppm, signal B) (*Figure 5.63*). Prior to the integration, phase correction and baseline correction were performed. All spectra were integrated using the following integration limits: [6.79 – 6.59 ppm] (signal A), [6.50 – 6.30 ppm] (signal B). The absolute values of the integration of signal A and B were collected. The molar ratio [B]/([A]+[B]) was calculated multiplied with the concentration of the solution (0.01522 mmol mL^{-1}) in the Young-NMR tube and plotted against the time of the recorded respective ^{1}H NMR spectrum.
The thermally induced isomerization of the ***Z,Z***-isomer into the ***E,E***-isomer can be described using the kinetics of a reaction first order (eq. 5.37) – (eq. 5.40).

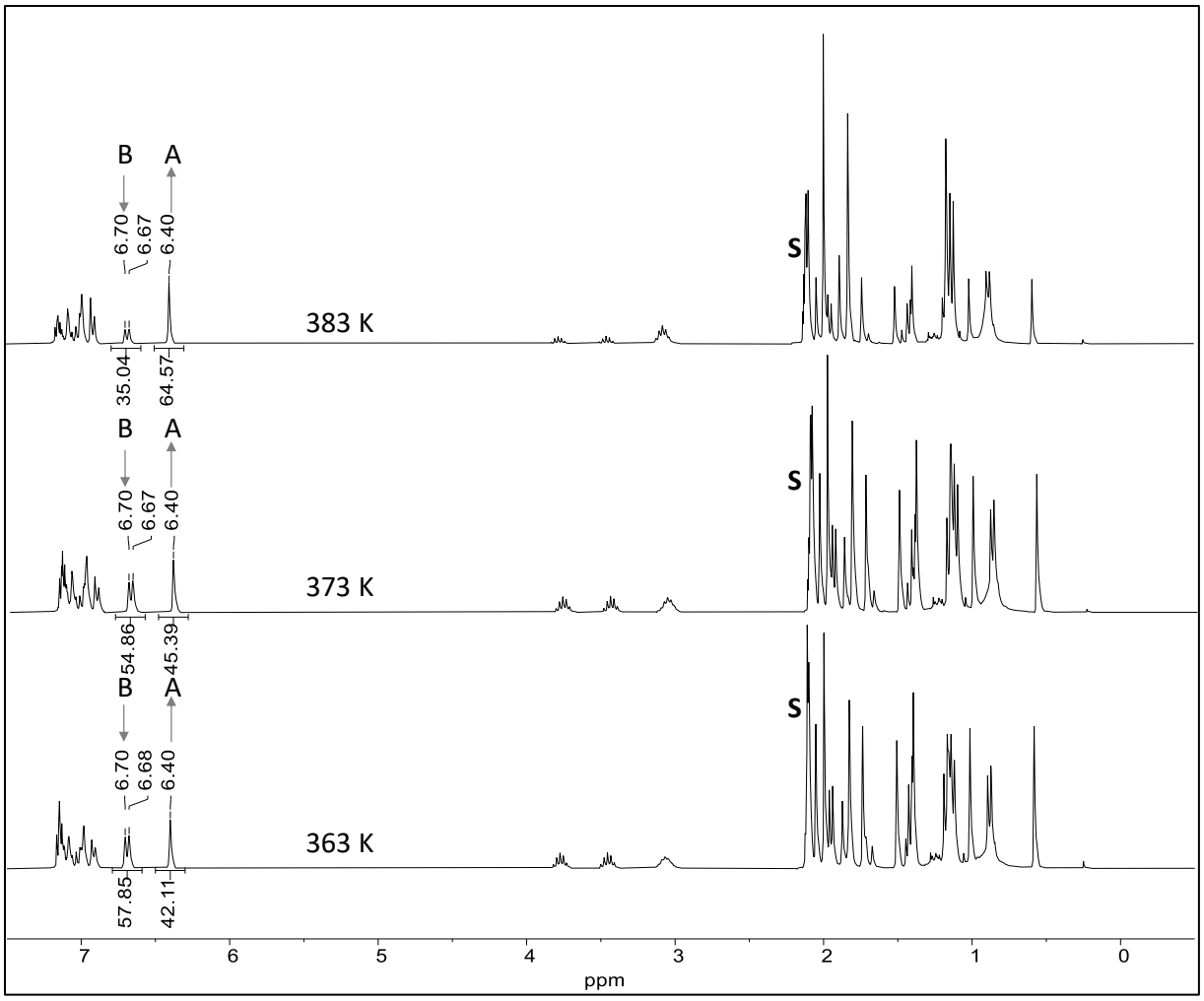

Figure 5.63. ^{1}H NMR spectra (300.13 MHz) of the isomeric mixture of $Si_2Mes_2(caac^{Me})_2$ (**9-Mes**) in (D_8)toluene at the beginning of the kinetic study at the different temperatures 383 K, 373 K and 363 K. The $C^{3,5}$-*H*, Mes resonance of the ***E,E***-isomer is marked with the letter A, the $C^{3,5}$-*H*, Mes resonance of the ***Z,Z***-isomer is marked with the letter B. The signal of the deuterated solvent is marked with the character **S**.

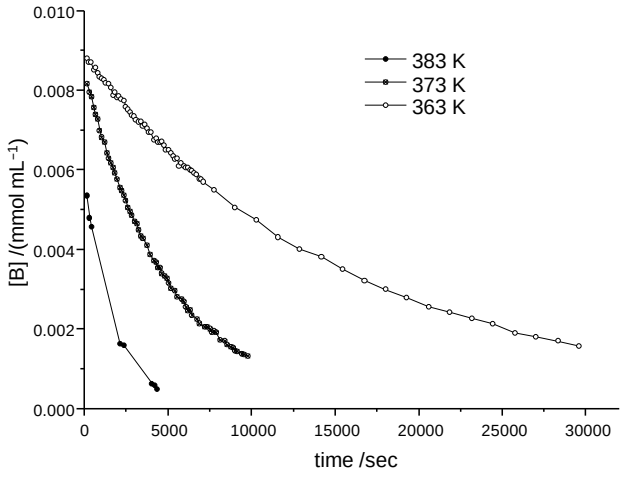

Figure 5.64. Determined concentration of the ***Z,Z***-isomer [B] in mmol mL^{-1} plotted against the time at different temperatures 363 K, 373 K and 383 K.

The reaction rate constants (k) and concentration of the ***Z,Z***-isomer at the beginning of the experiment [B_0] were obtained from the slope and the intercept of the linear fit (*Figure 5.65* and *Table 5.51*) using (eq. 5.39)and (eq. 5.40). The results are summarized in *Table 5.52*.

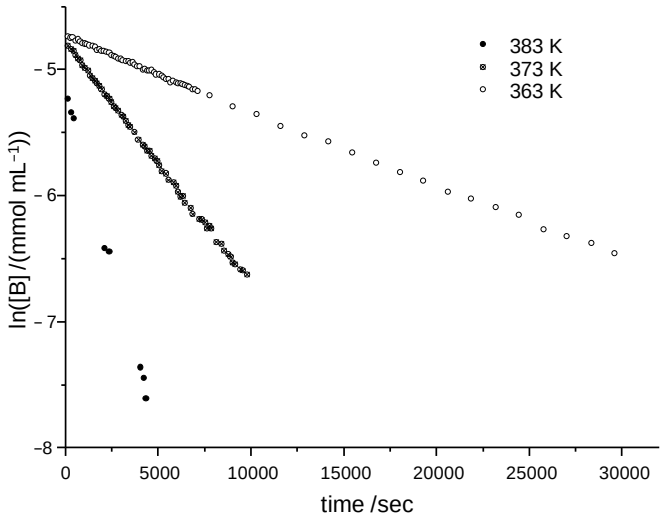

Figure 5.65. Plot of ln([B] /(mmol mL^{-1})) vs time, showing a linear correlation.

Table 5.51. Parameters of the linear regression of the plot ln([B]) versus t at different temperatures 363 K, 373 K, 383 K.

	383 K		**373 K**		**363 K**	
	slope	intercept	slope	intercept	slope	intercept
value	$-5.51\cdot10^{-4}$	−5.17	$-1.92\cdot10^{-4}$	−4.79	$-5.88\cdot10^{-5}$	−4.74
σ	$9.86\cdot10^{-6}$	$2.76\cdot10^{-2}$	$7.28\cdot10^{-7}$	$3.93\cdot10^{-3}$	$1.83\cdot10^{-7}$	$1.92\cdot10^{-3}$
r^2	0.998	0.0472	0.999	0.0164	0.999	0.0117

Table 5.52. Calculated reaction rate constants (k), concentrations of $Si_2(Mes)_2(caac^{Me})_2$ ***Z,Z*** [B_0] at the start of the experiment and mol% of the ***Z,Z***-isomer B_0 at different temperatures.

T /K	**k /sec^{-1}**	**σ(k) /sec^{-1}** [a]	**[B_0] /(mmol mL^{-1})**	**σ([B_0])**[b] **/(mmol mL^{-1})**	**mol% of B_0**[c]
383	$5.51\cdot10^{-4}$	$9.86\cdot10^{-6}$	$5.66\cdot10^{-3}$	$3.02\cdot10^{-5}$	37.2
373	$1.92\cdot10^{-4}$	$7.28\cdot10^{-7}$	$8.35\cdot10^{-3}$	$6.84\cdot10^{-6}$	54.8
363	$5.88\cdot10^{-5}$	$1.83\cdot10^{-7}$	$8.75\cdot10^{-3}$	$3.54\cdot10^{-6}$	57.5

[a]: Standard deviation of the reaction rate konstants σ(k), which was obtained by σ(k) = −σ(slope) (*Table 5.51*). [b]: Standard deviation of the concentration of **9-Mes-*Z,Z*** at the start of the experiment, which was obtained by σ([B_0]) = σ(y-intercept)/(y-intercept)·[B_0] (*Table 5.51*).

[c]: mol% of B_0= [B_0]/ (0.01522 mmol mL^{-1}) · 100 mol%. The obtained mol% perfectly fits with the corresponding relative integral B_0 of the first recorded ^{1}H NMR spectrum at the respective temperature (*Figure* 5.58).

Using the linearized form of the Eyring equation (eq. 2.5) the thermodynamic parameters of the irreversible isomerization can be calculated upon plotting ln(k/T) versus 1/T.

The enthalpy of activation ($\Delta H^{\ddagger}$) and entropy of activation ($\Delta S^{\ddagger}$) were obtained from the slope and the y-intercept of the linear fit (*Figure 5.66)*, respectively using (eq. 5.29) and (eq. 5.30). $\Delta G^{\ddagger}$ was calculated from the Gibb's Helmholtz (eq. 5.31). The activation parameters are summarized in *Table 5.54*.

Table 5.53. Reaction rate constants (k in sec^{-1}) for the ***Z,Z → E,E*** isomerization of $Si_2Mes_2(caac^{Me})_2$ (**9-Mes**) at different temperatures.

T /K	**k /sec^{-1}**	**σ(k) /sec^{-1}**	**ln(k/T)**	**1/T /K^{-1}**
383	$5.51 \cdot 10^{-4}$	$9.86 \cdot 10^{-6}$	–13.45	$2.61 \cdot 10^{-3}$
373	$1.92 \cdot 10^{-4}$	$7.28 \cdot 10^{-7}$	–14.48	$2.68 \cdot 10^{-3}$
363	$5.88 \cdot 10^{-5}$	$1.83 \cdot 10^{-7}$	–15.63	$2.75 \cdot 10^{-3}$

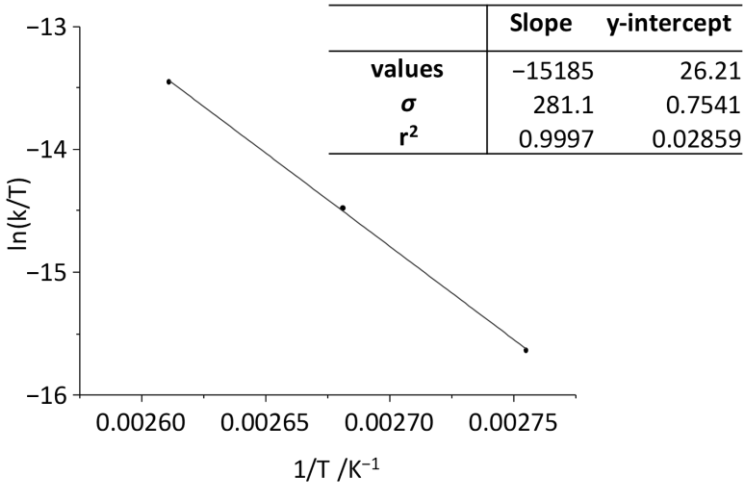

Figure 5.66. Eyring Plot of ln(k/T) versus 1/T for the ***Z,Z → E,E*** isomerization process in $Si_2Mes_2(caac^{Me})$ (**9-Mes**).

Table 5.54. Activation paramters of the irreversible ***Z,Z → E,E*** isomerization in $Si_2Mes_2(caac^{Me})_2$ (**9-Mes**).

Thermodynamic activation parameter	Calculated value[a] for the ***Z,Z → E,E*** isomerization
$\Delta G^{\ddagger}$(298K)	120.2 ± 2.3 kJ mol^{-1}
$\Delta G^{\ddagger}$(383K)	118.5 ± 2.3 kJ mol^{-1} (383 K)
$\Delta H^{\ddagger}$	126.3 ± 2.3 kJ mol^{-1}
$\Delta S^{\ddagger}$	20.4 ± 0.6 J K^{-1} mol^{-1}

[a]: The error was calculated using the variance formula given in reference [341]. The average error of the temperature (σ(T)) was estimated to be 0.2 K.

5.8 Evans Method of silicon(I) radical 3-Si

Three coaxial NMR tubes were constructed by inserting a one-end-sealed glass capillary tube of 1.0 mm diameter and approximately 10 cm in length into each J-young NMR tube. The capillary tube can be easily prepared from the Pasteur pipette.

Three solutions of radical **3-Si** in (D_6)benzene of known concentration (96.5 mM, 44.3 mM, 19.2 mM) were prepared separately and each filled upto 5 cm height into three capillary tubes. The tubes were inserted carefully into three J-Young NMR tubes containing 0.4 mL of (D_6)benzene each. ^{1}H NMR spectra were recorded under the standard conditions (300.13 MHz,Puls Sequence zg30, ns = 16, D1 = 1.000, Acq. Time = 5.4527). The presence of radical **3-Si** revealed a second C_6D_5H signal lower intensity, which was downfield shifted compared to the originated C_6D_5H solvent signal of (D_6)benzene in the ^{1}H NMR spectrum at ambient temperature.

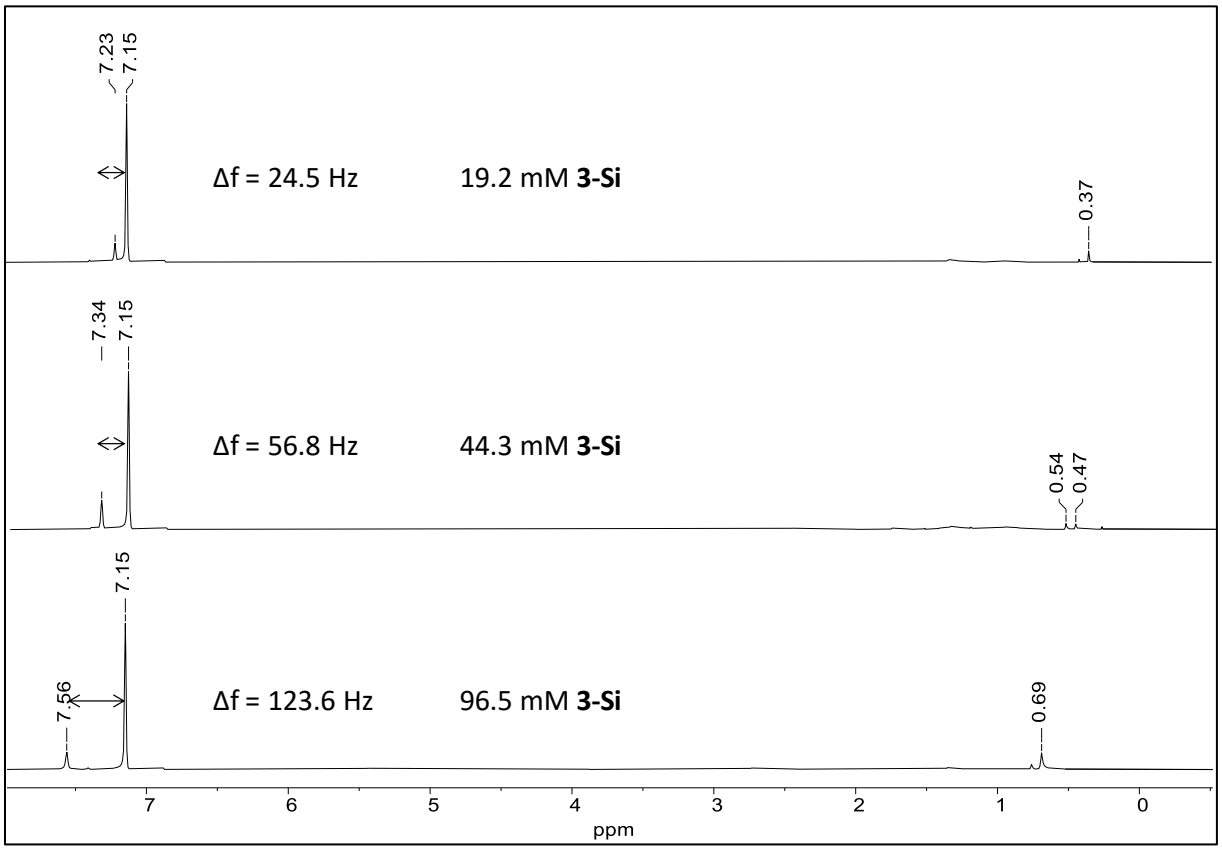

Figure 5.67. Recorded ^{1}H NMR spectra in (D_6)benzene of the prepared samples of Si($SiTMS_3$)($caac^{Me}$) (**3-Si**) at different concentrations after 0.5 h at ambient temperature.

Evans Equation:

$$\chi_{mol(meas)} = \frac{3\ \Delta f}{4\ \pi\ f\ c} + \ M\ \chi_{mass(solvent)} \qquad \text{(eq. 5.41)}$$

$\chi_{mol(meas)}$ is the molar susceptibility in cm^3mol^{-1}
Δf is the observed frequency difference in Hz
f is the spectrometer frequency in Hz
c is the concentration of the paramagnetic substance in $mol \cdot cm^{-3}$ (i.e. in mol/mL).
M is the molar mass of the paramagnetic compound in $g\ mol^{-1}$
$\chi_{mass(solvent)}$ mass susceptibility of the solvent

The term $\chi_{mass(solvent)}$, has always a negative value. This term can be neglected in case of a highly paramagnetic substance, resulting in the following simplified equation.

$$\chi_{mol(meas)} = \frac{3\ \Delta f}{4\ \pi\ f\ c} \qquad \text{(eq. 5.42)}$$

+
Molar diamagnetic susceptibility:

$$\chi_{(mol)Dia} = -\left(\frac{M}{2}\right) 10^{-6}\ cm^3/mol \qquad \text{(eq. 5.43)}$$

M is the molar mass of the paramagnetic substance.
This general equation can be used for a good estimation of the molar diamagnetic susceptibility. The resulting error in the effective magnetic moment (μ_{eff}) is within 1 – 2 % from that calculated using Pascal´s method.[51]

Diamagnetic correction:
The general equation of the molar diamagnetic susceptibility correction to the experimentally measured molar magnetic susceptibility is:

$$\chi_{(mol)meas} = \chi_{(mol)para} + \chi_{(mol)Dia} \qquad \text{(eq. 5.44)}$$

$\chi_{(mol)para}$ is the molar paramagnetic susceptibility of the paramagnetic substance.

$$\chi_{(mol)para} = \chi_{(mol)meas} - \chi_{(mol)Dia} \qquad \text{(eq. 5.45)}$$

51 Pascal proposed that the diamagnetism of a molecule could be determined in an additive fashion using values for the diamagnetic susceptibility of every atom (χ_{Di}) and bond (λ_i) in the molecule: $\chi_D = \sum_i \chi_{Di} + \sum_i \lambda_i$ see reference [342].

The value $\chi_{(mol)Dia}$ is always negative and therefore equation (eq. 5.45) turns into equation (eq. 5.46), where all values are positive.

$$\chi_{(mol)para} = \chi_{(mol)meas} + \left|\chi_{(mol)Dia}\right| \qquad \text{(eq. 5.46)}$$

Inserting equation (eq. 5.42) and (eq. 5.43) into equation (eq. 5.46) gives

$$\chi_{(mol)para} = \frac{3\ \Delta f}{4\ \pi\ f\ c} + \left(\frac{M}{2}\right) 10^{-6} \qquad \text{(eq. 5.47)}$$

Solving equation (eq. 5.47) for Δf gives, in order to insert the concentration in the equation in mM c has to be multiplied by 10^{-6}:

$$\Delta f = \frac{4\ \pi}{3\ f}\left(\chi_{(mol)para} - \left(\frac{M}{2}\right) 10^{-6}\right) 10^{-6}\ c \qquad \text{(eq. 5.48)}$$

c ... concentration in mM
f ... frequency of the spectrometer in Hz
M ... molecular weight of the radical g/mol[52]
$\chi_{(mol)para}$ ... molar susceptibility cm^3mol^{-1}

Since the overall molar susceptibility $\chi_{(mol)para)}$ is a constant it can be obtained of a linear correlation of given concentrations of the paramagnetic compound against the determined frequency shift in the residual proton signal of the deuterated solvent in the corresponding ^{1}H NMR spectrum.

$$\Delta f = a \cdot c \qquad \text{(eq. 5.49)}$$

Where the slope a of the linear correlation equals

$$a = \frac{4\ \pi}{3\ f}\left(\chi_{(mol)para} - \left(\frac{M}{2}\right) 10^{-6}\right) 10^{-6} \qquad \text{(eq. 5.50)}$$

Solving equation (eq. 5.50) for $\chi_{(mol)para}$ gives:

$$\chi_{(mol)para} = \frac{3}{4\ \pi\ f}\ a\ 10^6 + \left(\frac{M}{2}\right) 10^{-6} \qquad \text{(eq. 5.51)}$$

Under the assumption that the concentration of radical Si(SiTMS$_3$)(caac^{Me}) (**3-Si**) does not change after 0.5 h of the sample preparation in the deuterated solvent, which is in agreement with respect to the EPR-spectroscopy in benzene, ^{1}H-NMR spectroscopy in (D_6)benzene and UV/Vis spectroscopy in *n*-pentane, the molar susceptibility can be

calculated via the known concentration of the radical and the frequency shift of the residual proton signal of (D_6)benzene.

Table 5.55. Observed frequency shifts (Δf) of the deuterated solvent in the ^{1}H NMR spectrum or radical **3-Si** of known concentration after 0.5 h at ambient temperature (*Figure 5.67*).

Δf /Hz	**c(3-Si) /(mmol L^{-1})**
123.6	96.52
56.8	44.29
24.5	19.24

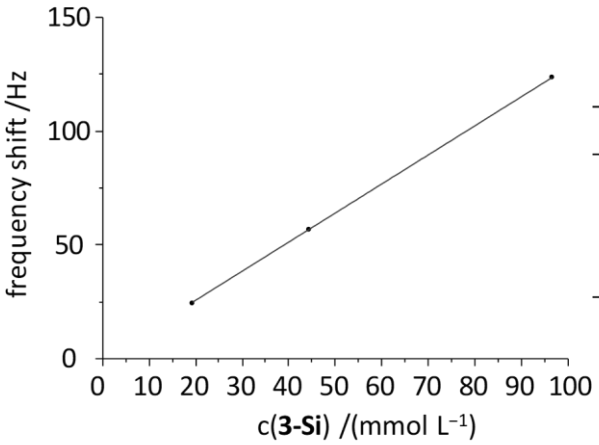

	Slope	Y-intercept
values	1.281	0
σ	0.00105	-
r²	0.999	0.113

Figure 5.68. Plot of the determined frequency shift of the residual proton signal of the deuterated solvent in (D_6)benzene against the concentration of Si(SiTMS$_3$)(caac^{Me}) (**3-Si**). Linear regression with the y-intercept set to 0. Parameters of the linear regression are given in the table.

Using equation (eq. 5.51) and inserting the ^{1}H NMR frequency of 300.13 MHz and the molecular weight of 561.21 g/mol of **3-Si**, the following result is obtained:

$$\chi_{(mol)para} = \frac{3}{4 \cdot \pi \cdot 300.13 \cdot 10^6}\, 1.281 \cdot 10^6 + \left(\frac{561.21}{2}\right) 10^{-6} = 1.30\ 10^{-3}\,\frac{\text{ml}}{\text{mol}}$$

This gives the magnetic susceptibility of Si(SiTMS$_3$)(caac^{Me}) (**3-Si**) without the mass susceptibility of the deuterated solvent, the result was obtained from equation (eq. 5.41).

Calculation of spin-only effective magnetic moment:

$$\mu_{\text{eff}} = 2.828\sqrt{\chi_{(mol)para}\, T} \qquad \text{(eq. 5.52)}$$

T is temperature of the spectrometer in Kelvin.

Calculation of the amount of unpaired electrons:
Assuming that the total orbital angular momentum (L) is completely quenched in the paramagnetic compound, the following equation can be applied:

$$\mu_{eff} = \sqrt{n(n+2)} \qquad \text{(eq. 5.53)}$$

n ... number of unpaired electrons in the system

Solving the equation for n, leads to a quadratic equation: $n^2 + 2n + \mu_{eff}^2 = 0$

The positive root of the quadratic equation was obtained from the quadratic formula:

$$n = \frac{-2 + \sqrt{4 - 4\ \mu_{eff}{}^2}}{2} \qquad \text{(eq. 5.54)}$$

Calculation of Magnetic susceptibility and effective magnetic moment of $Si(SiTMS_3)(caac^{Me})$ (**3-Si**) at 298 K:

Table 5.56. Calculated magnetic susceptibility and effective magnetic moment of silicon radical **3-Si** at ambient temperature.

	From (eq. 5.42)	From (eq. 5.41)[a]
$\chi_{mol(meas)}$ /(mL mol^{-1})	1020·10^{-6}	964·10^{-6}
$\chi_{(mol)para}$ /(mL mol^{-1})	1300·10^{-6}	1240·10^{-6}
μ_{eff}	1.76	1.72
unpaired electrons	1.02	0.99

[a]: For the calculation of $\chi_{mol(meas)}$ equation (eq. 5.41) was used: for the molar mass susceptibility ($M \cdot \chi_{mass(solvent)}$) of ($D_6$)benzene the value –54.8 10^{-6} mL mol^{-1} was inserted. [342]

5.8.1 Kinetic study of the decomposition of radical 3-Si

Since the linear function $\Delta f = a \cdot c$ describes the correlation between the frequency shift in the residual proton signal of the deuterated solvent and the corresponding concentration of the radical in solution, it can be used to calculate the concentration of a given solution of Si(SiTMS$_3$)(caac^{Me}) (**3-Si**) by deviding the frequency shift by the known slope (a).

$$c = \frac{\Delta f}{a} = \frac{\Delta f}{1.281} \qquad \text{(eq. 5.55)}$$

This way the decomposition of **3-Si** can be studied via the Evan's method by measurement of change the frequency shift over the time. Therefore ^{1}H NMR spectra of the three samples with the concentrations of 96.5 mM, 44.3 mM and 19.2 mM were measured at least twice a day during the time of two weeks. The frequency shifts of the residual proton peaks of (D_6)benzene were determined manually by each ^{1}H NMR spectrum and the concentration of radical **3-Si** in mM calculated by dividing it by the slope a (a = 1.282).

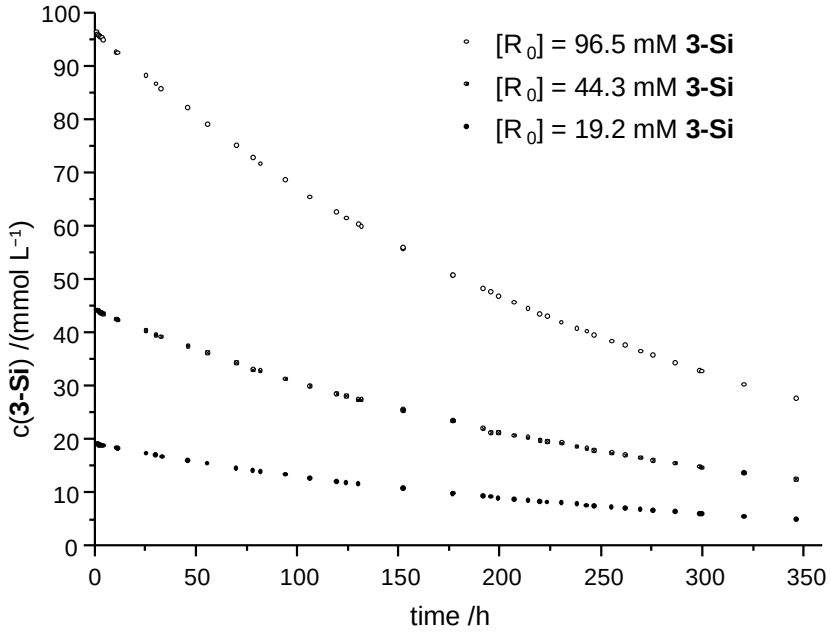

Figure 5.69. Plot of the determined concentrations of Si(SiTMS$_3$)(caac^{Me}) (**3-Si**) against the time.

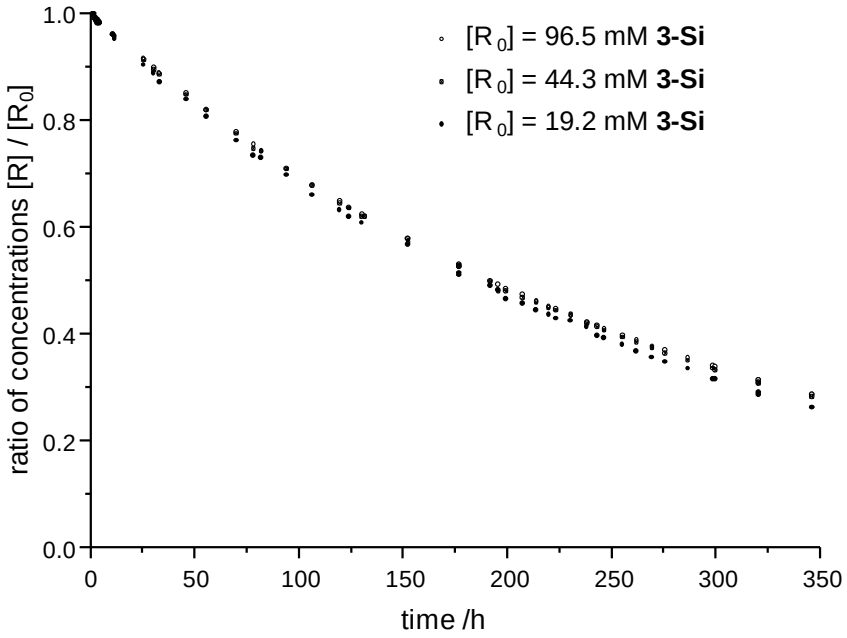

Figure 5.70. plot of the ratio of the determined concentrations of Si(SiTMS$_3$)(caac^{Me}) (**3-Si**) by the starting concentration [R]$_0$ against the time. The plot clearly shows that the decomposition of **3-Si** is independent from the starting concentration of the radical.

These preliminary results indicate, that radical **3-Si** most likely decomposes in a reaction pseudo-first order, which can be described the following way:

$$Rate = -\frac{d[R]}{dt} = k[R] \qquad \text{(eq. 5.56)}$$

Separation of the variables and integration gives:

$$\ln[R] - \ln[R]_0 = -kt \qquad \text{(eq. 5.57)}$$

This can be rearranged to:

$$\ln[R] = -kt + \ln[R]_0 \qquad \text{(eq. 5.58)}$$

This means that the plot of the ln of the determined concentration versus the time should give a linear correlation:

$$y = a\,x + b \qquad \text{(eq. 5.59)}$$

Where the slope (a) equals to the negative decomposition rate (a = –k) and the y-intercept (b) gives a relation to determine the start concentration (b = ln [R]$_0$).

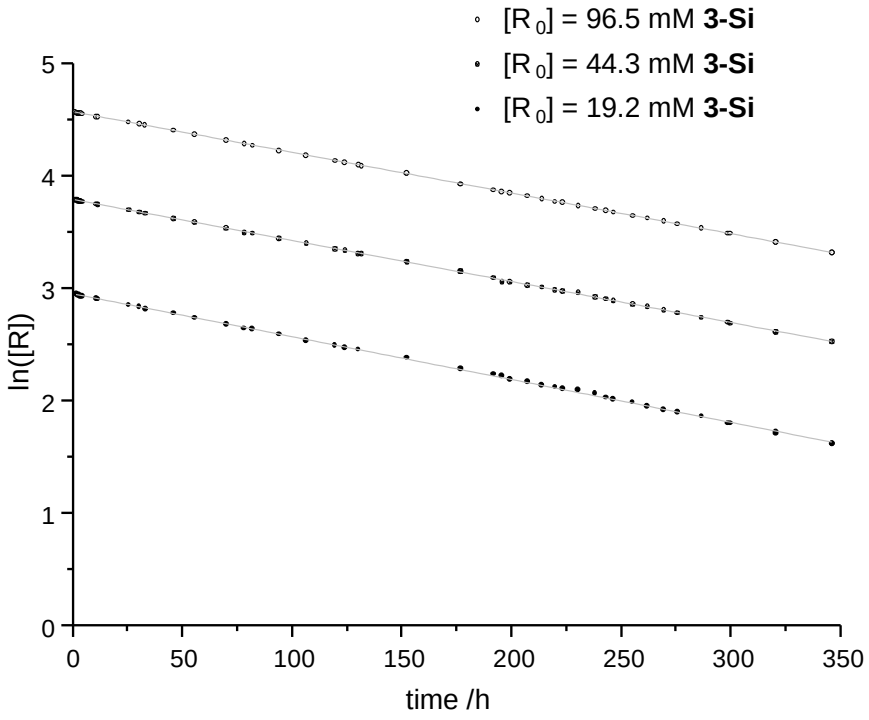

Figure 5.71. Plot of the ln of the determined concentrations [R] of the radical **3-Si** against the time. Linear regression lines are marked in grey.

The plot of ln[R] against time shows in case of the three starting concentrations three lines, which show roughly the same slope(a) and differ only by the different intercepts to the y-axis (b).

Table 5.57. Parameters of the linear regression of the three plots ln[R] versus time (h) in comparison. Via the relation a = −k, the rate constant k was calculated, as well from the relation b = $\ln[R]_0$ the start concentration of the radical **3-Si** could be calculated.

exp. $[R]_0$ [mM]	slope (a)		y-intercept (b)		r^2	k 10^{-3} [h^{-1}]	calc. $[R]_0$ [mM]
	value	σ	value	σ			
96.5	$-3.61 \cdot 10^{-3}$	$2.69 \cdot 10^{-6}$	4.569	$5.02 \cdot 10^{-4}$	0.999	3.61 ± 0.06	96.5 ± 0.1
44.3	$-3.65 \cdot 10^{-3}$	$6.07 \cdot 10^{-6}$	3.791	$1.13 \cdot 10^{-3}$	0.999	3.65 ± 0.12	44.3 ± 0.1
19.2	$-3.81 \cdot 10^{-3}$	$1.32 \cdot 10^{-5}$	2.956	$2.49 \cdot 10^{-3}$	0.999	3.81 ± 0.27	19.2 ± 0.1

The confidence interval (CI) for the rate constant (k) and start concentration (calc.$[R]_0$) was calculated the following way: CI(k) = −σ(slope) · *t* and CI($[R]_0$) = $e^{(\text{y-intercept})}$ · σ(y-interecept) · *t*, whereas student *t*-factor equals 2.011 for p = 95 % and n = 50 and f = 48.

The calculated start concentrations (calc.$[R]_0$, see *Table* 5.57), which were obtained from the linear regression, perfectly fit the experimental prepared concentrations of radical **3-Si**. This is a good sign for the reliability of the method. The calculated rate constants (k), seem to give the same constant value for each of the three starting concentrations, with respect to the confidence interval. This result clearly shows that radical **3-Si** decomposes via reaction pseudo first order regarding the concentration of the radical. It might be that the decomposition is still dependent with a rate first order regarding the deuterated solvent.

Using equation (eq. 5.57) and the known rate constant from *Table* 5.57 the half life can be calculated:

$$\ln\left(\frac{[R]}{[R]_0}\right) = -kt \qquad \text{(eq. 5.60)}$$

In order to calculate $t_{1/2}$ (eq. 5.60) turns into:

$$\ln(0.5) = -k\, t_{\frac{1}{2}} \qquad \text{(eq. 5.61)}$$

Solving equation (eq. 5.61) for $t_{1/2}$ gives:

$$t_{\frac{1}{2}} = -\frac{\ln(0.5)}{k} \qquad \text{(eq. 5.62)}$$

Which leads to the following result:

Table5.58. Calculated half life ($t_{1/2}$) of the three different concentrations of radical **3-Si**

exp. $[R]_0$ /mM	**k 10^{-3} /h^{-1}**	**$t_{1/2}$ /d**
96.5	3.61 ± 0.06	8.0
44.3	3.65 ± 0.12	7.9
19.2	3.81 ± 0.27	7.6

These results clearly show, that the radical **3-Si** decomposes via reaction first order and shows a half life of approx. 8 days.

5.9 Supplemental cw-X-band EPR spectra

5.9.1 EPR spectra of 3-Si

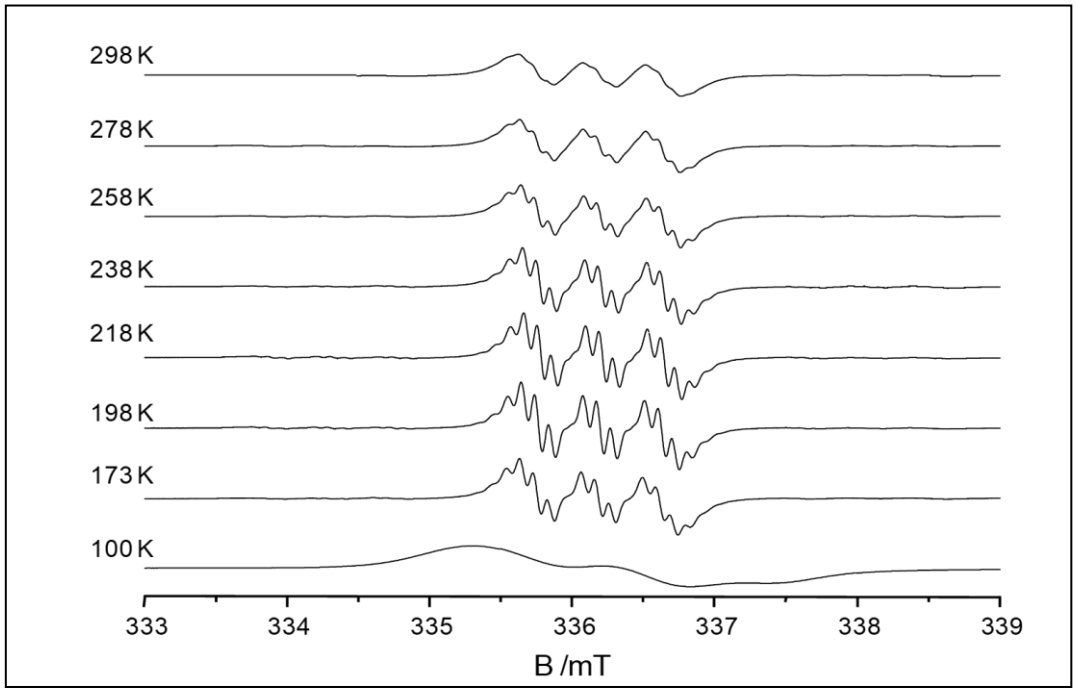

Figure 5.72. EPR spectra of Si(SiTMS$_3$)(caac^{Me}) (**3-Si**) in *n*-pentane (90 µmol L^{-1}) at variable temperatures (173 – 293 K), mod. frequency: 100 kHz.

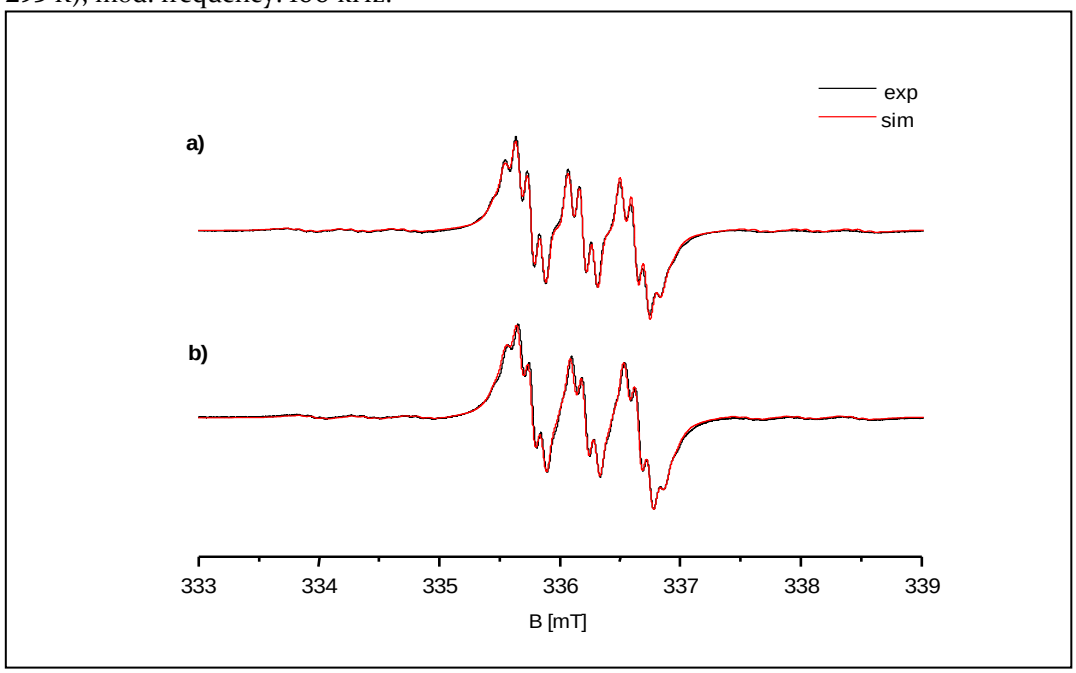

Figure 5.73. Comparison of experimental (-) and simulated (-) X-band EPR spectra of Si(SiTMS$_3$)(caac^{Me}) (**3-Si**) in a) *n*-pentane at 173 K (90 µmol L^{-1}) and b) benzene 298 K (100 µmol L^{-1}).

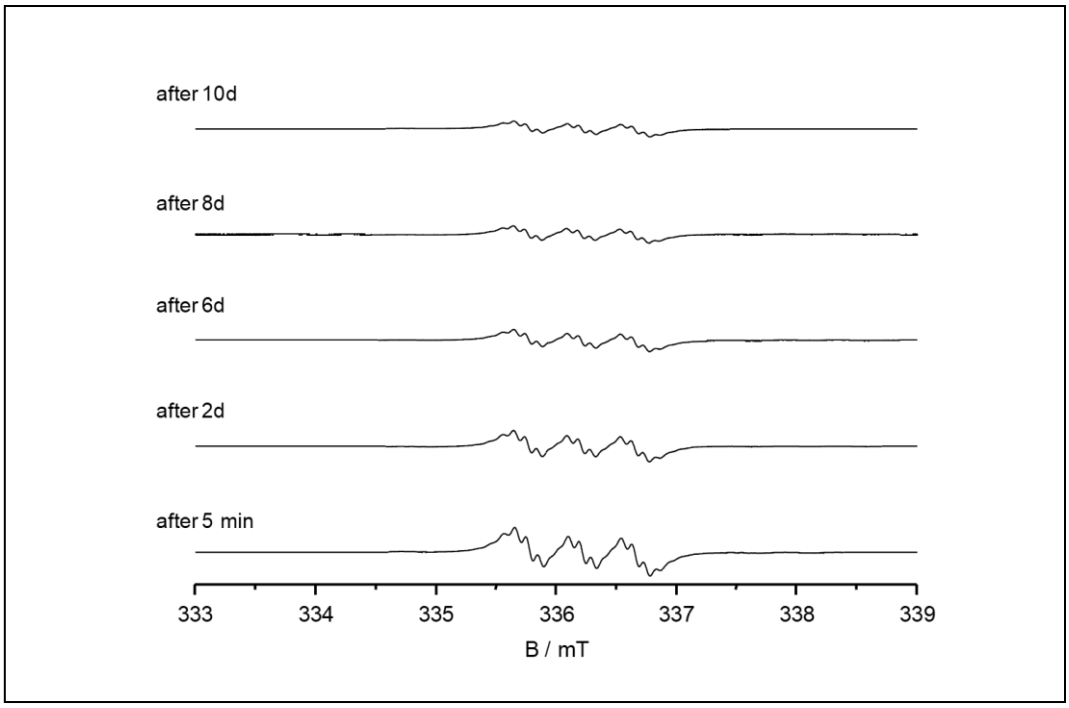

Figure 5.74. Selected EPR spectra of Si(SiTMS$_3$)(caac^{Me}) (**3-Si**) (c = 100 µmol L^{-1}) in benzene at r.t.

5.9.2 EPR spectra of 3-N

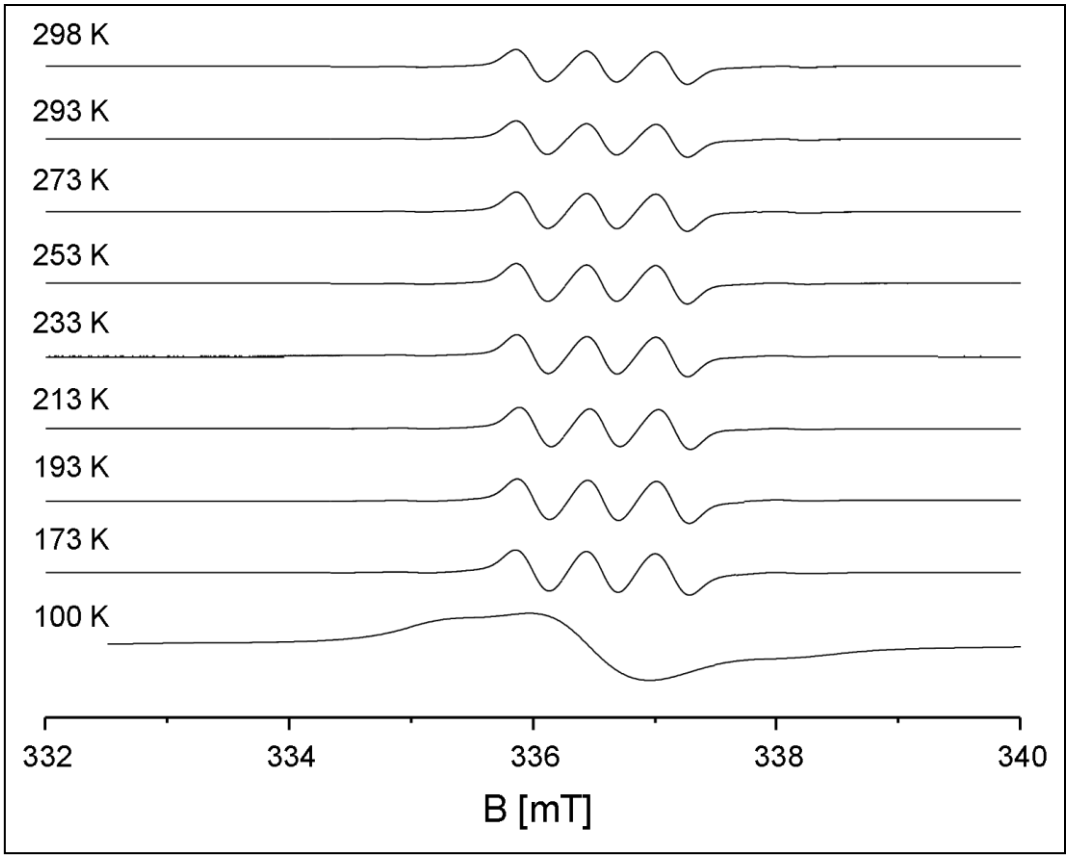

Figure 5.75. EPR spectra of Si(NTMS$_2$)(caac^{Me})·(**3-N**) in *n*-pentane (200 µmol L^{-1}) at variable temperatures (173 – 293 K), mod. frequency: 100 kHz.

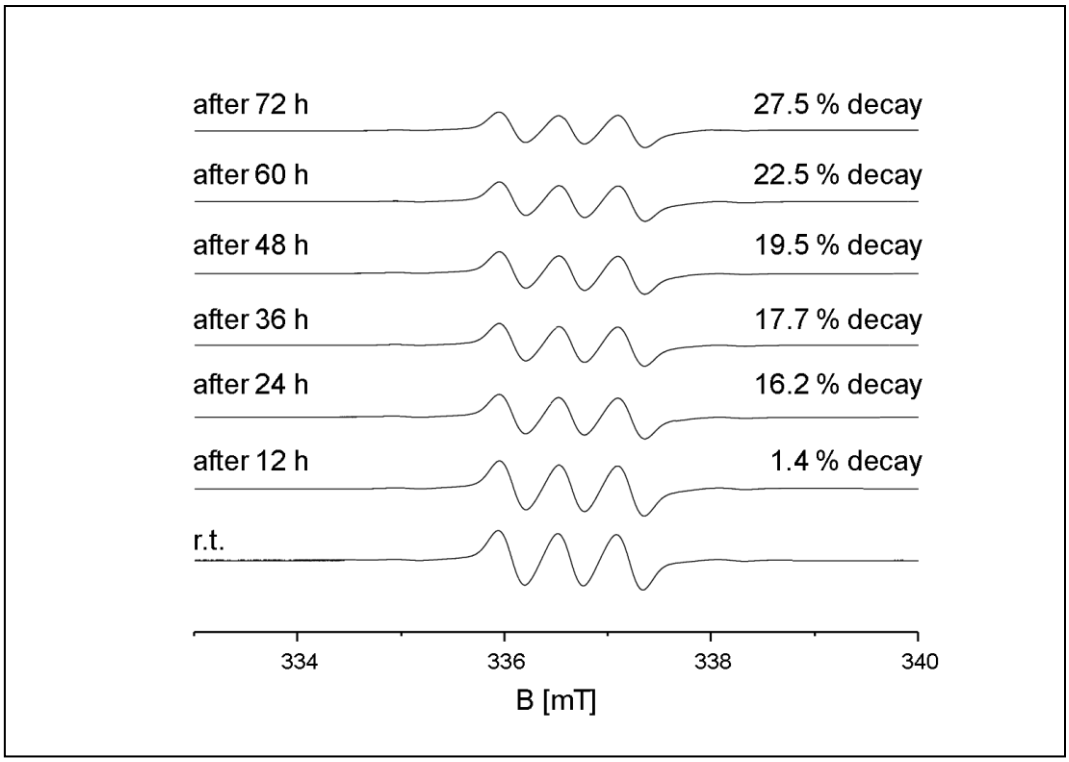

Figure 5.76. EPR spectra, showing the slow decomposition of radical Si(NTMS$_2$)(caac^{Me}) (**3-N**) in *n*-pentane (200 µmol L^{-1}) at ambient temperature. The percentage of the decomposition was determined upon integration of the EPR-signal and dividing the integrals by the first recorded EPR spectrum at ambient temperature.

5.9.3 EPR spectra of 3-O

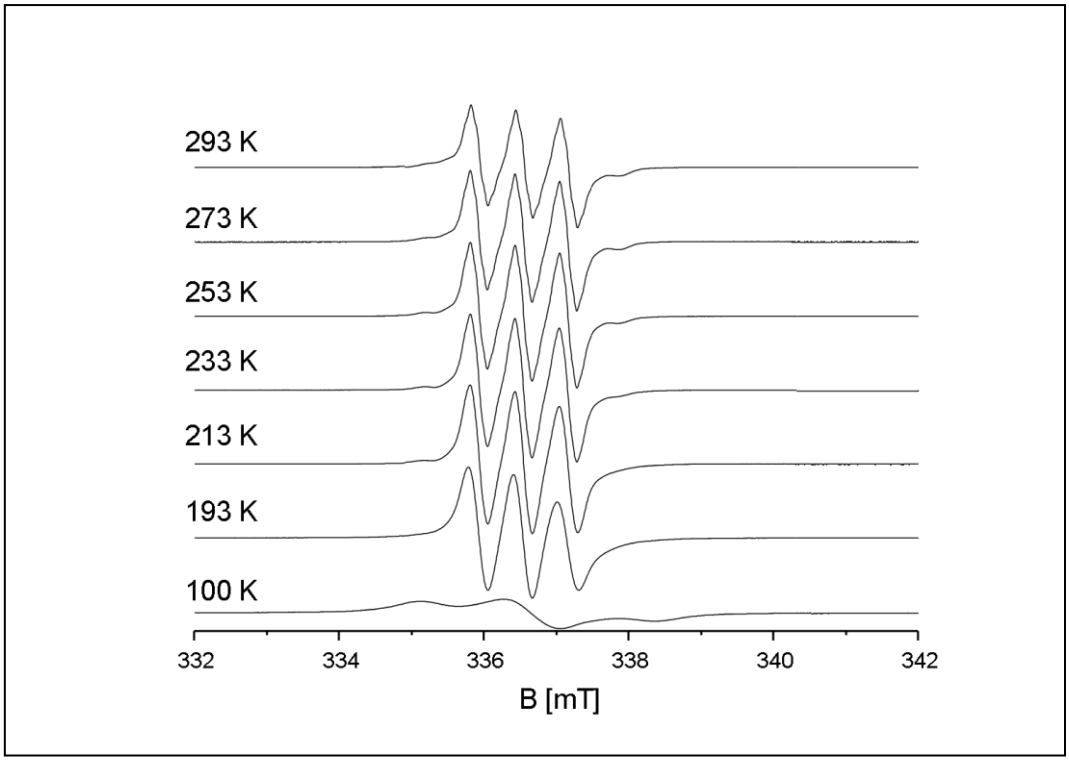

Figure 5.77. EPR spectra of radical Si(OMes*)(caac^{Me}) (**3-O**) in toluene (174 µmol L^{-1}) from 100 – 293 K.

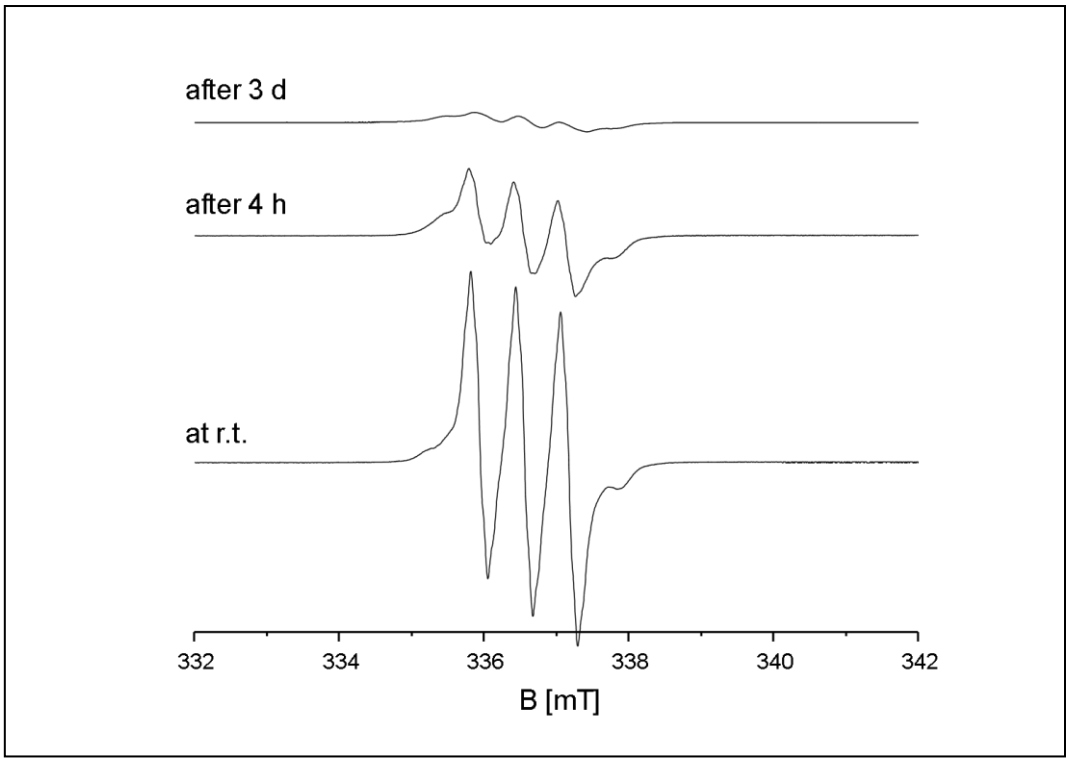

Figure 5.78. Selected EPR spectra of Si(OMes*)(caac^{Me}) (**3-O**) in toluene (174 µmol L^{-1}) at ambient temperature.

5.9.4 EPR spectra of 6

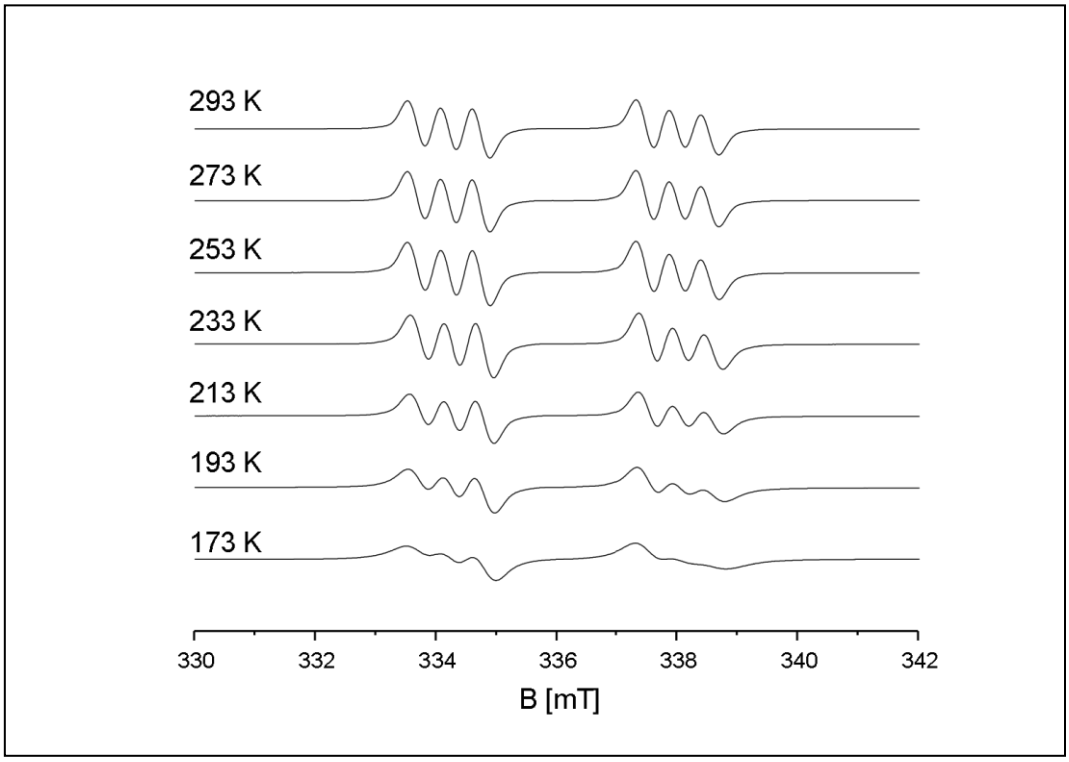

Figure 5.79. EPR spectra of radical (Mes)P–Si(Mes)(caac^{Me}) (**6**) (400 µmol L^{-1}) in *n*-pentane from 173 – 293 K.

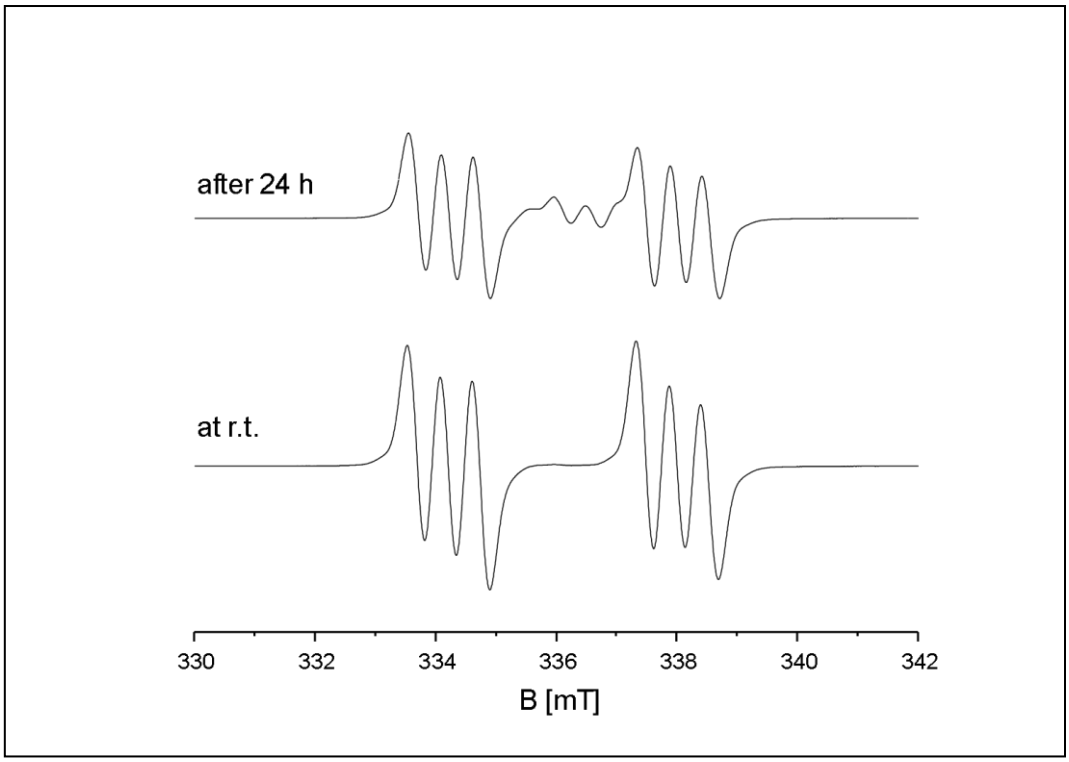

Figure 5.80. Selected EPR spectra of radical (Mes)P–Si(Mes)(caac^{Me}) (**6**) (400 µmol L^{-1}) in *n*-pentane at ambient temperature.

5.9.5 Cyclic voltammetric studies of compounds

5.9.6 CV study of 3-Si

The cyclic voltammograms of **3-Si** are depicted in *Figure* 5.81 and *Figure* 5.82, and show that the compound undergoes two major, electron transfers. One presumable reduction at $E_{1/2}$ = –1.941 V vs. $Fc^{+/0}$ ($E_{1/2}$ = –1.501 V vs. $DMFc^{+/0}$),[53] and another presumable oxidation at E_{pa} = –0.049 V vs. $Fc^{+/0}$, which is followed by an ECE process and could not be analyzed due to many overalpping peaks. This is most likely due to interactions of the analyte with the PF_6^- anion.

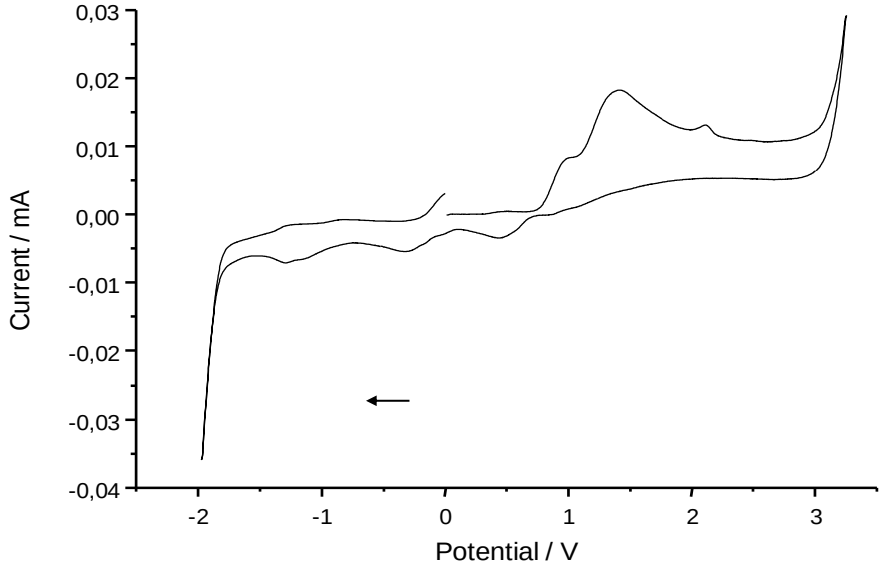

Figure 5.81. Full range electrochemical scan of **3-Si** in THF from (–2.0 V) to (3.0 V) at a scan rate of 100 mV/s shows the presence of the reduction peak at E_{pa} = –1.903 V vs. $Fc^{+/0}$, as well as an oxidation peak at E_{pa} = –0.049 V vs. $Fc^{+/0}$ followed by many overlapping electron transfers, which are probably formed due to interactions with the PF_6^- anion.

Table 5.59. Results of the cyclovoltammetric analysis of **3-Si**.[a]

V [mV s^{-1}]	ΔE [mV]	i_{pa}/i_{pc}	$E_{1/2}$ [V]
100	125	1.02	–1.941
200	146	1.02	–1.941
400	178	1.03	–1.941
800	220	1.05	–1.941

[a]: V = scan rate, $\Delta E = E_{pa} - E_{pc}$, where E_{pa} is the anodic peak potential and E_{pc} the cathodic peak potential; i_{pa}/i_{pc} = ratio of cathodic and anodic peak current, $E_{1/2} = (E_{pa} + E_{pc})/2$ = half-wave potential. Potentials are given versus the ferrocene $Fc^{+/0}$ redox pair.

53 The given value vs $DMFc^{+/0}$ in THF was converted to $Fc^{+/0}$ by subtraction of 440 mV as determined in reference [343].

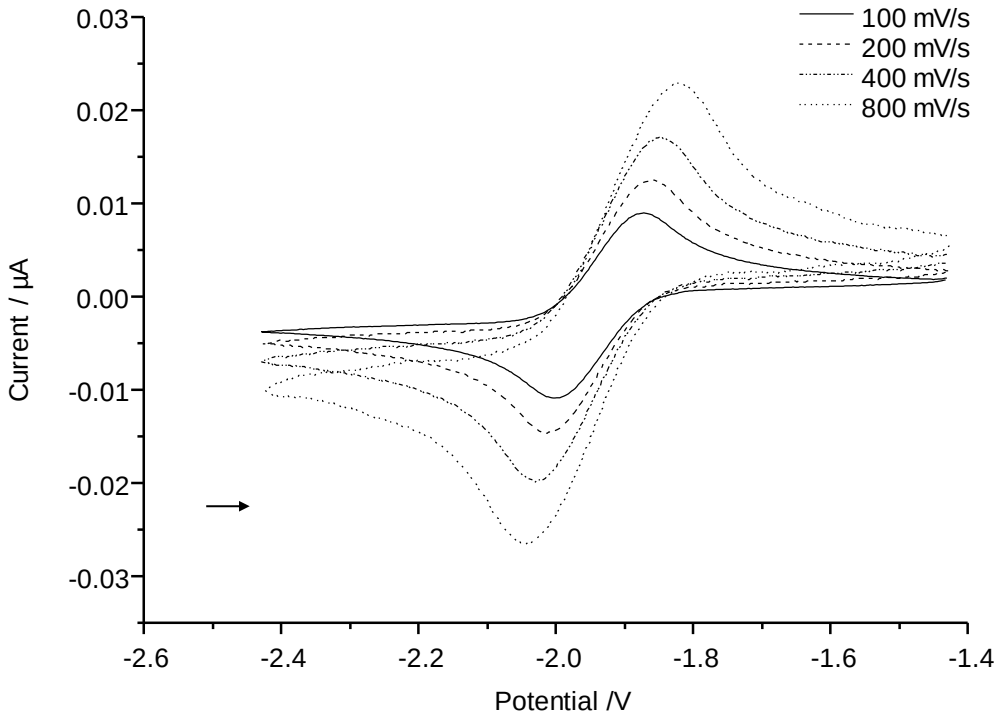

Figure 5.82. Measurement of **3-Si** in THF from –2.5 to –1.4 V at different scan rates l00 mV/s, 200 mV/s, 400 mV/s and 800 mV/s reveals a reversible le⁻-transfer at $E_{1/2}$ = –1.941 V vs. $Fc^{+/0}$. Reference electrode: ferrocene ($Fc^{+/0}$), electrolyte: [nBu_4N][PF_6] (0.1 mol/L).

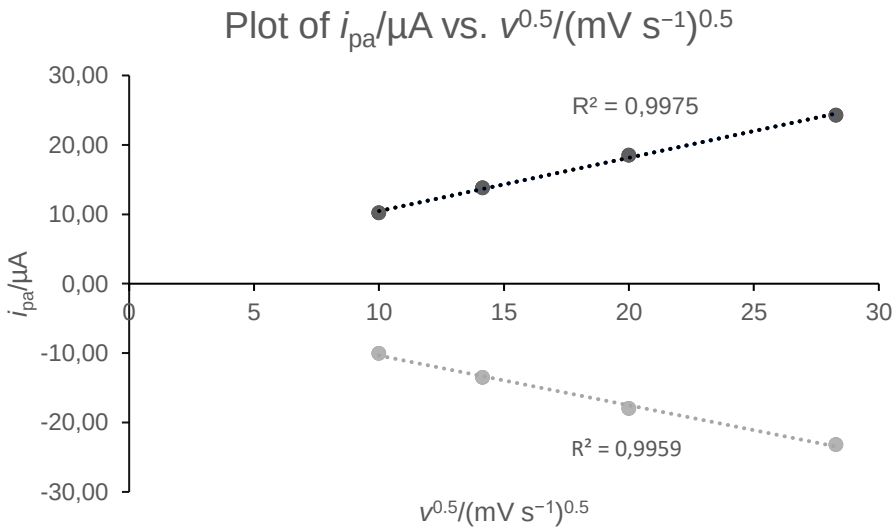

Figure 5.83. Plot of the anodic peak current (i_{pa}) against the square root of the scan rate $v^{1/2}$ for the reverse reduction of **3-Si**.

5.9.7 CV study of 3-N

The cyclic voltammograms of **3-N** are depicted in *Figure 5.84* and *Figure 5.85*, and show that the compound undergoes two major, electron transfers. One presumable reduction at $E_{1/2}$ = –1.727 V vs. $DMFc^{+/0}$, and another presumable oxidation at $E_{1/2}$ = –0.530 V vs. $DMFc^{+/0}$. The assignment (oxidation or reduction) cannot be truly determined with the methods used.

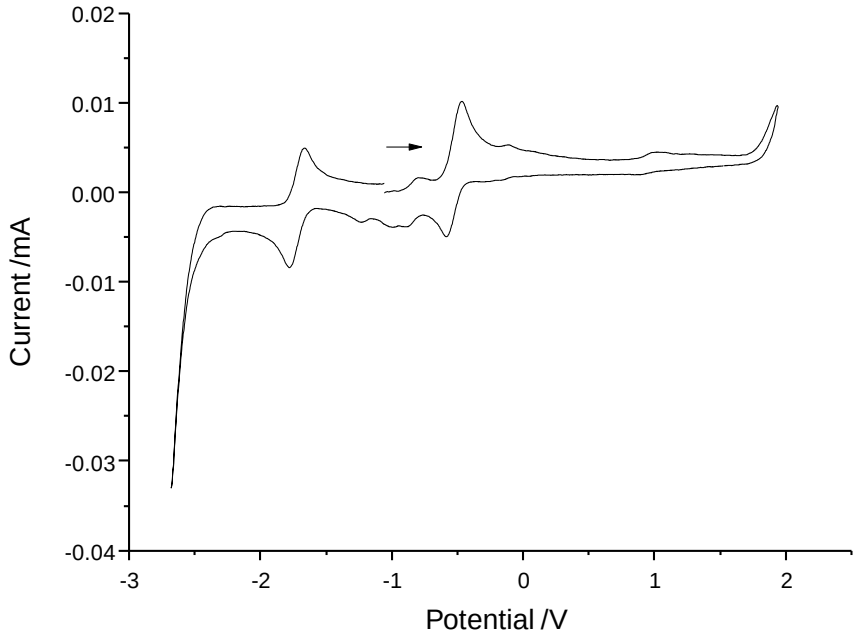

Figure 5.84. Full range electrochemical scan of **3-N** in fluorobenzene from (–3.0 V) to (2.2 V) at a scan rate of 100 mV/s shows the presence of the reduction peak at E_{pa} = –1.673 V vs. $DMFc^{+/0}$ and a oxidation peak at E_{pa} = –0.548 V vs. $DMFc^{+/0}$.

Table5.60. Results of the cyclovoltammetric analysis of the two processes in **3-N**[a]

V [mV s^{-1}]	ΔE [mV]	i_{pa}/i_{pc}	$E_{1/2}$ [V]	ΔE [mV]	i_{pa}/i_{pc}	$E_{1/2}$ [V]
50	93	0.83	–1.727	88	1,18	–0.530
100	105	0.89	–1.727	103	1,16	–0.530
200	127	0.93	–1.727	122	1,14	–0.530
400	156	0.96	–1.727	151	1,14	–0.530
800	198	0.97	–1.727	190	1,14	–0.530

[a]: V = scan rate, $\Delta E = E_{pa} - E_{pc}$, where E_{pa} is the anodic peak potential and E_{pc} the cathodic peak potential; i_{pa}/i_{pc} = ratio of cathodic and anodic peak current, $E_{1/2} = (E_{pa} + E_{pc})/2$ = half-wave potential. Potentials are given versus the ferrocene $Fc^{+/0}$ redox pair.

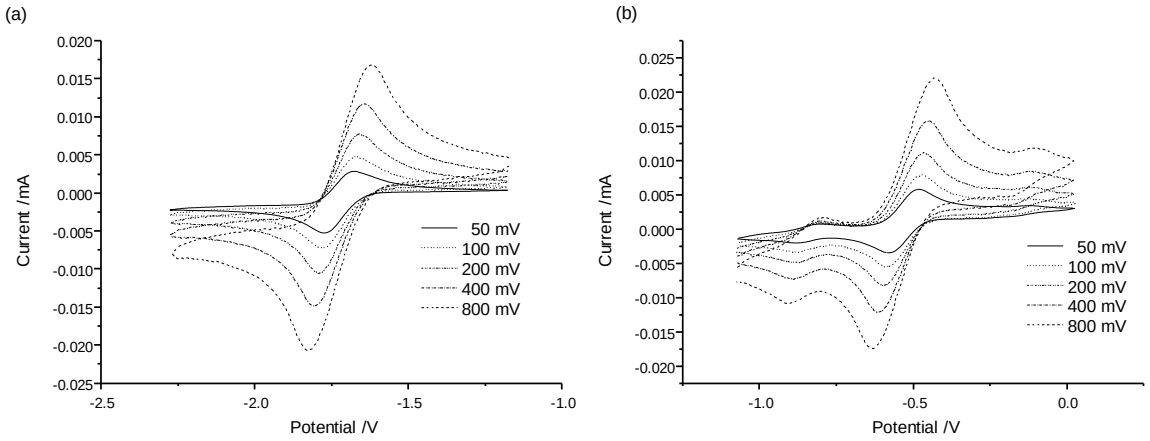

Figure 5.85. Measurement of **3-N** in fluorobenzene from –2.5 to –1.0 V (a) and –1.5 to 0.5 V at different scan rates 50 mV/s, 100 mV/s, 200 mV/s, 400 mV/s and 800 mV/s reveals a reversible $1e^-$-transfer at $E_{1/2}$ = –1.727 V (a) and –0.530 V (b) vs. $Fc^{+/0}$, respectively. Reference electrode: decamethylferrocene ($DMFc^{+/0}$), electrolyte: $[nBu_4N][Al(OC(CF_3)_3]$ (60 mmol L^{-1}).

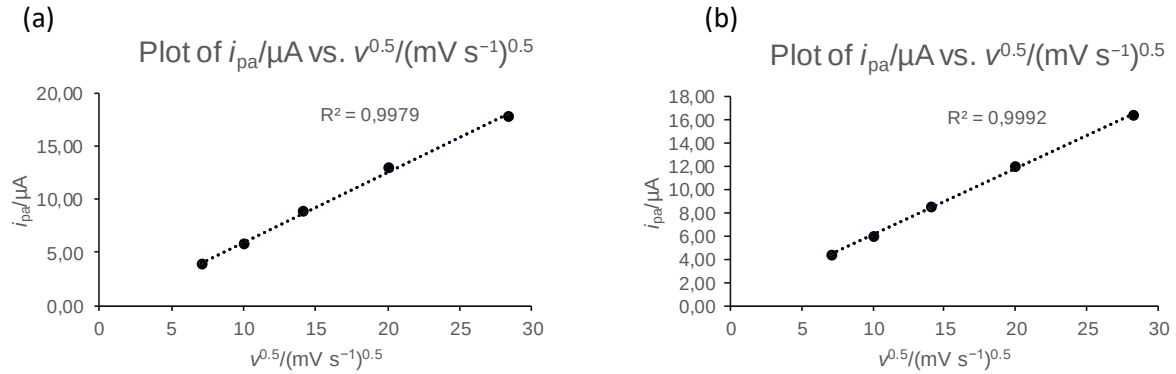

Figure5.86. Plot of the anodic peak current (i_{pa}) against the square root of the scan rate $v^{1/2}$ for the reverse reduction (a) and oxidation (b)of **3-N**.

5.9.8 CV study of 18

The cyclic voltammograms of **18** are depicted in *Figure* 5.87 and *Figure* 5.88 and show that the compound undergoes three major, electron transfers. One presumable reduction at $E_{1/2}$ = –1.388 V vs. $DMFc^{+/0}$ and one non-reversible oxidation at E_{pa} = 0.949 V vs. $DMFc^{+/0}$ in PhF/$(NBu_4)[Al(OC(CF_3)_3)_4]$. A second oxidative process is observed at E_{pa} = 1.534 V, but this could be the oxidation of the reaction product of the preceding oxidation, thus constituting an ECE-mechanism (E indicates an electron transfer step, C indicates a homogeneous chemical reaction).[344] The assignment of oxidative and reductive processes is confirmed by the determination of the open circuit potential at –1.041 V vs. $DMFc^{+/0}$.

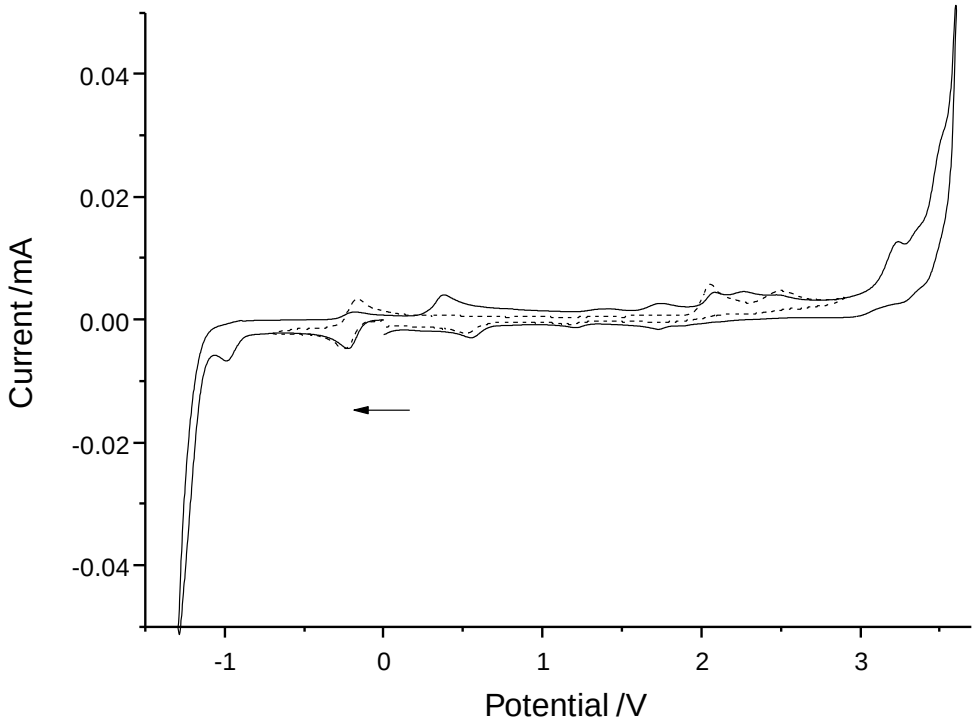

Figure 5.87. Full range electrochemical scan of **18** in fluorobenzene from (–1.5 V) to (4.0 V) at a scan rate of 100 mV/s. Major electron transfers are seen at ca. –0.2 V, 0.4 V, 0.6 V, 2.1 V, and 2.5 V. Reference electrode: decamethylferrocene ($DMFc^{+/0}$), electrolyte: $[nBu_4N][Al(OC(CF_3)_3]$ (60 mmol L^{-1}).

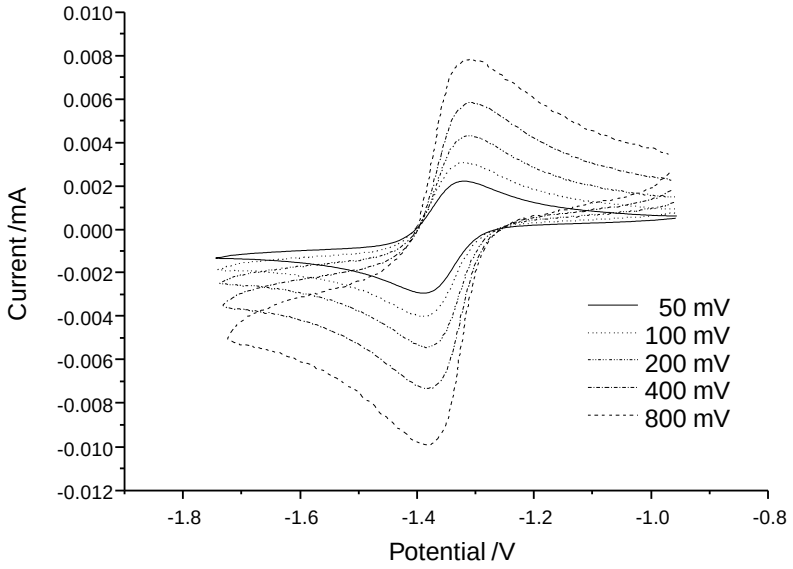

Figure 5.88. Measurement of **18** in fluorobenzene from –2.0 to –0.8 V at different scan rates 50 mV, 100 mV/s, 200 mV/s, 400 mV/s and 800 mV/s reveals a reversible $1e^-$-transfer at $E_{1/2}$ = –1.388 V vs. $DMFc^{+/0}$. Reference electrode: decamethylferrocene ($DMFc^{+/0}$), electrolyte: electrolyte: $[nBu_4N][Al(OC(CF_3)_3]$ (60 mmol L^{-1}).

Table 5.61. Results of the cyclovoltammetric analysis of **18**[a]

V [mV s^{-1}]	ΔE [mV]	i_{pa}/i_{pc}	$E_{1/2}$ [V]
50	62	0.99	–1.388
100	59	0.98	–1.388
200	60	0.97	–1.388
400	59	0.95	–1.388
800	75	0.93	–1.388

[a]: V = scan rate, $\Delta E = E_{pa} - E_{pc}$, where E_{pa} is the anodic peak potential and E_{pc} the cathodic peak potential; i_{pa}/i_{pc} = ratio of cathodic and anodic peak current, $E_{1/2} = (E_{pa} + E_{pc})/2$ = half-wave potential. Potentials are given versus the ferrocene $Fc^{+/0}$ redox pair.

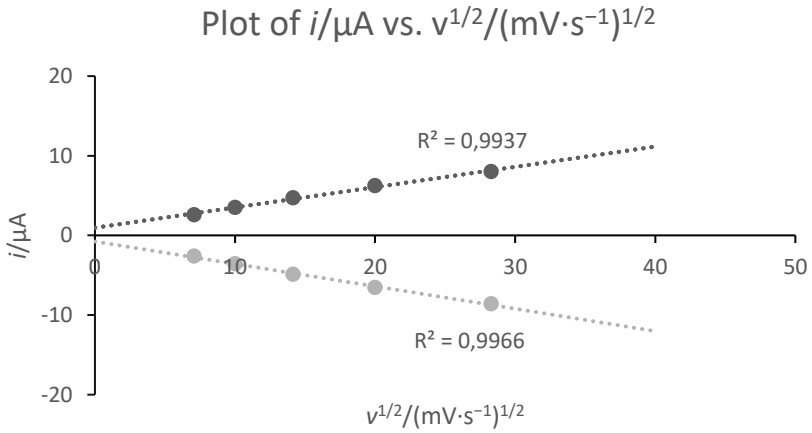

Figure 5.89. Plot of the anodic peak current (i_{pa}) against the square root of the scan rate $v^{1/2}$ for the reverse reduction of **18**.

5.10 UV/Vis NIR spectroscopy of compounds

5.10.1 UV/Vis-NIR spectra of 3-Si

The UV-Vis-NIR spectra of **3-Si** were recorded in *n*-hexane at ambient temperature and are depicted in *Figure* 5.90. The absorption maxima and corresponding molar extinction coefficients ελ are summarized in *Table* 5.62. The absorption bands were determined by means of band deconvolution assuming a Gaussian line profile. The corresponding deconvoluted absorption bands are displayed in *Figure 5.91* (**3-Si**) and the parameters used for the band deconvolution are summarized in *Table* 5.63 (**3-Si**).

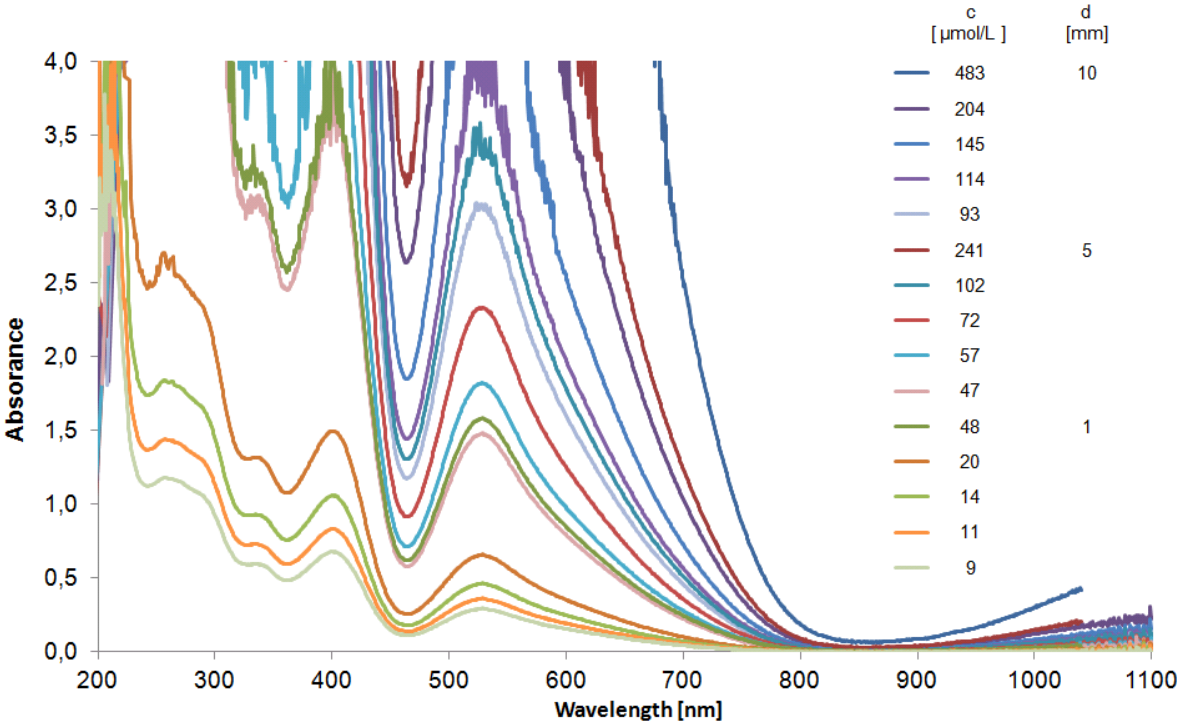

Figure 5.90. Experimental UV-Vis-NIR spectra of **3-Si** in *n*-hexane from 220 – 1100 nm at different concentrations c of **3-Si** and path lenghts d of the cuvette.

Table 5.62. Absorption maxima of the UV-Vis-NIR spectra of **3-Si** depicted in *Figure 5.81* and their corresponding molar extinction coefficients.

λ / nm	528.5	410	335.5	258
ε λ / L·mol^{-1}·cm^{-1}	3220.5	7305.7	6421.3	12681.4

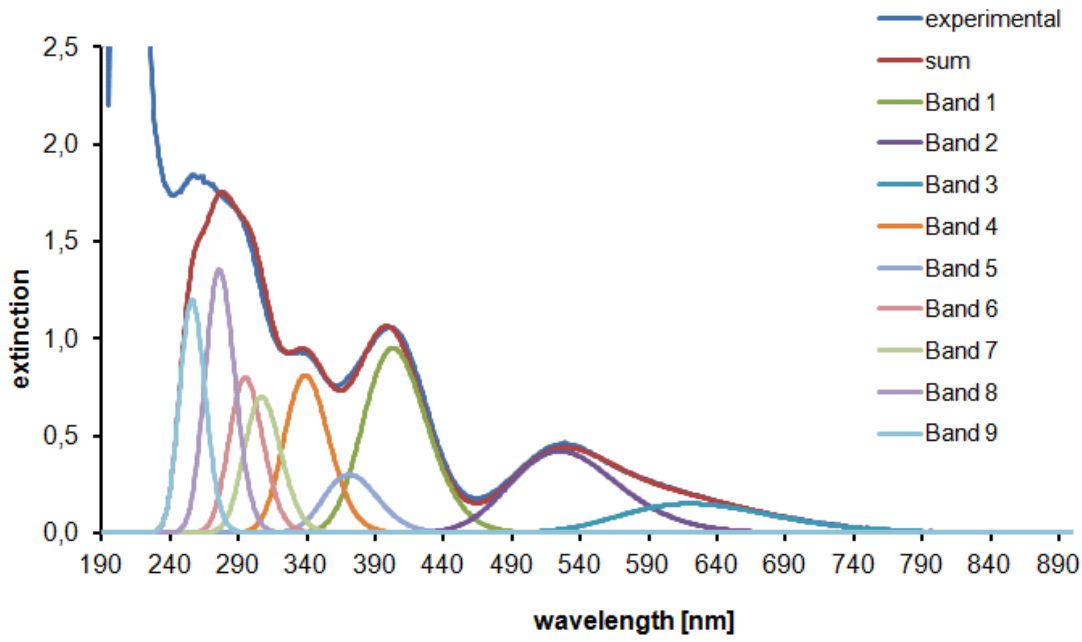

Figure 5.91. Deconvoluted and experimental UV-Vis-NIR spectra of **3-Si** in *n*-hexane at c = 14 µmol L^{-1} and d = 1 mm.

Table 5.63. Parameters used for the band deconvolution of the UV-Vis-NIR spectrum depicted in Figure 5.91.[a]

	Band 1	Band 2	Band 3	Band 4	Band 5	Band 6	Band 7	Band 8	Band 9
λ_{max}	403	525	620	339	371	295	307	276	256
E_{max}	0,950	0,420	0,150	0,810	0,300	0,800	0,700	1,354	1,200
σ_{max}	2000	2000	2000	2000	2000	2000	2000	2000	2000

[a] λ_{max} = wavelength in nm; E_{max} = extinction maximum; σ = linewidth in cm^{-1}.

The plots of extinction against concentration at the different wavelengths 258, 335.5, 401 and 528.5 nm were perfectly linear (r^2 = 1.000), which indicates that radical **3-Si** did not decompose during the UV/Vis measurement (up to 4 hours in *n*-hexane solution at different concentrations), which is in line with the ^{1}H NMR spectroscopic decomposition study which did not show any change in the ^{1}H NMR spectrum of radical **3-Si** in (D_6)benzene solution after 4 h (*Figure 5.92*).

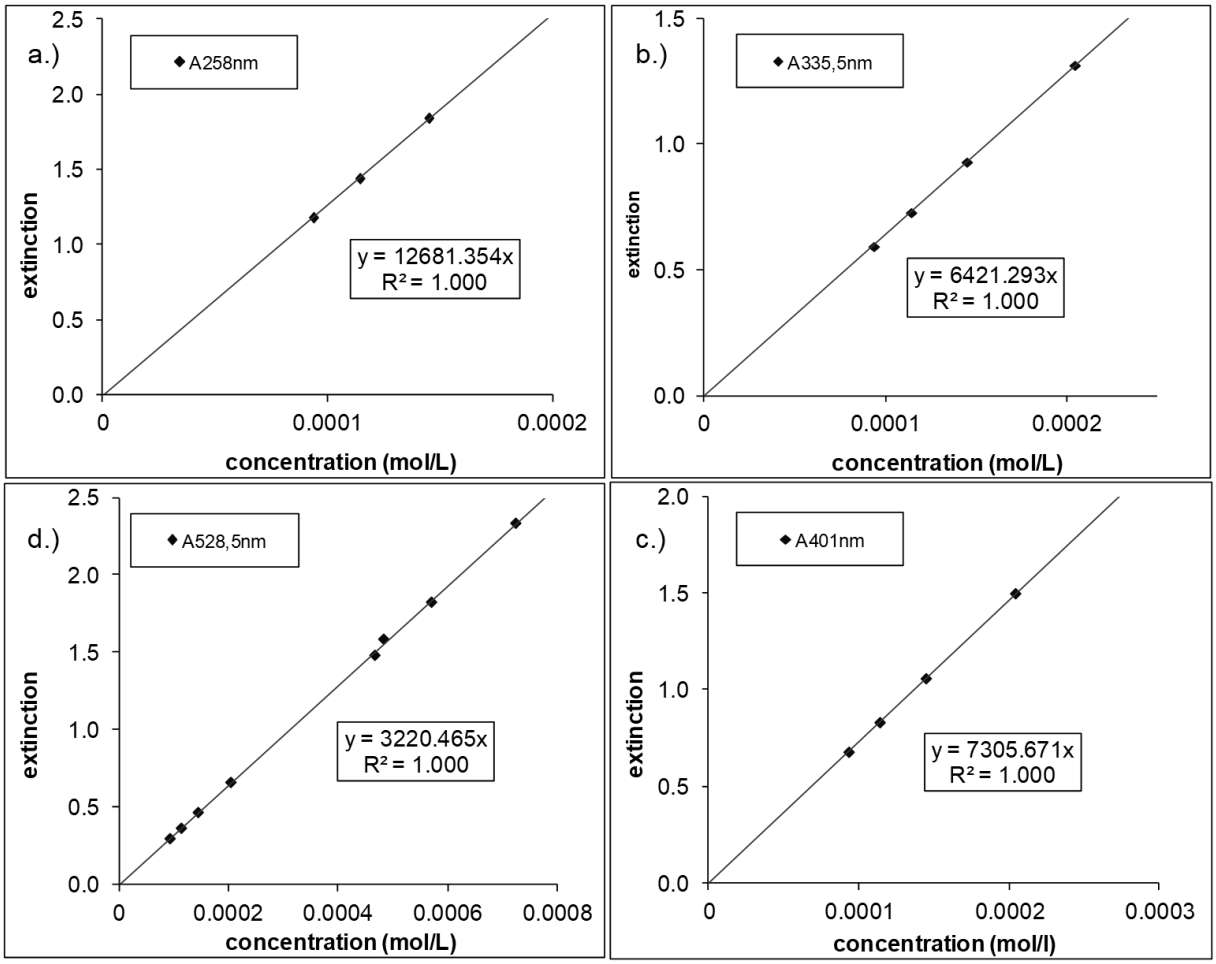

Figure 5.92. Charts a.) – d.) show the plots of extinction against concentration (mol L^{-1}) of the different maxima at 258, 335.5, 401 and 528.5 nm of **3-Si**.

5.10.2 UV/Vis-NIR spectra of 3-N

The UV-Vis-NIR spectra of **3-N** were recorded in *n*-hexane at ambient temperature and are depicted in *Figure 5.93*. The absorption maxima and corresponding molar extinction coefficients ελ are summarized in *Table 5.64*. The absorption bands were determined by means of band deconvolution assuming a Gaussian line profile. The corresponding deconvoluted absorption bands are displayed in *Figure 5.94* (**3-N**) and the parameters used for the band deconvolution are summarized in *Table 5.65* (**3-N**).

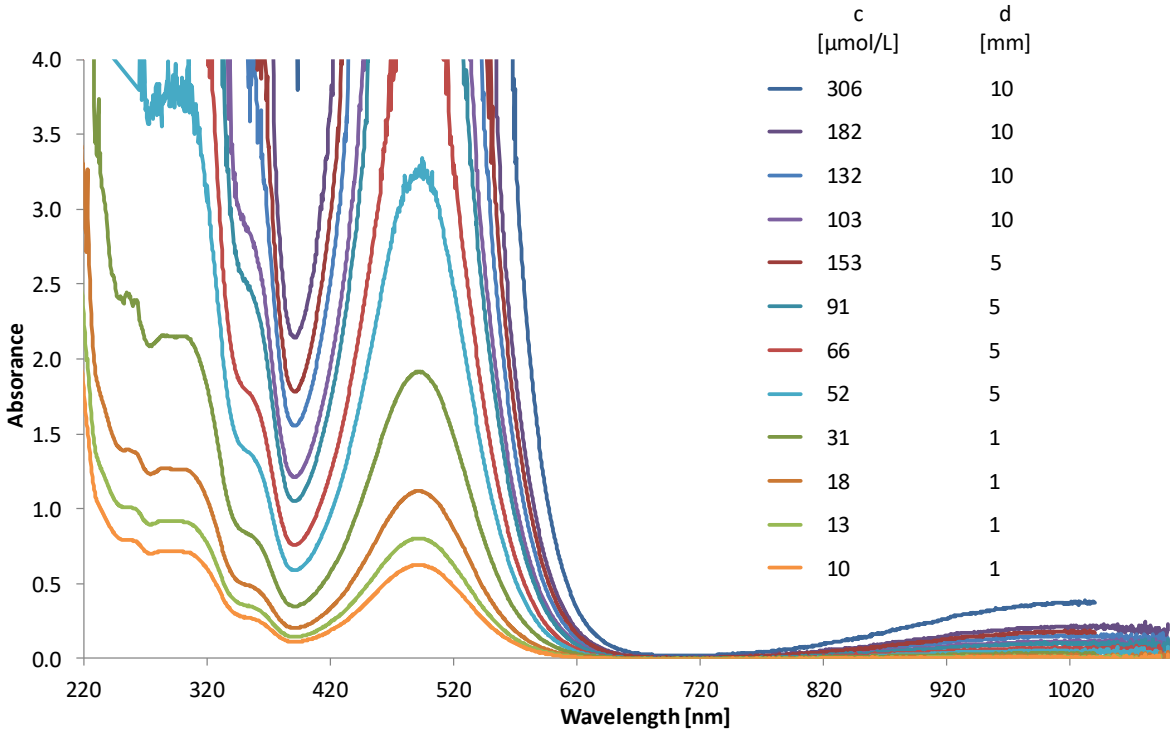

Figure 5.93. Experimental UV-Vis-NIR spectra of **3-N** in *n*-hexane from 220 – 1100 nm at different concentrations c of **3-N** and path lenghts d of the cuvette.

Table 5.64. Absorption maxima of the UV-Vis-NIR spectra of **3-N** depicted in *Figure 5.93* and their corresponding molar extinction coefficients.

λ / nm	492.5	355	285
ε_λ / L·mol^{-1}·cm^{-1}	6188.8	2692.6	7020.3

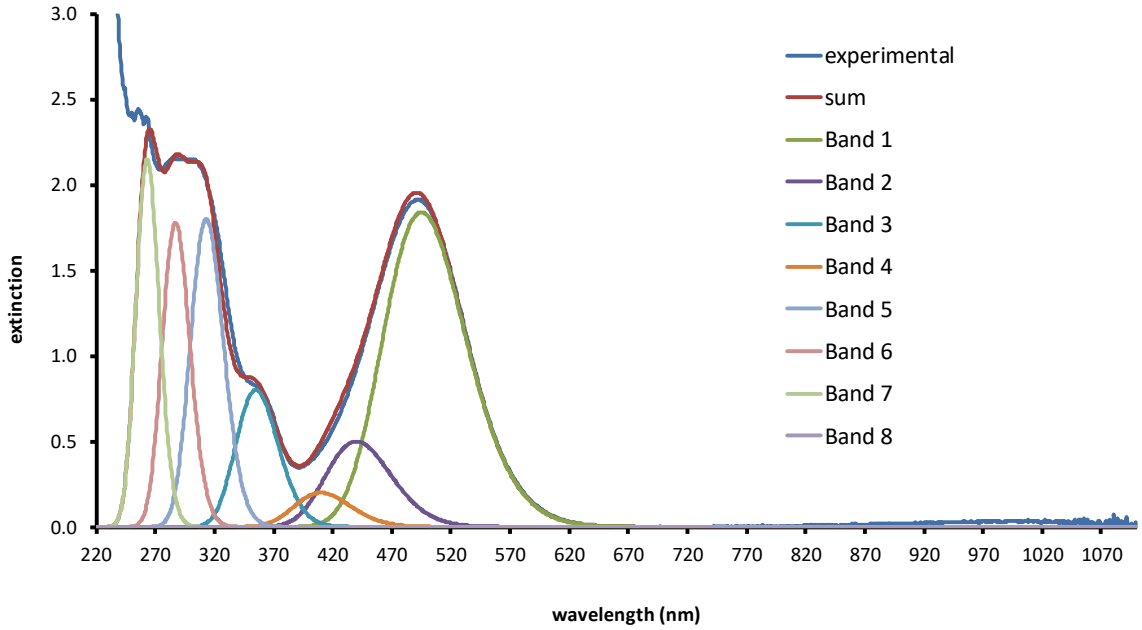

Figure 5.94. Deconvoluted and experimental UV-Vis-NIR spectra of **3-N** in *n*-hexane at c = 13 µmol L^{-1} and d = 1 mm.

Table 5.65. Parameters used for the band deconvolution of the UV-Vis-NIR spectrum depicted in *Figure 5.94*.[a]

	Band 1	Band 2	Band 3	Band 4	Band 5	Band 6	Band 7
λ_{max}	495	440	355	410	313	287	263
E_{max}	1.840	0.500	0.800	0.200	1.800	1.780	2.150
σ_{max}	2000	2000	2000	2000	2000	2000	2000

[a] λ_{max} = wavelength in nm; E_{max} = extinction maximum; σ = linewidth in cm^{-1}.

The plots of extinction against concentration at the different wavelengths 285, 355 and 492.5 nm were perfectly linear ($r^2 = 1.000$), which indicates that radical **3-N** did not decompose during the UV/Vis measurement (up to 4 h in *n*-hexane solution at different concentrations), which is in line with the ^{1}H NMR spectroscopic decomposition study which did not show any change in the ^{1}H NMR spectrum of radical **3-N** in (D_6)benzene solution after 4 h (*Figure 5.95*).

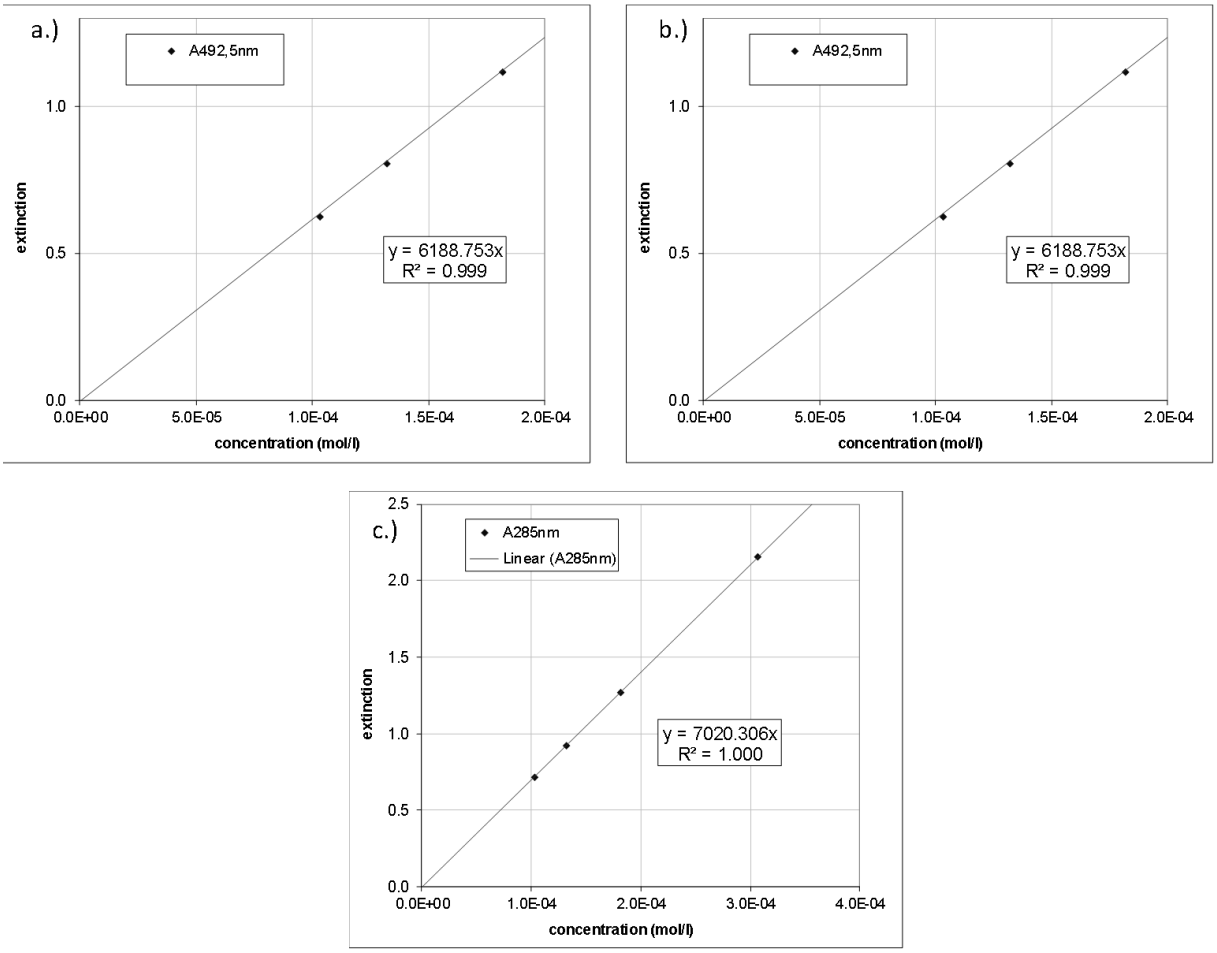

Figure 5.95. Charts a.) – c.) show the plots of extinction against concentration (mol L^{-1}) of the different maxima at 285, 355 and 492.5 nm of **3-N**.

5.10.3 UV/Vis-NIR spectra of 14-NHC

The NHC-stabilized disilavinylidene (SIDipp)SiSi(Br)Tbb (**14-NHC**) was obtained by a two-step procedure starting from $SiBr_2$(SIDipp) and TbbLi. Details on the synthesis are given in the literature.[118]

The UV/vis spectra of **14-NHC** were recorded in *n*-hexane at ambient temperature and are depicted in *Figure 5.96*. The absorption maxima and corresponding molar extinction coefficients ελ are summarized in *Table 5.66*. The absorption bands were determined by means of band deconvolution assuming a Gaussian line profile. The corresponding deconvoluted absorption bands are displayed in *Figure 5.97* (**14-NHC**) and the parameters used for the band deconvolution are summarized in *Table 5.67* (**14-NHC**).

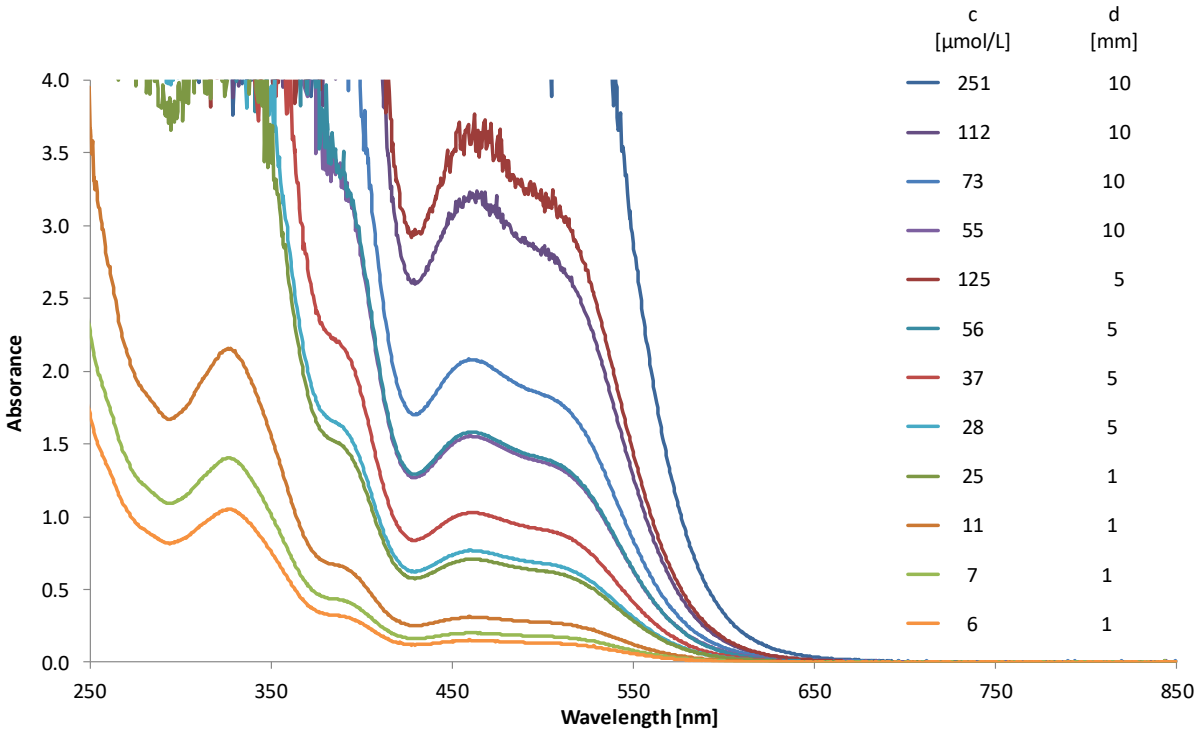

Figure 5.96. Experimental UV/vis spectra of **14-NHC** in *n*-hexane from 250 – 750 nm at different concentrations c of **14-NHC** and path lengths d of the cuvette.

Table 5.66. Absorption maxima of the UV/vis spectra of **14-NHC** depicted in *Figure 5.96* and their corresponding molar extinction coefficients.

λ / nm	515	460	388	326.5
ε λ / L·mol^{-1}·cm^{-1}	2361.8	2843.6	5958.7	19158.7

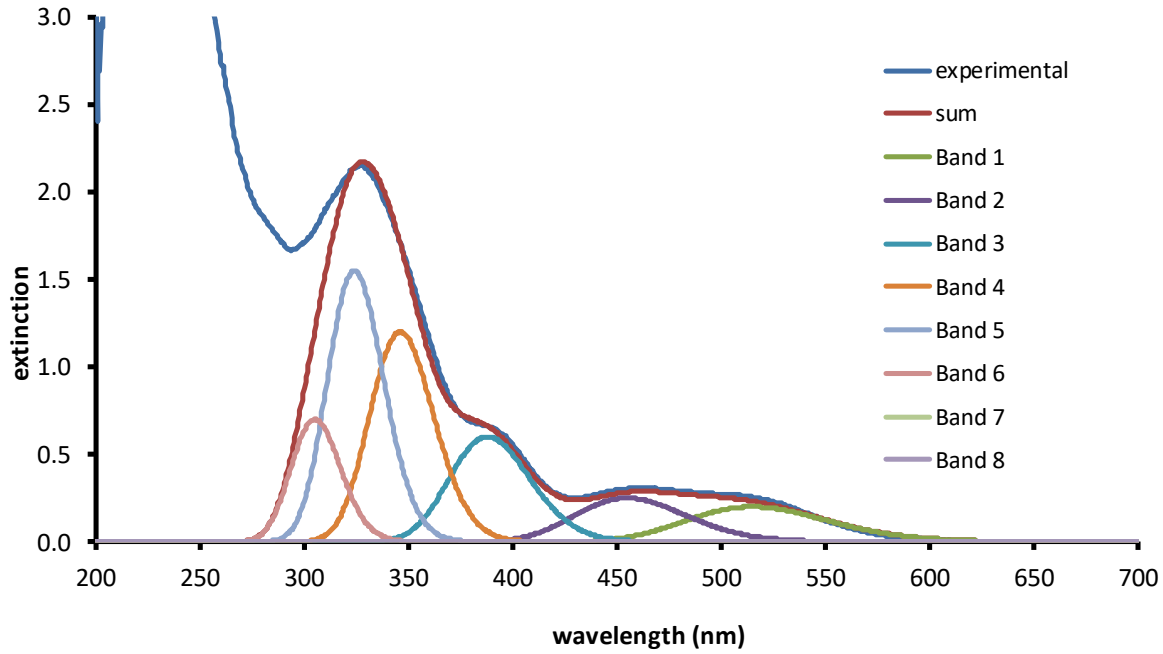

Figure 5.97. Deconvoluted and experimental UV/vis spectra of **14-NHC** in *n*-hexane at c = 11 µmol L^{-1} and d = 1 mm.

Table 5.67. Parameters used for the band deconvolution of the UV/vis spectrum depicted in *Figure 5.97*. λ_{max} = wavelength in nm; E_{max} = extinction maximum; σ_{max} = linewidth in cm^{-1}.

	Band 1	Band 2	Band 3	Band 4	Band 5	Band 6
λ_{max}	515	455	388	346	324	305
E_{max}	0.200	0.250	0.600	1.200	1.550	0.700
σ_{max}	1800	1800	1800	1800	1800	1800

5.10.4 UV/Vis-NIR spectra of 14

The UV-Vis-NIR spectra of **14** were recorded in *n*-hexane at ambient temperature and are depicted in *Figure 5.98*. The absorption maxima and corresponding molar extinction coefficients ελ are summarized in *Table 5.68*. The absorption bands were determined by means of band deconvolution assuming a Gaussian line profile. The corresponding deconvoluted absorption bands are displayed in *Figure 5.99* (**14**) and the parameters used for the band deconvolution are summarized in *Table 5.69* (**14**).

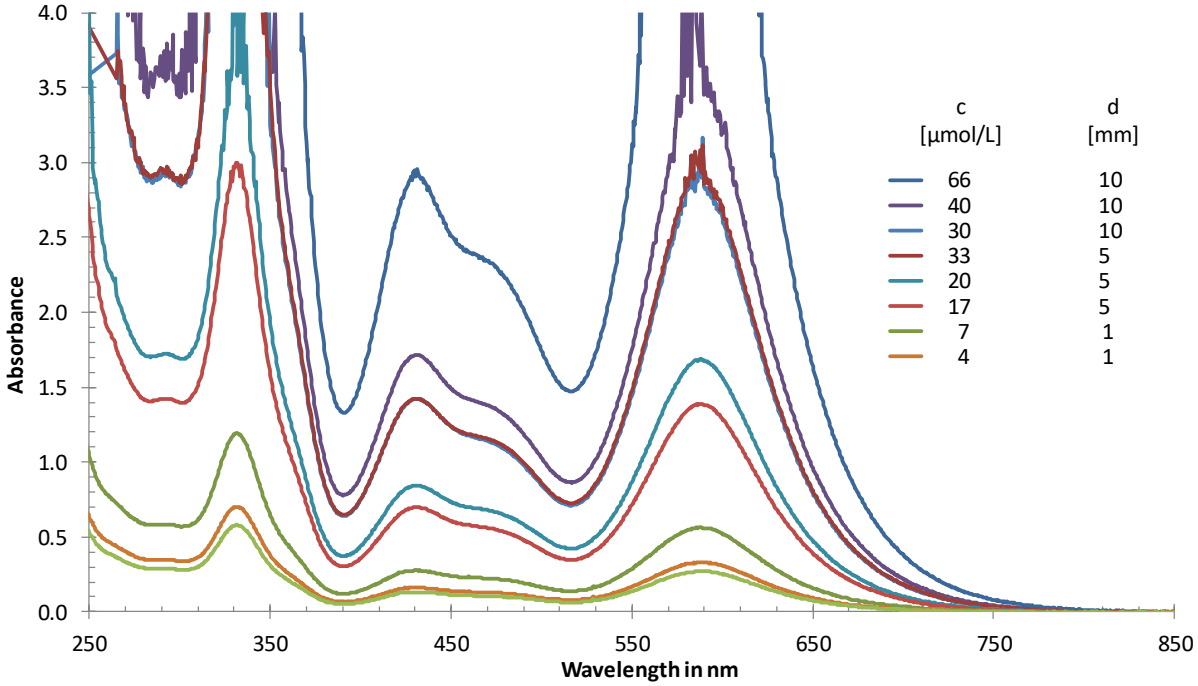

Figure 5.98. Experimental UV-Vis-NIR spectra of **14** in *n*-hexane from 250 – 850 nm at different concentrations c of **14** and path lenghts d of the cuvette.

Table 5.68. Absorption maxima of the UV-Vis-NIR spectra of **14** depicted in *Figure 5.98* and their corresponding molar extinction coefficients.

λ / nm	588	476	422	360	331	293
ε λ / L·mol^{-1}·cm^{-1}	8446.0	3415.0	4041.0	6751.0	17860.0	8652.0

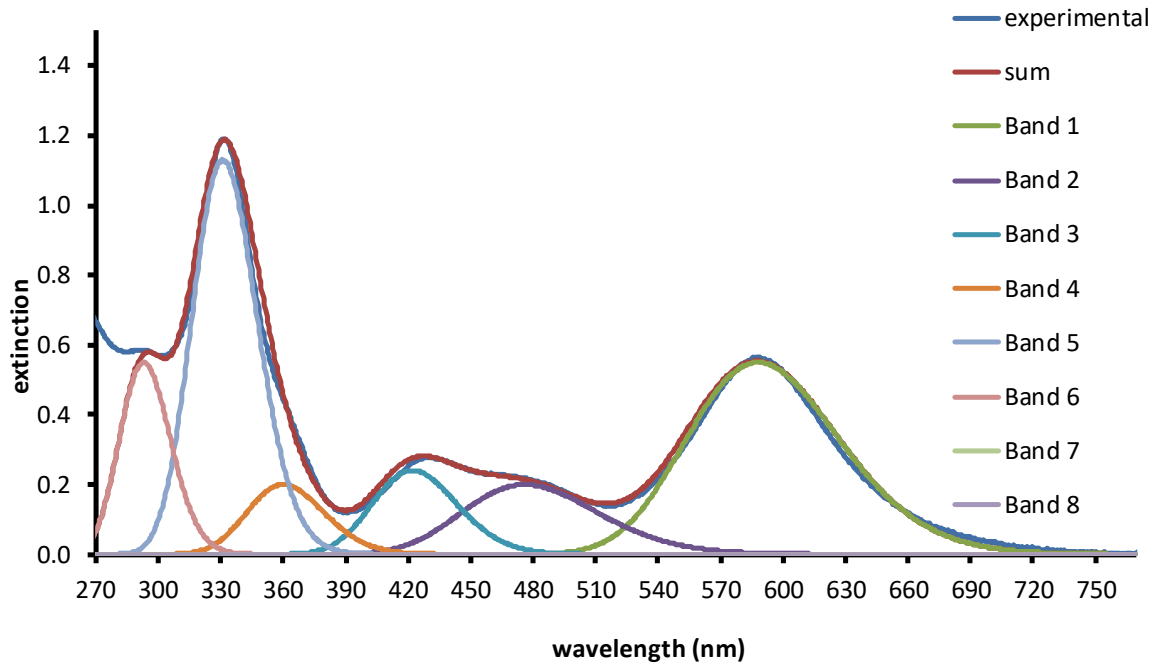

Figure 5.99. Deconvoluted and experimental UV-Vis-NIR spectra of **14** in *n*-hexane at c = 7 µmol L^{-1} and d = 1 mm.

Table 5.69. Parameters used for the band deconvolution of the UV-Vis-NIR spectrum depicted in Figure 5.99.[a]

	Band 1	Band 2	Band 3	Band 4	Band 5	Band 6
λ_{max}	588	476	422	360	331	293
E_{max}	0.550	0.200	0.240	0.200	1.130	0.550
σ_{max}	1480	2000	1600	2000	2000	2000

[a] λ_{max} = wavelength in nm; E_{max} = extinction maximum; σ = linewidth in cm^{-1}.

5.10.5 UV/Vis-NIR spectra of 14-Ge

The UV-Vis-NIR spectra of **14-Ge** were recorded in *n*-hexane at ambient temperature and are depicted in *Figure 5.100*. The absorption maxima and corresponding molar extinction coefficients ελ are summarized in *Table 5.70*. The absorption bands were determined by means of band deconvolution assuming a Gaussian line profile. The corresponding deconvoluted absorption bands are displayed in *Figure 5.101* (**14-Ge**) and the parameters used for the band deconvolution are summarized in *Table 5.71* (**14-Ge**).

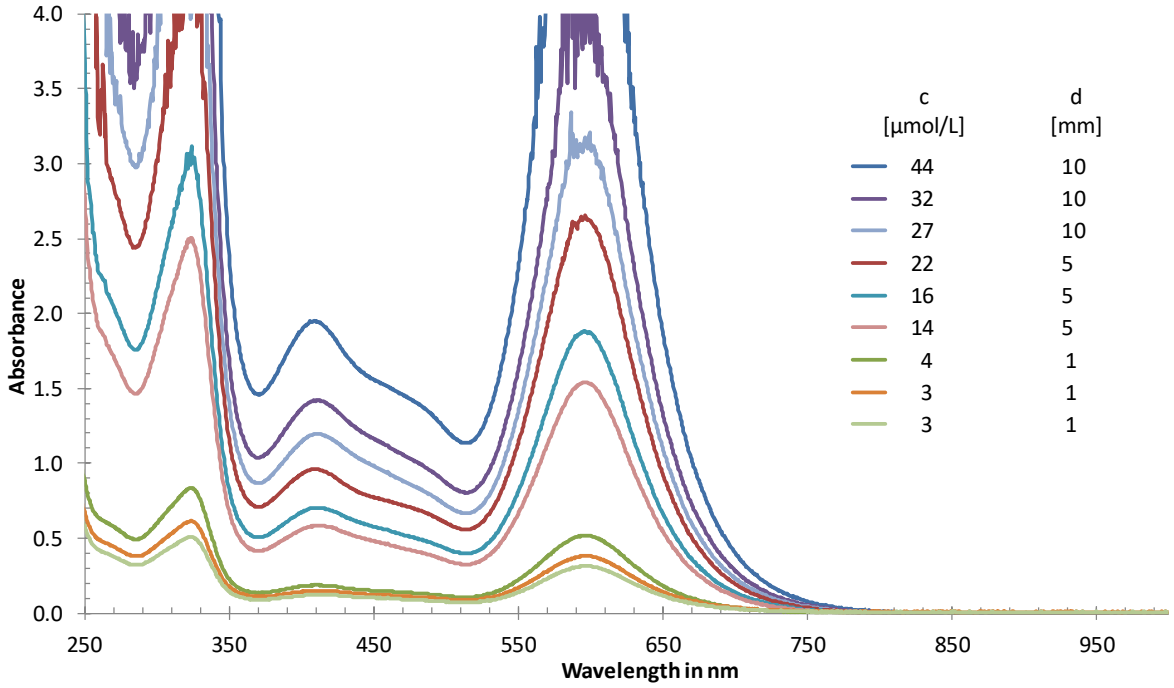

Figure 5.100. Experimental UV-Vis-NIR spectra of **14-Ge** in *n*-hexane from 250 – 1000 nm at different concentrations c of **14-Ge** and path lenghts d of the cuvette.

Table 5.70. Absorption maxima of the UV-Vis-NIR spectra of **14-Ge** depicted in *Figure 5.100* and their corresponding molar extinction coefficients.

λ / nm	597	526	480	410	325	331	300	267
ε_λ / L·mol^{-1}·cm^{-1}	11586	2777	3141	4398	18410	17860.0	13391	13180

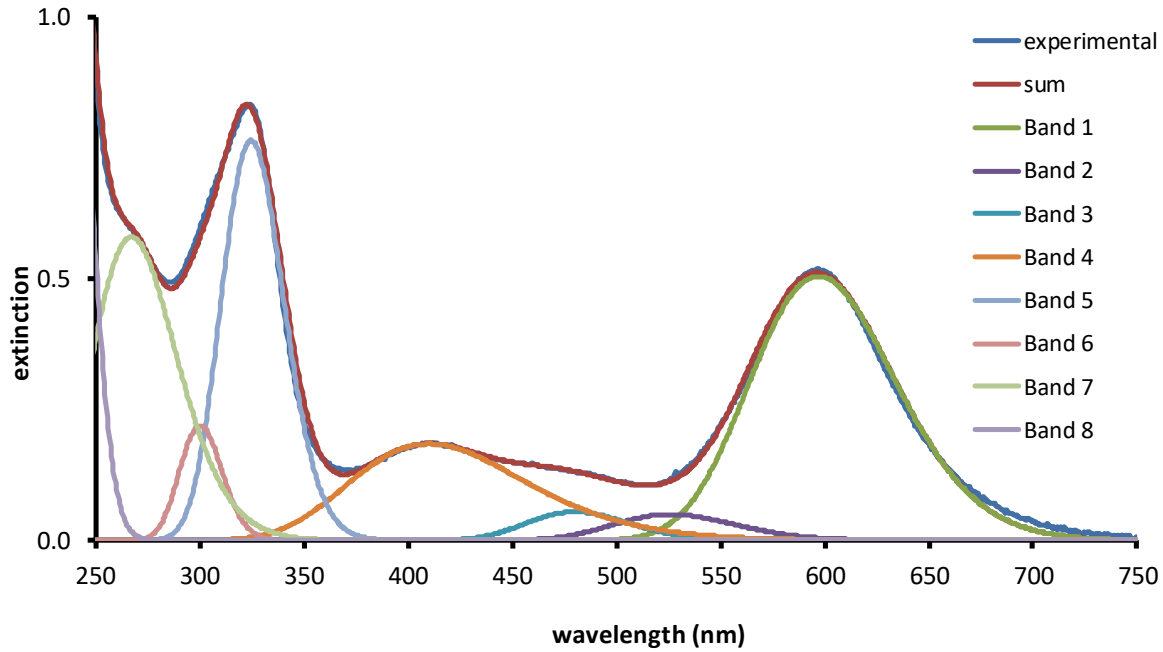

Figure 5.101. Deconvoluted and experimental UV-Vis-NIR spectra of **14-Ge** in *n*-hexane at c = 4 µmol L^{-1} and d = 1 mm.

Table 5.71. Parameters used for the band deconvolution of the UV-Vis-NIR spectrum depicted in *Figure 5.101.*[a]

	Band 1	Band 2	Band 3	Band 4	Band 5	Band 6	Band 7
λ_{max}	597	526	480	410	325	300	267
E_{max}	0.505	0.050	0.055	0.185	0.765	0.220	0.580
σ_{max}	1375	1500	1500	3500	2000	1600	4000

[a] λ_{max} = wavelength in nm; E_{max} = extinction maximum; σ = linewidth in cm^{-1}.

5.10.6 UV/Vis-NIR spectra of 19-Me

The UV-Vis-NIR spectra of **19-Me** were recorded in Et_2O at ambient temperature and are depicted in *Figure 5.102*. The absorption maxima and corresponding molar extinction coefficients ελ are summarized in *Table 5.72*. The absorption bands were determined by means of band deconvolution assuming a Gaussian line profile. The corresponding deconvoluted absorption bands are displayed in *Figure 5.103* (**19-Me**) and the parameters used for the band deconvolution are summarized in *Table 5.73* (**19-Me**).

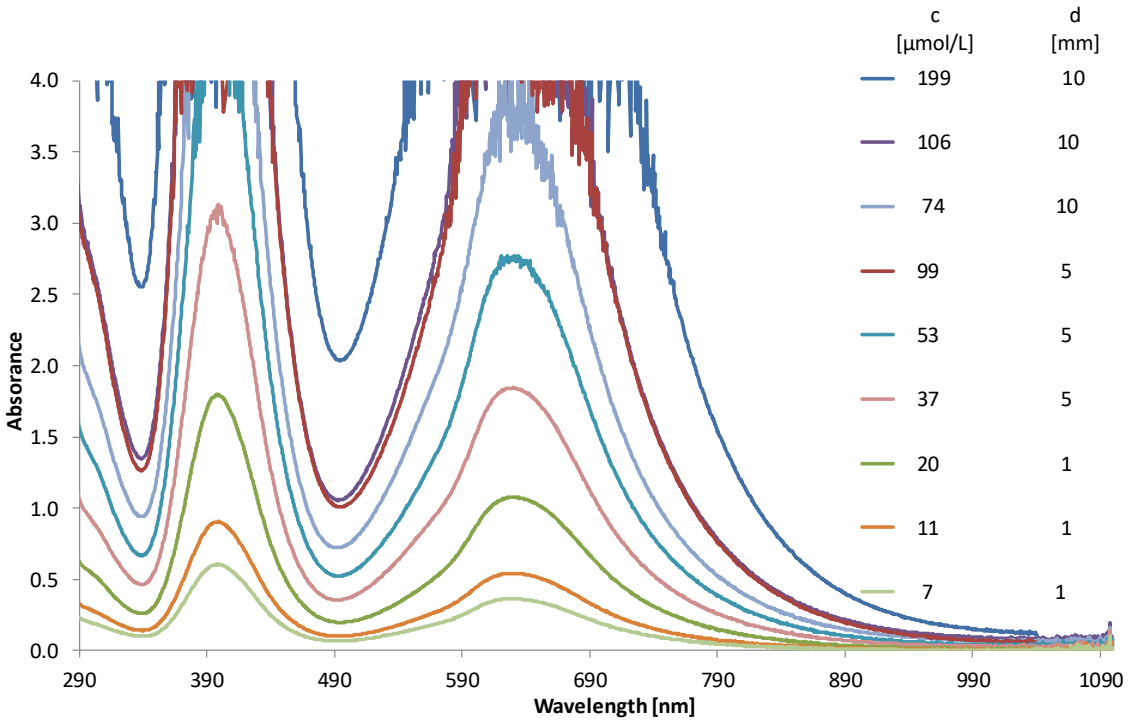

Figure 5.102. Experimental UV-Vis-NIR spectra of **19-Me** in Et_2O from 220 – 1100 nm at different concentrations c of **19-Me** and path lenghts d of the cuvette.

Table 5.72. Absorption maxima of the UV-Vis-NIR spectra of **19-Me** depicted in Figure 5.102 and their corresponding molar extinction coefficients.

λ / nm	631	399
ε_λ / $L \cdot mol^{-1} \cdot cm^{-1}$	5137.9	8854.7

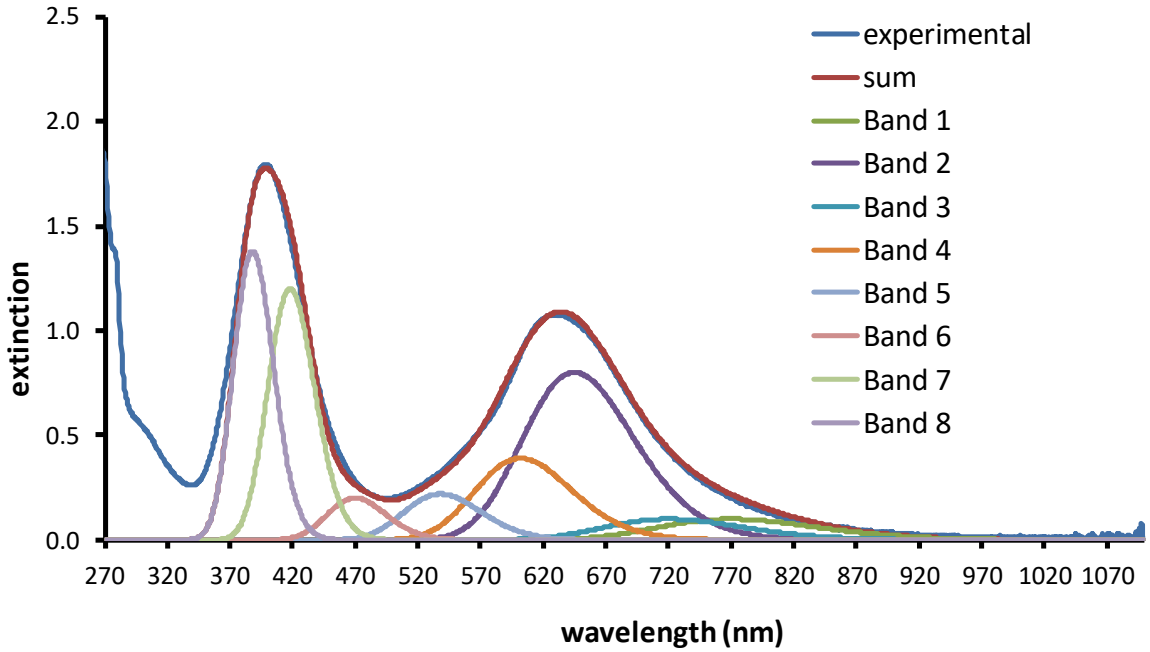

Figure 5.103. Deconvoluted and experimental UV-Vis-NIR spectra of **19-Me** in Et_2O at c = 11 µmol L^{-1} and d = 1 mm.

Table 5.73. Parameters used for the band deconvolution of the UV-Vis-NIR spectrum depicted in *Figure 5.103.* [a]

	Band 1	Band 2	Band 3	Band 4	Band 5	Band 6	Band 7	Band 8
λ_{max}	770	645	720	602	538	470	418	388
E_{max}	0.100	0.800	0.100	0.390	0.220	0.200	1.200	1.380
σ_{max}	1500	1500	1500	1500	1500	1500	1500	1500

[a] λ_{max} = wavelength in nm; E_{max} = extinction maximum; σ = linewidth in cm^{-1}.

5.11 Theoretical calculations of compounds

5.11.1Computational Details

Levels of Theory

level of theory (**I**)	B97-D3(BJ)^{ATM}/def2-TZVP	
functional set	B97-D	GGA
basis set	def2-TZVP	polarized triple-ζ
resolution of identity	RI-J	
auxiliary basis set	def2/J	Coulomb fitting basis
effective core potentials	def2-ECP	for Rb-Rn
dispersion correction	D3(BJ)	D3 with Becke-Johnson damping
three-body dispersion	ATM	Axilrod-Teller-Muto correction

Types of Calculations

structure optimization			
program	ORCA 5.0.0		
level of theory	B97-D3(BJ)^{ATM}/def2-TZVP		
grid settings	DEFGRID2		grid for exchange-correlation
convergence criteria	ΔE_{max}	$= 5 \cdot 10^{-6}$ E_H	max. energy change
	g_{max}	$= 3 \cdot 10^{-4}$ E_H/Bohr	max. gradient
	$RMS(g)_{max}$	$= 3 \cdot 10^{-4}$ E_H/Bohr	max. RMS gradient
	Δx_{max}	$= 4 \cdot 10^{-3}$ Bohr	max. displacement
	$RMS(\Delta x)_{max}$	$= 2 \cdot 10^{-3}$ Bohr	max. RMS displacement

frequency calculation		
program	ORCA 5.0.0	
level of theory	B97-D3(BJ)^{ATM}/def2-TZVP	
grid settings	DEFGRID2	grid for exchange-correlation
frequencies	harmonic, derived from two-sided numerical differentiation of the analytical gradients	

Ro-vibrational corrections to obtain free energies were obtained from quasi rigid rotor harmonic oscillator (Quasi-RRHO) statistical treatment (T = 298.15 K, p = 1 atm) based on harmonic frequencies calculated at the structure optimization level (B97-D3(BJ)^{ATM}/def2-TZVP). To avoid errors in the harmonic approximation, frequencies with wave numbers below 100 cm^{-1} were treated partially as rigid rotors.

ETS-NOCV		
program	ORCA 5.0.2	
level of theory	B97-D3(BJ)^{ATM}/def2-TZVP	
grid settings	DEFGRID3	grid for exchange-correlation

NBO/NRT analysis		
program	NBO 7.0.10	
level of theory	B97-D3(BJ)^{ATM}/def2-TZVP	

hyperfine coupling constants of silicon radicals		
program	ORCA 5.0.1	
level of theory	B97-D3(BJ)^{ATM}/def2-TZVP	
grid settings	DEFGRID3	grid for exchange-correlation
GIAOs used	yes	Gauge Including Atomic Orbitals
hfc settings	aiso, adip, aorb, fgrad, rho	calculate isotropic, dipolar, and spin-orbit coupling part of hfc, electric field gradient, and electron density at the nucleus

Dibromosilylenes $SiBr_2$(carbene) (carbene = $caac^{Me}$ (**1**), IDipp (**1-NHC^1**), SIDipp (**1-NHC^2**)), pyramidal monohalosilylenes SiBr(R)($caac^{Me}$) (R = $SiTMS_3$ (**2-Si**), Mes (**2-Mes**), $NTMS_2$ (**2-N**), $PMes_2$ (**2-P**)), silicon(I) radicals Si(R)($caac^{Me}$) (R = $SiTMS_3$ (**3-Si**), $NTMS_2$ (**3-N**), OMes* (**3-O**)) and phosphanyl-radical **6** were calculated by Jens Rump. Silenylgermylene **12**, carbene-stabilized disilavinylidenes (carbene)Si=SiBr(Tbb) (carbene = $caac^{Me}$ (**14**), SIDipp (**14-NHC**)) and ($caac^{Me}$)Ge=SiBr(Tbb) (**14-Ge**) as well as disilynylium cation **18**$^+$ were calculated by Leonard R. Maurer. The calculations of the UV/Vis spectra of the heavier tetrelavinylidenes **14**, **14-Ge** and **14-NHC** were performed by Dr. Gregor Schnakenburg.

5.11.2 Dibromosilylenes

Table 5.74. Selected structural parameters of the calculated gas phase structure (calc.) and the structure derived from single-crystal X-ray diffraction of **1** and $SiBr_2$(IDipp) (**1-NHC^1**).

	$SiBr_2(caac^{Me})$ (**1**)		$SiBr_2$(IDipp) (**1-NHC^1**)	
	calc.	exp.	calc.	exp.
Si–C^{carb}/Å	2.031	2.017(2)	2.028	1.989(3)
Si–Br1/Å	2.385	2.3541(7)	2.367	2.3379(8)
Si–Br2/Å	2.410	2.3591(7)	2.401	2.3606(9)
C^{carb}–N/Å	1.310	1.301(3)	1.367	1.363(4)
Br1–Si–Br2/ (deg)	102.5	99.27(2)	1.362	1.358(4)
Br1–Si–C^{carb}/ (deg)	98.3	96.97(6)	100.5	97.94(3)
Br2–Si–C^{carb}/ (deg)	87.1	93.71(6)	100.1	99.93(8)
Σ∢(Si)/ (deg)	287.9	289.95(5)	90.7	94.9(1)
Σ∢(C^{carb})/ (deg)	360.0	360.0(2)	291.3	292.77(7)

Table 5.75. Selected structural parameters of the calculated gas phase structure (calc.) and the structure derived from single-crystal X-ray diffraction of $SiBr_2$(SiDipp) (**1-NHC^2**).

	$SiBr_2$(SIDipp) (**1-NHC^2**).		
	calc.	exp.	
Si–C^{carb}/Å	2.053	2.009(2)	2.009(2)
Si–Br1/Å	2.369	2.3432(7)	2.3175(7)
Si–Br2/Å	2.403	2.3308(7)	2.3392(7)
C^{carb}–N1/Å	1.346	1.337(2)	1.336(2)
C^{carb}–N2/Å	1.336	1.328(2)	1.326(2)
Br1–Si–Br2/ (deg)	100.1	97.58(3)	98.25(3)
Br1–Si–C^{carb}/ (deg)	100.7	102.72(6)	101.66(6)
Br2–Si–C^{carb}/ (deg)	87.3	88.60(6)	91.28(6)
Σ∢(Si)/ (deg)	288.1	288.9(5)	291.2(5)
Σ∢(C^{carb})/ (deg)	360.0	359.9(1)	360.0(1)

5.11.3 Pyramidal Monohalosilenes SiBr(R)(caac^{Me})

Table 5.76. Selected structural parameters of the calculated gas phase structure (calc.) and the structure derived from single-crystal X-ray diffraction of **2-Si** and **2-Mes**.

	SiBr(SiTMS$_3$)(caac^{Me}) (**2-Si**)		SiBr(Mes)(caac^{Me}) (**2-Mes**)	
R = Si2, C^{Ar}	calc.	exp.	calc.	exp.
Si1–C^{carb}/Å	1.845	1.836(2)	1.844	1.843(1)
Si1–Br/Å	2.326	2.2921(5)	2.316	2.2952(4)
C^{carb}–N/Å	1.357	1.353(2)	1.357	1.350(2)
R–Si1–C^{carb}/ (deg)	123.2	124.15(5)	110.2	110.45(6)
∑∢(Si1) / (deg)	333.9	358.0(1)	329.0	332.33(4)
φ_{CAAC} [a]/°(deg)	31.3	28.06(6)	42.3	44.68(6)

[a]: φ_{CAAC} is the plane twist angle between the mean plane of the central five-membered ring of the caac^{Me} carbene and the plane of the atoms R, Si, C^{carb} (R = Si2, C^{Ar}).

Table 5.77. Selected structural parameters of the calculated gas phase structure (calc.) and the structure derived from single-crystal X-ray diffraction of **2-P** and **2-N**.

	SiBr(PMes$_2$)(caac^{Me}) (**2-P**)			SiBr(NTMS$_2$)(caac^{Me}) (**2-N**)	
R = P, N	calc.	exp.		calc.	exp.
Si–C^{carb}/Å	1.847	1.85(1)	1.861(9)	1.861	1.866(2)
Si–Br/Å	2.322	2.273(2)	2.286(2)	2.329	2.3108(6)
C^{carb}–N/Å	1.357	1.36(1)	1.34(1)	1.359	1.349(2)
R–Si–C^{carb}/ (deg)	108.6	109.9(2)	108.3(2)	115.2	113.67(6)
∑∢(Si) / (deg)	338.5	336.4(2)	333.5(2)	332.6	328.82(6)
φ_{CAAC} [a]/°(deg)	38.9	38.8(3)	138.4(4)	34.1	38.82(8)

[a]: φ_{CAAC} is the plane twist angle between the mean plane of the central five-membered ring of the caac^{Me} carbene and the plane of the atoms R, Si, C^{carb} (R = P, N).

5.11.4 Neutral silicon(I) radicals Si(R)(caac^{Me})

Table 5.78. Selected structural parameters of the calculated gas phase structure (calc.) and the structure derived from single-crystal X-ray diffraction of **3-Si** and **3-N**.

	Si(SiTMS$_3$)(caac^{Me}) (**3-Si**)		Si(NTMS$_2$)(caac^{Me}) (**3-N**)	
R = Si2, N	calc.	exp.	calc.	exp.
Si1–C^{carb}/Å	1.867	1.870(2)	1.906	1.895(4)
N–C^{carb}/Å	1.356	1.349(2)	1.358	1.361(4)
R–Si1–C^{carb}/ (deg)	113.9	112.9(1)	104.7	106.6(2)
φ_{CAAC} [a]/°(deg)	24.0	20.9(3)	0.7	4.0(6)

[a]: φ_{CAAC} is the plane twist angle between the mean plane of the central five-membered ring of the caac^{Me} carbene and the plane of the atoms R, Si, C^{carb} (R = Si2, N).

Table 5.79. Selected structural parameters of the calculated gas phase structure (calc.) and the structure derived from single-crystal X-ray diffraction of **3-O** and **6**.

	Si(OMes*)(caac^{Me}) (**3-O**)		(Mes)P=Si(Mes)(caac^{Me}) (**6**)	
R = O, P	calc.	exp.	calc.	exp.
Si–C^{carb}/Å	1.889	1.865(4)	1.818	1.813(2)
N–C^{carb}/Å	1.362	1.363(3)	1.376	1.369(3)
R–Si–C^{carb}/ (deg)	99.5	100.1(1)	125.6	122.3(7)
φ_{CAAC} [a]/ (deg)	3.8	0.5(1)	15.5	21.5(1)

[a]: φ_{CAAC} is the plane twist angle between the mean plane of the central five-membered ring of the caac^{Me} carbene and the plane of the atoms R, Si, C^{carb} (R = Si2, O, N).

Table 5.80. Calculated and experimental EPR spectroscopic parameters of **3-Si**, **3-N**, **3-O** and **6**.

	3-Si		**3-N**		**3-O**		**6**	
	calc.	exp.	calc.	exp.	calc.	exp.	calc.	exp.
multiplicity		three		three		three		d x t
g_{iso}	2.0051	2.0065	2.0035	2.0044	2.0031	2.0038	2.0056	2.0061
a_{iso}(^{29}Si)/mT	–4.67	3.81	–2.76	1.95	–1.93	1.24	0.74	–
a_{iso}(^{14}N)/mT	0.18	0.44	0.19	0.57	0.19	0.62	0.15	0.54
a_{iso}(^{31}P)/mT	–	–	–	–	–	–	4.31	3.74

5.11.5 Dynamics in silicon(I) radical 3-Si

Two types of dynamic processes could be modeled by means of relaxed potential energy surface scans. The first process involves the rotation of the Tris(trimethylsilyl)silyl group about the Si1–Si2 bond. This process is accompanied by a barrier of 19 kJ mol^{-1} and should therefore happen even at low temperatures in solution.
The second process displays the rotation of the carbene ligand around the Si1–C1 bond. A relaxed potential energy surface scan of the N–C1–Si1–Si2 dihedral angle starting from the calculated minimum values of 0° in 72 steps with a step size of 5° showed, that due to steric constrains between the hypersilyl-group and the Dipp ligand this process is better described as a precession movement of the C1–Si1 bond vector in relation to the C1–Si2 vector normal, as displayed in the figure below. The carbene ligand wobbles concomitantly and synchronously during this process in order to keep the sum of angles at the carbene carbon atom to the greatest possible extend unchanged.
Even though all structures have an enantiomeric counterpart denoted as (R_a)-**3-Si-x** and (S_a)-**3-Si-x**, the relaxed potential energy surface scan did not yield perfect enantiomers which were marked with the prime symbol (‘). However, an explicit calculation of the corresponding lowest energy pathway would be symmetric.

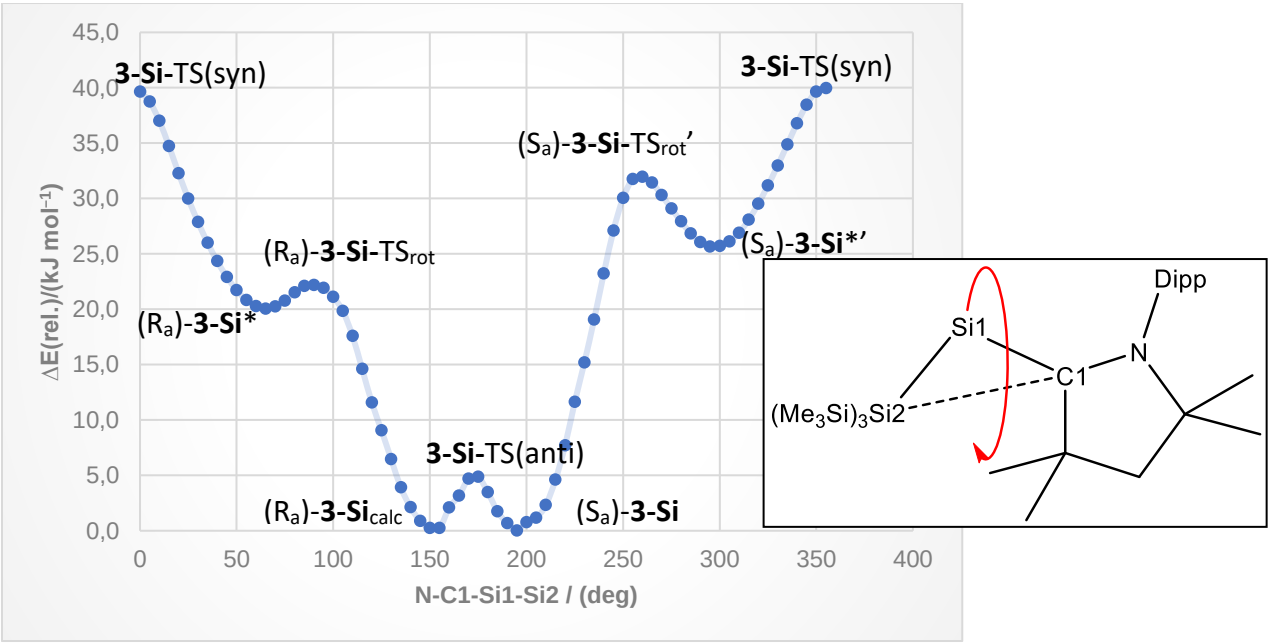

Figure 5.104. Energy profile of the relaxed potential energy surface scan of the N–C1–Si1–Si2 dihedral angle and schematic representation of the scan (lower right).

5.11.6 (Silenyl)germylen 12

Table 5.81. Selected structural parameters of the calculated gas phase structure (calc.) and the structure derived from single-crystal X-ray diffraction of **12**.

	(caac^{Me})Si(C≡CTMS)(GeAr^{Mes}) (**12**)		
	calc.	exp.	
Si–C^{carb}/Å	1.826	1.843(10)	1.801(14)
Si–Ge/Å	2.349	2.300(3)	2.302(4)
Ge–C^{Ar}/Å	2.039	2.015(9)	2.010(9)
Si–C$^{C\equiv C}$/Å	1.809	1.836(10)	1.779(10)
(C–C)$^{C\equiv C}$/Å	1.223	1.190(12)	1.1213(13)
C$^{C\equiv C}$–Si^{TMS}/Å	1.828	1.85(1)	1.891(9)
C^{carb}-Si-Ge / (deg)	117.6	117.9(3)	116.7(5)
Si-Ge-C^{Ar} / (deg)	97.7	101.0(3)	99.0(3)
C^{carb}-Si-C$^{C\equiv C}$ / (deg)	114.5	112.4(5)	115.2(6)
C^{carb}-Si-Ge-C^{Ar}/ (deg)	176.1	–179.7(4)	177.3(6)
N-C^{carb}-Si-Ge/ (deg)	–163.0	–161.5(7)	–161.6(12)

5.11.7 Carbene stabilized heavier tetrelavinylidenes

Table 5.82. Selected structural parameters of the calculated gas phase structure (calc.) and the structure derived from single-crystal X-ray diffraction of **14** and **14-Ge**.

	(caac^{Me})Si=SiBr(Tbb) (**14**)		(caac^{Me})Ge=SiBr(Tbb) (**14-Ge**)	
E= Si,Ge	calc.	exp.	calc.	exp.
E–C^{carb}/Å	1.867	1.878(5)	1.977	1.987
E–Si/Å	2.207	2.194(2)	2.278	2.249
Si–C^{Tbb}/Å	1.889	1.874(5)	1.893	1.890
Si–Br /Å	2.312	2.278(1)	2.314	2.281
C^{carb}-E-Si / (deg)	107.7	106.8(2)	106.7	105.5
E-Si-C^{Tbb} / (deg)	119.3	118.2(2)	117.9	119.3
E-Si-Br/ (deg)	128.3	127.8	129.9	128.1
C^{carb}-E-Si-C^{Tbb}/ (deg)°	179.3	178.2(1)	–178.4	180.0
N-C^{carb}-E-Si/ (deg)	–139.4	135.6(3)	140.5	136.4

Table 5.83. Selected structural parameters of the calculated gas phase structure (calc.) and the structure derived from single-crystal X-ray diffraction of (SIDipp)Si=SiBr(Tbb) (**14-NHC**)

	(SIDipp)Si=SiBr(Tbb) (**14-NHC**)	
	calc.	exp.
Si–C^{carb}/Å	1.923	1.937(4)
Si–Si/Å	2.178	2.167(2)
Si–C^{Tbb}/Å	1.892	1.882(3)
Si–Br /Å	2.307	2.286(2)
C^{carb}-Si-Si / (deg)	99.0	97.6(2)
Si-Si-C^{Tbb} / (deg)	120.8	123.4(2)
Si-Si-Br/ (deg)	128.4	127.2(1)
C^{carb}-Si-Si-C^{Tbb}/ (deg)	–176.7	177.3(2)
N-C^{carb}-Si-Si/ (deg)	111.9	101.0(3)
	–81.3	–90.1(3)

5.11.8 Rotation of the caac^{Me} substituent in 14 and 14-Ge

In order to rationalize the stereodynamics in **14** and **14-Ge** relaxed PES scans of the N^{CAAC}–C^{CAAC}–E–Si (E = Si, Ge) torsion angle in **14$_{calc}$** and **14-Ge$_{calc}$** were performed from –180° to 170° with a step size of 10° (*Figure 5.105*). Both compounds show a similar behaviour, upon rotation of the Si–C^{CAAC} bond.

The rotation of the caac^{Me} substituent about the Si–C^{CAAC} bond in **14** via the co-planar structure **14-a** proceeds via a low energy barrier of 14 kJ mol^{-1} and leads to a fast inversion of the two enantiomers (R_a)-**14** (τ = 140°) and (S_a)-**14$_{calc}$** (τ = –140°). In contrast a larger barrier of approximately 40 kJ mol^{-1} (via **14-b**) must be overcome to achieve the conversion to the almost co-planar structure **14**-0 (τ = –10°). Due to the symmetry, the enantiomer (R_a)-**14** can be reached by the same barrier, which is found to proceed via **14c** (*Figure 5.105*).

Likewise, the rotation of the caac^{Me} substituent about the Ge–C^{CAAC} bond in **14-Ge** via the co-planar structure **14-Ge-a** proceeds via a low energy barrier of 8 kJ mol^{-1} and leads to a fast inversion of the two enantiomers (R_a)-**14-Ge** (τ = 140°) and (S_a)-**14-Ge$_{calc}$** (τ = –140°). Similarly, a larger barrier of approximately 33 kJ mol^{-1} (via **14-b**) must be overcome to achieve the conversion to the almost co-planar structure **14-Ge-0** (τ = 10°).

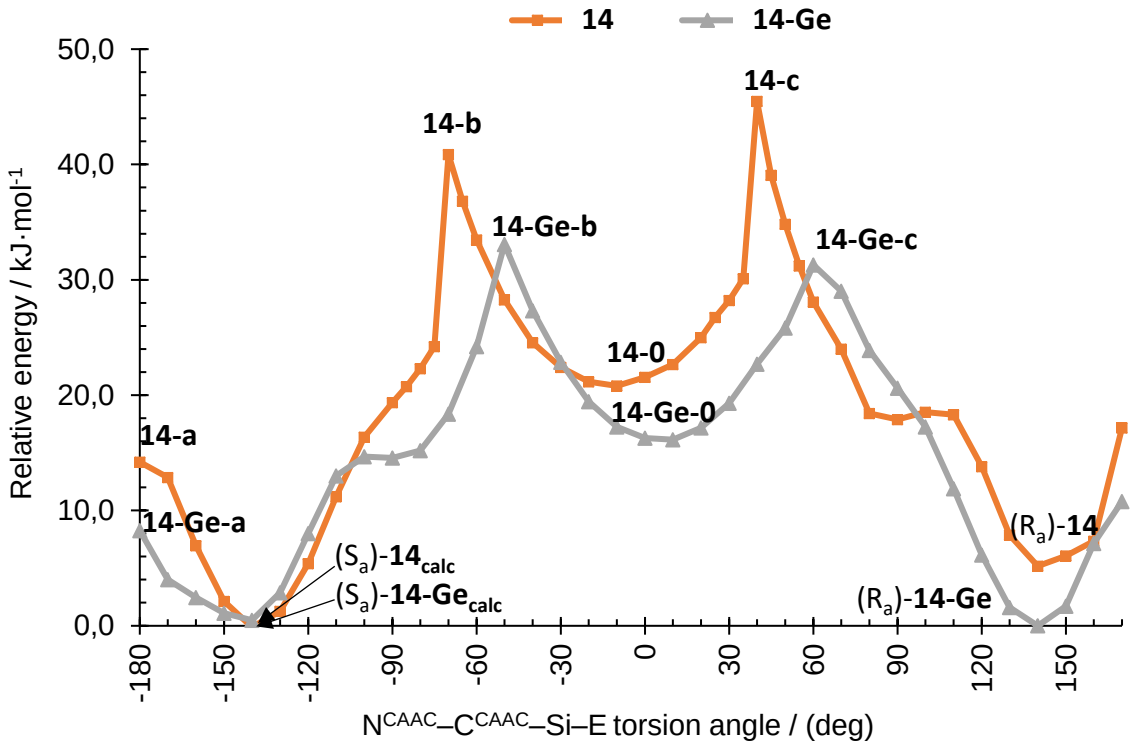

Figure 5.105. PES scans for the rotation of the caac^{Me} substituents abouth their Si–C^{CAAC} bonds in compounds **14** and **14-Ge**.

5.11.9 Disilynylium cation 18^+

Table 5.84. Selected structural parameters of the calculated gas phase structure (calc.) and the structure derived from single-crystal X-ray diffraction of **18**$^+$.

	$[(caac^{Me})Si{=}Si(IMe_4)(Tbb)]^+$ (**18**$^+$)	
	calc.	exp.
Si–C^{CAAC}/Å	1.882	1.896(3)
Si–Si/Å	2.213	2.203(2)
Si–C^{Tbb}/Å	1.889	1.885(3)
Si–C^{NHC} /Å	1.920	1.919(3)
C^{CAAC}-Si-Si / (deg)	109.3	109.0(1)
Si-Si-C^{Tbb} / (deg)	119.8	121.3(2)
Si-Si-C^{NHC}/ (deg)	130.9	131.2(2)
C^{CAAC}-Si-Si-C^{Tbb}/ (deg)°	–173.3	–168.5(2)
N-C^{CAAC}-Si-Si/ (deg)	–150.0	–155.2(2)

5.11.10 Calculated UV/Vis spectra of 14, 14-Ge and 14-NHC

Table 5.85. Experimental versus calculated absorbtions maxima of the UV/Vis spectrum of **14** in *n*-hexane at ambient temperature. Contributions with less than 5 % are not listed. Calculations were performed at the RI-B97-D3/def2-TZVP(CPCM/Hexane) level of theory by Dr. G. Schnakenburg.

(caac^{Me})Si=SiBr(Tbb) (**14**)

λexp /nm	λcalc /nm	excitation	contribution /%
588	557.9	HOMO → LUMO	62.6
		HOMO–1 → LUMO	16
		HOMO → LUMO+1	9.8
		HOMO–1 → LUMO+1	8.9
476	508.0	HOMO → LUMO+1	66.1
		HOMO → LUMO	10.1
		HOMO → LUMO+4	8.1
		HOMO–1 → LUMO	6.3
		HOMO–1 → LUMO+1	6.8
	459.5	HOMO → LUMO+2	97.6
	455.0	HOMO–2 → LUMO	98.2
	449.2	HOMO → LUMO+3	67.1
		HOMO–1 → LUMO	14.5
		HOMO → LUMO+4	14.5
	437.3	HOMO → LUMO+3	31.4
		HOMO → LUMO+4	30.5
422		HOMO–1 → LUMO	26.9
	400.0	HOMO–3 → LUMO	96.0
	386.7	HOMO → LUMO+4	37.3
		HOMO–1 → LUMO	25.2
		HOMO → LUMO+1	13.2
		HOMO–1 → LUMO+2	10.2
	381.5	HOMO–2 → LUMO+2	96.8
	375.8	HOMO → LUMO+5	97.7
360			
331			
293			

Table 5.86. Experimental versus calculated absorbtions maxima of the UV/Vis spectrum of **14-Ge** in *n*-hexane at ambient temperature. Contributions with less than 5 % are not listed. Calculations were performed at the RI-B97-D3/def2-TZVP(CPCM/Hexane) level of theory by Dr. G. Schnakenburg.

(caac^{Me})Ge=SiBr(Tbb) (**14-Ge**)

λexp /nm	λcalc /nm	excitation	contribution /%
597	558.0	HOMO → LUMO	61.6
		HOMO → LUMO+1	17.1
		HOMO–1 → LUMO	11.8
		HOMO–1 → LUMO+1	5.8
526	516.3	HOMO → LUMO+1	59.6
		HOMO → LUMO	13.7
		HOMO → LUMO+4	13.3
		HOMO–1 → LUMO+1	6.0
480	477.7	HOMO → LUMO+2	94.3
	466.0	HOMO → LUMO	94.4
	449.9	HOMO → LUMO+3	98.8
	439.8	HOMO → LUMO+4	52.5
410		HOMO–1 → LUMO	31.5
	396.2	HOMO–3 → LUMO	90.3
	391.3	HOMO–2 → LUMO	41.6
		HOMO → LUMO+4	22.3
		HOMO → LUMO+1	11.4
		HOMO–3 → LUMO	7.6
	386.6	HOMO → LUMO+5	95.1
325			
331			
300			
267			

Table 5.87. Experimental versus calculated absorbtions maxima of the UV/Vis spectrum of the NHC stabilized disilavinylidene **14-NHC** in *n*-hexane at ambient temperature. Contributions with less than 5 % are not listed. Calculations were performed at the RI-B97-D3/def2-TZVP(CPCM/Hexane) level of theory by Dr. G. Schnakenburg.

(SIDipp)Si=SiBr(Tbb) (**14-NHC**)

λexp /nm	λcalc /nm	excitation	contribution /%
515	568.8	HOMO → LUMO	87.1
		HOMO → LUMO+1	7.4
455	515.5	HOMO → LUMO+1	62.0
		HOMO → LUMO+3	13.8
		HOMO → LUMO+4	12.1
	502.3	HOMO → LUMO+2	94.2
	486.7	HOMO → LUMO+2	74.4
		HOMO → LUMO+3	5.1
		HOMO → LUMO+5	5.4
	480.3	HOMO → LUMO+4	93.0
	460.4	HOMO → LUMO+5	78.2
		HOMO → LUMO+6	17.4
	402.3	HOMO → LUMO+6	38.5
		HOMO-1 → LUMO	15.2
	394.5	HOMO → LUMO+7	77.5
388		HOMO–1 → LUMO	6.3
	385.0	HOMO–2 → LUMO	99.7
	369.4	HOMO–2 → LUMO	97.8
346			
324			
305			

5.12 List of Abbreviations

4-dmap	4-dimethylaminopyridine
Ar^R	2,6-R_2-C_6H_3
ATR	Attenuated total reflection
CAAC	cyclic(alkyl)(amino=carbene
$caac^{Me}$	:C[N(Dipp)(CMe_2)(CH_2)(CR_2)] R_2 = Me_2
$caac^{Et}$	:C[N(Dipp)(CMe_2)(CH_2)(CR_2)] R_2 = Et_2
$caac^{Cy}$	:C[N(Dipp)(CMe_2)(CH_2)(CR_2)] R_2 = $(CH_2)_5$
Cp	cyclopentadienyl
Cp*	pentamethylcyclopentadienyl
CV	Cyclic voltammetry
DFT	Density functional theory
Dipp	2,6-*i*Pr_2-C_6H_3
DME	dimethoxyethane
dmfc	Decamethylferrocene, [η^5-$C_5Me_5)_2Fe$]
Dsi	Disyl, $CH(SiMe_3)_2$
Eind	1,1,3,3,5,5,7,7-octaethyl-s-hydrindacen-4-yl
EMind	1,1,7,7-tetraethyl-3,3,5,5-tetramethyl-s-hydrindacen-4-yl
eq.	equivalent(s)
et al.	et alia
Et	ethyl
FTIR	Fourier-transform infrared spectroscopy
HOMO	highest occupied molecular orbital
IDipp	:C[N(Dipp)CH]$_2$
IDipp-Me_2	:C[N(Dipp)C(Me)]$_2$
*i*Pr	*iso*propyl
I*i*Pr_2Me_2	:C[N(*i*Pr)C(Me)]$_2$
IMe_4	:C[N(Me)C(Me)]$_2$
IMes	:C[N(Mes)CH]$_2$
I*t*Bu	:C[N(*t*Bu)CH]$_2$
LUMO	lowest unoccupied molecular orbital
Me	methyl
Mes	mesityl, 2,4,6-Me_3-C_6H_2
Mes*	2,4,6-*t*Bu_3-C_6H_2
NBO	natural bond orbital
n-Bu	*n*-butyl, C_4H_9
NHC	N-heterocyclic carbene

NHI	N-heterocylcic imine, :N=C[N(Dipp)CH]$_2$
NMR	nuclear magnetic resonance
NRT	natural resonance theory
OTf	triflate, $OSO_2(CF_3)$
Ph	phenyl
SIDipp	:C[N(Dipp)CH$_2$]$_2$
Tbb	2,4-Dsi$_2$-6-*t*Bu-C$_6$H$_2$
Tbt	2,4,6-(CH(SiMe$_3$)$_2$)$_3$-C$_6$H$_2$
*t*Bu	tert.-butyl
THF	tetrahydrofuran
TMS	SiMe$_3$
Tp	trispyrazolylborate
Tp'	tris(3,5-dimethyl-1-pyrazolyl)borate
Trip	2,4,6-*i*Pr$_3$-C$_6$H$_2$
Trp*	aliphatic substituent in a rigid triptcyclic framework: 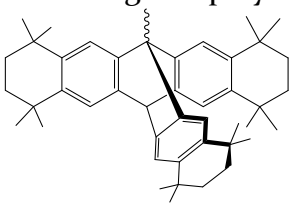
UV-Vis	ultraviolet-visible
WBI	Wiberg bond index
VT	Variable temperature

5.13 List of Figures

5.14 List of Schemes

5.15 List of Tables

5.16 Scientific Contributions

Peer-reviewed publications

Partial Synthesis of Coenzyme B_{12} from Cobyric Acid
Florian J. Widner*, F. Gstrein*, B. Kräutler, *Helv. Chim. Acta* **2017**, 100, e1700170, DOI: 10.1002/hlca.201700170; (*) contributed equally

Oral presentations

Silicon Compounds in Low Oxidation States Stabilized by a Cyclic (Alkyl)(Amino)Carbene: Synthesis, Structure and Reactivity
Contributed Talk, GDCh Kolloquium, Bonn, 21. June **2022**

Silicon(I) Chemistry: Isolation and Reactivity of the Two-coordinated Neutral Silicon(I) Radical Si(Tts)(caac^{Me})
Contributed Talk, Chemistry of Hypo and Hypercoordinated Compounds of the Group 14 (CCHC group 14) Conference, Rennes, France, 19.-21. June **2019**

Poster Presentations at International Conferences

Lewis Acidity and Redox Reactivity of a CAAC-stabilized Disilavinylidene
F. Gstrein, U. Das, G. Schnakenburg, L. R. Maurer, A. C. Filippou, The 19th International Symposium on Silicon Chemistry (Online ISOS 2021), Toulouse, France, 5.-7. July, **2021**

Reactions of SiBr$_2$(CAAC^{Me}) with Nucleophiles
F. Gstrein, U. Das, M. Straßmann, A. C. Filippou, Anglo-German Inorganic Chemistry Conference (AGICHEM 2017), Göttingen, 6.-9. August, **2017**

6 Bibliography

[1] A. F. Holleman, E. Wiberg, N. Wiberg, *Lehrbuch der Anorganischen Chemie*, De Gruyter, Berlin, **2007**.

[2] V. Gold, Ed. , *The IUPAC Compendium of Chemical Terminology: The Gold Book*, International Union Of Pure And Applied Chemistry (IUPAC), Research Triangle Park, NC, **2019**.

[3] M. Rahm, R. Hoffmann, N. W. Ashcroft, *Chem. Eur. J.* **2016**, *22*, 14625–14632.

[4] M. Rahm, R. Hoffmann, N. W. Ashcroft, *Chem. Eur. J.* **2017**, *23*, 4017–4017.

[5] D. Seyferth, *Organometallics* **2001**, *20*, 4978–4992.

[6] Y. Zhang, J. Li, H. Liu, Y. Ji, Z. Zhong, F. Su, *ChemCatChem* **2019**, *11*, 2757–2779.

[7] J. M. Jasinski, S. M. Gates, *Acc. Chem. Res.* **1991**, *24*, 9–15.

[8] K. S. Pitzer, *J. Am. Chem. Soc.* **1948**, *70*, 2140–2145.

[9] R. S. Mulliken, *J. Am. Chem. Soc.* **1950**, *72*, 4493–4503.

[10] R. S. Mulliken, *J. Am. Chem. Soc.* **1955**, *77*, 884–887.

[11] P. J. Davidson, D. H. Harris, M. F. Lappert, *J. Chem. Soc., Dalton Trans.* **1976**, 2268.

[12] R. West, M. J. Fink, J. Michl, *Science* **1981**, *214*, 1343–1344.

[13] A. G. Brook, F. Abdesaken, B. Gutekunst, G. Gutekunst, R. K. Kallury, *J. Chem. Soc., Chem. Commun.* **1981**, 191.

[14] M. Yoshifuji, I. Shima, N. Inamoto, K. Hirotsu, T. Higuchi, *J. Am. Chem. Soc.* **1981**, *103*, 4587–4589.

[15] G. Becker, G. Gresser, W. Uhl, *Z. Naturforsch. B* **1981**, *36*, 16–19.

[16] P. P. Power, *Chem. Rev.* **1999**, *99*, 3463–3504.

[17] R. C. Fischer, P. P. Power, *Chem. Rev.* **2010**, *110*, 3877–3923.

[18] V. Y. Lee, A. Sekiguchi, *Organometallic Compounds of Low-Coordinate Si, Ge, Sn, and Pb: From Phantom Species to Stable Compounds*, Wiley, Chichester, West Sussex, U.K, **2010**.

[19] A. Baceiredo, T. Kato, in *Organosilicon Compounds*, Elsevier, **2017**, pp. 533–618.

[20] C. Weetman, *Chem. Eur. J.* **2021**, *27*, 1941–1954.

[21] B. D. Shepherd, C. F. Campana, R. West, *Heteroat. Chem.* **1990**, *1*, 1–7.

[22] N. Wiberg, W. Niedermayer, G. Fischer, H. Nöth, M. Suter, *Eur. J. Inorg. Chem.* **2002**, *2002*, 1066–1070.

[23] K. Suzuki, T. Matsuo, D. Hashizume, K. Tamao, *J. Am. Chem. Soc.* **2011**, *133*, 19710–19713.

[24] M. Kira, *Proc. Jpn. Acad., Ser. B* **2012**, *88*, 167–191.

[25] T. Agou, N. Hayakawa, T. Sasamori, T. Matsuo, D. Hashizume, N. Tokitoh, *Chem. Eur. J.* **2014**, *20*, 9246–9249.

[26] A. Sekiguchi, R. Kinjo, M. Ichinohe, *Science* **2004**, *305*, 1755–1757.

[27] N. Wiberg, S. K. Vasisht, G. Fischer, P. Mayer, *Z. Anorg. Allg. Chem.* **2004**, *630*, 1823–1828.

[28] T. Sasamori, K. Hironaka, Y. Sugiyama, N. Takagi, S. Nagase, Y. Hosoi, Y. Furukawa, N. Tokitoh, *J. Am. Chem. Soc.* **2008**, *130*, 13856–13857.

[29] Y. Murata, M. Ichinohe, A. Sekiguchi, *J. Am. Chem. Soc.* **2010**, *132*, 16768–16770.

[30] S. Ishida, R. Sugawara, Y. Misawa, T. Iwamoto, *Angew. Chem. Int. Ed.* **2013**, *52*, 12869–12873; *Angew. Chem.* **2013**, *125*, 13107–13111.

[31] M. Asay, A. Sekiguchi, *Bull. Chem. Soc. Jpn.* **2012**, *85*, 1245–1261.

[32] N. Wienkenhöfer, 1,2-Dibromodisilenes: A Rich Soure for Titanium Silylidyne Complexes, Acyclic Silylenes and Silyne Dianions, Dissertation, University of Bonn, **2017**.

[33] R. Nishino, M. Minoura, Synthesis and Reaction of the Disilene Dianion Bearing Bulky Aliphatic Substituents, P154 posterpresentation, The 19th International Symposium on Silicon Chemistry (Online ISOS 2021), **2021**.

[34] M. Weidenbruch, S. Willms, W. Saak, G. Henkel, *Angew. Chem. Int. Ed.* **1997**, *36*, 2503–2504; *Angew. Chem.* **1997**, *109*, 2612–2613.

[35] D. Scheschkewitz, *Angew. Chem. Int. Ed.* **2004**, *43*, 2965–2967; *Angew. Chem.* **2004**, *116*, 3025–3028.

[36] K. Abersfelder, A. J. P. White, H. S. Rzepa, D. Scheschkewitz, *Science* **2010**, *327*, 564–566.

[37] H. Tanaka, S. Inoue, M. Ichinohe, M. Driess, A. Sekiguchi, *Organometallics* **2011**, *30*, 3475–3478.

[38] K. Suzuki, T. Matsuo, D. Hashizume, H. Fueno, K. Tanaka, K. Tamao, *Science* **2011**, *331*, 1306–1309.

[39] T. Iwamoto, M. Tamura, C. Kabuto, M. Kira, *Science* **2000**, *290*, 504–506.

[40] E. A. Carter, W. A. Goddard, *J. Phys. Chem.* **1986**, *90*, 998–1001.

[41] G. Trinquier, J. P. Malrieu, *J. Am. Chem. Soc.* **1987**, *109*, 5303–5315.

[42] J. P. Malrieu, G. Trinquier, *J. Am. Chem. Soc.* **1989**, *111*, 5916–5921.

[43] M. Driess, H. Grützmacher, *Angew. Chem. Int. Ed.* **1996**, *35*, 828–856; *Angew. Chem.* **1996**, *108*, 900–929.

[44] H. B. Wedler, P. Wendelboe, P. P. Power, *Organometallics* **2018**, *37*, 2929–2936.

[45] Y. Mizuhata, T. Sasamori, N. Tokitoh, *Chem. Rev.* **2009**, *109*, 3479–3511.

[46] M. Haaf, T. A. Schmedake, R. West, *Acc. Chem. Res.* **2000**, *33*, 704–714.

[47] P. Jutzi, D. Kanne, C. Krüger, *Angew. Chem. Int. Ed.* **1986**, *25*, 164–164; *Angew. Chem.* **1986**, *98*, 163–164.

[48] H. H. Karsch, U. Keller, S. Gamper, G. Müller, *Angew. Chem. Int. Ed.* **1990**, *29*, 295–296; *Angew. Chem.* **1990**, *102*, 297–298.

[49] P. Jutzi, A. Mix, B. Rummel, W. W. Schoeller, B. Neumann, H.-G. Stammler, *Science* **2004**, *305*, 849–851.[50] P. Ghana, M. I. Arz, G. Schnakenburg, M. Straßmann, A. C. Filippou, *Organometallics* **2018**, *37*, 772–780.

[51] P. Jutzi, *Chem. Eur. J.* **2014**, *20*, 9192–9207.

[52] M. Denk, R. Lennon, R. Hayashi, R. West, A. V. Belyakov, H. P. Verne, A. Haaland, M. Wagner, N. Metzler, *J. Am. Chem. Soc.* **1994**, *116*, 2691–2692.

[53] A. J. Arduengo, R. L. Harlow, M. Kline, *J. Am. Chem. Soc.* **1991**, *113*, 361–363.

[54] M. Kira, S. Ishida, T. Iwamoto, C. Kabuto, *J. Am. Chem. Soc.* **1999**, *121*, 9722–9723.

[55] M. Driess, S. Yao, M. Brym, C. van Wüllen, D. Lentz, *J. Am. Chem. Soc.* **2006**, *128*, 9628–9629.

[56] T. Kosai, S. Ishida, T. Iwamoto, *Angew. Chem. Int. Ed.* **2016**, *55*, 15554–15558; *Angew. Chem.* **2016**, *128*, 15783–15787.

[57] V. Lavallo, Y. Canac, C. Präsang, B. Donnadieu, G. Bertrand, *Angew. Chem. Int. Ed.* **2005**, *44*, 5705–5709; *Angew. Chem.* **2005**, *117*, 5851–5855.

[58] A. V. Protchenko, K. H. Birjkumar, D. Dange, A. D. Schwarz, D. Vidovic, C. Jones, N. Kaltsoyannis, P. Mountford, S. Aldridge, *J. Am. Chem. Soc.* **2012**, *134*, 6500–6503.

[59] B. D. Rekken, T. M. Brown, J. C. Fettinger, H. M. Tuononen, P. P. Power, *J. Am. Chem. Soc.* **2012**, *134*, 6504–6507.

[60] A. C. Filippou, B. Baars, O. Chernov, Y. N. Lebedev, G. Schnakenburg, *Angew. Chem. Int. Ed.* **2014**, *53*, 565–570; *Angewandte Chemie* **2014**, *126*, 576–581.

[61] Y. K. Loh, L. Ying, M. Ángeles Fuentes, D. C. H. Do, S. Aldridge, *Angew. Chem. Int. Ed.* **2019**, *58*, 4847–4851; *Angew. Chem.* **2019**, *131*, 4901–4905.

[62] D. Reiter, R. Holzner, A. Porzelt, P. J. Altmann, P. Frisch, S. Inoue, *J. Am. Chem. Soc.* **2019**, *141*, 13536–13546.

[63] A. Hinz, *Angew. Chem. Int. Ed.* **2020**, *59*, 19065–19069; *Angew. Chem.* **2020**, *132*, 19227–19231.

[64] R. C. Fischer, P. P. Power, *Chem. Rev.* **2010**, *110*, 3877–3923.

[65] C.-W. So, H. W. Roesky, J. Magull, R. B. Oswald, *Angew. Chem. Int. Ed.* **2006**, *45*, 3948–3950; *Angew. Chem.* **2006**, *118*, 4052–4054.

[66] S. S. Sen, S. Khan, P. P. Samuel, H. W. Roesky, *Chem. Sci.* **2012**, *3*, 659–682.

[67] D. Gau, T. Kato, N. Saffon-Merceron, F. P. Cossío, A. Baceiredo, *J. Am. Chem. Soc.* **2009**, *131*, 8762–8763.

[68] R. S. Ghadwal, H. W. Roesky, S. Merkel, J. Henn, D. Stalke, *Angew. Chem. Int. Ed.* **2009**, *48*, 5683–5686; *Angew. Chem.* **2009**, *121*, 5793–5796.

[69] A. C. Filippou, O. Chernov, G. Schnakenburg, *Angew. Chem. Int. Ed.* **2009**, *48*, 5687–5690; *Angew. Chem.* **2009**, *121*, 5797–5800.

[70] A. C. Filippou, Y. N. Lebedev, O. Chernov, M. Straßmann, G. Schnakenburg, *Angew. Chem. Int. Ed.* **2013**, *52*, 6974–6978; *Angew. Chem.* **2013**, *125*, 7112–7116.

[71] A. C. Filippou, O. Chernov, G. Schnakenburg, *Chem. Eur. J.* **2011**, *17*, 13574–13583.

[72] O. Chernov, Novel Molecular Si(II) Precursors for Synthesis of the First Compounds with Metal-Silicon-Triple Bonds, Dissertation, University of Bonn, **2012**.

[73] D. Martin, M. Melaimi, M. Soleilhavoup, G. Bertrand, *Organometallics* **2011**, *30*, 5304–5313.

[74] H. W. Roesky, *J. Organomet. Chem.* **2013**, *730*, 57–62.

[75] D. Scheschkewitz, Ed. , *Functional Molecular Silicon Compounds II*, Springer International Publishing, Cham, **2014**.

[76] G. Frenking, M. Hermann, D. M. Andrada, N. Holzmann, *Chem. Soc. Rev.* **2016**, *45*, 1129–1144.

[77] S. Würtemberger-Pietsch, U. Radius, T. B. Marder, *Dalton Trans.* **2016**, *45*, 5880–5895.

[78] V. Nesterov, D. Reiter, P. Bag, P. Frisch, R. Holzner, A. Porzelt, S. Inoue, *Chem. Rev.* **2018**, *118*, 9678–9842.

[79] S. Khan, H. W. Roesky, *Chem. Eur. J.* **2019**, *25*, 1636–1648.

[80] A. C. Filippou, O. Chernov, B. Blom, K. W. Stumpf, G. Schnakenburg, *Chem. Eur. J.* **2010**, *16*, 2866–2872.

[81] H. Cui, C. Cui, *Dalton Trans.* **2011**, *40*, 11937.

[82] S. M. I. Al-Rafia, R. McDonald, M. J. Ferguson, E. Rivard, *Chem. Eur. J.* **2012**, *18*, 13810–13820.

[83] Alain. Igau, Hansjorg. Grutzmacher, Antoine. Baceiredo, Guy. Bertrand, *J. Am. Chem. Soc.* **1988**, *110*, 6463–6466.

[84] A. Igau, A. Baceiredo, G. Trinquier, G. Bertrand, *Angew. Chem. Int. Ed.* **1989**, *28*, 621–622; *Angew. Chem.* **1989**, *101*, 617–618.

[85] M. N. Hopkinson, C. Richter, M. Schedler, F. Glorius, *Nature* **2014**, *510*, 485–496.

[86] K. M. Hindi, M. J. Panzner, C. A. Tessier, C. L. Cannon, W. J. Youngs, *Chem. Rev.* **2009**, *109*, 3859–3884.

[87] L. Mercs, M. Albrecht, *Chem. Soc. Rev.* **2010**, *39*, 1903.

[88] A. V. Zhukhovitskiy, M. J. MacLeod, J. A. Johnson, *Chem. Rev.* **2015**, *115*, 11503–11532.

[89] C. D. Martin, M. Soleilhavoup, G. Bertrand, *Chem. Sci.* **2013**, *4*, 3020.

[90] R. S. Ghadwal, R. Azhakar, H. W. Roesky, *Acc. Chem. Res.* **2013**, *46*, 444–456.

[91] Y. Wang, G. H. Robinson, *Inorg. Chem.* **2014**, *53*, 11815–11832.

[92] S. Roy, K. C. Mondal, H. W. Roesky, *Acc. Chem. Res.* **2016**, *49*, 357–369.

[93] R. Jazzar, M. Soleilhavoup, G. Bertrand, *Chem. Rev.* **2020**, *120*, 4141–4168.

[94] J. Morvan, M. Mauduit, G. Bertrand, R. Jazzar, *ACS Catal.* **2021**, *11*, 1714–1748.

[95] M. Soleilhavoup, G. Bertrand, *Acc. Chem. Res.* **2015**, *48*, 256–266.

[96] K. Chandra Mondal, S. Roy, H. W. Roesky, *Chem. Soc. Rev.* **2016**, *45*, 1080–1111.

[97] M. Melaimi, R. Jazzar, M. Soleilhavoup, G. Bertrand, *Angew. Chem. Int. Ed.* **2017**, *56*, 10046–10068; *Angew. Chem.* **2017**, *129*, 10180–10203.

[98] S. Kundu, S. Sinhababu, V. Chandrasekhar, H. W. Roesky, *Chem. Sci.* **2019**, *10*, 4727–4741.

[99] V. Lavallo, Y. Canac, B. Donnadieu, W. W. Schoeller, G. Bertrand, *Angew. Chem. Int. Ed.* **2006**, *45*, 3488–3491; *Angew. Chem.* **2006**, *118*, 3568–3571.

[100] G. D. Frey, V. Lavallo, B. Donnadieu, W. W. Schoeller, G. Bertrand, *Science* **2007**, *316*, 439–441.

[101] V. Lavallo, Y. Canac, A. DeHope, B. Donnadieu, G. Bertrand, *Angew. Chem. Int. Ed.* **2005**, *44*, 7236–7239; *Angew. Chem.* **2005**, *117*, 7402–7405.

[102] K. Denk, P. Sirsch, W. A. Herrmann, *J. Organomet. Chem.* **2002**, *649*, 219–224.

[103] C. A. Tolman, *Chem. Rev.* **1977**, *77*, 313–348.

[104] O. Back, M. Henry-Ellinger, C. D. Martin, D. Martin, G. Bertrand, *Angew. Chem. Int. Ed.* **2013**, *52*, 2939–2943; *Angew. Chem.* **2013**, *125*, 3011–3015.

[105] R. R. Rodrigues, C. L. Dorsey, C. A. Arceneaux, T. W. Hudnall, *Chem. Commun.* **2014**, *50*, 162–164.

[106] A. Liske, K. Verlinden, H. Buhl, K. Schaper, C. Ganter, *Organometallics* **2013**, *32*, 5269–5272.

[107] K. Verlinden, H. Buhl, W. Frank, C. Ganter, *Eur. J. Inorg. Chem.* **2015**, *2015*, 2416–2425.

[108] K. C. Mondal, S. Roy, B. Maity, D. Koley, H. W. Roesky, *Inorg. Chem.* **2016**, *55*, 163–169.

[109] D. Himmel, I. Krossing, A. Schnepf, *Angew. Chem. Int. Ed.* **2014**, *53*, 370–374; *Angew. Chem.* **2014**, *126*, 378–382.

[110] G. Frenking, *Angew. Chem. Int. Ed.* **2014**, *53*, 6040–6046; *Angew. Chem.* **2014**, *126*, 6152–6158.

[111] D. Himmel, I. Krossing, A. Schnepf, *Angew. Chem. Int. Ed.* **2014**, *53*, 6047–6048; *Angew. Chem.* **2014**, *126*, 6159–6160.

[112] L. Zhao, M. Hermann, N. Holzmann, G. Frenking, *Coord. Chem. Rev.* **2017**, *344*, 163–204.

[113] A. Nandi, S. Kozuch, *Chem. Eur. J.* **2020**, *26*, 759–772.

[114] Y. Wang, Y. Xie, P. Wei, R. B. King, H. F. Schaefer, P. von R. Schleyer, G. H. Robinson, *Science* **2008**, *321*, 1069–1071.

[115] K. C. Mondal, P. P. Samuel, H. W. Roesky, R. R. Aysin, L. A. Leites, S. Neudeck, J. Lübben, B. Dittrich, N. Holzmann, M. Hermann, G. Frenking, *J. Am. Chem. Soc.* **2014**, *136*, 8919–8922.

[116] K. Chandra Mondal, S. Roy, B. Dittrich, B. Maity, S. Dutta, D. Koley, S. K. Vasa, R. Linser, S. Dechert, H. W. Roesky, *Chem. Sci.* **2015**, *6*, 5230–5234.

[117] D. Geiß, M. I. Arz, M. Straßmann, G. Schnakenburg, A. C. Filippou, *Angew. Chem. Int. Ed.* **2015**, *54*, 2739–2744; *Angew. Chem.* **2015**, *127*, 2777–2782.

[118] P. Ghana, M. I. Arz, U. Das, G. Schnakenburg, A. C. Filippou, *Angew. Chem. Int. Ed.* **2015**, *54*, 9980–9985; *Angew. Chem.* **2015**, *127*, 10118–10123.

[119] K. C. Mondal, H. W. Roesky, M. C. Schwarzer, G. Frenking, B. Niepötter, H. Wolf, R. Herbst-Irmer, D. Stalke, *Angew. Chem. Int. Ed.* **2013**, *52*, 2963–2967; *Angew. Chem.* **2013**, *125*, 3036–3040.

[120] S. Roy, K. C. Mondal, L. Krause, P. Stollberg, R. Herbst-Irmer, D. Stalke, J. Meyer, A. C. Stückl, B. Maity, D. Koley, S. K. Vasa, S. Q. Xiang, R. Linser, H. W. Roesky, *J. Am. Chem. Soc.* **2014**, *136*, 16776–16779.

[121] Y. Li, Y.-C. Chan, Y. Li, I. Purushothaman, S. De, P. Parameswaran, C.-W. So, *Inorg. Chem.* **2016**, *55*, 9091–9098.

[122] K. C. Mondal, H. W. Roesky, M. C. Schwarzer, G. Frenking, I. Tkach, H. Wolf, D. Kratzert, R. Herbst-Irmer, B. Niepötter, D. Stalke, *Angew. Chem. Int. Ed.* **2013**, *52*, 1801–1805; *Angew. Chem.* **2013**, *125*, 1845–1850.

[123] K. C. Mondal, S. Roy, B. Dittrich, D. M. Andrada, G. Frenking, H. W. Roesky, *Angew. Chem. Int. Ed.* **2016**, *55*, 3158–3161; *Angew. Chem.* **2016**, *128*, 3210–3213.

[124] M. M. Siddiqui, S. Sinhababu, S. Dutta, S. Kundu, P. N. Ruth, A. Münch, R. Herbst-Irmer, D. Stalke, D. Koley, H. W. Roesky, *Angew. Chem. Int. Ed.* **2018**, *57*, 11776–11780; *Angew. Chem.* **2018**, *130*, 11950–11954.

[125] L. Zborovsky, R. Dobrovetsky, M. Botoshansky, D. Bravo-Zhivotovskii, Y. Apeloig, *J. Am. Chem. Soc.* **2012**, *134*, 18229–18232.

[126] D. Pinchuk, J. Mathew, A. Kaushansky, D. Bravo-Zhivotovskii, Y. Apeloig, *Angew. Chem. Int. Ed.* **2016**, *55*, 10258–10262; *Angew. Chem.* **2016**, *128*, 10414–10418.

[127] M. I. Arz, D. Geiß, M. Straßmann, G. Schnakenburg, A. C. Filippou, *Chem. Sci.* **2015**, *6*, 6515–6524.

[128] K. C. Mondal, H. W. Roesky, B. Dittrich, N. Holzmann, M. Hermann, G. Frenking, A. Meents, *J. Am. Chem. Soc.* **2013**, *135*, 15990–15993.

[129] C. Mohapatra, S. Kundu, A. N. Paesch, R. Herbst-Irmer, D. Stalke, D. M. Andrada, G. Frenking, H. W. Roesky, *J. Am. Chem. Soc.* **2016**, *138*, 10429–10432.

[130] S. Kundu, P. P. Samuel, A. Luebben, D. M. Andrada, G. Frenking, B. Dittrich, H. W. Roesky, *Dalton Trans.* **2017**, *46*, 7947–7952.

[131] Y. Liu, H. Keil, Z. Yang, R. Herbst-Irmer, H. W. Roesky, D. Stalke, *Eur. J. Inorg. Chem.* **2020**, *2020*, 2273–2278.

[132] M. I. Arz, M. Straßmann, A. Meyer, G. Schnakenburg, O. Schiemann, A. C. Filippou, *Chem. Eur. J.* **2015**, *21*, 12509–12516.

[133] M. I. Arz, G. Schnakenburg, A. Meyer, O. Schiemann, A. C. Filippou, *Chem. Sci.* **2016**, *7*, 4973–4979.[134] Y. Li, Y.-C. Chan, B.-X. Leong, Y. Li, E. Richards, I. Purushothaman, S. De, P. Parameswaran, C.-W. So, *Angew. Chem. Int. Ed.* **2017**, *56*, 7573–7578; *Angew. Chem.* **2017**, *129*, 7681–7686.

[135] F. Gstrein, U. Das, M. Straßmann, A. C. Filippou, Reactions of $SiBr_2(CAAC^{Me})$ with Nucleophiles, Anglo-German Inorganic Chemistry Conference (AGICHEM 2017), University of Göttingen, **2017**.

[136] S. Roy, P. Stollberg, R. Herbst-Irmer, D. Stalke, D. M. Andrada, G. Frenking, H. W. Roesky, *J. Am. Chem. Soc.* **2015**, *137*, 150–153.

[137] W. Li, C. Köhler, Z. Yang, D. Stalke, R. Herbst-Irmer, H. W. Roesky, *Chem. Eur. J.* **2018**, 1193–1197.

[138] S. Sinhababu, S. Kundu, A. N. Paesch, R. Herbst-Irmer, D. Stalke, I. Fernández, G. Frenking, A. C. Stückl, B. Schwederski, W. Kaim, H. W. Roesky, *Chem. Eur. J.* **2018**, *24*, 1264–1268.

[139] K. C. Mondal, P. P. Samuel, M. Tretiakov, A. P. Singh, H. W. Roesky, A. C. Stückl, B. Niepötter, E. Carl, H. Wolf, R. Herbst-Irmer, D. Stalke, *Inorg. Chem.* **2013**, *52*, 4736–4743.

[140] S. Kundu, P. P. Samuel, S. Sinhababu, A. V. Luebben, B. Dittrich, D. M. Andrada, G. Frenking, A. C. Stückl, B. Schwederski, A. Paretzki, W. Kaim, H. W. Roesky, *J. Am. Chem. Soc.* **2017**, *139*, 11028–11031.

[141] S. Sinhababu, S. Kundu, M. M. Siddiqui, A. N. Paesch, R. Herbst-Irmer, B. Schwederski, P. Saha, L. Zhao, G. Frenking, W. Kaim, D. Stalke, H. W. Roesky, *Chem. Commun.* **2019**, *55*, 4534–4537.

[142] K. C. Mondal, B. Dittrich, B. Maity, D. Koley, H. W. Roesky, *J. Am. Chem. Soc.* **2014**, *136*, 9568–9571.

[143] A. Schulz, *Dalton Trans.* **2018**, *47*, 12827–12837.

[144] C. Plett, Synthese Und Reaktivität Niedervalenter Siliziumverbindungen Mit Cyclischen Alkylaminocarbenen, Bachelorarbeit, University of Bonn, **2019**.

[145] W. Li, S. Kundu, C. Köhler, J. Li, S. Dutta, Z. Yang, D. Stalke, R. Herbst-Irmer, A. C. Stückl, B. Schwederski, D. Koley, W. Kaim, H. W. Roesky, *Organometallics* **2019**, *38*, 1939–1945.

[146] K. C. Mondal, H. W. Roesky, A. C. Stückl, F. Ehret, W. Kaim, B. Dittrich, B. Maity, D. Koley, *Angew. Chem. Int. Ed.* **2013**, *52*, 11804–11807; *Angew. Chem.* **2013**, *125*, 12020–12023.

[147] K. C. Mondal, P. P. Samuel, H. W. Roesky, B. Niepötter, R. Herbst-Irmer, D. Stalke, F. Ehret, W. Kaim, B. Maity, D. Koley, *Chem. Eur. J.* **2014**, *20*, 9240–9245.

[148] Z. R. Turner, J.-C. Buffet, *Dalton Trans.* **2015**, *44*, 12985–12989.

[149] Z. R. Turner, *Chem. Eur. J.* **2016**, *22*, 11461–11468.

[150] J.-S. Huang, W.-H. Lee, C.-T. Shen, Y.-F. Lin, Y.-H. Liu, S.-M. Peng, C.-W. Chiu, *Inorg. Chem.* **2016**, *55*, 12427–12434.

[151] B. Li, S. Kundu, A. C. Stückl, H. Zhu, H. Keil, R. Herbst-Irmer, D. Stalke, B. Schwederski, W. Kaim, D. M. Andrada, G. Frenking, H. W. Roesky, *Angew. Chem. Int. Ed.* **2017**, *56*, 397–400; *Angew. Chem.* **2017**, *129*, 407–411.

[152] M. M. Siddiqui, S. K. Sarkar, S. Sinhababu, P. N. Ruth, R. Herbst-Irmer, D. Stalke, M. Ghosh, M. Fu, L. Zhao, D. Casanova, G. Frenking, B. Schwederski, W. Kaim, H. W. Roesky, *J. Am. Chem. Soc.* **2019**, *141*, 1908–1912.

[153] O. Back, M. A. Celik, G. Frenking, M. Melaimi, B. Donnadieu, G. Bertrand, *J. Am. Chem. Soc.* **2010**, *132*, 10262–10263.

[154] R. Kretschmer, D. A. Ruiz, C. E. Moore, A. L. Rheingold, G. Bertrand, *Angew. Chem. Int. Ed.* **2014**, *53*, 8176–8179; *Angew. Chem.* **2014**, *126*, 8315–8318.

[155] S. Kundu, R. Yadav, S. Sinhababu, R. Yadav, *Dalton Trans.* **2022**, *51*, 2170–2202.

[156] A. Sidiropoulos, C. Jones, A. Stasch, S. Klein, G. Frenking, *Angew. Chem. Int. Ed.* **2009**, *48*, 9701–9704; *Angew. Chem.* **2009**, *121*, 9881–9884.

[157] C. Jones, A. Sidiropoulos, N. Holzmann, G. Frenking, A. Stasch, *Chem. Commun.* **2012**, *48*, 9855.

[158] D. C. Georgiou, B. D. Stringer, C. F. Hogan, P. J. Barnard, D. J. D. Wilson, N. Holzmann, G. Frenking, J. L. Dutton, *Chem. Eur. J.* **2015**, *21*, 3377–3386.

[159] L. Jin, M. Melaimi, L. L. Liu, G. Bertrand, *Org. Chem. Front.* **2014**, *1*, 351–354.

[160] Y. Li, K. C. Mondal, P. P. Samuel, H. Zhu, C. M. Orben, S. Panneerselvam, B. Dittrich, B. Schwederski, W. Kaim, T. Mondal, D. Koley, H. W. Roesky, *Angew. Chem. Int. Ed.* **2014**, *53*, 4168–4172; *Angew. Chem.* **2014**, *126*, 4252–4256.

[161] Y. Li, K. C. Mondal, H. W. Roesky, H. Zhu, P. Stollberg, R. Herbst-Irmer, D. Stalke, D. M. Andrada, *J. Am. Chem. Soc.* **2013**, *135*, 12422–12428.

[162] M. Arrowsmith, H. Braunschweig, M. A. Celik, T. Dellermann, R. D. Dewhurst, W. C. Ewing, K. Hammond, T. Kramer, I. Krummenacher, J. Mies, K. Radacki, J. K. Schuster, *Nature Chem* **2016**, *8*, 890–894.

[163] H. Braunschweig, R. D. Dewhurst, K. Hammond, J. Mies, K. Radacki, A. Vargas, *Science* **2012**, *336*, 1420–1422.

[164] G. Frenking, N. Holzmann, *Science* **2012**, *336*, 1394–1395.

[165] J. Böhnke, H. Braunschweig, W. C. Ewing, C. Hörl, T. Kramer, I. Krummenacher, J. Mies, A. Vargas, *Angew. Chem. Int. Ed.* **2014**, *53*, 9082–9085; *Angew. Chem.* **2014**, *126*, 9228–9231.

[166] J. Böhnke, H. Braunschweig, T. Dellermann, W. C. Ewing, K. Hammond, J. O. C. Jimenez-Halla, T. Kramer, J. Mies, *Angew. Chem. Int. Ed.* **2015**, *54*, 13801–13805; *Angew. Chem.* **2015**, *127*, 14006–14010.

[167] J. Böhnke, H. Braunschweig, P. Constantinidis, T. Dellermann, W. C. Ewing, I. Fischer, K. Hammond, F. Hupp, J. Mies, H.-C. Schmitt, A. Vargas, *J. Am. Chem. Soc.* **2015**, *137*, 1766–1769.

[168] M. Arrowsmith, J. Böhnke, H. Braunschweig, M. A. Celik, T. Dellermann, K. Hammond, *Chem. Eur. J.* **2016**, *22*, 17169–17172.

[169] Y. Wang, Y. Xie, P. Wei, R. B. King, H. F. Schaefer, P. v. R. Schleyer, G. H. Robinson, *J. Am. Chem. Soc.* **2008**, *130*, 14970–14971.

[170] O. Back, B. Donnadieu, P. Parameswaran, G. Frenking, G. Bertrand, *Nature Chem* **2010**, *2*, 369–373.

[171] M. Abraham, Y. Wang, Y. Xie, P. Wei, H. Schaefer, P. von R. Schleyer, G. Robinson, *Chem. Eur. J.* **2010**, *16*, 432–435.

[172] K. M. Melancon, M. B. Gildner, T. W. Hudnall, *Chem. Eur. J.* **2018**, *24*, 9264–9268.

[173] A. Aprile, R. Corbo, K. Vin Tan, D. J. D. Wilson, J. L. Dutton, *Dalton Trans.* **2014**, *43*, 764–768.

[174] R. Kinjo, B. Donnadieu, G. Bertrand, *Angew. Chem. Int. Ed.* **2010**, *49*, 5930–5933; *Angew. Chem.* **2010**, *122*, 6066–6069.

[175] U. Das, Reversible Coordination of $SiBr_2(caac^{Me})$ to $caac^{Me}$ and Its Conversion to Potassium Silenide $SiK(Tbb)(caac^{Me})$, manuscript, University of Bonn, **2019**.

[176] J. I. Schweizer, A. G. Sturm, T. Porsch, M. Berger, M. Bolte, N. Auner, M. C. Holthausen, *Z. Anorg. Allg. Chem.* **2018**, *644*, 982–988.

[177] A. Michalak, M. Mitoraj, T. Ziegler, *J. Phys. Chem. A* **2008**, *112*, 1933–1939.

[178] M. Radoń, *Theor Chem Account* **2008**, *120*, 337–339.

[179] M. P. Mitoraj, A. Michalak, T. Ziegler, *J. Chem. Theory Comput.* **2009**, *5*, 962–975.

[180] T. J. Hadlington, J. A. B. Abdalla, R. Tirfoin, S. Aldridge, C. Jones, *Chem. Commun.* **2016**, *52*, 1717–1720.

[181] S. Schwarzwald, Disilavinylidene Chemistry and Synthesis and Reactivty of Bisaryloxy-Silylenes, Dissertation, University of Bonn, **2022**.

[182] A. C. Filippou, B. Baars, O. Chernov, Y. N. Lebedev, G. Schnakenburg, *Angew. Chem. Int. Ed.* **2014**, *53*, 565–570; *Angew. Chem.* **2014**, *126*, 576–581.

[183] P. Ghana, M. I. Arz, U. Chakraborty, G. Schnakenburg, A. C. Filippou, *J. Am. Chem. Soc.* **2018**, *140*, 7187–7198.

[184] H. Ottosson, A. M. Eklöf, *Coord. Chem. Rev.* **2008**, *252*, 1287–1314.

[185] I. Hargittai, G. Schultz, J. Tremmel, N. D. Kagramanov, A. K. Maltsev, O. M. Nefedov, *J. Am. Chem. Soc.* **1983**, *105*, 2895–2896.

[186] R. West, J. D. Cavalieri, J. J. Buffy, C. Fry, K. W. Zilm, J. C. Duchamp, M. Kira, T. Iwamoto, T. Müller, Y. Apeloig, *J. Am. Chem. Soc.* **1997**, *119*, 4972–4976.

[187] Y. Apeloig, M. Karni, *J. Am. Chem. Soc.* **1984**, *106*, 6676–6682.

[188] H. Ottosson, *Chem. Eur. J.* **2003**, *9*, 4144–4155.

[189] S. Honda, Y. Kato, S. Ishida, T. Iwamoto, *Chem. Lett.* **2021**, *50*, 866–869.

[190] C. Dugave, L. Demange, *Chem. Rev.* **2003**, *103*, 2475–2532.

[191] D. H. Waldeck, *Chem. Rev.* **1991**, *91*, 415–436.

[192] H. Sakurai, H. Tobita, M. Kira, Y. Nakadaira, *Angew. Chem. Int. Ed.* **1980**, *19*, 620–620; *Angew. Chem.* **1980**, *92*, 632–632.

[193] M. J. Michalczyk, Robert. West, Josef. Michl, *Organometallics* **1985**, *4*, 826–829.

[194] B. D. Shepherd, D. R. Powell, R. West, *Organometallics* **1989**, *8*, 2664–2669.

[195] M. Kira, S. Ohya, T. Iwamoto, M. Ichinohe, C. Kabuto, *Organometallics* **2000**, *19*, 1817–1819.

[196] L. Zborovsky, A. Kostenko, D. Bravo-Zhivotovskii, Y. Apeloig, *Angew. Chem. Int. Ed.* **2019**, *58*, 14524–14528; *Angew. Chem.* **2019**, *131*, 14666–14670.

[197] *The Chemistry of Organic Silicon Compounds. 2,3*, Wiley, Chichester, **1998**.

[198] B. Tumanskii, M. Karni, Y. Apeloig, in *Organosilicon Compounds*, Elsevier, **2017**, pp. 231–294.

[199] S. S. Sen, A. Jana, H. W. Roesky, C. Schulzke, *Angew. Chem. Int. Ed.* **2009**, *48*, 8536–8538; *Angew. Chem.* **2009**, *121*, 8688–8690.

[200] D. Gau, R. Rodriguez, T. Kato, N. Saffon-Merceron, A. de Cózar, F. P. Cossío, A. Baceiredo, *Angew. Chem. Int. Ed.* **2011**, *50*, 1092–1096; *Angew. Chem.* **2011**, *123*, 1124–1128.

[201] T. Abe, S. Ishida, T. Iwamoto, *BCSJ* **2018**, *91*, 684–686.

[202] S. Inoue, M. Ichinohe, A. Sekiguchi, *J. Am. Chem. Soc.* **2007**, *129*, 6096–6097.

[203] S. Inoue, M. Ichinohe, A. Sekiguchi, *Organometallics* **2008**, *27*, 1358–1360.

[204] R. Kinjo, M. Ichinohe, A. Sekiguchi, *J. Am. Chem. Soc.* **2007**, *129*, 26–27.

[205] M. I. Arz, M. Straßmann, D. Geiß, G. Schnakenburg, A. C. Filippou, *J. Am. Chem. Soc.* **2016**, *138*, 4589–4600.

[206] D. Pinchuk, Y. Kratish, J. Mathew, L. Zborovsky, D. Bravo-Zhivotovskii, B. Tumanskii, Y. Apeloig, *Angew. Chem. Int. Ed.* **2019**, *58*, 7435–7439; *Angew. Chem.* **2019**, *131*, 7513–7517.

[207] D. S. Viswanath, Ed. , *Viscosity of Liquids: Theory, Estimation, Experiment, and Data*, Springer, Dordrecht, **2007**.

[208] S. Inoue, C. Eisenhut, *J. Am. Chem. Soc.* **2013**, *135*, 18315–18318.

[209] H. Tanaka, M. Ichinohe, A. Sekiguchi, *Chem. Lett.* **2008**, *37*, 1246–1247.

[210] S. Ozaki, T. Sasamori, N. Tokitoh, *Organometallics* **2008**, *27*, 2163–2165.

[211] P. P. Power, *Chem. Rev.* **2003**, *103*, 789–810.

[212] O. Back, B. Donnadieu, M. von Hopffgarten, S. Klein, R. Tonner, G. Frenking, G. Bertrand, *Chem. Sci.* **2011**, *2*, 858.

[213] P. Agarwal, N. A. Piro, K. Meyer, P. Müller, C. C. Cummins, *Angew. Chem. Int. Ed.* **2007**, *46*, 3111–3114; *Angew. Chem.* **2007**, *119*, 3171–3174.

[214] S. Ishida, F. Hirakawa, T. Iwamoto, *J. Am. Chem. Soc.* **2011**, *133*, 12968–12971.

[215] V. Nesterov, N. C. Breit, S. Inoue, *Chem. Eur. J.* **2017**, *23*, 12014–12039.

[216] E. Niecke, E. Klein, M. Nieger, *Angew. Chem. Int. Ed.* **1989**, *28*, 751–752; *Angew. Chem.* **1989**, *101*, 792–793.

[217] D. Lange, E. Klein, H. Bender, E. Niecke, M. Nieger, R. Pietschnig, W. W. Schoeller, H. Ranaivonjatovo, *Organometallics* **1998**, *17*, 2425–2432.

[218] D. Geiß, Neue Synthesestrategien Für Übergangsmetallkomplexe Mit Ungesättigter Germanium- Und Siliziumbasierter Ligandensphäre, Dissertation, University of Bonn, **2015**.

[219] M. J. S. Gynane, A. Hudson, M. F. Lappert, P. P. Power, H. Goldwhite, *J. Chem. Soc., Dalton Trans.* **1980**, 2428–2433.

[220] B. Çetinkaya, A. Hudson, M. F. Lappert, H. Goldwhite, *J. Chem. Soc., Chem. Commun.* **1982**, *0*, 609–610.

[221] R. Fleischer, Theoretische Studien Zu Carben Stabilisierten Silizium(I)-Verbindungen, Bachelorarbeit, University of Bonn, **2020**.

[222] L. Salem, J. Durup, G. Bergeron, D. Cazes, X. Chapuisat, H. Kagan, *J. Am. Chem. Soc.* **1970**, *92*, 4472–4474.

[223] L. Salem, *Acc. Chem. Res.* **1971**, *4*, 322–328.

[224] M. I. Arz, Molekulare Si(0)-Und Si(I) Verbindungen: Synthese, Struktur Und Reaktivität, Dissertation, University of Bonn, **2015**.

[225] S. P. Mallela, I. Bernal, R. A. Geanangel, *Inorg. Chem.* **1992**, *31*, 1626–1627.

[226] T. Sato, Y. Mizuhata, N. Tokitoh, *Chem. Commun.* **2010**, *46*, 4402.

[227] J. Bruckmann, C. Krüger, *Acta Cryst.* **1997**, *53*, 1845–1846.

[228] D. Scheschkewitz, *Chem. Lett.* **2011**, *40*, 2–11.

[229] C. Marschner, in *Organosilicon Compounds*, Elsevier, **2017**, pp. 295–360.

[230] M. Ichinohe, K. Sanuki, S. Inoue, A. Sekiguchi, *Organometallics* **2004**, *23*, 3088–3090.

[231] M. Ichinohe, K. Sanuki, S. Inoue, A. Sekiguchi, *Silicon Chem.* **2007**, *3*, 111–116.

[232] S. Inoue, M. Ichinohe, A. Sekiguchi, *Chem. Lett.* **2005**, *34*, 1564–1565.

[233] T. Iwamoto, M. Kobayashi, K. Uchiyama, S. Sasaki, S. Nagendran, H. Isobe, M. Kira, *J. Am. Chem. Soc.* **2009**, *131*, 3156–3157.

[234] T. Yamaguchi, M. Ichinohe, A. Sekiguchi, *New J. Chem.* **2010**, *34*, 1544.

[235] P. Willmes, M. J. Cowley, M. Hartmann, M. Zimmer, V. Huch, D. Scheschkewitz, *Angew. Chem. Int. Ed.* **2014**, *53*, 2216–2220.

[236] N. Akasaka, K. Fujieda, E. Garoni, K. Kamada, H. Matsui, M. Nakano, T. Iwamoto, *Organometallics* **2018**, *37*, 172–175.

[237] M. J. Cowley, K. Abersfelder, A. J. P. White, M. Majumdar, D. Scheschkewitz, *Chem. Commun.* **2012**, *48*, 6595.

[238] A. Rammo, I. Bejan, A. Meltzer, K. Radacki, H. Braunschweig, D. Scheschkewitz, *Aust. J. Chem.* **2013**, *66*, 1311.

[239] K. Abersfelder, H. Zhao, A. J. P. White, C. Praesang, D. Scheschkewitz, *Z. Anorg. Allg. Chem.* **2015**, *641*, 2051–2055.

[240] M. Majumdar, I. Omlor, C. B. Yildiz, A. Azizoglu, V. Huch, D. Scheschkewitz, *Angew. Chem. Int. Ed.* **2015**, *54*, 8746–8750; *Angew. Chem.* **2015**, *127*, 8870–8874.

[241] P. K. Majhi, V. Huch, D. Scheschkewitz, *Angew. Chem. Int. Ed.* **2021**, *60*, 242–246; *Angew. Chem.* **2021**, *133*, 246–250.

[242] Y. Kratish, D. Pinchuk, A. Kaushansky, V. Molev, B. Tumanskii, D. Bravo-Zhivotovskii, Y. Apeloig, *Angew. Chem. Int. Ed.* **2019**, *58*, 18849–18853; *Angew. Chem.* **2019**, *131*, 7513–7517.

[243] D. M. Jenkins, W. Teng, U. Englich, D. Stone, K. Ruhlandt-Senge, *Organometallics* **2001**, *20*, 4600–4606.

[244] A. G. Brook, F. Abdesaken, G. Gutekunst, N. Plavac, *Organometallics* **1982**, *1*, 994–998.

[245] K. M. Baines, A. G. Brook, R. R. Ford, P. D. Lickiss, A. K. Saxena, W. J. Chatterton, J. F. Sawyer, B. A. Behnam, *Organometallics* **1989**, *8*, 693–709.

[246] P. Jutzi, K. Leszczyńska, A. Mix, B. Neumann, B. Rummel, W. Schoeller, H.-G. Stammler, *Organometallics* **2010**, *29*, 4759–4761.

[247] A. Jana, V. Huch, D. Scheschkewitz, *Angew. Chem. Int. Ed.* **2013**, *52*, 12179–12182; *Angew. Chem.* **2013**, *125*, 12401–12404.

[248] A. Jana, M. Majumdar, V. Huch, M. Zimmer, D. Scheschkewitz, *Dalton Trans.* **2014**, *43*, 5175–5181.

[249] M. Igarashi, M. ıchinohe, A. Sekiguchi, *Heteroatom Chem.* **2008**, *19*, 649–653.

[250] J. Z. Xiong, D. Jiang, C. E. Dixon, K. M. Baines, T. K. Sham, *Can. J. Chem.* **1996**, *74*, 2229–2239.

[251] T. Yamaguchi, A. Sekiguchi, M. Driess, *J. Am. Chem. Soc.* **2010**, *132*, 14061–14063.

[252] A. Rit, J. Campos, H. Niu, S. Aldridge, *Nat. Chem.* **2016**, *8*, 1022–1026.

[253] S. Karwasara, L. R. Maurer, B. Peerless, G. Schnakenburg, U. Das, A. C. Filippou, *J. Am. Chem. Soc.* **2021**, *143*, 14780–14794.

[254] M. Lein, A. Krapp, G. Frenking, *J. Am. Chem. Soc.* **2005**, *127*, 6290–6299.

[255] M. M. Gallo, T. P. Hamilton, H. F. Schaefer, *J. Am. Chem. Soc.* **1990**, *112*, 8714–8719.

[256] H. Lee, J. H. Baraban, R. W. Field, J. F. Stanton, *J. Phys. Chem. A* **2013**, *117*, 11679–11683.

[257] A. J. Boone, D. H. Magers, J. Leszczyński, *Int. J. Quant. Chem.* **1998**, *70*, 925–932.

[258] P. O'Leary, J. R. Thomas, H. F. Schaefer, B. J. Duke, B. O'Leary, *Int. J. Quantum Chem.* **1995**, *56*, 593–604.

[259] P. P. Power, *Organometallics* **2007**, *26*, 4362–4372.

[260] H. K. Brody, D. H. Magers, J. Leszczyński, *Struct. Chem.* **1995**, *6*, 293–300.

[261] S. Nagase, K. Kobayashi, N. Takagi, *J. Organomet. Chem.* **2000**, *611*, 264–271.

[262] M. Bogey, H. Bolvin, C. Demuynck, J. Destombes, *Phys. Rev. Lett.* **1991**, *66*, 413–416.

[263] M. Cordonnier, M. Bogey, C. Demuynck, J. Destombes, *J. Chem. Phys.* **1992**, *97*, 7984–7989.

[264] D. Sülzle, H. Schwarz, *Chem. Phys. Lett.* **1989**, *156*, 397–400.

[265] K. M. Ervin, S. Gronert, S. E. Barlow, M. K. Gilles, A. G. Harrison, V. M. Bierbaum, C. H. DePuy, W. C. Lineberger, G. B. Ellison, *J. Am. Chem. Soc.* **1990**, *112*, 5750–5759.

[266] M. I. Bruce, *Chem. Rev.* **1991**, *91*, 197–257.

[267] T. Yang, B. B. Dangi, R. I. Kaiser, K.-H. Chao, B.-J. Sun, A. H. H. Chang, T. L. Nguyen, J. F. Stanton, *Angew. Chem. Int. Ed.* **2017**, *56*, 1264–1268; *Angew. Chem.* **2017**, *129*, 1284–1288.

[268] M. Stender, A. D. Phillips, R. J. Wright, P. P. Power, *Angew. Chem. Int. Ed.* **2002**, *41*, 1785–1787; *Angew. Chem.* **2002**, *114*, 1863–1865.

[269] Y. Sugiyama, T. Sasamori, Y. Hosoi, Y. Furukawa, N. Takagi, S. Nagase, N. Tokitoh, *J. Am. Chem. Soc.* **2006**, *128*, 1023–1031.

[270] J. Li, C. Schenk, C. Goedecke, G. Frenking, C. Jones, *J. Am. Chem. Soc.* **2011**, *133*, 18622–18625.

[271] T. J. Hadlington, M. Hermann, J. Li, G. Frenking, C. Jones, *Angew. Chem. Int. Ed.* **2013**, *52*, 10199–10203; *Angew. Chem.* **2013**, *125*, 10389–10393.

[272] T. Sasamori, T. Sugahara, T. Agou, J.-D. Guo, S. Nagase, R. Streubel, N. Tokitoh, *Organometallics* **2015**, *34*, 2106–2109.

[273] A. D. Phillips, R. J. Wright, M. M. Olmstead, P. P. Power, *J. Am. Chem. Soc.* **2002**, *124*, 5930–5931.

[274] L. Pu, B. Twamley, P. P. Power, *J. Am. Chem. Soc.* **2000**, *122*, 3524–3525.

[275] K. M. Krebs, D. Hanselmann, H. Schubert, K. Wurst, M. Scheele, L. Wesemann, *J. Am. Chem. Soc.* **2019**, *141*, 3424–3429.

[276] C. Wilhelm, D. Raiser, H. Schubert, C. P. Sindlinger, L. Wesemann, *Inorg. Chem.* **2021**, *60*, 9268–9272.

[277] R. Kobayashi, S. Ishida, T. Iwamoto, *Organometallics* **2021**, *40*, 843–847.

[278] A. C. Filippou, P. Ghana, personal communication, University of Bonn, **2015**.

[279] S.-H. Zhang, H.-X. Yeong, H.-W. Xi, K. H. Lim, C.-W. So, *Chem. Eur. J.* **2010**, *16*, 10250–10254.

[280] D. Dhara, V. Huch, D. Scheschkewitz, A. Jana, *Inorganics* **2017**, *6*, 6.

[281] Bochmann, M. J. Sarsfield, *Organometallics* **1998**, *17*, 5908–5912.

[282] J. Chen, E. Y.-X. Chen, *Dalton Trans.* **2016**, *45*, 6105–6110.

[283] K. W. Klinkhammer, *Chem. Eur. J.* **1997**, *3*, 1418–1431.

[284] T. Sasamori, J. S. Han, K. Hironaka, N. Takagi, S. Nagase, N. Tokitoh, *Pure Appl. Chem.* **2010**, *82*, 603–612.

[285] I. Papazoglou, Unprecedented Tetrylidyne Complexes of Group 6 and 10 Metals, Dissertation, University of Bonn, **2016**.

[286] S. Krämer, NHC-Stabilisierte Disilavinylidene Und Silylsilylene, Masterarbeit, University of Bonn, **2015**.

[287] S. Yao, Y. Xiong, M. Driess, *Acc. Chem. Res.* **2017**, *50*, 2026–2037.

[288] S. Yao, Y. Xiong, A. Saddington, M. Driess, *Chem. Commun.* **2021**, *57*, 10139–10153.

[289] S. Ishida, T. Iwamoto, C. Kabuto, M. Kira, *Nature* **2003**, *421*, 725–727.

[290] N. Takagi, T. Shimizu, G. Frenking, *Chem. Eur. J.* **2009**, *15*, 3448–3456.

[291] Y. Xiong, S. Yao, S. Inoue, J. D. Epping, M. Driess, *Angew. Chem. Int. Ed.* **2013**, *52*, 7147–7150; *Angew. Chem.* **2013**, *125*, 7287–7291.

[292] T. Sugahara, T. Sasamori, N. Tokitoh, *Angew. Chem. Int. Ed.* **2017**, *56*, 9920–9923; *Angew. Chem.* **2017**, *129*, 10052–10055.

[293] Y. Wang, M. Karni, S. Yao, A. Kaushansky, Y. Apeloig, M. Driess, *J. Am. Chem. Soc.* **2019**, *141*, 12916–12927.

[294] J. Keuter, A. Hepp, C. Mück-Lichtenfeld, F. Lips, *Angew. Chem. Int. Ed.* **2019**, *58*, 4395–4399; *Angew. Chem.* **2019**, *131*, 4440–4444.

[295] S. Yao, A. Kostenko, Y. Xiong, A. Ruzicka, M. Driess, *J. Am. Chem. Soc.* **2020**, *142*, 12608–12612.

[296] T. Koike, T. Nukazawa, T. Iwamoto, *J. Am. Chem. Soc.* **2021**, *143*, 14332–14341.

[297] Y. Xiong, S. Yao, R. Müller, M. Kaupp, M. Driess, *Angew. Chem.* **2015**, *127*, 10392–10395; *Angew. Chem.* **2015**, *127*, 10392–10395.

[298] L. C. Siemes, J. Keuter, A. Hepp, F. Lips, *Inorg. Chem.* **2019**, *58*, 13142–13149.

[299] A. Burchert, S. Yao, R. Müller, C. Schattenberg, Y. Xiong, M. Kaupp, M. Driess, *Angew. Chem. Int. Ed.* **2017**, *56*, 1894–1897; *Angew. Chem.* **2017**, *129*, 1920–1923.

[300] B. Prashant, Reactivity Studies on CaacMe Stabilized Silylone, Progress Report, University of Bonn, **2017**.

[301] R. S. Ghadwal, R. Azhakar, K. Pröpper, J. J. Holstein, B. Dittrich, H. W. Roesky, *Inorg. Chem.* **2011**, *50*, 8502–8508.

[302] G. Tavčar, S. S. Sen, R. Azhakar, A. Thorn, H. W. Roesky, *Inorg. Chem.* **2010**, *49*, 10199–10202.

[303] J. Li, S. Merkel, J. Henn, K. Meindl, A. Döring, H. W. Roesky, R. S. Ghadwal, D. Stalke, *Inorg. Chem.* **2010**, *49*, 775–777.

[304] S. M. I. Al-Rafia, A. C. Malcolm, R. McDonald, M. J. Ferguson, E. Rivard, *Chem. Commun.* **2012**, *48*, 1308–1310.

[305] T. Matsuo, K. Suzuki, T. Fukawa, B. Li, M. Ito, Y. Shoji, T. Otani, L. Li, M. Kobayashi, M. Hachiya, Y. Tahara, D. Hashizume, T. Fukunaga, A. Fukazawa, Y. Li, H. Tsuji, K. Tamao, *Bull. Chem. Soc. Jpn.* **2011**, *84*, 1178–1191.

[306] D. B. G. Williams, M. Lawton, *J. Org. Chem.* **2010**, *75*, 8351–8354.

[307] R. Inoue, M. Yamaguchi, Y. Murakami, K. Okano, A. Mori, *ACS Omega* **2018**, *3*, 12703–12706.

[308] J. Geier, H. Rüegger, H. Grützmacher, *Dalton Trans.* **2006**, 129–136.

[309] T. R. Hoye, B. M. Eklov, T. D. Ryba, M. Voloshin, L. J. Yao, *Org. Lett.* **2004**, *6*, 953–956.

[310] R. K. Harris, E. D. Becker, S. M. Cabral de Menezes, P. Granger, R. E. Hoffman, K. W. Zilm, *Pure Appl. Chem.* **2008**, *80*, 59–84.

[311] S. Stoll, A. Schweiger, *J. Magn. Reson.* **2006**, *178*, 42–55.

[312] D. F. Evans, *J. Chem. Soc.* **1959**, 2003.

[313] S. K. Sur, *J. Magn. Reson.* **1989**, *82*, 169–173.

[314] G. Brauer, *Handbuch Der Präparativen Anorganischen Chemie*, F. Enke, **1975**.

[315] K. Fredenhagen, G. Cadenbach, *Z. Anorg. Allg. Chem.* **1926**, *158*, 249–263.

[316] W. Rüdorff, E. Schulze, *Z. Anorg. Allg. Chem.* **1954**, *277*, 156–171.

[317] S. R. Bahr, P. Boudjouk, *J. Org. Chem.* **1992**, *57*, 5545–5547.

[318] N. A. Yakelis, R. G. Bergman, *Organometallics* **2005**, *24*, 3579–3581.

[319] M. Lehmann, A. Schulz, A. Villinger, *Angew. Chem. Int. Ed.* **2009**, *48*, 7444–7447; *Angew. Chem.* **2009**, *121*, 7580–7583.

[320] I. Tiritiris, T. Schleid, *Z. Anorg. Allg. Chem.* **2003**, *629*, 581–583.

[321] H. Gilman, C. L. Smith, *J. Organomet. Chem.* **1967**, *8*, 245–253.

[322] H.-M. Chen, J. P. Oliver, *J. Organomet. Chem.* **1986**, *316*, 255–260.

[323] R. A. Bartlett, M. M. Olmstead, P. P. Power, G. A. Sigel, *Inorg. Chem.* **1987**, *26*, 1941–1946.

[324] J. E. Borger, M. S. Bakker, A. W. Ehlers, M. Lutz, J. Chris Slootweg, K. Lammertsma, *Chem. Commun.* **2016**, *52*, 3284–3287.

[325] H. F. Holtzclaw, *Inorganic Syntheses. Volume 8 Volume 8*, **1966**.

[326] C. Stanciu, M. M. Olmstead, A. D. Phillips, M. Stender, P. P. Power, *Eur. J. Inorg. Chem.* **2003**, *2003*, 3495–3500.

[327] S. Marx, Homoleptische Und Heteroleptische Germanium(II)- Und Zinn(II)-Verbindungen Mit Alkoholat- Und Thiolat-Substituenten, Dissertation, Humboldt-Universität zu Berlin, **2005**.

[328] C. Lippmann, Untersuchung Der Reaktivität Eines Bis(Aryloxy)Silylens, Bachelorarbeit, University of Bonn, **2016**.

[329] *Handbuch der präparativen anorganischen Chemie. 2*, Enke, Stuttgart, **1978**.

[330] M. A. M. Fuhry, in *Encyclopedia of Reagents for Organic Synthesis* (Ed.: John Wiley & Sons, Ltd), John Wiley & Sons, Ltd, Chichester, UK, **2001**, p. rl150.

[331] K. K. Schönleber, Reaktivitätsstudien von [SiI_2(caac^{Me})], Bachelorarbeit, University of Bonn, **2017**.

[332] N. Kuhn, T. Kratz, *Synthesis* **1993**, *1993*, 561–562.

[333] R. S. Simons, L. Pu, M. M. Olmstead, P. P. Power, *Organometallics* **1997**, *16*, 1920–1925.

[334] T. Wiseman, S. Williston, J. F. Brandts, L.-N. Lin, *Anal. Biochem.* **1989**, *179*, 131–137.

[335] J. Abbenseth, D. Delony, M. C. Neben, C. Würtele, B. de Bruin, S. Schneider, *Angew. Chem. Int. Ed.* **2019**, *58*, 6338–6341; *Angew. Chem.* **2019**, *131*, 6404–6407.

[336] D. Delony, M. Kinauer, M. Diefenbach, S. Demeshko, C. Würtele, M. C. Holthausen, S. Schneider, *Angew. Chem. Int. Ed.* **2019**, *58*, 10971–10974; *Angew. Chem.* **2019**, *131*, 11087–11090.

[337] D. Delony, Reaction Analysis by Isothermal Titration Calorimetry, report, Göttingen, **2019**.

[338] G. A. Holdgate, *Biotechniques* **2001**, *31*, 164–166, 168, 170 passim.

[339] H. Kessler, *Angew. Chem. Int. Ed.* **1970**, *9*, 219–235.

[340] D. Kost, E. H. Carlson, M. Raban, *J. Chem. Soc. D* **1971**, 656.

[341] U. S. N. B. of Standards, *Journal of Research of the National Bureau of Standards: Engineering and Instrumentation*, U.S. Government Printing Office, **1966**.

[342] G. A. Bain, J. F. Berry, *J. Chem. Educ.* **2008**, *85*, 532.

[343] J. Ruiz Aranzaes, M.-C. Daniel, D. Astruc, *Can. J. Chem.* **2006**, 288–299.

[344] N. Elgrishi, K. J. Rountree, B. D. McCarthy, E. S. Rountree, T. T. Eisenhart, J. L. Dempsey, *J. Chem. Educ.* **2018**, *95*, 197–206.